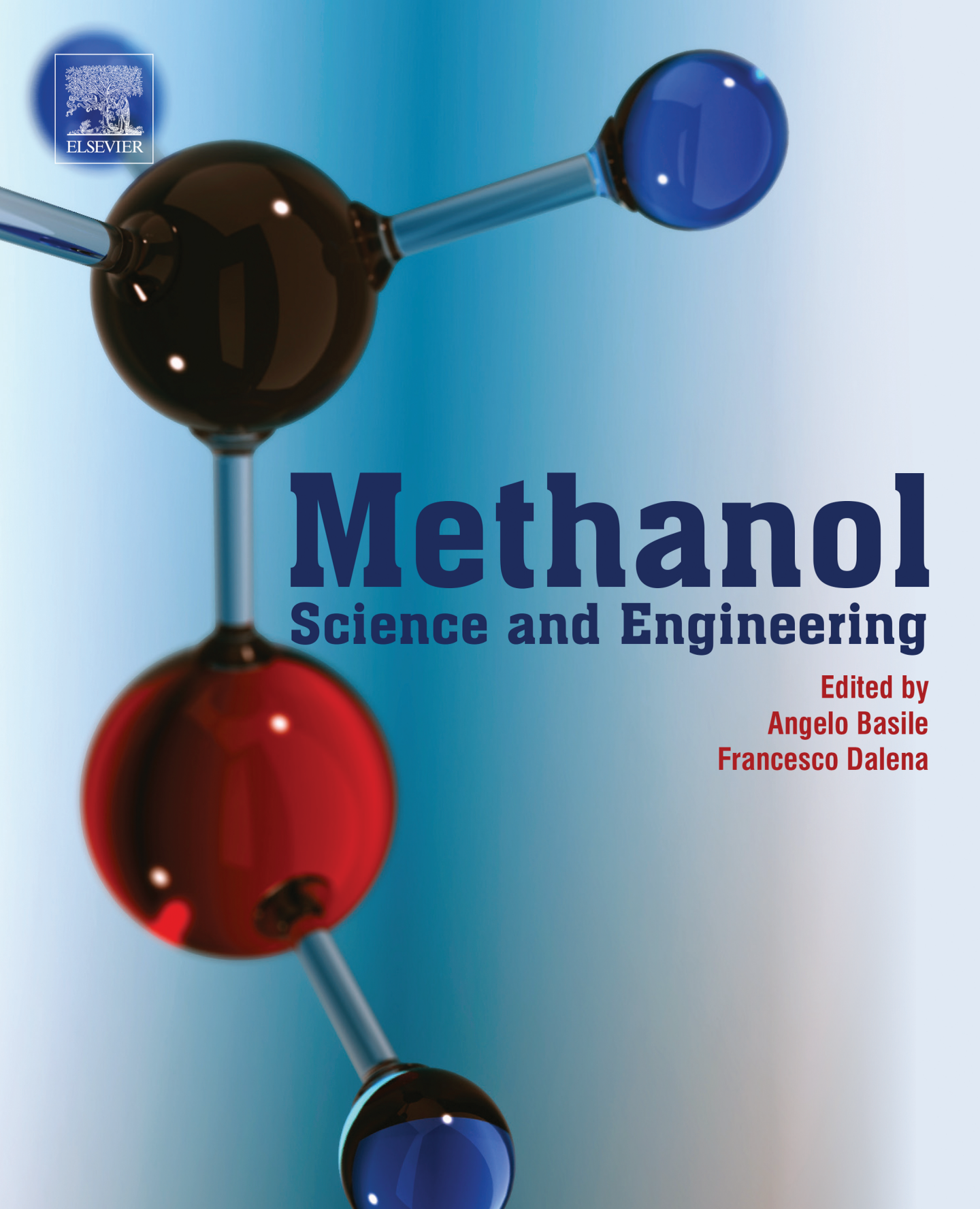
ELSEVIER
Methanol
Science and Engineering
Edited by
Angelo Basile
Francesco Dalena

Methanol

Science and Engineering

This page intentionally left blank

Methanol
Science and Engineering

Angelo Basile
Francesco Dalena

Elsevier
Radarweg 29, PO Box 211, 1000 AE Amsterdam, Netherlands
The Boulevard, Langford Lane, Kidlington, Oxford OX5 1GB, United Kingdom
50 Hampshire Street, 5th Floor, Cambridge, MA 02139, United States

Notices

Knowledge and best practice in this field are constantly changing. As new research and experience broaden our understanding, changes in research methods, professional practices, or medical treatment may become necessary.

Practitioners and researchers must always rely on their own experience and knowledge in evaluating and using any information, methods, compounds, or experiments described herein. In using such information or methods they should be mindful of their own safety and the safety of others, including parties for whom they have a professional responsibility.

To the fullest extent of the law, neither the Publisher nor the authors, contributors, or editors, assume any liability for any injury and/or damage to persons or property as a matter of products liability, negligence or otherwise, or from any use or operation of any methods, products, instructions, or ideas contained in the material herein.

Library of Congress Cataloging-in-Publication Data

A catalog record for this book is available from the Library of Congress

British Library Cataloguing-in-Publication Data

A catalogue record for this book is available from the British Library

ISBN: 978-0-444-63903-5

Publisher: John Fedor
Acquisition Editor: Kostas Marinakis
Editorial Project Manager: Carly Demetre
Production Project Manager: Maria Bernard
Cover Designer: Mark Rogers

Typeset by SPi Global, India

Contents

This page intentionally left blank

List of Contributors

Marjan Alavi Shiraz University, Shiraz, Iran
Francesco Arena Institute for Advanced Energy Technologies "Nicola Giordano" (ITAE-CNR); University of Messina, Messina, Italy
Vladimir Arutyunov Semenov Institute of Chemical Physics of Russian Academy of Sciences, Moscow; Institute of Problems of Chemical Physics of the Russian Academy of Sciences, Chernogolovka, Russia
Juan A. Baeza Universitat Autònoma de Barcelona, Bellaterra, Spain
Ali Bakhtyari Shiraz University, Shiraz, Iran
Marco Basile University of Calabria, Rende, Italy
Angelo Basile Institute on Membrane Technology (ITM-CNR), Rende, Italy
Giulia Bozzano Polytechnic of Milano, Milano, Italy
Mauro Capocelli University "Campus Bio-Medico" of Rome, Rome, Italy
Gabriele Centi University of Messina and INSTM/CASPE, Messina, Italy
Francesco Dalena University of Calabria, Rende, Italy
Marcello De Falco University "Campus Bio-Medico" of Rome, Rome, Italy
Francesco Falbo Institute on Membrane Technology (ITM-CNR), Rende, Italy
Alberto Figoli Institute on Membrane Technology (ITM-CNR), Rende, Italy
Francesco Galiano Institute on Membrane Technology (ITM-CNR), Rende, Italy
Fausto Gallucci Eindhoven University of Technology, Eindhoven, The Netherlands
Kamran Ghasemzadeh Urmia University of Technology, Urmia, Iran
Amalia Gordano Institute on Membrane Technology (ITM-CNR), Rende, Italy
Gianpiero Groppi Dipartimento di Energia, Politecnico di Milano, Milano, Italy
Albert Guisasola Universitat Autònoma de Barcelona, Bellaterra, Spain
Siddharth Gumber VIT University, Vellore, India
Anand V.P. Gurumoorthy VIT University, Vellore, India
Nazanin Hamedi Shiraz University, Shiraz, Iran
Gaetano Iaquaniello Processi Innovativi, L'Aquila; KT—Kinetics Technology S.p.A., Rome, Italy
Stefanie Kohler Total Refining & Chemicals, Paris La Défense Cedex, France
Kauko Leiviskä University of Oulu, Oulu, Finland
Flavio Manenti Polytechnic of Milano, Milano, Italy
Alessia Marino University of Calabria, Rende, Italy

Marco Martino University of Salerno, Fisciano, Italy
Outi Mäyrä University of Oulu, Oulu, Finland
Eugenio Meloni University of Salerno, Fisciano, Italy
Andrea Montebelli Dipartimento di Energia, Politecnico di Milano, Milano, Italy
Nuria Montpart EREP SA, Aclens, Switzerland; Universitat Autònoma de Barcelona, Bellaterra, Spain
Mojtaba Nasirinezhad Urmia University of Technology, Urmia, Iran
Alessandra Palella Institute for Advanced Energy Technologies "Nicola Giordano" (ITAE-CNR), Messina, Italy
Vincenzo Palma University of Salerno, Fisciano, Italy
Emma Palo KT – Kinetics Technology S.p.A., Rome, Italy
Carlo Pirola University of Milano, Milano, Italy
Mohammad R. Rahimpour Shiraz University, Shiraz, Iran
Behnaz Rahmatmand Shiraz University, Shiraz, Iran
Antonio Ricca University of Salerno, Fisciano, Italy
Concetta Ruocco University of Salerno, Fisciano, Italy
Seyyed M. Sadati Tilebon Iran University of Science and Technology, Tehran, Iran
Annarita Salladini University of Messina and INSTM/CASPE, Messina, Italy
Fereshteh Samimi Shiraz University, Shiraz, Iran
Alessandro Senatore University of Calabria, Rende, Italy
Lorenzo Spadaro Institute for Advanced Energy Technologies "Nicola Giordano" (ITAE-CNR); University of Messina, Messina, Italy
Enrico Tronconi Dipartimento di Energia, Politecnico di Milano, Milano, Italy
Carlo G. Visconti Dipartimento di Energia, Politecnico di Milano, Milano, Italy
Xudong Zhen Tianjin University of Technology and Education, Tianjin, China

Preface

Methanol, or methyl alcohol, is the simplest alcohol, which appears as a colorless liquid and with a distinctive smell. Traditionally, the primary uses of methanol have been for chemical production, as either a feedstock or a solvent or cosolvent. Nowadays, it is considered one of the most useful chemical compounds. In fact, it is one of the most promising building blocks for obtaining more complex chemical structures such as acetic acid, methyl tertiary butyl ether, dimethyl ether, and methylamine or for producing intermediates and synthetic hydrocarbons, including polymers and single-cell proteins. Furthermore, methanol is also considered a promising clean-burning fuel with a high number of octane:methanol can be mixed with conventional gasoline, without requiring any technical modification in the vehicle fleet. Nowadays, most vehicles use M85, a mixture of 85% of methanol and 15% of unleaded gasoline. Furthermore, methanol can also be used as a convenient energy carrier for hydrogen storage and transportation, as easily transportable as fuel.

Given the countless applications, many companies are trying to develop new technologies in order to produce methanol from different sources for the dual purpose of optimizing the production process and for the dual purpose of optimizing the production process and making it eco-sustainable.

Methanol can be synthesized from several carbon-containing feedstock, including natural gases, coal, biomass, or CO_2, with the latter one directly recovered from the atmosphere.

Knowing that there are CO_2 and H_2 among the precursors in the methanol synthesis, it is noteworthy that the conversion of CO_2 to methanol can be considered a promising method to significantly reduce CO_2 emissions and that methanol production can also be used as a convenient energy carrier for hydrogen storage and conservation. In fact, the methanol synthesis is the second source, after ammonia production, of hydrogen consumption (which has the highest energy content per weight) via several reactions, such as partial oxidation, steam reforming, autothermal reforming, methanol decomposition, and methanol-water solution electrolysis.

Finally, among the recent attractive applications of methanol, the most promising ones for the future are: production of Dimethyl Ether (DME), production of hydrogen, and the Direct Methanol Fuel Cell (DMFC).

The aim of this book is to provide, with contributions from some of the best scientists in the field, an overview on the status of the most recent research efforts. In fact, the book wants to provide a gradual knowledge starting from the production processes of methanol to arrive at the role of this molecule in the global market.

The volume is divided into four parts: Science and Production, Application and Innovation, Modeling and Technology, and Environment and Economy.

The first part (*Science and Production*) deals with production processes from various feedstocks to the formation of methanol. In detail, the volume opens with a chapter edited by the editors (Basile and Dalena) and their coworkers (Senatore, Marino, Gordano, and Basile). It provides an overview on the historical production processes of methanol (BASF and ICI), the last update of the production processes, and the most innovative application of methanol. Chapter 2 (Palma, Meloni, Ruocco, Martino, and Ricca) aims to explore the methanol synthesis process and the most relevant technologies available in the methanol industry. In Chapter 3 (Pirola, Bozzano, and Manenti) a comparison between the traditional, fossil-based process and the different biomass-based corresponding technologies is proposed. Furthermore, in this chapter there is a description of some selected processes together with the analysis of the different reactors and catalytic systems involved and the corresponding kinetic models interpretation. Chapter 4 (Iaquaniello, Centi, Salladini, and Palo) introduces the bio-methanol: the methanol produced via high temperature conversion of Refuse-derived-fuel (Rdf). Chapter 5 (De Falco and Capocelli) is focused on the methanol and the DME synthesis processes fed by a CO_2-rich syngas feedstock, derived from a biological process as fermentation or gasification of biomasses. Chapters 6–8 (Arutyunov) are focused on the conversion of natural gas (methane) into methanol. This process discussed in these three chapters is one of the most promising and well-developed fields with real technological experience and elaborated theoretical base. In particular Chapter 6 focuses on the historical and kinetics aspects; Chapter 7 discusses the products of direct conversion of natural gas into methanol and the effect of the gas composition on the Direct Methane To Methanol (DMTM); while Chapter 8 considers possible technological applications of the DMTM process. Chapter 9 (Spadaro, Arena, and Palella) provides an overview on the direct photo-conversion of CO_2. In particular, the chapter focuses on the advances in the photocatalytic CO_2 conversion. This chapter shows the development of efficient photocatalytic materials at higher "quantum yield," for improving the activity, selectivity, and the optimization of the photoreactor configuration enhancing the light transmission over the photocatalytic phase.

Part 2 of the book considers the application and the future innovative trends regarding this molecule. The first chapter of this part is Chapter 10 (Ghasemzadeh, Tilebon, and Basile). It is focused on extending the new technology applications such as solar energy systems, membrane reactors, and microreactors in hydrogen production from methanol feedstock during reforming processes. Chapter 11 (Bakhtyari and Rahimpour) treats the methanol dehydration for the

dimethyl ether production. This chapter reviews in detail the chemistry of methanol dehydration on the surface of solid-acid catalysts, the kinetic modeling for the derivation of rate expressions, conventional reactors, and also some innovative configurations. Chapter 12 (Zhen) describes the applications, such as methanol-gasoline, methanol-diesel, or other blends, that can be used on the internal combustion engines. Finally, it puts forward some new suggestions on the weakness in the research of methanol or methanol blends engines. Chapter 13 (Montpart, Baeza, and Guisasola) discusses the opportunities of methanol as a carbon source in bioelectrochemical systems, whereas Chapter 14 (Galiano, Falbo, and Figoli) introduces the Pervaporation (PV). The chemical process is described starting from the reactions and the transport mechanism, also illustrating the application of PV in organic/organic separation. The second part of the chapter also deals with the PV separation of methanol/organic and methanol/aqueous mixtures. Chapter 15 (Samimi and Rahimpour) provides a comprehensive overview of DMFC technology and presents different approaches to overcome its barriers for commercialization. Chapter 16 (Ghasemzadeh, Tilebon, and Basile) analyzes the Integrated Gasification Combined Cycles (IGCC) technology and, in particular, discusses the application of membrane processes in coproduction of methanol and electricity in IGCC plants.

Part 3 considers the modeling and the most innovative technology reactors for both the production and the application of methanol. Chapter 17 (Mäyrä and Leiviskä) introduces different mathematical model structures for methanol synthesis that have been developed and documented in the literature. Chapter 18 (Gallucci) describes the inorganic membrane reactors for methanol production. In particular it focuses on the main literature works dealing with methanol production. Chapter 19 (Visconti, Montebelli, Groppi, Tronconi, and Kohler) discusses the optimization of the conductive substrates for the methanol synthesis, as well as their catalytic activation by washcoating. In this chapter, an experimental work to confirm the feasibility of washcoating copper foams with a Cu-ZnO/Al_2O_3 industrial catalyst is also reported. The coated structures were, in fact, successfully tested at representative industrial methanol synthesis conditions. In Chapter 20 (Rahmatmand and Rahimpour) methanol synthesis processes by many and various types of methanol reactors have been proposed. Chapter 21 (Alavi, Hamedi, and Rahimpour) is focused on the modeling approaches toward dimethyl ether production reactors by having a short overview on the most recent findings in the literature.

The last part deals on the environment and economy of methanol. Chapter 22 (Iaquaniello, Centi, Salladini, and Palo) discusses more specifics of the economics of production of methanol from waste derived fuel like Rdf. Chapter 23 (Ghasemzadeh, Tilebon, Nasirinezhad, and Basile) is a comparative analysis of various methanol production methods and evaluation of the economic assessment of methanol production from renewable sources. Chapter 24 (Ghasemzadeh, Tilebon, Nasirinezhad, and Basile) is a comprehensive review on integrated systems for the coproduction of both electricity and methanol in IGCC plants with reference to

various aspects such as unit production capacity, CO_2 separation strategies, performance analysis, and especially economic assessment of this technology. The last chapter, Chapter 25 (Gumber and Gurumoorthy), is a comparative analysis of various methanol production methods and evaluation of economic assessment of methanol production from renewable sources.

To conclude, the Editors would like to express special thanks to each one of the authors for their valuable contributions to this volume. Other very special thanks are surely addressed to all the staff of Elsevier that helped us in all the various steps for realizing this work in the best way.

Francesco Dalena
Angelo Basile

PART 1

Science and Production

This page intentionally left blank

CHAPTER 1

Methanol Production and Applications: An Overview

Francesco Dalena*, Alessandro Senatore*, Alessia Marino*, Amalia Gordano†, Marco Basile*, Angelo Basile†

*University of Calabria, Rende, Italy †Institute on Membrane Technology (ITM-CNR), Rende, Italy

Acronyms

ACL	anode catalyst layer
ATR	autothermal reforming
BASF	Badische Anilin und Soda Fabrik
CCL	cathode catalyst layer
CMR	catalytic membrane reactor
DME	dimethyl ether
DMFC	direct methanol fuel cell
ETP	energy technology perspectives
GHG	greenhouse gases
IGCC	integrated gasification combined cycle
MD	methanol decomposition
MSR	methanol steam reforming
NCCC	National Carbon Capture Center
PEM	proton exchange membrane
PO	partial oxidation
POM	partial oxidation of methanol
SR	steam reforming
SW	solid wastes
WGS	water-gas shift
WTE	waste-to-energy

1 Introduction

In the last century, fossil fuels and natural gases have been our major source of energy. Unfortunately, these resources are not renewable and therefore limited. This creates instability in the global market, which leads to a corresponding instability in fuel price. Furthermore,

Methanol. https://doi.org/10.1016/B978-0-444-63903-5.00001-7

fossil fuels are primarily responsible for the emission of greenhouse gases (GHG) such as CO_2, CH_4, and N_2O, which contribute to global warming.

Nowadays, the main competitors appear to be hydrogen and methanol (as discussed in Chapter 25). The use of hydrogen appears to be the most promising from an energy point of view. In fact, it has the highest energy content per unit weight of any known fuel (142 kJ/g), and in comparison to the other known natural gases, it is environmentally safe. At present, the problems related to the use of hydrogen as a new energy resource are the costs of purification processes and the difficulties linked to infrastructure for storage and transport. The most important competitor appears to be methanol, which has an octane number of 113 and a density that is about half that of gasoline (Olah et al., 2009).

Among several uses, methanol can be mixed with conventional gasoline without requiring any technical modification in the vehicle fleet. Most of the methanol-fueled vehicles use M85, a mixture of 85% methanol and 15% unleaded gasoline (Cifre and Badr, 2007). Furthermore, methanol can be used as a convenient energy carrier for hydrogen storage and transportation, as an easily transportable fuel, and also in the chemical industry as a solvent and as a C1 building block for producing intermediates and synthetic hydrocarbons, including polymers and single-cell proteins (Bozzano and Manenti, 2016). For all these reasons, methanol is considered to be the transition molecule from fossil fuels to renewable energies.

Methanol, or methyl alcohol, is an organic compound, CH_3OH, with a molecular weight equal to 32.042 u.m.a. It is only slightly soluble in fat and oil and represents one of the most important chemical raw materials. Indeed, the primary use of methanol is in the chemical industry, as either a feedstock, solvent, or cosolvent.

Approximately 65% of the methanol produced worldwide is consumed for the production of acetic acid, methyl and vinyl acetates, methyl methacrylate, methylamines, methyl ter buthyl ether (MTBE), fuel additives, and other chemicals. The remaining portion is converted into formaldehyde and the resulting products, as shown in Fig. 1.1 (Khadzhiev et al., 2016; Ali et al., 2015).

Many technologies have been developed over the years to produce methanol from different sources. In fact, it can be synthesized from several carbon-containing feedstocks, including natural gases (it could even be produced right at the gas well by oxidative transformation), coal, biomass, or CO_2, the latter directly recovered from the atmosphere.

It is difficult to date precisely the first synthesis of methanol in history. We have tried to give a historical reconstruction of the methanol production processes afterward (Fig. 1.2).

Before the development of the modern industrial era, methanol, also called *wood spirit*, was prepared by wood heating in anaerobic condition. The wood distillation process provided an extract that contained many impurities besides the methyl alcohol. The process was

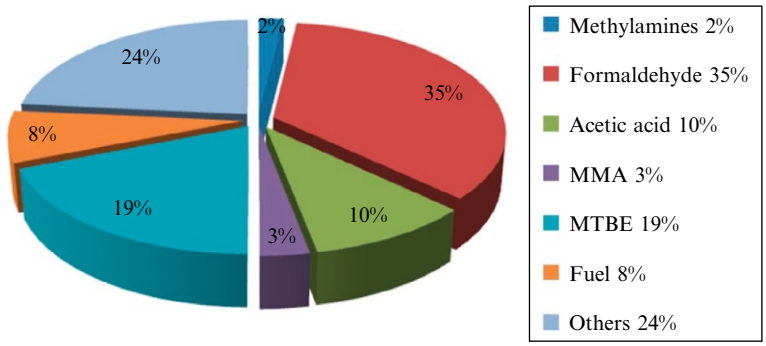

Fig. 1.1
Resulting products of methanol.

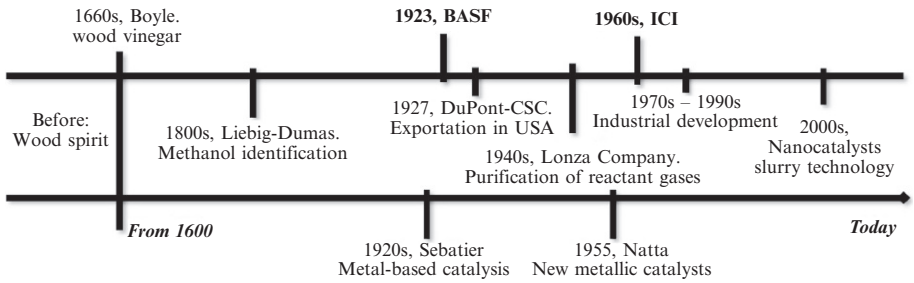

Fig. 1.2
Historical reconstruction of methanol production.

improved in the 1660s by scientist Sir Robert Boyle. He carried out a purification of the extract, called wood vinegar, by a reaction with milk of lime (an aqueous suspension of calcium hydroxide). However, this was not marketed for about two centuries (Fiedler et al., 2000). The exact composition of the wood vinegar remained unknown until the 1800s, when J.V. Liebig and J.B.A. Dumas independently identified the methanol molecule. On the basis of their works, in 1835 the term methyl was formally introduced into chemistry. In the same period, methanol began to be commercialized. A fundamental development in methanol synthesis came from the studies of Paul Sabatier. He found an important way to hydrogenate a large variety of functional groups by metal-based catalysis, and among the numerous compounds he studied, a nickel-based catalyst allowed him to obtain methyl alcohol by hydrogenation of carbon monoxide (Sabatier, 1926). However, the first break in methanol synthesis came in 1923 from a German company called Badische Anilin und Soda Fabrik (BASF). That company developed a metal-based catalytic hydrogenation at high pressure, called the BASF process (Tijm et al., 2001). This technology began to be exported, and in 1927 it was introduced by both DuPont and the Commercial Solvents Corporation in the United States. The BASF process not only represented the starting point in the industrial production of methanol, but it remained the dominant technology for more than 45 years. Over the following years, a great effort

has been made to develop new technologies to reduce pressure and temperature levels, with the aim of improving the economic process. In the 1940s, the Swiss Lonza Company began the industrial synthesis of methanol from electrolytic hydrogen and carbon dioxide, the latter derived from $Ca(NO_3)_2$ synthesis. For the first time, the reactant gases had been purified from nitrous vapors, and the reaction had been carried out using the ZnO-based catalyst, developed in Italy by Prof. Giulio Natta, for the methanol synthesis from CO and H_2 (Natta, 1955).

Thanks to the invention of steam methane reforming, which allowed the production of more pure *syngas* (a mixture of H_2, CO, and CO_2), a more active Cu/ZnO catalyst could be used, thus decreasing the process temperature and pressure to about 300°C and 100 bar, respectively. This significant improvement was proposed in the Imperial Chemical Industries (ICI) process in 1966 (Bozzano and Manenti, 2016). On this basis, many implementations were carried out through time and many new industrial plants were adapted to the singular production needs, such as the Lurgi, Haldor-Topsøe, and Linde plants.

Because of the increasing industrial production of methanol, it began to be used in several fields. In 1973, an oil embargo proclaimed by the Organization of Petroleum Exporting Countries (OPEC) in the U.S. and the Netherlands increased the interest in methanol as a new alternative automobile fuel. But while these studies have continued, the U.S. Clean Air Act was passed in 1990. This sanctioned the reduction of ozone and carbon monoxide emissions, which are the methanol combustion products. The use of methanol as a fuel was therefore banned. During the 1990s, market demand grew again when it was discovered that methyl alcohol can also be used as a fertilizer in agriculture for a great variety of products. Today, the global consumption of methyl alcohol is about 92Mt/year (Fig. 1.3), and since 1975 its production has grown at about 1433% (Zhen and Wang, 2015; Khadzhiev et al., 2016).

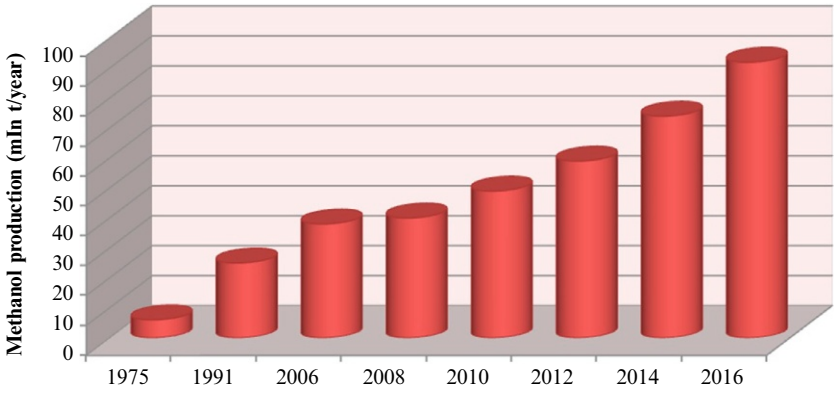

Fig. 1.3
Methanol production expressed in mln ton per year of production from 1975 to 2016.

This chapter seeks to give a general overview of methanol production, its historical production processes (BASF and ICI), and its most innovative trends with a particular focus on the production of dimethyl ether (DME), the production of hydrogen, and the application of methanol in the fuel cells.

2 Methanol Production

As mentioned above, methanol can be produced from several carbon-containing feedstocks, such as natural gas, coal, biomass, and CO_2. For each of them, the reactions and technologies involved are examined in detail.

2.1 Methanol From Natural Gas

Currently, about 90% of methanol is produced from natural gas (Blug et al., 2014). The process route for the production of the simplest alcohol is relatively straightforward, involving the three following basic steps (Tijm et al., 2001; Roan et al., 2004; Fiedler et al., 2005; Spath and Dayton, 2003):

- Production of synthesis gas;
- Conversion of the syngas into crude methanol;
- Distillation of the reactor effluent (crude methanol) to achieve the desired purity.

The mixture of syngas (H_2, CO, and CO_2) is mainly produced by steam reforming (SR) and autothermal reforming (ATR) of natural gas, as shown in Eqs. (1.1) and (1.2), respectively. However, it is also obtained by partial oxidation (PO) of methane (Eq. 1.4) or different carbon-based materials such as coal, heavy oils, or biogas (Wilkinson et al., 2016; Basile et al., 2015).

Steam reforming:

$$CH_4 + H_2O \rightleftarrows CO + 3H_2 \tag{1.1}$$

Autothermal reforming:

$$CH_4 + 2O_2 \rightarrow CO_2 + 2H_2O \tag{1.2}$$

which involves Eq. (1.1) and a *water gas shift (WGS)* reaction:

$$CO_2 + H_2 \rightleftarrows CO + H_2O \tag{1.3}$$

Partial oxidation:

$$CH_4 + {}^{1}/_{2}O_2 \rightarrow CO + 2H_2 \tag{1.4}$$

As reported by Bozzano and Manenti (2016), the composition of syngas is usually characterized by the stoichiometric number S, given by the ratio of two quantities: the difference between hydrogen and carbon dioxide moles, and the summation of the moles of CO_2 and CO.

$$S = \frac{\text{moles } H_2 - \text{moles } CO_2}{\text{moles } CO_2 + \text{moles } CO} \tag{1.5}$$

For the production of methanol and under ideal conditions, S should assume a value of 2. The stoichiometric value S takes into account the presence of CO_2 converted that consumes hydrogen via the reverse WGS reaction (Eq. 1.6).

$$CO_2 + 3H_2 \rightleftarrows CH_3OH + H_2O \quad \Delta H = -41.17 \text{kJ/mol} \tag{1.6}$$

The value of S depends on the adopted raw material. When syngas is produced by means of natural gas reforming, an S value of 2.8–3 is usually achieved.

The process of converting syngas into crude methanol occurs at a pressure of 50–100 bar and a temperature of 200–300°C. The main reactions involved in methanol synthesis are shown below (Klier, 1982):

Hydrogenation of carbon monoxide:

$$CO + 2H_2 \rightleftarrows CH_3OH \tag{1.7}$$

Divided into two consecutive steps:

$$CO + H_2 \rightleftarrows CH_2O \tag{1.8}$$

$$CH_2O + H_2 \rightleftarrows CH_3OH \tag{1.9}$$

Hydrogenation of carbon dioxide:

$$CO_2 + 3H_2 \rightleftarrows CH_3OH + H_2O \tag{1.10}$$

In which the first step involves the conversion of carbon dioxide in carbon monoxide as expressed in Eq. (1.2).

The reactions (1.7) and (1.10) are strongly exothermic (respectively $\Delta H = -100.46$ kJ/mol in Eq. (1.9) and $\Delta H = -61.59$ kJ/mol in Eq. 1.12) and, consequently, require significant cooling. The mixed gases are fed to the converter with H_2/CO maintained at a ratio from 3:1 to 5:1 for the conventional gas-phase process, which often requires equipment where the WGS is used to boost the hydrogen content (Eq. 1.5). The liquid-phase methanol process, through its superior heat management capabilities, can handle the synthesis gas straight from the generator, as it has a ratio of 1:1 to 1:2 as generated by coal gasifiers (Tijm et al., 2001). However, the ideal ratio H_2/CO_2 responds to Eq. (1.5).

In addition, the conversion of synthesis gas is subjected to a thermodynamic equilibrium that limits the process to a low conversion per pass and, therefore, implies a large recycle of unconverted gas. The resulting recycle and cooling duty are largely responsible for the investment costs of this process segment.

Over the years, several solid catalysts have been developed in order to maximize methanol yield and selectivity and minimize byproduct formation.

2.1.1 The BASF process—high-pressure method

On Jan. 16, 1923, while A. Mittasch and M. Pier were studying ammonia metal-catalyzed synthesis, (the Haber-Bosch process (Tour, 1920)), they discovered that the hydrogenation of carbon monoxide with an iron-based catalyst, over 500°C and 100 bar, provided methanol, among other products. They tried to synthesize methanol, therefore, by waste gases derived from the ammonia synthesis and the same iron-based catalyst. However, this reaction gives different products at the same time (Table 1.1), in which the methyl alcohol is the least thermodynamically favorite (Natta, 1955; Fiedler et al., 2000).

Furthermore, the yield was very low because of pollutants in the reactant gases such as chlorine, hydrogen sulphide, methane, and other hydrocarbons. This caused the deactivation of the iron catalyst and the reaction between carbon monoxide and iron, which can form penta-coordinated complexes (Natta, 1955). Since that time, a great variety of oxides and metals have been tested as hydrogenation catalysts, excluding only the eighth group of the periodic system. All reactions were carried out at high pressure, 250–300 bar, and high temperatures, 320–450°C. Among all, the two catalysts that gave the best results in these reaction conditions were ZnO/Cr_2O_3 and ZnO/CuO (Mittasch et al., 1925; Mittasch and Pier, 1926; Kung, 1980; Chinchen et al., 1988; Tijm et al., 2001; Fiedler et al., 2000). On this basis, many studies have been done to investigate the reaction mechanisms of the Eqs. (1.6)–(1.8), in presence of the above-mentioned solid catalysts (heterogeneous catalysis). As shown below, two different ways were proposed, both involving the adsorption of CO and H_2 (Kung, 1980): the mechanism A (Fig. 1.4) shows that the reaction takes place in four consecutive hydrogenation steps.

Table 1.1 Byproducts of methanol synthesis

Long-chain alcohols		$nCO + 2nH_2 \rightleftarrows CnH_{2n+1}OH + (n-1)H_2O$
Which can evolve in	Aldehydes	$RCH_2CH_2OH \rightleftarrows RCH_2CHO + H_2$
	Ketons	$2RCH_2CHO \rightleftarrows RCH_2COCHRCH_3 + O_{ads}$
Hydrocarbons:		$CO + 3H_2 \rightleftarrows CH_4 + H_2O$ $CO_2 + 4H_2 \rightleftarrows CH_4 + 2H_2O$ $nCO + (2n-1)H_2 \rightleftarrows CnH_{2n+2} + nH_2O$
DME		$2CO + 4H_2 \rightleftarrows CH_3OCH_3 + H_2O$

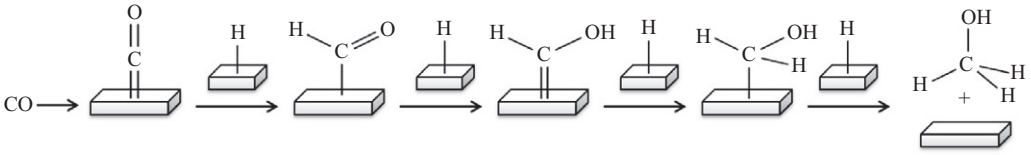

Fig. 1.4
Reaction mechanism A; the gray shape represents the catalyst surface.

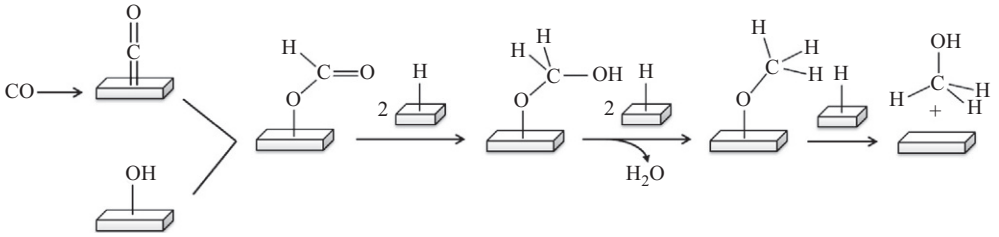

Fig. 1.5
Reaction mechanism B.

In mechanism B (Fig. 1.5) both CO and a hydroxyl group on the catalyst surface are involved. The first step takes place by an insertion of carbon monoxide to form a formate intermediate; subsequent hydrogenation and dehydration lead to the formation of methanol, passing through a methoxide intermediate.

It is noteworthy that the two mechanisms proposed differ not only for the intermediates formed, but also for the way in which they are bonded to the catalyst surface, that is with a carbon atom in mechanism A and with oxygen in B. As a result, catalytic cycles of ZnO/Cr_2O_3 and ZnO/CuO catalysts were proposed. As shown in Fig. 1.6, the active site was assumed to be a cluster of zinc ions with an oxygen vacancy. In accord with these studies, the interaction between the end oxygen of the adsorbed CO and the cluster electron-deficient vacancy allows the activation of the CO bond.

2.1.2 The ICI process—low-pressure method

In the 1960s, the BASF high-pressure method was overcome by a low-pressure method created by ICI (now Johnson Matthey). They developed a new route for methanol synthesis in a pressure range equal to 35–54 bar and at temperatures ranging from 200°C to 300°C. This was made possible not only by the discovery of a new, more active and selective copper-based catalyst ($Cu/ZnO/Al_2O_3$), but also by the development of new advanced purification processes for synthesis gases, which allowed them to use sulfur-chlorine-free syngas (Zhen and Wang, 2015; Van Bennekom et al., 2013).

Despite the fact that the catalytic power of copper/zinc catalysts in methanol synthesis was already well known, this was not exploited commercially due to their low lifetime and low

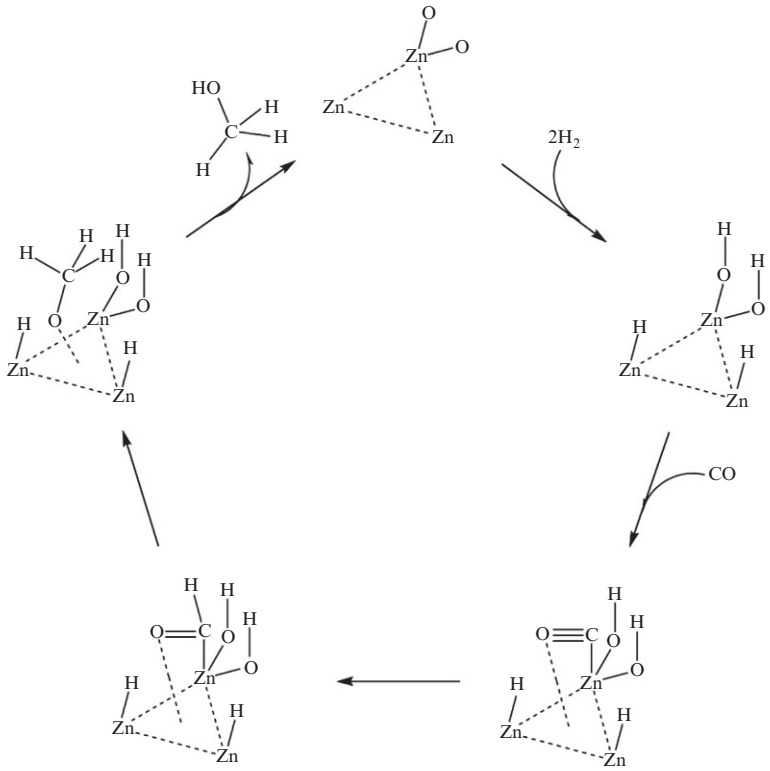

Fig. 1.6
Catalytic cycle of ZnO-catalyzed methanol synthesis.

thermal stability, mostly caused by their deactivation by poisoning (Chinchen et al., 1988; Sá et al., 2010). These problems were overcome thanks to the addition of alumina, which increases the stability of the Cu/ZnO catalyst and inhibits the thermal formation of Cu crystallites (Matsumura and Ishibe, 2009; Sá et al., 2010; Peppley et al., 1999).

Several studies have been carried out in order to investigate the catalytic behavior of the $Cu/ZnO/Al_2O_3$ catalyst, but today this mechanism is still not fully understood. Recent research confirms what is described above, that is that the oxygen vacancy in the ZnO lattice is responsible for a better adsorption and transformation of CO and CO_2, adding that this presence improves the Cu dispersion on the catalyst support (Ganesh, 2014; Nakamura et al., 2003; Yong et al., 2013).

Furthermore, it is well known that the active site of this kind of catalyst is copper, but there are controversies about its mechanism of action. Many studies suggested that metallic Cu sites are the active catalytic centers. On the other hand, during the methanol synthesis reaction, the migration from ZnO to Cu of the ZnO_x species leads to the formation of oxidized sites Cu^+, also considered as an active catalytic area. Furthermore, it has been shown that both the Cu and Cu^+

species are important in methanol formation, promoting CO_2 and CO hydrogenation respectively, and that the catalytic activity strongly depends on their ratio Cu^+/Cu^0 (Kanai et al, 1994; Fujitani et al., 1994; Ganesh, 2014; Kanai et al. 1996; Nakamura et al., 2003). On this basis, the catalytic cycle shown in Fig. 1.7 has been proposed. The microkinetic model shows that methanol can be produced by hydrogenation of carbon dioxide through the following intermediates HCOO, HCOOH, CH_2COOH, CH_2O, and CH_3O, and can also be produced from carbon monoxide hydrogenation by HCO, CH_2O, and CH_3O intermediates (Grabow and Mavrikakis, 2011).

In Table 1.2 some differences from feedstock and from a production point of view (expressed in t/day) of BASF, ICI, and other some useful production processes for obtaining methanol are reported. As can be seen, the evolution of the processes from the high pressure (BASF) to the low pressure (ICI) led to an increase of 10^5 t/day.

2.2 Methanol From Coal and Biomass

The use of biomass and char represents another route for methanol production. Nowadays, new industrial research is trying to solve the triple problem of energy demand, waste management, and GHG emissions. Waste-to-energy (WTE) technologies convert solid waste into various forms that can be used to supply energy, which can be derived by thermochemical processes. The latter is a better route than biochemical conversion, due to a

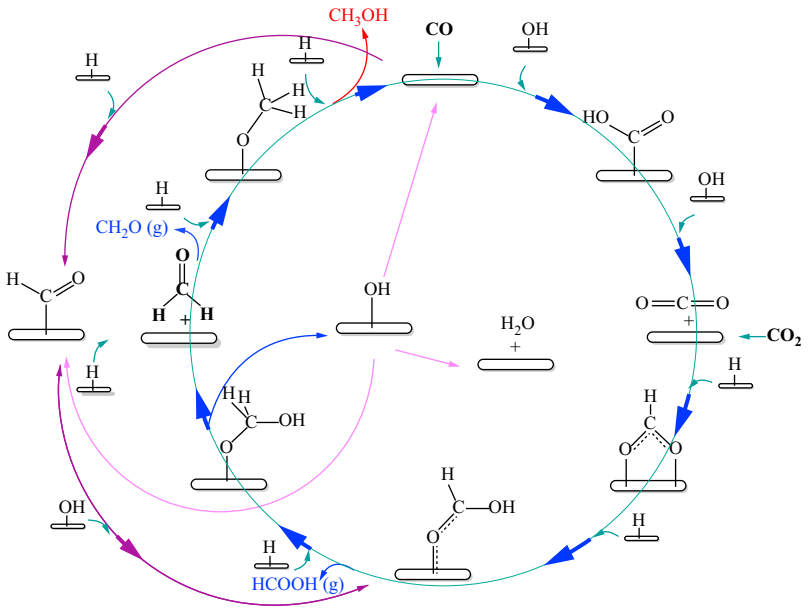

Fig. 1.7
Model of mechanism of methanol synthesis on Cu-based catalyst.

Table 1.2 Methanol yield (t/day) of the main historical industrial processes

Productive process	Feedstock	Yield	Reference
BASF	Syngas	0.07896 t/day	Klier (1982) and Kung (1980), and Mittasch and Pier (1926)
DuPont	Syngas	0.114 t/day	Klier (1982), Kung (1980), and Green (1973)
Haldor-Topsøe	Syngas	2400 t/day	Wilhelm et al. (2001) and Styhr (1972)
ICI	Carbonaceous feedstock	2500 t/day	Pinto (1983)

higher amount of feedstock transformed and a faster conversion rate (Shahbaz et al., 2017; Guan et al., 2016).

The production process for obtaining methanol from coal and biomass is similar to that for the production of methanol from natural gas, subdivided into the following three steps: syngas production, synthesis of the crude methanol, and purification.

In the first step, coal or biomass is converted inside a gasifier into the gaseous products, which consist of biogas (CH_4 and CO_2), syngas (H_2, CO_2 and CO), pure hydrogen, and alkaline gases (Dalena and Basile, 2015).

The gasification process is a thermochemical conversion technique that allows the conversion of solid biomass into gaseous mixtures with the help of gasifying agents such as air/oxygen, steam, and flue gases (Zhao et al., 2015; Dai et al., 2015). This process, using high temperatures in the presence of O_2, aims for a large-scale development to overcome the current limits (i.e., low hydrogen production and high tar content in the syngas (Chen et al., 2016;Shen and Yoshikawa, 2013)). In fact, the unwanted tar may cause the formation of tar aerosols and polymerization into more complicated structures, which are not favorable for hydrogen production through steam reforming (Ni et al., 2006). For this reason, several research groups have focused their studies on maximizing the hydrogen quantity produced and minimizing that of tar.

Under typical gasification conditions, oxygen levels are restricted to less than 30% of that required for complete combustion, and CO and H_2 are the major products (Milne et al., 1998).

Several works in the literature indicate the temperatures necessary to reduce underivatized mono-, di-, and poly-nuclear aromatics (which constitute the tar) to light gases. For example, it has been reported (Corella et al., 1999; Milne et al., 1998) that tar could be thermally cracked at temperature above 1000°C. These authors also carried out their research on biomass gasification under similar conditions but varied the gasifying agent. In fact, the use of some additives such as dolomite inside the gasifier helps tar reduction (Corella et al., 1999).

Generally, dolomite contains 30 wt% CaO, 21 wt% MgO, and 45 wt% CO_2, with others minerals such as SiO_2, Fe_2O_3, and Al_2O_3 (Dalena et al., 2017). It is a cheap disposable catalyst that can significantly reduce the tar content of the product gas from a gasifier.

As reported by Trop et al. (2014), torrefaction (also known as mild pyrolysis), was found to be another productive study aimed at the optimization of biomass properties. This process involves the combustion of the biomass at temperatures in the range of 200–300°C in anaerobic conditions. When the system reaches this temperature, the water and other volatile substances contained within the biomass evaporate, while the lignocellulose (the biopolymer of which is mainly composed the biomass) starts to degrade with a consequent loss of the initial mass equal to 20%. Torrefaction technology greatly reduces the tenacity of biomass; therefore the power consumption needed for grinding torrefied biomass is reduced by 80%–90% in comparison to raw biomass (Van der Stelt et al., 2011). Torrefaction is a promising process for increasing the amount of biomass used for gasification processes. The grindability of torrefied biomass is comparable to that of coal; therefore, it can be gasified in entrained flow gasifiers with high cold gas efficiencies (Trop et al., 2014), but results are environmentally friendly because it has zero carbon footprint.

Methanol is produced from syngas utilizing conventional gasification of biomass at high temperatures (800–1000°C); it can be made with any resource containing carbon, such as coal, or solid wastes (SW) (Balat, 2010).

The conversion of gaseous products involves many reactions described below (Shahbaz et al., 2017; Moghadam et al., 2014; Gao et al., 2012):

Char gasification reaction

$$C + H_2O \rightarrow CO + H_2 \quad \Delta H = 131.5\,\text{kJ/mol} \tag{1.10}$$

WGS reaction

$$CO + H_2O \rightleftarrows CO_2 + H_2 \quad \Delta H = -41\,\text{kJ/mol} \tag{1.3}$$

Steam reforming of methane

$$CH_4 + H_2O \rightleftarrows CO + 3H_2 \quad \Delta H = 206\,\text{kJ/mol} \tag{1.1}$$

Boudouard reaction

$$C + CO_2 \rightarrow 2CO \quad \Delta H = 172\,\text{kJ/mol} \tag{1.11}$$

Methanation reaction

$$C + 2H_2 \rightarrow CH_4 \quad \Delta H = -74.8\,\text{kJ/mol} \tag{1.12}$$

However, conventional gasification processes applied to biomass do not always produce a syngas with the quality required for methanol synthesis. One of the biggest problems in the

gasification of biomass is the formation of tar and char via reduction of carbon oxides, according to Eqs. (1.13) and (1.14):

$$CO + H_2 \rightarrow C + H_2O \tag{1.13}$$

$$CO_2 + 2H_2 \rightarrow C + 2H_2O \tag{1.14}$$

Tar and char formation during biomass gasification can be very problematic when using conventional biomass gasification systems (Shen et al., 2008). However, in order to use biomass in entrained flow gasifiers, the biomass must be pulverized to particle sizes of 100 μm, which is a necessity for these types of gasifiers (Prins et al., 2006; Chen and Kuo, 2010). Large energy consumption is needed to pulverize raw biomass (Trop et al., 2014).

The synthesis gas for methanol production should only contain a small proportion of inert gas components. In fact, the use of air as a gasification agent results in a syngas with a high nitrogen content. For methanol synthesis the optimal H_2:CO_2 molar ratio in the syngas is >2 (Specht and Bandi, 1999) and then the gasification of biomass always results in a gas with a too low H_2:CO_2 ratio. Usually the WGS process is the most frequently used process for ensuring a suitable ratio of CO_2:CO:H_2 and mainly to convert the CO into CO_2. If CO is present when the syngas is combusted in the gasificator, the CO_2 removal efficiency will be limited since the CO in syngas will be converted to CO_2 during the combustion process, as expressed in Eq. (1.3).

The reaction temperature for the WGS is 375°C and the pressure is 40 bar. Carbon monoxide is converted to carbon dioxide and hydrogen, as can be seen in Eq. (1.3). The carbon dioxide produced during the WGS process must be separated from the syngas in order to ensure a suitable ratio of CO_2:CO:H_2 for the commercially available methanol production catalyst required to be 5:28:63 (Zhang et al., 2010; Trop et al., 2014).

To optimize the stoichiometric ratio (Eq. 1.5) and to purify the syngas from substances harmful to the environment, several cleaning processes must be carried out before the gas enters the methanol production process, together with composition optimization. Firstly, sulfur must be removed from the syngas as sulfur is very hazardous for the catalyst used for methanol production and WGS reaction (Trop et al., 2014). Natural gas, in fact, can contain up to 30% hydrogen sulfide (Dalrymple et al., 1991). According to environmental regulations, negligible sulfur content would be allowed in the natural gas and fuels. H_2S, mercaptans, and, in some cases, COS and CS_2 are poisonous sulfur components associated with natural gas. They should be treated via appropriate technologies in gas refineries (Nabikandi and Fatemi, 2015).

In a 2002 report (Korens et al., 2002), SFA Pacific proposed two main methodologies for sulfur purification from commercially available syngas. These methods intend to transform hydrogen sulfide and CO_2 in a mixture of H_2, CO, H_2O, and S_2, according to Eq. (1.14):

$$2H_2S + CO_2 \rightleftarrows H_2 + CO + S_2 + H_2O \tag{1.14}$$

The two main technologies proposed by SPA Pacific are:

- *The sulfinol process*, which is based on a mixture of chemical solvents (aqueous amines) and the physical solvent Sulfolane (tetra-hydrothiophene dioxide). This method has been used in five projects since 1969, including two integrated gasification combined cycle (IGCC) plants and three chemical synthesis applications.
- *The rectisol process*, which is based on refrigerated methanol as the physical solvent. This method continues to be the predominant process used when very pure syngas is required for chemical synthesis. It is normally used where a deep desulfurisation of the synthesis gas is necessary, indicatively for feeds with H_2S composition greater than 30 mol % (in dry basis) (Marcum, 2012). Sulfur compounds are converted to elemental sulfur using a Claus plant and, once purified from sulfur compounds, the syngas is cooled before being introduced into the Rectisol process. The released heat is used to heat the synthesis gas after desulfurisation and to raise low-pressure steam. Part of it is used for the WGS reaction, and the remainder is expanded within a steam turbine. The low-pressure steam is added to the sulfur-free syngas and the mixture is conveyed to the WGS process (Trop et al., 2014).

Another process for the optimization of syngas from a methanol optimization point of view was proposed by the National Carbon Capture Center (NCCC) in 2012 (NCCC, 2012). The NCCC suggests a method to maximize CO_2 capture. In this process, the syngas is passed over a WGS catalyst in the presence of water to convert the CO to CO_2 (Eq. 1.3) prior to the CO_2 removal step. The NCCC is investigating the performance of WGS catalysts under a wide range of steam-to-CO ratios using a WGS reactor incorporated into a gasification power plant. The tests reported in this technical update show that high CO conversions are achieved at lower than recommended steam-to-CO ratios. Furthermore, as molar ratios are increased above about 1.6, the projected improvements in conversions become more marginal. Test data shows that no methane is formed and that no carbon is deposited in the reactor.

Another way to obtain the catalytic conversion of CO to CO_2 is by using a catalytic membrane reactor (CMR). This has possible applications in relation to the recovery of tritium from the blanket of a fusion reactor, to vehicular emission control, to removal of CO from combustion gases, and to conversion of water gas (Basile et al., 1996). By using a CMR, the hydrogen is recovered from the water by a catalytic shift reactor coupled with a membrane permeator. Extracting H_2 from the mixture reaction by using a palladium membrane or a Pd-Ag alloy membrane shifts the reaction toward the products, giving higher conversion with respect to the equilibrium values. The highest CO conversion obtained was 85% at a relatively low temperature (157°C) and at a permeate rate of 0.64 cm^3/min. As mentioned by Basile et al. (1996), it is possible to achieve an almost complete CO conversion (99.9%) at a feed pressure of 1.2 bar and 322°C through a 0.2 μm thick Pd/Al_2O_3 membrane

reactor (i.e., considerably mild operating conditions), revealing the dramatic advantage of a membrane reactor over a conventional reactor.

2.3 Methanol From Catalytic Hydrogenation of CO_2

As can be seen in Section 2.1, CO_2 is a linear molecule that is very stable and needs extra efforts to make it reactive. Owing to its high stability ($\Delta G^\circ = -400$ kJ mol^{-1}), a substantial energy input, optimized reaction conditions, and a catalyst with high stability and activity are required for converting CO_2 into value-added chemicals.

As reported by Ganesh (2014), converting one mole of CO_2 to methanol requires an energy input of about 228 kJ and six electrons to reduce C^{4+} of CO_2 to C^{2-} of methanol. The carbon-oxygen bonds are very strong, and high energy is required for breaking them. For this reason, in order to convert CO_2 into methanol, a good catalytic system is required, as expressed in Chapter 15.

The reaction of this catalytic conversion of CO_2 into methanol by hydrogenation is expressed in Eq. (1.10):

$$CO_2 + 3H_2 \rightleftarrows CH_3OH + H_2O \tag{1.10}$$

This method is a useful strategy for CO_2 utilization and a practical approach to sustainable development (Liu et al., 2003). In this conception, CO_2 can be captured from any natural or industrial source, human activities, or air by absorption, and chemically transformed into methanol, then using only renewable resources (*green chemistry*).

Regarding hydrogen, it can originate from water dissociation by electrolysis, as described in Eq. (1.15), using a renewable source of electricity as well (wind, solar, waves, etc.). In this way, it is also possible to store renewable energy on a large, long-term scale (Ganesh, 2014).

$$2H_2O \xrightarrow{\Delta,\ \text{electricity or } h\nu} 2H_2 + O_2 \tag{1.15}$$

Furthermore, other H_2 sources can be biomass pyrolysis or steam/oxygen gasification processes and reforming of biomass-derived products (Bozzano and Manenti, 2016). Other routes are still under investigation. For example, one of them involves the production of biological hydrogen by means of microorganisms activated by sunlight. This biological process of bioenergy conversion of algal biomass into other fuels includes alcoholic fermentation, such as the ABE process, anaerobic digestion, and photobiological hydrogen production. All biological processes are essentially dependent on the presence of enzymes suitable to convert the lignocellulosic biomass in hydrogen (Dalena et al., 2017).

Using CO_2 as a feedstock has many advantages. First of all, it is inexpensive, abundant, nontoxic, noncorrosive, and nonflammable and, therefore, safe to use. Furthermore, it can be

easily stored and transported in liquid form under mild pressure and processed in existing syngas conversion plants without any significant modification (Centi and Perathoner, 2009).

According to Olah (2005), methanol production from CO_2 is favorable not only for the use of nonfossil fuel sources (unlike syngas), but also because it allows the avoidance of CO_2 sequestration, which is a very expensive process, and offers mitigation of the greenhouse effect by means of an efficient recycling of CO_2. As reported in *Energy Technology Perspectives 2008* (ETP, 2008), the CO_2 emissions grown in thermal plants are a big problem for GHG emissions. For example, as reported in the review of Ganesh (2014), the CO_2 gas generated at major outlets such as thermal plants and cement industries generates about 4 t of CO_2 for each ton of coal burned. Nowadays, it is therefore necessary to develop a technology that can sequester CO_2 for reuse as a building block for other production cycles. Today, the only technology available to do this from large-scale fossil-fuel usage is CO_2 capture and storage (CCS).

The *Energy Technology Perspectives 2016* (ETP, 2016) scenarios demonstrate that CCS will need to contribute nearly one-fifth of the necessary emissions reductions to reduce global GHG emissions by 70% by 2050 at a reasonable cost. As reported by Tanaka (2008), CCS is therefore essential to the achievement of deep emission cuts. In a scenario that aims at emissions stabilization based on options with costs up to \$50/t CO_2, 27 gigatons (Gt) of CO_2 would need to be captured and stored by 2050, which is 70% of the total emissions. In the ETP scenario, which cuts global CO_2 emissions more than half and which considers emission abatement options with a cost of up to \$200/t CO_2, CCS accounts for 19% of total emissions reductions in 2050.

3 Methanol Application

As discussed in Section 1, the main methanol demand is in the chemical market; about 35% of it is consumed for formaldehyde production. The remaining volumes are consumed for the production of fuel additives, acetic acid, methyl and vinyl acetates, and other chemicals. Recently, methanol synthesis has become the second source of hydrogen consumption after ammonia production (Olah et al., 2011).

3.1 Methanol to DiMethylEther

In the last 10 years, one of the most promising technologies is the use of methanol as a C1 building block in the petrochemical industry, and a wide part of its production is consumed in the manufacturing of DME as an alternative fuel. DME has an octane number and ignition temperature close to that of diesel fuel. It leads to lower NO_X emissions, less smoke, and less engine noise than conventional diesel engines and, furthermore, can be easily transported (Semelsberger et al., 2006; Hosseininejad et al., 2012).

DME can also be used as a chemical feedstock for manufacturing many products, such as short olefins (ethylene and propylene), gasoline, hydrogen, acetic acid, and dimethyl sulfate. The current DME manufacturing process is a double-step (indirect) synthesis, in which methanol synthesis, carried out by one of the above-mentioned technologies, is followed by dehydration, according to Eq. (1.16).

$$2CH_3OH \rightarrow CH_3OCH_3 + H_2O \tag{1.16}$$

Another developing process involves the direct synthesis of DME from syngas. Research on this technology, capable of mass-producing DME at low cost, is underway by JFE Holdings. In this process, syngas CO and H_2, with a 1:1 molar ratio, are converted in DME in the presence of a catalyst. The overall reaction of the process (Eq. 1.17) is shown below (Ohno et al., 2006).

$$3CO + 3H_2 \rightarrow CH_3OCH_3 + CO_2 \tag{1.17}$$

In the late 20th century, the global production of DME was as low as 100–150 kt/year, but it is predicted, for example, that demand just in South Korea will exceed 6.5 Mt by 2020 (Khadzhiev et al., 2016). The production process of this promising fuel is widely discussed in Chapter 11.

3.2 Hydrogen Production

Hydrogen is considered a clean energy source that has an important role in refining, the chemical industry, and the electronic industry. Nevertheless, as seen in the introduction, hydrogen is difficult to store and transport, which seriously restricts its application. Its production from an easily transported liquid feedstock can be an efficient alternative. Methanol is considered an excellent liquid H_2 source with low toxicity and low chain-alcohols (Lü et al., 2012). For this reason, many research groups are developing various technologies that utilize methanol in the production of hydrogen.

These technologies are developing some thermochemical methods: direct decomposition (Lü et al., 2012; Choi and Kang, 2007; Usami et al., 1998), SR reaction (Sá et al., 2010; Yao et al., 2006; Chen and Lin, 2013; Iulianelli et al., 2014; Chen and Syu, 2011), PO (Chen et al., 2015) and also by methanol-water solution electrolysis (Damle, 2008).

3.2.1 Methanol decomposition

Methanol decomposition (MD) is an endothermic reaction to produce H_2 and CO, according to Eq. (1.18):

$$CH_3OH \rightleftarrows CO + 2H_2 \quad \Delta H = 90.1\,\mathrm{kJ\,mol^{-1}} \tag{1.18}$$

This is applicable to the recovery of waste heat of around 200°C from industries (Usami et al., 1998). For the development of heat-recovery systems, new catalysts that can be active even at

temperatures below 200°C are indispensable. Usami et al. (1998), for example, have tested 15% wt Pd/ZrO_2, Pd/Pr_2O_3, and Pd/CeO_2 catalysts. These catalysts, prepared by co-precipitation, can produce high catalytic activity in the selective decomposition of methanol to CO and H_2 at a temperature as low as 200°C.

3.2.2 Methanol steam reforming

The production process that is much used in the production of hydrogen is the methanol steam reforming (MSR) (Sá et al., 2010).

Compared to other fuels, methanol presents several advantages for hydrogen production. In fact, the absence of a strong C—C bond facilitates the reforming at low temperatures (200–300°C), a range of temperatures that is very low when compared to other common fuels (800–1000°C for methane and 400°C for ethanol) (Iulianelli et al., 2014).

The overall reaction of the MSR to the production of H_2 is expressed in Eq. (1.19):

$$CH_3OH + H_2O \rightleftarrows CO_2 + 3H_2 \quad \Delta H = 49.7\,\mathrm{kJ\,mol^{-1}} \tag{1.19}$$

In this reaction, two side reactions must be considered: the decomposition of methanol (Eq. 1.20) and the WGS (Eq. 1.3) as expressed below:

$$CH_3OH \rightleftarrows CO + 2H_2 \quad \Delta H = 90.2\,\mathrm{kJ\,mol^{-1}} \tag{1.20}$$

Even though the purpose of the MSR reaction is the production of hydrogen.

As indicated from the values of ΔH in the equations, only the WGS reaction is exothermal ($\Delta H = -41.2$ kJ mol^{-1}) and takes place without the variation of any mole number. The MSR reaction, besides being endothermic, takes place with an increase in the mole number. Unfortunately, the main drawback of this process is represented by the CO formation as a byproduct; this formation can deactivate the catalyst. Nowadays, there are several research groups that pay special attention to catalyst optimization in order to reduce the CO content (Iulianelli et al. 2014).

The steam reforming of methanol, the update of the use of catalysts for this technology, is widely discussed in Chapter 9.

3.2.3 Methanol-water solution electrolysis

Another way to produce hydrogen from methanol is by methanol-water solution electrolysis using an electrolytic cell. Generally, electrolysis of water is the best option for producing very pure hydrogen very quickly (Menia et al., 2017). As in the electrolysis of water, in the methanol-water system the hydrogen produced is very pure (hydrogen concentration is 95.5–97.2 mol%), but the theoretical voltage of the system is much lower than in water

electrolysis (1.23 V in water electrolysis compared to 0.03 V in methanol-water solution electrolysis). The full reaction system is well explained by Take et al. (2007).

In methanol-water solution electrolysis, hydrogen is produced by applying DC voltage to the electrolytic cell, as can be seen in Fig. 1.8.

In this system the overall reaction is:

$$CH_3OH + H_2O \rightarrow CO_2 + 3H_2 \tag{1.21}$$

The reaction at the anode and at the cathode are, respectively, Eqs. (1.22) and (1.23):

$$CH_3OH + H_2O \rightarrow CO_2 + 6H^+ + 6e^- \quad \text{anode} \tag{1.22}$$

$$6H^+ + 6e^- \rightarrow 3H_2 \quad \text{cathode} \tag{1.23}$$

At the anode, methanol reacts with water to produce carbon dioxide (exhausted outside the anode), protons, and electrons, according to the reaction (1.22).

The protons produced by the anode reaction move to the cathode of the electrolytic cell through the proton exchange membrane (PEM) and the electrons produced by the anode reaction move to the cathode through the external circuit containing the DC power supply.

At the cathode, protons supplied from the anode react with electrons supplied from the anode, according to Eq. (1.23).

Hydrogen production by methanol-water solution electrolysis is suitable for portable power applications because methanol-water solution electrolysis can start up and shut down in a moment and can produce hydrogen at a low temperature. The voltage needed in methanol-water is three times lower than that for water solution electrolysis. Furthermore, the work of Menia et al. (2017) shows that this technique must be improved by changing some parameters,

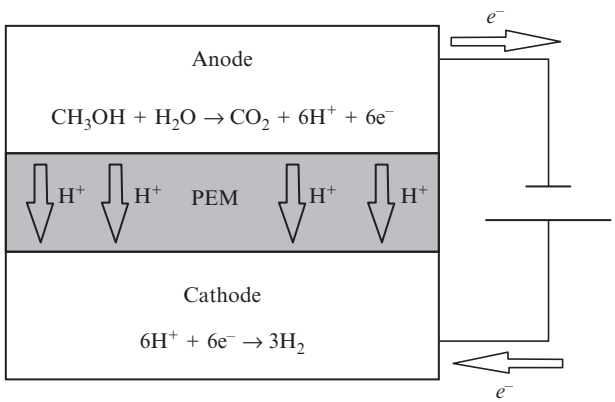

Fig. 1.8
Methanol-water solution electrolysis.

in particular the operating temperature, the cell voltage, the methanol concentration, and the nature of the catalysts.

3.2.4 Partial oxidation/autothermal reforming

Unlike MD and MSR, partial oxidation of methanol (POM) is an exothermic reaction, so no additional heat is needed. However, the temperature control can be difficult. The addition of steam into POM leads to the ATR of methanol. In other words, methanol ATR is a combined reaction of MSR and POM, and its H_2 yield is between the two reactions. The addition of steam in ATR intensifies H_2 production but lowers the reaction temperature and thereby the reaction rate.

On account of the simultaneous addition of oxygen and steam in methanol ATR, the thermal behavior and operating control become more complicated and intractable. In contrast to MSR and methanol ATR, relatively less H_2 is produced from POM.

POM is expressed as:

$$CH_3OH + {}^{1}/_{2}O_2 \rightleftarrows 2H_2 + CO_2 \quad \Delta H = 192.3\,\mathrm{kJ\,mol^{-1}} \tag{1.24}$$

Various studies of POM concerning a variety of catalysts are under development in order to optimize the experimental conditions. Normally, the reaction temperature is controlled at 150–300°C.

By virtue of more heat released from POM being employed for chemical reactions, POM is kinetically faster than MSR and methanol ATR, implying that a smaller reactor is achievable for POM.

Instead, ATR (Eq. 1.25) is a combination of MSR and POM. The overall reaction is:

$$4CH_3OH + 3H_2O + {}^{1}/_{2}O_2 \rightleftarrows 11H_2 + 4CO_2 \quad \Delta H = -44\,\mathrm{kJ/mol} \tag{1.25}$$

This process uses the energy produced from POM to supply the endothermic MSR reaction, and thus it can be run adiabatically (Kulprathipanja and Falconer, 2004). The heat released from POM can rapidly start up the reaction and drive the endothermic reaction of MSR. The overall reaction can be controlled to be thermo-neutral or slightly exothermic by adjusting the O_2/C molar ratio (Chen and Lin, 2013). This process is discussed in Chapter 9.

3.3 Methanol Fuel Cells

Nowadays, systems that require an external power supply for charging are constantly growing (computers, mp3 players, mobile devices, etc.). For this reason, researchers are looking for viable solutions to systems based on a rechargeable battery of Li and Ni. Methods to implement this technology from an energy point of view and especially to eliminate external sources

for charging fuel cells are under study. In particular, PEM fuel cells are electrochemical devices that convert chemical energy into electrical energy. One type of PEMFC is the direct methanol fuel cell (DMFC) that uses methanol or methanol solutions as fuel and works at an ambient temperature (Li and Faghri, 2013). The system is very similar to methanol-water solution electrolysis. The overall reaction is:

$$CH_3OH + 1.5O_2 \rightarrow CO_2 + 2H_2O \tag{1.26}$$

The structure of the DMFC consists of two porous electrocatalytic electrodes on both sides of a solid polymer electrolyte membrane. The thermodynamic reversible potential for the overall cell reaction is 1.214 V (Mallick et al., 2016).

Methanol and water are oxidized in the anode catalyst layer (ACL) and release electrons and protons, according to reaction (1.27):

$$CH_3OH + H_2O \rightarrow CO_2 + 6H^+ + 6e^- \tag{1.27}$$

The electrons are transported through an external circuit to the cathode, while the protons penetrate the electrolyte membrane to the cathode. In the cathode catalyst layer (CCL), the oxygen from the ambient atmosphere reacts with electrons and protons and generates water, according to reaction (1.28) (Mallick et al., 2015):

$$6H^+ + 6e^- + 1.5O_2 \rightarrow 3H_2O \tag{1.28}$$

This process and its applications, the use of catalysts, and future trends are widely discussed in Chapter 14.

Conclusions and Future Trends

A comprehensive overview of methanol's applications and production potential has been given in this chapter. This simple alcohol is one of the biggest future frontiers for green chemistry, both in terms of production and application.

From a production point of view, two of the three production cycles of methanol take biomasses or CO_2 as starting feeds. In each case, it's about new technological frontiers that are suitable for reducing GHG emissions. In fact, in the first case, GHGs are reduced by means of WTE technologies, in which solid wastes are converted into various forms that can be used to supply energy. This also helps solve at the same time the problem of waste management. In the second case, it can be possible to effect a direct reduction of the amount of one of the most important GHGs (CO_2), which can be captured from any natural or industrial source, human activity, or air by absorption, and chemically transformed into methanol. In addition, it is noteworthy that the production of methanol from CO_2 can be regarded as a completely green process, considering that the hydrogen necessary for this productive cycle can be

originated from water dissociation by electrolysis, also using a source of renewable electricity such as wind, solar, waves, etc.

As regards the application point of view, methanol is one of the most innovative and versatile molecules. Nowadays, it is not only used as a solvent and C1 building block for producing intermediates and synthetic hydrocarbons, including polymers and single-cell proteins, but also as an easily transportable fuel and convenient energy carrier for hydrogen storage and transportation.

This chapter, in which attention is paid to only some of the most innovative trends such as the production of DME, the production of hydrogen, and the DMFC, represents a necessary general overview for a better comprehension of this book. The production processes, the applications, the modeling, the most innovative technologies, and the role in the market of this molecule will be discussed in detail in the next chapters.

References

Ali, K.A., Abdullah, A.Z., Mohamed, A.R., 2015. Recent development in catalytic technologies for methanol synthesis from renewable sources: a critical review. Renew. Sustain. Energy Rev. 44, 508–518.

Balat, H., 2010. Prospects of biofuels for a sustainable energy future: a critical assessment. Energy Educ. Sci. Technol. 24 (2), 85–111.

Basile, A., Criscuoli, A., Santella, F., Drioli, E., 1996. Membrane reactor for water gas shift reaction. Gas Sep. Purif. 10 (4), 243–254.

Basile, A., Curcio, S., Bagnato, G., Liguori, S., Jokara, S.M., Iulianelli, A., 2015. Water gas shift reaction in membrane reactors: theoretical investigation by artificial neural networks model and experimental validation. Int. J. Hydrogen Energy 40, 5897–5906.

Blug, M., Leker, J., Pluss, L., Günter, A., 2014. Methanol generation economics. In: Bertau, M., Offermans, H., Plass, L., Schmidt, F., Wernicke, H.J. (Eds.), Methanol: The Basic Chemical and Energy Feedstock of the Future. Springer-Verlag, Berlin, Germany. ISBN 978-3-642-39709-7.

Bozzano, G., Manenti, F., 2016. Efficient methanol synthesis: perspectives, technologies and optimization strategies. Prog. Energy Combust. Sci. 56, 71–105.

Centi, G., Perathoner, S., 2009. Opportunities and prospects in the chemical recycling of carbon dioxide to fuels. Catal. Today 148, 191–205.

Chen, F., Wu, C., Dong, L., Vassallo, A., Williams, P.T., Huang, J., 2016. Characteristics and catalytic properties of Ni/CaAlOx catalyst for hydrogen-enriched syngas production from pyrolysis-steam reforming of biomass sawdust. Appl. Catal. B Environ. 183, 168–175.

Chen, W.H., Kuo, P.C., 2010. A study on torrefaction of various biomass materials and its impact on lignocellulosic structure simulated by a thermogravimetry. Energy 35 (6), 2580–2586.

Chen, W.H., Lin, B.J., 2013. Hydrogen production and thermal behaviour of methanol autothermal reforming and steam reforming triggered by microwave heating. Int. J. Hydrogen Energy 24, 9973–9983.

Chen, W.H., Shen, C.T., Lin, B.J., Liu, S.C., 2015. Hydrogen production from methanol partial oxidation over Pt/Al_2O_3 catalyst with low Pt content. Energy 88, 399–407.

Chen, W.H., Syu, Y.J., 2011. Thermal behaviour and hydrogen production of methanol steam reforming and autothermal reforming with spiral preheating. Int. J Hydrogen Energy 36, 3397–3408.

Chinchen, G.C., Denny, P.J., Jennings, J.R., Spencer, M.S., Waughr, K.C., 1988. Synthesis of methanol. Part 1. Catalysts and kinetics. Appl. Catal. A 36, 1–65.

Choi, H.J., Kang, M., 2007. Hydrogen production from methanol/water decomposition in a liquid photosystem using the anatase structure of Cu loaded TiO_2. Int. J. Hydrogen Energy 32, 3841–3848.
Cifre, P.G., Badr, O., 2007. Renewable hydrogen utilisation for the production of methanol. Energy Convers. Manage. 48 (2), 519–527.
Corella, J., Aznar, M.P., Gil, J., Caballero, M.A., 1999. Biomass gasification in fluidised bed: where to locate the dolomite to improve gasification? Energy Fuels 13 (6), 1122–1127.
Dai, J., Saayman, J., Grace, J.R., Ellis, N., 2015. Gasification of woody biomass. Annu. Rev. Chem. Biomol. Eng. 6, 77–99.
Dalena, F., Basile, A., 2015. Alcohols and bioalcohols: characteristics, production, and uses. Nova Publishers, New York (Chapter 1).
Dalena, F., Senatore, A., Tursi, A., Basile, A., 2017. Bioenergy production from second and third generation feedstock. In: Dalena, F., Basile, A., Rossi, C. (Eds.), Bioenergy Systems for the Future. Prospects for Biofuels and Biohydrogen. Elsevier Publishing, London, UK.
Dalrymple, D.A., Skinner, F.D., Meserole, N.P., 1991. Investigation of U.S. natural gas reserve demographics and gas treatment processes, 91. Gas Research Institute, USA. pp. 3-1–3-13.
Damle, A.S., 2008. Hydrogen production by reforming of liquid hydrocarbons in a membrane reactor for portable power generation—model simulations. J. Power Sources 180 (1), 516–529.
Fiedler, E., Grossmann, G., Kersebohm, D.B., Weiss, G., Witte, C., 2005. Methanol. In: Ullmann's encyclopaedia of industrial chemistry, seventh ed. Wiley-VCH Verlag GmbH & Co, Weinheim, Germany.
Fiedler, E., Grossmann, G., Kersebohm, D.B., Weiss, G., Witte, C., 2000. Methanol. doi:10.1002/14356007.a16 465.
Fujitani, T., Saito, M., Kanai, Y., Kakumoto, T., Watanabe, T., Nakamura, J., Uchijima, T., 1994. The role of metal oxides in promoting a copper catalyst for methanol synthesis. Catal. Lett. 25 (3), 271–276.
Ganesh, I., 2014. Conversion of carbon dioxide into methanol—a potential liquid fuel: fundamental challenges and opportunities (a review). Renew. Sustain. Energy Rev. 31, 221–257.
Gao, N., Li, A., Quan, C., Qu, Y., Mao, L., 2012. Characteristics of hydrogen-rich gas production of biomass gasification with porous ceramic reforming. Int. J. Hydrogen Energy 37 (12), 9610–9618.
Grabow, L.C., Mavrikakis, M., 2011. Mechanism of methanol synthesis on Cu through CO_2 and CO hydrogenation. ACS Catal. 1 (4), 365–384.
Green, R.V., 1973. Methanol Process With Recycle. US3763205.
Guan, G., Kaewpanha, M., Hao, X., Abudula, A., 2016. Catalytic steam reforming of biomass tar: prospects and challenges. Renew. Sustain. Energy Rev. 58, 450–461.
Hosseininejad, S., Afacan, A., Hayes, R.E., 2012. Catalytic and kinetic study of methanol dehydration to dimethyl ether. Chem. Eng. Res. Des. 90, 825–833. http://www.sciencedirect.com/science/article/pii/S036031991631299X (accessed 14 April 2017).
Iulianelli, A., Ribeirinha, P., Mendes, A., Basile, A., 2014. Methanol steam reforming for hydrogen generation via conventional and membrane reactors: a review. Renew. Sustain. Energy Rev. 29, 355–368.
Kanai, Y., Watanabe, T., Fujitani, T., Saito, M., Nakamura, J., Uchijima, T., 1994. Evidence for the migration of ZnO_x in a Cu/ZnO methanol synthesis catalyst. Catal. Lett. 27 (1), 67–78.
Kanai, Y., Watanabe, T., Fujitani, T., Uchijima, T., Nakamura, J., 1996. The synergy between Cu and ZnO in methanol synthesis catalysts. Catal. Lett. 38 (3), 157–163.
Khadzhiev, S.N., Kolesnichenko, N.V., Ezhova, N.N., 2016. Slurry technology in methanol synthesis (review). Pet. Chem. 56 (2), 77–95.
Klier, K., 1982. Methanol synthesis. Adv. Catal. 31, 243–313.
Korens, N., Simbeck, D.R., Wilhelm, D.J., 2002. Process screening analysis of alternative gas treating and sulphur removal for gasification. SFA Pacific, Inc. http://www.fischer-tropsch.org/DOE/DOE_reports/73965600100/SFA%20Pacific_Process%20Screening%20Analysis_Dec%202002.pdf (14 April 2017).
Kulprathipanja, A., Falconer, J.L., 2004. Partial oxidation of methanol for hydrogen production using ITO/Al_2O_3 nanoparticle catalysts. Appl. Catal. A 261 (1), 77–86.
Kung, H.H., 1980. Methanol synthesis. Catal. Rev. Sci. Eng. 22 (2), 235–259.

Li, X., Faghri, A., 2013. Review and advances of direct methanol fuel cells (DMFCs) part I: design, fabrication, and testing with high concentration methanol solutions. J. Power Sources 226, 223–240.
Liu, X.M., Lu, G.Q., Yan, Z.F., Beltramini, J., 2003. Recent advances in catalysts for methanol synthesis via hydrogenation of CO and CO_2. Ind. Eng. Chem. Res. 42, 6518–6530.
Lü, Y., Yan, W., Hu, S., Wang, B., 2012. Hydrogen production by methanol decomposition using gliding arc gas discharge. J. Fuel Chem. Technol. 40 (6), 698–706.
Mallick, R.K., Thombre, S.B., Shrivastava, N.K., 2015. A critical review of the current collector for passive direct methanol fuel cells. J. Power Sources 285, 510–529.
Mallick, R.K., Thombre, S.B., Shrivastava, N.K., 2016. Vapour feed direct methanol fuel cells (DMFCs): a review. Renew. Sustain. Energy Rev. 56, 51–74.
Marcum, L., 2012. Sulfur Process Technology. Linde Group, Linde Process Plants Inc., Tulsa, OK, USA, p. 3. http://www.linde-engineering.com/internet.global.lindeengineering.global/en/images/Sulfur%20Process%20Technology19_111155.pdf?v=1.0 (accessed 30 April 2017).
Matsumura, Y., Ishibe, H., 2009. High temperature steam reforming of methanol over $Cu/ZnO/ZrO_2$ catalysts. Appl. Catal. B 91 (1-2), 524–532.
Menia, S., Tebibel, H., Lassouane, L., Khellaf, A., Nouicer, I., 2017. Hydrogen production by methanol aqueous electrolysis using photovoltaic energy: Algerian potential. Int. J. Hydrogen Energy 42, 8661–8669.
Milne, T.A., Abatzoglou, N., Evans, R.J., 1998. Biomass Gasifier "Tars": Their Nature, Formation, and Conversion. Colorado, November 1998, NREL /TP-570-25357. http://www.ps-survival.com/PS/Gasifiers/Biomass_Gasifier_Tars_Their_Nature_Formation_And_Conversion_1998.pdf (accessed 30 April 2017).
Mittasch, A., Pier, M., 1926. Synthetic Manufacture Of Methanol. US1569775.
Mittasch, A., Winkler, K., Pier, M., 1925. Production of oxygenated organic compounds. US1558559.
Moghadam, R.A., Yusup, S., Uemura, Y., Chin, B.L.F., Lam, H.L., Shoaibi, A.A., 2014. Syngas production from palm kernel shell and polyethylene waste blend in fluidized bed catalytic steam co-gasification process. Energy 75, 40–44.
Nabikandi, N.J., Fatemi, S., 2015. Kinetic modelling of a commercial sulfur recovery unit based on Claus straight through process: comparison with equilibrium model. J. Ind. Eng. Chem. 30, 50–63.
Nakamura, J., Choi, Y., Fujitani, T., 2003. On the issue of the active site and the role of ZnO in Cu/ZnO methanol synthesis catalysts. Top. Catal. 22 (3), 277–285.
Natta, G., 1955. Catalysis. Reinhold Publishing Corporation, New York (Chapter 8).
NCCC, 2012. Technical update water-gas shift testing at the NCCC 2012. The National Carbon Capture Center at the Power Systems Development Facility, Wilsonville, AL.
Ni, M., Leung, D.Y.C., Leung, M.K.H., Sumathy, K., 2006. An overview of hydrogen production from biomass. Fuel Process. Technol. 87, 461–472.
Ohno, Y., Yoshida, M., Shikada, T., Inokoshi, O., Ogawa, T., Inoue, N., 2006. New Direct Synthesis Technology for DME (Dimethyl Ether) and Its Application Technology. JFE Technical Report. http://www.jfe-steel.co.jp/en/research/report/008/pdf/008-06.pdf (accessed 14 April 2017).
Olah, G.A., 2005. Beyond oil and gas: the methanol economy. Angew. Chem. Int. 44, 2636–2639.
Olah, G.A., Goeppert, A., Prakash, G.K.S., 2009. Beyond oil and gas: the methanol economy. Wiley-VCH, Weinheim, Germany.
Olah, G.A., Goeppert, A., Prakash, G.K.S., 2011. Beyond Oil and Gas: The Methanol Economy, 2nd ed., Updated and Enlarged Edition. John Wiley & Sons. ISBN: 978-3-527-64463-6.
Peppley, B.A., Amphlett, J.C., Kearns, L.M., Mann, R.F., 1999. Methanol steam reforming on $Cu/ZnO/Al_2O_3$ catalysts. Part 2. A comprehensive kinetic model. Appl. Catal. A 179 (1-2), 31–49.
Pinto, A., 1983. Method For Producing Methanol And Ammonia. Patent n. US4367206.
Prins, M.J., Ptasinski, K.J., Janssen, F.J.J.G., 2006. More efficient biomass gasification via torrefaction. Energy 31 (15), 3458–3470.
Roan, V., Betts, D., Twining, A., Dinh, K., Wassink, P., Simmons, T., 2004. An investigation of the feasibility of coal-based methanol for application in transportation fuel cell systems. Report. University of Florida, USA.

Sá, S., Silva, H., Brandão, L., Sousa, J.M., Mendes, A., 2010. Catalysts for methanol steam reforming—a review. Appl. Catal. B 99 (1–2), 43–57.

Sabatier, P., 1926. How I have been led to the direct hydrogenation method by metallic catalysts. Ind. Eng. Chem. 18 (10), 1005–1008.

Semelsberger, T.A., Borup, R.L., Greene, H.L., 2006. Dimethyl ether(DME) as an alternative fuel. J. Power Sources 156, 497–511.

Shahbaz, M., Yusup, S., Inayat, A., Patrick, D.O., Ammar, M., 2017. The influence of catalysts in biomass steam gasification and catalytic potential of coal bottom ash in biomass steam gasification: a review. Renew. Sustain. Energy Rev. 73, 468–476.

Shen, L., Gao, Y., Xiao, J., 2008. Simulation of hydrogen production from biomass gasification in interconnected fluidized beds. Biomass Bioenergy 32 (2), 120–127.

Shen, Y., Yoshikawa, K., 2013. Recent progresses in catalytic tar elimination during biomass gasification or pyrolysis—a review. Renew. Sustain. Energy Rev. 21, 371–392.

Spath, P.L., Dayton, D.C., 2003. Preliminary screening − technical and economic assessment of synthesis gas to fuels and chemicals with emphasis on the potential for biomass derived syngas. Technical Report NREL/TP-510-34929. NREL (National Renewable Energy Laboratory), DOE (US Department of Energy), Colorado, USA.

Specht, M., Bandi, A., 1999. The methanol cycle—sustainable supply of liquid fuels. Centre for Solar Energy and Hydrogen Research (ZSW), Stuttgart, Germany.

Styhr, P.H.J., 1972. Low Temperature Methanol Synthesis. GB1272798.

Take, T., Tsurutani, K., Umeda, M., 2007. Hydrogen production by methanol–water solution electrolysis. J. Power Sources 164 (1), 9–16.

Tanaka, N., 2008. Prospects for CO_2 capture and storage. In: International Energy Agency and Energy Technology Analysis. IEA Publications. https://www.iea.org/publications/freepublications/publication/CCS_2008.pdf (accessed 14 April 2017).

Tijm, P.J.A., Waller, F.J., Browna, D.M., 2001. Methanol technology developments for the new millennium. Appl. Catal. A. 221 (1–2), 275–282.

Tour, R.S., 1920. The direct synthetic ammonia process. Ind. Eng. Chem. 12 (9), 844–852.

Trop, P., Anicic, B., Goricanec, D., 2014. Production of methanol from a mixture of torrefied biomass and coal. Energy 77, 125–132.

Usami, Y., Kagawa, K., Kawazoe, M., Matsumura, Y., Sakurai, H., Haruta, M., 1998. Catalytic methanol decomposition at low temperatures over palladium supported on metal oxides. Appl. Catal. A 171 (1), 123–130.

Van Bennekom, J.G., Venderbosch, R.H., Winkelman, J.G.M., Wilbers, E., Assink, D., Lemmens, K.P.J., Heeres, H.J., 2013. Methanol synthesis beyond chemical equilibrium. Chem. Eng. Sci. 87, 204–208.

Van der Stelt, M.J.C., Gerhauser, H., Kiel, J.H.A., Ptasinski, K.J., 2011. Biomass upgrading by torrefaction for the production of biofuels: a review. Biomass Bioenergy 35 (9), 3748–3762.

Wilhelm, D.J., Simbeck, D.R., Karp, A.D., Dickenson, R.L., 2001. Syngas production for gas-to-liquids applications: technologies, issues and outlook. Fuel Process. Technol. 71 (1), 139–148.

Wilkinson, S.K., Van De Water, L.G.A., Miller, B., Simmons, M.J.H., Stitt, E.H., Watson, M.J., 2016. Understanding the generation of methanol synthesis and water gas shift activity over copper-based catalysts—a spatially resolved experimental kinetic study using steady and non-steady state operation under $CO/CO_2/H_2$feeds. J. Catal. 337, 208–220.

Yao, C.Z., Wang, L.C., Liu, Y.M., Wu, G.S., Cao, Y., Dai, W.L., He, H.Y., Fan, K.N., 2006. Effect of preparation method on the hydrogen production from methanol steam reforming over binary Cu/ZrO_2 catalysts. Appl. Catal. A 297, 151–158.

Yong, S.T., Ooi, C.W., Chai, S.P., Wub, X.S., 2013. Review of methanol reforming-Cu-based catalysts, surface reaction mechanisms, and reaction schemes. Int. J. Hydrogen Energy 38 (22), 9541–9552.

Zhang, X., Zhong, L., Guo, Q., Fan, H., Zheng, H., Xie, K., 2010. Influence of the calcination on the activity and stability of the $Cu/ZnO/Al_2O_3$ catalyst in liquid phase methanol synthesis. Fuel 89 (7), 1348–1352.

Zhao, Z., Lakshminarayanan, N., Swartz, S.L., Arkenberg, G.B., Felix, L.G., Slimane, R.B., Choi, C.C., Ozkan, U.S., 2015. Characterization of olivine-supported nickel silicate as potential catalysts for tar removal from biomass gasification. Appl. Catal. A. 489, 42–50.

Zhen, X., Wang, Y., 2015. An overview of methanol as an internal combustion engine fuel. Renew. Sustain. Energy Rev. 52, 477–493.

Further Reading

Bao, J., Liu, Z., Zhang, Y., Tsubaki, N., 2008. Preparation of mesoporous Cu/ZnO catalyst and its application in low-temperature methanol synthesis. Catal. Commun. 9 (5), 913–918.

David, R.L., 2005. CRC Handbook of Chemistry and Physics, 70th ed. CRC Press, Boca Raton, FL.

Galindo Cifre, P., Badr, O., 2007. Renewable hydrogen utilisation for the production of methanol. Energy Convers. Manag. 48 (2), 519–527.

International Energy Agency (IEA), 2008. Energy Technology Perspectives (ETP). OECD/IEA.

International Energy Agency (IEA), 2016. Energy Technology Perspectives (ETP). OECD/IEA. ISBN 978-92-64-26494-6/PDF: 978-92-64-26495-3.

Jingfa, D., Qi, S., Yulong, Z., Songying, C., Dong, W., 1996. A novel process for preparation of a Cu/ZnO/$A1_2O_3$ ultrafine catalyst for methanol synthesis from CO_2+H_2: comparison of various preparation methods. Appl. Catal. A 139 (1–2), 75–85.

CHAPTER 2

State of the Art of Conventional Reactors for Methanol Production

Vincenzo Palma, Eugenio Meloni, Concetta Ruocco, Marco Martino, Antonio Ricca
University of Salerno, Fisciano, Italy

List of Acronyms

AIST Advanced Industrial Science and Technology
ATR autothermal reforming
BASF Badische Anilin–und Soda Fabrik
BET Brunauer-Emmett-Teller
BFW boiler feed water
DMT dimethyl terephthalate
HM honeycomb monolith
ICI Imperial Chemical Industries
IFP Institut Francais du Petrole
LCC Lurgi combined converter
LER liquid entrained reactor
LNG liquefied natural gas
LPG liquefied petroleum gas
LPM liquid process methanol
MMA methyl methacrylate
MRF multistage radial flow
MTO methanol-to-olefin
MTP methanol-to-paraffin
OF open cell foam
PCHE printed circuit heat exchanger
RITE Research Institute for Innovative Technology for the Earth
RSR recirculation slurry reactor
UK United Kingdom
WGS water-gas shift
YKK Yoshida Kogyo Kabushikigaisha

Methanol. https://doi.org/10.1016/B978-0-444-63903-5.00002-9

1 Introduction

Methanol is one of the most important commodities in industrial chemistry; more than 90 production plants, worldwide, have a combined production capacity of 110 Mt, while according to IHS, the global demand reached 70 Mt in 2015 (2016). The rising worldwide demand for methanol is being pushed by growth in the Asian market, such that in the past 15 years, the demand for methanol has increased 500%, with a forecast of increasing further over the next five years. Today most of the methanol produced is used for emerging energy applications; however, methanol is still widely used in the polymer industry, for pharmaceutical applications, and more generally in organic synthesis. In particular, methanol is widely employed in the synthesis of formaldehyde, but also methyl methacrylate (MMA), dimethyl terephthalate (DMT), and other chemicals. Moreover, it can be used as a solvent or gasoline extender. In addition, use of methanol in the methanol-to-olefin and methanol-to-paraffin (MTO/MTP) processes is growing with an average growth rate of almost 7%, with an expectation of it becoming the second largest methanol derivate.

Methanol is industrially obtained through catalytic conversion of syngas, mainly from fossil fuel reforming. The production process consists of three main reactions: carbon monoxide (CO) and hydrogen (H_2), in presence of a catalyst react (2.1) to produce methanol (CH_3OH), while the excess of hydrogen, in the reformate gas, reacts with the carbon dioxide (CO_2) to produce further CO (2.2) and CH_3OH (2.3).

$$CO + 2H_2 \rightleftarrows CH_3OH; \quad \Delta H^{o}_{298K} = -90.8\,kJ/mol \tag{2.1}$$

$$CO + H_2O \rightleftarrows CO_2 + H_2; \quad \Delta H^{o}_{298K} = -41.6\,kJ/mol \tag{2.2}$$

$$CO_2 + 3H_2 \rightleftarrows CH_3OH + H_2O; \quad \Delta H^{o}_{298K} = -49.2\,kJ/mol \tag{2.3}$$

As shown in the preceding reactions, the synthesis of methanol is an exothermic process with a reduction of the moles; therefore it is favored at low temperatures and at high pressures (Dybkjær et al., 2006). An exhaustive experimental evaluation of the chemical equilibrium in methanol synthesis (2.1) and water gas shift reaction (2.2) was reported by Graaf et al. (Graaf et al., 1986). The authors studied a fixed-bed catalytic reactor at a pressure range of 10–80 bar and a temperature range of 200–270°C and described the equilibrium as being the result of ideal gas behavior, after a correction of the nonideality of the gas mixture using the Soave-Redlich-Kwong equation of state (Soave, 1972). A comparison with previously reported studies showed that this equation is in much more agreement with the experimental results than other equations, such as the Peng-Robinson equation (Peng and Robinson, 1976), the Lewis and Randall rule (Lewis and Randall, 1923), and the Redlich-Kwong equation (Redlich and Kwong, 1949). These data were subsequently partially revisited in a letter from Graaf to the editors of *Chemical Engineering Science,* in which the author affirmed that an error occurred during the calculation of the fugacity coefficients.

At any rate, the new data showed again that the best results were obtained with the Soave-Redlich-Kwong correction; however, the difference between it and the Peng-Robinson equation state was not significant (Graaf et al., 1990). As previously mentioned, the exothermicity of the process and the decrease of the moles during the reaction imply the need for low process temperatures and high pressures. When planning a plant, the main problem to solve is how to remove the reaction heat efficiently and economically. The presence of inert gases, such as methane, nitrogen, or argon, reduces the attainable conversion, and an increase in the carbon dioxide content decreases the maximum conversion. In any case, under normal synthesis conditions (7.5 MPa, 225°C), carbon conversion in traditional gas reactors cannot overcome the thermodynamic limit, which is more or less 60% (Dybkjær et al., 2006).

Two main types of reactors are used today in the synthesis of methanol, adiabatic and isothermal, and their use differs according to working conditions. Much less common are the slurry reactors used for liquid phase synthesis of methanol. The adiabatic systems commonly include a series of fixed bed reactors, with removal of the heat, operated downstream of each reactor. These kinds of reactors are characterized by low installation cost and high production capacity; however, because of the adiabatic process, the high equilibrium temperatures imply very low conversions for each cycle and, consequently, a high recycle ratio, a high dilution of the reagents, and a high volume of catalysts.

The isothermal reactor is continuously cooled through another source, water, or gas. It is primarily a heat exchanger, in which cooling is achieved by water circulation on the mantle of the tube bundle. The isothermal nature of this systems enables obtaining high conversions and a low volume of catalysts; however, to reach a useful reaction rate, the temperature needs to be 240°C–260°C, with a high recycle ratio. The installation costs are much higher than those of an adiabatic system, and the size of the plants are limited because of the tube bundle.

The design of typical reactors for methanol synthesis focus on these two approaches, with three typical categories of reactors defined. One of the most common is the indirect cooled reactor (Fig. 2.1) consisting of a series of adiabatic reactors separated by external coolers, aimed at reducing the temperature of the process stream (Dry, 1988). This simple approach assures very high productivity, and the use of the cooling system increases the external function of the system.

An alternative adiabatic reactor is the quench reactor (Fig. 2.2). It is one of the simplest systems for methanol synthesis, in which only a portion of the reactants are preheated and fed into the top of the reactor, which will then be converted, thus increasing the system's temperature. The rest of the reactants are fed cold and stepwise along the catalytic volume, which reduces the temperature of the process stream and further increases syngas conversion. Despite the easy management of the system, the quench reactor approach suffers from a non-uniform

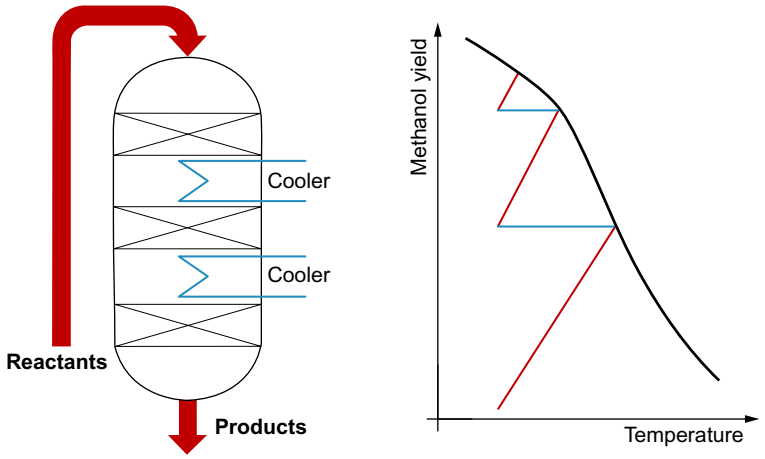

Fig. 2.1
Indirect cooled reactor.

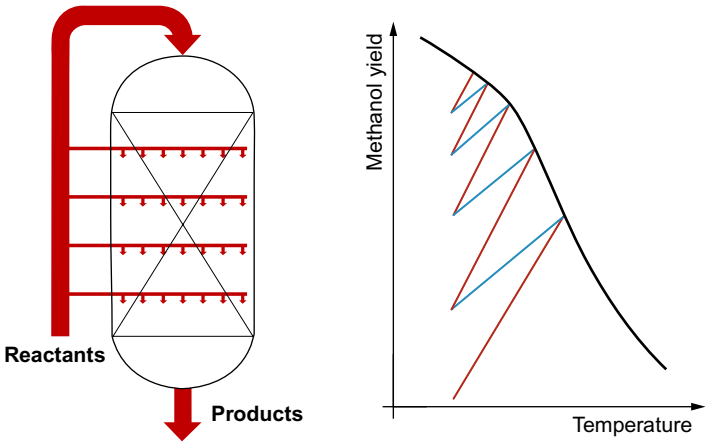

Fig. 2.2
Quench reactor.

exploitation of the catalytic volume: the reactants fed into the top of the reactor are processed by the total catalyst, while the reactants fed stepwise along the reactor skip time after time a part of the catalytic volume (Alberto et al., 2014).

The isothermal reactor approach is widely used in industrial processes, especially in a boiling water reactor (or internally cooled reactor) (Fig. 2.3). Its geometrical shape makes it very close to a tube shell heat exchanger, in which the catalyst is loaded on the tube side, while boiling water flows on the shell side. Such a scheme was developed and customized by several industries, such as Lurgi (Milani et al., 2015), Topsoe (Lahne and Lohmüller, 1986), Linde (Makihara et al., 1987), and Mitsubishi Heavy Industries (Shimomura and

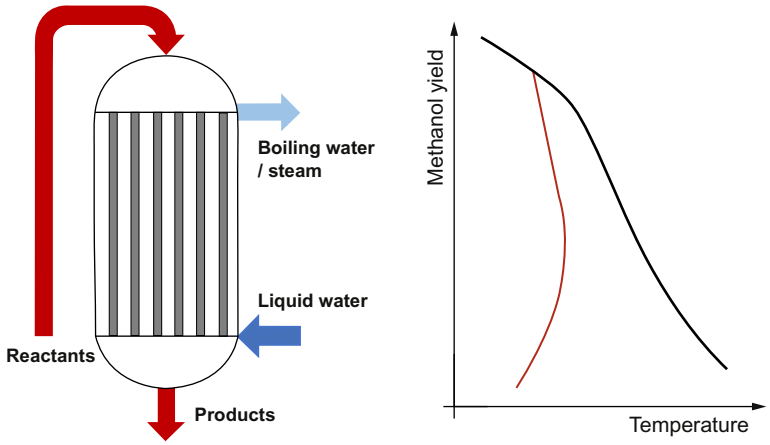

Fig. 2.3
Boiling water reactor.

Nojima, 1988). The plant concept assures an easy-to-manage process and a high conversion level, since an optimal reaction trajectory is achievable. Such a configuration, however, has several limitations, mainly because of the tube and the large shell that restrict the maximum methanol productivity to around 2000 t/d (Milani et al., 2015).

An interesting, but not widespread, alternative to the fixed bed are the slurry reactors, in which the system is in liquid phase, the catalyst is dispersed in an inert oil, and the heat is removed by an external thermal exchanger. The main obstacles to using a slurry reactor are the dimension of the plant and a high degree of retro-mixing that reduces the conversion.

In this chapter we provide a brief summary of the state-of-art conventional reactors for methanol production, focusing attention on the innovations of the past several decades, and we suggest ideas for further reading.

2 Catalysts for Methanol Synthesis

The first synthetic pathway for producing methanol from CO and H_2 was proposed in 1905 by Sabatier. In 1923 (Raudaskoski et al., 2009) BASF patented a methanol production process known as "high-pressure methanol synthesis," where the syngas used was supplied via coal gasification. In this process, performed at temperatures from 300°C to 400°C and pressures from 250 to 350 atm, a zinc/chromium oxide catalyst was employed. However, this catalyst also produced methane and other light hydrocarbons with a 2–5 wt% selectivity (Lange, 2001). In 1966 Imperial Chemical Industries (ICI) developed a process able to operate at a lower temperature and pressure (300°C and 100 atm), because of the production of a cleaner (sulfur-free) syngas via methane steam reforming, which assured the employment of a more active Cu/ZnO catalyst. With the reduction of the reaction temperature, it was also possible to

suppress the coproduction of light hydrocarbons. A few years later, Lurgi introduced a process operating under even less severe conditions (250–350°C and 40–50 atm). At first methanol was mostly produced via the catalytic hydrogenation of CO (Audibert and Raineau, 1928), with a feed gas of CO/H_2 or $CO/CO_2/H_2$. In the 1990s, it was found that a CO_2 hydrogenation reaction is faster than that of CO (Lee et al., 1993), and even starting from a $CO/CO_2/H_2$ feeding, CO_2 hydrogenation was much favored.

Most of the actual processes for methanol synthesis operate in gas phase and use copper-based catalysts. In particular, the most common catalyst adopted in the industry is a $CuO/ZnO/Al_2O_3$ formulation, and its composition depends on the manufacturer (Table 2.1). CuO content ranges between 20 and 80 wt%, while ZnO varies from 15 to 50 wt%; the alumina content is between 4 and 30 wt% (Bozzano and Manenti, 2016). Cu is usually regarded as the active site, whereas very small amounts of Zn atoms are reduced from ZnO and decorated on Cu nanoparticles at the interface (Li et al., 2016).

In particular, ZnO presence, along with a good interface between Cu and ZnO, improves copper dispersion and CO_2 adsorption. A synergistic effect between Cu and ZnO also exists, because of the combination of three different phenomena (Angelo et al., 2015): changing of Cu particles' morphology by a wetting/non-wetting effect of the Cu/ZnO system; migration of ZnO_x species on the surface of Cu particles because of the formation of a Cu-Zn surface alloy, which enhances copper activity; and hydrogen dissociation on ZnO, which is a source of H_2 storage (Grabow and Mavrikakis, 2011). Al_2O_3 is able to form zinc aluminate, which prevents the agglomeration of active sites and accelerates the adsorption and activation of CO, because of its

Table 2.1 Composition of methanol synthesis catalysts from different manufacturers (Bozzano and Manenti, 2016)

Manufacturer	Cu (wt%)	Zn (wt%)	Al (wt%)	Other
IFP	45–70	15–35	4–20	Zr-2–18
Synetix (formerly ICI)	20–35	15–50	4–20	Mg
BASF	38.5	48.8	12.9	Rare earth oxide-5
Shell	71	24	12	
Sud Chemie	65	22	31	
DuPont	50	19	17	
United Catalysts	62	21	17	
Haldor Topsoe MK-121	>55	21–25	8–10	
Mitsubishi Gas Chemical Company	63.6	33.4	3	
Ammonia Casale	30	50	3	Cr (16)
Lonza	40	20		Zr (40)
AIST, RITE	45.2	27.1	4.5	Zr (22.6) Si (0.6)
YKK Corporation	76.3	11	12.7	

disordered and defective surface domain (Liu et al., 2003). Moreover, the addition of Al^{3+} ions has been reported to increase the BET surface area and copper dispersion while inhibiting the sintering of Cu particles under on-stream conditions (Baltes et al., 2008).

Commercially, the ternary $Cu/ZnO/Al_2O_3$ catalyst is prepared via the co-precipitation method (Zhang et al., 1997). By using metal nitrate solutions and sodium carbonate as precipitation agents, it is possible to prepare Cu and Zn carbonate precursors. The precipitate is aged, recovered, and thermally decomposed in order to obtain a fine mixture of oxides. However, many researchers have developed unconventional preparation methods to improve catalyst activity, stability, and lifetime. In order to inherently increase the Cu/ZnO interface area, the citrate method, the decomposition of M(Cu, Zn) ammonia complexes, and the employment of oxalate-co-precipitated materials were proposed as suitable routes (Pori et al., 2016).

Other metals, including Pd and Au, as well as alternative supports were proposed for methanol synthesis. $Au\text{-}TiO_2$ catalysts enhanced CO_2 conversion rates but resulted in lower methanol selectivity. For $Pd\text{-}CeO_2$ catalysts, an improvement of activity because of ceria reducibility was observed (Fan and Fujimoto, 1995). Along with ZnO, ZrO_2 and SiO_2 are the most typical oxides employed as support for Cu (Liu et al., 2003). In particular, ZrO_2 is preferred because of its high stability under a reducing and oxidizing atmosphere, its ability to uniformly disperse CuO, and its capability to enhance the CO_2-hydrogenation functionality (Bonura et al., 2011); however, a slightly lower activity than ZnO for methanol formation was observed. On the other hand, SiO_2, selected for its acid-base nature and porosity texture, displays low selectivity toward methanol synthesis and is commonly employed together with additional metal oxides as promoters. In addition, the employment of magnesia as promoter helps to slow down thermal sintering and to improve catalyst selectivity. In particular, it was reported that Cu supported on SiO_2 and MgO is as active as Cu on ZnO (Chinchen et al., 1987). Zhang et al. (2012) also found that TiO_2 and $TiO_2\text{-}SiO_2$ addition to $Cu/Zn/Al_2O_3$ catalysts can assure a better CuO dispersion and adsorption of H_2 on the catalyst.

Different additives, including boron, chromium, manganese, rare earths, vanadium, titanium, yttrium gallium, and others, were proposed to further improve the surface area and dispersion of copper particle sizes (Xiao et al., 2017, Chinchen et al., 1988, Liu et al., 2006). For example, Cr was found to increase the copper surface area by changing the structure of skeletal copper (Huang et al., 2004). The addition of several modifiers (Rh, Ru, Co, Ag, Mo, and Mn) to $Cu/Zn/Al_2O_3$ was shown to change the coverage of copper surface intermediates, resulting in an improvement of methanol synthesis from CO_2/H_2 feed but not in the synthesis from CO/H_2 (Lee et al., 1995).

The preparation sequence also affects the catalytic performances. Single-staged co-precipitation of nitrate salts resulted in more active catalysts, but catalyst preparation split into two main stages ensured more stable formulation: in the first stage, a zinc aluminate was produced and then copper and zinc were precipitated (Liu et al., 2012). Other variants were also

investigated in catalyst preparation. Different techniques investigated (aerogel, sol-gel, solution combustion synthesis) (Zhang et al., 1997, Hong et al., 2002) appeared able to increase the surface area of the catalyst, but lower activity, selectivity, or stability were observed with respect to co-precipitated samples. Moreover, the presence of CO_2 in the mother liquid during the aging process of the co-precipitation method could improve the activity of the $Cu/ZnO/Al_2O_3$ catalyst (Wang et al., 2011) by increasing the surface area and the pores' volume, and avoiding crystallite growth. Other studies (Curry-Hyde et al., 1993) noted that very active catalysts can be obtained by leaching Cu, Zn, and Al alloys with a sodium hydroxide–sodium zincate solution.

The deactivation behavior of $Cu/ZnO/Al_2O_3$ catalysts, ascribable to both poisoning and thermal effects, has been extensively studied (Fichtl et al., 2015). Industrial plant data show a strong initial decrease in methanol formation, suggesting that the Cu-based catalysts undergo a relatively fast deactivation within the first hundred hours of operation (Kurtz et al., 2003). Poisons such as sulfur, and sometimes iron and nickel carbonyls, can be introduced into an reactor with fresh syngas. Sulfur content has to be as low as 5 ppm or even 1 ppm if possible (Bozzano and Manenti, 2016). Chloride impurities can also promote catalyst sintering as well. However, the innovations in syngas production technologies have drastically reduced the poisoning effects during methanol synthesis, but thermally induced mechanisms like sintering or phase segregation still remain crucial problems for the catalyst lifetime. The copper surface area was measured after exposing the $Cu/ZnO/Al_2O_3$ catalyst to a CO/H_2 stream, and the results suggested that Cu metal sintering was the cause of deactivation, with a loss of activity of 60% after 25 h and a nearly 60% loss of Cu surface area (Sun et al., 1999). Moreover, it was highlighted that sintering rates increase with temperature and in the presence of water. For methanol synthesis in a slurry phase, the H_2 consumption profile of a commercial fresh $Cu/ZnO/Al_2O_3$ catalyst was compared with that recorded after different hours of testing (Fig. 2.4); it was observed that the reduction peaks of the used catalyst became wider and the re-reduction became more difficult: during time-on-stream, CuO particles gradually grew, with a subsequent reduction of hydrogen uptake (Zhai et al., 2008).

3 Reactors for Methanol Synthesis

Since its commercial implementation in 1923, methanol synthesis was improved several times, mainly regarding reduction of the investment costs that dominate methanol production costs. Indeed, the conversion of remote gas to methanol offers a clear economic advantage on raw material costs compared to oil refining. However, this advantage is offset by larger investment costs. This trade-off is, in fact, a general characteristic of natural gas conversion processes (Lange, 2001).

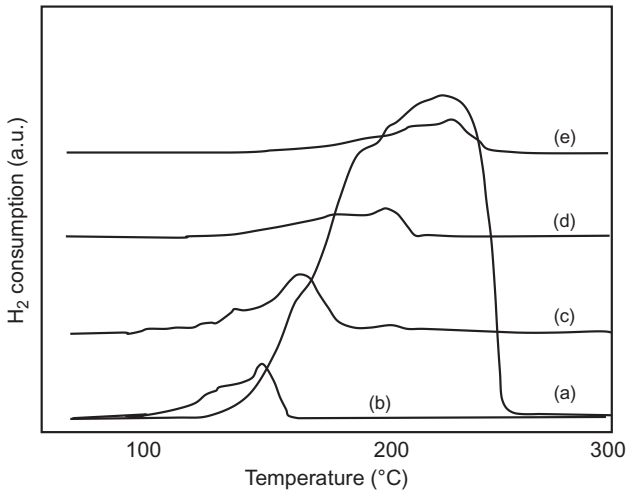

Fig. 2.4

H_2 consumption profile of $Cu/ZnO/Al_2O_3$ catalyst: (a) not reduced, (b) after 50 h reaction, (c) after 169 h reaction, (d) after 300 h reaction, and (e) after 500 h reaction. *After Zhai, X., Shamoto, J., Xie, H., Tan, Y., Han, Y., Tsubaki, N., 2008. Study on the deactivation phenomena of Cu-based catalyst for methanol synthesis in slurry phase. Fuel 87, 430–434.*

As already discussed, methanol synthesis can be achieved by reduction of carbon monoxide or carbon dioxide, according to several reaction mechanisms. For the conversion of CO_2 into methanol, the direct conversion route using CO_2 and H_2 was identified as more efficient than routes via carbon monoxide. In addition, the CO_2 reduction appeared more attractive than the CO processing since it employs carbon dioxide, which is considered as one of the most significant greenhouse gases. On one hand, methanol synthesis from carbon dioxide is typically done concurrent with the WGS (or reverse-WGS) reaction; the other hand, methanol is more unstable than many other compounds. Nevertheless, under certain operating conditions, the process is selected more than 99% of the time.

Both reactions have an exothermic nature and generate a reduction in the moles number. For these reasons, they are promoted at low temperature and high pressure. Such conditions counter several issues in terms of reaction kinetics and a plant's fixed and operative costs. It is worth noting that methanol synthesis from CO_2 is characterized by a less pronounced adiabaticity and by a minor decrease in volume, making temperature and pressure conditions less relevant.

Methanol is currently produced on an industrial-scale exclusively by catalytic conversion of synthesis gas. Processes are classified according to the pressure used:

(1) High-pressure process 25–30 MPa
(2) Medium-pressure process 10–25 MPa
(3) Low-pressure process 5–10 MPa

The main advantages of the low-pressure process are lower investment and production costs, improved operational reliability, and greater flexibility in the choice of plant size.

However, not all the synthesis gas is converted in one pass because of thermodynamic equilibrium limitations; therefore, after methanol and water are removed, the remaining synthesis gas must be recycled to the reactor. A simplified flow diagram for methanol synthesis can be summarized in this way: (a) the make-up synthesis gas is brought to the desired pressure in a multistage compressor (the unreacted recycle is added before the recycle stage); (b) a heat exchanger transfers energy from the hot gas leaving the reactor to the gas entering the reactor; (c) the exothermic formation of methanol takes place in the reactor at temperatures ranging from 200°C to 300°C (the heat of the reaction can be dissipated in one or more stages); (d) the mixture is cooled further (i) after passing through the heat exchanger (ii); and (e) the heat from condensation of the methanol and water can be utilized at another point in the process.

3.1 BASF High Pressure Process

The *BASF process*, also known as the high pressure process, for production of methanol is conducted at temperatures ranging from 320°C to 380°C and approximately 340 bar (Metzger, 2006). The process uses the $ZnO\text{-}Cr_2O_3$ catalyst. To avoid high temperatures (exothermic reaction), cold gas is injected in the catalyst bed. A short residence time (1–2 s) is used to prevent equilibrium from taking place. Conversions of 12%–15% for a single pass through the reactor are typical for this process.

The UK Wesseling process is similar to BASF process, but it operates at low CO partial pressure ($\asymp$13 bar in gas recycle) and reaction conditions at 300 bar and 350°C (Metzger, 2006).

3.2 ICI's 100 atm Methanol Synthesis Process

The ICI process was a milestone in the methanol synthesis field: it represents a concrete breakthrough toward the lower pressure processes for methanol synthesis. In the early 1900s, achieving efficient methanol synthesis by reducing operating pressure did not appear viable, because such solutions required overlarge equipment, and the chemical reaction was not as fast as desired. With the advancement and development of better materials and better designed equipment, a new objective focused on the search for a catalytic synthesis system that would be more active at about 100 atm. Based on technological advancements in the 1960s, Imperial Chemical Industries (ICI) proposed a $Cu/ZnO/Al_2O_3$ catalyst system that was able to ensure appreciable performances at very low temperatures (Metzger, 2006). This process was tested in August 1972 with great success and was a milestone in the methanol synthesis

approach and provided a foundation for later developments and designs. In the following years, continuous enhancements and optimizations of the process were carried out to achieve valuable improvements in terms of energy efficiency. In 2002 the ICI low-pressure methanol process was acquired by Johnson Matthey. By 2003 about 65% of the methanol production in the world was based on the ICI low-pressure process. This process is characterized by lower investment and process costs. The operating conditions in the converter range from 50 to 100 bar and 240–260°C.

This process's scheme (Fig. 2.5) is often split into two main parts, the first focuses on natural gas reforming and the second on syngas conversion into methanol. The separation of the two main macro-units in the process scheme, as widely diffused in the design of commercial methanol synthesis plants, remarks that capital investments of syngas manufacturing parts is typically higher than methanol synthesis. Therefore a plant's profit is related to its efficient integration of energy among the units involved in these two stages. The economics of the global process are heavily dependent on heat recovery and energy integration management, as well as the recycle scheme, refining, and separation. At the same time, the catalyst's lifetime

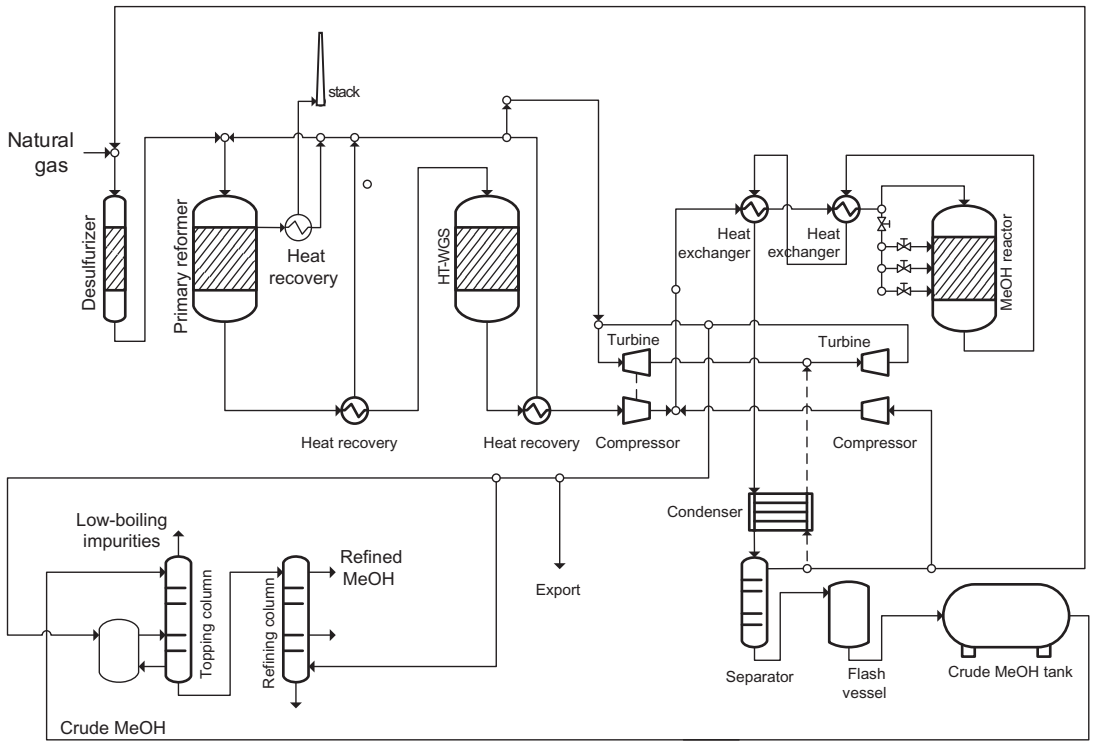

Fig. 2.5
The ICI low-pressure methanol process.

plays a crucial role in the process's maintenance and enhancement, thus directly affecting a plant's productivity.

3.3 Haldor Topsoe A/S Low-Pressure Methanol Synthesis Process

The Haldor Topsoe process (Fig. 2.6) is designed to produce methanol from natural or associated gas feedstock, based on a low-pressure synthesis approach. Associated gas is a natural gas produced by crude oil from the same reservoir. The syngas production is carried out in two stages: the first one, where a preheated mixture of natural gas and steam react in an externally heated high-temperature catalytic reactor (top-fired reactor); the second one, where fuel conversion is completed by adding an appropriate amount of oxygen to the process stream. The amount of oxygen fed to the process and the balance of conversion between the primary and secondary reformers are tuned in order to achieve a balanced syngas, characterized by a stoichiometric ratio of H_2/CO equal to 2 and a low content of inert gas.

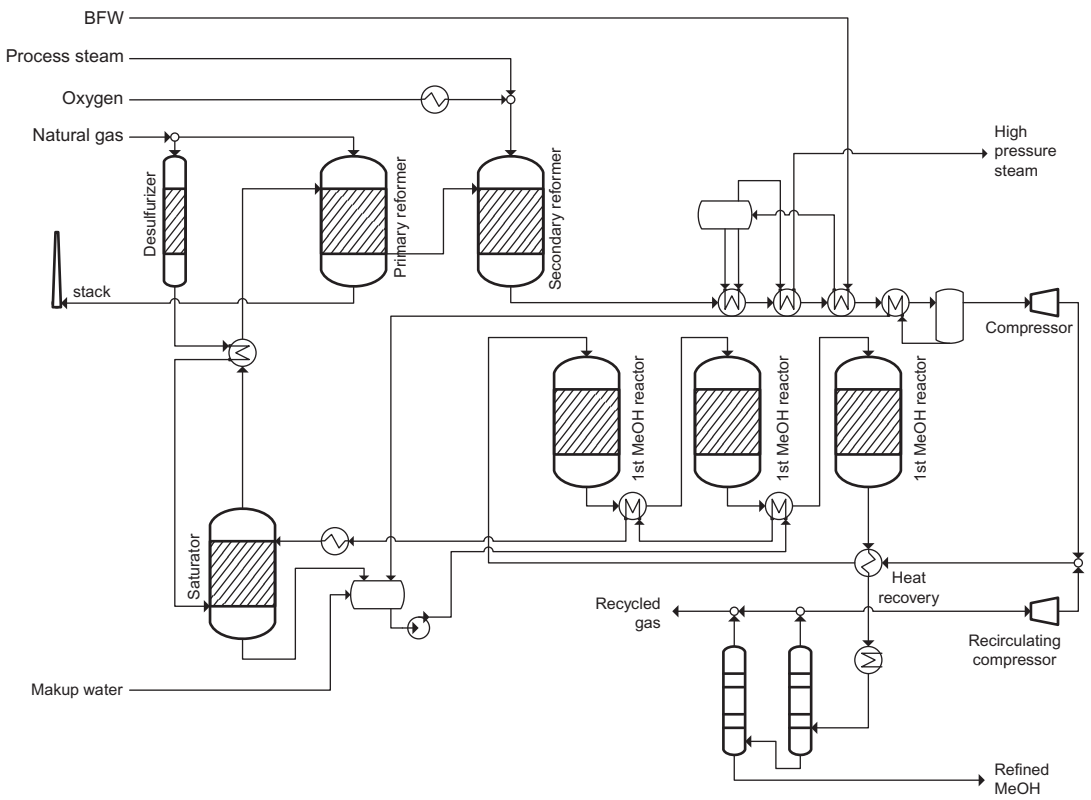

Fig. 2.6
Haldor Topsoe A/S Low-Pressure Methanol Synthesis process scheme.

Such an approach toward syngas production ensures up to 10% lower investment costs as compared with a conventional reforming scheme, even considering an oxygen plant.

The rationale behind the process is based on a complex heat recovery network: the heat content of the flue gas is recovered and used to preheat the reformer feed. Similarly, the heat content of the process gas is utilized for producing superheated high-pressure steam, for preheating boiler feed water (BFW), and for preheating process condensate before its entry into the saturator and reboiler in the distillation section. The methanol synthesis is achieved by means of three adiabatic reactors with heat exchangers between the catalytic stages: the exothermic heat of the reaction is recovered and used to heat saturator water. In addition, effluent stream from the last reactor is cooled, and heat is transferred by preheating the feed to the first reactor. This scheme can be applied in small to very large methanol plants (up to 10,000 t/d), with processes that require a total energy consumption of about 7.0 Gcal/t of product methanol, including oxygen production.

3.4 Kvaerner Methanol Synthesis Process

A different technology was developed by the Anglo-Norwegian Kvaerner company, based on a low-pressure process for methanol synthesis. Similar to the Haldor Topsoe process, in the Kvaerner process, the syngas production is carried out in two stages by processing natural or associated gas. Different from the other processes, in the Kvaerner process, carbon dioxide can be used in a methanol reactor plant in order to adjust the stoichiometric ratio of the syngas. Recent plants using this process in a typical range of 2000–3000 Mt/d have an energy efficiency ranging from 7.2 to 7.8 Gcal/t of product methanol (Lee and Sardesai, 2005), which is in line with Topsoe's published energy efficiency. The Kvaerner process scheme (Fig. 2.7) appears to be limited to regions where low-cost gas (such as CO_2-rich natural gas) is widely available, which significantly reduces capital costs.

3.5 Krupp Uhde's Methanol Synthesis Technology

A more versatile process scheme was developed by Thyssenkrupp in the 1970s. Today it is known as Krupp Uhde's Methanol Synthesis Technology. It is also based on the low-pressure synthesis chemistry of methanol and provides flexibility in choice of feedstock, including natural gas, LPG, and heavy naphtha. The steam reformer is uniquely designed by Krupp Uhde as a top-fired, box-type furnace with a cold outlet header system. The syngas generation is carried out by a nickel catalyst system, and the syngas obtained is cooled from 880°C to ambient temperature. The main part of the heat content is recovered by steam generation, BFW preheating, preheating of demineralized water, and heating of crude methanol for three-column distillation. The versatility of such a plant's operation results in a large range of energy consumption, which can be from 7 to 8 Gcal/t of methanol. The versatility of plants using this

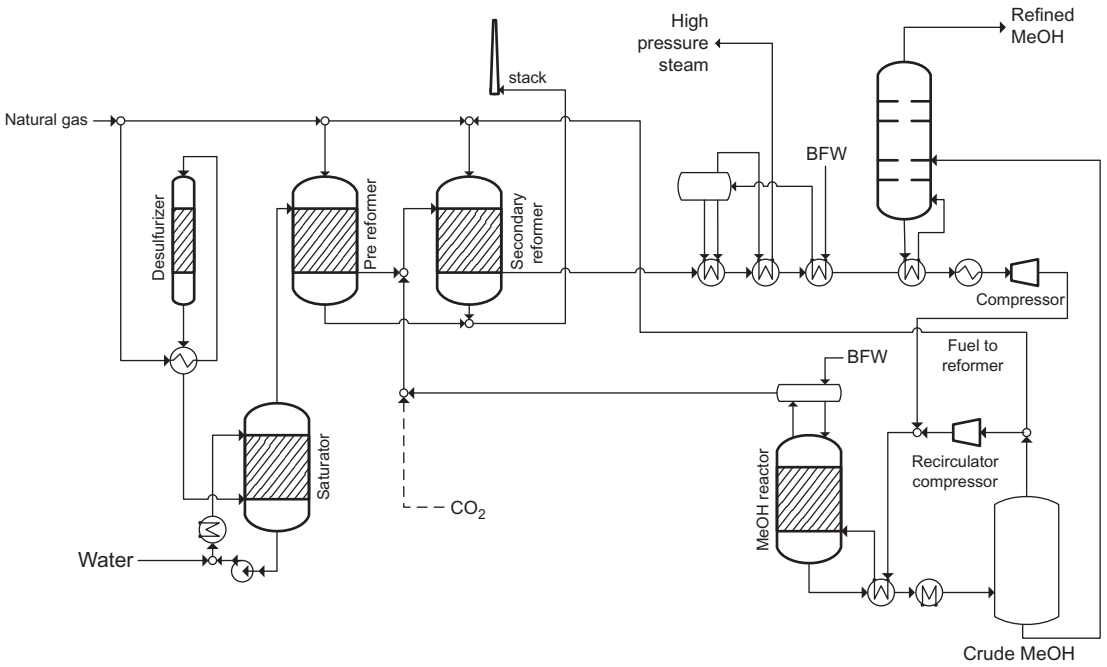

Fig. 2.7
Kvaerner Methanol Synthesis process scheme.

technology facilitates the diffusion of the technology; thus it is widely employed at methanol synthesis sites.

3.6 Lurgi Öl-Gas-Chemie GmbH Process

Lurgi Öl-Gas-Chemie GmbH proposed a process scheme (Fig. 2.8) aimed at producing methanol in a single-train plant starting from natural gas or oil-associated gas and capable of increasing the capacity of an existing methanol plant based on steam reforming. Syngas production is achieved in two stages: a prereforming stage, in which desulfurized natural gas, by reacting with steam, is partially converted in syngas; and an autothermal reforming unit, in which oxygen is added to the syngas in order to complete methane conversion and to achieve the final syngas mixture. Oxygen is involved in this reaction scheme in order to generate exothermic heat by partial oxidation of sacrificial natural gas to provide the necessary endothermic heat for the subsequent reforming reaction. Methanol synthesis takes place under quasi-isothermal conditions in the Lurgi water-cooled methanol reactor, in which a fixed bed catalyst is placed in tubes surrounded by boiling water. The reactor is fed by syngas produced in the reformer section, mixed with recycled gas from the synthesis loop; hydrogen from the pressure swing adsorption unit is added to the reactor to increase the H_2/CO ratio. The effluent stream is cooled down to 40°C to separate methanol and water from the unreacted process

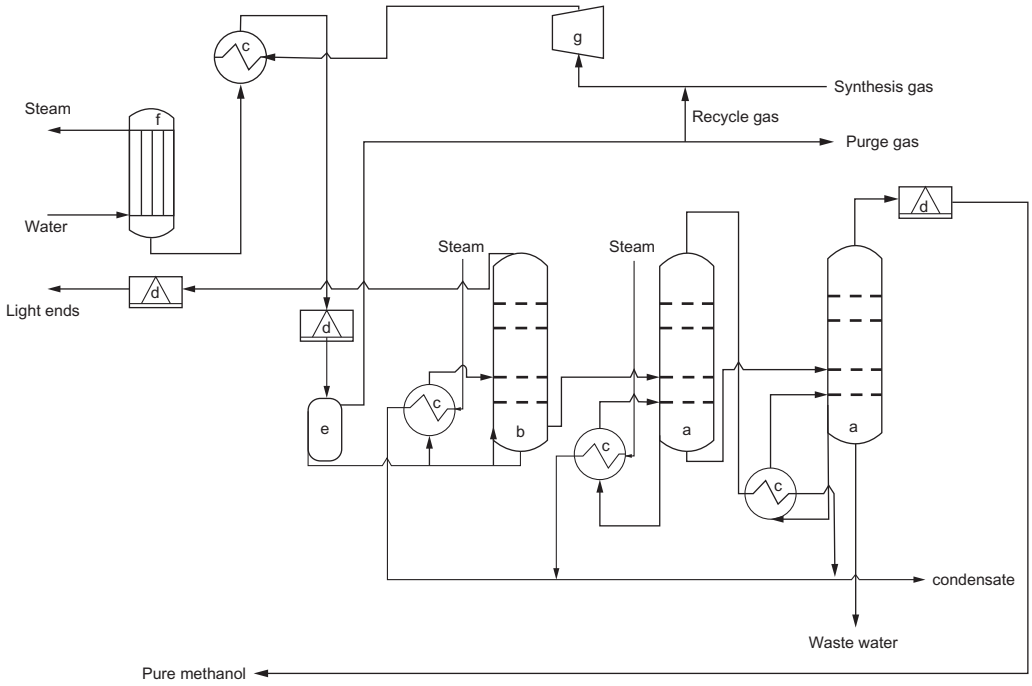

Fig. 2.8

Lurgi Öl-Gas-Chemie GmbH process scheme: (a) pure methanol columns, (b) light ends column, (c) heat exchanger, (d) cooler, (e) separator, (f) reactor, and (g) compressor recycle stage.

stream. Methanol and water are separated in distillation units, whereas the major portion of the gas is recycled back to the methanol synthesis reactor for higher overall conversion. The recycling of unreacted gas is unavoidable because of the very low kinetic of the conversion reaction, leading to a low degree of conversion per pass. Enhancements have been made, especially in the efficiency of the Lurgi combined converter (LCC), to reduce the recycle ratio down to about 2. The optimization has mainly focused on the capability to operate close to the maximum reaction rate zone. The process water is preheated in a fired heater and used as make-up water for the saturator, thus minimizing unnecessary water usage and treatment. Stream from the ATR unit contains a considerable amount of thermal energy that is recovered as high-pressure steam and partially exploited for the preheater and the reboiler. The overall process optimization ensures an energy consumption of approximately 7.1–7.2 Gcal/t of produced methanol, in a plant capable of producing up to 10,000 t/d.

3.7 Synetix LPM Process

To extend the operative field of its original process scheme, Synetix/ICI developed an improved scheme of the low-pressure methanol process that was able to produce a refined, high-purity methanol from a wide range of feedstock, such as natural gas, naphtha, coal, and

other petrochemical off-gas streams. The results of the proposed approach indicate that it is ideal for large capacities where conventional methanol processes may not be suitable or viable.

The scheme is characterized by three main processes: syngas preparation, methanol synthesis, and methanol purification. The feedstock is desulfurized before being fed into the reforming stage, in which a nickel-based catalyst very sensitive to sulfur poisoning is employed. Syngas is obtained through a steam reforming approach, similar to the Lurgi process, that leaves the reformer at about 880°C and 20 atm.

The methanol synthesis process is based on a recirculation approach: syngas is compressed and fed into the top of the reactor, at temperatures between 200°C and 290°C and pressures between 50 and 100 atm. It is well known that for temperatures close to 200°C, the chemical reaction rate is too low, whereas at temperatures close to 290°C, the employed copper-based catalyst can suffer from sintering effects. Such aspects limit the syngas conversion in the reactor module, in which only 7% of methanol is obtained. Therefore, downstream from the methanol reactor, the stream is cooled by a heat recovery module in order to separate the methanol (and water) from the unconverted reactants, which are recirculated at the top of the reactor. The condensed crude methanol, containing also water and a small amount of undesired by-products, is processed in a two-column distillation system to achieve high-purity methanol. The two columns comprise a topping and a refining column, in which the former removes all light ends, including dissolved gases, light hydrocarbons, and low-molecular-weight ethers, esters, and acetone; whereas the latter separates methanol from water and also eliminates higher hydrocarbons and alcohols through a side discharge from the column.

The proposed system is characterized by an overall energy consumption of about 7.8 Gcal/t of produced methanol; of course, the value is dependent on the type of feedstock used.

3.8 Liquid-Phase Methanol Process

The liquid-phase methanol process was originally developed by Chem Systems, Inc. in 1975 and was commercialized by Air Products and Chemicals, Inc., and Eastman Chemical Company in the 1990s. Based on the concept of the low-pressure methanol synthesis process, methanol synthesis is carried out in a slurry reactor, a liquid entrained reactor (LER), in which a fine powder catalyst ($Cu/ZnO/Al_2O_3$) is slurried in an inert high-boiling oil, typically white mineral oil. Gaseous reactants, which are fed to and dissolved in the inert oil, react with the catalytic surface in the slurry. The reaction temperature ranges between 230°C and 260°C, and the operating pressure ranges from 50 to 100 atm. The high capacity of the inert oil employed in the reactor implies that enhanced heat transfer management is required in the process scheme. The heat balance optimization could counter the requirement of adequate mass transfer conditions in the liquid phase. To enhance the mass transfer properties of the process, specially

developed, fine powder catalysts are used in order to minimize pore diffusional resistances and, in turn, mitigate mass transfer limitations. This process is unique in that it can handle unbalanced CO-rich gas and achieve high syngas conversion at each pass. As a result, the process can be packaged with advanced gasification technology such as the Texaco and Shell gasifiers.

4 Methanol Reactors

The most important part of the methanol synthesis process is the methanol reactor. Because the synthesis reaction is strongly exothermic, heat removal is an important step (Tijm et al., 2001), and so temperature control is important. A high heat flux leads to fewer tubes, smaller furnaces, and thus reduced costs (Aasberg-Petersen et al., 2001). The reactor technologies used extensively in commercial settings fall into two broad categories:

- multiple bed reactors
- single bed converters

4.1 Multiple Bed Reactors

Multiple catalyst bed reactors control the reaction temperature by separating the catalyst mass into several sections with cooling devices placed between the sections. Bed sizes are generally designed to allow the reaction to reach equilibrium conditions. The main multiple bed reactors are as follows (Tijm et al., 2001):

Haldor Topsoe's Collect, Mix, Distribute converter: This reactor, in which the synthesis gas flows radially through the catalyst beds, is characterized by catalyst beds separated by support beams. The gas leaving the upstream catalyst is collected and mixed with a quench gas for cooling. The mixed gas stream is spread evenly over the downstream catalyst bed. The reaction temperature is lowered, and the conversion per-pass rate is increased.

Kellog, Brown, and Root's adiabatic reactors in series: In these reactors, which are displaced in series, each catalyst layer is accommodated in a separate reactor vessel with intercoolers between each reactor. The feed gas enters directly into the first reactor, which increases the kinetic driving force for the reaction. This leads to a reduced catalyst volume as compared with a quench-type reactor.

Toyo Engineering Corporation's MRF-Z reactor: This reactor is a multistage radial flow reactor with intermediate cooling. This indirect cooling keeps the temperature close to the path of the maximum reaction rate curve (when the methanol concentration is plotted against temperature). Maximum, or close to maximum, conversion per pass is then achieved.

4.2 Single Bed Reactors

In single bed reactors, heat is continuously removed from the reactor by its transfer to a heat-removing medium, so the reactor runs effectively as a heat exchanger. In most commercial methanol production today, gas-phase reactor technology, which is a two-phase, gas-solid reactor, is in use. Recently, a three-phase, gas-solid-liquid technology was introduced (Hu et al., 2008): the reaction is performed with a solid catalyst suspended in a liquid medium that efficiently removes the reaction heat. Consequently, the reaction temperature in this type of reactor can be controlled more easily than in an ordinary solid reactor, and it has a higher single-pass conversion. Through the simplicity of their converter design, these liquid-phase technologies are reducing costs in the methanol industry. The main single bed reactors for methanol synthesis are as follows (Tijm et al., 2001):

Linde isothermal reactor: In this reactor's design, helically coiled tubes are embedded in the catalyst bed, which is very similar to LNGs (liquefied natural gas heat exchangers) with the catalyst around the tubes. The Linde isothermal reactor allows for up to 50% more catalyst-loading per unit of reactor volume. Compared to reactors with the catalyst inside the tubes, the heat transfer on the catalyst side is significantly higher for a Linde isothermal reactor. As a result, the cost of materials is less because less cooling area is required.

Lurgi Methanol Reactor: The Lurgi Methanol Reactor is much like a heat exchanger in that it has a vertical shell and tube heat exchanger with fixed tube sheets. The catalyst in the tubes rests on a bed of inert material. Steam is generated by the heat of reaction and drawn off below the upper tube sheet. To achieve precise control of the reaction temperature, steam pressure control is applied. Operating at isothermal conditions enables high yields at low recycles. In addition, the amount of by-products is minimized. For plant capacities above 3000 t/d, a two-stage converter system using two Lurgi Methanol Reactors in combination was developed. Because it needs to achieve only partial conversion of synthesis gas to methanol, the first converter can operate at higher space velocities and temperatures than a single-stage converter can. Operating at higher temperatures enables the production of high-pressure steam. Also, the converter can be made smaller. The exit gas is led into the second converter, which operates at a lower reaction rate.

Mitsubishi Gas Chemical/Mitsubishi Heavy Industry super converter: This super converter has double-tubes with the catalyst packed between the inner and outer tubes. The feed enters the inner tubes and is heated while flowing through the tubes. The gas then enters the space between the inner and outer tubes and flows through the catalyst bed. In addition to being cooled by the gas in the inner tubes, the catalyst is cooled by boiler water outside the double-tubes. Because the catalyst bed temperature is higher near the inlet of the reactor and then lowers toward the outlet, the gas proceeds along the maximum reaction rate line. This means that a higher conversion rate per pass is achieved (c. 14% methanol in the reactor outlet).

5 Conclusions and Future Trends

Methanol synthesis has been highly influenced by the process approach defined by Imperial Chemical Industries in the 1960s, which clearly posed a milestone in the methanol production field. All subsequent processes developed by several groups were based on the rationale defined by ICI and were characterized by the processed feedstock and by management of the recovery of energy.

Despite several attempts aimed at modifying catalytic formulations, copper-based catalysts still appear to be the favorite choice, mainly because of their relatively low cost and high selectivity toward methanol.

The research world is currently paying attention to the optimization of the methanol synthesis process. In past years, several researchers have studied the increase in methanol conversion and the decrease of the production costs. More recently, various schemes for *once-through* operations have been conceived to avoid the large amounts of recycled gas. Some once-through schemes are based on multiple reactors placed in series with interstage removal of methanol, e.g., by means of condensation (VAN Dijk and Fraley, 1993), by absorption in a liquid (Westerterp, 1992), or by reactive chromatography (Dandekar and Funk, 1995). Other once-through schemes attempt to remove the methanol inside the synthesis reactor, e.g., by means of a methanol permeating membrane (Struis et al., 1996), by means of a trickling liquid absorbent or trickling solid adsorbent particles (Westerterp et al., 1988, American Chemical Society, 1990), or by means of methanol condensation (Hansen and Joensen, 1991). Moreover, a new type of methanol synthesis reactor known as a recirculation slurry reactor (RSR) was studied (Hu et al., 2008). The catalyst slurry in the RSR is atomized to fine drops through a nozzle so that the intensive shearing action in a RSR has the effect of reducing the resistance to mass transfer from the gas to the liquid phase. Therefore the mass transfer rates are higher, and the rate of reaction in a RSR will be higher than in other slurry reactors at nominally identical conditions. Therefore it is expected that the recirculated slurry reactor will exhibit an increase in mass transfer rates, and thus an increase in the overall reaction rates as compared with traditional bubble slurry reactors.

As said previously, the modern low-temperature, low-pressure methanol synthesis is industrially carried out in externally cooled fixed bed multitubular reactors, from 8 to 12 m long, using $H_2/CO/CO_2$ mixtures and $Cu/ZnO/Al_2O_3$ pelletized catalysts. Because of the thermodynamic constraint, CO_x conversions per pass are limited, therefore requiring significant recycling of unconverted gas to ensure high overall syngas conversions, which results in high investment and operating costs and large pressure drops. In both reactor configurations, the accurate control of the temperature profile in the catalytic bed is a priority, in view of maximizing the syngas conversion per pass and the catalyst lifetime (i.e., minimizing the number of shutdowns per unit time), as well as minimizing the selectivity toward

by-products like dimethyl ether and methyl formate. Thanks to their high thermal efficiency, modularity, and reduced sensitivity to flow conditions, microchannel reactors are reported to be promising for converting biomass or stranded/associated gas into methanol (Montebelli et al., 2014). Regarding this aspect, the research of Tonkovich et al. (Tonkovich et al., 2008) looked at an innovative compact modular reactor for methanol synthesis based on microchannel technology. Furthermore, it is important to mention the printed circuit heat exchanger (PCHE) concept as well, which was developed and commercialized by Heatric and which finds specific application in highly exothermic catalytic processes (Montebelli et al., 2014). Other researchers addressed experimental investigations of novel microstructured methanol reactors, pointing out their superior heat transfer properties, which is particularly appealing for the design of small-scale methanol synthesis processes (Montebelli et al., 2014). So it is evident that the microchannel technology is an appealing technology, even if it presents some disadvantages related to its still early development stage, such as managing a number of reactors to handle large overall capacities, the high sensitivity to flow distribution, the scarce expertise in operating and maintaining such reactors, and the difficulty in loading/unloading the catalytic bed. Nevertheless, the use of structured catalysts seems to be a promising route to overcoming the problems encountered in methanol production. Structured catalysts usually consist of a thin catalyst layer (some tens of microns) deposited on a structured substrate, e.g., a honeycomb monolith (HM) or an open-cell foam (OF)—with both high void fractions and high volumetric surface areas, thus (i) enabling low-pressure drop, (ii) diminishing the risk of intraporous mass transfer limitations, and (iii) granting efficient heat removal when adopting conductive (e.g., metallic) substrates (Palma et al., 2016). In particular, structured catalysts made of highly conductive substrate materials, e.g., aluminum or copper, exhibit remarkably high radial effectiveness and thermal conductivities when employed in multitubular reactors. This topic can be further enhanced by adopting substrates with low void fractions and appropriate substrate geometries (Montebelli et al., 2014).

The adoption of such catalytic systems indeed causes a dramatic change in reactor heat transfer properties, which are found to differ from those typical of conventional random packings. Such differences are primarily related to the fact that heat exchange in conductive structured catalysts no longer relies on a convective mechanism, but on a conductive one within the continuous metallic matrix of the structured substrate, which is independent of the gas flow velocity inside the reactor tubes (Montebelli et al., 2014). Such properties make conductive structured catalysts promising for the intensification of a number of existing catalytic processes, especially those involving highly exothermic/endothermic reactions, gas/solid reactions, or gas/solid/liquid reactions in which large temperature gradients must be avoided to control selectivity and catalyst deactivation, such as methanol production.

References

Aasberg-Petersen, K., Bak Hansen, J.H., Christensen, T.S., Dybkjaer, I., Christensen, P.S., Stub Nielsen, C., Winter Madsen, S.E.L., Rostrup-Nielsen, J.R., 2001. Technologies for large-scale gas conversion. Appl. Catal. A Gen. 221, 379–387.

Alberto, M.-C.G., Emilio, R.-C.A., José, P.-A., 2014. Modelado matemático de un reactor de síntesis de metanol con interenfriamiento y desactivación de catalizador. Ingeniería, Investigación y Tecnología 15, 505–515.

American Chemical Society, 1990. Chemtech. American Chemical Society, Washington, DC.

Angelo, L., Kobl, K., Tejada, L.M.M., Zimmermann, Y., Parkhomenko, K., Roger, A.C., 2015. Study of CuZnMOx oxides (M = Al, Zr, Ce, CeZr) for the catalytic hydrogenation of CO_2 into methanol. C. R. Chim. 18, 250–260.

Audibert, E., Raineau, A., 1928. A study of the synthesis of methanol. Ind. Eng. Chem. 20, 1105–1110.

Baltes, C., Vukojević, S., Schüth, F., 2008. Correlations between synthesis, precursor, and catalyst structure and activity of a large set of $CuO/ZnO/Al_2O_3$ catalysts for methanol synthesis. J. Catal. 258, 334–344.

Bonura, G., Arena, F., Mezzatesta, G., Cannilla, C., Spadaro, L., Frusteri, F., 2011. Role of the ceria promoter and carrier on the functionality of Cu-based catalysts in the CO2-to-methanol hydrogenation reaction. Catal. Today 171, 251–256.

Bozzano, G., Manenti, F., 2016. Efficient methanol synthesis: perspectives, technologies and optimization strategies. Prog. Energy Combust. Sci. 56, 71–105.

Chinchen, G.C., Denny, P.J., Parker, D.G., Spencer, M.S., Whan, D.A., 1987. Mechanism of methanol synthesis from $CO_2/CO/H_2$ mixtures over copper/zinc oxide/alumina catalysts: use of14C-labelled reactants. Appl. Catal. 30, 333–338.

Chinchen, G.C., Denny, P.J., Jennings, J.R., Spencer, M.S., Waugh, K.C., 1988. Synthesis of methanol: part 1. Catalysts and kinetics. Appl. Catal. 36, 1–65.

Curry-Hyde, H.E., Sizgek, G.D., Wainwright, M.S., Young, D.J., 1993. Improvements to Raney copper methanol synthesis catalysts through zinc impregnation: IV. Pore structure and the influence on activity. Appl. Catal. A Gen. 95, 65–74.

Dandekar, H.W., Funk, G.A., 1995. Process for methanol production using simulated moving bed reactive chromatography. Google Patents.

Dry, R.J., 1988. Possibilities for the development of large-capacity methanol synthesis reactors for synfuel production. Ind. Eng. Chem. Res. 27, 616–624.

Dybkjær, I., Nø'Rgaard, T., Perregaard, J., Joensen, F., Topsøe, H., 2006. Tecnologie per la produzione di metanolo. In: Giavarini, C., Trifirò, F. (Eds.), Enciclopedia degli Idrocarburi. Istituto Della Enciclopedia Italiana Fondata Da Giovanni Treccani S.P.A, Rome (Italy).

Fan, L., Fujimoto, K., 1995. Development of active and stable supported noble metal catalysts for hydrogenation of carbon dioxide to methanol. Energy Convers. Manag. 36, 633–636.

Fichtl, M.B., Schlereth, D., Jacobsen, N., Kasatkin, I., Schumann, J., Behrens, M., Schlögl, R., Hinrichsen, O., 2015. Kinetics of deactivation on $Cu/ZnO/Al_2O_3$ methanol synthesis catalysts. Appl. Catal. A Gen. 502, 262–270.

Graaf, G.H., Sijtsema, P.J.J.M., Stamhuis, E.J., Joosten, G.E.H., 1986. Chemical equilibria in methanol synthesis. Chem. Eng. Sci. 41, 2883–2890.

Graaf, G.H., Sijtsema, P.J.J.M., Stamhuis, E.J., Joosten, G.E.H., 1990. On chemical equilibria in methanol synthesis. Chem. Eng. Sci. 45, 769–770.

Grabow, L.C., Mavrikakis, M., 2011. Mechanism of methanol synthesis on Cu through CO_2 and CO hydrogenation. ACS Catal. 1, 365–384.

Hansen, J.B., Joensen, F., 1991. High conversion of synthesis gas into oxygenates. Stud. Surf. Sci. Catal. 61, 457–467.

Hong, Z.-S., Cao, Y., Deng, J.-F., Fan, K.-N., 2002. CO2 hydrogenation to methanol over $Cu/ZnO/Al_2O_3$ catalysts prepared by a novel gel-network-coprecipitation method. Catal. Lett. 82, 37–44.
Hu, L.H., Wang, X.J., Yu, G.S., Wang, F.C., Yu, Z.H., 2008. Study of the characteristics of methanol synthesis in a recirculation slurry reactor–a novel three-phase synthesis reactor. Chem. Eng. Technol. 31, 33–37.
Huang, X., Ma, L., Wainwright, M.S., 2004. The influence of Cr, Zn and Co additives on the performance of skeletal copper catalysts for methanol synthesis and related reactions. Appl. Catal. A Gen. 257, 235–243.
Kurtz, M., Wilmer, H., Genger, T., Hinrichsen, O., Muhler, M., 2003. Deactivation of supported copper catalysts for methanol synthesis. Catal. Lett. 86, 77–80.
Lahne, U., Lohmüller, R., 1986. Schüttschichtreaktoren mit gewickelten Kühlrohren, eine konstruktive Neuentwicklung zur Durchführung exothermer katalytischer Prozesse. Chem. Ing. Tech. 58, 212–215.
Lange, J.-P., 2001. Methanol synthesis: a short review of technology improvements. Catal. Today 64, 3–8.
Lee, S., Sardesai, A., 2005. Liquid phase methanol and dimethyl ether synthesis from syngas. Top. Catal. 32, 197–207.
Lee, J.S., Lee, K.H., Lee, S.Y., Kim, Y.G., 1993. A comparative study of methanol synthesis from CO_2/H_2 and CO/H_2 over a $Cu/ZnO/Al_2O_3$ catalyst. J. Catal. 144, 414–424.
Lee, J.S., Moon, K.I., Lee, S.H., Lee, S.Y., Kim, Y.G., 1995. Modified $Cu/ZnO/Al_2O_3$ catalysts for methanol synthesis from CO_2/H_2 and CO/H_2. Catal. Lett. 34, 93–99.
Lewis, G.N., Randall, M., 1923. Thermodynamics and the Free Energy of Chemical Substances. McGraw-Hill Book Company Inc, New York.
Li, M.M.-J., Zeng, Z., Liao, F., Hong, X., Tsang, S.C.E., 2016. Enhanced CO_2 hydrogenation to methanol over CuZn nanoalloy in Ga modified Cu/ZnO catalysts. J. Catal. 343, 157–167.
Liu, X.-M., Lu, G.Q., Yan, Z.-F., Beltramini, J., 2003. Recent advances in catalysts for methanol synthesis via hydrogenation of CO and CO_2. Ind. Eng. Chem. Res. 42, 6518–6530.
Liu, X.-M., Yan, Z.-F., Lu, G.-Q., 2006. Role of nanosized zirconia on the properties of $Cu/Ga_2O_3/ZrO_2$ catalysts for methanol synthesis. Chin. J. Chem. 24, 172–176.
Liu, X., Bai, S., Zhuang, H., Yan, Z., 2012. Preparation of Cu/ZrO_2 catalysts for methanol synthesis from CO_2/H_2. Front. Chem. Sci. Eng. 6, 47–52.
Makihara, H., Niwa, K., Nagai, H., Morita, K., Horizoe, H., Kobayashi, K., Kuwada, C., 1987. Characteristics of a new methanol synthesis reactor. Energy Prog, 51–58.
Metzger, J.O., 2006. Beyond oil and gas: the methanol economy. By George A. Olah, Alain Goeppert, and G. K. Surya Prakash. Angewandte Chemie International Edition 45, 5045–5047.
Milani, D., Khalilpour, R., Zahedi, G., Abbas, A., 2015. A model-based analysis of CO_2 utilization in methanol synthesis plant. J. CO_2 Util. 10, 12–22.
Montebelli, A., Visconti, C.G., Groppi, G., Tronconi, E., Kohler, S., 2014. Optimization of compact multitubular fixed-bed reactors for the methanol synthesis loaded with highly conductive structured catalysts. Chem. Eng. J. 255, 257–265.
Palma, V., Ricca, A., Meloni, E., Martino, M., Miccio, M., Ciambelli, P., 2016. Experimental and numerical investigations on structured catalysts for methane steam reforming intensification. J. Clean. Prod. 111 (Part A), 217–230.
Peng, D.-Y., Robinson, D.B., 1976. A new two-constant equation of state. Ind. Eng. Chem. Fundam. 15, 59–64.
Pori, M., Likozar, B., Marinšek, M., Crnjak Orel, Z., 2016. Preparation of Cu/ZnO-based heterogeneous catalysts by photochemical deposition, their characterisation and application for methanol synthesis from carbon dioxide and hydrogen. Fuel Process. Technol. 146, 39–47.
Raudaskoski, R., Turpeinen, E., Lenkkeri, R., Pongrácz, E., Keiski, R.L., 2009. Catalytic activation of CO_2: use of secondary CO_2 for the production of synthesis gas and for methanol synthesis over copper-based zirconia-containing catalysts. Catal. Today 144, 318–323.
Redlich, O., Kwong, J.N.S., 1949. On the thermodynamics of solutions. V. An equation of state. Fugacities of gaseous solutions. Chem. Rev. 44, 233–244.
Shimomura, M., Nojima, S., 1988. Preparation of monolith-type catalyst for methanol steam reforming. Zeolites 8, 341.

Soave, G., 1972. Equilibrium constants from a modified redlich-kwong equation of state. Chem. Eng. Sci. 27, 1197–1203.
Struis, R.P.W.J., Stucki, S., Wiedorn, M., 1996. A membrane reactor for methanol synthesis. J. Membr. Sci. 113, 93–100.
Sun, J.T., Metcalfe, I.S., Sahibzada, M., 1999. Deactivation of $Cu/ZnO/Al_2O_3$ methanol synthesis catalyst by sintering. Ind. Eng. Chem. Res. 38, 3868–3872.
Tijm, P.J.A., Waller, F.J., Brown, D.M., 2001. Methanol technology developments for the new millennium. Appl. Catal. A Gen. 221, 275–282.
Tonkovich, A.L., Jarosch, K., Arora, R., Silva, L., Perry, S., Mcdaniel, J., Daly, F., Litt, B., 2008. Methanol production FPSO plant concept using multiple microchannel unit operations. Chem. Eng. J. 135 (Suppl 1), S2–S8.
Van Dijk, C.P., Fraley, L.D., 1993. Process for producing and utilizing an oxygen enriched gas. Google Patents.
Wang, D., Zhao, J., Song, H., Chou, L., 2011. Characterization and performance of $Cu/ZnO/Al_2O_3$ catalysts prepared via decomposition of M(Cu, Zn)-ammonia complexes under sub-atmospheric pressure for methanol synthesis from H_2 and CO_2. J. Nat. Gas Chem. 20, 629–634.
Westerterp, K.R., 1992. Multifunctional reactors. Chem. Eng. Sci. 47, 2195–2206.
Westerterp, K.R., Van Gelder, K.B., Janssen, H.J., Oyevaar, M.H., 1988. Development of catalytic hydrogenation reactors for the fine chemicals industry. Chem. Eng. Sci. 43, 2229–2236.
Xiao, S., Zhang, Y., Gao, P., Zhong, L., Li, X., Zhang, Z., Wang, H., Wei, W., Sun, Y., 2017. Highly efficient Cu-based catalysts via hydrotalcite-like precursors for CO2 hydrogenation to methanol. Catal. Today 281 (2), 327–336.
Zhai, X., Shamoto, J., Xie, H., Tan, Y., Han, Y., Tsubaki, N., 2008. Study on the deactivation phenomena of Cu-based catalyst for methanol synthesis in slurry phase. Fuel 87, 430–434.
Zhang, Y., Sun, Q., Deng, J., Wu, D., Chen, S., 1997. A high activity $Cu/ZnO/Al_2O_3$ catalyst for methanol synthesis: preparation and catalytic properties. Appl. Catal. A Gen. 158, 105–120.
Zhang, L., Zhang, Y., Chen, S., 2012. Effect of promoter SiO_2, TiO_2 or SiO_2-TiO_2 on the performance of CuO-ZnO-Al_2O_3 catalyst for methanol synthesis from CO_2 hydrogenation. Appl. Catal. A Gen. 415–416, 118–123.

Further Reading

The Methanol Industry–Methanol Institute, 2016. Methanol Institute. Available: http://www.methanol.org/the-methanol-industry/ (accessed 25.02.17).

This page intentionally left blank

CHAPTER 3

Fossil or Renewable Sources for Methanol Production?

Carlo Pirola*, Giulia Bozzano†, Flavio Manenti†

*University of Milano, Milano, Italy †Polytechnic of Milano, Milano, Italy

Acronyms

AG2S	Acid Gas to Syngas
CB	conduction band
CNR-ITAE	Consiglio Nazionale delle Ricerche—Istituto di Tecnologie Avanzate per l'Energia
CRI	Carbon Recycling International
GPLE	generalized power law expression
LCA	life cycle analysis
LHHW	Langmuir-Hinshelwod-Hougen-Watson
MPT	melting point temperature
MTBE	methyl-tert-butyl ether
PLE	power law expression
RDS	rate determining step
RTR	regenerative thermal reactor
USD	US dollar
UV-A	ultraviolet light, wavelength 315–400 nm
WGS	water-gas shift
WHB	waste heat boiler

Symbols

A, B, C, D, E, G, M	estimated constants
a	deactivation evaluated as the ratio r/r_0
a_{eq}	asymptotic deactivation
c	concentration
f	fugacity
k	kinetic constant

Methanol. https://doi.org/10.1016/B978-0-444-63903-5.00003-0

k_i	rate constant and of step *i*
K_i	equilibrium constant of step *i*
K, K^*, K_{eq}	equilibrium constant
n	order for the deactivation rate
p	pressure
r	rate of reaction
r_0	the rate of reaction at time 0
t	time
θ^*	coverage of the free sites

Subscripts

d	deactivation
eq	equilibrium
f	formation
w	water

1 Introduction

Methanol is one of the most important platform chemicals used as a building block for the production of several commodities and as fuel or additive. The most relevant synthetized chemicals that start from methanol are methyl-tert-butyl ether (MTBE), acetic acid, dimethyl ether, and formaldehyde. This last compound in particular consumes about 70% of the methanol produced in the world (Bozzano and Manenti, 2016). Several products, such as adhesives, plastics, paints, and silicones, are produced today using methanol as the main feedstock.

Methanol can be used potentially as transportation fuel, alone or mixed with gasoline. Respect pure gasoline or other fuels is considered safer and less toxic and the emission coming from its use in combustion engines are reduced in term of NO_x, SO_x, and particulate. Methanol is also one of the reactants in the production of biodiesel fuel manufactured from vegetable oils (Pirola et al., 2015) and MTBE via esterification. Based on its use as a hydrogen carrier, methanol can also be used in the automotive field in the development of fuel cell vehicles (McNicol et al., 1999).

Moreover, liquid methanol is becoming an increasingly attractive option for the storage of energy, as an alternative to hydrogen. In fact, the methanol economy, based on methanol produced by green synthetic procedures, can be proposed as an alternative to the hydrogen economy, which requires new storage and transportation technologies (Olah, 2005). Methanol is considered a suitable substance to promote the transition from fossil to renewable sources both on the basis of its intrinsic chemico-physical properties and on its ability to be produced by biomass technology

Table 3.1 Physical properties of hydrogen and methanol relevant to accident safety

	Hydrogen	Methanol
Molecular weight	2.016	32.04
Liquid density (g/mL)	0.074 (liquid) 1.3×10^{-6} (gas)	0.791
Boiling point (°C)	−253	65
Minimum ignition energy (mJ)	0.14	0.02
Diffusion coefficient (cm^2/s)	0.61	0.0042
Flammability limits (vol%)	4–75	6–36.5
Explosive limits (vol%)	18.3–59.0	6–36

(Olah et al., 2006). Methanol (octane number of 113) is characterized by a higher volumetric energy density than liquid hydrogen (99 and 71 g/L, respectively) and therefore does not require the use of a cryogenic container that must be maintained at a temperature of −253°C (Shamsul et al., 2014). The main physical properties of hydrogen and methanol relevant to accident safety are shown in Table 3.1, adapted from (Adamson and Pearson, 2000).

Methanol can be produced from different sources. The most important industrial processes for its synthesis are based on the use of traditional fossil fuel materials, natural gas and coal. New processes are now under development with intensive research in both academic and industrial laboratories, and they are based on the use of renewable biomass-based resources. The methanol process is one of the most important examples in industrial chemistry. It was proposed in 1923 by BASF, with a patent in which syngas, used for the methanol synthesis using a zinc/chromium oxide catalyst operating at 300–400°C and 250–350 atm, was supplied via coal gasification. Subsequent studies improved the performance of the process, and today the process is performed at lower temperatures and pressures (230–250°C, 40–50 atm) and has an energy efficiency of about 75% (Bozzano and Manenti, 2016). Obviously, the methanol process can be considered a well-established technology. Nevertheless, from an environmental and societal point of view, its main drawback is the use of fossil fuels as the raw materials. Fossil fuels, renewable materials, and nuclear energy are the three main categories of energy sources. Fossil fuels, that is, coal and natural gas, are nonrenewable materials that will be depleted in the future (Bhattacharyya et al., 2008), and their use is connected with global warming.

Several technologies and new processes are now under study to develop a new methanol production process based on the use of renewable sources, with biomass being the most important option.

In this chapter a comparison between the traditional, fossil based, process and the different biomass based corresponding technologies will be proposed. The description of some selected processes together with an analysis of the different reactors and catalytic systems involved and an interpretation of the corresponding kinetic models are presented.

2 Why Methanol From Biomass?

The enormous amount of fossil fuels burned worldwide is increasing the production of acid rain and photochemical smog, which are continuously increasing the amount of atmospheric carbon dioxide that is resulting in global warming. A parallel problem is the depletion of fossil fuels, although in recent years new oil resources have been discovered. The partial or complete substitution of fossil fuels with the direct or indirect use of solar energy is the most attractive option for stabilizing Earth's climate. The other possible option is nuclear energy, but this choice presents serious drawbacks. Nuclear fuels are nonrenewable energy resources, and also if a plant failure were to occur, large amounts of radioactive material could be released into the environment. In addition, nuclear waste remains radioactive for thousands of years, and its storage is very complex and dangerous. The use of renewable biofuel is attractive because it is based on solar energy, and it reduces carbon dioxide by photosynthesis. The combustion of biomass-derived fuels does not increase the total global CO_2. Moreover, liquid fuel, in particular ethanol and methanol, represents an alternative to petroleum fuels for different engines and is easy to store and manage. The carbon cycle of biomethanol is shown in Fig. 3.1, adapted from (Olah et al., 2006), and an overview of the most important methanol production processes from various carbon sources is shown in Fig. 3.2, adapted from (IEA-ETSAP and IRENA, 2013).

As mentioned earlier, the production of methanol from biomass is a challenging but important task, for both economical and societal reasons. By 2050 the most significant portion of greenhouse emissions will be derived from road transportation. From a legislative point of

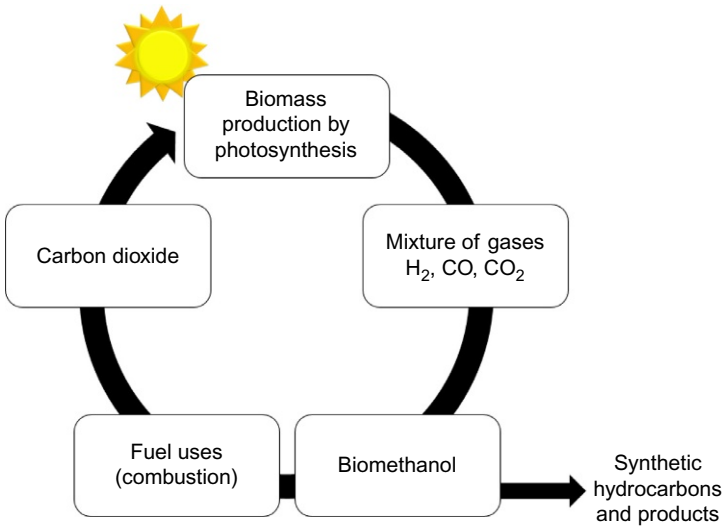

Fig. 3.1
The renewable carbon cycle of methanol.

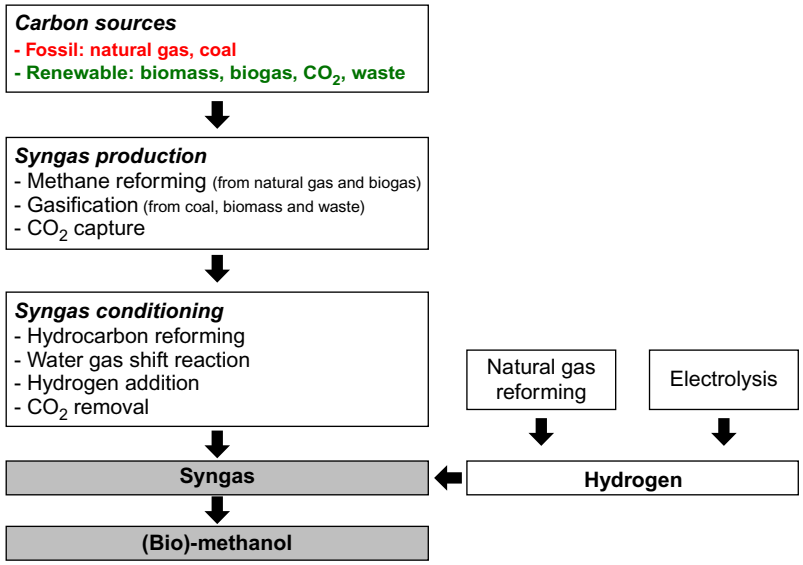

Fig. 3.2
Overview of the major production process of methanol and biomethanol.

view, the European Commission set a target of achieving 20% renewables by 2020. In 2010, 5.75% of the transportation fuels sold were renewable, and this percentage is expected to increase to 10% in 2020. If this trend continues, use of renewables is expected to reach 27% by 2025 (Shamsul et al., 2014). The role of biofuels will increase in the future, compared with the demand for gasoline and fossil diesel fuel (Leduc et al., 2010). Biomass-derived methanol is a promising option for the substitution of fossil petroleum in combustion engines, because it does not require complex modification in vehicles and its fuel distribution infrastructure is uncomplicated (Andersson et al., 2014).

It is not easy to determine the environmental performance of the biomethanol process because this technology is under development and is highly dependent on a plant's setup, on the kind of biomass used as raw material, and on the possible presence of valuable coproducts. However, based on several studies reported in the literature, a real estimate shows that biomethanol production can reduce greenhouse gas emissions by 25%–40% more than the same compound from fossil sources, if a life cycle analysis (LCA) is considered, that is, analyzing the entire life cycle "from cradle to grave" (IEA-ETSAP and IRENA, 2013).

Adamson and Pearson (2000) reported that biomass processing is the most convenient process (300–400 Euro/t) among all the processes developed for the production of methanol from renewable sources, which included a comparison with the cost of production of carbon dioxide (500–600 Euro/t). This is an approximate estimate, considering that the location, the kind of process, the capacity of the plant, and the purity of the final product influence in a significant way the economics of the methanol production. Some quantifications concerning the cost

of methanol produced from biomass are available in the literature, and as reported in (Shamsul et al., 2014), this parameter is strongly dependent on the scale of production, changing, for example, from $687/t for farm-scale production to $419/t (by partial oxidation) or $453/t (by steam reforming) for large-scale production. Production based on CO_2 conversion is estimated to be expensive, with costs ranging from $560/t to $1000/t. It is important to note that several aspects can significantly influence these estimations about biomethanol costs. For example, the coproduction of heat, electricity, or other chemical products can decrease the cost of the process. Moreover, when biomethanol is produced using industrial organic waste streams, the logistic of feedstocks is simplified, and the performance of the whole plant can be improved.

Concerning the methanol produced by fossil feedstock, more than 75% of this product is synthetized by syngas obtained from natural gas. Nearly 90 methanol plants are working worldwide with a total annual capacity of about 50 millions t and the price in 2011 ranging from $400/t to $500/t, with the expectation of increasing in the following years.

Several technologies for producing methanol from biomass materials are under development, but further study and innovations are necessary before these new processes can be used competitively for large-scale production. Presently, each year about 200 t of biomethanol are produced, but new strategies to increase the global capacity to well over 1,000,000 t in the coming years (IEA-ETSAP and IRENA, 2013) are being considered. Table 3.2, adapted from the preceding reference, presents an overview of the existing or planned facilities and processes for biomethanol synthesis.

The following sections presents the various types of biomass that can be obtained from waste products and that can be used as raw material for the biomethanol synthesis.

Table 3.2 Overview of the existing and planned facilities for biomethanol production

Country	Company	Start-Up Year	Capacity (kt/y)	Main Product	Feedstock
Currently in operation					
Netherlands	BioMCN	2010	200	Biomethanol	Glycerine
Sweden	BioDME	2011	1.5	BioDME	Black liquor
Canada	Enerkem	2011	4	Syngas, biomethanol	Treated wood
Under construction or proposed					
Sweden	Chemrec & Dom-sio Fabriker	Late 2012	100	BioDME, biomethanol	Black liquor
Sweden	Varmlands Metanol	2015	100	Biomethanol	Forest residue
Netherlands	Woodspirit	2015	400–900	Biomethanol	Wood
Poland	PKE & ZAK	2015	Up to 550	Heat & power, biomethanol, chemicals	Up to 10% biomass, coal
Germany	DeBioM			Biomethanol	Wood

3 Different Kinds of Biomass

Biomass refers to organic and carbonaceous materials that store sunlight via photosynthesis in the form of chemical energy. Biomass can be divided into five main categories: wood from natural forests, agricultural residue, energy crops (i.e., those cultivated exclusively for fuel production), urban solid waste/sewage, and food waste, as illustrated in Fig. 3.3, adapted from (Shamsul et al., 2014).

Biomass used as feedstock for biofuel production can be classified as first, second, and third generation biofuel. First generation biofuels are those produced directly from food crops. For example, crops such as wheat and sugar have been used in bioethanol production by fermentation, and oilseed rape has been one of the main raw materials in biodiesel synthesis. Second generation biofuels have been proposed to overcome the drawbacks of the first generation biofuels, primarily because they are produced from nonfood crops such as wood, organic waste, food crop waste, and specific biomass crops. Finally, third generation biofuels are based on improvements in their production, which is increasing the total yield of the process, and on taking advantage of specially engineered energy crops such as algae. The use of second and third generation biofuels helps to decrease the amount of food products devoted to fuel production, helps to decrease greenhouse gas emissions, and increases the selection of possible feedstocks (Cifre, 2007).

The two most important sources of biomass for fuel production are purpose-grown energy crops (woody crops and agricultural crops) and wastes (wood residues, forestry residues, sewage and/or municipal solid wastes, and animal wastes).

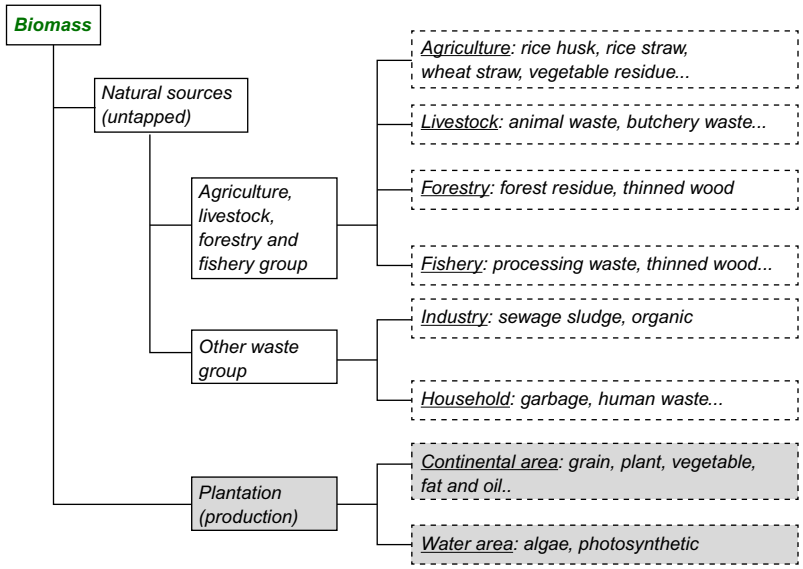

Fig. 3.3
Representation of different species and categories of biomass.

Biomass materials are composed of different amounts of cellulose, hemicellulose, lignin, and in smaller quantities, lipids, proteins, starches, and simple sugars (Saidur et al., 2011). Moreover, biomass comprises some inorganic compounds and obviously water. Cellulose, hemicellulose, and lignin (in combination referred to as "lignocellulose") are key factors in classifying biomass and in determining the main properties of raw materials used for biofuel production (Zhang et al., 2010). In lignocellulosic materials, the most abundant component is cellulose, then hemicellulose, and finally lignin. Cellulose and hemicellulose are macromolecules formed by several sugars, while lignin is an aromatic polymer. Knowing the structural composition of biomass, particularly for the lignocellulosic fraction, is crucial for the analysis, projection, and development of the production process of biofuel and biochemicals. Other techniques give very important information as to the ultimate and proximate analysis. The ultimate analysis determines the amount of N, S, and Cl, which is very important for estimating the ultimate environmental impact of a specific biomass, and the amount of C, H, and O, which makes it possible to calculate the heating values of the specific biomass. Proximate analysis enables the determination of the quantity of ash, fixed carbons, and volatile compounds in a specific biomass, thus giving valuable information for the study of biomass combustion and gasification. Biomass can be classified in terms of lignocellulosic constituents and by ultimate and proximate analysis. Some examples, taken from Zhang et al. (2010), are shown in Table 3.3.

Table 3.3 Examples of different biomasses characterized by lignocellulosic content, ultimate analysis, and proximate analysis

Lignocellulosic Residues (% on Dry Basis)						
	Hemicellulose		Cellulose		Lignin	
Rice straw	24		62		18	
Spruce wood	21		50		27	
Sugar cane bagasse	27–32		32–44		19–24	
Ultimate Analysis (% on Dry Basis)						
	C	H	O	N	S	Cl
Rice straw	38.45	5.28	–	0.88	–	–
Spruce wood	51.4	6.1	41.2	0.3	–	0.1
Sugar cane bagasse	44.8	5.4	39.6	0.4	0.01	–
Proximate Analysis (% On Dry Basis)						
	Fixed Carbon		Volatile Matter		Ash	
Rice straw	15.86		65.47		18.67	
Spruce wood	29.30		70.20		1.50	
Sugar cane bagasse	11.95		85.61		2.44	

Adapted from Zhang, L., Xu, C., Champagne, P., 2010. Overview of recent advances in thermos-chemical conversion of biomass. Energy Convers. Manag. 51, 969–982.

4 Traditional Process for Methanol Production

4.1 Chemistry

Methanol production is based on main three steps:

- Production of synthesis gas (syngas)
- Conversion of the synthesis gas into methanol
- Distillation of the reactor effluent

Reforming of natural gas is the most widely used process for producing syngas. However, there are alternatives for reforming of partial oxidation of other carbon-based materials, for instance coal, petroleum, heavy oil, petroleum coke, and biogas (Pino et al., 2014; Vita et al., 2015). The choice depends on economic, political, energy-consumption, and environmental considerations.

The composition of syngas, that is a mixture of CO, CO_2, and H_2, is given in terms of a stoichiometric number S, which is a ratio of two quantities: the difference between the moles of hydrogen and CO_2 and the summation of the moles of CO_2 and CO:

$$S = \frac{\text{moles}\,H_2 - \text{moles}\,CO_2}{\text{moles}\,CO_2 + \text{moles}\,CO} \tag{3.1}$$

Under ideal conditions, methanol production requires a value of S equal to 2; however, in most industrial applications, the value is slightly greater than 2, which indicates that a greater amount of hydrogen is required. The definition of the stoichiometric value S accounts for the consumption of hydrogen in the reverse water-gas shift reaction with CO_2. Different values of S are obtained, depending on the starting material; for example, syngas produced by natural gas reforming has an S value of 2.8–3.

The most diffused process for methanol production operates in gas phase at pressures of 50–100 atm and temperatures ranging from 200°C to 300°C. The catalyst is copper-based, constituted by a combination of CuO, ZnO, and Al_2O_3.

The macrokinetic mechanism of the methanol synthesis occurs in three reactions,

$$CO + 2H_2 \rightleftarrows CH_3OH \quad \left(\Delta H = -91\,\frac{\text{kJ}}{\text{mol}}\right) \tag{3.2}$$

$$CO_2 + 3H_2 \rightleftarrows CH_3OH + H_2O \quad \left(\Delta H = -49.5\,\frac{\text{kJ}}{\text{mol}}\right) \tag{3.3}$$

and the water-gas shift reaction:

$$CO + H_2O \rightleftarrows CO_2 + H_2 \quad \left(\Delta H = -41.0\,\frac{\text{kJ}}{\text{mol}}\right) \tag{3.4}$$

The microkinetic mechanism actually includes several reaction steps among the adsorbed species, and in the literature, up to about 50 reactions have been proposed. The Langmuir-Hinshelwood and Eley-Rideal mechanisms are usually adopted, and one or more of the steps are considered to be the rate determining step (RDS). In the first type of mechanism, the product is derived from the interaction of two adsorbed atoms or species and, in the second type of mechanism, from the interaction between one adsorbed atom or species and another atom/species (not adsorbed on the catalytic surface).

4.2 Catalytic Systems

In terms of $CuO/ZnO/Al_2O_3$, the composition of the catalyst can vary depending on the manufacturer, as shown in Table 3.4.

The CuO component ranges between 20% and 80%, the ZnO between 15% and 50%, and the Al_2O_3 from 4% to 30%. Additives, such as MgO, can also be present. The MgO was first adopted by Johnson Matthey, particularly in the Katalco 51-7 catalyst. MgO acts as a promoter and catalyst stabilizer, allows lower temperatures, and slows thermal sintering. MgO was incorporated in subsequent variants, Katalco 51-8 and Katalco 51-9. Today selectivity of catalyst is more than 99% (Moulijn et al., 2001; Hansen, 1997).

Metallic copper is the main active component (Ovesen, 1992; Rasmussen et al., 1994), while ZnO is believed to act as a supporter and Al_2O_3 a promoter. ZnO is also supposed to enhance

Table 3.4 Examples of compositions of the catalysts from different manufacturers, from Spath and Dayton (2015)

Manufacturer	Cu (wt%)	Zn (wt%)	Al (wt%)	Other
Johnson Matthey	20–35	15–50	4–20	Mg
IFP	45–70	15–35	4–20	Zr-2-18
BASF	38.5	48.8	12.9	Rare earth oxide-5
Shell	71	24	12	
Süd Chemie	65	22	31	
DuPont	50	19	17	
United Catalysts	62	21	17	
Haldor Topsoe MK-121	>55	21–25	8–10	
Mitsubishi Gas Chemical Company	63.6	33.4	3	
Ammonia Casale	30	50	3	Cr (16)
Lonza	40	20		Zr (40)
AIST, RITE	45.2	27.1	4.5	Zr (22.6) Si (0.6)
YYK Corporation	76.3	11	12.7	

Adapted from Wernicke, H.J., Plass, L., Schmidt, F., 2014. Methanol generation. In: Bertau, M., Offermanns, H., Plass, L., Schmidt, F., Wernicke, H.J. (Eds.), Methanol: The Basic Chemical and Energy Feedstock of the Future.

the dispersion of copper particles and stabilize the copper crystals. There is some discussion among authors about the real active site of the reactions: some believe Cu dissolved in ZnO (Klier, 1982), others believe that the metallic copper dispersed on the ZnO surface. The correlation between the catalyst activity and the metallic copper exposed area is quasilinear (Chinchen et al., 1987), which was also observed in situ with X-ray photoelectron spectroscopy (67) and surface X-ray diffraction studies (Clausen et al., 1991). The surface science techniques adopted by Fujitani and Nakamura (Fujitani and Nakamura, 2000), however, found a different effect of ZnO in the reactions; that is, they found that it constituted an active site other than that of dispersing Cu particles. This phenomenon was also observed by Ostrovskii (2002).

The catalyst activity in the methanol synthesis depends on the total exposed copper area, so variations in the CuO:Al_2O_3 ratio have a remarkable effect on the relative activity (Fitzpatrick and Hicks, 2010).

The efficiency of the CuO/ZnO/Al_2O_3 catalyst depends on its stability over time; thus efforts have been devoted to stabilizing the copper agglomerates on the catalytic surface under the process's operating conditions. Catalyst deactivation occurs mainly as a consequence of sintering and poisoning.

Poisons such as sulfur, and sometimes iron and nickel, carbonyls can be in fresh syngas. Because sulfur content has to be as low as 5 ppm or even 1 ppm, and chloride impurities can also promote catalyst sintering, the syngas is deeply purified before methanol synthesis so that sintering of Cu particles is considered the only responsible avenue for catalyst deactivation (Chincen et al., 1988). It is interesting to note that the fresh catalyst is black, because of the very restricted dimensions of dispersed Cu particles, whereas the sintered catalyst appears pink. The sintering of copper crystallites reduces the catalyst's active surface area, thus decreasing activity. In the case of methanol synthesis, the main mechanisms of crystallite growth result from crystallite and atomic migrations. In crystallite migration, entire crystallites move on the support surface, colliding and coalescing. In atomic migration, metal atoms move on the support surface and join larger crystallites. Atomic migration is favored at lower temperatures more than crystallite migration is. The global mechanism of sintering involves several elementary steps (Argyle and Bartholomew, 2015):

- Dissociation and emission of metal atoms from metal crystallites
- Adsorption and trapping of metal atoms on the surface
- Diffusion of metal atoms across the surface
- Metal or metal oxide particle dispersion
- Surface wetting by metal particles
- Metal particle nucleation
- Coalescence of metal particles

- Capture of atoms by metal particles
- Liquid formation
- Metal volatilization
- Splitting of crystallites
- Metal atom vaporization

The type of chemical process and the related operating conditions influence which of the abovementioned steps tend to occur. The increasing temperature and the presence of water enhance the sintering rate. Usually it is related to the absolute melting point temperature (MPT; copper = 1356 K). Two other temperatures, however, need to be taken into account: the Huttig temperature (0.3*MPT (K); copper = 407 K) and the Tamman temperature (0.5*MPT (K); copper = 678 K). In fact, at the Huttig temperature, surface atoms located at any lattice imperfection start dissociating and diffusing on the surface. At the Tamman temperature, bulk atoms become mobile. Therefore sintering is already active at the Huttig temperature and increases its rate up to the Tamman temperature. These temperatures support why Tohji et al. (1985) found sintering already active at 500 K. Supp (1981) reported that copper recrystallized at temperatures higher than 543 K, and Roberts found growth of copper crystals at 523 K. It is possible therefore to affirm that in methanol synthesis, sintering starts at 463–500 K and increases its rate at 543–573°C.

Sun et al. (1999) studied the effect of the feed composition on the catalyst's deactivation. In their experiments, they considered both differential and finite conversion reactors and adopted different feeds: CO_2/H_2 and CO/H_2. For differential conversion reactors, they found a rapid catalyst deactivation with CO/H_2 feeds caused by the reducing nature of CO, whereas CO_2/H_2 feeds induced hardly any deactivation. Opposite conclusions were obtained under finite conversion conditions. In particular, with CO/H_2 feeds, a slower catalyst deactivation was found, by virtue of the presence of reaction products (such as CO_2 produced by the WGS reaction), which slowed the overreduction of Cu and ZnO due to CO. Conversely, CO_2/H_2 feeds caused faster deactivation because of the presence of CO generated by the reverse WGS reaction. Other authors (e.g., Kung, 1992) found an optimal CO_2 concentration value for limiting catalyst deactivation, in the order of 2%–5%, which was connected with the optimal oxidation state of copper under such conditions. Higher CO_2 concentrations increase deactivation rates. Also, the production of H_2O disaggregates the catalyst matrix and reduces the surface of copper crystallites.

The deactivation through sintering is usually modeled by means of a power law expression (PLE)

$$\frac{da}{dt} = -k_d(T)a^n \tag{3.5}$$

where the deactivation order n varies from 1 to 16 and a is the ratio of the reaction rate at time t and the initial rate (at $t = 0$).

The kinetic constant k_d is a function of temperature following an Arrhenius-type expression. It has also been proposed (Forzatti and Lietti, 1999) to model the sintering rate by using a generalized power law expression (GPLE):

$$\frac{da}{dt} = -k_d(T)\left(a - a_{eq}\right)^n \tag{3.6}$$

In this manner, it is possible to confirm that deactivation is faster at the beginning and reaches a plateau after a proper timespan denoted by the term $-a_{eq}$. The order in this case is reduced to 1–2. Rahimpour et al. (1998), considering that CO and CO_2 adsorb on different active sites, proposed a mechanistic model for the catalyst deactivation. The deactivation occurred, in their model, because CO_2 occupied a CO site, and vice versa. They proposed a Langmuir-Hinshelwood-Hougen-Watson (LHHW)-type model to describe both kinetics and deactivation:

$$r_{CO} = a_1 \frac{k_{f1} K_{CO} K_H^2 K_{CH} p_{CO} p_{H_2}^2}{1 + K_{CO} p_{CO} + K_{CO} K_H^{3/2} K_{CH} p_{CO} p_{H_2}^{3/2}} \tag{3.7}$$

$$r_{CO_2} = a_2 \frac{k_{f2} K_{CO_2} K_H K_{HCO_2} p_{CO_2} p_{H_2}^{1/2}}{1 + K_{CO_2} p_{CO_2} + K_{CO_2} K_H^{1/2} K_{HCO_2} p_{CO_2} p_{H_2}^{1/2}} \tag{3.8}$$

$$\frac{da_1}{dt} = -a_1^{d1} \frac{k_{d1} p_{CO_2}^2}{1 + K_{CO} p_{CO} + K_{CO} K_H^{3/2} K_{CH} p_{CO} p_{H_2}^{3/2}} \tag{3.9}$$

$$\frac{da_2}{dt} = -a_2^{d2} \frac{k_{d2} p_{CO_2}^2}{1 + K_{CO_2} p_{CO_2} + K_{CO_2} K_H^{1/2} K_{HCO_2} p_{CO_2} p_{H_2}^{1/2}} \tag{3.10}$$

Løvik (2001) used this model in a pseudo-homogeneous reactor and found that after three months, a_2 was small and a_1 was nearly zero. Thus this coupled kinetic-deactivation model clearly overestimates the rate of deactivation. In fact, in industrial conditions, usually a catalyst lasts for three to four years. This mechanism disagrees with other findings in the literature (Kung, 1992) that indicate H_2O as responsible for deactivation.

4.3 Kinetic Modeling

Kinetic modeling is the core in the design and optimization of chemical reactors. Detailed knowledge about the reaction mechanism helps appropriate parties optimize the design and operation of a plant. The reaction kinetics and the mechanism involved in the production of methanol are still disputed. Many kinetic studies have been published, but they differ in terms of the composition of the feed gas and the operating conditions, thus conclusions concerning the kinetics and the mechanisms cannot be drawn yet. We will focus on the kinetics of the methanol production process based on a Cu/ZnO catalyst, which is widely used in the industry.

It is generally accepted that methanol is predominantly produced via hydrogenation of carbon dioxide, at least under typical operating conditions in industrial processes. However, the role of CO_2 and H_2O in methanol synthesis and the nature and number of the active sites and the chemical state of copper are still debated. After 45 years of study, the most reliable kinetic pathway is still being debated. However, the mechanism involving both CO and CO_2 hydrogenation seems to be the most likely one. Graaf et al. (1988) stated that, notwithstanding the role of CO_2 or CO in methanol synthesis, both hydrogenation reactions have to be considered in the kinetic scheme together with the WGS reaction and that rapidly interconverting CO and CO_2 does not make the three reactions independent (Bozzano and Manenti, 2016).

Natta (1955) and Bakemeier et al. (1970) began the first studies of the kinetics of methanol synthesis via $CO/CO_2/H_2$ mixtures and made reference to a "high pressure process" (taking place in the presence of ZnO/Cr_2O_3 catalysts). Natta's expression did not consider the presence of CO_2 in the feed, whereas Bakemaier et al.'s rate equation accounted for it, but not as a reactant.

Leonov et al. (1973) modeled for the first time low-pressure methanol synthesis on $Cu/ZnO/Al_2O_3$ catalysts. They considered CO as the only source of carbon for methanol generation, without taking into account the presence of CO_2 in the feed. Rozovskii et al. (1977) proposed the conversion of CO to CO_2 via the WGS reaction and the production of methanol via the hydrogenation of CO_2. The same authors found a significant production of methanol from CO_2 when operating at 495 K. In fact, CO_2 hydrogenation was faster than CO hydrogenation at lower temperatures and pressure. On the contrary, other researchers observed a faster dehydrogenation of CO under typical lab synthesis conditions, that is, 5–10 MPa and 500–575 K.

After the first correlative approaches, subsequent efforts were made to extend the kinetic models outside the usual experimental conditions. Gradually, the importance of CO_2 was recognized, and experimental data were collected by varying the CO/CO_2 ratio, which confirmed the maximum conversion rate at a fixed total pressure and hydrogen concentration (Klier et al., 1982). Vedage et al. (1985) used D_2O instead of H_2O to demonstrate a similar effect connected with H_2O. This maximum was not found in the experiments of Liu et al. (1985), where they found a decrease in the reaction with increasing CO_2. CO_2 prevented the reduction of some catalysts' active sites, thus increasing the catalytic activity, but at the same time, an excess of CO_2 produced too much water, which strongly adsorbed on the active sites, reducing the methanol production rates. Klier et al. (1982) demonstrated an initial methanol synthesis from the interaction of CO and H_2 adsorbed on the catalyst. They postulated the presence of an oxidized state (S_{ox}) and a reduced state (S_{red}) on the catalyst's active sites and suggested that the oxidized state, generated by the presence of CO_2: $CO_2 + S_{red} = CO + S_{ox}$, was the active one. Therefore they considered CO_2 as a promoter, postulating also a competitive adsorption mechanism of CO_2 and CO or H_2 on the catalyst's active sites. Their model's main

limitation was that the rate expression equaled zero in the absence of CO_2 in the feed, while the experiments showed methanol production.

Mochalin et al. (1984) investigated different models of some Russian research groups and finally reported a kinetic model; however, it unfortunately lacked the numerical values of the adopted parameters, so their model could not be used. Bardet et al. (1984) found that even small quantities of water accelerated methanol production when CO/H_2 feed mixtures were adopted, although this effect was not present when $CO/CO_2/H_2$ mixtures were used, which was connected to the WGS reaction producing CO_2. Dybkjaer (1985) suggested a rate expression based on a dual-site Langmuir-Hinshelwood mechanism: H_2 was adsorbed, dissociated, and reacted with the adsorbed CO_2. In this model, H_2 and H_2O competed for one specific active site, while CO and CO_2 adsorbed on a second and different active site.

The CO_2 hydrogenation at low temperature and low conversion can be the main source of methanol in the absence of water. In the presence of water and at high temperature and conversion, however, methanol is mainly produced via CO hydrogenation. Also, Villa et al. (1985) considered CO as the only source of methanol and included the water-gas shift reaction in their kinetic scheme.

Graaf et al. (1990) proposed the generation of methanol via successive hydrogenation of CO and CO_2, and the WGS reaction followed a formate-based path. In their model, CO/CO_2 and H_2/water adsorbed on two different active sites. In their kinetic expressions, some intermediates showed up in two different overall reactions, simultaneously providing two different concentrations for some intermediates, such as formyl and methoxy species. The rate expressions, however, are most commonly adopted in reactor modeling, and they fit well the experimental data Graaf et al. presented in their work.

Skrzypek et al. (1991) proposed a reaction mechanism based on the water-gas shift reaction and on the hydrogenation of CO_2. They presented interesting experiments with a CO and hydrogen feed at different concentrations, in which they did not find the production of methanol. In their analysis, the role of CO was restricted to participating in the WGS reaction and removing water with a beneficial effect on the synthesis reaction. The rate expression they proposed was a function of CO_2 and hydrogen in the feed and reproduced the observed presence of the maximum as a function of the CO_2 content.

Askgaard et al. (1995) proposed a kinetic model based on parameters evaluated by gas-phase thermodynamics. Only hydrogenation of CO_2 and water-gas shift reaction were included. Their work mainly addressed overcoming the big differences in pressure and temperature between the reactors and the industrial converters. Sixteen elementary steps were proposed. The RDS of the methanol synthesis was identified as the hydrogenation of formate, methoxide, and oxide. Upon adaptation to the process's actual operating conditions, their model fit well with experimental data. The reactions' self-inhibition to form methanol at temperatures lower than 500 K was

determined to be caused by the stable and abundant formate species blocking the active sites. Complex calculations are required in order to evaluate the model's parameters.

In 1996 Vanden Bussche and Froment proposed a mechanistic model based on a detailed reaction scheme that assumed CO_2 as the main carbon source (Vanden Bussche and Froment, 1996). After the dissociative adsorption of hydrogen and carbon dioxide on copper active sites, carbonate species were produced and suddenly hydrogenated to bicarbonates, which subsequently were reduced to formate, methoxy species, formaldehyde, and eventually methanol. As noted earlier, Klier et al. (1982) and Askgaard et al. (1995) also in their model the RDS is the hydrogenation of formate. The mechanistic nature of their model allowed careful extrapolation outside the experimental conditions with regard to which parameters were best fits for the model. This model accurately predicted the maximum conversion rate at 2% CO_2, and together with that of Graaf et al. (1988), is the most widely adopted model for methanol reactor simulation.

Ovesen et al. (1997) presented an advanced model that proposed a dynamic microkinetic model based on surface measurements in which the composition of the gas mixture in contact with the catalyst surface influenced the number of active sites. They started from Askgaard's model (a steady-state model) and applied the Wulff construction to evaluate the surface and interface free energies in order to clarify the rule for the changes in particle morphology and, in particular, the variation in the number of active sites under different operating conditions. The modifications observed were connected with a variation in the number of oxygen vacancies at the Zn-O-Cu interface. When larger CO/CO_2 ratios were employed, the number of available active sites increased on the (110) surface plane where methanol synthesis was faster. They used this model to reproduce the experimental data of Graaf et al. (1988) and obtained a better fit with respect to static microkinetic models and gave a better explanation of the behavior of the system in transient conditions. This model also seems to explain the apparently conflicting reaction orders reported in the literature. In fact, under dynamic conditions, the reaction orders are shown to depend on the oxidizing or reducing nature of the environment.

Kubota et al. (2001) also proposed a kinetic model with CO_2 as the leading actor for methanol generation. Reasonable accordance with experimental data produced in a test plant was obtained.

Lim et al. (2009) proposed a kinetic model based on the analysis of 48 elementary reactions, which took into account the surface reaction of methoxy species as the RDS for CO hydrogenation, whereas the hydrogenation of a formate intermediate was the RDS for the water gas-shift reaction.

Grabow and Mavrikakis (2011) developed an extended microkinetic model. They confirmed methanol to be produced by both CO and CO_2 hydrogenation, with CO_2 being the source of

two-thirds of the produced methanol under industrial operating conditions. Grabow and Mavrikakis mainly addressed CO_2 hydrogenation as a means for CO_2 fixation, but they included other CO and CO_2 hydrogenation pathways, the WGS reaction, and the reactions of the formation of some by-products and intermediates, such as formic acid (HCOOH) and formaldehyde (CH_2O). No assumptions based on RDS were adopted to calculate the model parameters, which came from DFT. The sensitivity of the catalytic activity to the WGS rate for $CO/CO_2/H_2$ mixtures was small, but larger WGS rates consumed CO and reduced the adsorption of CO_2. The beneficial effect of CO was found to be related to the removal of OH^*/H_2O^* (* indicates adsorbed species) shifting the CO_2 hydrogenation toward the production of methanol. Simulations with different feed compositions show that the carbon source, from which methanol originates, depends on the operating conditions, and a general rule does not exist.

Park et al. (2014) found that when both CO and CO_2 hydrogenation occurred, CO conversion was affected by temperature, pressure, and space velocity changes, whereas CO_2 conversion was only marginally influenced by these factors, thanks to the WSG reaction. Moreover, conversion was deeply influenced by the CO/hydrogen ratio. The contribution of each reaction was shown to be related to the CO content.

The rate equations of all the presented kinetic models are summarized in Table 3.5, along with the experimental conditions under which such models were derived/validated, from Bozzano and Manenti (2016).

4.4 Transport Phenomena Around and Inside the Catalyst

The mass transport limitations inside the catalyst are significant especially for the low-pressure methanol synthesis and when the $CuO/ZnO/Al_2O_3$ catalyst is used. Seyfert and Luft (1985) reported an effectiveness factor of 75% at 538 K and 80 bar (4.2 mm catalyst pellets), Graaf et al. (1990) evaluated effectiveness factors ranging from 32% to 92%, depending on the temperature and on the component, and observed a reduction in the effectiveness factor for increasing temperature.

Several researchers have studied the problem of intra-particle diffusion inside the catalyst. The pellets usually have an isotropic distribution of pore size, tortuosity, and thus conductivity. Lommerts et al. (2000) investigated different diffusion models to evaluate the efficiency of the catalyst and reported five principal approaches:

1. The dusty-gas model (Jackson, 1977)
2. The modified or extended Stefan-Maxwell equations (Maxwell, 1866)
3. The classic multicomponent pore diffusion (constant diffusion coefficients) model combined with convective mass transport

Table 3.5 Equation rates proposed for methanol synthesis, according to the operating conditions reported in first column

Operating Conditions (P, T)	Equation Rates	Author, Year
4–5.5 MPa 493–533 K	$r_{CO\rightarrow CH_3OH} = k\left(\frac{p_{CO}^{0.5}p_{H_2}}{p_{CH_3OH}^{0.66}} - \frac{p_{CH_3OH}^{0.34}}{p_{CO}^{0.5}p_{H_2}K_2^*}\right)$	Leonov et al. (1973)
2–8 MPa 483–538 K	$r_{CO\rightarrow CH_3OH} = \frac{k\left(f_{CO}f_{H_2}^2 - f_{CH_3OH}/K_{eq}\right)}{\left(1 + Af_{CO} + Bf_{H_2} + Cf_{CH_3OH} + Df_{CO_2}\right)^2}$	Schermuly and Luft (1977)
7.5 MPa 498–523 K	$r_{CO\rightarrow CH_3OH} = k_{r_{CO\rightarrow CH_3OH}}\left(1 + \frac{1}{k_{redox}^{eq}}\frac{p_{CO}}{p_{CO_2}}\right)^{-3}\frac{K_{CO}K_{H_2}^2\left(p_{CO}p_{H_2}^2 - p_{CH_3OH}/K_{r_{CO\rightarrow CH_3OH}}^{eq}\right)}{\left(1 + K_{CO}p_{CO} + K_{CO_2}p_{CO_2} + K_{H_2}p_{H_2}\right)}$	Klier et al. (1982)
	$r_{CO_2\rightarrow CH_3OH} = k_{r_{CO_2\rightarrow CH_3OH}}\left(p_{CO_2} - \frac{1}{K_{r_{CO_2\rightarrow CH_3OH}}^{eq}}\frac{p_{CH_3OH}p_{H_2O}}{p_{H_2}^3}\right)$	
8–14 MPa 503–538 K	$r_{CO\rightarrow CH_3OH} = \frac{k\left(f_{CO}f_{H_2}^2 - f_{CH_3OH}/K_{eq}\right)}{\left(1 + Af_{CO} + Bf_{H_2} + Cf_{CH_3OH} + Df_{CO}f_{H_2}^2 + Ef_{CO_2}\right)^2}$	Seyfert and Luft (1985)
3–9.5 MPa 488–518 K	$r_{CO\rightarrow CH_3OH} = \frac{f_{CO}f_{H_2}^2 - f_{CH_3OH}/K_2^*}{\left(A + Bf_{CO} + Cf_{H_2} + Gf_{CO_2}\right)^3}$	Villa et al. (1985)
	$r_{RWGS} = \frac{f_{CO_2}f_{H_2} - f_{CO}f_{H_2O}K_3^*}{M^2}$	
N/A	$r_{CO_2\rightarrow CH_3OH} = \frac{A_1A_2A_3^{0.5}\left[f_{CO_2}f_{H_2} - f_{CH_3OH}f_{H_2O}/\left(f_{H_1}^2K_{eq,CO_2}\right)\right]}{\left(1 + A_2f_{CO_2}\right)\left[1 + A_3^{0.3}f_{H_2}^{0.5} + A_4f_{H_2O}/\left(A_3f_{H_2}\right)^{0.5}\right]}$	Dybkjaer (1985)
	$r_{RWGS} = \frac{A_5A_2A_3^{1/2}\left(f_{CO_2}f_{H_2}^{1/2} - f_{CO}f_{H_2O}/f_{H_2}^{1/2}K_{eq,WGS}\right)}{\left(1 + A_2f_{CO_2}\right)\left[1 + A_3^{1/2}f_{H_2}^{0.5} + A_4f_{H_2O}/\left(A_3f_{H_2}\right)^{1/2}\right]}$	
0.3–1.5 MPa 523–563 K	$r_{CO\rightarrow CH_3OH} = k\left(p_{CO}p_{H_2}^{0.5}\right)^{-1.3}\left(p_{CO}p_{H_2}^2 - \frac{p_{CH_3OH}}{K_{eq}}\right)$	Agny and Takoudis (1985)
4–9.5 MPa 488–574 K	$r_{CO\rightarrow CH_3OH} = k_1\left(f_{CO}f_{H_2}^{2.5}\right)^{0.35}\left[1 - \left(\frac{f_{CH_3OH}}{K_{eq}}f_{CO}f_{H_2}^2\right)^{0.8}\right]$	Takagawa and Ohsugi (1987)

3–9 MPa 483–563 K	$r_{CO\rightarrow CH_3OH} = \frac{k\left(f_{CO}f_{H_2}^2 - f_{CH_3OH}/K_{eq}\right)}{\left(1 + K_{CO}f_{CO} + K_{H_2}f_{H_2}\right)^3}$	Kuczynski et al. (1987)
1.5–5 MPa 483–518 K	$r_{CO\rightarrow CH_3OH} = \frac{k_1K_{CO}\left[f_{CO}f_{H_2}^{3/2} - f_{CH_3OH}/\left(f_{H_2}^{1/2}K_1^{eq}\right)\right]}{\left(1 + K_{CO}f_{CO} + K_{CO_2}f_{CO_2}\right)\left[f_{H_2}^{1/2} + \left(K_{H_2O}/k_{H_2}^{1/2}\right)f_{H_2O}\right]}$ $r_{RWGS} = \frac{k_2K_{CO_2}\left[f_{CO_2}f_{H_2} - f_{H_2O}f_{CO}/K_2^{eq}\right]}{\left(1 + K_{CO}f_{CO} + K_{CO_2}f_{CO_2}\right)\left[f_{H_2}^{1/2} + \left(K_{H_2O}/k_{H_2}^{1/2}\right)f_{H_2O}\right]}$ $r_{CO_2\rightarrow CH_3OH} = \frac{k_3K_{CO_2}\left[f_{CO_2}f_{H_2}^{3/2} - f_{CH_3OH}f_{H_2O}/\left(f_{H_2}^{3/2}K_3^{eq}\right)\right]}{\left(1 + K_{CO}f_{CO} + K_{CO_2}f_{CO_2}\right)\left[f_{H_2}^{1/2} + \left(K_{H_2O}/k_{H_2}^{1/2}\right)f_{H_2O}\right]}$	Graaf et al. (1988)
2.89 MPa 4.38 MPa 513 K	$r_{CO/CO_2\rightarrow CH_3OH} = \frac{\left(p_{CO}p_{H_2}^2 - p_{CH_3OH}/K_{eq}\right)}{ap_{CO}p_{H_2}^{1.5} + bp_{H_2} + cp_{CO_2}} + \frac{\left(p_{CO_2}p_{H_2} - p_{CH_3OH}p_{H_2O}/\left(K''_{eq}p_{H_2}^2\right)\right)}{a'p_{CO_2}p_{H_2}^{0.5} + b'p_{CO_2}^2 + c'p_{H_2O}^3}$	McNeil et al. (1989)
3–9 MPa 460–550 K	$r_{CO_2\rightarrow CH_3OH} = k_1K_{H_2}^2K_{CO_2}\left[\frac{p_{H_2}^2p_{CO_2} - \frac{p_{CH_3OH}p_{H_2O}}{K_{eq}^{r_{CO_2\rightarrow CH_3OH}}p_{H_2}}}{\left(1 + K_{H_2}p_{H_2} + K_{CO_2}p_{CO_2} + K_{CH_3OH}p_{CH_3OH} + K_{H_2O}p_{H_2O} + K_{CO}p_{CO}\right)^3}\right]$ $r_{RWGS} = k_2K_{H_2}K_{CO_2}\left[\frac{p_{H_2}p_{CO_2} - \frac{p_{CO}p_{H_2O}}{K_{eq}^{r_{RWGS}}}}{\left(1 + K_{H_2}p_{H_2} + K_{CO_2}p_{CO_2} + K_{CH_3OH}p_{CH_3OH} + K_{H_2O}p_{H_2O} + K_{CO}p_{CO}\right)^2}\right]$	Skrzypek et al. (1991)
0.1–0.4 MPa 483–563 K	$r_+ = k_{-11}K_5^{-3/2}K_8^{-1}K_9K_{10}K_{11}\left(\frac{p_{H_2}}{p_o}\right)^{3/2}\left(\frac{p_{CO_2}}{p_o}\right)\theta_*^2$ $r_- = k_{-11}K_5^{-3/2}K_8^{-1}K_9K_{10}K_{11}\frac{1}{K_G}\frac{p_{CH_3OH}p_{H_2O}}{p_{H_2}^{3/2}p_o^{1/2}}\theta_*^2$ $r_{CO_2\rightarrow CH_3OH} = r_+ - r_-$ p_o is the thermodynamic reference pressure	Askgaard et al. (1995)

Continued

Table 3.5 Equation rates proposed for methanol synthesis, according to the operating conditions reported in first column—cont'd

Operating Conditions (P, T)	Equation Rates	Author, Year
1.5–5.1 MPa 453–553 K	$r_{CO_2\rightarrow CH_3OH} = \dfrac{k'_{5a}K'_2K_3K_4K_{H_2}p_{CO_2}p_{H_2}\left[1-\left({}^{1}/_{K^*}\right)\left({}^{p_{H_2O}p_{CH_3OH}}/_{p_{CO_2}p_{H_2}^3}\right)\right]}{\left(1+\left({}^{K_{H_2O}}/_{K_8K_9K_{H_2}}\right)\left({}^{p_{H_2O}}/_{p_{H_2}}\right)+\sqrt{K_{H_2}p_{H_2}}+K_{H_2O}p_{H_2O}\right)^3}$ $r_{RWGS} = \dfrac{k'_1p_{CO_2}\left[1-K_3^*\left({}^{p_{H_2O}p_{CO}}/_{p_{CO_2}p_{H_2}}\right)\right]}{\left(1+\left({}^{K_{H_2O}}/_{K_8K_9K_{H_2}}\right)\left({}^{p_{H_2O}}/_{p_{H_2}}\right)+\sqrt{K_{H_2}p_{H_2}}+K_{H_2O}p_{H_2O}\right)}$	Vanden Bussche and Froment (1996)
4.9 MPa 473–548 K	$r_{CO_2\rightarrow CH_3OH} = \dfrac{k_M\left\{p_{CO_2}p_{H_2}-{}^{p_{CH_3OH}p_{H_2O}}/_{\left[K_Mp_{H_2}^2\right]}\right\}}{\left[1+K_{CO_2}p_{CO_2}+K_{H_2O}p_{H_2O}\right]^2}$ $r_{RWGS} = \dfrac{k_R\left\{p_{CO_2}-{}^{p_{CO}p_{H_2O}}/_{\left[K_Rp_{H_2}\right]}\right\}}{\left[1+K_{CO_2}p_{CO_2}+K_{H_2O}p_{H_2O}\right]}$	Kubota et al. (2001)
3.4–4.1 MPa 473–513 K	$r_{CO_2\rightarrow CH_3OH} = A_{CH_3OH}e^{\left(-\frac{E_{CH_3OH}}{RT}\right)}\dfrac{c_{CO_2}\left(c_{H_2}-c_{H_2,eq}\right)}{\left(1+A_We^{\left(\frac{E_w}{RT}\right)}c_{H_2O}\right)^2}$ $r_{H_2O} = A_{H_2O}e^{\left(-\frac{E_{H_2O}}{RT}\right)}\dfrac{c_{CO_2}-c_{CO_2,eq}}{\left(1+A_We^{\left(\frac{E_w}{RT}\right)}c_{H_2O}\right)}$	Setinc and Levec (2001)
5.2 MPa 513 K	$r_{CO_2\rightarrow CH_3OH} = \dfrac{k_3p_{H_2}\left(1-\dfrac{p_{CH_3OH}p_{H_2O}}{K_{p(CH_3OH)}p_{H_2}^3p_{CO_2}}\right)}{1+K_{-2}p_{H_2O}+K_{-2}p_{H_2O}/(K_1p_{CO_2})}$	Rozovskii and Lin (2003)

5 MPa 523–553 K	$r_{CO\rightarrow CH_3OH}=\frac{k_{r_{CO\rightarrow CH_3OH}}K_{CO}K_{H_2}^2K_{CH,CO}\left(p_{CO}p_{H_2}^2-p_{CH_3OH}/K_{Pr_{CO\rightarrow CH_3OH}}\right)}{(1+K_{CO}p_{CO})\left(1+K_{H_2}^{0.5}p_{H_2}^{0.5}+K_{H_2O}p_{H_2O}\right)}$ $r_{CO_2\rightarrow CH_3OH}=\frac{k_{r_{CO_2\rightarrow CH_3OH}}K_{CO_2}K_{H_2}K_{CH,CO_2}\left(p_{CO_2}p_{H_2}^3-p_{CH_3OH}p_{H_2O}/K_{Pr_{CO_2\rightarrow CH_3OH}}\right)}{(1+K_{CO_2}p_{CO_2})\left(1+K_{H_2}^{0.5}p_{H_2}^{0.5}+K_{H_2O}p_{H_2O}\right)p_{H_2}^2}$ $r_{RWGS}=\frac{k_{r_{RWGS}}K_{CO_2}K_{H_2}^{0.5}(p_{CO_2}p_{H_2}-p_{CO}p_{H_2O}/K_{Pr_{RWGS}})}{\left(1+K_{H_2}^{0.5}p_{H_2}^{0.5}+K_{H_2O}p_{H_2O}\right)(1+K_{CO_2}p_{CO_2})p_{H_2}^{0.5}}$	Lim et al. (2009)
5–9 MPa 503–613 K	$r_{CO\rightarrow CH_3OH}=\frac{k'_{r_{CO\rightarrow CH_3OH}}K_{CO}\left[f_{CO}f_{H_2}^{0.5}-f_{CH_3OH}/\left(f_{H_2}^{0.5}K_{Pr_{CO\rightarrow CH_3OH}}\right)\right]}{(1+K_{CO}f_{CO})\left(1+K_{H_2}^{0.5}f_{H_2}^{0.5}+K_{H_2O}f_{H_2O}\right)}$ $r_{RWGS}=-\frac{k'_{r_{RWGS}}K_{CO_2}[f_{CO_2}f_{H_2}-f_{CO}f_{H_2O}/K_{Pr_{RWGS}}]}{(1+K_{CO_2}f_{CO_2})\left(1+K_{H_2}^{0.5}f_{H_2}^{0.5}+K_{H_2O}f_{H_2O}\right)}$ $r_{CO_2\rightarrow CH_3OH}=\frac{k'_{r_{CO_2\rightarrow CH_3OH}}K_{CO_2}\left[f_{CO_2}f_{H_2}^{1.5}-f_{H_2O}f_{CH_3OH}/\left(f_{H_2}^{1.5}K_{Pr_{CO_2\rightarrow CH_3OH}}\right)\right]}{(1+K_{CO_2}f_{CO_2})\left(1+K_{H_2}^{0.5}f_{H_2}^{0.5}+K_{H_2O}f_{H_2O}\right)}$	Park et al. (2014)

Adapted from Bozzano, G., Manenti, F., 2016. Efficient methanol synthesis: perspectives, technologies and optimization strategies. Prog. Energy Combust. Sci. 56, 71–105.

4. The classic multicomponent pore diffusion model (constant diffusion coefficients)
5. A model based on Thiele modulus and "first-order" kinetics for CH_3OH and H_2O production

Models 1 and 2 implicitly account for convective mass transport, whereas the other models take it into account explicitly. Models 1, 3, 4, and 5 allow for Knudsen diffusion. An analysis of the predictions of these models and their comparison to experimental data by Seyfert and Luft (1985) show that the convective mass transport appears to be negligible when compared with mass diffusion. The same conclusions apply to pressure and temperature gradients inside the particle. It is useful to apply the Thiele modulus to account for intra-phase diffusion and surface reaction phenomena, which enables easier implementation in methanol reactor models and reduces computation time. In fact, a comparison with more complex models, such as the dusty or the Stefan-Maxwell models, shows acceptable deviations in the effectiveness values of both methanol and water.

Rout et al. (2013) studied intra-particle multicomponent diffusion by comparing the Maxwell-Stefan, dusty-gas, Wilke, and Wilke-Bosanquet models. The dusty-gas model is an extension of the Maxwell-Stefan model, including Knudsen diffusion in which coefficients are related to the mean pore diameter of the pellets and are independent of pressure. The Wilke model uses the binary Fick's law, substituting the binary diffusivity with multicomponent diffusivity. It is a simplification of the Maxwell-Stefan equation in the Fickian form. The dusty-gas model can be simplified by using the Wilke-Bosanquet model. The latter comprises the Wilke model and the Bosanquet formula (1944). Dusty-gas and Wilke-Bosanquet models include Knudsen diffusion, whereas the Maxwell-Stefan and Wilke models disregard it and consider only bulk diffusion, which is independent of the mean pore diameter and inversely proportional to pressure. Knudsen diffusion prevails for Knudsen numbers (ratio of the molecular mean free path and the pore diameter) higher than 10. In commercial methanol plants, the Knudsen number is usually lower than 1. In practice, if the catalyst mean pore diameter exceeds 10 nm, Knudsen diffusion has a minor influence on diffusive mass transport (Rout et al., 2013). The same authors compared the mass- and mole-based models and found deviations between them to be less than 4%. Rout et al. (2013) found a discrepancy of 2%. In the case of mole-based models, this discrepancy was related to a contradiction between the species' boundary conditions and the total continuity equation. The authors also showed that the dusty-gas and Maxwell-Stefan models ensure slightly better agreement between mass- and mole-based pellet equations. The use of parallel or random pore models was also discussed by these authors. The parallel pore model assumes that the catalyst particle has cylindrical pores with plane surface. In the random pore model, the pellet is disassembled and reassembled, thus forming macro and micro structures. An analysis of the literature implies that the use of the simpler model based on the Thiele modulus is recommended for online optimization, control, and simulation purposes.

5 Biomass-Based Processes

5.1 Thermal Treatment of Biomasses

Production of methanol from biomasses for large-scale production is done primarily via gasification, which involves partial oxidation by steam and air to produce biosyngas. In large productions, gasification of biomasses is an appealing way to achieve methanol synthesis, except that it is a highly complex process with multiple components and with a multiphase (solid, liquid, and gas) and multiscale nature (Fig. 3.4). Moreover, the gasification process is the result of a series of steps that progressively transform the biomass particle into biosyngas and then into methanol by catalytic synthesis. The biomass particles are fed, for instance, from the top in an updraft gasifier (for other technologies and details, please refer to Ranzi et al. (2016)). Particles are partially dried, and the main moisture content is removed in the first step, thanks to the hot gas coming from the biomass layers beneath it. Particles are pyrolyzed next and then gasified before entering a char combustion zone where a certain (under-stoichiometric) amount of oxygen/air content is fed. The exothermicity of this step can energetically sustain the endothermicity of the gasification step. Finally, in the ash zone, heat is exchanged from the ashes to the inlet gas stream and then leaves the gasifier.

As can be easily seen, gasification operations require complex management and control, and many factors must be taken into account. One of the chief factors is biomass particle size, which is related to the residence time in the gasifier. In the case of lignocellulosic biomasses, thick (more than 1 cm) particles are often provided in the gasification process. An appropriate

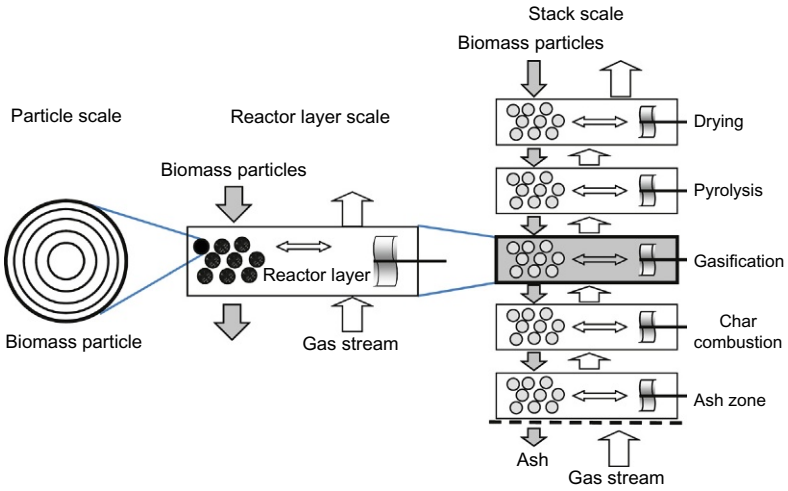

Fig. 3.4
Multiscale nature of biomass updraft gasifier.

counter-current stream of steam/air is provided to achieve a fuel ratio typical of gasification processes (one-third of the stoichiometric oxygen). If the thermal penetration time for thick particles is higher than the residence time, the biomass does not heat uniformly and only the external particle sectors can devolatilize. On the other hand, the particle kernel remains cold, and it does not react. This situation leads to poor performance of the gasifier in terms of the biosyngas produced and, therefore, in terms of the potential for methanol synthesis. The external sectors could react with the overall content of oxygen provided and achieve complete oxidation (combustion), because a large part of biomass conversion does not take place in the gasification process, and the effective biomass/air stoichiometry is completely biased. As a final result, large amounts of CO_2 and H_2O are produced on behalf of the expected biosyngas.

Interest has grown in using gasification processes as a practical and easy way to obtain biosyngas from biomasses of different natures and generations for methanol synthesis, and this interest has prompted several scientific communities to propose solutions for properly managing and optimizing these processes. Thermodynamic, strongly lumped kinetic, and lumped kinetic approaches have been proposed to support the operations involved in upgrading biomass to biosyngas. A recent model proposed by the authors (Corbetta et al., 2015; Cabianca et al., 2016), the GASDS Suite, is a field-proven dynamic model that accounts for a detailed kinetic scheme and that integrates different scales (the particle, the reactor layer, and the gasifier reactor). The model consists of a partial differential equation system that accounts for the mass, composition, and temperature gradients inside the biomass particles and in the biomass bed as well. The profiles can be calculated along the biomass bed into the gasifier, which enables monitoring the performance of the unit in terms of biosyngas production (Corbetta et al., 2015). Also, relevant information about the optimal feedstock, the optimal operating conditions, and the optimal biosyngas H_2/CO ratio are provided.

5.2 CO_2 Conversion

The conversion of carbon dioxide into hydrocarbons, including methanol, is highly appealing, and if performed using only solar energy, it is considered to be one of the most important research fields. This reaction contributes to the mitigation of carbon dioxide and its effect on global warming. This reaction produces energy in a renewable way and develops an excellent means for storing energy in liquid form, which is suitable for use in current transportation infrastructures. Hydrogen, a main reactant in the chemical conversion of CO_2, can originate by electrolysis from water dissociation, and the source of electricity for this reaction can be obtained from renewable processes or feedstocks, such as wind, solar, waves, or biomass. Alternative routes for the renewable production of hydrogen are biomass pyrolysis or steam/oxygen gasification processes, the biological production of H_2 using sunlight-activated microorganisms, and photocatalyzed water splitting (Ptasinski et al., 2002).

5.2.1 Biological processes

Methanol can be produced by starting from CO_2 and using biological processes. Nevertheless, the biological direct transformation of carbon dioxide into methanol is not possible by way of biological organisms. Methanotrophic bacteria can be used as biocatalysts for the production of methanol, starting from a mixture of CO_2 and CH_4, without the addition of H_2 (Duan et al., 2011). These organisms are able to convert methane to methanol by using oxygen and the methane monooxygenase enzyme and by operating in aqueous solutions at ambient temperature and pressure. Using this kind of bacteria, Xin et al. (2004) achieved maximal accumulation of methanol with 40% carbon dioxide in the mixed reaction gases, and defined an optimum gas mixture consisting of 20% methane, 20% oxygen, 20% nitrogen, and 40% carbon dioxide. The initial methanol concentration in the eluate buffer was 8.22 mmol/L, and the bioreactor was operated continuously for 198 h with constant productivity.

5.2.2 Catalytic hydrogenation

Carbon dioxide can be catalytically hydrogenated to methanol following the $CO_2 + 3H_2 \rightleftarrows CH_3OH + H_2O$ reaction. The main catalystic systems and the corresponding experimental parameters used to promote this reaction are shown in Table 3.6, taken from (Ganesh, 2014). The methanol produced can be transformed into dimethyl ether via the $2\,CH_3OH \rightleftharpoons CH_3OCH_3 + H_2O$ reaction; this reaction can also be performed simultaneously in the same reactor.

The production of methanol from CO_2/H_2 mixtures can be performed with a productivity about three to ten times lower than the traditional process of creating methanol from CO/H_2 syngas

Table 3.6 Catalyst used in catalytic hydrogenation of CO_2 to methanol with the corresponding experimental parameters

Catalyst	Reaction Temperature (°C)	CO_2 Conversion (%)	Methanol Selectivity (%)	Methanol Activity $\left(\frac{mol}{kg_{cat}\,h}\right)$
$Cu/Zn/Ga/SiO_2$	270	5.6	99.5	10.9
$Cu/Ga/ZnO$	270	6.0	88.0	11.8
Cu/ZrO_2	240	6.3	48.8	11.2
$Cu/Ga/ZrO_2$	250	13.7	75.5	1.9
$Cu/B/ZrO_2$	250	15.8	67.2	1.8
$Cu/Zn/ZrO_2$	250	19.4	29.3	–
$Cu/Zn/Ga/ZrO_2$	250	–	75.0	10.1
$Cu/Zn/Al/ZrO_2$	240	18.7	47.2	–
$Ag/Zn/ZrO_2$	220	2.0	97.0	0.46
$Pd/Zn/ZrO_2$	250	6.3	99.6	1.1

Adapted from Ganesh, I., 2014. Conversion of carbon dioxide into methanol- a potential liquid fuel: fundamental challenges and opportunities (a review). Renew. Sust. Energ. Rev. 31, 221–257.

(Arakawa et al., 2001). The difference in the yield is due to the inhibition of the kinetic rate by the water formed as coproduct. This limit can potentially be overcome by using catalytic distillation or a permoselective membrane for the continuous removal of water.

Copper is one of the most studied catalytic materials, and is particularly effective when loaded with other metals, for example, about 5 wt% of Zn and Al oxides. The best systems are copper-zinc oxides doped with ZrO_2, Ga_2O_3, and SiO_2 (Ganesh, 2014). The active center is the metallic Cu surface, and the activity of these samples is directly proportional to the exposed surface area of the metallic copper. The kind of support used also plays an important role in CO_2 conversion and methanol selectivity.

Similar to traditional conversion of syngas to methanol, CO_2 hydrogenation is an exothermic reaction and is favored at low operating temperatures. However, the kinetic energy of the reaction, following the Arrhenius law, increases with increasing temperatures. Considering these two different aspects, methanol formation from CO_2 reduction can be performed within an optimal temperature range. A positive effect on the pressure is also known. Temperatures that are too high can cause catalysts to deactivate because of sintering phenomena.

The limiting factor for this process for large-scale applications is the availability of carbon dioxide and hydrogen. In particular, the main problem is the availability of this last compound, and also the synthesis for methanol production needs three molecules of hydrogen per each molecule of carbon dioxide.

Some examples of producers of methanol by CO_2 hydrogenation are Mitsui Chemical Inc. and Carbon Recycling International (CRI) in Japan and Iceland, respectively. In both cases, hydrogen is produced by renewable resources: water splitting using solar, geothermal, hydro, and wind (Ganesh, 2014).

5.2.3 Acid gas conversion AG2S

A new technology was recently proposed for the production of syngas and then its conversion to methanol, starting from CO_2 and H_2S, that is, from acid gas (Bassani et al., 2016). This is a completely new technology for the reduction of and onsite reuse of CO_2. Rather than coupling the CO_2 with H_2 or other expensive reducing molecules (e.g., ammonia), this process combines CO_2 and another hydrogen-rich molecule: the H_2S. According to the filed patents and trademarks, CO_2 and H_2S react as

$$2H_2S + CO_2 \rightleftharpoons CO + H_2 + S_2 + H_2O \tag{3.11}$$

to give syngas and, as by-products, elemental sulfur and water, both innocuous. The reaction takes place in a regenerative thermal reactor (RTR), illustrated in Fig. 3.5, at relatively high temperatures. Energy sustainability is achieved by feeding a small amount of oxygen/air into the thermal chamber of the regenerative reactor. This technological advance is the completely new Acid Gas to Syngas (AG2S) process to remove emissions and produce syngas.

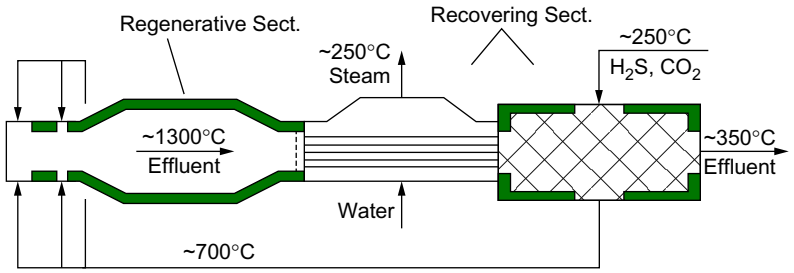

Fig. 3.5
Regenerative thermal reactor (RTR) consisting of regenerative and recovering sections (indicative temperatures).

This technology consists of different operations. The reaction between H_2S and CO_2 takes place at temperatures higher than 1000°C in a RTR gas-phase reactor; high temperatures are necessary to (i) activate the reactive system from a chemical-thermodynamic standpoint, (ii) quicken the kinetics, and (iii) obtain high yields. CO_2 and H_2S are injected into a thermal reactor. These waste gases are regenerated into valued products (CO and H_2). The regenerative thermal oxy-reduction reaction occurs in a refractory-lined chamber, assisted by a minor injection of either air or oxygen for energy sustainability. RTR effluents, comprised of products and unreacted feed species, are quenched in a waste heat boiler and heat exchanger train. These effluents are subsequently processed in catalytic reactors. Cooling allows for separating condensed species from a main gaseous stream, as elemental sulfur (Sx) and water. Catalytic reactors are necessary to convert the small amount of SO_2 into elemental sulfur (Claus reaction) and possible organosulfur compounds—ppm of COS and CS_2—back to H_2S and CO_2 according to hydrolysis reactions, thereby maintaining very high process selectivity overall. Finally, the gaseous stream undergoes a separation treatment in which the unreacted species and the H_2/CO mixture are split; resulting streams are recycled to RTR and exported to the next process, respectively.

Reaction mechanisms between CO_2 and H_2S are complex and involve thousands of chemical reactions and more than 100 molecular and radical species. The macro reaction steps of the AG2S technology to be experimentally investigated are (i) thermal decomposition of H_2S into hydrogenated free radicals (SH, H, etc.), that is, by thermal activation; (ii) CO_2 reduction to CO by free radicals (H, OH, etc.); (iii) the propagation of oxygen-based free radicals; (iv) the formation of sulfur oxides (e.g., SO); (v) the inhibition of backward reaction from CO to CO_2; (vi) the formation of stable SO_2 from SO; and (vii) the formation of H_2. Finally, the overall reaction is Eq. (3.11) plus unreacted feed species. RTR represents the key equipment for developing syngas synthesis starting from H_2S and CO_2. To ensure a proper production yield, it is essential to minimize regressive reactions (recombination) in the RTR effluent stream during cooling; a waste heat boiler (WHB) is best for this purpose. Moreover, installation of a WHB

allows for reducing the effluent temperature to a practical value for the thermo-mechanical design of a subsequent feed/effluent heat exchanger.

Because of the acidic behavior of the unreacted species, the split between the unreacted H_2S and CO_2 and the syngas is perceived as a chemical washing unit. An amine-based solution can be used in an absorber unit to knock down H_2S and CO_2 from the gaseous stream, while the syngas exits clean at the top. By way of a stripping column, H_2S and CO_2 are recovered as gas and then recycled to RTR. To help in cases where water is not removed from gaseous streams by upstream heat condensers, a contact condensing column can be installed.

5.2.4 CO_2 photoreduction to methanol

Photoreduction of CO_2 molecules, which is promoted by heterogeneous semiconductors in the presence of water and light irradiation, is seen as one of the most attractive routes for long-term production of methanol and other valuable products, such as hydrogen and methane (Habisreutinger et al., 2013). Interest in the process, known as artificial photosynthesis, has increased greatly because of advances in the nanotechnologies applied to the development of new high-performance photocatalysts.

The photoreduction reaction is a photocatalytic process caused by the formation of charge carriers (electron-hole pairs) on the catalyst's surface, when the latter is irradiated with light of suitable energy in terms of power and wavelength (typically, UV-A or visible light for some promoted photocatalysts). The resulting charge carriers are then separated on the semiconductor and transported to the surface of the particles where reaction with adsorbed molecules can take place (Chen et al., 2012). A simplified scheme of the photocatalytic process is shown in Fig. 3.6, adapted from Li et al. (2014).

When the photocatalyst, that is a semiconductor material, is irradiated with photons having energy equal to or greater than the band gap of the semiconductor, the electrons are excited from the valence band (VB) to the conduction band (CB). In this way, electrons and holes are generated and undergo intra-band transition. If these charges do not recombine, they can diffuse on the catalyst surface and react with the adsorbed molecules. The transformation of carbon monoxide into hydrocarbons happens only if the electrons on the photocatalysts have more negative chemical potential. The possible reactions involved in the process and the corresponding potentials at pH = 7 are shown in Table 3.7, taken from Li et al. (2014).

The reactions in the production of methane and methanol occur at lower potentials. For this reason, they can be considered more favorable from a thermodynamic point of view. Nevertheless, these reactions, with respect to the formation of CO, formic acid, and formaldehyde, require more electrons and are kinetically limited.

The great drawback of artificial photosynthesis has resulted from its limited conversion efficiency. The main problems with this technology are the catalysts' poor charge separation

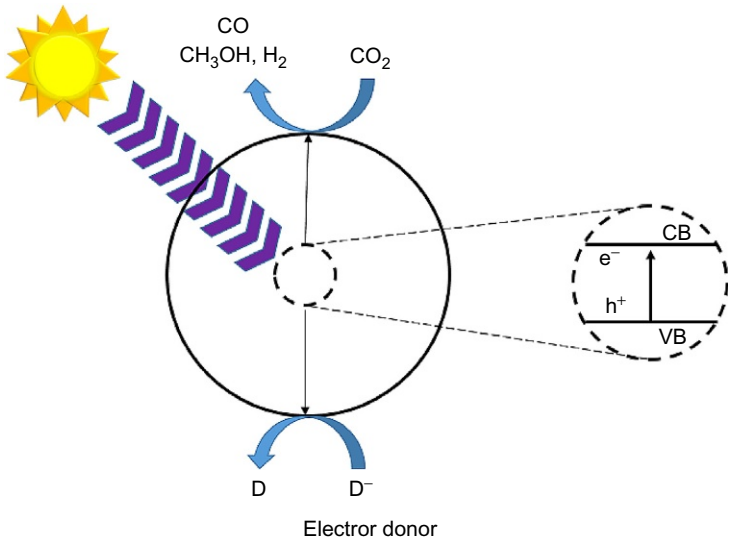

Fig. 3.6
Simplified schematic the photoreduction of carbon dioxide using semiconductor material created by light.

Table 3.7 Pathways for the CO_2 conversion on an irradiated semiconductor material (Li et al., 2014)

Reaction	E^0 (*V vs NHE*)
$CO_2 + 2e^- \rightarrow CO_2^-$	−1.90
$CO_2 + 2H^+ + 2e^- \rightarrow HCOOH$	−0.61
$CO_2 + 4H^+ + 4e^- \rightarrow HCHO + H_2O$	−0.53
$CO_2 + 6H^+ + 6e^- \rightarrow CH_3OH + H_2O$	−0.38
$CO_2 + 8H^+ + 8e^- \rightarrow CH_4 + 2H_2O$	−0.24
$2H_2O + 4h^+ \rightarrow O_2 + 4H^+$	+0.81
$2H^+ + 2e^- \rightarrow H_2$	−0.42

efficiency, only a limited portion of the solar spectrum being suitable for semiconductor activation, and the low solubility of carbon dioxide in water. Moreover, several reactions take place simultaneously in the photoreactor, and then the process results in poor selectivity.

The different photocatalysts comprise both oxides and ono-oxide compounds of titanium oxide (TiO_2), tungsten oxide (WO_3), zinc oxide (ZnO), gallum phosphide (GaP), cadmium sulfide (CdS), and silicon carbide (SiC) (Tahir and Saidina Amin, 2013). Photocatalysts can be doped with metal ions (Fe^{3+}, Zn^{2+}, etc.) and nonmetal ions (C, N, S, B, etc.) in order to shift from UV-A toward visible light adsorption, the spectra region suitable for their photoexcitation. Titanium dioxide is the most studied photocatalyst, and its efficiency

depends on its different physico-chemical characteristics (surface area, crystallographic composition, size of particles) (Ardizzone et al., 2007). Recent photoreactors suitable for working under pressures up to 20 bar allow a significant increase in the solubility of CO_2 in water, which increases the process's efficiency (Galli et al., 2017). Laboratory- and bench-scale studies of this reaction have suggested the use of fluidized bed, fixed bed, and surface coated reactors for CO_2 photoreduction (Li et al., 2014). The main characteristic of these photoreactors is that they provide a very large interaction surface area, which ensures effective harvesting and distribution of the light irradiation that maximizes the photolytic performance of desired products.

5.2.5 Biogas conversion by tri-reforming

The conversion of biogas, a renewable resource, to gasses with a high H_2 content is steadily increasing in importance. Biogas is a mixture of different gases produced from the anaerobic digestion of organic matter such as agricultural waste, municipal waste, plant material, sewage, and food waste. The components of biogas are mainly methane and carbon dioxide and also some impurities, such as H_2S, O_2, NH_3, H_2, and a quantity of water that is dependent on the producing conditions, as shown in Table 3.8.

Because biogas is composed mainly of CH_4 and CO_2, it can also be used to produce organic chemicals. This idea has driven many studies in recent years (Cho et al., 2009; Arab Aboosadi et al., 2011; Rahimpour et al., 2012; Zhang et al., 2013; Zhang et al., 2015). Most of the efforts have been directed toward methanol and dimethyl ether production, for the following reasons:

1. The relative simplicity of production from a mixture containing methane
2. A well-established market and an increasing demand for methanol

Here we propose the use of biogas tri-reforming (steam, dry reforming, and partial oxidation) to produce a mixture of syngas with unreacted CO_2. Because the reaction is entirely endothermic, the heat necessary is supplied by the combusted part of the biogas. The exiting stream can be used to directly produce methanol. The off-gases will be burned to produce electric energy (or to heat the reforming reaction). The mixture produced is then converted to methanol (a scheme of the proposed process is shown in Fig. 3.7).

Table 3.8 Biogas components

Compound	% Volume
CH_4	50–75
CO_2	25–50
N_2	0–10
H_2	0–1
H_2S	0–3
O_2	0–0.5
H_2O	1–2

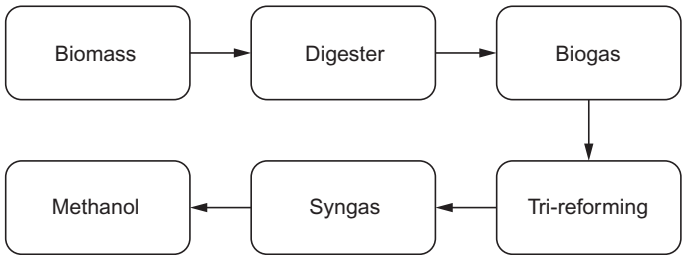

Fig. 3.7
Scheme of the proposed biogas to methanol plant.

There are two primary advantages of the proposed configuration: first, the carbon will be fixed in the product, which will lower carbon dioxide emissions; second, the carbon in the raw biogas can be used as a reactant for the production of methanol, which shifts its role from undesired compound to valuable reactant.

The tri-reforming process is aimed at the production of syngas from methane with water, carbon dioxide, and oxygen. It was first introduced by Song and W. Pan (2004) and since then has been extensively studied from the perspective of increasing the reforming efficiency and obtaining suitable outlet compositions. The idea is to combine steam, dry reforming, and partial oxidation following these reactions:

$$\text{Steam reforming} \quad CH_4 + H_2O \Rightarrow 3H_2 + CO \quad \Delta H^\circ_{298} = 206.3\,\text{kJ/mol}$$
$$\text{Dry reforming} \quad CH_4 + CO_2 \Rightarrow 2CO + 2H_2 \quad \Delta H^\circ_{298} = 247.3\,\text{kJ/mol}$$
$$\text{Partial oxidation} \quad CH_4 + 0.5O_2 \Rightarrow CO + 2H_2 \quad \Delta H^\circ_{298} = -36.6\,\text{kJ/mol}$$

This process was initially developed to reduce the CO_2 emissions from industrial electricity generators. The flue gases of a natural gas-powered system consist of (in volume) 8%–10% CO_2, 18%–20% H_2O, 2%–3% O_2, and 67%–72% N_2. There is no need to separate carbon dioxide from this stream in order for it to be reformed, which is why it holds such great potential. In fact, the system has all the co-reactants needed for the tri-reforming reactions. This process becomes even more attractive when the natural gas is burned with pure oxygen, not air, which leads to a syngas without N_2. The catalyst used by Song was based on Ni and was supported by oxides such as MgO, CeZrO, CeO_2. This process also provides a good way to limit coke formation on the catalyst. Use of only the dry reforming reaction produces more than negligible coking, which can be mitigated through the presence of water and oxygen. Tri-reforming can be performed in autothermal and isothermal conditions. In the autothermal configuration, it is possible to conduct the reactions without any source of external heat and is obtained by setting the oxygen content high enough to be sustainable throughout oxidation and the overall endothermic process. This is particularly significant for small-scale productions. The firebox, which is neither easily scaled to nor always economically feasible for small productions, is not in fact necessary in this case. The other point of strength is that there are no

heat diffusion limitations inside the pipe. The homogeneous production of heat inside the reactor avoids the generation of a radial temperature profile, as in a firebox. To accomplish this goal, an optimal temperature profile inside the reactor is mandatory; this is obtained by using the correct amount of oxygen, which burns CH_4 and produces H_2O and CO_2 that generate heat, which after the initial temperature peak will participate with the other components in methane reforming reactions. The reactor is subdivided in an exothermic section at the beginning, which provides heat for the endothermic section afterward. Much of the work reported in the literature was devoted to the reforming conditions needed to get a suitable product distribution model. Simulations were performed in order to obtain the optimal feed in order to produce syngas with the highest hydrogen yield for methanol production (Arab Aboosadi et al., 2011), with temperature constraints obtained experimentally in order to avoid sintering (Cho et al., 2009).

In the isothermal configuration, the reactor is heated externally. With this configuration, it is possible to obtain an outlet composition more suitable for methanol production. This technology is well accepted for large-scale production and was recently extended to a pilot small-scale production at CNR-ITAE (Pino et al., 2014). Methane conversion increases with temperature—because it is an endothermic equilibrium-limited reaction—and with the content of CO_2 in the biogas because of a mass action effect, even if this effect slightly modifies the process, because methane is already the limiting reactant for the reforming reactions. Carbon dioxide conversion increases with temperature for the same reason. The H_2/CO ratio decreases with temperature because the dry reforming reaction is more endothermic than the steam reforming reaction. It has the same behavior with increasing concentrations of CO_2 in the biogas because a mass action replaces water for the reforming reaction. The effect of pressure, related to the conversions, is similar to that of temperature, which is dictated by the facts that the reaction is equilibrium-limited and the overall number of moles increases. The H_2/CO ratio related to pressure does not have a linear behavior, but also depends on the initial composition of the biogas. The effect of water is straightforward. As its value increases, methane conversion increases, but the opposite happens to carbon dioxide because it is replaced by a more favorable reaction. Of course, the H_2/CO ratio increases. Oxygen increases methane conversion because of their reaction together, which is equilibrium favorable. It can also be said that there are no equilibria limitations, and this can be confirmed by the complete consumption of oxygen. The opposite effect can be tracked in carbon dioxide conversion because oxygen increases in content. The presence of oxygen is not important because of its increase in methane conversion, but because it reduces the endothermicity of the reaction. The added oxygen makes it possible to reform more biogas and to produce a higher quantity of syngas and methanol. Because of the high price of oxygen and the difficulty of using it in small-scale production, air is the best choice. From a purely thermodynamic analysis, the optimal syngas composition to make methanol is $H_2/CO = 2$. The real behavior of the reactor is, obviously, different. It has been found that in the absence of CO_2, the reaction does not proceed. The composition also needs to be able to deal with some

constraints in order to avoid excessive coking of the reactor. The optimal inlet CO_2 molar fraction must be between 2 and 8 and the $(H_2 - CO_2)/(CO + CO_2)$ ratio in the range of 2–3 (Rahimpour et al., 2012). A suitable link between the tri-reforming outlet and the methanol reactor inlet composition must be established in order to optimize the process; mainly the varying composition of the biogas to be treated must be taken into account.

6 Biomass-to-Methanol Process Design

Biomass conversion to biomethanol requires a series of steps: biomass drying, gasification, biosyngas sweetening, methanol synthesis, and purification. Biomass drying can be accomplished by means of screen-conveyor dryers to reduce the moisture content down to 5%–10% of free water. Often in the case of gasification, the biomass drying is directly carried out inside the gasifier, as illustrated in Fig. 3.4. Based on the applications of biosyngas, it would be better to use pure oxygen or air together with steam. In the case of methanol synthesis, pure oxygen is preferable so as to prevent any costly nitrogen separation before the synthesis process. Key parameters for lignocellulosic biomass gasification are as follows: the temperature of oxidizing gases at entrance is 600 K; the gasifier height is 20 m; the gasifier diameter is 2 m; the oxygen ratio is 10 %w; and the steam ratio is 10 %w.

Then biosyngas from gasification is sweetened by the H_2S and CO_2 removal process. According to Section 4.3, it is not necessary to completely remove the CO_2 because part of the methanol is synthesized by the CO_2 direct pathway. The relevant parameter to be fulfilled is the *S* ratio, previously defined, and the methanol synthesis requires *S* slightly larger than 2 as the optimal condition. Sometimes an unbalanced *S* ratio also requires the reverse water-gas shift operation to adjust the compositions before they enter the methanol synthesis reactor, but it is worth noting that the water-gas shift reaction is also active on the Cu-Zn–based catalysts in industrial synthesis. Other operations are combined with the sweetening to clean the biosyngas before the methanol synthesis. The chief ones are the removal of particulates by means of filters and cyclones, the tar reforming for the conversion of tar species into additional (and high *S* ratio) syngas, the removal of water, and the biosyngas compression. Finally, the cleaned and sweetened biosyngas enters the methanol reactor at the proper *S* ratio, and the synthesis takes place, as reported in the Section 4.1. Methanol is then purified to market grade. A scheme for methanol synthesis is shown in Fig. 3.8. Biosyngas is further compressed to the synthesis pressure (i.e., 80 bar), and the temperature is adjusted to feed the reactor at 230°C. The reaction exothermicity requires a special tubular reactor with boiling water in the shell-side (Lurgi or Haldor-Topsoe technology). Also, the reactor effluents are cooled down before entering a flash drum separator to split the liquid phase, biomethanol and water, from the gas phase, mainly unreacted biosyngas. A purge is required to remove incondensable and small quantities of methane that are generated in the methanol synthesis (methanation side reaction). The gas recycle is compressed to achieve the reactor pressure drops, whereas the liquid is laminated before entering methanol/water separation.

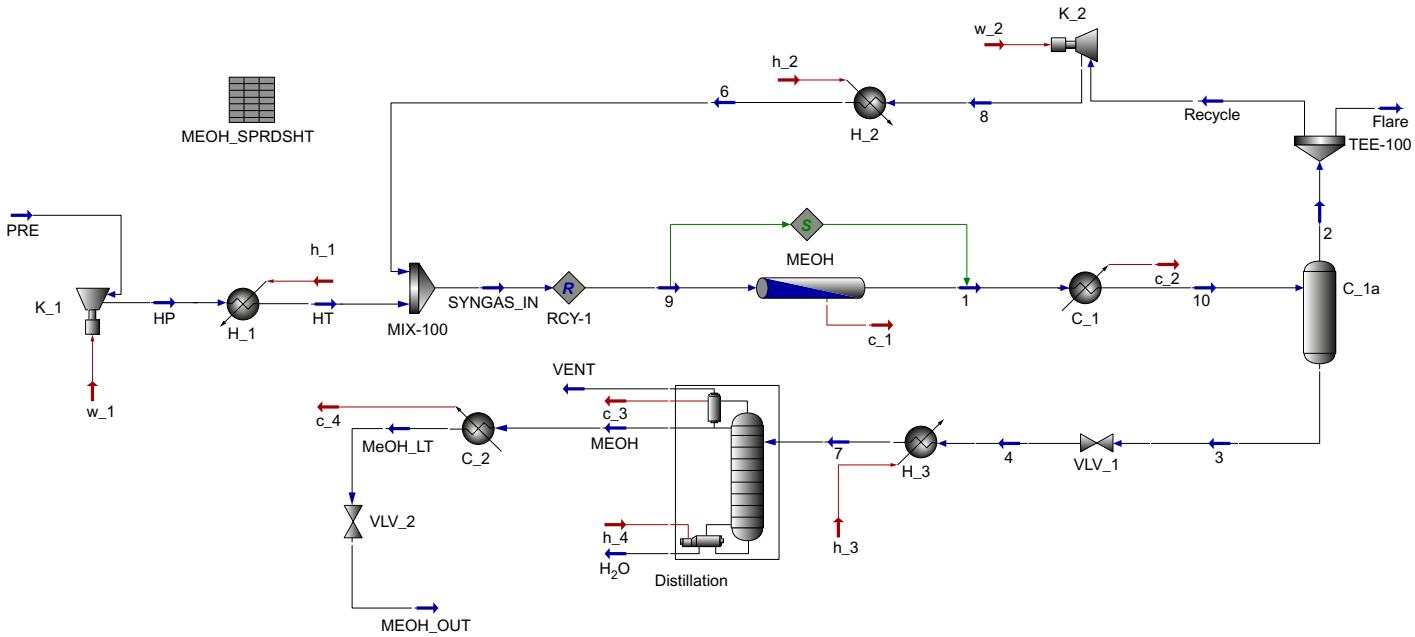

Fig.3.8
Methanol synthesis and purification flowsheet (AspenHysys).

Table 3.9 Yields for 100 kt of Arundo donax as feedstock

Product	Quantity (kt/y)	Yield
Input		
Biomass	100	–
Oxygen	10	–
Steam	10	–
Gasification		
Producer gas	94.3	90%
Sweetening		
Syngas	54	57%
Synthesis/purification		
Bio-MeOH	50	93%

Table 3.10 Payback time for biomethanol plant size

Plant Size (kt/y)	Investment Cost (M Eur)	Biomass Demand (kt/y)	Payback Time (Years)
50	19	88	5.8
100	30	175	3.5
150	41	262	3.0

The following analyses were made using Arundo donax as input for the sake of simplicity and because of its extensive characterization and productivity potential. Given the presented methods to simulate biomethanol and biochar coproduction, the economic assessment was done via CAPEX and OPEX calculations. Costs involving each specific operation (gasification, sweetening, etc.) were computed with the aid of the procedures described in (Turton et al., 2012). Biomass costs were acquired from the IRENA database, and biochar retail selling prices in Europe go from around $600 to $3400/t; as a conservative measure, a value of 500 Euro/t was considered here. The price considered for methanol was 330 Euro/t, in-between that of Shabangu et al. (2014) and the Methanex (2016) website. Biomass was considered with 7 %w moisture. Table 3.9 summarizes mass yields based on a yearly amount of 100 kt of biomass. Payback for different plant sizes is estimated and shown in Table 3.10.

An increasing plant size presents a considerable economy of scale, besides greatly increasing the profits. Nevertheless, large plants unavoidably require that more biomass is available near the plant. In fact, it would be more accurate to include the logistics costs and environmental impacts whenever the biomass is not local and comes from far regions. Whenever biomass availability justifies it and the budget allows it, the larger plants are preferable. Another factor that plays in the favor of larger plants is their smaller payback time for grassroots projects. Finally, it has been is proven that the larger plants are more resilient: their payback time is considerably less sensitive to the biomethanol selling price (and thus to market fluctuations).

7 Current Problems With Biomethanol Production and Conclusions

Currently, the high production cost and the substantial capital investment required for new processes limit commercial use of biomethanol. The cost of biomethanol will always be compared to that of methanol produced from fossil fuel. This comparison is not positive at this time, but it is reasonable to assume that it will be more favorable in the coming years because of the expected increase in the price of natural gas and the reducing availability of fossil fuels.

The syngas produced from biomass gasification is considered to be suitable for biomethanol production. However, this kind of process requires significant amounts of biomass for medium- and large-scale plants. For social and ethical reasons, it is also important to note that these biomass resources have to compete with foods crops.

Among all biomethanol processes, biomass gasification is considered to be the most complex and challenging one, and the gasification efficiency is expected to improve up to 10%, thanks to new research and optimization of the technology (IEA-ETSAP and IRENA, 2013).

The development of a market for biomethanol will be connected with the demand of biomass for other uses, such as other biofuels or power generation. In a biorefinery scenario, it will be important to optimize the use of biomass by selecting the most profitable uses, from both an economical and an environmental point of view. It is important to note that the chemical industry will always require a carbon resource (fossil, biomass, or waste), whereas power and automotive sectors can consider totally different alternatives, such as photovoltaics and electric vehicles, respectively.

The high capital costs involved with a new biomethanol process plant is mainly due to the impurities contained in the raw syngas produced from biomass. Compared to syngas produced from natural gas, biosyngas is more contaminated and requires additional cleaning technologies. Moreover, the molar ratio among the main constituents of syngas after the purification step, that is, H_2, CO, and CO_2, must be adjusted to a value suitable for methanol synthesis.

An important drawback of biomass gasification followed by biomethanol synthesis is the emission of pollutants into the environment. The main substances involved are ash, tar, particulates, and carbon dioxide (Shamsul et al., 2014). Consequently, plants must be provided with more advanced gas cleaning systems (metal filters, catalytic tar crackers, CO_2 capture system, sorbents) to minimize this disadvantage.

In general, several problems are connected with the bioproduction of methanol. Some technologies are already at a mature stage of development, and their main limitation is that their production costs are higher than those of fossil-based processes. More research in process systems engineering, in particular for heat integration, is the main avenue toward overcoming this economic limitation. A correct scale-up approach for all the biomass-based processes is

also very important, in particular for the advanced technologies recently introduced and proposed for biomethanol synthesis. The positive results obtained in bench-scale studies for these new technologies must now be confirmed on a larger scale, with new process configuration highly integrated.

References

Adamson, K.A., Pearson, P., 2000. Hydrogen and methanol: a comparison of safety, economics, efficiencies and emissions. J. Power Sources 86, 548–555.

Agny, R.M., Takoudis, C.G., 1985. Synthesis of methanol from carbon monoxide and hydrogen over a copper-zinc oxide-alumina catalyst. Ind. Eng. Chem. Prod. Res. Dev. 24, 50–55.

Andersson, J., Lundgren, J., Marklund, M., 2014. Methanol production via pressurized entrained flow biomass gasification—techno-economic comparison of integrated vs. stand-alone production. Biomass Bioenergy 64, 256–268.

Arab Aboosadi, Z., Jahanmiri, A.H., Rahimpour, M.R., 2011. Optimization of tri-reformer reactor to produce synthesis gas for methanol production using differential evolution (DE) method. Appl. Energy 8, 2691–2701.

Arakawa, H., Aresta, M., Armuor, J.N., Barteau, M.A., Beckman, E.J., Bell, A.T., 2001. Catalysis research of relevance to carbon management: progress, challenges and opportunities. Chem. Rev. 101–4, 953–996.

Ardizzone, S., Bianchi, C.L., Cappelletti, G., Gialanella, S., Pirola, C., Ragaini, V., 2007. Tailored anatase/brookite nanocrystalline TiO_2. The optimal particle features for liquid and Gas-phase photocatalytic reactions. J. Phys. Chem. C 111, 13222–13231.

Argyle, M.D., Bartholomew, C.H., 2015. Heterogeneous catalyst deactivation and regeneration: a review. Catalysts 5, 145–269.

Askgaard, T.S., Norskov, J.K., Ovesen, C.V., Stoltze, P., 1995. A kinetic model of methanol synthesis. J. Catal. 156, 229–242.

Bakemeier, H., Laurer, P.R., Schroder, W., 1970. Development and application of a mathematical model of the methanol synthesis. Chem. Eng. Prog. Symp. Ser. 66, 1–10.

Bardet, R., Thivolle-Cazat, J., Trambouze, Y., 1984. Hydrocondensation des oxydes de Carbone, à la pression atmosphérique, sur des catalyseurs Cu-ZnO-Al_2O_3. Influence de l'eau sur la formation du méthanol. C. R. Hebd. Seances Acad. Sci. 299, 423.

Bassani, A., Pirola, C., Maggio, E., Pettinau, A., Frau, C., Bozzano, G., Pierucci, S., Ranzi, E., Manenti, F., 2016. Acid gas to syngas $(AG2S)^{TM}$ technology applied to solid fuel gasification: cutting H_2S and CO_2 emissions by improving syngas production. Appl. Energy 184, 1284–1291.

Bhattacharyya, J.K., Kumar, S., Devotta, S., 2008. Studies on acidification in two-phase biomethanation processes of municipal solid waste. Waste Manag. 28, 164–169.

Bozzano, G., Manenti, F., 2016. Efficient methanol synthesis: perspectives, technologies and optimization strategies. Prog. Energy Combust. Sci. 56, 71–105.

Cabianca, L., Bassani, A., Furtado Amaral, A., Rossi, F., Bozzano, G., Ranzi, E., Telen, D., Logist, F., Van Impe, J., Manenti, F., 2016. Gasds: a kinetic-based package for biomass and coal gasification. Chem. Eng. Trans. 50, 247–252.

Chen, H., Nanayakkare, C., Grassian, V., 2012. Titanium dioxide photocatalysis in atmospheric chemistry. Chem. Rev. 112, 5919–5948.

Chincen, G.C., Denny, P.J., Jenning, J.R., Spencer, M.S., Waugh, K.C., 1988. Synthesis of methanol catalysts and kinetics. Appl. Catal. 36, 1–12.

Chinchen, G.C., Hay, C.M., Vandervell, H.D., Waugh, K.C., 1987. The measurement of copper surface areas by reactive frontal chromatography. J. Catal. 103, 79–86.

Cho, W., Song, T., Mitsos, A., Thomas McKinnon, J., Ko, G.H., Tolsma, J.E., Denholm, D., Park, T., 2009. Optimal design and operation of a natural gas tri-reforming reactor for DME synthesis. Catal. Today 139, 261–267.

Cifre, B., 2007. Renewable hydrogen utilization for the production of methanol. Energy Convers. Manag. 48, 519–527.
Clausen, B.S., Steffensen, G., Fabius, B., Villadsen, J., Feidenhans'l, R.H.T., 1991. In situ cell for combined XRD and on-line catalysis tests: studies of Cu-based water gas shift and methanol catalysts. J. Catal. 132, 524–535.
Corbetta, M., Bassani, A., Manenti, F., Pirola, C., Maggio, E., Pettinau, A., Deiana, P., Pierucci, S., Ranzi, E., 2015. Multi-scale kinetic modeling and experimental investigation of syngas production from coal gasification in updraft gasifiers. Energy Fuel 29, 3972–3984.
Duan, C., Luo, M., Xing, X., 2011. High rate conversion of methane to methanol by methylosinus trichosporium OB3b. Bioresour. Technol. 102, 7349–7353.
Dybkjaer, I., 1985. Design of ammonia and methanol synthesis reactors. In: NATO Conference on Chemical Reactor Design and Technology, Canada.
Fitzpatrick, T., Hicks, T., 2010. Catalysts with higher and more stable activity enable cost savings and boost output in methanol production, advances in methanol synthesis. Digital Refining, www.digitalrefining.com/article/1000297.
Forzatti, P., Lietti, L., 1999. Catalyst deactivation. Catal. Today 52, 165–181.
Fujitani, T., Nakamura, J., 2000. The chemical modification seen in the Cu/ZnO methanol synthesis catalysts. Appl. Catal. A Gen. 191, 111–129.
Galli, F., Compagnoni, M., Vitali, D., Pirola, C., Bianchi, C.L., Villa, A., Prati, L., Rossetti, I., 2017. CO_2 photoreduction at high pressure to both gas and liquid products over titanium dioxide. Appl. Catal., B 200, 386–391.
Ganesh, I., 2014. Conversion of carbon dioxide into methanol—a potential liquid fuel: fundamental challenges and opportunities (a review). Renew. Sust. Energ. Rev. 31, 221–257.
Graaf, G.H., Stamhuis, E.J., Beenackers, A.A.C.M., 1988. Kinetics of low-pressure methanol synthesis. Chem. Eng. Sci. 43, 3185–3195.
Graaf, G.H., Scholtens, H., Stamhuis, E.J., Beenackers, A.A.C.M., 1990. Intra-particle diffusion limitations in low-pressure methanol synthesis. Chem. Eng. Sci. 45, 773–783.
Grabow, L.C., Mavrikakis, M., 2011. Mechanism of methanol synthesis on Cu through CO_2 and CO hydrogenation. ACS Catal. 1, 365–384.
Habisreutinger, S.N., Schmidt-Mende, L., Stolarczyk, J., 2013. Photocatalytic reduction of CO_2 on TiO_2 and other semiconductors. Angew. Chem. Int. Ed. 52, 2–39.
Hansen, J.B., 1997. Methanol synthesis. In: Ertl, G., Knozinger, H., Weitkamp, J. (Eds.), Handbook of Heterogeneous Catalysis. In: 4Wiley-VCH, Weinheim.
IEA-ETSAP and IRENA, 2013. Production of bio-methanol technology brief. Technology brief 108.
Jackson, R., 1977. Transport in porous catalysts, In: Chemical Engineering Monographs, Vol. 4. Elsevier Scientific Publishing Co., New York.
Klier, K., 1982. Methanol synthesis. Adv. Catal. 31, 243–313.
Klier, K., Chatikavanij, V., Herman, R.G., Simmons, G.W., 1982. Catalytic synthesis of methanol from CO/H_2: IV. The effects of carbon dioxide. J. Catal. 74, 343–360.
Kubota, T., Hayakawa, I., Mabuse, H., Mori, K., Ushikoshi, K., Watanabe, T., 2001. Kinetic study of methanol synthesis from carbon dioxide and hydrogen. Appl. Organomet. Chem. 15, 121–126.
Kuczynski, M., van Ooteghem, A., Westerterp, K.R., 1987. Methanol adsorption by amorphous silica alumina in the critical temperature range. Colloid Polym. Sci. 264, 362–367.
Kung, H.H., 1992. Deactivation of methanol synthesis catalysts – a review. Catal. Today 11, 443–453.
Leduc, S., Lundgren, J., Franklin, O., Dotzauer, E., 2010. Location of a biomass based methanol production plant: a dynamic problem in northern Sweden. Appl. Energy 87, 68–75.
Leonov, E., Karabaev, M.M., Tsybina, E.N., Petrishcheva, G.S., 1973. Kinet. Katal. 14, 970–975.
Li, K., An, X., Park, K.H., Khraisheh, M., Tang, J., 2014. A critical review of CO_2 photoconversion: catalysts and reactors. Catal. Today 224, 3–12.

Lim, H.W., Park, M.J., Kang, S.H., Chae, H.J., Bae, J.W., Jun, K.W., 2009. Modeling of the kinetics for methanol synthesis using $Cu/ZnO/Al_2O_3/ZrO_2$ catalyst: influence of carbon dioxide during hydrogenation. Ind. Eng. Chem. Res. 48, 10448–10455.

Liu, G., Willcox, D., Garland, M., Kung, H.H., 1985. The role of CO_2 in methanol synthesis on Cu-Zn oxide: an isotope labeling study. J. Catal. 96, 251–260.

Lommerts, B.J., Graaf, G.H., Beenackers, A.A.C.M., 2000. Mathematical modeling of internal mass transport limitations in methanol synthesis. Chem. Eng. Sci. 55, 5589–5598.

Løvik, J.I., 2001. Modelling, Estimation and Optimization of the Methanol Synthesis with Catalyst Deactivation (Ph.D. thesis).

Maxwell, J.C., 1866. On the dynamic theory of gases. Philos. Trans. R. Soc. 157, 49–88.

McNeil, M.A., Schack, C.J., Rinker, R.G., 1989. Methanol synthesis from hydrogen, carbon monoxide and carbon dioxide over a $CuO/ZnO/Al_2O_3$ catalyst: II. Development of a phenomenological rate expression. Appl. Catal. 50, 265–285.

McNicol, B.D., Rand, D.A.J., Williams, K.R., 1999. Direct methanol-air fuel cells for road transportation. J. Power Sources 83, 15–31.

Methanex, 2016. Methanol price. https://www.methanex.com/our-business/pricing.

Mochalin, V.P., Lin, G.I., Rozovskii, A.Y., 1984. Kinetic-model of the process of methanol synthesis on the snm-1 catalyst. Khim. Prom-st. 1, 11.

Moulijn, J.A., Makkee, M., van Diepen, A., 2001. Chemical Process Technology. Wiley, Chichester.

Natta, G., 1955. Synthesis of methanol. Catalysis. Reinhold, NY, USA. p. 3.

Olah, G.A., 2005. Beyond oil and gas: the methanol economy. Angew. Chem. Int. Ed. Engl. 44, 2636–2639.

Olah, G.A., Goeppert, A., Surya Prakash, G.K., 2006. Beyond Oil and Gases: the Methanol Economy. Wiley-VCH, Weinheim.

Ostrovskii, V.E., 2002. Mechanisms of methanol synthesis from hydrogen and carbon oxides at Cu-Zn-containing catalysts in the context of some fundamental problems of heterogeneous catalysis. Catal. Today 77, 141–160.

Ovesen, C.V., 1992. Kinetic Modeling of Reactions on Cu Surfaces (Ph. D. thesis). Laboratory of Applied Physics, Technical University of Denmark, Lyngby.

Ovesen, C.V., Clausen, B.S., Schiøtz, J., Stoltze, P., Topsøe, H., Nørskov, J.K., 1997. Kinetic implications of dynamical changes in catalyst morphology during methanol synthesis over Cu/ZnO catalysts. J. Catal. 168, 133–142.

Park, N., Park, M.J., Lee, Y.J., Ha, K.S., Jun, K.W., 2014. Kinetic modeling of methanol synthesis over commercial catalysts based on three-site adsorption. Fuel Process. Technol. 125, 139–147.

Pino, L., Vita, A., Laganà, M., Recupero, V., 2014. Hydrogen from biogas: catalytic tri-reforming process with Ni/LaCe O mixed oxides. Appl. Catal. B Environ. 148–149, 91–105.

Pirola, C., Galli, F., Corbetta, M., Manenti, F., 2015. Robust kinetic modeling of the free fatty acid esterification using methanol and Amberlyst 46 resin as catalyst. Clean Techn. Environ. Policy 17, 1139–1147.

Ptasinski, H.J., Hamelinck, C., Kerkhoff, P.J.A.M., 2002. Exergy analysis of methanol from the sewage sludge process. Energy Convers. Manag. 43, 1445–1457.

Rahimpour, M.R., Fathikalajahi, J., Jahanmiri, A., 1998. Selective kinetic deactivation model for methanol synthesis from simultaneous reaction of CO_2 and CO with H_2 on a commercial copper/zinc oxide catalyst. Can. J. Chem. Eng. 76, 753–761.

Rahimpour, M.R., Arab Aboosadi, Z., Jahanmiri, A.H., 2012. Synthesis gas production in a novel hydrogen and oxygen perm-selective membranes tri-reformer for methanol production. J. Nat. Gas Sci. Eng. 9, 149–159.

Ranzi, E., Faravelli, T., Manenti, F., 2016. Pyrolysis, gasification and combustion of solid fuels. Adv. Chem. Eng. 49, 1–94.

Rasmussen, P.B., Holmblad, P.M., Askgaard, T., Ovesen, C.V., Stoltze, P., Norskov, J.K., 1994. Methanol synthesis on Cu(100) from a binary gas-mixture of CO_2 and H_2. Catal. Lett. 26, 373–381.

Rout, K.R., Hillestad, M., Jakobsen, H.A., 2013. A numerical study of pellet model consistency with respect to molar and mass average velocities, pressure gradients and porosity models for methanol synthesis process: effects of flux models on reactor performance. Chem. Eng. Res. Des. 91, 296–317.

Rozovskii, A.Y., Lin, G.I., 2003. Fundamentals of methanol synthesis and decomposition. Top. Catal. 22, 137–150.

Rozovskii, A.Y., Lin, G.I., Liberov, L.G., Slivinskii, E.V., Loktev, S.M., Kagan, Y.B., 1977. Mechanism of methanol synthesis from carbon dioxide and hydrogen. III. Determination of the rates of individual steps using carbon-14 monoxide. Kinet. Katal. 18, 691.

Saidur, R., Abdelaziz, E.A., Demirbas, A., Hossain, M.S., Mekhilef, S., 2011. A review on biomass as a fuel for a burner. Renew. Sust. Energ. Rev. 15, 2262–2289.

Schermuly, O., Luft, G., 1977. Methanol-syntheses im treibstrahlreaktor. Ger. Chem. Eng. 1, 222.

Setinc, M., Levec, J., 2001. Dynamics of a mixed slurry reactor for the three phase methanol synthesis. Chem. Eng. Sci. 56, 6081–6087.

Seyfert, W., Luft, G., 1985. Untersuchungen zur methnolsynthese im mitteldruckbereich. Chem. Ing. Tech. 57, 482–483.

Shabangu, S., Woolf, D., Fisher, E.M., Angenent, L.T., Lehmann, J., 2014. Techno-economic assessment of biomass slow pyrolysis into different biochar and methanol concepts. Fuel 117, 742–748.

Shamsul, N.S., Kamarudin, S.K., Rahman, N.A., Kofli, N.T., 2014. An overview on the production of bio-methanol as potential renewable energy. Renew. Sust. Energ. Rev. 33, 578–588.

Skrzypek, J., Lachowska, M., Moroz, H., 1991. Kinetics of methanol synthesis over commercial copper/zinc oxide/alumina catalysts. Chem. Eng. Sci. 46, 2809–2813.

Song, C., Pan, W., 2004. Tri-reforming of methane: a novel concept for catalytic production of industrially useful synthesis gas with desired H_2/CO ratios. Catal. Today 98, 463–484.

Spath, P.L., Dayton, D.C., 2015. Preliminary screening—technical and economic assessment of synthesis gas to fuels and chemicals with emphasis on the potential for biomass-derived syngas. www.nrelgov/docs/fy04osti/34929pdf.

Sun, J.T., Metcalfe, I.S., Sahibzada, M., 1999. Deactivation of Cu/ZnO/Al_2O_3 methanol synthesis catalyst by sintering. Ind. Eng. Chem. Res. 38, 3868–3872.

Supp, E., 1981. Improved methanol process. Hydrocarb. Process. 3, 71–75.

Tahir, M., Saidina Amin, N., 2013. Advances in visible light responsive titanium oxide-based photocatalysts for CO_2 conversion to hydrocarbon fuels. Energy Convers. Manag. 76, 194–214.

Takagawa, M., Ohsugi, M., 1987. Study on reaction rates for methanol synthesis from carbon monoxide, carbon dioxide, and hydrogen. J. Catal. 107, 161–172.

Tohji, K., Udagawa, Y., Mizushima, T., Ueno, A., 1985. The structure of the Cu/ZnO catalyst by an in situ EXAFS study. J. Phys. Chem. 89, 5671–5676.

Turton, R., Bailie, R.C., Whiting, W.B., Shaeiwitz, J.A., Bhattacharyya, D., 2012. Analysis, Synthesis, and Design of Chemical Processes, fourth ed. Prentice Hall, Upper Saddle River, NJ.

Vanden Bussche, K.M., Froment, G.F., 1996. A steady-state kinetic model for methanol synthesis and the water gas shift reaction on a commercial Cu/ZnO/Al_2O_3 catalyst. J. Catal. 161, 1–10.

Vedage, G.A., Herman, R.G., Klier, R., 1985. Chemical trapping of surface intermediates in methanol synthesis by amines. J. Catal. 95, 423–434.

Villa, P., Forzatti, P., Buzzi-Ferraris, G., Pasquon, I., 1985. Synthesis of alcohols from carbon oxides and hydrogen. 1. Kinetics of the low-pressure methanol synthesis. Ind. Eng. Chem. Process. Des. Dev. 24, 12–19.

Vita, A., Cristiano, G., Italiano, C., Pino, I., Specchia, S., 2015. Syngas production by methane oxy-steam reforming on Me/CeO_2 (Me = Rh, Pt, Ni) catalyst lined on cordierite monoliths. Appl. Catal. B Environ. 162, 551–563.

Xin, J.Y., Cui, J.R., Niu, J.Z., Hua, S.F., Xia, C.G., Li, S.B., Zhu, L.M., 2004. Production of methanol from methane by methanotrophic bacteria. Biocatal. Biotransform. 22, 225–229.

Zhang, L., Xu, C., Champagne, P., 2010. Overview of recent advances in thermos-chemical conversion of biomass. Energy Convers. Manag. 51, 969–982.

Zhang, Y., Cruz, J., Zhang, S., Lou, H.H., Benson, T.J., 2013. Process simulation and optimization of methanol production coupled to tri-reforming process. Int. J. Hydrog. Energy 38 (31), 13617–13630.

Zhang, Y., Zhang, Z.S., Benson, T., 2015. A conceptual design by integrating dimethyl ether (DME) production with trireforming process for CO_2 emission reduction. Fuel Process. Technol. 131, 7–13.

Further Reading

Chinchen, G.C., Waugh, K.C., Whan, D.A., 1986. The activity and state of the copper surface in methanol synthesis catalysts. Appl. Catal. 25, 101–107.

Solsvik, J., Jakobsen, H.A., 2011. Modeling of multicomponent mass diffusion in porous spherical pellets: application to steam methane reforming and methanol synthesis. Chem. Eng. Sci. 66, 1986–2000.

Wernicke, H.J., Plass, L., Schmidt, F., 2014. Methanol generation. In: Bertau, M., Offermanns, H., Plass, L., Schmidt, F., Wernicke, H.J. (Eds.), Methanol: The Basic Chemical and Energy Feedstock of the Future. Asinger's Vision Today.

This page intentionally left blank

CHAPTER 4

Waste as a Source of Carbon for Methanol Production

Gaetano Iaquaniello[*,‡], Gabriele Centi[†], Annarita Salladini[†], Emma Palo[‡]

[*] *Processi Innovativi, L'Aquila, Italy* [†] *University of Messina and INSTM/CASPE, Messina, Italy*
[‡] *KT – Kinetics Technology S.p.A., Rome, Italy*

Acronyms

DME	dimethyl ether
DMFC	direct methanol fuel cell
GHG	greenhouse gas
HT	high temperature (converter)
IRENA	International Renewable Energy Agency
kJ	kilojoule (10^3 joule)
KM-CDR	Kansai Mitsubishi carbon dioxide recovery
LHV	lower heating value
MEA	monoethanol amine
MSW	municipal solid waste
Mt	million tons
MTA	methanol-to-aromatics
MTBE	methyl tert-butyl ether
MTG	methanol-to-gasoline
MTO	methanol-to-olefin
MTP	methanol-to-propylene
MW	megawatt (10^6 watt)
NG	natural gas
PET	polyethylene terephthalate
PM	particulate matter
ppb	parts per billion
ppm	parts per million
PSA	pressure swing adsorption
RDF	residue-derived-fuel
t/d	ton per day (t/d)
TAME	tert-amyl-methyl-ether

Methanol. https://doi.org/10.1016/B978-0-444-63903-5.00004-2

WESP wet electrostatic precipitator
WGS water gas-shift reaction
WtE waste-to-energy
WtM waste-to-methanol

1 Introduction

The progressive decrease of conventional fossil fuel resources and an increase in waste generation (because of the world's growing population) poses the issue of developing economically viable and sustainable solutions for waste valorization. In terms of incineration, waste-to-energy (WtE) is a well-known technology, but its efficiency is largely dependent on the possibility of combined use of the heat and electricity produced (not always realized) (Ma et al., 2016; Astrup et al., 2015). On the other hand, a waste-to-chemical option is considered to be a less viable solution. However, we showed recently (Antonetti et al., 2017) that a new technology for producing urea from municipal solid wastes (MSW), particularly with the RDF fraction, is competitive with conventional urea production from fossil fuels (natural gas). We found that the estimated cost of production of urea was around 135 euro/t (internal rate of return $>10\%$), with a savings of about 113 t CH_4 and about 78 t CO_2 per ton of urea produced. This process is thus significantly more sustainable than that of the current urea production. The same approach is introduced here for the production of methanol with RDF.

Methanol is a large-volume chemical and energy vector, with a current world demand of more than 80 Mt (2016) and with a prediction of reaching about 100 Mt in 2020. Currently, the main methanol production route involves the synthesis of syngas (a mix of carbon monoxide, carbon dioxide, and hydrogen) from fossil sources (NG, especially) and its further catalytic conversion into methanol. About 80% of methanol production is based on NG, with the remainder derived from coal (17%) and small amounts of oil. Particularly in China (which accounted for about 60% of the world demand in 2016), coal-based methanol capacity is rapidly expanding. Chinese demand has grown significantly in terms of traditional methanol derivatives, such as formaldehyde and acetic acid, but also in new end uses, such as light olefins production, as well as expanded demand into energy applications, such as dimethyl ether (DME) and direct gasoline blending.

Feedstock for methanol production accounts for up to 90% of the production costs. Therefore the use of low-cost feedstock is key to the overall methanol economics. Historically, methanol production occurred mainly in Europe and North America, but additional methanol capacities have surged in other regions (Middle East, Africa, and South America), especially where there is access to low-cost natural gas or coal (limited mainly to China). Coal-based methanol production currently represents about 35% of the installed global capacity.

The methanol capacity additions in regions with more competitive/stranded gas economics triggered capacity rationalization in the more mature Western markets of North America and Europe in the early 2000s. In recent years, the exploitation of an unconventional natural gas (NG) supply through fracking in North America has enabled the region to regain its position as a methanol-production powerhouse, with an increased capacity with costs close to those of South America. However, the recent decrease in available shale gas, and thus a rapid realignment of NG costs with oil costs, has significantly depressed the outlook in this direction.

Therefore, in Europe and North America, competitiveness of methanol production relies on the identification of alternative, low-cost fossil-based feedstock. Global pricing originates in China, and the other regions are priced according to freight and duty differentials. Europe and the United States are the highest-priced regions because they pay a premium to pull tons of methanol from international markets. Now that methanol has a significant number of derivatives that compete as alternatives to products derived from crude oil, it becomes strategic for regions such as Europe to develop alternative routes for methanol production.

In addition, the use of methanol derived from sources other than fossil fuels must be considered. In fact, the current biofuels (mainly ethanol for gasoline and fuel derived from vegetable oils for diesel and aviation sectors) are too expensive for long-term, sustainable ways to meet the current targets for biofuels in regions such as Europe. It is thus imperative to find lower-cost routes for biofuel production (Lanzafame et al., 2015; Centi et al., 2011).

1.1 Biomethanol

The preceding factors have spurred interest in producing biomethanol, which can be produced from a wide range of biomass feedstocks via the production of syngas by gasification followed by (after purification, the main limit of the technology) catalytic conversion of the gas produced to methanol. For example, VärmlandsMetanol AB has developed a biomass-to-methanol process to gasify biomass (forest residue) and then purify and convert the syngas into fuel-grade methanol (http://www.varmlandsmetanol.se, accessed 24 January 2017). The process, which the plant announced in 2013, is still at the planning stage; however, it will produce 300 t/d fuel-grade methanol and deliver to districts heating water with a thermal duty of 15 MW. BioMCN (http://www.biomcn.eu, accessed 24 January 2017) was founded in the Netherlands about 10 years ago and was the first company in the world to produce, market, and sell industrial quantities of biomethanol using glycerin as a feedstock. Enerkem, a Canadian company located in Edmonton, produces biomethanol from waste (http://enerkem.com, accessed 24 January 2017). Since 2000 Enerkem has tested and validated a number of different feedstocks, from solid waste taken from municipalities to dozens of other types of residues.

In Enerkem's system, these feedstocks are converted into methanol, ethanol, or other renewable chemicals (Fig. 4.1). The first full-scale commercial biorefinery began operating in Edmonton (Canada) in 2015, with pilot and demonstration facilities in Canada, North America, and abroad (in development). The facility converts MSW to syngas, which is converted to methanol. The city of Edmonton will supply 100,000 t (dry) of sorted MSW per year to produce 43k t/y of methanol. The sorted MSW to be used is the ultimate residue after recycling and composting, which is saved from being put in a landfill. A methanol-to-ethanol conversion module was eventually added. This facility is part of a comprehensive municipal waste-to-biofuel initiative in partnership with the city of Edmonton and Alberta Innovates. Enerkem's four-step thermochemical process is as follows: (i) feedstock preparation, (ii) gasification, (iii) cleaning and conditioning of syngas, and (iv) catalytic synthesis.

The advantage of starting from MSW is that it uses a waste product, which must be treated anyway (incineration, landfill), to produce a valuable biofuel. Forest residues are costlier, because they need to be collected, transported, and treated to reach the necessary characteristics (size, humidity) for gasification. Glyceryl is a by-product of biodiesel (first generation) production, but because of the large number of applications, it is a valuable product and cannot be considered as a waste. MSWs represent a true opportunity, because of their negative or neutral cost (they need to collected and treated for incineration or landfilling), because of their widespread availability (unlike forest residue), and because of their added value, based on their use to produce chemicals and fuels, rather than just energy. It is worth noting that the efficiency of incineration is often low, around 35%–40% because the cogenerated heat can be used only is some cases. The situation is even worse for landfills because disposal adds a cost. The use of MSWs to produce chemicals and fuels also leads to significantly improved sustainability. For the cited waste-to-urea process (Antonetti et al., 2017), we showed that the production of urea from MSW will save about 113 t of CH_4 per t of urea and about 78 t of CO_2 per t of urea because of current technology and the alternative use of MSW to generate electrical energy. Thus there is a positive savings in energy and resources.

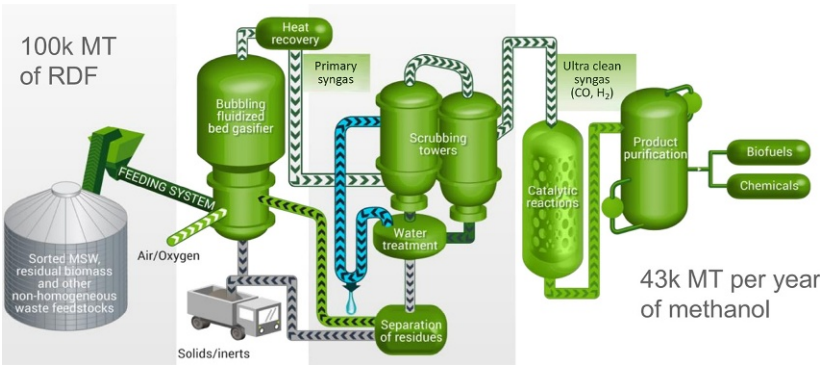

Fig. 4.1
Simplified scheme of the Enerkem waste-to-methanol plant using MSW. *Source: Enerkem, http://enerkem.com. Accessed 24 January 2017.*

However, data available for Enerkem's waste-to-methanol plant and process are very limited and, for example, are not available for assessing the techno-economics, the details of operations and process design, the applicability to different situations, and so on. Although the waste-to-methanol process is apparently based on established technologies, the process scheme and operation units have many peculiarities. For example, the gasification unit needs to be designed to avoid the formation of dioxins, chlorinated products, tars, and other compounds, which on the one hand, may create safety issues, and on the other hand, may deactivate the downstream catalytic process. The purification step of the gas stream after gasification is critical in terms of the purification level and energy efficiency. The water scrubbing system outlined in Fig. 4.1 is not ideal for reaching these objectives, and the water treatment unit after the scrubbing is likely difficult and complex, as can be seen in Fig. 4.1. The conventional catalysts for methanol synthesis from syngas are very sensitive to deactivation by even traces of pollutants, which may be present in the syngas derived from MSW. A specifically tailored catalyst is necessary. Catalysts for methanol synthesis need to operate at high pressure and at temperatures of about 220°C. Therefore it is not possible to send the gas directly to methanol synthesis after water scrubbing, as indicated in Fig. 4.1. There is an optimal amount of CO_2 and H_2O and a ratio of CO_x/H_2 in the feed to the methanol synthesis unit, and these values are typically not achieved in conventional gasification of MSW. It is thus evident that a number of questions are raised in regard to the Enerkem waste-to-methanol plant that are not dealt with in the available literature.

A small amount of literature relevant to the development of a waste-to-methanol plant exists. Brachi et al. (Brachi et al., 2014) investigated the fluidized-bed co-gasification of biomass and polymeric wastes for flexible end use of the syngas, with a focus on biomethanol. By using a prepilot, fluidized bed gasifier, they demonstrated that the co-gasification of regional biomass residues (e.g., dried olive husk) with PET or tire wastes provided a simplified process and a reduction in cost. The gas composition resulting from the presence of polymeric wastes allowed eliminating a water–gas shift reactor (to adjust CO_x/H_2 ratio) with only a CO_2 capture process being sufficient to meet the requirements for the downstream methanol production. However, the use of tire-based pellets rather than PET generates tar and particulates.

Gasification is a more complex process than waste incineration, but the reactors used for both processes are similar. In both cases, it is important to avoid the formation of substances like dioxins and furans, but the formation of these products needs sufficient oxygen to form or reform, and the oxygen-deficient atmosphere in a gasifier minimizes their formation. In addition, in gasification facilities, the syngas is quickly quenched such that there is insufficient residence time in the temperature range where dioxins or furans can reform. As a result, the need for a high-temperature zone (>1200°C) with relatively long residence times (>6 s) in incinerators is not necessary in gasifiers. On the other hand, in the latter case, it is necessary to limit the formation of CO_2 versus CO, whereas the opposite is true for incineration. Furthermore, as indicated, steam should be used to adjust the CO/H_2 ratio. Thus feed

composition and thermodynamics are different in the two cases. The main reactor types are fixed beds and fluidized beds. Fixed-bed reactors for incinerators typically have a grate to support the feed material and maintain a stationary reaction zone. They are relatively easy to design and operate and are therefore useful for small- and medium-scale power and thermal energy use. However, it is difficult to keep operating temperatures at constant levels and to ensure adequate gas mixing in the reaction zone. As a result, gas yields can be unpredictable and are not optimal for large-scale power purposes (i.e., more than 1 MW). In addition, this reactor design is not optimal for gasification to reduce tar formation. Smaller particle sizes are also necessary to limit this issue. For treatment of MSW in large-capacity gasifiers, fluid bed reactors are often indicated as preferable (Brachi et al., 2014) because they allow for variable fuel feed, uniform process temperatures, good interaction between gases and solids, and high levels of carbon conversion. However, the cost of grinding and uniform sieving of the MSW adds significant costs.

These considerations show that the question of an optimal gasifier design is still open and also that the process of transforming MSW to methanol is not a simple assembling of known technologies, but that a tailored design and optimization are required.

1.2 Biomethanol Uses and Advantages

Methanol has only half the energy content of gasoline, whereas ethanol has two-thirds of the energy intensity of gasoline. However, in situations like those in Europe, where the inexpensive production of first-generation ethanol is not possible, there is an advantage in terms of energy unit cost in the case of biomethanol versus bioethanol. If we consider the average cost of producing second-generation (lignocellulosic) bioethanol as being about 1000 to 1300 eruo/t and the average cost of biomethanol as being 200 to 400 euro/t (see Chapter 23), the energy unit cost in the case of biomethanol is about 0.2–0.3 times lower than for bioethanol. In addition, in Europe when a biofuel is made from a residue, the regulations indicate that the energy content is counted twice toward the renewable energy target (Renewable Energy Directive, art 21.2), because wastes, agricultural crop residues, and residues from processing are considered to have zero life-cycle greenhouse gas emissions up to the point the materials are collected). An overview on the production of biomethanol as potential renewable energy was reported by Shamsul et al. (Shamsul et al., 2014).

Methanol has attractive features for use in transportation:

1. It is a liquid fuel, which can be blended with gasoline and ethanol and can be used with today's vehicle technology at minimal incremental costs.
2. It can be blended in petrol at 10%–20%. In China, M10 and M85 are already used in thousands of vehicles. Methanol has also been investigated for use as a fuel in shipping.

3. It is a high-octane fuel with combustion characteristics that enable engines specifically designed for methanol fuel to match the best efficiencies of diesel engines, while meeting current pollutant emission regulations.
4. It is a safe fuel. The toxicity (mortality) is comparable to or better than gasoline. It also biodegrades quickly (compared to petroleum fuels) in case of a spill.
5. Produced from renewable biomass, methanol is an attractive option for low-carbon transportation fuel in the long term. Depending on the way it is produced and if the entire life cycle is taken into account, biomethanol could reduce greenhouse gas emissions by 25%–60%, compared with methanol from fossil fuels.
6. Multiple ways exist for introduction of methanol into the fuel infrastructure (light blends or heavy blends) and into vehicles (light-duty or heavy-duty applications). The optimal approaches are different in different countries and in different markets.

An analysis of the pros and cons of the production of biomethanol was made by IRENA, an intergovernmental organization dedicated to renewable energy (International Renewable Energy Agency (IRENA) and Production of Bio-methanol – Technology Brief, 2013). An analysis of methanol as an alternative transportation fuel in the United States was also made in a white paper by Bromberg and Cheng (Bromberg and Cheng, 2010). In both cases, however, the data are not well updated, and the possibility to produce methanol from MSW is not considered in detail.

2 Producing Biomethanol From MSW

Biorenewable resources have the potential to support the growing demand for chemical commodities and at the same time relax concerns about climate change and energy security. However, competing against products derived from low-priced oil and natural gas is a difficult if not impossible task. Bio-based materials are all more expensive than natural gas and cannot compete in making biofuels or chemical commodities. Fig. 4.2 depicts raw materials' price per million of Btu according to Bomgardner (Bomgardner, 2016).

Process developers therefore need to look at utilizing lower-cost bio-based feedstocks, including those traditionally classified as waste streams or fuel derived from MSW as RDF. As shown in Fig. 4.3, the amount of municipal waste will double in the next 15 years, and the cost for collecting and disposing waste is steadily increasing. From this point of view, RDF may represent a very interesting negative-cost feedstock for the production of chemicals, specifically for biomethanol. RDF is a sort of waste—basically what is left from MSW after recovering waste paper, glass, metals, and the organic fraction—with a LHV ranging from 12 to 16 and even 18,000 kJ per kg. Table 4.1 summarizes the chemical composition of RDF and the range of variation.

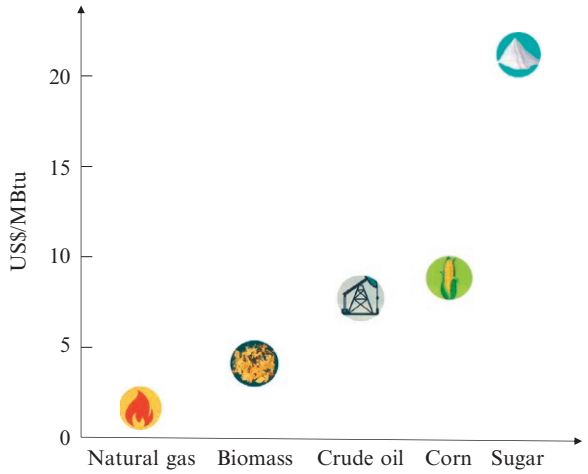

Fig. 4.2
Raw material prices per million Btu. *Source reference Bomgardner, H. M. (2016). Chem. Eng. News 94(18), 26.*

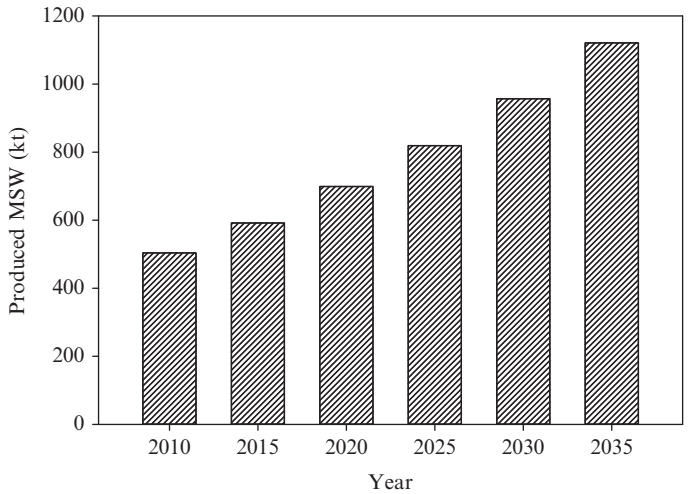

Fig. 4.3
Predicted increase in MSW production.

Today, RDF is disposed of either in landfills or through thermochemical treatment processes aiming to produce electricity, that is, WtE plants. A review of the advantages and disadvantages of the three main thermochemical conversion processes, combustion, pyrolysis, and gasification, was presented by Arena (Arena, 2012). In all these processes, a flue gas was generated at the end and released into the atmosphere. The environmental impact is specific for each process, and one of the greatest strengths of gasification technology is in its environmental performance. However, in such processes only the calorific value of RDF is

Table 4.1 Chemical composition of RDF and variation range (% wt.)

	Variation range	Typical
Wood	1–4	3
Paper	10–34	29
Plastic	26–36	31
Textile	7–8	7
Organic fraction	10–14	12
Inert fraction	10–27	18
C	29–38	33.5
H	4–5	4.5
O	14–18	16.5
H_2O	19–22	20.25
Ashes	17–30	25.25
LHV waste	MJ/kg 12–16	14.0

used. The energy efficiency, when the heat generated is used to produce electrical energy only, is around 27%–30%, depending on the type of reactor used for combustion. Energy efficiency may be higher in the case of coproduction of electrical energy and heat, but the use of the latter is possible only is some cases and climate conditions.

In a circular economy approach, however, waste should be a source of materials to make chemicals or usable materials (Stahel, 2016). RDF can be converted to syngas via adapted gasification (it is not a conventional gasification because it is necessary to obtain the right feedstock, for example, CO, CO_2, and H_2 ratios, for further processing); then after purification, it can be used for fuels or chemicals, such as methanol. The diagram in Fig. 4.4 shows a block scheme on how to make methanol from RDF.

Methanol can be then used in a variety of ways (see more details in Chapter 24):

- Direct blending in gasoline
- To produce other fuel components: MTBE, DME, for vegetable oil transesterification to produce biodiesel; for MTG process; etc.
- For chemicals, from light olefins through the MTO process or similar technologies (MTP, MTA) to other relevant chemicals, such as formaldehyde, acetic acid, acetate, etc.

An overview of the different possibilities is presented in Fig. 4.5. Out of the approximately 60 MMT of methanol sold globally in 2014, energy and fuel uses represented about 35%, a percentage that will further increase in the next decade. There are different types of uses for methanol in the energy area, in addition to direct use such as MTBE, TAME (tert-amyl-methyl-ether), low and high blends, to produce 1st generation biodiesel (by transesterification), DME, MTG, diesel blends and fuel additives as triptane. In general, in the area of energy and energy carriers (fuels), we can distinguish different paths to the utilization of methanol:

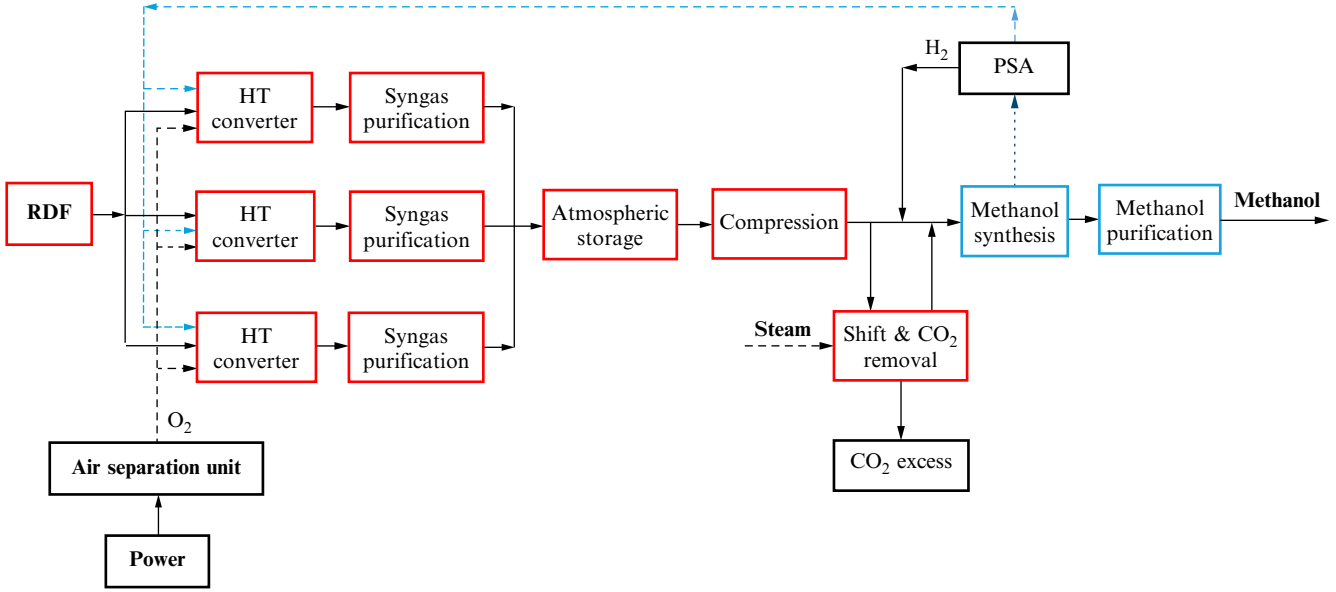

Fig. 4.4
Block diagram for WtM process.

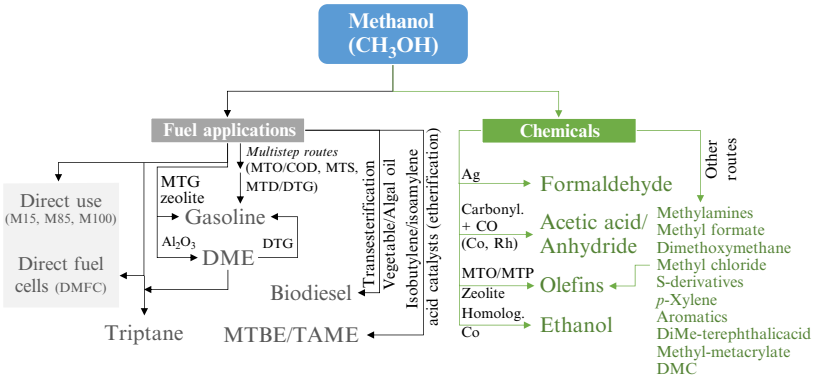

Fig. 4.5
Overview of the main routes to produce fuels and chemicals from methanol.

1. As direct energy carrier (gas turbines, heat generation, DMFC)
2. As component of the fuel mix (direct blending in gasoline or diesel)
3. As energy storage/transport chemical (via CO_2/H_2 conversion)
4. As raw material to produce other energy carriers (DME, gasoline by MTG)
5. As co-reactant to produce components of fuel mix (MTBE, TAME, biodiesel)

Methanol can also be used to produce H_2, but this is a use for niche applications.

3 Plant Configuration

The core of the process is the HT converter (modified gasifier), which is schematically presented in Fig. 4.6, where the RDF from battery limits is mixed with oxygen to produce a syngas whose major components are hydrogen, carbon monoxide, carbon dioxide, and methane. Such a stream also contains salts and particulates, HCl, COS and H_2S, and HCN. All these components need to be removed before any further catalytic treatment takes place.

Table 4.2 shows the experimental composition and variation range of the syngas produced by the high-temperature RDF converter. Looking at the composition, we see evidence of the higher impurity levels, all of which require additional purification and present processing challenges, such as the need for pretreatment steps and resolution of catalyst deactivation issues.

The high temperature and the appropriate temperature profile are the key parameters to achieving proper performance of the reactor (Iaquaniello, 2016). In particular, hydrogen content increases and tar content remarkably decreases at temperatures higher than 1000°C, methane and other hydrocarbons tend to decompose at temperatures above 600°C, and a small amount of char is present at temperatures as high as 1600°C and is discharged into the slag. Moreover, the absence of an oxidizing atmosphere eliminates one of the steps of the dioxins'

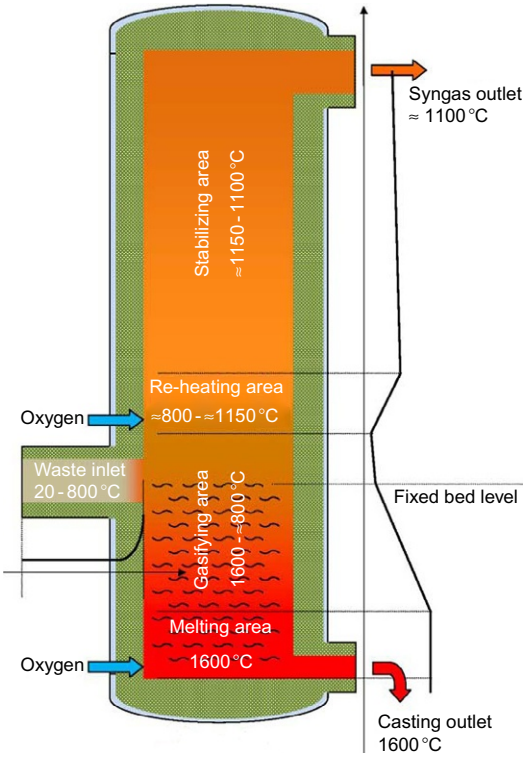

Fig. 4.6

HT converter together with required temperature profile. *Adapted from reference Iaquaniello, G., Salladini, A. (2016). Italian Patent Application n° 102016000100814, assigned to Processi Innovativi Srl.*

synthesis mechanisms (Stieglitz and Vogg, 1987) and strongly reduces their formation to an undetectable level.

The gas leaves the converter at around 1100°C and is quenched with water to reach near ambient temperature to enter into a first absorption tower containing water and then into a second tower containing an alkaline solution to remove particulates, salts, and HCl. A WESP will act as a final cleaning unit. The raw syngas coming from several different lines is routed to an atmospheric tank.

From the storage unit, the gas is compressed, COS is hydrolyzed to H_2S, which in turn is removed by a redox sulfur removal unit, followed by an H_2S deep polisher. The processed gas is split into two streams, one going directly to the methanol synthesis, the other routed to the shift reactor in order to convert CO into CO_2, which is then removed throughout the cryogenic unit. The excess CO_2 provides a CCS deployment option with little additional cost and represents one of the key "low-hanging fruits" for Bio-CCS (Vierhout, 2016). Raw hydrogen is added to the previous stream in order to get the proper CO/H_2 ratio before routing the streams to the methanol synthesis reactor. The purge gas will be recycled to the HT reactor to support the RDF conversion.

Table 4.2 Chemical composition and variation range of produced syngas

Parameter	Unit	Range	Expected	Notes
Molecular weight	g/mol	18–20	19.2	
Density	kg/Nm^3	0.75–0.90	0.85	
Pressure	mbarg	40–100	40.0	(1)
Temperature	°C	30–50	38.0	(2)
Composition	**Unit**	**Range**	**Expected**	**Notes**
H_2	vol.%	36–40	40.0	
CO	vol.%	37–43	41.0	
CO_2	vol.%	8–16	13.0	
H_2O	vol.%	6–8	5.0	(3)
N_2	vol.%	1–5	<4.0	
O_2	vol.%	<2	<1.0	
CH_4	vol.%	<5	<3.0	
Argon	vol.%	<2	<1.0	(4)
H_2S	mg/Nm^3	100–1500	<500	
COS	mg/Nm^3	10–150	<50.0	
Other sulfur compounds	mg/Nm^3	<10	<10.0	CS_2, etc.
HCl	mg/Nm^3	<5	<1.0	
HF	mg/Nm^3	<1	<1.0	HF, F^{-1}
HCN	mg/Nm^3	<10	<5.0	
Hg	mg/Nm^3	<0.2	<0.2	
Ti plus Cd	mg/Nm^3	<0.2	<0.2	
Heavy metals	mg/Nm^3	<1.0	<1.0	(5)
PM	mg/Nm^3	<3.0	<1.0	

(1) Safety element intervention threshold is fixed at 500 mbarg.
(2) Syngas temperature depends on the temperature of the cooling water circuit.
(3) Syngas is in saturation condition.
(4) Argon is entered into the system with oxygen.
(5) Sb, As, Pb, Cr, Co, Mn, NiV, Sn, Ca, Ta.

The overall material balance for a 300 t/d methanol plant is shown in Fig. 4.7, where around 716 t/d of RDF is used as feedstock.

3.1 Removal of Sulfur Components

Together with chlorides, which are removed downstream of the RDF conversion step, sulfur is a particularly severe poison for the WGS and the methanol synthesis reactors. A proper desulfurization system is required in order to reduce sulfur compounds to less than 0.1 ppm or even lower. The limit for chloride contamination is below 5 ppb.

Sulfur is present in RDF-generated syngas mainly as hydrogen sulfide (H_2S) and carbonyl sulfide (COS), although minor amounts of carbon disulfide and other sulfur compounds are also present. The H_2S/COS ratio is typically around 10 to 1. COS is thermally stable, and it may not be hydrogenated completely over a cobalt molybdate catalyst. Moreover, direct

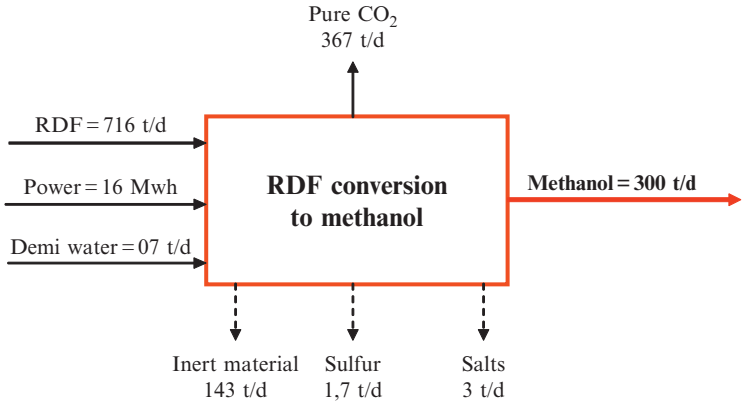

Fig. 4.7
Overall material balance for a 300 Mt/d plan.

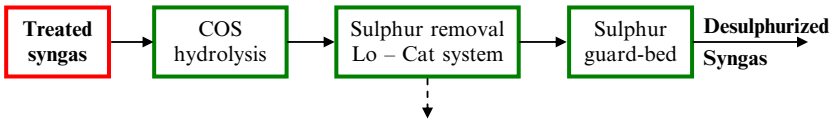

Fig. 4.8
Block diagram for the removal of sulfur compounds.

hydrogenation of other sulfur compounds over a nickel or cobalt molybdate catalyst in the presence of CO and H_2 may become problematic because of the possibility of methanation as a side reaction. In addition, the presence of significant amounts of H_2S does not allow the use of zinc oxide absorbents because of the high cost. The scheme indicated in Fig. 4.8 for removing sulfur components is thus based on the following steps: COS hydrolysis, H_2S removal throughout a redox system such as the Lo-Cat (Rouleau and Watson, n.d.), followed by a guard bed to remove all traces of sulfur contaminants (Biedermann et al., 2006).

3.2 The Correction of the R Ratio

The syngas composition from the RDF conversion step does not fit the requirements for methanol synthesis. Such a requirement is normally expressed via the *R* ratio

$$R = \frac{H_2 - CO_2}{CO + CO_2}$$

where *R* normally ranges from 2 to 2.1 and values are % in volumes.

The syngas composition range given in Table 4.2 shows that an excess of carbon is present, although the exact value depends on the chemical composition of the feed and RDF converter's operating conditions. In order to realign such an unbalance, two strategies can be implemented:

1. Add hydrogen
2. Remove the excess carbon

Adding hydrogen means either producing it separately by steam reforming, or by electrolysis of water, or by integrating the RDF conversion into a process in which an excess of hydrogen exists. The second scenario is well represented in the production of methanol, where the feedstock is natural gas. The economics of such integrations are presented elsewhere in this book (Chapter 24). Electrolysis is usually expensive, requiring 4–4.1 kWh per Nm^3 of hydrogen, although the oxygen coproduced can be used in the RDF conversion step, thus reducing the demand for pure oxygen. The use of electrolysis will make sense where the energy cost is quite low or when an excess of power exists in the grid, for instance during the night. In such a case, the electrolysis step will also act as a stabilizer for the power grid.

Steam reforming of natural gas is not a practical means of producing biomethanol. Therefore CO_2 removal is required to obtain the proper *R* ratio. CO should be reacted with water (WGS) with the formation of CO_2 and H_2 and with carbon dioxide removed in a following step. The CO_2 removal unit could be a conventional ammine sorption technology (based on MEA as solvent) or preferably the KM-CDR process based on the use of the sterically hindered ammine (KS-1) developed by Mitsubishi, which significantly reduces the cost of the process.
A cryogenic step is an alternative, whereas membrane separation technology and adsorption based on solid adsorbents are still under development (D'Alessandro et al., 2010).

The block diagram for *R* ratio adjustment is shown in Fig. 4.9, where only a fraction of the syngas is treated for such a purpose. In such a scheme, purge gas from the synthesis loop, after H_2 recovering with a PSA, is used as supporting fuel in the RDF conversion step. In such a way, the only carbon form leaving the system is the CO_2 stream.

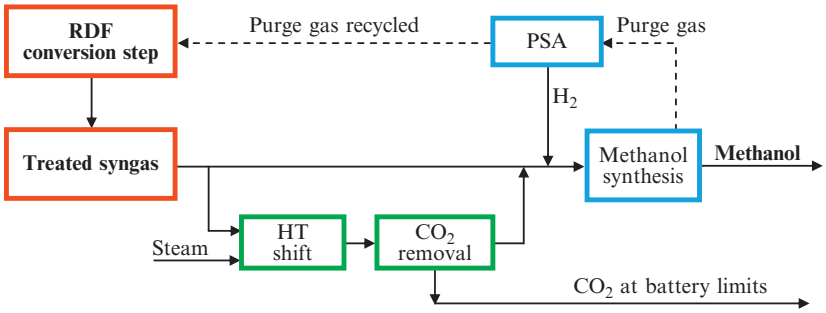

Fig. 4.9
Block diagram for the *R* ratio adjustment.

4 Energy Efficiency of the Conversion Process

The production of biomethanol will reduce the need for fossil fuel consumption and will reduce GHG emission. Generally, the energy efficiency of methanol production from natural gas ranges from about 60% to 70% (Biedermann et al., 2006). In the proposed scheme, the energy efficiency is estimated to be lower, between 56% and 57% in terms of feed + fuel LHV. This relates to the more complex process necessary to produce methanol from RDF rather than methane. However, this battery limit efficiency does not address the impact of the energy costs and GHG emissions associated with the extraction and distribution of natural gas; that is, fugitive methane emissions from the production, distribution, and use of natural gas have a significant impact (the GHG effect of CH_4 is about 30 times higher than that of CO_2).

The estimate of CO_2 emissions is roughly half the CO_2 emissions for a waste-to-energy application. If compared with methanol production from natural gas, the estimate is 1.2 kg CO_2 versus 2.18 kg CO_2 per kg of methanol in the latter case. This figure can be estimated by adding the emissions associated with methanol production (0.84 kg CO_2 per kg) and the ones associated with the combustion of methanol (1.34 kg CO_2 per kg). The emission reduction is then around 55%, higher than that reported in the literature (Biedermann et al., 2006; United Nations Industrial Development Organization (UNIDO), 2010). As a comparison, Japanese wood-based biomethanol production results in CO_2 emission reductions of 24%–40% compared to natural gas (Biedermann et al., 2006; United Nations Industrial Development Organization (UNIDO), 2010).

5 Conclusion

Biomethanol production via high-temperature conversion of RDF is a very promising process. Recent improvements in high-temperature conversion and in the use of multiple production lines allow alignment of the on-stream time in this section to the rest of plant (~8400 hours of operation per year). The energy efficiency is slightly lower than that of a natural gas-based plant on a battery limit, but its impact on energy cost and GHG emissions associated with the extraction and distribution of natural gas is better. The estimate of CO_2 emissions is roughly half that of CO_2 emissions for a waste-to-energy application and about 45% less if compared with methanol production from natural gas.

The last barrier to biomethanol commercialization, the relatively high capital costs, will be discussed in a separate chapter. One of the key parameters affecting the economics is the price of RDF disposal. Finally, it is necessary to establish a policy framework that fully credits the environmental advantages of bio-based materials.

References

Antonetti, E., Iaquaniello, G., Salladini, A., Spadaccini, L., Perathoner, S., Centi, G., 2017. Waste-to-chemicals for a circular economy: the case of urea production (waste-to-urea). ChemSusChem. https://doi.org/10.1002/cssc.201601555.

Arena, U., 2012. Process and technological aspects of municipal solid waste gasification. A review. Waste Manag. 32, 625–639.

Astrup, T.F., Tonini, D., Turconi, R., Boldrin, A., 2015. Life cycle assessment of thermal Waste-to-Energy technologies: review and recommendations. Waste Manag. 37, 104–115.

Biedermann, P., Grube, T., Höhlein, B., 2006. Methanol as an Energy carrier, Schriften des Forschungszentum Julich, Reihe Energietechnik/Energy Technology. vol. 55. Forschungszentrum Jülich Gmb, Germany. Available at https://www.deutsche-digitale-bibliothek.de/binary/REL5ILUDK4Y3GZSJ6WI4M42TCAVBC-32F/full/1.pdf.

Bomgardner, H.M., 2016. Renewables firms focus on cost squeeze. Chem. Eng. News 94 (18), 26.

Brachi, P., Chirone, R., Miccio, F., Miccio, M., Picarelli, A., Ruoppolo, G., 2014. Fluidized bed co-gasification of biomass and polymeric wastes for a flexible end-use of the syngas: focus on bio-methanol. Fuel 128, 88–98.

Bromberg, L., Cheng, W.K., 2010. Methanol as an Alternative Transportation Fuel in the US: Options for Sustainable and/or Energy-Secure Transportation. Sloan Automotive Laboratory/Massachusetts Institute of Technology (MIT), Cambridge, MA. 02139.

Centi, G., Lanzafame, P., Perathoner, S., 2011. Analysis of the alternative routes in the catalytic transformation of lignocellulosic materials. Catal. Today 167, 14–30.

D'Alessandro, D.M., Smit, B., Long, J.R., 2010. Carbon dioxide capture: prospects for new materials. Angew. Chem. Int. Ed. 49, 6058–6082.

Iaquaniello, G., Salladini, A. Italian Patent Application n° 102016000100814 (2016), assigned to Processi Innovativi Srl.

International Renewable Energy Agency (IRENA), Production of Bio-methanol – Technology Brief (2013). Available for download from the IEA-ETSAP and IRENA sites: iea-etsap.org/web/Supply.asp and www.irena.org/Publications.

Lanzafame, P., Centi, G., Perathoner, S., 2015. Catalysis for biomass and CO_2 use through solar energy: opening new scenarios for a sustainable and low-carbon chemical production. Chem. Soc. Rev. 43, 7562–7580.

Ma, H., Cao, Y., Lu, X., Ding, Z., Zhou, W., 2016. Review of typical municipal solid waste disposal status and energy technology. Energy Procedia 88, 589–594.

Rouleau, W., Watson, J. LO-CAT®: A Flexible Hydrogen Sulfide Removal Process. Available at http://www.merichem.com/LO-CAT-Flexible-H2S-Removal-Process.

Shamsul, N.S., Kamarudin, S.K., Rahman, N.A., Kofli, N.T., 2014. An overview on the production of bio-methanol as potential renewable energy. Renew. Sust. Energ. Rev. 33, 578–588.

Stahel, W.R., 2016. The circular economy. Nature 531, 435–438.

(a) Stieglitz, L., Vogg, H., 1987. Chemosphere 16, 1917–1922. (b) Mc Kay, G., 2002. Chem. Eng. J. 86, 343–348.

United Nations Industrial Development Organization (UNIDO), Global Industrial Energy Efficiency Benchmarking, UNIDO (2010). Available at https://www.unido.org/fileadmin/user_media/Services/Energy_and_Climate_Change/Energy_Efficiency/Benchmarking_%20Energy_%20Policy_Tool.pdf.

Vierhout, R. European Biofuels Technology Platform Meeting – Brussels, 21 June 2016. Available at http://biofuelstp.eu/spm7/160621_ENERKEM_Brussels_EBTP_final.pdf. Accessed 24 January 2017.

This page intentionally left blank

CHAPTER 5

Direct Synthesis of Methanol and Dimethyl Ether From a CO_2-Rich Feedstock: Thermodynamic Analysis and Selective Membrane Application

Marcello De Falco, Mauro Capocelli

University "Campus Bio-Medico" of Rome, Rome, Italy

Acronyms

DME	dimethyl ether
IMR	integrated membrane reactor
LPG	liquefied petroleum gas
MR	membrane reactor
SMR	staged membrane reactor
r-WGS	reverse water gas shift
WGS	water gas shift
ZSM5	Zeolite Socony Mobil-5

Symbols

F_{in}	inlet molar flow-rate
$F_{out,i}$	*i*-component outlet molar flow-rate
H_2/CO_x	hydrogen to CO_x ratio in the inlet feedstock
K_{eq}	equilibrium constants
p	partial pressure in the retentate side
$\overline{p}$	partial pressure in the permeate side
P	pressure
$Perm_{H_2O}$	water permeance across the membrane
S_{DME}	DME selectivity
T	temperature
X_{COx}	CO_x conversion

Methanol. https://doi.org/10.1016/B978-0-444-63903-5.00005-4

X_{H_2}	H_2 conversion
Y_{DME}	DME yield
$y_{CO_2,feed}$	inlet CO_2 molar fraction
y_i	i-component molar fraction

Greek symbols

α_i	i-component stoichiometric coefficient
ξ_j	j-reaction progress grade
ϕ_i	i-component fugacity coefficient

1 Introduction

Methanol is the simplest alcohol, being only a methyl group linked to a hydroxyl group (CH_3OH). It is a light, volatile, colorless, flammable liquid with a distinctive odor very similar to that of ethanol. It is used as an antifreeze, a solvent, a fuel, a denaturant for ethanol, and feedstock for a series of chemical productions (mainly for formaldehyde production and, consequently, for the production of plastics, paints, explosives, etc.).

Dimethyl ether (DME, C_2H_6O) is an organic compound used as an aerosol propellant and a reagent in the chemical industry for the synthesis of products such as dimethyl sulfate (a methylating agent), methyl acetate, and light olefins (Kang et al., 2008). Moreover, DME is a clean synthetic fuel that can be a substitute for liquefied petroleum gas (LPG) or that can be blended with diesel in fuel mixtures (Fleisch et al., 2012; Park and Lee, 2014). It has excellent combustion characteristics because of its low auto-ignition temperature, its high cetane number (55–60), and its ability to be burned in diesel engines, with only slight modifications.

Both methanol and DME are conventionally produced in a catalytic process from a syngas stream ($CO/CO_2/H_2$), generated from a fossil fuel (natural gas, coal, etc.) or from a biogas. The reactions involved in the methanol synthesis process are

$$CO + 2H_2 \leftrightarrow CH_3OH \quad \Delta H_o = -90.7\text{kJ/mol} \tag{5.1}$$

$$CO_2 + 3H_2 \leftrightarrow CH_3OH + H_2O \quad \Delta H_o = -49.4\text{kJ/mol} \tag{5.2}$$

$$CO + H_2O \leftrightarrow CO_2 + H_2 \quad \Delta H_o = -41.0\text{kJ/mol} \tag{5.3}$$

The process is exothermic (supported at high temperature) and is promoted by high pressures.

DME can be produced by two configurations:

– A two-step configuration, called the indirect method, which consists of a series of two separate steps: first, methanol is produced from a synthesis gas by reactions (5.1)–(5.3); then the methanol produced is dehydrated, producing DME.

– A one-step configuration, called the direct method, by which methanol and DME are simultaneously produced in an integrated reactor where a bifunctional catalyst is packed (Wang et al., 2006).

The direct method is more interesting and competitive from an industrial point of view, because of its lower operating costs and higher compactness and productivity, as reported by Arcoumanis et al. (2008).

The reactions of the DME synthesis one-step configuration are

$$CO_2 + 3H_2 \leftrightarrow CH_3OH + H_2O \quad \Delta H_o = -49.4\,kJ/mol \tag{5.4}$$

$$CO + H_2O \leftrightarrow CO_2 + H_2 \quad \Delta H_o = -41.0\,kJ/mol \tag{5.5}$$

$$2CH_3OH \leftrightarrow CH_3OCH_3 + H_2O \quad \Delta H_o = -23.0\,kJ/mol \tag{5.6}$$

$$CO + 2H_2 \leftrightarrow CH_3OH \quad \Delta H_o = -90.4\,kJ/mol \tag{5.7}$$

$$3CO + 3H_2 \leftrightarrow CH_3OCH_3 + CO_2 \quad \Delta H_o = -258.3\,kJ/mol \tag{5.8}$$

Among the five reactions, only three are independent: the reaction schemes are imposed on the following as CO_2 hydrogenation (5.4), water-gas shift (5.5), and methanol dehydration (5.6). It is worth noting that reactions (5.5) and (5.6) are also involved in the methanol production reaction schemes (5.2) and (5.3). All reactions are exothermic, and the process is thermodynamically feasible at low temperature and high pressure.

Conventionally, both methanol and DME industrial synthesis production processes are fed by a synthesis gas produced from fossil fuels consisting of a blend of CO, CO_2, and H_2. However, if the syngas is generated by a biological process from a biomass, the CO_2 content in the feedstock is much greater than in a traditional process (up to 40%–50%). Moreover, because CO_2 is a reactant, the process for producing methanol and DME can be included in the "CO_2 valorization" technologies, which means that those technologies are able to convert a greenhouse gas such as carbon dioxide into an added-value product, as described by Centi et al. (2013). Clearly, the greater the amount of CO_2 fed into a feedstock stream, the greater the environmental and economic benefits. For this reason, an interesting configuration provides for the enrichment of the syngas stream with pure CO_2, according to the block schemes shown in Figs. 5.1 and 5.2. An alternative, a reverse water-gas shift (r-WGS) reactor where

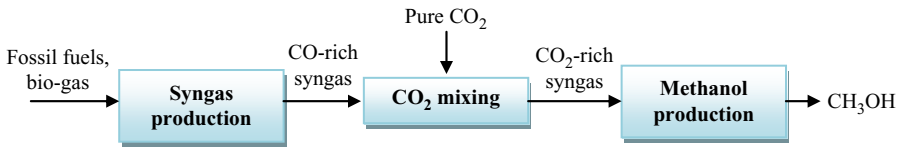

Fig. 5.1
Block diagram of a methanol production process fed by a high CO_2-content syngas stream.

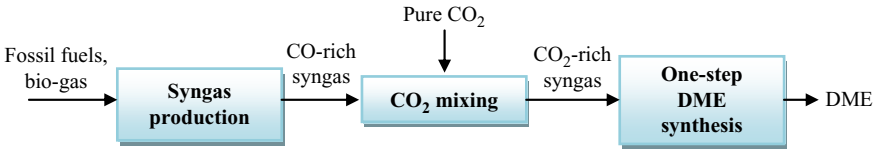

Fig. 5.2
Block diagram of a one-step DME production process fed by a high CO_2-content syngas stream.

reactions (5.3) and (5.5) are supported in the opposite direction, thus converting CO_2 in CO, can be placed before the methanol and DME production reactor, which allows modulation of the syngas composition in the inlet section, as described by De Falco et al. (2013).

For these reasons, methanol and DME production processes fed by a CO_2-rich stream have interesting potential uses, and assessing their behavior and performance is crucial to verifying the processes' feasibility.

As demonstrated in the following and as reported in a number of scientific papers (De Falco et al., 2013; Centi and Perathoner, 2013; Chen et al., 2012), CO_2 has a detrimental effect on the performance of methanol and DME production processes. This negative effect occurs because the higher CO_2 content in the reactor promotes the r-WGS reaction, thus increasing the water content and inhibiting the methanol production reaction (5.2) in the methanol synthesis process and the methanol dehydration (5.6) in the DME synthesis process. A solution is the integration of a steam water selective membrane able to selectively remove water from the reaction environment and supporting reactions (5.2) and (5.6) and, consequently, the methanol and DME production (Lee et al., 2006; Struis and Stucki, 2001; Samimi et al., 2013; Khajavi et al., 2010).

In the following section, we assess and evaluate the use of the membrane reactor (MR) for the production of methanol and for DME synthesis processes fed by a CO_2-rich reactant stream. First, a thermodynamic analysis of the one-step DME production process is discussed in order to quantify the detrimental effect of inlet CO_2 on the DME yield. Then a proper water-steam permselective membrane suitable for the processes' operating conditions is selected. Finally, process schemes are proposed and discussed.

2 Thermodynamic Analysis

Here we focus on the thermodynamic analysis of the one-step DME synthesis in order to describe the effect the CO_2 content has on the process's performance. We consider only the DME production process, but the same conclusions can be applied to methanol synthesis as well.

2.1 Thermodynamic Analysis of the Direct DME Synthesis Process

As previously mentioned, the reaction scheme of the DME synthesis process consists of CO_2 hydrogenation (5.4), water-gas shift (5.5), and methanol dehydration (5.6).

The thermodynamic model needed to evaluate the equilibrium threshold reactions is based on the solution of a set of three equations that describe the equilibrium constants K_{eq} of the reactions (5.4)–(5.6) as a function of the corresponding reactions' level of progress. The complete mathematical model of the DME production reaction schemes was reported by De Falco et al. (2016) and was based on the Van't Hoff equations for the calculation of the K_{eq} dependence on the temperature and also on the following equations for the definition of the equilibrium constant of reaction j ($K_{eq,j}$) as a function of the components' molar fractions and reaction pressures:

$$K_{eq,j}(T) = \prod_{i=1}^{c} \phi_i^{\alpha_i}(P,T,y_i) \cdot \prod_{i=1}^{c} y_i^{\alpha_i} \cdot P^{\sum \alpha_i} \tag{5.9}$$

where ϕ_i are the fugacity coefficients of the component i involved in the reaction (c is the total number of components involved), calculated according to the Tsonopoulos correlation as reported by De Santis (1980); α_i is the i-component stoichiometric coefficient; and P and T are the pressure and temperature, respectively. The molar fraction of the i-component y_i is calculated as a function of the reactions' levels of progress, imposing the material balances

$$\begin{aligned}
y_{CH_3OH} &= \frac{F_{in,CH_3OH} + \xi_1 - 2\xi_3}{F_{in,tot} - 2\xi_1} \\
y_{CH_3OCH_3} &= \frac{F_{in,CH_3OCH_3} + \xi_3}{F_{in,tot} - 2\xi_1} \\
y_{H_2} &= \frac{F_{in,H_2} - 3\xi_1 + \xi_2}{F_{in,tot} - 2\xi_1} \\
y_{CO} &= \frac{F_{in,CO} - \xi_2}{F_{in,tot} - 2\xi_1} \\
y_{CO_2} &= \frac{F_{in,CO_2} - \xi_1 + \xi_2}{F_{in,tot} - 2\xi_1} \\
y_{H_2O} &= \frac{F_{in,H_2O} + \xi_1 - \xi_2 + \xi_3}{F_{in,tot} - 2\xi_1}
\end{aligned} \tag{5.10}$$

where F_{in} is the inlet molar flow-rate and ξ_1, ξ_2, ξ_3 the progress grade of reactions (5.4), (5.5), and (5.6), respectively. By imposing Eq. (5.10) in Eq. (5.9) and fixing the inlet flow-rates, the temperature, and the pressure, it is possible to calculate the equilibrium progress levels by

numerically solving a set of three equations. Then the components outlet flow-rates are calculated as follows:

$$\begin{aligned}
F_{out,CH_3OH} &= F_{in,CH_3OH} + \xi_1 - 2\xi_3 \\
F_{out,CH_3OCH_3} &= F_{in,CH_3OCH_3} + \xi_3 \\
F_{out,H_2} &= F_{in,H_2} - 3\xi_1 + \xi_2 \\
F_{out,CO} &= F_{in,CO} - \xi_2 \\
F_{out,CO_2} &= F_{in,CO_2} - \xi_1 + \xi_2 \\
F_{out,H_2O} &= F_{in,H_2O} + \xi_1 - \xi_2 + \xi_3
\end{aligned} \tag{5.11}$$

Finally, the reactions' equilibrium behavior is assessed by quantifying the following:

$$X_{COx} = \frac{(F_{in,CO} - F_{out,CO}) + (F_{in,CO_2} - F_{out,CO_2})}{F_{in,CO} + F_{in,CO_2}} \quad CO_x \text{ conversion} \tag{5.12}$$

$$X_{H_2} = \frac{F_{in,H_2} - F_{out,H_2}}{F_{in,H_2}} \quad H_2 \text{ conversion} \tag{5.13}$$

$$Y_{DME} = \frac{2F_{out,CH_3OCH_3}}{F_{in,CO} + F_{in,CO_2}} \quad \text{DME yield} \tag{5.14}$$

$$S_{DME} = \frac{2F_{out,CH_3OCH_3}}{2F_{out,CH_3OCH_3} + F_{out,CH_3OH}} \quad \text{DME selectivity} \tag{5.15}$$

2.2 Results and Comments

The equilibrium conditions are assessed by imposing the following:

- A reaction's temperature within the range of 200–280°C
- A reaction's pressure within the range of 30–70 bar
- A ratio between the inlet hydrogen and the sum of the inlet CO and CO_2 (H_2/CO_x ratio) within a range of 2–4
- A CO_2 inlet molar fraction $y_{CO_2,feed}$ of 0%, 20%, and 40%

Figs. 5.3 and 5.4 show the CO_x conversion X_{COx} and H_2 conversion X_{H_2} with varying temperatures. Because all the reactions involved are exothermic, the conversions and the DME yield clearly decrease at higher temperatures. Moreover, a higher CO_2 content in the feedstock has a detrimental effect on the reactions' behavior in terms of conversions and DME yield, which is a result of the reverse water-gas shift and the subsequent accumulation of steam water, with a negative effect on both reactions (5.4) and (5.6). Increasing the $y_{CO_2,feed}$ greatly reduces both the CO_x conversion and the DME yield, thus limiting the process's

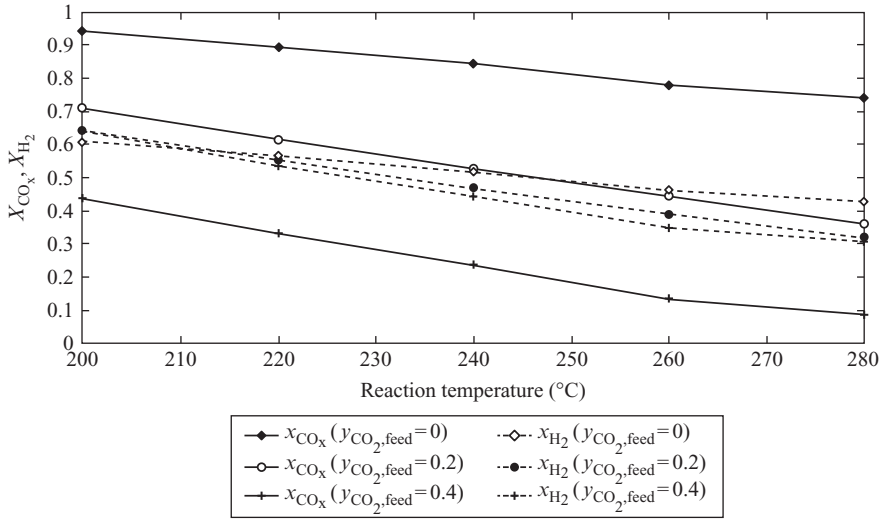

Fig. 5.3

CO_x and H_2 conversions versus reaction temperature and inlet feedstock CO_2 content (pressure = 50 bar, $H_2/CO_x = 3$).

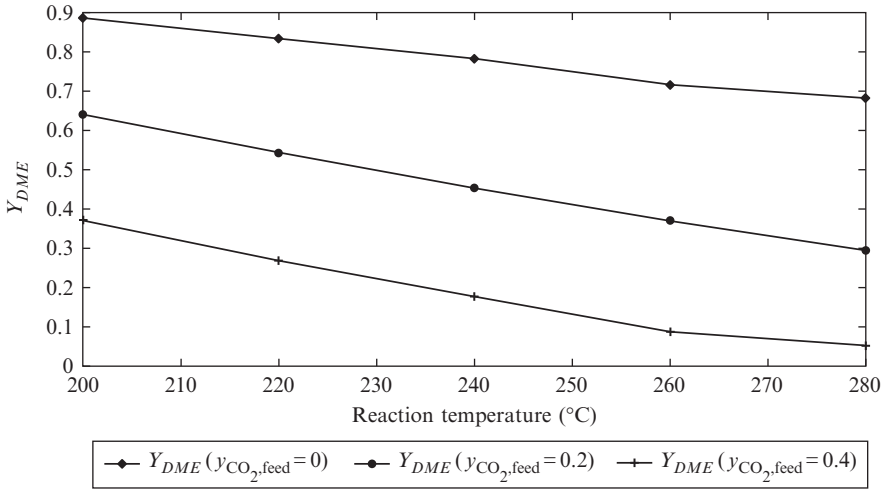

Fig. 5.4

DME yield versus reaction temperature and inlet feedstock CO_2 content (pressure = 50 bar, $H_2/CO_x = 3$).

potentialities. In DME selectivity, which is another parameter crucial to assessing the reactions' performance, both temperature and $y_{CO_2,feed}$ contribute to selectivity reduction: if $y_{CO_2,feed}$ is equal to 0, S_{DME} is 0.94 at 200°C and 0.915 at 280°C; if $y_{CO_2,feed}$ is equal to 20%, it is 0.9 at 200°C and 0.81 at 280°C; and if $y_{CO_2,feed}$ is 40%, it is 0.848 at 200°C and 0.56 at 280°C.

Figs. 5.5 and 5.6 show the reactions' behavior within a pressure range of 30–70 bar. The pressure has a positive effect on conversions and yield because the CO_2 dehydration reaction (5.4) leads to a reduction in the gas volume (Le Chatelier's principle). Cleary, the figures confirm the negative effect that the CO_2 composition in the inlet feedstock has on equilibrium conditions.

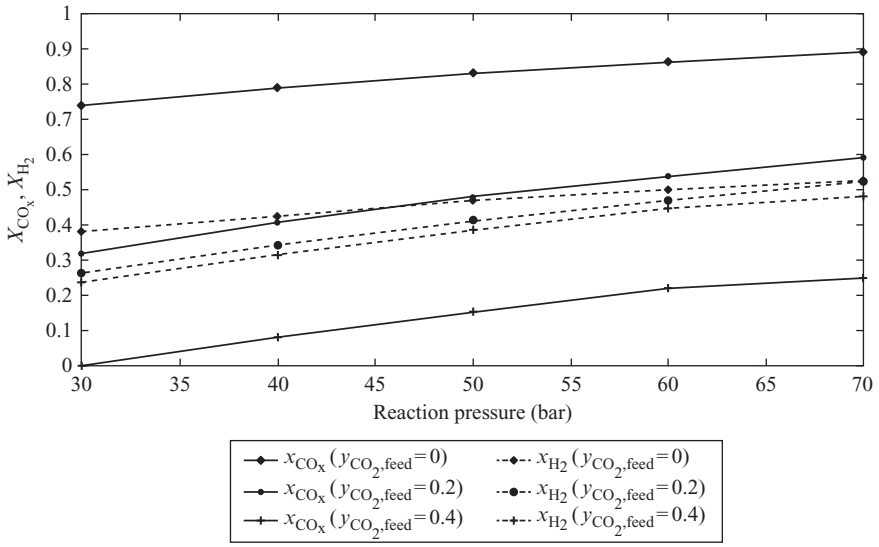

Fig. 5.5
CO_x and H_2 conversions versus reaction pressure and inlet feedstock CO_2 content (temperature = 240°C, $H_2/CO_x = 3$).

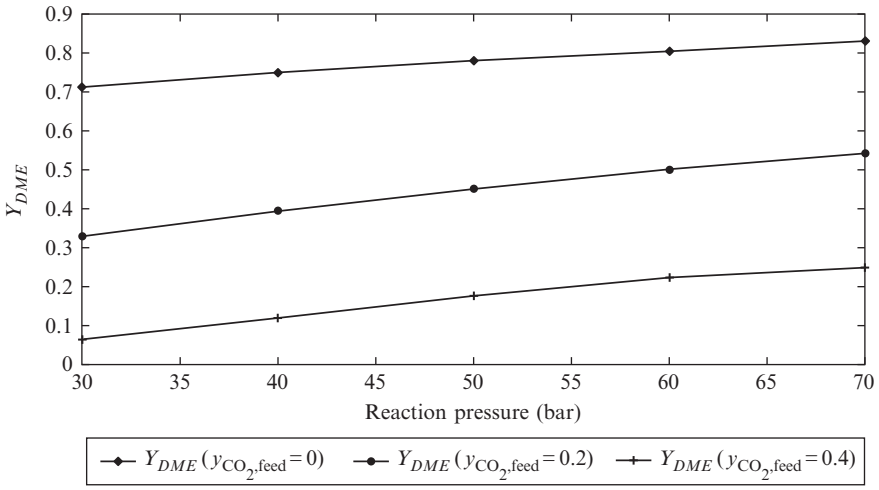

Fig. 5.6
DME yield versus reaction pressure and inlet feedstock CO_2 content (temperature = 240°C, $H_2/CO_x = 3$).

The pressure also has a slightly positive effect on the DME selectivity: imposing a temperature of 240°C and $y_{CO_2,feed}$ of 40% yields a S_{DME} of 0.645 at 30 bar and 0.772 at 70 bar.

Increasing the H_2/CO_x ratio in the feedstock leads to an increase of X_{COx}, a reduction of X_{H_2}, and an overall increase of the DME yield, as shown in Figs. 5.7 and 5.8. However, such an effect is negligible when the CO_2 content increases.

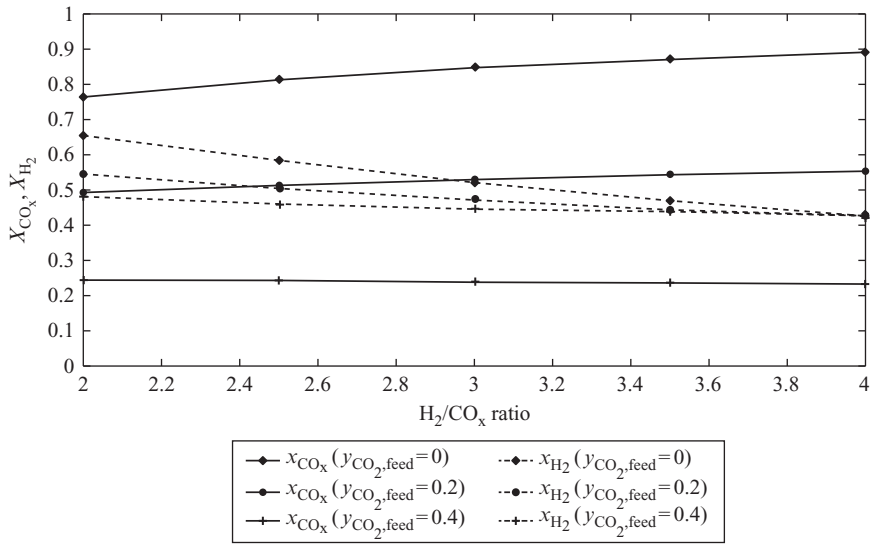

Fig. 5.7
CO_x and H_2 conversions versus inlet H_2/CO_x ratio and inlet feedstock CO_2 content (temperature = 240°C, pressure = 50 bar).

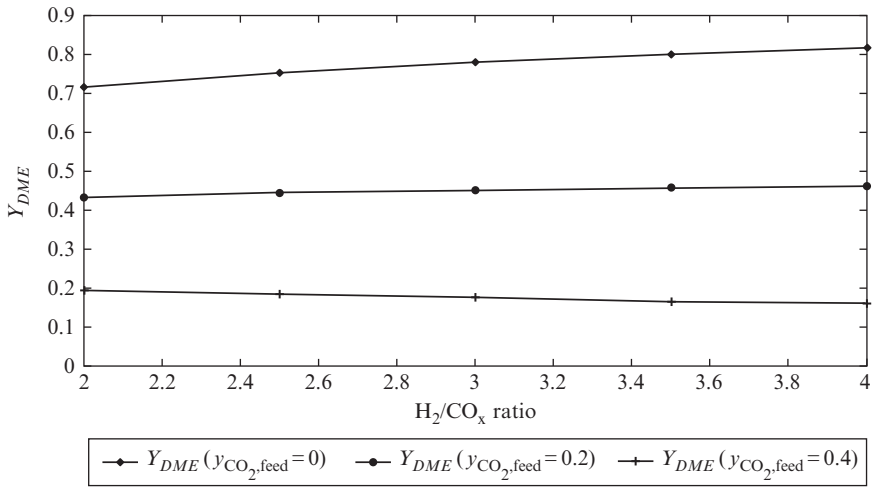

Fig. 5.8
DME yield versus inlet H_2/CO_x ratio and inlet feedstock CO_2 content (temperature = 240°C, pressure = 50 bar).

Moreover, the selectivity is slightly negatively affected by the H_2 content in the inlet feedstock: when the CO_2 molar fraction is 0.4, the DME selectivity is 0.796 at $H_2/CO_x = 2$ and 0.698 at $H_2/CO_x = 4$.

On the whole, the reactions' conversions and the DME yield are positively affected by low temperatures, high pressures, and a high H_2/CO_x ratio. Specifically, the negative effect of CO_2 on all the reactions' performance indices is evident. If a CO_2-rich stream must be fed to the one-step DME synthesis reactor, new solutions are needed to avoid limited conversions and production of DME.

3 Methanol/DME Synthesis Membrane Reactor Application

When a CO_2-rich stream is fed, a membrane reactor may be the best solution for improving the performance of a methanol or DME synthesis process.

As mentioned earlier, if a membrane selective to water steam is placed in a reaction's environment, the steam accumulated because of the r-WGS can be avoided, and the methanol and DME production reactions can always be supported, thanks to the low water content in the reaction's environment.

The following section presents the concept of a membrane reactor; then state-of-the-art technology related to water selective membranes is assessed, and membranes suitable for the production of methanol and DME are suggested.

3.1 Membrane Reactor Concept

A membrane reactor is a physical reactor in which a membrane selective to one or more products of a chemical reaction is installed. The basic concept is that removing a product of a reaction makes it possible to overcome a reaction's thermodynamic limits, because accumulation of products in the reactor is avoided.

The methanol synthesis process consists of reactions (5.1)–(5.3). The removal of water supports the CO_2 hydrogenation reaction (5.2), thus producing methanol and, simultaneously, the r-WGS with the conversion of CO_2 in CO, followed by the production of methanol via CO hydrogenation (5.1).

For the DME synthesis process, removing water from the catalyst promotes both CO_2 hydrogenation (5.4), with the production of methanol, and methanol dehydration (5.6), with the synthesis of DME.

In both cases, the removal of water makes it possible to overcome the stringent thermodynamic limits of the chemical processes, along with a significant positive effect on the reaction's conversion and on the CH_3OH or DME yield and selectivity.

The selective membrane can be installed in a chemical process in two potential configurations (De Falco et al., 2011a,b):

- Directly inside the reactor (integrated membrane reactor)
- By assembling a traditional catalytic reactor with an external separation module where the outlet reactor stream is cleaned and then fed to the next reaction step (staged membrane reactor)

An integrated membrane reactor performs better because the simultaneity of the reactions and the water removal leads to high conversions in a compact membrane reactor, as reported by De Falco et al. (2011a,b). On the other hand, integrating the selective membrane directly into the reaction's environment places thermal and mechanical stress on the membrane, which must be selected according to stringent operating conditions.

In the following section, proper water selective membranes able to operate at temperatures ranging from 200 to 300°C and at a transmembrane pressure difference of approximately 5–10 bar are presented and described.

3.2 Steam Water Selective Membranes Selection

In order for a membrane to be integrated in a methanol or DME synthesis reactor, it must have the following properties:

- Stability at the processes' operating temperatures (200–300°C)
- Stability at a transmembrane pressure difference of at least 5–10 bar in order to ensure a large fluctuation in water permeation
- High water selectivity, in particular, high water to hydrogen selectivity (>10)
- High water permeance ($>10^{-7}$ mol s^{-1} m^{-2} Pa^{-1})

Traditionally, steam water selective membranes are applied in processes such as water desalination, natural gas or air dehydration, and dehydration of organic compounds by pervaporation, which are all low-temperature processes ($T < 150$°C). Therefore the number of hydrophilic membranes developed for higher temperatures are limited.

Rohde et al. (2008) presented a detailed analysis on state-of-the-art applications of high-temperature water selective membranes (the Fischer-Tropsch process) characterized by operating conditions similar to those of the methanol/DME synthesis process. High temperature hydrophilic membranes were placed in three main categories:

1. Microporous zeolite membranes
2. Amorphous microporous membranes
3. Polymeric membranes

Both the polymeric membranes and the amorphous microporous membranes perform poorly at the processes' operating temperatures: for the polymeric membranes, water permeance is 4×10^{-8} mol s^{-1} m^{-2} Pa^{-1} at 200°C and H_2O/H_2 selectivity is <10 at 250°C, as reported by Struis and Stucki (2001); the amorphous microporous membranes are characterized by a permeance always $<10^{-7}$ mol s^{-1} m^{-2} Pa^{-1} and low H_2O/H_2 selectivity (<10) at temperatures >200°C, as reported by Lee et al. (2006).

Therefore the only type of membrane that can be applied in the methanol/DME production process is the microporous zeolite membrane, which is able to reach H_2O permeance ranging from 10^{-7} to 10^{-6} mol s^{-1} m^{-2} Pa^{-1} and a H_2O/H_2 selectivity >10 at a temperature of 250°C (Rohde et al., 2008).

The equation that regulates the flow of steam that permeates through the membrane is reported as

$$J_{H_2O} = Perm_{H_2O}\left(p_{H_2O} - \overline{p}_{H_2O}\right) \tag{5.16}$$

where p and $\overline{p}$ are the partial pressure in the retentate and permeate sides, respectively, and $Perm_{H_2O}$ is the permeance across the membrane. The dependence of water permeance on the temperature can be obtained by extrapolating from the experimental data, for example, those reported by Bernal et al. (2000) for a ZSM5/MFI membrane.

3.3 Membrane Reactor Process Configurations

As previously mentioned, the selective membrane can be applied internally or externally to the chemical reactor. Now we provide a detailed description of both architectures.

In the integrated membrane reactor (IMR) configuration, the reactor consists of two coaxial tubes. The internal tube is the selective membrane through which the water permeates to the inner section, called the permeation zone, where a sweep gas, which can be pure CO_2, is sent to carry out the permeated flux. The external tube is a metallic tube that is placed in contact with a service fluid for the removal of the heat generated by the exothermic reactions. The annular zone between the internal and external tubes is the reaction zone where the catalyst particles are packed and the reactions are supported.

Fig. 5.9 shows a conceptual block diagram of the IMR configuration, as follows:

- A syngas stream is fed to the IMR where it is converted into methanol or DME.
- The steam water that permeates through the selective membrane is carried from the permeation zone by a pure CO_2 stream.
- The reaction zone outlet stream is fed to a condensation unit where the CH_3OH and/or DME + H_2O components condensate and are separated from the gas components (CO, CO_2, H_2), which are recycled to the reactor. The stream from the permeation zone,

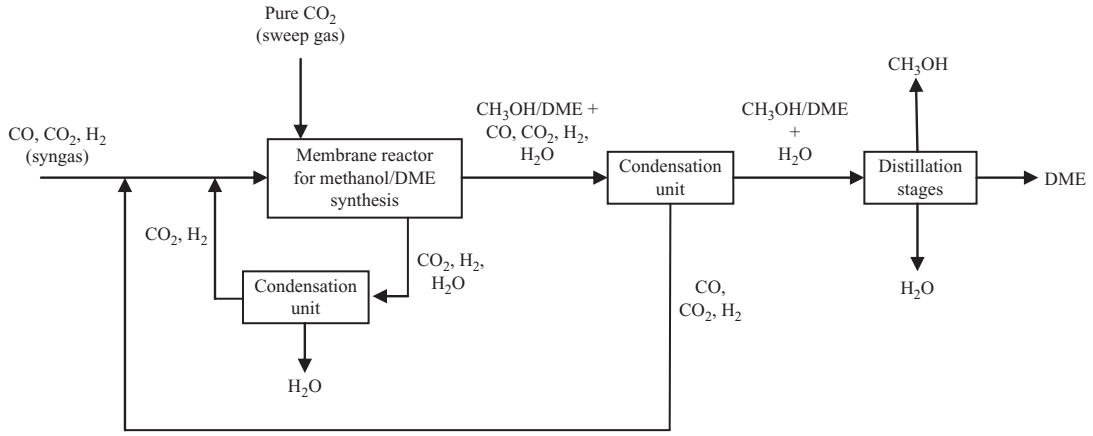

Fig. 5.9
Block scheme of an IMR configuration for methanol/DME production process.

consisting of the sweep gas CO_2 and the permeated components H_2O and H_2, is fed to a condensation unit where water condensates, while the CO_2 and H_2 are recycled to the membrane reactor.

– The condensed blend (CH_3OH/DME + H_2O) is sent to one or two distillation stages where the components are separated.

For a simulated analysis of the IMR for a DME synthesis process, refer to De Falco et al. (2017). Using a high CO_2 content in the membrane reactor's inlet and by setting optimal operating conditions (inlet temperature = 225°C, operating pressure = 70 bar, $H_2/CO_x = 3$), they found that the DME yield and the X_{COx} were both 75%, whereas the DME selectivity was close to 1, well beyond the thermodynamic limits.

Fig. 5.10 illustrates a similar block diagram for the staged membrane reactor (SMR), which consists of a series of conventional reactor + selective membrane modules.

The process consists of the following steps:

– The syngas stream is fed into the first synthesis catalytic reactor where the methanol or DME production process is supported.
– The outlet stream is sent to a membrane module, where water and an amount of hydrogen are separated and carried out by a pure CO_2 stream.
– The retentate is fed to the second reaction stage where the synthesis reactions are further promoted, thanks to the removal of the steam.
– Note that the number of reaction + separation steps depends on the final conversion target.
– Finally, the outlet stream in the last reactor is fed to the purification unit (condensation + distillation), as for the IMR configuration.

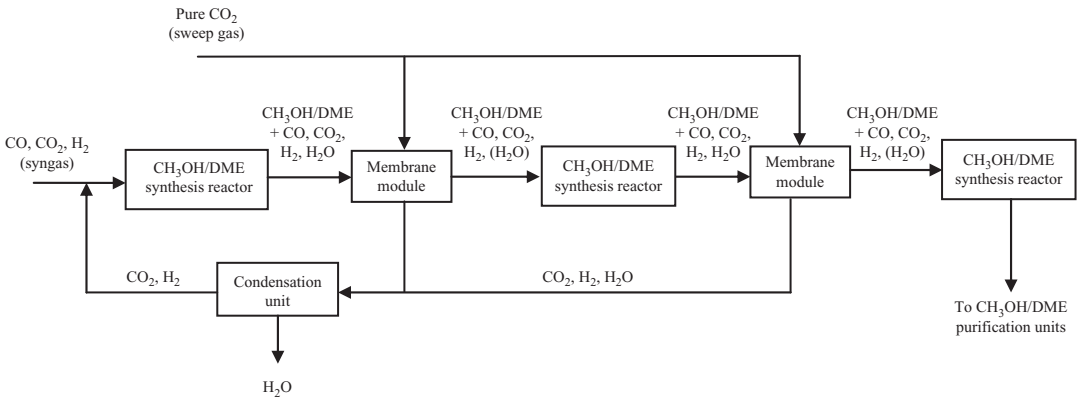

Fig. 5.10
Block scheme of a staged membrane reactor (SMR) configuration for methanol/DME production process.

The benefits of the SMR are mainly twofold:

- Because the membrane is separated from the reactor, the membrane is protected from unsuitable conditions, thus its operation and maintenance are safer.
- The number of reaction + separation steps means that the performance of the final process can be modulated.

4 Conclusions

In this chapter, we studied and analyzed the methanol and DME synthesis processes fed by a CO_2-rich feedstock. Our findings show that the CO_2-rich syngas can be derived from a biological process as fermentation or gasification of biomasses and can be fed to the production processes, thus valorizing the carbon dioxide and generating added-value products such as methanol and dimethyl ether (CO_2 valorization technology).

However, the thermodynamics analysis, which focused on the DME synthesis one-step process, highlighted the strong negative effect of CO_2 inlet composition on the reactions' conversion and DME yield, because of the promotion of the reverse water-gas shift and the subsequent accumulation of steam water in the reactions' environments, with a detrimental effect on the methanol and DME production reactions.

Integrating a membrane selective to water that is able to remove the generated steam may be the best solution for the support of methanol/DME production processes with high CO_2 contents, because this approach avoids the accumulation of water, thus overcoming the thermodynamic thresholds.

The water selective membrane study leads to the conclusion that only microporous zeolites are suitable to operating at the production conditions (200–300°C and 50–70 bar). Moreover, two different plant configurations are proposed: the integrated membrane reactor, where the membrane is directly installed in the synthesis catalytic reactor, and the staged membrane reactor, which consists of a series of reactor + water separation modules.

In order to apply the membrane reactor technology in the industrial methanol/DME processes, the selective membranes must ensure stable and durable performance in terms of water permeance ($>10^{-7}$ mol s^{-1} m^{-2} Pa^{-1}) and H_2O/H_2 selectivity (>10).

References

Arcoumanis, C., Bae, C., Crookes, R., Kinoshita, E., 2008. The potential of di-methyl ether (DME) as an alternative fuel for compression-ignition engines: a review. Fuel 87, 1014–1030.

Bernal, M.P., Piera, E., Coronas, J., Menéndez, M., Santamarìa, J., 2000. Mordenite and ZSM-5 hydrophilic tubular membranes for the separation of gas phase mixtures. Catal. Today 56, 221–227.

Centi, G., Perathoner, S., 2013. Advances in catalysts and processes for methanol synthesis from CO_2. In: De Falco, M., Iaquaniello, G., Centi, G. (Eds.), CO_2: A Valuable Source of Carbon, Green Energy and Technology. Springer-Verlag, London.

Centi, G., De Falco, M., Iaquaniello, G., Perathoner, S., 2013. Strategy and drivers for CO_2 (re)use. In: De Falco, M., Iaquaniello, G., Centi, G. (Eds.), CO_2: A Valuable Source of Carbon, Green Energy and Technology. Springer-Verlag, London.

Chen, W.H., Lin, B.J., Lee, H.W., Huang, M.H., 2012. One-step synthesis of dimethyl ether from the gas mixture containing CO_2 with high space velocity. Appl. Energy 98, 92–101.

De Falco, M., Capocelli, M., Basile, A., 2017. Selective membrane application for the industrial one-step DME production process fed by CO_2 rich streams: modeling and simulation. Int. J. Hydrog. Energy 42, 6771–6786.

De Falco, M., Iaquaniello, G., Salladini, A., 2011a. Reformer and membrane modules (RMM) for methane conversion: experimental assessment and perspectives of such novel architecture. ChemSusChem 4, 1157–1165.

De Falco, M., Iaquaniello, G., Salladini, A., 2011b. Experimental tests on steam reforming of natural gas in a reformer and membrane modules (RMM) plant. J. Membr. Sci. 368, 264–274.

De Falco, M., Giansante, S., Iaquaniello, G., 2013. Methanol production from CO_2 via reverse water gas shift reaction. In: De Falco, M., Iaquaniello, G., Centi, G. (Eds.), CO_2: A Valuable Source of Carbon, Green Energy and Technology. Springer-Verlag, London.

De Falco, M., Capocelli, M., Centi, G., 2016. Dimethyl ether production from CO_2 rich feedstocks in a one-step process: thermodynamic evaluation and reactor simulation. Chem. Eng. J. 294, 400–409.

De Santis, R., 1980. Introduzione al Calcolo degli Equilibri di Fasi Fluide. ESA.

Fleisch, T.H., Basu, A., Sills, R.A., 2012. Introduction and advancement of a new clean global fuel: the status of DME developments in China and beyond. J. Nat. Gas Sci. Eng. 9, 94–107.

Kang, S.W., Bae, J.W., Jun, K.W., Potdar, H.S., 2008. Dimethyl ether synthesis from syngas over the composite catalysts of Cu-ZnO-Al_2O_3/Zr-modified zeolites. Catal. Commun. 9, 2035–2039.

Khajavi, S., Jansen, J.C., Kapteijn, F., 2010. Application of a sodalite membrane reactor in esterification coupling reaction and separation. Catal. Today 156, 132–139.

Lee, K.H., Youn, M.Y., Sea, B., 2006. Preparation of hydrophilic ceramic membranes for a dehydration membrane reactor. Desalination 191, 296–302.

Park, S.H., Lee, C.S., 2014. Applicability of dimethyl ether (DME) in a compression ignition engine as an alternative fuel. Energy Convers. Manag. 86, 848–863.

Rohde, M.P., Schaub, G., Khajavi, S., Jansen, J.C., Kapteijn, F., 2008. Fischer-Tropsch synthesis with in situ H_2O removal—directions of membrane development. Microporous Mesoporous Mater. 115, 123–136.

Samimi, F., Bayat, M., Karimipourfard, D., Rahimpour, M.R., Keshavarz, P., 2013. A novel axial-flow spherical packed-bed membrane reactor for dimethyl ether synthesis: simulation and optimization. J. Nat. Gas Sci. Eng. 13, 42–51.

Struis, R.P.W.J., Stucki, S., 2001. Verification of the membrane reactor concept for the methanol synthesis. Appl. Catal. A Gen. 216, 117–129.

Wang, L., Fang, D., Huang, X., Zhang, S., Qi, Y., Liu, Z., 2006. Influence of reaction conditions on methanol synthesis and WGS reaction in the syngas-to-DME process. J. Nat. Gas Chem. 15, 38–44.

CHAPTER 6

Direct Methane to Methanol: Historical and Kinetics Aspects

Vladimir Arutyunov[*,†]

[*]*Semenov Institute of Chemical Physics of Russian Academy of Sciences, Moscow, Russia* [†]*Institute of Problems of Chemical Physics of the Russian Academy of Sciences, Chernogolovka, Russia*

Acronyms

CSTR	continuously stirred tank reactor
DMTM	direct metane (conversion) to methanol
OCM	oxidative coupling of methane
POM	partial oxidation of methane
SCMCR	simulated countercurrent moving bed chromatographic reactor

Symbols

P	pressure in atm or MPa
T, T°C	temperature in degees of Celsium
K	temperature in degees of Kelvin
t_r	time of reaction
d	diameter of reactor
τ_{ig}	ignition delay time
τ	time of diffusion
D	diffusion coefficient
D_o	diffusion coefficient under normal conditions
μ_1	first root of the Bessel function
k	rate constant of chemical reaction
W	rate of chemical reaction
φ	branching factor of branched-chain processes
X_A	conversion of reagent A
S_A	selectivity of formation of product A
Y_A	yield of product A
Q	methane flow rate

Methanol. https://doi.org/10.1016/B978-0-444-63903-5.00006-6

1 Introduction

The cost-effective conversion of methane, the dominant and most difficult-to-convert component of natural and associated gas, into chemical products is a major technological challenge. Because of the high thermodynamic stability of the methane molecule, there are very few thermodynamically favorable processes of chemical conversion of methane based on the use of only its own chemical energy without an additional supply, namely oxidation, halogenation, and sulfidation. Therefore, it is no wonder that these processes are considered to be a feasible initial stage of methane functionalization with its subsequent transformation into more valuable products.

Most of the industrial processes of chemical conversion of methane typically involve a complicated, capital- and energy-intensive step of its prereforming to syngas, and, therefore, have a low economic efficiency, which is one of the main constraints limiting the wider use of natural gas as a chemical raw material. That is why the direct conversion of methane into more valuable and high-demand products in some cases seems more appealing than conversion into syngas. Direct conversion to methanol and other oxygenates is among the most attractive and developed processes of functionalization of hydrocarbon gases into chemical products. Since the main product of the direct oxidative conversion of not only methane but also other light alkanes, C_2–C_4, is methanol, the process is traditionally referred to as direct methane to methanol (DMTM).

Extensive research and technological development in the field of direct conversion of natural gas into chemicals has been going on for a century. The reason for the unflagging interest in this problem is twofold. On one hand, the chemical conversion of light alkanes, which are the main components of natural and associated gas, is becoming one of the most important areas of modern petrochemistry, or rather a branched-off, self-contained booming industrial sector known as gas chemistry. On the other hand, it turned out that under certain conditions, the oxidation of even such a simple hydrocarbon as methane manifests a rapidly increasing complexity of the chemical system, which generates a virtually infinite variety of products ranging from water and carbon oxides to complex carbon-containing compounds up to fullerenes and carbon nanotubes. Thus, though studying the oxidation of methane and its closest homologues provided the main body of experimental data for the development of modern concepts of the kinetics of gas-phase reactions, even now these processes remain far from being perfectly understood, appearing almost as deep and endless as nature itself.

The direct conversion of methane to methanol (and to a lesser extent to formaldehyde) is dealt with in the vast majority of scientific studies and technological developments in this area, with the partial oxidation of methane's (POM) heavier homologues being considered only in a limited number of works. Therefore, in what follows we will mainly consider the DMTM process, generalizing it, where possible, to heavier alkanes.

We hope that this material will provide a complete understanding of the characteristics and potential of DMTM and will contribute to the growth of interest in the practical realization of its inherent technological capabilities. A more detailed discussion of the DMTM process can be found in the reviews (Arutyunov et al., 1995a, 1996a; Arutyunov, 2004; Arutyunov and Krylov, 2005) and monographs (Arutyunov and Krylov, 1998; Arutyunov, 2014).

2 Historical Aspects of the DMTM Process

Research on DMTM began at the start of the last century with studies carried out by Bone and coworkers (Bone and Wheeler, 1902, 1903; Bone and Allum, 1932) which demonstrated in principle the possibility of obtaining valuable oxygen-containing products (oxygenates) in the direct oxidation of methane. However, real interest in the problem arose only in the 1920–30s in connection with the advent of industrial processes for production of methanol and other oxygenates by the direct oxidation of natural gas (Walker and Malakoff, 1946; Bludworth, 1949). These were developed empirically, virtually unaffected by research. In the early 1930s, different groups (Yoshikawa, 1931; Newitt and Huffner, 1932; Pichler and Reder, 1933; Newitt and Szego, 1934; Newitt, 1937) almost simultaneously demonstrated the possibility of the occurrence of a high selectivity of the gas-phase oxidation of methane to methanol at high pressures. This has stimulated further efforts to increase the yield of oxygenates and to develop industrial processes for their production by the direct oxidation of natural gas. Along with patents on the catalytic oxidation of methane to oxygenates (formaldehyde, methanol, formic acid, etc.), the first patents were granted on the oxidation of methane to oxygenates at high pressure (Patent of Canada 291411, 1929; Patent US 1776771, 1930).

In a series of studies in the 1930s, Newitt and Huffner (1932), Newitt and Szego (1934), Newitt (1937), and Newitt and Schmidt (1937) thoroughly examined the gas-phase oxidation of methane and other hydrocarbons at high pressures. These studies demonstrated the possibility of obtaining a high yield of alcohols and aldehydes directly by the oxidation of alkanes. In fact, already in the works in the 1930s, a range of optimal conditions for DMTM was identified: high pressure (~100 atm) (Newitt and Huffner, 1932; Newitt and Szego, 1934; Wiezevich and Frolich, 1934), moderate temperature (400–450°C) (Paris, 1934), and a low concentration of oxygen (Pichler and Reder, 1933; Paris, 1934). A realistically achievable selectivity of methanol formation (up to 60%) was established (Newitt and Huffner, 1932; Newitt and Szego, 1934) and some kinetic characteristics of the process were determined: a rapid decline in the selectivity of methanol with increasing oxygen concentration (Pichler and Reder, 1933; Paris, 1934) and a high CO/CO_2 ratio in the products (Bone and Allum, 1932). Since then and up to now, the main goal is to identify conditions that would ensure a stable highest-yield production of the desired product, so that DMTM could compete with other technological processes.

In the 1940s in the United States and Canada, the industrial processes of POM, and then propane, butane, and mixtures thereof, extracted from associated gas and from gases released during oil stabilization and processing became widespread. In fact, it became one of the traditional petrochemical technologies (Asinger, 1958; Sittig, 1962). The subsequent decline of this technology in the late 1950s was associated with the rapid progress of a competing large-capacity technology based on the preconversion of hydrocarbons into syngas and subsequent catalytic synthesis of desired products. Another reason was the development of the market for propane and butane as domestic fuels and raw materials for a number of petrochemical processes, depriving the DMTM technology of a convenient and cheap raw material source. One more factor that contributed to this was associated with serious problems in isolating individual components from a wide variety of products of the nonselective gas-phase oxidation of C_3–C_4 hydrocarbons in the then-existing technologies. An important reason was that the partial oxidation technology of that period was based exclusively on the empirical data. A very limited number of fundamental studies and the lack of clear ideas about the mechanism of the process have become a serious obstacle to its technological refinement.

Although research on the POM continued and attempts to introduce new industrial processes such as the production of formaldehyde (Anisonian et al., 1957) were undertaken, none of them has found practical implementation. However, during this period, based on the theory of branched-chain process, developed in the 1930–50s by Semenov and his colleagues (Semenov, 1935), a fundamentally new level of understanding of the mechanism of oxidation of hydrocarbons began to emerge. The results of more than half a century's research on hydrocarbon oxidation and the ensuing ideas about the mechanism of these processes were summarized by Shtern in the monograph (Shtern, 1964).

In the mid-1980s, interest in the direct production of oxygenates from methane reemerged due to the increasing role of natural gas in the global energy sector, the oil crisis of the 1970s, and the need for environmentally friendly motor fuels. The fact that methanol is considered a component of cleaner fuels provided an impetus to a resurgance of interest in the technology of its production. To a considerable extent, interest in DMTM was reinvigorated by the publication of works (Gesser et al., 1985; Gesser and Hunter, 1992) and a number of others in which very high yields of methanol were reported.

In this period, the revival of interest in the problem of the direct oxidation of methane manifested itself in the almost simultaneous publication of a large group of review papers (Garcia and Loffer, 1984; Gesser et al., 1985; Foster, 1985; Pitchai and Klier, 1986; Sinev et al., 1989; Brown and Parkyns, 1991; Mackie, 1991). However, these reviews were devoted mainly to the catalytic oxidation of methane, reflecting the traditional focus on thermodynamic equilibrium catalytic processes and the absence at the time of clear ideas about the real mechanism of the DMTM process. Except for Gesser et al. (1985), they do not contain new data, being largely based on a compilation of the results of previous work.

The works (Arutyunov et al., 1995a, 1996a; Arutyunov, 2004) and monographs (Arutyunov and Krylov, 1998; Arutyunov, 2014) we published later summarized the available literature data based on the existing theoretical understanding of the mechanism of gas-phase DMTM. The problem of kinetic modeling of the homogeneous-heterogeneous oxidation of light alkanes was discussed in Sinev et al. (2007).

An important issue of the DMTM-based technologies is the assessment of their economic viability. According to the available economic assessments, for the DMTM process to successfully compete with the traditional technologies, it is necessary that, at a reasonable conversion of 7.5%–10.0%, the selectivity of methanol formation S_{CH3OH} (or the total of organic products) should be greater than 70% (Edwards and Foster, 1986; Foulds and Gray, 1995). However, until now, most of the experimental studies, the conditions of which can be transferred to the industrial scale, have shown that, at a methane conversion of more than 5%, the selectivity S_{CH3OH} of methanol formation does not exceed 50% (Arutyunov, 2014). Nevertheless, even these results offer real prospects for technological implementation. Although a number of works, for example, (Gesser et al., 1985; Gesser and Hunter, 1992), reported higher values of S_{CH3OH}, up to 60%–80%, they have not been reproduced by other researchers, and therefore, can hardly be regarded as credible.

To date, there are dozens of published experimental studies on the gas-phase POM, ethane, and their heavier homologues to oxygenates. Reactors of various types, including static reactors, perfect mixing reactors, and flow reactors of various sizes with a gas flow rate from a few liters to 1000 m^3/h and a diameter of 5–30 mm were used. The pressure range covered reaches thousands of atmospheres. In addition to the main parameters of the process, such as pressure, temperature, flow rate, and the mixture composition, the effects of reactor surface material, heterogeneous catalysts, homogeneous promoters, and a variety of physical methods of initiation of the process have been studied. Experiments have been performed with both premixed reagents and with those fed separately into the reactor. Preheated and cold gases have been introduced into the heated reactor. The oxidants were oxygen and air. A summary of the experimental conditions and the results of the most reliable and meaningful studies on DMTM is presented in Arutyunov (2014).

3 Key Features of the DMTM Mechanism

3.1 Oxidation of Methane at Moderate Temperatures

Now, when a complete picture of the DMTM mechanism is available, it is worthwhile to preface the discussion of the experimental results with a general theoretical outline of the process. The theoretical basis of oxidative gas chemical processes is the mechanism of the partial oxidation of rich hydrocarbon-oxygen mixtures. In contrast to the mechanism of the complete oxidation (combustion) of lean and stoichiometric mixtures of hydrocarbons,

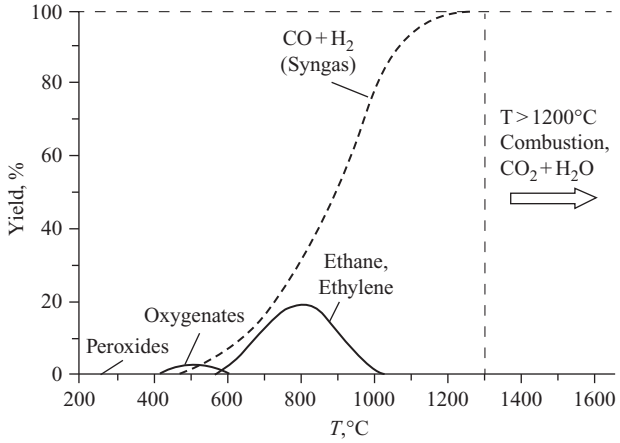

Fig. 6.1

Temperature ranges of formation and the yields of the main products of partial methane oxidation.

long-used in energetics and well studied, the above mechanism remains insufficiently studied. The core of this mechanism is the kinetics of the oxidation of hydrocarbons at medium temperatures, from ~300°C to ~1200°C (Fig. 6.1), that is well below typical combustion temperatures.

The difference between combustion and partial oxidation is of a fundamental nature. It is determined not only by a difference in the temperatures of the processes but, above all in their mechanisms. One of the main distinguishing features of the mechanism of the partial oxidation of alkanes in the medium temperature range is the significant role of peroxide compounds and radicals. At the low-temperature end of this range, a key role is played by $ROO^{\bullet}$ radicals and ROOH and R_1OOR_2 molecules (for methane, respectively, $CH_3O^{\bullet}$ and CH_3OOH), whereas at high temperatures, it belongs to the $HOO^{\bullet}$ radical and HOOH molecule. At the same time, the role of O, CH, CH_2, and C_2, as well as excited molecules, species important in the combustion processes, is insignificant in the partial oxidation.

In various regions of the indicated temperature range in which methane oxidation processes have been investigated more fully, different products dominate (Fig. 6.1). Note that, in moving toward higher temperatures, more and more thermodynamically stable products become abundant, with their maximum yield increasing monotonically, reaching almost 100% for syngas. An important feature of this region is that, at these temperatures, the processes on the surface of the heterogeneous catalyst and reactor walls compete successfully with those in the gas phase. Therefore, regardless of whether the catalyst is present, heterogeneous processes must be taken into account (Arutyunov and Strekova, 2017). However, despite a great diversity of conditions and products, we believe that, at present, the totality of processes of the POM at medium temperatures can be described on the basis of a single homogeneous-heterogeneous kinetic mechanism (Arutyunov and Krylov, 1998; Sinev et al., 2007).

In accordance with the dominance of particular products, the considered medium temperature range can be divided into three main subranges: preferential formation of oxygenates (DMTM, $T = 300–600°C$), oxidative coupling of methane (OCM) with preferential formation of C_2 hydrocarbons ($T = 600–900°C$), and POM to syngas ($T > 900°C$) (Fig. 6.1). This division corresponds to the significant changes in the kinetic mechanism with the changing temperature of the process.

The first, most difficult, and most energy-consuming step of any process of methane oxidation is obviously its activation, that is the rupture of the C—H bond to form $H^{\bullet}$ and $CH_3^{\bullet}$. However, depending on the conditions, the fate of methyl radicals, which determine the kinetics of the entire process, can vary greatly. At temperatures below 600°C, methyl radicals largely reversibly combine with molecular oxygen to form methylperoxy radicals

$$CH_3^{\bullet} + O_2 \Leftrightarrow CH_3OO^{\bullet} \tag{6.1}$$

which play a key role in the formation of oxygenates. At these temperatures, especially at elevated pressures, the equilibrium of reaction (1) is strongly shifted to the right, which gives rise to a sequence of reactions that lead to a preferential formation of oxygenates. However, at temperatures above 600°C, the equilibrium of reaction (1) shifts to the left and its role rapidly decreases (Fig. 6.2, left curve).

At the same time, the endothermic reactions of oxidation of methyl radicals

$$CH_3^{\bullet} + O_2 \rightarrow CH_3O^{\bullet} + O^{\bullet\bullet} \tag{6.2}$$

$$CH_3^{\bullet} + O_2 \rightarrow CH_2O + OH^{\bullet} \tag{6.3}$$

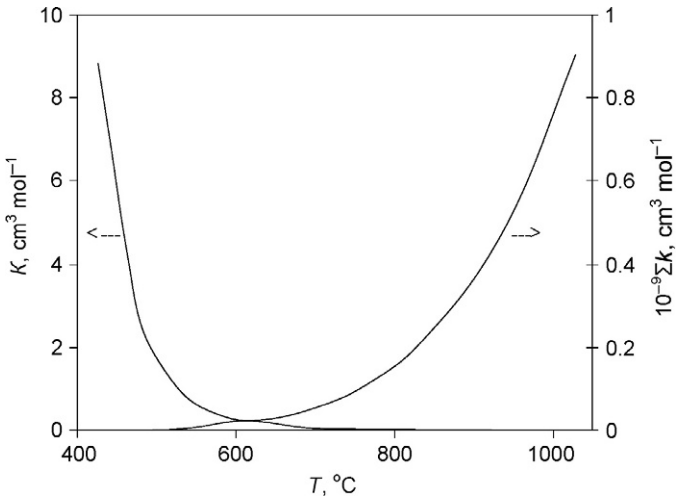

Fig. 6.2

Temperature range for the oxidative conversion of methane (Sinev et al., 2007). The left curve is the temperature dependence of the equilibrium constant of reaction (6.1). The right curve is the temperature dependence of the sum of rate constants of reactions (6.2) and (6.3).

at temperatures below 900°C are too slow (Fig. 6.2, right curve). Therefore, in the temperature range from 600°C to 900°C, known as the "ethylene window," despite a significantly higher concentration of oxygen compared to that of methyl radicals, the main channel for the consumption of methyl radicals is their recombination

$$CH_3^{\bullet} + CH_3^{\bullet} \rightarrow C_2H_6 \tag{6.4}$$

with the formation of ethane and then ethylene, OCM products. Above 900°C, reactions leading to products of deeper methane oxidation, including reactions (6.2) and (6.3) proceed at a sufficiently high rate, to eventually form carbon monoxide and hydrogen, that is, syngas (Sinev et al., 2007).

In accordance with these features of the mechanism of partial oxidation, it is currently applied to simulate three groups of processes: DMTM, OCM, and POM.

3.2 Mechanism of the Gas-Phase DMTM Process

Up until the 1950s, the DMTM process was studied largely experimentally, with the results being interpreted in terms of prevailing theories at that time. Since the 1970s, when the radical-chain nature of the process was no longer being questioned, even individual, unsystematic experimental data were often used as an occasion to speculate on the details of the mechanism. The situation changed dramatically with the advent of computer methods for the kinetic simulation of complex mechanisms, composed of dozens of species and hundreds of elementary reaction steps. Kinetic simulations of this complex nonlinear process showed a close coupling of the multitude of parallel processes of interconversion of intermediates.

The first and one of the most successful attempts at a kinetic analysis of the DMTM mechanism was apparently undertaken in a series of papers by Vedeneev et al. (1988a,b,c,d). A relatively compact but sufficiently complete model proposed in these works enabled the understanding of the specifics of this process while also describing its kinetics. The subsequent outline of the main kinetic features of the DMTM process largely relies on the analysis performed in this series of studies as well as on the subsequent research based on this model (Arutyunov et al., 1996c). Of the more recent works on simulating DMTM, it is worthwhile to mention (Chun and Anthony, 1993; Casey et al., 1994; Hunter et al., 1994; Vedeneev et al., 1994; Lødeng et al., 1995; Arutyunov et al., 1996b,c; Rasmussen et al., 2008; Rasmussen and Glarborg, 2008).

Currently, it is reliably established that methane oxidation at moderate temperatures, $T < 600$°C, occurs mainly through the intermediate formation of methylperoxy radicals $CH_3O_2^{\bullet}$

$$CH_4 \rightarrow CHCH_3^{\bullet} \rightarrow CH_3O_2^{\bullet} \tag{6.5}$$

Based on the mechanism proposed in Vedeneev et al. (1988a,b,c,d), it has been established that an important role is played n by the interaction of these radicals with molecular products, yielding peroxide compounds that, while decomposing, provide an effective chain branching in this reaction. No less important are radical-radical reactions involving $CH_3O_2^{\bullet}$·

In addition to temperature, an important parameter in the oxidation of hydrocarbons is pressure. An increase in the pressure affects gas-phase reactions for several reasons. As the pressure increases, so does the frequency of intermolecular collisions and, accordingly, the rate of the process, a factor that makes it possible to reduce the reaction temperature. This, in turn, opens up the possibility of "survival" of some intermediate products that otherwise would decompose or experience further transformations. The pressure also shifts the equilibrium of reversible reactions, the most important of which in the oxidation of hydrocarbons at such moderate temperatures are reactions of the type

$$R + O_2 \Leftrightarrow RO_2 \tag{6.6}$$

A change in the pressure may lead to an increase in the yield of radical recombination products and deactivation of the excited molecules. Finally, pressure is a critical factor for the branched-chain reactions.

The characteristics of methane oxidation at high pressures are determined by the initial stage of the process (Table 6.1), the mechanism of which was analyzed in detail in Vedeneev et al. (1988a,b,c,d). The reactions listed in Table 6.1 explain the formation of the main oxidation products, such of methanol, formaldehyde, and water, but does not account for their further transformation, since only the initial stage of the process is considered.

Table 6.1 The mechanism of the initial stage of the DMTM process

Initiation:

$$CH_4 + O_2 \xrightarrow{(I)} CH_3^{\bullet} + HO_2^{\bullet} \longrightarrow CH_3O_2^{\bullet}$$

Branching:

$$CH_3O_2^{\bullet} + \begin{cases} CH_4 & \xrightarrow{(II)} \\ CH_2O & \xrightarrow{(III)} \\ CH_3OH & \xrightarrow{(IV)} \\ H_2O_2 & \xrightarrow{(V)} \end{cases} CH_3OOH \xrightarrow{(VI)} CH_3O^{\bullet} + OH^{\bullet}$$

$$HO_2^{\bullet} + \begin{cases} CH_4 & \xrightarrow{(VII)} \\ CH_2O & \xrightarrow{(VIII)} \\ CH_3OH & \xrightarrow{(IX)} \end{cases} H_2O_2 \xrightarrow{(X)} OH^{\bullet} + OH^{\bullet}$$

Propagation:

$$CH_3O_2^{\bullet} + HO_2^{\bullet} \xrightarrow{(XI)} CH_3OOH + O_2$$

Termination:

$$CH_3O_2^{\bullet} + CH_3O_2^{\bullet} \begin{cases} \xrightarrow{(XII)} 2CH_3O^{\bullet} + O_2 \\ \xrightarrow{(XIII)} CH_2O + CH_3OH + O_2 \end{cases}$$

$$HO_2^{\bullet} + HO_2^{\bullet} \xrightarrow{(XIV)} H_2O_2 + O_2$$

$$CH_3O_2^{\bullet} \xrightarrow{(XV)} \text{heterogeneous termination}$$

Nevertheless, an analysis of Table 6.1 makes it possible to interpret the basic qualitative features of the DMTM process, although its quantitative description definitely requires using much more complex models that would take into account the totality of homogeneous and heterogeneous elementary steps important under the specified conditions, constructed according to the principle of an "open model." This means that the model includes all the relevant elementary steps and, at the same time, is open to the inclusion of new steps if necessary, with all the kinetic parameters being taken from independent databases, which can be modified only based on proper recommendations.

An analysis of the short model from Table 6.1 shows that the sequence of reactions (II) and (VI) leads to chain branching. In principle, branching occurs when hydrogen peroxide decomposes to $OH^{\bullet}$ radicals. However, in analyzing the initial stage, because of the characteristic long time of this process, exceeding 10^3 s under typical DMTM conditions, branching via reaction (X) can be disregarded. At high pressures, due to a slow diffusion of radicals to the reactor walls and a high concentration of methane, the branching rate always exceeds the rate of heterogeneous termination:

$$\varphi = k_{\mathrm{II}}[\mathrm{CH_4}] - k_{\mathrm{XV}} > 0 \tag{6.7}$$

Therefore, at the initial stage, the process develops according to a branched-chain mechanism, with the exponential increase of the concentration of radicals and, consequently, the reaction rate. Since the relationship

$$k_{\mathrm{VI}}[\mathrm{CH_3OOH}] \geq k_{\mathrm{II}}[\mathrm{CH_4}]\,[\mathrm{CH_3OO^{\bullet}}] \tag{6.8}$$

usually holds, that is the rate of decomposition of methyl hydroperoxide is higher than the rate of its formation, with the branching rate being controlled by the interaction of the methylperoxy radical with methane. Thus, at the initial stage, the kinetics of the process are mainly determined by reactions (I), (II), (VI), and (XV) (given in the parentheses are the subsequent fast reactions of radicals, which do not limit processes of their conversion):

$$\begin{aligned}
&\mathrm{CH_4 + O_2 \rightarrow CH_3^{\bullet} + HO_2^{\bullet}} \quad \left(\mathrm{CH_3^{\bullet} + O_2 \rightarrow CH_3OO^{\bullet}}\right)\\
&\mathrm{CH_3OO^{\bullet} + CH_4 \rightarrow CH_3OOH + CH_3^{\bullet}}\\
&\mathrm{CH_3OOH \rightarrow CH_3O^{\bullet} + OH^{\bullet}} \quad \left(\mathrm{OH^{\bullet} + CH_4 \rightarrow H_2O + CH_3^{\bullet}}\right)\\
&\mathrm{CH_3OO^{\bullet} \rightarrow \text{termination}}
\end{aligned} \tag{6.9}$$

However, the initial exponential autoacceleration of the reaction does not lead to an explosion, as in most other branched-chain reactions, due to the rapid growth of the rate of quadratic recombination of CH_3O_2 radicals (negative interaction of chains, nonlinear termination of chains) in reaction (XIII). Therefore, after the initial stage, the process becomes quasistationary, remaining so for some time (Fig. 6.3).

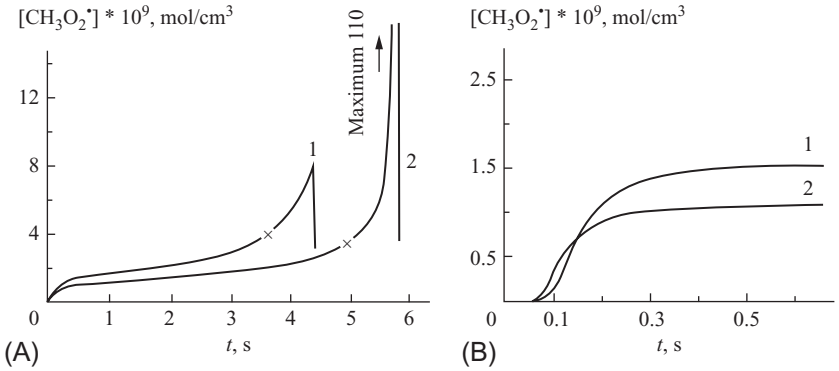

Fig. 6.3

Calculated time histories of the $CH_3O_2^{\bullet}$ radical concentration for (A) the process as a whole and (B) the first stage and beginning of the second at $P_{CH4} = 82$ atm, $T = 406°C$ and (1) $P_{O2} = 1.8$ atm and (2) $P_{O2} = 8.5$ atm (Vedeneev et al., 1988a,b,c,d).

The mechanism listed in Table 6.1 includes the most important reactions of the quadratic interaction of radicals, since throughout almost all stages of the reaction the concentration of methylperoxy and hydroperoxy radicals are commensurate and orders of magnitude higher that those of all other radicals.

The initial autoacceleration of the reaction is complete within a very short time (Fig. 6.3) at a negligibly small conversion of the reactants, and therefore is inaccessible to experimental observation. Note that the induction periods experimentally observed in the oxidation of methane at high pressures actually correspond to a steady-state branched-chain process, which is characterized by an approximate equality of the rates of chain-branching reactions (II)–(IX) and quadratic chain-termination reactions (XIII)–(XIV). Already at the initial stage of the reaction, a large number of various intermediates and almost all major stable molecular products are formed.

As the molecular products accumulate, the rates and contribution of the processes they are involved in increase, which leads to the gradual increase of the branching rate. At some point (marked with an "x" in Fig. 6.3), the steady-state mode gives way to the rapid growth of the rate of the process until the oxygen is consumed completely. This particular moment is typically considered as the end of the induction period, although it corresponds only to a change in the set of main chain-branching reactions (from reaction (II) to reactions (III)–(V)). The rapid growth rate of the process after the onset of the steady-state mode is, in fact, the return to the branched-chain reaction mode, not in methane-oxygen but in a more complex mixture containing, along with methane, appreciable concentrations of more reactive products, such as alcohols, aldehydes, and peroxides.

The model presented in Vedeneev et al. (1988a,b,c,d) enabled not only the qualitative description of almost all the main characteristics of the DMTM process, but also a number of

predictions experimentally confirmed later, which is of particular value. Of course, this model requires a serious refinement of the values of the rate constants and a gradual transformation into a full "open model" (Sinev et al., 2007). However, any model to replace it should at least give an adequate explanation of the phenomena that received a reasonable explanation in the framework of the previous model.

3.3 Main Kinetic Features of the DMTM

A kinetic analysis made it possible to interpret numerous, sometimes contradictory experimental results on the characteristics of the DMTM process in terms of a unified concept. At present, the POM at high pressure was reliably demonstrated to be a degenerate branched-chain process with a very short chain length and a long induction period. Branching is provided by a number of parallel pathways that lead to the formation and subsequent decomposition of the CH_3OOH and HOOH peroxides. Table 6.1 lists the reactions that play the most important role at the initial stage of the process, before the accumulation of high concentrations of intermediates.

The process consists of three major stages (Fig. 6.3). The oxidation begins as a typical branched-chain reaction with a pronounced exponential growth of radical concentrations with time. However, the accumulation of methylperoxy radicals $CH_3O_2^{\bullet}$ is soon completed due to an intense quadratic chain termination of these radicals, mostly through the recombination reaction (XIII) in Table 6.1.

$$CH_3OO^{\bullet} + CH_3OO^{\bullet} \rightarrow CH_3OH + CH_2O + O_2 \qquad (6.10)$$

In the second stage, which can be characterized as a steady-state branched-chain reaction in which chain branching is nearly counterbalanced by the quadratic removal of active species, intermediates gradually accumulate, especially formaldehyde and methanol, accompanied by a slow heating of the reaction mixture. When the critical concentration of these products, considerably more reactive than methane, reaches a critical point, the third stage sets in, manifesting itself through an explosive self-acceleration of the reaction. This is now due to the branching caused by the interaction of methylperoxy radicals with the products and by the heating of the mixture, resulting in a complete conversion of the oxygen. The quadratic interaction of methylperoxy radicals providing the onset of the steady-state branched-chain mode of the process can be seen as its most prominent feature. The first two stages can be regarded as an induction period of the ignition that occurs at the third stage due to an increase in the rate of branching during the interaction of peroxy radicals with the products formed at the second stage.

Nonlinear processes of interaction of chains give rise to two steady-state oxidation modes: simple-chain and branched-chain oxidation, with a critical transition between them caused by a

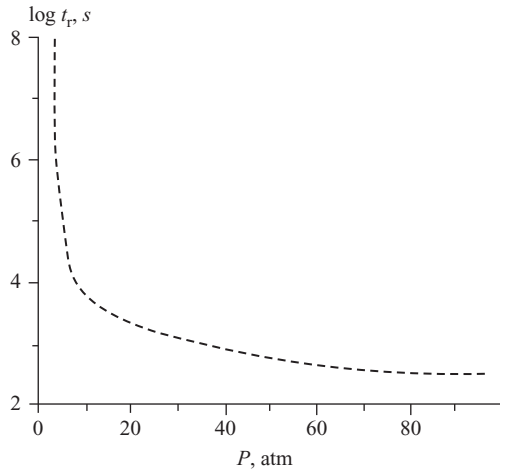

Fig. 6.4
Calculated pressure dependence of the reaction time t_r at $T = 650$ K (Vedeneev et al., 1994).

change in the reaction conditions, especially the pressure, with the rates of the two modes differing by a factor of $\sim 10^4$ (Fig. 6.4).

An increase in pressure transfers the reaction from a slow simple-chain mode to a much faster steady-state branched-chain mode and provides a further increase in the oxidation rate. The onset of a fast branched-chain steady-state reaction is the main factor that makes it possible to realize a noncatalytic gas-phase process and to create, on its basis, a stationary technological process. The steady-state branched-chain mode provides a noncatalytic reaction at relatively low temperatures, whereas the absence of the catalyst minimizes the effect of heterogeneous processes, which tend to produce deep oxidation products. Along with the critical transition between oxidation modes, other manifestations of the nonlinear nature of the DMTM process were found, such as cold flames, a negative temperature coefficient region, a temperature hysteresis of the reaction rate, and oscillatory modes (Arutyunov, 2014).

An important feature of the DMTM process demonstrated by kinetic simulations and confirmed experimentally is the decrease of its rate with increasing oxygen concentration. Thus in this oxidation process, oxygen behaves as an inhibitor, which is one of the factors that dictates the need for a low initial concentration of oxygen to provide a high rate for the process.

Simulations of the process also showed that an important aspect in achieving a high yield of oxygenates is to minimize heating of the initial mixture, that is to carry out the process in a quasi-isothermal mode. This is due to the fact that a temperature rise not only promotes secondary reactions, converting oxygenates already formed, but also reduces the rate of their formation, shifting the equilibrium to the left in reaction (6.1) (Arutyunov and Krylov, 1998; Arutyunov, 2014).

3.4 Catalysis and Promotion of the DMTM Process

A significant period in DMTM studies was dominated by traditional ideas about the possibility of increasing the selectivity of formation of desired products by selecting a proper catalytic system. Dozens of experimental studies have been conducted, the results of which are reflected, for example, in the reviews Foster (1985), Pitchai and Klier (1986), Sinev et al. (1989), Brown and Parkyns (1991), Krylov (1992), Arutyunov and Krylov (2005). Elucidation of the role of homogeneous and heterogeneous phases in this process and of the real possibilities of its promotion by catalysts and various physical methods has become one of the most important results of the kinetic modeling of DMTM.

Although reliably achievable selectivities of formation of CH_3OH and CH_2O in catalytic processes have not reached values of interest for practical applications (Tabata et al., 2002) and, at best, only approach the performance of the homogeneous process, such attempts are continuing. The authors of these studies do not take into account the main feature of the DMTM process: it is a branched-chain steady-state reaction occurring at such a high rate that the presence of a catalyst has no appreciable effect on its kinetics. In this case, the rate of generation of radicals is determined not by slow processes of thermal formation in the bulk or at a surface, but by a much faster process of chain branching, the rate of which is about 10^4 times greater than the rate of the initiation reactions (Arutyunov et al., 1996a; Arutyunov, 2004, 2014). Under these conditions, the catalyst can have a significant effect on the kinetics only if the rate of generation of radicals at the surface is comparable to the rate of their generation by the branched-chain reaction.

Kinetic simulations (Vedeneev et al., 1997; Arutyunov et al., 1999) have shown that, under typical DMTM conditions, an increase in the rate of formation of methyl radicals W_{eff} at the catalyst reduces the induction period and increases the methanol yield only if it exceeds the rate of their thermal generation W_{therm} in the gas phase by at least four orders of magnitude (Fig. 6.5). That is, it must exceed the rate of generation of methyl radicals in the gas-phase chain branching reactions.

If the rate of the additional generation of methyl radicals W_{eff} exceeds the rate of their thermal generation W_{therm} by less than 10^4-fold times, the additional formation of radicals has little effect on the process. However, near $\log(W_{\text{eff}}/W_{\text{therm}}) = 5$, a sharp reduction in the reaction time occurs, accompanied by an increase in the methanol yield. It is estimated that the maximum increase in the methanol yield due to an additional generation of methyl radicals can reach ~50%. However, this is achievable only if the rate of additional radical generation exceeds the rate of their thermal generation by about 10 orders of magnitude, which seems to be unrealistic.

Therefore, kinetic simulation showed a low probability of the creation of such a catalyst system that could really compete with the branched-chain DMTM process. In the "high-pressure"

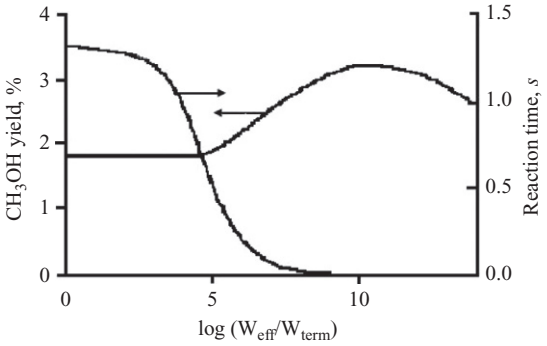

Fig. 6.5

Dependence of the calculated methanol yield and reaction time t_r on the ratio of the effective homogeneous generation rate of $CH_3^{\bullet}$ radicals to the rate of their thermal formation in the gas phase W_{eff}/W_{therm} at $T=410°C$, $P=100$ atm, and $[CH_4]/[O_2]=19$ (Arutyunov et al., 1999).

mode, introduction of a catalyst is not only useless but usually has a negative effect. This is because, concurrently with enhancing radicals generation, it increases the rate of their heterogeneous decay and, additionally, activates the decomposition of reaction products formed. Thus, simulations explain the low efficiency of heterogeneous catalysts in the DMTM process by their inability to compete with the branched-chain reaction in the gas phase.

All this fully applies to the other chemical and physical methods of initiation, which has seen a large number of attempts being undertaken in DMTM studies. A motivation for these efforts has been the known fact of an increase in the rate of the gas-phase oxidation of methane to formaldehyde at low pressures in the presence of nitrogen oxides (Layng and Soukop, 1928; Bibb and Lucas, 1929; Anisonian et al., 1957). Indeed, upon addition of NO_2, the induction period for the slow oxidation of methane and other alkanes at low pressures shortens and, starting from a certain NO_2 concentration, disappears completely, although the qualitative and quantitative composition of the oxidation products remains unchanged. Note, however, that the promotion effect manifests itself exclusively at low pressures; with increasing pressure, its magnitude becomes less and less pronounced (Takemoto et al., 2001). Even at a pressure of 10 atm, the decrease in the temperature of the process does not exceed 25°C, whereas the selectivity in oxygenates turns out to be practically independent of the NOx concentration. The selectivity of methanol formation (at a 4% methane conversion) in the presence of NOx is the same 30% as in the absence of promotion. This is consistent with the concepts of a nonessential role of additional initiation in the branched-chain mode, which sets in at high pressures. Nevertheless, efforts to promote the DMTM process continue, as can be judged from numerous studies on the topic.

Heavier homologues of methane have been considered as promoters of its oxidation, minor additives of which significantly reduce the reaction temperature without significantly affecting the output of basic products. The possibility of initiating the POM with ozone in a flow reactor

at $P \approx 1.5$ atm was examined in Zhu et al. (1993). Although ozone markedly promotes the reaction and increases the yield of methanol, a selectivity of 42% was achieved only at a methane conversion of less than 1%, which decreased sharply with the increase of conversion.

Hydrogen peroxide is an effective promoter of the oxidation of hydrocarbons with a relatively clear mechanism of chemical action. The initiation of the POM with hydrogen peroxide, the effect of which was also to decrease the process temperature or shorten the induction period, was studied in Eskendirov et al. (1997). In Davis and Schmidt (1999), H_2O_2 turned out to be the most effective of the molecular compounds tested in reducing the ignition delay time, twice outperforming methanol.

The possibility of initiating DMTM by various radicals was also explored (Davis and Schmidt, 1999). The concentration of radicals in the mixture did not exceed 0.1%, the introduction of which, like the introduction of ~2% various molecular promoters, reduced the ignition delay time but produced virtually no effect on the product yield. The nature of radicals introduced played no role, since the gas-phase processes quickly convert radicals into each other.

The most extensive study of the effect of different promoters on the DMTM process was carried out in Hunter et al. (1990) at a pressure of 10 atm. The promotional effect of 30 different compounds, including saturated, unsaturated, cyclic, and aromatic hydrocarbons as well as ethers, alcohols, ketones, aldehydes, water, peroxides, sulfur-containing compounds, and amines was studied. Many of these promoters significantly lowered the process temperature. The greatest effect was exerted by diethyl ether, in which an additive in the amount of 3.9% reduced the process temperatures from 402°C to 225°C. Another consequence of the effects of certain promoters was a significant increase in the formaldehyde yield, apparently at the expense of the corresponding decrease in the yield of methanol. In some cases, there was an increase in the selectivity of methanol and/or formaldehyde formation as compared to the unpromoted system. However, this required the introduction of such a large amount of promoter that would make it, in fact, one of the reagents, which radically changes the mechanism of the process and undermines the commercial prospects of increasing methanol output in this manner.

Discussing the promotion of DMTM, one cannot ignore numerous attempts to use physical methods to control its rate and selectivity. Especially numerous are works on microwave and plasmochemical activation of methane, which is probably due to the availability and simplicity of relevant technology, a large number of researchers in the field, and the relatively well-developed physics of gas-discharge processes. Most of the studies on the plasmochemical activation of methane are devoted to its conversion to syngas and oxidative coupling products. Works on the plasmochemical conversion of methane to oxygenates are noticeably scarcer. However, except for the technology for producing a number of thermodynamically equilibrium products (acetylene, syngas), the energy consumption and, accordingly, the economic cost of the gas-discharge and plasmochemical technologies for the conversion of natural gas, especially in light of the real efficiency of conversion of primary energy into the high-potential

energy of an electrical discharge, remains unacceptably high. Thus, it can hardly be expected that these techniques will be able to really compete with the autothermal branched-chain oxidation of natural gas.

4 Parameters of the Process

Although methane oxidation is a complex branched-chain reaction, the ratio between the major DMTM products for typical conditions can be illustrated by the following overall scheme, demonstrating the fundamental nonselectivity of this gas-phase process:

$$2CH_4 + 2O_2 \begin{cases} \nearrow 0.9CH_3OH + 0.1(CH_2O + H_2) \\ \searrow 0.9(CO + 2H_2O) + 0.1(CO_2 + H_2O + H_2) \end{cases} \quad (6.11)$$

With changing parameters, the ratio between the main channels and between the products in each channel can vary several-fold. Note that the scheme does not take into account all products. The main parameters affecting the yield of the products are the pressure, temperature, the CH_4/O_2 ratio, reaction time, and process pattern.

4.1 Effect of Pressure on the Temperature and Rate of the Process

High pressure, along with a low concentration of oxygen, is one of the two principal conditions for achieving a significant yield of alcohols. High pressure not only enhances the selectivity of formation of alcohols, but also reduces the temperature of the process, which contributes to the preservation of the oxygen-containing products formed. Fig. 6.6 shows the pressure

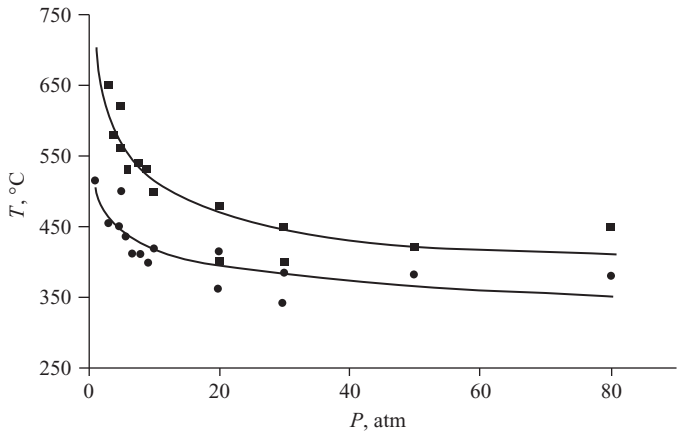

Fig. 6.6

Dependence of the temperatures of (■) onset of conversion and (●) complete oxygen conversion on the pressure plotted based on the data (Burch et al., 1989; Takemoto et al., 2002; Arutyunov et al., 2002).

dependences of the temperature of conversion at the outset and the temperature of complete conversion of oxygen from experiments in a quartz reactor reported in Burch et al. (1989), Takemoto et al. (2002), and Arutyunov et al. (2002). Although the experimental conditions in these works differ somewhat, Fig. 6.6 clearly demonstrates the pressure dependence of the process temperature. As can be seen, the temperature of the process changes most rapidly at low pressures. After 30 atm, this dependence becomes flatter, nearly disappearing above 80 atm. This experimental dependence is consistent with the theoretical dependence of the reaction time on the pressure (Fig. 6.4).

A detailed study of the slow reaction in very rich methane-air mixtures during the ignition delay period in the pressure range of 58–110 atm (Melvin, 1966) showed that auto-ignition occurs at $T \approx 350°C$, well below the auto-ignition temperature at low pressures. Increasing the pressure of an 88% CH_4 + 12% air ($[O_2]/([CH_4]+[O_2]) = 0.028$) mixture in the range from 58–110 atm at $T = 408°C$ was accompanied by a power reduction in the ignition delay time:

$$\tau_{ig} \sim P^{-1.4} \tag{6.12}$$

that is by the increase of the conversion rate.

The observed changes in the temperature and reaction time reflect changes in the mechanism caused by pressure rise, which are accompanied by the sharp increase of the methanol yield.

4.2 Effect of Pressure on the Yield of the Partial Methane Oxidation Products

A significant increase in the methanol (and formaldehyde) yield with the pressure in a copper reactor was observed in Furman (1946) and Furman and Shestakova (1956) (Fig. 6.7). The authors of this work emphasized the role of pressure in reducing the initial temperature and in the suppression of side reactions on the surface of the reactor. The methanol yield growth

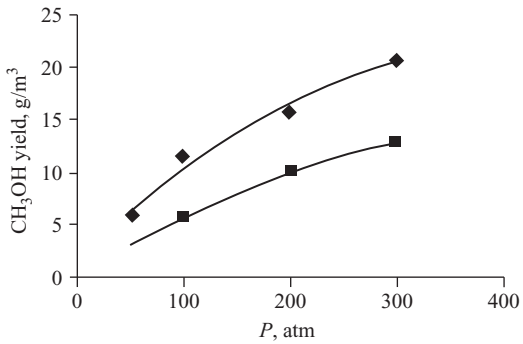

Fig. 6.7

Pressure dependence of the CH_3OH yield in a copper-surface reactor at $T = 475°C$, $[O_2]_0 = 3\%$: (◆) $t_r = 1.8$ s and (■) $t_r = 9.0$ s. *Based on data from Furman, M.S., Shestakova, A.D., 1956. Oxidation of methane under pressure. Tr. Gos. Inst. Azot. Promyshl. 6, 98–108 (in Russian).*

with increasing pressure gradually slows down, becoming practically undetectable at pressures of 300–500 atm. When the residence time of the reactants in the reactor was increased from 1.8 to 9.0 s, the methanol yield decreased significantly.

Experiments (Budymka et al., 1987) in a stainless steel flow reactor at a residence time of ~0.2 s, $T = 410°C$, and an O_2 concentration of 2.8% showed that the selectivity of formation of liquid organic products, total yield thereof, and the concentration of methanol and C_2–C_4 alcohols in the liquid product increase monotonically with the pressure. The content of aldehydes in the liquid product decreases monotonically with increasing pressure, and the content of organic acids remains almost unchanged. As in the other studies, the ratio of the sum of the concentrations of aldehydes to the sum of concentrations of alcohols in the liquid oxidate increased monotonically with the pressure.

The sum of the yields of liquid products and composition thereof (Fig. 6.8) in the pressure range from 30 to 230 atm were reported in Arutyunov et al. (1994).

The rapid increase of the yield of liquid organic products with the pressure was observed up to ~100 atm, after which it was slow. The concentration of methanol in the liquid oxidate showed a similar behavior, nearly reaching that of water at 100 atm. The formaldehyde concentration decreased slowly with increasing pressure up to 100 atm and then remained almost constant.

Several series of experiments in static-steel reactors at very high pressures, from 140 to 14,000 atm (Lott and Sliepcevich, 1967), as well as at pressures of 1700 and 3400 atm (Tripathy, 1975) do not show any specific features in the kinetics of the process or in the composition of resulting products, a behavior indicative of the "cellular effect" under these conditions (Gesser et al., 1995). The same turned out to be true when the process was conducted under supercritical conditions (Arutyunov, 2014; Arutyunov et al., 2007).

With decreasing pressure, the sum of the yields of liquid oxidation products and methanol decrease monotonically, as does the concentration of methanol in the liquid oxidation products (Fig. 6.9) (Arutyunov et al., 2002). In contrast, the concentration of formaldehyde increases with decreasing pressure while its yield remained practically constant despite the decrease of the total yield of liquid products. The yield of the products demonstrated a well-pronounced dependence on the material of the reactor surface. Although the maximum yield of methanol in quartz and stainless steel reactors at high pressures was almost identical, the quartz reactor required a higher initial concentration of oxygen to achieve it.

4.3 Factors Determining the Role of Pressure in the DMTM Process

The DMTM process is influenced by pressure through several mechanisms (Arutyunov, 2002). The degree of influence depends on a number of parameters, such as the time of the process(t_r) and the size and material of the reactor. Clearly, the main factor that determines

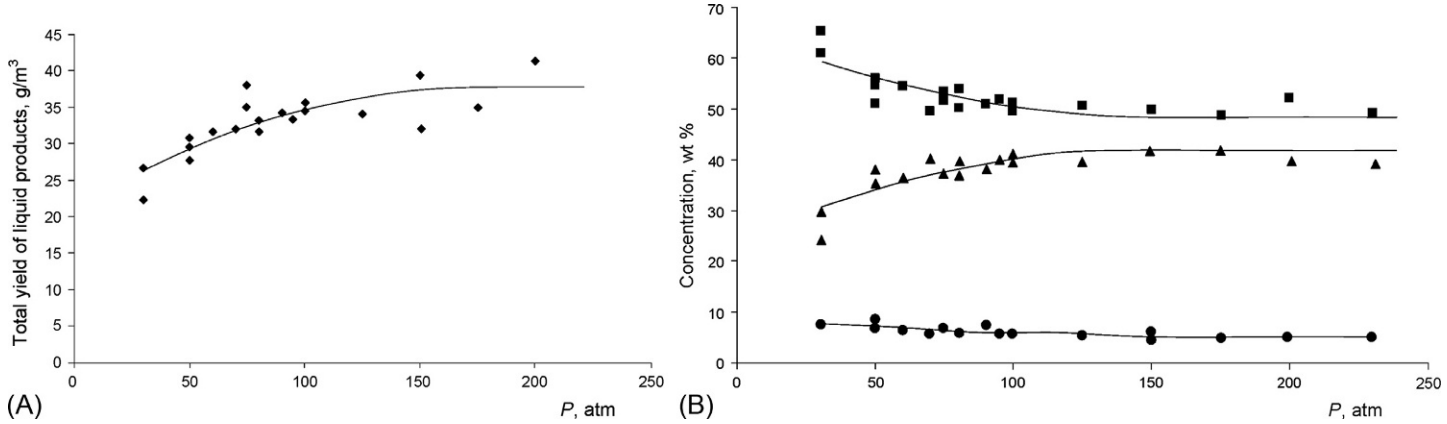

Fig. 6.8

Pressure dependence of the total yield of liquid oxidation products (A) and the composition of the liquid products (B) at $T = 400°C$ and $[O_2]_0 = 2.8\%$. (■) H_2O, (▲) CH_3OH, and (●) CH_2O (Arutyunov et al., 1994).

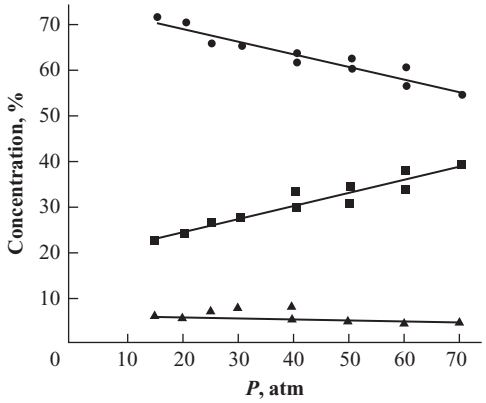

Fig. 6.9

Pressure dependence of the concentrations of (1) water, (2) methanol, and (3) formaldehyde in liquid products at $[O_2]_0 = 3.6\%$ and $T = 550°C$ in a quartz reactor (Arutyunov et al., 2002).

the effect of pressure on DMTM is the onset of the branched-chain reaction mode. Kinetics simulations for a CH_4: $O_2 = 9{:}1$ mixture at temperatures of 600–750 K and pressures of 1–100 atm (Vedeneev et al., 1988a,b,c,d) showed that a small change in pressure, by a few atmospheres, caused an abrupt decrease in the reaction time t_r by 3–4 orders of magnitude (Fig. 6.4), which is associated with the changeover from the radical-chain mode, controlled by a highly endothermic slow step of homogeneous chain initiation, to the branched-chain mode. In this mode, the oxidation rate is determined by chain-branching reactions, the rate of radical generation in which is several orders of magnitude higher than the rate of generation of radicals in homogeneous initiation reactions. Although the initial exponential growth of the radical concentration in the system is stopped quickly by the increasing rate of their mutual recombination, which transfers the reaction into a steady-state branched-chain mode (Fig. 6.3), the high rate of generation of radicals persists. The critical pressure of transition to the branched-chain steady-state mode depends on the process parameters, typically a few atmospheres, with the calculated pressure dependence of the reaction time (Fig. 6.4) being in good agreement with the experimental data.

After an abrupt transition of the system to the branched-chain steady-state mode, a further pressure rise is accompanied by a much slower monotonic increase in the methane oxidation rate (Fig. 6.4). The experimental pressure dependence of the ignition delay time for an 8.8:1.2 methane/air mixture was approximated by the expression $\tau_{ig} \sim P^{-1.4}$ (Melvin, 1966), which is consistent with the kinetic simulation results. For example, the pressure dependence of τ_{ig} for a 9:1 methane/oxygen mixture at pressures of 20–100 atm (Fig. 6.4) can be approximated by the formula $\tau_r \sim P^{-1.2}$.

At a constant residence time of the mixture in the reactor, a pressure rise leads to a decrease in the oxidation onset temperature and the temperature of complete oxygen conversion.

The data obtained in 4–7-mm-diameter flow reactors (Fig. 6.6), show that the pressure increase from 1 to 80 atm lowers the temperature of the onset of oxygen conversion and that of complete oxygen conversion on ~300°C. To a certain extent, the effect of the pressure increase is similar to the action of promoters on the reaction at low pressure.

The effect of pressure on the gas-phase process can manifest itself through the pressure dependence of the rate constants of some elementary reactions in the mechanism. However, at pressures above 10 atm, most of the rate constants occur in the high-pressure-limit mode, being insensitive to pressure changes.

A kinetic analysis shows that an increase in the pressure should lead not only to an increase in the methane conversion but also to an enhancement in the role of nonlinear radical gas-phase reactions, accompanied by an increase in the selectivity of methanol formation.

Fig. 6.10 and Table 6.2 show the most reliable experimental data on the pressure dependence of the methanol yield. All the experiments were performed at similar conditions, optimal for achieving a high methanol yield. We considered only those experiments in which the oxygen conversion is close to 100%. The results were compared in the methanol yield, as the most reliable experimentally measured quantity. Because of a low methane conversion, the methanol formation selectivity is typically determined with a significant uncertainty; moreover, in many practice-oriented works, it was not determined at all. The data from Lødeng et al. (1995)

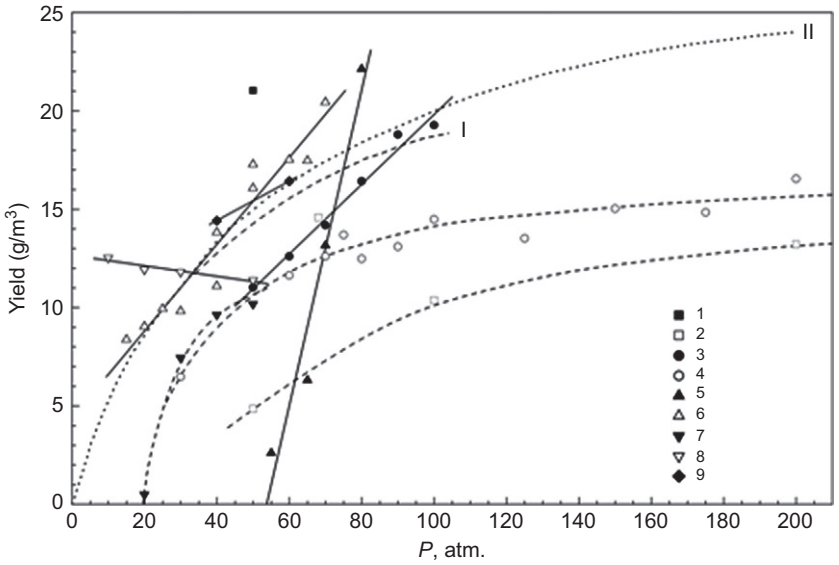

Fig. 6.10

Pressure dependence of the methanol yield in the partial oxidation of methane (POM) according to a number of studies. (I) calculated by the kinetic model described in Arutyunov et al. (1996a,b,c) at $T=480°C$, $[O_2]=3.5\%$ and a reactor diameter of 10 mm; (II) calculated by the equation $[CH_3OH]=[CH_3OH]_\infty/(1+P_{0.5}/P)$. References 1–9 and experimental conditions are given in Table 6.2.

Table 6.2 Experimental conditions and references for Fig. 6.10

No.	Reactor Diameter, (mm)	Reactor Material	Reaction Time, t_r (s)	Reference
1	3	Steel	5	Newitt (1937)
2	~10	Copper	1.8	Furman (1946)
3	25	Stainless steel	<1	Budymka et al. (1987)
4[a]	25	Stainless steel	~30–40	Arutyunov et al. (1994)
5	10	Stainless steel	~2	Arutyunov et al. (2002)
6	7	Quartz	~2	Arutyunov et al. (2002)
7[b]	4	Stainless steel	~100	Burch et al. (1989)
8[b]	4	Quartz	~100	Burch et al. (1989)
9[b]	20	Al_2O_3	~1	Lødeng et al. (1995)

[a]The values obtained at identical pressures are averaged.
[b]Estimation based on output data of the oxygen concentration and the selectivity of methanol formation.

and Burch et al. (1989), in which only the selectivity values are given, enabled the assessment of the methanol yield based on the ratio $\Delta[CH_4]/\Delta[O_2] \approx 1$. This makes it possible to evaluate the methanol yield Y_{CH3OH} from the expression

$$Y_{CH3OH} = QXS_{CH3OH} \tag{6.13}$$

where Q is the methane flow rate, X is its conversion, approximately equal to the initial concentration of oxygen, and S_{CH3OH} is the methanol formation selectivity.

The initial concentration of oxygen in these experiments ranged from 2.5% to 3.6%, while the temperature remained within 410–500°C. The reaction time ranged from 1 to 100 s. Reactors with stainless steel, copper, quartz, Pyrex, or Al_2O_3 (alsint) surface had a diameter from 4 to 25 mm. The presented data, with allowance for differences in the conversion and the size and surface material of the reactor, are in good agreement with each other and with the results of the kinetic simulation (Fig. 6.10, curve I). Despite the apparent incompleteness of accounting for the heterogeneous processes on the surface of the reactor, the simulation results satisfactorily describe the experimental pressure dependence of the methanol yield.

Another important factor determining the role of pressure in this process, at least for laboratory reactors with a small diameter at a low gas-flow rate, is the diffusion of the reaction mixture components to the surface. The degree of the influence of pressure is determined by a number of constructive characteristics of the reactor (diameter, surface material, residence time of the reactants in the reactor) and the partial pressure of the inert diluent.

Since in most laboratory experiments the gas flow is laminar, assessments can be made using expressions for molecular diffusion. The only exceptions are the experiments on a pilot facility (Budymka et al., 1987), wherein the flow was turbulent. For a laminar flow in a cylindrical reactor, the time of diffusion of components to the surface can be calculated by the formula

$$\tau = d^2/\mu_1 D \tag{6.14}$$

where d is the reactor diameter, μ_1 is the first root of the Bessel function, and D is the diffusion coefficient, given by

$$D = D_o(1/P)\,(T/273)^{1.5} \tag{6.15}$$

where D_o is the diffusion coefficient under normal conditions, P is the total pressure, and T is the reaction temperature (in K). For most of the experiments conducted on laboratory setups at pressures of ~50 atm, the characteristic time of diffusion τ is a few seconds, which is approximately equal to or smaller than the residence time of the mixture in the reactor. Therefore, at pressures below 50 atm, one can expect a significant interaction of the reacting mixture with the surface and a strong influence of the surface on the yield of the oxidation products, which is confirmed by data on the influence of the reactor surface material on the DMTM process.

The lowest methanol yield under flow reactor conditions at pressures of 50–300 atm was observed in a 10-mm-diameter copper reactor (Furman, 1946; Furman and Shestakova, 1956) (Fig. 6.10). In 25-mm-diameter stainless steel reactors, all other things being equal, the methanol yield was significantly higher (Budymka et al., 1987; Arutyunov et al., 1994). At approximately the same diameter of stainless steel reactors, at $t_r < 1$ s (Budymka et al., 1987), the methanol yield was higher than in experiments (Arutyunov et al., 1994) where t_r constituted tens of seconds. A comparison of the published data shows (Fig. 6.10) that the nature of the reactor surface material (stainless steel and quartz (Arutyunov et al., 2002); stainless steel, quartz, and Pyrex (Burch et al., 1989)) strongly influences the behavior of the pressure dependence of the yield and selectivity of methanol formation. At high pressure, the nature of reactor surface material is insignificant; however, with decreasing pressure the yield of methanol in stainless steel reactors reduces rapidly, whereas for quartz reactors, the pressure dependence is much weaker. The different behavior of these materials is not associated with differences in the rates of decomposition of methanol formed on the respective surfaces (Burch et al., 1989), being rather a result of the influence of the surface on the methane oxidation mechanism.

Along with increasing the rate of decay of free radicals involved in the branched-chain process, an increase in the rate of diffusion can enhance the contribution from catalytic reactions with the preferential formation of methane deep oxidation products (i.e., carbon oxides and water), which are formed on the surface of the reactor, especially metallic (Cu, Fe, or Ni). Experiments (Tulenin et al., 2001) showed that a supported platinum catalyst not only accelerates the reaction between methane and oxygen but also increases the fraction of deep oxidation products, that is, it decreases the selectivity of the gas-phase processes, including those leading to methanol formation. Since the POM to methanol occurs at a very low concentration of O_2, there is competition for oxygen between the gas-phase partial oxidation to oxygenates and the catalytic surface reaction of deep oxidation. At high pressures, the

catalytic reaction is controlled by the diffusion rate of the deficient reagent, oxygen, to the surface. The decreases of the competition between the surface reactions with the gas-phase partial oxidation for deficient oxygen can be described by a simple expression:

$$[CH_3OH] = [CH_3OH]_\infty/(1 + P_{0.5}/P) \tag{6.16}$$

where $[CH_3OH]_\infty$ is the methanol yield at infinite pressure, P is the total pressure, and $P_{0.5}$ is the pressure at which the methanol yield constitutes half of $[CH_3OH]_\infty$. The corresponding curve, plotted at $[CH_3OH]_\infty = 30$ g/m^3, and $P_{0.5} = 50$ atm, is shown in Fig. 6.10 (curve II). As can be seen, the above simple expression satisfactorily describes the course of most of the experimental curves displayed in Fig. 6.10.

Summarizing, we can recapitulate the reasons why the pressure affects the methanol yield in the POM:

- At pressures of a few atmospheres, the critical transition into the steady-state branched-chain reaction mode occurs, whereby the reaction rate abruptly increases by several orders of magnitude.
- With increasing pressure, the rates of the elementary mono- and trimolecular reactions increase to values corresponding to the high pressure limit.
- With increasing pressure, the contribution from nonlinear gas-phase reactions leading to the formation of methanol grows.
- The reduction of the diffusion rate with increasing pressure decreases the contribution of the heterogeneous processes leading to the predominant formation of deep oxidation products.

4.4 Effect of Temperature on the Yield of the Products

The temperature dependence of the methane conversion at a fixed length of the reactor (or reaction time) has a well-pronounced *S*-shape (Fig. 6.11) (Arutyunov et al., 1994). The transition from a negligible conversion to complete conversion occurs in a very narrow temperature range, reflecting the critical dependence of the rate of the branched-chain process on the temperature.

An increase in temperature leads to a reduction in the reaction time (the time of complete conversion of oxygen, almost coinciding with the induction period of the reaction). A nearly perfect Arrhenius dependence of the oxygen conversion time yields an effective activation energy of ~46 kcal/mol, with the heat-up of the mixture under these experimental conditions being close to the adiabatic, ~43°C per percent of oxygen in the reaction mixture. These experimental data are also almost identical to the results of the kinetic simulations reported in Arutyunov et al. (1996c). Very similar values of the activation energy of the process, ranging from 39 to 45 kcal/mol, were reported in Melvin (1966) and Kolbanovskii et al. (2011).

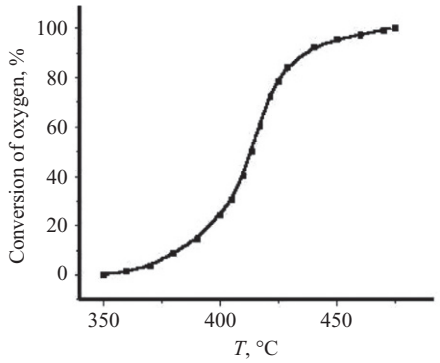

Fig. 6.11
Dependence of the oxygen conversion in the stainless steel reactor on the initial temperature of the reaction mixture at $P = 80$ atm, $[O_2]_0 = 3.3\%$, and $t_r \sim 1$ s (Arutyunov et al., 1994).

Note that the presence of even minor impurities of heavier hydrocarbons may lead to a significant reduction in the effective activation energy of the oxidation process. For example, according to (Simchenko et al., 1999), the content of ~6% C_2+ hydrocarbons in the gas results in a lowering of the activation energy to $E_a = 29$–33 kcal/mol.

Once the temperature of complete oxygen conversion is reached, a slight further rise in temperature has little effect on the methanol yield. Only with a significant temperature increase is a decline in the methanol yield observed, due to both a decrease in the selectivity of its formation and the decomposition of the formed product at the reactor surface. Nonetheless, the results of a number of works indicate that, in general, a decrease in temperature under the conditions of complete oxygen conversion is beneficial for the yield of oxygenates, although this effect is not very strong. A monotonic, although not a very significant, reduction in the methanol yield with increasing temperature was observed in Foral (1992). However, at temperatures above 600°C, the drop in the yield becomes significant.

According to the data obtained by studying the conversion of natural gas with a content of C_2+ hydrocarbons of ~5% in a pilot plant with a stainless steel flow reactor ($t_r \sim 0.2$ s, $P = 100$ atm, $[O_2]_0 = 2.8\%$) (Budymka et al., 1987), the dependences of the selectivity of formation of liquid organic products, total yield of liquid products, and concentrations of methanol and C_2–C_4 alcohols in the liquid product pass through a flat maximum at ~410°C. The yield of aldehydes slightly increases with the temperature.

According to the data from Arutyunov et al. (2002) (flow reactor with an internal quartz surface, $P = 20$–70 atm, and a reaction time of ~2 s), after reaching the temperature of complete oxygen conversion, the oxidation process is only moderately sensitive to the initial and maximum achievable temperature of the reactants. The yield of liquid products and the methanol concentration in the liquid phase increases insignificantly with the maximum heat-up

temperature of the mixture to $T \approx 520°C$, after which the methanol yield gradually decreases. This temperature dependence is consistent with the results of kinetic simulations of the process (Arutyunov et al., 1996c). The yields of formaldehyde and ethanol remained virtually unchanged as the maximum heat-up temperature of the mixture was increased from 480°C to 600°C. At temperatures significantly higher than 600°C, the DMTM process can be accompanied by noticeable soot formation.

The difference in the optimal temperatures reported in Arutyunov et al. (2002) and Budymka et al. (1987) is most likely due to differences in the composition of the gas mixtures, with that used in Budymka et al. (1987) containing a considerable amount of methane homologues. As shown in Simchenko et al. (1999), the changeover from natural gas containing ~6% C_2+ hydrocarbons to nearly pure methane (~0.2% C_2+), with the apparatus being the same, resulted in an increase in the process temperature by almost 90°C, that is just by a value corresponding to the difference in the optimal temperatures given in Arutyunov et al. (2002) and Budymka et al. (1987).

Of special interest in understanding the general nature of the effect of temperature on the PM are studies spanning a wide temperature range, covering, in particular, temperatures at which the transition from the preferential formation of DMTM products to the preferential formation of OCM products takes place. One of the most interesting studies in this respect, (Onsager et al., 1989), was performed in a flow reactor with an Al_2O_3 (alsint) coated internal surface at 500–750°C, 3–40 atm, $[O_2] < 9\%$, and reaction times of 0.1–1.0 s. Under these conditions, pressure variation within 10–25 atm only slightly affected the selectivity of product formation, while increasing the temperature caused fundamental changes. At temperatures below 500°C, only oxygenates were formed, while with increasing temperature, the selectivity of formation of C_2H_6 and C_2H_4 grew monotonically, in accordance with the temperature dependence of the equilibrium constant of reaction (6.1). However, with increasing methane conversion, the selectivity of formation of C_2 condensation products decreased rapidly, mainly due to their conversion into carbon oxides COx. The monotonic change of the composition of products with increasing temperature and increasing methane conversion is one of the major arguments in favor of a single mechanism of the POM at moderate temperatures, $T < 1000°C$.

A noticeable shift from oxygenates to C_2+ products occurs at 550–630°C, pressures from 30 to 100 atm, and a reaction time of ~1 s (Walsh et al., 1992a,b). However, due to a high initial concentration of oxygen, $[O_2]_0 = 14\%$, a complete oxygen conversion can raise the temperature by 500°C, so the final temperature can exceed 1000°C. Therefore, many of the described effects can be associated with the heating of the mixture.

As shown in Casey et al. (1994), with decreasing temperature, the selectivity of methanol formation increases up to a certain temperature, below which it remains practically constant if the reaction time is long enough to ensure a complete oxygen conversion (Fig. 6.12).

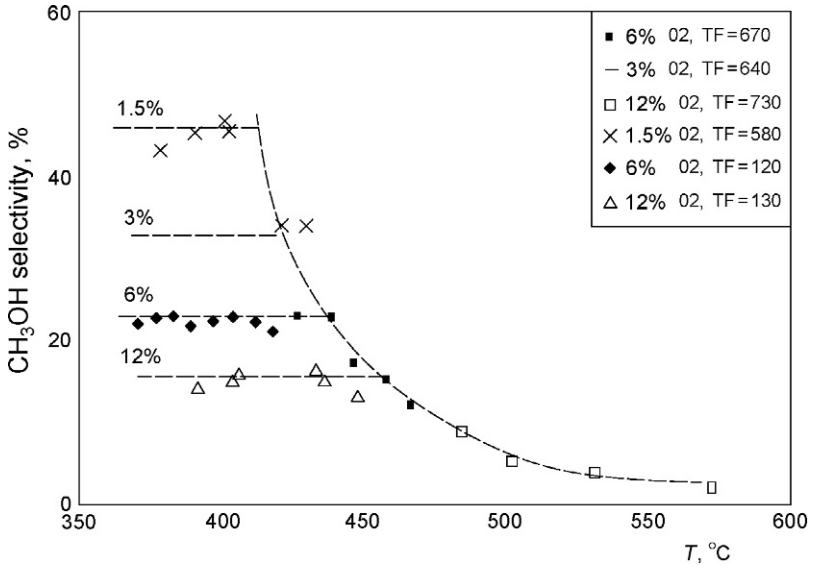

Fig. 6.12
Methanol selectivity as a function of the reactor temperature at different oxygen concentrations; TF is the total flow of the reactants, cm^3/min (Casey et al., 1994).

Thus, the available experimental data, supported by kinetic simulations (Arutyunov et al., 1996c) led us to conclude that, at the short times of the processes, ~1 s, an optimum temperature range for DMTM is 480–550°C. At temperatures above 550°C, the composition of the products shifts in favor of ethane and ethylene. At temperatures above 600°C, the methanol yield decreases and soot can form (Arutyunov et al., 2002), thereby contaminating the resulting liquid products. The high heat of the reaction imposes limits on the amount of oxygen supplied into the reactor; at an oxygen concentration above 3%, it is necessary to seek effective solutions for the problem of heat removal. On the other hand, a combination of high temperatures and relatively low pressures favors an increase in the formaldehyde yield.

4.5 Effect of the Oxygen Concentration (CH_4/O_2 Ratio) on the Selectivity and Yield of the Products

The decrease of the selectivity of methanol formation with increasing oxygen concentration (ratio of CH_4/O_2 in the feed) under high-pressure flow-reactor conditions was first observed in Pichler and Reder (1933). However, as described in the patent (Brockhaus and Franke, 1981), when a fast (76–268 m/s) preheated oxidant flow was ejected through a narrow nozzle at the center of a slower (1.3–2 m/s) preheated methane flow, the decrease of the selectivity of methanol formation with increasing oxygen concentration was less dramatic. The methane conversion in this study (Fig. 6.13) was proportional to the oxygen concentration, whereas the $\Delta CH_4/O_2$ remained constant, ~1 in most experiments, a feature indicative of the invariability

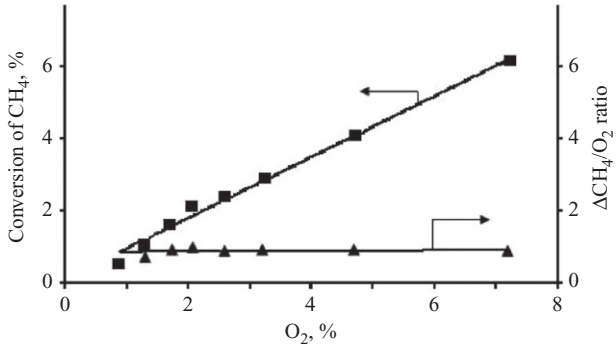

Fig. 6.13

Dependence of the (■) methane conversion and (▲) $\Delta CH_4/O_2$ ratio on the oxygen concentration at $P = 40$ atm, $T = 440$°C and 460°C, and $t_r = 0.6$–1.0 s. *Based on data from Brockhaus, R., Franke, H.J., 1981. Process for the manufacture of formaldehyde and methanol by partial oxidation of methane. US Patent 4243613.*

of the mechanism and of the formation of the main products according to the gross formula (6.11). In this case, the methanol yield reached ~2%, whereas the total yield of oxygenates was ~3%.

In experiments (Budymka et al., 1987) on the oxidation of natural gas in a stainless steel flow reactor ($t_r \sim 0.2$ s, $P = 100$ atm, $T = 410$–450°C), an increase in the oxygen concentration from 2% to 4% raised the yield of liquid products. However, the selectivity of formation of the sum of liquid organic products and the concentration of methanol in the liquid oxidation product passed through a maximum at an initial oxygen concentration of $[O_2] = 2.8\%$–3.0%. The concentration of C_2–C_4 alcohols passes through a maximum at a lower oxygen concentration, $[O_2] \approx 2.5\%$. At the same time, the concentration of aldehydes increased monotonically with the oxygen concentration. The concentration of acids in this range of oxygen concentrations remained virtually constant. The ratio of the concentration of the sum of aldehydes to that of alcohols in the liquid oxidate decreased monotonically with increasing oxygen concentration, from a ~7 at low O_2 concentrations to ~3 at higher oxygen concentrations.

Well-pronounced and unambiguous dependences of the basic parameters of the DMTM process on the oxygen concentration in a quartz flow reactor were obtained in Foral (1992) at $P = 91$ atm, $T = 427$°C, and $t_r = 35$ (Figs. 6.14 and 6.15).

With increasing methane conversion, the ratio of reacted methane to oxygen, $\Delta CH_4/O_2$, decreased monotonically from 1.4 to 1.0, which most likely reflects the observed (Fig. 6.15) reduction in the selectivity of methanol formation and the observed enhancement in the selectivity of CO_2 formation. Interestingly, while in these experiments, the selectivity of CO formation remains constant, the selectivities of the formation of methanol and CO_2 change

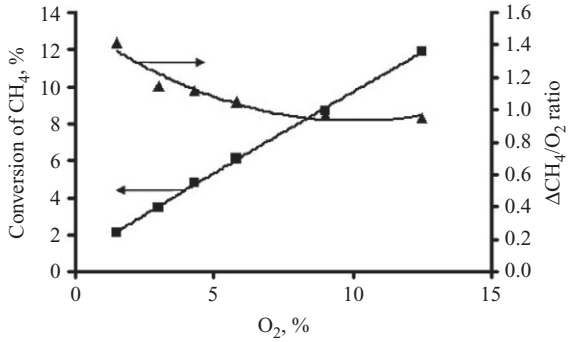

Fig. 6.14

Dependence of the (■) methane conversion and (▲) $\Delta CH_4/O_2$ ratio on the oxygen concentration at $P = 91$ atm, $T = 427°C$, and $t_r = 35$ s. *Based on data from Foral, M.J., April 5–10, 1992. The noncatalytic partial oxidation of natural gas to methanol. In: Preprints, Symposium on Natural Gas Upgrading II, 203d National Meeting of the American Chemical Society, Division of Petroleum Chemistry, San Francisco, CA. American Chemical Society, Washington, DC, pp. 34–40.*

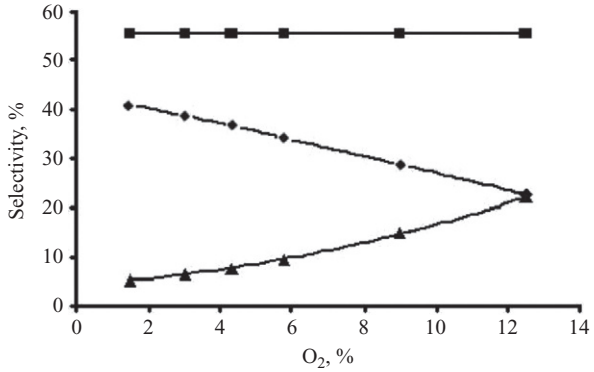

Fig. 6.15

Dependence of the selectivity of (◆) CH_3OH, (■) CO and (▲) CO_2 on the oxygen concentration. $P = 91$ atm, $T = 427°C$, $t_r = 35$ s. *Based on data from Foral, M.J., April 5–10, 1992. The noncatalytic partial oxidation of natural gas to methanol. In: Preprints, Symposium on Natural Gas Upgrading II, 203d National Meeting of the American Chemical Society, Division of Petroleum Chemistry, San Francisco, CA. American Chemical Society, Washington, DC, pp. 34–40.*

almost strictly antibatically, mutually compensating the amounts of carbon spent on their formation. These experiments produced no detectable amounts of formaldehyde or other products.

While the selectivity of methanol formation decreases almost linearly with increasing oxygen concentration, its yield reaches a 2.7% plateau at $[O_2] > 8\%$ and methanol formation selectivity of ~30%. The maximum selectivity in methanol, 42%, was achieved at the lowest oxygen concentration, $[O_2] = 1.5\%$.

The reduction of the selectivity of formation of liquid organic products with increased oxygen concentration expectedly gives rise to an extreme dependence of their yield. Attainment of a maximum in the yield of DMTM liquid products and its subsequent decrease with increasing oxygen concentration (with reduction of CH_4/O_2 ratio) at $P = 100$ atm was observed in Arutyunov et al. (1995b).

The dependence of the yield of the main liquid-phase oxidation products and of their concentrations in the liquid product on the oxygen concentration was obtained in Arutyunov et al. (2002). In a stainless steel reactor, the maximum concentration of methanol in the liquid-phase products reached 42% at an initial oxygen concentration of ~3.5%. The maximum yield of methanol, 20 g/m^3 of passed gas, was achieved at a somewhat higher initial oxygen concentration (~4.5%) (Fig. 6.16), which is due to an overall increase in the yield of liquid products with increasing conversion. In a quartz reactor, the maximum value of the methanol yield was about the same, but achieved at a higher initial oxygen concentration, above 6%, after which the yield gradually declined. Up to the initial oxygen concentration of 10%, the total yield of liquid products increased almost linearly, mainly due to the formation of water.

The concentration of methanol in the liquid oxidation products formed in a quartz reactor decreases almost linearly from the maximum value of ~42% at the initial oxygen concentration of 2%–3% (Fig. 6.17). The formaldehyde concentration decreases monotonically with increasing initial oxygen concentration from ~10% at $[O_2]_0 \approx 1\%$ to ~5% at $[O_2]_0 \approx 6\%$ and continues to decrease with a further increase in the oxygen concentration. A smoother

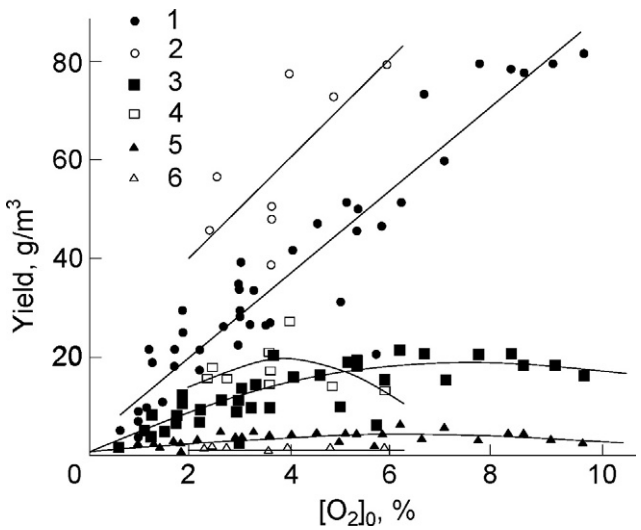

Fig. 6.16

Dependence of the yield Y (g/m^3) of (1, 2) the sum of liquid products, (3, 4) methanol, and (5, 6) formaldehyde on the initial oxygen concentration for the oxidation in a quartz (1, 3, 5) and stainless steel reactor (2, 4, 6) at $P = 80$ atm and $T = 550$°C (Arutyunov et al., 2002).

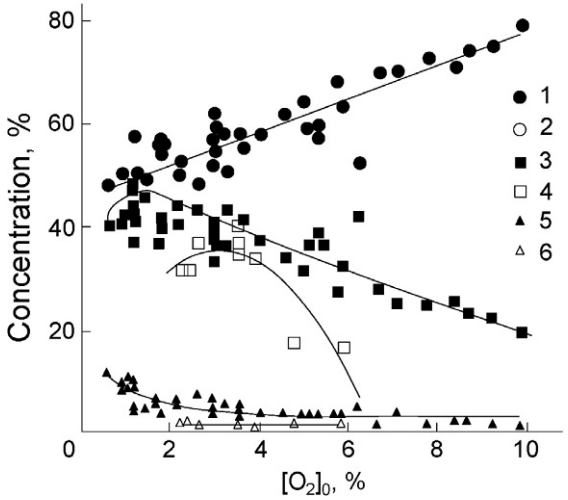

Fig. 6.17

Dependence of the concentrations of water (1, 2), methanol (3, 4), and formaldehyde (5, 6) in the liquid on the initial oxygen concentration for the oxidation in a quartz (1, 3, 5) and stainless steel (2, 4, 6) reactors at $P = 80$ atm and $T = 550°C$ (Arutyunov et al., 2002).

dependence on the oxygen concentration obtained in a quartz-surface reactor better matches the results of kinetic simulations of the process (Arutyunov et al., 1996c) and confirms the assumption of a substantial effect of the surface on the process in small-diameter reactors.

4.6 *Influence of the Oxygen Concentration on the Reaction Temperature and Reaction Rate*

A detailed study of the slow reaction of methane with air during the ignition delay period in a static stainless steel reactor (Melvin, 1966) showed not only quite regular increases in the methane conversion and in the final temperature of the reaction products with the oxygen concentration, but also an increase in the ignition delay time (Fig. 6.18). In other words, the increase of the air fraction in the methane-air mixture from 10% to 40% (increase in $[O_2]/([CH_4]+[O_2])$ from 0.019 to 0.088) clearly decreases the rate of the CH_4+O_2 reaction. The ignition delay time and heat-up temperature of the mixture grew linearly with the oxygen concentration. Processing of these results ($T_0 = 408°C$, $P = 72$–83 atm) yielded $\tau_{ig} \sim [O_2]^{0.6}$. This order of the ignition delay time in the oxygen concentration was found to be only weakly pressure dependent, varying by no more than 15%.

According to Foulds et al. (1997), the reaction initiation temperature increased with the oxygen concentration: from 401°C at $[O_2] = 2.5\%$ to 411°C at $[O_2] = 9.5\%$. A rapid growth of the

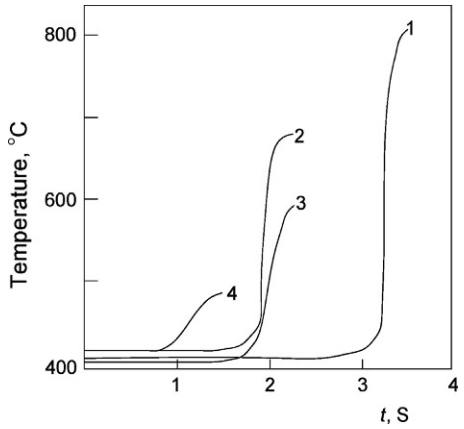

Fig. 6.18
Time history of the temperature for the ignition of methane-air mixtures at $P = 103$ atm and various air concentrations: (1) 40%, (2) 29%, (3) 21%, and (4) 10% (Melvin, 1966).

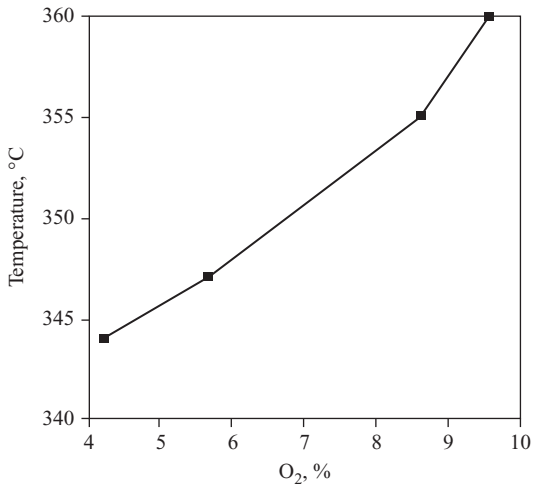

Fig. 6.19
Dependence of the minimal temperature required for complete oxygen conversion on the initial oxygen concentration at $P = 81$ atm (Gesser et al., 1995).

minimum temperature required for a complete oxygen conversion with the initial oxygen concentration was observed in Gesser et al. (1995) (Fig. 6.19).

The experimental data (Takemoto et al., 2001) show that the temperature of oxygen conversion increases with its concentration at $[O_2] = 2.7\%–5\%$ ($P = 10$ atm, $t_r = 11–15$ s). Kinetic simulations confirmed that the time it takes to convert the oxygen increases with its concentration.

4.7 Reaction Time

As discussed above, the duration of the process is of fundamental importance from the viewpoint of the relative role and mutual influence of the homogeneous and heterogeneous processes. At high rates of the flow of the reactants and their residence time in the reactor being not much greater than the time of their diffusion to the surface, within a few seconds, the reaction is expected to be substantially homogeneous, treatable within the framework of a gas-phase kinetic model. At a low reagent conversion rate and, accordingly, a long time in the reactor, on the order of minutes, significantly longer than the time of their diffusion to the surface, the role of heterogeneous phases becomes significant and the kinetics of the process become more complicated and difficult to analyze. However, in any case, it is desirable to limit the residence time of the mixture in the reactor by the period required for a complete conversion of oxygen. Within the limits of each of the two indicated groups of conditions in reactors with relatively inert surfaces (quartz, Pyrex, stainless steel), a small change in residence time of the mixture after a complete conversion of oxygen does not substantially affect the final yield of methanol and even that of formaldehyde, a compound less stable in these conditions. Even a rapid cooling (quenching) to stop the reaction in the mixture at the reactor outlet has not been successful in substantially increasing the methanol yield in any of the attempts reported in the literature.

An interesting experiment on the POM within a very short time (milliseconds), showing the primary set of oxidation products, was performed in Oberdorfer and Winch (1961) in an adiabatic compression reactor, more specifically, a cylinder of an engine driven by an electric motor. In this case, the initiation of a high-temperature reaction by compression and its rapid quenching by the subsequent expansion of the mixture occur near the top dead center of the piston stroke. The temperature of the mixture reached ~800°C, whereas the compression ratio was up to 45. The reaction time was estimated to be ~0.02 s. At the optimal concentration of oxygen (~8%) conversion was ~44%, whereas $\Delta CH_4/O_2 = 1.25$. A typical composition of the products was obtained with selectivity in carbon of $S_{CH3OH} \approx 22.5\%$, $S_{CH2O} \approx 15.2\%$, $S_{HCOOH} \approx 3.4\%$, and $S_{CO} \approx 33.3\%$. Hydrogen was also detected, but virtually no CO_2. A large content of formaldehyde in the products is probably due to a high temperature, low pressure, and relatively short duration of the reaction, factors favorable for the survival of this compound.

According to the results of work (Furman and Shestakova, 1956) (Fig. 6.7), even at pressures of 100–300 atm, increasing the residence time of the reaction mixture in the reactor with an active surface (copper) from 1.8 to 9.0 s significantly reduces the yields of methanol and formaldehyde. The kinetics of the accumulation of the reaction products (Fig. 6.20) show that the concentrations of the main products almost simultaneously achieve their maximum values and then decrease monotonically. As demonstrated by kinetic simulations (Vedeneev et al., 1988a,b,c,d; Chun and Anthony, 1993; Arutyunov et al., 1996c; Arutyunov and Krylov, 1998), the maximum concentration of oxygenates is reached at the time of a complete

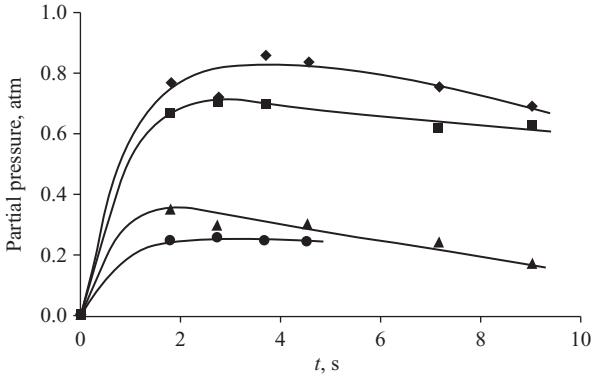

Fig. 6.20

Time evolution of the yield of various products in copper reactor at $P=300$ atm and $T=375°C$: (◆) CH_3OH, (■) CO, (▲) CH_2O, and (●) CHOOH. *Based on data from Furman, M.S., Shestakova, A.D., 1956. Oxidation of methane under pressure. Tr. Gos. Inst. Azot. Promyshl. 6, 98–108 (in Russian).*

conversion of oxygen, when the branched-chain oxidation reaction stops. The subsequent reduction in the concentration of oxygenates, apparently due to both their heterogeneous decomposition and continuing radical processes in the gas phase, likely under the action of OH radicals formed by the decomposition of hydrogen peroxide, accumulated during the branched-chain process. Most likely, the second reason dominates, since after a rapid initial decline, the subsequent change of the concentrations with time becomes slower.

Only a few studies reported the temperature profile of the reaction, which could be compared with the results of kinetic simulations. Along with (Foulds and Gray, 1995), reaction temperature profiles were presented in Casey et al. (1994). Although the residence time of the reactants in the reactor was not specified, it can be estimated from the available data as ~15 s. Fig. 6.21 shows how increasing the oxygen concentration forms a characteristic temperature profile of the reaction with a well-pronounced induction period and the subsequent rapid heat-up of the mixture.

Experiments (Lødeng et al., 1995) in a flow reactor lined inside with Al_2O_3 (Alsint) and equipped with five serially mounted thermocouples gave temperature profiles qualitatively consistent with the results of kinetic simulations of the process. In the absence of oxygen conversion, the preheated reactants cooled monotonically, whereas in the reaction mode, they are rapidly heated after an induction period. An important observation of this study is the instability and constant fluctuations in the temperature profile by ~5°C. The best results were obtained when the reaction zone was as close to the water-cooled quenching unit as possible.

In Simchenko et al. (1999), the reaction temperature profile was measured in a pilot plant with a gas flow rate of 760 m^3/h (stainless steel reactor, internal diameter 25 mm, length 10 m). The oxygen concentration was varied from 1 to 3%. The test gas contained only ~0.2% C_2+ methane homologues. The kinetic curves in Fig. 6.22 feature a long induction period,

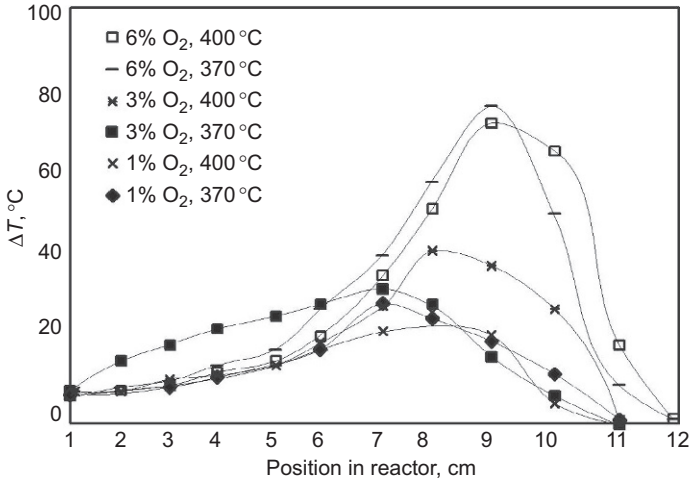

Fig. 6.21
Temperature profiles in the reactor at $P=50$ atm and various initial temperatures and oxygen concentrations (Casey et al., 1994).

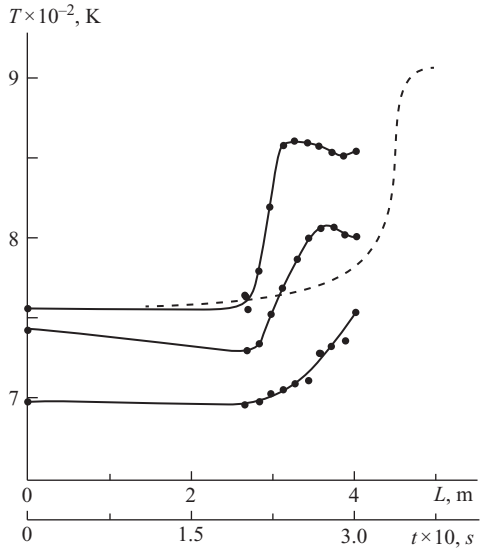

Fig. 6.22
Temperature profiles of the reaction at $P=100$ atm, $[O_2]_0=3\%$, and various initial temperature of the gas mixture (Simchenko et al., 1999). The dashed line represents the simulation results at $T=755$ K obtained using the model from Vedeneev et al. (1988a,b,c,d).

constituting ~80% of the total reaction time. Calculations within the framework of a kinetic model (Vedeneev et al., 1988a,b,c,d) showed good agreement with these experimental temperature profiles. However, the changeover to an unpurified test gas, containing ~6% C_2+ hydrocarbons, dramatically reduces the time (or reduces temperature) of complete oxygen

conversion, since the presence of even minor impurities of heavier hydrocarbons in methane greatly affects the rate of the process.

4.8 Specifics of the Organization of the Process

Analysis of DMTM suggests that, although frequent references to the structural features of the reactor as the cause of discrepancies are mentioned in the results of different studies, this is true only if the residence time of the reactants in the reactor is long. Consequently, heterogeneous reactions can play a significant role in the process. Nearly all the differences in the results of experiments at short residence times of the reactants in the reactor are normally well explained by differences in the experimental conditions, with the results themselves being satisfactorily described in the framework of gas-phase kinetic models. Apart from experiments in flow reactors, this conclusion is confirmed by experiments in adiabatic compression reactors (Oberdorfer and Winch, 1961; Torchian et al., 1974) and by experiments where the reactants are fed separately (Brockhaus and Franke, 1981).

As already noted, quenching the reaction mixture by cooling at the outlet of the reactor produces only a slight increase in the yield of methanol. A more effective structural measure to increase the methanol yield is to feed oxidant at several points along the reactor length. In Vedeneev et al. (1995), a flow pilot plant with a stainless steel reactor operating at a gas flow rate of $\sim$1000 m^3/h was used to perform experiments on the influence of stepwise oxidation, in which a fixed amount of oxidant was introduced through different number (from 1 to 4) points along the reactor length. Contrary to kinetic calculations, which predict a small but monotonic increase in the methanol yield with an increasing number of air inlets (Table 6.3), in fact an increase in the methanol yield was achieved only for two-stage oxidation, while for four-point oxidation the yield was even lower than for a single-point oxidant introduction. This discrepancy is probably associated with disregarding the real heat-up of the mixture in the simulation.

Fig. 6.23 shows how the methanol yield changes with the number of air inlets into the reactor at various total concentrations of oxygen supplied. Only at the lowest concentration, $[O_2] = 2\%$, is a slight monotonic growth of the methanol yield with the number of supply points

Table 6.3 Methanol yield as a function of the number of oxidant-supply inlets ($[O_2]_0 = 4\%$, $P = 100$ atm) (Vedeneev et al., 1995)

Number of Oxidant-Supply Inlets	Methanol Yield, g/m^3 of Gas	
	Calculation	Experiment
1	22.64	23.68
2	24.90	28.20
3	27.20	24.60
4	29.36	19.54

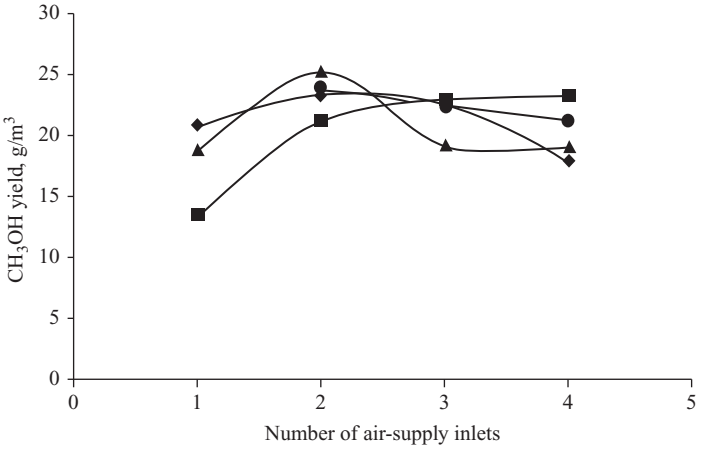

Fig. 6.23

Dependence of the methanol yield on the number of oxidant-supply inlets at $P = 65$ atm and various oxygen concentrations ($[O_2]_0$ in %): (■) 2, (▲) 3, (◆) 4, and (●) 5. *Based on data from Vedeneev, V.I., Simchenko, V.P., Shcherbakov, P.M., 1995. Production of methanol in the stepwise oxidation of natural gas. Gazov. Prom-st. 11, 30–31 (in Russian).*

observed. At higher concentrations of oxygen, at more than two points of air supply, the yield decreases. The maximum yield of methanol, 28.2 g/m^3 ($P = 100$ atm), was obtained by the introduction of 4% O_2 at two oxidant inlet points. Lack of the effect of distributed oxidant supply at higher oxygen concentrations is likely due to an overheating of the reaction mixture, which has no time to cool after the conversion of the previous oxygen portion at a short reaction time (~0.2 s) under these conditions. At an efficient heat sink between the oxidant feed points (Patent RU 2200731, 2001), distributed oxidant supply is expected to produce a greater effect.

Fig. 6.24, also plotted based on data from Vedeneev et al. (1995), shows how the yield of the main liquid-phase products changes after the supply of another portion of oxidant (4% oxygen introduced at four points). The yield of CH_3OH and C_2H_5OH alcohols reaches a maximum at 3% O_2 and begins to decrease at higher concentrations. The yield of aldehydes reaches its maximum value earlier. The yield of water increases monotonically.

The effect of the mode of oxygen supply into the DMTM reactor was investigated in detail in Casey et al. (1994). Of several designs, the distributed supply of oxygen through eight 0.6-mm-diameter holes arranged pairwise along a 30-mm length (Fig. 6.25) turned out to be the most successful. All other things being equal, this method of oxygen supply enabled reaching a maximum methanol yield of 1.8%, that is, it increased it by 50% compared to 1.2% for the conventional method of single-point oxidant supply.

One of the important technical problems is a significant carry-away of liquid-phase reaction products with the exhaust gases. According to phase equilibrium calculations, in the case

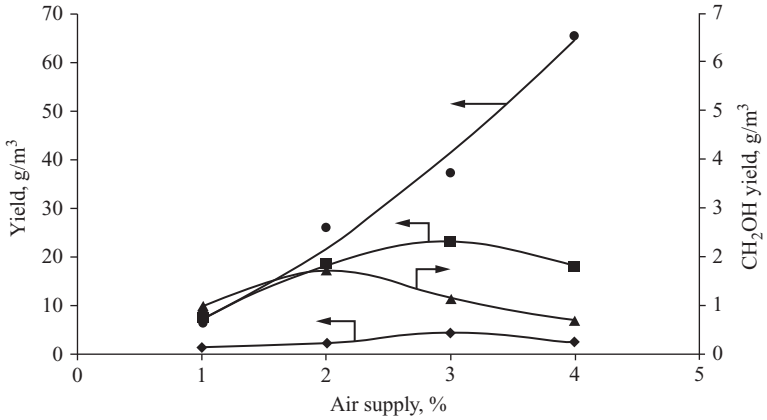

Fig. 6.24

Dependence of the yields of (●) water, (■) methanol, (◆) ethanol, and (▲) formaldehyde on the O_2, introduced in 1% portions to a total of $[O_2]_0 = 4\%$, at $P = 65$ atm. *Based on data from Vedeneev, V.I., Simchenko, V.P., Shcherbakov, P.M., 1995. Production of methanol in the stepwise oxidation of natural gas. Gazov. Prom-st. 11, 30–31 (in Russian).*

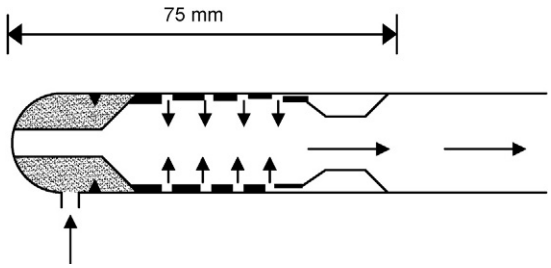

Fig. 6.25

Schematic diagram of a reactor with distributed oxygen supply (Casey et al., 1994).

of cooling with room-temperature water, 5%–10% of the methanol produced is carried away. In reality, this percentage can reach 15% or more, as can be seen from the data (Furman and Shestakova, 1956). A more complete extraction of condensable products is one of the most practical ways to increase the methanol yield. Note, however, that achieving a methanol carry-away percentage by the exhaust gas of less than 1% requires cooling to a temperature close to 0°C.

In Sokolovskii et al. (1998), the concentration and yield of methanol were increased by passing the reaction products through a trap filled with quartz crumb treated with boric acid. At a temperature of 120°C, such a trap efficiently removed methanol from the reactant flow. After a certain period, the trap was disconnected from the reactant flow and connected to a steam generator to extract the adsorbed methanol. The extraction efficiency was 80%, which made it possible to obtain a concentrated methanol solution.

Various methods for isolating the products formed in DMTM have been examined. Among them are various methods for continuous isolation or binding of the products formed and the separation of CH_4 and O_2 until their direct interaction, for example, on catalytic permeable membranes, and others. Unfortunately, no feasible methods for selective adsorption or membrane separation of methanol at temperatures close to the temperature of its formation in the DMTM process have been proposed.

As an interesting attempt at implementing one of these ideas, the authors of (Bjorklund and Carr, 2002) suggested using a simulated countercurrent moving bed chromatographic reactor (SCMCR) to extract the methanol formed during the partial oxidation of the methane. A process of methanol extraction with subsequent methane recycling was modeled using three successive switchable absorption columns filled with Supelcoport/10% Carbowax. This made it possible to achieve a more than eightfold increase in the overall conversion of methane, to 50% in the most favorable conditions as compared to 6% for a single pass through the reactor. The selectivity of methanol formation from a $CH_4/O_2 = 16.3$ mixture diluted to $\sim 60\%$ with helium in a thin ($d = 1$ mm) fused-silica capillary at a total pressure of $P = 100$ atm, $T = 477°C$, and $t_r = 10$ s was 40%–50%, that is, the yield exceeded 20%. Clearly, the implementation of such a process on a larger scale is technically very difficult, but can prove quite promising.

A number of studies pointed to the importance of a good mixing of the gases entering the reactor. In the patent (Gesser et al., 1986), oxygen and methane, supplied separately, were introduced into a special premixing chamber filled with Teflon shavings. A theoretical analysis, justifying the need for a rapid mixing of the reagents in order to achieve high degrees of conversion and selectivity, as well as to ensure the stable operation of the reactor, was carried out in Basevich et al. (1996). Kinetic simulations of the DMTM characteristics with consideration given to the molecular and turbulent diffusion of the reagents fed separately showed that a rapid mixing of the reagents within a time much shorter than the reaction time ($t_{mix} << t_r$) is a prerequisite for a high selectivity of methanol formation. Otherwise, during slow mixing, large volumes of mixture capable of self-ignition can arise, which makes the conversion process unstable.

5 Conclusions

Numerous experimental and theoretical investigations have demonstrated that, at properly chosen parameters and arrangements of the process, DMTM makes it possible to provide a yield of oxygenates, primarily methanol, high enough for practical applications.

References

Anisonian, A.A., Gudkov, S.F., Enikolopian, N.S., Kle'menov, N.A., Markevich, A.M., Nalbandian, A.B., et al., 1957. Production of formaldehyde by direct oxidation of natural gas by air. Gazov. Prom-st. 6, 32–40 (in Russian).

Arutyunov, V.S., 2002. The role of pressure in partial oxidation of methane. Russ. Chem. Bull. 51, 2170–2175.

Arutyunov, V.S., 2004. Recent results on fast flow gas-phase partial oxidation of lower alkanes. J. Nat. Gas Chem. 13, 10–22.
Arutyunov, V., 2014. Direct Methane to Methanol: Foundations and Prospects of the Process. Elsevier B.V., Amsterdam.
Arutyunov, V.S., Krylov, O.V., 1998. Oxidative Conversion of Methane. Nauka, Moscow (in Russian).
Arutyunov, V.S., Krylov, O.V., 2005. Oxidative conversion of methane. Russ. Chem. Rev. 74, 1111–1137.
Arutyunov, V.S., Strekova, L.N., 2017. The interplay of catalytic and gas-phase stages at oxidative conversion of methane: a review. J. Mol. Catal. A Chem. 426, 326–342.
Arutyunov, V.S., Vedeneev, V.I., Klimovetskaya, S.Y., Leonov, V.E., Pavlii, L.V., 1994. Influence of pressure on the formation of products of partial oxidation of methane. Theor. Found. Chem. Eng. 28, 563–568.
Arutyunov, V.S., Basevich, V.Y., Vedeneev, V.I., 1995a. Modern state of direct partial oxidation of natural gas to methanol. Ind. Eng. Chem. Res. 34, 4238–4243.
Arutyunov, V.S., Vedeneev, V.I., Klimovetskaya, S.Y., Leonov, V.E., Pavlii, L.V., 1995b. Effect of hydrogen, carbon monoxide and nitrogen on partial oxidation of methane. Theor. Found. Chem. Eng. 29, 63–67.
Arutyunov, V.S., Basevich, V.Y., Vedeneev, V.I., 1996a. Direct high pressure gas-phase oxidation of natural gas to methanol and other oxygenates. Russ. Chem. Rev. 65, 197–224.
Arutyunov, V.S., Basevich, V.Y., Vedeneev, V.I., Parfenov Yu, V., Sokolov, O.V., 1996b. Dependence of the kinetic of gas phase methane oxidation at high pressures on the concentration of oxygen and on temperature. Russ. Chem. Bull. 45, 45–48.
Arutyunov, V.S., Basevich, V.Y., Vedeneev, V.I., Romanovich, L.B., 1996c. Kinetic modeling of direct gas-phase methane oxidation to methanol at high pressures. Kinet. Catal. 37 (1), 20–27.
Arutyunov, V.S., Basevich, V.Y., Vedeneev, V.I., Krylov, O.V., 1999. On the role of catalyst in high temperature reactions of methane oxidation. Kinet. Catal. 40, 382–387.
Arutyunov, V.S., Rudakov, V.M., Savchenko, V.I., Sheverdenkin, E.V., Sheverdenkina, O.G., Zheltyakov, A.Y., 2002. Partial alkane oxidation at high pressures: methane oxidation in stainless steel and quartz reactors. Theor. Found. Chem. Eng. 36, 472–476.
Arutyunov, V.S., Zalepugin, D.Y., Sinev, M.Y., 2007. Oxidative conversion of light alkanes in supercritical conditions: first results, problems, and prospects. SKF-TP 2, 5–29 (in Russian).
Asinger, F., 1958. Chemie und technologie der paraffin-kohlenwasserstoffe. Akademie-Verlag, Berlin.
Basevich, V.Y., Vedeneev, V.I., Arutyunov, V.S., 1996. Radial and axial diffusion at gas phase oxidation of methane to methanol. Theor. Found. Chem. Eng. 30, 579–584.
Bibb, C.H., Lucas, H.J., 1929. Air oxidation of hydrocarbons catalyzed by nitrogen oxides. Ind. Eng. Chem. 21, 633–635.
Bjorklund, M.C., Carr, R.W., 2002. Enhanced methanol yields from the direct partial oxidation of methane in a simulated countercurrent moving bed chromatographic reactor. Ind. Eng. Chem. Res. 41, 6528–6536.
Bludworth, J.E., 1949. First tonnage oxygen plant ties in with petrochemical manufacture. Pet. Process. Petrochem. 4 (4), 377–379.
Bone, W.A., Allum, R.E., 1932. The slow combustion of methane. Proc. R. Soc. Lond. A134, 578–591.
Bone, W.A., Wheeler, R.V., 1902. J. Chem. Soc. 81, 535–549.
Bone, W.A., Wheeler, R.V., 1903. J. Chem. Soc. 83, 1074–1087.
Brockhaus, R., Franke, H.J., 1981. Process for the manufacture of formaldehyde and methanol by partial oxidation of methane. US Patent 4243613.
Brown, M.J., Parkyns, N.D., 1991. Progress in the partial oxidation of methane to methanol and formaldehyde. Catal. Today 8, 305–335.
Budymka, V.F., Egorov, S.A., Gavrya, N.A., Mochaev, A.S., Khomenko, G.A., Leonov, V.E., 1987. Effect of the process parameters on the gas-phase partial oxidation of natural gas. Khim. Prom-st. Segodnya 6, 10–11 (in Russian).
Burch, R., Squire, G.D., Tsang, S.C., 1989. Direct conversion of methane into methanol. J. Chem. Soc., Faraday Trans. 1 85, 3561–3568.
Casey, P.S., McAllister, T., Foger, K., 1994. Selective oxidation of methane to methanol at high pressures. Ind. Eng. Chem. Res. 33, 1120–1125.

Chun, J.-W., Anthony, R.G., 1993. Free radical kinetic model for homogeneous oxidation of methane to methanol. Ind. Eng. Chem. Res. 32, 796–799.
Davis, M.B., Schmidt, L.D., 1999. The seeding of methane oxidation. Combust. Flame 119, 182–188.
Edwards, J.H., Foster, N.R., 1986. The potential for methanol production from natural gas by direct catalytic partial oxidation. Fuel Sci. Technol. Int. 4, 365–390.
Eskendirov, I., Coville, N.J., Parmaliana, A., Sokolovski, V.D., 1997. Direct oxidative conversion of methane into higher hydrocarbons and oxy-products in the presence of hydrogen peroxide. Natural Gas Conversion IV. Studies in Surface Science and Catalysis. 107, Elsevier Sci. B.V., Amsterdam, pp. 301–306
Foral, M.J., 1992. The noncatalytic partial oxidation of natural gas to methanol. In: Preprints, Symposium on Natural Gas Upgrading II, 203d National Meeting of the American Chemical Society, Division of Petroleum Chemistry, San Francisco, CA. American Chemical Society, Washington, DC, pp. 34–40.
Foster, N.R., 1985. Direct catalytic oxidation of methane to methanol: a review. Appl. Catal. 19, 1–11.
Foulds, G.A., Gray, B.F., 1995. Homogeneous gas-phase oxidation of methane to methanol and formaldehyde. Fuel Process. Technol. 42, 129–150.
Foulds, G.A., Charlton, B.G., Le, B.T., Jones, J.C., Gray, B.F., 1997. The use of a jet-stirred continuously stirred tank reactor (CSTR) to study the homogeneous gas phase partial oxidation of methane to methanol. In: De Pontes, M., Espinoza, R.L., Nicolaides, C.P., Scurrell, M.S. (Eds.), Natural Gas Conversion IV. Studies in Surface Science and Catalysis. 107. Elsevier Science B.V., Amsterdam, pp. 3–8
Furman, M.S., 1946. Oxidation of methane under pressure. Khim. Prom-st. Segodnya 1–2, 24–26 (in Russian).
Furman, M.S., Shestakova, A.D., 1956. Oxidation of methane under pressure. Tr. Gos. Inst. Azot. Promyshl. 6, 98–108 (in Russian).
Garcia, E.Y., Loffer, D.A., 1984. Partial oxidation of methane. Lat. Am. J. Chem. Eng. Appl. Chem. 14, 267–284.
Gesser, H.D., Hunter, N.R., 1992. The direct conversion of methane to methanol (DMTM). In: Wolf, E.E. (Ed.), Direct Methane Conversion by Oxidative Processes: Fundamental and Engineering. Van Nostrad, New York, pp. 402–425.
Gesser, H.D., Hunter, N.R., Prakash, C.B., 1985. The direct conversion of methane to methanol by controlled oxidation. Chem. Rev. 85, 235–244.
Gesser, H.D., Hunter, N.R., Morton, L., 1986. Direct conversion of natural gas to methanol by controlled oxidation. US Patent 4618732.
Gesser, H.D., Hunter, N.R., Shigapov, A.N., 1995. Some characteristics of the partial oxidation of CH_4 to CH_3OH at high pressures. In: Bhasin, M.M., Slocum, D.W. (Eds.), Methane and Alkane Conversion Chemistry. Plenum Press, New York, pp. 271–286.
Hunter, N.R., Gesser, H.D., Morton, L.A., Yarlagadda, P.S., Fung, D.P.C., 1990. Methanol formation at high pressure by the catalyzed oxidation of natural gas and by the sensitized oxidation of methane. Appl. Catal. 57, 45–54.
Hunter, T.B., Wang, H., Litzinger, T.A., Frenklach, M., 1994. The oxidation of methane at elevated pressures: experiments and modeling. Combust. Flame 97, 201–224.
Kolbanovskii, Y.A., Bilera, I.V., Rossikhin, I.V., Borisov, A.A., Troshin, K.Y., 2011. Single-stage conversion of associated petroleum gas and natural gas to syngas in combustion and auto-ignition processes. Russ. J. Gen. Chem. 81, 2594–2603.
Krylov, O.V., 1992. The partial catalytic oxidation of methane to give oxygen-containing compounds. Russ. Chem. Rev. 61, 1118–1129.
Layng, T.E., Soukop, R., 1928. Ind. Eng. Chem. Res. 20, 1052.
Lødeng, R., Lindvag, O.A., Søraker, P., Roterud, P.T., Onsager, O.T., 1995. Experimental and modeling study of the selective homogeneous gas phase oxidation of methane to methanol. Ind. Eng. Chem. Res. 34, 1044–1059.
Lott, J.L., Sliepcevich, C.M., 1967. Partial oxidation of methane at high pressures. Ind. Eng. Chem. Process. Des. Dev. 6, 67–74.
Mackie, J.C., 1991. Partial oxidation of methane: the role of gas phase reaction. Catal. Rev. Sci. Eng. 33, 169.
Melvin, A., 1966. Spontaneous ignition of methaneeair mixtures at high pressure I. The ignition delay preceding explosion. Combust. Flame 10, 120–128.

Newitt, D.M., 1937. The oxidation of hydrocarbons at high pressures. Chem. Rev. 21, 299–317.
Newitt, D.M., Huffner, A.E., 1932. The formation of methyl alcohol and formaldehyde in the slow combustion of methane at high pressures. Proc. R. Soc. Lond. A134, 591–604.
Newitt, D.M., Schmidt, W.G., 1937. The oxidation of propane. Part II. The products of the slow oxidation at high pressure. J. Chem. Soc., 1665–1669.
Newitt, D.M., Szego, P., 1934. Slow oxidation at high pressures. Proc. R. Soc. Lond. A147, 555–571.
Oberdorfer, P.E., Winch, R.F., 1961. Chemicals from methane in a high compression engine. Ind. Eng. Chem. 53, 41–44.
Onsager, O.T., Lødeng, R., Søraker, P., 1989. The homogeneous gas phase oxidation of methane and the retarding effect of basic/inert surfaces. Catal. Today 4, 355–363.
Paris, A., 1934. Mild oxidation of methane under pressure. Chem. Abstr. 28, 5806 (Chim. Ind. April, 411–420).
Patent of Canada 291411, 1929.
Patent RU 2200731, 10.10, 2001.
Patent US 1776771, 1930.
Pichler, H., Reder, D.R., 1933. Uber die bildung von methylalkohol bei der partiellen oxydation von methan und athylen unter hohen druck. Angew. Chem. 11, 161–165.
Pitchai, P., Klier, K., 1986. Partial oxidation of methane. Catal. Rev. Sci. Eng. 28, 13–88.
Rasmussen, C.L., Glarborg, P., 2008. Direct partial oxidation of natural gas to liquid chemicals: chemical kinetic modeling and global optimization. Ind. Eng. Chem. Res. 47, 6579–6588.
Rasmussen, C.L., Jacobsen, J.G., Glarborg, P., 2008. Experimental measurements and kinetic modeling of CH_4/O_2 and $CH_4/C_2H_6/O_2$ conversion at high pressure. In. J. Chem. Kinet. 40, 778–807.
Semenov, N.N., 1935. Chemical Kinetics and Chain Reactions. Clarendon Press, Oxford.
Shtern, V.Y., 1964. Gas Phase Oxidation of Hydrocarbons. Pergamon Press, Oxford/London/New York.
Simchenko, V.P., Shcherbakov, P.M., Vedeneev, V.I., Arutyunov, V.S., 1999. The kinetics of methane oxidation at high pressures. Theor. Found. Chem. Eng. 33, 362–364.
Sinev, M.Y., Korchak, V.N., Krylov, O.V., 1989. The mechanism of the partial oxidation of methane. Russ. Chem. Rev. 58, 22–34.
Sinev, M., Arutyunov, V., Romanets, A., 2007. Kinetic models of C_1–C_4 alkane oxidation as applied to processing of hydrocarbon gases: principles, approaches and developments. In: Marin, G.B. (Ed.), Advances in Chemical Engineering. In: 36, Elsevier, Amsterdam, pp. 171–263.
Sittig, M., 1962. Combining Oxygen and Hydrocarbons for Profit. Gulf Pub. Co, Houston, TX (Sittig, M., 1970. Processes in the Oxidation of Hydrocarbon Raw Material, Khimiya, Moscow (in Russian)).
Sokolovskii, V.D., Coville, N.J., Parmaliana, A., Eskendirov, I., Makoa, M., 1998. Methane partial oxidation. Challenge and perspective. Catal. Today 42, 191–195.
Tabata, K., Teng, Y., Takemoto, T., Suzuki, E., Banares, M.A., Pena, M.A., et al., 2002. Activation of methane by oxygen and nitrogen oxides. Catal. Rev. 44, 1–58.
Takemoto, T., Tabata, K., Teng, Y., Nakayama, A., Suzuki, E., 2001. The effect of reaction pressure on the production of methanol trough the selective oxidation of methane in CH_4–O_2–NOx ($x = 1$ or 2). Appl. Catal. A205, 51–59.
Takemoto, T., He, D., Teng, Y., Tabata, K., Suzuki, E., 2002. The optimization of methanol yield in direct selective oxidation of methane with O_2 and NO in the presence of Cu-ZnO/Al_2O_3. J. Mol. Catal. A Chem. 179, 279–286.
Torchian, H.G., Mantashian, A.H., Nalbandian, A.B., 1974. Oxidation of methane under adiabatic compression conditions. Arm. Khim. Zh. 27, 271–278 (in Russian).
Tripathy, N., 1975. Slow combustion of methane at elevated pressures. Isr. J. Chem. 13, 190–196.
Tulenin, P.Y., Sokolov, O.V., Sinev, M.Y., Savkin, V.V., Arutyunov, V.S., Korchak, V.N., 2001. Interaction between heterogeneous and homogeneous processes in gas-phase methane oxidation by supported platinum catalysts. In: EvropCat Symposium 5. Alkane Activation. (Abstracts. Book 4. 5-P-12).
Vedeneev, V.I., Goldenberg, M.Y., Gorban, N.I., Teitelboim, M.A., 1988a. Quantitative model of the oxidation of methane at high pressures. I. Description of model. Kinet. Catal. 29, 1–8.

Vedeneev, V.I., Goldenberg, M.Y., Gorban, N.I., Teitelboim, M.A., 1988b. Quantitative model of the oxidation of methane at high pressures. II. Mechanism of autoacceleration. Kinet. Catal. 29, 8–14.
Vedeneev, V.I., Goldenberg, M.Y., Gorban, N.I., Teitelboim, M.A., 1988c. Quantitative model of the oxidation of methane at high pressures. III. Mechanism of formation of reaction products. Kinet. Catal. 29, 1121–1126.
Vedeneev, V.I., Goldenberg, M.Y., Gorban, N.I., Teitelboim, M.A., 1988d. Quantitative model of the oxidation of methane at high pressures. IV. Ignition delays. Kinet. Catal. 29, 1126–1133.
Vedeneev, V.I., Arutyunov, V.S., Basevich, V.Y., Goldenberg, M.Y., Teitelboim, M.A., Krymov, N.Y., 1994. Role of pressure in homogeneous and/or catalytic oxidation of methane. Catal. Today 21, 527–532.
Vedeneev, V.I., Simchenko, V.P., Shcherbakov, P.M., 1995. Production of methanol in the stepwise oxidation of natural gas. Gazov. Prom-st. 11, 30–31 (in Russian).
Vedeneev, V.I., Arutyunov, V.S., Bacevich, V.Y., 1997. Simulation of the gas-phase oxidation of methane: the kinetic limit of the yield of ethane and ethylene in the oxidative coupling of methane. Khim. Fiz. 16, 76–91 (in Russian).
Walker, J.C., Malakoff, H.L., 1946. Basic oxygenated chemicals from C_1, C_2 and C_3 paraffins and olefins. Oil Gas J. 45 (33), 59–65.
Walsh, D.E., Martenak, D.J., Han, S., Palermo, R.E., 1992a. Direct oxidative methane conversion at elevated pressure and moderate temperatures. Ind. Eng. Chem. Res. 31, 1259–1262.
Walsh, D.E., Martenak, D.J., Han, S., Palermo, R.E., Michaels, J.N., Stern, D.L., 1992b. Pressure, temperature, and product yield relationships in direct oxidative methane conversion at elevated pressure and moderate temperatures. Ind. Eng. Chem. Res. 31, 2422–2425.
Wiezevich, P.J., Frolich, P.K., 1934. Direct oxidation of saturated hydrocarbons at high pressures. Ind. Eng. Chem. 26, 267.
Yoshikawa, K., 1931. Oxidation of methane. II. The homogeneous oxidation of methane under high pressures. Bull. Inst. Phys. Chem. Res. 10, 305 (Chem. Abstr. 1931, 25, 4842).
Zhu, G., Gesser, H.D., Hunter, N.R., 1993. The O_3 sensitized partial oxidation of CH_4 to CH_3OH. Studies in surface science and catalysis. In: Curry-Hyde, H.E., Howe, R.F. (Eds.), Natural Gas Conversion III. Proceedings of the Third Natural Gas Conversion Symposium, Sydney, July 4–9. 81. Elsevier, Amsterdam.

Further Reading

Vedeneev, V.I., Goldenberg, M.Y., GorbanTeitelboim, N.I., Teitelboim, M.A., 1987. Mechanism of the initial stage of oxidation of methane at high pressures. Khim. Fiz. 6, 626–632 (in Russian).

CHAPTER 7

Direct Methane to Methanol: Reaction Products and Effect of Gas Composition

Vladimir Arutyunov[*,†]

[*]*Semenov Institute of Chemical Physics of Russian Academy of Sciences, Moscow, Russia* [†]*Institute of Problems of Chemical Physics of the Russian Academy of Sciences, Chernogolovka, Russia*

Acronyms

POM	partial oxidation of methane
DMTM	direct metane (conversion) to methanol
OCM	oxidative coupling of methane
GIAP	Russian State Institute of Nitrogen Industry

Symbols

P	pressure in atm or MPa
T, °C	temperature in Celsius
K	temperature in Kelvin
t_r	time of reaction
Q	methane flow rate

1 Introduction

The products obtained by the oxidative conversion of natural gas include hydrogen, syngas, acetylene, ethylene, oxygen-containing compounds, and aromatics. Especially attractive is the possibility of direct conversion of natural gas to oxygen-containing compounds (oxygenates), mainly methanol and formaldehyde, which are basic large-capacity petrochemical products. A cost-effective solution to this problem would greatly reduce the cost of producing not only these but also of many other chemicals derived from them; it would also make the use of the vast natural gas resources as chemical raw material much more attractive than it is now. Recently, this direction has been considered as promising way to solve the problems related to the utilization of the associated gas and the exploration of low-yield fields of natural gas, especially shale gas.

Methanol. https://doi.org/10.1016/B978-0-444-63903-5.00007-8

Because methanol is undoubtedly more important than other oxygen-containing compounds produced by the direct conversion of methane, this process was called *direct methane to methanol* (DMTM). The kinetic aspects of this process were considered in the previous chapter. In this chapter, the main DMTM products and the effect of the gas composition on the process are discussed. A high sensitivity of DMTMs to the initial gas composition and the great diversity in the composition of natural gases of different origins make the latter factor very important. A more detailed discussion of these aspects of the DMTM process can be found in the reviews (Arutyunov et al., 1995a, 1996; Arutyunov, 2004; Arutyunov and Krylov, 2005) and monographs (Arutyunov and Krylov, 1998; Arutyunov, 2014).

2 Oxidation Products

2.1 Main Products of the DMTM Process

At high pressures and moderate temperatures, the principal liquid-phase products of the oxidation of rich methane-oxygen mixtures ($[CH_4]/[O_2]$ ~10 to 30) are methanol, formaldehyde, and water. Methanol and formaldehyde, which are equally feasible primary products of the gas-phase oxidation of methane, are formed at similar rates, but through different pathways. This is especially evident in the initial stage of the process at a low conversion of methane in experiments at relatively low pressures, 1.5–3 atm (Han et al., 1995) (Fig. 7.1). In experiments in a 10-mm-diameter quartz flow reactor at 425–500°C and a low

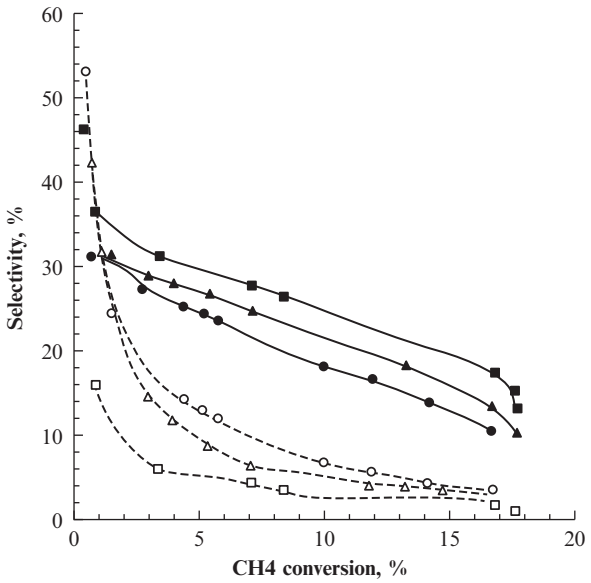

Fig. 7.1

Selectivity of methanol (closed symbols, solid lines) and formaldehyde (open symbols, dotted lines) formation as a function of the methane conversion at $P = 1.5$ (●), 2.0 (▲), and 3.0 (■) atm; $[O_2] = 20\%$, $t_r = 96$ s (Han et al., 1995).

methane conversion, the selectivity of formaldehyde formation is even superior to the selectivity of methanol formation. However, with increasing temperature (and, correspondingly, conversion), the overall selectivity of formaldehyde formation decreases more rapidly, which eventually makes methanol the predominant product.

At the beginning of the process ($T = 300$–$500°C$, $P = 21$–41 atm, and $[O_2] = 1$, 2–6, 5%), the only oxidation products are formaldehyde and methanol, with the selectivity of formaldehyde formation being twice that of methanol formation (Fig. 7.2). However, although the selectivity of formation of relatively stable methanol changes insignificantly with time, the selectivity of formation of less stable formaldehyde decreases rapidly, because it is consumed in secondary reactions leading to the formation of carbon oxides.

This was confirmed by the fact that carbon oxides were not observed among the primary products at short reaction times under specific conditions of adiabatic compression reactors (Torchian et al., 1974). The products of the partial oxidation of methane in those experiments were CH_3OH, CH_2O, CO, H_2, C_2H_6, C_2H_4, C_2H_2, C_3H_6, and C_2H_5OH.

The main gas-phase DMTM products are carbon oxides and hydrogen, with the yield of monoxide severalfold exceeding that of carbon dioxide. In this process, the main pathways for the formation of carbon dioxide are presumably not directly linked to carbon monoxide, as indicated by the fact that during the induction period in some experiments, it appeared before monoxide (Melvin, 1966). With increasing temperature, the yields of ethane and ethylene grow rapidly. In general, the ratio between the major DMTM products for the most typical conditions illustrates the schematic diagram (11) in the previous chapter, which demonstrated the fundamental nonselectivity of this gas-phase process.

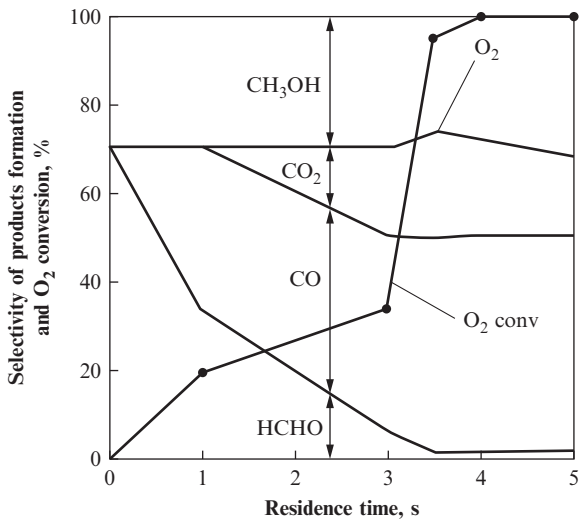

Fig. 7.2
Product selectivity as a function of the residence time at $T = 400°C$, $P = 41$ atm, and $CH_4/O_2/N_2 = 30{:}1{:}4$ (Omata et al., 1994).

2.2 CH_3OH/CH_2O Ratio

That formaldehyde, along with methanol, is the main product of the DMTM process, though quickly removed by secondary reactions, has been demonstrated in many studies. At low pressures, it prevails, apparently because of the peculiarities of the oxidation mechanism, which is also observed in appreciable quantities at high pressures in both gas-phase and catalytic experiments.

The catalytic partial oxidation of methane to formaldehyde, which has been the subject of many reviews (e.g., Baldwin et al., 1991) is beyond the scope of this chapter. It is, however, worth noting that on the surface of 5% V_2O_5-SiO_2 (one of the most efficient catalytic systems) at 650°C, atmospheric pressure, and a methane conversion per pass of 13.5%, the formaldehyde yield reached 4.73% (Parmaliana et al., 1993). A higher yield was obtained only by recycling the mixture and separating the accumulated product (Bafas et al., 2001). The work demonstrated the possibility of obtaining a formaldehyde yield of up to 50%, compared to 2% per pass on a V_2O_5-SiO_2-supported catalyst ($T = 840$ to 900 K, $P = 1$ atm), with a high selectivity of formaldehyde formation (up to 56%) and a 89% overall methane conversion.

One of the most detailed comparisons of the formation of formaldehyde in the presence of oxide catalysts and in an empty reactor was carried out by Baldwin et al. (1991). Fig. 7.3 shows the temperature dependences of the methane conversion, the selectivity of CH_2O formation, and its yield in an empty quartz reactor for a 1/5 methane-air mixture ratio at a pressure of $P = 5$ atm and a reaction time of $t_r = 2.3$ s.

As can be seen, the maximum CH_2O yield in an empty quartz reactor reached 3.46%, which was only slightly inferior to the best results obtained in the presence of oxide catalysts. The optimum

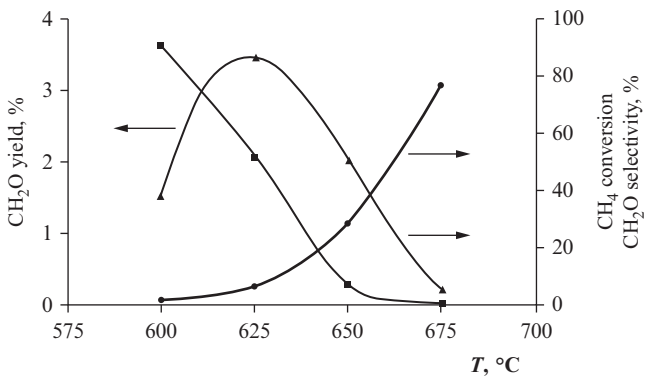

Fig. 7.3

Effect of temperature on the formaldehyde formation in an empty quartz reactor. Methane/air ratio 1:5, $P = 5$ atm, reaction time = 2.3 s (●) CH_4 conversion, (■) CH_2O selectivity, and (▲) CH_2O yield. *According to data from Baldwin, T.R., Burch, R., Squir, G.D., Tsang, S.C., 1991. Influence of homogeneous gas phase reactions in the partial oxidation of methane to methanol and formaldehyde in the presence of oxide catalysts. Appl. Catal., 74, 137–152.*

pressure for the noncatalytic conversion of methane to formaldehyde was about 5 atm. According to the authors of the paper, because of the subsequent thermal reactions involving formaldehyde, the upper limit of its yield under the conditions they used was unlikely to exceed 8%. In reality, it will be much lower, even when the reactants have very short residence times in the reaction zone. Thus, according to the findings of Baldwin et al. (1991), at slightly elevated pressures, ~5 atm, in an empty reactor, it was possible to obtain results that were not inferior to the best results obtained in the presence of catalysts. This was confirmed by the data from Irusta et al. (1994), in which the catalysis or promotion of the process with NO additives did not make it possible to surpass the results obtained in the gas-phase process. Filling the reactor with an "inert" solid phase or increasing the reaction time greatly reduces the formaldehyde yield.

The possibility of achieving in noncatalytic gas-phase partial oxidation of methane, at sufficiently high temperatures and short reaction times, practically the same results as in the catalytic oxidation was demonstrated in (Zhang et al., 2011). In a quartz flow reactor at $T = 1173–1273$ K, $P = 2$ atm, initial reagent ratio $[O_2]/[CH_4] = 0.5–15$ (at a 90% dilution with Ar), and a reaction time of 20–60 min, the highest formaldehyde yield was 2.4%. A marked formation of products under these conditions was observed only at temperatures above 1198 K. The first to appear, CH_2O and C_2H_6, were obviously the primary reaction products. Carbon oxides formed only at temperatures above 1223 K, after which the selectivity of CO formation passed through a maximum (35% at 1248 K), while the CO_2 yield increased sharply with temperature. The C_2H_6 and C_2H_4 (OCM products) also passed through a maximum (52%) at 1223 K and then within $T = 1233–1273$ K remain at 30%. According to the observations of the authors, in the investigated range, temperature had little effect on the ratio of the partial oxidation and OCM products, since the ancestors of the two groups of products were methyl radicals. An increase in the $[O_2]/[CH_4]$ ratio from 2, (which was already very high for normal conditions, with the main products being CH_2O and C_2H_6) to $[O_2]/[CH_4] = 5$ resulted in a very sharp decrease in the selectivity of their formation. With decreasing $[O_2]/[CH_4]$, the major products became OCM products, but the methane conversion decreased sharply. Kinetic simulations describe these results and indicate that, at such high temperatures, the main channel of CH_2O formation is the direct oxidation of methyl radicals $CH_3^{\bullet}$ with oxygen. In part, it is also formed in the dehydrogenation or oxidation of methoxy radicals $CH_3O^{\bullet}$.

Analysis of the homogeneous partial oxidation of methane at atmospheric pressure promoted by NOx in the framework of a detailed kinetic model (Zalc et al., 2006) confirmed the existence of a fundamental limitation on the CH_2O yield. The maximum predicted yield under all realistic conditions was below 10%. The addition of NOx, along with increasing the reaction rate, promotes the replacement of $HO_2^{\bullet}$ and $H^{\bullet}$, which are relatively slow reacting radicals, by more reactive $OH^{\bullet}$ radicals, thereby increasing the CH_2O yield. However, the CH_2O yield is limited by the rate of interaction of $OH^{\bullet}$, with CH_2O being higher than that with CH_4.

The effect of pressure on the calculated formaldehyde yield appeared to be small. At the same time, raising the pressure dramatically enhanced the methanol yield, thereby increasing the CH_3OH/CH_2O ratio in the products. According to the DMTM mechanism (Vedeneev et al., 1988a,b,c,d) (see the previous chapter), at high pressures, the ratio between the rates of formation of methanol and formaldehyde, and therefore their yields, is primarily determined by the competition between the reactions of $CH_3O^{\bullet}$ radicals, formed during the oxidation, with methane and oxygen, being dependent, among other things, on the CH_4/O_2 ratio and the temperature.

$$CH_3O^{\bullet} + CH_4 \rightarrow CH_3OH + CH_3^{\bullet} \tag{7.1}$$

$$CH_3O^{\bullet} + O_2 \rightarrow CH_2O + HO_2^{\bullet} \tag{7.2}$$

At temperatures typical of the DMTM process, the rate constant of reaction (7.2) is ~fivefold higher than that of reaction (7.1); however, a much higher (twentyfold to thirtyfold) methane concentration makes methanol the predominant product. For example, in Lødeng et al. (1995), at $P = 40$ and 60 atm, $T \approx 450°C$, $[O_2] = 2.8\%$, and a short reaction time ($t_r \approx 1.2$ s), the CH_3OH/CH_2O ratio in most experiments, especially at low conversions of the reactants, ranged within 3–5.

The pressure dependence of the CH_3OH/CH_2O ratio obtained based on data from Takemoto et al. (2002) and Arutyunov et al. (1994) is shown in Fig. 7.4. Due to the rapid growth of the methanol yield, this ratio increased rapidly with pressures up to 50–100 atm. At higher pressures, this dependence became weaker. These results indicate that the methanol/formaldehyde ratio in the oxidation products can be varied over a very wide range by

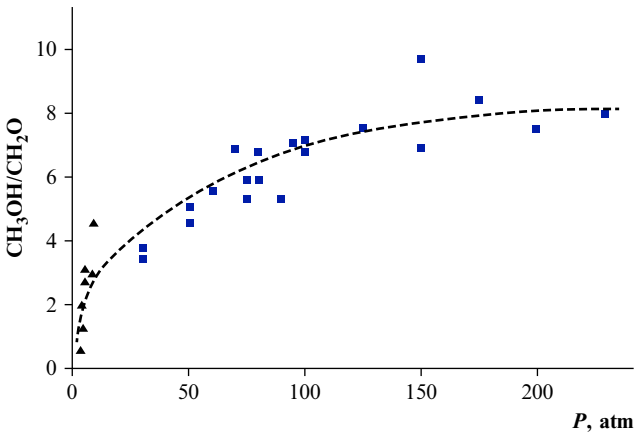

Fig. 7.4
Pressure dependence of the CH_3OH/CH_2O ratio: (▲) (Takemoto et al., 2002) and (■) (Arutyunov et al., 1994).

changing the process conditions, particularly pressure, temperature, and composition of the mixture.

2.3 CO/CO_2 Ratio

Although under typical DMTM conditions both carbon oxides are always among the main products of the partial oxidation of methane, in the vast majority of studies carbon monoxide noticeably prevails over dioxide. For example, in Lødeng et al. (1995), at $P = 40$ and 60 atm, $T = 450°C$, $[O_2] = 2.8\%$, $t_r \approx 1.2$ s, the ratio $CO/CO_2 \geq 10$. The predominance of carbon dioxide in some experiments with a long residence time of the reactants in a static reactor (e.g., Melvin, 1966) is likely due to a contribution from the heterogeneous oxidation of methane and heterogeneous conversion of the primary oxidation products. This probably explains why CO_2 appears earlier than CO (Melvin, 1966) during the ignition delay period. In any case, kinetic simulations predict (Arutyunov, 2003) a later appearance of CO_2 as compared with CO.

According to the experimental data from (Arutyunov et al., 1994), at an initial oxygen concentration of 2.8%, the concentration of carbon monoxide, the main gas-phase reaction product, at the reactor outlet reaches ~1.5%, remaining approximately constant in pressures ranging from 30 to 230 atm (Fig. 7.5). The concentration of carbon dioxide is severalfold lower, increasing slightly with the pressure, which leads to a decrease in the CO/CO_2 ratio. The increase of the CO_2 concentration with the pressure is probably partly associated with the formation and subsequent decomposition of formic acid, according to the mechanism proposed in (Vedeneev et al., 1992).

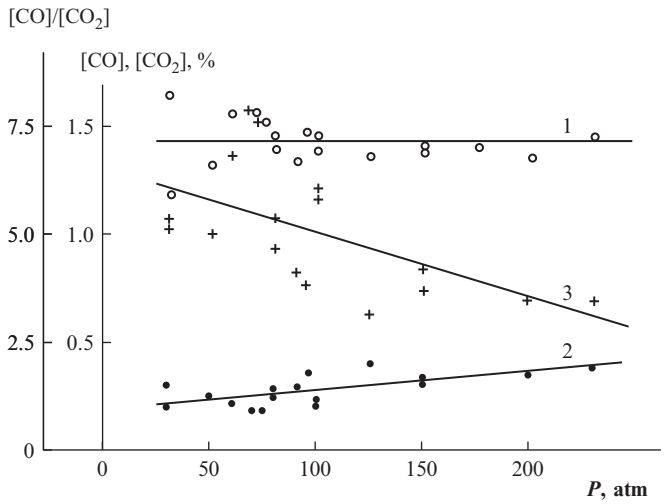

Fig. 7.5

Pressure dependence of the concentrations of carbon oxides and the $[CO]/[CO_2]$ ratio at $T = 400°C$ and $[O_2] \asymp 2.8\%$: (1) CO, (2) CO_2, and (3) $[CO]/[CO_2]$ (Arutyunov et al., 1994).

2.4 By-Products

In early studies, which especially focused on analysis of the composition of the DMTM products, a large number of various hydrocarbon and oxygen-containing products were identified. Later works have been aimed mainly at studying the yield and kinetics of the formation of the main products of the process. Therefore the scarce information about by-products in more current works may merely reflect a lack of interest in their production in this process. Note, however, that this may be due in part to the transition to more severe conditions and shorter reaction times, at which the formation of by-products is negligible.

Along with the main DMTM products just discussed, some studies have reported finding small amounts of liquid ethanol (up to 1.5%–2%), acetone (up to ~1%), and formic acid (up to ~0.8%). Small amounts of higher alcohols, aldehydes, and organic acids have also been detected. In the oxidation of gases with high concentrations of ethane and heavier alkanes, the yield of C_2–C_3 alcohols, aldehydes, and acids can be significant. Although hydrogen peroxide and organic peroxides are undoubtedly formed as intermediates in the oxidation process, even special attempts to identify them in the reaction products failed (Newitt and Huffner, 1932). Hydrogen peroxide, despite considerable effort, has not been detected during the induction period of the self-ignition of rich ($[O_2]/([CH_4]+[O_2]) = 0.019$–$0.088$) methane-air mixtures at pressures from 58 to 110 atm (Arutyunov et al., 2002). Only at atmospheric pressure were traces of these compounds detected (Chou and Albright, 1978).

Several studies have reported the detection of some complex organic compounds, such as methyl formate and methylal (Arutyunov, 2014). However, the most likely cause of their appearance may be a reaction in the isolated liquid phase. In any case, at very short reaction times in an adiabatic compression reactor (Torchian et al., 1974), complex organic products were not observed.

More logical and understandable is the formation of some gaseous by-products. At temperatures above 450–500°C, a marked yield of OCM products is observed, primarily ethylene and ethane (Onsager et al., 1989; Chun and Anthony, 1993; Casey et al., 1994); above 600°C, heavier homologues arise (Onsager et al., 1989).

The formation of hydrogen was mentioned in Lødeng et al. (1995), Chellappa et al. (1997), and Zhang et al. (2002a,b). In Zhang et al. (2002b), the H_2/CO ratio was ~0.4–0.5. A feasible source of H_2 is the dissociation of CH_2O to H_2 and CO.

At temperatures above 550°C, acetylene was detected (Walsh et al., 1992a,b).

In a number of studies, the exhaust gas was found to contain oxygen (see e.g., Arutyunov, 2014), a result difficult to explain within the framework of the branched-chain mechanism of gas-phase oxidation of methane, which invariably predicts a complete consumption of oxygen. The persistent presence of oxygen in the gaseous reaction products, on

average $\sim 0.05[O_2]_0$, was observed in (Arutyunov et al., 1994). Trivial reasons, such as oxygen leakage into the gas-handling system downstream of the reactor and analysis errors, were excluded. The most feasible explanation for the presence of oxygen in the exhaust gas is the production of secondary oxygen. Kinetic simulations of the process suggest that the source of secondary oxygen is the decomposition of hydrogen peroxide, which, by the time of complete oxygen conversion and actual stop of the branched-chain methane oxidation, can contain up to 20% of the oxygen present in the initial mixture:

$$2H_2O_2 \rightarrow 2H_2O + O_2 \tag{7.3}$$

In fact, this gross reaction does not reflect the radical-driven mechanism of hydrogen peroxide decomposition, which involves the formation of a large concentration of hydroxyl radicals. One of the main reasons for a decrease in the concentration of methanol and especially formaldehyde is the secondary reaction of hydroxyl radicals,

$$H_2O_2 \rightarrow 2OH^{\bullet} \tag{7.4}$$

$$OH^{\bullet} + CH_3OH \rightarrow H_2O + CH_3O^{\bullet} \tag{7.5}$$

$$OH^{\bullet} + CH_3OH \rightarrow H_2O + CH_2OH^{\bullet} \tag{7.6}$$

$$OH^{\bullet} + CH_2O \rightarrow H_2O + CHO^{\bullet} \tag{7.7}$$

which occurs after they reach the maximum values at the time of complete conversion of the initial oxygen and cessation of the branched-chain oxidation reaction. In the range of characteristic DMTM temperatures, 400 to 600°C, the reaction rate of gas-phase reaction (7.7) is more than twice that of reactions (7.5), (7.6), which may be one of the reasons for a more rapid decomposition of formaldehyde as compared with methanol.

2.5 $\Delta CH_4/\Delta O_2$ Ratio

Depending on the prevailing products, the stoichiometry of methane oxidation with oxygen can vary over a wide range: from $\Delta CH_4/\Delta O_2 = 1/2$ for the complete oxidation reaction

$$CH_4 + 2O_2 \rightarrow CO_2 + 2H_2O \tag{7.8}$$

to $\Delta CH_4/\Delta O_2 = 2$ for the hypothetical gross reactions

$$CH_4 + 1/2O_2 \rightarrow CO + 2H_2 \tag{7.9}$$

$$CH_4 + 1/2O_2 \rightarrow CH_3OH \tag{7.10}$$

$$CH_4 + 1/2O_2 \rightarrow CH_2O + H_2 \tag{7.11}$$

and even to higher values when the oxidation promotes the formation of a significant amount of oxygen-free conversion products, such as C_2H_6 or C_2H_4. According to the schematic

diagram (7.11) in the previous chapter, in the actual gas-phase DMTM process, the conversion of the reactants produces two main groups of products,

$$\begin{aligned} 2CH_4 + 2O_2 &\rightarrow CH_3OH \\ &\rightarrow CO + 2H_2O \end{aligned} \tag{7.12}$$

which lead to a conversion ratio of $\Delta CH_4/\Delta O_2 \approx 1$. If it is lower than that, one can conclude that the reaction is shifted in favor of the formation of CO and H_2O or that CO_2 is formed in an appreciable concentration, most likely by deep oxidation reactions at the surface of the reactor. The ratio $\Delta CH_4/\Delta O_2 > 1$ is indicative of the predominance of the formation of methanol and formaldehyde in the products or the C_2+ OCM products.

2.6 Yield of Methanol and Oxygenates

Because low oxygen concentration is a principal condition for high selectivity of methanol, which decreases rapidly with increasing initial oxygen concentrations, and therefore the methane conversion, the methanol yield per pass through the reactor is low, rarely exceeding 2.0%–2.5 %. Fig. 7.6 (Arutyunov, 2014) shows the results of many experiments carried out under fast flow conditions (residence time in the reactor was no more than 20 s) at a pressure of

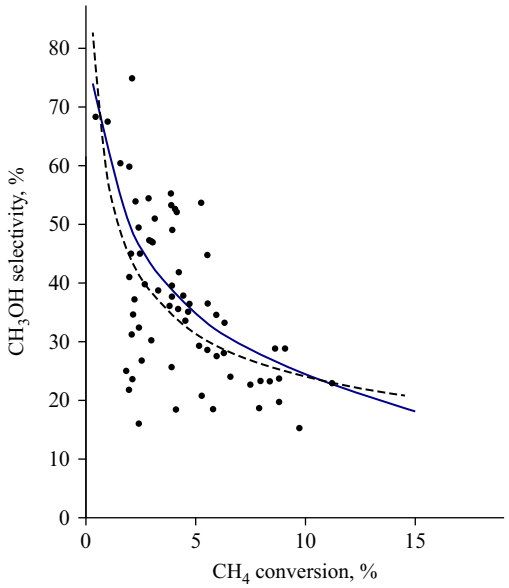

Fig. 7.6

Dependence of the CH_3OH selectivity on the CH_4 conversion obtained from fast-flow experiments with $t_r < 20$ s and $P \geq 30$ atm (Arutyunov et al., 1994). The dashed line is the trend of experimental data, whereas the solid line represents the results of kinetic simulations of the gas-phase DMTM process at $P = 100$ atm and $T = 420$°C (Arutyunov et al., 1996).

at least 30 atm. Despite the large data scatter, there is a clear trend of rapid decrease in the selectivity of methanol formation with increasing methane conversion. The overall trend line of the data presented is almost identical with the results of kinetic modeling of the gas-phase DMTM process (Arutyunov et al., 1996).

Fig. 7.7 is built on the same data dependence of the yield of methanol-from-methane conversion with a clear tendency to reach a yield limited to ~2.5%. As in the experimental data on the selectivity of methanol formation (Fig. 7.6), the trend line is in good agreement with the results of kinetic modeling of the gas-phase DMTM process.

The authors of Gesser et al. (1986, 1995), Yarlagadda et al. (1988), and Feng et al. (1994) claimed that they obtained a methanol yield of more than 6 to 7% per pass through the reactor, with the selectivity of its formation reaching 80% or even 90% (see, e.g., Arutyunov, 2014). However, the attempts of others (Burch et al., 1989), and sometimes the same authors, to reproduce these so-enticing results turned out to be unsuccessful. These experiments were performed at long reactant residence times in the reactor, about several minutes, and at relatively low temperatures (less than 400°C). It is hard to imagine any other explanation for the preceding results, especially a nearly 80% selectivity of methanol, except for a significant contribution from heterogeneous reactions occurring under these conditions. That a heterogeneous process takes place in these conditions was confirmed by the observation of

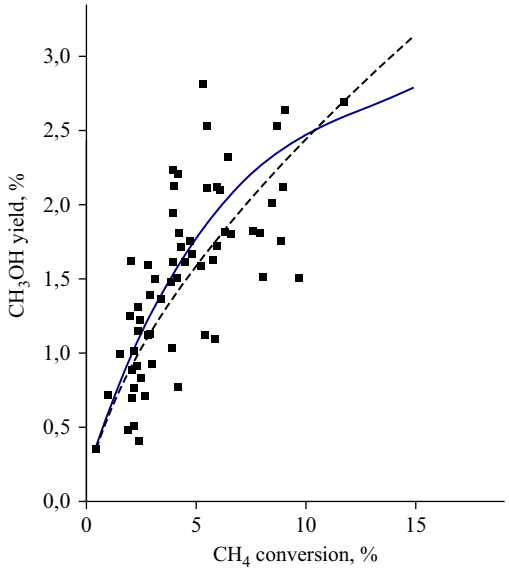

Fig. 7.7

Dependence of the CH_3OH yield on the CH_4 conversion obtained from fast-flow experiments at $t_r < 20$ s and $P \geq 30$ atm (Arutyunov, 2014). The dashed line is the trend of experimental data, and the solid line represents the results of kinetic simulations of the gas-phase DMTM process at $P = 100$ atm and $T = 420$°C (Arutyunov et al., 1996).

thermokinetic oscillations with a characteristic period of about 1 min (Yarlagadda et al., 1990). Another argument in favor of the heterogeneous nature of the process is a very weak pressure dependence of the selectivity of methanol formation at a complete oxygen conversion and a temperature of 340–350°C within 30–70 atm, which is not typical of the gas-phase process. A more detailed analysis of these experiments is given in Arutyunov (2014).

2.7 Oxidation Products of Methane Homologues

The number of works on the partial oxidation of methane homologues is much smaller than that on methane oxidation. A large variety of products produced by the oxidation of methane homologues makes it difficult to obtain a quantitative assessment of the fractions of individual products and their dependence on the particular parameters of the process. Generally, although the same basic classes of compounds (alcohols, aldehydes, organic acids) persist, the oxidation of methane homologues yields higher amounts of compounds with a larger number of carbon atoms, up to those present in the initial alkane.

One of the first studies of the oxidation of ethane under static conditions at pressures of 15–100 atm (Newitt and Bloch, 1933) showed that the composition of the oxidation of 9:1 C_2H_6-O_2 mixtures produces—along with carbon oxides, methane, and water-methanol, ethanol, formaldehyde, acetaldehyde, formic acid, and acetic acid. In this case, with increasing pressure, the yields of C_2 products (ethanol, acetaldehyde, and acetic acid) rise, whereas those of methanol and formaldehyde decrease. Practically the same products are formed in the partial oxidation of ethane in a static quartz reactor at atmospheric pressure (Newitt and Gardner, 1936).

The oxidation of propane at high pressures in static (Newitt, 1937; Newitt and Schmidt, 1937) and flow conditions (Wiezevich and Frolich, 1934) produced aldehydes (propionic and acetic), normal alcohols (methanol, ethanol, and propanol), and acids (mainly acetic and small amounts of propionic and formic). A pressure increase resulted in a significant increase in the yield of isopropyl alcohol, acetone, and organic acids, in a decrease in the yield of aldehydes and normal alcohols, in a redistribution of the ratio between normal alcohols in favor of propanol, in an increase in the CO_2 yield, and in a decrease in the CO yield; at pressures of 20 atm or higher, propylene became undetectable in the reaction product.

Only fragmentary information on the products of the gas-phase oxidation of butane, pentane, and heavier hydrocarbons at high pressures is available. In Wiezevich and Frolich (1934), the oxidation of pentanes, heptanes, and normal butane was studied. Along with the products of propane oxidation with oxygen, the products of the reaction of *n*-butane with oxygen at pressures from 33 to 160 atm were found to contain butyl alcohols, with its fraction increasing with the pressure. The oxidation of isobutane was reported (Sittig, 1962) to produce a variety of products, such as acetone, *tert*-butanol, and *tert*-butyl hydroperoxide.

3 Effect of the Gas Composition

3.1 Hydrocarbons

One of the main components affecting the nature of the partial oxidation of methane and the yield of its products is the presence of admixtures in its heavier homologues. Since the oxidation of methane homologues and mixtures with their high content will be considered separately, here we confine ourselves to an analysis of the influence of small concentrations of admixtures, only a few percent. In general, such admixtures cause an increase in the rate of oxidation or a decrease in the process temperature, in some cases significantly. The effect of small concentrations of additives of heavier hydrocarbons on the yield of the main products is substantially weaker.

In Burch et al. (1989), adding 5% of ethane to methane caused a decrease in temperature by 50°C at which the first products were detected, but it had no effect on the selectivity of methanol formation. In Simchenko et al. (1999), a changeover from natural gas containing ~6% C_2+ hydrocarbons to nearly pure methane (~0.2% C_2+) resulted in an increase in the process temperature by ~90°C, to a value almost identical to that predicted by kinetic simulations of DMTM.

The observed decrease in the temperature of the process was caused by a marked decrease in the effective activation energy of the oxidation in the presence of additives of heavy methane homologues. Based on the experimental data on the dependence of the time of complete oxygen conversion on the initial temperature for a gas containing ~6% C_2+ hydrocarbons (4.1% C_2H_6, 1.15% C_3H_8, and 0.45% C_4H_{10}), the activation energy was estimated to be $E_a = 29–33$ kcal/mol, which was significantly lower than the value characteristic of methane oxidation. The difference in the concentration of C_2+ hydrocarbons in the gas most likely explains the discrepancy in the optimal process temperature reported in different works (see, e.g., Budymka et al., 1987; Arutyunov et al., 2002).

Experiments with natural gas ($P = 91$ atm, $T = 427$°C, $t_r = 35$ s) containing ethane and ~1% C_3+ hydrocarbons (Foral, 1992) demonstrated that an increase in the ethane concentration in the mixture from 1% to 5% enhanced the overall conversion of hydrocarbons, but at the same time, the methane conversion decreased significantly, which was natural, given the higher reactivity of ethane and a significant deficit of oxygen. However, variations of the ethane concentrations within these limits produced no noticeable effect on the selectivity of formation of the products.

Perhaps the most detailed analysis of the effect of small (3%) additives of heavier alkanes on the methane conversion and methanol yield was performed in Omata et al. (1994). As expected, the main result was a decrease in the conversion temperature, by about 60, 50, and 30°C for *i*-butane, propane, and ethane, respectively (Fig. 7.8).

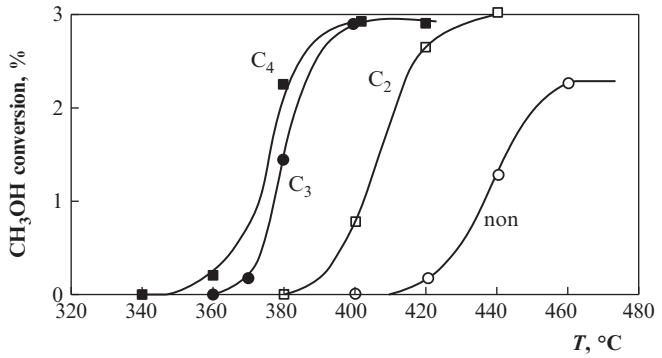

Fig. 7.8
Effect of addition of 3% C_2–C_4 hydrocarbons on the methane conversion at $P=41$ atm, $t_r=1$ s, and $CH_4:O_2:N_2=30:1:4$ (Omata et al., 1994).

More complicated was the question of the effect of hydrocarbon additives on the selectivity of conversion of methane to methanol. Although the methanol yield increased considerably (Fig. 7.9), much of this gain may have been due to the conversion of added alkane.

The influence of heavy methane homologues on the process temperature and reaction rate is well explained by their higher reactivity with respect to oxygen in the gas-phase reactions of initiation of the radical process:

$$C_nH_{2n+2} + O_2 \rightarrow C_nH^{\bullet}_{2n+1} + HO^{\bullet}_2 \qquad (7.13)$$

In the first approximation, this influence can be regarded as the promotion of methane oxidation, though the real picture is more complicated because of the complex interaction of the oxidation products (Sheverdenkin et al., 2004). However, in a typical DMTM temperature range, the initiation reaction rates for ethane and propane are, respectively, about two and three orders of magnitude higher than that for methane.

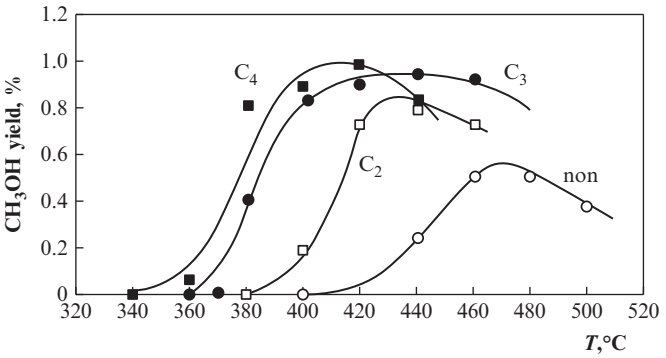

Fig. 7.9
Effect of addition of 3% C_2-C_4 hydrocarbons on the methanol yield at $P=4$ atm, $t_r=1$ s, and $CH_4:O_2:N_2=30:1:4$

3.2 Hydrogen

Hydrogen is one of the main DMTM gaseous products and is close to methane in terms of the typical conditions and mechanism of oxidation, which makes its possible impact on the process a very important issue. In Omata et al. (1994), hydrogen additives, unlike alkanes additives, caused no decrease in the initiation temperature. Although this paper argued that at low temperatures, 420–460°C, a hydrogen additive (4 mol% in methane) enhanced the methanol yield and inhibited the formation of CO_2, the data presented did not support this conclusion. In the presence of hydrogen, the yield was the same, except that the temperature at which it was achieved was ~10°C lower.

Simulations of the effect of a 10% H_2 additive at 34 atm, 430°C, $CH_4/O_2 = 16$, and a nearly complete conversion of oxygen showed a small decrease in the selectivity of methanol formation and virtually no effect on the methane conversion (Chellappa et al., 1997).

The effect of hydrogen on the DMTM process was studied in Arutyunov et al. (1995b) (Fig. 7.10). The presence of 5% hydrogen in the mixture had virtually no effect on the yield of liquid oxidation products. At higher concentrations of hydrogen, although the total amount of liquid products was the same, the methanol yield was substantially lower because of the corresponding increase in the water yield. The concentration of hydrogen remained essentially the same or increased slightly at the reactor inlet, with the gain not exceeding the hydrogen concentration in the absence of special hydrogen additives.

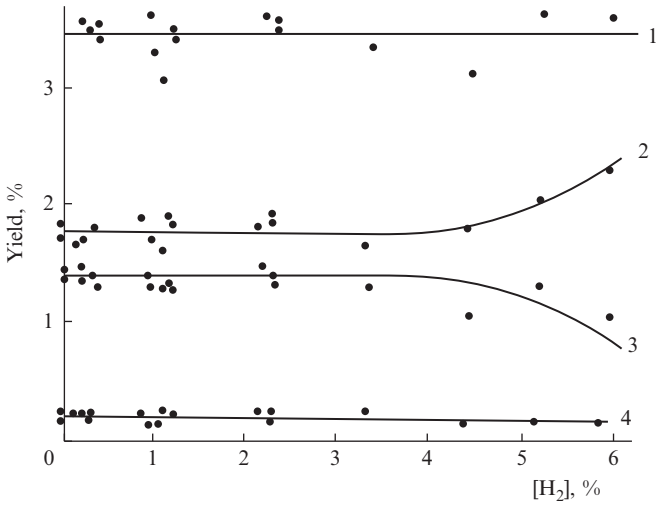

Fig. 7.10
Dependence of the yield of liquid oxidation products on the hydrogen concentration at $P = 100$ atm and $T = 400$°C: (1) total yield of liquid products, (2) H_2O, (3) CH_3OH, and (4) CH_2O (Arutyunov et al., 1995b).

3.3 Carbon Monoxide

Carbon monoxide is the main gaseous product of the process, being quite reactive under these conditions, so its effects may be very significant, especially at high methane conversion. The dependence of the yields of methanol and carbon oxides on the initial concentration of CO in the mixture were studied in (Furman and Shestakova, 1956) at $T = 375°C$, $P = 300$ atm, $t_r = 9$ s, and $[O_2] = 3.0\%–3.8\%$. The final concentration of carbon monoxide $[CO]_f$ in the products grew linearly with the initial concentration $[CO]_0$. However, the concentration of "oxidized carbon oxide" $[CO]_{ox}$, equal to the sum of the concentration $[CO]_r$ of CO formed in the reaction without special addition of CO and the concentration $[CO]_0$ of added CO minus the final concentration $[CO]_f$ ($[CO]_{ox} = [CO]_r + [CO]_0 - [CO]_f$), almost exactly corresponded to the CO_2 yield. These data suggest that CO_2 is mainly formed through the oxidation of CO. In this case, the methanol yield decreased monotonically with increasing $[CO]_0$, because at a given initial concentration of oxygen, an ever-increasing proportion of it was consumed to oxidize CO to CO_2 so that the conversion of methane decreased. It can be assumed that the correspondence between the CO conversion and the CO_2 yield in this study, where a reactor with a sufficiently active copper surface was used, occurred predominantly because of the heterogeneous oxidation of CO in the presence of hydrocarbons.

In Arutyunov et al. (1995b), the carbon monoxide additives, as well as the hydrogen additives, in concentrations of up to 5%, only slightly influenced the yield of products from the partial oxidation of methane (Fig. 7.11). A noticeable drop in the yield of liquid products after the addition of 5%–15% CO was observed. However, at high CO concentrations, at least in part, the effect was due to the reduction in the methane content in the mixture and, consequently, the CH_4/O_2 ratio, because in these experiments, the concentration of oxygen was constant. In the same range of CO concentrations, the difference between the initial and final CO concentrations decreased monotonically. Apparently, at these concentrations, an appreciable amount of CO reacts, thereby reducing the fraction of oxygen spent on the oxidation of methane. At still higher CO concentrations, its significant consumption in the reaction was observed. However, according to (Bjorklund and Carr, 2002), the reaction mixture can reasonably contain up to 12% CO.

3.4 Inerts

Because the ultimate goal of most works was the conversion of natural gas, relatively little experimentation was carried out with mixtures of highly diluted inert components. In the region of complete oxygen conversion, the temperature does not substantially affect the process; therefore dilution with inert components (while maintaining the total pressure and $[CH_4]/[O_2]$ ratio) apparently has little effect on the course of the reaction.

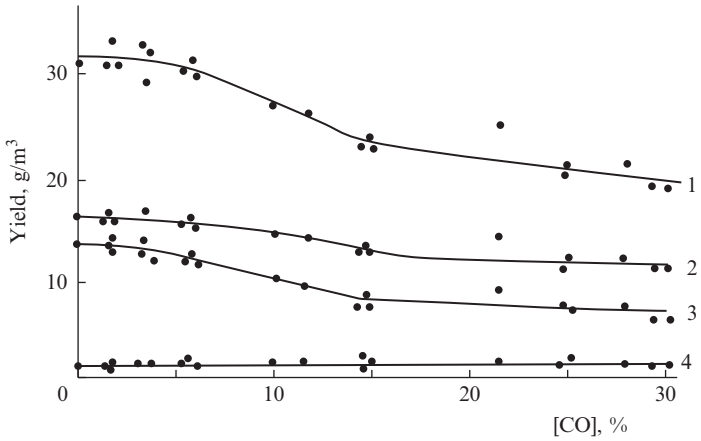

Fig. 7.11
Dependence of the yield of liquid oxidation products on the CO concentration at $P = 100$ atm and $T = 400°C$: (1) total yield of liquid products, (2) H_2O, (3) CH_3OH, and (4) CH_2O (Arutyunov et al., 1995b).

Comparison of the results reported in the patent of Brockhaus and Franke (1981), where oxygen, air, and air diluted with nitrogen were used as oxidants, did not reveal any systematic differences in the methane conversion or methanol yield because of a large data scatter. The authors of Burch et al. (1989) found no difference in the results obtained using mixtures containing and not containing nitrogen. The experiments performed in Chun and Anthony (1993) at a total pressure of $P = 50$ atm showed that diluting the test mixture with nitrogen (40%), CO, or CO_2 produced no effect on the selectivity of methanol formation.

It was demonstrated by Casey et al. (1994) that at $P = 50$ atm and $[O_2] = 6\%$, dilution of the reaction mixture with helium (degree of dilution was not specified) resulted in a barely noticeable change in the selectivity of methanol formation.

The author of Foral (1992) claimed that the addition of 10 mol% CO_2 to methane led to an increase in the yield of methanol. However, the data presented do not confirm, but rather refute, this conclusion. These data suggest that the addition of CO_2, like the addition of hydrogen, leaves the yield virtually the same as in the absence of the additives, only the temperature of reaching it is 20°C lower. The authors attempt to explain the allegedly "promoting" effect of CO_2 by the occurrence of the reaction

$$CO_2 + H \rightarrow CO + OH \tag{7.14}$$

is hardly reasonable, if only because the rate of the reaction under these conditions is low, as is the concentration of hydrogen atoms in the DMTM process; thus these two factors make the role of reaction (7.14) negligible.

In Feng et al. (1994), increasing the total pressure of a methane mixture with 6.5% O_2 from 10 to 50 atm by diluting it with CO_2 reduced the temperature of complete oxygen conversion and significantly increased the selectivity of methanol formation; however, these effects can be explained by a general increase of pressure in the system. In addition, in this study, heterogeneous processes might play a significant role.

4 Partial Oxidation of Methane Homologues

During production, transportation, and processing of hydrocarbons, significant amounts of gases with a high content or even a predominance of methane homologues are formed. A number of heavier hydrocarbons are formed during the oxidative conversion of methane or any other gaseous hydrocarbons, which influences the kinetics of the process. Therefore the investigation of the partial oxidation of methane homologues and mixtures of hydrocarbons corresponding to real natural gases is an important issue.

4.1 Ethane

The partial oxidation of ethane at high pressure was first performed in Newitt and Bloch (1933). The oxidation of mixtures containing 12%–15% O_2 in ethane was studied at pressures from 15 to 100 atm and temperatures from 260 to 315°C, at reaction times of a few minutes. In the oxidation of methane, the process featured a long induction period, significantly longer than the conversion itself. The predominant condensable product under these conditions was typically ethanol, of which the maximum concentration of reached was 36.5%, and the maximum yield of the sum of oxygenates was 71.7%. In addition to carbon oxides, methane, water, and ethanol, methanol, formaldehyde, acetaldehyde, formic acid, and acetic acid were formed.

With increasing pressure, the yield of ethanol, acetaldehyde, and acetic acid (i.e., C_2 products that do not require breaking the C-C bond) grew, whereas that of methanol and formaldehyde decreased. However, the reaction time in these experiments was maintained approximately constant (2.5–4.5 min) by significantly changing the temperature, an approach that did not provide the maximum yield of alcohols in each case. At pressures above 50 atm, the maximum yield of alcohols and acetaldehyde was only weakly dependent on pressure, whereas the acetic acid yield increased with pressure up to 100 atm, at which point, its maximum selectivity reached nearly 24%. The formaldehyde yield decreased monotonically with pressure up to 100 atm.

Experiments also showed a marked decrease in the selectivity of most (excluding formaldehyde) oxygenates, especially ethanol and acetic acid, when the initial concentration of oxygen in the mixture was increased from 11% to 15.5%. This was accompanied by an increase in the maximum heat-up of the mixture from 283.5 to 316.8°C, a factor that could

contribute significantly to this reduction. Upon the addition of successive portions of oxygen to the reacted mixture, the amount of formed ethanol, aldehydes, and acids, as well as methane, remained nearly constant, while the concentrations of methanol and carbon oxides increased monotonically (Newitt and Bloch, 1933).

The reaction conditions strongly affect the yield and composition of the products of the partial oxidation of ethane: not only the pressure, but also the temperature and, consequently, the duration of the oxidation. This is clearly seen from the pressure dependence of the composition of the products of the partial oxidation of ethane in a flow reactor (Table 7.1). In low-temperature static experiments, high pressure promotes a high yield of C_2 products, which dominate under these conditions. Under more severe conditions of flow experiments, with higher temperatures and much shorter reaction times, C_1 products dominate even at the highest pressures.

The experiments on the oxidation of ethane under flow conditions (Sheverdenkin et al., 2004) yielded results somewhat different from those obtained by Newitt and Gesser. As in the oxidation of methane, the main gaseous product of the ethane oxidation under these conditions was carbon monoxide. Its concentration grew with the initial oxygen concentration, reaching about 6 vol% at the maximum oxygen concentration. Hydrogen, ethylene, and carbon dioxide were also formed in appreciable quantities (Fig. 7.12). The concentration of hydrogen in the products increased approximately linearly with the initial oxygen concentration, reaching 3%. The ethylene concentration also rose sharply with the initial oxygen concentration, reaching almost 3%. Because the maximum heat-up was maintained nearly constant when the oxygen concentration was changed, the growth of the ethylene concentration was associated with the change of the initial oxygen concentration. The final concentration of carbon dioxide remained practically constant as the initial oxygen concentration was varied from 1.3% to 13.3%, being on average at least an order of magnitude lower than the carbon monoxide concentration (for methane oxidation, $CO/CO_2 \approx 6.7$). As in the oxidation of methane, the final reaction products' concentration of oxygen was a few percent of the initial concentration, which was apparently also of secondary origin.

Table 7.1 Effect of pressure and temperature on the yield of the main products of gas-phase oxidation of ethane (Sittig, 1962)

Compound	Composition of the Oxidation Products, mol%			
	7.03 atm 595°C	7.03 atm 460°C	70.3 atm 360°C	140.6 atm 340°C
Methanol	13	42	41	30
Ethanol	2	4	16	23
Formaldehyde	18	36	12	5
Acetaldehyde	3	5	4	4
Ethylene	46	0	0	0

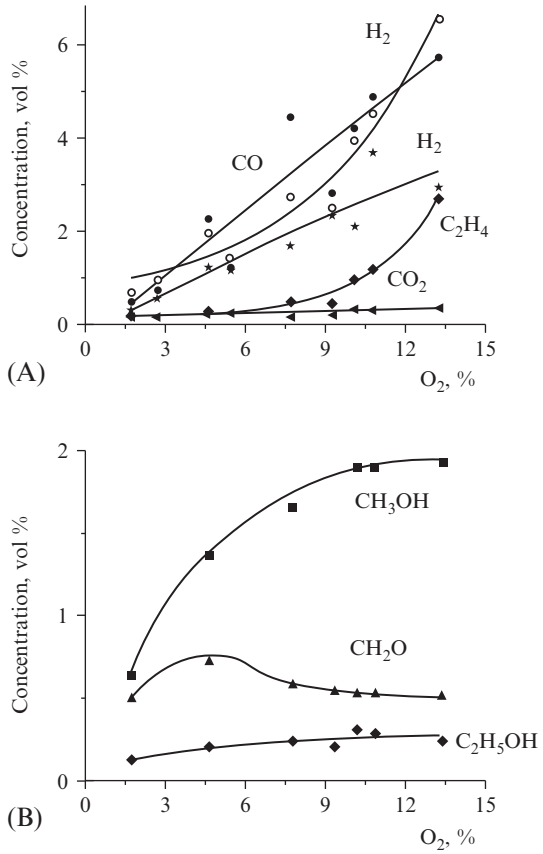

Fig. 7.12

Dependence of the concentrations of products of the gas-phase oxidation of ethane on the initial oxygen concentration at $P = 26$ atm, $Q = 400$ L/h, and $T_{max} = 550°C$: (A) (○) H_2O, (●) CO, (►) CO_2, (*) H_2, (◆) C_2H_4, (B) (■) CH_3OH, (▲) CH_2O, and (◆) C_2H_5OH (Sheverdenkin et al., 2004).

Also as in methane oxidation, the major organic liquid-phase product of ethane oxidation was methanol. At low initial oxygen concentrations (up to 5%), its concentration in the liquid products of methane and ethane oxidation was practically the same, ~40%. The main distinction between products formed from ethane oxidation and those from methane oxidation was a high concentration of formaldehyde, which reached almost 30% at a low oxygen concentration for the former and ~5.8% for the latter. However, with increasing initial oxygen concentration, the concentration of formaldehyde in the liquid products decreased sharply (Fig. 7.13).

As compared with methane oxidation, the ethanol concentration was almost tenfold higher, reaching ~10% under these conditions. Moreover, 0.2%–0.5% propanol was detected. In contrast to methanol, the content of C_2-C_3 alcohols in the liquid products changed

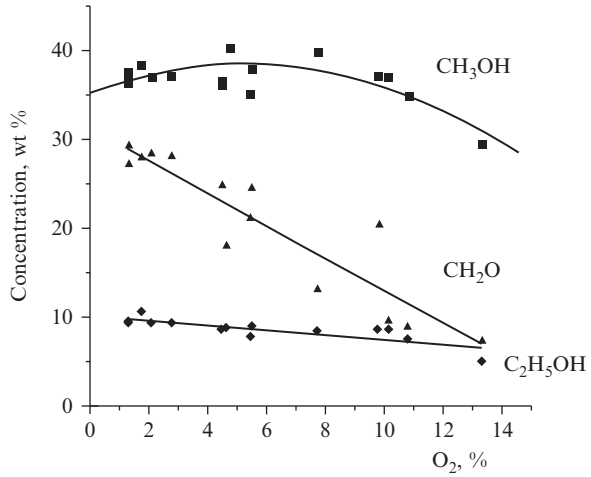

Fig. 7.13
Dependence of the concentrations of the main organic compounds in the liquid oxidation products on the initial oxygen concentration at $P = 26$ atm, $Q = 400$ L/h, and $T_{max} = 550°C$: (■) CH_3OH, (▲) CH_2O, (◆) C_2H_5OH (Sheverdenkin et al., 2004).

insignificantly as the initial oxygen concentration was increased from 1.3 to 13.3% (Fig. 7.13). The liquid oxidation products also contained 0.5%–1.5% formic acid. The total concentration of organic products in the liquid, mainly methanol, ethanol, and formaldehyde, reached 75% (i.e., it was significantly higher than in the oxidation of methane, which was <50%); however, it decreased with increasing initial oxygen concentration.

As the initial concentration of oxygen in the oxidation of ethane was increased, the yield of liquid products increased to an oxygen concentration of ~10% (Fig. 7.14). The methanol yield passed through a maximum at an oxygen concentration of above 6%, constituting, as in methane oxidation, ~20 kg per 1000 m^3 of gas passed through the reactor. With a further increase in the initial concentration of oxygen, the methanol yield went down slightly. The ethanol yield passed through a flat maximum at an initial oxidant concentration of ~6%–8%. In contrast to methane oxidation, the formaldehyde yield passed through a maximum at an oxygen content of ~4%–5%. The ratio of the yields of ethanol and methanol was ~0.2–0.3, which is consistent with the results obtained at the same pressures in Gesser et al. (1995).

An important advantage of the direct oxidation of ethane and mixtures thereof over methane oxidation is the possibility of carrying out the oxidation process at much lower pressures. Given that, in the gas-phase oxidation of ethane, its pressure is limited by the saturation vapor pressure, studies in a wide range of pressures have been typically performed with ethane-nitrogen mixtures. Dilution with nitrogen has not produced any significant effect on the kinetics of the process and the formation of the products. Fig. 7.15 shows the pressure dependences of the concentrations of the main organic oxidation products in the liquid oxidate

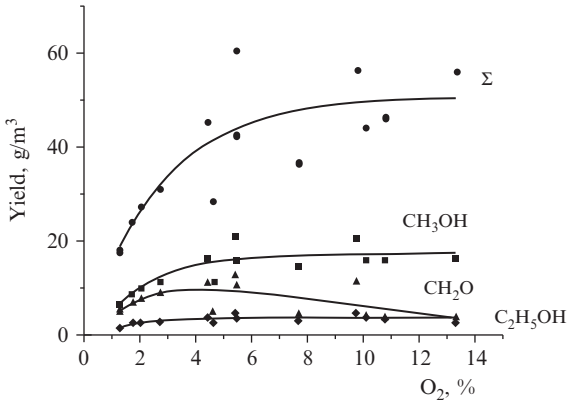

Fig. 7.14

Dependence of the yield (g/1000 L passed gas) of (●) the sum Σ of liquid products, (■) methanol, (▲) formaldehyde, and (◆) ethanol on the initial concentration of oxygen at $P = 26$ atm, $Q = 400$ L/h, and $T_{max} = 550°C$ (Sheverdenkin et al., 2004).

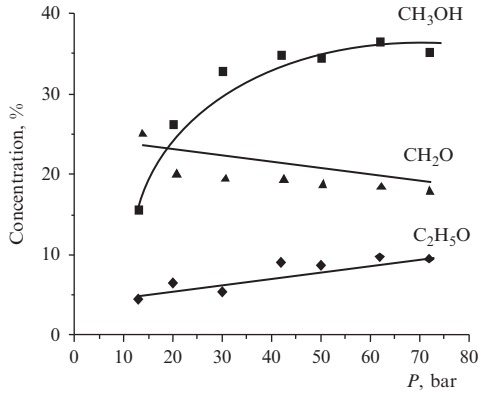

Fig. 7.15

Pressure dependence of the concentrations of (▪) methanol, (▲) formaldehyde, and (◆) ethanol in the liquid oxidate for the oxidation of an ethane-nitrogen mixture at $T_{max} = 460°C$, $[C_2H_6]_0 = 28.5\%$, and $[O_2]_0 = 11.5\%$ (the rest is nitrogen) (Sheverdenkin et al., 2004).

for a mixture containing 28.5% ethane in nitrogen. Similar dependences were obtained for the yields of these products.

It can be seen that significant changes occur only at pressures below 30 atm, whereas in the oxidation of methane, the pressure reduction from 70 to 30 atm resulted in a twofold drop in the yield of methanol and its concentration in the oxidate. Ethanol behaved similarly to methanol. The yield and percentage of formaldehyde remained constant as the pressure was decreased to 30 atm and even slightly increased with further decreasing pressure, making formaldehyde the major organic liquid oxidation product. As with changing oxygen

concentration, with changing pressure, the C_2H_5OH/CH_3OH ratio remained practically constant and significantly lower than unity, in contrast to the data reported in Gesser and Morton (1991), where this ratio increased sharply with the pressure, reaching a value of 6 at a pressure of 100 atm.

An almost fourfold decrease in gas flow rate Q, from 650 to 180 L/h, produced no change in the concentration of C_1-C_2 alcohols in the liquid products, while the concentration of formaldehyde dropped by more than twice. That the formaldehyde concentration decreases with increasing residence time of the mixture in the reactor is apparently due to an increase in the rate of its homogeneous-heterogeneous conversion to CO, the concentration of which increases with a decreasing gas flow rate.

4.2 Propane

Propane occupies an intermediate position between methane and ethane, which have no internal CH_2 groups, and the other members of the paraffin series. The oxidation of propane at high pressures under static conditions was studied in Newitt (1937) and Newitt and Schmidt (1937) and under flow conditions in Wiezevich and Frolich (1934). The data from Newitt (1937) and Newitt and Schmidt (1937) (Tables 7.2 and 7.3) showed that the aldehydes formed were represented by propionic and acetic aldehydes, normal alcohols, by methanol, ethanol, and propanol, and acids, and by acetic acid with small amounts of propionic and formic.

It should be noted that, in flow conditions at atmospheric pressure with a propane/oxygen ratio of 9/1 and $T = 465°C$, it was possible to provide high yields of peroxides: 15 mol per 100 mol of propane consumed, of which hydrogen peroxide accounted for 9 mol, with the rest falling mainly on propylene (Kooijman, 1947). Under similar conditions ($P = 1$ atm, $T = 350$–$475°C$, $[C_3H_8]/[O_2] = 5.6$–12.3, $\tau_r = 3.2$–11.8 s), a significant concentration of peroxides in the products (up to 1.7 mol %), represented almost entirely by hydrogen peroxide, was obtained in

Table 7.2 Effect of pressure and temperature on the yield of the main products of the gas-phase oxidation of propane (Newitt, 1937; Newitt and Schmidt, 1937)

	Composition of Oxidation Products, mol%			
Compound	1.055 atm 373°C	21.09 atm 281°C	63.28 atm 252°C	105.5 atm 250°C
Sum of aldehydes	20.5	21.8	13.5	13.7
Normal alcohols	19.7	21.0	17.5	15.2
Isopropanol	1.3	2.8	6.2	16.0
Acetone	0.5	4.3	12.5	7.9
Acids	4.3	17.0	19.0	18.9
Carbon dioxide	7.3	17.1	21.4	20.6
Carbon monoxide	21.3	16.9	9.9	7.7
Propylene	25.1	0	0	0

Table 7.3 Relative yields of alcohols in the oxidation of propane
air = 1:3.6 mixture (Newitt, 1937; Newitt and Schmidt, 1937)

Alcohol	Yield, %			
	5 atm	30 atm	30 atm	65 atm
CH_3OH	76.3	58.0	55.3	50.1
C_2H_5OH	19.1	17.6	13.2	9.8
n-C_3H_7OH	4.6	4.3	7.3	12.2
iso-C_3H_7OH	–	20.0	24.2	27.9

(Satterfield and Wilson, 1954). Under these conditions, at a large excess of propane, $[C_3H_8]/[O_2] = 5.6$, the propane-to-oxygen reaction molar ratio equaled ~1 and increased with temperature, from ~0.8 at 375°C to ~1.4 at 475°C. At the same time, the main saturated hydrocarbon product was methane, with small amounts of ethane ($[CH_4]/[C_2H_6] \approx 10$) and traces of normal isobutane also present. Olefins in the products were presented solely by ethylene (up to 8.9%) and propylene (up to 11.1%). Acetylene was completely absent. The oxygenates were represented by hydrogen peroxide, methanol (3%), and aldehydes (up to 3.8%), mainly formaldehyde.

As the pressure is increased, the yields of isopropanol, acetone, and organic acids grow significantly, the yields of aldehydes and normal alcohols decrease somewhat, with the proportion between them changing in favor of propanol, and the yield of CO_2 increases, whereas that of CO decreases. At pressures of 20 atm or higher, the reaction products contain no propylene (Table 7.2). The effect of pressure on the propane oxidation temperature is shown in Fig. 7.16.

Note that the data given in Tables 7.2 and 7.3 on the pressure dependence of the yield of the products of propane oxidation were not obtained under optimal conditions for the yield of

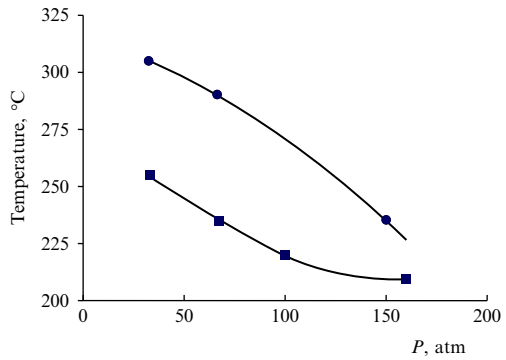

Fig. 7.16
Pressure dependence of the temperature of onset of the oxidation of (●) propane and (■) butane at $[O_2] = 6\%$ and a long reaction time. *Based on data from Wiezevich, P.J., Frolich, P.K., 1934. Direct oxidation of saturated hydrocarbons at high pressures. Ind. Eng. Chem., 26, 267.*

alcohols but at temperatures that provided an approximate constancy of the rate of the process. Given that, according to the same data, a temperature rise increased the overall yield of normal alcohols (at 30 atm, from 21% at 260°C to 40% at 286°C), the yield of alcohols under optimal conditions should be substantially higher.

As in the oxidation of methane and ethane, a decrease in the oxygen concentration in the mixture enhances the selectivity of formation of alcohols (Newitt and Schmidt, 1937). However, in the case of propane oxidation, a high selectivity of alcohols (30%–40%) can be achieved even when the propane/oxygen ratio is ~1/1 (Table 7.4). It is even claimed that the optimal conditions for producing alcohols are provided at the highest permissible concentration of oxygen from the perspective of the safety of the process (Wiezevich and Frolich, 1934).

A series of experimental studies on the direct oxidation of methane and its homologues, propane, and butane, aimed at studying the possibility of creating an industrial process, was carried out in 1950s in Russia at the State Institute of Nitrogen Industry (GIAP). In (Badrian and Furman, 1956, 1957), the yield of alcohols, aldehydes, and acids in the oxidation of propane with air in the isothermal mode was investigated. It has been shown that, as in the oxidation of ethane and methane, the main product is methanol, the yield of which is several times higher than the ethanol yield (Fig. 7.17).

The authors attributed this result to a lower energy of hydrogen abstraction from the central carbon atom as compared to the energy of its abstraction from the terminal atoms. In this case, the interaction with oxygen produced isopropylperoxy radicals, leading further to the formation of acetaldehyde and methoxy radicals and then to methanol. However, with an increasing reaction temperature, the probability of the reaction of a hydrogen atom of the terminal group

Table 7.4 Influence of the propane-to-air ratio on the yield of the main products of the gas-phase oxidation of propane at $P = 30$ atm and $T = 275$°C (Newitt, 1937)

	Composition of Oxidation Products, mol%				
Products	**1:20**	**1:5**	**1:3.6**	**1:1.25**	**1:0.5**
Sum of aldehydes	12.5	8.8	12.0	16.1	16.7
Normal alcohols	17.3	25.5	23.0	33.1	31.5
Isopropanol	2.7	6.9	5.2	5.2	14.4
Acetone	1.2	1.4	1.3	0.3	7.4
Acids	13.9	13.4	15.2	8.9	12.5
Carbon dioxide	31.5	25.0	22.1	10.5	7.0
Carbon monoxide	20.9	19.0	21.3	25.9	8.0
Sum of condensable products	47.6	56.0	56.7	63.6	85.5

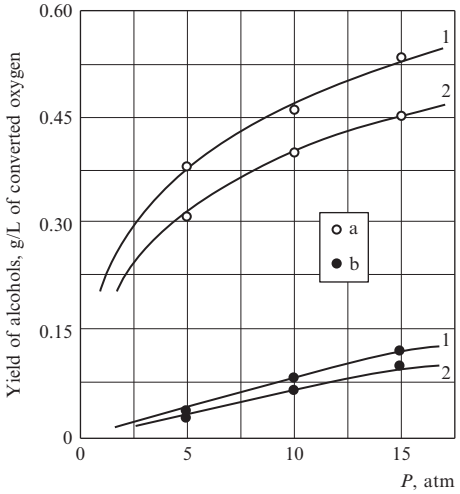

Fig. 7.17

Pressure dependence of the yield of (A) CH_3OH and (B) C_2H_5OH in the oxidation of propane at $T = 350°C$ and various reaction times s: (1) 16 s and (2) 4 s (Badrian and Furman, 1956).

increases, facilitating, respectively, the formation of ethanol, as was observed in the experiment.

The yield of alcohols increased markedly with pressure, with a maximum pressure of 15 atm used in the experiments probably being close to optimal. In the investigated range of temperatures, 325–375°C, the yield of alcohols was weakly dependent on the temperature rise: the methanol yield decreased slowly, whereas the ethanol yield increased even more slowly. As shown in Fig. 7.17, under these conditions, the reaction was practically complete within a few seconds. These same researchers used C^{14}-labeled methanol and aldehydes to show that the major product formed from methanol during propane oxidation was CO_2, more intensely at low pressure. Carbon monoxide was formed mostly from aldehydes. Note also that, in this case, acetaldehyde was partially converted into formaldehyde.

Another series of works on the oxidation of propane under pressure, performed at GIAP (Livshits, 1959; Livshits et al., 1959), showed that CO produced during the oxidation did not influence the yield and composition of the reaction products, if its concentration was less than 27 vol%, which made it possible to conduct the oxidation process in the circulation mode. At 350°C, $P = 10$ atm, an oxygen concentration of 3%, and a residence time of 2.7 s, the carbon selectivity of formation of useful products was 78%. The introduction of catalysts and various solid packings into the reaction zone did not result in any advantages over homogeneous oxidation.

As previously mentioned, even at elevated pressures, increasing the temperature causes a rapid changeover from oxygenates to unsaturated compounds.

4.3 Butane and Heavier Hydrocarbons

Only scattered data exist on the gas-phase oxidation of butane, pentane, and heavier hydrocarbons at high pressures, so only a general judgment on the expected yields of alcohols and the ratio between them can be made. The authors of Wiezevich and Frolich (1934), using the same equipment and approximately the same flow conditions as in studying the oxidation of propane, investigated the oxidation of normal butane, pentanes, and heptanes. As in the propane oxidation, increasing the pressure from 33 to 160 atm reduced the temperature of oxidation of *n*-butane from 255 to 210°C (Fig. 7.16). Among the products of the reaction of *n*-butane with oxygen at pressures ranging from 33 to 160 atm, along with the products formed in the oxidation of propane, butyl alcohols were found, a fraction of which increased with the pressure. The selectivity of formation of the oxidation products with respect to oxygen consumed was obtained at an industrial pilot flow plant at an oxygen content of 5–7 mol% (Table 7.5).

Based on these results, the authors concluded that the optimum conditions for the production of higher alcohols from a methane series of hydrocarbons are as follows: a pressure of 130–200 atm, a temperature as low as possible, a reaction time in the heated reactor of less than 10 s, and an oxygen concentration as high as possible (within the limits of safe operation). It was concluded that, for the oxidation of alkanes, low pressures favor the formation of lower alcohols and organic acids, whereas high pressures favor higher alcohols and aldehydes (Wiezevich and Frolich, 1934).

The effect of temperature on the yield of butane oxidation products is illustrated in Fig. 7.18. As can be seen, with decreasing temperature, the yield of oxygenates increases, whereas the yield of olefins decreases, first lower and then primary (Mitchell, 1956). It is particularly

Table 7.5 Selectivity of formation of the butane oxidation products with respect to oxygen (Wiezevich and Frolich, 1934)

Product	Selectivity, %	
	$P = 33$ atm	$P = 133$ atm
Acetone	1.4	0.7
Methanol	15.0	8.4
Ethanol	2.5	6.3
Propanol	3.2	8.9
Butanols	0.6	2.5
Aldehydes	6.9	15.9
Acids	16.7	4.6
Sum of target products	46.3	47.3
CO_2	9.4	6.1
CO	3.8	9.4
Unreacted oxygen	15.0	9.0

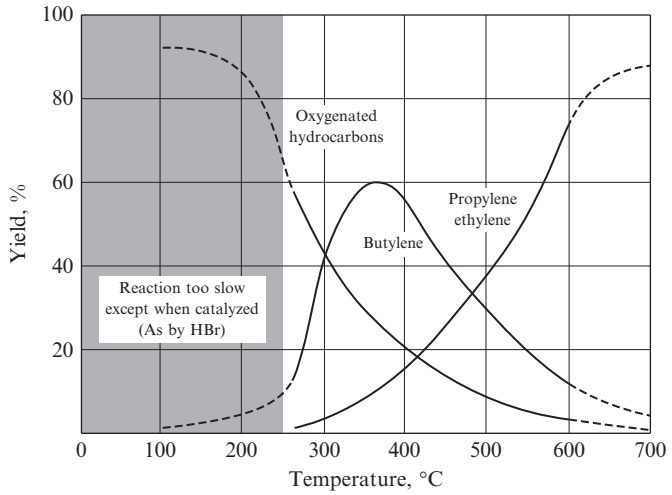

Fig. 7.18

Effect of temperature on the distribution of products for butane oxidation at atmospheric pressure and constant reactant ratio (Mitchell, 1956).

interesting that the composition of the products of the gas-phase oxidation of butane differs strikingly from the composition of its liquid-phase oxidation products at high pressure, which mainly contain acetic acid and methyl ethyl ketone, with the yield of alcohols being negligibly small (Emanuel et al., 1974).

In Quon et al. (1954), the oxidation of *n*-butane at 385°C, pressures of 3.5–12.5 atm, and process times of 0.8–4.5 s, performed under turbulent jet conditions to minimize concentration and temperature gradients, was quickly stopped by cooling with water. The concentration of each of the reagents, butane and oxygen, was varied within 1.5–6 mol%, with the remainder of the mixture being nitrogen. The pressure dependence of the yield of useful products (alcohols, aldehydes, acids, and acetone) passed through a maximum at $P \approx 8.8$ atm. With increasing pressure, the proportion between the different products remained essentially unchanged, except carbon monoxide, the yield of which increased. Examining how the yield of the products depended on the reaction time showed the presence of a distinct induction period of $\sim$1 s. The concentrations of the main oxygenates passed through a maximum at a reaction time of $\sim$2 s. Furthermore, the composition of the products had changed little.

The gas-phase oxidation of an *n*-butane-air mixture containing 18 vol% C_4H_{10}, 3 vol% O_2, and 79 vol% N_2 at pressures of 5, 10, and 15 atm and temperatures of 325, 350, and 375°C was studied in (Furman et al., 1958, 1959). The laboratory setup used made it possible to vary the residence time of the gases in the reaction zone from 2 to 12 s. The reactor was a massive stainless steel cylinder with a diameter of 100 mm and a wall thickness of 37.5 mm. The gases were fed into the reactor from a heated rapid-injection mixing vessel. Of the liquid products,

methanol, ethanol, and formaldehyde, the sum of higher aldehydes and the sum of acids were quantitatively analyzed. Acetone and esters were analyzed qualitatively.

The yield of liquid oxidation products increased with pressure, with that of aldehydes being the same in passing from 10 and 15 atm, with that of methanol continuing to grow (Fig. 7.19). The yield of liquid oxidation products was weakly temperature-dependent in the temperature range covered, whereas their selectivity of carbon decreased with increasing temperatures. The maximum yield of the products was achieved within 4–8 s and then decreased slightly up to 12 s, apparently because of the deeper oxidation of CO and CO_2.

The pressure dependence of the composition of the oxidation products of *iso*-butane is shown in Table 7.6.

The oxidation of butane was also studied in a pilot flow plant at a mixture circulation mode at a pressure of 15 atm, temperature of 370–390°C, and gas flow rate of 25 m^3/h. Oxygen was admixed to the circulating gas to its content in gas of 3−5 vol %. Gas circulation continued until the butane content in the mixture dropped to 12%, after which a fresh portion of butane was introduced into the gasholder. When the content of CO at the inlet of the reactor increased to 10%, which typically occurred after 4–5 cycles, the remaining gas mixture was discharged. The reactor was a steel tube 102 mm in diameter and 1.4 m in length. The data are in good agreement with the results obtained in the static laboratory setup (see Furman et al., 1958). On average, under these conditions, 2.6–2.9 kg of anhydrous liquid products were produced per

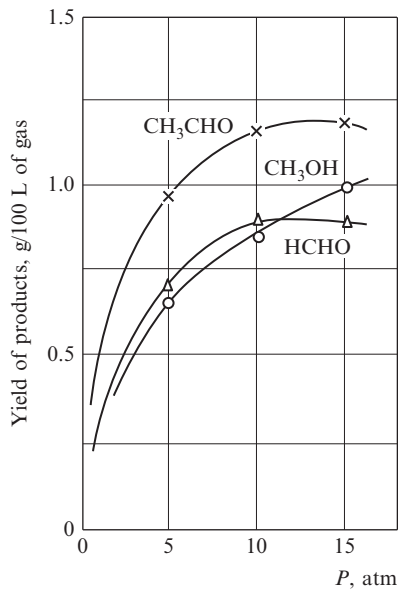

Fig. 7.19
Effect of pressure on the oxidation of *n*-butane at $T = 350$°C and $\tau = 8$ s (Furman et al., 1958).

Table 7.6 Effect of pressure and temperature on the composition of the gas-phase isobutane oxidation products (Sittig, 1962)

Products	Composition of Oxidation Products, mol% With Respect to Introduced Isobutane			
	7.03 atm 452°C	35.15 atm 350°C	140.6 atm 265°C	140.6 atm 215°C
Methanol	44	44	33	17
Formaldehyde	44	19	1	1
Acetaldehyde	30	20	9	2
Acetone	31	47	53	37
tert-Butanol	2	6	30	43
tert-Butyl hydroperoxide	0	0	2	9
Water	155	70	42	8

100 m^3 of reaction gas mixture, including 0.75–0.8 kg of methanol, 0.9–1.1 kg of acetaldehyde, 0.9–1.0 kg of formaldehydes, and 0.03–0.04 kg of organic acids. Higher alcohols (propionic and possibly butyric) and ketones were not analyzed, which reduced the yield of useful products somewhat. It was shown that the decrease of the temperature to 340−350°C increased the efficiency of using the hydrocarbon, whereas an increase in the pressure raised the yield of desired products, especially methanol. A significant accumulation of carbon dioxide in the circulating gas (up to 10–12 vol%) did not affect the oxidation process. The yield of useful products in experiments with different CO contents in the gas remained at the same level.

Because of the complexity of the mechanism of the low- and medium-temperature gas-phase oxidation of butane-rich mixtures with oxygen at elevated pressures, there are no in-depth works on the kinetic simulation of the process.

For the gas-phase oxidation of heavier alkanes into oxygenates in rich mixtures, virtually no reliable quantitative data are available. It is known that the oxidation products of 60% *n*-pentane and 40% *iso*-pentane mixtures with 5%–6% oxygen consist mainly of alcohols, aldehydes, acetone, and acids with 2–3 carbon atoms. In contrast, the oxidation products of heptane (fraction boiling within 70–97°C and containing almost all of heptane isomers present in the gasoline fraction head) mainly contained hexyl-heptyl alcohols boiling in the range of 140–180°C. The inconsistency of these data with the results for the oxidation of pentane is presumably associated with the reaction occurring in the liquid phase (Wiezevich and Frolich, 1934).

4.4 General Features of the Oxidation of Alkanes at High Pressures

Note that, in the series of normal paraffinic hydrocarbons, their relative rate of oxidation increases rapidly with the hydrocarbon chain length and that branched paraffinic hydrocarbons are oxidized more slowly than normal ones with the same number of hydrocarbon atoms.

This may seem surprising, since a hydrogen atom is more easily abstracted from a tertiary carbon atom than from a secondary one, let alone a primary carbon atom. Apparently, in this case, the rupture of the C-H bond is not a limiting step, with the process rate being determined by the stability of intermediate oxidation products. The oxidation of normal paraffinic hydrocarbons gives more reactive aldehydes, whereas the oxidation of isoparaffinic hydrocarbons produces more stable ketones. This dependence of the relative reactivity of paraffinic hydrocarbons on their structure is directly related to their motor fuel properties (octane number) and explains why the branched paraffins exhibit better antiknock properties (Sittig, 1962).

The mechanism of the oxidation of hydrocarbons depends on the temperature range in which the oxidation is carried out. Below ~300°C, the oxidation of C_4+ hydrocarbons proceeds according to the low-temperature mechanism with the predominant formation of various oxygen-containing compounds, such as aldehydes, ketones, alcohols, CO, and CO_2. At 300–450°C, in the transition zone, the formation of oxygen-containing products slows down, whereas the yield of olefins with the same number of carbon atoms as the initial hydrocarbon increases. Above 450°C, cracking occurs to form lower olefins and partial paraffins. In the transition zone, the reaction rate decreases with increasing temperatures (NTC phenomenon). For propane, ethane, and especially methane, the boundaries of the indicated areas are noticeably shifted to higher temperatures, while the overall pattern of change of the oxidation mechanism persists.

The type and structure of the oxidized hydrocarbons are the most important parameters affecting the yield of the products. For example, acetone is formed much more efficiently from isobutane than from normal butane, whereas the yield of methanol and formaldehyde during the oxidation of isobutene is markedly lower than in the case of normal hydrocarbons (Table 7.7) under identical conditions.

Another important parameter of the process is the ratio between the reagents, that is, oxygen and hydrocarbon. Changing the propane-to-air ratio from 1/20 to 1/0.5 results in a nearly

Table 7.7 Influence of the type and structure of the hydrocarbon on the yield of the product (Mitchell, 1956)

Products	Yield of Liquid Products, wt%		
	Propane	*n*-Butane	*i*-Butane
Acetaldehyde	28.0	30.6	17.0
Formaldehyde	26.4	22.9	19.8
Methanol	23.8	19.4	13.8
Acetone	1.7	4.9	26.0
C_3-aldehydes	2.9	4.5	3.8
Propylene oxide	2.5	–	3.0
Butylene oxide	–	2.8	1.1

twofold increase in the selectivity of formation of the desired liquid oxidation products, from 47.6% to 85.5% under the isothermal conditions of a static reactor ($P = 30$ atm, $T = 275$°C), which is due mainly to an increase in the yield of alcohols and acetone. A similar effect was also observed in the oxidation of propane under adiabatic conditions in a flow reactor. With an increasing hydrocarbon-to-oxygen ratio, the desired products had a higher molecular weight; that is, the degree of degradation of the initial hydrocarbon was smaller.

The pressure has a significant effect on the rate of oxidation of hydrocarbons by increasing the rate of oxidation (lowering the oxidation initiation temperature) (Fig. 7.20) and changing the composition of the products (Tables 7.5, 7.6, and 7.8). A rise in pressure and decrease in temperature lead to an increase in the yield of oxygen-containing products with the same number of carbon atoms in the molecule as in the starting hydrocarbon.

Fig. 7.18 shows how temperature influences the yield of the partial oxidation products of alkanes. There are three main groups of oxidation products: oxygen-containing compounds (their formation is favored by low temperatures), olefins corresponding to the initial hydrocarbon, and olefins formed through the destruction of the skeleton of the hydrocarbon molecule. With increasing pressure, the temperature limits of the areas of formation of these groups of products shift to higher temperatures. For example, at a pressure of 7 atm, the peak for the yield of butenes in the oxidation of butane is located at ~600°C, as compared to 375°C at 1 atm (Fig. 7.18).

An interesting feature of the oxidation of lower alkanes is the mutual promoting effect of methane and heavier homologues, as seen from experiments and kinetic simulations. The reason for this effect is that not only more reactive alkanes promote methane oxidation but also, under certain conditions, methane promotes the oxidation of its gaseous homologues, because it provides more effective chain branching. The promotion of the oxidation of methane by its

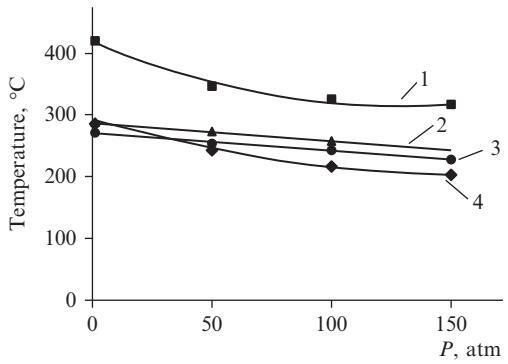

Fig. 7.20

Temperature of onset of the oxidation of C_1–C_4 alkanes as a function of the pressure: (1) methane, (2) ethane, (3) propane, and (4) butane. *Based on data Mitchell, R.L., 1956. Make petrochemicals from air and LPG. Pet. Refin., 179–182.*

Table 7.8 Influence of pressure on the oxidation onset temperature (Mitchell, 1956)

Hydrocarbon	Oxidation Onset Temperature, °C			
	1 atm	50 atm	100 atm	150 atm
Methane	420	350	330	320
Ethane	285	276	260	–
Propane	270	255	245	232
n-Butane	–	248	220	210

heavier homologues is well known, and is mainly due to their ability to provide a higher initiation rate of radicals than is characteristic of methane oxidation, which makes heavier alkanes more reactive in low-temperature oxidation. An increase in the rate of oxidation of less stable hydrocarbons caused by additives of more stable methane is apparently due to more effective chain branching in the methane oxidation mechanism, which manifests itself at higher temperatures. Indeed, methylperoxy radicals formed during methane oxidation are more effective in chain branching realized through the following sequence:

$$CH_3^{\bullet} \rightarrow CH_3OO^{\bullet} \rightarrow CH_3OOH \rightarrow CH_3O^{\bullet} + OH^{\bullet} \tag{7.15}$$

In the case of heavier alkanes, along with this branching mechanism, there are additional possibilities, such as the rapid decay of the corresponding peroxide radicals to form an olefin and the $HO_2^{\bullet}$ radical (weakly reactive in these conditions)

$$C_nH_{2n+1}^{\bullet} \rightarrow CnH_{2n+1}OO^{\bullet} \rightarrow C_nH_{2n} + HO_2^{\bullet} \tag{7.16}$$

This channel is equivalent to switching off branching and switching on an additional chain termination. Therefore the addition of methane, for which the pathway leading to olefin is absent, leads to an increase in the overall rate of the process. This effect is supported by the results of calculations of the electronic structure, according to which the concerted formation of $HO_2^{\bullet}$ and C_2H_4,

$$CH_3CH_2OO^{\bullet} \leftrightarrow C_2H_4 + HO_2^{\bullet} \tag{7.17}$$

dominates over the isomerization of this radical,

$$CH_3CH_2OO^{\bullet} \leftrightarrow C^{\bullet}H_2CH_2OOH \tag{7.18}$$

because at similar values of the preexponential factor, the barrier for reaction (7.17) is several kcal/mol lower than that for reaction (7.18) (Rienstra-Kiracofe et al., 2000). A similar mechanism is likely operative for heavier alkylperoxy radicals (Naik and Dean, 2006).

Based on the preceding data, we can draw some general conclusions on the optimal conditions (Table 7.9) and the basic features of the oxidation of methane and its homologues to oxygenates at high pressures:

Table 7.9 Optimal parameters for the formation of liquid organic products in the oxidation of alkanes at high pressures

Hydrocarbon	Oxidation Onset Temperature, °C			
	P, atm	Initial Reaction Temperature, °C	C_nH_{2n+2}/O_2	Conversion to Useful Products Per Passage, %
Methane	70–100	450	30	2
Ethane	25–30	400	10	5
Propane	15–20	350	1	20
n-Butane	7–10	350	1	20

(1) For the oxidation of C_1-C_4 alkanes in optimum conditions, a selectivity of formation of liquid organic products of 50% or higher can be achieved.
(2) Increasing the oxygen concentration reduces the selectivity of formation of liquid organic products; however, the changeover from methane to butane is accompanied by a sharp decrease in the hydrocarbon-to-oxygen ratio (∼30 for methane, ∼10 for ethane, and ∼1 for propane and butane) at which the selectivity is still high. At the same time, the conversion of hydrocarbons to useful products increases (∼2% for methane, ∼5% for ethane, and ∼20% for propane and butane).
(3) In the series from methane to butane, the temperature and pressure optimal for the production of liquid hydrocarbon products decrease monotonically (100 atm and 450°C for methane, 30 atm and 400°C for ethane, 20 atm and 350°C for propane, and 10 atm and 350°C for butane). These data correspond to the occurrence of the process in flow conditions, at reaction durations from a fraction of a second to several seconds.
(4) In the series from methane to butane, the effect of pressure on the composition of the products diminishes.
(5) In the oxidation of mixtures of alkanes, even small impurities of higher alkanes substantially lower the temperature of the process to the temperature characteristic of their oxidation.

5 Conclusions

The process for the direct conversion of metane to methanol is very flexible and can be used to process hydrocarbon gases of practically any composition. The higher the content of heavier hydrocarbons, the more favorable the conditions of the process and the greater the yield of oxygenates. The process is also flexible in regard to the possibility of readily adjusting the composition and parameters of the product.

References

Arutyunov, V.S., 2003. On catalysis of homogeneous-heterogeneous processes of oxidizing hydrocarbon conversion. Catal. Ind. 3, 3–9 (in Russian).

Arutyunov, V.S., 2004. Recent results on fast flow gas-phase partial oxidation of lower alkanes. J. Nat. Gas Chem. 13, 10–22.

Arutyunov, V., 2014. Direct Methane to Methanol: Foundations and Prospects of the Process. Elsevier BV, Amsterdam.

Arutyunov, V.S., Krylov, O.V., 1998. Oxidative Conversion of Methane. Nauka, Moscow (in Russian).

Arutyunov, V.S., Krylov, O.V., 2005. Oxidative conversion of methane. Russ. Chem. Rev. 74, 1111–1137.

Arutyunov, V.S., Vedeneev, V.I., Klimovetskaya, S.Yu., Leonov, V.E., Pavlii, L.V., 1994. Influence of pressure on the formation of products of partial oxidation of methane. Theor. Found. Chem. Eng. 28, 563–568.

Arutyunov, V.S., Basevich, V.Ya., Vedeneev, V.I., 1995a. Modern state of direct partial oxidation of natural gas to methanol. Ind. Eng. Chem. Res. 34, 4238–4243.

Arutyunov, V.S., Vedeneev, V.I., Klimovetskaya, S.Yu., Leonov, V.E., Pavlii, L.V., 1995b. Effect of hydrogen, carbon monoxide and nitrogen on partial oxidation of methane. Theor. Found. Chem. Eng. 29, 63–67.

Arutyunov, V.S., Basevich, V.Ya., Vedeneev, V.I., 1996. Direct high pressure gas-phase oxidation of natural gas to methanol and other oxygenates. Russ. Chem. Rev. 65, 197–224.

Arutyunov, V.S., Rudakov, V.M., Savchenko, V.I., Sheverdenkin, E.V., Sheverdenkina, O.G., Zheltyakov, A.Yu., 2002. Partial alkane oxidation at high pressures: methane oxidation in stainless steel and quartz reactors. Theor. Found. Chem. Eng. 36, 472–476.

Badrian, A.S., Furman, M.S., 1956. Effect of pressure on the formation of intermediate propane oxidation products. Dokl. Akad. Nauk SSSR 108, 861–863 (in Russian).

Badrian, A.S., Furman, M.S., 1957. Kinetics and mechanism of the oxidation of propane under pressure. Tr. GIAP 7, 79–100 (in Russian).

Bafas, I.C., Constantinou, I.E., Vayenas, C.G., 2001. Partial oxidation of methane to formaldehyde with 50% yield in a continuous recycle reactor separator (CRRS). Chem. Eng. J. 109–115.

Baldwin, T.R., Burch, R., Squir, G.D., Tsang, S.C., 1991. Influence of homogeneous gas phase reactions in the partial oxidation of methane to methanol and formaldehyde in the presence of oxide catalysts. Appl. Catal. 74, 137–152.

Bjorklund, M.C., Carr, R.W., 2002. Enhanced methanol yields from the direct partial oxidation of methane in a simulated countercurrent moving bed chromatographic reactor. Ind. Eng. Chem. Res. 41, 6528–6536.

Brockhaus, R., Franke, H.J., 1981. Process for the manufacture of formaldehyde and methanol by partial oxidation of methane. US Patent 4243613.

Budymka, V.F., Egorov, S.A., Gavrya, N.A., Mochaev, A.S., Khomenko, G.A., Leonov, V.E., 1987. Effect of the process parameters on the gas-phase partial oxidation of natural gas. Khim. Prom-st 6, 10-1 (in Russian).

Burch, R., Squire, G.D., Tsang, S.C., 1989. Direct conversion of methane into methanol. J. Chem. Soc. Faraday Trans. I 85, 3561–3568.

Casey, P.S., McAllister, T., Foger, K., 1994. Selective oxidation of methane to methanol at high pressures. Ind. Eng. Chem. Res. 33, 1120–1125.

Chellappa, A.S., Fuangfoo, S., Viswanath, D.S., 1997. Homogeneous oxidation of methane to methanol: effect of CO_2, N_2, and H_2 at high oxygen conversions. Ind. Eng. Chem. Res. 36, 1401–1409.

Chou, T.-C., Albright, L.F., 1978. Partial oxidation of methane in glass and metal tubular reactors. Ind. Eng. Chem. Process. Des. Dev. 17, 454–459.

Chun, J.-W., Anthony, R.G., 1993. Partial oxidation of methane, methanol, and mixtures of methane and methanol, methane and ethane, and methane, carbon dioxide, and carbon monoxide. Ind. Eng. Chem. Res. 32, 788–795.

Emanuel, N.M., Denisov, E.T., Maizus, Z.K., 1974. Chain reactions of oxidation of hydrocarbons in the liquid phase. Nauka, Moscow (in Russian).

Feng, W., Knopf, F.C., Dooley, K.M., 1994. Effects of pressure, third bodies, and temperature profiling on the non-catalytic partial oxidation of methane. Energy Fuels 8, 815–822.

Foral, M.J., 1992. The noncatalytic partial oxidation of natural gas to methanol. In: Preprints, Symposium on Natural Gas Upgrading II, 203d National Meeting of the American Chemical Society, Division of Petroleum Chemistry, San Francisco, CA, April 5–10. American Chemical Society, Washington, DC, pp. 34–40.

Furman, M.S., Shestakova, A.D., 1956. Oxidation of methane under pressure. Tr. Gos. Inst. Azot. Promyshl. 6, 98–108 (in Russian).

Furman, M.S., Badrian, A.S., Gol'tyaeva, N.A., Savchuk, S.N., 1958. Gas-phase oxidation of *n*-butane under pressure. Gazov. Prom. 10, 36–43. (in Russian).

Furman, M.S., Badrian, A.S., Gol'tyaeva, N.A., 1959. Oxidation of *n*-butane under pressure. Tr. GIAP 9, 238–247 (in Russian).

Gesser, H.D., Morton, L.A., 1991. The dehydrogenative coupling of methane to form higher hydrocarbons in a hot wire thermal diffusion column. Catal. Lett. 11, 357–363.

Gesser, H.D., Hunter, N.R., Morton, L., 1986. Direct conversion of natural gas to methanol by controlled oxidation. US Patent 4618732.

Gesser, H.D., Hunter, N.R., Shigapov, A.N., 1995. Some characteristics of the partial oxidation of CH_4 to CH_3OH at high pressures. In: Bhasin, M.M., Slocum, D.W. (Eds.), Methane and Alkane Conversion Chemistry. Plenum Press, NY, pp. 271–286.

Han, L.-B., Tsubota, S., Kobayashi, T., Haruta, M., 1995. Formation of methanol by the gas phase partial oxidation of methane under normal pressures. J. Chem. Soc. Chem. Commun. 93–94.

Irusta, S., Lomatmdo, E.A., Miro, E.E., 1994. Effect of NO and solids on the oxidation of methane to formaldehyde. Catal. Lett. 29, 339–348.

Kooijman, P.L., 1947. The preparation of peroxides by the oxidation of propane. Recueil 66 (1/2), 5–23.

Livshits, V.D., 1959. Effect of the solid phase of "catalysts" on the oxidation of propane. Tr. GIAP 9, 216–222 (in Russian).

Livshits, V.D., Sokolova, N.P., Beskova, A.P., 1959. Oxidation of propane under pressure. Tr. GIAP 9, 223–237 (in Russian).

Lødeng, R., Lindvag, O.A., Søraker, P., Roterud, P.T., Onsager, O.T., 1995. Experimental and modeling study of the selective homogeneous gas phase oxidation of methane to methanol. Ind. Eng. Chem. Res. 34, 1044–1059.

Melvin, A., 1966. Spontaneous ignition of methaneeair mixtures at high pressure. I. The ignition delay preceding explosion. Combust. Flame 10, 120–128.

Mitchell, R.L., 1956. Make petrochemicals from air and LPG. Pet. Refin. 1956, 179–182.

Naik, C.V., Dean, A.V., 2006. Detailed kinetic modeling of ethane oxidation. Combust. Flame 145, 16–37.

Newitt, D.M., 1937. The oxidation of hydrocarbons at high pressures. Chem. Rev. 21, 299–317.

Newitt, D.M., Bloch, A.M., 1933. The slow combustion of ethane at high pressures. Proc. R. Soc. A140, 426–439.

Newitt, D.M., Gardner, J.B., 1936. The initial formation of alcohols during the slow combustion of methane and ethane at atmospheric pressure. Proc. R. Soc. A154, 329–335.

Newitt, D.M., Huffner, A.E., 1932. The formation of methyl alcohol and formaldehyde in the slow combustion of methane at high pressures. Proc. R. Soc. Lond. A134, 591–604.

Newitt, D.M., Schmidt, W.G., 1937. The oxidation of propane. Part II. The products of the slow oxidation at high pressure. J. Chem. Soc., 1665–1669.

Omata, K., Fukuoka, N., Fujimoto, K., 1994. Methane partial oxidation to methanol. 1. Effects of reaction conditions and additives. Ind. Eng. Chem. Res. 33, 784–789.

Onsager, O.T., Lødeng, R., Søraker, P., 1989. The homogeneous gas phase oxidation of methane and the retarding effect of basic/inert surfaces. Catal. Today 4, 355–363.

Parmaliana, A., Frusteri, F., Mezzapica, A., Scurrell, M.S., Giordano, N., 1993. Novel high activity catalysts for partial oxidation of methane to formaldehyde. J. Chem. Soc. Chem. Commun. 751–753.

Quon, D., Dalla Lana, I., Govier, G.W., 1954. The vapor phase partial oxidation of *n*-butane—effect of pressure, reaction time, and inlet gas composition. Can. J. Chem. 32, 880–895.

Rienstra-Kiracofe, J.C., Allen, W.D., Schaefer III, H.F., 2000. The $C_2H_5+O_2$ reaction mechanism: high level ab initio characterization. J. Phys. Chem. A. 104, 9823–9840.

Satterfield, C.N., Wilson, R.E., 1954. Partial oxidation of propane. The role of hydrogen peroxide. Ind. Eng. Chem. 46, 1001–1007.

Sheverdenkin, E.V., Arutyunov, V.S., Rudakov, V.M., Savchenko, V.I., 2004. Kinetics of partial oxidation of alkanes at high pressures: oxidation of ethane and methane-ethane mixtures. Theor. Found. Chem. Eng. 38, 311–315.

Simchenko, V.P., Shcherbakov, P.M., Vedeneev, V.I., Arutyunov, V.S., 1999. The kinetics of methane oxidation at high pressures. Theor. Found. Chem. Eng. 33, 362–364.

Sittig, M., 1962. Combining Oxygen and Hydrocarbons for Profit. Houston, Texas: Gulf Pub. Co.; 1962 (Sittig, M., 1970. Processes in the Oxidation of Hydrocarbon Raw Material. Khimiya, Moscow (in Russian)).

Takemoto, T., He, D., Teng, Y., Tabata, K., Suzuki, E., 2002. The optimization of methanol yield in direct selective oxidation of methane with O_2 and NO in the presence of Cu-ZnO/Al_2O_3. J. Mol. Catal. A Chem. 179, 279–286.

Torchian, H.G., Mantashian, A.H., Nalbandian, A.B., 1974. Oxidation of methane under adiabatic compression conditions. Arm. Khim. Zh. 27, 271–278 (in Russian).

Vedeneev, V.I., Goldenberg, M.Ya., Gorban', N.I., Teitelboim, M.A., 1988a. Quantitative model of the oxidation of methane at high pressures. I. Description of model. Kinet. Catal. 29, 1–8.

Vedeneev, V.I., Goldenberg, M.Ya., Gorban', N.I., Teitelboim, M.A., 1988b. Quantitative model of the oxidation of methane at high pressures. II. Mechanism of autoacceleration. Kinet. Catal. 29, 8–14.

Vedeneev, V.I., Goldenberg, M.Ya., Gorban', N.I., Teitelboim, M.A., 1988c. Quantitative model of the oxidation of methane at high pressures. III. Mechanism of formation of reaction products. Kinet. Catal. 29, 1121–1126.

Vedeneev, V.I., Goldenberg, M.Ya., Gorban', N.I., Teitelboim, M.A., 1988d. Quantitative model of the oxidation of methane at high pressures. IV. Ignition delays. Kinet. Catal. 29, 1126–1133.

Vedeneev, V.I., Arutyunov, V.S., Krymov, N.Yu., Cherbakov, P.M., Sedykh, A.D., 1992. Some features of methane oxidation at high pressures. Catal. Today 13, 613–616.

Walsh, D.E., Martenak, D.J., Han, S., Palermo, R.E., 1992a. Direct oxidative methane conversion at elevated pressure and moderate temperatures. Ind. Eng. Chem. Res. 31, 1259–1262.

Walsh, D.E., Martenak, D.J., Han, S., Palermo, R.E., Michaels, J.N., Stern, D.L., 1992b. Pressure, temperature, and product yield relationships in direct oxidative methane conversion at elevated pressure and moderate temperatures. Ind. Eng. Chem. Res. 31, 2422–2425.

Wiezevich, P.J., Frolich, P.K., 1934. Direct oxidation of saturated hydrocarbons at high pressures. Ind. Eng. Chem. 26, 267.

Yarlagadda, P.S., Morton, L., Hunter, N.R., Gesser, H.D., 1988. Direct conversion of methane to methanol in a flow reactor. Ind. Eng. Chem. Res. 27, 252–256.

Yarlagadda, P.S., Morton, L.A., Hunter, N.R., Gesser, H.D., 1990. Temperature oscillations during the high-pressure partial oxidation of methane in a tubular flow reactor. Combust. Flame. 79, 216–217.

Zalc, J.M., Green, W.H., Iglesia, E., 2006. NOx-mediated homogeneous pathways for the synthesis of formaldehyde from CH_4-O_2 mixtures. Ind. Eng. Chem. Res. 45, 2677–2688.

Zhang, Q., He, D., Li, J., Xu, B., Han, Z., Liang, Y., et al., 2002a. Comparatively high yield methanol production from gas phase partial oxidation of methane. Appl. Catal. A 224, 201–207.

Zhang, Q., He, D., Zhang, X., Zhu, Q., 2002b. Methanol production from partial oxidation of methane in a special designed reactor. ACS Fuel Chem. Div. Prepr. 47 (1), 334.

Zhang, J., Burkle-Vitzthum, V., Marquaire, P.M., Wild, G., Commenge, J.M., 2011. Direct conversion of methane in formaldehyde at very short residence time. Chem. Eng. Sci. 66, 6331–6340.

This page intentionally left blank

CHAPTER 8

Direct Methane to Methanol: Promising Technologies Based on the DMTM Process

Vladimir Arutyunov[*,†]

[*]*Semenov Institute of Chemical Physics of Russian Academy of Sciences, Moscow, Russia* [†]*Institute of Problems of Chemical Physics of the Russian Academy of Sciences, Chernogolovka, Russia*

Acronyms

POM	partial oxidation of methane
DMTM	direct metane (conversion) to methanol
OCM	oxidative coupling of methane
PSA	pressure swing adsorption
NTP	at normal temperature and pressure
EER	energy and environmental research corporation (USA)
SCR	selective catalytic reduction
WCF	water-coal fuel

1 Introduction

As an industrial technology, the direct oxidation of natural gas to oxygenates experienced a rapid upsurge, a subsequent decline, and even a near-total oblivion. Nowadays, however, the situation is changing rapidly, not least because of significant changes expected in the role of natural gas and gas chemistry in the world's economy and energy and in the structure of the world's gas resources. A tendency toward the reduction of the average capacity of newly discovered natural gas fields; an increase in the proportion of low-yield gas fields, associated gas, and gas from unconventional sources; and the complexity and high cost of gas transportation; enhance interest in more flexible and low-capacity processing technologies, such that could be implemented directly at the site of natural gas production. In this technological niche of relatively simple low-tonnage processes, the direct partial oxidation of natural and associated gas to methanol is still one of the most promising directions. Along with advances in studying the mechanism of hydrocarbon oxidation at moderate temperatures and high pressures, this gives a good opportunity to return DMTM to the rank of industrial technologies.

Methanol. https://doi.org/10.1016/B978-0-444-63903-5.00008-X

There is the fundamental difference of methane chemistry from the traditional "destructive" petrochemistry, which is mainly based on the processes of pyrolysis, cracking, dehydrogenation, and isomerization of heavy hydrocarbons of petroleum. The chemistry of methane is essentially "constructive" in its nature. Its purpose is to produce from CH_4, the most simple and stable hydrocarbon molecule, a vast variety of more complex and less stable products, such as modern petrochemicals. Due to the high thermodynamic stability of methane, the possibilities of using traditional petrochemical catalytic processes aimed at producing thermodynamically equilibrium target products in the gas chemistry of methane are limited. This explains ever-increasing attention to thermodynamically nonequilibrium kinetic processes occurring due to high energy released in the oxidation of methane.

Autothermal processes of partial oxidation, such as DMTM, provide heat release in the same volume in which the target reaction occurs, making it possible to avoid using costly and metal-consuming heat exchange equipment. It enables minimizing the energy spent for methane activation, which requires significantly greater energy for breaking strong C—H bonds, as compared to conventional petrochemical processes. Given that one of the cheapest and most available energy sources is the oxidation of natural gas itself, the chemical processing of natural gas should rely, as far as possible, on the use of autothermal processes such as DMTM, in which the heat required for the desired reaction is produced by the partial oxidation of natural gas itself. From the standpoint of these basic principles governing the current trends in the gas chemistry, the appeal of DMTM based on the partial oxidation of natural gas is growing.

In this chapter, promising technologies based on the DMTM process—which were more thoroughly described in the two previous chapters—will be considered. A more detailed discussion of kinetics aspects of the DMTM process can be found in the reviews (Arutyunov et al., 1995, 1996; Arutyunov, 2004; Arutyunov and Krylov, 2005) and monographs (Arutyunov and Krylov, 1998; Arutyunov, 2014).

2 Industrial Experience of the Partial Oxidation of Hydrocarbon Gases to Oxygenates

At the time, the partial oxidation of gaseous hydrocarbons to oxygenates was one of those technological areas in which practical implementation was much ahead of the level of theoretical understanding of this chemical processes. Industrial processes based on the gas-phase partial oxidation of hydrocarbons came into existence almost immediately after the first data on the possibility of obtaining high yields of oxygenates and other products by direct oxidation had appeared. The first pilot plant of Cities Service Company was built in Tallant, Oklahoma, as early as 1926 (Walker and Malakoff, 1946; Bludworth, 1949), only a few years after the birth of the petrochemical industry. However, it turned out to be ineffective

because it produced too many low-value byproducts. Then the Celanese Corporation built three plants, two in Texas (Bishop and Pampa) and one in Canada (Edmonton). At that time, it was the cheapest method for producing three basic oxygen-containing petrochemical products: methanol, formaldehyde, and acetaldehyde (Meyer, 1955). These processes were estimated to account for a quarter to a third of the total production of methanol and formaldehyde in the United States in 1941 (Weiss, 1941).

By the middle of the last century, the process of partial oxidation of propane, butane, and mixtures thereof produced from associated gas and oil processing and stabilization gases had become widespread in the United States, in *fact, it became one of the traditional petrochemical industries*. Initially, the oxidation was carried out by air, but in 1949, oxygen was first used. The main products of the oxidation of associated gas were formaldehyde, methanol, acetaldehyde, acetic acid, acetone, and a mixture of liquid oxygenates, used as a solvent or raw material for producing other products. Unfortunately, there are no reports that would give a clear idea of the large installations operated in the United States by the Celanese, McCarthy, Warren, and Cities Service Oil firms. The techniques developed at the research laboratories of these companies had been kept secret (Bludworth, 1949).

In general, the technological schemes of the gas-phase oxidation of oil gas were similar to those for oxidation of methane. Oil gas was mixed with recycled gas and oxidant, and the mixture was heated to 355–370°C at a pressure of 7.0–10.5 atm and then fed into a low-carbon steel reactor. In the reactor, the heat release by the reaction raised the temperature to 425–455°C, which was considered optimal for the formation of oxygenated products. The gas mixture from the reactor flowed into cooling, separation, and purification systems. The conversion of gas per pass was ~20%–25%. The optimal gas–phase oxidation mode was achieved with a short contact time, 0.25–2.0 s, and the maximum oxygen conversion. Although a number of processes occur in the presence of heterogeneous catalysts, they have not become widely used in the gas-phase oxidation of oil gases. Despite the fact that many catalysts have been patented, no significant advantages due to their use have been achieved (Bludworth, 1949). An approximate composition of liquid C_2—C_4 hydrocarbon oxidation products is shown in Table 8.1.

The results indicate that a moderate pressure of ~7 atm prevents the formation of olefins while promoting higher yields of oxygenated products. Oxidation at elevated pressures and low temperatures makes it possible to provide the maximum yield of the products with the same number of carbon atoms as in the original hydrocarbon, i.e., without the destruction of the hydrocarbon molecule. Increasing the pressure raises the yield of alcohols at the expense of aldehydes. The oxidation of hydrocarbons heavier than ethane increases the yield of secondary and tertiary alcohols. The process was carried out at a low oxygen/hydrocarbon ratio: 1 kg of oil gas was oxidized with 1 kg of oxygen. An advantage of using oxygen was to ensure a smaller size of equipment for oxidized gas recirculation, lower losses of hydrocarbons into the exhaust gas, and a higher yield of oxidation products.

Table 8.1 Approximate composition of the products of gas-phase oxidation of C_2—C_4 hydrocarbons (mol % of initial hydrocarbon converted) (Paushkin et al., 1973)

	Ethane	Propane	*n*-Butane	Isobutane
Methanol	15–60	25–50	8–25	5–25
Formaldehyde	5–20	10–15	5–12	5–10
Acetaldehyde	1–6	10–20	2–10	2–4
Ethanol	1–8	2–4	–	–
Acetone	–	3–7	1–6	15–35
Glycols	–	–	5–15	1–10
Other oxygen-containing products	1–4	3–6	7–25	3–27

The industrial processes of the production of formaldehyde from methane have been developed in Germany. The oxidation of methane with molecular oxygen was performed in the presence of 1%–2% nitrogen oxides or using heterogeneous catalysts (94% Cu–6% Sn) (Paushkin et al., 1973). In 1942 the Gutehoffnungshutte Company constructed the first industrial-scale plant for producing formaldehyde by direct oxidation of natural gas in Copsa Mica, Romania. However, because it was almost immediately incapacitated due to military actions, there are no reliable published data on the results of its operation.

A gas-phase process of oxidation of natural gas to formaldehyde promoted by NO_2 was developed in the 1950s at the Institute of Chemical Physics of Russian Academy of Sciences by Nalbandyan and coworkers (Paushkin et al., 1973; Anisonian et al., 1957). The process was based on the accelerating effect of potassium tetraborate on methane oxidation and the inhibitory effect of packing on the oxidation of formaldehyde to CO_2. Based on the results of the operation of a pilot plant with a capacity of 150–180 m^3 of gas mixture per hour, in 1956–57, a pilot plant with capacity up to 2000 tons of formaldehyde per year was designed and built. However, for reasons not related to technological issues, the work on the process was stopped.

Since the mid-1950s, for a number of reasons, the industrial use of the direct oxidation of gaseous hydrocarbons to oxygenates virtually ceased. First, propane-butane fraction, formerly a byproduct of natural gas production, has become a widespread domestic fuel and raw material for the petrochemical industry, thereby depriving the process of direct oxidation of low-cost and user-friendly raw material. At the same time, the partial oxidation of dry natural gas, requiring much more stringent conditions and providing a lower yield of the desired products, has not been implemented commercially. Additionally, a low selectivity in certain products and a wide variety thereof, especially in the oxidation of C_3—C_4 hydrocarbons, required greater effort to separate the individual components. Most importantly, there was no clear understanding of the mechanism of the process, the concept of which was largely based on scattered and often contradictory empirical data.

For these reasons, DMTM technology has been superseded by the competing process for producing methanol and other chemicals from natural gas through its conversion to syngas, which, despite greater technological complexity, provides a highly selective mass production of many basic chemicals given today's easy access to huge gas resources. However, rapid change in the raw material basis of the gas industry and the inevitable increase of the role of remote low-capacity sources (shale gas, gas hydrates, marginal fields, associated petroleum gas, etc.) requires new, simpler, light-duty, and flexible technologies. The use of most of these resources on the basis of existing natural gas transportation and processing technologies is almost impossible.

As a promising direction in creating a new generation of technologies for the in-field processing of resources from unconventional sources of hydrocarbon gases with low output rates and a short operation life of individual wells, spatial dispersion, and remoteness from consumers, the DMTM technology can regain practical significance. In what follows, we consider problems where the solution would best contribute to the application of DMTM as well as those areas in which this technology would be most effective for a wide variety of applications.

3 Conceptual Schemes of the Partial Oxidation of Natural Gas to Oxygenates

With the development of the theory of the branched-chain processes of hydrocarbon oxidation and the progress in understanding the DMTM mechanism, new variants of technological processes based on it—with consideration given to these basic concepts—have been proposed. The most economically and technologically promising niches where its use can provide tangible benefits have been identified (Arutyunov, 2011, 2014). These technologies are based on the conceptual schemes of the flow and circulation variants of the process.

The flow mode of the process with the use of air as the oxidant (Fig. 8.1) is the most simple and attractive, *especially for small plants intended for procuring the necessities of gas companies in*

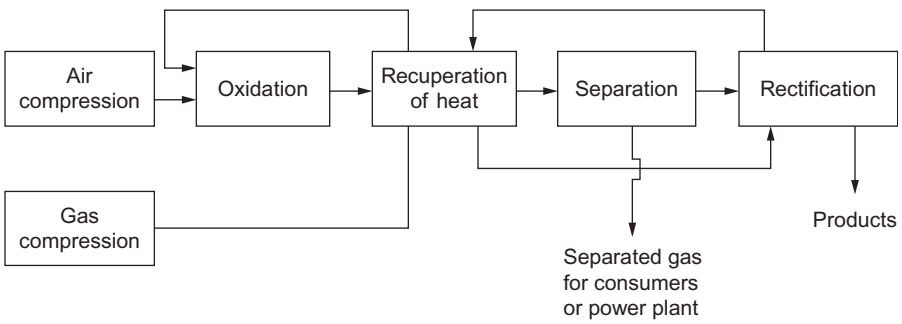

Fig. 8.1
Flow diagram of the process of partial oxidation of natural gas.

methanol as an inhibitor of hydrate formation. For Russia's gas fields, the consumption of methanol for this purpose reaches 1–2 kg per 1000 m^3 of produced gas (Bukhgalter, 1986). On average, a complex gas pretreatment plant consumes ~4–5 thousand tons of methanol per year. Given the fact that the delivery of methanol to remote areas doubles its price on average, supplementing such a plant by its own facility for the production of crude methanol would provide a significant economic benefit. Due to the high heat effect of the reaction, recuperation of heat from the exhaust gas is not only sufficient for heating the fresh reaction mixture, but also can provide the required amount of steam to heat up the liquid products entering the rectification unit and can meet the heat needs of the entire gas production facility.

According to the data presented in the previous two chapters, the optimum process conditions are as follows: the gas temperature at the reactor inlet ~450°C, pressure 7–10 MPa, and initial oxygen concentration of 4.3%. Without special preventive measures, the temperature of the reaction mixture rises by 120–160°C at such an oxygen concentration. The methanol yield per pass through the reactor is 17–20 kg per 1000 m^3 of gas passed. An approximate composition of the resulting liquid products was found to be (in wt.%) 38–42 methanol, 4.8 formaldehyde, 0.5–1 ethanol, 0.2–0.5 acids, with the rest being water. The conversion of methane is almost equal to the initial oxygen concentration, with the exhaust gas containing ~1% CO, 0.2% CO_2, and a small amount of hydrogen, with the nitrogen concentration corresponding to the volume of air supplied. This gas can be used as a gaseous fuel *for own* needs of gas producing facilities, which is the best option. It can also be returned back to the pipeline if its calorific value and nitrogen content are acceptable. In the latter case, since the aim is only to obtain a certain amount of methanol and the unreacted gas is returned, there is no need to intensify the oxidation process. It suffices to provide even a low degree of oxidation, for example 3%–5%, achievable in a single pass through the reactor. At an inlet gas pressure of not less than 5 MPa, there is no need to compress it further. Using a single distillation column makes it possible to produce crude methanol with a methanol concentration of not less than 91% and a water concentration of not more than 9%, which is quite suitable for use as a hydrate formation inhibitor (Bukhgalter, 1986). As a byproduct formed in the distillation residue, weak (8%–12%) formalin solution is formed. This has numerous applications, including in the gas and oil fields. For example, it can be used as a hardener of phenol-formaldehyde resins, for processing wells against flooding, and as a germicide for suppressing sulfate-reducing bacteria, which cause the degradation of the collecting properties of the reservoir.

If the exhaust gas cannot be returned to the pipeline and its energy content substantially exceeds the existing energy needs, the degree of conversion of the gas can be increased. The most obvious way is to increase the number of consecutive reactors (cascade connection). However, this requires multiple cooling, separations, and reheating the reaction mixture, i.e., an excessive complication of the technological scheme. That makes this approach unlikely to be economically feasible. A more effective method may be an incomplete cooling of the reagents

combined with the absorption (adsorption) removal of methanol. A similar scheme was proposed to avoid the recirculation of technological gas during the production of methanol from syngas. As the most suitable absorbent, tetraethylene glycol dimethyl ether (tetraglyme, TEGDME) was proposed, a compound with a high boiling point (275°C) and a good thermal stability (Westerterp et al., 1988). However, in the cascade scheme, due to the gradual increase of the reaction gas volume because of nitrogen addition, the volume of which is about four times the amount of the converted methane, the performance in methanol drops so that the size of the reactors of the consecutive cascades must be increased.

A more promising variant is the distributed supply of oxygen at several points along the reactor. This makes it possible to not only provide a high rate of the process and, hence, to reduce the size of the reactor, but also to increase the yield of methanol at the same flow rate of oxygen. Another important prerequisite for a high selectivity of methanol formation at a relatively high conversion of methane is to limit the heating of the reaction mixture to ~550–570°C. At $T > 600$°C, along a reduction of the yield of oxygenates, a noticeable amount of soot is formed, which contaminates the liquid oxidation products. This limits the initial oxygen concentration, and accordingly, the conversion of natural gas per pass through the reactor to 4%–5%. One solution to the problem is to carry out the oxidation in a sectioned reactor with spread oxidant supply and excess heat removal between the sections, for example by generating steam (Fig. 8.2). Two options are possible: to carry out the reaction in the void volume followed by driving the gas mixture into the steam generator section or conducting the process directly in the steam generator with continuous heat removal (Patent RU, 2200731, 2001).

By changing the parameters of steam supplied, it is possible to reliably and smoothly adjust the temperature of the oxidation process. To increase the overall conversion of natural gas,

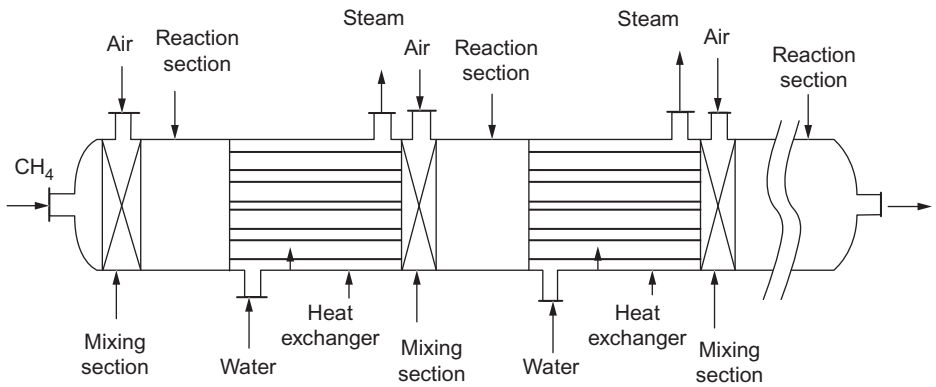

Fig. 8.2
Reactor-generator for the partial oxidation of natural gas with stepped heat removal (Patent RU, 2200731, 2001).

particularly if it is necessary to spend energy on its compression, it is advantageous in some cases, even for oxidation with air, to resort to partial recycling of the exhaust gas. For example, such a scheme, implemented in a three-section reactor (Fig. 8.2) with a supply of 3%–4% oxygen in each section and excess heat removal between the sections, enables bringing the total conversion up to 9%–10% per pass, nearly without reducing the selectivity.

A three-section reactor with distributed oxygen supply operating at a flow rate of natural gas of 13 thousand m^3/h (110 million m^3/year) will actually consume only about 10 million m^3 of gas, whereas the remainder may be used for energy production or returned to the pipeline. Along with 5 thousand ton/year of methanol, ~0.5 thousand ton/year of formaldehyde can be produced, which in terms of 37% commercial formalin constitutes ~1.4 thousand ton/year. However, the production of commercial formalin and rectified methanol at small-scale plants is hardly justified, since it requires additional stages of rectification and, consequently, appropriate equipment. The ethanol yield is less than 100 tons/year, and therefore, its separation from methanol is unreasonable. A high-calorie exhaust gas with a heat content of ~7400 kcal/m^3 is suitable for use in all types of power engines.

Using a steam generator to remove the heat released by the reaction, although effective, is not the only way of controlling the temperature of the oxidation process. If only a small part of the pipeline gas is used for methanol production, the oxidation is carried out nearly at the pressure of the incoming gas, with only small additional compression. If the exhaust gas is discharged back into the pipeline, the volume of gas passing through the reactor is unimportant. In this case, a simple scheme of cooling the reaction mixture by supplying additional cold gas into the reactor is suitable (Fig. 8.3) (Patent RU, 2568113, 2015).

Natural gas from the pipeline is additionally compressed with compressor 1 to the reaction pressure, mixed with the circulating gas, heated to the reaction temperature in recuperative heat exchanger 2, and fed into the first mixer of sectional reactor 3, wherein the corresponding amount of air is also supplied by air compressor 4. In addition to mixer 5, each section of the reactor has a reaction zone and a cooling zone. At the beginning of each cooling zone 6, an annular manifold for feeding and forming a cylindrical near-wall flow of cold gas (shown by dashed lines) is mounted. The gradual mixing of cold gas with heated reaction mixture limits the heat-up of the latter. In addition, the displacement of the reaction by cold gas from the reactor near-wall layer reduces the negative effect of the metal surface of the reactor on the oxidation process, in particular lowering the rate of heterogeneous deep-oxidation processes that lead to the formation of mainly carbon oxides and water, thereby increasing the process selectivity. At the same time, the corrosion of the reactor walls slows down and their temperature lowers, which makes it possible to reduce the requirements for the material of the reactor.

For more reliable temperature control and for ensuring the formation of a cylindrical cold gas layer, each section of the reactor can be equipped with several manifolds, with thermocouple 7

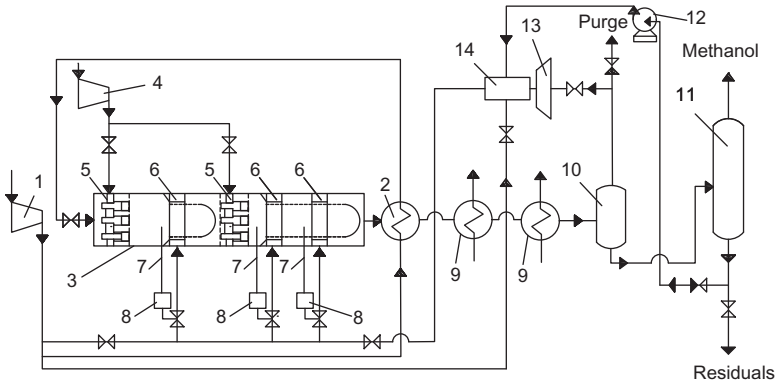

Fig. 8.3

Flow diagram of the flowthrough process of methanol production by the partial oxidation of natural gas in a sectioned reactor with temperature control by means of introducing cold gas into the reactor (Patent RU, 2568113, 2015). (1) Compressor, (2) recuperative heat exchanger, (3) reactor, (4) air compressor, (5) mixers, (6) cold gas supply collectors, (7) thermocouples, (8) adjusting devices of cold gas supply, (9) heat exchangers, (10) separator, (11) distillation column, (12) pump for pumping liquid by-products to additional oxidation, (13) booster compressor, and (14) mixer.

and control device 8 (to adjust the volume of cold gas supplied) placed ahead of each manifold. Cold gas fed into the reactor may be natural gas, process exhaust gas, or any combination thereof. Furthermore, oxidation byproducts from the bottom of distillation column 11 may be supplied by pump 12 to mixer 14, from which they, together with circulation or initial gas (compressed with a compressor 13) are transported, as a part of the cooling gas flow, to be oxidized. Based on the idea of regulating the temperature of the process by supplying an additional volume of cold gas into the reactor, the Amtek engineering company designed a flow plant with a capacity of ~5 thousand tons of methanol per year.

The circulation process of natural gas oxidation is an implementation of the standard technological approach in the case of a low conversion of the reactants per pass. However, the use of recirculation of the gases in the partial oxidation of hydrocarbons to oxygenates involves certain difficulties. First, recycling implies the need to use oxygen, which increases the capital costs by 30%–40% and makes the entire process more complex. That, in turn, tightens the requirements for its operational service and staff. Apparently, for DMTM plants with a capacity of up to 20 thousand tons/year, the most appropriate oxygen generation technology is pressure swing adsorption (PSA). It makes it possible to produce relatively pure technical oxygen containing more than 90% O_2 in the amount of several hundred to several thousand cubic meters per hour. However, the cost is still high.

Apart from the need to use oxygen of at least technical purity, a serious problem is the purification of the circulation gas from carbon oxides, the main gas-phase reaction products. Estimates show (Basevich et al., 1997) that, although the circulation mode provides a much

higher degree of conversion of methane and a higher yield of methanol while maintaining a high selectivity of its formation, the concentration of gaseous reaction products in the circulation gas increases rapidly. Moreover, while the concentrations of CO and H_2 reactive products level off onto a plateau with time, that of CO_2, an inert product, continues to accumulate monotonously with the number of cycles.

Although it has been experimentally shown that the presence of 5% of CO and H_2 in the reaction mixture only slightly affects the yield of methanol (Arutyunov and Krylov, 1998), with evidence reported (Bjorklund and Carr, 2002) that CO concentrations as high as 12% do not reduce the methanol yield, for the cyclic process to occur effectively, it is at least partially necessary to remove carbon oxides, even when part of the recirculated mixture is discharged. This requirement greatly complicates the process. While the methods of purification from carbon dioxide are well developed, for example, by absorption in solutions of ethanol amines, there are practically no efficient methods for purification from carbon monoxide. The known methods, such as copper-ammonia treatment, methanation, selective oxidation, etc., are too complex and make the circulation process ineffective in small capacity installations. Since the partial oxidation of oxygenates to carbon oxides, mainly CO, accounts for nearly 50% of the selectivity in carbon, the development of more effective methods for removal, and especially extraction, of CO as one of the products of the process would be of great importance for this technology.

Fig. 8.4 shows a flowchart of the circulation-mode oxidation of natural gas in a three-section reactor with the removal of excess heat between the oxidation stages due to steam formation. The resulting steam is used for heating the distillation columns, whereas its excess can be offered to external consumers. The exhaust gases can be used for energy production.

In order to at least partially take advantage of the circulation mode while avoiding purification from carbon oxides, a number of combinations of cyclic and continuous-flow methods (semirecycle) have been proposed. In this case, only part of the exhaust gas is directed to recirculation, whereas the problem of accumulation of products, including carbon oxides and nitrogen, is solved by blowing off a larger volume of gas. Fig. 8.5 displays the calculated dependence of the methanol yield and the concentration of nitrogen in the blow-off gas for the cyclic process of partial oxidation of natural gas with atmospheric air in a two-section reactor at a methane conversion of 4% in each section on the fraction of blow-off gas.

With decreasing blow-off gas fraction, the methanol yield increases while the calorific value of exhaust gas decreases and the volume of gases passing through the reactor rises, a factor that makes it necessary to increase the size and productivity of the equipment. For oxidation with air, the optimal fraction of blow-off gas is ~50%. In this case, the calculated methanol yield reaches 60 kg/m^3 per 1000 m^3 of methane consumed, with the CO content at the reactor inlet constituting less than 3%. The air consumption is ~1400 m^3/h per 1000 m^3/h

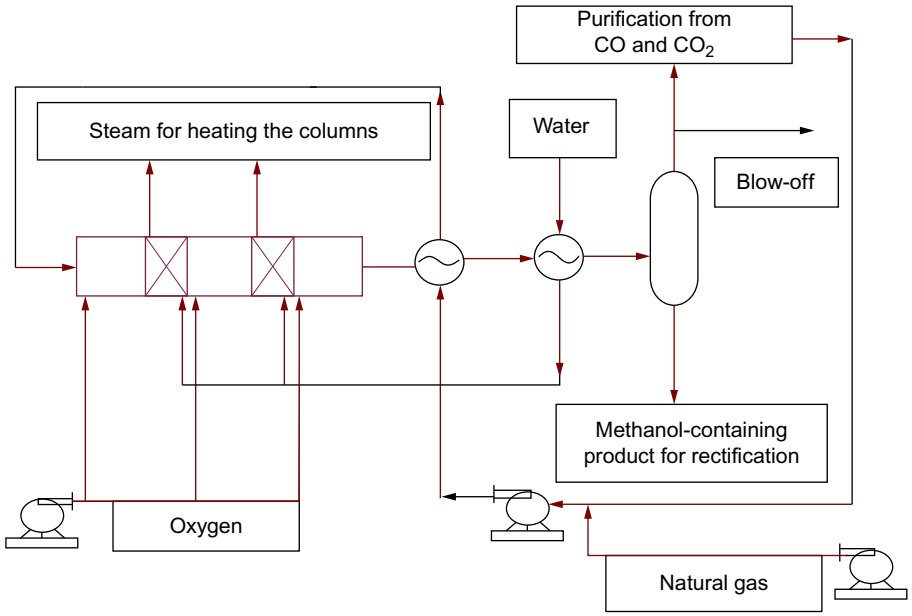

Fig. 8.4
Flowsheet of the circulation process of methanol production.

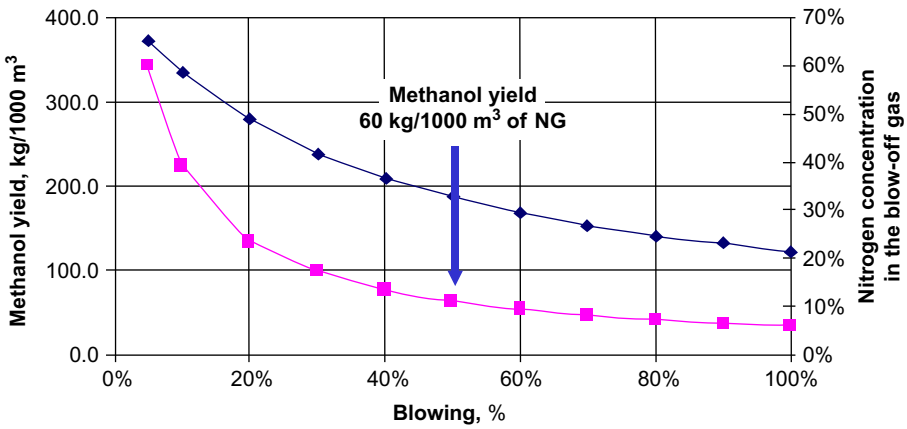

Fig. 8.5
Calculated dependences of the methanol yield (per 1000 m^3 NTP/h of supplied natural gas at a methane content of 98%) and nitrogen concentration in blow-off gas on the fraction of blow-off gas for the cyclic partial oxidation of natural gas with atmospheric air.

of converted gas. The blow-off gas, containing ~30% nitrogen, has a high calorific value, 20 MJ/m^3 (the blow-off gas volume is ~1600 m^3 NTP per 1000 m^3 NTP of converted gas) and can be used as high-quality power generation fuel with reduced production of nitrogen oxides.

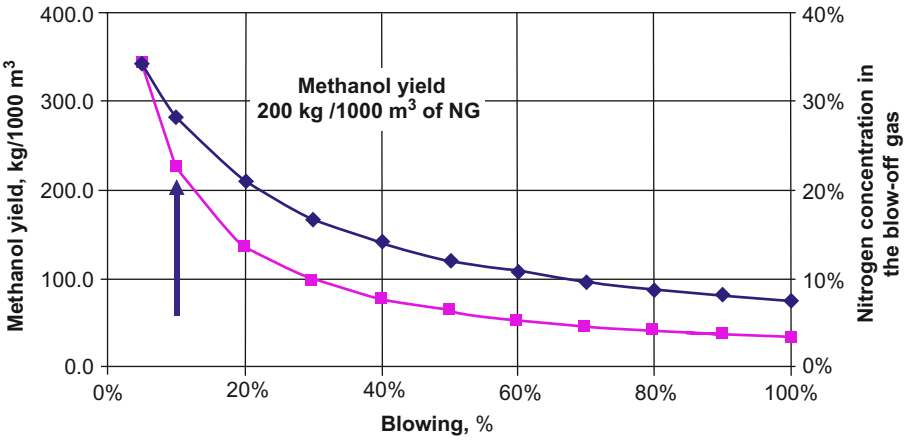

Fig. 8.6

Calculated dependences of the methanol yield (per 1000 m^3 NTP/h of introduced gas at a methane content of 98%) and nitrogen concentration in the blow-off gas on the fraction of blow-off gas for the cyclic partial oxidation of natural gas with oxygen-enriched air ($[O_2] = 50\%$).

The methanol yield can be increased significantly by using oxygen-enriched air, which makes it possible to increase the multiplicity of gas circulation (decrease the blow-off gas volume). By using enriched air with an oxygen content of ~50%, which can be obtained by membrane separation, the fraction of blow-off gas can be reduced to 10% (Fig. 8.6). In this case, the calculated methanol yield increased to ~200 kg per 1000 m^3 of methane consumed. The calorific value of the blow-off gas is ~16 MJ/m^3, whereas its volume is ~1560 m^3 NTP per 1000 m^3 of feed gas. The use of technical oxygen (~90% O_2) enables further reduction of the fraction of blow-off gas, which, however, is a technically complex and capital-intensive solution.

4 Innovative Technologies Based on the Gas-Phase Oxidation of Hydrocarbon Gases to Oxygenates

The present state of the technology of partial oxidation of gaseous hydrocarbons to oxygenates is still far from perfect, mainly due to insufficient research and development efforts. Nevertheless, it is currently possible to clearly outline the areas (Fig. 8.7) in which this technology has good prospects, in some cases providing the only feasible solution to the existing problems. Some of these applications are discussed below.

The prevention of hydrate formation during the production and transportation of natural gas is one of the most promising applications of DMTM. The prevention of hydrate formation is a serious problem in the gas industry. According to some estimates, the expenditure for these purposes constitutes up to 20% of the costs of the production and transportation of natural gas. The total consumption of methanol for this purpose in Russia already exceeds 400

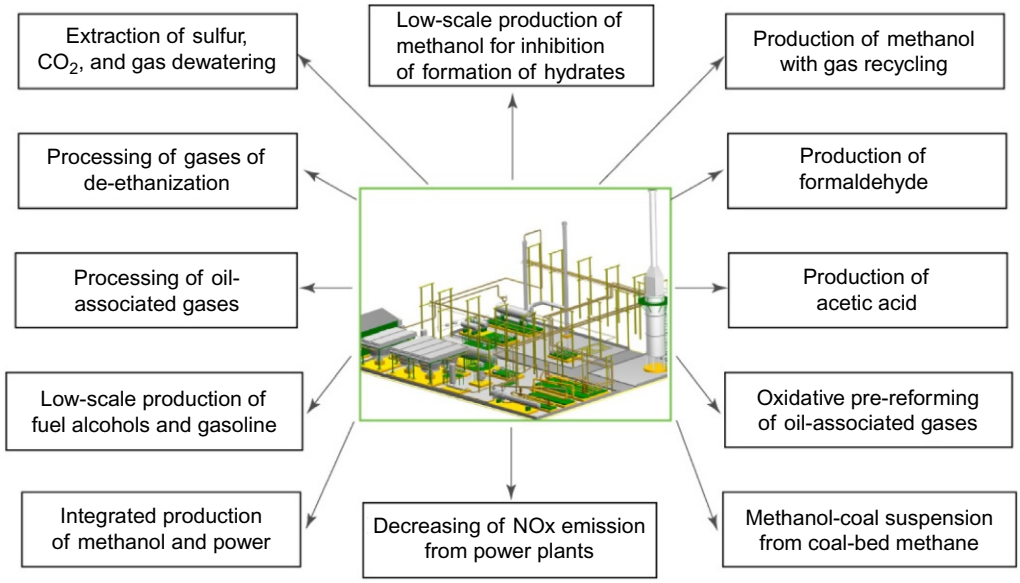

Fig. 8.7
Promising technologies based on the direct oxidation of natural and associated gas.

thousand tons/year. The main consumers of methanol are numerous distantly spaced remote gas-producing facilities, each of which consumes only a few thousand tons of methanol annually. Under these conditions, methanol delivery to remote locations, thousands of kilometers away from the place of its production, entails high costs, so low-tonnage production at the site of production provides tangible economic benefits. No less important a factor is the reliability of deliveries. In addition, as an inhibitor, crude methanol is quite suitable, the production of which by the method described in the previous section is much simpler than the technology of manufacturing the commercial product.

However, the prevention of hydrate formation includes not only the production of methanol but as well the methods for its introduction into gas wells or gas pipelines. A method for preventing hydrate formation in the gas transported through a pipeline by the partial oxidation of part of the gas and the subsequent return of the partially converted gas containing, apart from everything else, methanol into the transport pipeline is described in Patent RU 2051202 (1995). This eliminates the steps of isolation and distillation of liquid products; however, it excludes the possibility of the production of methanol for the antihydrate treatment of the upstream parts of the gas transport system and gas production wells. Moreover, along with methanol, water, and other oxidation products, including carboxylic acid, occur in the transport line. Therefore, there is a more interesting method, a schematic diagram of which in displayed in Fig. 8.8. In this method, concurrently with processing the transported gas, liquid methanol is isolated, a procedure accompanied by the optimization of the operation of the system for the separation and rectification of methanol.

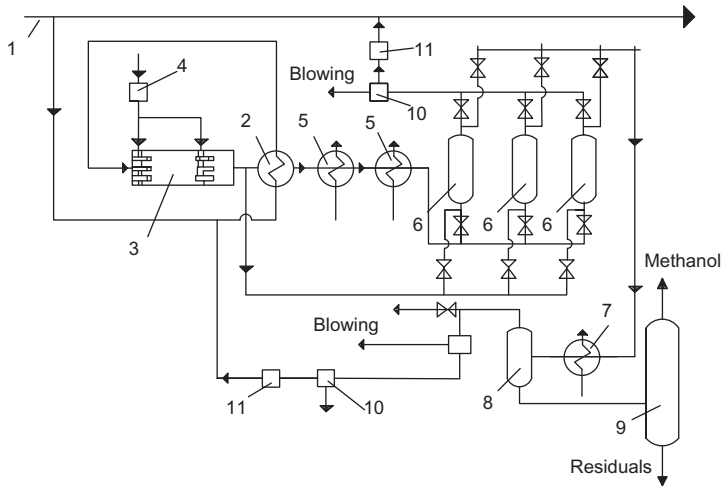

Fig. 8.8
Flow diagram of the production of methanol and its simultaneous introduction into the pipeline. (1) Gas pipeline, (2) recuperative heat exchanger, (3) reactor, (4) air compressor, (5) heat exchangers, (6) adsorption columns, (7) heat exchanger, (8) separator, (9) rectification column, (10) separators of nitrogen-containing gas, and (11) units for separation of carbon oxides.

Part of the transported gas from pipeline line 1 is supplied through recuperative heat exchanger 2, into sectional reactor 3, wherein concurrently air or oxygen is fed from compressor 4, and the partial oxidation of gas takes place with a conversion of 5%–6%. The partially oxidized gas is divided at the reactor outlet into two flows. One flow is cooled in heat exchangers 2 and 5 and then is fed into one of batch adsorption columns 6, where it is purified from water and organic reaction byproducts (formaldehyde and acids) and excess methanol, after which the flow containing the desired concentration of methanol vapor is returned to the transport pipeline. The other hot gas flow is used to desorb the products adsorbed from the first stream, followed by its cooling in heat exchanger 7 and recovering methanol by a standard technique, using separator 8 and distillation column 9. The resulting liquid methanol can be introduced into gas production wells and gas pipelines. The separated gas can be returned to pipeline 1, recycled to the oxidation reactor, or used to generate energy. A reduction of the concentration of nitrogen in the gas returned into the pipeline or subjected to recirculation can be accomplished by isolating from it, in separators 10, a low-calorie nitrogen-containing gas, which can be used as a fuel. Furthermore, carbon oxides can be removed in separators 11.

The purification of natural gas from sulfur-containing compounds may also become one of the most attractive areas for DMTM application in field conditions. Drying natural gas and removal of sulfur compounds and carbon dioxide from it are among the most important stages of gas production. This is accomplished by means of a large number of industrial processes involving various adsorbents, including methanol. The widely known Rectisol process

(licensors are the Linde AG and Lurgi GmbH companies) is designed for removing the acidic gases with an organic solvent at temperatures below 0°C. Hydrogen sulfide, carbonyl sulfide, and carbon dioxide are typically extracted with methanol, although, in some cases, other solvents are used. The process produces purified gas with a sulfur content of less than 10^{-6} and even a lower carbon dioxide concentration. The main advantages of this method are the use of a cheap and readily available solvent, simplicity of the technology, and low energy consumption (A Handbook of Modern Processes of Gas Processing, 1992). The Rectisol process is economically efficient, capable of significantly reducing the specific consumption of energy as compared with other purification methods, such as absorption by ethanol amines.
A significantly higher solubility of H_2S in methanol as compared to CO_2 makes it possible, on one hand, to separate them with high selectivity and, on the other, to provide a high degree of purification from sulfur compounds in the presence of CO_2. The process is best suited for the purification of gases containing a large number of different contaminants. Another process for extracting acidic gases with methanol is the Ifpexol process, developed and patented by the French Institute of Petroleum (Benayoun, 2001).

In field conditions, the extraction of undesirable impurities with methanol becomes attractive if methanol is produced directly from the extracted gas and on the equipment integrated into the gas processing plant, such as by using the opportunities provided by the DMTM process.
A flowsheet of the combined process is shown in Fig. 8.9 (Patent RU, 2385180, 2010).

The first part of the scheme realizes the conventional process of methanol production by means of the DMTM. Purified natural gas is fed into compression and heating unit 1 and then into reactor unit 2, where air or oxygen is also pumped by oxidant compression unit 3. In separation unit 4, liquid products are extracted and then directed into distillation unit 5. Methanol and vat residue come into receptacles 6 and 7, respectively. The separated gas is returned to the gas line. From receptacle 6, the resulting methanol, under a pressure of 6 MPa, enters ammonia or propane refrigerator 8, where it is cooled to −15°C. The cooled methanol is supplied for refluxing into absorption column 9, where it encounters raw natural gas that counterflows from the bottom, being supplied by source 10. Hydrogen sulfide-containing methanol after heat exchange with lean methanol is regenerated in column 11. The hydrogen sulfide fraction is sent for utilization into Claus apparatus 12, while purified methanol is returned by pump 13 into the process. Purified hydrocarbon gas is sent to consumer 14 and to conversion into methanol. The residual methanol content in the purified gas may be adjusted so as to prevent hydrate formation during its further transportation. Thus, application of such a technology, based on a combination of the DMTM and Rectisol processes, enables carrying out three important operations: to effectively and economically purify natural gas from acidic components, to introduce methanol into it in the amount required for its further transportation, and to obtain liquid methanol for inhibition of hydrate formation in the gas transporting system upstream of the plant.

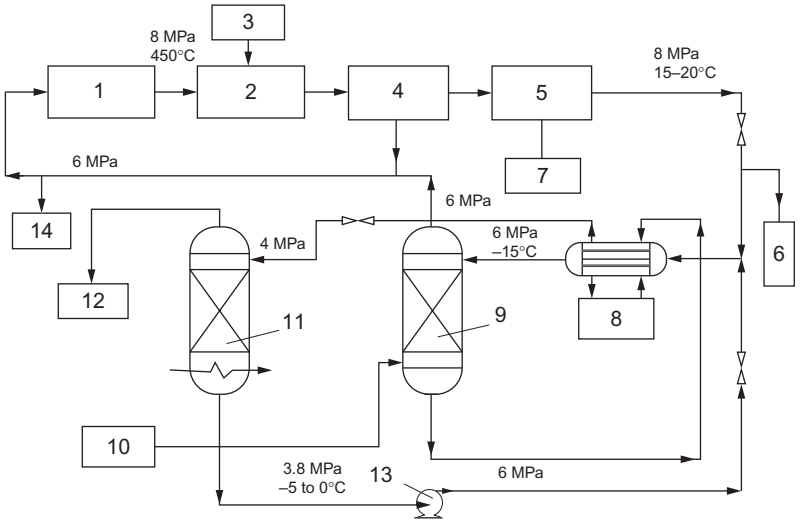

Fig. 8.9

Technological scheme for the purification of natural gas from sulfur components with concurrent production of methanol by the DMTM (Patent RU, 2385180, 2010): (1) gas compression and heating unit, (2) reactor unit, (3) air compression unit, (4) separation unit, (5) rectification unit, (6) receptacle for methanol, (7) receptacle for vat residue, (8) ammonia refrigerator, (9) absorption column, (10) raw gas source, (11) regeneration column, (12) hydrogen sulfide utilization unit, (13) pump, (14) sweet gas consumer.

Processing of de-ethanization gases from gas fractionation plants can also become an area of practical applications of the DMTM process. Virtually all the natural gas produced is processed to extract higher hydrocarbons and valuable raw materials as well as to prevent their condensation in the cold units of the gas transporting system. Therefore, according to Russian Standard OST 51.40-93 for natural gas supplied to the gas–main pipelines, its hydrocarbon dew point must not exceed 0°C, or even −10°C in the winter in cold-climate areas. This is achieved by extracting ethane, at least partially, propane, butane, and higher hydrocarbons, valuable chemical raw materials, and high-calorific ecological household and motor fuel. This treatment also provides a homogeneous and stable composition of natural gas transported through pipelines irrespective of its origin.

Despite a wide variety of technologies used for the fractionation of hydrocarbon gases, all derived products fall into four main groups: dry natural gas purified in accordance with the requirements of transportation, liquefied gases (propane-butane fraction), liquid products (gas condensate), and de-ethanization gases. The first three fractions are highly marketable and relatively easily transportable commercial products. However, the latter fraction, which contains most of the ethane removed from natural gas as well as some amounts of methane and propane, in many cases cannot be used other than as fuel for local needs or, in some cases,

is simply flared. At the same time, this fraction is an ideal raw material for the DMTM process, readily convertible at pressures below 30 atm with a high yield of products. Therefore, the integration of a partial oxidation unit with a gas fractionation plant would allow producing valuable oxygen-containing products from otherwise waste raw material.

Formaldehyde production from ethane-containing gases, primarily separated on gas fractionation plants, may become one of the promising approaches to processing the ethane fraction. At relatively low pressures, <30 atm, and a high total yield of oxygenates, the concentration of formaldehyde in the liquid products reaches more than ≈30%. This high figure makes it possible to consider the gas-phase oxidation of ethane-containing gas as a potential one-step method of formaldehyde production. A flowchart of this process is given in Patent RU 2283829 (2005). Nowadays, formaldehyde is produced by the oxidative dehydrogenation of methanol, which consumes more than 20% of the world's production.

Production of acetic acid and other carbonylation products is one of the most feasible ways to improve the selectivity of the partial oxidation of methane by using, along with oxygenates, carbon monoxide formed for the carbonylation of methanol and other liquid-phase reaction products. Canada's CANMET Company proposed a method for the production of acetic acid by the direct oxidation of methane, bypassing the step of producing synthesis gas (Patent US 5659077, 1997; Mac Farlan and Liu, 2001). Methane is oxidized in the gas phase to methanol, which is then separated and carbonylated on a deposited catalyst with carbon monoxide contained in the reaction gases formed in the same oxidation process:

$$2CH_4 + 2O_2 \rightarrow CH_3OH + CO + 2H_2O \quad (8.1)$$

$$CH_3OH + CO \rightarrow CH_3COOH \quad (8.2)$$

The technology (Fig. 8.10) was based on the DMTM process described in Arutyunov et al. (1996), with a conversion of methane per pass through the reactor of 6%–12%, a complete oxygen consumption at a temperature greater than 400°C, and working pressure of ~7 MPa. The resultant steam was used for technological purposes. At this pressure and $T = 200–250$°C, methanol was carbonylated to CH_3COOH and CH_3COOCH_3 on a Pd/C catalyst in the presence of CH_3I. The catalytic activity persisted for 600 h, indicative that the carbonylation takes place in the gas phase. According to authors' estimates, the cost of production of 1 kg of CH_3COOH by this method must be 30% lower than that for the conventional method.

Acetic acid production based on DMTM with the use of methanol carbonylation by CO formed in the oxidation process itself is especially promising because it enables nearly a 100% in-carbon selectivity of formation of the desired liquid products; i.e., it eliminates one of the major drawbacks of the process. If industrial methods for extracting CO from recycled gas are in place, acetic acid can be produced by directly using the well-known method of methanol carbonylation developed by the Monsanto Company.

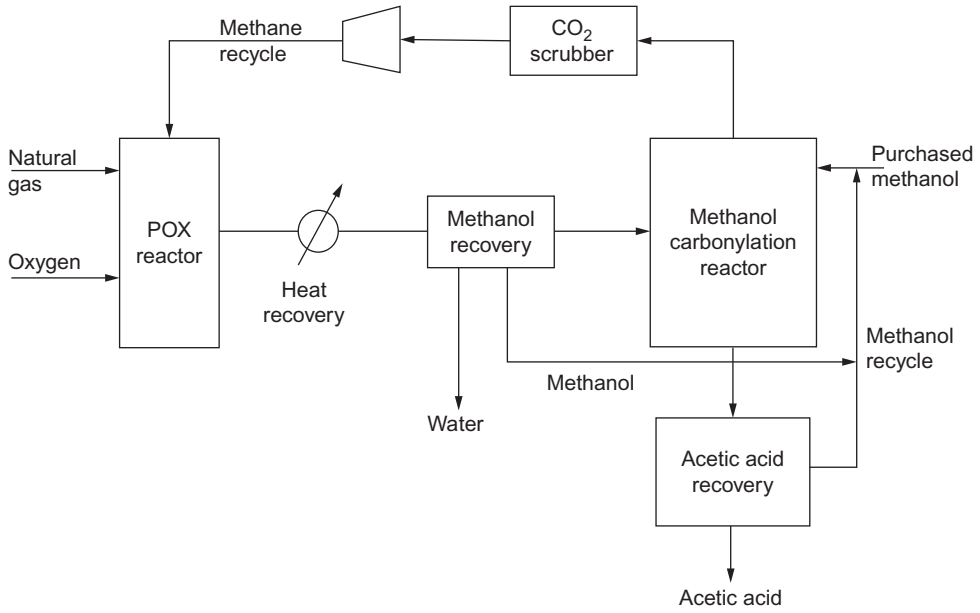

Fig. 8.10
CANMET Integrated process for converting methane to acetic acid (Patent US 5659077, 1997; Mac Farlan and Liu, 2001).

Research on the possibility of methanol carbonylation to other products, such as methyl formate (Chen et al., 2004) and dimethyl carbonate (Ma et al., 2003), is also underway. Should an additional source of hydrogen be available, the possibility of using CO to increase the yield of methanol through the intermediate formation of methyl formate, proposed by Christiansen as long ago as 1919 (Olah et al., 2006), can also be considered:

$$\begin{aligned} CH_3OH + CO &\rightarrow HCOOCH_3 \\ \underline{HCOOCH_3 + 2H_2 &\rightarrow 2CH_3OH} \\ CO + 2H_2 &\rightarrow CH_3OH \end{aligned} \qquad (8.3)$$

Methanol is first carbonylated to methyl formate, which is then hydrogenated to form twice the amount of methanol. The carbonylation reaction proceeds in the liquid phase in the presence of sodium or potassium methoxide ($NaOCH_3$ or $KOCH_3$) as a homogeneous catalyst. This fine-tuned industrial technology is used in the production of formic acid. Recently, the possibility of efficient use of heterogeneous catalysts was demonstrated. The subsequent process of hydrogenation of methyl formate can take place in the liquid or gas phase over copper-containing catalysts. With a suitable choice of catalyst, the process can occur in a single reactor. According to the available patents of a number of firms, the process of production of methanol via methyl formate occurs at 80–120°C and pressures from 10 to 50 atm (Olah et al., 2006), which makes it very compatible with the process of direct oxidation.

There are other possibilities of processing the mixture of methanol, formaldehyde, and formic acid obtained by direct oxidation of methane without prior separation, which leads to expectations of a significant increase in the yield of methanol and, accordingly, the commercial attractiveness of the process. Formaldehyde may be subjected to dimerization into methyl formate on TiO_2 and ZnO_2 catalysts.

$$2HCHO \xrightarrow{TiO_2 \text{ and } ZnO_2} HCOOCH_3 \tag{8.4}$$

Another possibility involves its conversion over CaO and MgO to methanol and formic acid, which rapidly react with each other to form methyl formate:

$$\begin{aligned} 2HCHO &\xrightarrow{H_2O} CH_3OH + HCO_2H \\ CH_3OH + HCO_2H &\xrightarrow{H_2O} HCOOCH_3 \end{aligned} \tag{8.5}$$

The resulting methyl formate can be catalytically hydrogenated or electrochemically reduced to form two molecules of methanol without any byproducts:

$$HCOOCH_3 + 2H_2 \rightarrow 2CH_3OH \tag{8.6}$$

Formic acid produced by the oxidation can serve as a source of hydrogen for the hydrogenation of formaldehyde in an aqueous solution at 250°C in the presence of a suitable catalyst:

$$HCHO + HCO_2H \rightarrow CH_3OH + CO_2 \tag{8.7}$$

A suitable combination of the above reactions makes it possible to substantially increase the yield and selectivity of methanol formation in the direct oxidation process (Olah et al., 2006).

The energochemical production of methanol at thermal power plants makes it possible not only to simplify and optimize the process of production of methanol, but also to significantly reduce nitrogen oxide (NOx) emissions in the production of electricity. NOx is among the most dangerous anthropogenic emissions, which is one of the main components of photochemical smog. For the power plant and gas-pumping compressor stations operating on natural gas, they are a major hazard for ecosystems. Therefore, reducing NOx emissions from power plants is one of the most important global environmental problems. The cost of reducing NOx emissions into the atmosphere by power plants is quite large, 0.5–2 cents/kWh. Nowadays, only a small number of power plants have equipment for removing nitrogen oxides. Therefore, in the future, hundreds of power plants will have to significantly reduce NOx emission.

Flue gases from power plants with a gas consumption of 35–80 thousand m^3/h contain 700–1500 mg/m^3 of nitrogen oxides (Druskin, 1992). Of the three main kinetic mechanisms of the formation of nitrogen oxides during the combustion of hydrocarbon fuels, thermal (Zeldovich mechanism), prompt NOx (Fenimore mechanism), and fuel NOx, the major role in the combustion of natural gas is played by the thermal mechanism (Hill and Smoot, 2000). This mechanism is described by the two main reactions

$$N_2 + O = NO + N \tag{8.8}$$

$$N + O_2 = NO + O \tag{8.9}$$

It is characterized by a strong temperature dependence. The formation of "thermal" NO decreases sharply as the combustion temperature drops below 1800 K. Therefore, reducing the combustion temperature is one of the most effective ways to decrease the concentration of NOx in the flue gas. This is accomplished using various methods, including the creation of combustion zones with a significant deviation of the fuel-to-oxidant ratio from the stoichiometric value, dilution of the reagents with steam, and partial recirculation of flue gases (Druskin, 1992; Hill and Smoot, 2000). Reducing the concentration of NOx by 50% on average entails additional expenditures of $5–$50 per kilowatt of the burner unit (Hill and Smoot, 2000).

The recirculation of combustion products into the combustion zone is one of the most studied and widespread methods of reducing nitrogen oxides, currently widely used in combustion technology. The admixing of 20% of the recycle gas to the blow air can halve the yield of nitrogen oxides (Druskin, 1992). The maximum flame temperature is thereby reduced by nearly 200°C. Since the introduction of recycle gas into the combustion chamber results in a certain decrease in the temperature of the exhaust gas and in a reduction in the efficiency of power plants by about 0.02%–0.03% per 1% recycle gas added, it is believed that, under the condition of steady combustion, flue gas recirculation should be limited to 20%–30% (Druskin, 1992).

As an effective alternative to flue gas recirculation in reducing NOx emissions for all types of power plants fueled by natural gas, it is possible to combine a power plant with the DMTM process into an integrated chemical-power production. Energochemical technology, combining the direct oxidation of natural gas into methanol with the production of electricity from the outgoing gas of the chemical process, makes it possible to greatly simplify the equipment. In fact, it bypasses the main drawbacks of the DMTM process, such as low conversion per pass and a low selectivity of methanol formation in this process. The simplicity of the equipment and the use of air as the oxidant instead of expensive oxygen make the process economically efficient. At the same time, power plants become able to reduce NOx emissions without additional capital and operational costs for these purposes. Using the off-gas from the DMTM process, containing methane and a small admixture of other combustible gases (CO and H_2) and about 30% nitrogen (from the air spent for the oxidation) as a fuel for the power plant, makes it possible to reduce NOx emissions due to a lower temperature of combustion of a nitrogen-diluted fuel.

According to thermodynamic calculations, for a stoichiometric mixture, a 30% dilution of methane with nitrogen leads to a reduction in the NO concentration by ~20%, whereas a 60% dilution leads to a decrease of more than 50%. These results are very consistent with those

obtained in experiments with General Electric gas turbines operating on natural gas diluted with nitrogen. The increase in the molar concentration of N_2 to 48% resulted in an almost twofold decrease in the emission of NOx (Cocchi et al., 2008).

Various types of modern power plants can operate on natural gas highly diluted with nitrogen, up to methane content below 50% in electrochemical generators (fuel cells), 40% in spark ignition engines, 30% in conventional gas turbines, 5% in diesel engines, and 1% in gas turbines with catalytically assisted combustion (Su et al., 2005).

Thus, the dilution of natural gas with nitrogen in its partial oxidation conversion to methanol can significantly reduce NOx emissions. To further reduce the NOx emissions to a level of a few percent of the initial concentration, it is advantageous to use the primary (unfractionated) liquid products from the DMTM process, containing ~40% methanol and ~5% formaldehyde, introduced into the flue duct at temperatures from 320°C to 820°C. As shown in (Zamansky et al., 1996), the introduction of methanol and some other compounds into flue gases at these temperatures results in the oxidation of nitric oxide to nitrogen dioxide, which then can be removed in scrubbers. The process is mainly controlled by the reactions

$$CH_3OH + OH = CH_2OH + H_2O \tag{8.10}$$

$$CH_2OH + O_2 = CH_2O + HO_2 \tag{8.11}$$

$$HO_2 + NO = OH + NO_2 \tag{8.12}$$

There is a very pronounced "temperature window" of the process near 850 K within which the concentration of NO can be decreased to a few percent of the initial level (Fig. 8.11). The amount of methanol needed to effectively reduce the NO concentration is approximately equal to the content of NO in the flue gases, meaning it should be about 0.1% of their volume.

The range of initial concentrations of NO in which it is effectively oxidized to NO_2 is quite wide, covering almost the entire range of NO concentrations interesting for the energy industry. The Energy and Environmental Research Corporation (EER) in the United States, which specializes in the field of environment and power production, has developed the CombiNOx process, which consists of the three-stage combustion of natural gas, selective noncatalytic oxidation of NO by supplying methanol in the boiler flue, and purification of the flue gas from NO_2 (and SO_2) in a wet scrubber. According to EER specialists, at a methanol-to-NO molar ratio of 1.5, it is possible to obtain the same effect as when using the selective catalytic reduction (SCR) of NOx with ammonia, but at significantly lower cost. According to estimates, the method developed by EER specialists is three times cheaper than the SCR (Kotler and Pein, 1995).

Such a process is especially advantageous if methanol is produced directly at a power plant in an integrated energochemical production. If natural gas is received directly from a gas pipeline at a pressure of 5.5–6.5 MPa, the installation can do without energy expenditures on gas

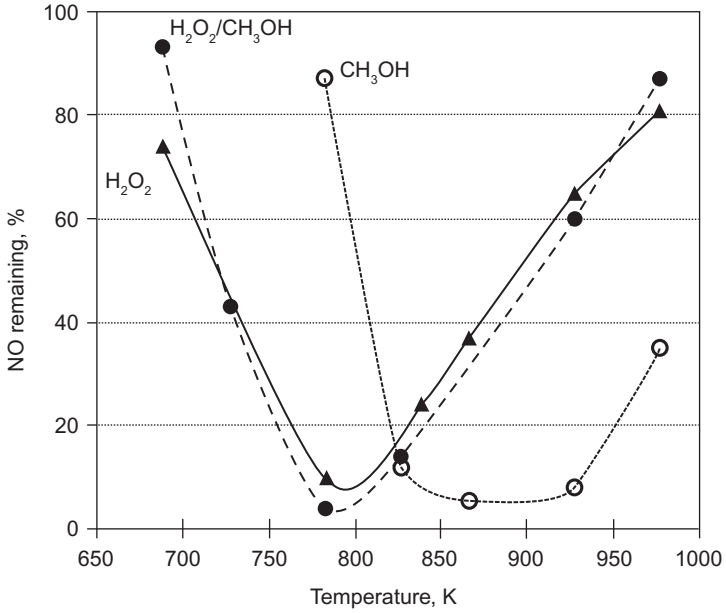

Fig. 8.11

Temperature window of NO conversion by introducing H_2O_2, CH_3OH, and a 1:1 mixture thereof. [NO] = 200 ppm, additive/[NO] = 1.5, and $[O_2]$ = 3.8% (Zamansky et al., 1996).

compression. After standard oxidation with air and separation of the liquid oxidation products, the high pressure of the discharge gas to be burnt in the power installation can be advantageously released in a turboexpander to drive an air compressor. The resulting cold gas flow can be advantageously used for the final cooling of the reaction gases before separation, which makes cumbersome air coolers redundant while enhancing by ~10% the recovery of liquid oxidation products due to a deeper cooling of the gas-liquid mixture to be separated. A scheme of such integrated production of methanol at a power plant is shown in Fig. 8.12.

Given the use of the off-gas of the DMTM process for energy generation and the possibility of utilization of steam produced directly at the power plant, the efficiency of carbon use in such an integrated energochemical process is expected to be close to 100%. A complete use of the reaction heat and calorific value of the exhaust gas actually eliminates the two main drawbacks of the DMTM method associated with the low selectivity of methanol formation and low conversion of gas per pass. At the same time, its benefits, such as the one-step nature of the process and relatively low capital and operating costs, make the DMTM-based integrated method of methanol production quite competitive with the existing methods of commercial methanol production. It should be noted that the properties of methanol are similar to petroleum distillate fuel. Currently, there are assurances of the main manufacturers of gas turbines about the possibility of using methanol as a fuel. Methanol can fuel almost any type of boiler

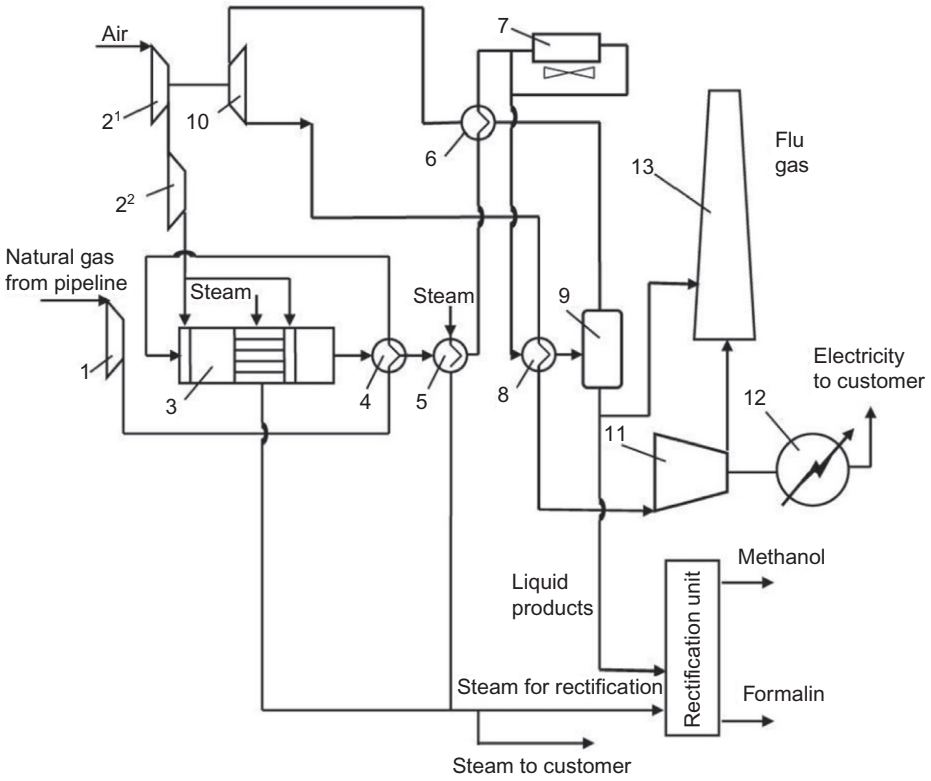

Fig. 8.12

Flow diagram of the integrated process for the production of methanol and electricity with removal nitrogen oxides from the flue gas: (1) booster compressor, (2^1, 2^2) stages of air compressor, (3) two-sectioned reactor, (4) recuperative heat exchanger, (5) steam generator, (6) heat exchanger, (7) air cooler, (8) end heat-exchanger refrigerator, (9) separator, (10) turboexpander, (11) gas turbine, (12) generator, and (13) smokestack.

installation. The main advantage of methanol compared to the conventional distillate fuel is that it contains no sulfur. Therefore, one additional advantage of integrated chemical-power methanol production at power plants is the possibility of using methanol produced as a clean backup liquid fuel. As a result, the supply of reserve fuel to power plants, for example mazut, can be curtailed or completely avoided.

The integrated energochemical production of methanol can be launched at dozens of power plants fueled by natural gas. According to technical-economic assessments, the cost of methanol and specific investment expenditures will be significantly lower than the values typical of modern plants. In this case, the environmental performance of power plants will be improved without additional expenditures, and, at the same time, the reliability of providing them with reserve fuel will be enhanced.

Utilization of coalbed methane for the production of methanol-coal slurries may also be a promising niche for the use of light-duty installations based on the DMTM process. During coal metamorphism, which is accompanied by a low-temperature thermochemical decomposition of organic matter, coal produces large amounts of methane. Methane accumulates due to its adsorption in coal. One ton of coal typically contains 6–8 m^3 of gas. Since the world's coal resources are approximately 10^4 billion tons, the gas content of coal deposits is comparable to its content in the gas fields. Therefore, even a moderate gas production from coal could make a significant contribution to the world's production of natural gas. In addition, the coalbed methane released to the atmosphere constitutes about 8% of all anthropogenic methane emissions (Su et al., 2005).

In the United States, active coalbed methane extraction has been carried out since the 1950s, and its annual output accounts for about 7% of the total production of natural gas. The use of coalbed methane wells is complicated by a low flow rate and its large spread, which can vary from 2 to more than 200 thousand m^3/day. DMTM offers the possibility of an integrated utilization of coalmining waste, including not only methane but also fine coal slime.

Since the 1970s, a number of countries have launched research on the use of water-coal fuel (WCF) to replace coal and mazut in power plants and even as a fuel for turbine and diesel power plants. In addition to being a useful method for utilization of waste coal, WCF makes it possible to transport coal in railway tanks and through pipelines. A lot of experience in this area has already been acquired in Russia, the United States, and China. However, in terms of the calorific value, performance, stability and other properties, another kind of slurry is more promising: coal-methanol slurry. The technology regarding production, applications, and properties of methanol-coal slurries have been described in a number of patents (Patent JP 55304, 1978; Patent JP 45283, 1983; Patent US 861439, 1986; Patent US 4802891, 1988).

As compared to WCF, the use of methanol-coal slurries reduces transportation costs per unit of energy delivered and eliminates the problem of transportation in winter conditions (the freezing point of methanol is −98°C) and makes it possible to use low-grade and wet coals. Coal and methanol are mixed well, with many components of coal being partially eluted into methanol, which leads to complex interactions or modifications of both the solid and liquid phases. Methanol effectively penetrates into pores and cracks in coal, making it easier to disintegrate during combustion due to its explosive expansion on heating. Methanol-coal slurries exhibit a high stability and long storage time, more than 2 months even without periodic stirring, as well as good transport properties due to a sufficiently low viscosity. Their effectiveness as a fuel exceeds that of pulverized coal fuel. The use of such slurries is particularly effective in the case of coals capable of adsorbing a large amount of methanol, such as bituminous and subbituminous coals.

This combination of properties of methanol-coal fuel makes the use of DMTM for the joint utilization of coalbed methane and coal waste in the small-tonnage process an attractive option. One advantage is that methanol-coal slurries can be prepared from methanol containing various impurities formed during its production, including heavier alcohols and water (Patent US 4802891, 1988). That is, the liquid oxidate from the DMTM unit, containing up to 40% methanol and 5%–8% of other organic compounds, can be used without any pretreatment or rectification together with crushed and enriched waste coal. In addition, the methane-containing off-gas from the DMTM process with a methane concentration not less than 25% can be used to generate electricity for the entire complex and the needs of the coal mine (Fig. 8.13).

The properties of the resulting fuel are largely determined by the preparation method. In particular, the high activity of coal in its interaction with methanol and other oxygenates leads to the alkylation of coal and its depolymerization (Zherebtsov, 2007). Therefore, when mechanochemical and especially cavitation technologies are used to produce methanol-coal fuel, one can expect not only the trivial formation of a slurry but also significant changes in the structure of the original coal and the fuel composition, the appearance of new liquid fraction, and significant enhancement in the stability and storage time of the fuel. The conceptual scheme of preparation of methanol-coal slurries is considered in (Arutyunov, 2011).

It is also interesting to examine the interaction of coal with methanol and other oxygenates under supercritical conditions. In this case, the interaction of coal with oxygenates (Adschiri et al., 2000) is accompanied by coal hydrolysis with supercritical water to produce liquid and gaseous products, including resins, lower alkanes, and aromatic compounds (Vostrikov et al., 2007). This process is expected to give rise to a fundamentally new stable liquid hydrocarbon product with high consumer characteristics.

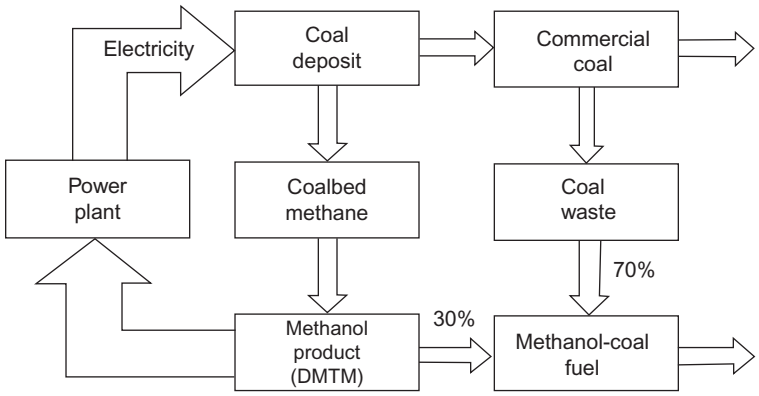

Fig. 8.13
Flow diagram of the production of methanol-coal fuel from coalbed methane and coal waste.

5 Conclusions

Currently, the method of partial oxidation of hydrocarbon gases to oxygenates does not exist as an industrial technology, a circumstance that predetermines the basic problems of its further progress. Many of the technological, engineering, and scientific problems have not been solved not because they are intractable, but simply because there has been no demand for such solutions. For comparison, in recent years, leading oil and gas companies have invested billions of dollars in the development of various aspects of the production of syngas and accompanying processes; this area employs tens of thousands of highly skilled professionals. It is not surprising, therefore, that modern methods of syngas production are technologically the most advanced chemical processes.

There is no doubt that as soon as a new wave of industrial applications of technology of partial oxidation begins to gain strength, most of the technical issues that impede or limit the capabilities of this technology will be successfully resolved. That this technology will experience a renaissance is beyond doubt, since the need for simple low-scale methods for processing hydrocarbon gases is great. In this respect, the DMTM has no economically and technologically feasible alternatives. The small deposits of natural gas with reserves of less than 7 billion m^3, the number of which in the world exceeds 25,000, account for 12% of all resources.

A significant influence on the progress in DMTM circulation technology will be produced by creating effective methods for removing CO from the circulation gases. However, a more attractive prospect of drastically increasing the selectivity of the process is to use resulting CO, for example, as a carbonylation agent for production from methanol acetic acid or other products (Arutyunov et al., 2015). The possibility of catalytic hydrogenation of formaldehyde directly in the gas flow, considered in a number of works, is also noteworthy for increasing the methanol yield. Of certain interest, especially for designing simple technologies of production of methanol for inhibiting hydrate formation in gas fields, are simple methods for the conversion of diluted formalin (vat residue) into products consumed locally or readily transportable, such as paraformaldehyde or urotropin. In some cases, it may be advantageous to combine the DMTM process with the subsequent conversion of methanol into products that can be used as engine fuel for local needs, such as dimethyl ether or heavier alcohols; or to increase the octane number of petroleum fuels by alkylating or etherifying them with methanol; or to modify biodiesel fuel by etherifying vegetable oils with methanol.

Of considerable interest is the possibility of extracting formed oxygenates from the gas flow without using cumbersome and energy-intensive processes of heat transfer and separation, for example by adsorption in a moving adsorbent bed (chromatographic reactor), in cyclic adsorbers, or by chemical bonding. Should it become possible to remove oxygenates without using cycles of complete cooling and subsequent heating of the reaction mixture, the problem of low conversion per passage of gas through the reactor would be mostly solved.

Interesting prospects are associated with a further study of the mechanism of the oxidation of hydrocarbons, especially in nonsteady and oscillatory regimes, which provide an increase in the selectivity to methanol. It is equally interesting to study the possibility of controlling this nonlinear process by means of short-time catalytic or physical impacts Arutyunov, 2014.

Now we are at the very beginning of the new stage of development of DMTM technology and its applications, and it is difficult to predict what real technological processes will be created on its basis. However, with a high degree of confidence, it is possible to predict a significant role of the DMTM technology in the development of the world's natural gas resources.

References

A Handbook of Modern Processes of Gas Processing, 1992. Oil, Gas and Petrochemistry Abroad 9, 76–97 (in Russian).

Adschiri, T., Sato, T., Shibuichi, H., Okazaki, S., Arai, K., 2000. Extraction of Taiheiyo coal with supercritical water-HCOOH mixture. Fuel 79, 243–248.

Anisonian, A.A., Gudkov, S.F., Enikolopian, N.S., Kle'menov, N.A., Markevich, A.M., Nalbandian, A.B., et al., 1957. Production of formaldehyde by direct oxidation of natural gas by air. Gazov. Prom-st 6, 32–40 (in Russian).

Arutyunov, V.S., 2004. Recent results on fast flow gas-phase partial oxidation of lower alkanes. J. Nat. Gas Chem. 13, 10–22.

Arutyunov, V.S., 2011. Oxidative Conversion of Natural Gas. KRASAND, Moscow (in Russian).

Arutyunov, V., 2014. Direct Methane to Methanol: Foundations and Prospects of the Process. Elsevier B.V, Amsterdam.

Arutyunov, V.S., Krylov, O.V., 1998. Oxidative Conversion of Methane. Nauka, Moscow (in Russian).

Arutyunov, V.S., Krylov, O.V., 2005. Oxidative conversion of methane. Russ. Chem. Rev. 74, 1111–1137.

Arutyunov, V.S., Basevich, V.Ya., Vedeneev, V.I., 1995. Modern state of direct partial oxidation of natural gas to methanol. Ind. Eng. Chem. Res. 34, 4238–4243.

Arutyunov, V.S., Basevich, V.Ya., Vedeneev, V.I., 1996. Direct high pressure gas-phase oxidation of natural gas to methanol and other oxygenates. Russ. Chem. Rev. 65, 197–224.

Arutyunov, V.S., Savchenko, V.I., Sedov, I.V., Fokin, I.G., Nikitin, A.V., Strekova, L.N., 2015. New conceptions for small-scale GTL. Chem. Eng. J. 282, 206–212.

Basevich, V.Ya., Vedeneev, V.I., Arutyunov, V.S., Romanovich, L.B., 1997. Gas phase oxidation of methane to methanol in cyclic mode. Theor. Found. Chem. Eng. 31, 68–71.

Benayoun, D., 2001. Ifpecsol—simple method for gas processing. Gazov. Prom. 5, 50–53 (in Russian).

Bjorklund, M.C., Carr, R.W., 2002. Enhanced methanol yields from the direct partial oxidation of methane in a simulated countercurrent moving bed chromatographic reactor. Ind. Eng. Chem. Res. 41, 6528–6536.

Bludworth, J.E., 1949. First tonnage oxygen plant ties in with petrochemical manufacture. Pet. Process. 4 (4), 377–379.

Bukhgalter, E.B., 1986. Methanol and Its Use in the Gas Industry. Nedra, Moscow (in Russian).

Chen, L., Zhang, J., Ning, P., Chen, Y., Wu, W., 2004. Kinetics of methanol carbonylation to methyl formate catalyzed by sodium methoxide. J. Nat. Gas Chem. 13, 225–230.

Cocchi, S., Giannini, N., Provenzale, M., Zucca, A., Romano, C., Ceccherini, G., 2008. A simple model for NOx formation in diffusion gas turbine combustors: rig test validation with a wide range of fuel gases. In: 31st Meeting on Combustion, Italian Section of the Combustion Institute. GE Oil &Gas e Nuovo Pignone S.p.A, Firenze e Italy. VII-1. http://143.225.115.225/proc/proc2008/data/papers/VII/VII-1.pdf.

Druskin, L.I., 1992. Efficient Use of Natural Gas at Industrial Installations. A Handbook. Energoatomizdat (in Russian).
Hill, S.C., Smoot, L.D., 2000. Modeling of nitrogen oxides formation and destruction in combustion systems. Prog. Energy Combust. Sci. 26, 417–458.
Kotler, V.R., Pein, R., 1995. Reduction of waste gases without flue gas purification at thermal power plants (USA experience). Fuel Energy Abstr. 36, 356–362 (in Russian).
Ma, X., Li, Z., Wang, B., Xu, G., 2003. In-situ IR studies on the oxidative carbonylation of methanol to dimethyl carbonate. ACS Fuel Chem. Div. Prepr. 48 (1), 426–427.
Mac Farlan, A., Liu, D., 2001. CANMET integrated acetic acid process: coproduction of chemicals and power from natural gas. In: Iglesia, E., Fleish, T.H. (Eds.), Studies in Surface Science and Catalysis. Proceedings of the 6th Natural Gas Conversion Symposium, Girdwood, AL, 2001. Natural Gas Conversion VI, vol. 136, Elsevier Science B.V, Amsterdam-London-New York-Oxford-Paris-Shannon-Tokyo.
Meyer, R.E., 1955. LPG to chemicals by oxidation. Oil Gas J. 7, 82–86.
Olah, G.A., Goeppert, A., Prakash, G.K.S., 2006. Beyond Oil and Gas: The Methanol Economy. Wiley-VCH Verlag GmbH & Co. KGaA, Weinheim.
Patent JP 45283/1983.
Patent JP 55304/1978.
Patent RU 2051202; 27.12.1995.
Patent RU 2200731; 10.10.2001.
Patent RU 2283829; 24.02.2005.
Patent RU 2385180; 27.03.2010.
Patent RU 2568113; 09.02.2015.
Patent US 4802891; 21.03.1988.
Patent US 5659077; 19.08.1997.
Patent US 861439; 09.05.1986.
Paushkin, Ya.M., Adelson, S.V., Vishnyakova, T.P., 1973. Technology of Petrochemical Synthesis. Part I. Chemistry, Moscow (in Russian).
Su, S., Beath, A., Guo, H., Mallet, C., 2005. An assessment of mine methane mitigation and utilization technologies. Prog. Energy Combust. Sci. 31, 123–170.
Vostrikov, A.A., Fedyaeva, O.N., Dubov, D.Yu., Psarov, S.A., Sokol, M.Yu., 2007. Dynamic and static conversion of brown coal in water in supercritical conditions. SKF-TP 2, 70–84 (in Russian).
Walker, J.C., Malakoff, H.L., 1946. Basic oxygenated chemicals from C_1, C_2 and C_3 paraffins and olefins. Oil Gas J. 45 (33), 59–65.
Weiss, J.M., 1941. After the present emergence what? Chem. Ind. 49 (3), 348–352.
Westerterp, K.R., Bodewes, T.N., Vrijland, M.S.A., Kuczynski, M., 1988. To new methanol converters. Hydrocarbon Process. 11, 69–73.
Zamansky, V.M., Ho, Loc, Maly, P.M., Seeker, W.R., 1996. Gas phase reactions of hydrogen peroxide and hydrogen peroxide/methanol mixtures with air pollutants. In: 26th Symposium (International) on Combustion/ Combustion Institute, pp. 2125–2132.
Zherebtsov, S.I., 2007. Interaction of low-metamorphic coals with methanol. Khim. Tverd. Topl. 3, 60–70 (in Russian).

CHAPTER 9

Reforming and Partial Oxidation Reactions of Methanol for Hydrogen Production

Kamran Ghasemzadeh*, Seyyed M. Sadati Tilebon†, Angelo Basile‡

*Urmia University of Technology, Urmia, Iran †Iran University of Science and Technology, Tehran, Iran ‡Institute on Membrane Technology (ITM-CNR), Rende, Italy

Acronyms

ATR	autothermal reforming
CFD	computational fluid dynamics
CI-NP	co-impregnation with nanoparticle precursor
CI	co-impregnation
CNT	carbon nanotube
CP	co-precipitation
CPOX	catalytic partial oxidation
CT	carbon template
GHSV	gas hourly space velocity
HP	homogeneous precipitation
HS	hydrothermal synthesis
HT-PEMFC	high temperature polymer electrolyte membrane fuel
LDH	layered double hydroxides
IMP	impregnation
IMP-BD	modified impregnation with 1,3-butanediol
LT-PEMFC	low temperature polymer electrolyte membrane fuel
MATR	methanol autothermal reforming
MD	methanol decomposition
MHS	modified hydrothermal synthesis;
MSR	methanol steam reforming
NG	natural gas
OGCP	oxalate gel co-precipitation
P.T	pretreatment temperature
PEMFC	polymer electrolyte membrane fuel cell
POX	partial oxidation
PTSG	polymer template sol–gel method

Methanol. https://doi.org/10.1016/B978-0-444-63903-5.00009-1

SF	sweep factor
SQ	sequential impregnation
SR	steam reforming
SRG	soft reactive grinding technique
SRG-N	soft reactive grinding of oxalic acid with Cu/Zn nitrate precursors
SRG-C	soft reactive grinding of oxalic acid with Cu/Zn carbonate precursors
ST	silica template
R	traditional reactor
WGS	water gas shift
WHSV	weight hourly space velocity
WT	wet impregnation

Symbols

K	reaction rate constant
$L1$	metal loading of 1 wt%.
$L2$	metal loading of 10 wt%.
r_i	rate for species i
R	global gas constant
P_i	partial pressure of species i
$P1$	inlet partial pressure of water and methanol equal to 10.1 kPa.
$P2$	inlet partial pressure of water and methanol equal to 24.3 kPa.

1 Introduction

Nowadays, environmental problems are one of the world biggest concerns, with the most important factor being emissions from fossil-fuel combustion. Therefore, research in the field of clean energy is necessary. In other words, environmentally friendly power sources are required to overcome environmental problems. Many researchers have noted that electrical power produced from fuel cells is environmentally friendly and can eliminate a wide range of concerns about the future of the world (Cacciola et al., 2001; King and O'Day, 2000; Ramirez et al., 2008). Regarding a fuel cell's structure, they require a hydrogen source. This is one main cause of a variety of experiments in the field of hydrogen production. The biggest problem with hydrogen is the high density of energy (see Table 9.1; Sadati et al., 2015), which increases the risk of storing it. Despite the advantages of fuel cells such as low or zero gas emissions, hydrogen storage problems have prevented the development of fuel cells.

On the other hand, the transport of hydrogen because of these noted problems is very difficult or impossible to do in regards to fuel cells application. For this problem, there is one solution; In situ production of hydrogen. Microreactors and membrane reactors (MRs) including

Table 9.1 Energy contents of different fuels

Fuel	Energy Content (MJ/kg)
Hydrogen	120
Liquefied natural gas	54.4
Propane	49.6
Aviation gasoline	46.8
Automotive gasoline	46.4
Automotive diesel	45.6
Ethanol	29.6
Methanol	19.7
Coke	27
Wood (dry)	16.2
Bagasse	9.6

reforming processes can eliminate these noted problems (Brown, 2001; Ghenciu, 2002; Olah et al., 2011; Iulianelli et al., 2008a; Basile et al., 2008; Ghasemzadeh et al., 2013b; Ghasemzadeh et al., 2015a; Tosti et al., 2008; Damle, 2008; Löffler et al., 2003; Sun, 2004; Pattekar and Kothare, 2004).

Another main problem of fuel cell technology is the harsh operational conditions of hydrogen production (usually at a high temperature). Reforming alcohols and hydrocarbons allows in situ hydrogen production. The main industrial feed for hydrogen production is natural gas. Another hydrogen carrier that can be used for hydrogen production is methanol. It should be noted that this matter has some advantages compared with other hydrogen carrier hydrocarbons, including:

- Relatively low operational temperature
- Relatively simple reactions in reformer
- Low required feed volume compared with gaseous matters
- High hydrogen-to-carbon ratio
- Biodegradability, etc.

The operation temperature of methanol steam reforming (MSR) is relatively low, between 200°C and 300°C. The main reason for the low temperature for this process is the absence of strong carbon-carbon bonds. The operational temperature is low when compared to other common fuels such as methane, which is reformed above 500°C (Dittmar et al., 2013; Wu et al., 2013; Xu et al., 2013; Zhu and Fan, 2015), and ethanol, with a reforming temperature around 400°C (Dittmar et al., 2013; Contreras et al., 2014; Garbarino et al., 2013; Li et al., 2013; Palma et al., 2014). Of course, the difficulty of methanol purification because of miscibility in water and high toxicity are some of the disadvantages of methanol (Sá et al., 2010). Nevertheless, according to the literature, methanol was introduced as a high potential feedstock for in situ hydrogen production systems. Therefore, in this chapter, after discussing different methods of

hydrogen production from methanol, we will focus on developing new technologies for hydrogen production during steam reforming and partial oxidation of methanol.

2 Hydrogen Production

In recent years, more than 90% of the world's hydrogen production has been accomplished by reforming and oxidating fossil fuels and alcohols (Haryanto et al., 2005; Palo et al., 2007). However, in addition to these sources of hydrogen production, water splitting (Agrafiotis et al., 2005; Ni et al., 2007b; Norman et al., 1981) and biomass gasification (Navarro et al., 2007; Ni et al., 2006) processes can produce hydrogen. Regarding the main purpose of this chapter, a summary about fuel processing technologies will be discussed in the following.

2.1 Fuel Processing

Typically, convectional fuels contain hydrogen and carbon. One of the most important methods for hydrogen production is decomposition of the fuel molecules to achieve the hydrogen. Usually, this process occurs in the presence of oxygen and/or water steam. However, there are some methods where adding the water or oxygen is not required. Many technologies for processing fuels to achieve hydrogen have been developed. In the following section, some of the most important methods for fuel processing are discussed.

2.1.1 Steam reforming, partial oxidation, and autothermal reforming

A wide range of processes called fuel processing can convert the hydrocarbons and alcohols to hydrogen (plus other byproducts). Reforming and oxidation of hydrocarbons and alcohols, pyrolysis (Muradov and Veziroğlu, 2005; Muradov, 1998), plasma reforming (Benilov and Naidis, 2006; Chen et al., 2008), aqueous phase reforming, and ammonia reforming (Choudhary et al., 2001) are some of the processes for hydrogen production. It should be noted that steam reforming and partial oxidation are the main processes for hydrogen production on an industrial scale. However, many materials such as methane, gasoline, methanol, ethanol, or ammonia can be used in this process as a feed. Fuel processing of methane is the most common hydrogen production method in commercial use today (Dittmar et al., 2013; Patrascu and Sheintuch, 2015; Wu et al., 2013). However, as mentioned before, for in situ production strategy, methanol has more advantages. A conceptual flow sheet of hydrogen production technologies is shown in Fig. 9.1.

The first method in fuel processing that should be discussed is steam reforming (SR). The SR process is a catalytic process that converts the hydrocarbon or alcohols to hydrogen and carbon monoxide in the presence of steam (Eq. 9.1). Water molecules are highly stable; therefore breaking their molecular chain requires a high level of energy. So the SR process is endothermic. On the other hand, partial oxidation (POX) is a partial combustion of fuels

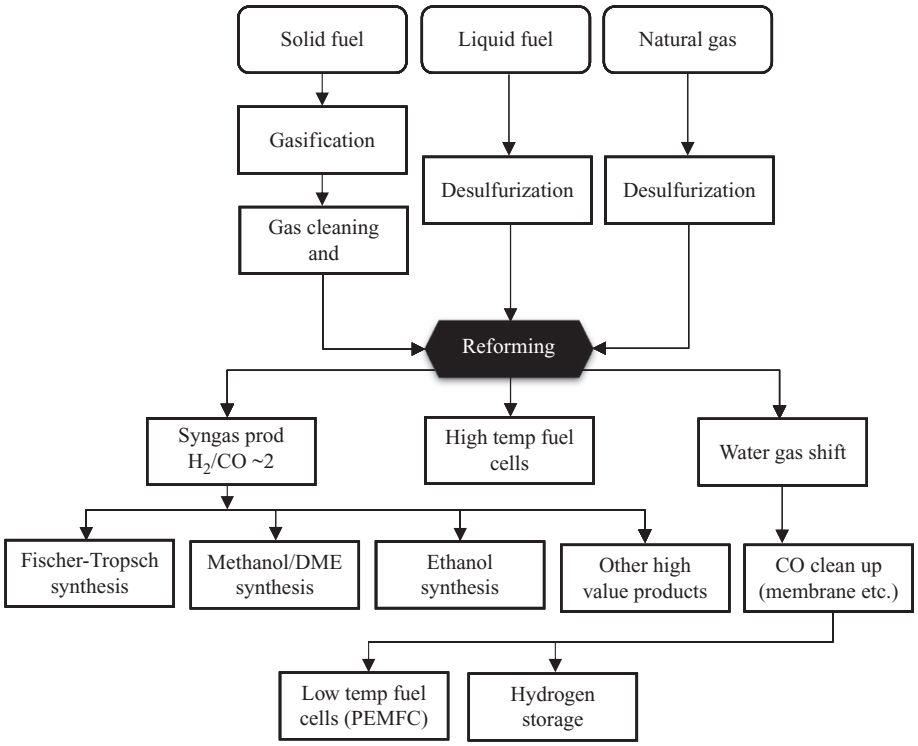

Fig. 9.1
Fuel processing of gaseous, liquid, and solid fuels for hydrogen production.

(Eq. 9.2). It is clear that this process will produce heat. So, POX is exothermic. But, autothermal reforming (ATR) (Eq. 9.3) is the optimum process for SR and POX. On an industrial scale, this process occurs in a two-step reactor. The first step of the reactor is the POX zone and the second step is the SR section. This integration will lead to the decreasing need for an external source to remove or add heat. Of course, all these processes have other advantages and disadvantages in addition to heat source requirement (Divins et al., 2013; Khila et al., 2013).

It should be noted that in addition to the main reactions for POX, SR, and ATR processes, many side reactions can be taken in commercial reactors. Water gas shift (WGS) is one of the main reactions that should be considered in fuel processing systems. The main reaction of WGS is noted in Eq. 9.4 (Jeong et al., 2013; LeValley et al., 2014). This reaction can change the ratio of CO/H_2 as an important parameter in syngas production systems. On the other hand, one of the most important problems in hydrogen production is carbon (coke) formation (Eq. 9.5). This phenomenon can cause catalyst deactivation, reduction of the total volume of the reactor, reduction of the heat transfer, and an increase in the gas hour space velocity (GHSV) (Holladay et al., 2009; Ni et al., 2007a).

Steam reforming

$$C_mH_n + m\,H_2O \rightarrow m\,CO + (m + 0.5n)H_2 \quad (9.1)$$

ΔH = endothermic (absolute amount is hydrocarbon dependent)

Partial oxidation

$$C_mH_n + 0.5mO_2 \rightarrow m\,CO + 0.5H_2 \quad (9.2)$$

ΔH = exothermic (absolute amount is hydrocarbon dependent)

Autothermal reforming

$$C_mH_n + 0.5mH_2O + 0.25mO_2 \rightarrow mCO + (0.5m + 0.5n)H_2 \quad (9.3)$$

ΔH = thermally neutral (absolute amount is hydrocarbon dependent)

Water gas shift (WGS)

$$CO + H_2O \rightarrow CO_2 + H_2 \quad (9.4)$$

$\Delta H = -41.1$ kJ/mol

Coke formation

$$C_mH_n \rightarrow xC + C_{m-x}H_{n-2x} + xH_2 \quad (9.5)$$

ΔH = hydrocarbon dependent

In hydrogen production reactors, the engineering design should lead to an increase in the SR, POX, or ATR reactions while preventing the occurrence of coke formation reactions. There are several parameters that can change the coke formation. The ratio of carbon to steam in SR and carbon to steam and feed composition are some important parameters. The most important parameter for coke formation is temperature. Therefore, detailed temperature control is necessary. For different operational conditions and different feeds, there is an optimum temperature for minimizing the coke formation.

As a general point of view, the SR, POX, and ATR are different common methods for hydrogen production on a commercial scale. Each of these processes has advantages and challenges, summarized in Table 9.2.

The reforming process produces a gas stream composed primarily of hydrogen, carbon monoxide, and carbon dioxide. Regarding Table 9.2, endothermic SR of hydrocarbons or alcohols requires an external heat source. The SR does not require oxygen. It also has a lower operating temperature than POX and ATR and produces reformate with a high H_2/CO ratio ($\sim$3:1), which is beneficial for hydrogen production. However, it does have the highest emissions of the three processes. The POX process converts hydrocarbons or alcohols to hydrogen by partially oxidizing (combusting) the feed with oxygen. The heat is provided by the "controlled" combustion. It does not require a catalyst for operation, has minimal methane slip, and is more sulfur-tolerant than the other processes. The process occurs at high temperatures with some soot formation. Also, the H_2/CO ratio (1:1 to 2:1) is favored for the feeds to hydrocarbon synthesis reactors such as Fischer-Tropsch. The ATR process uses POX to provide the heat and SR to increase the hydrogen production, resulting in a thermally neutral process.

Table 9.2 Comparison of reforming technologies

Technology	Advantages	Disadvantages
SR process	Most extensive industrial experience Oxygen not required Lowest process temperature Best H_2/CO ratio for H_2 production	Highest air emissions
ATR process	Lower process temperature than POX Low methane slip	Limited commercial experience Requires air or oxygen
POX process	Decreased desulfurization requirement No catalyst required Low methane slip	Low H_2/CO ratio Very high processing temperatures Soot formation/handling adds process complexity

The ATR is typically conducted at a lower pressure than POX reforming and has a low methane slip. Since POX is exothermic and ATR incorporates POX, these processes do not need an external heat source for the reactor. However, they require an expensive and complex oxygen separation unit in order to feed pure oxygen to the reactor or the product gas is diluted with nitrogen. The SR is typically the preferred process for hydrogen production in industry (Holladay et al., 2009; Dauenhauer et al., 2006; Deluga et al., 2004; Horn et al., 2007; Rabenstein and Hacker, 2008).

2.1.2 Hydrogen production from methanol feedstock

As mentioned before, methanol can be converted to hydrogen at lower temperatures (150–350°C) (Busetto et al., 1984; Matter et al., 2004) than most other fuels (>500°C) (Li et al., 2015; Mondal et al., 2015; Silva et al., 2015) because it contains no carbon-carbon bonds that must be broken, and, unlike methane, it is easily activated at low temperatures. Low-temperature conversion leads to low levels of CO formation, even if the catalyst provides no special mechanism for selectivity of CO_2 over CO. However, it should be noted that operation at low temperature without a catalyst and at long residence times will lead to high levels of methane, which defeats the purpose of reforming the methanol in the first place (Palo et al., 2007). In general, for in situ hydrogen production systems, this feedstock presents promising potential.

2.1.2.1 Steam reforming of methanol

There are several catalytic reactions available for liberating hydrogen from methanol. A wide range of reactions may occur in the reformer. Of course, some of them are more important. In other words, used catalysts are selective and the possibility of them is much higher than another (a large number of side reactions are deniable). The main reactions of reformers includes (Behrens and Armbrüster, 2012):

$$\text{Methanol decomposition (MD):}\quad CH_3O \rightarrow CO + 2H_2,\quad \Delta H^\circ = +90\ \text{kJ/mol} \tag{9.6}$$

$$\text{Methanol steam reforming:}\quad CH_3OH + H_2O \rightarrow CO_2 + 2H_2,\quad \Delta H^\circ = +49\ \text{kJ/mol} \tag{9.7}$$

As discussed previously, a WGS (Eq. 9.4) reaction is a favorable reaction and always happens in a reformer.

On the other hand, catalysts play an important role in the overall process performance. Therefore, a detailed study of catalysts is necessary. Catalysts play one of the most important roles in the reforming process. Process temperature, selectivity of hydrogen, and the amount of carbon dioxide are some highlighted specifications of hydrogen production by steam reforming. Ideally, the catalyst should be highly active in order to achieve large amounts of hydrogen, highly selective so that the carbon monoxide produced is negligible, and, finally, it should present long-term stability. Copper-based catalysts are the most commonly used for the MSR reaction due to their high activity and selectivity. However, these catalysts are known for their pyrophoric characteristics and deactivation by thermal sintering, which motivates the search for other types of catalysts. In comparison with the Cu-based, group 8–10 catalysts have been reported in the literature (Agarwal et al., 2005; Chiarello et al., 2010; Conant et al., 2008; Papavasiliou et al., 2005; Sá et al., 2010) as highly stable and with similar selectivity. However, concerning the catalytic activity, the later catalysts have the disadvantage of producing less hydrogen than the copper-based ones.

On the other hand, the performance of copper-based catalysts is affected by the status of copper. More specifically, high values of copper dispersion and metal surface area, along with small particle sizes, are the targets to attain for the production of highly active catalysts. A summary of the physicochemical properties of various catalysts found in the literature is presented in Table 9.3.

In its turn, the influence of the preparation method and promoter types of the Cu-based catalysts on the performance of the MSR reaction is presented in Tables 9.4 and 9.5. To facilitate the comparison between different catalysts, some authors use the commercially available $CuO/ZnO/Al_2O_3$ catalyst as a reference.

Regarding the literature, carbon nanotubes (CNTs) have been used as supports for Cu-based catalysts due to their structural morphology and characteristics. In the work of Yang and Liao (2007), multiwalled CNTs were used to prepare a Cu/ZnO-CNT nanocatalyst, presenting high catalytic activities of approximately 400 μmol g^{-1} s^{-1}, for reaction temperatures around 400°C. Concerning their results, the catalytic activity of the Cu/ZnO/CNT increased with the total metal loading until the value of 30 wt%, after which it decreased. It was suggested that

Table 9.3 Physicochemical properties of copper catalysts found in the literature

Catalyst	Preparation Method	S_{BET} ($m^2\ g^{-1}$)	S_{Cu} ($m^2\ g^{-1}$)	Cu Dispersion (%)	Reference
Cu/Zn/Al	WT	63.9	–	–	(Shen and Song, 2002)
Cu/Zn/Al	HS	84.5	–	–	(Shen and Song, 2002)
Cu/Zn/Al	CP	93.7	–	–	(Shen and Song, 2002)
Cu/ZnO	CP	48.6	20.8	9.6	(Agrell et al., 2003)
$Cu/ZnO/Al_2O_3$	CP	91.9	22.2	11.3	(Agrell et al., 2003)
$Cu/ZnO/ZrO_2$	CP	81.8	15.5	13.2	(Agrell et al., 2003)
$Cu/ZnO/ZrO_2/Al_2O_3$	CP	116.2	23.3	23.2	(Agrell et al., 2003)
Cu/ZnO	CP	40.7	16.0	–	(Shishido et al., 2004)
Cu/ZnO	HP	76.4	41.6	–	(Shishido et al., 2004)
$Cu/ZnO/Al_2O_3$	HP	97.5	47.0	–	(Shishido et al., 2004)
Cu/ZrO_2	IMP	13.1	1.0	–	(Yao et al., 2006)
Cu/ZrO_2	CP	64.2	3.5	–	(Yao et al., 2006)
Cu/ZrO_2	OGCP	71.5	18.4	–	(Yao et al., 2006)
Cu/ZnO	CP	47.5	20.8	–	(Jeong et al., 2006)
$Cu/ZnO/Al_2O_3$	CP	90.8	23.7	–	(Jeong et al., 2006)
$Cu/ZnO/ZrO_2/Al_2O_3$	CP	129.7	25.9	–	(Jeong et al., 2006)
Cu/Zn/Al	WT	152	–	–	(Patel and Pant, 2006a)
Cu/Zn/Ce/Al	WT	162	–	–	(Patel and Pant, 2006a)
CuO/CeO_2	CT	153	–	–	(Valdes-Solis et al., 2006)
$CuMn_2O_4$	ST	144	–	–	(Valdes-Solis et al., 2006)
$CuO/ZnO/Zr_2O_2$	CP	64	–	–	(Valdes-Solis et al., 2006)
Cu-Mn	CP	9.6	–	–	(Liu et al., 2008)
Cu-Mn	CP	55.2	–	–	(Liu et al., 2008)
Cu-Mn spinel	SRG	118.1	–	–	(Liu et al., 2008)
$CuO/ZnO_{Ac\text{-}300}$	MHS	64	–	–	(Mateos-Pedrero et al., 2015)
$CuO/ZnO_{Ac\text{-}350}$	MHS	71	–	–	(Mateos-Pedrero et al., 2015)
$CuO/ZnO_{Ac\text{-}375}$	MHS	80	–	–	(Mateos-Pedrero et al., 2015)
$CuO/ZnO_{Ac\text{-}400}$	MHS	54	–	–	(Mateos-Pedrero et al., 2015)
$CuO/ZnO_{N\text{-}375}$	MHS	77	–	–	(Mateos-Pedrero et al., 2015)

CP, co-precipitation; *CT*, carbon template; *HP*, homogeneous precipitation; *HS*, hydrothermal synthesis; *IMP*, impregnation; *OGCP*, oxalate gel co-precipitation; *SRG*, soft reactive grinding technique; *ST*, silica template; *WT*, wet impregnation; *MHS*, modified hydrothermal synthesis.

Table 9.4 Influence of the preparation method on the performance of different Cu-based catalysts for MSR

Catalyst	Preparation Method	T (°C)	X_{MeOH} (%)	Activity ($\mu molH_2\ gcat^{-1}\ s^{-1}$)	y_{CO}	S_{CO} (%)	Reference
Cu/ZnO	CP	250	46.4	51	–	0.4	(Shishido et al., 2004)
Cu/ZnO	HP	250	94.2	105	–	0.4	(Shishido et al., 2004)
Cu/ZnO/Al_2O_3	HP	250	97.3	109	–	1	(Shishido et al., 2004)
CuO/ZrO_2	PTSG	250	92	–	0.002	–	(Purnama et al., 2004)
CuO/ZnO/Al_2O_3 (commercial)	–	250	92	–	0.1	–	(Purnama et al., 2004)
CuZn	IMP	230	0	–	–	–	(Jakdetchai et al., 2005)
CuZn	IMP	300	36.8	–	–	7.1	(Jakdetchai et al., 2005)
CuZn	IMP-BD	230	59.5	–	–	0	(Jakdetchai et al., 2005)
Cu/ZrO_2	IMP	260	10	3	0	–	(Yao et al., 2006)
Cu/ZrO_2	CP	260	62	56	0.009	–	(Yao et al., 2006)
Cu/ZrO_2	OGCP	260	100	90	0.005	–	(Yao et al., 2006)
Cu/Zn/Zr/Al	WT	260	60	159	0.016	–	(Patel and Pant, 2006b)
Cu/Zn/Zr/Al	CP	260	97	261	0.008	–	(Patel and Pant, 2006b)
Cu/ZnO	CP	240	43.0	36	0.0018	–	(Wang et al., 2007)
Cu/ZnO	CP	240	48.6	41	0.0022	–	(Wang et al., 2007)
Cu/ZnO	SRG-C	240	52	44	0.0016	–	(Wang et al., 2007)
Cu/ZnO	SRG-N	240	70.9	59	0.0026	–	(Wang et al., 2007)
Cu-Mn	OGCP	260	59.7	51	–	1.4	(Liu et al., 2008)
Cu-Mn	CP	260	65.7	56	–	1.1	(Liu et al., 2008)
Cu-Mn spinel	SRG	260	92.9	79	–	0.7	(Liu et al., 2008)
CuZnZrAl	SQ	260	61	–	–	4.5	(Jones and Hagelin-Weaver, 2009)

Table 9.4 Influence of the preparation method on the performance of different Cu-based catalysts for MSR—cont'd

Catalyst	Preparation Method	T (°C)	X_{MeOH} (%)	Activity ($\mu molH_2$ $gcat^{-1}$ s^{-1})	y_{CO}	S_{CO} (%)	Reference
CuZnZrAl	CI-NP	260	63	–	–	3.0	(Jones and Hagelin-Weaver, 2009)
CuZnZrAl	CI	260	65	–	–	7.0	(Jones and Hagelin-Weaver, 2009)
$Cu/Zn/Al_2O_3$ (commercial)	–	260	60	–	–	3.2	(Jones and Hagelin-Weaver, 2009)

CP, co-precipitation; *CI*, co-impregnation; *CI-NP*, co-impregnation with nanoparticle precursor; *HP*, homogeneous precipitation; *IMP*, impregnation; *IMP-BD*, modified impregnation with 1,3-butanediol; *OGCP*, oxalate gel co-precipitation; *PTSG*, polymer template sol–gel method; *SQ*, sequential impregnation; *SRG*, soft reactive grinding technique; *SRG-N*, soft reactive grinding of oxalic acid with Cu/Zn nitrate precursors; *SRG-C*, soft reactive grinding of oxalic acid with Cu/Zn carbonate precursors; *WT*, wet impregnation.

Table 9.5 Influence of the type of promoter on the performance of different Cu-based catalysts for MSR

Catalyst	T (°C)	X_{MeOH} (%)	Activity ($\mu mol\ H_2$ g_{cat}^{-1} s^{-1})	y_{CO}	S_{CO} (%)	Reference
$Cu/Cr/Al_2O_3$	300	63	117	0.011	–	(Lindström et al., 2002)
$Cu/Zr/Al_2O_3$	300	44	81	0.0075	–	(Lindström et al., 2002)
Cu/ZnO	308	90	–	0.0014	–	(Agrell et al., 2003)
$Cu/ZnO/Al_2O_3$	305	90	–	0.0011	–	(Agrell et al., 2003)
$Cu/ZnO/ZrO_2$	295	90	–	0.0005	–	(Agrell et al., 2003)
$Cu/ZnO/ZrO_2/Al_2O_3$	278	90	–	0.00045	–	(Agrell et al., 2003)
Cu/CeO_2	260	91	135		2.3	(Liu et al., 2003)
Cu/ZnO	260	67	99		0.9	(Liu et al., 2003)
Cu/Zn(Al)O	260	58	86		0.8	(Liu et al., 2003)
Cu/Al_2O_3	260	22	32		0.4	(Liu et al., 2003)
$Cu\text{-}Cr_2O_3$	240	–	28		5	(Huang et al., 2004)
Cu-ZnO	240	–	24		7	(Huang et al., 2004)
Cu-CoO	240	–	17		14	(Huang et al., 2004)

Continued

Table 9.5 Influence of the type of promoter on the performance of different Cu-based catalysts for MSR—cont'd

Catalyst	T (°C)	X_{MeOH} (%)	Activity (μmol H_2 g_{cat}^{-1} s^{-1})	y_{CO}	S_{CO} (%)	Reference
Cu/Zn/Al	250	39	–	–	0.6	(Yong-Feng et al., 2004)
Cu/Zn/Zr/Al	250	61	–	–	0.4	(Yong-Feng et al., 2004)
Cu-Mn-O	240	99	–		3.1	(Papavasiliou et al., 2005)
Cu-Ce-O	240	37	–		0.8	(Papavasiliou et al., 2005)
CuO/CeO_2	250	80	75		–	(Oguchi et al., 2005)
$CuO/CeO_2/ZrO_2$	250	–	97		–	(Oguchi et al., 2005)
Cu/Zn/Al	260	76	203	0.011	–	(Patel and Pant, 2006a)
Cu/Zn/Ce/Al	260	90	244	0.0006	–	(Patel and Pant, 2006a)
$Cu/Zn/Al_2O_3$	300	100	185	0.012	–	(Patel and Pant, 2006a)
Cu/ZnO	260	75	–	0.0073	–	(Jeong et al., 2006)
$Cu/ZnO/Al_2O_3$	260	79	–	0.0073	–	(Jeong et al., 2006)
$Cu/ZnO/ZrO_2/Al_2O_3$	260	92	–	0.0010	–	(Jeong et al., 2006)
CuZn	250	39	–	0.0011[a]	–	(Bichon et al., 2007)
Pd/CuZn	250	47	–	0.003[a]	–	(Bichon et al., 2007)
Cu/SiO_2	300	50	–	–	0.15	(Matsumura and Ishibe, 2009a)
$ZnO/Cu/SiO_2$	300	75	–	–	0.6	(Matsumura and Ishibe, 2009a)
$Cu/Zn/Al_2O_3$ (commercial)	300	57	–	–	1.1	(Matsumura and Ishibe, 2009a)
$Cu/ZnO/Al_2O_3$ (commercial)	270	59.0	–	–	–	(Huang et al., 2009)
$Cu/ZnO/Al_2O_3$	270	89.2	–	–	0.92	(Huang et al., 2009)
$Cu/ZnO/ZrO2/Al_2O_3$	270	92.4	–	–	0.97	(Huang et al., 2009)
$Cu/ZnO/CeO_2/ZrO_2/Al_2O_3$	270	89.4	–	–	0.85	(Huang et al., 2009)
$Cu/ZnO/CeO_2/Al_2O_3$	270	79.3	–	–	0.66	(Huang et al., 2009)
CuMn-spinel	213	77	–		0.2	(Fukunaga et al., 2009)
Non-spinel CuMn	214	61	–		0.1	(Fukunaga et al., 2009)

[a]Dry gas.

the high content of metal could cause a partial destruction of the structure or a metal aggregation, resulting in the decrease of activity. A minimum content of ZnO (20%) was required to maintain the CO concentration below 1% (Yang and Liao, 2007; Liao and Yang, 2008).

According to the work of Liao and Yang (2008), three catalysts were prepared with similar composition: a Ni–Cu alloy supported on carbon nanotubes (Ni-Cu/CNT), a bimetal catalyst of Ni and Cu supported on carbon nanotubes (Ni/Cu/CNT), and an Ni-Cu catalyst supported on activated carbon (Ni-Cu/C). Liao et al. justified this due to a better metallic distribution and lower aggregation of metal particles when CNTs were used as supports instead of activated carbon. Comparing both CNT-supported catalysts, the formation of Ni–Cu alloys is responsible for the difference in the catalytic activity. In the absence of a Ni–Cu alloy, hydrogen strongly adsorbs on Ni, reducing the contact of methanol with Ni, thus decreasing the activity.

Finally, a different type of catalyst was prepared by Gao et al. (2008) where single-walled CNT were used not as a support, but as a template. A nanofiber La_2CuO_4 catalyst was prepared and compared to a La_2CuO_4 bulk powder catalyst. Their results indicated that the performance of the nanofiber catalyst is clearly superior, especially at low temperatures (150°C), where all methanol was converted with no CO formation. Moreover, they reported oxygen vacancies in the nanofiber catalyst and the generation of trapped electrons on the vacancy sites. It was suggested that the oxygen vacancy along with the trapped electron can stabilize the intermediates of HCO and H_2CO which decompose to CO and H_2, preventing the formation of CO. It is important to highlight the high activity of 290.2 μmol g^{-1} s^{-1}, especially at low temperature, which is among the highest values found in the literature. Regarding the catalyst stability, a decrease of approximately 2% in methanol conversion was reported during the 60 h lifetime test, but a long-term stability test was not presented.

On the other hand, reduction is another important parameter for the preparation of a catalyst before adding to the MSR process. The aim of reduction is converting the metal oxide to active metal in the surface of the catalyst. The temperature of reduction can change the activity of the catalyst. Some authors report that the lower the temperature needed for the reduction, the easier the reduction is, which may result from a high dispersion and large surface area of the catalyst. Several authors have corroborated this trend with their work, namely Shen, Song, Breen, and Ross (Günter et al., 2001; Shen and Song, 2002; Yao et al., 2006) whose results are presented in Table 9.6. A linear correlation cannot be established between the activity and the reduction temperature, but the trend indicates that easier reducibility follows higher activity. In contrast, other authors concluded that the reducibility of the copper species does not indicate any information about the catalyst activity, and in some cases the catalysts that were more difficult to reduce tended to be more active.

As an example, in Jones and Hagelin-Weaver (2009), the catalyst with the best performance was the one with the highest reduction temperature. Cu-based catalysts are described as easily deactivated. Deactivation is generally attributed to a change in oxidation state, catalyst

Table 9.6 Influence of the reduction temperature in the catalytic activity

Catalyst	S_{BET} ($m^2\ g^{-1}$)	Reduction Peak (°C)	T (°C)	X_{MeOH} (%)	Activity (μmol H_2 $g_{cat}^{-1}\ s^{-1}$)	Reference
Cu/Zn/Al	94.0	265	255	–	127	(Breen and Ross, 1999)
Cu/Zn/Zr	94.7	240	255	–	165	(Breen and Ross, 1999)
Cu/Zn/Zr/Al	103.3	240	255	–	186	(Breen and Ross, 1999)
Cu/Zn/Al	63.9	477	230	15	–	(Shen and Song, 2002)
Cu/Zn/Al	84.5	230	230	85	–	(Shen and Song, 2002)
Cu/Zn/Al	93.7	233	230	100	–	(Shen and Song, 2002)
Cu/Zn/ Al2O3 (commercial)	68.0	250	300	55	–	(Jones and Hagelin-Weaver, 2009)
Cu/Zn/Zr	19.0	280	300	46	–	(Jones and Hagelin-Weaver, 2009)
Cu/Zn/Zr/Al	48.0	322	300	48	–	(Jones and Hagelin-Weaver, 2009)

sintering, or coke deposition. Poisoning of the catalyst can also occur if there are foreign species in the feed mixture such as chloride and sulfur. In the work of Valdes-Solis et al. (2006) deactivation was related to the specific feed composition and space velocity. In this study, simultaneous coke formation and phase sintering reported. Both of them are cause of catalyst deactivation. Deactivation by the presence of coke was also reported by Cao et al. (2006) when water was absent in the feed. In a study of deactivation of supported copper catalysts for methanol synthesis, Kurtz et al. (2003) found that high concentrations of CO led to an enhanced sintering of the metallic Cu particles. It was also reported that Al_2O_3 is a structural promoter for Cu/ZnO catalysts, which inhibits thermal sintering of Cu crystallites. Matsumura and Ishibe (2009b) reported that the growth of ZnO and ZrO_2 particles was accompanied by catalyst deactivation. The Zn/Cu ratio was analyzed by Jones et al. (2008) and correlated to catalyst deactivation. After a reductive treatment and exposure to reaction conditions, the ratio between Zn/Cu increased and a less-active Cu phase was exposed, which led to deactivation. Copper-alumina catalysts can be stabilized by cerium as suggested in the work of Patel and Pant (2006a). They performed studies comparing cerium-promoted Cu-Zn-Ce-Al-oxide catalysts with catalysts containing only a zinc promoter. The long run-time performance of the ceria-containing catalysts was superior due to its high oxygen storage capacity. Under MSR reductive conditions, partially reduced ceria sites are formed producing mobile oxygen that facilitates the coke gasification, inhibiting coke deposition. The addition of oxygen to the feed mixture (oxidative MSR) helps to reduce catalyst deactivation because oxygen reduces or even suppresses coke formation. As described above, the increase of the steam-to-carbon ratio is also favorable to decrease the catalyst deactivation.

The group 8–10 metal-based catalysts were first studied by Iwasa et al. (1998) (as seen in Table 9.7). Based on their preliminary findings, other authors have later studied the influence of several factors on the catalytic performance for MSR. The most commonly used catalyst in this

Table 9.7 A summary of various supported group 8–10 catalysts used for MSR

Catalyst	T (°C)	P.T. (°C)	Activity ($\mu molH_2\ gcat^{-1}\ s^{-1}$)	S_{CO}	X_{MeOH} (%)	S_{metal} ($m^2\ g^{-1}$)	Dispersion (%)	Reference
Pd [P2, L1]	200	–	2.0	99.9	–	–	2.1	(Iwasa et al., 1993)
Pd/SiO_2 [P2, L1]	200	–	0.13	100	–	–	7.2	(Iwasa et al., 1993)
Pd/Al_2O_3 [P2, L1]	200	–	1.9	98.6	–	–	13.1	(Iwasa et al., 1993)
Pd/La_2O_3 [P2, L1]	200	–	3.1	92	–	–	5	(Iwasa et al., 1993)
Pd/Nd_2O_3 [P2, L1]	200	–	3.7	93	–	–	25.3	(Iwasa et al., 1993)
Pd/Nb_2O_5 [P2, L1]	200	–	1.5	95.8	–	–	19.6	(Iwasa et al., 1993)
Pd/ZnO [P2, L1]	200	–	8.3	3	–	–	10.7	(Iwasa et al., 1993)
Pd/ZrO_2 [P2, L1]	200	–	4.0	80	–	–	28.9	(Iwasa et al., 1993)
Pd/ZnO [P1, L2]	220	500	–	1.9	56.3	–	–	(Iwasa et al., 1995)
Pd/ZnO [P2, L2]	220	500	–	0.5	20.5	–	–	(Iwasa et al., 1995)
Pd/SiO_2 [P2, L2]	220	500		100	0.09	–	–	(Iwasa et al., 1995)
Pd/SiO_2 [P2, L2]	220	–	0.37	100	–	–	1.4	(Takezawa and Iwasa, 1997)
Pt/SiO_2 [P2, L2]	220	–	0.42	74.4	–	–	2.1	(Takezawa and Iwasa, 1997)
Pd [P1, L2]	220	500	–	100	10.9	9.9	2.1	(Iwasa et al., 1998)
Pd/SiO_2 [P1, L2]	220	500		100	15.7	42.4	9	(Iwasa et al., 1998)
Pd/MgO [P1,L2]	220	500	–	93.4	41	49	10.4	(Iwasa et al., 1998)
Pd/In_2O_3 [P1, L2]	220	500	–	4.5	28.3	9.9	2.1	(Iwasa et al., 1998)
Pd/Ga_2O_3 [P1, L2]	220	500	–	5.4	21.2	12.3	2.6	(Iwasa et al., 1998)
Pd/CeO_2 [P1, L2]	220	500	–	77.3	62.4	170.6	36.2	(Iwasa et al., 1998)
Pd/ZrO_2 [P1, L2]	220	500	–	81.6	64.3	31.1	6.6	(Iwasa et al., 1998)
Pd/ZnO [P1, L2]	220	500	–	0.8	54.2	10.4	2.2	(Iwasa et al., 1998)
Pd/A.C. [P1, L2]	220	500	–	100	2.3	–	–	(Iwasa and Takezawa, 2003)
Pd/HfO_2 [P1, L2]	220	500	–	100	13.6	–	–	(Iwasa and Takezawa, 2003)
Pd/Ta_2O_5 [P1, L2]	220	500	–	100	6.0	–	–	(Iwasa and Takezawa, 2003)
Pt [P1, L2]	220	500	–	43.3	3	1.65	0.6	(Iwasa et al., 1998)
Pt/ZnO [P1, L2]	220	500	–	4.4	27.9	–	–	(Iwasa et al., 1995)
Pt/SiO_2 [P2, L2]	220	500	–	74.4	0.3	–	–	(Iwasa et al., 1995)
Pt/Ga_2O_3 [P1, L2]	220	500	–	24.5	5.4	7.2	2.63	(Iwasa et al., 1998)
Pt/In_2O_3 [P1, L2]	220	500	–	1.7	30.6	7.7	2.81	(Iwasa et al., 1998)
Pt/ZnO [P1, L2]	220	500	–	4.6	27.6	7.1	2.58	(Iwasa et al., 1998)
Pt/SiO_2 [P1, L2]	220	500	–	81.2	10.3	92.3	33.5	(Iwasa et al., 1998)
Ni/SiO_2 [P2, L2]	220	–	2.0	98.9	–	–	10.6	(Takezawa and Iwasa, 1997)
Ni/ZnO [P1, L2]	220	500	–	97	19.1	2.7	0.4	(Iwasa et al., 1998)
Co/ZnO [P1, L2]	220	500	–	91.1	20.3	–	–	(Iwasa et al., 1995)
Co/ZnO [P1, L2]	220	500	–	86.7	13.1	6.2	0.92	(Iwasa et al., 1998)

Continued

Table 9.7 A summary of various supported group 8–10 catalysts used for MSR—cont'd

Catalyst	T (°C)	P.T. (°C)	Activity ($\mu molH_2$ $gcat^{-1}$ s^{-1})	S_{CO}	X_{MeOH} (%)	S_{metal} (m^2 g^{-1})	Dispersion (%)	Reference
Ru/ZnO [P1, L2]	220	500	–	96.2	9.5	–	–	(Iwasa and Takezawa, 2003)
Ir/ZnO [P1, L2]	220	500	–	79.6	2.6	–	–	(Iwasa and Takezawa, 2003)

*P*1: inlet partial pressure of water and methanol equal to 10.1 kPa. *P*2: inlet partial pressure of water and methanol equal to 24.3 kPa. *L*1: metal loading of 1 wt%. *L*2: metal loading of 10 wt.%.

group is the palladium supported in zinc oxide (Pd/ZnO), due to its anomalous high performance. Accordingly, the preparation method and the pretreatment conditions of the Pd/ZnO catalysts have been thoroughly studied in the literature. A different approach focused on the search for new types of supports, which presented higher surface areas than the commercially available ZnO support.

Finally, other authors have synthesized catalysts based on different alloy species and studied the effect of Zn addition on bimetallic catalysts. The effects of Pd or PdZn particle's size and their distribution on the support surface have been investigated.

In this case, Karim et al. (2006) varied the reduction pretreatment temperature in order to prepare Pd/ZnO catalysts with different particle sizes. At higher temperatures, a higher percentage of the PdZn alloy phase was formed, increasing the selectivity for MSR reaction. The formation of the PdZn alloy was not the only reason for the increase of the CO_2 selectivity. In some cases, catalysts with higher amounts of metallic palladium had better selectivity. The key difference in these cases was the structural presence of small palladium particles (<2 nm diameter). It is found that monometallic palladium particles promote the methanol decomposition reaction instead of the MSR reaction. As this trend is more pronounced with small palladium particles, the relative importance of monometallic Pd diminishes with their growth.

Bimetallic impregnation effects was also studied in the MSR process and required catalysts. The PdZn alloy formation is attributed to the high Pd/ZnO catalytic performance. In this case, Iwasa et al. (2003) studied the effect of zinc addition to a series of other palladium-supported catalysts. Fig. 9.2 illustrates the Zn addition effect to both MSR selectivity and activity. The Zn-modified Pd catalysts presented significantly improved selectivity, more pronounced when supported on CeO_2 or activated carbon. Activity was also higher for Zn-modified Pd/CeO_2 and Pd/AC. Besides Zn, other metals were added to the Pd/CeO_2 catalyst, such as Cd, In, Pb, Bi, Sn, Cu, and Ga. For hydrogen production, Zn and Ga had the highest rates. On the other hand, Cd originated the catalyst with higher selectivity values, even higher than the Zn-based catalyst. The catalysts containing In had equal selectivity when compared to the Zn-containing catalyst. These results were attributed to the alloy formation between Cd, In, Ga and Pd.

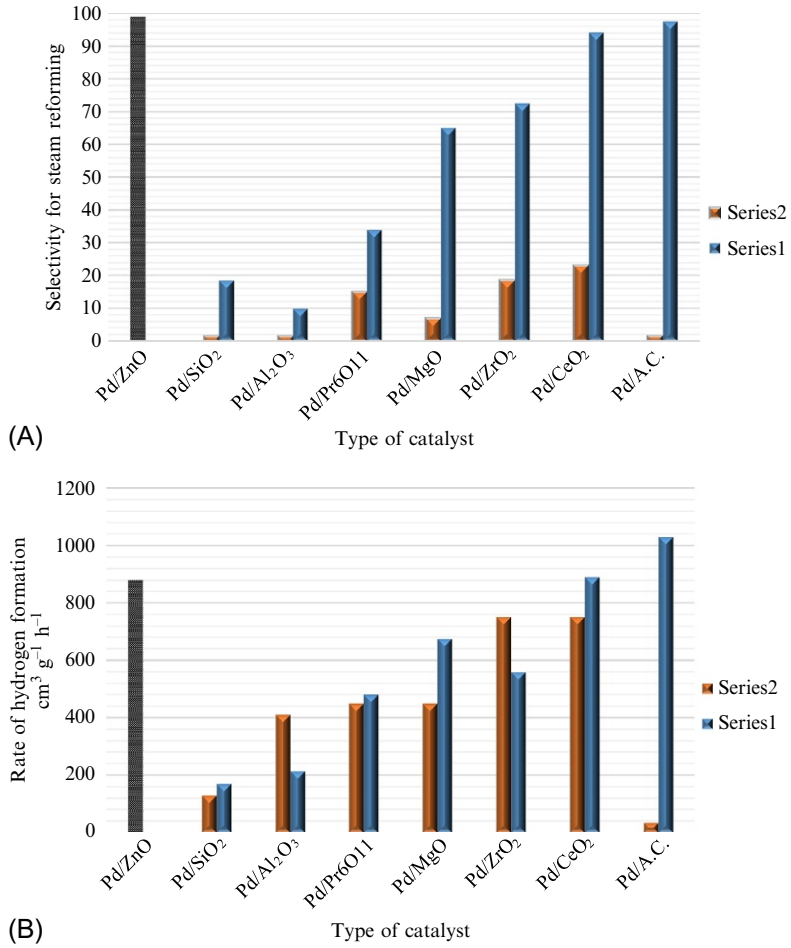

Fig. 9.2

Effect of the Zn addition to supported Pd catalysts upon the steam reforming reaction performance. *From Iwasa, N., et al., 2003. Effect of Zn addition to supported Pd catalysts in the steam reforming of methanol. Appl. Catal. A: Gen. 248 (1), 153–160.*

Ito et al. (2003), similarly to Iwasa and Takezawa (2003), tested platinum-supported catalysts in carbon black, using promoters such as Zn and Ga. Carbon black allows an increase in the catalyst surface area for bimetallic impregnation when compared to the ZnO support. The Zn promoter enhanced both CO_2 selectivity and methanol conversion, whereas the Ga promoter only presented good results regarding the selectivity. In another work, Suwa et al. (2004) studied the Zn-modified catalysts using a palladium precursor supported on carbon black. Pd/ZnO jointly with Zn-modified Pd/C showed higher activities. A better Zn promoter dispersion resulted in higher selectivity values towards CO_2.

Recently, a biometallic Pd-In catalyst was tested by Men et al. (2010) without any reduction pretreatment in a microstructured reactor. This catalyst was active and highly selective to CO_2 at temperatures above 350°C. Additionally, after impregnating with Pd, a critical Pd:In ratio of

5:10 was found. Below this value, the PdInAl catalyst is very selective to CO_2 and keeps low CO concentration (<1%). The methanol conversion at 350°C was 40%. Finally, a metal wall-coated bimetallic $PdZn/Al_2O_3$/FeCrAl catalyst was investigated for hydrogen production in a microreformer. A methanol conversion of 100% and 99% selectivity for H_2 with a low CO molar concentration (0.5%) was achieved under 350°C reaction temperature (Sá et al., 2010; Men et al., 2010).

Layered double hydroxides (LDH) correspond to a class of anionic clays having a hydrocalcite-like structure. Qi et al. (2005) investigated NiAl and Ni(M)Al (M = Au, Rh, Ir) LDH-derived catalyst for MSR and obtained as major products H_2, CO, CO_2, and CH_4. They concluded that the NiAl-LDH exhibited high selectivity to CO_2 and H_2, whereas partial substitution of Al by Au, Rh, or Ir considerably catalyzed the methanation reaction and consequently reduced the production of H_2. In further studies the NiAl LDH-derived catalysts were investigated, taking into account the following factors: hybrid-atom addition, calcination temperature, reaction temperature, pretreatment temperature and pressure, water/methanol ratios, and inorganic ions. The optimization of the described parameters led to an activity comparable to Cu-based catalysts at 390°C, with low fractions of methane and carbon monoxide (as reported in Table 9.8) (Qi et al., 2007a; Qi et al., 2006; Qi et al., 2007b).

A thermodynamic evaluation of the MSR process was done by Faungnawakij et al. (2006). The thermodynamic consideration for MSR via Gibbs free minimization to evaluate the effect of reforming temperature (25–1000°C), pressure (0.5–3 atm), and plausible product species has been studied. The principal set of compounds involved in the calculation were methanol, water, hydrogen, carbon dioxide, and carbon monoxide. Based on the thermodynamic calculation, the conclusions are summarized in the following:

- MeOH SR provided hydrogen-rich feeds for fuel cell application. A complete MeOH conversion and hydrogen concentration exceeding 70% on a dry basis was obtained at S/C = 1 when the temperature was in the range of 200–500°C at atmospheric pressure. The maximum concentration and yield of hydrogen could be achieved at almost 75% on a dry basis and 100%, respectively.
- On the basis of the reforming efficiency, the operating condition was optimized in the temperature range of 100–225°C, S/C of 1.5–3, and pressure at 1 atm. The calculation showed that the requirement from sufficiently low CO concentration (<10 ppm) is too severe for the existing catalysts (Tr = 50°C).
- At equilibrium, only methane and coke thermodynamically coexist with H_2O, H_2, CO, and CO_2, while C_2H_6, C_3H_8, i-C_4H_{10}, n-C_4H_{10}, CH_3OH, C_2H_5OH, C_3H_7OH, i-C_4H_9OH, n-C_4H_9OH, and DME were suppressed at essentially zero. The temperature for the coke-free region decreased by increasing the S/C ratio.
- At a given the temperatures higher than ca. 150°C, varying pressures from 0.5–3 atm did not affect the MeOH conversion and hydrogen yield since MeOH conversion attained the maximum at 100%.

Table 9.8 Summary of NiAl-LDH derived catalysts performance for MSR

Catalysts	T (°C)	X_{MeOH} (%)	Activity ($\mu molH_2 g_{cat}^{-1} s^{-1}$)	$Y_{CO\ dry}$	$Y_{CH4\ dry}$	S_{CO} (%)	S_{CH4} (%)	$T_{pre\text{-}activation}$ (°C)	Reference
NiAl	340	16.1	42.7	–	–	6.4	0	–	(Qi et al.,
	380	35.0	95.0	–	–	4.6	0	–	2005)
NiAl-Au	280	27.1	54.3	–	–	28.9	0	–	
	340	829	128.7	–	–	29.0	5.5	–	
	380	99.4	56.9	–	–	1.6	36.2	–	
NiAl-Rh	280	36.7	65.8	–	–	35.4	0.6	–	
	340	80.2	50.0	–	–	8.7	33.6	–	
	380	82.6	40.2	–	–	0.3	41.4	–	
NiAl-Ir	280	44.6	77.6	–	–	35.5	1.6	–	
	340	85.3	73.0	–	–	20.9	22.9	–	
	380	92.9	61.3	–	–	0.3	33.9	–	
NiAl-LDH	340	18.1	–	0.022	0.000	–	–	200	(Qi et al.,
	360	57.9	–	0.321	0.013	–	–		2006)
	380	65.5	–	0.298	0.013	–	–		
	340	16.0	–	0.025	0.000	–	–	300	
	360	55.6	–	0.292	0.012	–	–		
	380	47.8	–	0.266	0.015	–	–		
	340	18.5	–	0.023	0.000	–	–	340	
	360	50.1	–	0.240	0.018	–	–		
	380	446.4	–	0.211	0.020	–	–		
	360	97	–	0.073	0.217	–	–	360	
	380	100	–	0.045	0.237	–	–	–	
NiAl-LDH	390	87.6	179.2	0.06	0.05	–	–	–	(Qi et al.,
	390	84.4	75.6	0.16	0.00	–	–	–	2007a)
NiAl-LDH	390	87.6	179.7	0.062	0.054	–	–	–	(Qi et al.,
NiAl-LDH + KOH	390	77.5	183.2	0.096	0.005	–	–	–	2007b)
NiAl-LDH + K_2CO_3	390	91.0	201.1	0.127	0.005	–	–	–	
NiAl-LDH + KCl	390	83.5	193.7	0.138	0.004	–	–	–	

The reforming zone contains a variety of reactions. It is clear that experimental data for different operation conditions is not achievable. Therefore, simulation study is required. The first requirement for simulation of the reactive process is reaction kinetics. Many researchers proposed kinetic of steam reforming reactions that are accessible in references (Amphlett et al., 1985; Peppley et al., 1999a; Agrell et al., 2002; Jiang et al., 1993a; Lee et al., 2004; Peppley et al., 1999b). Jiang et al. (1993a, 1993b) proposed a kinetic for steam reforming of methanol. This model is based on a simple empirical rate law expression for the $Cu/ZnO/Al_2O_3$ catalyst from BASF (S3-85), sold commercially for methanol synthesis. The catalyst used in their study consisted of 31.7% CuO, 49.5% ZnO, and 18.8% Al_2O_3 and possessed a BET surface area of 83 $m^2\ g^{-1}$. The rate equation proposed by these authors is divided into two parts, depending on the H_2 partial pressure:

$$r_{MSR} = kP_{CH_3OH}^{0.26} P_{H_2O}^{0.03} \left(P_{H_2} < 7kPa\right) \tag{9.8}$$

$$r_{MSR} = kP_{CH_3OH}^{0.26} P_{H_2O}^{0.03} P_{H_2}^{-0.2} \left(P_{H_2} > 7kPa\right) \tag{9.9}$$

$$k(T) = 1.9{*}10^{12} \exp\left(\frac{-100.9 kJ mol^{-1}}{RT}\right) \tag{9.10}$$

Obviously, the reaction kinetic in catalytic reactions is dependent on the type of catalyst. In the other study, Cao et al. (2006) studied Pd/ZnO catalyst application in steam reforming of methanol. The proposed kinetic is:

$$-r_A = 2.9047{*}10^{10} \exp\left(\frac{-94800}{RT}\right) P_{CH_3OH}^{0.715} P_{H_2O}^{0.088} \tag{9.11}$$

In this kinetic r_A is based on "mmol/kg_{cat}/s" and temperature range is 160–310°C. This result provides kinetic data for the design of a miniature fuel processor for small fuel cell applications. The rate equation has been applied to a three-dimensional pseudo-homogeneous model to simulate temperature profiles in both microchannel and conventional fixed-bed reactors. Some of the proposed kinetics are listed in Table 9.9.

Table 9.9 The most proposed kinetics reaction rates of MSR process

Rate expression	Catalyst	Activation Energy (kJ/mol)	Reference
$-r_M = k\sqrt{P_M P_W} P_H^{-1.3}$	$Cu/ZnO/Cr_2O_3/Al_2O_3$	116.1	(Barton and Pour, 1980)
$-r_M = \frac{kK_M P_M}{1 + K_M P_M + K_W P_W}$	$Cu/ZnO/Al_2O_3$ (BASF)	102.6	(Santacesaria and Carra, 1983)
$-r_M = \frac{kK_M P_M - k'^{P_{CO}} P_M^2}{1 + KP_{CO}}$	Cu/ZnO (Girdler G66B)	96	(Amphlett et al., 1985)
$-r_M = \left(\frac{kK_1 P_M}{\sqrt{K_3 P_H}}\right) / \left(1 + \frac{K_1 P_M}{\sqrt{K_3 P_H}} + \frac{1}{\sqrt{K_3 P_H}}\right)^2$	$Cu/ZnO/Al_2O_3$ (BASF S3-85)	110	(Jiang et al., 1993b)
$-r_M = kP_M^{0.04}$	$Cu/MnO/Al_2O_3$	79.7	(Idem and Bakhshi, 1996)
$-r_M = \frac{k\left(P_M - \frac{P_C P_H^3}{K_E P_W}\right)}{1 + KP_M}$	$Cu/MnO/Al_2O_3$	77.3	(Idem and Bakhshi, 1996)
$-r_M = kP_M^{0.28} P_C^{-0.99}$	$Cu/MnO/Al_2O_3$	77.7	(Idem and Bakhshi, 1996)
$-r_M = \left(k\left(\frac{P_M P_W}{P_H} - \frac{P_C P_H^2}{K_E}\right)\right) / (1 + KP_M)^4$	$Cu/MnO/Al_2O_3$	116.6	(Idem and Bakhshi, 1996)
$-r_M = \frac{kK_1 \left(\frac{P_M}{\sqrt{P_H}}\right)\left(1 - \left(\frac{P_H^3 P_C}{K_E P_M P_W}\right)\right)}{DEN}$	$Cu/ZnO/Al_2O_3$ (BASF K3-110)	102.8	(Idem and Bakhshi, 1996)
$-r_M = kP_M^{0.4}\left(1 - \left(\frac{P_C P_H^3}{K_E P_M P_W}\right)\right)$	$Cu/ZnO/Al_2O_3$	83	(Peppley et al., 1999b)
$-r_M = kP_M^{0.63} P_W^{0.39} P_H^{-0.23} P_C^{-0.07}$	$Cu/ZnO/Al_2O_3$ (BASF K3-110)	74	(Geissler et al., 2001)
$-r_M = \frac{kK_1 \left(\frac{P_M}{\sqrt{P_H}}\right)\left(1 - \left(\frac{P_H^3 P_C}{K_E P_M P_W}\right)\right)}{DEN}$	$Cu/ZnO/Al_2O_3$ (BASF K3-110)	122.4	(Samms and Savinell, 2002)

C, carbon dioxide; *H*, hydrogen; *M*, methanol; *W*, water.

$$DEN = \left[1 + K_1\left(\frac{P_M}{\sqrt{P_H}}\right) + K_2 P_C\sqrt{P_H} + K_3\left(\frac{P_W}{\sqrt{P_H}}\right)\right]\left(1 + \sqrt{K_4 P_H}\right)$$

2.1.2.2 Partial oxidation (POX) of methanol

There are two type of partial oxidation in catalyst usage point of view. Noncatalytic partial oxidation (POX) and catalytic partial oxidation (CPOX). The CPOX has many advantages compared with conventional POX. The operating temperature of POX reactions is usually the temperature of fire flame and is a high operational temperature. Therefore, in high temperature, many operational problems such as a hot spot will occur. On the other hand, there is not a suitable mechanism for controlling selectivity and conversion of feed. Without a catalyst, the reactor will produce random product and the repeatability of the process will decrease. However, nowadays, most such studies take place in the field of CPOX (Hohn and Lin, 2009; York et al., 2003; Enger et al., 2008).

The application of CPOX of methanol to yield hydrogen was first reported in 1976 by Houseman and Cerini (1976a, 1976b), who used catalysts containing mixtures of nickel, palladium, platinum, and silver oxide. The CPOX of methanol has been the major path to make formaldehyde since the 1890s. With a methanol-rich mixture, the reactant stream is passed through a fixed catalyst bed reactor under atmospheric pressure. The resulting formaldehyde is quickly quenched in water prior to further decomposition to CO and H_2. For the purpose of hydrogen production, the overall reaction can be described by Eq. 9.12 (Hohn and Lin, 2009):

$$CH_3OH + 0.5O_2 \rightarrow CO_2 + 2H_2 \qquad (9.12)$$

$$\Delta H^\circ = -155 \text{ kJ/mol}$$

The reaction is exothermic with a rapid reaction rate. Under certain conditions, part of the feed can be fully oxidized (Eq. 9.13), which generates further heat to provide autothermal operation. This process renders a self-sustained system that does not require any external heat source.

$$CH_3OH + \frac{3}{2}O_2 \rightarrow CO_2 + 2H_2O, \quad \Delta H^\circ_{298K} = -675.5 \text{ kJ/mol} \qquad (9.13)$$

The POM reaction mechanism is rather complex. Several authors (Lyubovsky and Roychoudhury, 2004; Otsuka et al., 2003) proposed that there existed some intermediate reactions in POX of methanol (Eq. 9.12), MSR (Eq. 9.7), MD (Eq. 9.6), revers of WGS (Eq. 9.14), and methanol combustion (Eq. 9.13), methanation (Eqs. 9.15, 9.16), and oxidative dehydrogenation of methanol (Eq. 9.17).

$$CO_2 + H_2 \leftrightarrow CO + H_2O, \quad \Delta H_{298} = -41.16 \text{ kJ/mol} \qquad (9.14)$$

$$CO + 3H_2 \leftrightarrow CH_4 + H_2O, \quad \Delta H_{298} = -206.2 \text{ kJ/mol} \qquad (9.15)$$

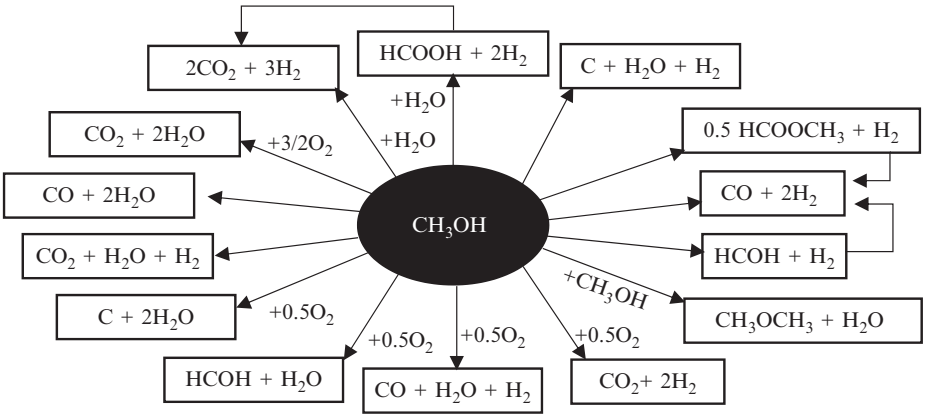

Fig. 9.3
Reaction network mechanism of methanol POX.

$$CO_2 + 4H_2 \leftrightarrow CH_4 + 2H_2O, \quad \Delta H_{298} = -164.9 \text{ kJ/mol} \tag{9.16}$$

$$CH_3OH + 0.5\ O_2 \rightarrow HCHO + H_2O, \quad \Delta H_{298} = -157 \text{ kJ/mol} \tag{9.17}$$

Accordingly, CPOX is a complex system. Zum Mallen and Schmidt (1996) proposed that catalytic POX possesses both equilibrium conversion and nonequilibrium regimes. That is, different paths for methanol conversion, such as oxidation, steam reforming, and decomposition may take place simultaneously. Fig. 9.3 illustrates a plausible reaction network when conducting CPOX of methanol (Hohn and Lin, 2009).

However, the POX process is a possible choice for hydrogen production. There are many disadvantages for POM processes compared with MSR processes. Therefore, the majority of commercial plants are based on MSR reaction.

3 New Technologies for Hydrogen Production From Methanol

New technologies and new ideas can improve the overall efficiency of the process. Many researchers around the world are working on the reforming process to improve it. One of the most important points for improving the hydrogen production process is an energy source to supply the required energy. The best choice is renewable energies. Recently, many studies focused on using solar energy as a renewable source in the hydrogen production process. In this case, five thermochemical routes for solar hydrogen production are depicted in Fig. 9.4. As indicated in this figure, the chemical source of H_2 is water for the solar thermolysis and the solar thermochemical cycles, fossil fuels for the solar cracking, and a combination of fossil fuels and H_2O for solar reforming and solar gasification. All of these routes involve

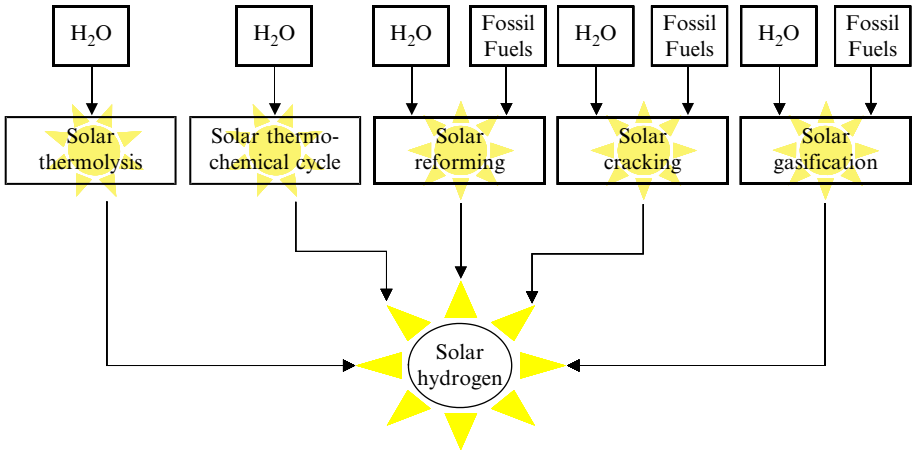

Fig. 9.4
Five thermochemical routes for the production of solar hydrogen.

endothermic reactions that make use of concentrated solar radiation as the energy source for high-temperature process heat (Steinfeld, 2005).

The economics of solar hydrogen production have been assessed for H_2 produced via solar thermochemical hydrogen production. These assessments indicate that the solar thermochemical production of hydrogen can be competitive with the electrolysis of water using solar-generated electricity, and, under certain conditions, might become competitive with conventional fossil-fuel based processes at current fuel prices, even before the application of credit for CO_2 mitigation and pollution avoidance. The weaknesses of these economic evaluations are related primarily to the uncertainties in the viable efficiencies and investment costs of the various components due to their early stage of development and their economy of scale. Further development and large-scale demonstration are warranted (Steinfeld, 2005).

H_2 from H_2O by solar thermolysis: The single-step thermal dissociation of water is known as water thermolysis,

$$H_2O \rightarrow H_2 + 0.5\,O_2 \tag{9.18}$$

Although conceptually simple, the noted reaction has been impeded by the need for a high-temperature heat source above 2500 K for achieving a reasonable degree of dissociation, and by the need for an effective technique for separating H_2 and O_2 to avoid ending up with an explosive mixture (Steinfeld, 2005; Baykara, 2004).

H_2 from H_2O by solar thermochemical cycles: Water-splitting thermochemical cycles bypass the H_2/O_2 separation problem and further allow operating at relatively moderate upper temperatures. Previous studies (Steinfeld, 2005; Steinfeld, 2002; Abanades and Flamant, 2006) performed on H_2O-splitting thermochemical cycles were mostly characterized by the use of

process heat at temperatures below about 1200 K, available from nuclear and other thermal sources. These cycles required multiple steps and suffered from inherent inefficiencies associated with heat transfer and product separation at each step.

In recent years, significant progress has been accomplished in the development of optical systems for large-scale solar concentration capable of achieving mean solar-concentration ratios exceeding 5000 suns. Such high radiation fluxes correspond to $T_{stagnation} > 3000$ K and allow the conversion of solar energy to thermal reservoirs at 2000 K and above, which are needed for the more efficient two-step thermochemical cycles using metal oxide redox reactions (M denotes metal):

$$\text{First step (solar)}: M_xO_y \rightarrow xM + 0.5yO_2. \tag{9.19}$$

$$\text{Second step (nonsolar)}: xM + yH_2O \rightarrow M_xO_y + yH_2 \tag{9.20}$$

On the other hand, the carbothermal reduction of metal oxides using coke, natural gas (NG), and other carbonaceous materials as reducing agents brings about the reduction of oxides at much more moderate temperatures. The corresponding overall chemical reactions may be represented as:

$$M_xO_y + yC \rightarrow xM + yCO \tag{9.21}$$

$$M_xO_y + yCH_4 \rightarrow xM + y(2H_2 + CO) \tag{9.22}$$

The H_2 by decarbonization of fossil fuels: Three solar thermochemical processes for H_2 production using fossil fuels as the chemical source are considered: cracking, reforming, and gasification. These routes are schematically illustrated in Fig. 9.5.

The solar cracking route refers to the thermal decomposition of hydrocarbons and alcohols that can be represented by the simplified net reaction (Steinfeld, 2005; Steinfeld, 2002; Abanades and Flamant, 2006):

$$CxHy \leftrightarrow xC + 0.5yH_2 \tag{9.23}$$

Usually, gasification is used for solid fossil fuels (or heavy liquid fuels). This process should be done in a gasifier. The product of this process is syngas. It's clear that converting the fuels to H_2 and CO requires an external energy source. This energy or a part of the required energy can be supplied by solar radiations.

Another potential for hydrogen production by use of solar energy (plus fossil fuels) is reforming. As noted previously, this process is endothermic; that amount of required energy is dependent on the hydrocarbon and alcohol type. However, when solar energy as an external energy source is utilized in the reforming process, the process will be a solar reforming for hydrogen production. Of course, there are some different details that are not in the scope of this chapter.

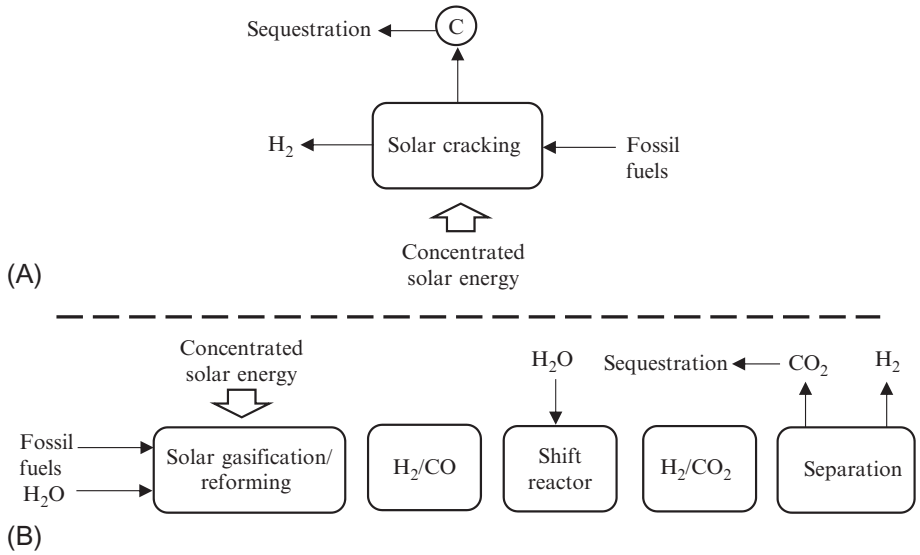

Fig. 9.5
Schematic of solar thermochemical routes for H_2 production using fossil fuels and H_2O as the chemical source: (A) solar cracking, and (B), solar reforming and gasification.

As mentioned before, fuel cells have become a focus in recent years. Hydrogen production microchannels and MRs via MSR have some advantages that make them a valuable method for usage as fuel cells. Relatively low required temperature in atmospheric pressure and in situ hydrogen production are some of the desirable qualifications of MSR MRs or microchannels. In this case, Park et al. (2004) worked on a development reformer of MSR. Three types of patterned sheets were prepared to construct a base structure. The aspect ratio of microchannels can be regulated by changing the number of microchannel sheets. The catalyst was deposited inside the microchannel of a reformer unit. Electric heaters provided heat for the endothermic reaction and the vaporization of liquid fuel. A vaporizer and a reformer unit were connected serially to make a prototype microreactor. The MSR reaction was conducted with the microreactor. The performance of the microreactor was investigated at various operating conditions. The developed fuel processor generated enough hydrogen for a power output of 15 We. The base case performance and operating conditions are presented in Table 9.10.

3.1 Membrane and Membrane Reactor

The application of a membrane in hydrogen production processes can be categorized into two groups: (A) membrane as a separator for separation of produced hydrogen; (B) application of MRs for hydrogen production. The application of a membrane as a separator is studied

Table 9.10 Base case performance and operating conditions of developed microreactor

Vaporizer temperature	120°C
Steam to carbon ratio, S/C	1.1
Feed flow rate	12 (cm^3/h)
Reformer temperature	260°C
Pressure	1 atm
Methanol conversion	>90%
Gas composition, dry basis	73.4% H_2
	25% CO_2
	1.6% CO
H_2 production rate	0.498 (mol/h)
	186 sccm
	33 Wt
Estimated electric power assumptions: fuel cell efficiency = 60%, H_2 utilization = 80%	15We

Table 9.11 Some of the most significant benefits and drawbacks of MRs utilization

MRs Benefits	MRs Drawbacks
Compact unit in combining both reaction and hydrogen purification with a consequent capital cost reduction	High costs and low mechanical resistance in case of dense palladium MRs
Conversion enhancement of equilibrium limited reactions. Higher conversions than CRs (exercised at the same MRs conditions) or at the same conversion of CRs reached at milder operating conditions	Not high-purity hydrogen production in the case of composite Pd-based MRs. Not high hydrogen perm-selectivity in the case of non Pd-based MRs utilization
Direct production of high-purity hydrogen in a single unit (in the case of dense Pd-based MR)	Hydrogen embrittlement at $T < 300$°C in the case of dense Pd-MRs
Retentate stream of MRs rich in CO_2 (i.e. the stream not permeated through the membrane when performing reforming reactions)	Contamination of H_2S, coke CO, etc. in the case of Pd-MRs

and use+d widely. It is also reported in many experimental and simulation studies. On the other hand, MRs are relatively new technology with many advantages compared with conventional reactors. Some of the most significant benefits and drawbacks of MRs utilization are presented in Table 9.11 (Iulianelli et al., 2014).

Several types of reactors can be used in MSR processes. The reactor design has a direct effect on reaction conversion, but many other qualifications in addition to conversion (such as technical complexity, cost of manufacturing, etc.) should be considered. Experimental works indicate that microreactors have suitable conditions for application in MSR process.

A microreactor is defined as a device that contains microstructured features, with a submillimeter use, in which chemical reactions are performed in a continuous manner.

This type of reactor is ideal for using in fuel cells. However, it is noted that the microreactor range in an area from 0.1 to 10 cm^2 (between 10 and 200 cm^2 named minireactor) (Iulianelli et al., 2014). Packed bed reactors are commonly used in MSR processes. It is clear that, for utilizing the catalyst in microreactors, the size of the catalyst should be smaller than the microreactor area. However, the design of a reactor targets the maximization of the conversion and selectivity at the lowest costs and its performance is influenced by the flow pattern, velocity profile, pressure drop, and heat transfer. Therefore all these aspects must be considered. For conducting an MSR reaction, most of the used reactor designs are rectilinear channels, pinhole, coil-based, and radial (see Fig. 9.6) (Iulianelli et al., 2014).

Recently, many scientists have proposed the application of membranes combined to chemical and biochemical reactions in order to intensify the whole process. Most of the approaches may be classified concerning the role of membranes towards the removal/addition of the various chemical species as: (a) extractor, (b) distributor, and (c) contactor. Membranes are generally categorized by referring to materials or structures, giving particular relevance to the selectivity of the permeation of such a product with respect to other ones. However, in this study, our attention is devoted to the discussion on dense and porous inorganic MRs, able to integrate MSR reaction with a membrane process (H_2 separation). Commonly, the role of the membrane in an MR can be described as:

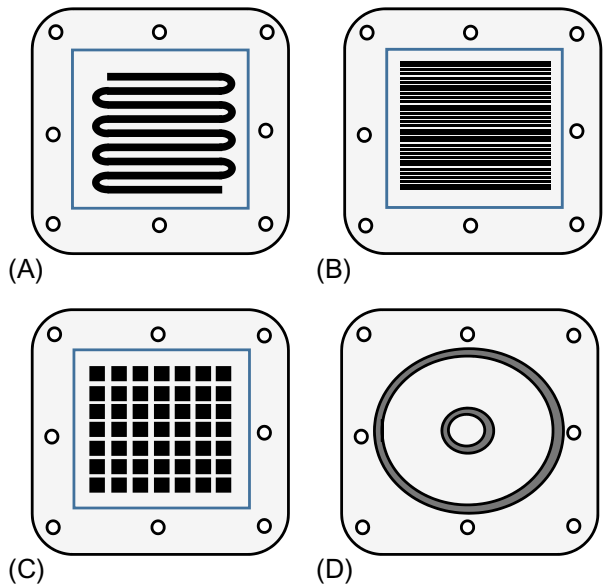

Fig. 9.6
Different flow field designs of CRs. (A) Coiled-serpentine; (B) Parallel multichannel; (C) Pinhole; and (D) Radial.

- Extractor, when it selectively removes the desired products from the reaction mixture for permeation.
- Distributor, when it controls the addition of reactants to the reaction mixture.
- Contactor, when it intensifies the contact within reactants and catalyst.

Iulianelli et al. (2008a), investigated the MSR in a dense Pd-Ag MR: the pressure and GHSV effects on CO-free H_2 production. They experimented a dense tubular Pd-Ag MR used for carrying out the MSR reaction for producing a CO-free hydrogen stream. A noncommercial Cu/Zn/Mg-based catalyst used in the lumen side of the MR and the experimental tests were performed at a reaction temperature of 300°C and H_2O/CH_3OH feed molar ratio of 3/1 and compared with the efficiency of concurrent and countercurrent configurations. Moreover, at the best operative conditions corresponding to a reaction pressure of 3.0 bar, GHSV = 0.36 h^{-1} and countercurrent flow configuration, the MR was able to achieve almost 93.0% of CO-free hydrogen recovery, a hydrogen selectivity of around 75% and 77% of hydrogen yield. In another work, Iulianelli et al. (2008b) compared the efficiency of MRs and traditional reactors (TRs). As a result, they noted that MR has better performance than TRs. The MR is able to achieve 94% of CO-free hydrogen recovery, almost 75% of hydrogen selectivity, 65% of hydrogen yield, and almost 60% of CO-free hydrogen yield. At any rate, the MR indicates better performance than the TR, asserting itself as the best solution to carry out the MSR reaction in an MR for a CO-free hydrogen production. In the other work, they studied the efficiency of a new catalyst in MR. In this work, Basile et al. (2008) compared the MR and fixed-bed reactor. The MR showed better performances in terms of methanol conversions and hydrogen productions than the FBR one working at the same operative conditions. The $CuO/Al_2O_3/ZnO/MgO$ catalyst exhibited high reaction activity in the temperature range 250–300°C. Complete methanol conversion was achieved in the MR at 300°C and H_2O/CH_3OH ratio higher than 5/1, while in both the FBR and MR the carbon monoxide selectivity was lower than 1%. In order to optimize the hydrogen recovery in the MR, the effect of operative parameters such as the sweep gas flow rate and the reaction pressure will be evaluated with a deeper scouting in a future work.

Moreover, several studies showed that supports can play an efficient role in thin membrane performance. Liguori et al. (2014) reported the MSR in an Al_2O_3 supported thin Pd-layer MR over $Cu/ZnO/Al_2O_3$ catalyst. In this experimental study, an MR housing a composite membrane constituted by a thin Pd-layer supported onto Al_2O_3 is utilized to perform an MSR reaction to produce high-grade hydrogen for PEM fuel cell applications. The influence of various parameters such as temperature, from 280°C to 330°C, and pressure, from 1.5 to 2.5 bar, is analyzed. A commercial Cu/Zn-based catalyst is packed in the annulus of the MR and the experimental tests are performed at space velocity of 18,500 h^{-1} and H_2O:CH_3OH molar ratio of 2.5:1 (in feed). As a best result of this work, 85% of methanol conversion and a highly pure hydrogen stream permeated through the membrane while a CO content lower than 10 ppm was reached at 330°C and 2.5 bar.

In Table 9.12, the most representative results in terms of conversion, hydrogen recovery, and so on are reported about MSR resaction performed in MRs. In detail, this table summarizes the different typology of membranes used in MRs for conducting MSR reaction besides the type of catalyst used and other important parameters such as: H_2/N_2 ideal selectivity, H_2O/MeOH feed ratio, reaction pressure, reaction temperature, etc (Iulianelli et al., 2014).

Silica membranes are one of the most valuable membranes for the hydrogen separation process. Simulations studies showed that silica membrane can be used in MSR. Ghasemzadeh et al. (2013b) investigated a simulation study of the silica MR performance for the MSR process. In addition to the simulation study, they did HAZOP analysis. It could be concluded that the methanol conversion realized in silica MR was increased by reaction temperature and feed molar ratio, while feed flow rate and reaction pressure effects were different.

In particular, it was found that methanol conversion is decreased by increasing the reaction pressure from 1.5 to 4.0 bar, whereas over 4.0 bar, it is improved. Moreover, methanol conversion was continuously decreased by increasing the feed flow rate. It appears clear that, working at low feed molar ratio, this is more suitable for the silica MR from a hydrogen recovery point of view. Regarding the modeling results and safety aspects, reaction temperature, pressure, feed molar ratio, and feed flow rate were considered as key parameters for HAZOP analysis. In particular, a PID temperature controller was strongly recommended for use in a silica MR heating system. As a general conclusion, the safety assessment combined with a modeling study in the processes involving high-risk possibilities (e.g. hydrogen production in the MRs systems) seems to be necessary. In the other work (Ghasemzadeh et al., 2013c), H_2/N_2 selectivity in silica MR was reported higher than 100. A modeling study indicated that hydrogen permeability can be about $1*10^{-7}$ - $5 * 10^{-7}$ mol/m^2 Pa s. Moreover, silica MR performance in MSR processes was studied by Ghasemzadeh et al. (2015b). The conversion of methanol was reported in several operation conditions. In particular, at 553 K, SF = 6 and 1.5 bar, 94.68% methanol conversion and 32.6% hydrogen recovery were achieved with respect to SF = 0, where 90.39% methanol conversion and 4.03% hydrogen recovery were obtained. Therefore, the hydrogen recovery is more sensible to SF values over methanol conversion.

Moreover, in the same year, silica MR performance in MSR was studied by Ghasemzadeh et al. (2015b). They fabricated the microporous silica membrane using polymeric sol–gel method. To achieve a high quality of silica membrane, a new strategy used for surface modification of ceramic support, in which a particle-sized control of boehmite sol applied. After evaluation of modified alumina supports, the synthesized silica membrane was characterized and its performance was investigated. The performance analysis of the silica membrane in hydrogen purification shows that the H_2/N_2, H_2/CO_2 and H_2/Ar permselectivity increase sufficiently to 26.18, 22.13, and 29.42, at 200°C, respectively, so that the hydrogen permeance measured around 1.1×10^{-6} mol m^{-2} s Pa at the corresponding conditions. These promising results indicate a high quality of silica membrane for hydrogen production.

Table 9.12 Some of the most representative experimental results about MSR reaction in MRs from the open literature

Membrane Types	Membrane Preparation	H_2/N_2 Selectivity	Catalyst	H_2O/CH_3OH	GHSV (h^{-1})	T (°C)	p (bar)	Conv. (%)	H_2 Recovery (%)	H_2 Permeate Purity (%)	Reference
Pd (20–25 μm layer)/PSS	ELP	Infinite	Cu-based	1.2/1	–	350	–	99	–	~100	(Lin et al., 1998)
Pd (20 μm layer)/PSS	ELP	4000	Cu/ZnO/Al_2O_3	1.2/1	10[b]	350	6	~95	97	99.9	(Lin and Rei, 2001)
Dense Pd–Cu (25 μm thickness)	–	Infinite	Cu–Zn based	–	–	300	10	90	~38	~100	(Wieland et al., 2001)
Dense Pd–Ru–In (200 μm thickness)	–	Infinite	Cu/ZnO/Al_2O_3	1.2/1	–	200	7	~99	~24	~100	(Itoh et al., 2002)
SiO_2/g-Al_2O_3/Pt-SiO_2/PSS	Soaking-rolling	–	Cu–Zn/ based	1.3/1	–	230	–	100	9.1	–	(Lee et al., 2006)
Pd–Ag/TiO_2-Al_2O_3	ELP	–	Ru–Al_2O_3	4.5/1	–	550	1.3	65	–	~72	(Basile et al., 2006)
Carbon-self supported	–	–	Cu/ZnO/Al_2O_3	1.5/1	1[b]	250	2	~99	–	97	(Zhang et al., 2006)
SiO_2/g–Al_2O_3	Soaking-rolling	~37	Cu-Zn/ based	3/1	–	260	–	42	5	98	(Lee et al., 2008)
Dense Pd–Ag (50 μm thickness)	Cold-rolling	Infinite	CuO/Al_2O_3/ZnOMgO	3/1	~0.4[b]	300	3	–	80	~100	(Iulianelli et al., 2008a)
Pd–Ag (3.9 μm thickness)/ a-Al_2O_3	ELP	Infinite	CuO/ZnO/Al_2O_3	1/1	600[a]	250	3 10	100	45 95	~100	(Israni and Harold, 2011)
Pd–Ag (20–25 μm thickness)/PSS	ELP	–	CuO/ZnO/Al_2O_3	1.2/1	5[b]	240	10	36.1	18	–	(Rei et al., 2011)
Carbon molecular sieve	Pyrolysis	62[c]	CuO/ZnO/Al_2O_3	4/1	–	200	1	~95	~84	–	(Sá et al., 2011)

Carbon-self supported	Pyrolysis	~5.5	$CuO/Al_2O_3/ZnOMgO$	3/1	–	250	2	55	–	~80	(Briceño et al., 2012)
Dense Pd-Ag	Cold-rolling	Infinite	$Cu/ZnO/Al_2O_3$	3/1	1800	280	2.5	100	46	~100	(Ghasemzadeh et al., 2013a)
Pd (3.9 μm thickness) / Al_2O_3	–	~6000	$Cu/ZnO/Al_2O_3$	2.5/1	18,500	330	2.5	85	40	~100	(Liguori et al., 2014)
SiO_2/ g–Al_2O_3/ α-Al_2O_3	Sol-gel	26.18	$Cu/ZnO/Al_2O_3$	3	6000	200	1.5	~85	37.9	–	(Ghasemzadeh et al., 2015b)

[a][sccm/h/g-cat).
[b]WHSV.
[c]H_2/Ar selectivity.

Advantages were numerous for autothermal reforming. On the other hand, MRs can improve the process to achieve different benefits. Ghasemzadeh et al. (2016) reported on the performance of dense Pd-Ag MR during MSR in comparison with ATR using computational fluid dynamics (CFD) analysis. The effects of some important operating parameters (temperature, pressure, sweep gas ratio) on the performance of Pd-Ag MR were studied in terms of methanol conversion and hydrogen recovery. The CFD results showed that the Pd-Ag MR during the methanol autothermal reforming (MATR) reaction presents higher performance in term of the methanol conversion and hydrogen recovery with respect to ones obtained in the MSR reaction. In particular, in the best operating condition, the hydrogen production rate in the reaction zone shows an enhancement around 11% in the MATR reaction over ones achieved in the MSR reaction.

The fuel cells are very efficient for converting chemical into electric energy and hydrogen is the ideal fuel for this application. However, hydrogen has a low energy density, making it difficult to store and transport. Furthermore, an entirely new distribution infrastructure and storage is needed. Previous reasons directed the scientific community to search for new energy vectors and methanol was demonstrated to be a good alternative. In fact, it has higher energy density than hydrogen, it is easier to handle and store and, especially, it shows relatively low reforming temperature (240–260°C) due to the absence of C–C bonds. As a result, many authors have been studying MSR for in situ hydrogen production to feed fuel cells. Commercial power supplies are already available combining in situ hydrogen generation by MSR to supply high temperature fuel cells, namely by Ultracell, AixCellSys, and Serenergy. The fuel cell and the reformer can be defined as external reforming (the MSR operated as a stand-alone system) or internal reforming (the MSR is part of the fuel cell stack) (Iulianelli et al., 2014). MSR for in situ hydrogen production for fuel cell applications has been studied mostly as a stand-alone process. An external reformer system consists of a combustor where a small fraction of fuel is burned and provides heat for the following steps: a vaporizer to heat and vaporize the fuel, a reformer to carry out the reforming reaction, and a carbon monoxide converter to carbon dioxide such as a preferential oxidation (PROX) reactor (Fig. 9.7). The hydrogen purification can be achieved by pressure swing adsorption (PSA) or metal membrane processes (Iulianelli et al., 2014).

AixCellSys and Serenergy used similar strategies to produce power supplies that combine external reforming and high temperature polymer electrolyte membrane fuel (HT-PEMFC). These systems integrate a combustor, which burns the nonreacted hydrogen from the fuel cell outstream; a vaporizer to heat and vaporize the fuel (water/methanol molar ratio of 1.5:1); and a reformer loaded with $CuO/ZnO/Al_2O_3$ and HT-PEMFC (see Fig. 9.8).

These power supplies do not require CO removal due to the high CO tolerance of HT-PEMFC, up to ca. 1% for fuel cells operating at 170°C or above. The startup period is slightly longer for HT-PEMFC systems (5–15 min) due to the acid nature of polymeric membranes

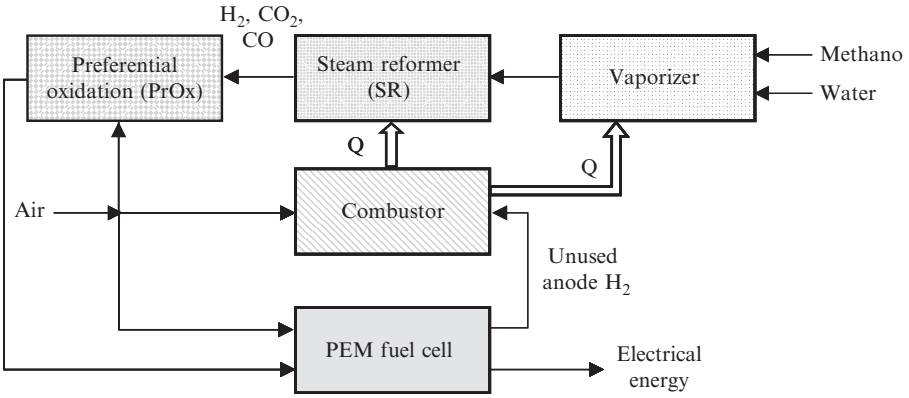

Fig. 9.7
Standard setup for external reforming.

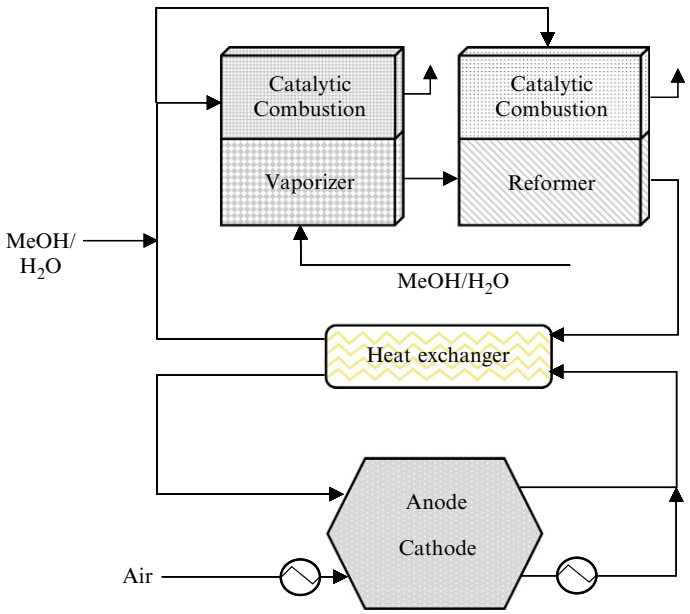

Fig. 9.8
Integrated MSR-FC.

(Polybenzimidazole—PBI) that requires materials suitable for operating under corrosive conditions, increasing the size of the fuel cell stack. During the startup period, a lithium battery provides the energy for two heaters until the operation temperature is reached. Both systems are compact and represent an important step toward the commercialization of power supplies based on MSR/FC systems. However, the maximum electric power output is 0.2 W cm^2 for both systems, which is half the performance for a fuel cell fed with pure hydrogen (Iulianelli et al., 2014). Last but not least, Basile et al. (2015) noted that integration of MRs and the hydrogen

production process leads to using fuel cells instead of conventional electricity production. Power plants are the main greenhouse gas producers in the world. Therefore, the utilization of fuel cells may reduce the greenhouse gas emissions.

4 Conclusion and Future Trends

It is evident that there is a growing need for hydrogen. Hydrogen will play a key role in the manufacture of better transportation fuels. It may also play a role in the introduction of a "hydrogen economy," provided CO_2-sequestration is accepted. Technologies are available that offer a high degree of feedstock flexibility. The conversion of methanol is the most economic route to hydrogen for the small scale. Among different methods of hydrogen production from methanol, the steam reforming process appears to be the most feasible technology. The enormous potential of waste heat is available, and MSR with its characteristics of endothermic reaction and lowest exergy rate/reaction temperature could serve as a way to recover this enormous waste energy into hydrogen energy. Hence, in this chapter, the fundamentals of MSR with respect to POX reaction were introduced. Specifically, the thermodynamic equilibrium and catalyst modifications were extensively discussed. After that, the application of new technologies such as MRs and microreactors for extending MSR efficiency improvement were evaluated. The fundamentals of experimental and modeling works about carrying out MSR reaction in MRs and microreactors were conducted, giving much needed understanding of the effects of operating parameters and further understanding regarding membrane types, MRs configurations, and catalyst kinetics.

Hence, future directions to improve MRs and microreactors should be focused on membrane technologies for hydrogen separation by developing high-performing and cost-effective membranes that could achieve high selectivity and permeability, with recognition of the tradeoff that exists between these two parameters. Moreover, presenting multistage or cascaded process designs to reach the desired selectivity and recovery—with the aim of reducing the membrane area, which would decide its footprint, capital cost and feasibility of MR and microreactor applications in in-situ hydrogen production systems—can decrease the total cost of the integrated system for hydrogen production from methanol.

Therefore, possibilities are still open for future works and research, in the hope of achieving a future advanced and sustainable energy system for methanol conversion to hydrogen.

References

Abanades, S., Flamant, G., 2006. Thermochemical hydrogen production from a two-step solar-driven water-splitting cycle based on cerium oxides. Sol. Energy 80 (12), 1611–1623.

Agarwal, V., Patel, S., Pant, K.K., 2005. H_2 production by steam reforming of methanol over $Cu/ZnO/Al_2O_3$ catalysts: transient deactivation kinetics modeling. Appl. Catal. A Gen. 279 (1), 155–164.

Agrafiotis, C., et al., 2005. Solar water splitting for hydrogen production with monolithic reactors. Sol. Energy 79 (4), 409–421.
Agrell, J., et al., 2003. Production of hydrogen from methanol over Cu/ZnO catalysts promoted by ZrO_2 and Al_2O_3. J. Catal. 219 (2), 389–403.
Agrell, J., Birgersson, H., Boutonnet, M., 2002. Steam reforming of methanol over a $Cu/ZnO/Al_2O_3$ catalyst: a kinetic analysis and strategies for suppression of CO formation. J. Power Sources 106 (1), 249–257.
Amphlett, J.C., et al., 1985. Hydrogen production by the catalytic steam reforming of methanol: Part 2: kinetics of methanol decomposition using girdler G66B catalyst. Can. J. Chem. Eng. 63 (4), 605–611.
Barton, J., Pour, V., 1980. Kinetics of catalytic conversion of methanol at higher pressures. Collect. Czechoslov. Chem. Commun. 45 (12), 3402–3407.
Basile, A., et al., 2006. Co-current and counter-current modes for methanol steam reforming membrane reactor: experimental study. Catal. Today 118 (1), 237–245.
Basile, A., et al., 2008. Hydrogen production by methanol steam reforming carried out in membrane reactor on Cu/Zn/Mg-based catalyst. Catal. Today 137 (1), 17–22.
Basile, A., Iulianelli, A., Tong, J., 2015. Membrane reactors for the conversion of methanol and ethanol to hydrogen. Membrane Reactors for Energy Applications and Basic Chemical Production. Elsevier, pp. 187–208.
Baykara, S.Z., 2004. Experimental solar water thermolysis. Int. J. Hydrog. Energy 29 (14), 1459–1469.
Behrens, M., Armbrüster, M., 2012. Methanol steam reforming. Catalysis for Alternative Energy Generation. Springer, pp. 175–235.
Benilov, M.S., Naidis, G.V., 2006. Modeling of hydrogen-rich gas production by plasma reforming of hydrocarbon fuels. Int. J. Hydrog. Energy 31 (6), 769–774.
Bichon, P., et al., 2007. Hydrogen from methanol steam-reforming over Cu-based catalysts with and without Pd promotion. Int. J. Hydrog. Energy 32 (12), 1799–1805.
Breen, J.P., Ross, J.R.H., 1999. Methanol reforming for fuel-cell applications: development of zirconia-containing Cu–Zn–Al catalysts. Catal. Today 51 (3), 521–533.
Briceño, K., et al., 2012. Carbon molecular sieve membranes supported on non-modified ceramic tubes for hydrogen separation in membrane reactors. Int. J. Hydrog. Energy 37 (18), 13536–13544.
Brown, L.F., 2001. A comparative study of fuels for on-board hydrogen production for fuel-cell-powered automobiles. Int. J. Hydrog. Energy 26 (4), 381–397.
Busetto, C., et al., 1984. Catalysts for low-temperature methanol synthesis. Preparation of Cu-Zn-Al mixed oxides via hydrotalcite-like precursors. J. Catal. 85 (1), 260–266.
Cacciola, G., Antonucci, V., Freni, S., 2001. Technology up date and new strategies on fuel cells. J. Power Sources 100 (1), 67–79.
Cao, W., et al., 2006. Methanol-steam reforming over a $ZnO\text{-}Cr_2O_3/CeO_2\text{-}ZrO_2/Al_2O_3$ catalyst. Chem. Eng. J. 119 (2), 93–98.
Chen, H.L., et al., 2008. Review of plasma catalysis on hydrocarbon reforming for hydrogen production—interaction, integration, and prospects. Appl. Catal. B Environ. 85 (1), 1–9.
Chiarello, G.L., Aguirre, M.H., Selli, E., 2010. Hydrogen production by photocatalytic steam reforming of methanol on noble metal-modified TiO_2. J. Catal. 273 (2), 182–190.
Choudhary, T.V., Sivadinarayana, C., Goodman, D.W., 2001. Catalytic ammonia decomposition: COx-free hydrogen production for fuel cell applications. Catal. Lett. 72 (3), 197–201.
Conant, T., et al., 2008. Stability of bimetallic Pd-Zn catalysts for the steam reforming of methanol. J. Catal. 257 (1), 64–70.
Contreras, J.L., et al., 2014. Catalysts for H_2 production using the ethanol steam reforming (a review). Int. J. Hydrog. Energy 39 (33), 18835–18853.
Damle, A.S., 2008. Hydrogen production by reforming of liquid hydrocarbons in a membrane reactor for portable power generation—model simulations. J. Power Sources 180 (1), 516–529.
Dauenhauer, P.J., Salge, J.R., Schmidt, L.D., 2006. Renewable hydrogen by autothermal steam reforming of volatile carbohydrates. J. Catal. 244 (2), 238–247.
Deluga, G.A., et al., 2004. Renewable hydrogen from ethanol by autothermal reforming. Science 303 (5660), 993–997.

Dittmar, B., et al., 2013. Methane steam reforming operation and thermal stability of new porous metal supported tubular palladium composite membranes. Int. J. Hydrog. Energy 38 (21), 8759–8771.
Divins, N.J., et al., 2013. Bio-ethanol steam reforming and autothermal reforming in 3-μm channels coated with $RhPd/CeO_2$ for hydrogen generation. Chem. Eng. Process. Process Intensif. 64, 31–37.
Enger, B.C., Lødeng, R., Holmen, A., 2008. A review of catalytic partial oxidation of methane to synthesis gas with emphasis on reaction mechanisms over transition metal catalysts. Appl. Catal. A Gen. 346 (1), 1–27.
Faungnawakij, K., Kikuchi, R., Eguchi, K., 2006. Thermodynamic evaluation of methanol steam reforming for hydrogen production. J. Power Sources 161 (1), 87–94.
Fukunaga, T., et al., 2009. Characterization of CuMn-spinel catalyst for methanol steam reforming. Catal. Commun. 10 (14), 1800–1803.
Gao, L., Sun, G., Kawi, S., 2008. A study on methanol steam reforming to CO_2 and H_2 over the La_2CuO_4 nanofiber catalyst. J. Solid State Chem. 181 (1), 7–13.
Garbarino, G., et al., 2013. Cobalt-based nanoparticles as catalysts for low temperature hydrogen production by ethanol steam reforming. Int. J. Hydrog. Energy 38 (1), 82–91.
Geissler, K., et al., 2001. Autothermal methanol reforming for hydrogen production in fuel cell applications. Phys. Chem. Chem. Phys. 3 (3), 289–293.
Ghasemzadeh, K., Liguori, S., et al., 2013a. H_2 production by low pressure methanol steam reforming in a dense Pd-Ag membrane reactor in co-current flow configuration: experimental and modeling analysis. Int. J. Hydrog. Energy 38 (36), 16685–16697.
Ghasemzadeh, K., Morrone, P., Iulianelli, A., et al., 2013b. H_2 production in silica membrane reactor via methanol steam reforming: modeling and HAZOP analysis. Int. J. Hydrog. Energy 38 (25), 10315–10326.
Ghasemzadeh, K., Morrone, P., Liguori, S., et al., 2013c. Evaluation of silica membrane reactor performance for hydrogen production via methanol steam reforming: modeling study. Int. J. Hydrog. Energy 38 (36), 16698–16709.
Ghasemzadeh, K., et al., 2015a. A simulation study on methanol steam reforming in the silica membrane reactor for hydrogen production. Int. J. Hydrog. Energy 40 (10), 3909–3918.
Ghasemzadeh, K., et al., 2015b. Hydrogen production via silica membrane reactor during the methanol steam reforming process: experimental study. RSC Adv. 5 (116), 95823–95832.
Ghasemzadeh, K., Andalib, E., Basile, A., 2016. Evaluation of dense Pd-Ag membrane reactor performance during methanol steam reforming in comparison with autothermal reforming using CFD analysis. Int. J. Hydrog. Energy 41 (20), 8745–8754.
Ghenciu, A.F., 2002. Review of fuel processing catalysts for hydrogen production in PEM fuel cell systems. Curr. Opinion Solid State Mater. Sci. 6 (5), 389–399.
Günter, M.M., et al., 2001. Redox behavior of copper oxide/zinc oxide catalysts in the steam reforming of methanol studied by in situ X-ray diffraction and absorption spectroscopy. J. Catal. 203 (1), 133–149.
Haryanto, A., et al., 2005. Current status of hydrogen production techniques by steam reforming of ethanol: a review. Energy Fuel 19 (5), 2098–2106.
Hohn, K.L., Lin, Y.-C., 2009. Catalytic partial oxidation of methanol and ethanol for hydrogen generation. ChemSusChem 2 (10), 927–940.
Holladay, J.D., et al., 2009. An overview of hydrogen production technologies. Catal. Today 139 (4), 244–260.
Horn, R., et al., 2007. Methane catalytic partial oxidation on autothermal Rh and Pt foam catalysts: oxidation and reforming zones, transport effects, and approach to thermodynamic equilibrium. J. Catal. 249 (2), 380–393.
Houseman, J., Cerini, D.J., 1976a. onboard hydrogen generation for automobiles. In: 11th Intersociety Energy Conversion Engineering Conference.1, pp. 6–16.
Houseman, J., Cerini, D.J., 1976b. Hydrogen-Rich Gas Generator. Patent.
Huang, G., et al., 2009. Steam reforming of methanol over $CuO/ZnO/CeO_2/ZrO_2/Al_2O_3$ catalysts. Appl. Catal. A Gen. 358 (1), 7–12.
Huang, X., Ma, L., Wainwright, M.S., 2004. The influence of Cr, Zn and Co additives on the performance of skeletal copper catalysts for methanol synthesis and related reactions. Appl. Catal. A Gen. 257 (2), 235–243.
Idem, R.O., Bakhshi, N.N., 1996. Kinetic modeling of the production of hydrogen from the methanol-steam reforming process over Mn-promoted coprecipitated Cu-Al catalyst. Chem. Eng. Sci. 51 (14), 3697–3708.

Israni, S.H., Harold, M.P., 2011. Methanol steam reforming in single-fiber packed bed Pd-Ag membrane reactor: experiments and modeling. J. Membr. Sci. 369 (1), 375–387.
Ito, S., et al., 2003. Steam reforming of methanol over Pt–Zn alloy catalyst supported on carbon black. Catal. Commun. 4 (10), 499–503.
Itoh, N., Kaneko, Y., Igarashi, A., 2002. Efficient hydrogen production via methanol steam reforming by preventing back-permeation of hydrogen in a palladium membrane reactor. Ind. Eng. Chem. Res. 41 (19), 4702–4706.
Iulianelli, A., 2014. Methanol steam reforming for hydrogen generation via conventional and membrane reactors: a review. Renew. Sust. Energ. Rev. 29, 355–368.
Iulianelli, A., Longo, T., Basile, A., 2008a. Methanol steam reforming in a dense Pd-Ag membrane reactor: the pressure and WHSV effects on CO-free H_2 production. J. Membr. Sci. 323 (2), 235–240.
Iulianelli, A., Longo, T., Basile, A., 2008b. Methanol steam reforming reaction in a Pd-Ag membrane reactor for CO-free hydrogen production. Int. J. Hydrog. Energy 33 (20), 5583–5588.
Iwasa, N., et al., 2003. Effect of Zn addition to supported Pd catalysts in the steam reforming of methanol. Appl. Catal. A Gen. 248 (1), 153–160.
Iwasa, N., et al., 1993. Highly selective supported Pd catalysts for steam reforming of methanol. Catal. Lett. 19 (2), 211–216.
Iwasa, N., et al., 1998. New catalytic functions of Pd-Zn, Pd-Ga, Pd-In, Pt-Zn, Pt-Ga and Pt-In alloys in the conversions of methanol. Catal. Lett. 54 (3), 119–123.
Iwasa, N., Masuda, S., Takezawa, N., 1995. Steam reforming of methanol over Ni, Co, Pd and Pt supported on ZnO. React. Kinet. Catal. Lett. 55 (2), 349–353.
Iwasa, N., Takezawa, N., 2003. New supported Pd and Pt alloy catalysts for steam reforming and dehydrogenation of methanol. Top. Catal. 22 (3–4), 215–224.
Jakdetchai, O., Takayama, N., Nakajima, T., 2005. Activity enhancement of CuZn-impregnated FSM-16 by modification with 1,3-butanediol for steam reforming of methanol1. Kinet. Catal. 46 (1), 56–64.
Jeong, D.-W., et al., 2013. H_2 production from a single stage water gas shift reaction over Pt/CeO_2, Pt/ZrO 2, and Pt/Ce (1- x) Zr (x) O_2 catalysts. Int. J. Hydrog. Energy 38 (11), 4502–4507.
Jeong, H., et al., 2006. Hydrogen production by steam reforming of methanol in a micro-channel reactor coated with $Cu/ZnO/ZrO_2/Al_2O_3$ catalyst. J. Power Sources 159 (2), 1296–1299.
Jiang, C.J., et al., 1993a. Kinetic study of steam reforming of methanol over copper-based catalysts. Appl. Catal. A Gen. 93 (2), 245–255.
Jiang, C.J., et al., 1993b. Kinetic mechanism for the reaction between methanol and water over a $Cu\text{-}ZnO\text{-}Al_2O_3$ catalyst. Appl. Catal. A Gen. 97 (2), 145–158.
Jones, S.D., Hagelin-Weaver, H.E., 2009. Steam reforming of methanol over CeO_2-and ZrO_2-promoted Cu-ZnO catalysts supported on nanoparticle Al_2O_3. Appl. Catal. B Environ. 90 (1), 195–204.
Jones, S.D., Neal, L.M., Hagelin-Weaver, H.E., 2008. Steam reforming of methanol using Cu-ZnO catalysts supported on nanoparticle alumina. Appl. Catal. B Environ. 84 (3), 631–642.
Karim, A., Conant, T., Datye, A., 2006. The role of PdZn alloy formation and particle size on the selectivity for steam reforming of methanol. J. Catal. 243 (2), 420–427.
Khila, Z., et al., 2013. A comparative study on energetic and exergetic assessment of hydrogen production from bioethanol via steam reforming, partial oxidation and auto-thermal reforming processes. Fuel Process. Technol. 112, 19–27.
King, J.M., O'Day, M.J., 2000. Applying fuel cell experience to sustainable power products. J. Power Sources 86 (1), 16–22.
Kurtz, M., et al., 2003. Deactivation of supported copper catalysts for methanol synthesis. Catal. Lett. 86 (1–3), 77–80.
Lee, D.W., et al., 2006. Preparation of Pt-loaded hydrogen selective membranes for methanol reforming. Catal. Today 118 (1–2), 198–204.
Lee, D.-W., et al., 2008. Study on methanol reforming-inorganic membrane reactors combined with water-gas shift reaction and relationship between membrane performance and methanol conversion. J. Membr. Sci. 316 (1), 63–72.
Lee, J.K., Ko, J.B., Kim, D.H., 2004. Methanol steam reforming over $Cu/ZnO/Al_2O_3$ catalyst: kinetics and effectiveness factor. Appl. Catal. A Gen. 278 (1), 25–35.

LeValley, T.L., Richard, A.R., Fan, M., 2014. The progress in water gas shift and steam reforming hydrogen production technologies–a review. Int. J. Hydrog. Energy 39 (30), 16983–17000.
Li, D., et al., 2015. Metal catalysts for steam reforming of tar derived from the gasification of lignocellulosic biomass. Bioresour. Technol. 178, 53–64.
Li, S., et al., 2013. A Ni@ ZrO_2 nanocomposite for ethanol steam reforming: enhanced stability via strong metal–oxide interaction. Chem. Commun. 49 (39), 4226–4228.
Liao, P.-H., Yang, H.-M., 2008. Preparation of catalyst Ni–Cu/CNTs by chemical reduction with formaldehyde for steam reforming of methanol. Catal. Lett. 121 (3-4), 274–282.
Liguori, S., et al., 2014. Methanol steam reforming in an Al_2O_3 supported thin Pd-layer membrane reactor over $Cu/ZnO/Al_2O_3$ catalyst. Int. J. Hydrog. Energy 39 (32), 18702–18710.
Lin, Y.-M., Lee, G.-L., Rei, M.-H., 1998. An integrated purification and production of hydrogen with a palladium membrane-catalytic reactor. Catal. Today 44 (1), 343–349.
Lin, Y.-M., Rei, M.-H., 2001. Study on the hydrogen production from methanol steam reforming in supported palladium membrane reactor. Catal. Today 67 (1), 77–84.
Lindström, B., Pettersson, L.J., Menon, P.G., 2002. Activity and characterization of Cu/Zn, Cu/Cr and Cu/Zr on γ-alumina for methanol reforming for fuel cell vehicles. Appl. Catal. A Gen. 234 (1), 111–125.
Liu, Q., et al., 2008. Waste-free soft reactive grinding synthesis of high-surface-area copper–manganese spinel oxide catalysts highly effective for methanol steam reforming. Catal. Lett. 121 (1-2), 144–150.
Liu, Y., et al., 2003. Steam reforming of methanol over Cu/CeO_2 catalysts studied in comparison with Cu/ZnO and Cu/Zn (Al) O catalysts. Top. Catal. 22 (3-4), 205–213.
Löffler, D.G., Taylor, K., Mason, D., 2003. A light hydrocarbon fuel processor producing high-purity hydrogen. J. Power Sources 117 (1–2), 84–91.
Lyubovsky, M., Roychoudhury, S., 2004. Novel catalytic reactor for oxidative reforming of methanol. Appl. Catal. B Environ. 54 (4), 203–215.
Mateos-Pedrero, C., et al., 2015. CuO/ZnO catalysts for methanol steam reforming: the role of the support polarity ratio and surface area. Appl. Catal. B Environ. 174, 67–76.
Matsumura, Y., Ishibe, H., 2009a. Suppression of CO by-production in steam reforming of methanol by addition of zinc oxide to silica-supported copper catalyst. J. Catal. 268 (2), 282–289.
Matsumura, Y., Ishibe, H., 2009b. High temperature steam reforming of methanol over $Cu/ZnO/ZrO_2$ catalysts. Appl. Catal. B Environ. 91 (1), 524–532.
Matter, P.H., Braden, D.J., Ozkan, U.S., 2004. Steam reforming of methanol to H_2 over nonreduced Zr-containing CuO/ZnO catalysts. J. Catal. 223 (2), 340–351.
Men, Y., et al., 2010. Methanol steam reforming over bimetallic $Pd\text{-}In/Al_2O_3$ catalysts in a microstructured reactor. Appl. Catal. A Gen. 380 (1), 15–20.
Mondal, T., Pant, K.K., Dalai, A.K., 2015. Catalytic oxidative steam reforming of bio-ethanol for hydrogen production over Rh promoted $Ni/CeO_2\text{-}ZrO_2$ catalyst. Int. J. Hydrog. Energy 40 (6), 2529–2544.
Muradov, N.Z., 1998. CO_2-free production of hydrogen by catalytic pyrolysis of hydrocarbon fuel. Energy Fuel 12 (1), 41–48.
Muradov, N.Z., Veziroğlu, T.N., 2005. From hydrocarbon to hydrogen–carbon to hydrogen economy. Int. J. Hydrog. Energy 30 (3), 225–237.
Navarro, R.M., Pena, M.A., Fierro, J.L.G., 2007. Hydrogen production reactions from carbon feedstocks: fossil fuels and biomass. Chem. Rev. 107 (10), 3952–3991.
Ni, M., Leung, D.Y.C., Leung, M.K.H., 2007a. A review on reforming bio-ethanol for hydrogen production. Int. J. Hydrog. Energy 32 (15), 3238–3247.
Ni, M., Leung, M.K.H., et al., 2007b. A review and recent developments in photocatalytic water-splitting using TiO_2 for hydrogen production. Renew. Sust. Energ. Rev. 11 (3), 401–425.
Ni, M., et al., 2006. An overview of hydrogen production from biomass. Fuel Process. Technol. 87 (5), 461–472.
Norman, J.H., Basenbruch, G.E., O'keefe, D.R., 1981. Thermochemical water-splitting for hydrogen production. Final report 1 Jan 75–31 Dec 80.[Sulfur-iodine cycle].
Oguchi, H., et al., 2005. Steam reforming of methanol over $Cu/CeO_2/ZrO_2$ catalysts. Appl. Catal. A Gen. 281 (1), 69–73.

Olah, G.A., Goeppert, A., Prakash, G.K.S., 2011. Beyond Oil and Gas: The Methanol Economy. John Wiley & Sons, Weinheim, DE.

Otsuka, K., Ina, T., Yamanaka, I., 2003. The partial oxidation of methanol using a fuel cell reactor. Appl. Catal. A Gen. 247 (2), 219–229.

Palma, V., et al., 2014. CeO_2-supported Pt/Ni catalyst for the renewable and clean H_2 production via ethanol steam reforming. Appl. Catal. B Environ. 145, 73–84.

Palo, D.R., Dagle, R.A., Holladay, J.D., 2007. Methanol steam reforming for hydrogen production. Chem. Rev. 107 (10), 3992–4021.

Papavasiliou, J., Avgouropoulos, G., Ioannides, T., 2005. Steam reforming of methanol over copper–manganese spinel oxide catalysts. Catal. Commun. 6 (7), 497–501.

Park, G.-G., et al., 2004. Development of microchannel methanol steam reformer. Chem. Eng. J. 101 (1), 87–92.

Patel, S., Pant, K.K., 2006a. Activity and stability enhancement of copper-alumina catalysts using cerium and zinc promoters for the selective production of hydrogen via steam reforming of methanol. J. Power Sources 159 (1), 139–143.

Patel, S., Pant, K.K., 2006b. Influence of preparation method on performance of Cu (Zn)(Zr)-alumina catalysts for the hydrogen production via steam reforming of methanol. J. Porous. Mater. 13 (3–4), 373–378.

Patrascu, M., Sheintuch, M., 2015. On-site pure hydrogen production by methane steam reforming in high flux membrane reactor: experimental validation, model predictions and membrane inhibition. Chem. Eng. J. 262, 862–874.

Pattekar, A.V., Kothare, M.V., 2004. A microreactor for hydrogen production in micro fuel cell applications. J. Microelectromech. Syst. 13 (1), 7–18.

Peppley, B.A., et al., 1999a. Methanol–steam reforming on $Cu/ZnO/Al_2O_3$. Part 1: the reaction network. Appl. Catal. A Gen. 179 (1), 21–29.

Peppley, B.A., et al., 1999b. Methanol–steam reforming on $Cu/ZnO/Al_2O_3$ catalysts. Part 2. A comprehensive kinetic model. Appl. Catal. A Gen. 179 (1), 31–49.

Purnama, H., et al., 2004. Activity and selectivity of a nanostructured CuO/ZrO_2 catalyst in the steam reforming of methanol. Catal. Lett. 94 (1–2), 61–68.

Qi, C., Amphlett, J.C., Peppley, B.A., 2007a. Hydrogen production by methanol reforming on NiAl layered double hydroxide derived catalyst: effect of the pretreatment of the catalyst. Int. J. Hydrog. Energy 32 (18), 5098–5102.

Qi, C., Amphlett, J.C., Peppley, B.A., 2007b. K (Na)-promoted Ni, Al layered double hydroxide catalysts for the steam reforming of methanol. J. Power Sources 171 (2), 842–849.

Qi, C., Amphlett, J.C., Peppley, B.A., 2005. Methanol steam reforming over NiAl and Ni (M) Al layered double hydroxides (M=Au, Rh, Ir) derived catalysts. Catal. Lett. 104 (1–2), 57–62.

Qi, C., Amphlett, J.C., Peppley, B.A., 2006. Product composition as a function of temperature over NiAl-layered double hydroxide derived catalysts in steam reforming of methanol. Appl. Catal. A Gen. 302 (2), 237–243.

Rabenstein, G., Hacker, V., 2008. Hydrogen for fuel cells from ethanol by steam-reforming, partial-oxidation and combined auto-thermal reforming: a thermodynamic analysis. J. Power Sources 185 (2), 1293–1304.

Ramirez, D., et al., 2008. Distributed generation system with PEM fuel cell for electrical power quality improvement. Int. J. Hydrog. Energy 33 (16), 4433–4443.

Rei, M.-H., et al., 2011. Catalysis-spillover-membrane. III: the effect of hydrogen spillover on the palladium membrane reactor in the steam reforming reactions. J. Membr. Sci. 369 (1), 299–307.

Sá, S., et al., 2010. Catalysts for methanol steam reforming—a review. Appl. Catal. B Environ. 99 (1), 43–57.

Sá, S., Sousa, J.M., Mendes, A., 2011. Steam reforming of methanol over a $CuO/ZnO/Al_2O_3$ catalyst part II: a carbon membrane reactor. Chem. Eng. Sci. 66 (22), 5523–5530.

Sadati, S., et al., 2015. Hydrogen production: overview of technology options and membrane in auto-thermal reforming including partial oxidation and steam reforming. Int. J. Membr. Sci. Technol. 2 (1), 56–67.

Samms, S.R., Savinell, R.F., 2002. Kinetics of methanol-steam reformation in an internal reforming fuel cell. J. Power Sources 112 (1), 13–29.

Santacesaria, E., Carra, S., 1983. Kinetics of catalytic steam reforming of methanol in a CSTR reactor. Appl. Catal. 5 (3), 345–358.

Shen, J.-P., Song, C., 2002. Influence of preparation method on performance of Cu/Zn-based catalysts for low-temperature steam reforming and oxidative steam reforming of methanol for H_2 production for fuel cells. Catal. Today 77 (1), 89–98.
Shishido, T., et al., 2004. Active Cu/ZnO and Cu/ZnO/Al_2O_3 catalysts prepared by homogeneous precipitation method in steam reforming of methanol. Appl. Catal. A Gen. 263 (2), 249–253.
Silva, J.M., Soria, M.a., Madeira, L.M., 2015. Challenges and strategies for optimization of glycerol steam reforming process. Renew. Sust. Energ. Rev. 42, 1187–1213.
Steinfeld, A., 2002. Solar hydrogen production via a two-step water-splitting thermochemical cycle based on Zn/ZnO redox reactions. Int. J. Hydrog. Energy 27 (6), 611–619.
Steinfeld, A., 2005. Solar thermochemical production of hydrogen – a review. Sol. Energy 78 (5), 603–615.
Sun, J., 2004. Hydrogen from steam reforming of ethanol in low and middle temperature range for fuel cell application. Int. J. Hydrog. Energy 29 (10), 1075–1081.
Suwa, Y., et al., 2004. Comparative study between Zn–Pd/C and Pd/ZnO catalysts for steam reforming of methanol. Appl. Catal. A Gen. 267 (1), 9–16.
Takezawa, N., Iwasa, N., 1997. Steam reforming and dehydrogenation of methanol: Difference in the catalytic functions of copper and group VIII metals. Catal. Today 36 (1), 45–56.
Tosti, S., et al., 2008. Low temperature ethanol steam reforming in a Pd-Ag membrane reactorPart 1: Ru-based catalyst. J. Membr. Sci. 308 (1-2), 250–257.
Valdes-Solis, T., Marban, G., Fuertes, A.B., 2006. Nanosized catalysts for the production of hydrogen by methanol steam reforming. Catal. Today 116 (3), 354–360.
Wang, L.-C., et al., 2007. Production of hydrogen by steam reforming of methanol over Cu/ZnO catalysts prepared via a practical soft reactive grinding route based on dry oxalate-precursor synthesis. J. Catal. 246 (1), 193–204.
Wieland, S., Melin, T., Lamm, A., 2001. Membrane reactors for hydrogen production. Chemie Ingenieur Technik 73 (6), 768.
Wu, H., et al., 2013. Ni-based catalysts for low temperature methane steam reforming: recent results on Ni-Au and comparison with other bi-metallic systems. Catalysts 3 (2), 563–583.
Xu, Y., et al., 2013. In silico search for novel methane steam reforming catalysts. N. J. Phys. 15 (12), 125021.
Yang, H.-M., Liao, P.-H., 2007. Preparation and activity of Cu/ZnO-CNTs nano-catalyst on steam reforming of methanol. Appl. Catal. A Gen. 317 (2), 226–233.
Yao, C.-Z., et al., 2006. Effect of preparation method on the hydrogen production from methanol steam reforming over binary Cu/ZrO_2 catalysts. Appl. Catal. A Gen. 297 (2), 151–158.
Yong-Feng, L., Xin-Fa, D., Wei-Ming, L., 2004. Effects of ZrO_2-promoter on catalytic performance of CuZnAlO catalysts for production of hydrogen by steam reforming of methanol. Int. J. Hydrog. Energy 29 (15), 1617–1621.
York, A.P.E., Xiao, T., Green, M.L.H., 2003. Brief overview of the partial oxidation of methane to synthesis gas. Top. Catal. 22 (3–4), 345–358.
Zhang, X., et al., 2006. Methanol steam reforming to hydrogen in a carbon membrane reactor system. Ind. Eng. Chem. Res. 45 (24), 7997–8001.
Zhu, L., Fan, J., 2015. Thermodynamic analysis of H_2 production from CaO sorption-enhanced methane steam reforming thermally coupled with chemical looping combustion as a novel technology. Int. J. Energy Res. 39 (3), 356–369.
Zum Mallen, M.P., Schmidt, L.D., 1996. Oxidation of methanol over polycrystalline Rh and Pt: rates, OH desorption, and model. J. Catal. 161 (1), 230–246.

PART 2

Application and Innovation

This page intentionally left blank

CHAPTER 10

Methanol to Dimethyl Ether

Ali Bakhtyari, Mohammad R. Rahimpour
Shiraz University, Shiraz, Iran

Acronyms

ATR	autothermal reforming
CDR	carbon dioxide reforming
CFC	chlorofluorocarbon
CLR	chemical looping reforming
DEW	dimethyl ether enhanced waterflooding
DME	dimethyl ether
ER	Eley-Rideal
FTIR	Fourier transform infrared
H-SOD	hydroxy sodalite
IER	ion exchange resin
IUPAC	International Union of Pure and Applied Chemistry
LH	Langmuir-Hinshelwood
LHSV	liquid hourly space velocity
LNG	liquefied natural gas
LPG	liquefied petroleum gases
MF	methyl formate
MGC	Mitsubishi gas chemical company
PI	process intensification
PID	proportional/integral/derivative
PO	partial oxidation
RDS	rate determining step
SR	steam reforming
TCR	thermally coupled reactor
TEC	Toyo engineering corporation
TR	tri reforming
WGS	water-gas shift
WHSV	weight hourly space velocity

Methanol. https://doi.org/10.1016/B978-0-444-63903-5.00010-8

1 Methanol: A Key Building Block

Methanol, also called methyl alcohol, is the simplest alcohol with a methyl group attached to a hydroxyl one. At moderate condition, methanol is a volatile, colorless, and polar liquid with a unique smell, and is highly flammable and toxic. Methanol as a significant liquid petrochemical that is mainly utilized as feedstock for manufacturing valuable compounds such as fuels, solvents, and antifreeze agents. Dimethyl ether (DME), methyl formate, formalin, acetic acid, and formaldehyde are some of the major products obtained from methanol in direct or indirect routes. It could also be utilized for biodiesel production through transesterification reactions. Methanol potential as a medium for hydrogen storage and delivery makes it interesting in energy applications. In the current status, methanol acts as an important building block in the petrochemical industry and thus a great deal of attention is being paid to it (Semelsberger et al., 2006; Arcoumanis et al., 2008; Riaz et al., 2013; Su et al., 2013; Bakhtyari et al., 2015, 2016a,b,c). A considerable portion of produced methanol is consumed in the manufacturing of DME.

2 DME: Fuel of the 21st Century

DME (IUPAC name is methoxymethane) has the chemical formula of CH_3OCH_3. DME, which is the simplest alkyl ether, and is considered the isomer of ethanol. At ambient condition, it exists in the vapor phase. However, under the pressures of greater than 5 bar, it is liquefied at room temperature (Shikada et al., 1998; Azizi et al., 2014). Hence, it is easy and safe to store and deal with. Physical properties and combustion characteristics of DME are summarized in Tables 10.1 and 10.2, respectively. DME is colorless, almost non-toxic, highly flammable, and resistant to auto oxidation and formation of peroxides (Azizi et al., 2014; Raoof et al., 2008). DME has the heating characteristics similar to those of liquefied petroleum gases (LPG) such as propane and butane (Azizi et al., 2014; Zhang et al., 2010). Accordingly, DME is applicable in both domestic and industrial applications as an energy source. The key properties of DME are compared with those of conventional fuels in Table 10.3.

A major part of DME is consumed in the production of dimethyl sulfate through the reaction with sulfur trioxide. Besides, it could be efficiently converted to acetic acid through carbonylation reaction (Muller and Hubsch, 2005). DME is a key building block for the production of downstream chemicals such as ethanol (Liu et al., 2013; Yang et al., 2011), light olefins (Pérez-Uriarte et al., 2016; Pérez-Uriarte et al., 2017; Al-Dughaither and de Lasa, 2014; Idemitsu process uses DME to produce olefins, 2007), methyl acetate (Liu et al., 2013; Zhou et al., 2016; Park et al., 2016), and aromatics (Zhang et al., 2013; Wang et al., 2016). Due to the environmentally friendly nature of DME, it is suggested as an aerosol and refrigerant in cooling facilities. In fact, DME makes zero ozone defects and thus does not intensify

Table 10.1 Physical properties of DME (Perry and Green, 1999; Cousins and Laesecke, 2012)

Property	Quantity	Unit
Molecular		
Volume	0.06312	$(nm)^3$
Surface area	0.8457	$(nm)^2$
Accessible surface area	0.7250	$(nm)^2$
Polar surface area	0.0916	$(nm)^2$
Dipole moment	1.30	debye
Acentric factor	0.192	–
Critical point		
Critical temperature	400.1	K
Critical pressure	5.27	MPa
Critical density	5.85	$kmol/m^3$
Compressibility factor	0.271	–
Gas (or vapor)		
Saturated density (242.5–350.1)	0.0398–0.9993	$kmol/m^3$
Ideal constant pressure heat capacity (200–1500 K)	54.36–165.81	J/mol K
Viscosity (293.15 K)	0.925×10^{-2}	mPa s
Enthalpy (233–313 K)	810.5–887.5	kJ/kg
Entropy (233–313 K)	5.9–5.7	kJ/kg K
Liquid		
Triple point	131.7	K
Normal boiling point	249.0	K
Vapor pressure (131.7–400.1 K)	3.05×10^{-6}–5.27	MPa
Heat of vaporization (131.7–400 K)	26.03–1.64	kJ/mol
Saturated density (131.7–400.1)	18.95–5.59	$kmol/m^3$
Constant pressure heat capacity (131.7–250)	98.36–103.14	J/mol K
Viscosity	0.2166–0.07814	mPa s
Enthalpy (233–313 K)	324.6–517.3	kJ/kg
Entropy (233–313 K)	3.8–4.5	kJ/kg K

Table 10.2 Combustion characteristics of DME (Mikkelsen et al., 1996; Kustrin and Tuma, 1996; Ohno, 1997; Fleisch et al., 1997; Fleisch and Meurer, 1995)

Property	Quantity	Unit
Burning velocity	50	cm/s
Ignition energy	45	MJ
Ignition temperature	508	K
Net calorific value	6903	kcal/kg
Heat of combustion	27–31	MJ/kg
Volumetric heat value	18.2×10^3	MJ/m^3
Low heating value	27.6	MJ/kg
Cetane number	55–60	–
Flame color	Visible blue	–

Table 10.3 Comparing the properties of conventional fuels (Mikkelsen et al., 1996; Kustrin and Tuma, 1996; Ohno, 1997; Fleisch et al., 1997; Fleisch and Meurer, 1995)

Property	Unit	DME	Diesel	CNG	LNG	Fischer-Tropsch	Gasoline
Low heating value	MJ/kg	27.6	43	50	50	43	43
Volumetric heat value	MJ/lit	18.2	36.5	8	21.1	33.1	32.2
Density	$(mol/m^3) \times 10^{-6}$	0.660	0.850	0.160[a]	0.422	0.770	0.750
Cetane number	–	55–60	45	–	–	80	–

[a]At 3000 psi.

global warming issues. Therefore, in competition with the conventional refrigerants such as Freon, CFCs (i.e., chlorofluorocarbon), and R-134, DME is acquiring popularity (Onaka et al., 2010; Afroz et al., 2008; Park et al., 2008; Granryd, 2001). DME could be utilized as a solvent in the extraction of various compounds such as green crude (Kanda and Li, 2011), lipids (Kanda et al., 2012), and hydrocarbons (Kanda et al., 2013). Although the low boiling point of DME (249 K) limits its application, it makes the regeneration step easy. DME is also a precursor to trimethyloxonium tetrafluoroborate, which is useful in alkylating reactions (Curphey, 1971). DME is expected to be a suitable hydrogen resource for the application in the direct fuel cells. Due to the relatively large molecular weight of DME (46.07 g/mol) and its low solubility in water (71 kg DME/m^3 water at 293 K), energy loss is reduced by utilizing DME in fuel cells. Easy vaporization of DME in the moderate condition leads to the elimination of liquid pumps in the fuel cell facilities (Yoo et al., 2006). Pesticide and polishing and anti-rust agents are other applications of DME in daily life.

The slight polarity of DME, which leads to miscibility with hydrocarbons and partial solubility in water, is introducing it as a promising candidate in oil recovery. Enhanced waterflooding is managed by injecting DME-brine solutions into hydrocarbon reservoirs. In fact, swelling and the further decrease of oil viscosity are the results of DME partitioning from the DME-brine solutions into the oil phase. Consequently, the mobility of oil is improved and thus oil recovery is enhanced. In this regard, Shell developed a novel technology called DME enhanced waterflooding (DEW) (Ratnakar et al., 2017; Ratnakar et al., 2016).

In parallel with numerous applications of DME, it is well known as a clean fuel. In fact, DME possesses several merits that make it attractive for clean and efficient energy generation (Fleisch et al., 2012; Yoon and Han, 2009). As said beforehand, DME does not show a tendency to be oxidized and in this manner to produce explosive peroxides. There is no carbon-carbon bond in the structure of DME. Due to the presence of less than 40% oxygen, such a characteristic leads to the lower formation of carbon oxides during combustion. The emissions of unburned hydrocarbons are less when compared with conventional energy sources such as natural gas (Fleisch et al., 2012; Yoon and Han, 2009). DME has higher cetane number (55–60) compared with diesel fuels (50) (Ogawa et al., 2004). The cetane number is a criterion for the ignitibility of fuels in the compression ignition engines. Therefore, it could be a promising alternative to the

conventional fuels in the transportation section (Azizi et al., 2014; Tokay et al., 2012). Furthermore, emission of toxic pollutants such as nitrogen oxides and sulfur oxides is eliminated by extensively utilizing DME. Based on the recent techno economic assessments in the international market, DME production is comparable in costs with LPG (Sousa-Aguiar et al., 2005). Besides, due to similar vapor pressure of DME to that of LPG, it could be processed within the available equipment in the storage and transportation sections (Azizi et al., 2014; Fleisch et al., 2012; Yoon and Han, 2009). Such merits lead to the superiority of DME in energy delivery. As stated by Sousa-Aguiar et al. (2005), DME is currently known as the "*Fuel of the 21st Century*."

3 Routes of DME Production

A variety of raw materials could be utilized to produce DME. In this regard, natural gas (Ogawa et al., 2004), synthesis gas (Shikada et al., 1998; Seddon, 2011), methanol (Bakhtyari et al., 2016b; Bakhtyari et al., 2015; Sabour et al., 2014; Ghavipour and Behbahani, 2014; Farsi et al., 2014; Samimi et al., 2013a, 2014a), and biomass (Higo and Dowaki, 2010; Peral and Martín, 2015) are the most investigated ones. In fact, the conversion of natural gas to DME by direct or indirect routes is the most thriving one for large scale production (Sousa-Aguiar et al., 2005). This is because DME production forms natural gas that allows the costs to be independent of the fluctuation of oil price. The availability of natural gas reservoirs is another advantage. However, biomass to DME could be an efficient alternative due to the reducing cost of feedstock and availability of biomass (Higo and Dowaki, 2010; Peral and Martín, 2015).

3.1 Direct Route

In the direct route for conversion of natural gas (i.e., methane) to DME, reactions of autothermal reforming (or CO_2 reforming) and DME synthesis occur simultaneously. Based on the following stoichiometry, methane is converted to syngas and water with further DME and water generation form syngas (Ogawa et al., 2004).

Autothermal reforming

$$2CH_4 + O_2 + CO_2 \rightleftarrows 3CO + 3H_2 + H_2O \tag{10.1}$$

DME synthesis

$$3CO + 3H_2 \rightleftarrows CH_3OCH_3 + CO_2 \tag{10.2}$$

Overall

$$2CH_4 + O_2 \rightleftarrows CH_3OCH_3 + H_2O \tag{10.3}$$

In this case, methane is converted to a syngas with a hydrogen to carbon monoxide ratio of 1 (i.e., $H_2/CO = 1$) in the presence of oxygen or even carbon dioxide. Then equimolar hydrogen and

carbon monoxide are combined to form DME with carbon dioxide as by-product. The generated carbon dioxide in the DME synthesis reaction is consumed and thus, enhances the reforming reaction. Overall, reaction (10.3) occurs and DME and water are produced from methane.

According to an elegant route, DME could be produced directly from methane in two steps. In the first step, methyl halides, typically chloromethane (i.e., CH_3Cl) or bromomethane (i.e., CH_3Br), are produced as a result of oxidative bromination of methane with oxygen and hydrogen halides. The typical catalyst of this step is Rh-SiO_2. The produced methyl halides are converted to methanol and DME by hydrolysis on a silica supported metal chloride catalyst. Producing large quantities of methanol and corrosion of facilities as a result of the hydrolysis of methyl halides are the major drawbacks of this route (You et al., 2009; Olah et al., 1985; Prakash et al., 2009).

It is not conventional to carry out the reforming and DME synthesis reactions in a single reactor. In fact, the processing needs of these two reactions are quite distinct from each other. Accordingly, DME synthesis from synthesis gas (syngas), which is known as the direct or one-step DME synthesis route, is brought up. Syngas, which is a mixture of hydrogen, carbon monoxide, and carbon dioxide, is conventionally produced from hydrocarbons. Natural gas (i.e., methane), coal, naphtha, liquefied natural gas (LNG), and biomass are the feedstocks converted to syngas (Peng et al., 2017; Mujeebu, 2016; Souza and Schmal, 2005; Seo et al., 2007; Abdoulmoumine et al., 2015). The most conventional reforming processes for large scale syngas production are steam reforming (SR) (Seo et al., 2007; Ko et al., 1995), autothermal reforming (ATR) (Souza and Schmal, 2005; Ding and Chan, 2008), partial oxidation (PO) (Dissanayake et al., 1991; Vernon et al., 1990), carbon dioxide reforming (CDR) (Wang et al., 1996; Richardson and Paripatyadar, 1990), tri reforming (TR) (Song and Pan, 2004; Rahimpour et al., 2012a; Farniaei et al., 2014), and chemical looping reforming (CLR) (Hafizi et al., 2016).

All the probable reactions for direct or one-step DME synthesis as well as their enthalpies are below. However, some reactions would be dominant due to catalyst activity in the process condition (Shikada et al., 1998; Ogawa et al., 2004; Sousa-Aguiar et al., 2005):

Hydrogenation of carbon monoxide to methanol

$$CO + 2H_2 \rightleftarrows CH_3OH \quad \Delta H = -90.7\,\text{kJ/mol} \tag{10.4}$$

$$2CO + 4H_2 \rightleftarrows 2CH_3OH \quad \Delta H = -182.0\,\text{kJ/mol} \tag{10.5}$$

Hydrogenation of carbon dioxide to methanol

$$CO_2 + 3H_2 \rightleftarrows CH_3OH + H_2O \quad \Delta H = -49.4\,\text{kJ/mol} \tag{10.6}$$

Water-gas shift (WGS)

$$CO + H_2O \rightleftarrows CO_2 + H_2 \quad \Delta H = -40.9\,\text{kJ/mol} \tag{10.7}$$

Dehydration of methanol to DME

$$2CH_3OH \rightleftarrows CH_3OCH_3 + H_2O \quad \Delta H = -23.4 kJ/mol \tag{10.8}$$

Hydrogenation of carbon monoxide to DME

$$2CO + 4H_2 \rightleftarrows CH_3OCH_3 + H_2O \quad \Delta H = -204.8 kJ/mol \tag{10.9}$$

$$3CO + 3H_2 \rightleftarrows CH_3OCH_3 + CO_2 \quad \Delta H = -245.7 kJ/mol \tag{10.10}$$

The equilibrium conversions of these reactions are at maximum state when the syngas feedstock with stoichiometric hydrogen to carbon monoxide ratio (i.e., H_2/CO) is utilized (Azizi et al., 2014). According to this reaction set, methanol synthesis (i.e., Eqs. 10.4–10.6), WGS (i.e., Eq. 10.7), and methanol dehydration (i.e., Eq. 10.8) occur simultaneously on the hybrid catalysts. However, direct syngas to DME reactions (i.e., Eqs. 10.9 and 10.10) compete with the other reactions. Due to the highly exothermic nature of the one-step DME synthesis process, appropriate control of the system is of great importance. In-situ methanol generation and consumption could help to eliminate the thermodynamic constrains of methanol synthesis. The intermediate methanol separation unit, which is highly energy intensive, could be omitted (Shikada et al., 1998; Seddon, 2011). In spite of the less waste of hydrocarbon feedstock in the one-step DME synthesis, it is of high complexity. In fact, DME purification and elimination of unreacted syngas and carbon dioxide are the inconveniences of this process. They are even more difficult in the presence of methanol in the product stream (Shikada et al., 1998; Azizi et al., 2014; Seddon, 2011). Weak catalyst stability in the process condition, which leads to decay in the activity and selectivity of the catalyst, beside the necessity of reducing carbon dioxide from syngas leads to doubts concerning the technical feasibility of the one-stage route. Additionally, due to the WGS reaction (i.e., Eq. 10.7), the stoichiometric amount of carbon monoxide is consumed to generate carbon dioxide and hydrogen. In this regard, some effort was made to produce DME from carbon dioxide rich syngas (De Falco et al., 2016). In a commercial point of view, this route is not yet proven. However, there are some instances claiming to overcome the technical problems of the one-step route for large scale DME production from syngas. NKK (Ogawa et al., 2004; Shikada et al., 2000; Shikada et al., 2005), Haldor Topsoe (Haugaard and Voss, 2001), and Air Products (Peng et al., 2002; Peng et al., 2000; Peng et al., 1998) are of these kinds. Seddon (Seddon, 2011) summarized the characteristics of these processes.

3.2 Indirect Route

Due to the aforementioned drawbacks of the direct route in the large-scale production, DME synthesis from methanol, that is, the indirect or two-step method, is brought up. In this route, the as-produced and purified methanol is converted to DME in a single reactor. Accordingly, the following reaction is accomplished on the surface of solid-acid catalysts:

Dehydration of methanol to DME

$$2CH_3OH \rightleftarrows CH_3OCH_3 + H_2O \quad \Delta H = -23.4 kJ/mol \tag{10.11}$$

The exothermic nature of this reaction causes enhanced equilibrium conversion at lower temperatures. Higher temperatures lead to production of undesired by-products such as syngas, ethylene, and coke (Azizi et al., 2014). In this process, purified methanol is heated to vapor and then passes through the catalytic reactor. The product, which is a mixture of DME and water, is cooled to condense water and separate it partially. The remaining mixture is sent to the distillation unit to purify the DME in two distinct steps. Production of DME from methanol is well known in figure. It is implemented typically at 10–20 bar using a γ-alumina catalyst with inlet temperature range of 493–523 K and outlet temperature range of 573–623 K. Toyo Engineering Corporation (TEC) (Shoji and Terai, 2007) invented a two-step process for the production of DME including vapor phase dehydration of methanol on activated alumina particles with an average pore diameter of 5–10 nm and 0.07 wt% content of sodium oxide. Toyo managed manufacturing of fuel-used DME in Sichuan Province in China in 2003 (Yoon and Han, 2009). Other licensors include Haldor Topsoe, Linde/Lurgi, Uhde, and Mitsubishi Gas Chemical Company (MGC) (Azizi et al., 2014; Fleisch et al., 2012).

Based on the importance of DME in the chemical industry, numerous studies are available focusing on the reactors, catalysts, and process of DME synthesis. Azizi et al. (2014) presented a critical review on the studies of DME in the 1965–2013 period. Based on their evaluation, the publications on the DME synthesis focused on the catalyst type and then on the reactor configuration. As stated by Yoon and Han (Yoon and Han, 2009), the concentrated research on the technologies of DME manufacturing includes improving activities of prepared catalysts as well as presenting reactor configurations such as fixed bed, fluidized bed, and slurry reactors. Besides inventing innovating methods for the elimination of reaction heat, improving process efficiency by optimization, and efforts to scale up the process are the objectives of recent studies on DME.

In the following sections, kinetics of reaction, catalysts, reactor configurations, novel systems, and the effect of operating parameters with the focus on the indirect method are investigated.

4 Chemistry of Methanol Dehydration

Over the years, various catalysts have been investigated for the conversion of methanol to DME in the pilot or commercial scales. In one of the earlier studies, Adkins and Perkins (1928) reported the formation of DME from methanol inside alumina (i.e., Al_2O_3) at 573–623 K. As stated by Chang (1983), the activities of silica gel, alumina, and hybrid alumina silica with 30% alumina and 70% silica were evaluated for the conversion of methanol to DME. Carbon oxides, ethane, and ethylene were the byproducts of methanol

conversion to DME at 673 K. More investigations showed that the conversion of methanol to hydrocarbons is initiated by fast and reversible formation of DME and water (Mole and Whiteside, 1982; Wolthuizen et al., 1980). The review study of Spivey (Spivey, 1991) confirms such a statement. Bandiera and Naccache (1991) investigated the kinetic of methanol dehydration over H-mordenite catalyst. They conducted the experiments in a fixed bed reactor at atmospheric pressure and a temperature range of 473–573 K. The obtained data confirmed the hypothesis of dual-site catalysis. In fact, a Brønsted acid site is responsible for the formation of $[CH_3 \cdot OH_2]^+$ intermediate, which is then converted to $[CH_3]^+$ and water. The neighbor Lewis basic site forms $[CH_3O]^-$ and $[OH]^-$ intermediates. The combination of two neighbor intermediates (i.e., $[CH_3]^+$ and $[CH_3O]^-$) leads to the production of DME. On the other hand, simultaneous adsorption and dissociation of two methanol molecules with production of DME and water is achieved in a one-step pathway. The competition of DME and water formation with methanol adsorption leads to the methanol kinetic order of less than unity (Bandiera and Naccache, 1991).

Another hypothesis was proposed by Kubelková et al. (1990). Based on their FTIR spectroscopy study on the alumina modified HY and HZSM-5 zeolites, early adsorption of methanol on the zeolite surface is followed by transmission of the zeolitic proton, which leads to the formation of the methoxonium ion (i.e., $[H_3COH_2]^+$). Dehydration of methoxonium ion leaves a methyl group, which is attached to the surface of zeolite and in combination with zeolitic oxygen, generates a methoxy group. The methoxy group could then react with a second methanol molecule to produce DME. Accordingly, a single-site catalysis is implemented. This pathway was then confirmed by density functional theory calculations of Blaszkowski and Van Santen (1995). According to this pathway, the rate determining step (RDS) of DME production from methanol is the dehydration of the first methanol molecule (Blaszkowski and Santen, 1996).

On the other hand, both mechanisms of Langmuir-Hinshelwood and Eley-Rideal are reported in literature. In the Langmuir-Hinshelwood (LH) mechanism, the reaction between two surface intermediates is considered the RDS, while the Eley-Rideal (ER) mechanism proposes the reaction between a surface intermediate and a methanol molecule in the gas phase (Spivey, 1991).

In a further study, Blaszkowski and Santen (1996) demonstrated that the hybrid pathway is possible. In this regard, a parallel reaction pathway composed of two-step single-site paths of Kubelková et al. (1990) and a one-step dual-site path of Bandiera and Naccache (1991) was proposed. More details are provided in the studies of Blaszkowski and Van Santen (1995) and Blaszkowski and Santen (1996).

Xu et al. (1997) conducted an experimental study to investigate the impact of temperature, water content, and catalyst acidity on the catalyst activity and rate of methanol dehydration to DME. In this regard, a series of catalysts with different acidity (i.e., silica content) were

considered. γ-$A1_2O_3$, amorphous alumina silica, H-ZSM-5, and titania-modified zirconia were the evaluated solid-acid catalysts. Water exhibited a strong inhibiting effect on the catalyst's activity with the greatest effect on the γ-Al_2O_3 and a less significant effect on the H-ZSM-5. Such observation is due to active site blockage by water molecules. In fact, the competitive adsorption of water molecules with those of methanol increases by increasing water content. Increasing catalyst acidity was also shown to increase the catalytic activity. Water is preferentially absorbed on the Lewis acid sites and thus, γ-$A1_2O_3$ with strong Lewis acidity is strongly affected by water formation (Fu et al., 2005).

Addition of silica to alumina ratio could strongly affect the performance of a catalyst. Enhanced surface area and increasing surface acidity are the outcomes of increasing silica content in the alumina structure (Yaripour et al., 2005a). Modification of alumina with 6 wt% silica exhibited the best methanol conversion with no hydrocarbon byproduct (Yaripour et al., 2005a). Similar trends were observed in the modification of γ-Al_2O_3 by phosphorus (i.e., alumina phosphate) with an Al/P molar ratio of 2 (Yaripour et al., 2005b). Fu et al. (2005) improved the performance of the γ-Al_2O_3 catalyst by modification. In this regard, γ-Al_2O_3 modified by titanium(IV) sulfate (i.e., $Ti(SO_4)_2$) exhibited great improvement for surface Brønsted acidity and thus, the activity for DME formation. However, improving surface acidity did not make the reaction proceed toward the formation of coke and byproduct hydrocarbons for the temperatures of 513–593 K.

Methanol conversion to DME is mainly attributed to the sites with weak to medium acidity (Yaripour et al., 2005a). Both the Brønsted and Lewis acid sites could be incorporated into the catalysis of methanol to DME reaction (Spivey, 1991). However, the Brønsted acid sites possessing suitable strength are believed to be those responsible for DME formation (Fu et al., 2005). During the dehydration of methanol to DME over the γ-Al_2O_3 catalyst, due to the propensity of the Lewis acid sites' catalyst to adsorb water molecules more than methanol, water is more preferentially involved in the reaction. Such a negative effect leads to the reduction of catalytic activity of methanol and selectivity of DME with increasing water content (i.e., with time on stream). The kinetic data proving the increase in the activation energy with increasing water content confirms the blockage of active sites by water molecules (Vishwanathan et al., 2004). High stability of the H-ZSM-5 catalyst in the presence of water introduces it as a rival for γ-Al_2O_3 (Vishwanathan et al., 2004; Roh et al., 2004; Jun et al., 2003). In fact, the hydrophobic nature of the H-ZSM-5 catalyst is the main reason for stability in the presence of water (Vishwanathan et al., 2004; Jun et al., 2003). H-ZSM-5 with the Si/Al ratio range of 15–25 exhibits excellent catalytic activity and stability in methanol dehydration to DME. Although this catalyst includes strong acid sites, it is resistant toward coke formation because of shape selectivity (Jun et al., 2003). However, the presence of strong acid sites leading to the formation of other hydrocarbons and less for the selectivity for DME is the main disadvantage of this catalyst (Vishwanathan et al., 2004). As mentioned previously, DME formation is mainly caused by the sites with weak or medium

acidity. Brønsted acid sites with suitable strength are believed to be responsible for the selectivity of the catalyst for DME (Fu et al., 2005; Yaripour et al., 2005a). The dealuminated H-Y zeolite with Si/Al ratio of 7.8 shows strong Brønsted surface acidity. Such a characteristic leads to the superiority of side reactions that are responsible for hydrocarbons and coke formation (Fu et al., 2005).

A possible strategy to eliminate the formation of hydrocarbons and thus, to increase the selectivity of H-ZSM-5 for DME up to 100%, is the reduction of the strength of acid sites. Accordingly, in order to avoid the formation of hydrocarbons alongside retaining the stability, a tailored H-ZSM-5 is suggested. In this regard, Vishwanathan et al. (2004) prepared a series of H-ZSM-5 catalysts, which were modified with different contents of sodium (i.e., Na). Sodium content of up to 80 mol% was added to the H-ZSM-5 by the impregnation method. The Na-impregnated H-ZSM-5 catalysts exhibited the optimum activity as well as 100% selectivity for the DME in the whole studied temperature range (i.e., 503–613 K). The water content had no significant effect on the catalyst performance in the reaction time of 65 hours. On the one hand, partial substitution of sodium in the H-ZSM-5 catalyst leads to the elimination of coke and hydrocarbon formation and invariant activity with time on stream. Immutability of such characteristics could potentially lead to the elimination or even reduction of the methanol purifying units and thus, the direct use of crude methanol (i.e., pure and anhydrous methanol containing up to 20 mol% water) for DME manufacturing.

Efforts have been made to adjust the catalyst surface acidity, Brønsted/Lewis acidity ratio, and textural properties of various catalysts with the aim of obtaining higher methanol conversion and DME selectivity and lower hydrocarbons and coke formation (Sabour et al., 2014; Fei et al., 2006; Jin et al., 2007; Kim et al., 2006; Hosseini and Nikou, 2014; Akarmazyan et al., 2014; Said et al., 2014; Dębek et al., 2015; Catizzone et al., 2015; Wei et al., 2015; Rutkowska et al., 2016).

Ion exchange resins (IER) are even applicable in the conversion of methanol to DME. Typical compositions of IER are copolymers of divinyl benzene/styrene in the structure of which sulfonic acid groups are involved (Hosseininejad et al., 2012). These macroreticular resins with macroporous structure were prepared to reduce significantly the limited diffusion by small pores (Kunin et al., 1962). The distinguished characteristic of these resins is the lower required temperature for dehydration reaction. In fact, the dehydration of alcohols could be carried out in the temperature range of 303–423 K (Winterbottom, 1981; Kemball et al., 1981). The activity of these resins for DME production from methanol is obtained by the presence of sulfonic acid groups which are enabling the DME production without the coupled basic sites. In fact, the hydroxyl groups of sulfonic acid sites provide the basic function (Spivey, 1991). Introducing Lewis acid sites to these resins through reaction with boron trifluoride (i.e., BF_3) or aluminum chloride (i.e., $AlCl_3$) could effectively increase the activity for dehydration of alcohols (Spivey, 1991;

Magnotta and Gates, 1977a,b). Different types of IER were evaluated for DME production by Hosseininejad et al. (Hosseininejad et al., 2012). A specific IER, called Amberlyst 35, was, in terms of physical stability and catalytic properties, superior to γ-Al_2O_3 and zeolites.

Water content could strongly affect the performance of IER in the dehydration of alcohols through a dual action process, that is, swelling the resin and participating in the reaction mechanism. On the one hand, water molecules firs open the pores leading to reduction of mass transfer resistance and then compete with the molecules of alcohol to achieve the reaction sites. In methanol dehydration to DME, the swelling phenomenon is inevitable due to water production. However, the intense competition of methanol molecules to achieve the dehydration sites minimizes the inhibition effect of water molecules (Spivey, 1991; Stiles, 1987).

In spite of the obvious achievements in the catalysis of methanol dehydration reaction, there still exist some issues that must be cured. In almost all the cases, the surface acidity of practical catalysts such as γ-alumina and zeolites is adjusted by adding alkaline, alkaline earth, transition, and rare earth metals or even their combinations. Hence, the heat stability of catalysts for long time-on-stream applications in the commercial scale is a cause of worry and thus, is worthy of investigation (Sun et al., 2014).

5 Kinetic Study of Methanol Dehydration

A series of studies have been implemented to determine the rate of methanol dehydration on various catalysts. From a practical point of view, obtaining an intrinsic rate of reaction is of great importance. In fact, accurate evaluations of reactor performance in both pilot and industrial scales strongly depend on the accuracy of reaction rate expressions. The most important kinetic studies are presented in this section.

Gamma type alumina (i.e., γ-Al_2O_3), which is the most studied catalyst for methanol dehydration to DME, was investigated by Bercic and Levec (1992). Their experiments were conducted at 1.46 bar and 563–633 K in a differential fixed-bed reactor. They conducted a kinetic modeling based on the well-known Langmuir-Hinshelwood approach and correlated the experimental results with different kinetic equations. Accordingly, the obtained data was found to be consistent with the hypothesis of surface controlled reaction and dissociative methanol adsorption. The calculated activation energy and heat of methanol and water adsorption were 143.7, 70.5, and 42.1 kJ/mol, respectively. In the further study, the accuracy of kinetic expression was evaluated by applying a mathematical model. The results of numerical simulation were compared with those of experiments in a similar temperature range and 2.1 bar (Bercic and Levec, 1993). Fazlollahnejad et al. (2009) evaluated the accuracy of this kinetic expression by developing a one-dimensional heterogeneous plug flow mathematical model. The numerical results of the model were compared with those of experiments at the temperature range of 543–603 K and 1 atm pressure. A good consistency between the experiments and model was observed.

Mollavali et al. (2008) evaluated the performance of a series of commercial γ-Al_2O_3 catalysts under a practical operating condition (i.e., 573 K, 17 bar, and weight hourly space velocity (WHSV) of 26.07 h^{-1}). In addition to testing the available kinetic expressions against the experiments, a new kinetic expression was developed. In fact, they modified the kinetic model of Lu et al. (2004) by a multiple RDS assumption. The performance of their model was shown to be superior to almost all the previous models. The state of the mass transfer resistance was determined by varying feed flow rate and particle size. Invariant methanol conversion by WHSV showed the insignificant external mass transfer resistances. The catalyst particle sizes of below 0.8 mm did not have a significant effect on the methanol conversion leading to negligible intra-particle resistance. Hence, under the experiments conditions, both internal and external mass transfer resistances were insignificant.

Considering wide ranges of temperature (i.e., 533–653 K), pressure (i.e., 2–17 bar), and feed composition (i.e., 0–20 wt% of water), Moradi et al. (2010) investigated the kinetic behavior of a commercial γ-Al_2O_3 sample for DME production from crude methanol. The hypothesis of negligible heat and mass internal and external resistances were confirmed by varying the feed flow rate and catalyst size during the experiments. A reaction rate expression fitting their experiments better than other available equations was introduced. This expression was a modification of the one presented by Bercic and Levec (1992). According to their statistical analysis, the following order of significance was obtained for the impact of input variables on the DME yield:

$$\text{Temperature} > \text{wt.}\% \text{ of water} > \text{Pressure}$$

In a similar study, Zhang et al. (2011) conducted an experimental procedure to study the methanol dehydration over a commercial Al_2O_3 catalyst in a fixed bed reactor at isothermal condition. They studied temperature, pressure, and liquid hourly space velocity (LHSV) were 513–613 K, 1–10 bar, and 0.9–2.1 h^{-1}, respectively. In addition to the evaluation of available reaction rate expressions, a new one based on LH dissociative adsorption was developed. The temperature and flow rate of the feed stream were shown to have significant impact on the methanol conversion, while the pressure of feed showed little impact. The insignificance of the pressure was in accordance with the previous studies (Moradi et al., 2010).

With the aim of searching for a proper catalyst for commercial methanol dehydration to DME at moderate temperatures (i.e., 383–408 K) and pressures (i.e., up to 9 bar), Hosseininejad et al. (2012) investigated the activity of available solid-acid catalysts such as γ-Al_2O_3, zeolites (HY, HM, and HZSM-5), and IER (Amberlyst 15, Amberlyst 35, Amberlyst 36, and Amberlyst 70) in an autoclave batch. Due to its superiority, Amberlyst 35 was selected for kinetics studies in the absence of mass transfer resistances. Therefore, the dual-site LH model was applied for the reaction rate expression. Their applied mechanism was in accordance with that of Gates and Johanson (1971). As mentioned previously, simultaneous occupation of the adjacent acid sites by two methanol molecules and the inhibiting effect of

water molecules due to adsorption tendency on the acid sites are the principles of this model. This model was found to have the best fit for experimental data of methanol dehydration over the Amberlyst 35 catalyst.

In a comprehensive study, Tavan et al. (2013) showed that the kinetic model of Bercic and Levec (1992) is not valid for methanol dehydration over γ-Al_2O_3 for temperatures below 583 K. Hence, they developed a simple first order equilibrium reaction rate expression by applying their experimental data. This simple model showed unacceptable deviation in the case of HZSM-5 application. They applied the model previously developed by Ha et al. (2011) to fit their experimental data at 485, 505, and 525 K.

There are other efforts in research to develop reaction rate expressions for methanol dehydration over various catalysts. A summary of developed equations is provided in Table 10.4. As can be seen, there is a basic difference between the developed models, which implies the behavior of considered RDS. On the one hand, considering the RDS as an equilibrium limited step leads to appearing the equilibrium constant (i.e., K_{eq}) in the reaction rate expression. In this regard, the equilibrium constant must be considered. The equilibrium constants of methanol dehydration over the γ-Al_2O_3 catalyst were reviewed and modified by Ghavipour and Behbahani (2014). It is worth mentioning that each developed model is the representative of a specific temperature, pressure, and feed composition. On the other hand, none of the models possess the generality to be applied in any desired condition. However, almost all the investigations have a consensus on the negligible impact of pressure on the methanol conversion. As a consequence, considering the consistency between the extent of model and the desired condition of application is essential.

6 Reactors of Methanol Dehydration

Process intensification (PI), which is a novel design approach in chemical industry, is applied to enhance production rate and quality of products alongside reducing energy and feed consumption. Chemical reactors play a vital role in PI (Rossiter, 2003; Smith, 2000). Accordingly, various configurations applied for DME production from methanol are discussed in this section. Conventional systems like fixed bed reactors are reviewed and then, the innovative configurations such as thermally coupled reactors, membrane reactors, and divided wall columns are introduced.

6.1 Fixed Bed Reactors

Fixed beds of catalyst particles are the most prevalent reactor configuration for gas (or vapor) phase reactions in the commercial applications. This prevalence is due to simple operation, lower capital and operating costs, and easy maintenance (Fogler, 1999; Levenspiel and Levenspiel, 1972; Andrigo et al., 1999). There are a number of classifications in practice, but it

Table 10.4 A summary of developed kinetic rate expressions

Catalyst	Rate Expression	Temp. (K)	Pres. (bar)	Feed	Ref.
IER[a]	$-r_M = \frac{k(K_M P_M)^2}{[1 + K_M P_M + K_D P_D + K_W P_W]^2}$	392	1.01325	MeOH + DME + Water + Ar[b]	Gates and Johanson (1971)
IER[c]	$-r_M = \frac{kK_M P_M}{[1 + 2(K_M P_M)^{0.5} + K_D P_D + K_W P_W]^2}$	413	1.01325	MeOH + DME + Water + N[d]	Klusáček and Schneider (1982)
IER[c]	$-r_M = \frac{kK_M P_M^2}{[1 + 2(K_M P_M)^{0.5} + K_D P_D + K_W P_W]^3}$	413	1.01325	MeOH + DME + Water + N[d]	Klusáček and Schneider (1982)
IER[c]	$-r_M = \frac{kK_M P_M^2}{[1 + 2(K_M P_M)^{0.5} + K_D P_D + K_W P_W]^4}$	413	1.01325	MeOH + DME + Water + N[d]	Klusáček and Schneider (1982)
IER[c]	$-r_M = \frac{kK_M P_M}{[1 + 2(K_M P_M)^{0.5} + K_D P_D + K_W P_W]^3}$	413	1.01325	MeOH + DME + Water + N[d]	Klusáček and Schneider (1982)
IER[c]	$-r_M = \frac{k(K_M P_M)^{0.5}}{[1 + 2(K_M P_M)^{0.5} + K_D P_D + K_W P_W]^2}$	413	1.01325	MeOH + DME + Water + N[d]	Klusáček and Schneider (1982)
IER[c]	$-r_M = \frac{k(K_M P_M)^{0.5}}{[1 + 2(K_M P_M)^{0.5} + K_D P_D + K_W P_W]}$	413	1.01325	MeOH + DME + Water + N[d]	Klusáček and Schneider (1982)
SiO_2–Al_2O_3	$-r_M = \frac{kK_M P_M^{0.5}}{[1 + K_M P_M{}^{0.5} + K_W P_W]}$	433	–	MeOH + Water	Figueras et al. (1971)
γ-Al_2O_3	$-r_M = \frac{kK_M^2 [C_M^2 - (C_D C_W / K_{eq})]}{[1 + 2(K_M C_M)^{0.5} + K_W C_W]^4}$	563–633	1.46	MeOH + Water	Bercic and Levec (1992)
γ-Al_2O_3	$-r_M = \frac{kK_M^2 [P_M^2 - (P_D P_W / K)]}{[1 + 2(K_M P_M)^{0.5} + K_W P_W]^4}$	543–643	2–17	MeOH + Water	Mollavali et al. (2008)
γ-Al_2O_3	$-r_M = \frac{k[P_M - (P_D P_W / K_{eq} P_M)]}{[1 + K_M P_M + K_W^{-1} P_W]}$	543–643	2–17	MeOH + Water	Mollavali et al. (2008)
γ-Al_2O_3	$-r_M = \frac{k(K_M C_M)^2}{[1 + K_M C_M + K_W C_W]^2}$	533–653	2–17	MeOH + Water	Moradi et al. (2010)

Continued

Table 10.4 A summary of developed kinetic rate expressions—cont'd

Catalyst	Rate Expression	Temp. (K)	Pres. (bar)	Feed	Ref.
γ-Al_2O_3	$-r_M = \frac{k(K_M C_M)^2}{\left[1 + 2(K_M C_M)^{0.5} + K_W C_W\right]^4}$	533–653	2–17	MeOH + Water	Moradi et al. (2010)
γ-Al_2O_3	$-r_M = \frac{k(K_M C_M)^2}{\left[1 + 2(K_M C_M)^{2/3} + K_W C_W\right]^3}$	533–653	2–17	MeOH + Water	Moradi et al. (2010)
Commercial Al_2O_3	$-r_M = \frac{kP_M\left[1 - \left(P_D P_W / K_{eq} P_M^2\right)\right]}{\left[1 + (K_M P_M)^{0.5} + K_W P_W\right]^2}$	513–613	1–10	Pure MeOH	Zhang et al. (2011)
IER[e]	$-r_D = \frac{k(K_M C_M)^2}{\left[1 + K_M C_M + (K_W C_W)^n\right]^m}$	383–408	9	MeOH + Water + THF[f]	Hosseininejad et al. (2012)
IER[e]	$-r_D = \frac{k(K_M C_M)^2}{\left[1 + K_M C_M + K_W C_W + K_D C_D\right]^2}$	343–403	8.2	MeOH + Water + *o*-Xylene	An et al. (2004)
IER[e]	$-r_D = \frac{k(K_M C_M)^2}{\left[1 + K_M C_M + K_W C_W + K_D C_D\right]}$	343–403	8.2	MeOH + Water + *o*-Xylene	An et al. (2004)
γ-Al_2O_3	$-r = k_1 C_M - k_2 C_W$	485–525	1	Pure MeOH	Tavan et al. (2013)
HZSM-5	$-r = \frac{kK_M P_M\left[1 - \left(P_D P_W / K_{eq} P_M^2\right)\right]}{\left[1 + K_M P_M + K_W P_W\right]}$	485–525	1	Pure MeOH	Tavan et al. (2013)
Clinoptilolite	$-r_M = \frac{k(K_M P_M)^2 - k' K_W P_D P_W}{\left[1 + K_M P_M + K_W P_W + K_N K_M P_M^{m+1} + K_{NN} K_M P_M P_W^{n+1}\right]^2}$	583–623	1	MeOH + N[d]	Royaee et al. (2008)
Commercial γ-Al_2O_3	$-r_M = k f_M^{0.55}\left[1 - \frac{f_D f_W}{K_{eq} f_M^2}\right]$	513–613	1–10	Pure MeOH	Li et al. (2009)

[a]Polystyrene sulfonic acid.
[b]Argon.
[c]Macroreticular sulfonated styrene divinyl benzene copolymer (25% divinyl benzene).
[d]Nitrogen.
[e]Amberlyst 35.
[f]Tetrahydrofuran.

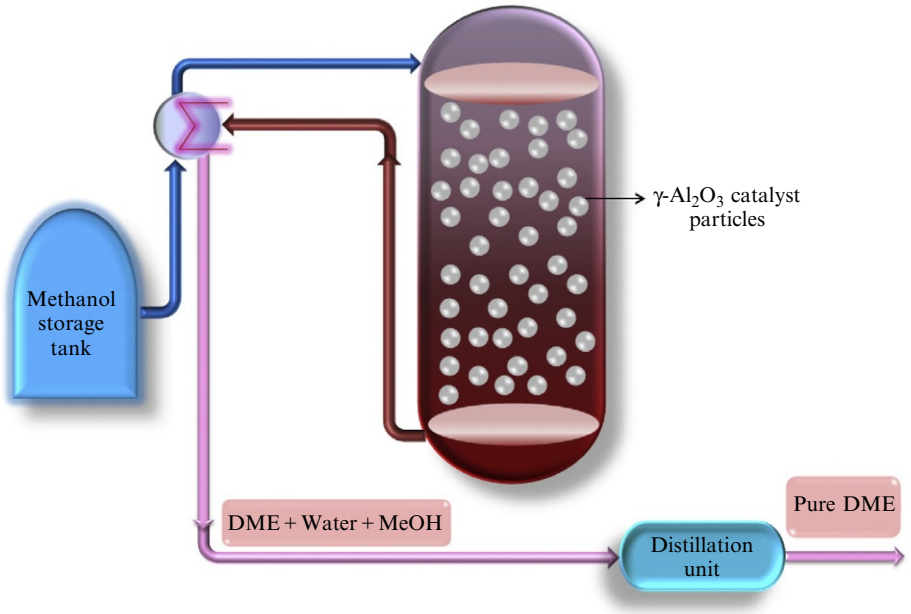

Fig. 10.1
Schematic diagram of adiabatic DME reactor.

is common to classify the fixed bed reactors according to adiabatic or non-adiabatic operation. For the reactions with low to medium heat of reaction, the adiabatic operation is suggested (Froment and Bischoff, 1979). In fact, adiabatic operation is utilized in the case of the insignificant effect of temperature rise on the selectivity or yield of desired product. Such a condition appears in the reaction with a small heat of reaction or systems with a single reaction pattern. In adiabatic operation, the catalyst particles are surrounded by an outer insulation layer preventing heat loss (Andrigo et al., 1999). The adiabatic operation for methanol dehydration is schematically presented in Fig. 10.1. In the adiabatic fixed bed reactors, it is possible to employ the optimum axial temperature profile from the upper section to the lower section. In fact, in the upper section of the reactor (i.e., reactor entrance), due to fresh feed and catalyst, the rate of reaction is high. Through the reactor length, the driving force of reaction decreases due to the consumption of reactants and generation of products and thus, the rate of reaction tends to decrease. Increasing temperature due to the exothermic nature of methanol dehydration leads to the increasing of the reaction rate and compensates for the fall in the driving force.

Plenty of studies investigated the different aspects of the fixed bed methanol dehydration reactor. The commercial reactor of methanol dehydration over the γ-Al_2O_3 catalyst equipped with a feed preheater was numerically simulated under dynamic condition (Farsi et al., 2011a). They employed a heterogeneous one dimensional unsteady state mathematical model to

evaluate the performance of the reactor. To examine the accuracy of the proposed model, the numerical results were compared with the output data of a commercial DME reactor at a steady state condition. It was claimed that the kinetic model of Bercic and Levec (1992) was employed. By implementing a sensitivity analysis, the impact of possible disturbances on the DME production was determined. A feedback proportional/integral/derivative (PID) controller was employed to investigate the controllability of the process. It was shown that by applying a 10 K increase in the input temperature, the response at the output is observed with a time delay of about 15 seconds and the new steady state condition is established after about 50 seconds and about a 8 K increase in the output temperature was observed. The change in the output DME molar fraction was negligible. Decreasing output temperature and DME molar fraction with decreasing input molar fraction of methanol and tiny effect of input pressure change are the results of their simulation study.

Tavan and Hosseini (2013) conducted a simulation study to evaluate the vapor phase of DME production and cost analysis in a process with a fixed bed reactor of the HZSM-5 catalyst. They employed the Hysys simulation package and the kinetic expression developed in their previous study (Tavan et al., 2013). Based on their cost analysis, the major part of the capital investment in the conventional DME process pertains to the distillation towers of the purifying step.

In order to obtain the optimum condition for DME production, a number of numerical studies were carried out by different authors. In this regard, sensitivity analysis or optimization procedures were employed. Numerical simulations by solving the governing equations or computational fluid dynamic calculations were the applied tools (Ghavipour and Behbahani, 2014; Golshadi et al., 2013; Alavi et al., 2013). The modified process of DME production was well investigated by Bai et al. (2013). They employed the PRO/II platform to simulate the reaction section and further rectifying the section of process. The results were compared with a set of real plant data collected from an industrial DME plant with 200,000 tons per year production capacity. By further investigation, they determined the suitable feed stages and reflux ratios in the rectifying section. Then, the optimum operating condition for desired product purity was obtained.

In a recent study, Hamidi et al. (2015) proposed a new system of DME production with an adsorptive agent for in-situ water removal from the reacting mixture. A schematic diagram of this system is well presented in Fig. 10.2. The interesting feature of this system is the shifting of the equilibrium reaction toward higher methanol conversion due to the elimination of water from the reacting mixture. Zeolite 4A was employed for in-situ water adsorption. The difference between this system and the commercial one is the flowing adsorbent particles. These particles are continuously regenerated and fed to the fixed catalyst bed. More than an 11% increase in the DME production capacity was reported.

Although the tubular structure of fixed bed reactors is conventional, some drawbacks such as high pressure drop and low production capacity impose extra charges and limit the applications.

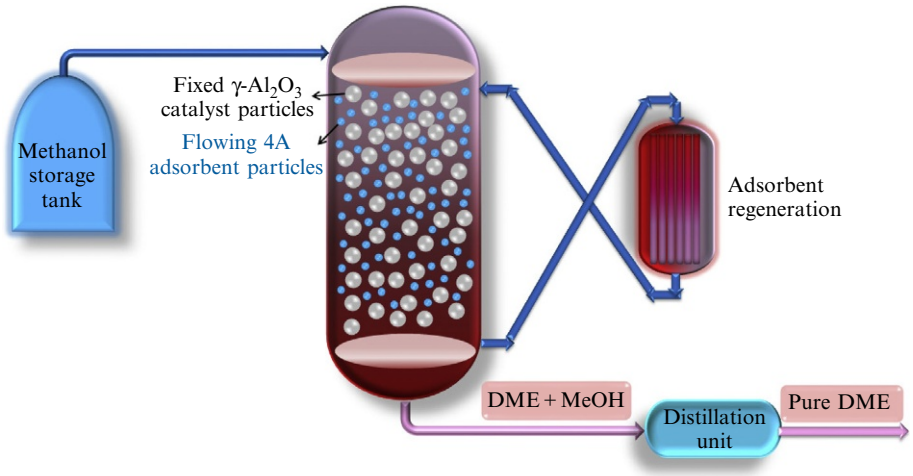

Fig. 10.2
Schematic diagram of adiabatic DME reactor with in-situ water adsorption.

To avoid such drawbacks, spherical fixed bed reactors are promising alternatives. The reacting mixture could flow axially through the catalyst bed (Farsi et al., 2014; Samimi et al., 2013a, 2014a). Fig. 10.3 shows the schematic diagram of the axial flow spherical fixed bed reactor for DME production from methanol. As shown, catalyst particles are loaded into the space between two perforated plates in the upper and lower sections of the reactor. The perforated plates have the role of mechanical supports beside the uniform feed distribution. As stated by Samimi et al. (2014a), utilizing catalyst particles with a smaller size and thus, a higher effectiveness factor, is a major advantage of spherical fixed bed reactors. In fact, due to a lower

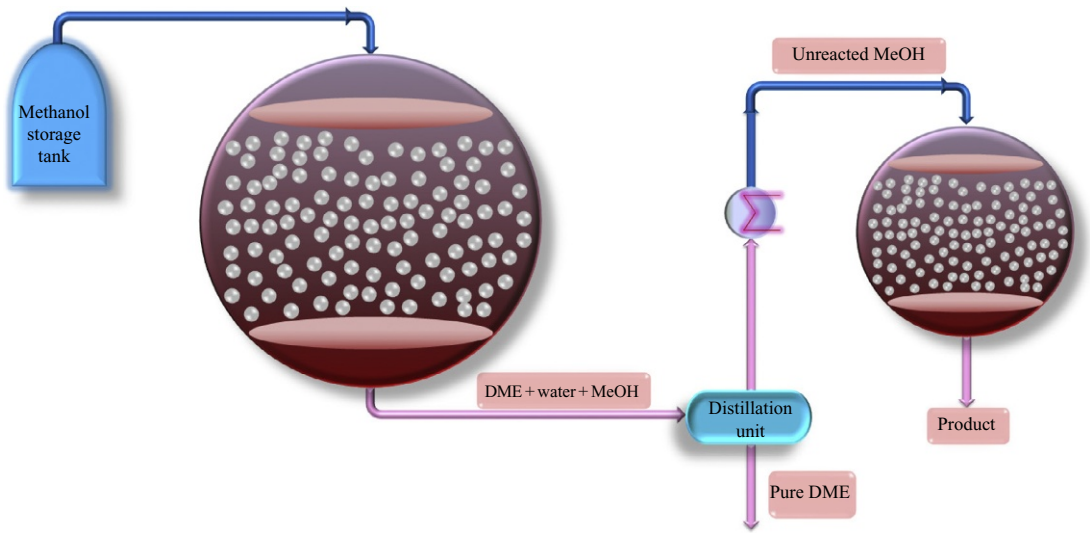

Fig. 10.3
Schematic diagram of axial flow spherical fixed bed DME reactor.

pressure drop in such a structure, the application of smaller pellets is possible. The lower pressure drop allows for the injecting of higher feed flow rates, leading to higher production capacity. Therefore, the cost of recompression is effectively reduced. Lower wall thickness is the other advantage of spherical fixed bed reactors leading to lower capital cost (Farsi et al., 2014; Samimi et al., 2013a, 2014a). Based on the rearch, spherical fixed bed reactors are economically more favorable than the tubular ones (Farsi et al., 2014; Samimi et al., 2013a, 2014a; Hartig and Keil, 1993). The capability of multi stage spherical fixed bed configurations for DME production was examined by different authors (Farsi et al., 2014; Samimi et al., 2013a, 2014a). They all claimed that the kinetic model of Bercic and Levec (1992) for the rate of reaction on γ-Al_2O_3 was employed in their simulations. More than a 16% increase in the DME production capacity was reported by two series spherical reactors working under optimum conditions (Samimi et al., 2014a).

6.2 Membrane Assisted and Thermally Coupled Reactors

Based on the PI approach, process integration could lead to a considerable decrease in the process costs and even an increase in energy efficiency. Hence, the recuperative multifunctional reactors are introduced. Membrane assisted reactors and integrated thermally coupled reactors (TCR) are types of these.

Membranes play an important role in the implementation of PI strategy by novel design and process development techniques aimed at reducing process costs, equipment size, and energy requirements (Bernardo et al., 2009). Membranes are well developed in the theoretical studies for in-situ separation of products from the reaction media. Such a strategy could result in higher yield and selectivity of products. Due to the elimination of products from the reacting mixture, the equilibrium conversion is enhanced. Hence, higher conversion is achieved. In addition to the reaction proceeding toward a higher conversion of feedstocks, highly energy efficient separation is implemented. Therefore, energy extensive separation units such as distillation are significantly reduced or even become smaller. Conventional separation units such as distillation utilizes the phase change and thus, require heat exchanger facilities. Accordingly, in-situ membrane separation eliminates such facilities. In a general point of view, membrane separation competes with almost all the conventional separation techniques based on the overall economy, process safety, environmental issues, and technical aspects (Bernardo et al., 2009; Bernardo and Clarizia, 2013; Rahimpour, 2015a,b).

In the methanol dehydration to DME, water is produced as an undesired product. As mentioned previously, the presence of water to the catalyst surface has a negative effect on the methanol access to the acidic sites. If water vapor is selectively eliminated from the reacting mixture, loss of catalyst activity may be prevented and thus, enhanced product yield would be obtained. Furthermore, the DME purifying step is omitted or even becomes smaller (Samimi et al., 2013a; Sea and Lee, 2006). The flowing sweep gas around the catalyst bed

could capture the generated heat of reaction and hence, increase the equilibrium conversion. The capability of water selective membranes to enhance the production rate of reactions was widely studied in the reacting systems containing water vapor (Rohde et al., 2008; Khajavi et al., 2010). In the current status, hydrophilic membranes such as amorphous silica, hydroxy sodalite (H-SOD), polymers, ZMS-5, F-4SF resin, MOR, and SIL are the candidates for water removal from reaction media. Based on the work of Rohde et al. (2006, 2008), amorphous silica membranes showed low hydrothermal stability and perm-selectivity. Blocking of the pores due to wax deposition is a common occurrence in polymeric membranes. The low thermal resistance of polymeric membranes limits their application (Gascon et al., 2012; Téllez and Menéndez, 2011). Microporous zeolites were shown to be, in terms of permeation rate and perm-selectivity, superior to both amorphous silica and polymer membranes (Iliuta et al., 2010). H-SOD, which is a zeolite type membrane, found application in the water removal due to outstanding characteristics such as almost a 100% selectivity for water in the mixtures of hydrogen and carbon oxides and appropriate thermal and mechanical stabilities. Small molecules such as water (kinetic diameter is 2.68 °A) are efficiently separated by H-SOD membranes (Rohde et al., 2006, 2008).

In order to develop the idea of utility of spherical reactors, Samimi et al. (2013a) proposed an axial flow fixed bed spherical reactor equipped with an H-SOD membrane for DME production. They developed a mathematical model for the evaluation of this system. It was claimed that the kinetic model of Bercic and Levec (1992) was employed. As a result of water removal during the reaction, higher methanol conversion was obtained. The new configuration working under optimum condition produced a product stream with more than a 13% increase in the molar fraction of DME.

The integrity of water perm-selective membranes with the TCR is currently state of the art. In fact, the idea of water elimination from the reaction media is well developed in the theoretical studies of TCR. TCR is akin to shell and tube heat exchangers. The difference is in the contents of hot and cold regions. A reacting system undergoing exothermic reactions plays the role of heat source, while the cold side contains a reacting system with endothermic reactions. Hence, autothermality and energy saving is managed in the system (Rahimpour et al., 2012b). In the case of equilibrium reactions, heat transfer could enhance the equilibrium conversion in both reaction sides. A schematic diagram of a shell and tube heat exchanger reactor for simultaneous production of DME and methyl formate (MF) is presented in Fig. 10.4. Since methanol dehydration is an exothermic reaction, it could be coupled with endothermic reactions, such as dehydrogenation of organic compounds. In a theoretical study of a novel recuperative configuration, methanol dehydration coupled with the dehydrogenation of cyclohexane (Farsi et al., 2010, 2011b). The heat generated by methanol dehydration in the hot side provides the required heat for dehydrogenation reaction. In addition to production of diverse compounds such as benzene and hydrogen, higher conversion of methanol and DME molar fraction were obtained.

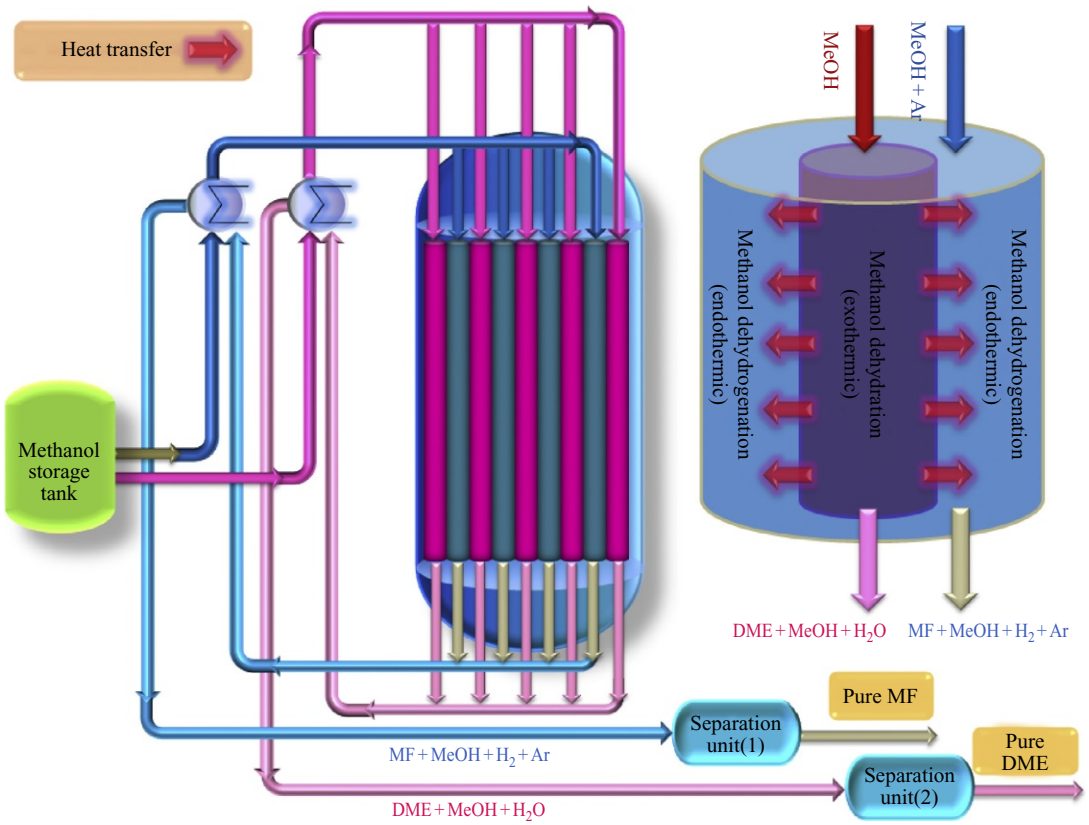

Fig. 10.4
Schematic diagram of thermally coupled reactor of DME and MF.

Integrity of water perm-selective membranes with the thermally coupled reactors for DME production is an interesting field of study. In this regard, a thermally coupled reactor equipped with two distinct membranes was proposed by Samimi et al. (2013b). Dehydrogenation of decalin was proposed as the endothermic reaction. In addition to autothermality, water elimination by H-SOD membrane was applied. Furthermore, the generated hydrogen was aimed to be eliminated by a palladium/silver membrane (Itoh, 1987). A considerable increase in the DME production rate was reported. The concept of double thermally coupling was introduced in their further study (Samimi et al., 2014b), in which two exothermic reactions (i.e., methanol and DME synthesis) were applied for the heat source of endothermic reaction (i.e., dehydrogenation of methyl cyclohexane). By applying H-Sod membrane for in-situ water removal, considerable increases in methanol conversion and DME molar fraction were reported.

In a series of studies, simultaneous production of DME and MF from pure methanol feedstock was theoretically investigated by Bakhtyari et al. (2015, 2016a,b). In the first work, the

TCR with exothermic methanol dehydration to DME and endothermic methanol dehydrogenation to MF was proposed (Bakhtyari et al., 2015). Furthermore, the impact of hydrogen separation from the endothermic side was investigated. Through the sensitivity analysis, impacts of various operating conditions were determined. Enhancement of methanol conversion to 85% and 87% were obtained by TCR and TCR with hydrogen separation, respectively. In a further study, a heat exchanger reactor equipped with two distinct membranes for simultaneous conversion of methanol to DME and MF as well as in-situ separation of water vapor and hydrogen was numerically simulated (Bakhtyari et al., 2016b). The optimum operating condition was obtained by an optimization procedure. Hence, the proposed system operating under optimum condition enhanced the methanol conversion to DME to 95.1% and methanol conversion to MF to 99.6%. Such conditions provided a high purity of desired compounds in the product streams. The interesting feature of these two systems was multi production, i.e., production of diverse value-added compounds from a single feedstock. The concept of double thermally coupling was proposed by introducing the syngas to DME as the second exothermic reaction in the system (Bakhtyari et al., 2016a). In this regard, two DME production reactions (i.e., methanol to DME and syngas to DME) provided the heat sources of methanol dehydrogenation reaction. H-SOD membrane was applied to remove water from both DME synthesis reactions. The advancements of this study were 97%, 66%, and 17% conversion of methanol to DME, conversion of methanol to MF, and hydrogen conversion, respectively. The structure of this reactor is schematically shown in Fig. **10.5**. In these studies, the kinetic expression of Bai et al. (2013) was applied for methanol to DME reaction.

It is worth mentioning that the advancements of TCR and membrane assisted TCR that were reported in the literature show the feasibility of these processes. However, more investigations and economic assessments are required to determine the capabilities and operability of such standpoint in the practical large-scale applications.

6.3 Reactive Distillation

Reactive or catalytic distillation is a combination of reaction and separation units. Such an approach is efficient in methanol dehydration due to higher conversion, higher selectivity for DME, and lower process costs (Azizi et al., 2014; Tavan and Hosseini, 2013; Kiss, 2011). The advantageous feature of catalytic distillation is moderate operating conditions, that is, 313–453 K and 8–12 bar. However, the available catalysts of methanol dehydration suffer from very low activity in this temperature range. In fact, the selective catalysts of DME such as zeolites tend to be active in temperatures above 523 K. IERs are the promising alternatives for the operation in the lower temperatures. Therefore, developing highly selective catalysts that are active in the suitable temperature range for reactive distillation is currently of a great interest. Thermally coupled distillation towers, dividing wall towers, and cyclic distillation are the modified reactive distillation strategies that are proposed to decrease energy consumption

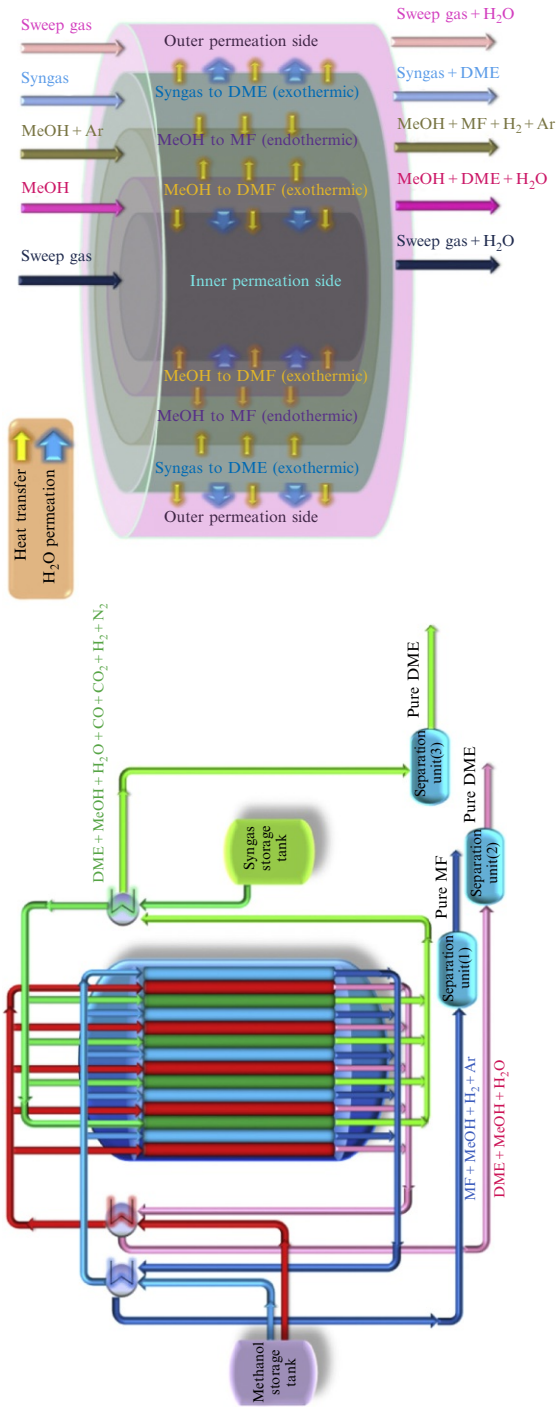

Fig. 10.5
Schematic diagram of thermally double coupled double membrane reactor of DME and MF.

(Olujić et al., 2009; Harmsen, 2010; Dejanović et al., 2010). Divided wall columns have found application due to simultaneous separation of various components in a single system and thus, decreasing the cost of multiple system separation. It was estimated that by utilizing the technology of divided wall columns, up to a 30% decrease in the capital cost, up to a 40% decrease in the operating cost, and up to a 30% decrease in energy consumption is managed (Tavan and Hosseini, 2013; Harmsen, 2010; Isopescu et al., 2008). Tavan and Hosseini (2013) reported more than a 44% decrease in the operating costs of a DME production unit applying a divided wall column.

7 Conclusions and Future Trends

The present contribution investigated the conventional route for DME production, that is, methanol dehydration, from different points of view such as chemistry, kinetics, available reactor configurations, and process intensification. Although the commercial units employ this route for large scale production, it is evident that a large number of research is devoted to the investigation of syngas to DME process. Currently, hybrid catalysts are attracting attention due to the elimination of intermediate facilities of methanol purification. Economic assessment of recuperative alternatives is also necessary. It is obvious that the profitability of DME manufacturing strongly depends on the feedstock. Hence, extensive research is required to determine the efficient process and economics of DME production from various feedstocks such as natural gas, syngas, carbon dioxide rich syngas, coal, and biomass. In the current status, developing the roots of DME production from bio based material (i.e., biomass and bio-oil) is being given a great deal of attention (Wang et al., 2016; Higo and Dowaki, 2010; Peral and Martín, 2015; Chang et al., 2012; Parvez et al., 2016). Providing such technology could lead to higher profitability. Consequently, green chemistry is the irrefutable future of chemical processes like DME production.

References

Abdoulmoumine, N., et al., 2015. A review on biomass gasification syngas cleanup. Appl. Energy 155, 294–307.

Adkins, H., Perkins, P.D., 1928. The behavior of methanol over aluminum and zinc oxides. J. Phys. Chem. 32 (2), 221–224.

Afroz, H.M.M., Miyara, A., Tsubaki, K., 2008. Heat transfer coefficients and pressure drops during in-tube condensation of CO_2/DME mixture refrigerant. Int. J. Refrig. 31 (8), 1458–1466.

Akarmazyan, S.S., et al., 2014. Methanol dehydration to dimethylether over Al_2O_3 catalysts. Appl. Catal. B Environ. 145, 136–148.

Alavi, M., Jazayeri-rad, H., Behbahani, R., 2013. Optimizing the feed conditions in a DME production process to maximize the methanol conversion. Sci. Technol. 3 (2), 61–66.

Al-Dughaither, A.S., de Lasa, H., 2014. Neat dimethyl ether conversion to olefins (DTO) over HZSM-5: effect of SiO_2/Al_2O_3 on porosity, surface chemistry, and reactivity. Fuel 138, 52–64.

An, W., Chuang, K.T., Sanger, A.R., 2004. Dehydration of methanol to dimethyl ether by catalytic distillation. Can. J. Chem. Eng. 82 (5), 948–955.

Andrigo, P., Bagatin, R., Pagani, G., 1999. Fixed bed reactors. Catal. Today 52 (2), 197–221.
Arcoumanis, C., et al., 2008. The potential of di-methyl ether (DME) as an alternative fuel for compression-ignition engines: a review. Fuel 87 (7), 1014–1030.
Azizi, Z., et al., 2014. Dimethyl ether: a review of technologies and production challenges. Chem. Eng. Process. Process Intensif. 82, 150–172.
Bai, Z., et al., 2013. Process simulation of dimethyl ether synthesis via methanol vapor phase dehydration. Pol. J. Chem. Technol. 15 (2), 122–127.
Bakhtyari, A., Mohammadi, M., Rahimpour, M.R., 2015. Simultaneous production of dimethyl ether (DME), methyl formate (MF) and hydrogen from methanol in an integrated thermally coupled membrane reactor. J. Nat. Gas Sci. Eng. 26, 595–607.
Bakhtyari, A., Haghbakhsh, R., Rahimpour, M.R., 2016a. Investigation of thermally double coupled double membrane heat exchanger reactor to produce dimethyl ether and methyl formate. J. Natural Gas Sci. Eng. 32, 185–197.
Bakhtyari, A., Parhoudeh, M., Rahimpour, M.R., 2016b. Optimal conditions in converting methanol to dimethyl ether, methyl formate, and hydrogen utilizing a double membrane heat exchanger reactor. J. Nat. Gas Sci. Eng. 28, 31–45.
Bakhtyari, A., Darvishi, A., Rahimpour, M., 2016c. A heat exchanger reactor equipped with membranes to produce dimethyl ether from syngas and methyl formate and hydrogen from methanol. Int. J. 3 (2), 65.
Bandiera, J., Naccache, C., 1991. Kinetics of methanol dehydration on dealuminated H-mordenite: model with acid and basic active centres. Appl. Catal. 69 (1), 139–148.
Bercic, G., Levec, J., 1992. Intrinsic and global reaction rate of methanol dehydration over gamma-alumina pellets. Ind. Eng. Chem. Res. 31 (4), 1035–1040.
Bercic, G., Levec, J., 1993. Catalytic dehydration of methanol to dimethyl ether. Kinetic investigation and reactor simulation. Ind. Eng. Chem. Res. 32 (11), 2478–2484.
Bernardo, P., Clarizia, G., 2013. 30 years of membrane technology for gas separation. Chem. Eng. 32.
Bernardo, P., Drioli, E., Golemme, G., 2009. Membrane gas separation: a review/state of the art. Ind. Eng. Chem. Res. 48 (10), 4638–4663.
Blaszkowski, S.R., Santen, R.A.v., 1996. The mechanism of dimethyl ether formation from methanol catalyzed by zeolitic protons. J. Am. Chem. Soc. 118 (21), 5152–5153.
Blaszkowski, S., Van Santen, R., 1995. Density functional theory calculations of the activation of methanol by a Brønsted zeolitic proton. J. Phys. Chem. 99 (30), 11728–11738.
Catizzone, E., et al., 2015. Dimethyl ether synthesis via methanol dehydration: effect of zeolite structure. Appl. Catal. A Gen. 502, 215–220.
Chang, C.D., 1983. Hydrocarbons from methanol. Catal. Rev. Sci. Eng. 25 (1), 1–118.
Chang, J., Fu, Y., Luo, Z., 2012. Experimental study for dimethyl ether production from biomass gasification and simulation on dimethyl ether production. Biomass Bioenergy 39, 67–72.
Cousins, D.S., Laesecke, A., 2012. Sealed gravitational capillary viscometry of dimethyl ether and two next-generation alternative refrigerants. J. Res. Natl. Inst. Stan. Technol. 117, 231.
Curphey, T., 1971. Trimethyloxonium tetrafluoroborate. Org. Synth. 142.
De Falco, M., Capocelli, M., Centi, G., 2016. Dimethyl ether production from CO_2 rich feedstocks in a one-step process: thermodynamic evaluation and reactor simulation. Chem. Eng. J. 294, 400–409.
Dębek, R., et al., 2015. Dehydration of methanol to dimethyl ether over modified vermiculites. C. R. Chim. 18 (11), 1211–1222.
Dejanović, I., Matijašević, L., Olujić, Ž., 2010. Dividing wall column—a breakthrough towards sustainable distilling. Chem. Eng. Process. Process Intensif. 49 (6), 559–580.
Ding, O., Chan, S., 2008. Autothermal reforming of methane gas—modelling and experimental validation. Int. J. Hydrog. Energy 33 (2), 633–643.
Dissanayake, D., et al., 1991. Partial oxidation of methane to carbon monoxide and hydrogen over a Ni/Al_2O_3 catalyst. J. Catal. 132 (1), 117–127.
Farniaei, M., et al., 2014. Syngas production in a novel methane dry reformer by utilizing of tri-reforming process for energy supplying: modeling and simulation. J. Nat. Gas Sci. Eng. 20, 132–146.

Farsi, M., et al., 2010. Novel recuperative configuration for coupling of methanol dehydration to dimethyl ether with cyclohexane dehydrogenation to benzene. Ind. Eng. Chem. Res. 49 (10), 4633–4643.
Farsi, M., Eslamloueyan, R., Jahanmiri, A., 2011a. Modeling, simulation and control of dimethyl ether synthesis in an industrial fixed-bed reactor. Chem. Eng. Process. Process Intensif. 50 (1), 85–94.
Farsi, M., et al., 2011b. Optimal conditions for hydrogen production from coupling of dimethyl ether and benzene synthesis. Int. J. Hydrog. Energy 36 (1), 299–310.
Farsi, M., Asemani, M., Rahimpour, M., 2014. Mathematical modeling and optimization of multi-stage spherical reactor configurations for large scale dimethyl ether production. Fuel Process. Technol. 126, 207–214.
Fazlollahnejad, M., et al., 2009. Experimental study and modeling of an adiabatic fixed-bed reactor for methanol dehydration to dimethyl ether. Chin. J. Chem. Eng. 17 (4), 630–634.
Fei, J., et al., 2006. Synthesis of dimethyl ether (DME) on modified HY zeolite and modified HY zeolite-supported Cu–Mn–Zn catalysts. Appl. Catal. A Gen. 304, 49–54.
Figueras, F., et al., 1971. Dehydration of methanol and tert-butyl alcohol on silica-alumina. Trans. Faraday Soc. 67, 1155–1163.
Fleisch, T.H., Meurer, P.C., 1995. DME: the diesel fuel for the 21st century? In: AVL Conference on Engine and Environment.
Fleisch, T.H., et al., 1997. Dimethyl ether: a fuel for the 21st century. In: de Pontes, R.L.E.C.P.N.J.H.S.M., Scurrell, M.S. (Eds.), Surface Science and Catalysis. Elsevier, London, United Kingdom, pp. 117–125.
Fleisch, T.H., Basu, A., Sills, R.A., 2012. Introduction and advancement of a new clean global fuel: the status of DME developments in China and beyond. J. Nat. Gas Sci. Eng. 9, 94–107.
Fogler, H.S., 1999. Elements of chemical reaction engineering. Prentice Hall, New Jersey, United States.
Froment, G.F., Bischoff, K.B., 1979. Chemical reactor analysis and design. Wiley, Hoboken, NJ, United States.
Fu, Y., et al., 2005. Surface acidity and the dehydration of methanol to dimethyl ether. Thermochim. Acta 434 (1), 22–26.
Gascon, J., et al., 2012. Practical approach to zeolitic membranes and coatings: state of the art, opportunities, barriers, and future perspectives. Chem. Mater. 24 (15), 2829–2844.
Gates, B., Johanson, L., 1971. Langmuir-hinshelwood kinetics of the dehydration of methanol catalyzed by cation exchange resin. AIChE J. 17 (4), 981–983.
Ghavipour, M., Behbahani, R.M., 2014. Fixed-bed reactor modeling for methanol to dimethyl ether (DME) reaction over γ-alumina using a new practical reaction rate model. J. Ind. Eng. Chem. 20 (4), 1942–1951.
Golshadi, M., Mosayebi Behbahani, R., Irani, M.R., 2013. CFD simulation of dimethyl ether synthesis from methanol in an adiabatic fixed-bed reactor. Iranian J. Oil Gas Sci. Technol. 2 (2), 50–64.
Granryd, E., 2001. Hydrocarbons as refrigerants—an overview. Int. J. Refrig. 24 (1), 15–24.
Ha, K.-S., et al., 2011. New reaction pathways and kinetic parameter estimation for methanol dehydration over modified ZSM-5 catalysts. Appl. Catal. A Gen. 395 (1), 95–106.
Hafizi, A., Rahimpour, M., Hassanajili, S., 2016. Hydrogen production by chemical looping steam reforming of methane over Mg promoted iron oxygen carrier: optimization using design of experiments. J. Taiwan Inst. Chem. Eng. 62, 140–149.
Hamidi, M., Samimi, F., Rahimpour, M., 2015. Dimethyl ether synthesis in a gas–solid–solid trickle flow reactor with continuous adsorbent regeneration. J. Taiwan Inst. Chem. Eng. 47, 105–112.
Harmsen, J., 2010. Process intensification in the petrochemicals industry: drivers and hurdles for commercial implementation. Chem. Eng. Process. Process Intensif. 49 (1), 70–73.
Hartig, F., Keil, F.J., 1993. Large-scale spherical fixed bed reactors: modeling and optimization. Ind. Eng. Chem. Res. 32, 424.
Haugaard, J., Voss, B., 2001. Process for the synthesis of a methanol/dimethyl ether mixture from synthesis gas. Google Patents.
Higo, M., Dowaki, K., 2010. A life cycle analysis on a bio-DME production system considering the species of biomass feedstock in Japan and Papua New Guinea. Appl. Energy 87 (1), 58–67.
Hosseini, S.Y., Nikou, M.R.K., 2014. Investigation of different precipitating agents effects on performance of γ-Al_2O_3 nanocatalysts for methanol dehydration to dimethyl ether. J. Ind. Eng. Chem. 20 (6), 4421–4428.

Hosseininejad, S., Afacan, A., Hayes, R., 2012. Catalytic and kinetic study of methanol dehydration to dimethyl ether. Chem. Eng. Res. Des. 90 (6), 825–833.
Idemitsu process uses DME to produce olefins, BTX. Focus on Catalysts, 2007. 2007(10), 6.
Iliuta, I., Larachi, F., Fongarland, P., 2010. Dimethyl ether synthesis with in situ H_2O removal in fixed-bed membrane reactor: model and simulations. Ind. Eng. Chem. Res. 49 (15), 6870–6877.
Isopescu, R., Woinaroschy, A., Draghiciu, L., 2008. Energy reduction in a divided wall distillation column. Rev. Chim. 59 (1), 812–815.
Itoh, N., 1987. A membrane reactor using palladium. AIChE J. 33 (9), 1576–1578.
Jin, D., et al., 2007. Dimethyl ether synthesis via methanol and syngas over rare earth metals modified zeolite Y and dual Cu–Mn–Zn catalysts. Fuel 86 (17), 2707–2713.
Jun, K.-W., et al., 2003. Highly water-enhanced H-ZSM-5 catalysts for dehydration of methanol to dimethyl ether. Bull.-Korean Chem. Soc. 24 (1), 106–108.
Kanda, H., Li, P., 2011. Simple extraction method of green crude from natural blue-green microalgae by dimethyl ether. Fuel 90 (3), 1264–1266.
Kanda, H., et al., 2012. Lipids extracted from several species of natural blue-green microalgae by dimethyl ether: extraction yield and properties. Fuel 95, 88–92.
Kanda, H., et al., 2013. Wet extraction of hydrocarbons from *Botryococcus braunii* by dimethyl ether as compared with dry extraction by hexane. Fuel 105, 535–539.
Kemball, C., Dowden, D., Winterbottom, J., 1981. Hydration and dehydration by heterogeneous catalysts. The Royal Society of Chemistry, London, United Kingdom.
Khajavi, S., Jansen, J.C., Kapteijn, F., 2010. Application of a sodalite membrane reactor in esterification—coupling reaction and separation. Catal. Today 156 (3), 132–139.
Kim, S.D., et al., 2006. Effect of γ-alumina content on catalytic performance of modified ZSM-5 for dehydration of crude methanol to dimethyl ether. Appl. Catal. A Gen. 309 (1), 139–143.
Kiss, A.A., 2011. Heat-integrated reactive distillation process for synthesis of fatty esters. Fuel Process. Technol. 92 (7), 1288–1296.
Klusáček, K., Schneider, P., 1982. Stationary catalytic kinetics via surface concentrations from transient data: methanol dehydration. Chem. Eng. Sci. 37 (10), 1523–1528.
Ko, K.-D., et al., 1995. Kinetics of steam reforming over a Ni/alumina catalyst. Korean J. Chem. Eng. 12 (4), 478–480.
Kubelková, L., Nováková, J., Nedomová, K., 1990. Reactivity of surface species on zeolites in methanol conversion. J. Catal. 124 (2), 441–450.
Kunin, R., Meitzner, E., Bortnick, N., 1962. Macroreticular ion exchange resins. J. Am. Chem. Soc. 84 (2), 305–306.
Kustrin, I., Tuma, M., 1996. Dimethyl ether-new perspective working fluid for organic rankine cycle power plants. In: Powergen-Conference 1996. Pennwell Conferences & Exhibitions.
Levenspiel, O., Levenspiel, C., 1972. Chemical reaction engineering. vol. 2. Wiley, New York.
Li, R., et al., 2009. Research on the intrinsic kinetics of methanol dehydration to dimethyl ether. Nat. Gas Chem. Ind. 39 (5), 9–12.
Liu, Y., et al., 2013. Synthesis of ethanol from methanol and syngas through an indirect route containing methanol dehydrogenation, DME carbonylation, and methyl acetate hydrogenolysis. Fuel Process. Technol. 110, 206–213.
Lu, W.-Z., Teng, L.-H., Xiao, W.-D., 2004. Simulation and experiment study of dimethyl ether synthesis from syngas in a fluidized-bed reactor. Chem. Eng. Sci. 59 (22), 5455–5464.
Magnotta, V., Gates, B., 1977a. Superacid polymers: paraffin isomerization and cracking in the presence of $AlCl_3$-sulfonic acid resin complexes. J. Catal. 46 (3), 266–274.
Magnotta, V., Gates, B., 1977b. Superacid polymers: synthesis and analysis of $AlCl_3$–sulfonic acid resin complexes. J. Polym. Sci.: Polym. Chem. Ed. 15 (6), 1341–1347.
Mikkelsen, S.-E., Sorenson, S.C., Hansen, J., 1996. Dimethyl ether as an alternate fuel for diesel engines. Application of Powertrain and Fuel Technologies to Meet Emissions Standards. Institution of Mechanical Engineers, London.
Mole, T., Whiteside, J., 1982. Conversion of methanol to ethylene over ZSM-5 zeolite in the presence of deuterated water. J. Catal. 75 (2), 284–290.

Mollavali, M., et al., 2008. Intrinsic kinetics study of dimethyl ether synthesis from methanol on γ-Al_2O_3 catalysts. Ind. Eng. Chem. Res. 47 (9), 3265–3273.
Moradi, G., et al., 2010. Intrinsic reaction rate and the effects of operating conditions in dimethyl ether synthesis from methanol dehydration. Korean J. Chem. Eng. 27 (5), 1435–1440.
Mujeebu, M.A., 2016. Hydrogen and syngas production by superadiabatic combustion—a review. Appl. Energy 173, 210–224.
Muller, M., Hubsch, U., 2005. Dimethyl ether. Ullmann's Encyclopedia of Industrial Chemistry. In: seventh ed. Wiley-VCH, Weinheim.
Ogawa, T., et al., 2004. Direct dimethyl ether (DME) synthesis from natural gas. In: Xinhe, B., Yide, X. (Eds.), Studies in Surface Science and Catalysis. Elsevier, London, United Kingdom, pp. 379–384.
Ohno, Y., 1997. New clean fuel from coal. Dimethyl ether. In: Fuel and Energy Abstracts.
Olah, G.A., et al., 1985. Electrophilic reactions at single bonds. 20. Selective monohalogenation of methane over supported acidic or platinum metal catalysts and hydrolysis of methyl halides over gamma-alumina-supported metal oxide/hydroxide catalysts. A feasible path for the oxidative conversion of methane into methyl alcohol/dimethyl ether. J. Am. Chem. Soc. 107 (24), 7097–7105.
Olujić, Ž., et al., 2009. Equipment improvement trends in distillation. Chem. Eng. Process. Process Intensif. 48 (6), 1089–1104.
Onaka, Y., Miyara, A., Tsubaki, K., 2010. Experimental study on evaporation heat transfer of CO_2/DME mixture refrigerant in a horizontal smooth tube. Int. J. Refrig. 33 (7), 1277–1291.
Park, K.-J., Jung, D., Seo, T., 2008. Flow condensation heat transfer characteristics of hydrocarbon refrigerants and dimethyl ether inside a horizontal plain tube. Int. J. Multiphase Flow 34 (7), 628–635.
Park, S.Y., Shin, C.-H., Bae, J.W., 2016. Selective carbonylation of dimethyl ether to methyl acetate on Ferrierite. Catal. Commun. 75, 28–31.
Parvez, A.M., et al., 2016. Synthesis of bio-dimethyl ether based on carbon dioxide-enhanced gasification of biomass: process simulation using Aspen plus. Energy Technol. 4 (4), 526–535.
Peng, X.-D., et al., 1998. Use of aluminum phosphate as the dehydration catalyst in single step dimethyl ether process. Google Patents.
Peng, X.-D., A.W. Wang, and B.A. Toseland, Single step synthesis Gas-to-Dimethyl ether process with methanol introduction. 2000, Google Patents.
Peng, X.-D., et al., 2002. Separation process for one-step production of dimethyl ether from synthesis gas. Google Patents.
Peng, W., et al., 2017. Hydrogen and syngas production by catalytic biomass gasification. Energy Convers. Manag. 135, 270–273.
Peral, E., Martín, M., 2015. Optimal production of dimethyl ether from switchgrass-based syngas via direct synthesis. Ind. Eng. Chem. Res. 54 (30), 7465–7475.
Pérez-Uriarte, P., et al., 2016. Kinetic model for the reaction of DME to olefins over a HZSM-5 zeolite catalyst. Chem. Eng. J. 302, 801–810.
Pérez-Uriarte, P., et al., 2017. Deactivation kinetics for the conversion of dimethyl ether to olefins over a HZSM-5 zeolite catalyst. Chem. Eng. J. 311, 367–377.
Perry, R.H., Green, D.W., 1999. Perry's Chemical Engineers' Handbook. McGraw-Hill Professional, New York, United States.
Prakash, G.K.S., et al., 2009. Poly(4-vinylpyridine) catalyzed hydrolysis of methyl bromide to methanol and dimethyl ether. J. Mol. Catal. A Chem. 310 (1–2), 180–183.
Rahimpour, M.R., 2015a. Membrane reactors for biodiesel production and processing. Membrane Reactors for Energy Applications and Basic Chemical Production. Woodhead Publishing, Cambridge, United Kingdom, pp. 289–312.
Rahimpour, M.R., 2015b. 21 – Butene oligomerization, phenol synthesis from benzene, butane partial oxidation, and other reactions carried out in membrane reactors. Membrane Reactors for Energy Applications and Basic Chemical Production. Woodhead Publishing, Cambridge, United Kingdom, pp. 641–660.
Rahimpour, M., Aboosadi, Z.A., Jahanmiri, A., 2012a. Synthesis gas production in a novel hydrogen and oxygen perm-selective membranes tri-reformer for methanol production. J. Nat. Gas Sci. Eng. 9, 149–159.
Rahimpour, M., et al., 2012b. Assessment and comparison of different catalytic coupling exothermic and endothermic reactions: a review. Appl. Energy 99, 496–512.

Raoof, F., et al., 2008. Effects of temperature and feed composition on catalytic dehydration of methanol to dimethyl ether over γ-alumina. Fuel 87 (13–14), 2967–2971.
Ratnakar, R.R., Dindoruk, B., Wilson, L., 2016. Experimental investigation of DME–water–crude oil phase behavior and PVT modeling for the application of DME-enhanced waterflooding. Fuel 182, 188–197.
Ratnakar, R.R., Dindoruk, B., Wilson, L.C., 2017. Phase behavior experiments and PVT modeling of DME-brine-crude oil mixtures based on Huron-Vidal mixing rules for EOR applications. Fluid Phase Equilib. 434, 49–62.
Riaz, A., Zahedi, G., Klemeš, J.J., 2013. A review of cleaner production methods for the manufacture of methanol. J. Clean. Prod. 57, 19–37.
Richardson, J., Paripatyadar, S., 1990. Carbon dioxide reforming of methane with supported rhodium. Appl. Catal. 61 (1), 293–309.
Roh, H.-S., et al., 2004. Superior dehydration of CH_3OH over double layer bed of solid acid catalysts—a novel approach for dimethyl ether (DME) synthesis. Chem. Lett. 33 (5), 598–599.
Rohde, M., et al., 2006. Fischer−Tropsch synthesis with in-situ H_2O removal by a new hydrophilic membrane: an experimental and modelling study. DGMK Tagungsber 4, 215.
Rohde, M., et al., 2008. Fischer–Tropsch synthesis with in situ H_2O removal–directions of membrane development. Microporous Mesoporous Mater. 115 (1), 123–136.
Rossiter, A.P., 2003. Succeeding in process integration. In: Process Industries Expo User Conference.
Royaee, S.J., et al., 2008. A new Langmuir–Hinshelwood mechanism for the methanol to dimethylether dehydration reaction over clinoptilolite-zeolite catalyst. Appl. Catal. A Gen. 338 (1), 114–120.
Rutkowska, M., et al., 2016. Hierarchically structured ZSM-5 obtained by optimized mesotemplate-free method as active catalyst for methanol to DME conversion. Catal. Sci. Technol. https://doi.org/10.1039/C6CY00040A.
Sabour, B., et al., 2014. Catalytic dehydration of methanol to dimethyl ether (DME) over Al-HMS catalysts. J. Ind. Eng. Chem. 20 (1), 222–227.
Said, A.E.-A.A., El-Wahab, M.M.A., El-Aal, M.A., 2014. The catalytic performance of sulfated zirconia in the dehydration of methanol to dimethyl ether. J. Mol. Catal. A Chem. 394, 40–47.
Samimi, F., et al., 2013a. A novel axial-flow spherical packed-bed membrane reactor for dimethyl ether synthesis: simulation and optimization. J. Nat. Gas Sci. Eng. 13, 42–51.
Samimi, F., et al., 2013b. Simultaneous dimethyl ether synthesis and decalin dehydrogenation in an optimized thermally coupled dual membrane reactor. J. Nat. Gas Sci. Eng. 14, 77–90.
Samimi, F., et al., 2014a. Mathematical modeling and optimization of DME synthesis in two spherical reactors connected in series. J. Nat. Gas Sci. Eng. 17, 33–41.
Samimi, F., Kabiri, S., Rahimpour, M.R., 2014b. The optimal operating conditions of a thermally double coupled, dual membrane reactor for simultaneous methanol synthesis, methanol dehydration and methyl cyclohexane dehydrogenation. J. Nat. Gas Sci. Eng. 19, 175–189.
Sea, B., Lee, K.-H., 2006. Synthesis of dimethyl ether from methanol using alumina–silica membrane reactor. Desalination 200 (1), 689–691.
Seddon, D., 2011. Methanol and dimethyl ether (DME) production from synthesis gas A2. In: Khan, M.R. (Ed.), Advances in Clean Hydrocarbon Fuel Processing. Woodhead Publishing, Cambridge, United Kingdom, pp. 363–386.
Semelsberger, T.A., Borup, R.L., Greene, H.L., 2006. Dimethyl ether (DME) as an alternative fuel. J. Power Sources 156 (2), 497–511.
Seo, J.G., Youn, M.H., Song, I.K., 2007. Hydrogen production by steam reforming of LNG over Ni/Al_2O_3–ZrO_2 catalysts: effect of Al_2O_3–ZrO_2 supports prepared by a grafting method. J. Mol. Catal. A Chem. 268 (1), 9–14.
Shikada, T., et al., 1998. Direct synthesis of dimethyl ether form synthesis gas. In: Parmaliana, D.S.F.F.A.V.A., Arena, F. (Eds.), Surface Science and Catalysis. Elsevier, London, United Kingdom, pp. 515–520.
Shikada, T., et al., 2000. Method and apparatus for producing dimethyl ether. Google Patents.
Shikada, T., et al., Method for producing dimethyl ether. 2005, Google Patents.
Shoji, K., Terai, S., 2007. Process for producing dimethyl ether. Google Patents.
Smith, R., 2000. State of the art in process integration. Appl. Therm. Eng. 20 (15–16), 1337–1345.
Song, C., Pan, W., 2004. Tri-reforming of methane: a novel concept for catalytic production of industrially useful synthesis gas with desired H_2/CO ratios. Catal. Today 98 (4), 463–484.

Sousa-Aguiar, E.F., Appel, L.G., Mota, C., 2005. Natural gas chemical transformations: the path to refining in the future. Catal. Today 101 (1), 3–7.
Souza, M.M., Schmal, M., 2005. Autothermal reforming of methane over $Pt/ZrO_2/Al_2O_3$ catalysts. Appl. Catal. A Gen. 281 (1), 19–24.
Spivey, J.J., 1991. Review: Dehydration catalysts for the methanol/dimethyl ether reaction. Chem. Eng. Commun. 110 (1), 123–142.
Stiles, A.B., 1987. Catalyst Supports and Supported Catalysts. Butterworth-Heinemann, Oxford, United Kingdom.
Su, L.-W., Li, X.-R., Sun, Z.-Y., 2013. The consumption, production and transportation of methanol in China: a review. Energy Policy 63, 130–138.
Sun, J., et al., 2014. Catalysis chemistry of dimethyl ether synthesis. ACS Catal. 4 (10), 3346–3356.
Tavan, Y., Hosseini, S.H., 2013. From laboratory experiments to simulation studies of methanol dehydration to produce dimethyl ether reaction—Part II: Simulation and cost estimation. Chem. Eng. Process. Process Intensif. 73, 151–157.
Tavan, Y., et al., 2013. From laboratory experiments to simulation studies of methanol dehydration to produce dimethyl ether—Part I: Reaction kinetic study. Chem. Eng. Process. Process Intensif. 73, 144–150.
Téllez, C., Menéndez, M., 2011. Zeolite membrane reactors. Membranes for Membrane Reactors. John Wiley & Sons, Ltd, Hoboken, NJ, United States, pp. 243–273.
Tokay, K.C., Dogu, T., Dogu, G., 2012. Dimethyl ether synthesis over alumina based catalysts. Chem. Eng. J. 184, 278–285.
Vernon, P.D., et al., 1990. Partial oxidation of methane to synthesis gas. Catal. Lett. 6 (2), 181–186.
Vishwanathan, V., et al., 2004. Vapour phase dehydration of crude methanol to dimethyl ether over Na-modified H-ZSM-5 catalysts. Appl. Catal. A Gen. 276 (1), 251–255.
Wang, S., Lu, G., Millar, G.J., 1996. Carbon dioxide reforming of methane to produce synthesis gas over metal-supported catalysts: state of the art. Energy Fuel 10 (4), 896–904.
Wang, Z., et al., 2016. Design and operation of a pilot plant for biomass to liquid fuels by integrating gasification, DME synthesis and DME to gasoline. Fuel 186, 587–596.
Wei, Y., et al., 2015. Enhanced catalytic performance of zeolite ZSM-5 for conversion of methanol to dimethyl ether by combining alkaline treatment and partial activation. Appl. Catal. A Gen. 504, 211–219.
Winterbottom, J., 1981. Hydration and dehydration by heterogeneous catalysts. Catalysis 4, 141–174.
Wolthuizen, J., et al., 1980. Catalysis by Zeolites. Elsevier, Amsterdam, p. 85.
Xu, M., et al., 1997. Synthesis of dimethyl ether (DME) from methanol over solid-acid catalysts. Appl. Catal. A Gen. 149 (2), 289–301.
Yang, G., et al., 2011. A new method of ethanol synthesis from dimethyl ether and syngas in a sequential dual bed reactor with the modified zeolite and Cu/ZnO catalysts. Catal. Today 164 (1), 425–428.
Yaripour, F., et al., 2005a. Catalytic dehydration of methanol to dimethyl ether (DME) over solid-acid catalysts. Catal. Commun. 6 (2), 147–152.
Yaripour, F., et al., 2005b. Synthesis of dimethyl ether from methanol over aluminium phosphate and silica–titania catalysts. Catal. Commun. 6 (8), 542–549.
Yoo, J.-H., et al., 2006. Fuel cells using dimethyl ether. J. Power Sources 163 (1), 103–106.
Yoon, E.S., Han, C., 2009. A review of sustainable energy—recent development and future prospects of dimethyl ether (DME). In: Rita Maria de Brito Alves, C.A.O.d.N, Evaristo Chalbaud, B. (Eds.), Computer Aided Chemical Engineering. Elsevier, London, United Kingdom, pp. 169–175.
You, Q., et al., 2009. Synthesis of dimethyl ether from methane mediated by HBr. J. Nat. Gas Chem. 18 (3), 306–311.
Zhang, L., et al., 2010. Synthesis of dimethyl ether via methanol dehydration over combined Al_2O_3-HZSM-5 solid acids. Chin. J. Catal. 31 (8), 987–992.
Zhang, L., et al., 2011. Intrinsic kinetics of methanol dehydration over Al_2O_3 catalyst. Eng. Technol. 59, 1538–1543.
Zhang, Q., et al., 2013. Characterization and catalytic application of $MnCl_2$ modified HZSM-5 zeolites in synthesis of aromatics from syngas via dimethyl ether. J. Ind. Eng. Chem. 19 (3), 975–980.
Zhou, H., et al., 2016. In situ DRIFT study of dimethyl ether carbonylation to methyl acetate on H-mordenite. J. Mol. Catal. A Chem. 417, 1–9.

This page intentionally left blank

CHAPTER 11

Methanol As An Internal Combustion on Engine Fuel

Xudong Zhen

Tianjin University of Technology and Education, Tianjin, China

Acronyms

BSFC	brake specific fuel consumption
BTE	brake thermal efficiency
CA	crank angle
CFD	computational fluid dynamics
CI	compression ignition
CNG	compressed natural gas
CR	compression ratio
DISI	direct injection spark ignition
DME	dimethyl ether
EGR	exhaust-gas recirculation
HC	hydrocarbon compounds
HCCI	homogenous charge compression ignition
IC	internal combustion
IMEP	indicated mean effective pressure
ISFC	indicated specific fuel consumption
IT	ignition timing
LES	large eddy simulation
LPG	liquefied petroleum gas
MBD	blend of methanol (20%)-biodiesel (40%)-diesel (40%)
MBD-5DEE	blend of MBD with 5% diethyl ether
MIE	minimum ignition energy
MIT	minimum ignition temperature
MON	motor octsne number
NO_x	nitrogen oxides
NTP	normal temperature and pressure
PCCI	premixed charge compression ignition

Methanol. https://doi.org/10.1016/B978-0-444-63903-5.00011-X

PM	particulate matter
RCCI	reactivity controlled compression ignition
RON	research octane number
SI	spark ignition
SFC	specific fuel consumption
SOI	start of injection
UHC	unburnt hydrocarbons
ULSD	ultra-low sulfur diesel
VOCs	volatile organic compounds

1 Introduction

As atmospheric environmental pollution becomes more and more serious today, many countries have enacted various emission regulations to improve the atmospheric environment. It is generally accepted that automobile and internal combustion (IC) engine emissions are some of the main sources of atmospheric pollution. Therefore, in order to improve the atmospheric environment, it is a good idea to reduce the exhaust emissions of IC engines. In addition, with the depletion of conventional oil resources, various alternative resources such as natural gas, methanol, and biodiesel need to be developed to replace conventional fossil fuels (gasoline or diesel) for IC engines (Celik et al., 2011; Li et al., 2010a,b; Vancoillie et al., 2013; Zhen et al., 2012).

Today, methanol fuel is considered a viable green fuel for IC engines because of its low soot emissions and the possibility of it being produced in a CO_2-neutral manner. Methanol as a fuel for IC engines has attracted interest throughout history, with much research conducted during the oil crisis in the 1970s (Li et al., 2010a,b). Methanol is a colorless, pure substance, and its structure is the simplest saturated alcohol. Methanol can be produced from biomass, natural gas, or coal (Clausen et al., 2010; Holmgren et al., 2012; Li et al., 2010a,b; Reno et al., 2011). The basic properties of methanol, diesel, and gasoline are illustrated in Table 11.1. In Table 11.1, it can be seen that because the octane rating of methanol fuel is 109, it has a higher antiknock performance. Also, the engine geometry compression ratio (CR) can be increased significantly when using methanol as fuel (Zhen et al., 2013a,b). This is because a higher octane rating allows a significant increase in the CR and a higher heat vaporization value may cool down the incoming fuel-air charge, increasing the volumetric efficiency and promoting the power output.

Methanol is considered to be one of the most favorable fuels for IC engines, in several ways: it can be used in a high CR spark ignition (SI) engine that could replace diesels in certain vocational applications; it can be used in an inlet port injection SI engine; it can be used in

Table 11.1 The properties of methanol, gasoline and diesel

Fuel Property	Methanol	Gasoline	Diesel
Formula	CH_3OH	$C_{5–12}$	$C_{10–26}$
Molecular weight (g/mol)	32	95–120	180–200
Oxygen content	50%	0	0
Stoichiometric air/fuel ratio	6.45	14.6	14.5
Low calorific value (MJ/kg)	19.66	44.5	42.5
High calorific value (MJ/kg)	22.3	46.6	45.8
Freezing point (°C)	−98	−57	−1∼-4
Boiling point (°C)	64.8	30–220	175–360
Flash point (°C)	11	−45	55
Auto-ignition temperature (°C)	465	228–470	220–260
Research octane number	108.7	80–98	
Motor octane number	88.6	81–84	
Cetane number	3	0–10	40–55
Flammability limits (vol)	6.7–36	1.47–7.6	1.85–8.2
Specific heat (20°C) (kJ/kg K)	2.55	2.3	1.9
Latent heat (kJ/kg)	1109	310	270
Viscosity (20°C) (cP)	0.6	0.29	3.9

a high-compression direct-injection stratified charge SI engine; it can be used in a direct-injection SI engine; and it can be used in a turbocharged, port-fuel-injected, high CR medium duty engine (Clausen et al., 2010; Holmgren et al., 2012; Reno et al., 2011; Surawski et al., 2012; Zhen et al., 2013a,b). Although it has half the volumetric energy density of gasoline or diesel, methanol is an excellent fuel, and it can be blended with gasoline (M15: 85% methanol and 15% gasoline) or used as pure methanol (M100: 100% methanol) (Olah, 2005; Vancoillie et al., 2012a,b). Compared with the hydrogen and gasoline fuels, methanol is a transportation fuel and has many significant advantages. It has better fuel conversion efficiencies than gasoline thanks to the larger vaporization heat as well as a much better resistance to knock that makes it the best option for small, turbocharged, high power density, directly injected stoichiometric engines (Boretti, 2013).

Currently, the conventional gasoline or diesel engines can be modified to use pure methanol (M100) or dual-fuel (petrol-methanol or diesel-methanol blends, etc.) through some specific techniques. The modified methanol engines are widely used in various passenger cars. The modified conventional diesel engines fueled with M100 or blends (methanol-diesel) will become the main alternative power for diesel passenger cars and trucks. The study of combustion and emissions is the core scientific engineering technology issue relating to the development of methanol engines. This chapter systematically presents the methanol applications for IC engines. Finally, it puts forward some new prospects and suggestions in the development of methanol engines.

2 Methanol Fuel Used on IC Engines

2.1 Engine Using Pure Methanol (M100) as Fuel

From the engineering application perspective, methanol is an ideal alternative, renewable, environmentally and economically attractive fuel (Zhen and Wang, 2015a,b,c). For the development of high-power and high-efficiency methanol engines, in the 1990s the Southwest Research Institute proposed a high CR SI methanol engine program that provides a new idea for replacing the traditional diesel engines (Brusstar et al., 2002). Fig. 11.1 shows the measured brake thermal efficiency (BTE) of the engine operating with methanol fuel and the baseline diesel engine. It is clearly seen from Fig. 11.1 that, compared with the original diesel engine, the methanol engine exhibits peak efficiency of nearly 43%, and maintains over 40% efficiency over a much wider range of speeds and loads (Brusstar et al., 2002). Zhen et al. (2013a,b,c) and Zhen and Wang (2015b) studied the ignition, combustion, and emission performances for a high-compression methanol engine. The studied methanol engine was modified from a conventional four-cylinder, four-stroke, and direct-injection diesel engine. The spray pattern was changed from the original direct-injection mode into the intake port injection mode. In the research on the ignition process for the high CR methanol engine, it was found that species such as CH_2O, OH, and H_2O_2 were quickly generated and consumed during combustion. Using a smaller flame kernel could increase the demand for minimum ignition temperature (MIT), and using a smaller flame kernel could decrease the demand for minimum ignition energy (MIE). Zhen and Wang (2015a,b,c) also studied the knock during homogenous charge compression ignition (HCCI) in a high CR methanol engine based on large eddy simulation (LES) with detailed chemical kinetics. It was found that the knocking combustion burnt faster during HCCI than the SI methanol engine. The HCO reaction rate was different from an SI engine. It had two obvious peaks: one was positive, the other negative.

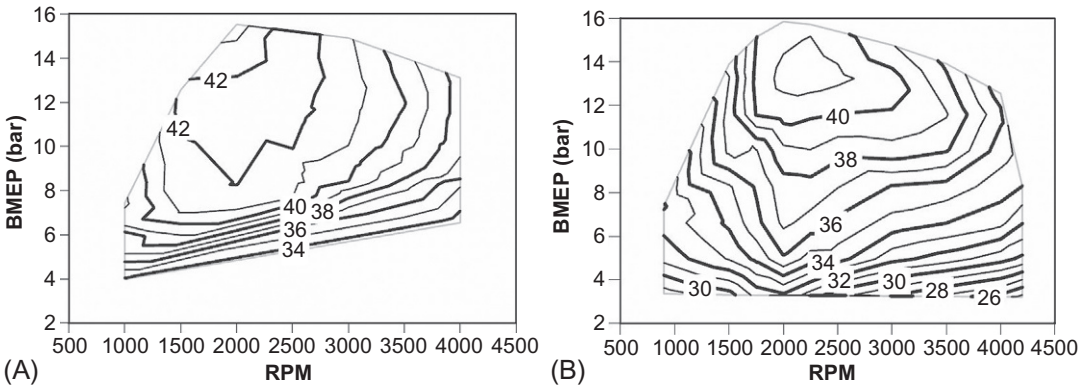

Fig. 11.1

The measured break thermal efficiency of the engine operating with methanol fuel and the baseline diesel engine. (A) Methanol: BTE (%) as a function of BMEP, RPM. (B) Baseline stock 1.9 L VW TDI Diesel: BTE (%) as a function of BMEP, RPM.

Zhang and Wu (2016) studied the combustion characteristics and performance of an HCCI engine fueled with methanol, considering the intake charge temperature, fuel-air equivalence ratio, and engine speed. Fig. 11.2 shows the experimental setup (Zhang and Wu, 2016). It was found that the intake charge temperature was the most sensitive parameter among tested parameters for methanol HCCI combustion. The maximum thermal efficiency occurred near 7.5º crank angle (CA) and the combustion duration was less than 11ºCA. Qu et al. (2015) studied the regulated and unregulated emissions from a direct injection spark ignition (DISI) methanol engine under homogeneous combustion and light load. The experiments were conducted on a four-cylinder DISI methanol engine. The variations in emitted HCHO and unburned methanol showed opposite tendencies with the variations in the methanol injection timing, ignition timing (IT), excess air ratio, intake air temperature, and engine speed. Retarding methanol injection timing, advancing IT, using lean mixture, and reducing intake air temperature could decrease HCHO emissions. Vice versa, unburned methanol emission decreased. Gong et al. (2016a,b) modified a single-cylinder, four-stroke, water-cooled, stratified-charge DISI methanol engine from a diesel engine. It was found that decreasing CR can decrease its maximum pressure rise rate and improve the BTE at low load. As a result, decreasing CR from 16 to 14, the BTE of the methanol engine increased by 18% at low load.

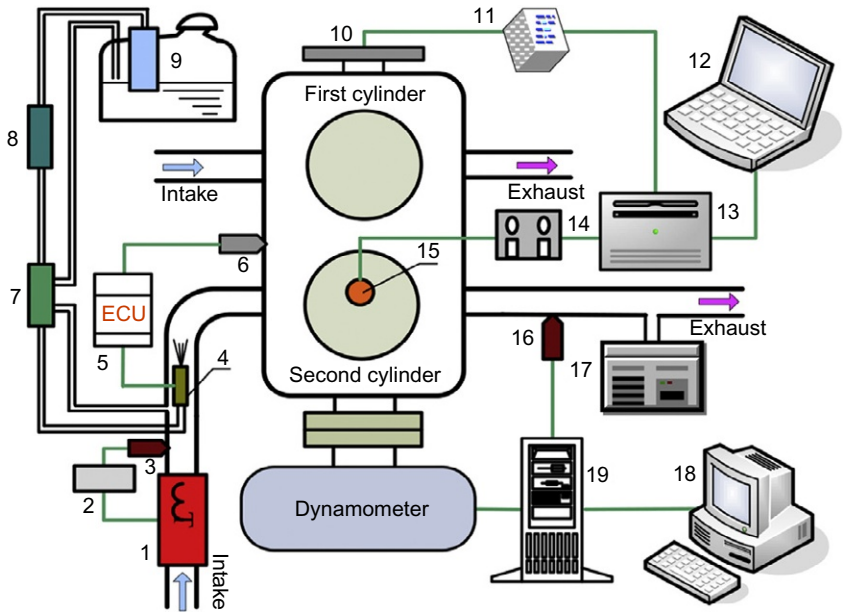

Fig. 11.2

Experimental setup. (1) Electric heater; (2) intake charge temperature controller; (3) temperature sensor; (4) injector; (5) injection ECU; (6) hall sensor; (7) injection pressure regulator; (8) fuel filter; (9) fuel tank and pump; (10) photoelectricity transducer; (11) crank-angle encoder; (12) computer 1; (13) combustion analyzer; (14) charge amplifier; (15) pressure transducer; (16) temperature sensor; (17) exhaust gas analyzer; (18) computer 2; (19) dynamometer and control cabinet.

BTE decreased by 6% and the maximum pressure rise rate decreased up to 60% at high load and maximum torque engine speed. Li et al. (2015) studied the critical firing and misfiring boundary in an SI methanol engine during cold start based on single-cycle fuel injection. For ambient temperatures below 16°C, methanol engines must use auxiliary start aids during a cold start. Optimal control of the methanol injection and IT can realize ideal next cycle firing combustion after injection. Resistance wire and glow plug preheating can provide critical firing down to ambient temperatures of 5°C and 0°C, respectively. Using an additional liquefied petroleum gas (LPG) injection into the intake manifold could provide critical firing down to an ambient temperature of 13°C during cold start.

Wang et al. (2016a,b) studied the effects of engine misfire on regulated and unregulated emissions from a methanol-fueled vehicle. It was found that the CO, hydrocarbon compounds (HC), unburned methanol, carbonyls, and volatile organic compounds (VOCs) were increased with the misfire rate, and the CO, toluene, xylene, and formaldehyde were the leading contributors. Xie et al. (2016) studied the influence of air and exhaust-gas recirculation (EGR) dilutions on improving the performance of high CR SI engines with methanol at a light load. It was found that air and cooled EGR dilutions could possibly improve engine fuel consumption, and the hot EGR had better combustion and relation between output torque and nitrogen oxides (NO_x) than cooling EGR. Dhaliwal et al. (2000) studied the emissions effects of alternative fuels in light-duty and heavy-duty vehicles. The reformulated gasoline, compressed natural gas (CNG), LPG, M85, and M100 with conventional gasoline and diesel fuels were compared. The results showed that using M100 in heavy-duty vehicles produced variable emissions trends concerning THC and CO. However, M100 offered large and consistent emissions benefits for NO_x and particulate matter (PM), which were the more serious problems for the baseline diesel vehicles. The use of pure methanol as fuel at high CR in a single-cylinder gasoline engine was studied by Celik et al. (2011). They found that by increasing the CR from 6:1 to 10:1 with methanol, the engine power and BTE increased by up to 14% and 36%, respectively. Moreover, CO, CO_2, and NO_x emissions were reduced by about 37%, 30%, and 22%, respectively.

2.2 Engine Using Methanol-Gasoline Blends as Fuel

Methanol fuel can be blended with many various fuels. For instance, it can be blended with gasoline fuel in an SI engine. It can be blended with M15 (15% methanol and 85% gasoline) or many other proportions. The methanol can be blended with gasoline fuel, which can improve the engine performance such as power performance, fuel economy performance, and emissions performances (Canakci et al., 2013; Cay et al., 2013; Gravalos et al., 2013; Liu et al., 2007; Siwale et al., 2014). For instance, methanol can suppress knocking combustion (Liu et al., 2014); decrease HC, CO, PM, and NO_x emissions; and improve the thermal efficiency (Liang et al., 2013; Wu et al., 2016).

The combustion process can be improved in SI engines because of the oxygen content in methanol. The methanol-gasoline fuel blends can cause a decrease in CO and unburned HC emissions significantly (Canakci et al., 2013). The aldehydes and methanol emission mechanisms from methanol-gasoline fueled SI engines are also studied (Wei et al., 2009; Zhang et al., 2011a,b). Liu et al. (2015) studied the methanol-gasoline dual-fuel spark ignition combustion for reducing particle number emissions and improving fuel economy in a high CR gasoline engine. The results showed that it achieved high particle number reduction and low fuel consumption for methanol-gasoline engines. Wang et al. (2015a,b) evaluated the toxic reduction and fuel economy of a gasoline direct-injection powered passenger car fueled with methanol-gasoline blends, and various substitution ratios were considered in the study. It was found that as the methanol fuel was added into the gasoline, the CO, HC, CO_2, and PM from the engine were decreased.

2.3 Engine Using Methanol-Diesel Blends as Fuel

Because the methanol fuel is an oxygenated and renewable fuel, it is receiving increasing attention for diesel engines. Methanol fuel can be blended with diesel in various proportions. For instance, it can be blended with diesel fuel with M15D85 (15% methanol and 85% diesel) or other proportions. Many dual fuel (methanol-diesel) engines have been studied, including combustion behaviors (Huang et al., 2004; Li et al., 2013; Nagafi and Yusaf, 2009; Sayin, 2010), regulated and unregulated emission performances (Chao et al., 2000; Sayin et al., 2009, 2010), methanol fumigation (Cheng et al., 2008a,b; Zhang et al., 2010a,b, 2011a,b, 2013), etc.

To meet more stringent emission norms, Soni and Gupta (2016) investigated a two-stage strategy to achieve a higher level of emission reduction in a methanol-diesel engine. It was found that, compared with the base fuel (diesel-methanol blend), the water-blend method tended to reduce NO_x emission by 95% and soot by 14%. It is generally accepted that the combustion process is highly affected by intake temperature and injection timing, especially for diesel-methanol dual engines (Pan et al., 2015). Wang et al. (2015a, 2015b) studied the effects of intake preheating and injection on combustion and emission characteristics of a diesel-methanol dual-fuel engine. It was found that as the injection timing retarded, the combustion become a single-stage combustion. Also, the soot-NO_x trade-off was completely broken at a low intake temperature and a high methanol substitution percentage. Wang et al. (2016a,b) also examined the cyclic variability of diesel-methanol dual-fuel combustion. It was found that a high methanol substitution percentage increased the cyclic variations at light loads while the effect of diesel injection timing had no effect on cyclic variations. Increasing engine speed could decrease cylinder-to-cylinder variation (Chen et al., 2016).

Wei et al. (2016) investigated the effects of methanol-to-diesel ratio and diesel injection timing on combustion, performance, and emissions in diesel-methanol engines. It was found that by retarding diesel injection timing, HC emissions firstly increased and then decreased while

CO emissions always increased. Li et al. (2016a,b) investigated the effects of diesel injection parameters on a six-cylinder, heavy-duty, common-rail diesel-methanol dual-fuel engine. The methanol was premixed with air in the intake pipe and afterward ignited by the direct-injected diesel in the cylinder. The results showed that smoke emission could be further reduced by coupling the high diesel injection pressure and the advanced diesel injection timing. However, NO_x emission may be increased. In the diesel-methanol dual-fuel engine, the vibration was affectedly greatly by the rapid burning characteristics. The vibration could be reduced by optimizing the diesel injection timings and pressures (Li et al., 2016a,b). Prashant et al. (2016) investigated the ignition delay, the maximum rate of pressure rise, and the temperature and cylinder peak pressure in a four-cylinder, turbocharged and intercooled diesel-methanol engine. It was found that the in-cylinder pressure rise was higher in the case of 20% substitution, and the ignition delay was found to decrease.

2.4 Engine Using Methanol-Hydrogen Blends as Fuel

It is effective to improve the performance of methanol engines through the hydrogen addition. Compared with methanol fuel, hydrogen has a much wider flammability limit that enables the fuel to be fast and completely combusted at lean and high residual gas conditions (Hu et al., 2009a,b). Due to the lean flammability limits of hydrogen and the chemical quality of methanol in reference to gasoline, it has higher efficiencies and a reduction in exhaust emissions (Schafer, 1981). The high flame temperature and propagation speed of hydrogen also help shorten the combustion duration while increasing the cylinder temperature. These properties of hydrogen may be helpful for the full evaporation and combustion of methanol fuel at low load and lean conditions (Zhang et al., 2014a,b). Methanol fuel can be blended with hydrogen in the engine. For example, it can be blended with hydrogen in M85H15 (85% methanol and 15% hydrogen) or other proportions. Table 11.2 shows the physical and chemical properties of methanol and hydrogen (Vancoillie et al., 2012a,b). Because hydrogen possesses high thermal and mass diffusivities, the hydrogen enrichment can improve the formation of fuel-air mixtures in the engine intake manifolds. Meanwhile, because of the high flame speed and wide flammability limits of hydrogen, the hydrogen enrichment can also promote the turbulent combustion in conventional fuel engines (Hu et al., 2009a,b; Ji and Wang, 2009; Liu et al., 2013; Wang et al., 2010).

Li et al. (2013) proposed a laminar flame speed correlation of hydrogen-methanol blends using the computational fluid dynamics (CFD) simulation. The results demonstrated that, compared with the experimental results, the proposed new correlation was suitable for the engine simulation. Ji et al. (2013) investigated the effects of hydrogen addition on enhancing the performance of a methanol engine at part load and lean conditions. The test results illustrated that the engine combustion cycle variation was easily, the BTE was enhanced, and the HC and CO emissions were generally reduced after the hydrogen blending. Zhang et al. (2014a,b)

Table 11.2 The properties of methanol and hydrogen

Fuel Property	Methanol	Hydrogen
Chemical structure	CH_3OH	H_2
Oxygen content by mass (%)	50	0
Density at NTP (kg/L)	0.79	0.00008
Lower heating value (MJ/kg)	20.09	120
Volumetric energy content (MJ/L)	15.9	0.010
Stoichiometric air to fuel ratio (kg/kg)	6.5	34.2
Energy per unit mass of air (MJ/kg)	3.12	3.51
Research octane number	109	130 ($\lambda=2.5$)
Motor octane number	88.6	NA
Sensitivity (RON-MON)	20.4	NA
Boiling point at 1 bar (°C)	65	−253
Heat of vaporization (kJ kg)	1100	461
Reid vapor pressure (psi)	4.6	NA
Mole ratio of products to reactants	1.061	0.852
Flammability limits in air (λ)	0.23–1.81	0.15–10.57
Laminar flame speed at NTP, $\lambda=1$ (cm/s)	42	210
Adiabatic flame temperature (°C)	1870	2117
Specific CO_2 emissions (g/MJ)	68.44	0.00

studied the idling characteristics of a hydrogen-blended methanol engine under lean conditions and three hydrogen volume fractions in the intake of 0%, 1%, and 2%. The results showed that both flame development and propagation periods were shortened, and HC and CO emissions were reduced after the addition of hydrogen for the methanol engine at the idle and lean conditions. Ji et al. (2016) developed a two-zone quasidimensional model for predicting the performance of a hydrogen-enriched methanol engine. The results showed that hydrogen enrichment could improve the flame propagation speed, reduce the exhaust loss, and enhance BTE. Gong et al. (2016a,b) investigated the combustion, CO, NO, HCHO and unburned methanol emissions characteristics in a direct-injection SI methanol engine with a hydrogen addition ratio from 5% to 15%. The results showed that as the hydrogen addition goes from 0% to 15%, CO emission, formaldehyde, and the unburned methanol were decreased, whereas the NO emission was increased.

2.5 Engine Using Methanol-Biodiesel Blends as Fuel

Methanol fuel can be blended with biodiesel in an engine. It can be blended with biodiesel in M85B15 (85% methanol and 15% biodiesel) or other proportions. Biodiesel is an alternative fuel for IC engines. Compared with diesel fuel, it can reduce HC, CO, and PM emissions by using methanol-biodiesel blends. Biodiesel has been a lucrative commodity in the current global economic trade as there is mounting concern over issues relating to the environment and oil depletion. Biodiesel has been proven to be the next alternative renewable fuel as it is

environmentally friendly, sustainable, and possesses similar combustion characteristics to petroleum diesel. However, due to the higher density and viscosity of biodiesel, pure biodiesel is not widely used in diesel engines (Mat Yasin et al., 2014). Therefore, the method of methanol-biodiesel blends is widely used. Table 11.3 shows the physical and chemical properties of methanol and biodiesel (Cheung et al., 2009).

Datta et al. (2016) studied the performance of biodiesel-methanol blends in a variable CR engine by using optimized engine parameters. The operational and performance parameters were all considered in the study. It was found that the biodiesel-methanol blends had maximum efficiency and minimum emissions by optimizing engine parameters. Zhou et al. (2015) investigated knocking combustion phenomena in a reactivity controlled compression ignition (RCCI) engine fueled with biodiesel-methanol blends. A reduced biodiesel-methanol chemical reaction mechanism was developed and applied to capture local pressure and species concentrations. The results showed that the knocking combustion could be suppressed by retarding the start of injection (SOI) and lowering premixed methanol mass fraction. Cheng et al. (2008a,b) studied the emissions of a four-cylinder naturally aspirated direct-injection diesel engine fueled with biodiesel-methanol blends (biodiesel with 10% methanol and 10% fumigation methanol). The results showed higher BTE than ultra-low sulfur diesel (ULSD). The blended mode tended to further improve the efficiency at low load condition but at high load condition the cooling effect of methanol reduced the efficiency; the fumigation mode had the opposite effect.

Yilmaz (2012a,b) investigated the effects of intake air preheat and fuel blend ratio in a diesel engine operating on biodiese-methanol blends. The fuel concentrations of B85M15 (85% biodiesel and 15% methanol), B90M10 (90% biodiesel and 10% methanol), B95M5 (95% biodiesel and 5% methanol), and B100 (100% biodiesel) were considered in the study. The results showed that the high heat of vaporization of methanol affected CO and HC emissions significantly. Anand et al. (2011) investigated the combustion and emission characteristics of neat biodiesel and its methanol blend in a turbocharged, direct-injection, multicylinder truck diesel engine fitted with a mechanical distributor-type fuel injection pump. The experimental

Table 11.3 The properties of methanol and biodiesel

Fuel Property	Methanol	Biodiesel
Cetane number	<5	51
Lower heating value (MJ/kg)	19.7	37.5
Density (kg/m^3)@20°C	792	871
Viscosity (mPa s) 40°C	0.59	4.6
Heat of evaporation (kJ/kg)	1178	300
Carbon content (% mass)	37.5	77.1
Hydrogen content (% mass)	12.5	12.1
Oxygen content (% mass)	50	10.8
Sulfur content (mg/kg)	0	<10

results indicated that with the methanol addition in the biodiesel, the maximum thermal efficiency could be increased while the nitricoxide and smoke emissions were decreased. Cheung et al. (75) studied the regulated and unregulated emissions in a diesel engine operating on Euro V diesel fuel, pure biodiesel, and biodiesel-methanol blends. The blends contain 5%, 10%, and 15% by volume of methanol. It was found that the blended fuels could lead to higher CO and HC emissions than biodiesel as well as higher CO emissions but lower HC emissions than the diesel fuel. There were simultaneous reductions of NO_x and PM to a level below those of the diesel fuel. Compared with diesel fuel, the blended fuels generated higher formaldehyde, acetaldehyde, and unburned methanol emissions and lower 1,3-butadiene and benzene emissions, while the toluene and xylene emissions were not significantly different.

Yilmaz and Sanchez (2012) studied the emission characteristics in a two-cylinder, four-cycle, direct-injected, water-cooled diesel engine fueled with B85E15 (85% biodiesel and 15% ethanol) and B85M15 (85% biodiesel and 15% methanol) blends. It was found that compared with the biodiesel-methanol blends, biodiesel-ethanol blends were more effective for emissions reduction. The unregulated emission species were responsible for an adverse environmental impact and health hazards upon prolonged exposure. Agarwal et al. (2016) studied the unregulated emissions and health risk potential from biodiesel and methanol blends in a four-cylinder, 1.4-liter compression ignition engine. The results showed that, compared with the baseline mineral diesel, there was an increasing trend for some of the unregulated species from blends of biodiesel such as formaldehyde, acetaldehyde, ethanol and *n*-butane. However, methane was reduced upon using these oxygenated fuel blends except methanol. Nevertheless, there were no significant changes for sulfur dioxide, iso-butane, *n*-octane, *n*-pentane, formic acid, benzene, acetylene, and ethylene upon using biodiesel and methanol blends. Zhu et al. (2010) studied the emissions characteristics of a diesel engine operating on biodiesel and biodiesel blended with ethanol and methanol in a four-cylinder naturally aspirated direct-injection diesel engine. The results showed that, compared with Euro V diesel fuel, the blended fuels could lead to the reduction of both NO_x and PM emissions of a diesel engine, and the methanol-biodiesel blends were more effective than the biodiesel-ethanol blends.

2.6 Engine Using Methanol-Dimethyl Ether (DME) Blends as Fuel

Methanol fuel can be blended with DME in the engine. It can be blended with DME in M85D15 (85% methanol and 15% DME) or other proportions. Compared with other alternatives, DME and methanol are suitable alternative fuels for compression ignition (CI) and SI engines, respectively. DME can be produced from a variety of feedstock such as natural gas, coal, crude oil, residual oil, waste products, and biomass. Table 11.4 shows the physical and chemical properties of methanol and DME (Liang et al., 2011). The high cetane number and low boiling point of DME symbolize the short ignition delay, low auto-ignition temperature, and almost instantaneous vaporization when DME is injected into the cylinder. Moreover, as DME is

Table 11.4 The properties of methanol and DME

Fuel Property	Methanol	DME
Chemical structure	CH_3OH	CH_3OCH_3
Density (kg/m^3)	790 (liquid)	206 (gaseity)
Boiling point (°C)	65	−25.1
Auto-ignition temperature (°C)	450	235
Lower heating value (MJ/kg)	19.9	27.6
Vaporization heat (kJ/kg)	1110	460
Research octane number	111	–
Cetane number	<15	55–60
Stoichiometric air/fuel ratio	6.5	9.0
Oxygen content (wt.%)	50	34.8
Carbon content (wt.%)	37.5	52.2
Flame speed (cm/s)	45–52.3	45–52

nontoxic and environmentally benign, whether at low or high mole fractions (percent by volume) in air, it hardly has any odor and causes negative health effects. The DME has a low carbon-to-hydrogen ratio (C:H), a high oxygen content (around 35% by mass), and no carbon-carbon bonds in its molecular structure. Therefore, it can realize smoke-free combustion while also being used as an ignition promoter in order to ignite a low cetane number fuel in some studies (Hou et al., 2006; Kajitani et al., 1997; Kim et al., 2004; Orenson and Mikkelsen, 1995; Park and Lee, 2014; Yu and Bae, 2003).

Liang et al. (2011) studied the combustion and emissions performance of a DME-enriched SI methanol engine at idling conditions. The engine was modified to be fueled with the mixture of methanol and DME that was injected into the engine intake ports simultaneously (see Fig. 11.3 (Liang et al., 2011)). The experimental results showed that with the increase of the DME enrichment level at idling conditions, both flame development and propagation durations were shortened. Meanwhile, compared with the original methanol engine at stoichiometric condition, the largest drop of HC emissions was nearly 50%. However, with the addition of DME, the CO and NO_x emissions increased. Yao et al. (2006a,b) applied DME to the CNG and methanol HCCI combustion processes to promote ignition. It was found that as the DME was added, the ignition and operating range of CNG and methanol HCCI engines were improved. Zhang et al. (2014a,b) investigated the spray characteristics of methanol and DME on the swirl nozzle of a Stirling engine by comparing with traditional ULSD under different fuel injection rates and different surrounding back pressures in a constant volume pressure vessel. The results showed that the atomization quality of DME under atmospheric back pressure was much better than that of methanol and ULSD, while it became worse when ambient back pressure was higher than the saturated vapor pressure. Additionally, higher back pressure and a larger injection flow rate were beneficial to the atomization quality of

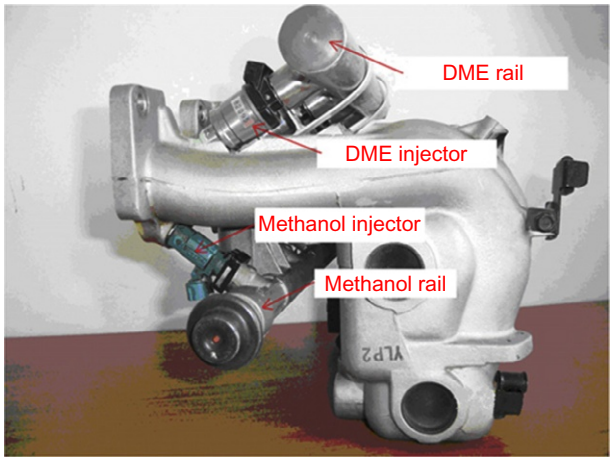

Fig. 11.3
Methanol and DME fuel rails and injectors installed on the intake manifolds.

ULSD, whereas those factors seem to have a relatively small influence on the droplet size distribution of methanol.

2.7 Engine Using Methanol-LPG Blends as Fuel

Methanol fuel can be blended with LPG in the engine. It can be blended with LPG in M85%L15 (85% methanol and 15% LPG) or other proportions. LPG is a by-product of natural gas production and crude oil refineries. LPG refers to the propane (C_3H_8) or butane (C_4H_{10}) or the mixtures of propane and butane in the same container with a specific ratio (Sulaiman et al., 2013; World LP Gas Association and United Nation Environment Programme, 2008). LPG can be blended with methanol fuel in an IC engine. Table 11.5 shows the physical and chemical properties of methanol and LPG (Gong et al., 2011).

Gong et al. (2011) studied the effects of the ambient temperature on the firing behavior and unregulated emissions of electronically controlled inlet port injection SI methanol and LPG-methanol engines. It was found that the LPG only played a part of start aids in the LPG-methanol engine. Using additional LPG injected into the inlet port resulted in a reliable firing of the LPG-methanol engine at a low ambient temperature during cold start. When the ambient temperature dropped, the mass ratio of injected LPG-methanol for the reliable firing of the LPG-methanol engine during cold start increased rapidly. Patil et al. (2014) studied the emission and performance enhancement of a multicylinder SI engine fueled with LPG and vaporized water methanol induction. The results showed that as the percentage of the water-methanol induction level of the engine increased, there was a slight increase in the

Table 11.5 The properties of methanol and LPG

Fuel Property	Methanol	LPG
Molecular weight	32	44
Composition (% m) C	37.5	81.8
H	12.5	18.2
O	50	0
Density (kg/m^3)	790	504
Boiling point (°C)	65	−30
Stoichiometric air/fuel ratio	6.5	15.7
Auto-ignition temperature (°C)	470	466
Research octane number	111	105
Flammability limit (%v)	6.7–36.2	4–9.5
Latent heat of vaporization (kJ/kg)	1110	406
Lower heating value (MJ/kg)	19.6	46.4
Flame speed (m/s)	0.523	0.37

percentage of useful work, while the NO_x decreased drastically, about 47%. Additionally, the engine BTE was increased.

2.8 Engine Using Methanol-Water Blends as Fuel

Methanol fuel can be blended with water in various proportions in SI engines. For example, it can be blended with M85W15 (85% methanol and 15% water) or other proportions. Methanol fuel is prone to absorb water when it is exposed to the atmosphere for a considerable amount of time, such as during transport or storage. Methanol-water blends, used as fuel for IC engines, could have an economic advantage compared to pure methanol because the methanol does not have to be fully dried in the production process (Sileghem et al., 2013).

Donnelly et al. (1976) concluded that, when as little as 0.1 vol% water was added to an M20 (20% methanol and 80% gasoline) blend, phase separation could occur at a temperature of 20°C. Because cof this very small water tolerance of the methanol-gasoline blend, water contamination during the methanol transport and storage had to be avoided. Besides the dependence of water content, it was also found that the tendency for phase separation was a strong function of methanol content and gasoline composition (Sileghem et al., 2013). Sileghem et al. (2013) studied the performance and emissions from a production-type four-cylinder SI gasoline engine running on gasoline, pure methanol, and methanol-water blends. Methanol-water blends of 2.5% v/v, 5% v/v, and 10% v/v water were tested. It was indicated that the BTE did not differ significantly for all methanol fuels and was still higher than the gasoline fuels. Additionally, with the higher water addition in the fuel, the NO_x emissions were decreased substantially. Breda et al. (2015) studied the potential as a knock suppressor of port-injected methanol-water mixtures and water in a high-turbocharged DISI engine. In order to find the best trade-off between fuel consumption, performance, and knock tendency, some different strategies in terms of methanol-water ratios of

the port-injected mixture were compared. It was found that at the analyzed operating condition, the best strategy seemed to be the injection of pure water, which led to the lowest indicated specific fuel consumption (ISFC).

2.9 Engine Using Methanol-Ethanol-Gasoline Blends as Fuel

Methanol fuel can be blended with ethanol-gasoline in an IC engine, and it can be blended with ethanol-gasoline. Using liquid alcohols such as methanol and ethanol in SI engines is a promising approach to transportation and securing the domestic energy supply. Methanol and ethanol are compatible with the existing fueling and distribution infrastructure and are easily stored in a vehicle. They can be used in IC engines with only minor adjustments and have the potential to increase the efficiency and decrease noxious emissions compared to gasoline engines (Sileghem et al., 2013). Table 11.6 shows the physical and chemical properties of methanol and ethanol (Sileghem et al., 2013).

Turkcan et al. (2013) studied the effects of second injection timing on combustion characteristics of a two-stage direct-injection gasoline-alcohol HCCI engine. The methanol and ethanol were blended with gasoline fuel. It was found that the combustion and emissions characteristics could be directly controlled while the HCCI operating range could be extended

Table 11.6 The properties of methanol and ethanol

Fuel Property	Methanol	Ethanol
Chemical structure	CH_3OH	C_2H_5OH
Oxygen content by mass (%)	50	34.8
Density at NTP (kg/L)	0.79	0.79
Lower heating value (MJ/kg)	20.09	26.95
Volumetric energy content (MJ/L)	15.9	21.3
Stoichiometric air to fuel ratio (kg/kg)	6.5	9
Energy per unit mass of air (MJ/kg)	3.12	3.01
Research octane number	109	109
Motor octane number	88.6	89.7
Sensitivity (RON-MON)	20.4	19.3
Boiling point at 1 bar (°C)	65	79
Heat of vaporization (kJ kg)	1100	838
Reid vapor pressure (psi)	4.6	2.3
Mole ratio of products to reactants	1.061	1.065
Flammability limits in air (λ)	0.23–1.81	0.28–1.91
Laminar flame speed at $NTP_{sss}=1$ (cm/s)	42	40
Adiabatic flame temperature (°C)	1870	1920
Specific CO_2 emissions (g/MJ)	68.44	70.99

by the second fuel injection timing. Compared with the gasoline case at a low equivalence ratio, the better combustion characteristics, lower NO_x, unburnt hydrocarbons (UHC) and CO emissions, and higher indicated mean effective pressure (IMEP) and indicated efficiency values were obtained based on the optimization of the second fuel injection timings. Balki et al. (2014) studied the effects of different alcohol (methanol and ethanol) fuels on the performance, emissions, and combustion characteristics in a low-power single-cylinder engine. The results showed that, compared with the conventional gasoline operation, the use of alcohol fuels increased the engine torque, brake specific fuel consumption (BSFC), thermal efficiency, and combustion efficiency. In addition, the cylinder gas pressure and heat release rate occurred earlier; CO_2 emission increased while HC, CO, and NO_x emissions decreased.

Iliev (2015) analyzed the performance and emissions characteristics for different blends of ethanol, methanol, and gasoline (by volume) by using a one-dimensional engine model. The results indicated that, compared with gasoline fuel, the brake power decreased and the BSFC increased when using alcohol-gasoline fuel blends. In addition, with the increase of fuel blends proportions, the CO and HC concentration decreased. As the fuel blends proportions increased up to 30% (E30M30), there was a significant increase in NO_x emissions. Elfasakhany (2015) investigated the performance and exhaust emissions from an SI engine fueled with ethanol-methanol-gasoline blends. The results showed that, compared with the neat gasoline fuel, the concentrations of CO and UHC emissions were significantly decreased. The lowest emissions of CO and UHC among all test fuels were presented by using methanol-gasoline blends. Balki et al. (2016) optimized the operating parameters based on the Taguchi method in an SI engine using pure gasoline, ethanol, and methanol. According to the result, the optimum CR and engine speed value were found to be 9.0 and 2400 rpm for all fuels. While the optimum IT was also 20ºCA for alcohol fuels, it is 26ºCA in gasoline.

2.10 Engine Using Methanol-Ethanol-Diesel Blends as Fuel

Alcohols, mainly methanol and ethanol, in combination with diesel fuel have been widely investigated for reducing NO_x and PM emissions (Agarwal, 2007). The solubility of ethanol in diesel fuel is affected by temperature and the water content of the fuel (2005). Due to many reasons such as low cetane number, high latent heat of vaporization, and high ignition temperature, methanol fuel has a low ability for self-ignition (Byraktar, 2008). Methanol fuel can be blended with ethanol-diesel in engines, and it can be blended with ethanol-diesel. Karabektas et al. (2013) studied the effects of blends containing low ratios of alternative fuels on the performance and emission characteristics in a naturally aspirated, direct-injection diesel engine. The considered parameters were brake power, specific fuel consumption (SFC), and thermal efficiency as well as carbon monoxide, hydrocarbon, and nitrogen oxide emissions. The experimental results showed that the ethanol and methanol blends yielded lower brake power while resulting in higher SFC and lower CO emissions.

2.11 Engine Using Methanol-Diesel-Isopropyl Alcohol Blends as Fuel

Among various developments in reducing emissions, the application of oxygenated fuels to diesel engines is an effective way to reduce smoke emissions. The addition of oxygen-containing compounds to diesel fuel has been proposed as a way to complete the oxidation of carbonaceous particulate matter and associated hydrocarbons. In addition, many oxygenates have a high cetane number and their association with diesel results in a high cetane number and hence lower CO and HC emissions with little variation in NO_x emission (Yu et al., 2011). Methanol fuel can be blended with diesel-isopropyl alcohol in the engine. Table 11.7 shows the physical and chemical properties of methanol, diesel, and isopropyl alcohol (Chockalingam and Ganapathy, 2012).

Chockalingam and Ganapathy (2012) studied the performance and emission of a single-cylinder constant-speed diesel engine fueled with diesel, methanol, and isopropyl alcohol blends. Four fuel blends—namely 80:10:10, 70:20:10, 60:20:20, and 50:30:20 proportions by volume of diesel, methanol, and isopropyl alcohol—were considered in the diesel engine. The mixing protocol consisted of first blending the additive isopropyl alcohol into the methanol and then blending this mixture into the diesel fuel. The results showed that, compared with the neat fuel, the engine performance fueled with blends was improved. As a cetane number improver, isopropyl alcohol was acting as a surfactant to retain the homogeneity of the methano-diesel mixture. With the addition of the isopropyl alcohol, the HC emissions were decreased. As the methanol was increased in the blend, the smoke density was decreased significantly.

2.12 Engine Using Methanol-Diesel-Biodiesel Blends as Fuel

Methanol fuel can be blended with diesel-biodiesel in an IC engine. The addition of higher oxygen content and high volatility methanol can be a promising technique for using the biodiesel-diesel blend efficiently in diesel engines without any modifications in the engine. Qi et al. (2010) investigated the performance and combustion characteristics of a

Table 11.7 The properties of methanol, diesel and isopropyl alcohol

Fuel Property	Methanol	Diesel	Isopropyl alcohol
Molecular formula	CH_3OH	C_xH_y	C_3H_8O
Molecular weight	32.042	190-220	60.09
Specific gravity	0.796	0.83	0.7851
% of oxygen by weight	50	0	26
Heat of evaporation (kJ/kg)	1100	260	666
Cetane number	<5	45–50	–
Lower heating value (kJ/kg)	11,770	42,600	24,040

biodiesel-diesel-methanol blend fueled engine. The BD50 (50% biodiesel and 50% diesel in vol.) was prepared as the baseline fuel. Methanol was added to BD50 as an additive by volume percent of 5% and 10% (denoted as BDM5 and BDM10). The results showed that the addition of higher oxygen content and high volatility methanol could be a promising technique for using biodiesel-diesel blend efficiently in diesel engines without any modifications in the engine. Mat Yasin et al. (2014) studied the characterization of a diesel engine operating with a small proportion of methanol as a fuel additive in the biodiesel blend. The results showed that with the addition of biodiesel to methanol, the combustion pressure was improved. Compared with the diesel, the brake SFC was higher; however, the NO_x was increased while CO and CO_2 were decreased.

Yilmaz (2012a,b) studied the stand B45D45M10 (45% biodiesel, 45% diesel, and 10% methanol), B40D40M20 (40% biodiesel, 40% diesel, and 20% methanol), B45D45E10 (45% biodiesel, 45% diesel, and 10% ethanol) and B40D40E20 (40% biodiesel, 40% diesel, and 20% ethanol) blends in a compression-ignited engine under the same operating conditions. The results showed that biodiesel-alcohol-diesel blends showed higher BSFC than diesel as alcohol concentrations in blends increased, CO and HC emissions increased while NO emission decreased. Methanol blends were more effective than ethanol blends for reducing CO and HC emissions. Yasin et al. (2015) studied the biodiesel-methanol-diesel low proportion blends operating with a multicylinder diesel engine. The results showed that biodiesel-methanol-diesel blends showed higher BSFC than mineral diesel. In addition, a biodiesel-diesel blend with 5% of methanol was more effective for reducing CO emissions than a biodiesel blend with 20%. Zaglinskis et al. (2016) investigated the properties of a compression ignition engine fueled by biodiesel, methanol, and diesel fuel. It was found that BSFC increased for B30 (30% biodiesel in vol) and B3010M (30% biodiesel and 10% methanol in vol) BTE increased. Both blends showed reduced soot concentration and ambiguous distribution of incomplete combustion product emission values.

Venu and Madhavan (2017) studied the influence of diethyl ether addition in ethanol-biodiesel-diesel and methanol-biodiesel-diesel blends in a diesel engine. It was found that as the diethyl ether was added in MBD (blend of methanol (20%)-biodiesel (40%)-diesel (40%)), it decreased the combustion duration and HC and NO_x emissions. The lowest NO_x and BSFC were recorded for MBD-5DEE (blend of MBD with 5% diethyl ether).

2.13 Engine Using Methanol-Diesel-Dodecanol Blends as Fuel

Methanol fuel can be blended with diesel-dodecanol in an IC engine. Methanol can be used in CI engines purely or by blending with conventional diesel fuel. Problems concerning the use of methanol in diesel engines can be resolved by different approaches. Using it in CI engines as diesel-methanol blends is the simplest method. The most important problem encountered in

this case is the phase separation. This problem can be prevented by adding some solvent into the mixture (Murayama et al., 1982). Table 11.8 shows the physical and chemical properties of diesel, methanol, and 1-dodecanol (Byraktar, 2008). Byraktar (2008) investigated the performance parameters of an experimental compression ignition engine fueled with diesel-methanol-dodecanol blends. The methanol concentration in the blend has been changed from 2.5% to 15% with increments of 2.5%, and 1% dodecanol was added into each blend to solve the phase-separation problem. It was found that among the different blends, the blend including 10% methanol was the most suited for CI engines from the engine performance point of view. Methanol caused improvements in the engine's effective power. Many parameters such as torque and SFC were improved about 7% with the blend of DM10. The optimum proportion of methanol was determined to be 10%. If some cetane improver was added into the blends, the cetane rating could be raised, which may obtain the better results.

2.14 Engine Using Methanol-Gasoline-n-Butanol Blends as Fuel

Compared with the methanol fuel, *n*-butanol has some advantages. Butanol is less corrosive than methanol, and it can be distributed using the same infrastructure used to transport gasoline. If the butanol alcohol can be demonstrated for use in the IC engine designed for use with gasoline with some minor modifications (Szwaja and Naber, 2010). Elfasakhany and Mahrous (2016) investigated the performance and emissions assessment of *n*-butanol-methanol-gasoline blends in an SI engine. It was concluded that higher rates of *n*-butanol-methanol blended in gasoline could improve the SI engine performance parameters and emission concentration. The performance (higher performance and lower emissions) of dual alcohol-gasoline blends could exceed single alcohol-gasoline blends and pure gasoline at higher rates.

Table 11.8 The properties of diesel, methanol and dodecanol

Fuel Property	Diesel	Methanol	1-Dodecanol
Molecular formula	$C_{14.342}H_{24.75}$	CH_3OH	$C_{12}H_{26}O$
Molecular weight (kg/kmol)	197.21	32.042	186.339
Stoichiometric fuel/air ratio	0.06924	0.15393	0.07462
Cetane number	45–55	3–5	–
Flash point (°C)	78	11	107
Ignition temperature (°C)	235	470	527
Viscosity at 298.15 K (mPa s)	3.35	0.59	16.136
Density (g/cm^3)	0.83	0.79	0.83
Lower heating value (MJ/kg)	42.740	20.270	39.860
Heat of vaporization (MJ/kg)	0.270	1.110	–

3 Conclusions and Recommendations

This section systematically introduces methanol fuel as an alternative in IC engines. Many various applications such as pure methanol, methanol-gasoline, and methanol-diesel blends that can be used in the IC engines are summarized. Compared with the conventional fossil fuels such as gasoline or diesel, methanol fuel has the potential to reduce vehicle emissions, and consequently to improve the atmospheric environment and reduce pressure on energy demand.

From the engineering application perspective, methanol is an ideal alternative: renewable as well as an environmentally and economically attractive fuel for IC engines. Despite great efforts made by researchers, methanol applications are still a crucial topic concerning the design and development for IC engines, and they need further improvements. The development of new methanol storage and transportation technologies would play an important role in the promotion and application of IC engines. The development of high CR engines (pure methanol or methanol blends) to replace the high-power, high-efficiency vehicle engines (for instance, diesel engine), would have great realistic significance. For the development of the methanol engine, the study of combustion and emission mechanisms of methanol fuel or methanol blends is the core scientific engineering technology issue. It is a good idea to develop some new combustion modes such as HCCI, premixed charge compression ignition (PCCI), and RCCI, which play an important role in the development of methanol engines. So, it is believed that future studies should focus on these areas, which not only could help explain the combustion and emission mechanisms of methanol fuel or methanol blends but also make an important contribution to the development and application for methanol engines so as to meet the market demand.

References

Agarwal, A.K., Shukla, P.C., Patel, C., Gupta, J.G., Sharma, N., Prasad, R.K., Agarwal, R.A., 2016. Unregulated emissions and health risk potential from biodiesel (KB5, KB20) and methanol blend (M5) fuelled transportation diesel engines. Renew. Energy 98, 283–291.

Agarwal, A.K., 2007. Biofuels (alcohols and biodiesel) applications as fuels for internal combustion engines. Prog. Energy Combust. Sci. 33, 233–271.

Anand, K., Sharma, R.P., Mehta, P.S., 2011. Experimental investigations on combustion, performance and emissions characteristics of neat karanji biodiesel and its methanol blend in a diesel engine. Biomass Bioenergy 35, 533–541.

Balki, M.K., Sayin, C., Sarikaya, M., 2016. Optimization of the operating parameters based on Taguchi method in an SI engine used pure gasoline, ethanol and methanol. Fuel 180, 630–637.

Balki, M.K., Sayin, C., Canakci, M., 2014. The effect of different alcohol fuels on the performance, emission and combustion characteristics of a gasoline engine. Fuel 115, 901–906.

Boretti, A., 2013. Renewable hydrogen to recycle CO_2 to methanol. Int. J. Hydrog. Energy 38, 1806–1812.

Breda, S., Berni, F., d'Adamo, A., Testa, F., Severi, E., Cantore, G., 2015. Effects on knock intensity and specific fuel consumption of port water/methanol injection in a turbocharged GDI engine: Comparative analysis. Energy Procedia 82, 96–102.

Brusstar, M., Stuhldreher, M., Swain, D., Pidgeon, W., 2002. High efficiency and low emissions from a port-injected engine with neat alcohol fuels. SAE Technical Paper No 2002-01-2743.

Byraktar, H., 2008. An experimental study on the performance parameters of an experimental CI engine fueled with diesel-methanol-dodecanol blends. Fuel 87, 158–164.

Canakci, M., Ozsezen, A.N., Alptekin, E., Eyidogan, M., 2013. Impact of alcohol-gasoline fuel blends on the exhaust emission of an SI engine. Renew. Energy 52, 111–117.

Cay, Y., Korkmaz, I., Cicek, A., Kara, F., 2013. Prediction of engine performance and exhaust emissions for gasoline and methanol using artificial neural network. Energy 50, 177–186.

Celik, M.B., Ozdalyan, B., Alkan, F., 2011. The use of pure methanol as fuel at high compression ratio in a single cylinder gasoline engine. Fuel 90, 1591–1598.

Chao, H.R., Lin, T.C., Chao, M.R., Chang, F.H., Huang, C.I., Chen, C.B., 2000. Effect of methanol-containing additive on the emission of carbonyl compounds from a heavy-duty diesel engine. J. Hazard. Mater. B73, 39–54.

Chen, Z., Yao, C., Wang, Q., Han, G., Dou, Z., Wei, H., Wang, B., Liu, M., Wu, T., 2016. Study of cylinder-to-cylinder variation in a diesel engine fueled with diesel/methanol dual fuel. Fuel 170, 67–76.

Cheung, C.S., Zhu, L., Huang, Z., 2009. Regulated and unregulated emissions from a diesel engine fueled with biodiesel and biodiesel blended with methanol. Atmos. Environ. 43, 4865–4872.

Cheng, C.H., Cheung, C.S., Chan, T.L., Lee, S.C., Yao, C.D., 2008a. Experimental investigation on the performance, gaseous and particulate emissions of a methanol fumigated diesel engine. Sci. Total Environ. 389, 115–124.

Cheng, C.H., Cheung, C.S., Chan, T.L., Lee, S.C., Yao, C.D., Tsang, K.S., 2008b. Comparison of emissions of a direct injection diesel engine operating on biodiesel with emulsified and fumigated methanol. Fuel 87, 1870–1879.

Chockalingam, S., Ganapathy, S., 2012. Performance and emissions analysis of a single cylinder constant speed diesel engine fuelled with diesel-methanol-isopropyl alcohol blends SAE Technical Paper No. 2012-01-1683.

Clausen, L.R., Houbak, N., Elmegaard, B., 2010. Technoeconomic analysis of a methanol plant based on gasification of biomass and electrolysis of water. Energy 35, 2338–2347.

Datta, B.Y., Govinda Rao, B., Dharma Rao, Anusha, C., 2016. Alexandria Eng. J. 55, 1201–1209.

Dhaliwal, B., Yi, N., Checkel, D., 2000. Eissions effects of alternative fuels in light-duty and heavy-duty vehicles. SAE Technical Paper No. 2000-01-0692.

Donnelly, R.G., Heywood, J.B., LoRusso, J., O'Brien, F., Reed, T.B., 1976. Methanol as an automotive fuel: a summary of research in the M. I. T. Energy Laboratory. Final Report.

Elfasakhany, A., Mahrous, A.F., 2016. Performance and emissions assessment of *n*-butanol-methanol-gasoline blends as a fuel in spark-ignition engines. Alexandria Eng. J. 55, 3015–3024.

Elfasakhany, A., 2015. Investigations on the effects of ethanol-methanol-gasoline blends in a spark-ignition engine: performance and emissions analysis. Eng. Sci. Technol. Int. J. 18, 713–719.

Gong, C.M., Li, D., Li, Z., Liu, F.H., 2016a. Numerical study on combustion and emission in a DISI methanol engine with hydrogen addition. Int. J. Hydrog. Energy 41, 647–655.

Gong, C.M., Liu, F.H., Sun, J.Z., Wang, K., 2016b. Effect of compression ratio on performance and emissions of a stratified-charge DISI (direct injection spark ignition) methanol engine. Energy 96, 166–175.

Gong, C.M., Li, J., Li, J.K., Li, W.X., Gao, Q., Liu, X.J., 2011. Effects of ambient temperature on firing behavior and unregulated emissions of spark-ignition methanol and liquefied petroleum gas/methanol engines during cold start. Fuel 90, 19–25.

Gravalos, I., Moshou, D., Gialamas, T., Xyradakis, P., Kateris, D., Tisiropoulos, Z., 2013. Emissions characteristics of spark ignition engine operating on lower-higher molecular mass alcohol blended gasoline fuels. Renew. Energy 50, 27–30.

Holmgren, K.M., Berntsson, T., Andersson, E., Rydberg, T., 2012. System aspects of biomass gasification with methanol synthesis—process concepts and energy analysis. Energy 45, 817–828.

Hou, Y.C., Ji, L.B., Zu, L.L., Huang, Z., 2006. Heat release analysis on combustion and parametric study on emissions of HCCI engines fueled with 2-propanol/*n*-heptane blend fuels. Energy Fuel 20, 1870–1878.

Hu, E., Huang, Z., He, J., Miao, H., 2009a. Experimental and numerical study on lean premixed methane-hydrogen-air flames at elevated pressures and temperatures. Int. J. Hydrog. Energy 34, 6951–6969.
Hu, E., Huang, Z., Liu, B., Zheng, J., Gu, X., Huang, B., 2009b. Experimental investigation on performance and emissions of a spark-ignition engine fuelled with natural gas/hydrogen blends combined with EGR. Int. J. Hydrog. Energy 34, 528–539.
Huang, Z.H., Lu, H.B., Jiang, D.M., Zeng, K., Liu, B., Zhang, J.Q., et al., 2004. Combustion behaviors of a compression-ignition engine fuelled with diesel/methanol blends under various fuel delivery advance angles. Bioresour. Technol. 95, 331–341.
Iliev, S., 2015. A comparison of ethanol and methanol blending with gasoline using a 1-D engine model. Procedia Eng. 100, 1013–1022.
Ji, C., Yang, J., Liu, X., Zhang, B., Wang, S., Gao, B., 2016. A quasi-dimensional model for combustion performance prediction of an SI hydrogen-enriched methanol engine. Int. J. Hydrog. Energy 41, 17676–17686.
Ji, C., Wang, S., 2009. Effect of hydrogen addition on combustion and emissions performance of a spark ignition gasoline engine at lean conditions. Int. J. Hydrog. Energy 34, 7823–7834.
Ji, C.W., Zhang, B., Wang, S.F., 2013. Enhancing the performance of a spark-ignition methanol engine with hydrogen addition. Int. J. Hydrog. Energy 38, 7490–7498.
Kajitani, S., Chen, Z., Konno, M., Rhee, K.T., 1997. Engine performance and exhaust characteristics of direct-injection diesel engine operated with DME. SAE Technical Paper No. 972973.
Karabektas, M., Ergen, G., Hosoz, M., 2013. Effects of the blends containing low ratios of alternative fuels on the performance and emission characteristics of a diesel engine. Fuel 112, 537–541.
Kim, D., Kim, M., Lee, C., 2004. Effect of premixed gasoline fuel on the combustion characteristics of compression ignition engine. Energy Fuel 18, 1213–1219.
Li, G., Zhang, C., Li, Y., 2016a. Effects of diesel injection parameters on the rapid combustion and emissions of an HD common-rail diesel engine fueled with diesel-methanol dual-fuel. Appl. Therm. Eng. 108, 1214–1225.
Li, Y., Zhang, C., Yu, W., Wu, H., 2016b. Effects of rapid burning characteristics on the vibration of a common-rail diesel engine fueled with diesel-methanol dual-fuel. Fuel 170, 176–184.
Li, Z., Gong, C.M., Qu, X., Liu, F., Sun, J., 2015. Critical firing and misfiring boundary in a spark ignition methanol engine during cold start based on single cycle fuel injection. Energy 89, 236–243.
Li, Y.P., Jia, M., Liu, Y.D., Xie, M.Z., 2013. Numerical study on the combustion and emission characteristics of a methanol/diesel reactivity controlled compression. Appl. Energy 106, 184–197.
Li, J., Gong, C.M., Su, Y., Dou, H.L., Liu, X.J., 2010a. Effect of injection and ignition timings on performance and emissions from a spark-ignition engine fueled with methanol. Fuel 89, 3919–3925.
Liang, C., Ji, C.W., Liu, X.L., 2011. Combustion and emissions performance of a DME-enriched spark-ignited methanol engine at idle condition. Appl. Energy 88, 3704–3711.
Li, H.Q., Hong, H., Jin, H.G., Cai, R.X., 2010b. Analysis of a feasible polygeneration system for power and methanol production taking natural gas and biomass as materials. Appl. Energy 87, 2846–2853.
Liang, B., Ge, Y., Tan, J., Han, X., Gao, L., Hao, L., Ye, W., Dai, P., 2013. Comparison of PM emissions from a gasoline direct injected (GDI) vehicle and a port fuel injection (PFI) vehicle measured by electrical low pressure impactor (ELPI) with two fuels: gasoline and M15 methanol gasoline. J. Aerosol Sci. 57, 22–31.
Liu, H., Wang, Z., Long, Y., Xiang, S., Wang, J., Wagnon, S.W., 2015. Methanol-gasoline Dual-fuel Spark Ignition (DFSI) combustion with dual-injection for engine particle number (PN) reduction and fuel economy improvement. Energy 89, 1010–1017.
Liu, H., Wang, Z., Wang, J., 2014. Methanol-gasoline DFSI (dual-fuel spark ignition) combustion with dual-injection for engine knock suppression. Energy 73, 686–693.
Liu, X.L., Ji, C.W., Gao, B.B., Wang, S.F., Liang, C., Yang, J.X., 2013. A laminar flame speed correlation of hydrogen-methanol blends valid at engine-like conditions. Int. J. Hydrog. Energy 38, 15500–15509.
Liu, S.H., Eddy, R.C.C., Hu, T.G., Wei, Y.J., 2007. Study of spark ignition engine fueled with methanol/gasoline fuel blends. Appl. Therm. Eng. 27, 1904–1910.
Mat Yasin, M.H., Yusaf, T., Mamat, R., Fitri Yusop, A., 2014. Characterization of a diesel engine operating with a small proportion of methanol as a fuel additive in biodiesel blend. Appl. Energy 114, 865–873.

Murayama, T., Miyamoto, N., Yamada, T., Kawashima, J.I., 1982. A method to improve the solubility and combustion characteristics of alcohol-diesel fuel blends. SAE Technical Paper No. 821113.

Nagafi, G., Yusaf, T.F., 2009. Experimental investigation of using methanol-diesel blended fuels in diesel engine. In: Proceedings of the Fourth International Conference on Thermal Engineering: Theory and Applications, Abu Dhabi, UAE, pp. 1–5.

Olah, G.A., 2005. Beyond oil and gas: the Methanol Economy. Angew. Chem. Int. Ed. 44 (18), 2636–2639.

Orenson, S.C., Mikkelsen, S.E., 1995. Performance and emissions of a 0.273 liter direct injection diesel engine fuelled with neat dimethyl ether. SAE Technical Paper No. 950064.

Pan, W., Yao, C., Han, G., Wei, H., Wang, Q., 2015. The impact of intake air temperature on performance and exhaust emissions of a diesel methanol dual fuel engine. Fuel 162, 101–110.

Park, S.H., Lee, C.S., 2014. Applicability of dimethyl ether (DME) in a compression ignition engine as an alternative fuel. Energy Convers. Manag. 86, 848–863.

Patil, B., Nayak, V., Padmanabha, M., 2014. Emission and performance enhancement of multi-cylinder SI engine fuelled with LPG and vaporized water methanol induction. SAE Technical Papers No. 2014-01-2764.

Prashant, G.K., Lata, D.B., Joshi, P.C., 2016. Investigations on the effect of methanol blend on the combustion parameters of dual fuel diesel engine. Appl. Therm. Eng. 103, 187–194.

Qi, D.H., Chen, H., Geng, L.M., Bian, Y.Z.H., Ren, X.C.H., 2010. Performance and combustion characteristics of biodiesel-diesel-methanol blend fuelled engine. Appl. Energy 87, 1679–1686.

Qu, X., Gong, C.M., Liu, J.J., Cui, F.Y., Liu, F.H., 2015. Regulated and unregulated emissions from a DISI methanol engine under homogenous combustion and light load. Fuel 158, 166–175.

Reno, M.L.G., Lora, E.E.S., Palacio, J.C.E., Venturini, O.J., Buchgeister, J., Almazan, O., 2011. A LCA (life cycle assessment) of the methanol production from sugarcane bagasse. Energy 36, 3716–3726.

Sayin, C., Ozesezen, A.N., Canakci, M., 2010. The influence of operating parameters on performance and emissions of a DI diesel engine using methanol-blended-diesel fuel. Fuel 89, 1407–1414.

Sayin, C., 2010. Engine performance and exhaust gas emissions of methanol and ethanol-diesel blends. Fuel 89, 3410–3415.

Sayin, C., Ilhan, M., Canakci, M., Gumus, M., 2009. Effect of injection timing on the exhaust emissions of a diesel engine using diesel-methanol blends. Renew. Energy 34, 1261–1269.

Schafer, F., 1981. An investigation of the addition of hydrogen to methanol on the operation of an unthrottled otto engine. SAE Technique No., 810776.

Sileghem, L., Huylebroeck, T., Van den Bulcke, A., Vancoillie, J., Verhelst, S., 2013. Performance and emissions of a SI engine using methanol-water blends. SAE Technical Paper No. 2013-01-1319.

Siwale, L., Kristof, L., Bereczky, A., Mbarawa, M., Kolesnikov, A., 2014. Performance, combustion and emission characteristics of *n*-butanol additive in methanol-gasoline blend fired in a naturally-aspirated spark ignition engine. Fuel Process. Technol. 118, 318–326.

Soni, D.K., Gupta, R., 2016. Numerical investigation of emission reduction techniques applied on methanol blended diesel engine. Alexandria Eng. J. 55, 1867–1879.

Sulaiman, M.Y., Ayob, M.R., Meran, I., 2013. Performance of single cylinder spark ignition engine fueled by LPG. Procedia Eng. 53, 579–585.

Surawski, N.C., Ristovski, Z.D., Brown, R.J., Situ, R., 2012. Gaseous and particle emissions from an ethanol fumigated compression ignition engine. Energy Convers. Manag. 54, 145–151.

Szwaja, S., Naber, J.D., 2010. Combustion of *n*-butanol in a spark ignition IC engine. Fuel 89, 1573–1582.
Elfasakhany, A., 2015. Experimental investigation on SI engine using gasoline and a hybrid iso-butanol/gasoline fuel. Energy Convers. Manag. 89, 398–405.

Turkcan, A., Ozsezen, A.N., Canakci, M., 2013. Effects of second injeciton timing on combustion characteristics of a two stage direct injection gasoline-alcohol HCCI engine. Fuel 111, 30–39.

Vancoillie, J., Demuynck, J., Sileghem, L., Van De Ginste, M., Verhelst, S., Brabant, L., et al., 2013. The potential of methanol as a fuel for flex-fuel and dedicated spark-ignition engines. Appl. Energy 102, 140–149.

Vancoillie, J., Demuynck, J., Sileghem, L., Van De Ginste, M., Verhelst, S., 2012a. Comparison of the renewable transportation fuels, hydrogen and methanol formed from hydrogen, with gasoline—engine efficiency study. Int. J. Hydrog. Energy 92, 628–636.

Vancoillie, J., Demuynck, J., Sileghem, L., Van De Ginste, M., Verhelst, S., 2012b. Comparison of the renewable transportation fuels, hydrogen and methanol formed from hydrogen, with gasoline—engine efficiency study. Int. J. Hydrog. Energy 37, 9914–9924.

Venu, H., Madhavan, V., 2017. Influence of diethyl ether (DEE) addition in ethanol-biodiesel-diesel (EBD) and methanol-biodiesel-diesel (MBD) blends in a diesel engine. Fuel 189, 377–390.

Wang, Q., Wang, B., Yao, C., Liu, M., Wu, T., Wei, H., Dou, Z., 2016a. Study on cyclic variability of dual fuel combustion in a methanol fumigated diesel engine. Fuel 164, 99–109.

Wang, Q., Yao, C., Dou, Z., Wang, B., Wu, T., 2015a. Effect of intake pre-heating and injection timing on combustion and emission characteristics of a methanol fumigated diesel engine at part load. Fuel 159, 796–802.

Wang, X., Ge, Y., Zhang, C., Tan, J., Hao, L., Liu, J., Gong, H., 2016b. Effects of engine misfire on regulated, unregulated emissions from a methanol-fueled vehicle and its ozone forming potential. Appl. Energy 177, 187–195.

Wang, X., Ge, Y., Liu, L., Peng, Z., Hao, L., Yin, H., Ding, Y., Wang, J., 2015b. Evaluation on toxic reduction and fuel economy of a gasoline direct injection- (GDI-) powered passenger car fueled with methanol-gasoline blends with various substitution ratios. Appl. Energy 157, 134–143.

Wang, S., Ji, C., Zhang, B., 2010. Effect of hydrogen addition on combustion and emissions performance of a spark-ignited ethanol engine at idle and stoichiometric conditions. Int. J. Hydrog. Energy 35, 9205–9213.

Wei, L., Yao, C., Han, G., Pan, W., 2016. Effects of methanol to diesel ratio and diesel injection timing on combustion, performance and emissions of a methanol port premixed diesel engine. Energy 95, 223–232.

Wu, B., Wang, L., Shen, X., Yan, R., Dong, P., 2016. Comparison of lean burn characteristics of an SI engine fueled with methanol and gasoline under idle condition. Appl. Therm. Eng. 95, 264–270.

Wei, Y., Liu, S., Liu, F., Liu, J., Zhu, Z., Li, G., 2009. Aldehydes and methanol emission mechanisms and characteristics from a methanol/gasoline-fueled spark-ignition (SI) engine. Energy Fuel 23, 6222–6230.

World LP Gas Association and United Nation Environment Programme, 2008. Guidelines for Good Safety Practices in the LP Gas Industry. France.

Xie, F., Li, X., Su, Y., Hong, W., Jiang, B., Han, L., 2016. Influence of air and EGR dilutions on improving performance of a high compression ratio spark-ignition engine fueled with methanol at light load. Appl. Therm. Eng. 94, 559–567.

Yao, M.F., Zheng, Z.Q., Qin, J., 2006a. Experimental study on homogeneous charge compression ignition combustion with fuel of dimethyl ether and natural gas. J. Eng. Gas Turbines Power 128, 414–420.

Yao, M.F., Chen, Z., Zheng, Z.Q., Zhang, B., Xing, Y., 2006b. Study on the controlling strategies of homogeneous charge compression ignition combustion with fuel of dimethyl ether and methanol. Fuel 85, 2046–2056.

Yasin, M.H.M., Mamat, R., Yusop, A.F., Aziz, A., Najafi, G., 2015. Comparative study on biodiesel-methanol-diesel low proportion blends operating with a diesel engine. Energy Procedia 75, 10–16.

Yilmaz, N., 2012a. Performance and emission characteristics of a diesel engine fuelled with biodiesel-ethanol and biodiesel-methanol blends at elevated air temperatures. Fuel 94, 440–443.

Yilmaz, N., Sanchez, T.M., 2012. Analysis of operating a diesel engine on biodiesel-ethanol and biodiesel-methanol blends. Energy 46, 126–129.

Yilmaz, N., 2012b. Comparative analysis of biodiesel-ethanol-diesel and biodiesel-methanol-diesel blends in a diesel engine. Energy 40, 210–213.

Yu, W., Chen, G., Huang, Z.H., 2011. Influence of cetane number improver on performance and emissions of a common-rail diesel engine fueled with biodiesel-methanol blend, Front. Energy 5 (4), 412–418.

Yu, J., Bae, C., 2003. Dimethyl ether (DME) spray characteristics in a common-rail fuel injection system. Proc. Inst. Mech. Eng. D: J. Autom. Eng. 217, 113–144.

Zaglinskis, J., Lukacs, K., Bereczky, A., 2016. Comparison of properties of a compression ignition engine operating on diesel-biodiesel blend with methanol additive. Fuel 170, 245–253.

Zhang, C., Wu, H., 2016. Combustion characteristics and performance of a methanol fueled homogeneous charge compression ignition (HCCI) engine. J. Energy Inst. 89, 346–353.
Zhang, B., Ji, C., Wang, S., Zhou, X., 2014a. Idling performance of a hydrogen-blended methanol engine at lean conditions. Energy Procedia 61, 331–334.
Zhang, W., Chen, X., Gu, G., Hu, H., Liu, T., Huang, Z., 2014b. Experimental study of the spray characteristics of USLD, methanol and DME on the swirl nozzle of a Stirling engine. Fuel Process. Technol. 119, 1–9.
Zhang, Z.H., Cheung, C.S., Yao, C.D., 2013. Influence of fumigation methanol on the combustion and particulate emissions of a diesel engine. Fuel 111, 442–448.
Zhang, F., Shuai, S., Wang, Z., Zhang, X., Wang, J., 2011a. A detailed oxidation mechanism for the prediction of formaldehyde emission from methanol-gasoline SI engines. Proc. Combust. Inst. 33, 3151–3158.
Zhang, Z.H., Tsang, K.S., Cheung, C.S., Chan, T.L., Yao, C.D., 2011b. Effect of fumigation methanol and ethanol on the gaseous and particulate emissions of a direct-injection diesel engine. Atmos. Environ. 45, 2001–2008.
Zhang, Z.H., Cheung, C.S., Chan, T.L., Yao, C.D., 2010a. Experimental investigation of regulated and unregulated emissions from a diesel engine fueled with Euro V diesel fuel and fumigation methanol. Atmos. Environ. 44, 1054–1061.
Zhang, Z.H., Cheung, C.S., Chan, T.L., Yao, C.D., 2010b. Experimental investigation on regulated and unregulated emissions of a diesel/methanol combustion engine with and without diesel oxidation catalyst. Sci. Total Environ. 408, 865–872.
Zhen, X.D., Wang, Y., 2015a. An overview of methanol as an internal combustion engine fuel. Renew. Sust. Energ. Rev. 52, 477–493.
Zhen, X.D., Wang, Y., 2015b. Numerical analysis on original emissions for a spark ignition methanol engine based on detailed chemical kinetics. Renew. Energy 81, 43–51.
Zhen, X.D., Wang, Y., 2015c. Numerical analysis of knock during HCCI in a high compression ratio methanol engine based on LES with detailed chemical kinetics. Energy Convers. Manag. 96, 188–196.
Zhen, X.D., Wang, Y., Xu, S.Q., Zhu, Y.S., 2013a. Study of knock in a high compression ratio spark-ignition methanol engine by multi-dimensional simulation. Energy 50, 150–159.
Zhen, X.D., Wang, Y., Zhu, Y.S., 2013b. Study of knock in a high compression ratio SI methanol engine using LES with detailed chemical kinetics. Energy Convers. Manag. 75, 523–531.
Zhen, X.D., Wang, Y., Xu, S.Q., Zhu, Y.S., 2013c. Numerical analysis on knock for a high compression ration spark-ignition methanol engine. Fuel 103, 892–898.
Zhen, X.D., Wang, Y., Xu, S.Q., Zhu, Y.S., Tao, C.J., Xu, T., et al., 2012. The engine knock analysis—an overview. Appl. Energy 92, 628–636.
Zhou, D.Z., Yang, W.M., An, H., Li, J., 2015. Application of CFD-chemical kinetics approach in detecting RCCI engine knocking fuelled with biodiesel/methanol. Appl. Energy 145, 255–264.
Zhu, L., Cheung, C.S., Zhang, W.G., Huang, Z., 2010. Emissions characteristics of a diesel engine operating on biodiesel and biodiesel blended with ethanol and methanol. Sci. Total Environ. 408, 914–921.

Further Reading

Hansen, A.C., Zang, Q., Lyne, P.W.L., 2005. Ethanol-diesel fuel blends—a review. Bioresour. Technol. 96, 277–285.
Svensson, E., Li, C., Shamun, S., Johansson, B., Tuner, M., Perlman, C., Lehtiniemi, H., Mauss, F., 2016. Potential Levels of Soot, NO_x, HC and CO for methanol combustion. SAE Technical Papers No. 2016-01-0887.
Zhen, X.D., Wang, Y., 2013. Study of ignition in a high compression ratio SI (spark ignition) methanol engine using LES (large eddy simulation) with detailed chemical kinetics. Energy 59, 549–558.

This page intentionally left blank

CHAPTER 12

From Methanol to Electricity and Hydrogen Through Bioelectrochemical Systems

Nuria Montpart[*,†], **Juan A. Baeza**[†], **Albert Guisasola**[†]

[*] *EREP SA, Aclens, Switzerland* [†] *Universitat Autònoma de Barcelona, Bellaterra, Spain*

List of Acronyms

AEM	anion exchange membrane
ARB	anode respiring bacteria
BES	bioelectrochemical system
CE	Coulombic efficiency
CEM	cation exchange membrane
COD	chemical oxygen demand
MEC	microbial electrolysis cell
MFC	Microbial fuel cell
rRNA	ribosomal ribonucleic acid
SHE	standard hydrogen electrode

List of Symbols

b	number of electrons exchanged during oxidation reaction
E	voltage
E_{emf}	overall cell electromotive force
E_{ps}	power source applied voltage
F	Faraday's constant
G	Gibbs free energy
I	current intensity
J	current density
M	molar concentration
n	mol
P	power output
r_{CAT}	cathodic gas recovery
r_{H_2}	overall efficiency

Methanol. https://doi.org/10.1016/B978-0-444-63903-5.00012-1

R_{ext} external electric resistance
S substrate concentration
t time
V voltage
V_R reactor volume
η energy recovery
ΔH combustion enthalpy

1 Introduction

Methanol is present in some wastewaters and, as any conventional biodegradable substrate, is generally treated under aerobic conditions. However, methanol contains a significant amount of energy in its chemical bounds (20.2 kJ kg^{-1} COD), which nowadays is wasted in oxygen reduction. The new paradigm in environmental engineering deals with resource recovery rather than waste treatment. Therefore, technologies aiming at recovering the energy contained in wastewaters, such as bioelectrochemistry, are getting more attention. This chapter deals with the opportunities for methanol in bioelectrochemical systems. The chapter shows that the utilization of methanol as substrate in bioelectrochemical systems for energy valorization is feasible as long as the adequate syntrophic consortium is enriched in the anode. Successful results for electricity or hydrogen obtainment from methanol as sole substrate are detailed and discussed.

1.1 Bioelectrochemical Systems: Fundamentals

Bioelectrochemical systems (BES) comprise emerging technologies that combine the metabolism of some microorganisms with electrochemistry. They are considered promising systems and have the potential to occupy a prominent place in the future of renewable energy generation, bioremediation, and wastewater treatment.

As an electrochemical cell, the system is comprised of two electrodes: an anode, where an oxidation reaction takes places (loss of electrons from a chemical compound), and a cathode, where a reduction reaction occurs (gain of electrons by another chemical compound). The electrical connection of both electrodes allows the flow of electrons from the anode to the cathode. The electrodes are surrounded by an electrolyte, a conductive aqueous solution where charged species diffuse. An ion exchange membrane can physically separate both electrodes in an anodic and a cathodic half-cell or chamber, containing the anolyte and the catholyte respectively.

The particularity of BES is in the fact that either oxidation and/or reduction reactions can be catalyzed microbiologically. The metabolism of these microorganisms is linked to the electrodes and, therefore, they are generally called electroactive microorganisms. Microorganisms whose metabolism is related to anodic processes are the ones with the most studied and best understood metabolic mechanisms. The so-called anode respiring bacteria (ARB) or exoelectrogens oxidize the organic matter available and use an insoluble anode as the

terminal electron acceptor in anaerobic conditions (i.e., in absence of other possible electron acceptors such as oxygen, nitrate, and sulfate). Species comprised in ARB include the genus *Geobacter* and *Shewanella* (Hurst and Crawford, 2007), to cite the most studied ones.

The oxidation of organic matter by ARB on the anode is coupled with a reduction reaction on the cathode. Depending on the reduction reaction, the thermodynamics of the overall process is favored or it requires some energy input to drive it, leading to two main types of BES. Shown in Fig. 12.1, they are microbial fuel cell (MFC) and microbial electrolysis cell (MEC). In an MFC, oxygen is reduced to water in the cathode, which leads to a thermodynamically favored process. The electrical connection of the anode with a cathode produces an electron flow that can be used elsewhere as electricity. On the contrary, in an MEC, the cathodic reaction (usually hydrogen formation) requires an energy input to drive the process and, thus, to obtain the product of interest.

The thermodynamics of the overall reaction can be evaluated in terms of Gibbs free energy, ΔG_r (J), but it can also be evaluated in terms of overall cell electromotive force, E_{emf} (V), defined as the difference in reduction potential between the cathode and the anode, which is positive for a thermodynamically favorable reaction. E_{emf} also indicates the maximum attainable power generation in MFC and the minimum energy input required in MEC, according to thermodynamics.

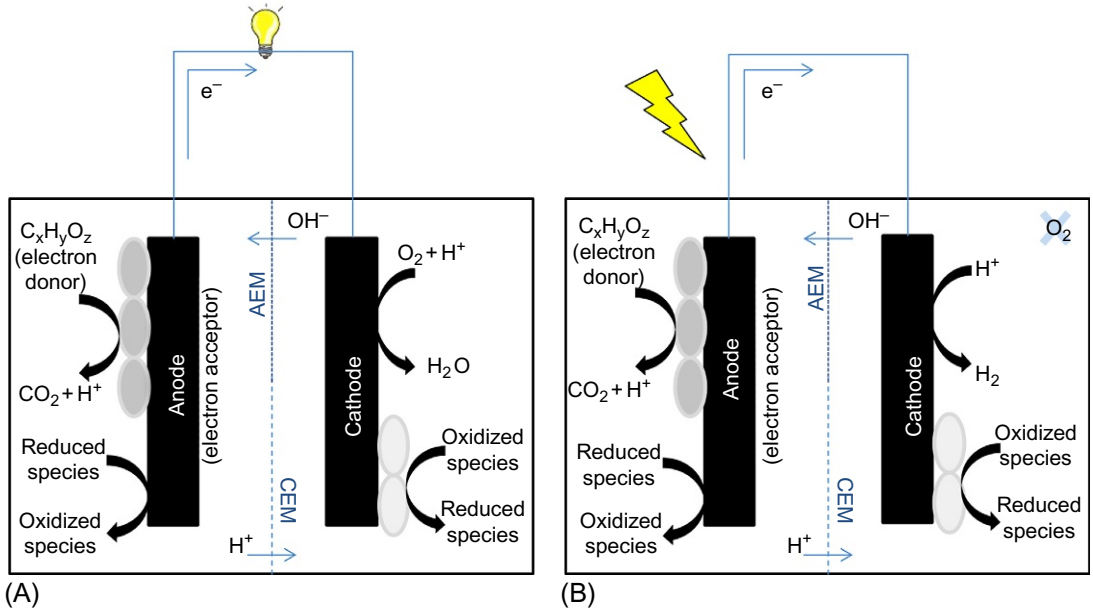

Fig. 12.1

Schematics of (A) a microbial fuel cell (MFC) and (B) a microbial electrolysis cell (MEC). Oxidation and reduction processes can occur electrochemically or can be catalyzed microbiologically. Both processes can be physically separated by an ion exchange membrane, selectively allowing cations flow (cation exchange membrane, CEM) or anions flow (anion exchange membrane, AEM).

In an MFC (Fig. 12.1A), a carbon source is oxidized under anaerobic conditions by ARB, using the anode as a final electron acceptor. Electrons flow along the electrical circuit to the cathode. Protons produced during the substrate oxidation diffuse to the cathode, where they are consumed in the oxygen reduction reaction. Different conditions are therefore met in both electrodes, requiring an anaerobic environment in the anode surroundings and aerobic conditions around the cathode. When acetate is the electron donor, the reactions occurring in each electrode can be expressed as in Eqs. (12.1) and (12.2).

Anode, oxidation reaction:

$$\begin{gathered} CH_3COO^- + 4H_2O \rightarrow 2HCO_3^- + 8e^- + 9H^+ \\ \left(E_{HCO_3^-|CH_3COO^-} = -0.28\,V \text{ vs. SHE at pH} = 7 \text{ and } T = 25°C\right) \end{gathered} \tag{12.1}$$

Cathode, reduction reaction:

$$O_2 + 4H^+ + 4e^- \rightarrow 2H_2O \quad \left(E_{O_2|H_2O} = 0.82\,V \text{ vs. SHE at pH} = 7 \text{ and } T = 25°C\right) \tag{12.2}$$

With an overall cell electromotive force of $E_{emf} = E_{cathode} - E_{anode} = 1.1$ V.

The same oxidation reaction occurs in the anode of an MEC when using acetate as the electron donor (Fig. 12.1B). However, anaerobic conditions are maintained in the cathode of an MEC, and the cathodic reaction occurring is the reduction of protons to hydrogen as in Eq. (12.3).

Cathode, reduction reaction:

$$2H^+ + 2e^- \rightarrow H_2 \quad \left(E_{H^+/H_2} = -0.41\,V \text{ vs. SHE at pH} = 7 \text{ and } T = 25°C\right) \tag{12.3}$$

With an overall cell electromotive force of $E_{emf} = E_{cathode} - E_{anode} = -0.13$ V.

Therefore, in an MFC about 1.1 V can be theoretically produced from acetate based on thermodynamic values, whereas in an MEC for hydrogen production a minimum energy input of about 0.13 V is required to drive the process (at 25°C and pH 7).

Besides electrons, protons are also produced during the biodegradation of organic matter. The transport of electrons from the anode to the cathode needs to be compensated to meet the electroneutrality condition, meaning that the solution is electrically neutral. The fact that not only protons and hydroxyls but other charged species can be responsible for maintaining the electroneutrality leads to pH gradients in the system, experiencing a pH drop in the anodic environment (due to proton formation), and a pH increase in the cathodic environment (due to proton consumption/hydroxyls formation). Such pH gradients are more significant when an ion exchange membrane (AEM or CEM) is present in the system. In contrast, when the system lacks a membrane, pH gradients affect in a rather local scale. The reduction potential of both the oxidation and the reduction reactions will vary according to pH, leading to changes in the attainable or required thermodynamic values (Gil et al., 2003; Rozendal et al., 2007; Ruiz et al., 2016).

In practice, the voltage that can be obtained or that is required in BES under conventional conditions differs from the thermodynamically possible values because of a whole variety of

voltage losses occurring in the system (Rozendal et al., 2008). These losses decrease the attainable voltage in MFCs and increase the voltage requirements in MECs. For instance, reported values of attained voltage in MFC are not higher than 0.9 V and applied voltages for hydrogen production in MEC are not lower than 0.4 V.

The use of ion exchange membranes in BES physically separates the anode and the cathode. A configuration with a membrane increases voltage losses, which Rozendal estimated to be between 0.26 and 0.38 V (Rozendal et al., 2007). The removal of the membrane not only can simplify the construction, operation, and maintenance of BES, but it also decreases the internal resistance and reduces the gradient of pH, theoretically increasing the output of the system. However, the membrane also separates the anodic and cathodic chamber and prevents the mixing of the reaction products. Without the membrane, oxygen (in MFC) and hydrogen (in MEC) could be transferred to the anode and the cell performance would be severely deteriorated. Throughout this chapter a membrane-less configuration will be referred to as single-chamber system, as opposed to a double-chamber system.

MFC and MEC share a common anode environment which comprises a mixed culture. The microbial distribution in the anode depends on the operational conditions of the cell (from pH and temperature to the organic substrate in the feed). As in many mixed-culture biological processes, the proliferation of undesired microbial species is an essential issue to face. Anaerobic methanogenic populations are able to grow in the anodic environment competing with ARB for acetate (acetoclastic methanogens). Methanogenesis buildup in BES has been reported as a major failure in some scale-up attempts (Cusick et al., 2011). Moreover, in a membrane-less MEC, undesired biological processes can also appear using hydrogen as a substrate (e.g., hydrogenotrophic methanogens, homoacetogenic bacteria, hydrogen oxidizing ARB) (Ruiz et al., 2013). Substrate utilization by microorganisms other than ARB would lead, in MFC, to a lower electrical current generation whereas in MEC net hydrogen production will decrease and the gas obtained will be less rich in hydrogen. The addition of chemical inhibitors of hydrogen scavengers is not an economically feasible option in view of a future full-scale use of the process and may lead to the development of resistances (Rago et al., 2015). Fig. 12.2 summarizes the microbial ecosystem found in BES driven by fermentable substrates. As an example, the interactions between the different existing communities in MEC are schematized in Fig. 12.3.

The most common parameters used to evaluate the performance of BES are detailed below.

- Cell *current intensity* and *power output* of an MFC are calculated according to Ohm's law based on voltage monitored (Eqs. 12.4 and 12.5):

$$I = V/R_{\text{ext}} \tag{12.4}$$

$$P = V \cdot I \tag{12.5}$$

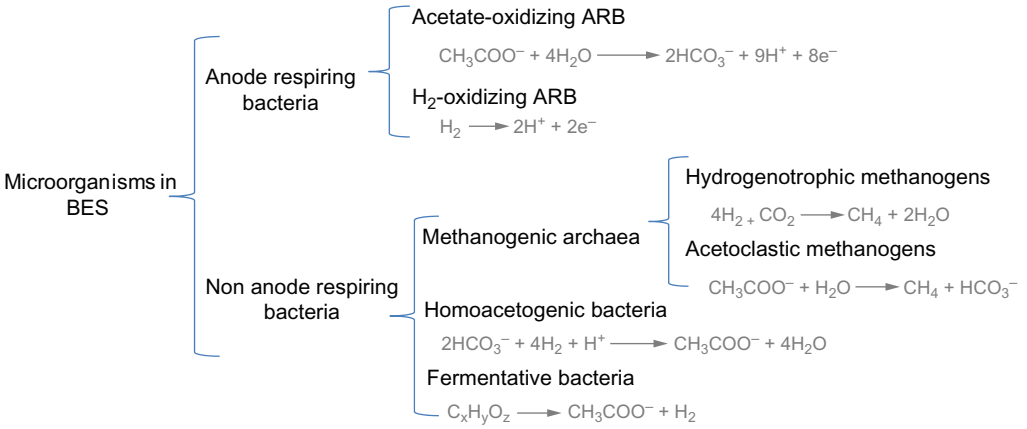

Fig. 12.2
Microbial distribution in a common BES anode driven by fermentable substrates.

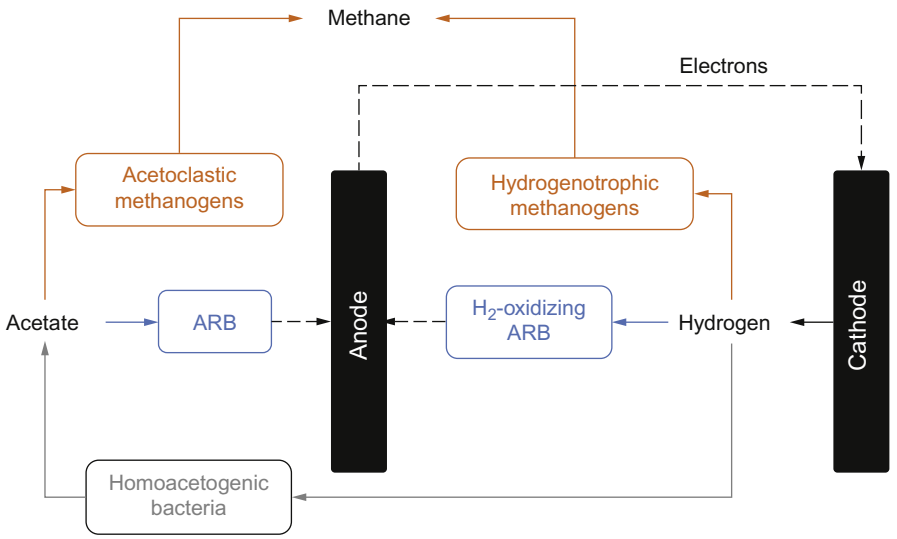

Fig. 12.3
Microbial metabolic interactions in single chamber MECs. *Continuous arrows* indicate hydrogen, acetate, and methane flows. *Discontinuous arrows* represent the flow of electrons.

where V is the voltage drop in the resistance (V), R_{ext} is the external resistance (Ω), I is the current intensity (A), and P is the power output (W). Maximum power output (P_{max}) is calculated with Eq. (12.5) considering the maximum voltage reached during a batch cycle. Current intensity is often normalized to the electrode area, referred to as current density, J (A m^{-2}), or normalized to the reactor or cell volume (A m^{-3}).

- *Coulombic efficiency* (CE) defines the ratio of coulombs contained in the substrate consumed that are recovered as electrical current intensity (Eq. 12.6).

$$\mathrm{CE} = \frac{\int_{t_0}^{t} I(t)dt}{F \cdot b \cdot \Delta S \cdot V_R} \tag{12.6}$$

where t is time (s), F is Faraday's constant (96,485 C/mol-e^-), b is the stoichiometric number of electrons produced per mole of substrate (e.g., 8 mol e^-/mol acetate), ΔS is the substrate consumption (mol/L), and V_R the liquid volume (L). For a mixed substrate, CE can be calculated based on COD consumption ($b = 4$ mol-e^-/mol O_2).

- *Cathodic gas recovery* (r_{CAT}) of an MEC is calculated as the ratio of moles of hydrogen measured and moles of hydrogen that can be produced based on current intensity measured (Eq. 12.7).

$$r_{\mathrm{CAT}} = \frac{n_{\mathrm{H_2}}}{\frac{\int_{t_0}^{t} I(t)dt}{2F}} \tag{12.7}$$

where $n_{\mathrm{H_2}}$ is the number of moles of hydrogen measured and is calculated according to the ideal gases law ($PV = nRT$) knowing the hydrogen volume measured and 2 is the number of moles of electrons per mole of hydrogen.

- *Overall efficiency* ($r_{\mathrm{H_2}}$) of an MEC calculated as stated in Eq. (12.8).

$$r_{\mathrm{H_2}} = r_{\mathrm{CAT}} \cdot \mathrm{CE} \tag{12.8}$$

- *Energy recovery* in an MEC, i.e., the amount of energy added that is recovered as hydrogen. It can be calculated based on electricity input (η_W) and based on both electricity and substrate inputs (η_{WS}) according to Eqs. (12.9) and (12.10), respectively.

$$\eta_W = \frac{\Delta H_{\mathrm{H_2}} \cdot n_{\mathrm{H_2}}}{\int_{t_0}^{t} \left(I \cdot E_{ps} - I^2 R_{\mathrm{ext}}\right) dt} \tag{12.9}$$

where $\Delta H_{\mathrm{H_2}}$ is the heat of combustion for hydrogen (286 kJ/mol, upper heating value), E_{ps} is the applied voltage (V) and R_{ext} is the external resistance used for monitoring (Ω).

$$\eta_{WS} = \frac{\Delta H_{\mathrm{H_2}} \cdot n_{\mathrm{H_2}}}{\int_{t_0}^{t} \left(I \cdot E_{ps} - I^2 R_{\mathrm{ext}}\right) dt + \Delta H_S \cdot n_S} \tag{12.10}$$

where ΔH_S is the heat of combustion of the substrate and n_S is the number of moles of substrate consumed during the period of time considered.

1.2 Wastewater Treatment and Valorization in Bioelectrochemical Systems

Real wastewater contains a wide range of substrates with different biodegradability. Hence, the opportunities for wastewater treatment and valorization using BES lay in their capability to use the chemical energy contained in both nonfermentable and fermentable carbon sources. When fermentable or complex substrates are present in the system, an initial hydrolysis and fermentation step is necessary to break macromolecules to simpler molecules and to convert them to acetate and other readily biodegradable substrates, which will be further metabolized by ARB. Therefore, a syntrophic consortium between fermentative bacteria and ARB needs to be developed. Syntrophic interactions between fermentative bacteria and ARB have been reported to allow the utilization of complex organic matter in BES, where different substrates entail the development of different microbial communities (Kiely et al., 2011; Lu et al., 2012; Montpart et al., 2015).

A great variety of substrates has been used in BES under very different conditions, ranging from pure substrates in synthetic wastewaters to complex mixtures of substrates with real wastewaters. The utilization of wastewater containing methanol (e.g., from paper and glycerol production or from chemical industries) and its possible utilization as a substrate in BES has also been reported. Table 12.1 summarizes these works, which are further discussed in the following sections focusing on the role of methanol.

Table 12.1 Works published in indexed scientific publications related to methanol utilization in BES, ordered according to the type of BES used

Substrate	Reference
Valorization in microbial fuel cell	
Methanol and ethanol	Kim et al. (2007)
Biodiesel wastewater	Clauwaert et al. (2008)
Synthetic biodiesel wastewater	Feng et al. (2011)
Methanol	Montpart et al. (2014)
Wastewater containing methanol	Liu and Li (2014)
Wastewater containing methanol	Liu et al. (2014)
Crude glycerol	Chookaew et al. (2014)
Valorization in microbial electrolysis cell	
Glycerol	Sakai and Yagishita (2007)
Glycerol	Escapa et al. (2009)
Glycerol and biodiesel wastewater	Selembo et al. (2009)
Biodiesel wastewater	Chignell and Liu (2011)
Methanol-rich industrial wastewater	Tenca et al. (2013)
Glycerol	Speers et al. (2014)
Methanol	Montpart et al. (2014)
Crude glycerol	Chookaew et al. (2014)
Methanol	Yamamuro et al. (2014)
Glycerol	Montpart et al. (2015)

2 Electricity Production From Methanol in Bioelectrochemical Systems

The first tests using methanol as a substrate to produce electricity in MFC are reported by Kim et al. (2007). A comparative study of direct methanol and ethanol utilization in double-chambered MFC showed a successful power generation with ethanol but a nonappreciable response with methanol (Fig. 12.4). The system had been inoculated with anaerobic sludge from a municipal wastewater treatment plant.

Clauwaert et al. (2008) operated an MFC using as the carbon source analytical glycerol or industrial glycerol coming from a biodiesel producing plant. No significant change was observed in the current and power production, in spite of the more complex composition of the industrial glycerol, including sulfate. However, the possible methanol content in this stream was not reported. In any case, using industrial glycerol as the carbon source, a current intensity production of 111 A/m^3 was obtained.

Feng et al. (2011) stated that electricity production with biodiesel wastewater was comparable to electricity production using glycerol as the sole carbon source (Fig. 12.5), reaching 38 A/m^3. In this work, biodiesel was prepared from waste bean oil and methanol, although the remaining amount of methanol in the synthetically prepared biodiesel wastewater was not reported.

These previous works showed that the methanol presence did not produce inhibitory effects when treating glycerol as the carbon source. However, it was not proven that methanol could

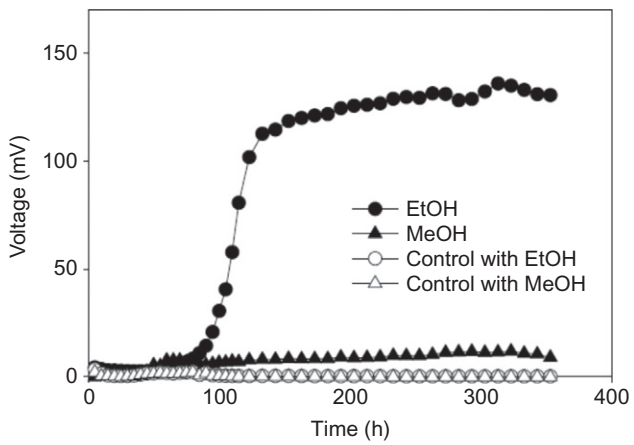

Fig. 12.4

Voltage generation in two-chamber MFCs using 10 mM of ethanol or methanol during start-up. The inoculum was anaerobic sewage sludge, with autoclaved sludge used as an abiotic control. *Extracted from Kim, J.R., Jung, S.H., Regan, J.M., Logan, B.E., 2007. Electricity generation and microbial community analysis of alcohol powered microbial fuel cells. Bioresour. Technol. 98, 2568–2577. https://doi.org/10.1016/j.biortech.2006.09.036.*

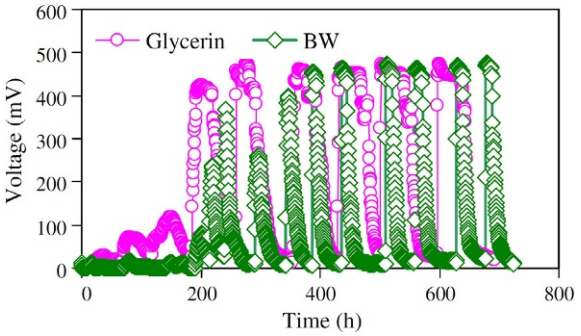

Fig. 12.5

MFC enrichment with a mixed solution of 50 mM PBS containing 1400 mg COD/L BW (biodiesel wastewater) or glycerin with domestic wastewater as bacteria source. *Extracted from Feng, Y., Yang, Q., Wang, X., Liu, Y., Lee, H., Ren, N., 2011. Treatment of biodiesel production wastes with simultaneous electricity generation using a single-chamber microbial fuel cell. Bioresour. Technol. 102, 411–415. https://doi.org/10.1016/j.biortech.2010.05.059.*

generate some electricity when using it as the sole carbon source. Montpart et al. (2014) was the first work demonstrating direct methanol utilization in an MFC. Three different strategies were tested: (i) direct replacement of acetate for methanol; (ii) progressive replacement of acetate for methanol; and (iii) a two-step syntrophic consortium development with bioaugmentation of ARB with methanol-fermenting bacteria. The idea beneath the syntrophic consortium of anaerobic methanol-degraders and ARB was that fermentative bacteria (essentially, acetogens) would degrade methanol, while ARB would live off the degradation byproducts (such as acetate) generating current intensity in the MFC.

Although the three strategies showed current intensity when operating with methanol as the sole carbon source after an inoculation period of 80 days, the bioaugmentation strategy was the most efficient in terms of higher CE, higher power density, and lower internal resistance. This strategy enhanced the syntrophic consortium because methanol-degrading acetogens were selected against other methanol degraders (essentially methanogens) from an anaerobic sludge. This selected culture was used as a bioaugmentation agent in an MFC where an acetate-degrading population had been previously developed, i.e., an MFC already enriched in ARB.

Using methanol as the sole carbon source, the system performance increased up to a steady power output of 220 μW and 16.7 A/m^3 (i.e., it reached potential of 470 mV when operating with a 1000 Ω external resistance, Fig. 12.6). These results were comparable to previous values (250–300 μW) obtained using acetate as the sole carbon source in other studies with the same reactors. In addition, these values were also comparable to those reported with conventional carbon sources. In analogous configurations, Logan et al. (2007) obtained a power output of 325 μW feeding acetate as the carbon source and Liu and Logan (2004) obtained 270.4 μW feeding glucose.

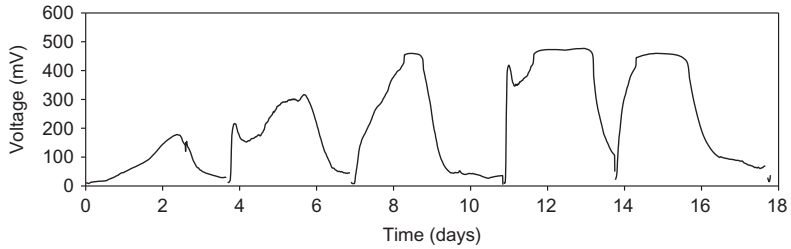

Fig. 12.6

Performance evolution of the methanol-driven MFC with a syntrophic consortium. *Extracted from Montpart, N., Ribot-Llobet, E., Garlapati, V.K., Rago, L., Baeza, J.A., Guisasola, A., 2014. Methanol opportunities for electricity and hydrogen production in bioelectrochemical systems. Int. J. Hydrog. Energy 39, 770–777. https://doi.org/10.1016/j.ijhydene.2013.10.151.*

The proposed chemical reaction scheme occurring in the system comprised the conversion of methanol to acetate (Eq. 12.11), and the subsequent utilization of acetate by ARB (Eq. 12.12).

$$4CH_3OH + 2HCO_3^- \rightarrow 3CH_3COO^- + H^+ + 4H_2O \quad (12.11)$$

$$CH_3COO^- + 4H_2O \rightarrow 2HCO_3^- + 9H^+ + 8e^- \quad (12.12)$$

This work also showed how methanol and acetate, the only metabolite detected, evolved during a batch cycle in an MFC (Fig. 12.7). Methanol degradation was fast whereas acetate concentration was low indicating that the process was not limited by ARB (i.e., the fermentation products were rapidly consumed by ARB). However, the presence of other acetate sinks different from ARB could not be ruled out. The low acetate presence in the bulk was

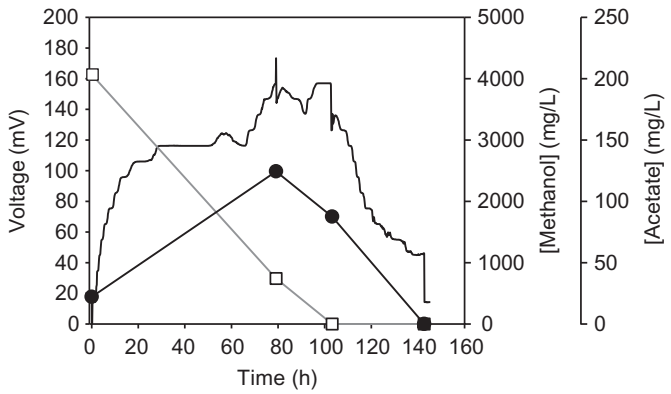

Fig. 12.7

Voltage and metabolites evolution in a methanol driven MFC. *Solid line*, voltage; ●, acetate; □, methanol concentration. *Extracted from Montpart, N., Ribot-Llobet, E., Garlapati, V.K., Rago, L., Baeza, J.A., Guisasola, A., 2014. Methanol opportunities for electricity and hydrogen production in bioelectrochemical systems. Int. J. Hydrog. Energy 39, 770–777. https://doi.org/10.1016/j.ijhydene.2013.10.151.*

consistent with the fact that the immobilization of the consortium as an anodic biofilm was enhanced throughout the cell operation. Thus, only the surplus acetate that had not been consumed by ARB inside the biofilm could diffuse into the bulk.

Liu and Li (2014) and Liu et al. (2014) also presented positive results of electricity generation in single-chamber MFCs using municipal wastewater amended with methanol in concentrations from 0.005 to 0.04 M. Municipal wastewater was also used for anode acclimation for 2 months before the tests. Stable power generation (0.2–0.3 A m^{-3}) was achieved in the MFCs, linked to methanol degradation efficiencies of 100% at all methanol concentrations tested. The effluent chemical oxygen demand (COD) was 82–118 mg COD/L and probably corresponded to refractory organics from the municipal wastewater. Methanol losses in MFCs by volatilization were discarded.

The increase in methanol concentration prolonged the cycle duration of MFCs. For instance, the cycle duration was extended from 60 h at 0.005 M up to over 250 h at 0.04 M, clearly showing conversion of part of the methanol to electricity by ARB. However, the increase of methanol concentration led to lower pH inside the MFCs and lower CE (from 11.5% without methanol to 5.1% at 0.04 M), which was attributed to the switch from exoelectrogenic reactions to anaerobic fermentation. Hence, anaerobic degradation was concluded as the main pathway for methanol removal in MFCs. On the other hand, the cathodic open circuit potential results showed that methanol had toxic effects on the cathodic Pt catalyst, although it was considered that this effect was not at a significant extent.

Yamamuro et al. (2014) also studied methanol degradation in single-chamber MFCs linked to electricity production, although their focus was more on analyzing by metagenomics the microbial community involved. The inoculum used in this work was activated sludge from a wastewater-treatment facility located within a chemical plant. They developed MFCs that generated electricity from methanol at the maximum power density of 220 mW m^{-2} (based on the projected area of the anode). Their results suggested that methanol was anaerobically catabolized by a syntrophic bacterial consortium comprised of *Sporomusa* and *Geobacter* with the anode as the electron acceptor. As in the work of Montpart et al. (2014), acetate was also detected as an intermediate in the MFC. The authors also proposed Eq. (12.11) for explaining the acetate generated by *Sporomusa* that was further degraded by *Geobacter* (Eq. 12.12). In spite of the complete degradation of methanol, the CE was around 13%, indicating that other metabolic pathways not related to electricity generation were also responsible for methanol disappearance.

Additional works developed by Montpart (2014) and Montpart et al. (2015) showed that electricity generation in MFC from biodiesel wastewater with crude glycerol (203 g L^{-1} glycerol and 23.4 g L^{-1} methanol in the raw solution) was possible. The system was previously inoculated to develop the proper syntrophic consortium and synthetic glycerol was used during the start-up of the system. A stable maximum current intensity of 0.4 mA was obtained from the beginning, not significantly lower than when synthetic glycerol was used (0.45 mA).

Table 12.2 Single-chamber MFC performance with methanol-containing feedings

Wastewater Treated	Current Intensity ($A\ m^{-3}$)	Power per Anode Volume ($W\ m^{-3}$)	Power Density per Anode Surface ($mW\ m^{-2}$)	CE (%)	COD Removal (%)	Reference
Methanol	16.7	0.75	0.1	26.7	100	Montpart et al. (2014)
Municipal wastewater with added methanol	2.1	0.2–0.3	16	5–11	80–95	Liu et al. (2014), Liu and Li (2014)
Methanol	1.18	1.32	220	13	100	Yamamuro et al. (2014)
Biodiesel wastewater	57.1	9.1	1.22	39.4	57	Montpart (2014)

The parameters evaluating the system performance were even better using biodiesel wastewater as the substrate rather than using synthetic glycerol.

Table 12.2 summarizes the performance of the different aforementioned MFCs fed with methanol, synthetic glycerol, and municipal wastewater with added methanol and biodiesel wastewater. Methanol output in terms of electricity generation was low as compared to glycerol as the carbon source, but a successful complete degradation could be observed when there was a proper development of a syntrophic consortium (Montpart et al., 2014; Yamamuro et al., 2014). Biodiesel wastewater as a carbon source in MFC allowed higher CE and current intensity, although COD removal was lower, which was attributed to products other than glycerol or methanol contained in the wastewater.

Regarding the two works found in the literature using methanol as the sole carbon source, the maximum CE of 26.7% was obtained in the work by Montpart et al., compared to the 13% obtained by Yamamuro et al. (2014). CE around 30% is a typical value obtained when using complex organic compounds such as glycerol, dairy wastewater, or starch in MFCs (Montpart et al., 2015). A value of CE lower than 30% indicates the degradation of methanol by methanogenesis or other nonbioelectrochemical processes. The maximum current intensity per volume of cell (16.7 A m^{-3}) was also observed by Montpart et al. (2014). The power obtained per volume of cell was of the same order of magnitude (0.75 vs. 1.32 W m^{-3}), but when expressed per anode surface the work of Yamamuro et al. (2014) was much higher (220 vs 0.1 mW m^{-2}). The reason for this high discrepancy was the type of anode (graphite felt vs brush), with a much higher theoretical surface for the brush anode used by Montpart et al. (2014). In any case, these works demonstrate that electricity generation in MFCs using methanol as the only carbon source is possible if a proper syntrophic consortium is developed.

3 Hydrogen Production From Methanol in Bioelectrochemical Systems

3.1 Hydrogen Production in Single-Chamber MEC

Glycerol has been reported to be an interesting substrate in BES for hydrogen production. However, biodiesel wastewater containing glycerol, methanol, and other compounds has provided lower performance, raising suspicion about the possible effect of methanol in these cells. Sakai and Yagishita (2007) demonstrated the possibility of obtaining both hydrogen and ethanol from biodiesel wastes using a pure culture of *Enterobacter aerogenes*, whose electroactivity was promoted with thionine as a chemical mediator. Speers et al. (2014) showed that hydrogen can be obtained in an MEC cell while glycerol was partially oxidized to ethanol in the anode by a selected consortium of two pure cultures. The work of Escapa et al. (2009) focused on the production of hydrogen from glycerol in a single-chamber MEC provided with a gas-phase cathode. The main advantage of this configuration was the minimization of hydrogen availability in the electrolyte. Hydrogen produced reached 0.6 $m^3\ m^{-3}$ reactor d^{-1} and current intensity 10.7 A m^{-3} at an applied voltage of 1 V. Chookaew et al. (2014) proposed a two-stage process for treating crude glycerol with 1%–3% of methanol, consisting of dark fermentation and a BES (MFC or MEC). The first step involved glycerol and methanol fermentation to volatile fatty acids, which were used as the carbon source in the MFC or the MEC. Both dark fermentation and MEC steps contributed to hydrogen production. Methanol was removed in the dark fermentation process; therefore, its effect on hydrogen production in MEC was not evaluated.

Selembo et al. (2009) compared the performance of a single-chamber MEC fed with glycerol and biodiesel wastewater to produce hydrogen. At 0.9 V of applied voltage, 2 $m^3\ m^{-3}\ d^{-1}$ of hydrogen were produced from glycerol whereas 0.41 $m^3\ m^{-3}\ d^{-1}$ were produced when biodiesel wastewater was used as the carbon source. Methanol and its possible toxic effects were suggested to be responsible for the differences in system performance. Similarly, Chignell and Liu (2011) observed a decrease in hydrogen production yield in a single-chamber MEC when methanol was present in biodiesel wastewater. Montpart (2014) also tested biodiesel wastewater as a substrate to produce hydrogen in a single-chamber MEC with an applied voltage of 0.8 V. From the first fedbatch cycle tested, the system exhibited a very long current intensity response. Neither hydrogen nor methane were detected (Fig. 12.8), indicating an electron recycling situation. Such electron recycling entails the use of hydrogen produced as an electron donor for ARB and/or as a substrate for homoacetogenic bacteria, observing as a result a lower or even inexistent net hydrogen production. Electron recycling is also identified when CE surpasses 100%, meaning that the electrons available in the substrate fed to the system are being reused and, therefore, they flow more than once through the electrical circuit. In the tests performed, an average CE of 240% was measured. The initial existence of H_2-oxidizing ARB and/or homoacetogenic bacteria microorganisms in the system was only expected as a result of hydrogen production from glycerol fermentation.

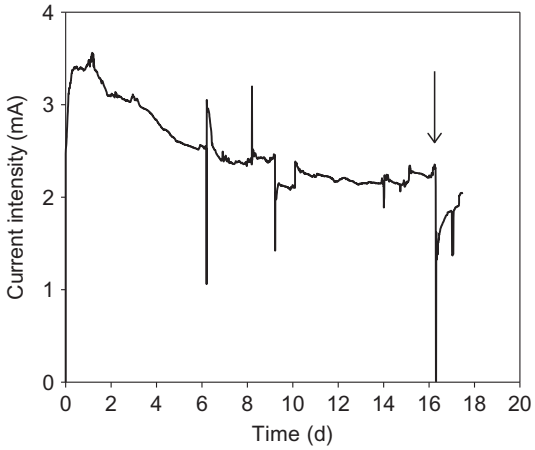

Fig. 12.8
Current intensity profile for a conventional cycle in MEC fed with biodiesel wastewater. *Arrow* indicates change of media and feeding of fresh carbon source.

Tenca et al. (2013) presented the performance of a single-chamber MEC fed with methanol-rich wastewater (1.5 g methanol L^{-1}) from a chemical manufacturing facility. The anodic biofilm was initially enriched and acclimated to the wastewater in MFC configuration. At 0.7 V of applied voltage, the MEC current intensity response reached 2.1 A m^{-2} (based on cathode surface), yielding up to 1.8 m^3 m^{-3} d^{-1} of gas, mainly composed of methane (55% methane, 32% hydrogen, 13% carbon dioxide). No methanol was detected in the effluent and CE reached about 10%. The authors suggested that high rates of methane production were due to the biological conversion of methanol to methane. In such a situation, methanol would be initially metabolized to acetate, which would afterwards be degraded to methane. Also low CE indicated a large contribution of nonanode-related processes to organic matter degradation.

The work of Montpart et al. (2014) specifically investigated the role of methanol, presenting the opportunities of this carbon source for hydrogen production in MEC. The work studied the response of a single-chamber MEC fed with methanol as the sole carbon source. The system was started with an anode already enriched with a methanol-degrading microbial syntrophic consortium and methanogenesis was chemically inhibited by the addition of 2-bromoethanesulfonate. The results (Fig. 12.9) showed a similar trend to those observed by the same authors with biodiesel wastewater: CE was 296%, the cycle was remarkably long (about 28 days), and, despite the significant current density obtained (1.7 A m^{-2} and 5.7 mA m^{-2} based on cathode and anode surface respectively), no hydrogen was detected during the fedbatch cycle. Again, these observations were attributed to the occurrence of hydrogen recycling from the cathode to the anode (i.e., electron recycling phenomena).

The presence of homoacetogenic bacteria contributing to the electron recycling phenomena in these methanol-fed systems was confirmed with microbiological techniques. Results from

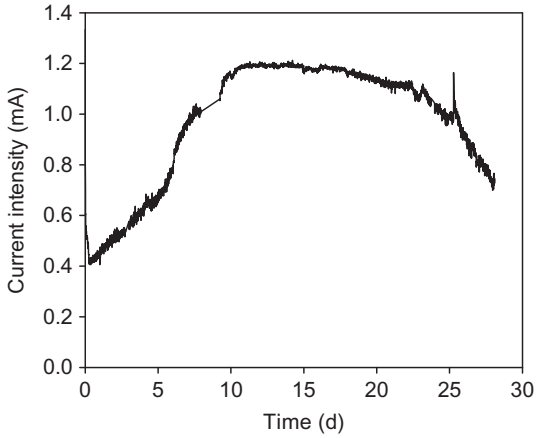

Fig. 12.9

Current intensity evolution in a single chamber methanol-driven MEC. *Extracted from Montpart, N., Ribot-Llobet, E., Garlapati, V.K., Rago, L., Baeza, J.A., Guisasola, A., 2014. Methanol opportunities for electricity and hydrogen production in bioelectrochemical systems. Int. J. Hydrog. Energy 39, 770–777. https://doi.org/10.1016/j.ijhydene.2013.10.151.*

high-throughput 16S rRNA gene pyrosequencing (Fig. 12.10) showed that a microbial community with high diversity was present in the anodic biofilm. The main genus detected was *Geobacter* sp. (39%), which is commonly found in high proportion (around 70%) in similar BES fed with acetate (Parameswaran et al., 2011), hence reinforcing the hypothesis that acetate was a degradation metabolite of methanol. Regarding homoacetogenic bacteria, *Acetobacterium* sp. were the homoacetogens present in higher proportion. Indeed, their presence could be expected, since it is known that acetogens metabolize C1-compounds, such as CO_2 and methanol, to acetate (Diekert, 1994; Heijthuijsen, 1986). *Desulfovibrio* sp. (standing for 6% of anode population) are also homoacetogenic bacteria and can excrete acetate into the medium from hydrogen (Ljungdahl, 1986). Homoacetogenic bacteria were also found in the methanol-fed MFC of Yamamuro et al. (2014). They found *Sporomusa*, a member of the phylum *Firmicutes*, as the second most abundant genus. *Sporomusa* has metabolic features as homoacetogenesis and utilization of C1 compounds, including methanol and decarboxylation of dicarboxylic acids. It is also known to oxidize methanol to form acetate according to Eq. (12.11).

The study of Montpart et al. (2014) also showed that the activity of H_2-oxidizing ARB was minimal and that therefore the electron recycling was mainly caused by the presence of homoacetogenic bacteria.

According to these studies, net hydrogen production from methanol in a single-chamber MEC does not seem possible, since (i) in absence of methanogenic activity, homoacetogenic bacteria will enhance an electron recycling situation, which cannot be avoided (homoacetogenic bacteria are in charge of methanol conversion to acetate) and (ii) in the presence of

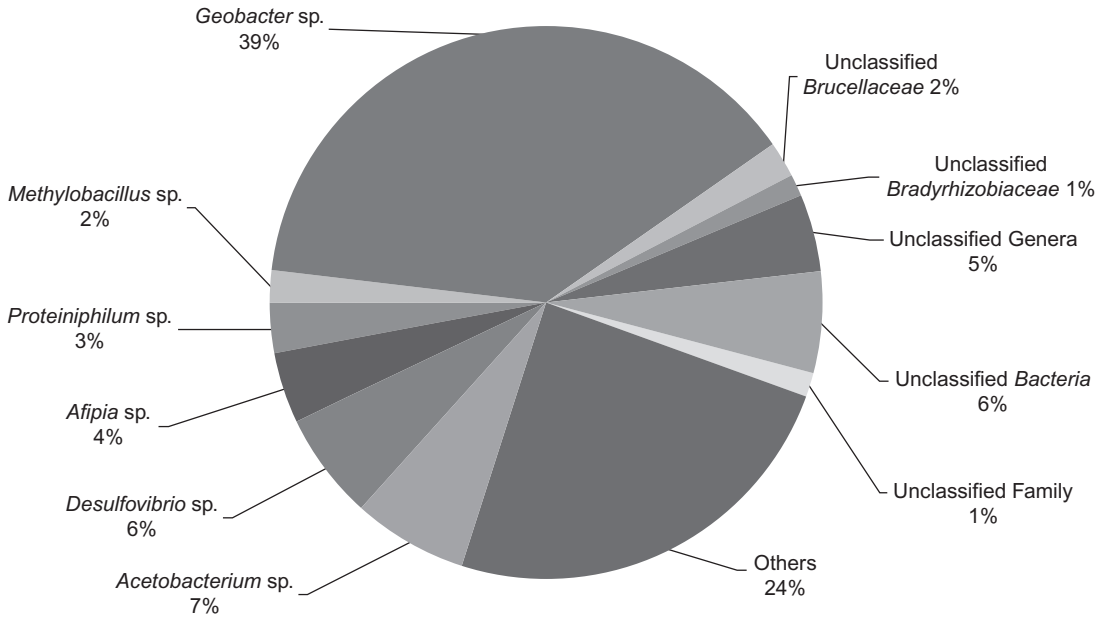

Fig. 12.10

Anodic genus microbial distribution through high-throughput 16S rRNA gene pyrosequencing. Genera making less than 1% of total sequences were classified as others. *Extracted from Montpart, N., Ribot-Llobet, E., Garlapati, V.K., Rago, L., Baeza, J.A., Guisasola, A., 2014. Methanol opportunities for electricity and hydrogen production in bioelectrochemical systems. Int. J. Hydrog. Energy 39, 770–777. https://doi.org/10.1016/j.ijhydene.2013.10.151.*

methanogenic activity, the production of methane will be favored. In terms of wastewater treatment and energetic valorization, the second scenario is not necessarily negative. In fact, methane production under this configuration has been previously proposed and named as electromethanogenesis (Cheng et al., 2009), although operating costs as compared to anaerobic digestion may limit the use of this technology with such a carbon source.

3.2 Hydrogen Production in Double-Chamber MEC

To avoid the problem of electron recycling, the work of Montpart et al. (2014) also performed tests in the double-chamber MEC configuration. Under this arrangement, a clear current intensity profile was obtained for each batch cycle (Fig. 12.11), meaning that the cell experienced a current intensity increase as methanol was being converted to acetate and a decrease when the substrate was being depleted. This evidenced that electron recycling was avoided. Also hydrogen was detected during this period and CE was assessed to be lower than 100% for each batch cycle. Throughout the double-chamber operational period, maximum current intensity achieved in every batch cycle increased, obtaining at the steady state 10.7 mA m^{-2} (based on anode surface) and CE of 90%, with a production of 0.1 m^3 H_2 m^{-3}

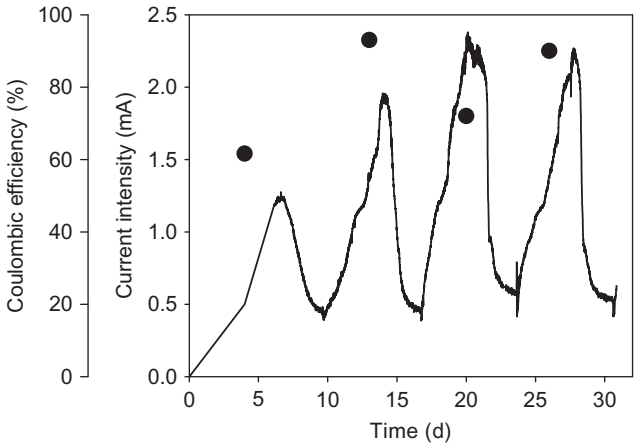

Fig. 12.11

Current intensity evolution in a double chamber methanol-driven MEC. *Solid*, current intensity; ●, coulombic efficiency. *Extracted from Montpart, N., Ribot-Llobet, E., Garlapati, V.K., Rago, L., Baeza, J.A., Guisasola, A., 2014. Methanol opportunities for electricity and hydrogen production in bioelectrochemical systems. Int. J. Hydrog. Energy 39, 770–777. https://doi.org/10.1016/j.ijhydene.2013.10.151.*

reactor d^{-1}. Energy recovery based on electricity input stabilized around 60% and energy recovery based on both electricity and substrate input was only around 20%, still far from considering the system energetically feasible and leaving an open door to further optimization.

As a consequence of physically separating both anolyte and catholyte, a pH change was observed. pH decreased in the anolyte (final pH about 6.5), where protons were produced, and increased in the catholyte (final pH about 11), where hydroxides were produced. Methanol was not detected when the cycle was over, i.e., when current intensity decreased. Besides, during the cycle, maximum current intensity remained rather constant. These observations permitted the inference that the decrease in current intensity was not a consequence of the change in pH but of the complete depletion of the substrate.

The authors concluded that net hydrogen production from biodiesel wastewater would also be possible in a double-chamber configuration regardless of the presence of methanol and methanol-metabolizing bacteria.

Regarding the perspectives of methanol utilization in BES at full-scale, one has to keep in mind that, up to date, bioelectrochemical hydrogen production from domestic/industrial wastewater has been only successfully achieved under well-controlled lab conditions. BES scaling-up is nowadays the focus of many researchers in view of bridging the gap between lab experiments and industrial application. Few efforts have been done so far and the values obtained in terms of organic matter removal and hydrogen production are still one or two orders of magnitude lower than those required for considering bioelectrochemical hydrogen production as industrially feasible.

Besides other optimization strategies, such as reactor configuration (materials, design, hydrogen separation), special care will be required when selecting operational parameters. Indeed, since the periodic addition of chemical methanogenesis inhibitors is not economically feasible, other operational parameters such as the hydraulic retention time of the system or the hydrogen gas retention time will need to be selected to minimize the loss of organic matter for nonanode-related processes.

4 Conclusion and Future Trends

The opportunities to energetically valorize methanol or methanol containing wastewater in bioelectrochemical systems have been presented and discussed throughout this chapter. Both the electricity generation and hydrogen production from methanol in microbial fuel cells and microbial electrolysis cells have been presented as feasible in the literature. The importance of a syntrophic consortium able to metabolize this carbon source and make it available for anode-related microorganisms is imperative. In regards to the microbial interactions within microbial electrolysis cells, net hydrogen production is only favored in a double-chamber configuration. Nevertheless, given the novelty of the technology, large optimization work still needs to be done so that electricity generation is boosted and the production of undesired products, such as methane, is minimized.

Future real implementation of bioelectrochemical systems for wastewater treatment and valorization will only be a reality if the overall technology costs can compete with current costs for wastewater treatment.

References

Cheng, S., Xing, D., Call, D.F., Logan, B.E., 2009. Direct biological conversion of electrical current into methane by electromethanogenesis. Environ. Sci. Technol. 43, 3953–3958.

Chignell, J.F., Liu, H., 2011. Biohydrogen production from glycerol in microbial electrolysis cells and prospects for energy recovery from biodiesel wastes. In: ASME 2011 International Manufacturing Science and Engineering Conference, MSEC 2011, pp. 693–701.

Chookaew, T., Prasertsan, P., Ren, Z.J., 2014. Two-stage conversion of crude glycerol to energy using dark fermentation linked with microbial fuel cell or microbial electrolysis cell. New Biotechnol. 31, 179–184.

Clauwaert, P., Van Der Ha, D., Verstraete, W., 2008. Energy recovery from energy rich vegetable products with microbial fuel cells. Biotechnol. Lett. 30, 1947–1951. https://doi.org/10.1007/s10529-008-9778-2.

Cusick, R., Bryan, B., Parker, D., Merrill, M., Mehanna, M., Kiely, P., Liu, G., Logan, B., 2011. Performance of a pilot-scale continuous flow microbial electrolysis cell fed winery wastewater. Appl. Microbiol. Biotechnol. 89, 2053–2063. https://doi.org/10.1007/s00253-011-3130-9.

Diekert, G., 1994. Metabolism of homoacetogens. Antonie Van Leeuwenhoek 66, 209–221. https://doi.org/10.1007/BF00871640.

Escapa, A., Manuel, M.F.-F., Morán, A., Gómez,, X., Guiot, S.R., Tartakovsky, B., Morán, A., Gómez, X., 2009. Hydrogen production from glycerol in a membraneless microbial electrolysis cell. Energy Fuel 23, 4612–4618. https://doi.org/10.1021/ef900357y.

Feng, Y., Yang, Q., Wang, X., Liu, Y., Lee, H., Ren, N., 2011. Treatment of biodiesel production wastes with simultaneous electricity generation using a single-chamber microbial fuel cell. Bioresour. Technol. 102, 411–415. https://doi.org/10.1016/j.biortech.2010.05.059.

Gil, G.-C., Chang, I.-S., Kim, B.H., Kim, M., Jang, J.-K., Park, H.S., Kim, H.J., 2003. Operational parameters affecting the performance of a mediator-less microbial fuel cell. Biosens. Bioelectron. 18, 327–334. https://doi.org/10.1016/S0956-5663(02)00110-0.

Heijthuijsen, J.H.F.G., 1986. Interspecies hydrogen transfer in co-cultures of methanol-utilizing acidogens and sulfate-reducing or methanogenic bacteria. FEMS Microbiol. Lett. 38, 57–64.

Hurst, C.J., Crawford, R.L., 2007. Manual of Environmental Microbiology, third ed. ASM Press, Washington, DC.

Kiely, P.D., Cusick, R., Call, D.F., Selembo, P.A., Regan, J.M., Logan, B.E., 2011. Anode microbial communities produced by changing from microbial fuel cell to microbial electrolysis cell operation using two different wastewaters. Bioresour. Technol. 102, 388–394. https://doi.org/10.1016/j.biortech.2010.05.019.

Kim, J.R., Jung, S.H., Regan, J.M., Logan, B.E., 2007. Electricity generation and microbial community analysis of alcohol powered microbial fuel cells. Bioresour. Technol. 98, 2568–2577. https://doi.org/10.1016/j.biortech.2006.09.036.

Liu, B., Li, B., 2014. Single chamber microbial fuel cells (SCMFCs) treating wastewater containing methanol. Int. J. Hydrog. Energy 39, 2340–2344. https://doi.org/10.1016/j.ijhydene.2013.11.111.

Liu, H., Logan, B.E., 2004. Electricity generation using an air-cathode single chamber microbial fuel cell in the presence and absence of a proton exchange membrane. Environ. Sci. Technol. 38, 4040–4046.

Liu, B., Brückner, C., Lei, Y., Cheng, Y., Santoro, C., Li, B., 2014. Cobalt porphyrin-based material as methanol tolerant cathode in single chamber microbial fuel cells (SCMFCs). J. Power Sources 257, 246–253. https://doi.org/10.1016/j.jpowsour.2014.01.117.

Ljungdahl, L.G., 1986. The autotrophic pathway of acetate synthesis in acetogenic bacteria. Annu. Rev. Microbiol. 40, 415–450.

Logan, B., Cheng, S., Watson, V., Estadt, G., 2007. Graphite fiber brush anodes for increased power production in air-cathode microbial fuel cells. Environ. Sci. Technol. 41, 3341–3346.

Lu, L., Xing, D., Liu, B., Ren, N., 2012. Enhanced hydrogen production from waste activated sludge by cascade utilization of organic matter in microbial electrolysis cells. Water Res. 46, 1015–1026. https://doi.org/10.1016/j.watres.2011.11.073.

Montpart, N., 2014. Hydrogen Production from Wastewater in Single Chamber Microbial Electrolysis Cells: Studies Towards Its Scaling-up. Universitat Autònoma de Barcelona, Bellaterra, Spain.

Montpart, N., Ribot-Llobet, E., Garlapati, V.K., Rago, L., Baeza, J.A., Guisasola, A., 2014. Methanol opportunities for electricity and hydrogen production in bioelectrochemical systems. Int. J. Hydrog. Energy 39, 770–777. https://doi.org/10.1016/j.ijhydene.2013.10.151.

Montpart, N., Rago, L., Baeza, J.A., Guisasola, A., 2015. Hydrogen production in single chamber microbial electrolysis cells with different complex substrates. Water Res. 68, 601–615. https://doi.org/10.1016/j.watres.2014.10.026.

Parameswaran, P., Torres, C.I., Lee, H.-S., Rittmann, B.E., Krajmalnik-Brown, R., 2011. Hydrogen consumption in microbial electrochemical systems (MXCs): the role of homo-acetogenic bacteria. Bioresour. Technol. 102, 263–271. https://doi.org/10.1016/j.biortech.2010.03.133.

Rago, L., Guerrero, J., Baeza, J.A., Guisasola, A., 2015. 2-Bromoethanesulfonate degradation in bioelectrochemical systems. Bioelectrochemistry 105, 44–49. https://doi.org/10.1016/j.bioelechem.2015.05.001.

Rozendal, R.A., Hamelers, H.V.M., Molenkamp, R.J., Buisman, C.J.N., 2007. Performance of single chamber biocatalyzed electrolysis with different types of ion exchange membranes. Water Res. 41, 1984–1994. https://doi.org/10.1016/j.watres.2007.01.019.

Rozendal, R.A., Hamelers, H.V.M., Rabaey, K., Keller, J., Buisman, C.J.N., 2008. Towards practical implementation of bioelectrochemical wastewater treatment. Trends Biotechnol. 26, 450–459.

Ruiz, Y., Baeza, J.A., Guisasola, A., 2013. Revealing the proliferation of hydrogen scavengers in a single-chamber microbial electrolysis cell using electron balances. Int. J. Hydrog. Energy. 38, 15917–15927.

Ruiz, Y., Baeza, J.A., Guisasola, A., 2016. Microbial electrolysis cell performance using non-buffered and low conductivity wastewaters. Chem. Eng. J. 289, 341–348. https://doi.org/10.1016/j.cej.2015.12.098.

Sakai, S., Yagishita, T., 2007. Microbial production of hydrogen and ethanol from glycerol containing wastes discharged from a biodiesel fuel production plant in a bioelectrochemical reactor with thionine. Biotechnol. Bioeng. 98, 340–348.

Selembo, P.A., Perez, J.M., Lloyd, W.A., Logan, B.E., 2009. High hydrogen production from glycerol or glucose by electrohydrogenesis using microbial electrolysis cells. Int. J. Hydrog. Energy 34, 5373–5381.

Speers, A.M., Young, J.M., Reguera, G., 2014. Fermentation of glycerol into ethanol in a microbial electrolysis cell driven by a customized consortium. Environ. Sci. Technol. 48, 6350–6358.

Tenca, A., Cusick, R.D., Schievano, A., Oberti, R., Logan, B.E., 2013. Evaluation of low cost cathode materials for treatment of industrial and food processing wastewater using microbial electrolysis cells. Int. J. Hydrog. Energy 38, 1859–1865. https://doi.org/10.1016/j.ijhydene.2012.11.103.

Yamamuro, A., Kouzuma, A., Abe, T., Watanabe, K., 2014. Metagenomic analyses reveal the involvement of syntrophic consortia in methanol/electricity conversion in microbial fuel cells. PLoS ONE 9, 1–8. https://doi.org/10.1371/journal.pone.0098425.

This page intentionally left blank

CHAPTER 13

Methanol Separation From Liquid Mixtures Via Pervaporation Using Membranes

Francesco Galiano, Francesco Falbo, Alberto Figoli

Institute on Membrane Technology (ITM-CNR), Rende, Italy

1 Introduction on Pervaporation

In recent years, membrane separation by pervaporation (PV) has gained interest thanks to its low environmental impact, low production costs, possibility of operating at low temperature, energy saving, easy scale-up, and high selectivity toward the molecules of interest to be separated. PV is a process which allows the separation of liquid mixtures by using a membrane (Crespo and Brazinha, 2015). When the membrane is in contact with a liquid mixture, one of the components is preferentially separated from the mixture due to its higher affinity with, and/or, quicker diffusivity in the membrane. As a result, both the more permeable species in the permeate, and the less permeable species in the feed, can be concentrated. In order to ensure the continuous mass transport, very low absolute pressures are usually maintained at the downstream side of the membrane, removing all the molecules migrating to the face, and thus, rendering a concentration difference across the membrane.

The PV process usually uses nonporous polymeric membranes or molecularly porous inorganic membranes (such as membranes containing zeolites) (Vane, 2005).

PV is a competitive technology to conventional energy intensive processes such as distillation and evaporation, which are energy intensive processes for the separation of close-boiling liquids or liquids forming azeotropes. However, a number of azeotropic mixtures cannot be efficiently separated by common distillation and PV, thus, can be used in combination with membrane distillation process.

The separation is not based on relative volatilities as in the case of thermal processes, but on the relative rates of permeation through a membrane (Khow and Mitra, 2010).

The driving force for PV process is the difference in chemical potential, corresponding to the concentration gradient between phases on the opposite sides of the interfacial barrier.

Methanol. https://doi.org/10.1016/B978-0-444-63903-5.00013-3

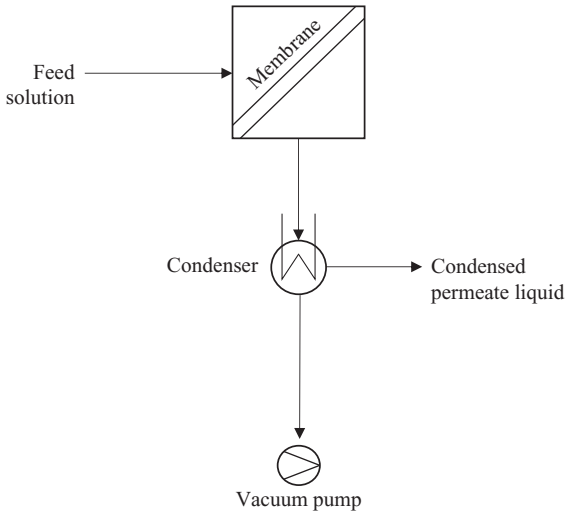

Fig. 13.1
Typical scheme of PV set-up.

So PV could be effectively utilized as an economical substitute for azeotropic separations (Feng and Huang, 1997).

Fig. 13.1 shows a typical set-up of a generic separation by PV.

Depending on the liquid mixture to separate, PV can be divided into three main types: (1) hydrophilic PV; (2) hydrophobic PV; and (3) organic/organic PV (Cassano et al., 2013). In particular, polymers that are highly hydrophilic, such as polyvinylalcohol (PVA), polyacrylonitryle (PAN), or chitosan (CS), are used in hydrophilic PV. These materials promote the diffusion and permeation of water molecules through the membrane (Verhoef et al., 2008; Gómez et al., 2006; van Veen et al., 2011). In hydrophobic PV, hydrophobic polymers, such as polydimethylsiloxane (PDMS), polystyrene-butadiene-co-styrene (SBS), and poly(1-trimethylsilyl-1-propyne) (PTMSP), are employed. In this case, the separation of nonpolar organic compounds from water (Kujawski, 2000; Catarino and Mendes, 2011a,b; Peng et al., 2003; Simone et al., 2012) is enhanced. Finally, in organic/organic PV, both hydrophilic and hydrophobic polymers can be used depending on the type of separation (polar/nonpolar, polar/polar or nonpolar/nonpolar) (Falbo et al., 2016; Zereshki et al., 2010a,b, c, 2011a,b; Kopec et al., 2013).

Based on the above-mentioned separations, PV can be used for different applications: (1) dehydration of aqueous-organic mixtures (W/O), (2) removal of organic compounds from aqueous solutions (O/W), and (3) separation of organic-organic solvent mixtures (O/O).

However, the O/O separation has been less investigated and there is still a possibility for improvement mainly due to the lack of solvent resistant polymers. In fact, the need of materials

with superior chemical resistance towards aggressive organic mixtures has limited such application.

Separation of O/O solvent mixtures, and particularly the ethanol purification from methanol, is the main objective of this chapter and it is widely described in the following sections.

2 Transport Mechanism in PV

The proposed mechanism to describe the permeation of different species through a dense membrane in PV is the solution-diffusion model (Wijmans and Baker, 1995).

Permeation through the membrane consists of the following steps:

1. Absorption of the target component from the liquid phase to the membrane interface on the basis of its chemical affinity;
2. Diffusion of the permeating compound through the membrane matrix;
3. Desorption (evaporation) of the species as a vapor to the downstream interface.

These three fundamental phases also govern the mass transport through the membranes (Binning et al., 1961).

When a PV membrane is in contact with a liquid feed mixture, it is generally believed that the thermodynamic equilibrium reaches instantly at the membrane-feed interface therefore,

$$S = \frac{C_{\text{membrane}}}{C_{\text{feed}}} \tag{13.1}$$

where C_{membrane} and C_{feed} represent the concentrations of a species in the membrane surface and the feed, respectively, and S is thus the partition coefficient or solubility of a species between the membrane and the feed phase, which is a characteristic parameter dependent upon the interaction of the species with the membrane. Membrane transport is a rate-controlling process, which is generally governed by Fick's first law:

$$J = -D\frac{dC_{\text{membrane}}}{dx} \tag{13.2}$$

where (J) is the total permeation flux of a species through the membrane, (D) is the diffusion coefficient of the species in the membrane, and x is the position variable. By introducing the solubility (S) of the species at the membrane/feed and membrane/permeate interface, the concentrations of a species in the faces of the membrane can be expressed in its concentrations in the feed and the permeate, respectively, and thus Fick's first law becomes:

$$J = \frac{DS}{x}\Delta C \tag{13.3}$$

where the diffusion and the solubility are treated as constant. If the trans membrane concentration (ΔC) is taken as the driving force for the mass transport, the permeability P of the species in the membrane can thus be defined as:

$$P = DS \tag{13.4}$$

Clearly, the permeability is an index measuring the intrinsic mass transport capability of a membrane for a species. Experimentally, the total and partial flux (J_a and J_b) can be obtained from the following expressions:

$$J = \frac{Q}{A \cdot t} \tag{13.5}$$

$$J_a = J \cdot X_a \tag{13.6}$$

$$J_b = J \cdot X_b \tag{13.7}$$

where Q is the weight of permeate obtained at time t, A is the effective membrane area, X_a and X_b are the weight fraction of component in the permeate side (Ghosh et al., 2010).

Another important parameter is the selectivity (α) which defines the separation characteristics of the membrane and can be expressed as:

$$\alpha_{a/b} = \frac{Y_a/Y_b}{X_a/X_b} \tag{13.8}$$

where X and Y are the weight fractions of the components in the feed and permeate, respectively, while the subscripts a and b indicate the two components that have to be separated.

The enrichment factor is used as an indicator of the separation selectivity for component a:

$$\beta = \frac{Y_a}{X_a} \tag{13.9}$$

Moreover, in order to evaluate the performance of the process, PV separation index (PSI), and taking both selectivity and total flux of a membrane into account Eq. (13.10) can be used:

$$\mathrm{PSI} = J(\alpha - 1) \tag{13.10}$$

The operational variables are critical to control the PV process (Smitha et al., 2004). For example, a change in the feed concentration directly affects the sorption phenomena at the liquid-membrane interface and also the permeation characteristics dictated by the solution-diffusion principle. Pressure at the feed and permeate side is also important. PV operation is carried out by applying vacuum or sweep gas to the permeate side of the membrane, which creates a chemical potential difference. This can be explained by the increase in driving force in the hand term of Eq. (13.5). Temperature affects all of the steps in the analytic transport process mentioned above, and also alters the driving force for mass transfer. Arrhenius-type

relationships have been used to describe the effect of the temperature on the flux as follows (Wijmans and Baker, 1995):

$$J = J_i \exp\left(\frac{E}{RT}\right) \tag{13.11}$$

3 Application of PV in Organic/Organic (O/O) Separation

The organic-organic (O/O) mixture separation is of main interest in the petrochemical industries (Ravanchi et al., 2009). Molecular separation processes are responsible for c.40% of the total energy consumption worldwide in the petrochemical industry (Kreiter et al., 2008). Subsequently, this chemical sector is searching for more energy-efficient separation processes to decrease energy consumption.

PV has been explored for the recovery of aromatics from naphtha stream, the reduction of benzene content in C6 reformates and the fractionation of alcohols/alkanes and alcohols/ether mixtures, considered critical issues in the refiners (van Veen et al., 2011). However, this type of separation is less investigated in research due to the lack of solvent resistant polymers; therefore, there it can be still improved. In fact, the need of materials with superior chemical resistance towards aggressive organic mixtures has limited the application of organic/organic PV.

However, several PV plants for O/O mixture separation have been installed and commercial membranes are available today (Peivasti et al., 2008; Sridhar et al., 2005).

Pervaporative O/O separation is classified in four categories: (1) separation of polar/nonpolar solvent mixtures, (2) separation of aromatic/alicyclic mixtures, (3) separation of aromatic isomers, and (4) separation of polar/polar mixture which is discussed in detail in Section 4.

3.1 Separation of Polar/Nonpolar Solvent Mixtures

The first industrial application of PV to polar/nonpolar separation was the methanol methyl-*tert*-butyl ether (MTBE) separation. In the traditional MTBE production process, methanol in excess is used to achieve a high conversion of isobutene and to minimize side reactions. Unfortunately, it forms a minimum-boiling azeotrope with MTBE at a composition of 14.3 wt% of the alcohol at atmospheric pressure. PV can be used to break this azeotrope (Mahdi et al., 2015; Smitha et al., 2004), which is problematic to separate by simple distillation. Most of the works on methanol/MTBE separation were carried out by using different polymers.

Polymers with high hydrophilicity (CA) (Wu et al., 2008; Wang et al., 2009; Ma et al., 2008), and PVA (Kim et al., 2003; Gozzelino and Malucelli, 2004), were used in many studies to prepare the membranes. Other studies were carried out by using poly-4-vinyl-pyridine (P4VP)

and PVA grafted on alumina to prepare the membranes (Yoshida and Cohen, 2003). Therefore, CS (Kim et al., 2002; Huang et al., 2001) and some other polymers have also been studied for methanol/MTBE separation.

Further works were carried out using a glassy polymer as a poly-ether-ether-ketone with cardo group (PEEKWC) (Zereshki et al., 2011a,b), these membrane materials showed very good processability, high thermal stability, and excellent mechanical properties at high temperatures.

Moreover, very high methanol/MTBE selectivity of 764 and 511 were obtained, using acrylic acid based copolymers, by Zhang et al. (2003) and Ray and Ray (2006), respectively.

Kopec et al. (2013) used polyamide-6 (PA6) based PV membranes which showed a methanol/MTBE selectivity of c.20. More recently, composite membranes from blended CS were developed by Nawawi et al. (Nawawi Mohd et al., 2013; Nawawi Mohd and Zamrud, 2014). A selectivity of c.80 and flux of 0.060 kg m^{-2} h^{-1} was obtained by operating at 50°C with 30 wt% of methanol as a starting feed solution.

The ethanol/ethyl-*tert*-butyl ether (ETBE) separation is an additional industrial application in which PV can be used as a valuable process as an alternative to separation by conventional methods.

ETBE is preferred to MTBE due to its lower water solubility (<26 g L^{-1}) with respect to MTBE (43–54 g L^{-1}), and is much more biodegradable than the latter thanks to the presence of a hydrogen atom in β-position to the ether group (Noureddini, 2002). ETBE can be obtained from the reaction of ethanol with isobutene to ensure a high isobutene conversion toward ether production (Jonquieres et al., 2000). When ETBE is found from bio-ethanol, it is also now considered as one of the most promising bio-fuels.

Nevertheless, the azeotropic mixture constituted by ethanol/ETBE (20/80 wt%) is difficult to separate by traditional technologies such as distillation. Numerous studies on ethanol/ETBE separation by PV were carried out. In particular, French researchers studied this separation by using CA membranes (Billy et al., 2010; Nguyen et al., 1997, 1998). Poly(pyrrolidinone) (Touchal et al., 2006) and polyamide-imides (PAI) based membranes (Jonquieres et al., 2000; Jonquières et al., 2005) were also used for the same separation. In 2002, Ortiz et al. (2002) used the commercial PERVAP 2256® membrane from Sulzer Chemtech.

Cellulose based blends (PVP-poly(vinyl-acetate)/CA) (Nguyen et al., 1997, 1998) and poly (acrylic-acid/CA phthalate) (Luo et al., 1997) membranes showed similar results with low flux at higher selectivity. The selectivity and the flux of graft copolymers CA-g-PEGDMA with different architectures (Billy et al., 2010) were 28–329 and 0.23–1.09 kg m^{-2} h^{-1}, respectively.

Pyrrolidinone-based membranes PVP/tetra-methyl-piperidinyloxy-methacrylate (TMPM) were able to efficiently separate ethanol/ETBE mixture with high flux (6.06–20.21 kg m^{-2} h^{-1} at 50°C)

(Touchal et al., 2006; Jonquieres et al., 2000). Interesting results were obtained for PU-PAI block copolymers with a flux ranging from 8.24 to 0.035 kg m^{-2} h^{-1} (Jonquières et al., 2005).

S. Zereshki et al. used PLA/PVP blend membranes to separate the ethanol from ETBE (Zereshki et al., 2011a,b). The works demonstrated that the ethanol/ETBE selectivity were not acceptable. However, the fluxes were acceptable at 0.05–1.36 kg m^{-2} h^{-1}.

PV can be used also in ethanol (30.5 wt%) cyclohexane (69.5 wt%) azeotropic mixture separation.

This separation was studied initially by Suzuki et al. (1987) and by Sakohara et al. (1994).

Zhou et al. (1995) obtained an ethanol/cyclohexane selectivity of 230 by using a poly(pyrrole) membrane. Zereshki et al. (2010a,b,c) reported a total flux of 0.16 kg m^{-2} h^{-1} and an ethanol/cyclohexane selectivity of 255 by using PEEK-PVP blend membranes; while a total flux of 0.19 kg m^{-2} h^{-1} and an ethanol/cyclohexane selectivity of 45 was obtained by using PLA/PVP blend membranes.

Moreover, Falbo et al. (2016), by using ethylene chlorotrifluoroethylene (ECTFE), have developed membranes with very high resistance to organic solvents and high ethanol flux c.1.7 kg m^{-2} h^{-1}. These membranes also showed good ethanol/cyclohexane selectivity with a value of c.30.

3.2 Separation of Aromatic/Alicyclic Mixtures

Separation of benzene and cyclohexane is among the most important and most difficult processes in the petrochemical industry. Cyclohexane is produced by catalytic hydrogenation of benzene. The unreacted benzene is present in the reactor's effluent stream and must be removed for pure cyclohexane recovery. Benzene cyclohexane separation is very problematic when using the conventional distillation process because these components form close boiling point mixtures at the entire range of their compositions. Presently, azeotropic distillation and extractive distillation are used for this separation. These two processes, however, suffer from complexity and high energy consumption. For all these reasons, the industry has always been eager to look for a viable alternative to the conventional benzene/cyclohexane separation processes.

Many studies were carried out to estimate the PV properties of membrane materials and interesting experiments were conducted to separate this mixture. Martin and Kelly (1961) and Martin et al. (1964) used revised cellulose membranes and a flux of c.1 kg m^{-2} h^{-1} was found. In another study, Cabasso et al. (1974) obtained very good flux values too. A shift from dealing with cellulose ester based compounds was brought forth by Elfret et al. (1978). Inui et al. (1999) working with polymethyl methacrylate-co-methacrylic acid membranes ionically

crosslinked achieved high flux and good selectivity. With the basic idea of grafting, Terada et al. (1982) synthesized graft copolymer membranes of 2-hydroxyethylmethylacrylate-methylacrylate of 10 μm thickness. The experiments were conducted having 50 wt% of benzene in the feed, and these membranes showed a flux of 0.7 1.3 kg m^{-2} h^{-1} and an exceptional selectivity (benzene concentration in permeate was 100 wt%). Park et al. (1994) prepared a blend membrane of PVA and polyallyl amine and tested them in PV by using a feed with 10 wt% of benzene. The membrane showed a flux of 1.3 kg m^{-2} h^{-1} and a benzene/cyclohexane selectivity of 62.

3.3 Separation of Aromatic Isomers Mixtures

The aromatic isomers mixture separation has increased extensive significance since the 1980s. Initial inroads were made by Mulder et al. (1982) which achieved high fluxes but a low selectivity. McCandless and Downs (1987) modified hydrophilic polymers for achieving high selectivity. About 12 polymeric membranes for the separation of the C8-aromatics at different temperatures were tested and the selectivity for p- to m-xylene were below 1.69 for all membranes. Wytcherley and McCandless (1992) separated m- and p-xylene mixtures using commercial PVA membrane in the presence of CBr4 as a selective feed complexing agent. In 1991, Westing et al., using polyethylene membranes, studied the separation of aromatic C8-isomers (Westing et al., 1991). The rate of mass transport across the membrane increased for the aromatic C8-isomers in the order *o*-xylene < ethylbenzene < *m*-xylene < *p*-xylene, and the flux of the components depended strongly on the downstream pressure. The very small separation factors (c.2) obtained restricted the use of PVA membranes for the purification of mixed xylenes at industrial levels. The separation of aromatic isomers continues to be an active research area because the present separation methods in use are both complex and use a lot of energy.

4 Methanol Purification by PV

4.1 Methanol/Organic Separations

Methanol is the simplest molecule, with the chemical formula CH_3OH, belonging to the family of organic compounds called "alcohols." It is formed by a methyl group bonded to a hydroxyl group. Methanol is, nowadays, produced at industrial level using carbon monoxide, carbon dioxide, and hydrogen through a catalytic process. It was once produced from the distillation of the wood and it is a colorless, volatile liquid. It finds its main applications in the production of other chemicals (acetic acid, formaldehyde, and various intermediates) and it is largely applied in the fuel sector (Sridhar et al., 2005). Methanol and isobutene are the reagents used for the production of the methyl *tert*-butyl ether (MTBE) which is used as a gasoline additive and antiknock agent, and able to enhance the octane number of gasoline, improving driving

performances and reducing the carbon monoxide emissions (Collignon et al., 1999). The reaction conversion is generally favored by adding larger amounts of methanol (up to 20%) in the reactor. However, the excess of methanol causes purification problems since methanol and MTBE form an azeotropic mixture at 14.3 wt% of methanol at atmospheric pressure. The distillation process, which is the dominant separation method for organic mixtures separation, becomes inefficient for the separation of close boiling liquids or azeotropes (such as methanol/MTBE). PV, on the contrary, demonstrated to be a valid and simple approach for this type of separation. PV is able, in fact, to break the azeotrope by using a membrane selective towards methanol, allowing the purification of MTBE. The selection of the appropriate membrane, suitable for this type of separation, is generally carried out considering the solubility of both components in the polymer material. Methanol is more polar than MTBE and it tends to establish hydrogen bondings with the polar groups present in the membrane matrix. MTBE, on the contrary, is slightly hydrophobic and its solubility in a membrane, with a polar moiety, is less pronounced (Sridhar et al., 2005). Extensive studies have been carried out on the research of the optimal membrane material able to successfully accomplish the methanol/MTBE separation by using PV. Zereshki et al. (2010a,b,c) applied poly(lactic aid) (PLA) as a material for the fabrication of dense membranes for the methanol/MTBE separation by PV. PLA is a thermoplastic polyester biopolymer derived from the lactic acid. In general, the selection of the most suitable polymer for a given separation is based on the Hansen solubility parameter (vectorial distance) obtained from the contributions of δ_d, δ_p and δ_h representing respectively the dispersive, the polar, and the hydrogen bonding contributions (Table 13.1).

From the solubility parameters of methanol, MTBE and PLA, is, therefore, possible to determine the type of interactions which can be established between the two solvents and the polymer, predicting the favored permeating compound through the membrane.

In this case, the polar contribution δ_p of the solubility parameter of PLA (9.7 $MPa^{1/2}$) was closer to that of methanol (12.27 $MPa^{1/2}$) than that of MTBE (3.63 $MPa^{1/2}$). This behavior favored the selective permeation of methanol through the membrane despite the hydrogen contribution δ_h. The PLA membrane presented a selectivity of more than 30 at low concentrations of methanol (1 wt%) at the temperature of 30°C and at the feed flow rate of 50 L h^{-1}. The selectivity, however, decreased at higher concentrations of methanol due to a swelling phenomenon of the membrane.

Table 13.1 Solubility parameters and vectorial distance between methanol, MTBE, and PLA

Compound	Solubility Parameters ($MPa^{1/2}$)			Vectorial Distance ($MPa^{1/2}$)
	δ_d	δ_p	δ_h	
Methanol	15.13	12.27	22.29	16.83
MTBE	15.48	3.63	5.22	6.78
PLA	18.5	9.7	6	

In another work, Zhou et al. (2013) studied the PV separation of methanol/MTBE mixture at the azetropic point (methanol concentration of 15 wt%) by using poly(vinyl alcohol) (PVA)/cellulose acetate (CA) blended membranes. The PVA/CA range composition was varied from 0 to 100 wt% of CA. The pristine PVA membrane exhibited the lowest flux and the highest selectivity (about 4000), while the CA pristine membrane presented the highest flux and the lowest selectivity (about 500). The observed decrease of the selectivity with increasing CA loading was attributed to the change in membrane morphology and, in particular, to the formation of enlarged free volumes which allowed a higher indiscriminate permeation of both compounds (methanol and MTBE).

The same PV separation (with 20 wt% of methanol) was also investigated by Wu et al. (2008) with CA/poly(vinyl) pyrrolidone (PVP) blended membranes prepared at different compositions. The effect of PVP influenced both the flux and the selectivity of the prepared membranes. From swelling tests, it was evidenced a preferential sorption of CA and CA/PVP blended membrane for methanol with respect to MTBE. This behavior was observed up to 15 wt% of PVP dispersed in the membrane matrix. At higher PVP concentrations, however, due to an enlargement of membrane free volume, the preferential sorption of methanol was reduced allowing more MTBE to be absorbed. This effect was also evidenced in PV tests. The selectivity of the membrane increased by increasing the PVP concentration in the membrane matrix (up to 15 wt%) where it reached the maximum value of 411. The increase of permeation flux with the increase of PVP content was related to the plasticizing effect of the additive on the CA polymer producing a higher amount of amorphous regions allowing the permeation of more methanol and MTBE molecules.

A summary of research data on methanol/MTBE mixture separations by using PV is reported in Table 13.2.

The separation of methanol from other organics, such as toluene, is of great interest in many petrochemical and pharmaceutical industries. Both methanol and toluene selective membranes have been developed so far and applied in PV for this type of organic/organic separation. Das and Ray (2016) recently fabricated hybrid elastomeric membranes (selective for toluene) by using natural rubber as a polymer and three types of fillers such as carbon black, organophilic clay, and organophilic zeolite. The produced membranes were then applied for the PV separation of toluene (in the range concentration of 3–40 wt%) from methanol. All the evaluated membranes presented a total flux that increased by increasing the toluene concentration in the feed solution (ranging from about 0.03 to 0.35 kg m^{-2} h^{-1}) due to its plasticizing effect on the rubber membrane. Also the toluene selectivity presented a similar trend for all the membranes considered, ranging from a maximum of 150 (at low toluene concentrations) to a minimum of about 90 (at high toluene concentrations). The decrease of selectivity, at high feed concentration of toluene, was related to the extensive swelling of

Table 13.2 Summary of literature data about methanol/MTBE separation by PV

Separation	Membrane Material	Selectivity (α)	Total Flux (kg µm m^{-2} h^{-1})	Temperature (°C)	Ref.
Methanol (5–40 wt%)-MTBE	Polyarylethersulfone with cardo (PES-C)	3124–99.6	1.2.–4.52	40	Han et al. (2013)
Methanol (20 wt%)-MTBE	Chitosan composite modified with surfactant	231.29	7.05	25	Yong and Lee (1999)
Methanol (20 wt%)-MTBE	Chitosan composite modified with H_2SO_4	9.33	1.5	25	Yong and Lee (1999)
Methanol (5–35 wt%)-MTBE	Triacetate (TCA)	1200–20	0.1–6	–	Cao et al. (1999)
Methanol (21 wt%)-MTBE	Modified polyethylene oxide (PPO)	5.4–7.8	3–4.8	40	Doghieri et al. (1994)
Methanol (10–30 wt%)-MTBE	PERVAP® 2256	180–25	1.35–2.7	25	Yong and Lee (1999)
Methanol (31 wt%)-MTBE	CA with metal oxide particles Al_2O_3 (0–10 wt%)	550–859	1–2.5	40	Wang et al. (2009)
Methanol (31 wt%)-MTBE	CA with metal oxide particles ZnO (0–14 wt%)	550–800	1–4.5	40	Wang et al. (2009)
Methanol (20 wt%)-MTBE	Poly(3-hydroxybutyrate) (PHB)	14.5	3.98	50	Villegas et al. (2011)

the membrane. Methanol selective membranes were developed, on the contrary, by Singha et al. (2009) for its separation from toluene by using PVA membranes chemically modified by cross-linking polymerization of acrylic acid and hydroxyethylmethacrylate. Methanol concentration was varied in the feed solution from 1.8 to 18.66 wt%. The tested membranes presented superior fluxes and selectivity when compared with various membranes reported in research. The selectivity reached, in fact, the value of 622.

Research data about the PV separation of methanol/alcohols mixtures are very limited. Pulyalina et al. (2015), for instance, studied polybenzoxazinoneimide (PBOI) membranes for the purification of methanol/ethanol mixtures via PV. The concentration of methanol in the feed mixtures was varied from 5 to 20 wt% at the temperatures of 20, 50, and 70°C. Membranes were found to be more permeable for methanol than for ethanol with a selectivity ranging from about 900 to about 300 (at 20°C). The preferable methanol sorption was attributed to the

fact that the smaller size of the methanol molecules allowed them to diffuse more easily through the membrane in comparison to ethanol ones. The selectivity decreased while the total flux increased with the growth of methanol concentration in the feed. This behavior was explained by considering the swelling effect of the membrane matrix, which caused an increase in the free volume fraction responsible of higher sorption of both permeants.

Bettens et al. (2010) investigated the PV performances of two methylated microporous silica membranes for the separation of methanol/alcohol mixtures (ethanol, isopropanol, and butanol) as a function of methanol feed composition (0–15 vol% of methanol) and of temperature. The methylated silica membrane (M1) presented a total flux which increased by increasing the methanol concentration in the feed. At low methanol concentrations, in fact, the other alcohols could hinder the methanol molecules to get in contact with the pores, therefore limiting its permeation. However, when the methanol concentration was increased, the competition between methanol and the alcohols decreased, resulting in a higher methanol permeation. The highest total flux was obtained for the smallest alcohol (ethanol) (about 0.9 kg m^{-2} h^{-1} at 15% methanol and at 60°C) while lower and similar values were obtained with isopropanol/methanol and butanol/methanol binary mixtures (total flux of about 0.35 and 0.45 kg m^{-2} h^{-1}, respectively). At 5 wt% of methanol the selectivity of the membrane for ethanol/methanol, isopropanol/methanol, and butanol/methanol mixtures was 9, 58, and 131, respectively.

Among the O/O separations in which methanol is involved, the separation of methanol/*n*-butyl acetate was studied by Luis et al. (2013). *N*-Butyl acetate is an important solvent in the chemical industry. One of the most convenient ways to produce it derives from the transesterification reaction of methyl acetate (a by product of PVA synthesis) with butanol, according to the following reaction:

$$\underset{\text{Methylacetate}}{CH_3COOCH_3} + \underset{\text{Butanol}}{CH_3CH_2CH_2CH_2OH} \rightleftarrows \underset{\text{Butylacetate}}{CH_3COOCH_2CH_2CH_2CH_3} + \underset{\text{Methanol}}{CH_3OH}$$

The concomitant production of methanol is also important in that the methanol can be reused as a feedstock for the production of PVA or in other applications (Steinigeweg and Gmehling, 2004). The transesterification reaction is, however, reversible. For this reason, in order to increase the yield, it is necessary to constantly remove butylacetate or methanol, allowing to shift the equilibrium towards the formation of the products. Luis et al. (2013), therefore, evaluated the performances of several commercial membranes for the methanol/butyl acetate PV separation. Ten different commercial membranes were tested: eight composite membranes supplied by PolyAn GmbH (Germany), specific for organic/organic separation, and two PVA based membranes (Pervap 1201 and Pervap 2255-50). Removing the effect of the driving force, all the considered membranes resulted in selecting butyl acetate. The affinity of the membranes for butyl acetate was higher when its concentration was increased in the feed side. In particular, the best performances were obtained for two PolyAn\GmbH membranes (named

as Poly OL M1 and M2) presenting a permeance of 70,000 and 80,000 GPU, respectively ($1\ \text{GPU} = 1 \times 10^{-6}\ \text{cm}^3\ (\text{STP})/(\text{cm}^2\ \text{s cm Hg}) = 7.5005 \times 10^{-12}\ \text{ms}^{-1}\ \text{Pa}^{-1}$) and a selectivity of 20 (measured at 20 mol% of methanol feed concentration).

4.2 Methanol/Water Separation

The PV separation of alcohol/water mixtures is of great importance for the chemical industry. In spite of the ethanol/water separation, which is already well applied and diffused at the industrial level representing a consolidate technique, methanol/water separation is still a challenge. Methanol, in fact, has a greater polarity in comparison to ethanol, with a molecular size closer to that of water. For these reasons, methanol can compete with water molecules in permeating through the membrane and specific selective membranes have to be, therefore, applied (Toth and Mizsey, 2015). Polydimethyl siloxane (PDMS) and mixed matrix membranes have been, so far, the most diffused membrane types used in methanol/water separation.

Mohammadi et al. (2005), for instance, applied PDMS membranes for the PV separation of ethanol/water and methanol/water mixtures. It was observed that by increasing the alcohol feed concentration (from 0.3 to 3 wt%), the total flux also increased (from 0.5 to 0.9 kg $\text{m}^{-2}\ \text{h}^{-1}$ for ethanol/water mixture and from about 0.35 to 0.5 kg $\text{m}^{-2}\ \text{h}^{-1}$ for methanol/water mixture). This behavior was explained considering the higher swelling of the membrane at higher alcohol concentrations, which promoted the diffusion of more molecules to pass through. The methanol flux was slightly higher than the ethanol one because of the higher diffusion coefficient of the methanol flux due to its smaller molecular size. The separation factor was, however, negatively affected by the increase of alcohol concentration in the feed solution. It decreased from 8 to about 2.5 for the methanol/water mixture and from 3 to about 1.8 for the ethanol/water mixture. This could be due to the fact that the increase of alcohol concentration results in the increase of membrane free-volume. The permeation of water molecules with a smaller molecular diameter, and therefore responsible of the selectivity decrease, was, thus, enhanced. The higher selectivity of the membrane toward methanol/water solution can be explained considering its higher swelling degree in ethanol/water solutions.

In order to increase membrane performances, mixed matrix membranes (MMMs) have been developed by incorporating different types of fillers (silicalites, silica, zeolite, …) into the polymeric matrix. Metal-organic frameworks (MOFs) are a class of crystalline and microporous materials made up of metal ions linked together by organic ligands (James, 2003). Membranes prepared with MOFs received great attention in PV and gas separation applications (Li et al., 2011; Basu et al., 2010; Ibrahim and Lin, 2016). A particular sub-class of MOFs, zeolitic imidazolate frameworks (ZIFs) made up of a tetrahedral metal ion bridged by imidazolate, were incorporated in PDMS membranes for the separation of alcohol (methanol, ethanol, isopropanol, and sec-butanol) aqueous solutions mixtures by PV (Li et al., 2014).

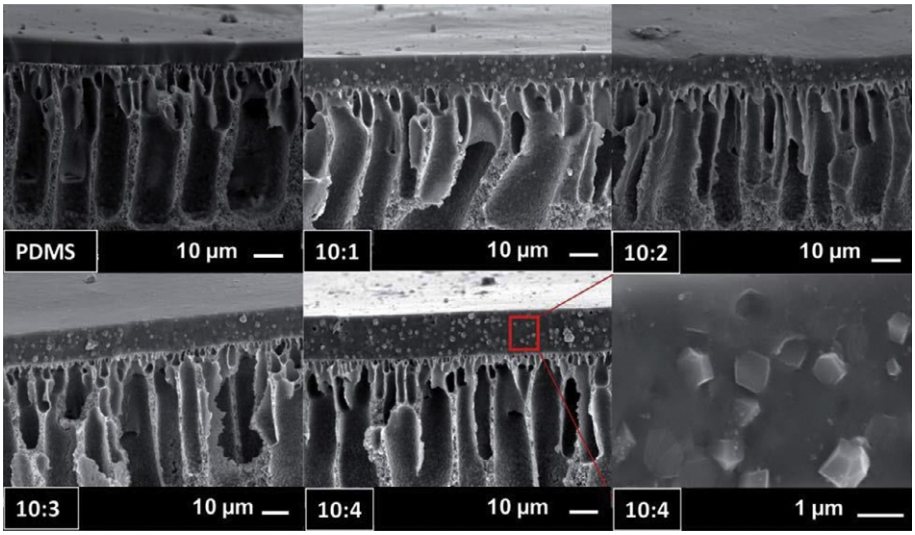

Fig. 13.2
Cross-sectional images of filled PDMS membranes with different ZIF-71 loadings. The picture at the bottom right is a detailed image of the selective layer of the ZIF-71 filled membrane (PDMS: ZIF-71 = 10: 4) (Li et al., 2014).

In particular ZIFs-71, having super-hydrophobic pore-channels and already known for their potentiality in bio-alcohols separations by PV (Liu et al., 2013), were evaluated for the preparation of PDMS MMMs membranes at different PDMS/ZIF-71 ratio (from 10:0 to 10:4 wt/wt). The ZIFs-71 presented a homogeneous distribution into the PDMS membrane at all the loadings considered (Fig. 13.2). The thickness of the PDMS membranes increased by increasing the ZIF-71 loading.

The separation factor of the PDMS pristine membrane increased (from 5.3 to 16.3) by moving from methanol to sec-butanol due to the higher swelling of the membrane in alcohols with a longer carbon chain. For filled PDMS membranes, the separation factor increased by increasing the ZIF-71 loading but up to a certain value (PDMS:ZIF-71 = 10:2) when it started to decrease probably due to the formation of defects into the membrane. For methanol/water solution, the highest separation factor of 8 was reached when the PDMS:ZIF-71 ratio was equal to 10:3 and in any case it was superior to the separation factor obtained with the un-filled PDMS membrane. The methanol flux also increased at a higher ZIF content into the membrane. This was probably due to the fact that methanol kinetic diameter (0.39 nm) is much smaller than ZIF-71 pore window (0.48 nm), favoring its permeation through ZIF rather than through the PDMS dense membrane. In Table 13.3 a summary of research data on methanol/water PV separation are reported.

Table 13.3 Summary of research data about methanol/water separation by PV

Separation	Membrane Material	Separation Factor (β)	Total Flux (kg m^{-2} h^{-1})	Temperature (°C)	Ref.
Methanol (5 wt%)/water	PDMS + ZIF-71 (10:0)	5.3	0.486	50	Li et al. (2014)
	PDMS + ZIF 71 (10:1)	6.1	0.469		
	PDMS + ZIF 71 (10:2)	7	0.611		
	PDMS + ZIF 71 (10:3)	8	0.458		
	PDMS + ZIF 71 (10:4)	7.7	0.417		
Methanol (0.3–3 wt%)/water	PDMS	2–8	0.35–0.5	30	Mohammadi et al. (2005)
Methanol (20–60 vol%)/ water	PVA/*N*-3-(trimethoxysilyl) propyl ethylenediamine (TMSPEDA) (2 mL)	0.95–1.2	2.5–3.4	30	Hu et al. (2013)
	PVA/*N*-3-(trimethoxysilyl) propyl ethylenediamine (TMSPEDA) (3 mL)	1–1.3	1.9–2.4		
	PVA/*N*-3-(trimethoxysilyl) propyl ethylenediamine (TMSPEDA) (4 mL)	1.1–1.3	1.4		
	PVA/*N*-3-(trimethoxysilyl) propyl ethylenediamine (TMSPEDA) (5 mL)	1.6–1.3	0.75		
Methanol (4 wt%)/water	Chitosan	5	0.08	30	Zieliń ska et al. (2011)
Methanol (4 wt%)/water	PDMS/silica	25	0.09	30	Shirazi et al. (2012)
Methanol (3 m/m%)/water	Sulzer PERVAP™ 4060	4.6–5	2	70	Toth and Mizsey (2015)
	Sulzer PERVAP™ 2211	1.2	8–10		
Methanol (0–90 wt%)/water	Sulzer PERVAP™ 2201	2.5–10	0.3–1.5	60	Van Baelen et al. (2005)
Methanol (0–50 wt%)/water	Zeolite NaA	100–1000	0–2	60	Shah et al. (2000)
Methanol (85 wt%)/water	Sulfonated (5%) polyphenylsulfone	11.1	0.033	60	Tang et al. (2012)

5 Conclusions

The more stringent regulations regarding environmental safeguard and natural resources preservation make PV technology more and more attractive for its low environmental impact in terms of energy requirements and high efficiency in green applications, like the removal of pollutants from water, the separation of organic solvents from industrial wastewaters, and the solvent dehydration. PV in particular, thanks to the development of novel membrane materials

more accomplished and more resistant to harsh conditions, is increasing interest, at an industrial level, in the field of organic/organic separations. Methanol is one of the most used solvents in the chemical, automotive, and pharmaceutical industries. However, at the same time, methanol is toxic, flammable, and highly reactive. The recovery and reuse of this solvent, together with the treatment of the effluents contaminated, are, therefore, of great importance in reducing the production costs and protecting the environment. PV, in this context, plays a crucial role. Several research data reports on the application of PV in treating organic/organic solutions for the separation of methanol/organic mixtures and in breaking methanol/organic azeotropes. The methanol/MTBE mixtures separation is, for instance, one of the most studied and is also one of the most interesting at an industrial level. Moreover, the necessity of methanol recovery from other organics such as ethanol, toluene, and butyl acetate is also highly considered.

The separation of methanol from water, in comparison to methanol/organic separations, is still a challenge, from some points of view, due to the similarities between the two molecules in terms of polarity and molecule dimension. However, PDMS and novel MMMs are also showing good and promising results for this type of separation.

References

Basu, S., Khan, A.L., Cano-Odena, A., Liu, C., Vankelecom, I.F.J., 2010. Membrane-based technologies for biogas separations. Chem. Soc. Rev. 39, 750–768.

Bettens, B., Verhoef, A., Van Veen, H.M., Vandecasteele, C., Degreve, J., Van der Bruggen, B., 2010. Pervaporation of binary water-alcohol and methanol-alcohol mixtures through microporous methylated silica membranes: Maxwell-Stefan modelling. Comput. Chem. Eng. 34, 1775–1788.

Billy, M., Costa, A.R.D., Lochon, P., Clément, R., Dresch, M., Jonquières, A., 2010. Cellulose acetate graft copolymers with nano-structured architectures: application to the purification of bio-fuels by pervaporation. J. Membr. Sci. 348, 389–396.

Binning, R.C., Lee, R.J., Jenning, J.F., Martin, E.C., 1961. Separation of liquid mixtures by permeation. Ind. Eng. Chem. 53 (45), 6–50.

Cabasso, L., Jayur-Grodzinski, L., Vofsi, P., 1974. Polymeric alloys of polyphosphonates and acetyl celluloses I-sorption and diffusion of benzene cyclohexane. J. Appl. Polym. Sci. 18, 2137.

Cao, S., Shi, Y., Chen, G., 1999. Pervaporation separation of MeOH/MTBE through CTA membrane. J. Appl. Polym. Sci. 71, 377–386.

Cassano, A., Figoli, A., Galiano, F., Argurio, P., Molinari, R., 2013. Membrane operations in wastewater treatment: complexation reactions coupled with membranes, pervaporation and membrane bioreactors. In: Basile, A. (Ed.), Membrane Reactors in Environmental Engineering, Biotechnology and Medicine. Woodhead Publishing Limited, Sawston, Cambridge, UK, pp. 731–762 (Chapter 19).

Catarino, M., Mendes, A., 2011a. Non-alcoholic beer—a new industrial process. Sep. Purif. Technol. 79, 342–351.

Catarino, M., Mendes, A., 2011b. Dealcoholizing wine by membrane separation processes. Innovative Food Sci. Emerg. Technol. 12, 330–337.

Collignon, F., Loenders, R., Martens, J.A., Jacobs, P.A., Poncelet, G., 1999. Liquid phase synthesis of MTBE from methanol and isobutene over acid zeolites and amberlyst-15. J. Catal. 182, 302–312.

Crespo, J.G., Brazinha, C., 2015. Fundamentals of pervaporation. In: Basile, A., Figoli, A., Khayet, M. (Eds.), Pervaporation, Vapour Permeation and Membrane Distillation, first ed. Woodhead Publishing, Elsevier, Amsterdam, The Netherlands (Chapter 1).

Das, P., Ray, S.K., 2016. Separation of toluene-methanol mixtures by pervaporation using filled elastomeric membranes. J. Taiwan Inst. Chem. Eng. 64, 89–105.
Doghieri, F., Nardella, A., Sarti, G.C., Valentini, C., 1994. Pervaporation of methanol-MTBE mixtures through modified poly(phenylene oxide) membranes. J. Membr. Sci. 91, 283–291.
Elfret, K., Rusenkranz, J.H., Rudolf, H., 1978. US Patent, 4, 115, 465.
Falbo, F., Santoro, S., Galiano, F., Simone, S., Davoli, M., Drioli, E., Figoli, A., 2016. Organic/organic mixture separation by using novel ECTFE polymeric pervaporation membranes. Polymer 98, 110–117.
Feng, X., Huang, R.Y.M., 1997. Liquid separation by membrane pervaporation: a review. Ind. Eng. Chem. Res. 36, 1048–1066.
Ghosh, U.K., Narayan Pradhan, C., Adhikari, B., 2010. Pervaporation separation of furfural from aqueous solution using modified polyurethaneurea membrane. Desalination 252, 1–7.
Gómez, P., Ibáñez, R., Ortiz, I., Grossmann, I., 2006. Optimum design of PV processes for dehydration of organic mixtures. Desalination 193, 152–159.
Gozzelino, G., Malucelli, G., 2004. Permeation of methanol/methyl-t-butyl ether mixtures through poly(ethylene-co-vinyl acetate) films. Colloids Surf. A Physicochem. Eng. Asp. 235, 35–44.
Han, G.L., Zhang, Q.G., Zhu, A.M., Liu, Q.L., 2013. Pervaporation separation of methanol/methyl *tert*-butyl ether mixtures using polyarylethersulfone with cardo membranes. Sep. Purif. Technol. 107, 211–218.
Hu, K., Nie, J., Liu, J., Zheng, J., 2013. Separation of methanol from methanol/water mixtures with pervaporation hybrid membranes. J. Appl. Polym. Sci. 128, 1469–1475.
Huang, R.Y.M., Moon, G.Y., Pal, R., 2001. Chitosan/anionic surfactant complex membranes for the pervaporation separation of methanol/MTBE and characterization of the polymer/surfactant system. J. Membr. Sci. 184, 1–15.
Ibrahim, A., Lin, Y.S., 2016. Pervaporation separation of organic mixtures by MOF-5 membranes. Ind. Eng. Chem. Res. 55, 8652–8658.
Inui, K., Noguchi, K., Miyata, T., Uragami, T., 1999. J. Appl. Polym. Sci. 71, 233–241.
James, S.L., 2003. Metal-organic frameworks. Chem. Soc. Rev. 32, 276–288.
Jonquieres, A., Dole, C., Clement, R., Lochon, P., 2000. Synthesis and characterization of new highly permeable polyamideimides from dianhydride monomers containing amide functions: an application to the purification of a fuel octane enhancer (ETBE) by pervaporation. J. Polym. Sci. A Polym. Chem. 38, 614–630.
Jonquières, R., Clément, P., Lochon, 2005. New film-forming poly(urethane-amideimide) block copolymers: influence of soft block on membrane properties for the purification of a fuel octane enhancer by pervaporation. Eur. Polym. J. 41, 783–795.
Khow, O.S., Mitra, S., 2010. Pervaporation in chemical analysis. J. Chromatogr. A 1217, 2736–2746.
Kim, S.G., Kim, Y.I., Jegal, J., Lim, G.T., Lee, K.H., 2002. Characterization and preparation of polyion complex composite membranes for the separation of methyl *tert*-butyl ether/methanol mixtures. J. Appl. Polym. Sci. 85, 714–725.
Kim, S.G., Kim, Y.I., Yun, H.G., Lim, G.T., Lee, K.H., 2003. Preparation of asymmetric PVA membranes using ternary system composed of polymer and cosolvent. J. Appl. Polym. Sci. 88, 2884–2890.
Kopec, R., Meller, M., Kujawski, W., Kujawa, J., 2013. Polyamide-6 based pervaporation membranes for organic-organic separation. Sep. Purif. Technol. 110, 63–73.
Kreiter, R., Wolfs, D.P., Engelen, C.W.R., van Veen, H.M., Vente, J.F., 2008. High-temperature pervaporation performance of ceramic-supported polyimide membranes in the dehydration of alcohols. J. Membr. Sci. 319, 126–132.
Kujawski, W., 2000. Pervaporative removal of organics from water using hydrophobic membranes. Binary mixtures. Sep. Sci. Technol. 35, 89–108.
Li, J.-R., Sculley, J., Zhou, H.-C., 2011. Metal-organic frameworks for separations. Chem. Rev. 112, 869–932.
Li, Y., Wee, L.H., Martens, J.A., Vankelecom, I.F.J., 2014. ZIF-71 as a potential filler to prepare pervaporation membranes for bio-alcohol recovery. J. Mater. Chem. A 2, 10034–10040.
Liu, S., Liu, G., Zhao, X., Jin, W., 2013. Hydrophobic-ZIF-71 filled PEBA mixed matrix membranes for recovery of biobutanol via pervaporation. J. Membr. Sci. 446, 181–188.

Luis, P., Degrève, J., Van der Bruggen, B., 2013. Separation of methanol-*n*-butyl acetate mixtures by pervaporation: potential of 10 commercial membranes. J. Membr. Sci. 429, 1–12.
Luo, G.S., Niang, M., Schaetzel, P., 1997. Sorption and pervaporation separation of ethyl *tert*-butyl ether and ethanol mixtures through a blended membrane. J. Appl. Polym. Sci. 66, 1631–16381.
Ma, X., Hu, C., Guo, R., Fang, X., Wu, H., Jiang, Z., 2008. HZSM5-filled cellulose acetate membranes for pervaporation separation of methanol/MTBE mixtures. Sep. Purif. Technol. 59, 34–42.
Mahdi, T., Ahmad, A., Nasef, M., Ripin, A., 2015. State-of-the-art technologies for separation of azeotropic mixtures. Sep. Purif. Rev. 44, 308–330.
Martin, E.C., Kelly, L.T. 1961. US Patent, 2, 981, 730.
Martin, E.C., Binning, R.C., Adams, L.M., Lee, R.J., 1964. US patent, 3, 150, 456.
McCandless, F.P., Downs, W.B., 1987. Separation of C_8 aromatic isomers by pervaporation through commercial polymer films. J. Membr. Sci. 30, 111–116.
Mohammadi, T., Aroujalian, A., Bakhshi, A., 2005. Pervaporation of dilute alcoholic mixtures using PDMS membrane. Chem. Eng. Sci. 60, 1875–1880.
Mulder, M.H.V., Kruitz, F., Smolders, C.A., 1982. Separation of isomeric xylenes by pervaporation through cellulose ester membranes. J. Membr. Sci. 11, 349–363.
Nawawi Mohd, M.G., Zamrud, Z., 2014. Composite chitosan membranes for the separation of methanol/methyl *tert*-butyl ether mixtures. J. Teknol. 67 (2), 23–30.
Nawawi Mohd, M.G., Zamrud, Z., Idham, G., Hassan, Z., Mohd Sakri, O.N., 2013. Blended chitosan and polyvinyl alcohol membrane for pervaporation separation methanol/methyl *tert*-butyl ether mixture. (II) Effect of operating parameters. J. Teknol. 65 (1), 39–43.
Nguyen, Q.T., Noezar, I., Clément, R., Streicher, C., Brueschke, H., 1997. Poly(vinyl pyrrolidone-co-vinyl acetate)-cellulose acetate blends as novel pervaporation membranes for ethanol-ethyl tertio-butyl ether separation. Polym. Adv. Technol. 8, 477–486.
Nguyen, Q.T., Clement, R., Noezar, I., Lochon, P., 1998. Performances of poly(vinylpyrrolidone-co-vinyl acetate)-cellulose acetate blend membranes in the pervaporation of ethanol-ethyl *tert*-butyl ether mixtures: simplified model for flux prediction. Sep. Purif. Technol. 13, 237–245.
Noureddini, H., 2002. Ethyl *tert*-butyl ether and methyl *tert*-butyl ether: status, review, and alternative use exploring the environmental issues of mobile, recalcitrant compounds in gasoline. ACS Symp. Ser. 799, 107–124.
Ortiz, I., Alonso, P., Urtiaga, A., 2002. Pervaporation of azeotropic mixtures ethanol/ethyl *tert*-butyl ether: influence of membrane conditioning and operation variables on pervaporation flux. Desalination 149, 67–72.
Park, C.K., Lee, M.Y., Oh, B., Choi, M., 1994. Separation of benzene/cyclohexane by pervaporation through chelate poly(vinyl alcohol)/poly (allyl amine) blend membrane. Polym. Bull. 33, 591–598.
Peivasti, M., Madandar, A., Mohammadi, T., 2008. Effect of operating conditions on pervaporation of methanol/methyl *tert*-butyl ether mixtures. Chem. Eng. Process. Process Intensif. 47, 1069–1074.
Peng, M., Vane, L.M., Liu, S.X., 2003. Recent advances in VOCs removal from water by pervaporation. J. Hazard. Mater. B 98, 69–90.
Pulyalina, A.Y., Polotskaya Galina, A., Veremeychik, K.Y., Goikhman, M.Y., Podeshvo, I.V., Toikka, A.M., 2015. Ethanol purification from methanol via pervaporation using polybenzoxazinoneimide membrane. Fuel Process. Technol. 139, 178–185.
Ravanchi, M.T., Kaghazchi, T., Kargari, A., 2009. Application of membrane separation processes in petrochemical industry: a review. Desalination 235, 199–244.
Ray, S., Ray, S.K., 2006. Synthesis of highly methanol selective membranes for separation of methyl tertiary butyl ether (MTBE)-methanol mixtures by pervaporation. J. Membr. Sci. 278, 279–289.
Sakohara, S., Sakai, S., Maekawa, Y., Asaeda, M., 1994. Separation of organic solvent mixtures by dimethylacrylamide gel polymerized in pores of a thin, porous ceramic membrane. Kobunshi Ronbunshu 51, 540–546.
Shah, D., Kissick, K., Ghorpade, A., Hannah, R., Bhattacharyy, D., 2000. Pervaporation of alcohol-water and dimethylformamide-water mixtures using hydrophilic zeolite NaA membranes: mechanisms and experimental results. J. Membr. Sci. 179, 185–205.

Shirazi, Y., Ghadimi, A., Mohammadi, T., 2012. Recovery of alcohols from water using polydimethylsiloxane-silica nanocomposite membranes: characterization and pervaporation performance. J. Appl. Polym. Sci. 124, 2871–2882.

Simone, S., Figoli, A., Santoro, S., Galiano, F., Alfadul, S.M., Al-Harbi, O.A., Drioli, E., 2012. Preparation and characterization of ECTFE solvent resistant membranes and their application in pervaporation of toluene/water mixtures. Sep. Purif. Technol. 90, 147–161.

Singha, N.R., Kuila, S.B., Das, P., Ray, S.K., 2009. Separation of toluene-methanol mixtures by pervaporation using crosslink IPN membranes. Chem. Eng. Process. 48, 1560–1565.

Smitha, B., Suhanya, D., Sridhar, S., Ramakrishna, M., 2004. Separation of organic-organic mixtures by pervaporation—a review. J. Membr. Sci. 241, 1–21.

Sridhar, S., Smitha, B., Shaik, A., 2005. Pervaporation-based separation of methanol/MTBE mixtures—a review. Sep. Purif. Technol. 34, 1–33.

Steinigeweg, S., Gmehling, J., 2004. Transesterification processes by combination of reactive distillation and pervaporation. Chem. Eng. Process. 43, 447–456.

Suzuki, F., Onozato, K., Yaegashi, H., Masuko, T., 1987. Pervaporation of organic solvents by poly[bis(2,2,2-trifluoroethoxy) phosphazene] membrane. J. Appl. Polym. Sci. 34, 2197–2204.

Tang, Y., Widjojo, N., Shi, G.M., Chung, T.-S., Weber, M., Maletzko, C., 2012. Development of flat-sheet membranes for C1–C4 alcohols dehydration via pervaporation from sulfonated polyphenylsulfone (sPPSU). J. Membr. Sci. 415–416, 686–695.

Terada, J., Hohjoh, T., Yoshimasu, S., Ikemi, I.M., Shinohara, T., 1982. Separation of benzene/cyclohexane azeotropic mixture through polymeric membranes with microphase separated structures. Eur. Polym. J. 14 (5), 347–353.

Toth, A.J., Mizsey, P., 2015. Methanol removal from aqueous mixture with organophilic pervaporation: experiments and modelling. Chem. Eng. Res. Des. 98, 123–135.

Touchal, S., Roizard, D., Perrin, L., 2006. Pervaporation properties of polypyrrolidinone based membranes for EtOH/ETBE mixtures separation. J. Appl. Polym. Sci. 99, 3622–3630.

Van Baelen, D., Van der Bruggen, B., Van den Dungen, K., Degreve, J., Vandecasteele, C., 2005. Pervaporation of water-alcohol mixtures and acetic acid-water mixtures. Chem. Eng. Sci. 60, 1583–1590.

van Veen, H.M., Rietkerk, M.D.A., Shanahan, D.P., van Tuel, M.M.A., Kreiter, R., Castricum, H.L., ten Elshof, J.E., Vente, J.F., 2011. Pushing membrane stability boundaries with HybSi pervaporation membranes. J. Membr. Sci. 380, 124–131.

Vane, L.M., 2005. A review of pervaporation for product recovery from biomass fermentation processes. J. Chem. Technol. Biotechnol. 80, 603–629.

Verhoef, A., Figoli, A., Leen, B., Bettens, B., Drioli, E., Van der Bruggen, B., 2008. Performance of a nanofiltration membrane for removal of ethanol from aqueous solutions by pervaporation. Sep. Purif. Technol. 60, 54–63.

Villegas, M., Castro Vidaurre, E.F., Habert, A.C., Gottifredi, J.C., 2011. Sorption and pervaporation with poly(3-hydroxybutyrate) membranes: methanol/methyl *tert*-butyl ether mixtures. J. Membr. Sci. 367, 103–109.

Wang, Y., Yang, L., Luo, G., Dai, Y., 2009. Preparation of cellulose acetate membrane filled with metal oxide particles for the pervaporation separation of methanol/methyl *tert*-butyl ether mixtures. Chem. Eng. J. 146, 6–10.

Westing, M., Werner, U., Huang, S.T., 1991. Pervaporation of aromatic C_8-isomers. J. Membr. Sci. 57, 257–270.

Wijmans, J.G.R., Baker, W., 1995. The solution-diffusion model: a review. J. Membr. Sci. 107, 1–21.

Wu, H., Fang, X., Zhang, X., Jiang, Z., Li, B., Ma, X., 2008. Cellulose acetate-poly(*N*-vinyl-2- pyrrolidone) blend membrane for pervaporation separation of methanol/MTBE mixtures. Sep. Purif. Technol. 64, 183–191.

Wytcherley, R.W., McCandless, F.P., 1992. The separation of meta- and para-xylene by pervaporation in the presence of CBr4, a selective feed-complexing agent. J. Membr. Sci. 67, 67–74.

Yong, N.S., Lee, Y.M., 1999. Pervaporation separation of methanol/MTBE through chitosan composite membrane modified with surfactants. J. Membr. Sci. 157, 63–71.

Yoshida, W., Cohen, Y., 2003. Ceramic-supported polymer membranes for pervaporation of binary organic/organic mixtures. J. Membr. Sci. 213, 145–157.

Zereshki, S., Figoli, A., Madaeni, S.S., Simone, S., Drioli, E., 2010a. Pervaporation separation of methanol/methyl *tert*-butyl ether with poly(lactic acid) membranes. J. Appl. Polym. Sci. 118, 1364–1371.

Zereshki, S., Figoli, A., Madaeni, S.S., Simone, S., Jansen, J.C., Esmailinezhad, M., Drioli, E., 2010b. Poly(lactic acid)/poly(vinyl pyrrolidone) blend membranes: effect of membrane composition on pervaporation separation of ethanol/cyclohexane mixture. J. Membr. Sci. 362, 105–112.

Zereshki, S., Figoli, A., Madaeni, S.S., Simone, S., Esmailinezhad, M., Drioli, E., 2010c. Effect of polymer composition in PEEKWC/PVP blends on pervaporation separation of ethanol/cyclohexane mixture. Sep. Purif. Technol. 75, 257–265.

Zereshki, S., Figoli, A., Madaeni, S.S., Simone, S., Esmailinezhad, M., Drioli, E., 2011a. Pervaporation separation of MeOH/MTBE mixtures with modified PEEK membrane: effect of operating conditions. J. Membr. Sci. 371, 1–9.

Zereshki, S., Figoli, A., Madaenib, S.S., Galiano, F., Drioli, E., 2011b. Pervaporation separation of ethanol/ETBE mixture using poly(lactic acid)/poly(vinyl pyrrolidone) blend membranes. J. Membr. Sci. 373, 29–35.

Zhang, L., Chen, H.L., Pan, Z.R., 2003. Study on swelling behavior and pervaporation properties of AA-MMA-BA copolymers for separation of methanol/MTBE/C5 mixtures. J. Appl. Polym. Sci. 87, 2267–2271.

Zhou, M., Persin, M., Kujawski, W., Sarrazin, J., 1995. Electrochemical preparation of polypyrrole membranes and their application in ethanol-cyclohexane separation by pervaporation. J. Membr. Sci. 108, 89–96.

Zhou, K., Zhang, Q.G., Han, G.L., Zhu, A.M., Liu, Q.L., 2013. Pervaporation of water-ethanol and methanol-MTBE mixtures using poly(vinylalcohol)/cellulose acetate blended membranes. J. Membr. Sci. 448, 93–101.

Zielińska, K., Kujawski, W., Chostenko, A.G., 2011. Chitosan hydrogel membranes for pervaporative dehydration of alcohols. Sep. Purif. Technol. 83, 114–120.

CHAPTER 14

Direct Methanol Fuel Cell

Fereshteh Samimi, Mohammad R. Rahimpour
Shiraz University, Shiraz, Iran

Acronyms

ACC	anode current collector
ACL	anode catalyst layer
ADL	anode diffusion layer
AFC	alkaline fuel cell
CCC	cathode current collector
CCL	cathode catalyst layer
DLFC	direct liquid fuel cell
DMFC	direct methanol fuel cell
EOD	electro-osmotic drag
H_2-PEMFC	hydrogen-fueled PEMFC
MCFC	molten carbonate fuel cell
MCO	Methanol crossover
MEA	membrane electrode assembly
MOR	methanol oxidation reaction
ORR	oxygen reduction reaction
PAFC	phosphoric acid fuel cell
PEM	polymer electrolyte membrane
PEMFC	polymer electrolyte membrane fuel cell
SOFC	solid oxide fuel cell

1 Introduction to Fuel Cell

Global depletion of fossil fuel resources like petroleum, coal, and natural gas has driven researchers to seek sustainable energy and efficient energy conversion devices (Kamarudin et al., 2009; Radenahmad et al., 2016; Vasquez, 2007). The prospect of a fuel cell as an efficient energy device has attracted much attention recently. William Grove was the first one who discovered the basic principle of fuel cells in 1839. Fuel cells convert the chemical energy of a fuel directly into electrical energy through a catalytic reaction (Hoogers, 2002; Sharaf and

Methanol. https://doi.org/10.1016/B978-0-444-63903-5.00014-5

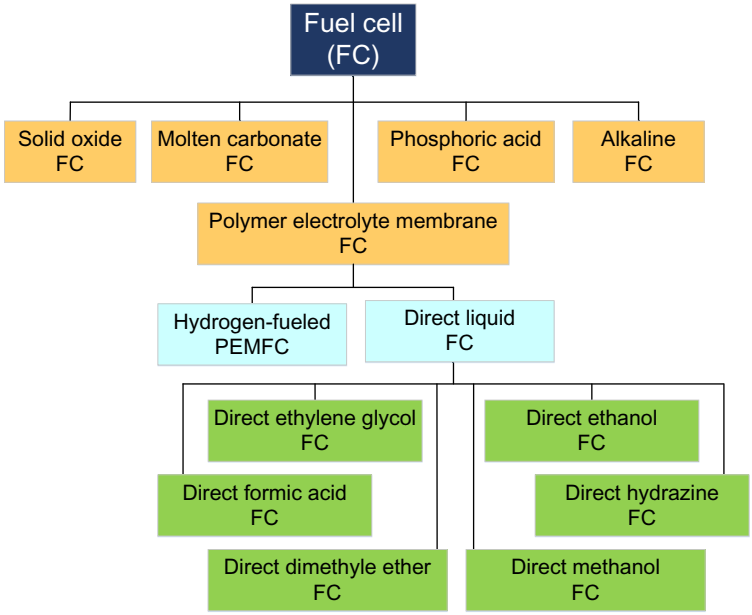

Fig. 14.1
Different types of fuel cells.

Orhan, 2014). A fuel cell is composed of an anode, a cathode, and an electrolyte between the anode and cathode side. As presented in Fig. 14.1, there are several fuel cell technologies, based on material used as the electrolyte: solid oxide fuel cell (SOFC), polymer electrolyte membrane fuel cell (PEMFC), phosphoric acid fuel cell (PAFC), molten carbonate fuel cell (MCFC), and alkaline fuel cell (AFC) (Acres, 2001; Kirubakaran et al., 2009; Lucia, 2014; Mekhilef et al., 2012; Sharaf and Orhan, 2014; Stambouli, 2011; Von Spakovsky and Olsommer, 2002). The selection of these fuel cells depends on their typical applications, power outputs, operating temperatures, costs, and efficiencies (McGrath et al., 2004; Shrivastava et al., 2016). Among them, PEMFCs have the highest power density and fastest start-stop capability (Giddey et al., 2005; Nachiappan et al., 2013; Padmavathi and Sangeetha, 2013). Based on the fuel applied, PEMFCs are classified as direct liquid fuel cell (DLFC) and hydrogen-fueled PEMFC (H_2-PEMFC) (Demirci, 2007; Jayakumar et al., 2015; Qian et al., 2006).

Liquid fuels (i.e., dimethyl ether, methanol, formic acid, etc.) are used in DLFC instead of gaseous hydrogen. High theoretical energy density, easy storage, transportation, and distribution of liquid fuel, and the elimination of fuel reformer and humidifiers are the superiorities of DLFC compared to H_2-PEMFC (Demirci, 2007; Lamy et al., 2002; Qian et al., 2006). Currently, solid oxide fuel cell (SOFC), direct methanol fuel cell (DMFC), and H_2-PEMFC are the most common fuel cell types. However, there are some differences among them, and the advantages and disadvantages of each type for portable power supply systems are summarized in Table 14.1 (Hsueh et al., 2012).

Table 14.1 Comparison of DMFC, H_2-PEMFC, and SOFC

	DMFC	H_2-PEMFC	SOFC
Operating temperature (°C)	<120	<120	800–1000
Type of electrolyte	Nafion membrane	Nafion membrane	Yttria stabilized zirconia (YSZ)
Charge carrier in the electrolyte	H^+	H^+	O^{2-}
Anode reaction	$CH_3OH + H_2O \rightarrow CO_2 + 6H^+ + 6e^+$	$H_2 \rightarrow 2H^+ + 2e^-$	$H^2 + O^{2-} \rightarrow H_2O + 2e^-$
Cathode reaction	$3/2O_2 + 6H^+ + 6e^+ \rightarrow 3H_2O$	$1/2O_2 + 2H^+ + 2e^- \rightarrow H_2O$	$1/2O_2 + 2e^- \rightarrow O^{2-}$
Cathode electrode	Pt	Pt	Lanthanumstrotium manganite (LSM)
Anode electrode	Pt. PtRu	Pt. PtRu	Ni-YSZ
Released power	<5 kW	5–250 kW	100–250 kW
Advantages	Easy fuel storage, simple structure without thermal management	High-power density	Diversified fuel, non-noble metal for catalyst
Disadvantages	Low-power density	Low energy density of storing hydrogen at high pressure or in metal hydride	Slow startup due to high operating temperature

Among the fuel cell family, DMFC is under rapid development. This is primarily because of its structural simplicity, low pollution, fast operation, and high energy density. In DMFC, CH_3OH as the anode fuel and O_2 as the cathode fuel are utilized to produce electricity without a reformer or humidifier (Lu et al., 2005; Wee, 2007). DMFC is a promising candidate to be used in portable electronic devices such as a laptop, mobile phone, digital camera, etc.
A replacement cartridge is used for fuel storage and the replenishment is performed either by replacing or refilling the cartridge within seconds (Hsueh et al., 2012; Lu et al., 2005). The theoretical energy density of DMFCs is 15 times more than a lithium (Li)-ion battery. Despite ethanol and other liquid fuels having the same energy density as methanol, they cannot be utilized due to their slow electrochemical oxidation reaction and extremely low power output (Hsueh et al., 2012). DMFC can be divided into active or passive based on the feed mode (Kamarudin et al., 2009; Li and Faghri, 2013; Mallick et al., 2015; Qian et al., 2006; Shrivastava et al., 2014; Shrivastava et al., 2013) and liquid feed or vapor feed based on the state of methanol input (Faghri et al., 2012; Li and Faghri, 2013; Scott et al., 1999; Yuan et al., 2014b).

2 Direct Methanol Fuel Cell (DMFC) Components

A schematic representing the principles of a DMFC is illustrated in Fig. 14.2. DMFC is mainly comprised of an anode current collector (ACC), membrane electrode assembly (MEA), and cathode current collector (CCC) (Kamarudin and Hashim, 2012). ACC and CCC are used to

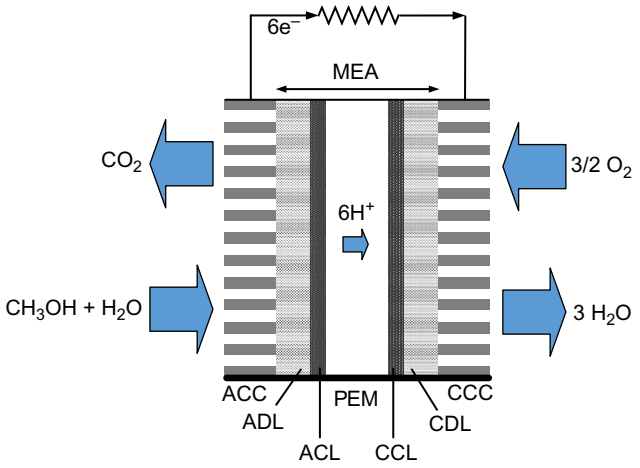

Fig. 14.2
A schematic of DMFC components (Shrivastava et al., 2016).

collect generated current in the MEA, to hold the MEA, and permit transmission of reactants and products. The current collector is generally a stainless steel perforated plate to provide carbon dioxide leaving and fuel injection. MEA consists of an anode diffusion layer (ADL), anode catalyst layer (ACL), polymer electrolyte membrane (PEM), cathode catalyst layer (CCL), and cathode diffusion layer (CDL). The roles of anode and cathode DL provide a porous surface for maintaining the catalyst layer, uniform distribution of the reactants, and electron conduction toward current collector (Shrivastava et al., 2016). The function of the anode and cathode CL is to establish a triple phase boundary between reactants, a proton conductor, and catalyst. Fig. 14.3 shows a complete classification of catalysts studied by the researchers. More information is available in the study of Munjewar et al. (2016). Typically, Pt-Ru and Pt catalysts are loaded at the anode and the cathode sides, respectively.

PEM, located between the anode and cathode compartment, provides the passage of proton and restricts electron transmission. Nafion perfluorosulfonic acid polymer is the most currently used membrane in DMFC because of its excellent thermal and chemical stability and high proton conductivity (Ahmad et al., 2010; Yuan et al., 2014b). However, Nafion membranes suffer from transmission of methanol through the membrane; a phenomenon called "methanol crossover," which significantly reduces the performance of DMFC. Nafion membranes are classified into Nafion 117, Nafion 115, and Nafion 112 based on their thickness; the thickest membrane is Nafion 117 (Heinzel and Barragan, 1999). The following specifications of DMFC membranes are required for their commercialization: low methanol crossover (Azad et al., 2015; Cowan et al., 2008; Kannan et al., 2013; Stambouli and Traversa, 2002), low cost (Jamsak et al., 2007; Jung et al., 1998; Souza and Muccillo, 2010), high chemical and thermal stability, excellent mechanical strength (Azad et al., 2014; Jung et al., 1998; Yamasaki et al., 2014), and high ionic conductivity (Cowan et al., 2008; Fergus et al., 2016; Kamaruddin et al., 2013).

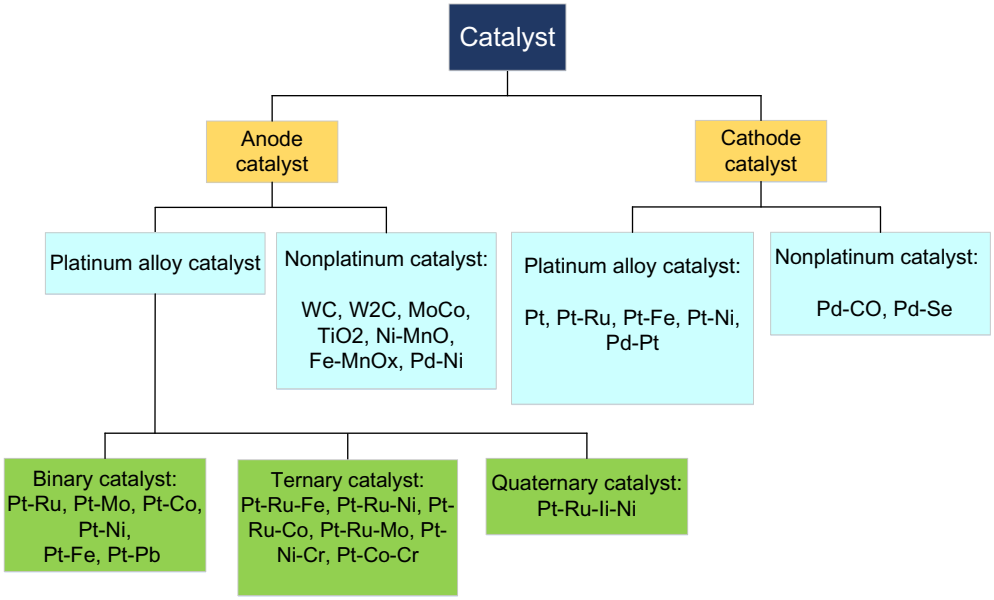

Fig. 14.3
Classification of catalyst (Munjewar et al., 2016).

3 Configuration and Basic Principles of DMFC

A mixture of methanol and water should be provided in the fuel cell system as shown in Fig. 14.4. The original fuel in form of pure methanol must be supplied to gain a high energy density and then the methanol can be added to the water. The mixture of methanol and water is transported through the anode CC, mostly due to diffusion and arrives at the anode CL. Some part of methanol is oxidized to CO_2 at the anode CL and releases electrons, protons, and heat during the reaction. This is called methanol oxidation reaction (MOR) and is given by Eq. (14.1). The produced carbon dioxide travels in the direction of the fuel reservoir and then leaves the cell. The electrons move via an external circuit to the cathode to generate electricity and the protons migrate through the PEM to the cathode (Kamarudin and Hashim, 2012; Yuan et al., 2014b).

On the other hand, oxygen from the atmospheric air is reduced at the cathode. Water and heat are produced through the reaction of oxygen with protons and electrons. This is called oxygen reduction reaction (ORR), as described in Eq. (14.2). Water vapor at the cathode leaves the cell mainly by diffusion and natural convection. The released heat is dissipated to the methanol solution on the anode side and to the ambient air on the cathode side. The net reaction is equivalent to methanol combustion, as seen in Eq. (14.3) (Hsueh et al., 2012; Kamarudin and Hashim, 2012).

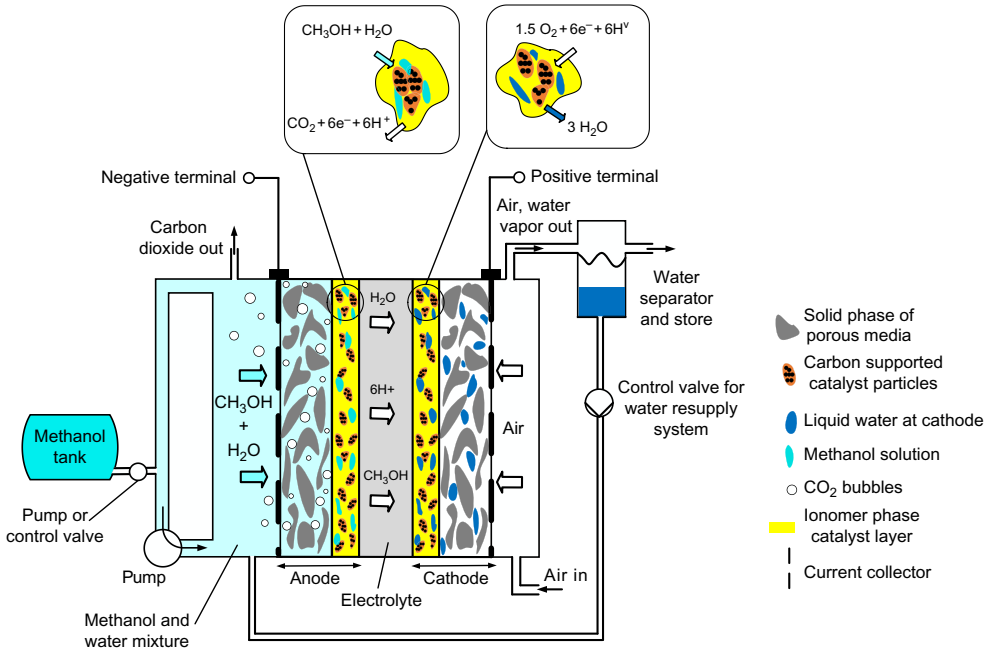

Fig. 14.4
A schematic of DMFC system (Bahrami and Faghri, 2013; Larminie et al., 2003).

At the anode:

$$CH_3OH + H_2O \rightarrow CO_2 + 6H^+ + 6e^- + \text{heat} \tag{14.1}$$

At the cathode:

$$3/2O_2 + 6H^+ + 6e^- \rightarrow 3H_2O + \text{heat} \tag{14.2}$$

The overall reaction:

$$3/2O_2 + CH_3OH \rightarrow CO_2 + 2H_2O + \text{heat} \tag{14.3}$$

4 Electrochemical Processes in DMFC

Methanol oxidation at the anode side generates carbon dioxide and produces six protons and six electrons (Carrette et al., 2001; Hamnett, 1997). The MOR given by Eq. (14.1), demonstrates an overall reaction scheme, not a detailed mechanism. Bagotzky et al. (1977) have presented the stages and different possibilities of methanol oxidation, as given in Fig. 14.5. Methanol as the fuel is at the top, and carbon dioxide as the product is at the bottom. Although methanol can reach the carbon dioxide by all the routes, the most preferred route is the one contains the stable compounds, formaldehyde (CH_2O) and formic acid (HCOOH). Notice from

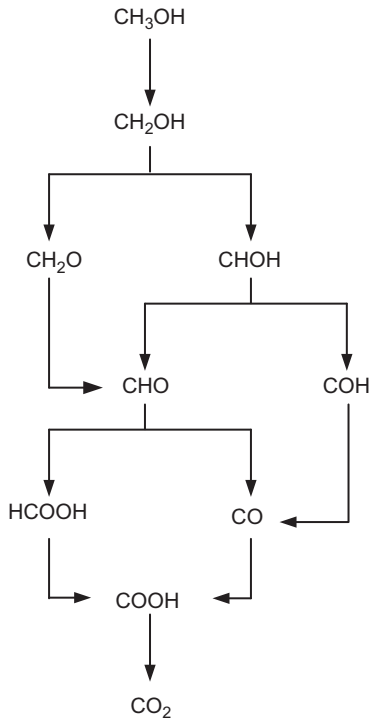

Fig. 14.5
Different pathways of methanol oxidation at the anode side of DMFC (Carrette et al., 2001; Hamnett, 1997).

the figure that methanol oxidation reaction may generate carbon monoxide (CO) as an intermediate product. CO acts as a poison for the platinum (Pt) catalyst. The reaction sites are occupied by the adsorbed CO and thus the methanol oxidation rate is reduced. This reveals the importance of choosing a catalyst. To get rid of catalyst-poisoning, a more active alloy catalyst, Pt-Ru (with atomic ratio of 1:1), is currently used in the anode compartment of DMFC. The oxygen-containing molecules absorb the Ru atoms and facilitate CO oxidation reaction into CO_2 (Liu et al., 2006a; Ochal et al., 2011; Watanabe and Motoo, 1975).

5 State of Fuel Input

DMFCs typically operate between 40 and 80°C, and methanol can be provided in either a liquid or a vapor form (Ren et al., 2000; Thomas et al., 2002). However, there are several differences in the nature of liquid and vapor feed DMFCs. In a liquid feed DMFC, diluted methanol solution is directly used in the fuel cell, whereas in a vapor feed DMFC, the concentrated methanol solution transfers from the fuel reservoir to the vaporizer and then the methanol vapor is fed to the anode (Mallick et al., 2016). In vapor feed DMFC, a mixture of methanol and water

vapor can be fed directly to the fuel cell, or the liquid methanol solution is first vaporized and is then fed to the fuel cell (Li and Faghri, 2013). In the vapor feed DMFC, the methanol vapor may condense into diluted methanol solution in the anode DL and anode CL, while in the liquid feed DMFC, the liquid methanol may vaporize into the gaseous phase containing CO_2 molecules (Mallick et al., 2016).

There are some advantages of vapor feed DMFC over liquid feed DMFC (Fukunaga et al., 2004; Lobato Bajo et al., 2008; Rice and Faghri, 2008). Higher reaction rates are attained at higher temperatures when applying vapor feed methanol (Lobato Bajo et al., 2008; Scott et al., 1999). Compared to the liquid phase, vapor feed has a lower start-up time due to considerably higher mass transfer (Rice and Faghri, 2008). The higher mass diffusivity of methanol, the superior gas release at the catalyst surface, and the less localized cooling of the anode catalyst in vapor feed leads to significantly higher power density than in liquid feed (Fukunaga et al., 2004; Scott et al., 1999). The vapor phase has a higher activity than liquid phase because of the higher methanol feed concentration. Also lower methanol crossover occurs in vapor feed compared to liquid feed (Arico et al., 1996; Hogarth et al., 1997; Shukla et al., 1995).

However, methanol supplied in the vapor form consumes energy and makes the system more complex. On the other hand, the typical operating range of liquid feed DMFC is close to room temperature and there are several different benefits associated with utilizing liquid feed such as a more compact and simple structure, better thermal management, and lower parasitic power losses. Generally, liquid phase fuels are more desirable in portable power supply systems because of their transportability and higher energy density than gas fuels (Li and Faghri, 2013; Shrivastava et al., 2016).

6 Feed Mode

DMFC is classified based on methanol and oxygen supply modes as passive, semi-passive, and active. In active DMFC, assistant devices such as a fuel cell stack, fuel pump, sensors, CO_2 separator, electronic controls, air blower, heaters, and humidity components and circulation apparatus are required (Guo and Faghri, 2006; Shrivastava et al., 2016). The purpose of an active system is quantitative monitoring of temperature, flow rate, concentration, etc. to provide the highest performance (Arico et al., 2001; Mekhilef et al., 2012). However, such equipment not only makes the system more complicated and increases the construction cost but also increases the parasitic energy consumption, which obviously reduces the total system efficiency. Therefore, in view of real application, an active DMFC is more preferred for the bulky high-power system in vehicular and stationary power plants (Arico et al., 2001).

Hence, for the development of portable electrical devices, researchers are more interested in passive DMFCs because of their autonomy feature. Passive DMFCs work without the help of auxiliary equipment for the supply of fuel and oxidant. It uses the natural mechanisms

such as capillary forces, gravity, concentration, or osmosis to deliver methanol, water, and oxygen. Ambient air diffuses into the cathode through a kind of air-breathing mechanism, and methanol transports to the anode from the reservoir via concentration gradient (Mekhilef et al., 2012; Zhong et al., 2008). Passive modes are more simple and reliable with a compact structure (Li and Faghri, 2013). In 2009, Toshiba demonstrated the feasibility in using DMFC as the power source of a mobile fuel cell. A methanol solution was supplied by filling a cartridge and oxygen was provided from the ambient air (Radenahmad et al., 2016). Semi-passive DMFCs have an active anode and a passive cathode or vice versa; the anode or the cathode side can only be controlled (Kannan et al., 2013).

7 Challenges and Barrier Issues of DMFC

7.1 Methanol Cross Over

Methanol crossover (MCO) is defined as methanol transport through the membrane from anode to the cathode side. It has been acknowledged as the most notable technical barrier causing major performance losses of DMFC. In fact, the inherent water diffusion feature of the Nafion membrane and methanol solubility in water causes MCO. Consequently, only some parts of the methanol oxidizes at the anode CL and the rest diffuses through the membrane (Jewett et al., 2007; Jung et al., 1998; Springer et al., 1993). This transport process is mainly carried out by diffusion and electro-osmotic drag (EOD) mechanism. The diffusive mass transport is the prevailing mechanism in the MCO issue, which is proportional to methanol feed concentration (Basri et al., 2009; Gholami et al., 2015; Kho et al., 2005). EOD is created when protons are transferred from anode to cathode and drag a number of methanol molecules. The EOD contribution in MCO increases while increasing the amount of methanol fraction at the anode CL-PEM interface and the current created by the cell.

When the methanol arrives at the cathode, it reacts with oxygen via combustion reaction, resulting in a lower cathode potential, and thus lower fuel cell performance since it does not generate electricity (Hikita et al., 2001; Liu et al., 2006b). There are several requirements for the reduction of MCO. Diluted methanol solution should be supplied in a DMFC, which is operated at high current density (Chen et al., 2006). Lower MCO is caused by using a thicker membrane (Nafion 117), because of a lower methanol concentration gradient across the membrane (Liu et al., 2006b; Yuan et al., 2012). Also by applying an extremely active anode catalyst, methanol oxidation rate at the anode side increases and, therefore, methanol concentration at the anode CL can be retained at a lower amount for MCO reduction (Li and Faghri, 2013). In order to reduce MCO and to design a perfect DMFC, mass management also seems to be a critical issue. However, the interactions between the species (CH_3OH, H_2O, CO_2 and O_2) as well as the phase change phenomena make the mass management and fuel cell design more complex.

7.2 Methanol Management

Uniform distribution of methanol at the anode CL is necessary for a desired performance of DMFC. If methanol distributes non-uniformly, several fuel starving locations may be created at the anode CL, and as a result there are many unused catalyst particles; therefore, the cell performance is reduced. The uniform distribution of methanol at the anode CL depends primarily on the anode CC structure. An anode CC with a higher open ratio offers a more uniform methanol distribution (Achmad et al., 2011).

As mentioned before, methanol crossover depends on methanol feed concentration and it is reduced in low methanol concentration ($\leq$4 M). On the other hand, high methanol concentration reduces the mass transport loss, which improves the cell performance and increases the operation time. Also, concentrated methanol feed increases the cell temperature which enhances the electrochemical activity and the cell performance. Hence, obtaining an optimum methanol concentration in the reservoir and at the anode side is an important issue for effective cell performance. This optimum concentration relies on the resistance of methanol from the fuel reservoir to the anode CL (Chen et al., 2006; Gholami et al., 2013; Li et al., 2010). An external methanol transport barrier can be utilized between the fuel reservoir and anode CC to allow operating at a high methanol feed concentration (Munjewar et al., 2017).

Total methanol consumption in DMFC consists of three parts: methanol used for generating the cell current, methanol diffused through PEM (MCO), and methanol vapor left in the cell with carbon dioxide at the anode side. To reduce methanol wastage, researchers are using the term "fuel efficiency" in their studies, which means "the ratio of part of methanol converted into useful electricity to the total amount of methanol used." High fuel efficiency is desirable for effective operation (Shrivastava et al., 2016).

7.3 Carbon Dioxide Management

According to the reaction in Eq. (14.1), carbon dioxide is generated during an anode electrochemical reaction. Because of buoyancy force, it transports counter-currently towards the fuel reservoir and leaves the cell from the vent provided in the fuel tank. Inefficient removal of CO_2 yields to its accumulation at the anode CL and reduces the active sites of catalyst for anode oxidation reaction. Moreover, CO_2 may block the pores of anode DL and covers the openings of anode CC, which increases the mass transport resistance and reduces the cell performance (Chetty et al., 2010). Consequently, continuous and complete removal of carbon dioxide prevents the blocking of the reaction area and helps to improve the performance of DMFC.

Carbon dioxide removal is a function of operating conditions, anode CC structure, and anode DL. The rate of CO_2 generation is proportional to current generation; which means CO_2 production increases at higher current density. The researchers indicated that CO_2 removal is more complicated at high current density (Chen et al., 2008). Several researchers studied the orientation of the passive DMFCs for effective removal of carbon dioxide (Lai et al., 2008;

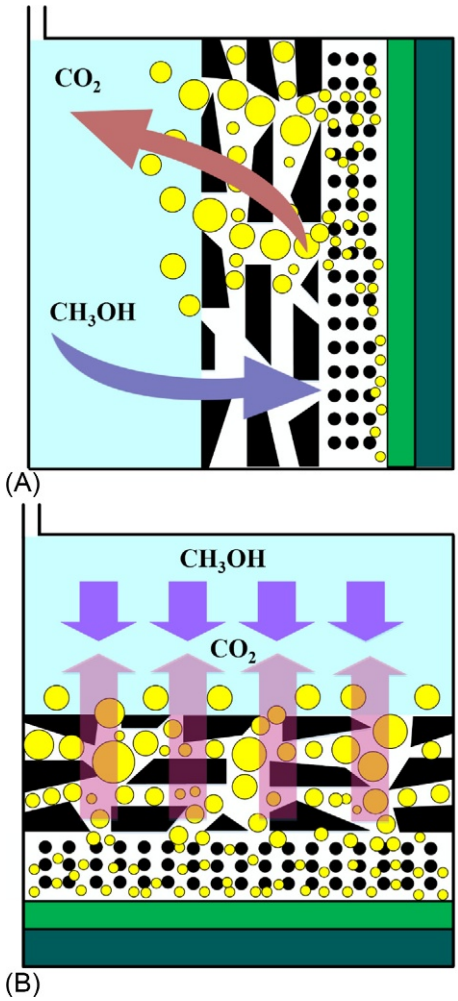

Fig. 14.6
Effect of DMFC different orientations on the anodic mass transfer process. (A) Vertical and (B) horizontal (Yuan et al., 2012).

Yuan et al., 2012). Yuan et al. (2012) found that passive DMFC with the vertical orientation exhibits a better performance at the lower methanol concentration by increasing methanol transferring. Nevertheless, the horizontal orientation is suggested for higher methanol concentration which improves the performance of fuel cell by reducing MCO with CO_2 gas blockage as illustrated in Fig. 14.6.

7.4 Water Management

One molecule of water at the anode side is needed for oxidation of one molecule of methanol. However, water to methanol molar ratio in the passive DMFC considerably exceeds 1:1 for a complete methanol oxidation reaction which generates 6e. Insufficient water results in

incomplete methanol oxidation, formation of intermediate compounds such as formic acid, formaldehyde, and methylformate while releasing a lower number of electrons (4e). These intermediate species lead to catalyst poisoning and deterioration of the cell performance. Hence, sufficiently diluted methanol is crucial (Nakagawa et al., 2009; Sanicharane et al., 2002).

Uniform distribution of water should be provided over anode CL. A non-uniform water distribution may cause several unused locations in the anode CL and thus, reduce the cell performance (Shrivastava et al., 2016). Sufficient water is required in the membrane for proton conductance. This is due to reducing Nafion membrane resistance for proton conduction by increasing its water content (Sone et al., 1996).

Water generated at the cathode side escapes out of the cell through the natural convection. If water is not efficiently removed, it may accumulate on the cathode side, causing a serious water flooding problem. The liquid water occupies the pores of cathode DL and prevents the oxygen flow, which reduces the cell performance. Moreover, water crossover through the membrane and oxidation of MCO contribute to water flooding at cathode CL. This problem is more serious in a diluted methanol solution compared to a concentrated methanol solution (Munjewar et al., 2017). Effective water management is crucial in order to supply water at the anode, to remove produced water at the cathode, and to maintain enough water in the membrane (Yuan et al., 2014a).

7.5 Oxygen Management

Oxygen from the ambient air transfers through the cathode DL and cathode CC by diffusion and natural convection. A sufficient quantity of oxygen should be available for the reduction reaction at the cathode side. An inadequate amount of oxygen may cause an increase of concentration polarization, which leads to poor cell performance. An adequate amount of oxygen can be provided by the reduction of the oxygen mass transport resistance between the cathode CL and cathode CC. This resistance depends on water flooding and the structure of the cathode side. Water accumulated at the cathode CL may occupy the penetration holes and causes a non-uniform distribution of oxygen which leads to several oxygen starving locations, resulting in inferior cell performance (Munjewar et al., 2017).

The open cathode in passive DMFC is exposed to the surrounding atmosphere and therefore may be damaged by dust and chemical particles in the air. Consequently, the cathode pores may be blocked and the oxygen transport inhibited. To solve this problem, using air filters at the cathode side for the enhancement of overall cell performance is offered (Jewett et al., 2007; Xu and Faghri, 2010).

8 Durability and Stability

One of the main concerns associated with commercial development of DMFCs is long-term stability of a cell. The desired life-time is near 5000 operating hours for portable applications (Wee, 2007). Passive DMFC is now far away from this requirement, because of the severe

performance decay during operation. Therefore, durability and stability play a significant role in the commercialization of DMFC (Guo and Faghri, 2008).

There are two classifications of performance degradation: permanent degradation (irrecoverable) and temporary degradation (recoverable). Catalyst degradation, CL and DL degradation, PEM degradation, and current collector degradation result in permanent degradation. The temporary degradation which is recovered after operation interruption includes CO_2 accumulation at anode, cathode water flooding, etc. (Bresciani et al., 2014; Feng et al., 2012; Zainoodin et al., 2014).

9 Cost and Commercialization

To make DMFC commercially feasible, manufacturing and energy consumption costs are the two major obstacles for any manufacturer (Kamarudin et al., 2009). A passive DMFC system has a higher cost compared to its competitor, like the Li-ion battery, because of the following main reasons: use of precious platinum catalysts at both electrodes to reach a high power density, use of costly Nafion membrane, and current collector coating with highly valuable metals (such as platinum, gold, etc.) (Shrivastava et al., 2016). The coating on current collectors with highly expensive metals such as Pt and Au is performed to enhance its corrosion resistance and to reduce the contact resistance between MEA and current collector. The cost related to the Pt catalyst can be decreased either by reducing the Pt loading of the catalyst or by applying a non-Pt catalyst. Although non-noble catalysts have been suggested for DMFCs, they cannot compete with platinum catalysts because of their significantly lower activities (Kamarudin et al., 2009).

Numerous studies have been done over the years for the barrier issues and many alternative solutions have been proposed, but still the cost is a major hurdle for DMFC commercialization and hence more extensive research is expected in this direction (Shrivastava et al., 2016). Although DMFCs have superiorities to rechargeable batteries, powering portable electronic devices are still governed by a rechargeable Li-ion battery.

10 Conclusion and Future Trends

Among the fuel cell types, direct methanol fuel cell (DMFC) is the most feasible candidate to Li-ion batteries as the power source for portable applications in the future, and is now under rapid development. This is mainly because of its high energy density, simple structure, and rapid operation. However, there are several major obstacles for the widespread applications of DMFC that need to be addressed. Methanol crossover (MCO) through the membrane is one of the most remarkable technical hurdles resulting in major losses in the cell performance. MCO is a function of membrane structure and thickness, methanol feed concentration, and the cell operating conditions. Diluted methanol solution and high current density can effectively reduce MCO. Durability, stability, and cost are also the main factors affecting the commercialization

of DMFC. The use of a considerable amount of platinum catalysts at both electrodes for more favorable electrochemical activities makes commercialization of DMFC much further away. More research should be conducted on these major concerns to result in a reliable DMFC technology for a broad range of applications.

References

Achmad, F., Kamarudin, S.K., Daud, W.R.W., Majlan, E., 2011. Passive direct methanol fuel cells for portable electronic devices. Appl. Energy 88, 1681–1689.

Acres, G.J., 2001. Recent advances in fuel cell technology and its applications. J. Power Sources 100, 60–66.

Ahmad, H., Kamarudin, S.K., Hasran, U.A., Daud, W.R.W., 2010. Overview of hybrid membranes for direct-methanol fuel-cell applications. Int. J. Hydrog. Energy 35, 2160–2175.

Arico, A., Creti, P., Kim, H., Mantegna, R., Giordano, N., Antonucci, V., 1996. Analysis of the electrochemical characteristics of a direct methanol fuel cell based on a Pt-Ru/C anode catalyst. J. Electrochem. Soc. 143, 3950–3959.

Arico, A., Srinivasan, S., Antonucci, V., 2001. DMFCs: from fundamental aspects to technology development. Fuel Cells 1, 133–161.

Azad, A.K., Kruth, A., Irvine, J.T., 2014. Influence of atmosphere on redox structure of BaCe0.9Y0.1O2.95—insight from neutron diffraction study. Int. J. Hydrog. Energy 39, 12804–12811.

Azad, A.K., Setsoafia, D., Ming, L., Petra, I., 2015. Synthesis and characterization of high density and low temperature sintered proton conductor $BaCe_{0.5}Zr_{0.3}5In_{0.1}Zn_{0.05}O_{3-\delta}$. Adv. Mater. Res. 1098, 104–109.

Bagotzky, V., Vassiliev, Y.B., Khazova, O., 1977. Generalized scheme of chemisorption, electrooxidation and electroreduction of simple organic compounds on platinum group metals. J. Electroanal. Chem. Interfacial Electrochem. 81, 229–238.

Bahrami, H., Faghri, A., 2013. Review and advances of direct methanol fuel cells. Part II: Modeling and numerical simulation. J. Power Sources 230, 303–320.

Basri, S., Kamarudin, S.K., Daud, W.R.W., Yaakub, Z., Ahmad, M., Hashim, N., Hasran, U.A., 2009. Unsteady-state modelling for a passive liquid-feed DMFC. Int. J. Hydrog. Energy 34, 5759–5769.

Bresciani, F., Rabissi, C., Casalegno, A., Zago, M., Marchesi, R., 2014. Experimental investigation on DMFC temporary degradation. Int. J. Hydrog. Energy 39, 21647–21656.

Carrette, L., Friedrich, K., Stimming, U., 2001. Fuel cells—fundamentals and applications. Fuel Cells 1, 5–39.

Chen, R., Zhao, T., Liu, J., 2006. Effect of cell orientation on the performance of passive direct methanol fuel cells. J. Power Sources 157, 351–357.

Chen, R., Zhao, T., Yang, W., Xu, C., 2008. Two-dimensional two-phase thermal model for passive direct methanol fuel cells. J. Power Sources 175, 276–287.

Chetty, R., Scott, K., Kundu, S., Muhler, M., 2010. Optimization of mesh-based anodes for direct methanol fuel cells. J. Fuel Cell Sci. Technol. 7031011.

Cowan, L.A., Morcos, R.M., Hatada, N., Navrotsky, A., Haile, S.M., 2008. High temperature properties of $Rb_3H(SO_4)_2$ at ambient pressure: absence of a polymorphic, superprotonic transition. Solid State Ionics 179, 305–313.

Demirci, U.B., 2007. Direct liquid-feed fuel cells: thermodynamic and environmental concerns. J. Power Sources 169, 239–246.

Faghri, A., Li, X., Bahrami, H., 2012. Recent advances in passive and semi-passive direct methanol fuel cells. Int. J. Therm. Sci. 62, 12–18.

Feng, L., Cai, W., Li, C., Zhang, J., Liu, C., Xing, W., 2012. Fabrication and performance evaluation for a novel small planar passive direct methanol fuel cell stack. Fuel 94, 401–408.

Fergus, J., Hui, R., Li, X., Wilkinson, D.P., Zhang, J., 2016. Solid Oxide Fuel Cells: Materials Properties and Performance. CRC Press, Boca Raton, FL.

Fukunaga, H., Ishida, T., Teranishi, N., Arai, C., Yamada, K., 2004. Impedance of vapor feed direct methanol fuel cells—polarization dependence of elementary processes at the anode. Electrochim. Acta 49, 2123–2129.
Gholami, O., Imen, S.J., Shakeri, M., 2013. Effect of non-uniform parallel channel on performance of passive direct methanol fuel cell. Int. J. Hydrog. Energy 38, 3395–3400.
Gholami, O., Imen, S.J., Shakeri, M., 2015. Effect of anode and cathode flow field geometry on passive direct methanol fuel cell performance. Electrochim. Acta 158, 410–417.
Giddey, S., Ciacchi, F., Badwal, S., 2005. Fuel quality and operational issues for polymer electrolyte membrane (PEM) fuel cells. Ionics 11, 1–10.
Guo, Z., Faghri, A., 2006. Miniature DMFCs with passive thermal-fluids management system. J. Power Sources 160, 1142–1155.
Guo, Z., Faghri, A., 2008. Development of a 1 W passive DMFC. Int. Commun. Heat Mass Transfer 35, 225–239.
Hamnett, A., 1997. Mechanism and electrocatalysis in the direct methanol fuel cell. Catal. Today 38, 445–457.
Heinzel, A., Barragan, V., 1999. A review of the state-of-the-art of the methanol crossover in direct methanol fuel cells. J. Power Sources 84, 70–74.
Hikita, S., Yamane, K., Nakajima, Y., 2001. Measurement of methanol crossover in direct methanol fuel cell. JSAE Rev. 22, 151–156.
Hogarth, M., Christensen, P., Hamnett, A., Shukla, A., 1997. The design and construction of high-performance direct methanol fuel cells. 2. Vapour-feed systems. J. Power Sources 69, 125–136.
Hoogers, G., 2002. Fuel Cell Technology Handbook. CRC Press, Boca Raton, FL.
Hsueh, K.L., Tsai, L.D., Lai, C.C., Peng, Y.M., 2012. Direct methanol fuel cells. Electrochem. Technol. Energy Storage Convers. 1&2, 701–727.
Jamsak, W., Assabumrungrat, S., Douglas, P., Laosiripojana, N., Suwanwarangkul, R., Charojrochkul, S., Croiset, E., 2007. Performance of ethanol-fuelled solid oxide fuel cells: proton and oxygen ion conductors. Chem. Eng. J. 133, 187–194.
Jayakumar, A., Sethu, S.P., Ramos, M., Robertson, J., Al-Jumaily, A., 2015. A technical review on gas diffusion, mechanism and medium of PEM fuel cell. Ionics 21, 1–18.
Jewett, G., Guo, Z., Faghri, A., 2007. Water and air management systems for a passive direct methanol fuel cell. J. Power Sources 168, 434–446.
Jung, D.H., Lee, C.H., Kim, C.S., Shin, D.R., 1998. Performance of a direct methanol polymer electrolyte fuel cell. J. Power Sources 71, 169–173.
Kamaruddin, M., Kamarudin, S.K., Daud, W.R.W., Masdar, M., 2013. An overview of fuel management in direct methanol fuel cells. Renew. Sust. Energ. Rev. 24, 557–565.
Kamarudin, S.K., Hashim, N., 2012. Materials, morphologies and structures of MEAs in DMFCs. Renew. Sust. Energ. Rev. 16, 2494–2515.
Kamarudin, S.K., Achmad, F., Daud, W.R.W., 2009. Overview on the application of direct methanol fuel cell (DMFC) for portable electronic devices. Int. J. Hydrog. Energy 34, 6902–6916.
Kannan, R., Singh, K., Gill, S., Fürstenhaupt, T., Thangadurai, V., 2013. Chemically stable proton conducting doped $BaCeO_3$—no more fear to SOFC wastes. Sci. Rep. 3, 2138.
Kho, B.K., Bae, B., Scibioh, M.A., Lee, J., Ha, H.Y., 2005. On the consequences of methanol crossover in passive air-breathing direct methanol fuel cells. J. Power Sources 142, 50–55.
Kirubakaran, A., Jain, S., Nema, R., 2009. A review on fuel cell technologies and power electronic interface. Renew. Sust. Energ. Rev. 13, 2430–2440.
Lai, Q.-Z., Yin, G.-P., Zhang, J., Wang, Z.-B., Cai, K.-D., Liu, P., 2008. Influence of cathode oxygen transport on the discharging time of passive DMFC. J. Power Sources 175, 458–463.
Lamy, C., Lima, A., LeRhun, V., Delime, F., Coutanceau, C., Léger, J.-M., 2002. Recent advances in the development of direct alcohol fuel cells (DAFC). J. Power Sources 105, 283–296.
Larminie, J., Dicks, A., McDonald, M.S., 2003. Fuel Cell Systems Explained. J. Wiley, Chichester.
Li, X., Faghri, A., 2013. Review and advances of direct methanol fuel cells (DMFCs). Part I: Design, fabrication, and testing with high concentration methanol solutions. J. Power Sources 226, 223–240.
Li, X., Faghri, A., Xu, C., 2010. Water management of the DMFC passively fed with a high-concentration methanol solution. Int. J. Hydrog. Energy 35, 8690–8698.

Liu, H., Song, C., Zhang, L., Zhang, J., Wang, H., Wilkinson, D.P., 2006a. A review of anode catalysis in the direct methanol fuel cell. J. Power Sources 155, 95–110.
Liu, J., Zhao, T., Liang, Z., Chen, R., 2006b. Effect of membrane thickness on the performance and efficiency of passive direct methanol fuel cells. J. Power Sources 153, 61–67.
Lobato Bajo, J., Linares León, J.J., Cañizares Cañizares, P., Rodrigo, R., Andrés, M., López-Vizcaíno López, R., 2008. Performance of a vapor-fed polybenzimidazole (PBI)-based direct methanol fuel cell. Energy Fuels 22 (5), 3335–3345.
Lu, G., Liu, F., Wang, C.-Y., 2005. Water transport through Nafion 112 membrane in DMFCs. Electrochem. Solid-State Lett. 8, A1–A4.
Lucia, U., 2014. Overview on fuel cells. Renew. Sust. Energ. Rev. 30, 164–169.
Mallick, R.K., Thombre, S.B., Shrivastava, N.K., 2015. A critical review of the current collector for passive direct methanol fuel cells. J. Power Sources 285, 510–529.
Mallick, R.K., Thombre, S.B., Shrivastava, N.K., 2016. Vapor feed direct methanol fuel cells (DMFCs): a review. Renew. Sust. Energ. Rev. 56, 51–74.
McGrath, K.M., Prakash, G.S., Olah, G.A., 2004. Direct methanol fuel cells. J. Ind. Eng. Chem. 10, 1063–1080.
Mekhilef, S., Saidur, R., Safari, A., 2012. Comparative study of different fuel cell technologies. Renew. Sust. Energ. Rev. 16, 981–989.
Munjewar, S.S., Thombre, S.B., Mallick, R.K., 2016. A comprehensive review on recent material development of passive direct methanol fuel cell. Ionics, 1–18.
Munjewar, S.S., Thombre, S.B., Mallick, R.K., 2017. Approaches to overcome the barrier issues of passive direct methanol fuel cell—review. Renew. Sust. Energ. Rev. 67, 1087–1104.
Nachiappan, N., Kalaignan, G.P., Sasikumar, G., 2013. Effect of nitrogen and carbon dioxide as fuel impurities on PEM fuel cell performances. Ionics 19, 351–354.
Nakagawa, N., Sekimoto, K., Masdar, M.S., Noda, R., 2009. Reaction analysis of a direct methanol fuel cell employing a porous carbon plate operated at high methanol concentrations. J. Power Sources 186, 45–51.
Ochal, P., de la Fuente, J.L.G., Tsypkin, M., Seland, F., Sunde, S., Muthuswamy, N., Rønning, M., Chen, D., Garcia, S., Alayoglu, S., 2011. CO stripping as an electrochemical tool for characterization of Ru@ Pt core-shell catalysts. J. Electroanal. Chem. 655, 140–146.
Padmavathi, R., Sangeetha, D., 2013. Design of novel SPEEK-based proton exchange membranes by self-assembly method for fuel cells. Ionics 19, 1423–1436.
Qian, W., Wilkinson, D.P., Shen, J., Wang, H., Zhang, J., 2006. Architecture for portable direct liquid fuel cells. J. Power Sources 154, 202–213.
Radenahmad, N., Afif, A., Petra, P.I., Rahman, S.M., Eriksson, S.-G., Azad, A.K., 2016. Proton-conducting electrolytes for direct methanol and direct urea fuel cells—a state-of-the-art review. Renew. Sust. Energ. Rev. 57, 1347–1358.
Ren, X., Zelenay, P., Thomas, S., Davey, J., Gottesfeld, S., 2000. Recent advances in direct methanol fuel cells at Los Alamos National Laboratory. J. Power Sources 86, 111–116.
Rice, J., Faghri, A., 2008. Analysis of a passive vapor feed direct methanol fuel cell. Int. J. Heat Mass Transf. 51, 948–959.
Sanicharane, S., Bo, A., Sompalli, B., Gurau, B., Smotkin, E., 2002. In situ 50 C FTIR spectroscopy of Pt and PtRu direct methanol fuel cell membrane electrode assembly anodes. J. Electrochem. Soc. 149, A554–A557.
Scott, K., Taama, W., Argyropoulos, P., 1999. Engineering aspects of the direct methanol fuel cell system. J. Power Sources 79, 43–59.
Sharaf, O.Z., Orhan, M.F., 2014. An overview of fuel cell technology: fundamentals and applications. Renew. Sust. Energ. Rev. 32, 810–853.
Shrivastava, N.K., Thombre, S.B., Wasewar, K.L., 2013. Nonisothermal mathematical model for performance evaluation of passive direct methanol fuel cells. J. Energy Eng. 139, 266–274.
Shrivastava, N.K., Thombre, S.B., Mallick, R.K., 2014. Effect of diffusion layer compression on passive DMFC performance. Electrochim. Acta 149, 167–175.

Shrivastava, N.K., Thombre, S.B., Chadge, R.B., 2016. Liquid feed passive direct methanol fuel cell: challenges and recent advances. Ionics 22, 1–23.
Shukla, A., Christensen, P., Hamnett, A., Hogarth, M., 1995. A vapour-feed direct-methanol fuel cell with proton-exchange membrane electrolyte. J. Power Sources 55, 87–91.
Sone, Y., Ekdunge, P., Simonsson, D., 1996. Proton conductivity of Nafion 117 as measured by a four-electrode AC impedance method. J. Electrochem. Soc. 143, 1254–1259.
Souza, E.C.C.d, Muccillo, R., 2010. Properties and applications of perovskite proton conductors. Mater. Res. 13, 385–394.
Springer, T.E., Wilson, M.S., Gottesfeld, S., 1993. Modeling and experimental diagnostics in polymer electrolyte fuel cells. J. Electrochem. Soc. 140, 3513–3526.
Stambouli, A.B., 2011. Fuel cells: the expectations for an environmental-friendly and sustainable source of energy. Renew. Sust. Energ. Rev. 15, 4507–4520.
Stambouli, A.B., Traversa, E., 2002. Solid oxide fuel cells (SOFCs): a review of an environmentally clean and efficient source of energy. Renew. Sust. Energ. Rev. 6, 433–455.
Thomas, S.C., Ren, X., Gottesfeld, S., Zelenay, P., 2002. Direct methanol fuel cells: progress in cell performance and cathode research. Electrochim. Acta 47, 3741–3748.
Vasquez, L., 2007. Fuel Cell Research Trends. Nova Publishers, New York.
Von Spakovsky, M., Olsommer, B., 2002. Fuel cell systems and system modeling and analysis perspectives for fuel cell development. Energy Convers. Manag. 43, 1249–1257.
Watanabe, M.a., Motoo, S., 1975. Electrocatalysis by ad-atoms: Part II. Enhancement of the oxidation of methanol on platinum by ruthenium ad-atoms. J. Electroanal. Chem. Interfacial Electrochem. 60, 267–273.
Wee, J.-H., 2007. A feasibility study on direct methanol fuel cells for laptop computers based on a cost comparison with lithium-ion batteries. J. Power Sources 173, 424–436.
Xu, C., Faghri, A., 2010. Water transport characteristics in a passive liquid-feed DMFC. Int. J. Heat Mass Transf. 53, 1951–1966.
Yamasaki, K., Koizumi, M., Maekawa, K., 2014. Laser-sintered porous structures for samarium-based solid oxide fuel cells. Procedia Mater. Sci. 4, 103–108.
Yuan, W., Tang, Y., Yang, X., Liu, B., Wan, Z., 2012. Structural diversity and orientation dependence of a liquid-fed passive air-breathing direct methanol fuel cell. Int. J. Hydrog. Energy 37, 9298–9313.
Yuan, W., Deng, J., Zhang, Z., Yang, X., Tang, Y., 2014a. Study on operational aspects of a passive direct methanol fuel cell incorporating an anodic methanol barrier. Renew. Energy 62, 640–648.
Yuan, W., Zhou, B., Deng, J., Tang, Y., Zhang, Z., Li, Z., 2014b. Overview on the developments of vapor-feed direct methanol fuel cells. Int. J. Hydrog. Energy 39, 6689–6704.
Zainoodin, A., Kamarudin, S.K., Masdar, M., Daud, W.R.W., Mohamad, A.B., Sahari, J., 2014. Investigation of MEA degradation in a passive direct methanol fuel cell under different modes of operation. Appl. Energy 135, 364–372.
Zhong, L., Wang, X., Jiang, Y., Zhang, Q., Qiu, X., Zhou, Y.a., Liu, L., 2008. A micro-direct methanol fuel cell stack with optimized design and microfabrication. Sensors Actuators A Phys. 143, 70–76.

Further Reading

Ren, X., Wilson, M.S., Gottesfeld, S., 1996. High performance direct methanol polymer electrolyte fuel cells. J. Electrochem. Soc. 143, L12–L15.

This page intentionally left blank

CHAPTER 15

Coproduction of Electrical Energy and Methanol in IGCC Plants

Kamran Ghasemzadeh[*], Seyyed M. Sadati Tilebon[†], Angelo Basile[‡]

[*] *Urmia University of Technology, Urmia, Iran* [†] *Iran University of Science & Technology, Tehran, Iran*
[‡] *Institute on Membrane Technology (ITM-CNR), Rende, Italy*

Acronym

AER	absorption enhanced reforming
AGR	acid gas removal
ASU	air separation unit
C	carbon
CCS	CO_2 capture and storage
CF	capacity factor
COE	cost of electricity
DME	dimethyl ether
DOE	Department of Energy in USA
EOR	enhanced oil recovery
FGD	flue gas desulfurization
GEE	general electric energy
GT	gas turbine
H	hydrogen
HHV	higher heating value
HRSG	heat recovery steam generator
IEA	International Energy Agency
IGCC	integrated gasification combined cycles
ITM	ion transport membranes
LCOE	levelized cost of electricity
LHV	lower heating value
MMMs	mixed matrix membranes
MR	membrane reactor
N	nitrogen
PC	pulverized coal

Methanol. https://doi.org/10.1016/B978-0-444-63903-5.00015-7

PCC	pulverized coal combustion
PSA	pressure swing adsorption
PrCC	precombustion capture
PVA	poly (vinyl alcohol)
SC	supercritical
SRU	sulfur recovery unit
TASC	total as-spent cost
TOC	total overnight cost
TPC	total plant cost
TPD	ton per day
VAM	vinyl acetate
VM	volatile matter

1 Introduction

Global warming and the production of greenhouse gases are considered to be the most serious challenges the world is facing today. Many gases play greenhouse effect, however one of the most important of them is CO_2. Electricity generation contributes approximately 30% of global CO_2 emissions and fossil fuels produce 60% of the world's electricity and 38% of it is generated using coal. The use of coal as a primary fuel is expected to grow by roughly 30% between 2010 and 2030 and the worldwide capacity of coal fuel power plants are expected to increase by over 40% in the next 20 years and will generate over 1400 GWe of electricity by 2025. Therefore, in the future it is necessary to develop more efficient coal-based power plants with a CO_2 capture facility to reduce greenhouse gas emissions which cause global warming. Lignite fueled power plants ensure power generation for another 80 years. However, in order to use lignite as fuel, more advanced technologies are required for the reduction in greenhouse gas emissions and to produce costs of electricity comparable to other power generation plants. The efficiency of the lignite fuel power plants has been achieved up to 43% with technological developments (Beér, 2007; Chiesa et al., 2005; Leidich et al., 2005; Mondol et al., 2009; Romeo et al., 2008).

On the other hand, coal is an accessible source for required energy in power plants, but there are some problems using coal as an energy source. Coal combustion will be emit huge amounts of impurities into the atmosphere. Therefore, it is necessary to design a system with a low level of CO_2 emission. integrated gasification combined cycles (IGCC) technology offers a significant advantage over conventional coal-based power plants in terms of CO_2 capture. IGCC technology has proved to be commercially viable against conventional coal-fired power plants. Indeed, the IGCC coal-based power plants have high thermal efficiency (Emun et al., 2010), low environmental impact (Ratafia-Brown et al., 2002), and can produce power as well as synthetic fuels (Ratafia-Brown et al., 2002), chemicals (Zhang et al., 2013), and marketable

by-products (Mondol et al., 2009) making IGCC an attractive technology for the next century. At present, the cost of electricity (COE) produced by IGCC plants with CO_2 capture and storage (CCS) is lower than a conventional plant (pulverized coal (PC) plant) for high rank coal but comparable or higher for low rank coal. The thermal efficiency of IGCC plants is very high, approximately in the region of 46%–47% and for advanced new technologies, the efficiency can go up to 55%. The IGCC plants with CCS will produce electricity at a competitive price when the IGCC plant efficiency is achieved up to 50% and the CO_2 sequestration is commercially available (Grainger and Hägg, 2008; Christou et al., 2008; Rubin et al., 2007; Shinada et al., 2002).

Overall, CCS processes can reduce the efficiency of IGCC plants because additional technology, capital cost, and operating cost is required. But new methods of energy recovery and new applications of separated CO_2 can improve the cost of IGCC systems. IGCC–CCS systems are a technology for the future of the world. This process can be an ideal solution for many crises for the future of life, such as the environment and energy. Methanol production is one of the latest and newest applications of captured carbon dioxide that is hoped to improve the efficiency and cost affectivity of process. In fact, separation of carbon dioxide is a key point for simultaneous methanol and electricity production. Variety of separation methods such as cryogenic (Aaron and Tsouris, 2005; Zanganeh et al., 2009), sorption (adsorption (Yang et al., 2008; Aaron and Tsouris, 2005), and absorption (Chiesa and Consonni, 1998; Rezvani et al., 2009)), and membrane separation (Carbo et al., 2006; Kaldis et al., 2004) were used. Each of these noted processes have advantages and disadvantages, but membrane separation is a next generation separation technology that is the best choice for application in the IGCC process in the future.

Despite all of the advantages of the IGCC process and membrane separation, there are some worries about the efficiency and cost affectivity of them. Fortunately, in recent years, several industrial cases of IGCC power plants were constructed that can be suitable bases for future developments. However, improvement in operation and capital cost of process can make the IGCC process the best process for electricity production and maybe a variety of chemicals production. In this chapter, IGCC power plants in the case of coproduction of methanol and electricity has been studied. Moreover, membrane separation and economic studies as two important and effective parameters in IGCC power plants are investigated.

2 IGCC Plant Technology

The IGCC plant is a process with purpose of using hydrocarbon fuels in solid or liquid phases to produce electrical power in a cleaner and more efficient way via gasification, compared to directly combusting the fuels. Main usable hydrocarbons for the IGCC process include coal, biomass (Rhodes and Keith, 2005), refinery bottom residues (such as petroleum coke, asphalt, visbreaker tar, etc.) (Huth et al., 2000), and municipal wastes (Ionescu et al., 2013). The

approach to achieve a "cleaner" production of power is to convert solid/liquid fuels to gas first, so that they can be cleaned before they are burned by removing mainly particulates, sulfur, mercury, and other trace elements. The cleaned gas, called synthetic or synthesis gas (syngas) can then be sent to a conventional combined cycle to produce electricity. A simplified IGCC process diagram comprising of three major "islands"—gasification, gas cleanup, and power—is shown in Fig. 15.1. The ultimate goal for the IGCC process is to achieve a lower COE than conventional PC power plants and/or to be competitive with natural gas-fired combined-cycle systems with comparable emissions. While "clean" power generation is the primary driving motivation for entering the business of IGCC, "increasing plant efficiency" to a level higher than that of PC plants is the second driving motivation. To obtain higher efficiency, "integration" between sub-systems becomes necessary. Integration consists of all aspects of the operation, including mechanical, thermal, and dynamic process control (Wang, 2017).

In general, several types of feeds can be used in IGCC systems. Coals, liquid petroleum, petroleum cock, and biomass are main feeds for the IGCC plant. Environmental aspects are sustainability highlighted properties of the IGCC process. Therefore, biomass is very attractive and can be defined as "animal and plant resources and the wastes deriving from their treatment, which could be used directly or after a pretreatment as a source of energy." Main biomasses and their characteristics are noted in Table 15.1 (Dahlquist, 2013).

It should be noted that the IGCC processes are approximately complex and there are many units for operating them. Indeed, gasification is one of the most important sections of the IGCC

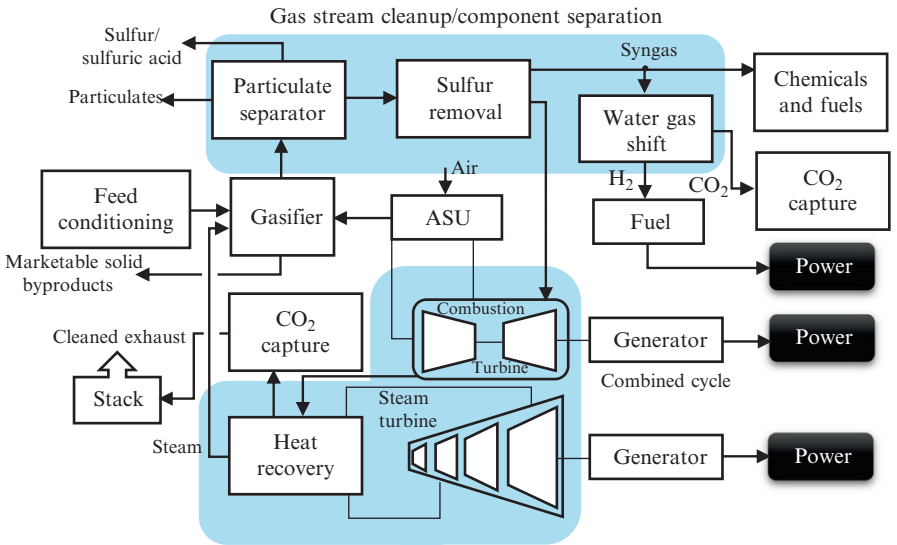

Fig. 15.1
Simplified block diagram of an IGCC system.

Table 15.1 The main biomass and their characteristics

Characteristic	Moisture (%) wb	VM (%)	Ashes (%)	C (%)	H (%)	N (%)	HHV (MJ/kgdb)	LHV (MJ/kgdb)	Bulk density (kg/m^3)
Oak wood	6.2	86.0	0.9	49.7	6.5	0.2	20.4	18.9	750
Pine wood	9.5	89.3	0.7	51.3	6.1	0.2	19.2	–	440–560
Pine bark	–	–	1.8	46.9	5.3	–	–	–	–
Sawdust pellet	10.0	85.6	0.8	49.8	6.4	0.3	18.5	17.4	650
Sorghum	–	–	2.1	43.9	6.2	0.2	16.8	–	220–260
Salix wood	7.9	85.7	1.9	49.1	6.2	0.3	18.8	–	300–400
Poplar wood	8.6	80.3	1.3	49.7	6.5	0.2	19.6	19.3	420
Fire wood	7.7	77.0	5.8	48.6	6.5	0.2	18.9	–	700–800
Birch wood	7.4	80.9	2.6	48.3	8.3	0.1	19.3	–	600
Vine pruning	45.0	86.0	2.3	46.5	6.4	0.4	18.6	17.1	790–900
Olive tree pruning	40.0	86.0	3.9	49.3	5.5	0.6	18.5	17.4	800–900
Sawdust	11.6	81.5	0.8	49.5	6.8	0.4	19.7	–	100
Bamboo	8.5	76.5	0.8	50.6	5.3	0.2	19.3	–	200–250
Wood chips	9.3	88.0	1.0	50.0	5.8	0.3	19.3	–	150
Giant reed	40.0	–	8.5	45.5	5.7	0.2	18.0	17.5	180–200
Black locust	30.0	85.7	3.6	50.7	5.7	0.5	19.7	18.5	625
Straw	8.7	72.3	14.9	43.0	6.3	0.8	16.0	14.9	100–180
Wheat	6.4	75.0	8.0	43.0	10.85	0.3	16.0	–	–
Rice husk	–	69.3	19.0	36.7	5.0	0.9	14.5	13.9	75
Sugarcane	–	85.2	2.2	52.5	6.8	0.5	18.9	–	130–150
Rapeseed	6.1	77.6	3.8	42.4	7.1	0.2	16.6	–	–
Stone fruit residues	6.9	85.6	0.5	51.6	6.0	0.5	21.6	–	–
Almond shell	8.7	81.7	2.8	52.4	6.7	0.5	19.0	17.7	–
Hazelnut shell	9.3	71.0	7.9	42.8	5.15	0.6	15.7	–	–
Walnut shell	6.7	76.1	3.6	51.5	7.3	0.7	–	–	–
Tomato	7.0	86.1	3.8	52.3	7.6	3.4	–	–	–
Olive husk	8.3	78.4	6.4	49.6	5.5	1.4	20.9	19.1	–
Bagasse	–	77.0	2.1	51.5	6.0	1.0	18.2	–	–

processes. There is an important difference between gasification and combustion. The purpose of combustion is to produce heat, whereas the purpose of gasification is to produce fuels or chemicals. Therefore, during a combustion process, the stoichiometric (or theoretical) amount of oxidant is used to completely oxidize the feedstock and obtain the maximum thermal energy output (heat); whereas, during a gasification process, as little thermal energy as possible is intended to be used (and, thus, limited oxidant is needed) to convert the feedstock to useful fuels, preserving as much of the original fuel's chemical energy (or heating value) as desired.

Typically, a stoichiometric ratio of 0.25–0.35 (i.e., 25%–35% of the oxygen theoretically needed for complete combustion) is implemented in a gasification process. A variety of products can be achieved by a gasifier outlet stream. Products that can be derived from gasifying coal or any carbon source are shown in Fig. 15.2 (Wang, 2017).

In fact, there are various gasifiers in design and operation point of view. The key process in any IGCC technology is the production of clean synthesis gas from the feedstock. Therefore, the role of gasifiers is highlighted and each of the gasifiers have special qualities. As an example, general electric is a successful technology and can be used quite effectively to gasify higher-rank coals and petroleum coke. For a typical IGCC plant that is engineered to generate about 600 MW of net power, two GE RSC gasifiers would be used. The gasifier throughput would be about 2500 Ton per day (TPD) of coal. The gasifiers would typically operate at a pressure of about 600 psig and a temperature of about 1316°C (2400°F) to produce the synthesis gas. Another important parameter is product stream characteristics. The characteristics of feed and product stream for several gasifiers are noted in Table 15.2.

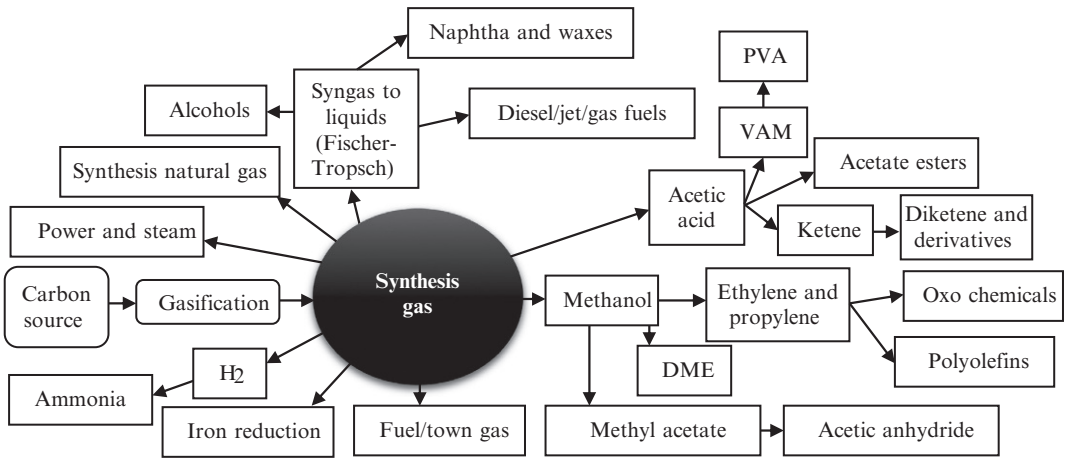

Fig. 15.2
Products that can be derived from gasifying coal or any carbon source.

Table 15.2 Stream characteristics for several gasifier products

Components	GE		SCGP		Siemens SFG		CB&I E-Gas			
	Syngas (dry basis)	Coal (dry basis)	Syngas (dry basis)[a]	Syngas (dry basis)[b]	Syngas (dry basis)[a]	Syngas (dry basis)[b]	Syngas by lignite (wet basis)	Syngas by sub. coal (wet basis)	Syngas by bit. coal (wet basis)	Syngas by pet. coal (wet basis)
Carbon monoxide	43.53	4.99	65.39	72.52	63.69	56.31	26.4	18–28	20–38	30–44
Hydrogen	37.49	4.99	28.83	21.08	30.85	32.99	30.6	26–35	22–32	18–30
Carbon dioxide	18.23	–	1.22	5.63	3.74	3.79	17.0	16–22	7.5–15	6.1–15
Methane	0.05	–	0.06	0.01	0.02	0.02	0.2	1.6–3.7	1.0–2.0	0.8–1.1
Nitrogen + argon	0.50	1.01	4.29	0.43	0.72	5.94	0.7	0.9–2.8	0.3–2.8	0.9–2.8
Hydrogen sulfide + carbonyl sulfide	0.20	–	0.21	0.21	–	–	0.1	0.1–0.4	0.6–1.1	1.1–1.3
Moisture	–	–	–	–	–	–	25	20–30	20–30	20–30
NH_3	–	–	–	–	–	–	0.1	0.6–0.8	0.5–0.7	0.4–0.6
Carbon	–	74.05	–	–	–	–	–	–	–	–
Sulfur	–	0.64	–	–	–	–	–	–	–	–
Oxygen		10.37	–	–	–	–	–	–	–	–
Ash or trace		8.37	–	–	0.99	0.96	–	–	–	–

[a] N_2 is transport gas.
[b] CO_2 is transport gas.

Additional information about different gasifiers are accessible in literature (Gray, 2017). On the other hand, various gasifiers need different feeds and these feed characteristics should be considered. As an example, typical particle size distributions used in various gasifiers are noted in Table 15.3.

Energy is one of the main crises for the future of the world. Usage of light fossil fuels is not wise. However, burning a light fossil fuel is the worst choice because it is nonrenewable and limited and there are variety of valuable applications for it. Low quality fuels such as coals are a suitable solution for this problem. According to the International Energy Agency report, more than 30% of total energy demand and 40% of global electricity comes from coal. But there are some problems in using coal as fuel. Difficulty of coal burning and huge pollutant emission are some of them.

The IGCC system is a suitable solution for the energy crisis in future of the world. The overall efficiency of an IGCC plant is dependent on matching coal properties to the type of gasifier to be used in the process. An in-depth understanding of coal characteristics, the plant configuration, which includes coal preparation, and the coal feeding system is necessary to improve the overall efficiency of the gasification process. In the following section, we will discuss the coal characteristics pertaining to coal gasification—coal preparation and coal feeding systems. The many characteristics of coal include chemical composition, petrographic properties, grindability, friability, caking properties, reactivity, char morphology, and inorganic species. These parameters separate different coals into two groups (low and high rank coals for IGCC). The comparison of low rank and high rank coals is denoted in Table 15.4 (Gray, 2017).

Advantages of IGCC power plants compared with conventional plants is producing impressive developments. Now several commercialized IGCC such as Tampa, Wabash, Buggenum, and Puertollano are in operation (Wang, 2017). The development of IGCC technology started with the first generation in the 1970s, induced by the oil crisis and this was followed by a number of commercial-scale demonstration plants during the second generation in the 1990s. The process units of these earlier IGCC power plants are considered mature technology

Table 15.3 Typical particle size distribution used in various gasifiers

Gasifier type	Particle size
Dry feed entrained flow gasifier (low reactivity feed)	50–90% <63 μm and 100% <200 μm
Dry feed entrained flow gasifier (highly reactive feed)	94% <250 μm and 100% <500 μm
Slurry based entrained flow gasifier	15% >425 μm and 29% <75 μm
Dry feed fluidized bed gasifier	<6 mm
Dry feed transport gasifier	85% in 0.043–1 mm
Dry feed fixed-bed gasifier	Top size: <100 mm Bottom size: 5–8 mm

Table 15.4 Comparison of low rank and high rank coals

Properties	Low rank coals	High rank coals	Comments
Grindability	Lower	Higher	High rank coals are easier to grind compared to low rank coals and therefore preferred for dry feed entrained flow gasifiers
Slurriability	Higher slurry viscosity for a given solid loading	Lower slurry viscosity for given solid loading	High rank coals are preferred for high solids loading in slurry for a given particle size distribution
Reactivity	High	Medium to low	Reactivity of the chars decreases with increase in the coal rank
Ash fusion temperature	Low	Can vary	The presence of reactive inorganic species in low rank coals can generate highly reactive slag that interacts with the refractory of the slagging gasifiers
Caking characteristics	Non caking	Only vitrinite-rich bituminous coals show caking characteristics	Caking characteristics of bituminous coals are not preferred in fixed and fluidized bed gasifiers due to char agglomeration
Heating value	Lower	Higher	A higher amount of coal feed is required for low rank coals for a given syngas production rate

and a lot of lessons learned are available for further improvements of the next IGCC generation after 2010. However, the integration of all components to build an IGCC power plant is still challenging because there are no standardized systems available (Wolfersdorf and Meyer, 2017).

As noted previously, the main advantage of the IGCC system is it's environmentally friendly. In addition to usage biomass, IGCC systems can be integrated with CCS in the reduction or elimination of CO_2 emission. Three types of CCS process can be used in IGCC plants. CO_2 capture systems are divided into three major categories. They are postcombustion, where the CO_2 removal occurs after hydrocarbon combustion; precombustion, where the CO_2 is separated prior to combustion; and oxy or oxygen fuel, where the CO_2 is removed as part of the fuel derivation and not part of the combustion process. The carbon dioxide capture technology discussion occurs in this order based on the

maturity of the three types of technologies, pilot testing results, experience in commercial applications, and cost of application. The technologies used to capture the CO_2 include sorption processes (absorption and adsorption), selective membranes, and cryogenic capture. General flow sheet of IGCC–CCS process is shown in Fig. 15.3 (Carpenter and Long, 2017).

The feasibility of several product productions in one system is a positive parameter for the system. The IGCC plant design is similar to that of coal-based chemicals or fuels production. Synthesis products usually realize a higher added value in comparison to pure electricity generation. Polygeneration plants combine both syngas-based power generation and the production of chemicals or fuels, aiming for an increase of product flexibility and resource utilization for higher total efficiencies and improved economics of the overall plant. Consequently, syngas-based chemicals production in combination with a coal-fired power block for electricity and steam generation is not referred to as polygeneration. Currently, most coal-to-X plants (where X is fuels, chemicals, power, etc.) or refinery projects are polygeneration plants. A general flow sheet of a coal-based polygeneration plant, primarily focusing on the output of synthesis product, is illustrated in Fig. 15.4. However, a large variety of different polygeneration configurations can be distinguished. As reported by Laugwitz et al. (2011), existing refinery polygeneration power plants achieve significantly higher availabilities in comparison to IGCC power plants.

A refinery IGCC usually reaches an availability of 85%–90% after three years of operation, while most coal-based IGCC power plants needed more than five years of operation to reach an average availability of approximately 75%. Polygeneration plants usually emit less CO_2 than conventional coal-based power plants, because carbon is stored partially in the product,

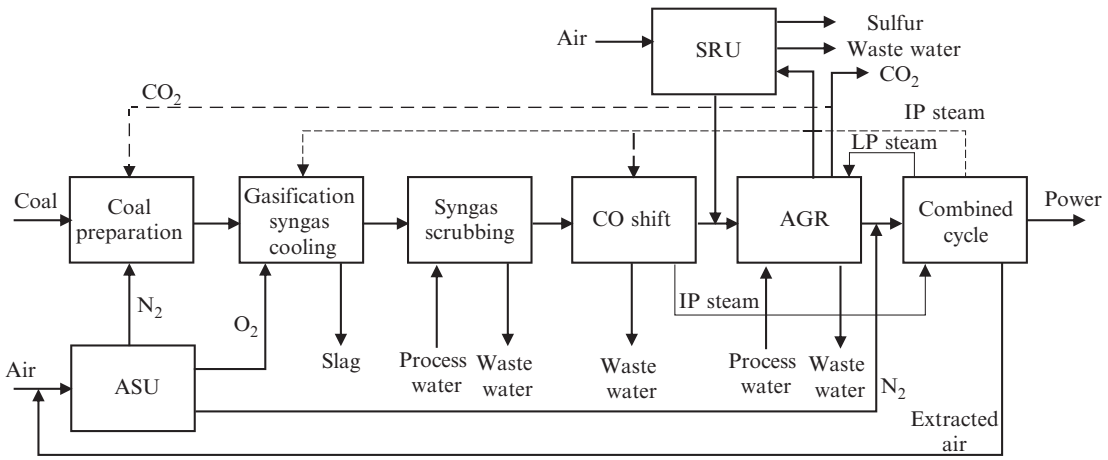

Fig. 15.3
General flow sheet of IGCC–CCS power plant.

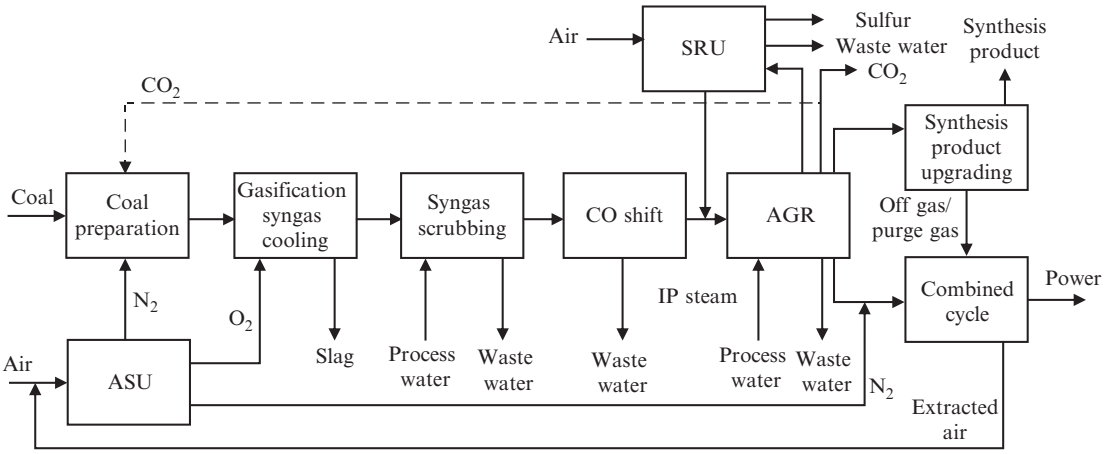

Fig. 15.4
Flow sheet of polygeneration plant producing chemicals and power.

except in ammonia coproduction. In addition, the removal of CO_2 is usually a necessary part of the process chain because of the requirements for gas composition for subsequent synthesis. The removed CO_2 could be stored easily, leading to a comparatively low efficiency penalty (Wolfersdorf and Meyer, 2017).

As noted previously, several separation technologies can be used in IGCC-CCS power plants. Pressure swing adsorption (PSA) is a valuable process in gas separation systems. The addition of a PSA unit to the IGCC plant requires a higher degree of integration compared to the postcombustion scenario. A major difference is that the CO_2-lean gas stream leaving the PSA process (i.e., the H_2-rich gas stream) is further processed in the plant, constituting the fuel for the gas turbine. The additional units, with respect to the reference IGCC plant, consist of a water-gas shift section, a PSA process, and a compression stage for CO_2 transport. The plant layout is represented in Fig. 15.5.

2.1 Methanol as Byproducts of the IGCC Plant

As noted previously, IGCC power plant is one of most promising strategies for the future of the earth. Carbon dioxide capture from IGCC process can improve sustainability and the reuse of them can improve the efficiency. Indeed, there are variety of applications for captured CO_2 such as methanol production and enhanced oil recovery (EOR). However, methanol production is considered the most valuable application of captured CO_2 from the IGCC power plant.

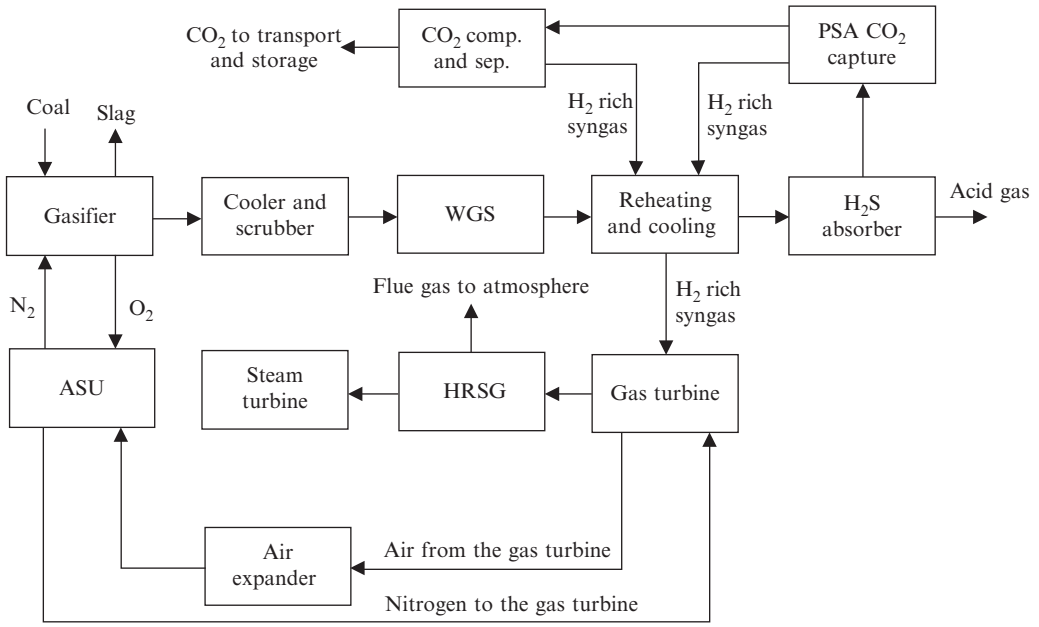

Fig. 15.5
The IGCC plant with an integrated PSA unit for CO_2 capture and a CO_2 compression unit.

3 Application of Membrane Processes in Coproduction of Methanol and Electricity

Membrane is defined as a phase that can separate the streams selectively and in molecular scale. Membrane processes have many advantages compared with conventional separation methods. High level of energy consumption, low efficiency, low product purity, need to change phase, and high required space are some challenges of common separation methods. In comparison, membrane separation technology is a good option to achieve valuable separation process. In coproduction of electricity and methanol systems by the IGCC plant, many points for membrane applications can be focused on. Overall, the application of membranes for these systems can be classified in two groups; namely the IGCC process and methanol plant.

3.1 Membrane Applications for IGCC Process

The most highlighted applications of membrane process in IGCC power plant are related to CO_2 separation. However, hydrogen separation for syngas plant could be applied. Fig. 15.6 shows plant layouts for an IGCC system using a conventional liquid solvent-based CO_2 capture system, and a system using a membrane-based clean-up.

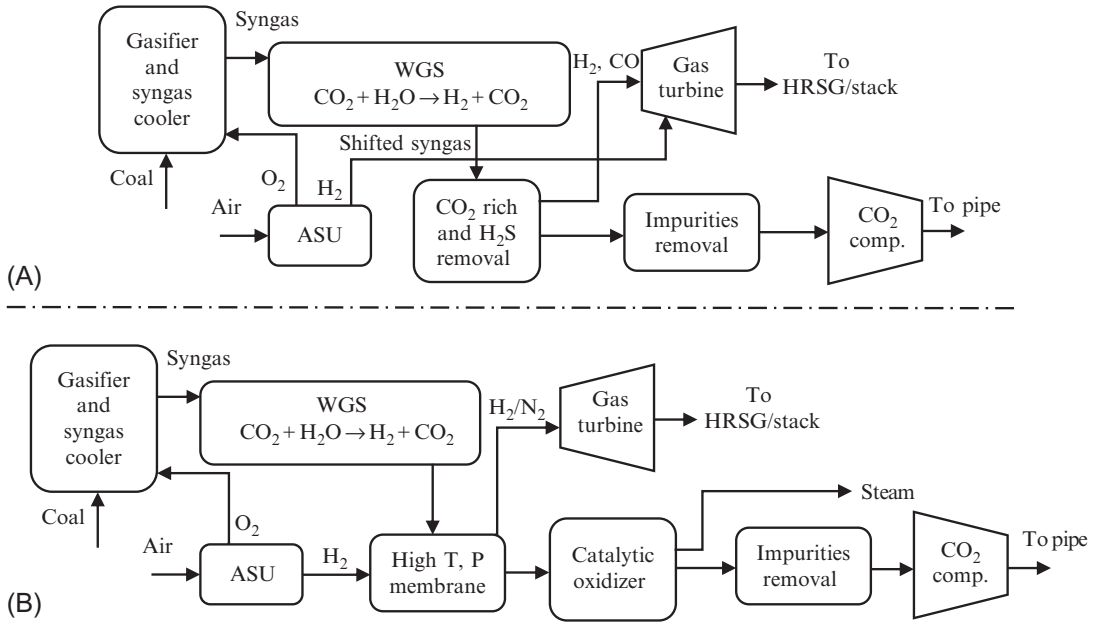

Fig. 15.6
System layouts for IGCC system with conventional liquid solvent-based CO_2 capture (A) and membrane-based CO_2 capture (B).

3.1.1 H_2 selective membrane

A simple diagram of the IGCC power plant with a H_2 separation membrane is illustrated in Fig. 15.7. In precombustion capture (PrCC), CO_2 has to be separated from H_2-containing streams. To produce large-scale electricity using gas turbines, the gasification is typically carried out at very high pressures (>50 bars). From a membrane process point of view, higher pressure means larger driving force for separation. However, the challenging part is to separate CO_2 from H_2, which is a much smaller molecule than N_2. For this reason, several types of H_2 selective membrane such as mixed matrix, Pd based, and silica membranes can be used in this application (Ramasubramanian et al., 2013).

In this case, Chiesa et al. (2007), investigated metallic membrane applications in IGCC. This paper investigates novel IGCC plants that employ hydrogen separation membranes in order to capture carbon dioxide for long-term storage. The thermodynamic performance of these membrane-based plants are compared with similar IGCCs that capture CO_2 using conventional (i.e., solvent absorption) technology. The basic plant configuration employs an entrained-flow, oxygen-blown coal gasifier with quench cooling, followed by an adiabatic water gas shift (WGS) reactor which converts most of the CO contained in the syngas into CO_2 and H_2. The syngas then enters a WGS membrane reactor where the syngas undergoes further shifting; simultaneously, the H_2 in the syngas permeates through the

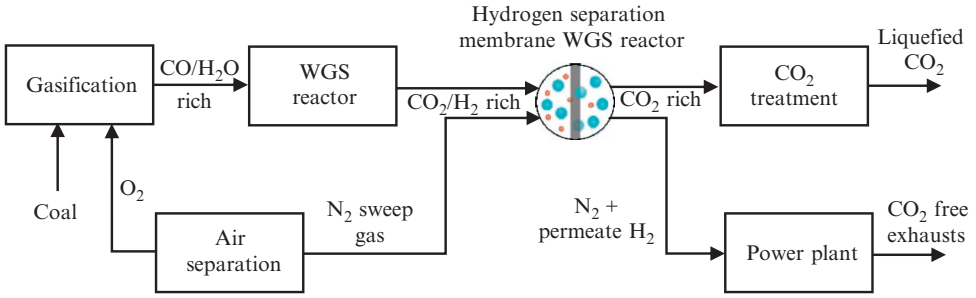

Fig. 15.7
Conceptual scheme of a low CO_2 emission IGCC plant based on a hydrogen separation membrane reactor.

hydrogen-selective, dense metal membrane into a counter-current nitrogen "sweep" flow. The permeated H_2, diluted by N_2, constitutes a decarbonized fuel for the combined cycle power plant whose exhaust is CO_2 free. Exiting the membrane reactor is a hot, high pressure "Raffinate" stream composed primarily of CO_2 and steam, but also containing "fuel species" such as H_2S, unconverted CO, and unpermeated H_2. Two different schemes (oxygen catalytic combustion and cryogenic separation) have been investigated to both exploit the heating value of the fuel species and to produce a CO_2-rich stream for long-term storage. Our calculations indicate that, when 85 vol% of the H_2+CO in the original syngas is extracted as H_2 by the membrane reactor, the membrane-based IGCC systems are more efficient by ~1.7 percentage points than the reference IGCC with CO_2 capture based on commercially ready technology.

Ku et al., in 2011, studied membrane performance requirements for carbon dioxide capture using hydrogen-selective membranes in IGCC power plants. Membranes can provide a significant boost in the performance by separating CO_2 at high temperature and at high pressure, provided they are properly integrated into a power plant. In this study, membrane performance targets were derived for CO_2 capture using H_2-selective membranes in IGCC power plant systems. Three key differences were found relative to plants configured for the production of industrial-grade H_2. First, the H_2/CO_2 selectivity requirement is lower when the permeate is combusted in a gas turbine, as opposed to purified for industrial use. Second, the membrane is subject to additional selectivity requirements. For example, CO_2 product purity specs impose a H_2/N_2 selectivity requirement. Third, the plant design must account for the energy associated with unshifted CO, CH_4, and other fuel components that are not separated by the membrane. In contrast to H_2 production systems where the high H_2/CO_2 selectivity requirement favors ultra-high selectivity metal-based membranes, the requirements for IGCC indicate a wider range of materials, including ceramic, zeolite, and polymeric membranes, should be considered (Ku et al., 2011).

3.1.2 CO_2 selective membrane

CO_2 selective membranes can be used in various carbon dioxide processes, as shown in Fig. 15.8. It should be noted that H_2 and CO_2 purity are two important parameters for increasing the overall efficiency of the IGCC process. CO_2 selective membranes can provide the high purity CO_2 stream. This means that the process product will be more valuable (Favre, 2007; Merkel et al., 2012; Shekhawat et al., 2003).

On the other hand, permeability and selectivity are two main performance characteristics for membranes. Regarding literatures, several polymeric and inorganic membrane presented suitable performance for this application. For instance, Pebax and Polyactive are the most commonly studied commercial block copolymers with polyamide and polybutyleneterephthalate hard segments, respectively. In particular, CO_2 permeability and CO_2/N_2 selectivity for these materials tend to be 100–150 Barrers and about 45, respectively, at 35°C (Ku et al., 2011).

Facilitated transport membranes are other types of membranes that can be used in CO_2 separation (Huang et al., 2008; LeBlanc et al., 1980; Quinn et al., 1995; Zhang et al., 2002). In facilitated transport membranes, the CO_2 molecule reacts with carrier molecules in the membrane through a selective reversible chemical reaction by which its solubility is greatly enhanced. The nonreactive gases like N_2, H_2, and CO get transported purely by solution-diffusion. Consequently, high selectivities for CO_2/nonpolar gases can be readily

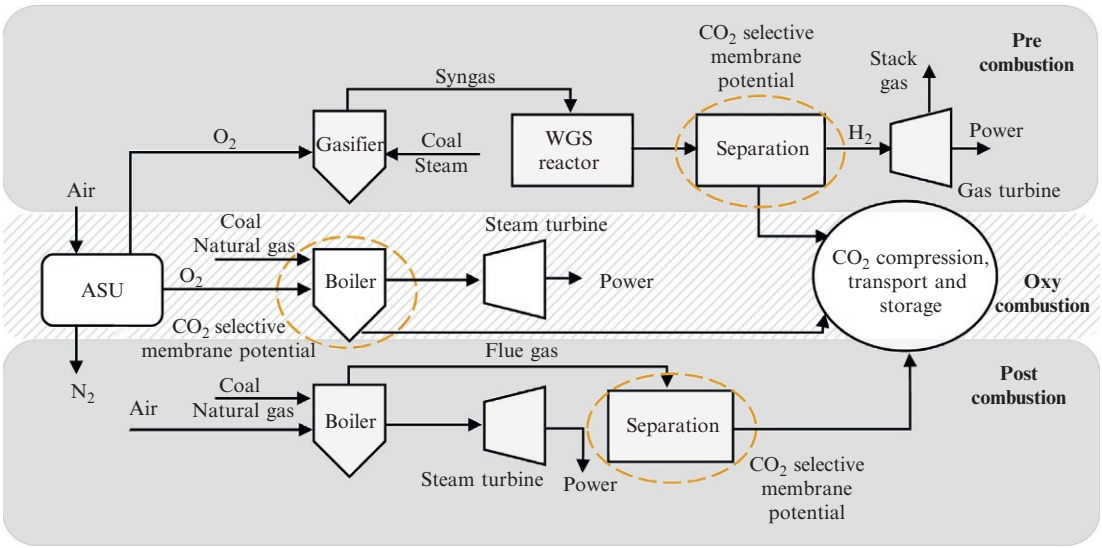

Fig. 15.8
Potential of CO_2 selective membranes for various CCS processes in IGCC plant.

achieved. This type of membranes was depicted to have extraordinary separation properties with best CO_2 permeances and selectivities greater than 1000 GPU and 200, respectively at 35° (Ku et al., 2011).

Most of the inorganic membranes studied for CO_2/N_2 separation have a microporous structure (Shekhawat et al., 2003; Yang et al., 2008; Zou et al., 2007). In general, separation is achieved by either molecular sieving or selective surface diffusion through the pores or both. Molecular sieving is relatively ineffective due to the comparable sizes for CO_2 and N_2, and the permeances in pure molecular sieving are small. In selective surface diffusion, CO_2 preferentially adsorbs and diffuses along a surface concentration gradient. The pore area available for N_2 is then effectively reduced or, in some cases, blocked. Such microporous transport can comfortably cross the upper bound for polymeric materials (Huang et al., 2008; Zou and Ho, 2006). Zeolites (Venna and Carreon, 2009; Yang et al., 2008), microporous silica (Yang et al., 2008; Ramasubramanian et al., 2013), and carbon are important materials in this context.

Mixed matrix membranes (MMMs) (Li et al., 2013; Rodenas et al., 2014; Zornoza et al., 2011) composed of inorganic particles dispersed uniformly in a continuous polymer matrix have attracted considerable attention for CO_2 separations. They can potentially realize a synergistic combination of advantages of polymers (easy processability, defect-free film formation, low cost) and inorganic materials (superior gas separation performance, mechanical strength, thermal stability).

Overall, there are some advantages for using the CO_2 selective membranes. Some of the important advantages of CO_2-selective membranes are summarized here (Ku et al., 2011):

I. Along with H_2, residual CO and N_2 in the syngas can be separated from CO_2. This can help to reach higher CO_2 purity in the stream to be sequestered.
II. Recovery target of 90% CO_2 is somewhat arbitrary and is more susceptible to change than the purity target of at least 95%. For a lower CO_2 recovery requirement, the amount of CO in the fuel stream will be higher due to a lower conversion in the WGS reactor. To tackle this, an additional combustion step will be needed after CO_2 capture for H_2-selective membranes. Since CO is retained by the fuel stream for CO_2-selective membranes, they can provide more flexibility on CO_2 recovery or CO conversion target for the WGS reactor.
III. Applying the same rationale to N_2, it can easily be concluded that they also provide greater flexibility on the purity of O_2 obtained from the air separation unit (ASU) for the gasification. H_2- selective membranes cannot take too much nitrogen since it will have to be separated from CO_2 in an additional step before the capture. This flexibility can also reduce the energy consumption of the ASU.
IV. Plasticization of polymeric solution-diffusion membranes due to high H_2O and/or CO_2 partial pressures as in syngas can increase the CO_2/H_2 selectivity of rubbery

CO_2-selective membranes while hampering the H_2/CO_2-selectivity of glassy H_2-selective membranes.

V. There is a greater scope to increase the reverse gas CO_2/H_2 selectivity by using facilitated transport membranes since they are not limited by the upper bound.

3.1.3 O_2 selective membrane

In the pre combustion process, high purity O_2 should be provided by ASU. Nowadays, most of commercial ASU plants are cryogenic. Cryogenic systems consume a high level of energy and are not suitable for small or medium industries. On the other hand, cryogenic processes are very complex. In the meantime, the membrane separation process is a simple, efficient, and proportional low energy consumer. Ion transport membranes (ITM) are main membrane modules that can be used in ASU. The main commercial application of ITM is in IGCC process (Baker, 2000; Dyer et al., 2000; Vente et al., 2006).

The ITM Oxygen technology is ideally suited to integration with power generation processes that require oxygen as a feedstock for combustion or gasification, or in any oxygen-based application with a need for power or an export power market. As a result, the IGCC process is an ideal application for ITM Oxygen coproduction technology. Fig. 15.9 depicts a flowsheet for the integration of ITM Oxygen in an IGCC facility (Schwarz et al., 2001).

It should be mentioned that Ghasemzadeh et al. (2015), reported a detailed study about membrane applications for the IGCC power plant. The discussion indicated that simplifications

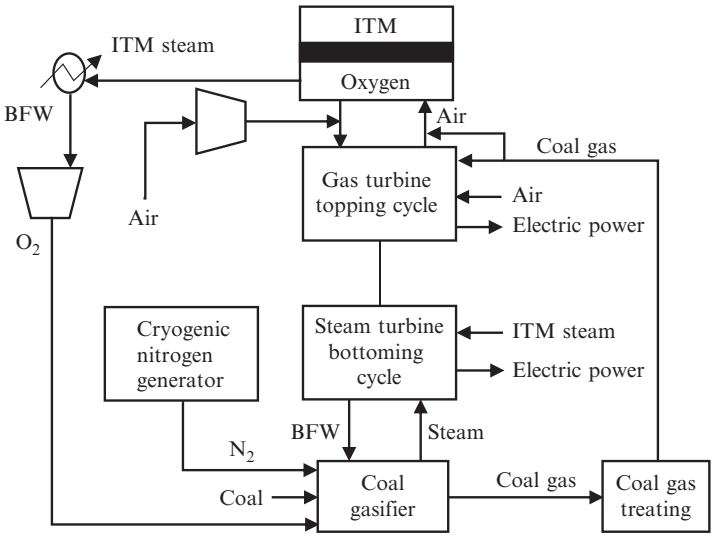

Fig. 15.9
ITM Oxygen/IGCC integration.

in IGCC plant design and efficiency improvements of a few percentage points can be achieved by doing the following:

- replacing the ASU with the ITM membrane system that provides the oxygen for gasification;
- integrating low temperature polymeric hydrogen membranes downstream in a WGS process;
- intensifying the CO_2 formation and separation by combining H_2 selective (Pd-based or silica) membranes with the WGS reaction process;
- integrating CO_2 selective membrane (silica and zeolite membranes) for precombustion process.

Also the potential economics of membrane separation in electricity production appear to be positive even though the membrane lifetime duration is still an open issue, which may affect this aspect. Therefore, the main challenge to employing CO_2 capture strategies is the development of membrane materials. If higher permeance, and especially more selective, membranes can be developed, the cost of the technology described will decrease even further. Moreover, the advantages of H_2 separation membranes in IGCC plants can be discovered if hydrogen succeeds as an extensive decarbonized energy carrier on the road to reducing CO_2 emissions in the fight against climate change. In this context their many potential benefits may accelerate their deployment compared to plants for simple power generation with CO_2 capture. It is clear that usage of CO_2 for methanol production can improve the system efficiency (Ghasemzadeh et al., 2015).

3.2 Membrane Applications for Methanol Production From Captured CO_2

The reactions of methanol production from syngas are mainly CO and CO_2 hydrogenation and reverse water–gas shift reaction (Sadati Tilebon et al., 2015; Ghasemzadeh et al., 2016).

$$CO + 2H_2 \Leftrightarrow CH_3OH \tag{15.1}$$

$$CO_2 + 3H_2 \Leftrightarrow CH_3OH + H_2O \tag{15.2}$$

$$CO_2 + H_2 \Leftrightarrow CO + H_2O \tag{15.3}$$

Regarding the literatures, for a practical point of view, it should be mentioned that there is no study for the evaluation of membrane applications in the methanol production process. However, several works from modeling aspects were presented by Farsi and Jahanmiri (2011, 2012a,b). In their works, a palladium membrane in a membrane reactor (MR) system was considered as a hydrogen distributer for reaction zone and a water-selective membrane such as silica membrane was assumed for removing steam from reaction zone, simultaneously. Their results indicated that membrane application can improve methanol production rate.

4 Economic Evaluation of IGCC Plant

Mondol et al., in 2009, presented an economic study of the IGCC plant with low rank coal. The techno-economic evaluation of four novel IGCC power plants fuelled with low rank lignite coal with CO_2 capture facility has been investigated using an ECLIPSE process simulator. The performance of the proposed plants was compared with two conventional IGCC plants with and without CO_2 capture. The proposed plants included an advanced CO_2 capturing process based on the absorption enhanced reforming (AER) reaction and the regeneration of sorbent materials avoiding the need for a sulphur removal component, shift reactor, and/or a high temperature gas cleaning process. The results showed that the proposed CO_2 capture plants efficiencies were 18.5%–21% higher than the conventional IGCC plant. For the proposed plants, the CO_2 capture efficiencies were found to be within 95.8%–97%. The CO_2 capture efficiency for the conventional IGCC plant was 87.7%. The specific investment costs for the proposed plants were between 1207 and 1479€/kWe and 1620€/kWe and 1134€/kWe for the conventional plants with and without CO_2 capture, respectively. Overall, the proposed IGCC plants were cleaner, more efficient, and produced electricity at cheaper price than the conventional IGCC process (Mondol et al., 2009).

Economic analysis for IGCC plants is very complicated and uncertain because the technologies are not fully matured. The four commercialized IGCC plants—Tampa, Wabash, Buggenum, and Puertollano—were all started as demonstration plants. Thus, the experiences learned from these four plants are extremely valuable for advancing the technologies but might not be as helpful for the cost analysis. This is because the costs of materials and labor are constantly changing and new technologies are continuously implemented. This is compounded by current and potential future emissions policies and many other factors that can affect the international and domestic financial structures. Therefore, there have always been concerns about the uncertainty of the economic analyses associated with different kinds of IGCC plants (Wang, 2017).

Among many economic analyses for IGCC plants, the following 2013 report from the U.S. Department of Energy provides the most comprehensive. Basically, twelve power plant configurations were analyzed, including six IGCC cases utilizing the General Electric Energy (GEE), ConocoPhillips (CoP, E-Gas, now owned by Chicago Bridge & Iron (CB&I)), and Shell Global Solutions (Shell) gasifiers, each with and without CO_2 capture; four PC cases, two subcritical and two supercritical (SC), each with and without CO_2 capture; and two natural gas combined cycle (NGCC) plants, both with and without CO_2 capture. The net power output ranged from 500 to 750 MW. The capacity factor (CF), defined as the fraction of the annual available day of the power plant, was 80% for the IGCC cases and 85% for the PC and NGCC cases. The CO_2 capture efficiency was about 90%. The cost for coal was US$1.55/GJ ($1.64/Million Btu) for coal (Illinois No. 6) and US$6.21/GJ ($6.55/Million Btu) for natural gas, both on higher heating value (HHV) basis in 2007 USD. The 2013 analyses were

further updated in 2015 (US DOE, 2015a,b). The fuel prices were adjusted to US$2.78/GJ ($2.94/Million Btu) for Illinois No. 6 coal and US$5.81/GJ ($6.13/Million Btu) for natural gas, both on an HHV basis in 2011 US dollars. It is interesting to show the earlier results side by side with the updated results for comparison, as indicated in Fig. 15.10. Indeed, Fig. 15.10A shows the net plant efficiency (HHV). The IGCC plant using the dry-fed Shell gasifier had the highest efficiency 42.1% (HHV) in comparison with the slurry-fed GE or E-Gas gasifiers. However, the Shell case was penalized more—a reduction of about 11 percentage

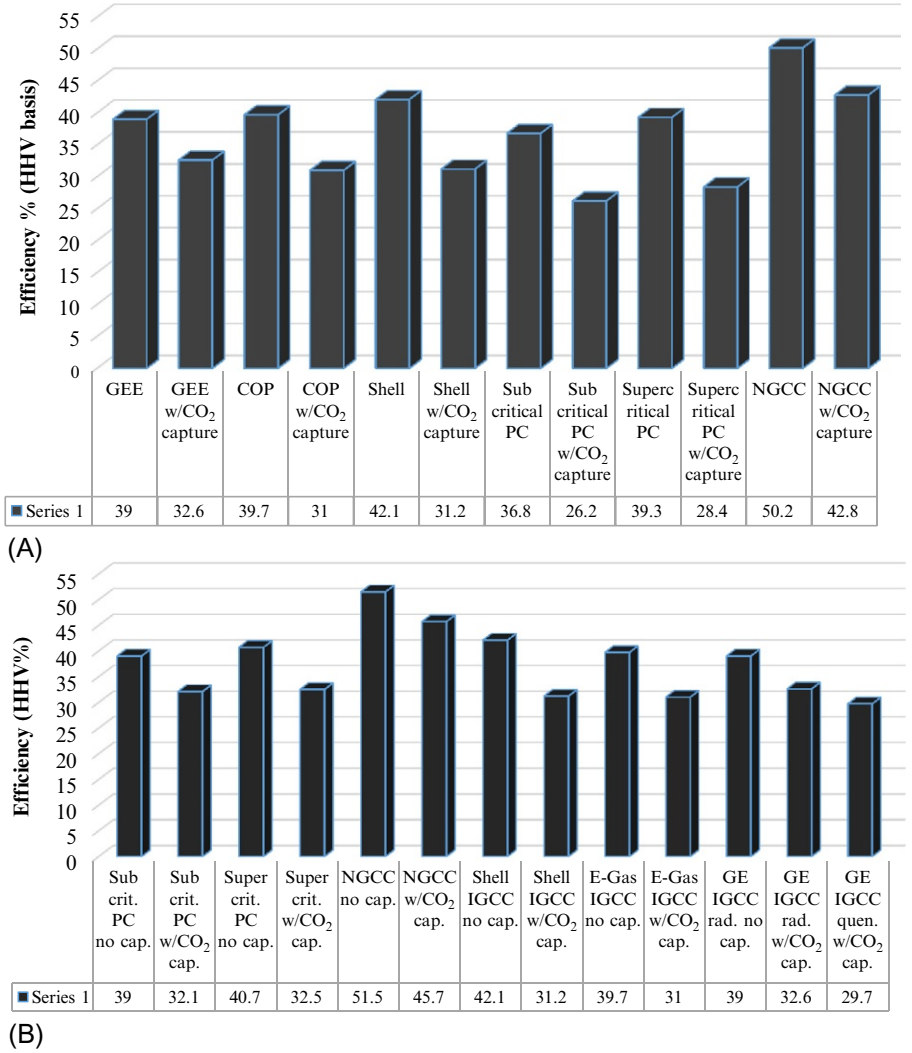

Fig. 15.10
Comparison of net plant thermal efficiency (HHV) with and without CO_2 capture. (A) from US DOE (2013) and (B) from US DOE (2015).

points of efficiency—by CO_2 capture than the slurry-fed GE or E-Gas processes, which only lost 7–8 percentage points of efficiency. The penalty for employing postcombustion carbon capture was about 10–11 percentage points of efficiency reduction for sub- and supercritical PC plants and 7.4 percentage points for NGCC plants. A comparison between the 2013 and 2015 analyses (Fig. 15.10A vs. Fig. 15.10B) illustrates that there were not many changes in efficiency of the identical plants (Wang, 2017).

Moreover, as shown in Fig. 15.11, the capital cost ($/kW) for building different power plants with and without carbon capture in terms of total overnight cost (TOC) and total as-spent cost

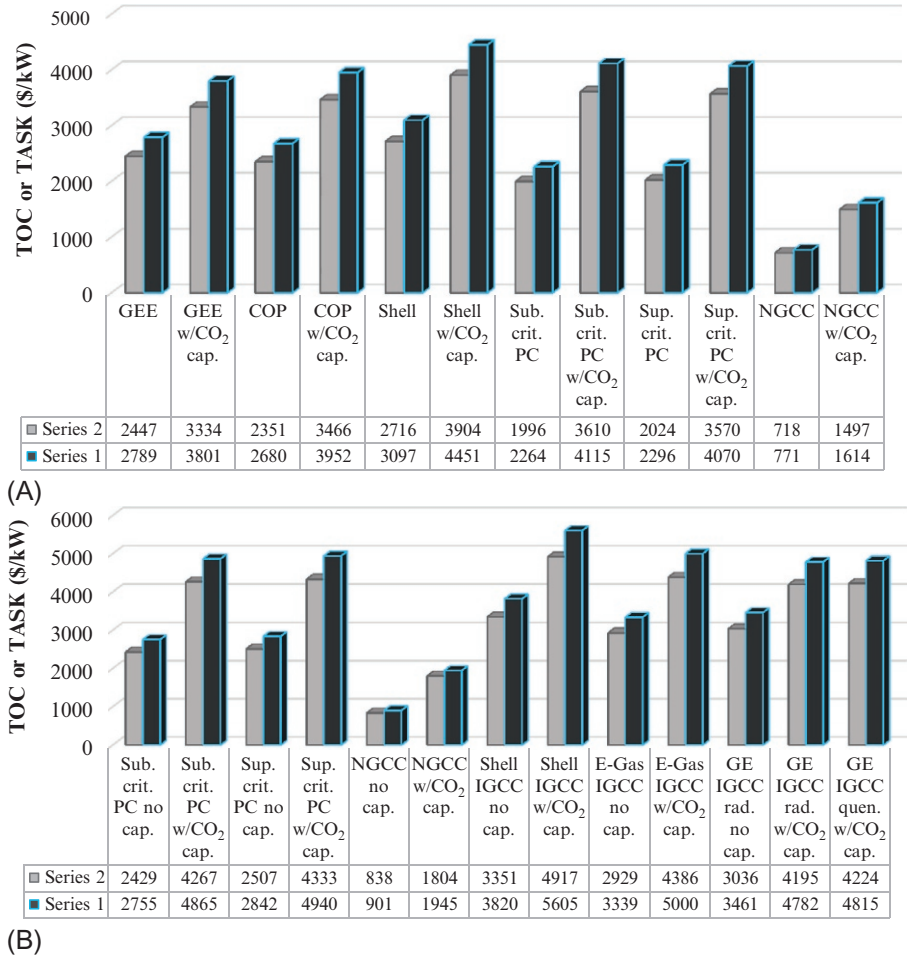

Fig. 15.11

(A) Comparison of capital cost ($/kW) in terms of total as-spent cost (TASC Series 1) and total overnight cost (TOC – Series 2). (Note: TOC is expressed in 2007 dollars. TASC is expressed in mixed-year 2007–2011 year dollars for coal plants and 2007–2009 mixed-year dollars for NGCC plants.) (US DOE, 2013). (B) Comparison of capital cost ($/kW) in 2011 USD (US DOE, 2015).

(TASC) were compared. The total plant cost (TPC) included all equipment (complete with initial chemical and catalyst loadings), materials, labor (direct and indirect), engineering and construction management, and contingencies (process and project). The TOC was calculated by adding the owner's costs to the TPC. Escalation and interest on debt incurred during the capital expenditure period were estimated and added to the TOC to calculate the TASC.

Cormos et al. (2015), considered an IGCC system, in which coal was used only as feedstock in Case 1, coal in addition with sawdust (80/20% wt. blending ratio) was used for Case 2, coal in addition with meat and bone meal (80/20% wt. blending ratio) was sued for Case 3, coal in addition with municipal solid waste (80/20% wt. blending ratio) was used for Case 4, coal in addition with sewage sludge (80/20% wt. blending ratio) was used for Case 5, and coal in addition with waste paper (80/20% wt. blending ratio) was used for Case 6. About 90% value was considered for carbon dioxide capturing in each case and some of the most important results is noted in Table 15.5.

Meanwhile, as an economic aspect, Brouwer et al., in 2015, investigated operational flexibility and economics of power plants in future low-carbon power systems. Several parameters for IGCC, NGCC, PC (-CCS), and GT (gas turbine) were reported. The minimum load level is the lowest level at which a power plant can operate for an extended time whilst meeting emission limits, expressed as a percentage of the maximum capacity. The ramp rate is the average speed at which power output can be increased or decreased between the minimum and maximum load levels, expressed as a % of the maximum capacity per minute. The startup time is defined as the time it takes from turn-on to reach the minimum load level. Startup costs consist of a number of components. Depending on the definition used, only the direct costs are included (the narrow definition) or also indirect costs (the broad definition) (Brouwer et al., 2015). As reported in Table 15.6, flexibility parameters of various power plants are summarized.

4.1 Membrane Process Role in Economics of the IGCC Plant

Merkel et al., in 2012, presented a carbon dioxide capture unit with membranes in the IGCC power plant, in which, CO_2-permeable membranes were used with less membrane area, but slightly more compression power than the hydrogen-selective membrane. Regarding their reports, in comparison to the Selexol plant, both used membrane processes that presented slightly less total energy. Indeed, the real difference of Selexol plant is in the expected plant cost. The total cost of the membrane units including CO_2 compression is about 50% of those of a Selexol plant. The cost differential is due mainly to the simple flow scheme of the membrane processes compared to the more complex Selexol system, which uses a number of large high-pressure columns (see Table 15.7). The net result is that the increase in the levelized cost of electricity (LCOE) for 90% CO_2 capture is about 20% for the two membrane

Table 15.5 Overall plant performance indicators (precombustion capture) for each assumed cases

Main plant data	Units	Case 1	Case 2	Case 3	Case 4	Case 5	Case 6
Solid fuel flowrate (as received)	kg/h	165704	180.455	168.453	187.400	192.000	182.900
Gasification island power consumption	MW_e	8.08	8.27	8.11	8.35	8.59	8.23
Power island power consumption	MW_e	19.00	19.05	18.95	19.05	19.11	18.62
Total ancillary power consumption (E)	MW_e	111.87	112.99	110.68	113.99	119.13	112.01
Net electric power output (F = D − E)	MW_e	420.41	421.93	420.23	421.72	420.70	422.93
Carbon capture rate	%	92.35	92.83	92.24	93.02	93.57	92.26
CO_2 specific emissions	kg/MWh	76.12	71.19	72.23	70.68	68.29	78.11
Total investment cost	MM€	1102.31	1131.33	1092.95	1148.21	1178.61	1133.75
Total investment cost per kW gross	€/kW	2070.92	2114.95	2058.63	2143.34	2183.31	2119.40
Total investment cost per kW net	€/kW	2621.99	2681.31	2600.83	2722.69	2801.55	2680.71
Total fixed O&M costs (year)	M€/y	38.22	39.03	38.06	39.48	40.17	39.12
Total fixed O&M costs (kWh net)	€/kWh	0.01212	0.01233	0.01208	0.01248	0.01273	0.01233
Total variable O&M costs (year)	M€/y	79.18	73.95	135.79	74.24	85.35	94.51
Total variable O&M costs (kWh net)	€/kWh	0.02511	0.02337	0.04309	0.02347	0.02705	0.02980
Total fixed and variable costs (year)	M €/y	117.40	112.98	113.72	173.85	125.52	133.63
Total fixed and variable costs (kWh net)	€/kWh	0.03723	0.03570	0.05517	0.003595	0.03978	0.04213

Table 15.6 Flexibility parameters of power plants per technology

Technology	Minimum load (% of max capacity)	Ramp rate (% of max capacity (min))	Startup time (h)			Startup cost (€/MW installed per start)		
Decade of commissioning			Hot start	Warm start	Cold start	Hot start	Warm start	Cold start
PC(-CCS)								
2000	40±10	2.5±1.5	2±0.5	4±1	8±2	39±12	46±14	75±23
2010	35±10	4±2	2±0.5	4±1	8±2	39±12	46±14	75±23
2020	25±10	5±2	2±0.5	4±1	8±2	39±12	46±14	75±23
2030	20±10	6±2	2±0.5	4±1	8±2	39±12	46±14	75±23
IGCC								
2000	50±10	2.5±2	6±2	n/a	90±10	n/a	n/a	n/a
2010	50±10	3±2	6±2	n/a	90±10	n/a	n/a	n/a
2020	45±10	4±2	5±2	n/a	90±10	n/a	n/a	n/a
2030	40±10	4±2	5±2	n/a	90±10	n/a	n/a	n/a
NGCC(-CCS)								
2000	45±10	5±3	2±0.5	3±0.5	4±1	27±11	39±20	57±29
2010	45±10	6±2	1±0.5	2±0.5	3±1	27±11	39±20	57±29
2020	40±15	7±2	1±0.25	2±0.5	3±1	27±11	39±20	57±29
2030	25±10	9±2	1±0.25	2±0.5	3±1	27±11	39±20	57±29
GT								
2000	40±15	15±5	0.25	0.25	0.5	13±6	16±8	23±12
2010	40±15	15±5	0.25	0.25	0.5	13±6	16±8	23±12
2020	35±15	15±5	0.25	0.25	0.5	13±6	16±8	23±12
2030	20±10	20±5	0.25	0.25	0.5	13±6	16±8	23±12

Table 15.7 Comparison of energy use and capital costs for CO_2 capture from a 556 MWe IGCC plant using Selexol and various CO_2-selective and hydrogen-selective membrane processes (cost basis is 2007 US$) (Merkel et al., 2012)

System parameter (unit)	Selexol + CO_2 com.	CO_2 selective membrane	H_2 selective membrane
Compression power (MWe)	31	31	18
Refrigeration or steam (MWe)	19	14	20
Total power (MWe)	50	45	38
Membrane area (m^2)	–	16,000	25,000
Membrane or Selexol equipment cost ($ million)	74	8	12.5
Compression and/or refrigeration equipment cost ($ million)	18	45	48
Bare erected plant cost ($ million)	166	88	100
Engineering fees ($ million)	16	8	9
Contingencies ($ million)	69	21	26
Total plant cost ($ million)	252	117	135
Estimated increase in LCOE (%)	31	20	21

designs, compared to 30% for Selexol. It is noted that cost estimates at this conceptual stage typically have an accuracy of ±30% (Merkel et al., 2012).

Furthermore, several studies have been based on the technical and economic feasibility of membrane-based pulverised coal combustion PCC. Flue gas after desulfurization (FGD) in a typical coal-based power plant is humid and at close to 1 atm pressure and 50–60°C with CO_2 and N_2 concentrations at 10%–15% and close to 70%, respectively. The low CO_2 partial pressure of 0.1–0.15 bar implies an inherently low driving force for CO_2 transport. Permeability and selectivity are two main parameters of membranes in this application. The most important problem in membrane application in IGCC–PCC is the tradeoff between selectivity and permeability. To overcome this problem, recycling the retentate will provide a high recovery of product and high purity. Researchers have shown that a higher CO_2/N_2 selectivity (>100) is required to achieve high CO_2 purities ($>90\%$ purity).

Detailed economic analysis targeted toward achieving the DOE cost targets shows that a purely membrane-based simpler air-sweep process can achieve the targets at a CO_2/N_2 selectivity of about 150 and a CO_2 permeance of 3000 GPU (1 GPU = 3.35 3×10^{-10} mol/(m^2 s Pa)) at the flue gas feed pressure of about 1 atm (Ramasubramanian et al., 2013).

As noted previously, ITM systems can be used in the IGCC process for supplementing the required oxygen. Table 15.8 indicates the cost and performance comparison for the cryogenic based system and the ITM oxygen-integrated IGCC facility (Safdarnejad et al., 2015). Regarding their results, the cryogenic plant consumes 3180 TPD of Illinois coal and 2565 TPD of oxygen (purity 95%), whilst the ITM Oxygen-integrated plant consumes 3176 TPD of Illinois coal and 2420 TPD of oxygen (purity 99+%). The ITM Oxygen plant, including the supplemental air compressor, the additional combustor, ITM Oxygen modules, oxygen coolers, oxygen compressors, and the cryogenic nitrogen plant, saves 31% of the installed cost for air separation equipment. In fact, the economic benefits of ITM Oxygen technology for the IGCC plant are a 2.9% improvement in thermal efficiency with a 6.5% decrease in the cost of generated electric power. The efficiency increase also produces a concomitant reduction in carbon dioxide and sulfur emissions. Therefore, integration of ITM Oxygen technology with IGCC offers the benefits of further improving system efficiency, resulting in better environmental performance and lower costs (Schwarz et al., 2001).

On the other hand, Kaldis et al., in 2004, investigated the energy and capital cost analysis of CO_2 capture in coal IGCC processes via gas separation membranes. In this study, the use of a hybrid coal IGCC system, consisting of a gasifier, a shift reactor, and a membrane separator, was examined. Two alternative separation options were studied: (a) low temperature separation, using polymer membranes, and (b) high temperature separation, by ceramic membranes. Single and multistage separation were examined for operation at 16 and 23 bar. The energy and cost analysis of the alternative cases showed that CO_2 removal in this hybrid IGCC scheme is technically feasible. Incorporation of shift reaction and membrane separators results in an energy penalty of 8%–14% units, depending on pressure and staging, and an increased capital cost, especially for the ceramic membranes. However, this technology would permit reduction of CO_2 emissions exceeding 50%, compared to conventional IGCC. Some of the results of this study are presented in Table 15.9 (Kaldis et al., 2004).

Table 15.8 Benefits of ITM Oxygen for the IGCC application

	Cryogenic O_2 case	ITM O_2 case	Delta	% Change
IGCC facility capital investment ($million)	641	610	31	4.8
IGCC facility capital investment ($/kW)	1567	1453	114	7.3
Power production (MW)	409	420	11	2.7
Thermal efficiency (%HHV)[a]	45.2	46.5	1.3	2.9
Cost of electricity (mills/kWh)	55.5	51.9	3.6	6.5

[a]Higher heating value.

Table 15.9 Capital cost analysis for IGCC-shift-membranes process

	Base case (w/o shift) (M $)		Polymer membranes (M $)				Ceramic membranes (M $)			
			$P = 16$ bar		$P = 23$ bar		$P = 16$ bar		$P = 23$ bar	
Equipment	$P = 16$ bar	$P = 23$ bar	One stage	Multistage	One stage	Multistage	One stage	Multistage	One stage	Multistage
Heat exchangers	10.8	10.10	21.8	24.2	18.8	21.2	19.8	23.8	18.0	20.6
Cyclones	110.0	110.0	110.0	110.0	110.0	110.0	110.0	110.0	110.0	110.0
Compressors	42.3	50.3	54.0	61.9	63.8	73.1	65.0	71.0	76.8	90.7
Turbines	34.2	38.1	30.5	36.2	36.9	44.2	34.5	39.7	41.7	50.6
Gasifier	0.7	0.7	0.7	0.7	0.7	0.7	0.7	0.7	0.7	0.7
Membranes	–	–	111.0	591.9	76.0	503.1	810.0	1188.0	540.0	859.5
Shift reactor	–	–	2.0	2.0	2.2	2.2	2.0	2.0	2.2	2.2
Total Equipment cost	198.0	209.1	330.0	826.9	308.4	754.5	1042	1435	789.4	1134
Capital investment cost	545.5	576.1	909.2	2278	849.7	2079	2871	3954	2175	3125
Specific capital investment ($/kW)	1240	1263	2851	6521	2591	5700	9284	11,491	6837	8891

5 Conclusion and Future Trends

In present study, a process for satisfying variable power demand and a method for maximizing the monetary value of a synthesis gas stream of methanol production were disclosed. As a general consequence, in the IGCC plant equipped with methanol production unit, the power-producing zone and the methanol production zone operated cyclically and substantially out of phase in which one or more of the combustion turbines are shut down during a period of off-peak power demand and the syngas fuel diverted to the methanol producing zone. Membrane processes, as one of the most promising separation technologies, indicated that they can improve the efficiency of the IGCC plant and methanol production capacity. This out of phase cyclical operational procedure maximized electricity output with high thermodynamic efficiency and maximized methanol production with high stoichiometric efficiency. In this case, it seems that the economic potential of the combined power and methanol producing zones is enhanced. On the other hand, it was evident that applying H_2-selective and CO_2-selective membranes in the IGCC plants for separation of syngas can increase the economic potential of coproduction of electricity energy and methanol strategy. However, upgrading the membrane performance for H_2 and CO_2 separation in industrial scale is one of the main challenges of this way.

References

Aaron, D., Tsouris, C., 2005. Separation of CO_2 from flue gas: a review. Separ. Sci. Technol. 40 (1-3), 321–348.
Baker, R.W., 2000. Membrane technology. Wiley Online Library, United States.
Beér, J.M., 2007. High efficiency electric power generation: the environmental role. Prog. Energy Combust. Sci. 33 (2), 107–134.
Brouwer, A.S., et al., 2015. Operational flexibility and economics of power plants in future low-carbon power systems. Appl. Energy 156, 107–128.
Carbo, M.C., et al., 2006. Advanced membrane reactors in IGCC: H_2 or CO_2 separation. In: Fifth Annual Conference on Carbon Capture and Sequestration, Virginia.
Carpenter, S.M., Long, H.A., 2017. Integration of carbon capture in {IGCC} systems. In: Integrated Gasification Combined Cycle (IGCC) Technologies. Woodhead Publishing, United Kingdom, pp. 445–463.
Chiesa, P., et al., 2005. Co-production of hydrogen, electricity and CO_2 from coal with commercially ready technology. Part A: performance and emissions. Int. J. Hydrog. Energy 30 (7), 747–767.
Chiesa, P., Consonni, S., 1998. Shift reactors and physical absorption for low-CO_2 emission IGCCs. In: ASME 1998 International Gas Turbine and Aeroengine Congress and Exhibition. V003T08A026.
Chiesa, P., Kreutz, T.G., Lozza, G.G., 2007. CO_2 sequestration from IGCC power plants by means of metallic membranes. J. Eng. Gas Turbines Power 129 (1), 123–134.
Christou, C., Hadjipaschalis, I., Poullikkas, A., 2008. Assessment of integrated gasification combined cycle technology competitiveness. Renew. Sust. Energ. Rev. 12 (9), 2459–2471.
Cormos, A.-M., Dinca, C., Cormos, C.-C., 2015. Multi-fuel multi-product operation of IGCC power plants with carbon capture and storage (CCS). Appl. Therm. Eng. 74, 20–27.
Dahlquist, E., 2013. Technologies for Converting Biomass to Useful Energy: Combustion, Gasification, Pyrolysis, Torrefaction and Fermentation. CRC Press, Boca Raton, FL.

Dyer, P.N., et al., 2000. Ion transport membrane technology for oxygen separation and syngas production. Solid State Ionics 134 (1), 21–33.
Emun, F., et al., 2010. Integrated gasification combined cycle (IGCC) process simulation and optimization. Comput. Chem. Eng. 34 (3), 331–338.
Farsi, M., Jahanmiri, A., 2012a. Dynamic modeling of a H_2O-permselective membrane reactor to enhance methanol synthesis from syngas considering catalyst deactivation. J. Nat. Gas Chem. 21 (4), 407–414.
Farsi, M., Jahanmiri, A., 2012b. Application of water vapor-permselective alumina–silica composite membrane in methanol synthesis process to enhance CO_2 hydrogenation and catalyst life time. J. Ind. Eng. Chem. 18 (3), 1088–1095.
Farsi, M., Jahanmiri, A., 2011. Methanol production in an optimized dual-membrane fixed-bed reactor. Chem. Eng. Process. Process Intensif. 50 (11), 1177–1185.
Favre, E., 2007. Carbon dioxide recovery from post-combustion processes: can gas permeation membranes compete with absorption? J. Membr. Sci. 294 (1), 50–59.
Ghasemzadeh, K., Basile, A., Tilebon, S.M.S., 2015. Membranes for IGCC power plants. In: Integrated Membrane Systems and Processes. John Wiley & Sons, Ltd., Oxford. p.255.
Ghasemzadeh, K., Tilebon, S.M.S., Basile, A., 2016. Membrane reactors for hydrogen production from biomass-derived oxygenates. In: Membrane Technologies for Biorefining. Woodhead Publishing, United Kingdom, p. 435.
Grainger, D., Hägg, M.-B., 2008. Techno-economic evaluation of a PVAm CO_2-selective membrane in an IGCC power plant with CO_2 capture. Fuel 87 (1), 14–24.
Gray, D.D., 2017. Major gasifiers for (IGCC) systems. In: Integrated Gasification Combined Cycle (IGCC) Technologies. Woodhead Publishing, United Kingdom, pp. 305–355.
Huang, J., Zou, J., Ho, W.S.W., 2008. Carbon dioxide capture using a CO_2-selective facilitated transport membrane. Ind. Eng. Chem. Res. 47 (4), 1261–1267.
Huth, M., et al., 2000. Operation experiences of Siemens IGCC gas turbines using gasification products from coal and refinery residues. In: ASME Turbo Expo 2000: Power for Land, Sea, and Air. V002T01A011.
Ionescu, G., et al., 2013. Integrated municipal solid waste scenario model using advanced pretreatment and waste to energy processes. Energy Convers. Manag. 76, 1083–1092.
Kaldis, S.P., Skodras, G., Sakellaropoulos, G.P., 2004. Energy and capital cost analysis of CO_2 capture in coal IGCC processes via gas separation membranes. Fuel Process. Technol. 85 (5), 337–346.
Ku, A.Y., et al., 2011. Membrane performance requirements for carbon dioxide capture using hydrogen-selective membranes in integrated gasification combined cycle (IGCC) power plants. J. Membr. Sci. 367 (1–2), 233–239.
Laugwitz, A., Gräbner, M., Meyer, B., 2011. Availability analysis of integrated gasification combined cycle (IGCC) power plants. In: Power Plant Life Management and Performance Improvement. Woodhead Publishing, United Kingdom, pp. 110–142.
LeBlanc, O.H., et al., 1980. Facilitated transport in ion-exchange membranes. J. Membr. Sci. 6, 339–343.
Leidich, F.U., et al., 2005. Development of a lignite-fired power plant concept with integrated pressurised fluidised-bed drying and fuel cells. Int. J. Energy Technol. Policy 3 (1–2), 39–49.
Li, T., et al., 2013. Carbon dioxide selective mixed matrix composite membrane containing ZIF-7 nano-fillers. J. Membr. Sci. 425, 235–242.
Merkel, T.C., Zhou, M., Baker, R.W., 2012. Carbon dioxide capture with membranes at an IGCC power plant. J. Membr. Sci. 389, 441–450.
Mondol, J.D., et al., 2009. Techno-economic evaluation of advanced IGCC lignite coal fuelled power plants with CO_2 capture. Fuel 88 (12), 2495–2506.
Quinn, R., Appleby, J.B., Pez, G.P., 1995. New facilitated transport membranes for the separation of carbon dioxide from hydrogen and methane. J. Membr. Sci. 104 (1–2), 139–146.
Ramasubramanian, K., Zhao, Y., Winston Ho, W.S., 2013. CO_2 capture and H_2 purification: Prospects for CO_2-selective membrane processes. AIChE J. 59 (4), 1033–1045.
Ratafia-Brown, J.A., et al., 2002. An environmental assessment of IGCC power systems. In: Nineteenth Annual Pittsburgh Coal Conference, p. 27.

Rezvani, S., et al., 2009. Comparative assessment of coal fired IGCC systems with CO_2 capture using physical absorption, membrane reactors and chemical looping. Fuel 88 (12), 2463–2472.
Rhodes, J.S., Keith, D.W., 2005. Engineering economic analysis of biomass IGCC with carbon capture and storage. Biomass Bioenergy 29 (6), 440–450.
Rodenas, T., et al., 2014. Visualizing MOF mixed matrix membranes at the nanoscale: towards structure-performance relationships in CO_2/CH_4 separation over NH2-MIL-53 (Al)@ PI. Adv. Funct. Mater. 24 (2), 249–256.
Romeo, L.M., Bolea, I., Escosa, J.M., 2008. Integration of power plant and amine scrubbing to reduce CO_2 capture costs. Appl. Therm. Eng. 28 (8), 1039–1046.
Rubin, E.S., Chen, C., Rao, A.B., 2007. Cost and performance of fossil fuel power plants with CO_2 capture and storage. Energy Policy 35 (9), 4444–4454.
Sadati Tilebon, S.M., et al., 2015. Hydrogen production: overview of technology options and membrane in auto-thermal reforming including partial oxidation and steam reforming. Int. J. Membr. Sci. Technol. 2 (1), 56–67.
Safdarnejad, S.M., Hedengren, J.D., Baxter, L.L., 2015. Plant-level dynamic optimization of cryogenic carbon capture with conventional and renewable power sources. Appl. Energy 149, 354–366.
Schwarz, H.-H., Apostel, R., Paul, D., 2001. Membranes based on polyelectrolyte-surfactant complexes for methanol separation. J. Membr. Sci. 194 (1), 91–102.
Shekhawat, D., Luebke, D.R., Pennline, H.W., 2003. A review of carbon dioxide selective membranes. US Department of Energy, United States, pp. 9–11.
Shinada, O., Yamada, A., Koyama, Y., 2002. The development of advanced energy technologies in Japan: IGCC: a key technology for the 21st century. Energy Convers. Manag. 43 (9), 1221–1233.
US DOE, US Department of Energy (DOE), 2013. Cost and performance baseline for fossil energy plants volume 1: bituminous coal and natural gas to electricity, revision 2a, Report DOE/NETL-2010/1397.
US DOE, US Department of Energy (DOE), 2015a. Cost and performance baseline for fossil energy plants volume 1a: bituminous coal (PC) and natural gas to electricity, revision 3, Report DOE/NETL-2015/1723, July 6.
US DOE, US Department of Energy, 2015b. Cost and performance baseline for fossil energy plants volume 1b: bituminous coal (IGCC) to electricity-year dollar update, revision 2b, Report DOE/NETL-2015/1727, July 31.
Venna, S.R., Carreon, M.A., 2009. Highly permeable zeolite imidazolate framework-8 membranes for CO_2/CH_4 separation. J. Am. Chem. Soc. 132 (1), 76–78.
Vente, J.F., et al., 2006. On the full-scale module design of an air separation unit using mixed ionic electronic conducting membranes. J. Membr. Sci. 278 (1), 66–71.
Wang, T., 2017. An overview of IGCC systems. In: Integrated Gasification Combined Cycle (IGCC) Technologies. Woodhead Publishing, United Kingdom, pp. 1–80.
Wolfersdorf, C., Meyer, B., 2017. The current status and future prospects for IGCC systems. In: Integrated Gasification Combined Cycle (IGCC) Technologies. Woodhead Publishing, United Kingdom, pp. 847–889.
Yang, H., et al., 2008. Progress in carbon dioxide separation and capture: a review. J. Environ. Sci. 20 (1), 14–27.
Zanganeh, K.E., Shafeen, A., Salvador, C., 2009. CO_2 capture and development of an advanced pilot-scale cryogenic separation and compression unit. Energy Procedia 1 (1), 247–252.
Zhang, X., et al., 2013. Carbon chain analysis on a coal IGCC—CCS system with flexible multi-products. Fuel Process. Technol. 108, 146–153.
Zhang, Y., Wang, Z., Wang, S.C., 2002. Selective permeation of CO_2 through new facilitated transport membranes. Desalination 145 (1–3), 385–388.
Zornoza, B., et al., 2011. Functionalized flexible MOFs as fillers in mixed matrix membranes for highly selective separation of CO_2 from CH_4 at elevated pressures. Chem. Commun. 47 (33), 9522–9524.
Zou, J., Ho, W.S.W., 2006. CO_2-selective polymeric membranes containing amines in crosslinked poly (vinyl alcohol). J. Membr. Sci. 286 (1), 310–321.
Zou, J., Huang, J., Ho, W.S.W., 2007. CO_2-selective water gas shift membrane reactor for fuel cell hydrogen processing. Ind. Eng. Chem. Res. 46 (8), 2272–2279.

CHAPTER 16

Which Future Route in the Methanol Synthesis? Photocatalytic Reduction of CO_2, the New Challenge in the Solar Energy Exploitation

Lorenzo Spadaro[*,†], **Francesco Arena**[*,†], **Alessandra Palella**[*]

[*] *Institute for Advanced Energy Technologies "Nicola Giordano" (ITAE-CNR), Messina, Italy*
[†] *University of Messina, Messina, Italy*

Acronyms

ATP	adenosine-triphosphate
BG	band gap
CB	conduction band
CST-Pr	continuous stirred tank photoreactors
CSTR	continuous stirred tank reactors
HER	hydrogen evolution reaction
HOMO	highest occupied molecular orbital
LDH	layered double hydroxide
LUMO	lowest unoccupied molecular orbital
LPG	liquefied petroleum gas
NADPH	nicotinamide-adenine-dinucleotide-phosphate
NHE	normal hydrogen electrode
QDs	quantum dots
PB-Pr	packed-bed photoreactors
PCET	proton-coupled electron transfer
PGA	poly-galacturonic acid
PME	pectin methylesterase enzyme
PSII	photosystem II
UV	ultraviolet
UVA	ultraviolet A

Methanol. https://doi.org/10.1016/B978-0-444-63903-5.00016-9

UVC ultraviolet C
VB valence band
Vis visible

Symbols

$\mathbf{A}^-$ anion
$\mathbf{D}^+$ cation
d_{vs} average diameter of the bubble
$\mathbf{e}^-$ electron
ΔE° standard potential (V)
E_{app} apparent activation energy (kJ/mol)
F Faraday's constant, 96,485 (C/mol)
ΔG° Gibbs's free energy (kJ/mol)
ΔH° enthalpy (kJ/mol)
$\mathbf{h}^+$ hole
h Plank constant, 6.63 (J s)
K equilibrium constant
n number of electron per mole of product
ΔS° entropy (J/mol K)
ν light frequency (Hz)
ξ gas hold-up coefficient

1 Introduction

Methanol is a very important chemical intermediate widely used in many industrial manufacture processes (Larson and Tingjin, 2003; Liu et al., 2003; Song, 2006; Wang et al., 2011). It is a valuable fuel alternative to LPG (Liquefied Petroleum Gas), gasoline, and gas oil (Fiedler et al., 2000; Larminie and Dicks, 2003; Olah et al., 2009; Pontzen et al., 2011), and in perspective, it is an energy carrier better than hydrogen, because of much easier handling, storage, and transportation issues.

Therefore, also in consideration of evident environmental benefits, the potential use of CO_2 as a carbon-source for the synthesis of methanol has attracted a great scientific attention in recent years (Arena et al., 2014; Pérez-Fortes et al., 2016). However, the use of CO_2 as a raw material is currently hindered by poor hydrogen production from renewable sources and thermodynamic stability, requiring high energy inputs to attain appreciable conversion levels into chemicals (Arena et al., 2014). Therefore, even if "renewable hydrogen" (Rossi and Nicolini, 2012) could turn industrial concerns into hydrogenation processes, the photocatalytic conversion using water as a "reagent" and sunlight as an energy source looks like a simple and attractive route to obtain CH_3OH from CO_2.

Although the biomass conversion can be considered as an indirect utilization of the solar source, the commercial exploitation of the sun is still addressed to the energetic purposes by the photovoltaic and solar-thermal sectors. As is well known, the energy which reaches Earth from the sun is impressively high, and in fact it represents more than 100 times greater than that is necessary for human needs. In particular, at 40 degrees of latitude, the radiated power in summer is about 600 W/m^2, which means a net power of 4.8 kW/m^2 in 8 h of full solar exposition, which is equivalent to the energy generated by approximately 0.5 L of gasoline in a thermal engine. On the other side, the exploitation of solar energy requires huge spaces and investment costs for the large-scale conversion, due to poor conversion efficiency (10%–30%) into thermal or electrical forms. As an example, for a family home with a photovoltaic roof of less than 100 m^2, if it is well exposed (or exposed to south), it may provide less than 50% of the energy needed in winter. All this data renders the photochemical conversion of CO_2 to methanol particularly attractive from both scientific and practical points of view (*methanol-based economy*).

Since the pioneering work of Inoue et al. (1979), a great research concern has been focused on solar fuels obtained by photosynthetic processes using CO_2. However, the direct conversion of solar energy into methanol is still quite challenging, due to the low efficacy of the photoconversion process, which is also accompanied by a lack of selectivity. In fact, the photocatalytic process involves not only the activation and reduction of the thermodynamically stable CO_2 molecule but also proton transfers and hydrogenation reactions (Yuan and Xu, 2015). Hence, two alternative strategies are currently being pursued to overcome such drawbacks; namely, the development of high "quantum-yield" photocatalysts, and the photoreactor optimization to improve the light transmission efficiency (Ola and Maroto-Valer, 2015a).

With particular regard to photocatalytic materials, several metal oxide semiconductors, such as TiO_2 (Tahir and Amin, 2013), ZnO (Guo et al., 2016), CdS (Liu et al., 1998; Navalón et al., 2013) and others, have been explored in the direct CO_2 photoconversion. Among these, TiO_2 is generally considered the best semiconductor because of its nontoxicity, low cost, and stability. Nevertheless, its solar energy conversion efficiency is limited by a band gap of 3.2 eV, corresponding to a maximum absorption in the UV region being only c.3% of the sunlight spectrum (Carp et al., 2004). Thus, dye sensitisation (Zhao et al., 2009), doping (Li et al., 2016; Zhang et al., 2015), and oxygen-defect generation (He et al., 2016; Tan et al., 2016) are the approaches adopted to improve the light absorption capacity and the photoreactivity of TiO_2 samples. As a rule, metal doping improves the charge carrier separation and lifetime, favoring higher conversion of adsorbed species (Tseng and Wu, 2005; Ola and Maroto-Valer, 2014; Slamet et al., 2005). In fact, Tseng and Wu (2005) argued that copper acts as an electron trap that prevents the electron-hole pair recombination, attaining methanol yields of 20 μmol/g h and 0.3 μmol/g h, using a 2% Cu/TiO_2 catalyst under UVC and UVA

irradiation, respectively. Recently, Paulino et al. (2016) investigated the influence of both CuO and ZnO deposition on the photoactivity of TiO_2 prepared by slow-hydrolysis technique, pointing out that the two promoters enhance the CH_4 formation rate from c.5 to 8 μmol/g h.

Different aspects of the CO_2 photoreduction process are still under debate. In particular, the effects of process conditions are strongly disputed, while the key factors governing product distribution are still unclear (Tseng et al., 2002). Generally, the CO_2 photoreduction in aqueous medium leads to methanol as a main product over Cu/TiO_2 photocatalysts under UV radiation (Spadaro et al., 2013; Tseng et al., 2004; Tseng and Wu, 2005; Wang et al., 2014), while Ola and Maroto-Valer (2015b, 2016) observed the formation of hydrogen, methanol, acetaldehyde, and ethanol over metal-doped TiO_2 materials deposited on quartz plates under batch conditions. The same authors indicated the prevalent formation of gas phase CH_4 and acetaldehyde, using optical fibers coated with metal/TiO_2 monoliths under continuous flow.

The configuration of the photoreactor can strongly influence the photocatalytic efficiency. In particular the relevance of the photoreactor design is substantiated by Wang et al (2010b) who performed the photocatalytic reduction of CO_2 over Pd-Rh/TiO_2 photocatalysts in fixed bed configuration, reaching a methanol yield one order of magnitude higher than that obtained in aqueous medium.

Therefore, advances in the photocatalytic CO_2 conversion deserve systematic efforts in the fields of material science and reactor engineering in order to make the process economically practical and industrially scalable.

2 Mimic Mather Nature Work: Methanol From Photosynthesis Processes

2.1 Natural Photosynthesis

Photosynthesis is a natural process driving chemical reactions or processes occurring under the catalytic effect of chemical species that come to be activated by photons with adequate energy. The cycle of *chlorophyll* is the most important and known example of natural photosynthesis, responsible for plant growth; plants take various nutrients and water mostly from the soil, and carbon dioxide from the atmosphere, transforming them into glucose and oxygen, which produces wood-cellulose for the development of roots, trunks, and leaves.

As shown in Fig. 16.1, photosynthesis represents the natural way to store the solar energy by producing organic compounds from H_2O and CO_2 as glucose (Eq. 16.1):

$$6CO_2 + 6H_2O + \text{sun light} \rightarrow C_6H_{12}O_6 + 6O_2 \tag{16.1}$$

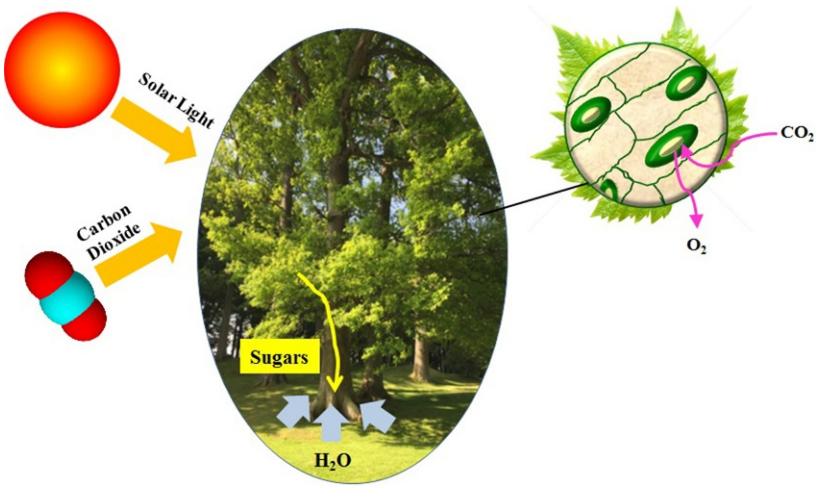

Fig. 16.1
Representation of the plant growth.

The required electrons for the synthesis are generated through several redox cycles, involving various chemical species. Namely, the solar energy promotes the evolution of oxygen by water oxidation, generating protons and electrons, which in turn produce hydrogen and reduce CO_2 into products of adequate redox potential (i.e., sugars, carbohydrates, and lipids). In particular, this process involves two cyclic reactions inside of the chloroplast of the green plant. Namely, the chlorophyll pigment captures the solar energy, then it converts and stores this energy through the use of ATP (Adenosine-triphosphate) and NADPH (Nicotinamide-Adenine-Dinucleotide-Phosphate) molecules and, in turn, releases oxygen and protons by the water splitting process. In a second concerted cycle, the atmospheric CO_2 is then reduced to glucose in a dark reaction (Calvin cycle), using hydrogen atoms carried via NADPH source (Lee et al., 2013).

Plants have developed different mechanisms and functionalities which symbiotically work to perform the photosynthetic process (Concepcion et al., 2012; Gust et al., 2009), as shown in Fig. 16.2.

An "Antenna" system selects the light of the appropriate wavelength and carries its energy in the place where electrons and charges are formed. In respect to this, the action of ATP in combination with several enzymes is fundamental for the energy transportation and the generation of trans-membrane proton gradients, realized through several reduction mechanisms. The photosystem II (PSII) reaction center drives the splitting of water into O_2 and protons by the capture of four photons, while the NADPH molecule triggers the reduction of H^+ and CO_2 (Nikokavoura and Trapalis, 2017).

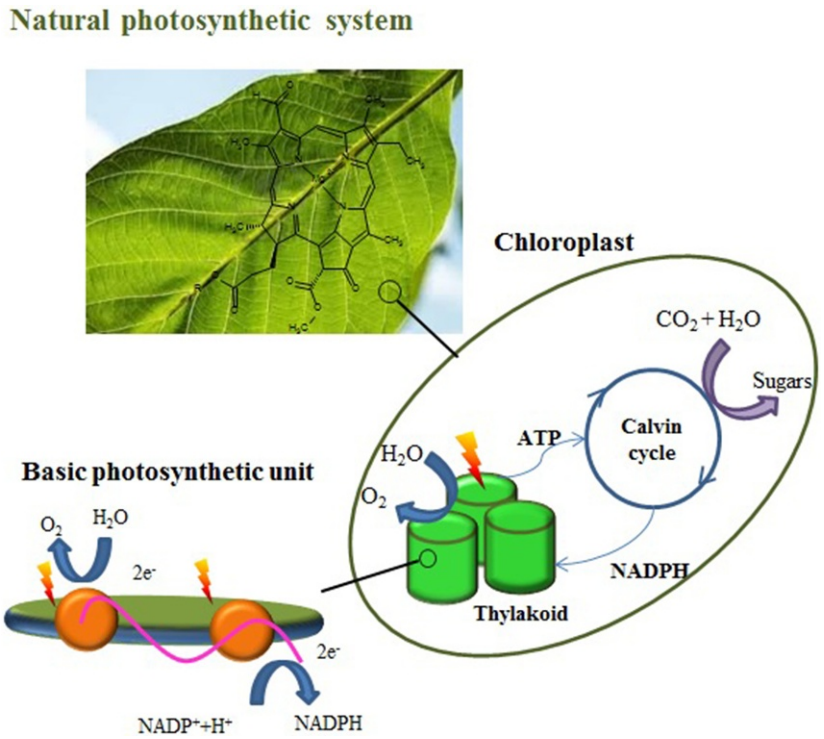

Fig. 16.2
Representation of mechanisms and functionalities of plant involved in the natural photosynthesis.

Obviously, being not directly involved in the life cycle of plants, the natural photosynthesis cannot form alcohols, like methanol, which are naturally produced by microbial metabolic cycles (i.e., fermentation) of organic molecules, mainly carbohydrates (Zhou et al., 2016).

In particular, methanol is produced in nature toward the anaerobic metabolism of many bacteria or as a by-product in the ethanol fermentation process which occurs in many fruits. For instance, microbial fermentation of pectin-rich substrates can lead to methanol, as widely reported in literature. Furthermore, the methanol synthesis can be also associated with the stabilization of pectins in the cell walls of plants, which are formed in the early stages of cell development (Doong et al., 1995). Similar to polymers, the structure of PGA (poly-galacturonic acid) based pectin is variable among plant species, and even within the tissues of the same plant, with different degrees of methyl esterification. During the cell growth, several strands of cellulose and hemicellulose are produced, because the pectin substrate must adapt itself to the new structure by cross-linking reduction, which can occur through PGA methylation. Then, PGA is demethylated through the action of the pectin methylesterase enzyme (PME), yielding residues of ionized galacturonic acid and methanol, as displayed in the reaction scheme reported in Fig. 16.3 (Galbally and Kirstine, 2002).

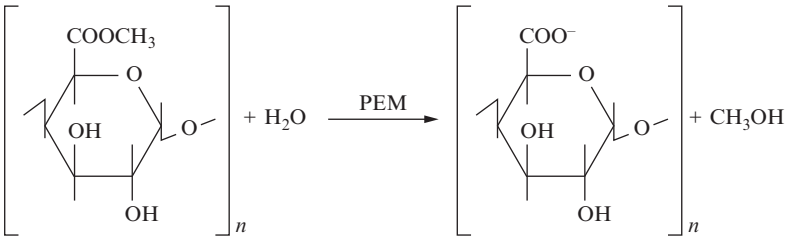

Fig. 16.3
Scheme of methanol formation via PGA demethylation.

The same enzyme is also responsible for the methanol formation by alcoholic fermentation. During the fermentation process, PME de-esterifies naturally, according to the scheme of Fig. 16.3 (Ohimain, 2016). In general, pectin enzymes are widely present in nature and are also produced by bacteria, fungi, and yeast as is the case of *Saccharomyces cerevisiae*, which is the dominating yeast in traditional fermentation of food and beverages.

Therefore, to date the methanol production via biological routes is not feasible on a large commercial scale (Nikokavoura and Trapalis, 2017), because of a poor efficiency of the natural photosynthetic process resulting in very low yield and very high costs for extraction-purification.

2.2 Methanol via Artificial Synthesis

Since the late 1970s, many studies have been proposed for artificially reproducing the photosynthesis process, aiming to convert CO_2 into high value products. Despite the biological organism's ability to self-repair for maintaining their unchanged photoactivity, the artificial photosynthesis can directly lead to high yields of methanol, without any intermediate products. Similar to that occurring in nature, the artificial "photosynthesis" exploits the energy of light to induce the formation of "radical" or "redox" species, which can act as highly active reactants. In particular, at variance with the natural process leading mostly to carbohydrate compounds, CO_2 and H_2O are converted at the surface of a proper semiconductor photocatalyst into methanol and/or methane, showing that water is both the reducing agent and the electron/proton source, according to the following reactions:

$$CO_{2(g)} + 2H_2O_{(l)} \rightarrow CH_3OH_{(l)} + 3/2O_{2(g)} \tag{16.2}$$

$$CO_{2(g)} + 2H_2O_{(l)} \rightarrow CH_{4(g)} + 2O_{2(g)} \tag{16.3}$$

The artificial photocatalytic process involves a network of reaction steps, consisting of: (i) the adsorption of CO_2; (ii) the photo-generation of electron-hole pairs; (iii) the separation and the transportation of charge carriers; and (iv) the chemical interactions between different chemical species leading to reaction products.

2.2.1 CO_2 adsorption

The photosynthesis process starts with the absorption of light radiation (i.e., UV or visible) and the surface adsorption of CO_2 on the photocatalyst, whose activation is crucial for the reduction process. The factors that affect CO_2 chemisorption are many: the electronic configuration of the adsorbent system, the work function associated to the electron transfer, and the local geometry (Vitillo, 2015). Literature data indicate an average C—O bond order of 1.5 for the chemisorbed species, against a value of 2.0 typical of the gas phase CO_2, in the light of greater C—O distance (e.g., 1.24 vs. 1.15 Å) and lower bond energy indicating the stabilization of adsorbed species in a meta-stable anionic form, though the anion results are kinetically stable (Freund and Roberts, 1996). Actually, CO_2 chemisorption on the photocatalyst surface occurs via carbon or oxygen coordination, thus acting as either electron donor or acceptor species (Fig. 16.4). Indeed, the chemisorption process can involve the electron lone pair of oxygen, forming a bond with the Lewis acid centers of photocatalyst (i.e., oxygen coordination), or the carbon atoms, gaining electrons from Lewis basic centers and generating carbonate-like species (i.e., carbon coordination) (Chang et al., 2016).

As shown, the chemisorbed $CO_2^{\delta\bullet-}$ species loses the linear symmetry of free CO_2, driving to a decrease in the energy barrier, since the LUMO (lowest unoccupied molecular orbital) level decreases as the molecule bends, as illustrated in the scheme by Freund and Roberts (1996), reported in Fig. 16.5.

Overall, the CO_2 molecule contains 22 electrons, 6 of which occupy the three core level orbitals of C_{ls} and O_{1s}, and the other 16 are delocalized in the valence σ and π orbitals. Therefore, $l\pi_{gx}$ represents the highest occupied molecular orbital (HOMO), while the LUMO level is the $2\pi_u$ orbital. When the geometry shifts from linear to bent, the energy of the orbitals sensibly changes, resulting in the energy of each π-orbital being split into two degeneracies.

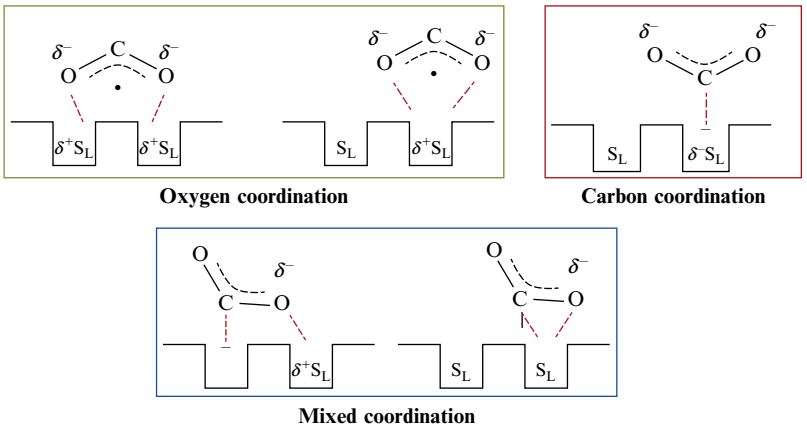

Fig. 16.4
Representation of CO_2 interactions on the photocatalyst surface.

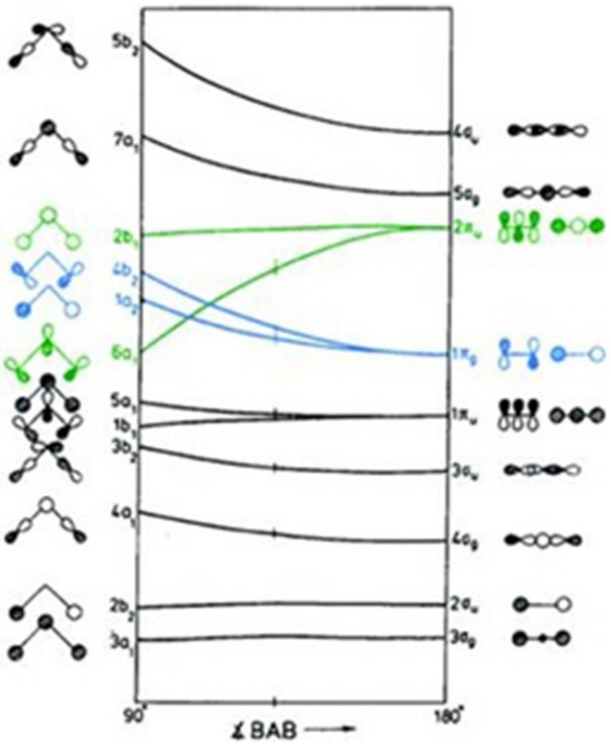

Fig. 16.5

Walsh diagram of CO_2 orbital energies in linear and bent geometries. *Reported from Freund, H.J., Roberts, M.W., 1996. Surface chemistry of carbon dioxide. Surf. Sci. Rep. 25, 225–273.*

In particular, the energy of the two degeneracies of HOMO level increases, confirming the more stability of the linear geometry. On the contrary, the energy of $2\pi_u$ orbitals of LUMO level is split into components, which are 2b1 level, whose energy remains almost unchanged, and 6a1 energy level, characterized by energy even lower than that of HOMO level. Therefore, the electronic configuration $6a_1$ of $2\pi_u$ is the only valence orbital for which the bent geometry is strongly preferred to the linear one for the adsorption and activation of CO_2 on the semiconductor surface. On this account, the chemisorption process of CO_2 can be promoted by several factors such as the larger exposure of the surface area, the presence of basic sites and surface defects.

2.2.2 Electron-hole pair photo-generation

Generally, solid materials are classified as insulators, conductors, and semiconductors, depending on their energy transport properties (e.g., electricity and heat). Referred to the electronic structure, the "Band Theory" explains such properties in terms of delocalized orbitals and relative energy levels, considering a filled Valence Band (VB) and a higher empty Conduction Band (CB), as shown in Fig. 16.6. In particular, high conducting materials, like

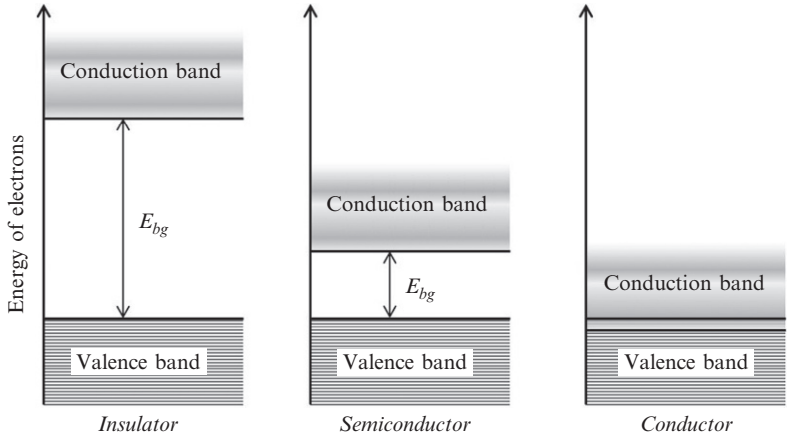

Fig. 16.6
Energy diagram of VB and CB of conductors, insulators, and semiconductors materials.

metals, are characterized by the overlap of the band of Valence with that of Conduction. Therefore, the electrons of the metals can move freely across the material. On the other hand, in the insulator material, the Valance Band is completely filled and the energy gap between VB and CB is so high that the electrons cannot be admitted to the conducting zone. The electronic structures of semiconductors represent a good compromise between the different properties of the former two materials. In fact, as in the case of the insulators, the VB in the semiconductors are well separated from the CB; however, the relative gap of energy is generally lower than 4 eV. Therefore, the mobility of electrons from the ground state to the conduction level can be induced by proper excitation/stimulation, as through illumination with photons of appropriate energy (Kondarides, 2010; White et al., 2015).

Indeed, the light that irradiates the surface of a semiconductor, through its energy, may prompt many electronic transitions in the material and energetic processes, which allow the jump of electrons from ground state orbitals to excited ones at higher energy. Then, electronic-hole pairs are generated in the material, determining an electron's current by photo-induction (Eq. 16.4):

$$h\nu + \text{semiconductor} \rightarrow \text{hole}^+ + \text{e}^- + \text{energy} \tag{16.4}$$

Conforming to the Quantum Laws, the photo-induced current can reduce the adsorbed species, carbonic, and carboxyl groups (i.e., CO_2, HCO_3^-, $CO_3^=$), and, therefore, convert them into methanol by the presence of hydrogen. Nevertheless, the energy associated to the incident light must be higher than that needed to overcome the energy barrier represented by the photocatalyst band gap (BG) (Low et al., 2016).

The hole-electron recombination represents the major limitation to the reduction process of the molecule chemisorbed on the surface of the photocatalyst. In fact, the charge carriers can recombine on the surface and in the bulk of the semiconductor before reacting with the adsorbed species, dissipating energy as heat or light.

2.2.3 Charge carriers' separation and transportation

After charge carriers' generation, electrons can reduce the chemisorbed species through the transfer of these charges from the semiconductor surface to the adsorbed or chemisorbed molecules, Fig. 16.7. Indeed, if the electron-hole lifetime overcomes the length of the nanosecond and the surface of semiconductor is in deep contact with the reactant solution or the reactant gas mixture, the abstraction of electrons (e^-) from their orbitals leads to an electronic current moving in the opposite way with respect to positive charges (h^+). The probability that the charges transfer occurs, and its rate, depends on the BG and redox potential of chemisorbed species (Linsebigler et al., 1995). Semiconductors having high band gap, as TiO_2 (c.3.2 eV), can only exploit UV radiation (±4% of the total solar energy), while the materials with a narrower band gap, like CdS (c.2.4 eV), are photoactive under visible light.

From a mechanistic point of view, the charge transfer is in competition with the electron-hole recombination. However, the electron-hole pair could evolve by recombination at the surface (case A, Fig. 16.7) or in the bulk (case B, Fig. 16.7), while the reduction of chemisorbed species (i.e., CO_2, HCO_3^-, $CO_3^=$) leads to heat release (case C, Fig. 16.7) and oxidation of some other chemisorbed species (i.e., H_2O, OH^-, sacrificial agents, etc.) by positively charged holes (case D, Fig. 16.7).

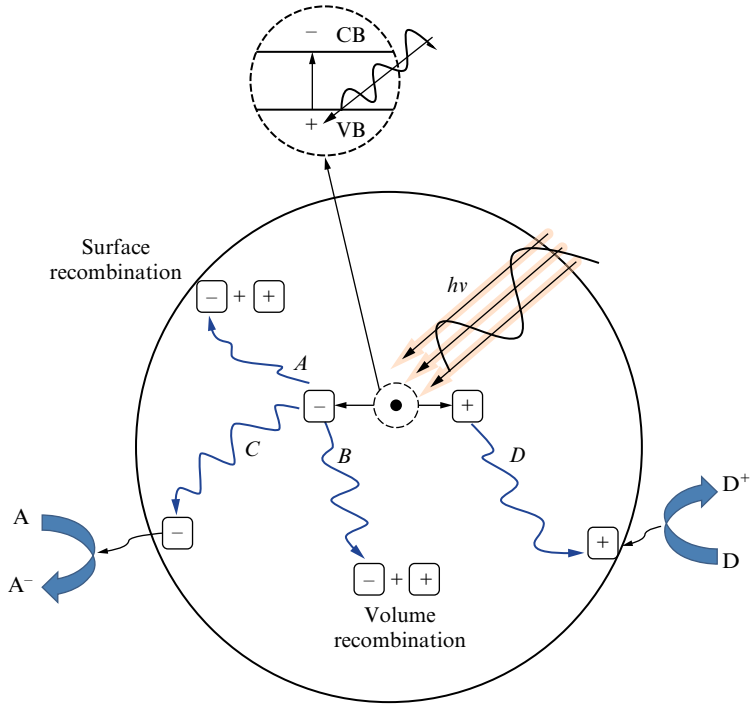

Fig. 16.7
Representation of the processes of photo-generation of electron-hole pairs and the separation and the transportation of charge carriers.

As already known, the transfer and recombination of electrons and holes are two competitive processes, among which the recombination is the critical aspect of any photocatalytic reaction that strongly limits the efficiency of the photoreduction process and leads to the dissipation, as heat or light, of the energy previously acquired through the absorption of photons. The electron–hole pairs normally have a lifetime of about 10^{-9} s. On the other hand, the chemisorption process requires between 10^{-8} and 10^{-3} s. Therefore, the recombination of the photo-excited electron-hole pair should be retarded to enhance the charge transfer process and, consequently, the photocatalytic production of H_2 and the photoreduction of CO_2. However, the rate of recombination of e^--h^+ pairs is extremely faster than that of their separation (Fan et al., 2013), contributing for the low efficiency of CO_2 conversion. The processes of charges separation and transfer are closely related to the crystal morphology, to the presence of defects, disorders, and material modifications for many photocatalysts such as TiO_2-based ones (Liu and Li, 2014). In particular, the irregularities in the crystal structure of TiO_2 can induce surface electron states, different from that of bulk, which can act as charge carrier traps, suppressing the recombination of electrons and holes (Linsebigler et al., 1995).

The interface between the surface of semiconductor and the adsorbed or chemisorbed species commonly induces a redistribution of electric charges and the formation of a double layer. The transfer of mobile charge carriers between the semiconductor and the contact phase, or the trapping of charge carriers in surface states at the interface, produce a space charge layer. In particular, in the case of n-type semiconductors in gas phase interactions, such as TiO_2, the interface becomes negatively charged, making the surface states accessible for electron trapping (Linsebigler et al., 1995). Hence, composite photocatalysts have been recently developed by coupling different types of semiconductors (e.g., diodes). In fact, the contact of two semiconductors generates a "heterojunction" through the coupling of their BG allowing the charges to move from the VB of the first semiconductor to the CB of the second one, because of their different potential (Chen et al, 2014). On this account, for the composite TiO_2-ZnO system Xi et al. (2011) recently documented a six-fold higher CO_2 photoreduction activity with respect to bare TiO_2. This was explained by the fact that electrons move from ZnO with lower CB (−0.31 V) to TiO_2 with higher CB (−0.29 V), meanwhile holes move from TiO_2 with higher VB (2.91 V vs. NHE) to ZnO having a lower VB (2.89 V vs. NHE) (Liu and Li, 2014).

2.2.4 Chemical reactions between surface species and charge carriers

Similarly to any other redox cycle, for allowing the transits of the electron towards the chemisorbed CO_2, the semiconductor must "purchase" electrons from sacrificial agent, guaranteeing the electronic neutrality of the material. In particular, the oxidation of water to O_2 is the main route for providing to the needed electrons, Fig. 16.8.

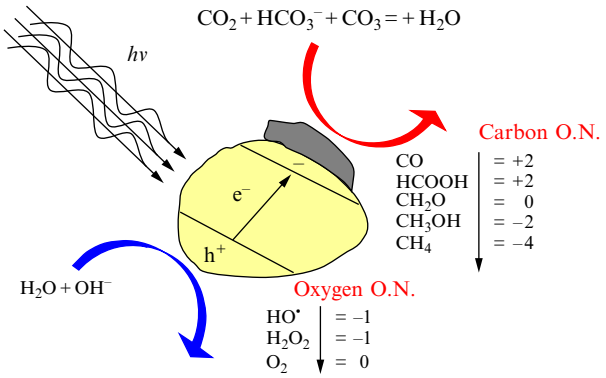

Fig. 16.8
Reaction scheme of the photoreduction mechanism of CO_2.

Therefore, the methanol synthesis involves the reduction of electron "acceptor" reactants (i.e., CO_2, H_2O, etc.) to form methanol, H_2, CO, and other organic compounds, and the oxidation of donor species (i.e., H_2O, and OH^-), through the combined action of holes and electrons which move on the surface of the photocatalyst (Ola and Maroto-Valer, 2015c).

As well known, the initial excitation, which occurs in any semiconductor during the photocatalytic process if properly photo-stimulated, drives to electron transfer and/or energy transfer phenomena as a natural consequence of the inverse process of de-excitation. In respect of this, electron transfer represents the driving power of any chemical reaction which occurs on the surface of the heterogeneous photocatalyst. Basically, the photoactivity involves specific "reactive centers", which are reactive sites placed on the surface of the heterogeneous photocatalyst, where the electrons jump from the occupied orbital of the donor species to the empty orbital of the acceptor reactants.

As shown in the scheme of Fig. 16.9, the electron transfer process occurs through the overlap of the orbitals of the donor and acceptor species, also partially filled. This process is realized through the relocation of an electron from the donor to the acceptor, leading to the formation of cation (D^+) and anion (A^-) species. Differently, the energy transfer occurs by the phenomena of electron exchange or dipole-dipole resonant coupling. If equally favored by the thermodynamic, the process of electron transfer results larger than that of the electron exchange, because the latter needs the concomitant overlap of two orbital pairs. While the dipole-dipole coupling, occurring via Coulombic resonance interactions, is easily achieved because this process doesn't involve a real orbital overlapping and also acts in a wider range of 10–100 Å (Linsebigler et al., 1995).

Among the different donor species (i.e., reductants and/or hole scavengers) H_2O is still the more powerful, inexpensive, and safe hydrogen source. Indeed, the water splitting provides the hydrogen required for the reduction of CO_2 into methanol, as follows (Eqs. 16.5–16.7):

$$H_2O + h^+ \rightarrow H^+ + OH^- \tag{16.5}$$

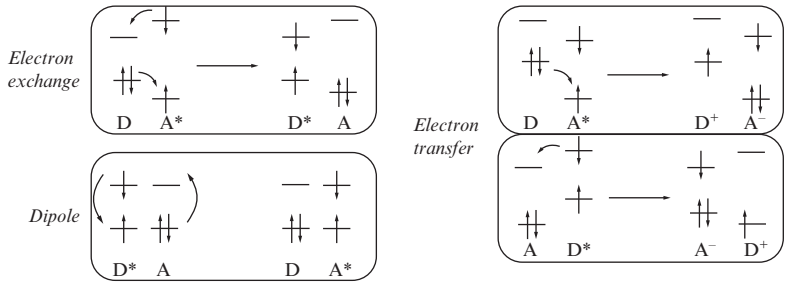

Fig. 16.9

Scheme of different interactions between different reactive centers in excited state (*) or in ground state. *Adapted from Linsebigler, A.L., Lu, G., Yates, J.T., Jr., 1995. Photocatalysis on TiO_2 surfaces: principles, mechanisms, and selected results. Chem. Rev. 95, 735–758.*

$$H^+ + e^- \rightarrow H^\bullet \tag{16.6}$$

$$H^\bullet + H^\bullet \rightarrow H_2 \tag{16.7}$$

Then, one of the first reaction mechanisms recognized in the methanol photosynthesis accounts for the formation of CO_2 radical species ($CO_2^{\bullet-}$) as a main intermediate because of its larger negative potential (Eq. 16.8):

$$CO_2 + e^- \rightarrow CO_2^{\bullet-} \quad (-1.90\,\text{V vs. NHE, pH}\,0) \tag{16.8}$$

On the other hand, the formation of the $CO_2^{\bullet-}$ species is also considered the limiting step of the whole process, because of the high energy necessary for bending the linear CO_2 and for assuming the anionic radical symmetry.

The theory of multiple "Proton-Coupled Electron Transfer" (PCET) processes otherwise prefigures an alternative way for limiting the activation barrier for the intermediate formation and the energy restructuring. Indeed, the high activation barrier would be attenuated through a series of electrons and protons transfer processes. On the other hand, the PCET processes are kinetically dependent by the photocatalyst surface availability of protons and electrons. Then, in large competition with H_2 evolution, PCET processes need the transfer of six electrons for each molecule of methanol formed, against the two required for water splitting, which can explain the lower conversion and efficiency (Chang et al., 2016).

Irrespectively to the formation of the $CO_2^{\bullet-}$ precursor, many reaction mechanisms are still under debate because of the adopted process conditions and/or the characteristics of the photocatalyst.

In 1995, explaining the photocatalytic behavior in CO_2 photoreduction of TiO_2 supported on zeolite, Anpo et al. (1995) have proposed a multi-step reactive interaction mechanism in which

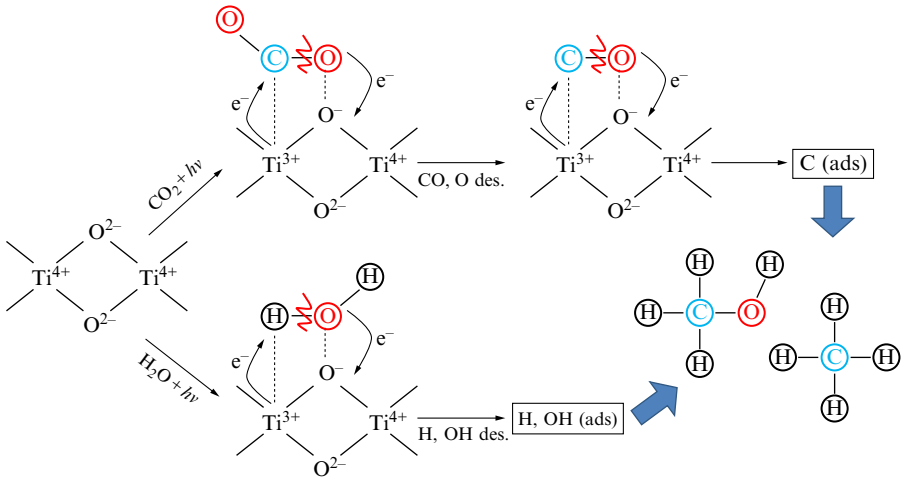

Fig. 16.10

Schematic representation of the photocatalytic reduction of CO_2 with H_2O on TiO_2 surface. *Adapted from Anpo, M., Yamashita, H., Ichihashi, Y., Ehara, S., 1995. Photocatalytic reduction of CO_2 with H_2O on various titanium oxide catalysts. J. Electroanal. Chem. 396, 21–26.*

photo-excited Ti^{3+}–O^{-}*sites are involved as reactive centers. Specifically, through the action of these sites, the photoreduction process can first lead to radical intermediate formation such as H•, OH•, CO•, and O•, which can react each other on the photocatalyst, yielding CH_4 and CH_3OH as main products (Fig. 16.10). In this case, reduction and oxidation processes can proceed competitively on the same Ti^{3+}–O^{-}* sites, as confirmed by the straight dependence of the reaction rate with the H_2O/CO_2 rate.

Other authors, such as Wu (2009), have invoked a further mechanism which combines the water splitting process with that of a super oxygen species (O_2^-) generated on the photocatalytic surface, where H atoms are generated and then chemisorbed on the same photocatalyst surface (Cu-TiO_2) starting from the H^+ form. At first, the OH^- ions are converted into the radical form through the release of an electron on each electronic hole photogenerated. Then the radicals species (OH•) react each other for forming H_2O_2, which is further converted into the super oxygen specie (O_2^-). The oxygen evolution by donation of an electron to an electronic hole complete this cycle (Eqs. 16.9–16.15).

$$TiO_2 + h\nu \rightarrow e^- + h^+ \tag{16.9}$$

$$H_2O \rightarrow H^+ + OH^- \tag{16.10}$$

$$H^+ + e^- \rightarrow TiO_2 - H \text{ or } Cu - H \tag{16.11}$$

$$OH^- + h^+ \rightarrow OH^{\bullet} \tag{16.12}$$

$$2OH^{\bullet} \rightarrow H_2O_2 \tag{16.13}$$

$$H_2O_2 + h^+ \rightarrow O_2^- + 2H^+ \quad (16.14)$$

$$O_2^- + h^+ \rightarrow O_2 \quad (16.15)$$

On this route, the adsorbed hydrogen would reduce $CO_2^{\bullet -}$ radical species to hydrocarbons, as shown in the scheme reported in Fig. 16.11.

Relying on the fact that the CO_2 photoreduction requires six moles of electrons for one mole of methanol, the author argues that half of these electrons should be progressively transferred to the chemisorbed CO_2, while the rest would be furnished through the action of hydrogen atoms during the formation of a methoxy group. The OH^- and H_2O_2 species would cover the six holes photogenerated during the process, resulting in two H_2O consumed for the production of 1.5 O_2. In particular, through the acceptance of an electron and the adding of one hydrogen atom generated by water splitting, the chemisorbed CO_2 would be converted into $HCOO^-$ species, which should then evolve to H_2COO^- through the insertion of another atom of hydrogen. Then, interacting with the neighboring reactive center (i.e., TiO_2 sites, activated by the presence of oxygen vacancy), the H_2COO^- species would break the carbon-oxygen double-bond, removing one oxygen, producing formaldehyde. Afterwards, a further addition of hydrogen atom would lead to the methoxy group formation, which will be then converted into methanol by the action of "free" H_2O on the photocatalyst surface (Wu, 2009).

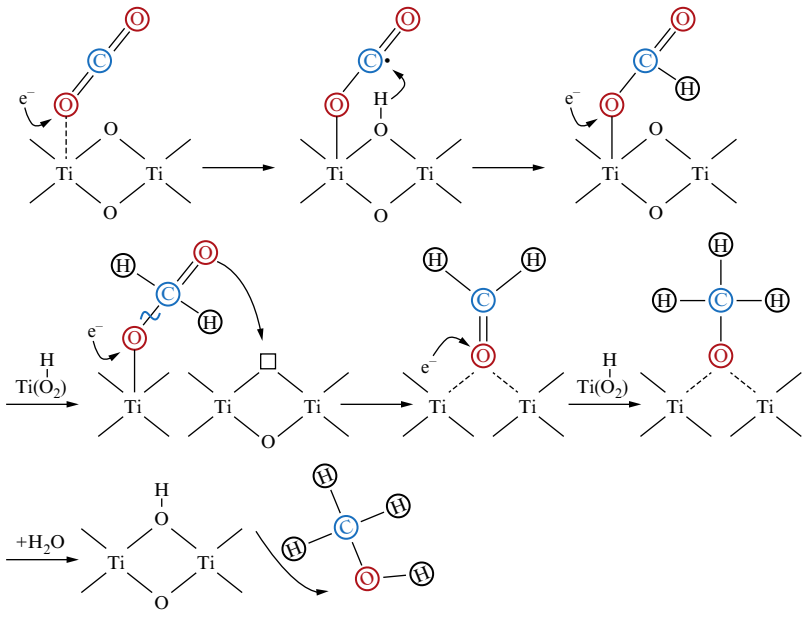

Fig. 16.11

Mechanism of photocatalytic reduction of adsorbed CO_2, over TiO_2 surface. *Adapted from Wu, J.C.S., 2009. Photocatalytic reduction of greenhouse gas CO_2 to fuel. Catal. Surv. Asia 13, 30–40.*

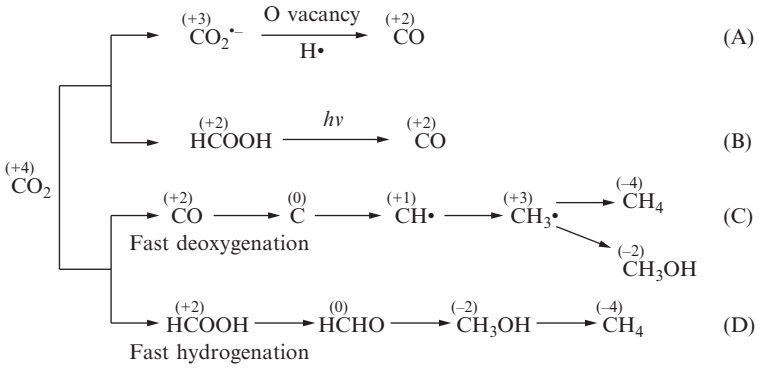

Fig. 16.12

Proposal of reaction pathways for the formation of CO, CH_4, and CH_3OH in the photocatalytic CO_2 reduction. *Adapted from Dhakshinamoorthy, A., Navalon, S., Corma, A., Garcia, H., 2012. Photocatalytic CO_2 reduction by TiO_2 and related titanium containing solids. Energy Environ. Sci. 5, 9217–9233.*

In a closer study, Dhakshinamoorthy et al. (2012) suggested another hypothesis of reaction pathways, prefiguring a mechanism in which both CO_2^- and HCOOH intermediates are produced on the surface of a photocatalyst to form CO, CH_4, and CH_3OH products, as displayed in the following scheme of Fig. 16.12.

In particular, CO should be the first product formed either via HCOOH or $CO_2^{\bullet-}$ intermediate species, both preliminarily generated starting from the chemisorbed CO_2 towards two alternative reaction mechanisms. In particular, the $CO_2^{\bullet-}$ species would further evolve to CO (Fig. 16.12A) through the action of radicals H• and the dissociative activity operated by oxygen vacancy sites. On the other parallel side, the CO molecule could be obtained also by the photodecomposition of HCOOH (Fig. 16.12B).

Starting from the CO, both CH_4 and CH_3OH products would be therefore formed through several subsequent processes of deoxygenation and hydrogenation by the which the oxidation state of carbon changes progressively from 2^+ to 3^- of CO and CH_3, respectively. After that, the CH_3• radical would also add $OH^{\bullet}$ or $H^{\bullet}$ species available on the photocatalyst surface for forming CH_3OH or CH_4 products, respectively (Fig. 16.12C).

In a parallel way, starting directly from HCOOH, CH_3OH and CH_4 could be formed by several consecutive hydrogenation stages, which count the reduction of the oxidation state of carbon from 2^+ (HCOOH), to 2^- (CH_3OH) and then 4^- (CH_4), crossing the zero state of formaldehyde (Fig. 16.12D). As a conclusion, the authors argue that a faster hydrogenation process would favor the HCOOH conversion, while a larger deoxygenation activity would majorly push the reaction rate of CO (Dhakshinamoorthy et al., 2012; Liu and Li, 2014).

3 Influence of Process Conditions in Multiphase Reactions, Aqueous Medium Versus Gas-Vapor Stream

Different aspects of the CO_2 photoreduction process are still under debate. In particular, the effects of process conditions are strongly disputed, whereas the key factors governing the product distribution still remain unclear (Liu et al., 2015). Indeed, several physical and procedural factors can interfere and affect the photoreduction process of CO_2, many of these are related to the mass transfer phenomena/limitations occurring between molecules and species in different physical states (i.e., CO_2 as gas, H_2O as liquid or vapor, photocatalyst as solid, and $HCO_3^-/CO_2^=/HO^-/H_3O^+$ as ions dissolved in liquid media).

3.1 CO_2 Photoreduction in Three-Phase System

In general, the three-phase process configuration consists in a slurry batch-reactor system in which CO_2 is bubbled (continuous flow) or recirculated (semi-continuous) in an aqueous solution, while the photocatalyst is dispersed in the solution and maintained suspended by constant stirring, ensuring the saturation of CO_2 by pressure regulation.

Very complex relationships influence the mass transfer in the three-phase processes, which is affected by the kinetics of the reaction, the thermodynamics of the process, the fluid dynamics conditions, and the inter-phase, intra-phase, and intra-particle transport of reagents and products. In recent years, several mathematical models have been developed to allow the defining of the influence of physical factors such as the wettability of the photocatalyst, the mass transfer at the interface, the intra-particle diffusion, and the axial dispersion factors for the different types of reactors.

In particular, as described in Fig. 16.13, the kinetics of a three-phase reaction is strongly influenced by the rate of diffusion of reactants and products between the different interfaces. As a rule, a three-phase process consists of different steps, as follows:

1. mass transfer of gaseous species towards gas-liquid interface;
2. mass transfer of gas and liquid into photocatalytic granule;
3. intra-particle diffusion of the reactants;
4. adsorption of the reactants on photocatalytic surface and reaction towards active sites (reaction center);
5. desorption of products from surface and diffusion into the liquid phase.

The mass transfer phenomena-limitations are related to the extent of interfacial area generated between the gas and liquid phase. In a bubbling bed reactor, the gas-liquid specific surface area is defined through the following expression:

$$\text{Gas} - \text{liquid surface area} = 6\xi/d_{vs} \tag{16.16}$$

where d_{vs} is the average diameter of the bubble and ξ is the gas hold-up coefficient.

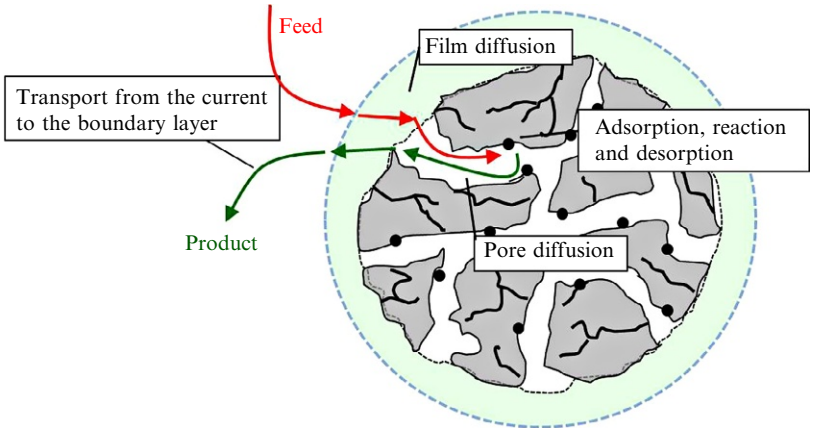

Fig. 16.13
Diagram of mass transfer phenomena in three-phase process.

The hold-up coefficient determines the limit of the available interfacial area for mass transfer, the higher the hold-up value, the wider the available interfacial area. The hold-up value is affected by:

- the gas flow rate (an increase of the flow rate leads to a higher ξ, but also to a rise in the cost of pumping);
- the bubbles rate, which is determined by their size (smaller bubbles are characterized by a faster rate and a larger surface area for mass transfer).

The size of the bubbles depends primarily on the bubble generator, on the flow regime, on the fluid properties, and on the operating conditions. At atmospheric pressure, the hold-up value can vary as a function of the geometry of the generator used, being higher for a porous plate distributor, which generates the smallest bubbles. In the bubbling columns, an increase of the operating pressure involves a decrease of the bubbles size. This effect is much more pronounced in the perforated plates distributors, rather than in the porous ones. However, with the pressure increase, the influence due to the type of the bubble generator used diminishes, becoming negligible for pressures greater than 10 MPa. Moreover, the bubbles traveling through the liquid tend to join together through coalescence, therefore the use of porous distributors is totally inefficient for large columns and it is difficult to scale up for industrial reactors.

Under normal conditions, the carbon dioxide is characterized by a relatively low saturation value in water (1.45 g/L). Therefore, the increase of the CO_2 concentration in the solution is one of the most successful ways for improving the efficiency and yield of the photoreduction process in a three-phase system. Currently, two effective methods are known to increase the CO_2 saturation. The first one consists of varying the pH of the solution, while the second method is based on the increase of the CO_2 pressure in the reactor. The former approach is widely used at the laboratory testing level since it is easy to adopt and it has the advantage of

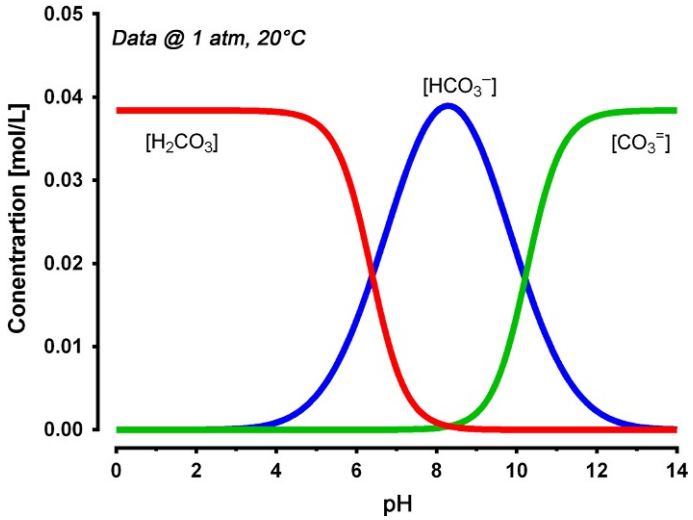

Fig. 16.14
CO_2 equilibrium at different pH.

being quite inexpensive, although the basic pH influences the surface charge of the photocatalyst. Nevertheless, the maximum concentration of CO_2 obtainable by varying the pH of the solution is still low, since it is limited by chemical equilibrium, as depicted in Fig. 16.14.

Namely, this method benefits from the different solubility of CO_2 in water at various pHs as a consequence of the well-known acid-base neutralization and hydrolysis processes, as specified in the reactions of Eqs. (16.17)–(16.20).

$$CO_{2(g)} + H_2O \rightleftarrows H_2CO_{3(acq)} \quad (\text{solubility } 1.45\,\text{stp g/L}) \tag{16.17}$$

$$H_2CO_{3(acq)} + 2H_2O \rightleftarrows H_3O^+ + HCO_3^- \quad \left(K_{a1} = 4.3 \times 10^{-7}\right) \tag{16.18}$$

$$HCO_3^- + 2H_2O \rightleftarrows H_3O^+ + CO_3^{=} \quad \left(K_{a2} = 5.6 \times 10^{-11}\right) \tag{16.19}$$

$$H_3O^+ + OH^- \rightleftarrows 2H_2O \quad \left(K_W = 1.0 \times 10^{-14}\right) \tag{16.20}$$

The addition of a strong base, such as NaOH, into the reaction solution brings a left shift of the equilibria (16.17)–(16.19), due to the neutralization of carbonic acid, with an increase of the carbonyl ions in solution. Then, taking into account that the concentration of the different carbonyl species (CO_2, H_2CO_3, HCO_3^-, CO_3^{2-}) changes with the pH of the solution (Fig. 16.14), it emerges that the selectivity and the methanol yield of the process can be strongly influenced by the addition of an alkaline agent. Several authors, in fact, have reported significant increases in methanol yield through the addition of NaOH or KOH in the liquid media (Jeyalakshmi et al., 2016; Tahir and Amin, 2013; Tseng et al., 2004; Tseng and

Wu, 2005; Xiong et al., 2015). Furthermore, considering the overall photochemical process, working with basic pH implies further positive effects related to the mechanism of water photo-oxidation and to the "hole scavenger" capacity of the semiconductor. In fact, the holes photogenerated in the semiconductor can oxidize hydroxyl ions (OH^-) to hydroxyl radicals ($OH^\bullet$), inhibiting, therefore, the electron-hole recombination rate.

Other procedural parameters that influence the performance of the CO_2 photoreduction process in "Continuous Stirred Tank Reactors" (CSTR) are the pressure and the reaction temperature. In general, the increase of CO_2 pressure in the CSTR reactors has the immediate effect of improving the CO_2 solubility in the solution, as reported by the graph of Fig. 16.15.

The increase of the operating pressure determines, therefore, a larger CO_2 amount which should lead to a consequent increase of the total productivity of the process, although, in some studies a "volcano-shape" relationship has been reported, plotting methanol yield values at various CO_2 pressures. In particular, Tseng et al. (2002) justify this trend with the "possible" formation of hydrocarbons at a higher carbon number such as ethanol, even though, many studies have been conducted in very low and narrow range of pressures (1.0–1.4 atm). More recently, Rossetti et al. (2014, 2015) and Galli et al. (2017) have developed a new batch photoreactor, which allows running CO_2 photoreduction up to 20 bar. In the study, the authors have referred to a remarkable improvement of product yield by the rising of operating pressure, which also leads to the formation mainly of liquid products such as methanol, ethanol,

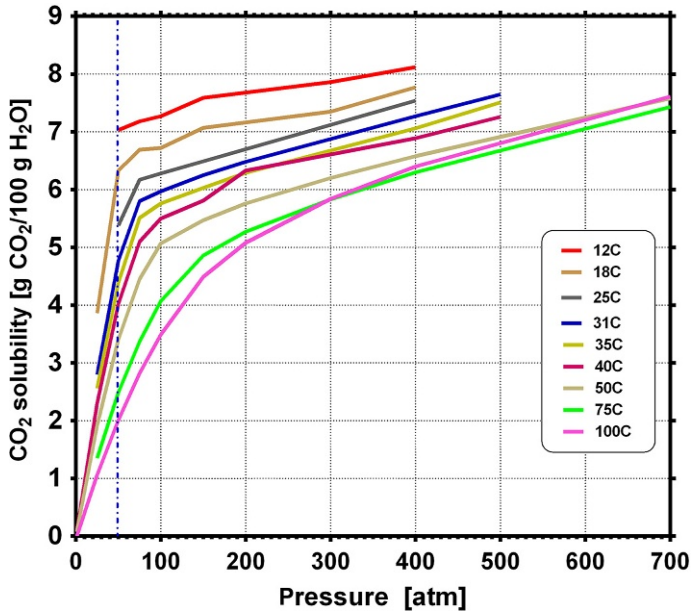

Fig. 16.15
Solubility of CO_2 in water vs. pressure.

and formic acid. On the other hand, gas products (e.g., CH_4 and H_2) would be more favorably formed at middle pressures, although no linear or clear relationship has been documented.

Reaction temperature has more a complex influence on the performance of the CO_2 photoreduction process. Indeed, the increase in the reaction temperature leads to a decrease of the solubility of CO_2, as reported by the graph of Fig. 16.16.

Therefore, this process is favored at a low temperature regime, which is also more cost-effective. In fact, the majority of the experiments in the literature are performed at room temperature (Dai et al., 2015; Lee et al., 2013; Su et al., 2017). Furthermore, the photo-excitation process does not need a thermal energy supply for the electron-hole pair generation, although, the fraction of "effective" collision between the photocatalyst and reagents increase with the reaction temperature. On the other hand, a remarkable amount of energy is needed for chemisorption of refractory CO_2 molecules on the photocatalyst surface. Indeed, the adsorption process of CO_2 requires the overcoming of an activation energy, generally ranging from 10 to 100 kJ/mol, supplied through temperature. Even the desorption process need to be energetically sustained, so that the products can leave the photocatalyst surface and diffuse in the liquid phase. On this address, several authors report beneficial effects provided by the temperature growth. In particular, Slamet et al. (2005), by varying the reaction temperature between 40°C and 100°C, noted a sensible enhancement of the methanol yield, principally justified by the products desorption improvement in the adsorption/desorption

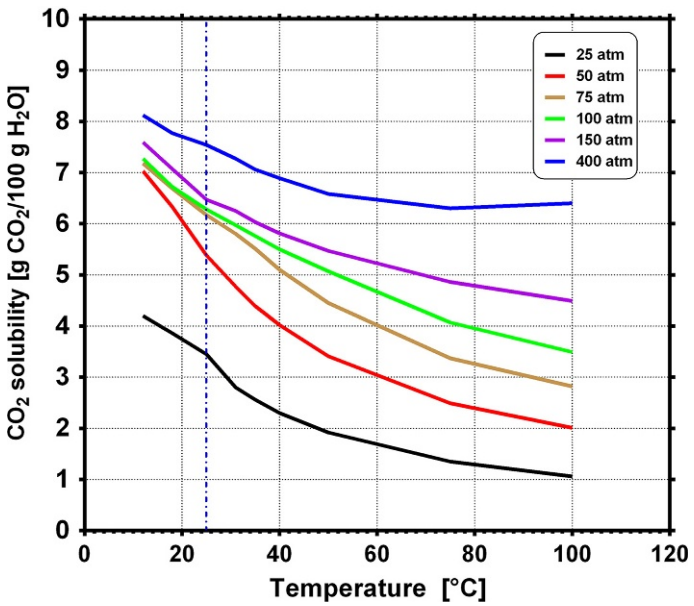

Fig. 16.16
Solubility of CO_2 in water vs. temperature.

equilibria of all species involved in the reaction. At low temperature, the surface of the photocatalyst is largely covered by products, resulting in positive apparent activation energy (E_{app}). On the contrary, at high temperature the desorption process of products improves, as proved by a negative E_{app} value (Saladin and Alxneit, 1997; Slamet et al., 2005).

3.2 CO_2 Photoreduction in Biphasic System

For many reasons due to the process, it can be useful to lead the CO_2 photoreduction in a biphasic system, and also obtaining a sensible growth in the methanol yield. Since the fact that smaller reactor volumes are needed, the reaction rates are enhanced by orders of magnitude by improved process conditions and better selectivities. The CO_2 photoreduction with water for the methanol synthesis can be conducted under gas-solid conditions, wherein the gas phase represents the reagent phase containing properly humidified CO_2, while the solid phase consists in the photocatalyst. The latter is confined in a small volume, like catalytic bed, or supported on the surface of inert materials (i.e., plates, beads, fibers, and monoliths) or on the walls of the photoreactor, instead of the multiphase system where the solid photocatalyst is dispersed in the large volume of reaction medium, normally water, which acts in the dual role of reactant and reaction phase. Allowing to overcome many drawbacks which strongly afflict the photoreduction process, several advantages are associated to the biphasic process such as ease of conducting reactions, increased rates of reactions, high yield and selectivity, elimination of solvent/water phase, simplified separation of products, and simplicity of process and equipment. Indeed, the biphasic system consists of a flow apparatus, in which the photocatalyst is fed continuously by the gas reactant mixture, humidified CO_2, generally obtained at saturated pressure by bubbling CO_2 in column water maintained at constant temperature. This process configuration is not affected by limitations due to the solubility of the CO_2 in water and allows improving the control of process conditions such as contact time and water/CO_2 ratio, increasing the photocatalyst stability and life, enhancing light irradiation efficiency and CO_2 chemisorption on the photocatalyst surface.

4 Thermodynamic Aspects of Methanol Photosynthesis From CO_2 and H_2O

The process of reduction of CO_2 into methanol is quite a big challenge, due to its unfavorable equilibrium. With a linear geometry, CO_2 is one of the most chemically stable and inert molecules in nature. In fact, the strong refractory character of the CO_2 molecule can be easily proven through thermodynamic analysis. In particular, according to Hess's cycle (Table 16.1), at standard condition of temperature and pressure (i.e., T/298 K and P/1 atm) the formation of methanol required a free Gibbs's energy ($\Delta G°$) of circa 726 kJ/mol towards CO_2 reduction and water oxidation to O_2, due to the large endothermic character (i.e., $\Delta H°$ c.702 kJ/mol) and low entropy (i.e., $\Delta S°$ c.81 J/mol K) of this reaction, respectively.

Table 16.1 Thermodynamic data at standard conditions (Haynes, 2014)

Molecule	ΔH_f° (kJ/mol)	S° (J/mol K)	ΔG_f° (kJ/mol)
$CH_3OH_{(l)}$	−239.032	127.235	−166.816
$O_{2(g)}$	0	205.029	0
$CO_{2(g)}$	−393.505	213.677	−394.384
$H_2O_{(l)}$	−285.830	69.915	−237.178

Indeed, the breaking of C═O bonds and the bending of the linear molecular geometry needs a large contribution of energy and the use of an appropriate photocatalyst (Lee et al., 2013). Then, as a consequence of the lower free Gibbs's energy necessary for the water splitting reaction (c.237 kJ/mol), at standard conditions the hydrogen evolution reaction (HER) is in strong competition with the CO_2 photoreduction (Chang et al., 2016).

The energetic aspects of the thermodynamic also reflect the driving power of the redox processes, according to Eq. (16.21):

$$\Delta G^\circ = -nF\Delta E^\circ \tag{16.21}$$

where ΔG° is the free Gibbs's energy (in J/mol); n is the number of electron per mole of product, F is the Faraday's constant (i.e., 96,485 C/mol), while ΔE° is the standard potential of a given redox reaction, ascertaining the spontaneity of the same reaction.

The reaction mechanism in the CO_2 photoreduction is still controversial, since the final oxidation state of carbon is determined by the specific reaction pathway and by the number and rates of electrons transferred between photogenerated carriers and species inside the reaction system (Yuan and Xu, 2015).

Considering the thermodynamic redox potentials, the photoreduction of CO_2 can lead to different products involving diverse redox processes, as provided in the Eqs. (16.22)–(16.27).

$$CO_2 + e^- \rightarrow CO_2^\bullet \quad (-2.00\,V) \tag{16.22}$$

$$CO_2 + 2e^- + 2H^+ \rightarrow HCOOH \quad (-0.61\,V) \tag{16.23}$$

$$CO_2 + 2e^- + 2H^+ \rightarrow CO + H_2O \quad (-0.48\,V) \tag{16.24}$$

$$CO_2 + 4e^- + 4H^+ \rightarrow HCHO + H_2O \quad (-0.52\,V) \tag{16.25}$$

$$CO_2 + 6e^- + 6H^+ \rightarrow CH_3OH + H_2O \quad (-0.38\,V) \tag{16.26}$$

$$CO_2 + 8e^- + 8H^+ \rightarrow CH_4 + H_2O \quad (-0.24\,V) \tag{16.27}$$

The CO_2 photoreduction would mainly occur through the multi-electronic transfer mechanism because of the high thermodynamic stability of CO_2, as mirrored by the highest potential required for the formation of radical $CO_2^\bullet$ species (−2.00 V, Eq. 16.21). Furthermore, the redox potentials proportionally decrease with the rising of the number of electrons acquired

(Eqs. 16.22–16.27), because the reduction processes with a larger electron exchange are more thermodynamically favored. Therefore, methanol and methane products would be thermodynamically preferred due to the greater reduction grade of carbon.

The value of pH can affect sensibly the photoactivity and product distribution of the reaction, according to the thermodynamic equilibria and the reactant species involved. In particular, the molecule of CO_2 is in equilibrium with the carbonic acid form (H_2CO_3) in solution and with its two conjugated bases (i.e., HCO_3^-, CO_3^{2-}), especially at basic pH. Therefore, all these species can be reduced under the surface of photocatalyst, jointly with CO_2. Namely, as shown in Eqs. (16.28)–(16.30), the reduction of carbonic acid follows the same multi-electronic mechanism of CO_2, although it occurs at higher potential, indicating that the reduction of H_2CO_3 is more thermodynamically favored than that of CO_2.

$$H_2CO_3 + 2e^- + 2H^+ \rightarrow HCOOH + H_2O \quad (-0.166\,V) \tag{16.28}$$

$$H_2CO_3 + 4e^- + 4H^+ \rightarrow HCHO + 2H_2O \quad (-0.050\,V) \tag{16.29}$$

$$H_2CO_3 + 6e^- + 6H^+ \rightarrow CH_3OH + 2H_2O \quad (+0.044\,V) \tag{16.30}$$

Even the anion carbonate takes part in the multi-electronic reduction process, leading to the formation of the oxalate anion (Eq. 16.31), formate anion (Eq. 16.32), and methanol (Eq. 16.33). In addition, both the oxalate and the formate ions can lead to the formation of methanol (Eqs. 16.34, 16.35), with the total transfer of 6 electrons.

$$2CO_3^{=} + 2e^- + 4H^+ \rightarrow C_2O_4^{=} + 2H_2O \quad (+0.478\,V) \tag{16.31}$$

$$CO_3^{=} + 4e^- + 3H^+ \rightarrow HCOO^- + 2H_2O \quad (+0.311\,V) \tag{16.32}$$

$$CO_3^{=} + 6e^- + 8H^+ \rightarrow CH_3OH + 2H_2O \quad (+0.209\,V) \tag{16.33}$$

$$C_2O_4^{=} + 2e^- + 2H^+ \rightarrow 2HCOO^- \quad (+0.145\,V) \tag{16.34}$$

$$HCOO^- + 4e^- + 5H^+ \rightarrow CH_3OH + H_2O \quad (+0.157\,V) \tag{16.35}$$

The redox potentials of the semi-reactions in Eqs. (16.31)–(16.35) are greater than those previously reported for both the carbonic acid and CO_2, therefore they are the most thermodynamically favored among all the possible processes. In other words, the potential of the formation of different products changes according to the starting carbonyl species (CO_2, H_2CO_3, HCO_3^-, $CO_3^{=}$), resulting in a more positive moving from CO_2 to the ion $CO_3^{=}$, as shown in Fig. 16.17.

Actually the most known photocatalysts possess band gap values ranging between −0.5 V and 0.2 V, which are therefore consistent with the methanol and methane formation. It should also be noted that in the CO_2 photoreduction process, protons are consumed in an equal number of electrons, and they are provided, apart from the hydrolysis of CO_2, from the photo-oxidation of water.

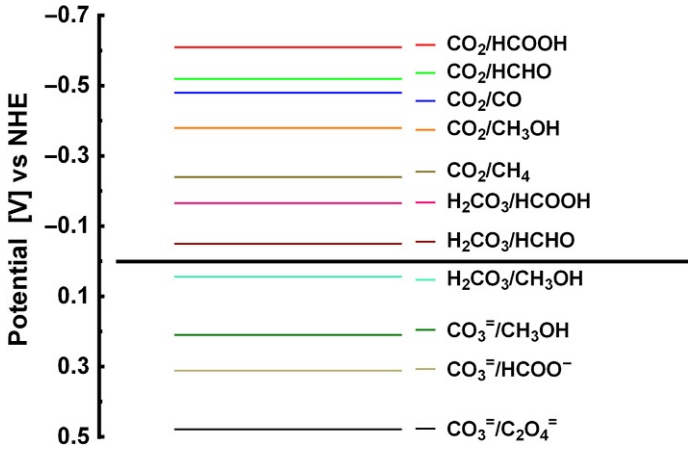

Fig. 16.17
Thermodynamic potentials at the variance of carbonyl species.

5 Photocatalysts for Methanol Synthesis

The efficiency of any photocatalytic process depends primarily on the choice of photocatalyst. Besides the large photo-stability, a photocatalyst must have a thermodynamic potential sufficiently positive for acting as an electron acceptor and a redox potential negative enough to allow the electron donor function. The photocatalysts active in the methanol synthesis via CO_2 photoreduction belong to a restricted category of materials based on semiconductor oxides or sulfides, eventually promoted and/or doped by the addition of various transition metals, such as copper, zinc, nickel, cobalt, and cadmium. In spite of the fact that the efficiency of many photocatalysts is actually far from the targets required for a commercial use, either TiO_2-based or non-TiO_2-based photocatalytic systems have been successfully valued in diverse photoreactor configurations and with different operative conditions, as summarized in Tables 16.2 and 16.3. In particular, semiconductor materials, such as TiO_2, $SrTiO_3$, $CaFe_2O_4$, SiC, ZnS, CdS, $InTaO_4$, Ti/(MCM-41), Ti/(MCM-48), and TiO_2/(SBA-15), have shown in recent literature that band gap energies are suitable for the direct photocatalytic reduction of carbon dioxide. Indeed, the electrons located in the conduction band of these materials can generate, by photo-stimulation, a continuous current of electrons, available for the effective photoreduction reactions of CO_2 chemisorbed molecules, acquiring other electrons by oxidative processes of sacrificial molecules such as water. Accordingly, photocatalyst takes a direct part of the entire redox cycle, acting in the dual role of electron-donor (reduction process) and electron-acceptor (oxidation process).

5.1 TiO_2-Based Photocatalysts

Among the photocatalysts, TiO_2 is the most promising based-material for the methanol synthesis via CO_2 photoconversion, due to its own chemical-physical properties, which include powerful oxidation properties and good charge transfer potentials. Moreover, it

Table 16.2 Summary of recent literature in the methanol synthesis via CO_2 photoreduction processes in three-phase systems

Photocatalyst	Light Source	Test Details	CH_3OH Productivity ($\mu mol/h\ g_{cat}$)	Ref.
Cu/TiO_2	8 W Hg lamp 254 and 365 nm	Slurry reactor; Cat. weight: 0.3 g; 0.2 N NaOH; $P_{CO2}=101.3–135.6$ kPa; 30 h; discontinuous mode	20	Tseng et al., 2004
Cu doped TiO_2	6 UV lamps (@10 W)	Slurry reactor; Cat. weight: 0.3 g; 1 M $KHCO_3$; 6 h; discontinuous mode	442	Slamet et al., 2005
Cu/TiO_2	8 W Hg lamp 254 nm	Slurry reactor; Cat. weight: 0.3 g; 0.2 N NaOH; $P_{CO2}=101.3–135.6$ kPa; 30 h; discontinuous mode	23.3	Tseng and Wu, 2005
$CoPc/TiO_2$	500 W tungsten-halogen lamp	Slurry reactor; Cat. weight: 0.15 g; 0.1 M NaOH; 10 h; discontinuous mode	0.1	Liu et al., 2007
TiO_2 anatase	8 W Hg lamp 254 nm	Slurry reactor; Cat. weight: 0.1 g; 0.2 N NaOH; $P_{CO2}=110$ kPa; discontinuous mode	0.04	Kočí et al., 2009
$AgBr/TiO_2$	150 W Xe lamp; visible light with $\lambda>420$ nm	Slurry reactor; Cat. weight: 0.5 g; 0.2 M $KHCO_3$; $P_{CO2}=7.5$ MPa; 5 h; discontinuous mode	15.6	Asi et al., 2011
Cu_2O/SiC	500 W Xe lamp with UV filter (400–700 nm)	XPAII reactor; Cat. weight: 0.2 g; 0.1 M NaOH and 0.1 M Na_2SO_3; 5 h; continuous	38.2	Li et al., 2011
WO_3, $Pt/SrTiO_3$:Rh, $CuAlGaO_4$ or, $Pt/CuAlGaO_4$	300 W Xe lamp with AM1.5G filter	Twin photoreactor; 0.15 g of $Pt/CuAlGaO_4$ and $Pt/SrTiO_3$:Rh; 0.3 g WO_3; pH 2.6; 6 h	3.9	Lee et al., 2013

Continued

Table 16.2 Summary of recent literature in the methanol synthesis via CO_2 photoreduction processes in three-phase systems—cont'd

Photocatalyst	Light Source	Test Details	CH_3OH Productivity ($\mu mol/h\ g_{cat}$)	Ref.
TiO_2-nitrogen modified	UV-vis lamp 300–600 nm	Slurry reactor; Cat. weight: 0.6 g; 2 h; discontinuous mode	23	Michalkiewicz et al., 2014
Cu_2O/TiO_2 nanotubes	Pulsed Nd:YAG laser 355 nm	Slurry reactor; 3 cm × 3 cm catalyst; $P_{CO2} = 3.4$ atm; 6 h; discontinuous mode	0.9	Wang et al., 2014
CeO_2-TiO_2	500 W Xe lamp, visible light	Slurry reactor; Cat. weight: 0.15 g; 0.1 M NaOH; 6 h; discontinuous mode	3.1	Abdullah et al., 2015
WO_3, Pt/$SrTiO_3$:Rh, Pt/$CuAlGaO_4$	300 W Xe lamp with AM1.5G filter	Twin photoreactor; 0.15 g of Pt/$CuAlGaO_4$ and Pt/$SrTiO_3$:Rh; 0.30 g WO_3; pH 2.6; 8 h	1.0	Cheng et al., 2015
Bi_2WO_6 microspheres with conductive polymers	500 W Xe arc lamp, visible light ($\lambda \geq 420$ nm)	Quartz cuvette; Cat. weight: 0.05 g; $T = 4°C$ $F_{CO2} = 50$ mL/min; 4 h; continuous mode	13.8	Dai et al., 2015
Ce doped TiO_2	9 W Hg lamp 254 nm	Slurry reactor; Cat. weight: 0.5 g; 0.2 N NaOH; $F_{CO2} = 5$ mL/min; 8 h; discontinuous mode	23.5	Xiong et al., 2015
$Na_{(1-x)}La_xTaO_{(3+x)}$ with Pt, Ag, Au, CuO, NiO and RuO_2	450 W Xenon lamp-300–700 nm	Slurry reactor; Cat. weight: 0.4 g; 0.2 M NaOH; pH 8; 20 h; discontinuous mode	60	Jeyalakshmi et al., 2016
Pt/WO_3, GaN: ZnO–Ni/NiO	300 W Xe lamp with AM1.5G filter	Twin photoreactor; Pt/WO_3 (0.3 g) and GaN:ZnO-Ni/NiO (0.3 g); 8 h	7.5	Yu et al., 2016
$Cd_{0.2}Zn_{0.8}S$@UiO-66-NH_2 nanocomposites	300 W Xe lamp with 420 nm cut-off filter	Slurry reactor; Cat. weight: 0.1 g; 0.1 M NaOH; discontinuous mode	6.8	Su et al., 2017

Table 16.3 Summary of recent literature in the methanol synthesis via CO_2 photoreduction processes in biphasic systems

Photocatalyst	Light Source	Test Details	CH_3OH Productivity ($\mu mol/h\ g_{cat}$)	Ref.
Pt-Ti-oxide/ Y-zeolite	Hg lamp-280 nm	Quartz cell reactor; Cat. weight: 0.15 g; CO_2 (24 μmol) and gaseous H_2O (120 μmol); discontinuous mode	5.0	Yamashita et al., 1998
Cu/TiO_2	Hg lamp (365 nm)	Optical fibers reactor; $F_{CO2}=3$ mL/min; $T_{sat}=75°C$; $P_{CO2}=1.29$ bar; $P_{H2O}=0.026$ bar; continuous mode	0.45	Wu et al., 2005
$NiO/InTaO_4$	Liquid phase: Circular fluorescent lamp (452, 543, 611 nm). Gas phase: Halogen lamp (400–1100 nm)	Liquid phase: Stirred batch reactor; Cat. weight: 0.3 g; 0.2 M NaOH; $P_{CO2}=101$ kPa; 10 h; discontinuous mode. Gas phase: Optical fibers reactor; $P_{tot}=120$ kPa; $P_{H2O}=2.4$ kPa; $\tau=5000$ s; continuous mode.	2.8 (liquid phase) 11.3 (gas phase)	Wang et al., 2010b
Cu-ZnO	8 W fluorescent lamp 369 nm	Fixed bed reactor; 0.01 g catalyst deposited on a glass microfiber filter; $T=50°C$; $P=2$ bar $CO_2/H_2O=6.7$; discontinuous mode	0.27	Núñez et al., 2013
Ni^{2+}/TiO_2	Halogen lamp (500 W, 400–1100 nm) and Hg lamp (200 W–365 nm)	Optical fibers reactor catalyst; loaded on monoliths or quartz plates; $F_{CO2}=4$ mL/min; H_2O content = 50 mL; 4 h; continuous mode	5.58	Ola and Maroto-Valer, 2014
V-, Cr- Co-TiO_2	Halogen lamp (500 W) 380–1100 nm	Fixed bed reactor; 0.2 g of catalyst dispersed on quartz plate; $F_{CO2}=4$ mL/min; $P=1$ atm; 4 h; continuous mode	26.1	Ola and Maroto-Valer, 2015b

Continued

Table 16.3 Summary of recent literature in the methanol synthesis via CO_2 photoreduction processes in biphasic systems—cont'd

Photocatalyst	Light Source	Test Details	CH_3OH Productivity (μmol/h g_{cat})	Ref.
Au nanoparticles/ TiO_2 nanowires	35 W Xenon car head lamp-visible light	Batch reactor; Cat. weight: 0.01 g; $P_{CO2}=P_{H2}=0.25$ bar; 100°C; 2 h; discontinuous mode	12.7	Tahir et al., 2015

presents several attractive features, such as a relative low cost and the resistance offered against the corrosion of aggressive media (Tahir and Amin, 2013). The TiO_2 properties in photocatalysis have been widely investigated either for environment application, such as in the degradation of organic pollutants, or in the energetic field, such as for hydrogen generation by the water splitting process. On the other hand, some studies recognize its alone use for the methanol synthesis (Han et al., 2009). The performances of the alone TiO_2 are significantly limited, especially regarding the adsorption and reduction of CO_2 and the activation of the photo-induced process, which can be partially improved through a fine tuning of the particle size and the introduction of oxygen vacancies. Another route to enhance the photoactivity of TiO_2 is the preferential exposure of crystal facets. Indeed, it has been found that the Anatase (1 0 1) facet plays a critical role in adsorbing CO_2 and facilitating the electron transfer from the surface of TiO_2 to the adsorbed molecule, even if, the (1 0 1) surface plane is less photoactive than (0 0 1), due to the presence of highly active unsaturated Ti atoms and surface oxygen species on (0 0 1) facet. On this account, recently Yu et al. (2014) achieved the best compromise between adsorption capacity and photocatalytic activity by obtaining the optimal 45:55 ratio in the exposure of (1 0 1) and (0 0 1) facets, which would allow the formation of a surface heterojunction inside the single particle for the transfer of photogenerated electrons and holes from (1 0 1) to (0 0 1) facets, respectively.

The size of TiO_2 particles rules the exposure of the specific surface area of the photocatalyst, affecting charge–carrier dynamics and light absorption efficiency. To address this, Kočí et al. (2009) have investigated the influence of crystallite size of TiO_2 nanoparticles in the CO_2 photoreduction under UV light, observing the growth in methane and methanol products with the decrease in the particle size up to 14 nm and reporting 9.5 and 1.15 μmol/g_{cat} as maximum yield values for CH_4 and CH_3OH, respectively. Improved effects can be derived from the inclusion of TiO_2 nanoparticles into a clay mineral structure or within the

zeolite cavities and framework (Yamashita et al., 1998). These composite materials can achieve generally two important advantages, a higher effective surface area and a lower crystallite size of the TiO_2 particles, driving to the reduction of electron-hole pairs recombination rate and a change of the acid-base properties of the catalyst surface. In particular, Kaolinite-TiO_2 composites have reported an activity 4 times higher in the photocatalytic reduction of CO_2 than that of alone TiO_2 (Kočí et al., 2011).

The photoactivity of TiO_2 requires photons with a wavelength less than 380 nm, which corresponds to only 5% circa of the solar spectrum. Besides the low adsorption of visible light, the main limit of TiO_2 in the methanol photosynthesis is the value of the redox potential (c.−0.25 eV at pH 0), which is lower than that required for the reduction of CO_2 to CO_2^- (i.e., −1.9 eV at pH 0). In order to overcome such strong limitations, various techniques have been developed in the last few years, which include doping with metals and nonmetals (Guan et al., 2003; Liu et al., 2012), sensitization using dyes, the use of supports and promoters, such as combination with metal oxides (i.e., CeO_2, ZnO, etc.), nanocarbons (Xia et al., 2007), graphene (Ai et al., 2011), enzymes (Woolerton et al., 2011), and novel sensitizers (Ettedgui et al., 2010).

Similarly to the role of chlorophyll in the natural photosynthesis, the employment of organic complexes like dye sensitizers is a valuable route to increase TiO_2 light absorption efficiency. By photons capture, dye sensitizers are oxidized, transferring the electrons generated on TiO_2, leading to charge separation. The use of phthalocyanines (Pc-s) have received great attention, due to their excellent photoconductivity properties, chemical stability, and optical absorption in the UV-vis region. Even the employment of CoPc complexes has been investigated. In particular, Zhao et al. (2009) documented that the addition of CoPc to TiO_2 promotes the photoresponse of TiO_2 in the visible region, narrowing the band gap from 3.22 eV of pure TiO_2 to 2.14 eV of the CoPc/TiO_2 system.

A well-established strategy for improving the photoactivity of TiO_2 accounts for the deposition of metal nanoparticles, such as copper, which can also enhance selectivity towards CH_3OH. On the contrary, Pd or Pt doping would favor the selectivity towards CH_4 and CO (Dhakshinamoorthy et al., 2012). The deposition of metal nanoparticles on TiO_2 aims to generate redox couples and, at the same time, to favor the adsorption of CO_2 molecules on metal sites, enhancing the reduction process against that of recombination (Tahir et al., 2015).

Compared with others, copper oxides have been demonstrated to be the most performing co-photocatalysts of TiO_2. Aside from an electron trap that prevents the electron-hole pairs recombination (Tseng and Wu, 2005), the key role played by copper can be ascribed to a combination of different effects, such as electronic promotion, as demonstrated by the decrease of the band-gap energy, and the larger electron mobility, consequent to the improved redox properties. Furthermore, the chemisorption of CO_2 is more favored on the copper catalytic

surface, as proved by the vast literature regarding methanol synthesis by catalytic hydrogenation (Arena et al., 2007, 2009, 2013; Xiao et al., 2015). On this account, CuO phase can act as co-photocatalyst, enhancing CO_2 availability on the photocatalytic surface and improving the electron transfer in the hole-electron generation process (Slamet et al., 2005).

The peculiar activity of the electronic promoter of Cu^{II} with regard to the other species with different oxidation state (i.e., Cu^0 and Cu^I) has been explained by Slamet et al. (2005), considering that Cu^{2+} ion has an unfilled 3d shell which makes electrons trapping feasible by Cu^{II} on the surface of TiO_2, according to the redox cycle reported in Eqs. (16.36)–(16.37).

$$Cu^{II}O \xrightarrow{e^-} Cu^{I}O \tag{16.36}$$

$$Cu^{I}O \xrightarrow{O_2/H^+} Cu^{II}O \tag{16.37}$$

During the photoreduction process, the electrons generated in the conduction band of TiO_2 by photoexitation, are trapped into the 3d core level of Cu^{2+}, towards reduction of Cu^{II} to Cu^I (Eq. 16.36), therefore, Cu^I as the second step (Eq. 16.37) is oxidized to Cu^{II} by the action of proton or O_2, forming $H^\bullet$ and $O_2^{\bullet -}$ radical species.

More recently, Wang et al. (2014) in opposition to Slamet et al. (2005) have argued that Cu^I species is an effective active phase in the CO_2 photocatalytic reduction process, due to the higher charge separation efficiency.

Photocatalytic tests carried out with different electronic promoters (M) have shown a progressive rise of the photoconversion rate by varying the M loading in the M-TiO_2 system up to 1.0–1.50 wt%. A further increase of the metal loading would have a negative effect on the photocatalytic activity under visible light, probably due to the metal ion species acting as multiple trap sites and thus facilitating electron–hole recombination (Ola and Maroto-Valer, 2015b).

Even the use of quantum dot (QDs) sensitizers for photocatalytic application has been recently valued because of thermal-photo stability and large adsorption cross sections. In particular, Wang et al. (2010a), combining CdSe and Pt doping with (QD)-sensitized TiO_2 heterostructures, have synthesized c-CdSe/Pt/TiO_2 photocatalysts in which a type II band alignment with TiO_2 is realized, leading to the direct injection into TiO_2 lattice of the photo-excited electrons of the QDs, for initiating the photocatalytic process.

The promotion of TiO_2 with ZnO or CeO_2 can lead to both structural and electronic benefits. In particular, cerium oxide can inhibit the growth of TiO_2 particles and promote the exposure of the specific surface area, thus favoring the adsorption of CO_2 and water. Furthermore, the natural coexistence of Ce^{3+} and Ce^{4+} ions in the lattice of ceria, combined with the oxygen-storage properties of the material, would enhance the charge separation and favor the formation of surface oxygen species with strong reduction capability, thus promoting the CO_2 reduction reaction (Abdullah et al., 2015; Xiong et al., 2015).

5.2 Non-TiO_2 Based Photocatalysts

Not many semiconductors exhibit band gap energies suitable for the methanol synthesis via CO_2 photoconversion, as shown in Fig. 16.18. In particular, several metal oxides and sulfides such as ZnO, WO_3, Fe_2O_3, ZrO_2, Cu_2O, $ATaO_4$ (A = Li, Na, In, K), CdS, Bi_2S_3, and ZnS have proven photocatalytic properties in the methanol photosynthesis under UV/Vis irradiation.

At the moment, zinc and nickel oxides represent the most investigated TiO_2 substitutes because of their larger photoactivity. The comparative study carried out by Yahaya et al. (2004) referred to the superior performance of both NiO and ZnO in the CO_2 photoreduction with water with respect of TiO_2 under monochromatic irradiation at 355 nm. NiO, ZnO, and TiO_2 achieved in the study, after 9 h of irradiation, a maximum methanol yield of c.180 μmol, c.150 μmol, and 100 μmol, respectively.

Among the oxides with wolframite-type structures, $InTaO_4$, whose band gap is c.2.6 eV, can be utilized for performing the reduction of CO_2, exploiting a larger part of sunlight spectrum, as shown in Fig. 16.19.

However, if alone, the $InTaO_4$ photocatalyst has demonstrated a very low activity in the methanol synthesis. Aiming at overcoming these limits and improving the methanol yield,

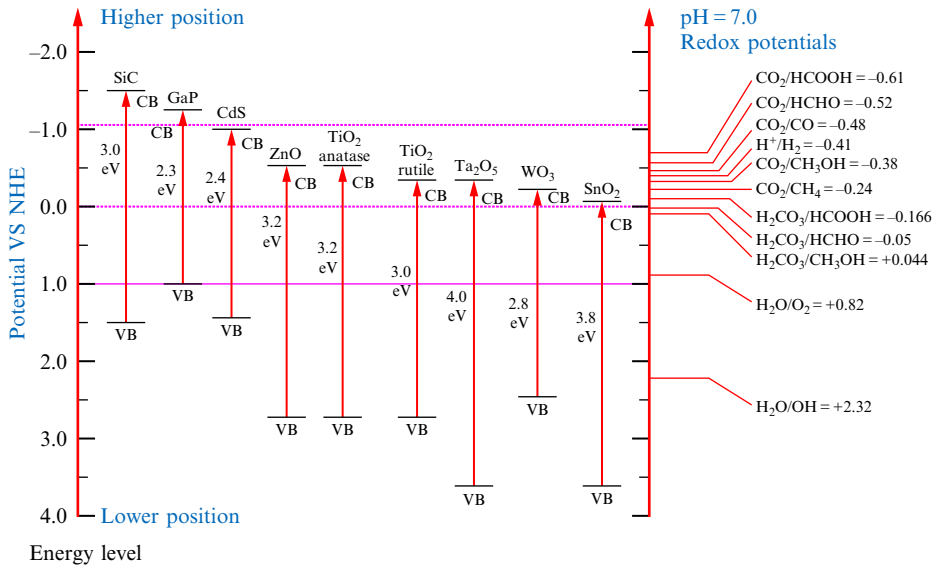

Fig. 16.18

Schematic representation of conductance band potentials of semiconductors and thermodynamic reduction potentials of various compounds measured at pH 7. *Reported from Tahir, M., Amin, N.A.S., 2013. Advances in visible light responsive titanium oxide-based photocatalysts for CO_2 conversion to hydrocarbon fuels. Energy Convers. Manag. 76, 194–214.*

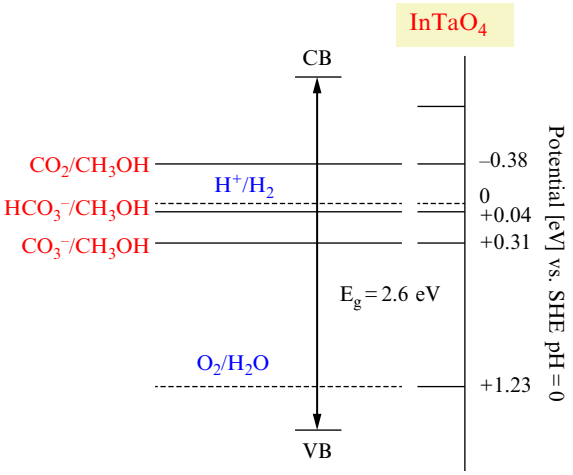

Fig. 16.19
Diagram reporting CB and VB levels of $InTO_4$ semiconductor and thermodynamic reduction potentials of various compounds at pH 0.

several studies have been carried out for enhancing the $InTaO_4$ proprieties by realizing a metal oxide heterojuction. In this respect, the study of Pan and Chen (2007) performed with a NiO-$InTaO_4$ photocatalyst, at 1.0 wt%. NiO of loading, has proven a significant improvement of the photocatalytic activity with respect to that of the pure $InTaO_4$, reporting in the 0.2 M $KHCO_3$ aqueous phase a methanol production rate of 1.394 μmol/g_{cat} h. These findings were then confirmed by the study of Wang et al. (2010b), who compared the photocatalytic performance of pure $InTiO_4$ with that of NiO/$InTiO_4$ system, obtaining a comparable methanol production rate by the use of NiO/$InTiO_4$ photocatalyst (1.11 μmol/g_{cat} h). The authors argued that interaction between the particles of NiO and the $InTaO_4$ phase, can act as electron trap creating a Schottky barrier that would suppress the electron-hole recombination.

The exploitation of Bi_2WO_6 Aurivillius oxides with a layered structure in the methanol synthesis has received recent considerable attention, due to the significant achievement in the photocatalytic water splitting and in the photodegradation of organic pollutants under visible light irradiation (Dai et al., 2015).

In particular, Cheng et al (2012) reported that Bi_2WO_6 microspheres, synthesized through an anion exchange route starting from BiOBr, displayed promising results, with a methanol yield of 32.6 μmol/g after 2 h of irradiation. A further improvement of activity of Bi_2WO_6 photocatalyst was achieved by Dai et al. (2015), through the addition of several conductive polymers (i.e., polyaniline, polypyrrole, and polythiophene) during the synthesis of Bi_2WO_6. Namely, the PTh/Bi_2WO_6 composite exhibited a methanol yield of 56.5 μmol/g_{cat} in 4 h of irradiation, resulting in the total yield of hydrocarbons c.3 times higher than that of pure

Bi_2WO_6. Such findings pointed out the improvement of visible light absorption ability obtained with the introduction of conducting polymers, which can promote even the charge transfer efficiency.

More recently, layered double hydroxides (LDHs), with octahedral structure, have received considerable attention as useful materials in the CO_2 photoconversion process because of their high CO_2 sorption capacity in the layered space, and their semiconductor properties, opportunely tuneable by changing the composition of the layer (Guo et al., 2016). In particular, this new class of compounds has the general formula below:

$$\text{LDHs} = \left[M^{2+}{}_{1-x}M^{3+}{}_{x}(OH)_2\right]^{x+}\left(A_{n-}{}^{x/n}\right)\cdot yH_2O \quad (0.20 < x < 0.33)$$

where M^{2+} and M^{3+} are divalent and trivalent cations (Cu^{2+}, Mg^{2+}, Al^{3+}, Fe^{3+}, etc.), while A_{n-} is n^--valent anion and y is the number of water molecule.

The energy gap of these materials can be favorably narrowed through the replacing of Mg in the octahedral structure with other elements, such as Zn, Cu, and Ti, which drives the formation of conductors with metal oxide structures like O—Cu—O, enabling an easy electrons excitation with visible light and, therefore, increasing the photocatalytic performance of the system. Accordingly, Lv and Liu (2016) have successfully synthesized a CuNiAl-LDHs photocatalyst, which has achieved the largest methanol yield (0.6 mmol/g_{cat}) compared to that of CuMgAl-LDHs and CuZnAl-LDHs systems, because of its narrower band gap (2.62 eV) and its larger surface area (101.9 m^2/g) than that of the other two LDHs compounds (2.97 eV and 83.7 m^2/g; 2.90 eV and 92.8 m^2/g), respectively.

6 Photoreactor

In addition to the development of visible-light responsive photocatalytic materials, the design and engineering of new photoreactors today represent the most suitable approaches to enhance the efficiency of the CO_2 photoreduction process. The ideal photoreactor should ensure a uniform light distribution throughout the entire photocatalytic system, it should provide a large area of exposure for irradiation and, at the same time, it should facilitate the separation/recovery of photocatalyst and products from the reaction medium. The photoreactors can be generally classified according to the phases involved in the reaction (i.e., three phase systems (gas-liquid-solid) or biphasic ones (gas-solid)), and to the mode of operation (i.e., batch, semi-batch, and continuous) (Li et al., 2014; Ola and Maroto-Valer, 2015a).

The three-phase photoreactors are the most employed systems in photocatalysis because of their simplicity and easy handling. In a laboratory, a three-phase apparatus generally consists of a quartz Continuously Stirred Tank Photoreactor (CST-Pr), in which the photocatalyst is suspended in the aqueous reaction medium through vigorous agitation, as shown in the photos of Figs. 16.20 and 16.21 (Spadaro et al., 2017). The most important

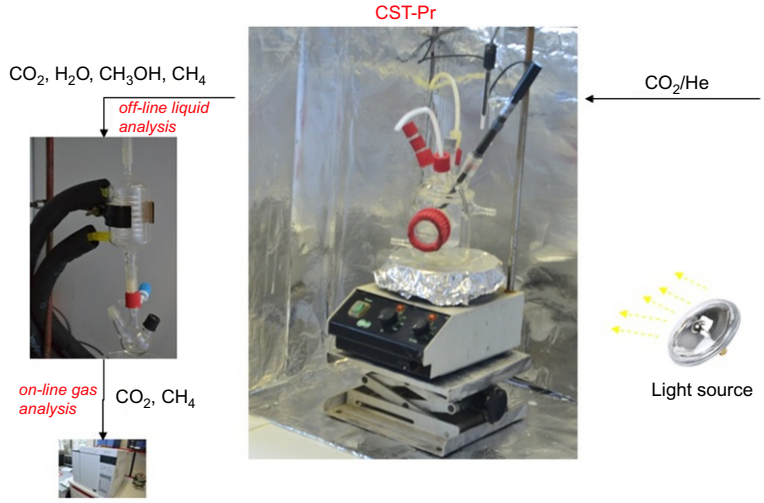

Fig. 16.20
Photo of "Continuously Stirred Tank" photoreactor configuration.

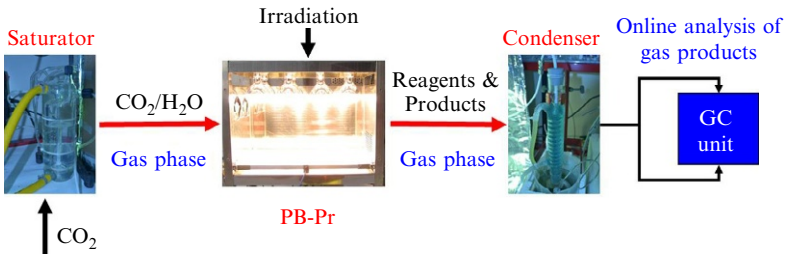

Fig. 16.21
Photo of "Packed bed" photoreactor configuration.

advantage of the CST-Pr system is the possibility to run the photoreduction process with an high catalyst loading. In addition, a superior illumination exposure can be achieved, increasing the light responsive to the photocatalyst, if the particle size of the material is sufficiently small and the solution is homogeneously mixed. On the contrary, the main drawbacks are related to the lower pressure of CO_2 available, the catalyst recovery from the reaction ambient, and the adsorption of light by the organic products in the solution, which limits the intensity of the radiation that effectively reaches the catalyst particles (Ola and Maroto-Valer, 2015a).

Alternatively, the biphasic system usually includes a Packed Bed Photoreactor (PB-Pr), in which the photocatalyst is physically confined longitudinally to the inner section of the reactor, separately from the CST-Pr configuration in which the photocatalyst is dispersed in the whole volume of the reactor. The surface of the photocatalytic bed is crossed and contacted by a continuous flow of gas/vapors reagents, as shown in Fig. 16.21. This type of photoreactor

configuration avoids the use of the liquid medium and, therefore, all limitations due to the solubility of the CO_2 in water, and the problems related to the mass transfer phenomena and to the stability of the photocatalyst. Furthermore, the biphasic system overcomes the drawback of the catalyst recovery from reaction medium, because the photocatalyst is confined or immobilized onto fixed supports such as plates, beads, fibers, and monoliths.

On this account, Spadaro et al. (2017) have recently compared the performance of CST-Pr configuration with that of the PB-Pr system, running the photoreduction of CO_2 for more than 120 h of irradiation under UV-visible light and over the same Cu-TiO_2 photocatalyst. In particular, the study clearly proves that both the reactor configuration and the operative conditions, like the reaction media/phase, can strongly act on the process yield and the selectivity of the reaction, also intervening on the photocatalyst stability. Indeed, CST-Pr leads almost exclusively to the formation of methanol, while in gas-vapor stream the conversion of CO_2 is also accomplished through notable evolution of methane and CO. Furthermore, at the lower contact time (<0.3 s) methane prevails with respect to the CO or to other by-products in the outlet-stream of PB-Pr configuration. On the other hand, providing the photoreduction process at a higher contact time (>22.0 s), no methanol is observed. Comparing the performance, CST-Pr system has shown a total hydrocarbon yield of 72 μmol/g_{cat}, which is lower than two orders with respect to that recorded by PB-Pr configuration (2430 μmol/g_{cat}). The remarkably higher productivity of the photosystems in the gas-vapor configuration is largely due to the lesser photo-deactivation phenomena which, in turn, occurs rapidly in the liquid media, driving to completely cut off the CO_2 conversion after about 10 h, as shown in Fig. 16.22A. This finding also mirrors a lower stability of the photocatalysts versus the photo-corrosion operated by water (Ola and Maroto-Valer, 2016). Indeed, in spite of a comparable methanol yield in the first hours of irradiation, the photocatalyst exhibits a higher stability in the humidified stream, running the CO_2 conversion almost firmly for more than 120 h, as shown in Fig. 16.22B.

Another important advantage of the biphasic system is related to the higher efficiency in the light absorption, since the fact that one of the parameters that most influences the photocatalytic yield is the number of photons absorbed by the catalyst (Ola et al., 2012; Ola and Maroto-Valer, 2014). On this account, the more recent reactor solutions are seeing the photocatalysts as the coating phase of a support matrix placed inside the reactor around the light source or directly on the photoreactor wall. In particular, Wu et al (2005) for the first time proposed a new photoreactor design, in which the photocatalyst, supported on the surface of the optical fibers, receives the photons transmitted from the fibers through the contact interface between the two phases, assuring a homogeneous distribution of light throughout the photoreactor. Indeed, as shown in Fig. 16.23, when the light is transmitted into the optical fibers, the beam is split into two components, due to the difference of the refraction index between the photocatalyst coating and the quartz wall. On this account, a portion of the light is reflected and transmitted along the fibers, while the rest of light passes through the quartz wall,

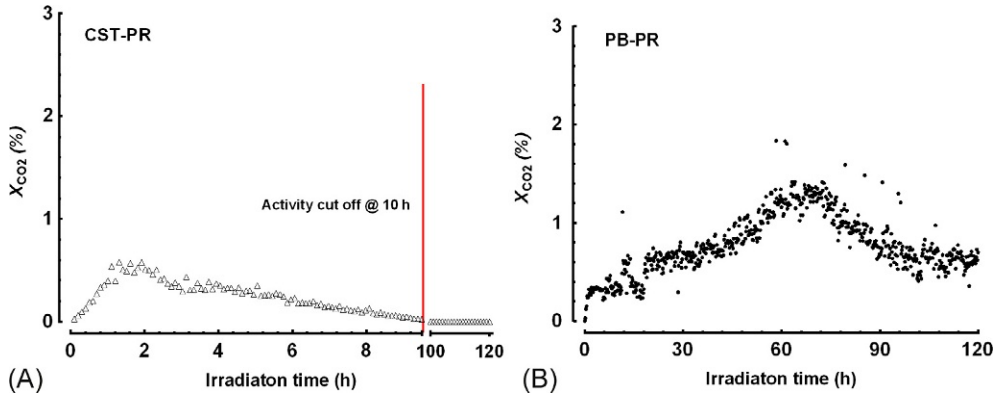

Fig. 16.22

Results of CO_2 photocatalytic reduction tests over Cu-TiO_2 photocatalyst: carbon dioxide conversion vs. irradiation time in ideal batch reactor (A) and in gas-vapor phase system (B). *Reported from Spadaro, L., Arena, F., Negro, P., Palella, A., 2017. Synthesis of fuels by photocatalytic reduction of CO_2 from industrial exhausts emissions: from laboratory size to the pilot scale. Appl. Catal. B: Environ. (in preparation).*

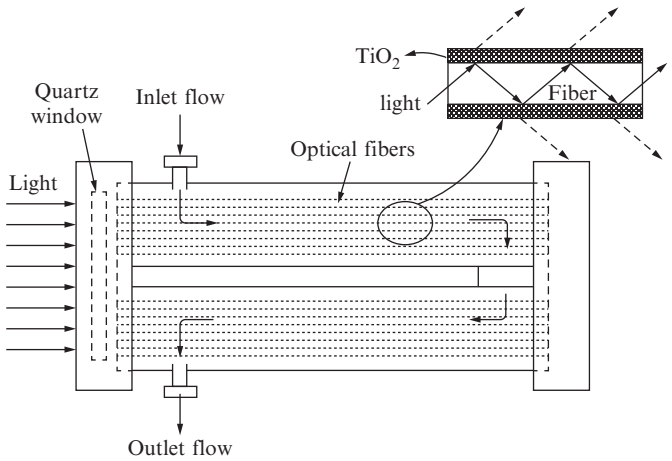

Fig. 16.23

Optical-fibers photoreactor. *Reported from Wu, J.C.S., Lin, H.M., Lai, C.L., 2005. Photo reduction of CO_2 to methanol using optical-fiber photoreactor. Appl. Catal. A: Gen. 296, 194–200.*

exciting the catalyst layer at the interface. Furthermore, Wang et al. (2010b) have compared the performance in the CO_2 photoreduction with respect to that of the tank photoreactor in the aqueous phase using the NiO/$InTaO_4$ catalyst under visible light and real sunlight irradiation, reporting a quantum efficiency value for the optical-fiber reactor 14 times higher than that of the aqueous phase reactor (0.0045% and 0.063%, respectively), which the authors have ascribed to the improved light-energy utilization of the catalyst film.

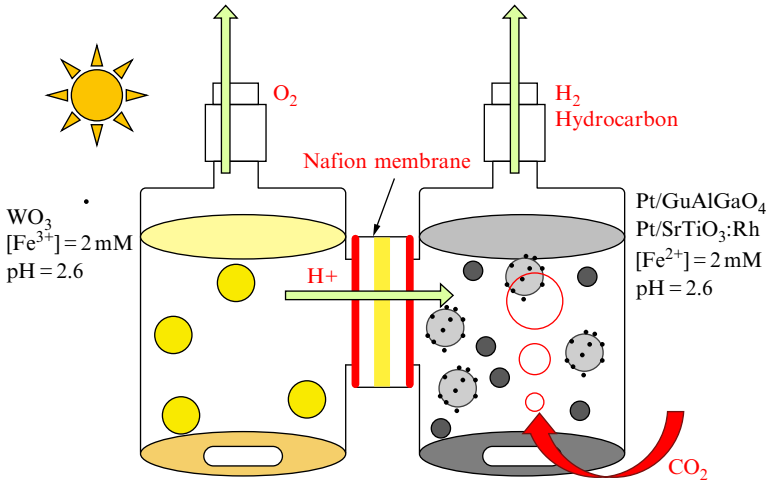

Fig. 16.24

Twin photoreactor. *Reported from Lee, W.H., Liao, C.H., Tsai, M.F., Huang, C.W., Wu, J.C.S., 2013. A novel twin reactor for CO_2 photoreduction to mimic artificial photosynthesis. Appl. Catal. B: Environ. 132–133, 445–451.*

Then, in 2013 the research team led by Wu introduced a new twin-reactor for photo-driven CO_2 hydrogenation into methanol, as shown in Fig. 16.24 (Lee et al., 2013). The heart of this technology was constituted by two quartz compartments divided by a membrane, containing two different photocatalysts for the production of hydrogen and oxygen, respectively. By including a CO_2 reduction photocatalyst in the H_2-generating compartment of the reactor, the hydrogen generated from water splitting can be used directly for the CO_2 hydrogenation. In this way, the addition of extra-hydrogen to drive the CO_2 complete reduction is avoided, achieving sustainable operation. Moreover, hydrogen and oxygen are produced separately, preventing the water-formation backward reaction, and avoiding the oxidation of hydrocarbons product due to the presence of oxygen in the same vessel (Yu et al., 2016).

With this reaction apparatus, a further enhancement of the efficiency of CO_2 hydrogenation was achieved by feeding a gaseous mixture of CO/CO_2, reaching a methanol production rate of 1 $\mu mol/g_{cat}$ h and a quantum efficiency of 0.0035%, with respect to the one using only CO or CO_2 (quantum efficiencies of 0.0005% and 0.001%, respectively). In fact, the presence of CO co-fed prompted the production of methyl formate, which was assumed by the authors as an intermediate product of CH_3OH, therefore enhancing both the methanol yield and the quantum efficiency (Cheng et al., 2015).

7 Conclusions and Future Trends

The practical exploitation of solar energy for the methanol synthesis is a very attractive research topic for its extraordinary impacts from energetic and environmental points of view.

Low photoconversion efficiency and poor product selectivity represent the main process drawbacks, due to a combination of thermodynamic, kinetic, and engineering factors.

New photocatalytic materials at high "quantum yield" and innovative photoreactor configurations are under scrutiny to overcome the technological limits of methanol synthesis, especially considering a 100% quantum efficiency of the current solar panels technology.

A strongly rising concern in the artificial "methanol photosynthesis" is conceivable in the next future, considering the recent significant advances on materials and reactors development.

References

Abdullah, H., Khan, M.R., Pudukudy, M., Yaakob, Z., Ismail, N.A., 2015. CeO_2-TiO_2 as a visible light active catalyst for the photoreduction of CO_2 to methanol. J. Rare Earths 33 (11), 1155–1161.

Ai, Z.H., Ho, W.K., Lee, S., 2011. Efficient visible light photocatalytic removal of NO with BiOBr-graphene nanocomposites. J. Phys. Chem. C 115, 25330–25337.

Anpo, M., Yamashita, H., Ichihashi, Y., Ehara, S., 1995. Photocatalytic reduction of CO_2 with H_2O on various titanium oxide catalysts. J. Electroanal. Chem. 396, 21–26.

Arena, F., Barbera, K., Italiano, G., Bonura, G., Spadaro, L., Frusteri, F., 2007. Synthesis, characterization and activity pattern of Cu-ZnO/ZrO_2 catalysts in the hydrogenation of carbon dioxide to methanol. J. Catal. 249, 185–194.

Arena, F., Italiano, G., Barbera, K., Bonura, G., Spadaro, L., Frusteri, F., 2009. Basic evidences for methanol-synthesis catalyst design. Catal. Today 143, 80–85.

Arena, F., Mezzatesta, G., Zafarana, G., Trunfio, G., Frusteri, F., Spadaro, L., 2013. Effects of oxide carriers on surface functionality and process performance of the Cu-ZnO system in the synthesis of methanol via CO_2 hydrogenation. J. Catal. 300, 141–151.

Arena, F., Mezzatesta, G., Spadaro, L., Trunfio, G., 2014. Latest advances in the catalytic hydrogenation of carbon dioxide to methanol/dimethylether. In: Bhanage, B.M., Arai, M. (Eds.), Transformation and Utilization of Carbon Dioxide, Green Chemistry and Sustainable Technology. Springer-Verlag, Berlin, Heidelberg, pp. 103–130.

Asi, M.A., He, C., Su, M., Xia, D., Lin, L., Deng, H., Xiong, Y., Qiu, R., Li, X.Z., 2011. Photocatalytic reduction of CO_2 to hydrocarbons using AgBr/TiO_2 nanocomposites under visible light. Catal. Today 175, 256–263.

Carp, O., Huisman, C.L., Reller, A., 2004. Photoinduced reactivity of titanium dioxide. Prog. Solid State Chem. 32, 33–177.

Chang, X., Wang, T., Gong, J., 2016. CO_2 photo-reduction: insights into CO_2 activation and reaction on surfaces of photocatalysts. Energy Environ. Sci. 9, 2177–2196.

Chen, S., Hub, Y., Meng, S., Fu, X., 2014. Study on the separation mechanisms of photogenerated electrons and holes for composite photocatalysts g-C_3N_4-WO_3. Appl. Catal. B Environ. 150–151, 564–573.

Cheng, H.F., Huang, B.B., Liu, Y.Y., Wang, Z.Y., Qin, X.Y., Zhang, X.Y., Dai, Y., 2012. An anion exchange approach to Bi_2WO_6 hollow microspheres with efficient visible light photocatalytic reduction of CO_2 to methanol. Chem. Commun. 48, 9729–9731.

Cheng, Y.H., Nguyen, V.H., Chan, H.Y., Wu, J.C.S., Wang, W.H., 2015. Photo-enhanced hydrogenation of CO_2 to mimic photosynthesis by CO co-feed in a novel twin reactor. Appl. Energy 147, 318–324.

Concepcion, J.J., House, R.L., Papanikolas, J.M., Meyer, T.J., 2012. Chemical approaches to artificial photosynthesis. PNAS 109, 15560–15564.

Dai, W., Xu, H., Yu, J., Hu, X., Luo, X., Tu, X., Yang, L., 2015. Photocatalytic reduction of CO_2 into methanol and ethanol over conducting polymers modified Bi_2WO_6 microspheres under visible light. Appl. Surf. Sci. 356, 173–180.

Dhakshinamoorthy, A., Navalon, S., Corma, A., Garcia, H., 2012. Photocatalytic CO_2 reduction by TiO_2 and related titanium containing solids. Energy Environ. Sci. 5, 9217–9233.

Doong, R., Liljebjelke, L.K., Fralish, G., Kumar, A., Mohnen, D., 1995. Cell-free synthesis of pectin. Plant Physiol. 109, 141–152.

Ettedgui, J., Diskin-Posner, Y., Weiner, L., Neumann, R., 2010. Photoreduction of carbon dioxide to carbon monoxide with hydrogen catalyzed by a rhenium(I) phenanthroline-polyoxometalate hybrid complex. J. Am. Chem. Soc. 133, 188–190.

Fan, W., Zhang, Q., Wang, Y., 2013. Semiconductor based nanocomposites for photocatalytic H_2 production and CO_2 conversion. Phys. Chem. Chem. Phys. 15, 2632–2649.

Fiedler, E., Grossmann, G., Kersebohm, D.B., Weiss, G., Witte, C., 2000. Methanol. In: Ullmann's Encyclopedia of Industrial Chemistry. Wiley, New York.

Freund, H.J., Roberts, M.W., 1996. Surface chemistry of carbon dioxide. Surf. Sci. Rep. 25, 225–273.

Galbally, I.E., Kirstine, W., 2002. The production of methanol by flowering plants and the global cycle of methanol. J. Atmos. Chem. 43, 195–229.

Galli, F., Compagnoni, M., Vitali, D., Pirola, C., Bianchi, C.L., Villa, A., Prati, L., Rossetti, I., 2017. CO_2 photoreduction at high pressure to both gas and liquid products over titanium dioxide. Appl. Catal. B Environ. 200, 386–391.

Guan, G.Q., Kida, T., Yoshida, A., 2003. Reduction of carbon dioxide with water under concentrated sunlight using photocatalyst combined with Fe-based catalyst. Appl. Catal. B Environ. 41, 387–396.

Guo, Q., Zhang, Q., Wang, H., Liu, Z., Zhao, Z., 2016. Core-shell structured ZnO@Cu-Zn-Al layered double hydroxides with enhanced photocatalytic efficiency for CO_2 reduction. Catal. Commun. 77, 118–122.

Gust, D., Moore, T.A., Moore, A.L., 2009. Solar fuels via artificial photosynthesis. Acc. Chem. Res. 42 (12), 1890–1898.

Han, X., Kuang, Q., Jin, M., Xie, X., Zheng, L., 2009. Synthesis of titania nanosheets with a high percentage of exposed (001) facets and related photocatalytic properties. J. Am. Chem. Soc. 131, 3152–3153.

Haynes, W.M. (Ed.), 2014. Handbook of Chemistry and Physics, 95th ed. CRC Press, Boca Raton.

He, Z., Tang, J., Shen, J., Chen, J., Song, S., 2016. Enhancement of photocatalytic reduction of CO_2 to CH_4 over TiO_2 nanosheets by modifying with sulfuric acid. Appl. Surf. Sci. 364, 416–427.

Inoue, T., Fujishima, A., Konishi, A., Honda, K., 1979. Photoelectrocatalytic reduction of carbon dioxide in aqueous suspensions of semiconductor powders. Nature 277, 637–638.

Jeyalakshmi, V., Mahalakshmy, R., Krishnamurthy, K.R., Viswanathan, B., 2016. Photocatalytic reduction of carbon dioxide in alkaline medium on La-modified sodium tantalate with different co-catalysts under UV-visible radiation. Catal. Today 266, 160–167.

Kočí, K., Obalová, L., Plachá, D., Lacný, Z., Jirkovský, J., 2009. Effect of TiO_2 particle size on the photocatalytic reduction of CO_2. Appl. Catal. B Environ. 89, 494–502.

Kočí, K., Matějka, V., Kovář, P., Lacný, Z., Obalová, L., 2011. Comparison of the pure TiO_2 and kaolinite/TiO_2 composite as catalyst for CO_2 photocatalytic reduction. Catal. Today 161, 105–109.

Kondarides, D.I., 2010. Photocatalysis. In: Centi, G. (Ed.), Catalysis. Encyclopedia of Life Support Systems (EOLSS), Developed under the Auspices of the UNESCO. EOLSS Publishers, Oxford.

Larminie, J., Dicks, A., 2003. Fuel Cell Systems Explained, second ed. Wiley, New York.

Larson, E.D., Tingjin, R., 2003. Synthetic fuel production by indirect coal liquefaction. Energy Sustain. Dev. 7, 79–102.

Lee, W.H., Liao, C.H., Tsai, M.F., Huang, C.W., Wu, J.C.S., 2013. A novel twin reactor for CO_2 photoreduction to mimic artificial photosynthesis. Appl. Catal. B Environ. 132–133, 445–451.

Li, H., Lei, Y., Huang, Y., Fang, Y., Xu, Y., Zhu, L., Li, X., 2011. Photocatalytic reduction of carbon dioxide to methanol by Cu_2O/SiC nanocrystallite under visible light irradiation. J. Nat. Gas Chem. 20, 145–150.

Li, K., An, X., Park, K.H., Khraisheh, M., Tang, J., 2014. A critical review of CO_2 photoconversion: catalysts and reactors. Catal. Today 224, 3–12.

Li, K., Peng, T., Ying, Z., Song, S., Zhang, J., 2016. Ag-loading on brookite TiO_2 quasi nanocubes with exposed {210} and {001} facets: activity and selectivity of CO_2 photoreduction to CO/CH_4. Appl. Catal. B Environ. 180, 130–138.

Linsebigler, A.L., Lu, G., Yates Jr., J.T., 1995. Photocatalysis on TiO_2 surfaces: principles, mechanisms, and selected results. Chem. Rev. 95, 735–758.
Liu, L., Li, Y., 2014. Understanding the reaction mechanism of photocatalytic reduction of CO_2 with H_2O on TiO_2-based photocatalysts: a review. Aerosol Air Qual. Res. 14, 453–469.
Liu, B.J., Torimoto, T., Yoneyama, H., 1998. Photocatalytic reduction of CO_2 using surface-modified CdS photocatalysts in organic solvents. J. Photochem. Photobiol. A Chem. 113, 93–97.
Liu, X.M., Lu, G.Q., Yan, Z.F., Beltramini, J., 2003. Recent advances in catalysts for methanol synthesis via hydrogenation of CO and CO_2. Ind. Eng. Chem. Res. 42, 6518–6530.
Liu, S., Zhao, Z., Wanga, Z., 2007. Photocatalytic reduction of carbon dioxide using sol-gel derived titania-supported CoPc catalysts. Photochem. Photobiol. Sci. 6, 695–700.
Liu, S., Guo, E., Yin, L., 2012. Tailored visible-light driven anatase TiO_2 photocatalysts based on controllable metal ion doping and ordered mesoporous structure. J. Mater. Chem. 22, 5031–5041.
Liu, D., Fernández, Y., Ola, O., Mackintosh, S., Maroto-Valer, M.M., Parlett, C.M.A., Lee, A.F., Wu, J.C.S., 2015. On the impact of Cu dispersion on CO_2 photoreduction over Cu/TiO_2. Catal. Commun. 25, 78–82.
Low, J., Cheng, B., Yu, J., Jaroniec, M., 2016. Carbon-based two-dimensional layered materials for photocatalytic CO_2 reduction to solar fuels. Energy Storage Mater. 3, 24–35.
Lv, M., Liu, H., 2016. Photocatalytic property and structural stability of CuAl-based layered double hydroxides. J. Solid State Chem. 227, 232–238.
Michalkiewicz, B., Majewska, J., Kądziołka, G., Bubacz, K., Mozia, S., Morawski, A.W., 2014. Reduction of CO_2 by adsorption and reaction on surface of TiO_2-nitrogen modified photocatalyst. J. CO_2 Util. 5, 47–52.
Navalón, S., Dhakshinamoorthy, A., Álvaro, M., Garcia, H., 2013. Photocatalytic CO_2 reduction using non-titanium metal oxides and sulphides. ChemSusChem 6, 562–577.
Nikokavoura, A., Trapalis, C., 2017. Alternative photocatalysts to TiO_2 for the photocatalytic reduction of CO_2. Appl. Surf. Sci. 391, 149–174.
Núñez, J., O'Shea, V.A., Jana, P., Coronado, J.M., Serrano, D.P., 2013. Effect of copper on the performance of ZnO and $ZnO_{1-x}N_x$ oxides as CO_2 photoreduction catalysts. Catal. Today 209, 21–27.
Ohimain, E.I., 2016. Methanol contamination in traditionally fermented alcoholic beverages: the microbial dimension. Springerplus 5 (1), 1607.
Ola, O., Maroto-Valer, M.M., 2014. Role of catalyst carriers in CO_2 photoreduction over nanocrystalline nickel loaded TiO_2-based photocatalysts. J. Catal. 309, 300–308.
Ola, O., Maroto-Valer, M.M., 2015a. Review of material design and reactor engineering on TiO_2 photocatalysis for CO_2 reduction. J Photochem Photobiol C: Photochem Rev 24, 16–42.
Ola, O., Maroto-Valer, M.M., 2015b. Transition metal oxide based TiO_2 nanoparticles for visible light induced CO_2 photoreduction. Appl. Catal. A Gen. 502, 114–121.
Ola, O., Maroto-Valer, M.M., 2015c. Review of material design and reactor engineering on TiO_2 photocatalysis for CO_2 reduction. J Photochem Photobiol C: Photochem Rev 24, 16–42.
Ola, O., Maroto-Valer, M.M., 2016. Synthesis, characterization and visible light photocatalytic activity of metal based TiO_2 monoliths for CO_2 reduction. Chem. Eng. J. 283, 1244–1253.
Ola, O., Maroto-Valer, M., Liu, D., Mackintosh, S., Lee, C.W., Wu, J.C.S., 2012. Performance comparison of CO_2 conversion in slurry and monolith photoreactors using Pd and Rh-TiO_2 catalyst under ultraviolet irradiation. Appl. Catal. B Environ. 126, 172–179.
Olah, G.A., Goeppert, A., Surya Prakash, G.K., 2009. Chemical recycling of carbon dioxide to methanol and dimethyl ether: from greenhouse gas to renewable, environmentally carbon neutral fuels and synthetic hydrocarbons. J. Org. Chem. 74, 487–498.
Pan, P.W., Chen, Y.W., 2007. Photocatalytic reduction of carbon dioxide on $NiO/InTaO_4$ under visible light irradiation. Catal. Commun. 8, 1546–1549.
Paulino, P.N., Salim, V.M.M., Resende, N.S., 2016. Zn-Cu promoted TiO_2 photocatalyst for CO_2 reduction with H_2O under UV light. Appl. Catal. B Environ. 185, 362–370.
Pérez-Fortes, M., Schöneberger, J.C., Boulamanti, A., Tzimas, E., 2016. Methanol synthesis using captured CO_2 as raw material: techno-economic and environmental assessment. Appl. Energy 161, 718–732.

Pontzen, F., Liebner, W., Gronemann, V., Rothaemel, M., Ahlers, B., 2011. CO_2-based methanol and DME efficient technologies for industrial scale production. Catal. Today 171, 242–250.

Rossetti, I., Villa, A., Pirola, C., Pratia, L., Ramis, G., 2014. A novel high-pressure photoreactor for CO_2 photoconversion to fuels. RSC Adv. 4, 28883–28885.

Rossetti, I., Villa, A., Compagnoni, M., Prati, L., Ramis, G., Pirola, C., Bianchi, C.L., Wang, W., Wang, D., 2015. CO_2 photoconversion to fuels under high pressure: effect of TiO_2 phase and of unconventional reaction conditions. Catal. Sci. Technol. 5, 4481–4487.

Rossi, F., Nicolini, A., 2012. An experimental investigation to improve the hydrogen production by water. Appl. Energy 97, 763–770.

Saladin, F., Alxneit, I., 1997. Temperature dependence of the photochemical reduction of CO_2 in the presence of H_2O at the solid/gas interface of TiO_2. J. Chem. Soc. Faraday Trans. 93 (23), 4159–4163.

Slamet, Nasution, H.W., Purnama, E., Kosela, S., Gunlazuardi, J., 2005. Photocatalytic reduction of CO_2 on copper-doped Titania catalysts prepared by improved-impregnation method. Catal. Commun. 6, 313–319.

Song, C., 2006. Global challenges and strategies for control, conversion and utilization of CO_2 for sustainable development involving energy, catalysis, adsorption and chemical processing. Catal. Today 115, 2–32.

Spadaro, L., Arena, F., Bonura, G., Mezzapica, A., Palella, A., Frusteri, F., 2013. Cu-TiO_2 photocatalysts for the direct conversion of CO_2 into methanol. In: 23rd North American Catalysis Society Meeting, Louisville, Kentucky, June 2–7.

Spadaro, L., Arena, F., Negro, P., Palella, A., 2017. Synthesis of fuels by photocatalytic reduction of CO_2 from industrial exhausts emissions: from laboratory size to the pilot scale. Appl. Catal. B Environ. (in preparation).

Su, Y., Zhang, Z., Liu, H., Wang, Y., 2017. $Cd_{0.2}Zn_{0.8}S$@UiO-66-NH_2 nanocomposites as efficient and stable visible-light-driven photocatalyst for H_2 evolution and CO_2 reduction. Appl. Catal. B Environ. 200, 448–457.

Tahir, M., Amin, N.A.S., 2013. Advances in visible light responsive titanium oxide-based photocatalysts for CO_2 conversion to hydrocarbon fuels. Energy Convers. Manag. 76, 194–214.

Tahir, M., Thair, B., Amin, N.A.S., 2015. Gold-nanoparticle-modified TiO_2 nanowires for plasmon-enhanced photocatalytic CO_2 reduction with H_2 under visible light irradiation. Appl. Surf. Sci. 356, 1289–1299.

Tan, L.L., Ong, W.J., Chai, S.P., Mohamed, A.R., 2016. Visible-light-activated oxygen-rich TiO_2 as next generation photocatalyst: importance of annealing temperature on the photoactivity toward reduction of carbon dioxide. Chem. Eng. J. 283, 1254–1263.

Tseng, I.H., Wu, J.C.S., 2005. Chemical states of metal-loaded titania in the photoreduction of CO_2. Catal. Today 97, 113–119.

Tseng, I.H., Chang, W.C., Wu, J.C.S., 2002. Photoreduction of CO_2 using sol-gel derived titania and titania-supported copper catalysts. Appl. Catal. B Environ. 37, 37–48.

Tseng, I.H., Wu, J.C.S., Chou, H.Y., 2004. Effects of sol-gel procedures on the photocatalysis of Cu/TiO_2 in CO_2 photoreduction. J. Catal. 221, 432–440.

Vitillo, J.G., 2015. Magnesium-based systems for carbon dioxide capture, storage and recycling: from leaves to synthetic nanostructured materials. RSC Adv. 5, 36192–36239.

Wang, C., Thompson, R.L., Baltrus, J., Matranga, C., 2010a. Visible light photoreduction of CO_2 Using CdSe/Pt/TiO_2 heterostructured catalysts. J. Phys. Chem. Lett. 1, 48–53.

Wang, Z.Y., Chou, H.C., Wu, J.C.S., Tsai, D.P., Mul, G., 2010b. CO_2 photoreduction using NiO/$InTaO_4$ in optical-fiber reactor for renewable energy. Appl. Catal. A Gen. 380, 172–177.

Wang, W., Wang, S., Ma, X., Gong, J., 2011. Recent advances in catalytic hydrogenation of carbon dioxide. Chem. Soc. Rev. 40, 3703–3727.

Wang, J., Ji, G., Liu, Y., Gondal, M.A., Chang, X., 2014. Cu_2O/TiO_2 heterostructure nanotube arrays prepared by an electrodeposition method exhibiting enhanced photocatalytic activity for CO_2 reduction to methanol. Catal. Commun. 46, 17–21.

White, J.L., Baruch, M.F., Pander III, J.E., Hu, Y., Fortmeyer, I.C., Park, J.E., Zhang, T., Liao, K., Gu, J., Yan, Y., Shaw, T.W., Abelev, E., Bocarsly, A.B., 2015. Light-driven heterogeneous reduction of carbon dioxide: photocatalysts and photoelectrodes. Chem. Rev. 115, 12888–12935.

Woolerton, T.W., Sheard, S., Pierce, E., Ragsdale, S.W., Armstrong, F.A., 2011. CO_2 photoreduction at enzyme-modified metal oxide nanoparticles. Energy Environ. Sci. 4, 2393–2399.

Wu, J.C.S., 2009. Photocatalytic reduction of greenhouse gas CO_2 to fuel. Catal. Surv. Asia 13, 30–40.

Wu, J.C.S., Lin, H.M., Lai, C.L., 2005. Photo reduction of CO_2 to methanol using optical-fiber photoreactor. Appl. Catal. A Gen. 296, 194–200.

Xi, G.C., Ouyang, S.X., Ye, J., 2011. General synthesis of hibrid TiO_2 mesoporus "French Fries" toward improved photocalytic conversion of CO_2 into hydrocarbon fuel: a case of TiO_2/ZnO. Chem. Eur. J. 17, 9057–9061.

Xia, X.H., Jia, Z.H., Yu, Y., Liang, Y., Wang, Z., Ma, L.L., 2007. Preparation of multi-walled carbon nanotube supported TiO_2 and its photocatalytic activity in the reduction of CO_2 with H_2O. Carbon 45, 717–721.

Xiao, J., Mao, D., Guo, X., Yu, J., 2015. Effect of TiO_2, ZrO_2 and TiO_2-ZrO_2 on the performance of CuO-ZnO catalyst for CO_2 hydrogenation to methanol. Appl. Surf. Sci. 338, 146–153.

Xiong, Z., Zhao, Y., Zhang, J., Zheng, C., 2015. Efficient photocatalytic reduction of CO_2 into liquid products over cerium doped titania nanoparticles synthesized by a sol-gel auto-ignited method. Fuel Process. Technol. 135, 6–13.

Yahaya, A.H., Gondal, M.A., Hameed, A., 2004. Selective laser enhanced photocatalytic conversion of CO_2 into methanol. Chem. Phys. Lett. 400, 206–212.

Yamashita, H., Fujii, Y., Ichihashi, Y., Zhang, S.G., Ikeue, K., Park, D.R., Koyano, K., Tatsumi, T., Anpo, M., 1998. Selective formation of CH_3OH in the photocatalytic reduction of CO_2 with H_2O on titanium oxides highly dispersed within zeolites and mesoporous molecular sieves. Catal. Today 45, 221–227.

Yu, J., Low, J., Xiao, W., Zhou, P., Jaroniec, M., 2014. Enhanced photocatalytic CO_2-reduction activity of anatase TiO_2 by coexposed {001} and {101} facets. J. Am. Chem. Soc. 136, 8839–8842.

Yu, S.H., Chiu, C.W., Wu, Y.Y., Liao, C.H., Nguyen, V.H., Wu, J.C.S., 2016. Photocatalytic water splitting and hydrogenation of CO_2 in a novel twin photoreactor with IO_3^-/I^- shuttle redox mediator. Appl. Catal. A Gen. 518, 158–166.

Yuan, L., Xu, Y., 2015. Photocatalytic conversion of CO_2 into value-added and renewable fuels. Appl. Surf. Sci. 342, 154–167.

Zhang, Z., Huang, Z., Cheng, X., Wang, Q., Chen, Y., Dong, P., Zhang, X., 2015. Product selectivity of visible-light photocatalytic reduction of carbon dioxide using titanium dioxide doped by different nitrogen-sources. Appl. Surf. Sci. 355, 45–51.

Zhao, Z., Fan, J., Xie, M., Wang, Z., 2009. Photo-catalytic reduction of carbon dioxide with in-situ synthesized CoPc/TiO_2 under visible light irradiation. J. Clean. Prod. 17, 1025–1029.

Zhou, H., Li, P., Liu, J., Chen, Z., Liu, L., Dontsova, D., Yan, R., Fan, T., Zhang, D., Ye, J., 2016. Biomimetic polymeric semiconductor based hybrid nanosystems for artificial photosynthesis towards solar fuels generation via CO_2 reduction. Nano Energy 25, 128–135.

PART 3

Modeling and Technology

This page intentionally left blank

CHAPTER 17

Modeling in Methanol Synthesis

Outi Mäyrä, Kauko Leiviskä
University of Oulu, Oulu, Finland

Acronyms

ICI	Imperial Chemical Industries
BASF	Badische Anilin–& Soda Fabrik
CO_2	carbon dioxide
H_2	hydrogen
CO	carbon monoxide
CH_3OH	methanol
H_2O	water
Cu	copper
ZnO	zinc oxide
Cr_2O_3	chromium oxide
Al_2O_3	aluminum oxide
CuO	copper oxide
Zr	zirconium
ANN	artificial neural network
MPC	model predictive control
DE	differential evolution
DMMR	dual-bed multifunctional methanol reactor
CMR	conventional methanol reactor
RWGS	reverse water-gas shift reaction

Symbols

C_i	concentration of substance i [mol/dm^3]
$C_{i,in}$	concentration of substance i in feed flow [mol/dm^3]
F	feed flow [dm^3/s]
k_j	rate constant
A_j	kinetic parameter for Arrhenius equation
B_j	kinetic parameter for Arrhenius equation
$K_j = A_j \exp\left(\frac{B_j}{RT}\right)$	Arrhenius equation for parameter identification

Methanol. https://doi.org/10.1016/B978-0-444-63903-5.00017-0

K_i	equilibrium constant
R	ideal gas constant 8.31446 J K^{-1} mol^{-1}
n_i	the amount of substance i [mol]
$\dot{n}_i$	the molar flow rate i [mol/s]
R_i	the specific production/consumption rate of the substance i [mol/s]
p	pressure [bar]
T	temperature [K]
V	volume [dm^3]

1 Introduction

Methanol synthesis is a widely studied process and the product, methanol, is commonly utilized as a fuel, a solvent, an energy storage medium, and a feedstock in the industry. Especially in energy-related conversion, methanol is assumed to play an important role in the future. To meet the demands of the future, that makes requirements for process development to achieve sustainable and energy-efficient ways to produce methanol a necessity.

Known as the "high-pressure" process, the first commercial methanol synthesis plant was opened in 1923 in Germany by Badische Anilin–& Soda Fabrik (BASF). The operational point in this process was at 320–450°C and 250–350 bar (Gallucci and Basile, 2007). The applied catalyst was based on chromate. The so-called "low-pressure" process replaced the old one in the 1960s, when the ability to produce sulfur-free synthesis gas made it possible to use the more active copper-based catalysts. This process was operated in the lower pressures and temperatures, namely 60–80 bar and 250–280°C (Lange, 2001). Since then, the markets have been dominated by two low-pressure processes: ICI (Imperial Chemical Industries) and Lurgi-processes (Løvik, 2001).

The traditional industrial methanol production process via synthesis gas includes three production steps: production of the synthesis gas, conversion of the synthesis gas into methanol, and distillation of the reactor effluent. Nowadays, most of the commercial processes are operated in gas phase using the copper-based catalysts. The main differences among the processes are in reactor design and catalyst arrangements. The desired purity of the produced methanol affects the distillation configuration and the adopted feedstock. When considering the known processes for methanol production, the production and the purification of the synthesis gas are crucial because of their overall cost effect (Bozzano and Manenti, 2016). The existing technologies for producing methanol, identified in Bozzano and Manenti (2016), can be listed as:

- Gas-phase technologies
  - Adiabatic reactors
  - Isothermal reactors (for example, the Lurgi process)
  - Gas-phase fluidized bed converter

- Liquid-phase technologies
- Membrane reactors
- One-step technologies.

Even though methanol synthesis has been a commercial process since 1923, there is still discussion about the reaction mechanism and kinetic modeling of the system (Rozovskii and Lin, 2003; Peter et al., 2012; Bozzano and Manenti, 2016). However, many studies assume that the methanol is produced primarily through CO_2 hydrogenation (Skrzypek et al., 1995; Coteron and Hayhurst, 1994; Vanden Bussche and Froment, 1996; Wu et al., 2001; Šetinc and Levec, 1999, 2001). In Šetinc and Levec (1999), it is stated that the role of CO is to remove absorbed oxygen from the catalyst surface, which leads to a reaction between CO_2 and H_2.

The main reactions involved in methanol production from synthesis gas are

$$CO + 2H_2 \Leftrightarrow CH_3OH, \tag{17.1}$$

$$CO_2 + 3H_2 \Leftrightarrow CH_3OH + H_2O, \tag{17.2}$$

$$CO + H_2O \Leftrightarrow CO_2 + H_2. \tag{17.3}$$

The alternative feedstock and production routes have also been studied. There, the utilization of the biomass, wood, or garbage (Gallucci and Basile, 2007), and CO_2 in methanol production is the attractive and current research topic. The use of CO_2 as a feedstock has especially drawn a lot of attention (Skrzypek et al., 1995; Vanden Bussche and Froment, 1996; Kokubu et al., 2000; Løvik, 2001; Ganesh, 2014). One reason for this is the strict regulation of CO_2 emissions stated in the Kyoto agreement (Løvik, 2001). In general, research related to the methanol synthesis has mainly focused on the catalyst-developing (Lachowska and Skrzypek, 2004; Li et al., 2014; Li and Jens, 2013; Jadhav et al., 2014; Xu et al., 2016) and feedstock-producing processes. The use of biomass is one of the research topics at the moment (Tock et al., 2010; Göransson et al., 2011; Holmgren et al., 2012; Bozzano and Manenti, 2016; Manenti et al., 2016).

A couple of interesting examples of the utilization of CO_2 as a feedstock in methanol synthesis have been published. In Iceland, methanol is produced from hydrogen and carbon dioxide utilizing geothermal energy (Halper, 2011; Olah 2013; Kauw et al., 2015). On the other hand, in Japan the pilot facility for methanol synthesis from hydrogen and carbon dioxide has been running since 2009 (Mitsui Chemicals, 2010).

2 Process Identification for Modeling

The identification of dynamic and variable interactions of the studied process often includes experimental campaigns in connection with mathematical modeling that consists of the estimation of model parameters and structure. In this context, many authors have examined the reaction kinetics of methanol synthesis by process identification. The studies usually involve

experiments with varying reaction conditions (temperature and pressure), feedstock, and applied catalysts. Some derived mathematical model structures found in the literature are based on the synthesis from CO and H_2 while others take CO_2 into account as a feed. Thus, a variety of kinetic equations exist with different levels of reaction or condition details. The basic form of the presented model structure, namely the resulting kinetic equations, may also vary due to different assumptions about the limitations affecting reactions. Some authors consider thermodynamics to limit the reaction rate the most, while others base the model identification on the mass transfer limitations. For example, in Lommerts et al. (2000) different kinds of diffusion models of varying complexity have been compared with conclusions that usually the internal mass transport can be adequately modeled with simple models.

Already the high-pressure methanol synthesis with the ZnO/Cr_2O_3 catalyst and its kinetics have been studied. An example of the early research is the equation proposed by Natta (Vanden Bussche and Froment, 1996). Natta observed only CO hydrogenation and represented the kinetic equation based on the fugacity of components and estimated constants. A typical assumption was that only the hydrogenation of CO occurred in the synthesis but later it was noticed that CO_2 also was involved in the reaction kinetics. Leonov et al. (1973) published the first model of methanol synthesis kinetics over a $Cu/ZnO/Al_2O_3$ catalyst. Since then, models have been generated for the low-pressure synthesis over the Cu-based catalysts. In Villa et al. (1985), it was noticed that the water-gas shift reaction must be taken into account, but still methanol was assumed to form only through CO hydrogenation.

Graaf et al. (1986, 1988a, 1988b, 1990) and Graaf and Beenackers (1996) have derived a kinetic model considering both CO and CO_2 hydrogenation and the water-gas shift reaction (in the two- and three-phase methanol synthesis), and further modeled the mass transport limitations and recalculated the values of the developed model parameters as well as studied the chemical equilibria in methanol synthesis. Authors identified the equations for the equilibrium constants by assuming the ideal gas behavior and compensating the nonideality with the Soave-Redlich-Kwong equation of state. The equations for the chemical equilibria derived by Graaf et al. (1986) have been used in other studies as well, for example by Vanden Bussche and Froment (1996). Also Skrzypek et al. (1990) used the equations presented by Graaf et al. (1986) while they examined the dependence between the initial feed composition, temperature, and pressure on the equilibrium concentrations of the components. Skrzypek et al. (1990) noticed that the temperature and pressure have a considerable influence on equilibrium conversions: the increasing temperature decreases the conversion of the main reaction (the production of methanol) while the increasing pressure has the opposite effect.

The mass transport limitations have also been modeled and documented by Skrzypek et al. (1985), where a rather complex dusty gas diffusion model was presented. Later, in Skrzypek et al. (1991), the Langmuir-Hinshelwood-type kinetic equation for low-pressure methanol synthesis over the Polish commercial catalyst, CuO (60% wt)-ZnO (30%)–Al_2O_3 (7.5%) was

presented. According to this research, the methanol synthesis favors CO_2 instead of CO as a carbon source, and then the kinetic model was based on reactions (17.2) and (17.3). For evidence, a couple of experiments were performed. It was noticed that when only CO_2 and H_2 were used as the feed, methanol formed without difficulty and the selectivity of synthesis was high. When the feed flow included CO and H_2 without CO_2 and H_2O and steam was completely removed from the feed, methanol was not formed. As the water was introduced into the feed, methanol synthesis initiated due to the water-gas shift reaction. Skrzypek et al. (1985, 1990, 1991, 1995) have a lot of reported studies in the area of methanol synthesis, including kinetic and mechanistic studies but also studies about catalysts.

In Coteron and Hayhurst (1994), the kinetic equations are derived for the methanol synthesis from H_2 and CO and also from H_2, CO, and CO_2. They studied the process with varying CO_2 concentrations while the H_2/CO ratio was kept constant in the feed flow and the amorphous catalysts of composition $Cu_{70}Zr_{30}$ and $Cu_{70}Zn_{30}$ (subscripts indicates atom percent) were applied. There, the increasing CO_2 content in the feed increased the rate of methanol synthesis over the Zr catalyst. On the other hand, a slight decrease in the rate of synthesis was observed with the CO_2 content higher than 10 mol%. Over the Cu/Zn catalyst, the decrease in the rate of synthesis was observed when the CO_2 content exceeded 2 mol%. The developed model indicated that methanol is produced through CO_2 hydrogenation and the role of CO is the removal of oxygen absorbed on the catalyst surface.

In Šetinc and Levec (2001), the kinetics of methanol synthesis in a well-mixed slurry reactor were studied. The authors used a commercial $Cu/ZnO/Al_2O_3$ catalyst and further proposed a model for the liquid-phase methanol synthesis with the Langmuir–Hinshelwood mechanism. According to this research, the behavior of the liquid phase methanol synthesis can be described if the Langmuir–Hinshelwood mechanism is utilized to describe the elementary steps on the catalyst surface. The methanol production in the liquid phase was proportional to the CO_2 concentration, not to the CO concentration. Also the role of water was found to be significant in this type of liquid-phase synthesis.

Considering the low-pressure methanol synthesis and the $CuO/ZnO/Al_2O_3$ catalyst, the mass transport limitations inside the catalyst have to be noticed (Bozzano and Manenti, 2016). A few research results about the catalyst's effectiveness factor can be found from (Graaf et al., 1990). Also, the intraparticle diffusion inside the catalyst has been studied in Lommerts et al. (2000), Solsvik and Jakobsen (2011) and Solsvik et al. (2013).

In Manenti et al. (2011), the different steady-state models for Lurgi's fixed-bed shell and tube-boiler reactors have been proposed and compared. The mathematical modeling of the methanol synthesis, its challenges, and the most common simplifications were thoroughly discussed. The three different model structures (two pseudohomogenous and one heterogeneous) with different assumptions were presented and validated. According to the authors, the pseudohomogenous model based on mass balances results in good modeling accuracy with the

necessary computational effort (Manenti et al., 2011). There, the dynamic model for the methanol synthesis fixed-bed reactor was presented and compared to the corresponding steady-state model. The dynamic model is built-up in the mass balances of each reactant and of the whole system's energy balance. The main route and the instructions for the methanol synthesis dynamic model generation were documented very well. Moreover, the need for further study was noticed to find the balance of the modeling accuracy and the required computational effort (Manenti et al., 2013).

Some microkinetic models have been documented and discussed, for example in Askgaard et al. (1995), Ovesen et al. (1997) and Grabow and Mavrikakis (2011). In addition, two global kinetic models, the power law and the Langmuir-Hinshelwood-Hougen-Watson models taken from Vanden Bussche and Froment (1996), including the micro kinetic model adopted from Ovesen et al. (1997) for the methanol synthesis over the ternary copper catalyst are derived and analyzed in Peter et al. (2012). The 13 elementary steps included in the microkinetic model were adopted from Ovesen et al. (1997). The conclusion then was that the rate of methanol synthesis is described more accurately with the global models than with the microkinetic model structure. According to the results, the prediction of the global models could be usable in the reaction design while the microkinetic model can be used to discuss the existing dynamic changes during the methanol synthesis. The parameters (of all three models) influencing mostly for methanol production rate were further evaluated with the sensitivity analysis. The interesting observation was that the driving force in reverse water-gas shift reaction differs between the presented global models (Peter et al., 2012).

A very extensive literature review about methanol synthesis is proposed in Bozzano and Manenti (2016). The review is focused on technologies and procedures of modeling and optimizing the methanol synthesis reactor, especially the packed bed units. In the article, the history of methanol synthesis, the catalyst development, the existing technologies, the possible carbon sources, different reactor types, and the kinetic and modeling studies were summarized and the synthesis limiting phenomena were discussed. An interesting comparison of different model structures and kinetic assumptions is proposed. The rate equations, operating conditions, and the catalyst deactivation models found from literature are summarized and discussed. In the conclusions, both CO and CO_2 are assumed to be involved in methanol synthesis. Finally they compared two commonly used model structures developed by Graaf et al. and Vanden Bussche and Froment. Of those, the Vanden Bussche and Froment rate equation was found to be more convincing (Bozzano and Manenti, 2016).

The most discussed research on the modeling of methanol synthesis and its kinetics is briefly summarized in Table 17.1, according to corresponding authors. Among these studies the modeling approach has mainly been the simulation of physical phenomena in the form of kinetic equations as a basic model structure.

Recently, newer modeling approaches have been introduced to the field of process identification related to methanol synthesis. In this context, the following process identification

Table 17.1 The summary of the research on methanol synthesis modeling in the chronological order

Author (Reference)	Assumptions	Conditions	Catalyst/Other
Natta (1955)	CO hydrogenation	High-pressure methanol synthesis	ZnO/Cr_2O_3 catalyst
Bakemeier et al. (1970)	The reactions of CO and CO_2 noticed	High-pressure methanol synthesis	ZnO/Cr_2O_3 catalyst
Brown et al. (1984)	The liquid-phase methanol synthesis	$T=473–543$ K, $P=35–70$ bar	Powdered, Cu/Zn/Al catalyst
Weimer et al. (1987)	The liquid-phase methanol synthesis	$T=523$ K, $p=20–60$ bar	United catalyst
Leonov et al. (1973)	CO hydrogenation	Low-pressure methanol synthesis	Cu-based catalyst
Villa et al. (1985)	CO hydrogenation, water-gas shift reaction included		
Klier et al. (1982)	Primarily CO hydrogenation, also CO_2 included in the kinetic equation	$T=498–523$ K, $p=75$ bar	CuO–ZnO catalyst and tubular, integral, fixed-bed reactor
Agny and Takoudis (1985)	CO hydrogenation	$T=523–563$ K, $P=3–15$ bar	Commercial $Cu/ZnO/Al_2O_3$ catalyst
Graaf et al. (1988a, 1990), Lommerts et al. (2000)	CO and CO_2 hydrogenation and the water-gas shift reaction	$T=480–550$ K, $p=15–50$ bar	The comparison of the two- and three-phase methanol synthesis, mass transport limitations
Vanden Bussche and Froment (1996)	CO_2 hydrogenation and the water-gas shift reaction	$T=453–553$ K, $p=15–51$ bar	$Cu/ZnO/Al_2O_3$ catalyst, tubular reactor
Von Wedel et al. (1988)	CO hydrogenation	$T=493–523$ K, $p=20–60$ bar	The gradientless autoclave, commercial catalyst
Ledakowicz et al. (1992)	CO hydrogenation	$T=490–533$ K, $p=20–60$ bar	The stirred autoclave and bubble-column slurry reactor, commercial catalyst
Skrzypek et al. (1991)	CO_2 hydrogenation and the water-gas shift reaction	$T=460–550$ K, $p=30–90$ bar	The fixed-bed (and also differential) reactor, commercial catalyst
Coteron and Hayhurst (1994)	CO_2 hydrogenation, the role of CO related to the catalyst surface reactions	$T=473–523$ K, $p=10$ bar	The continuous, tubular, differential reactor
Šetinc and Levec (2001)	The liquid-phase methanol synthesis with Langmuir-Hinshelwood mechanism	$T=473–513$ K, $p=34–41$ bar	The slurry reactor, the commercial catalyst
Kubota et al. (2001)	CO_2 hydrogenation	$T=473–548$ K, $p=3.5–5.7$ MPa	Cu/ZnO-based catalyst
Park et al. (2014)	CO and CO_2 hydrogenation	$T=493–613$ K, $p=50–90$ bar	$Cu/ZnO/Al_2O_3$ catalyst (Süd-Chemie, MegaMax 700)

examples are related with methanol synthesis modeling with the artificial neural networks (ANN). ANN is the effective computing architecture mimicking the network of nerve cells and simulating the method of information processing in the human brain. The ANNs can be used to model the dependency of the numerical input and output values identified with experimental data. There are different types of ANN structures sorted by architecture of a network, by the applied activation functions, by the network topology, and by the learning algorithms. The details of ANNs can be found in Dayhoff (1990).

The ANN model was utilized in the case study of the network of forced unsteady-state ring reactors. In that case the ANN model parameters were estimated to simulate the performance of the three-reactor network in the low-pressure methanol synthesis system. The results showed that an advanced process control is required to maximize the yield and selectivity of the methanol and to fulfill the process constraints. For this reason, the suitability of the model predictive control (MPC) in the three-reactor network was also discussed. There, the ANN model was assumed to be a useful control model for implementing MPC into the documented system (Fissore et al., 2004). In general, the MPC is a widely adopted control method for dynamic processes with the capability of handling large time delays. More about MPC can be found from Camacho and Alba (2013).

The ANN modeling has also been applied in the methanol synthesis research, for example to estimate the catalyst deactivation (Kito et al., 2004), to optimize the composition, and to identify the preparation conditions for the Cu-oxide catalyst in the catalyst development case (Omata et al., 2004; Watanabe et al., 2004). In addition, the ANN was utilized in the kinetic studies and modeling of the methanol dehydration in dimethyl ether synthesis (Alamolhoda et al., 2012) including the methanol oxidation to formaldehyde (Papes Filho and Maciel Filho, 2010).

3 Case Example on the Simulator for Methanol Synthesis

3.1 Process Simulation

Simulators—steady state and dynamic—are used to gain new knowledge of the studied process. Steady-state simulations can be utilized, for example, to solve the mass and energy balances of the system and also to evaluate different system configurations. Steady-state simulators can provide valuable information for design purposes. On the other hand, the time-dependent behavior of the process can be examined with the dynamic simulators that include derivate terms, enabling the predictive study of a process. Simulators are also commonly applied to provide information for the optimization, to evaluate different control strategies, and to study the complex and time-dependent interactions of the process variables in the different operating ranges.

In the methanol production process, simulations have been utilized for optimizing process conditions, the flow rate of reactants, or simulating the whole process chain. An interesting optimization case and simulation results with discussion are presented in Hoseiny et al. (2016). In the same way, a dynamic mathematical model of a membrane-gas-flowing solids-fixed-bed reactor in a Matlab environment is presented. The process optimization with a differential evolution (DE) algorithm is also performed and discussed in Bayat et al. (2014a). Differential evolution consists of an optimization method mimicking biological evolution with mutation, crossover, and selection. A DE algorithm generates new, real valued parameter vectors by adding the weighted difference between two population vectors to a third vector in the mutation phase. The mutated vector's parameters are then mixed with the parameters of another predetermined vector, the target vector, to yield the so-called trial vector. In the following generation, the target vector is replaced with the trial vector if the trial vector yields a lower cost-function value than the target vector. Each population vector serves once as the target vector in one generation. Mutated vectors can be selected for a next generation randomly or the population member with the lowest cost-function value can be applied. Also the different kind of crossover schemes can be utilized (Storn and Price, 1997).

The long-term catalyst deactivation in a dual-bed multifunctional methanol reactor (DMMR) is investigated with simulations and the optimization is carried out with the DE algorithm. The temperature profile in the DMMR reactor is compared to the temperature profile of a conventional methanol reactor (CMR) to optimize the catalyst activity and service life (Bayat et al., 2014b). Several reactor type comparisons and catalyst deactivation simulations are also presented in Rahimpour et al. (2010).

3.2 Simulation of Methanol Synthesis Process: A Case Study

In Mäyrä and Leiviskä (2008), the steady state and the dynamic simulators based on mass balances and the kinetic equation from Vanden Bussche and Froment (1996) are presented for methanol synthesis. The mass balances were based on the flow conditions and the assumed reaction scheme and were written as:

$$\begin{bmatrix}\text{change of the}\\ \text{substance}\end{bmatrix} = \begin{bmatrix}\text{the flow rate of}\\ \text{the substance in}\end{bmatrix} - \begin{bmatrix}\text{the flow rate of}\\ \text{the substance out}\end{bmatrix} + \begin{bmatrix}\text{production of}\\ \text{the substance}\end{bmatrix} \tag{17.4}$$

With mathematical notations, the mass balance for substance i was

$$\frac{dn_i}{dt} = \dot{n}_{i,in} - \dot{n}_i + R_i, \tag{17.5}$$

where n [mol] is the amount of substance, $\dot{n}$ [mol/s] is the molar flow rate, and R [mol/s] is the specific production/consumption rate of the substance.

Often the mass balance is expressed in concentrations of the substances obtained through equation

$$n_i = C_i V, \tag{17.6}$$

where C is the concentration and V is the volume. Substituting Eq. (17.6) into Eq. (17.5) and assuming the constant volume, the mass balance equation can be written as

$$V\frac{dC_i}{dt} = F(C_{i,in} - C_i) + R_i. \tag{17.7}$$

The common assumption is that the temperature dependency follows the Arrhenius equation. This was also assumed in the presented simulation case.

$$k_j = A_j \exp\left(\frac{B_j}{RT}\right). \tag{17.8}$$

The kinetic equation for the simulation study, adopted from Vanden Bussche and Froment (1996), was modified as presented in Eqs. (17.9) and (17.10).

$$r_{CH_3OH} = \frac{k_1 p_{CO_2} p_{H_2}\left(1 - p_{CH_3OH} p_{H_2O}/K_1^{eq} p_{CO_2} p_{H_2}^3\right)}{\left(1 + K_{WH} p_{H_2O}/p_{H_2} + \sqrt{K_{H_2} p_{H_2}} + K_{H_2O} p_{H_2O}\right)^3} \tag{17.9}$$

$$r_{RWGSR} = \frac{k_2 p_{CO_2}\left[1 - K_3^{eq}(p_{CH_2O} p_{CO}/p_{CO_2} p_{H_2})\right]}{\left(1 + K_{WH} p_{H_2O}/p_{H_2} + \sqrt{K_{H_2} p_{H_2}} + K_{H_2O} p_{H_2O}\right)} \tag{17.10}$$

The related parameters from Vanden Bussche and Froment (1996) and from Graaf and Beenackers (1996) are presented in Table 17.2 for this simulation. The developed simulators apply the kinetic model, operating conditions, and feed compositions presented by Vanden Bussche and Froment (1996). First, the steady-state concentrations were simulated with varying pressure and temperature. Then, the process dynamics and the impact of the pressure were studied with the dynamic simulator. The detailed dynamic simulator with the results is presented here, while the details of steady-state simulation can be further found in Mäyrä and Leiviskä (2008).

Table 17.2 The model parameters for the presented simulation case

	A	B	Feed Composition [mol %]
k_1	0.499	17,197	CO: 4
k_2	$6.62e^{-11}$	124,119	H_2O: 0
K_{WH}	3453.38	–	CH_3OH: 0
KH_2	1.07	36,696	H_2: 82
KH_2O	$1.22e^{10}$	−94,765	CO_2: 3
K_1^{eq}	$2.391e^{-13}$	98,388	Inert: 11
K_3^{eq}	$2.554e^{-11}$	58,705	

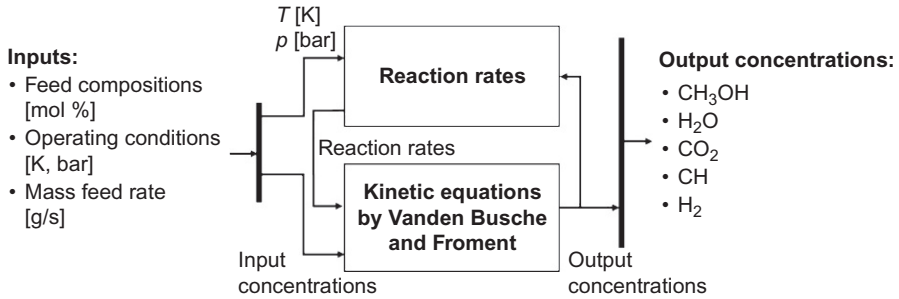

Fig. 17.1
The schematic of the simulation environment.

The simulator was constructed in a Matlab Simulink environment and the solver type was variable-step (minimum step size was 1×10^{-3}) with the Adams-Bashforth-Moulton PECE solver. The principle of the simulator is presented in (Fig. 17.1). The feed composition, the operating conditions, and the mass feed rate (adopted from Vanden Bussche and Froment) were set as the inputs. The reaction rates based on the operating conditions (p and T) and the mass balances were utilized while simulating the output concentrations. In this simulating case, the used operating conditions were

- $T = 493.2$ K,
- $p = 50$ bar and
- the mass feed rate $= 2.8 \times 10^{-11}$ g/s.

The reactor length was set to 0.016 m, the diameter 0.15 m, and the catalyst mass was 34.8 g.

In general, the simulation is a way to get insight about the studied process and its dynamics, including the response in output when changing the feed composition or the operating conditions. In this case, the earlier mentioned simulation parameters were applied (Table 17.2) and the model by Vanden Bussche and Froment was adopted. In the results after the simulation run, the output concentration characteristics related the above presented input concentrations and operating conditions were obtained (Fig. 17.2).

It can be concluded that the obtained final methanol concentrations in the end of the simulation are on the same level with the original ones and time-dependent behavior of the output concentrations are similar with those presented in Vanden Bussche and Froment (1996). After this, the sensitivity analysis was performed with the identified simulator (See Chapter 3.3 and Mäyrä and Leiviskä (2008, 2009)).

To further explore the effects of the pressure, the simulations were also carried out with the varied pressure, $p = 15$ bar. All other operating conditions and feed compositions were kept the same as in the first simulation run. The simulated trajectories of the output concentrations with the applied lower pressure are presented in Fig. 17.3.

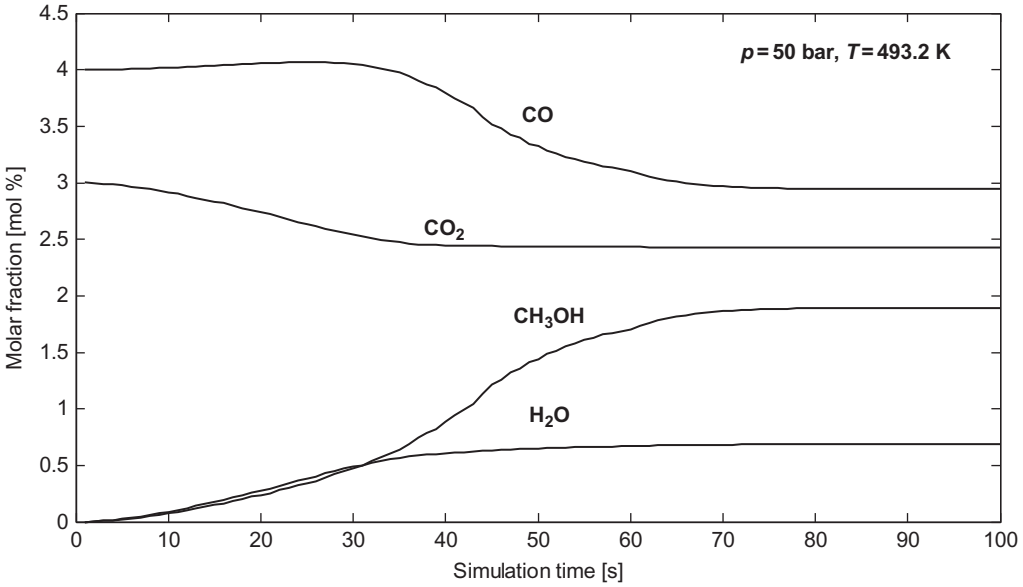

Fig. 17.2

Simulated output concentrations at $p = 50$ bar and $T = 493.2$ K, with the initial feed concentrations and the selected model parameters (Table 17.2).

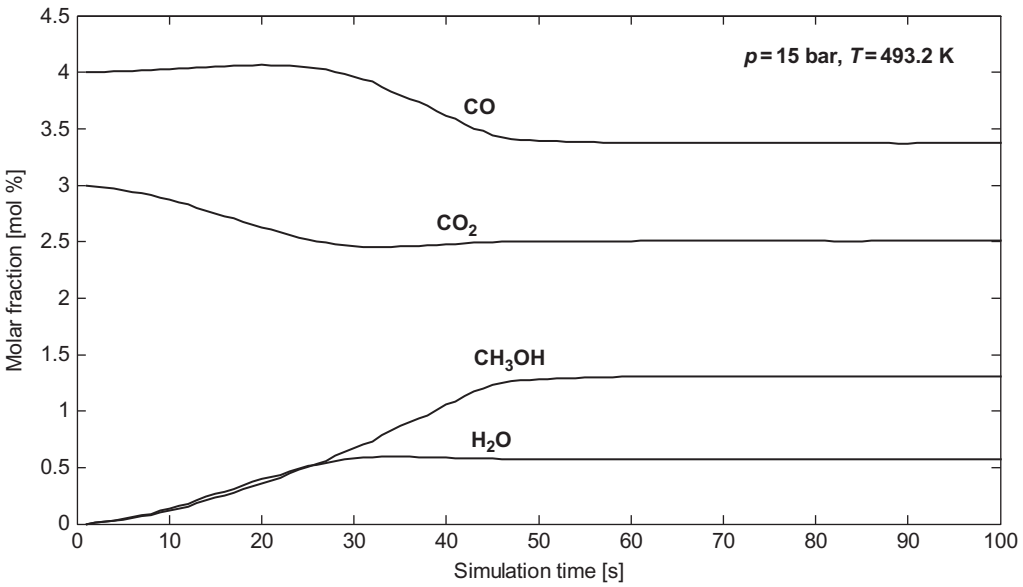

Fig. 17.3

Simulated output concentrations, $p = 15$ bar, $T = 493.2$ K, with the initial feed concentrations and the selected model parameters (Table 17.2).

According to these simulations, the decrease of the pressure has an effect on the methanol synthesis output concentrations. When decreasing the pressure, the methanol yield tends to decrease while the amount of the feed components increase in the output flow. Corresponding results have been documented in the original article by Vanden Bussche and Froment (1996) and also in Skrzypek et al. (1990). These similarities with the simulation results strengthen the applicability of the presented simulation approach to become an efficient tool for process design and optimization.

3.3 Sensitivity Analysis

Next in the presented simulation case (Section 3.2), the sensitivity analysis was applied to gain knowledge about the parameters most affecting the model output. In general, sensitivity analysis is a tool for estimating the uncertainty of the system (real process, for example) or model. It can be used to increase knowledge of the relationship between the input and output variables or to find out the critical variables of the selected system. The details of sensitivity analysis can be found from Saltelli et al. (2004). A typical procedure for the sensitivity analysis includes the following steps (Corrêa et al., 2005), also applied to the presented case study here as:

1. Selection of the parameters for testing,
2. Selection of the studied values for the variables,
3. Definition of the ranges for the parameter values,
4. Generation of a random (uniform distribution) data set for each parameter within the defined range,
5. Execution of the simulations with the above generated data for calculating the objective function,
6. Determination of the relative importance of the parameters with different values of the studied variables,
7. Evaluation of the sensitivity related to each analyzed parameter.

Sensitivity analysis can be utilized in methanol production modeling to analyze dependencies between model inputs and outputs or its parameters. For example, sensitivity analysis was used to gain knowledge from the interactions between operational parameters and emissions in fluidizing catalytic cracking units employed in the petroleum industry (Whitcombe et al. 2003), the catalytic fixed-bed reactors (Quina and Quinta Ferreira 1999), the catalytic plate reactors (Zanfir and Gavriilidis 2002), and the fuel-cell applications (Nagel et al. 2008; Corrêa et al. 2005).

The kinetic equation proposed by Vanden Bussche and Froment (1996) has five parameters, all of which are temperature-dependent and follow the Arrhenius equation. The sensitivity in this case was analyzed with respect to each parameter's A and B terms, whereas the studied outputs were the reaction rates and the methanol yield. The relative importance was

calculated with varying operational conditions (temperature and pressure) and the overall sensitivity of each parameter was also determined. The details of this particular sensitivity analysis can be found in Mäyrä and Leiviskä (2008, 2009).

According to simulation runs for the sensitivity analysis, the B term of the k_2 is the most significant affecting parameter and overall the B terms are more sensitive than the A terms. The sensitivities of the two most significant parameters, B terms in k_2 and k_1, were then studied with different temperatures and pressures. It was found that the sensitivities were higher with lower temperatures and higher pressures. This result indicates that modification of the model parameters in lower temperature and higher pressure leads to a greater change in the model output. This observation can be used, for example, when adapting the same model structure into the new case or to a new data set. Instead of the whole model parameter estimation, the identification could be focused on the most sensitive model parameters.

Based on the sensitivity analysis, the response of the simulated output was studied by changing the values of the kinetic parameters in the model. The tested maximum difference between the original values (Table 17.2) and the modification range of the values was $\pm 15\%$. In Fig. 17.4 the simulated output flow concentrations are presented for the case where the kinetic parameters were decreased 10% from their original values.

For the comparison, the operating conditions and the feed compositions during both simulations (Figs. 17.2 and 17.4) were kept the same. However, the kinetic parameters were modified. According to simulation results, the 10% decrease in kinetic parameters will increase the methanol concentration from 1.9 mol% (Fig. 17.2) to 2.6 mol% (Fig. 17.4) in the output flow. In practice, this information can be used when performing test runs with new catalysts or with new testing equipment. There is no need to identify the whole process again but only to fit the kinetic parameters to the new situation.

4 Conclusions

In this chapter, the research on the modeling of methanol synthesis is first introduced with the literature review. The following simulation example is based on the mass balance and the kinetics presented by Vanden Bussche and Froment. The simulation results and the parameter sensitivity analysis are performed with discussion, and the overall results are compared to the existing literature.

The research of methanol synthesis includes various topics, such as catalyst development, sustainable synthesis gas process development, and alternative feedstock studies. The kinetic studies, process modeling, and whole process chain development are closely related with those and therefore seem to be under wide investigation. Also the development of a sustainable, more energy efficient, and environmental friendly methanol production process is the ambition of the current research. The cleaner and more cost-effective production processes and the utilization

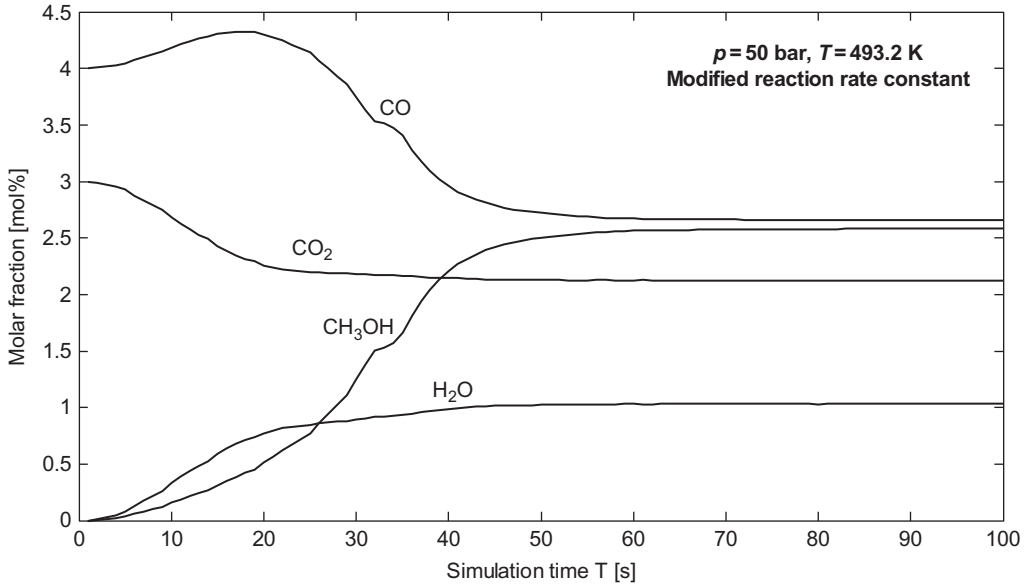

Fig. 17.4
Simulated output concentrations with modified kinetic parameters (−10% of original).

of the alternative feed stock—garbage, for example—put more expectations and requirements for process design and thus also for process modeling, control, and optimization.

According to the recent research topics, the debate about the carbon source and reaction kinetics is ongoing. The generated models are related to the current research and the easily adapted model structure seems to remain a future aim. However, the balance between the modeling accuracy and the demand for computing effort must be taken into account in the model development.

The new catalysts and alternative feedstocks cause changes to the methanol production chain and the new process models are needed for process development and optimization. It is obvious that an accurate process model is a valuable tool for process design, playing an important role when achieving the sustainable processes based on methanol synthesis against future requirements.

References

Agny, R.M., Takoudis, C.G., 1985. Synthesis of methanol from carbon monoxide and hydrogen over a copper-zinc oxide-alumina catalyst. Ind. Eng. Chem. Prod. Res. Dev. 24, 50–55.

Alamolhoda, S., Kazemeini, M., Zaherian, A., Zakerinasab, M.R., 2012. Reaction kinetics determination and neural networks modeling of methanol dehydration over nano γ-Al_2O_3 catalyst. J. Ind. Eng. Chem. 18, 2059–2068.

Askgaard, T.S., Norskov, J.K., Ovesen, C.V., Stoltze, P., 1995. A kinetic model of methanol synthesis. J. Catal. 156, 229–242.

Bakemeier, H., Laurer, P.R., Schroder, W., 1970. Chem. Eng. Prog. Symp. Ser. 66 (98), 1.
Bayat, M., Dehghani, Z., Rahimpour, M.R., 2014a. Membrane/sorption-enhanced methanol synthesis process: dynamic simulation and optimization. J. Ind. Eng. Chem. 20, 3256–3269.
Bayat, M., Dehghani, Z., Rahimpour, M.R., 2014b. Sorption-enhanced methanol synthesis in a dual-bed reactor: dynamic modeling and simulation. J. Taiwan Inst. Chem. Eng. 45, 2307–2318.
Bozzano, G., Manenti, F., 2016. Efficient methanol synthesis: perspectives, technologies and optimization strategies. Prog. Energy Combust. Sci. 56, 71–105.
Brown, D.M., Gottier, G.N., Upadhye, R.S., Bauer, J.V., Cilen, N.A., Markiewicz, G.S., 1984. Modeling of methanol synthesis in the liquid phase. Inst. Chem. Engng Symp. Ser. (Chem. React. Engng.) 87, 699–708.
Camacho, E.F., Alba, C.B., 2013. Model Predictive Control. Springer-Verlag, London.
Corrêa, J.M., Farret, F.A., Popov, V.A., Simoes, M.G., 2005. Sensitivity analysis of the modeling parameters used in simulation of proton exchange membrane fuel cells. IEEE Trans. Energy Convers. 20 (1), 211–218.
Coteron, A., Hayhurst, A.N., 1994. Kinetics of the synthesis of methanol from $CO+H_2$ and $CO+CO_2+H_2$ over copper-based amorphous catalysts. Chem. Eng. Sci. 49 (2), 209–221.
Dayhoff, J.E., 1990. Neural Network Architectures: An Introduction. Van Nostrand Reinhold, New York.
Fissore, D., Barresi, A.A., Manca, D., 2004. Modelling of methanol synthesis in a network of forced unsteady-state ring reactors by artificial neural networks for control purposes. Chem. Eng. Sci. 59, 4033–4041.
Gallucci, F., Basile, A., 2007. A theoretical analysis of methanol synthesis from CO_2 and H_2 in a ceramic membrane reactor. Int. J. Hydrog. Energy 32, 5050–5058.
Ganesh, I., 2014. Conversion of carbon dioxide into methanol—a potential liquid fuel: fundamental challenges and opportunities (a review). Renew. Sust. Energ. Rev. 31, 221–257.
Göransson, K., Söderlind, U., He, J., Zhang, W., 2011. Review of syngas production via biomass DFBGs. Renew. Sust. Energ. Rev. 15, 482–492.
Graaf, G.H., Beenackers, A.A.C.M., 1996. Comparison of two-phase and three-phase methanol synthesis processes. Chem. Eng. Process. 35, 413–427.
Graaf, G.H., Sijtsema, P.J.J.M., Stamhuis, E.J., Joosten, G.E.H., 1986. Chemical equilibria in methanol synthesis. Chem. Eng. Sci. 41 (11), 2883–2890.
Graaf, G.H., Stamhuis, E.J., Beenackers, A.A.C.M., 1988a. Kinetics of low-pressure methanol synthesis. Chem. Eng. Sci. 43 (12), 3185–3195.
Graaf, G.H., Winkelman, J.G.M., Stamhuis, E.J., Beenackers, A.A.C.M., 1988b. Kinetics of the three phase methanol synthesis. Chem. Eng. Sci. 43 (8), 2161–2168.
Graaf, G.H., Scholtens, H., Stamhuis, E.J., Beenackers, A.A.C.M., 1990. Intra-particle diffusion limitations in low-pressure methanol synthesis. Chem. Eng. Sci. 45 (4), 773–783.
Grabow, L.C., Mavrikakis, M., 2011. Mechanism of methanol synthesis on Cu through CO_2 and CO hydrogenation. ACS Catal. 1 (4), 365–384.
Halper, M., 2011. Forget storing carbon; re-use it: a company in Iceland is turning CO_2 into methanol to power cars. Renew. Energy Focus 12, 56–58.
Holmgren, K.M., Berntsson, T., Andersson, E., Rydberg, T., 2012. System aspects of biomass gasification with methanol synthesis—process concepts and energy analysis. In: The 24th International Conference on Efficiency, Cost, Optimization, Simulation and Environmental Impact of Energy, ECOS 2011. 45, pp. 817–828.
Hoseiny, S., Zare, Z., Mirvakili, A., Setoodeh, P., Rahimpour, M.R., 2016. Simulation–based optimization of operating parameters for methanol synthesis process: application of response surface methodology for statistical analysis. J. Nat. Gas Sci. Eng. 34, 439–448.
Jadhav, S.G., Vaidya, P.D., Bhanage, B.M., Joshi, J.B., 2014. Catalytic carbon dioxide hydrogenation to methanol: a review of recent studies. Chem. Eng. Res. Des. 92, 2557–2567.
Kauw, M., Benders, R.M.J., Visser, C., 2015. Green methanol from hydrogen and carbon dioxide using geothermal energy and/or hydropower in Iceland or excess renewable electricity in Germany. Energy 90, 208–217.
Kito, S., Satsuma, A., Ishikura, T., Niwa, M., Murakami, Y., Hattori, T., 2004. Application of neural network to estimation of catalyst deactivation in methanol conversion. Catal. Today 97, 41–47. Advanced Methods in Characterization of Catalysts and Materials.
Klier, K., Chatikavanij, V., Herman, R.G., Simmons, G.W., 1982. Catalytic synthesis of methanol from CO/H_2: IV. The effects of carbon dioxide. J. Catal. 74 (2), 343–360.

Kokubu, Y., Fujiwara, K., Ono, H., Sugawara, H., Yamamoto, K., Oomatsuzawa, T., Inomata, M., 2000. US Patent 6,028,119, 22 Feb 2000.

Kubota, T., Hayakawa, I., Mabuse, H., Mori, K., Ushikoshi, K., Watanabe, T., Saito, M., 2001. Kinetic study of methanol synthesis from carbon dioxide and hydrogen. Appl. Organometal. Chem. 15, 121–126.

Lachowska, M., Skrzypek, J., 2004. Methanol synthesis from carbon dioxide and hydrogen over Mn-promoted copper/zinc/zirconia catalysts. React. Kinet. Catal. Lett. 83, 269–273.

Lange, J.-P., 2001. Methanol synthesis: a short review of technology improvements. Catal. Today 64, 3–8.

Ledakowicz, S., Stelmachowski, M., Chacuk, A., 1992. Methanol synthesis in bubble column slurry reactors. Chem. Eng. Process. 31, 213–219.

Leonov, V.E., Karavaev, M.M., Tsybina, E.N., Petrischeva, G.S., 1973. Kinet. Katal. 14, 848.

Li, B., Jens, K.J., 2013. Liquid-phase low-temperature and low-pressure methanol synthesis catalyzed by a Raney Copper-Alkoxide system. Top. Catal. 56, 725–729.

Li, C., Yuan, X., Fujimoto, K., 2014. Development of highly stable catalyst for methanol synthesis from carbon dioxide. Appl. Catal. A Gen. 469, 306–311.

Lommerts, B.J., Graaf, G.H., Beenackers, A.A.C.M., 2000. Mathematical modeling of internal mass transport limitations in methanol synthesis. Chem. Eng. Sci. 55 (23), 5589–5598.

Løvik, I., 2001. Modelling, estimation and optimization of the methanol synthesis with catalyst deactivation. Doctoral thesis, Norwegian University of Science and Technology.

Manenti, F., Cieri, S., Restelli, M., 2011. Considerations on the steady-state modeling of methanol synthesis fixed-bed reactor. Chem. Eng. Sci. 66, 152–162.

Manenti, F., Cieri, S., Restelli, M., Bozzano, G., 2013. Dynamic modeling of the methanol synthesis fixed-bed reactor. Comput. Chem. Eng. 48, 325–334.

Manenti, F., Adani, F., Rossi, F., Bozzano, G., Pirola, C., 2016. First-principles models and sensitivity analysis for the lignocellulosic biomass-to-methanol conversion process. Comput. Chem. Eng. 84, 558–567.

Mäyrä, O., Leiviskä, K., 2008. Modelling in methanol synthesis. Report A No 37. University of Oulu.

Mayra, O., Leiviska, K., 2009. Modelling in methanol synthesis. In: Pierucci, S. (Ed.), Icheap-9: 9th International Conference on Chemical and Process Engineering. Pts 1–3, pp. 1413–1418.

Mitsui Chemicals. Annual Report 2010, 2010. Available from: http://www.mitsuichem.com/ir/library/ar/pdf/en_ar10_all.pdf?1464866458066 (accessed 22.09.16.).

Nagel, F.P., Schildhauer, T.J., Biollaz, S.M.A., Stucki, S., 2008. Charge, mass and heat transfer interactions in solid oxide fuel cells operated with different fuel gases-A sensitivity analysis. J. Power Sources 184, 129–142.

Natta, G., 1955. Catalysis. vol. 3. Reinhold, New York. p. 349.

Olah, G.A., 2013. Towards oil independence through renewable methanol chemistry. Angew. Chem. Int. Ed. 52, 104–107.

Omata, K., Hashimoto, M., Watanabe, Y., Umegaki, T., Wagatsuma, S., Ishiguro, G., Yamada, M., 2004. Optimization of Cu oxide catalyst for methanol synthesis under high CO_2 partial pressure using combinatorial tools. Appl. Catal. A Gen. 262, 207–214.

Ovesen, C.V., Clausen, B.S., Schiøtz, J., Stoltze, P., Topsøe, H., Nørskov, J.K., 1997. Kinetic implications of dynamical changes in catalyst morphology during methanol synthesis over Cu/ZnO catalysts. J. Catal. 168, 133–142.

Papes Filho, A.C., Maciel Filho, R., 2010. Hybrid training approach for artificial neural networks using genetic algorithms for rate of reaction estimation: application to industrial methanol oxidation to formaldehyde on silver catalyst. Chem. Eng. J. 157, 501–508.

Park, N., Park, M.-J., Lee, Y.-J., Ha, K.-S., Jun, K.-W., 2014. Kinetic modeling of methanol synthesis over commercial catalysts based on three-site adsorption. Fuel Process. Technol. 125, 139–147.

Peter, M., Fichtl, M.B., Ruland, H., Kaluza, S., Muhler, M., Hinrichsen, O., 2012. Detailed kinetic modeling of methanol synthesis over a ternary copper catalyst. Chem. Eng. J. 203, 480–491.

Quina, M.M.J., Quinta Ferreira, R.M., 1999. Model comparison and sensitivity analysis for a fixed bed reactor with two catalytic zones. Chem. Eng. J. 75, 149–159.

Rahimpour, M.R., Bayat, M., Rahmani, F., 2010. Dynamic simulation of a cascade fluidized-bed membrane reactor in the presence of long-term catalyst deactivation for methanol synthesis. Chem. Eng. Sci. 65, 4239–4249.

Rozovskii, A.Y., Lin, G.I., 2003. Fundamentals of methanol synthesis and decomposition. Top. Catal. 22, 137–150.

Saltelli, A., Tarantola, S., Campolongo, F., Ratto, M., 2004. Sensitivity analysis in practice: a guide to assessing scientific models. John Wiley & Sons.
Šetinc, M., Levec, J., 1999. On the kinetics of liquid-phase methanol synthesis over commercial $Cu/ZnO/Al_2O_3$ catalyst. Chem. Eng. Sci. 54, 3577–3586.
Šetinc, M., Levec, J., 2001. Dynamics of a mixed slurry reactor for the three-phase methanol synthesis. Chem. Eng. Sci. 56, 6081–6087.
Skrzypek, J., Grzesik, M., Szopa, R., 1985. Analysis of the low-temperature methanol synthesis in a single commercial isothermal Cu-Zn-Al catalyst pellet using the dustygas model. Chem. Eng. Sci. 40 (4), 671–673.
Skrzypek, J., Lachowska, M., Serafin, D., 1990. Methanol synthesis from CO_2 and H_2: dependence of equilibrium conversions and exit equilibrium concentrations of components on the main process variables. Chem. Eng. Sci. 45, 89–96.
Skrzypek, J., Lachowska, M., Moroz, H., 1991. Kinetics of methanol synthesis over commercial copper/zinc oxide/alumina catalysts. Chem. Eng. Sci. 46, 2809–2813.
Skrzypek, J., Lachowska, M., Grzesik, M., Słoczyński, J., Nowak, P., 1995. Thermodynamics and kinetics of low pressure methanol synthesis. Chem. Eng. J. Biochem. Eng. J. 58, 101–108.
Solsvik, J., Jakobsen, H.A., 2011. Modeling of multicomponent mass diffusion in porous spherical pellets: application to steam methane reforming and methanol synthesis. Chem. Eng. Sci. 66, 1986–2000.
Solsvik, J., Tangen, S., Jakobsen, H.A., 2013. Evaluation of weighted residual methods for the solution of the pellet equations: the orthogonal collocation, Galerkin, tau and least-squares methods. Comput. Chem. Eng. 58, 223–259.
Storn, R., Price, K., 1997. Differential evolution—a simple and efficient heuristic for global optimization over Continuous Space. J. Glob. Optim. 11, 341–359.
Tock, L., Gassner, M., Maréchal, F., 2010. Thermochemical production of liquid fuels from biomass: thermo-economic modeling, process design and process integration analysis. Biomass Bioenergy 34, 1838–1854.
Vanden Bussche, K.M., Froment, G.F., 1996. A steady-state kinetic model for methanol synthesis and the water gas shift reaction on a commercial $Cu/ZnO/Al_2O_3$ catalyst. J. Catal. 161 (1), 1–10.
Villa, P., Forzatti, P., Buzzi-Ferraris, G., Garone, G., Pasquon, I., 1985. Synthesis of alcohols from carbon oxides and hydrogen. 1. Kinetics of the low-pressure methanol synthesis. Ind. Eng. Chem. Proc. Des. Dev. 24, 12–19.
Von Wedel, W., Ledakowicz, S., Deckwer, W.-D., 1988. Kinetics of methanol synthesis in the slurry phase. Chem. Eng. Sci. 43 (8), 2169–2174.
Watanabe, Y., Umegaki, T., Hashimoto, M., Omata, K., Yamada, M., 2004. Optimization of Cu oxide catalysts for methanol synthesis by combinatorial tools using 96 well microplates, artificial neural network and genetic algorithm. Catal. Today 89, 455–464. Synthesis of Ecological High Quality Transportation Fuels.
Weimer, R.F., Terry, D.M., Stepanhoff, P., 1987. Laboratory kinetics and mass transfer in the liquid-phase methanol process. In: A.I.Ch.E. Annual Meeting, New York, November 16. Paper 25d.
Whitcombe, J.M., Cropp, R.A., Braddock, R.D., Agranovski, I.E., 2003. Application of sensitivity analysis to oil refinery emissions. Reliab. Eng. Syst. Saf. 79, 129–224.
Wu, J., Saito, M., Takeuchi, M., Watanabe, T., 2001. The stability of Cu/ZnO-based catalysts in methanol synthesis from CO_2-rich feed and from CO-rich feed. Appl. Catal. A Gen. 218, 235–240.
Xu, J., Su, X., Liu, X., Pan, X., Pei, G., Huang, Y., Wang, X., Zhang, T., Geng, H., 2016. Methanol synthesis from CO_2 and H_2 over $Pd/ZnO/Al_2O_3$: catalyst structure dependence of methanol selectivity. Appl. Catal. A Gen. 514, 51–59.
Zanfir, M., Gavriilidis, A., 2002. An investigation of catalytic plate reactors by means of parametric sensitivity analysis. Chem. Eng. Sci. 57, 1653–1659.

CHAPTER 18

Inorganic Membrane Reactors for Methanol Synthesis

Fausto Gallucci

Eindhoven University of Technology, Eindhoven, The Netherlands

Acronyms

CI	current indicator
DME	dimethyl ether
dP	differential pressure indicator
FI	flow indicator
FT	Fisher-Tropsch
IZA	International Zeolite Association
MISC	multi in situ crystallization
MTO	methanol to olefins
PCV	pressure control valve
PI	pressure indicator
STP	standard temperature and pressure
RITE	research institute of innovative technology for earth
TI	temperature indicator
TREC	thermodynamic equilibrium of conventional reactor
V	valve
WGS	water gas shift reaction
MFI, MEL, CHA, ERI, FAU, LTA, AFI, MOR, TON	framework structures of zeolite (see IZA website for more info)

1 Introduction

Methanol, also known as methyl alcohol or wood alcohol, is a very important chemical compound that can be used as a platform molecule and as an energy carrier (Gallucci et al., 2007). The interest in methanol as an energy carrier has increased recently with the "hype" of carbon dioxide reuse. The idea is to convert the CO_2 captured from power plants and other

Methanol. https://doi.org/10.1016/B978-0-444-63903-5.00018-2

energy-intensive industries with the hydrogen produced "for free" with the excess of renewable electricity (in the moments of peak production). This methanol can then be used as an energy carrier. While the idea is interesting, there is a strong debate on the techno-economic viability of this route. The main arguments in favor of this route are the possibility of storing CO_2 in a liquid form for its reuse and the fact that a lot of electricity can be generated in peak times that cannot be used otherwise. Arguments against this route are the fact that hydrogen will not be free even in peak times, the electrolyzers will work at low capacity, and the methanol, if used as additives for fuels, will result in the distributed generation of CO_2. An interested reader is referred to the long list of literature on CO_2 reuse. It is worth mentioning here that the same concept was suggested many years ago by the Research Institute of Innovative Technology for Earth (RITE) in Japan (RITE, 2017).

Methanol is also produced naturally in the anaerobic metabolism by many varieties of bacteria. For this reason, there is a small amount of methanol vapor in the atmosphere. However, atmospheric methanol is slowly oxidized by oxygen (with sunlight energy) into water and carbon dioxide (Hanson and Hanson, 1996).

Methanol was first synthetized by M. Berthelot in 1857 using dry wood distillation. Referring to this research, methanol was commonly called "wood alcohol" (Gallucci et al., 2007).

2 Methanol Production

Several techniques have been developed to produce methanol. As already noted, the first route was the distillation of vinegar on wood and then dry wood distillation. These techniques were used as long as the first catalytic process was discovered. However, nowadays the market and price of methanol are increasing (Methanol.org, 2017). Along with this, the required reduction of greenhouse gas emissions makes the production of methanol via partial oxidation of biomass (wood or solid waste) a very attractive and promising route.

The feasibility of this process was demonstrated in a large-scale system in which a product gas is initially produced by pyrolysis of the waste material. The product yield for the conversion process is estimated to be 185 kg of methanol per metric ton of solid waste.

The global methanol demand is nowadays dictated by methanol to olefins (MTO) and formaldehyde production (see Fig. 18.1).

The catalytic processes for methanol production were studied since the 1920s, especially by the German chemical company BASF. The first methanol was produced as an undesired byproduct of ammonia production using an iron-oxide catalyst. The study of such processes drove the research at BASF toward a selective catalyst for methanol production. In the 1920s they produced a selective Zn/Cr catalyst and patented the high-pressure methanol synthesis process operated at up to 350 bar and 400°C (Farbenindustrie Akt-Ges, 1932).

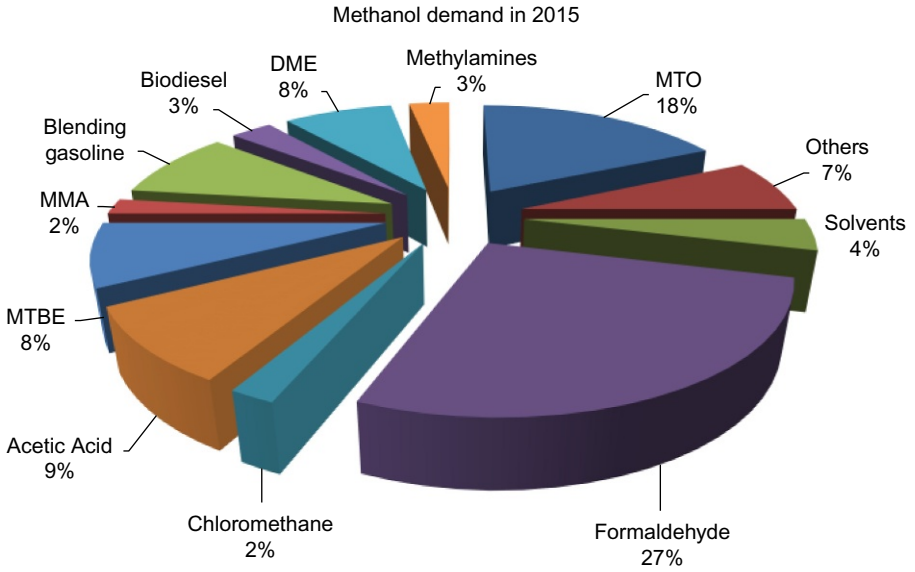

Fig. 18.1
Global methanol demand by end users in 2015 (Methanol.org, 2017).

In the 1960s, ICI developed a low-pressure process by replacing the Cr-based catalyst with a Cu-based catalyst. The process, which operates at 35–55 bar and 200–300°C, is the only one used today in a market for large-scale methanol production (Tijm et al., 2001).

Nowadays, the highest active and selective catalysts for methanol production are $Cu/ZnO/Al_2O_3$ catalysts. These catalysts present good activity starting from 200°C and are selective toward the formation of methanol from H_2 and CO_2. All the catalysts actually used in the low-pressure methanol synthesis contain copper oxide, zinc oxide, and one or more stabilizer compounds. A typical composition of the catalysts used for the synthesis with respect to the producers is reported in Table 18.1.

Being that the methanol synthesis catalyst is a well-established catalyst, the research is nowadays focused toward reaction engineering in order to increase the yield per pass, thus decreasing the recycle of unconverted syngas.

Table 18.1 Typical composition for methanol synthesis catalysts

Producer	Cu (%)	Zn (%)	Al (%)
BASF	65–75	20–30	5–10
Süd Chemie	65–75	18–23	5–10
ICI	61	30	9
DuPont	50	19	31
Haldor Topsøe	50–60	21–25	15–28

The methanol synthesis is indeed an equilibrium system that is best represented by the following reactions:

$$CO + 2H_2 \Leftrightarrow CH_3OH \quad \Delta H_{298K} = -90.7 \text{ kJ/mol} \tag{18.1}$$

$$CO_2 + H_2 \Leftrightarrow CO + H_2O \quad \Delta H_{298K} = 41.19 \text{ kJ/mol} \tag{18.2}$$

$$CO_2 + 3H_2 \Leftrightarrow CH_3OH + H_2O \quad \Delta H_{298K} = -49.51 \text{ kJ/mol} \tag{18.3}$$

CO_2 is always present either in the syngas, or produced in situ. The third reaction is also very interesting as it is the base for the CO_2 reuse into chemical building blocks.

To circumvent the thermodynamic limitation that reduces the yield of conventional systems, two possible routes can be used: (i) smart recycling of the unconverted synthesis and (ii) in situ product removal of the products of the reaction.

In situ product removal can be achieved by selective adsorption of one or both liquid products. While removing the methanol would only simplify the final product purification, the removal of water is very important as well. By removing water, one can indeed achieve higher methanol production (as the Le Chatelier's effect on the equilibrium reactions is higher), and at the same time can prevent unwanted methanol reforming reactions and deactivation of the catalyst (as water accelerates the crystallization of Cu and ZnO contained in a Cu/ZnO-based catalyst) (Wu et al., 2001).

The methanol and water separation can be made possible by using a novel reactor that allows in situ condensation of water and methanol as described by Bos and Brilman (2015). The authors recently used this reactor for the conversion of CO_2 into methanol using hydrogen that could be produced by renewable energy.

The schematic of the reactor is reported in Fig. 18.2. By using two temperature zones in the reactor, the authors were able to condense the product and boost the conversion of carbon at $>99.5\%$ with almost complete selectivity toward methanol.

When the recovery of methanol and water is not possible inside the reactor, it should be done downstream from the reactor in a way that the energy required for the separation and recycling of the unconverted gas is minimized. Recently Kiss et al. (2016) reported a new process for methanol synthesis by CO_2 hydrogenation (see Fig. 18.3). In this process, the authors used a stripping unit at high pressure with wet hydrogen as a stripping agent so that the unconverted CO/CO_2 is completely removed from the product and steam is not accumulating in the reaction zone (thus allowing high conversion rates).

Many other processes using the removal of methanol with conventional systems have been investigated but are not part of this chapter.

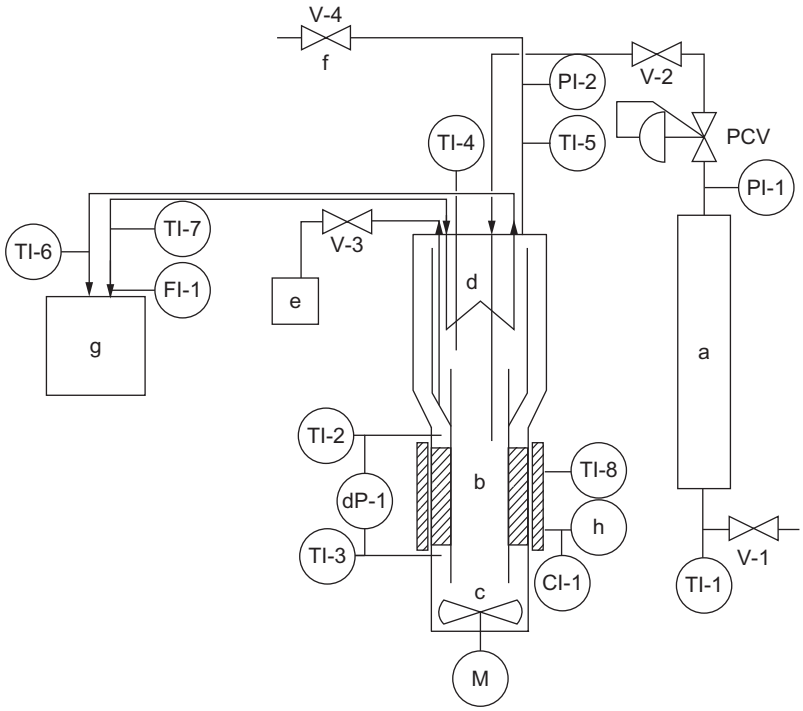

Fig. 18.2

Schematic overview of the setup: (a) buffer vessel, (b) catalyst section (annulus), (c) fan, (d) cooler, (e) liquid outlet, (f) purge, (g) water bath, (h) oven temperature controller, (TI) temperature indicator, (PI) pressure indicator, (CI) current indicator, (dP) differential pressure indicator, (FI) flow indicator, (PCV) pressure control valve, (V) valve. *Reproduced from Bos, M.J., Brilman, D.W.F., 2015. A novel condensation reactor for efficient CO_2 to methanol conversion for storage of renewable electric energy. Chem. Eng. J., 278, 527–532. https://doi.org/10.1016/j.cej.2014.10.059 with permission of Elsevier.*

The scope of this chapter is to discuss the membrane reactor concept for methanol production. A continuous product removal from the reaction zone making use of membranes improves both the reactant's conversion and methanol yield as indicated by Struis et al. (1996).

These authors used a Nafion membrane to separate in situ methanol in a methanol synthesis reactor. The removal of products clearly has an important effect on the conversion of methanol, and the membrane reactor can achieve higher yields than the conventional reactor without membranes. However, the applicability of this membrane reactor is hampered by the temperature limitations of the membranes used. These are stable at around 150°C, too low for the methanol catalyst to be active. Therefore, there is a need to go to higher temperatures for such membranes to be industrially interesting.

The low temperature resistance is a typical problem affecting polymeric membranes. This is why more research effort is spent on inorganic membranes that can separate water/methanol at temperatures interesting for the reactions.

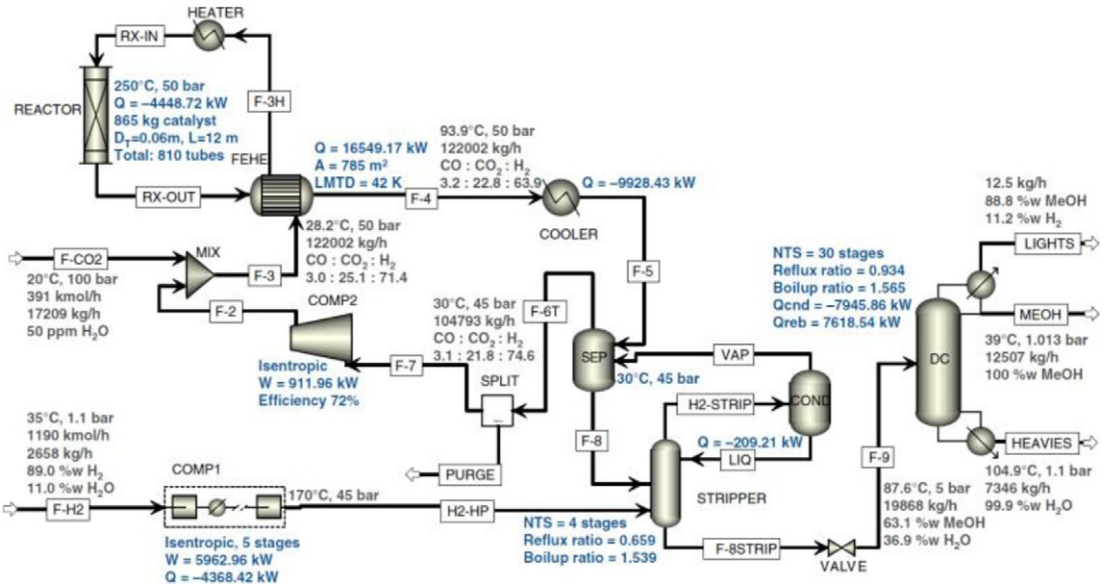

Fig. 18.3

Aspen Plus flowsheet of an efficient process for methanol synthesis by CO_2 hydrogenation. *Reproduced by Kiss, A.A., Pragt, J.J., Vos, H.J., Bargeman, G., de Groot, M.T., 2016. Novel efficient process for methanol synthesis by CO_2 hydrogenation. Chem. Eng. J., 284, 260–269. https://doi.org/10.1016/j.cej.2015.08.101 with permission of Elsevier.*

For methanol synthesis the temperatures of operation are typically around 250°C (200–320°C). In this range there are several inorganic membranes under investigation. The most interesting at the moment seem to be carbon membranes and zeolite membranes.

3 Carbon Membranes

Microporous carbon membranes are very good candidates for methanol synthesis. These membranes have excellent permeation selectivity, high hydrothermal stability, and high corrosion resistance. But most importantly, these membranes have high tenability, as their porous structure and hydrophobicity/hydrophilicity can be modified by working at the appropriate temperature and selecting the right polymer precursors (Llosa Tanco et al., 2015). Due to their highly porous structures with a sharp distribution of pore sizes ranging from 0.3–0.6 nm, the carbon membranes are suitable for the gas separations such as H_2/N_2, O_2/N_2, CO_2/N_2, and CO_2/CH_4.

Although most of the research on this kind of membrane is focused on the recovery of hydrogen from the methanol reforming reaction (Zhang et al., 2015), with proper modification of the structure the membranes are also applied for methanol and water removal (Tanaka et al., 2011). More research is required in this sense to apply the carbon molecular sieve membranes to methanol production.

4 Zeolite Membranes for Membrane Reactors

In the last 30 years membrane reactors have attracted a lot of attention because of their superior performance compared to conventional systems. This is especially due to the combination of reaction and in situ removal of products in a single system. This allows a tremendous reduction of reactor volumes and energy use. This has been reported by several authors. For instance, for water-gas shift reactions (WGS) Brunetti et al. reported a decrease of volume by 80% when using membrane reactors at high pressure compared with a conventional two-stage WGS reaction system (see Fig. 18.4) (Brunetti et al., 2007).

Among the different membrane reactors, zeolite membrane reactors, which mainly belong to the area of inorganic membrane reactors, gained increasing interest during the last 20 years, as demonstrated by the growing number of scientific publications and patents (Fig. 18.5).

Membranes based on zeolite are very interesting as they can be used as a molecular sieve, due to the well-defined and narrow pore size distribution of the zeolites.

These hydrated alumino-silicates, with an open crystalline structure of tetrahedral SiO_4 and AlO_4^- units linked by oxygen atoms, with cavities or pores of molecular dimension (Meier, 1986; Weitkamp, 2000).

Zeolites belong to a more general class of microporous materials called "molecular sieves," since they can selectively separate molecules based on their size. The main characteristic of zeolites is their very regular pore structure of molecular dimensions. Around 50 zeolites have been found in nature and more than 1500 types of zeolite have been synthesised. The Structure Commission of the International Zeolite Association (IZA) is in charge of approving zeolite structures, which are classified using a three-letter code included in the

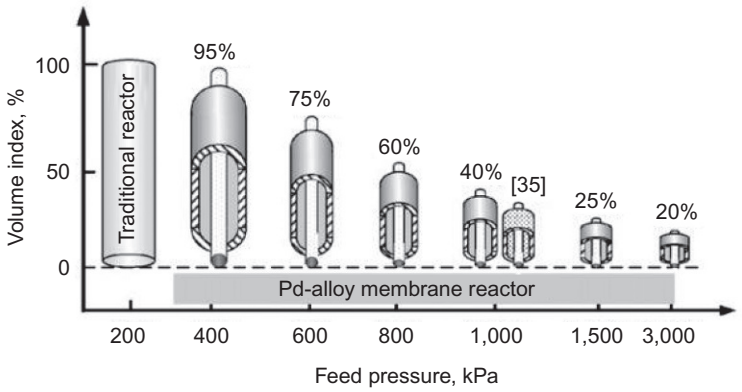

Fig. 18.4
Volume index as a function of feed pressure for the mixture 1. Furnace temperature = 280°C. Set CO conversion 90% of the TREC.

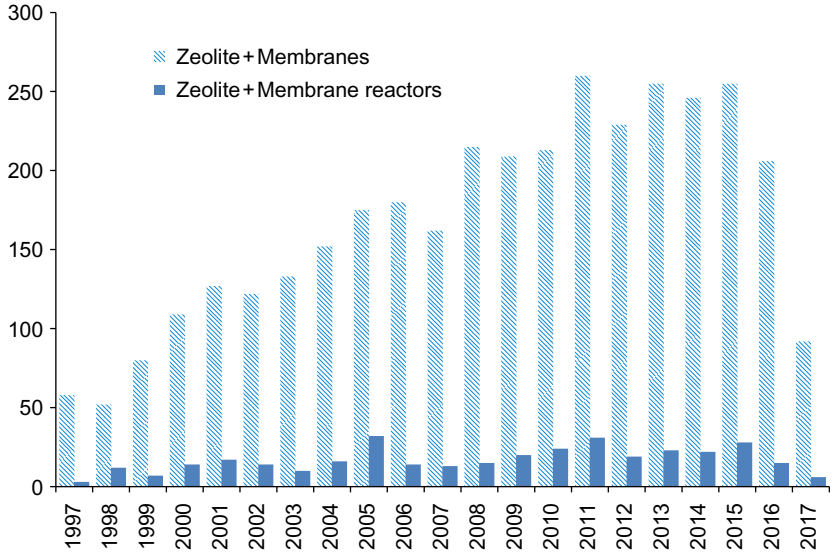

Fig. 18.5

Scientific publications on zeolite membranes and membrane reactors over the last 20 years. The search has been performed using the Scopus search engine with the keywords "zeolite AND membrane" and "zeolite AND membrane reactor."

"Atlas of Zeolite Structure Types" (Meier, 1991). A complete list of zeolites and structures can be found on the IZA structure commission website.

The pore size of zeolites range from 0.2 to about 1 nm. They have a very narrow pore size distribution (as shown in Fig. 18.6) which makes these materials ideal for either catalyst supports or membrane materials.

As already well described by Krishna (2006), the zeolite structures can be grouped into three main categories:

(a) Zeolites with intersecting channel structure in which the pore structure presents different channels, intersecting each other to form a three-dimensional network. The structure can be based on straight and zigzag channels. The types of framework that may belong to this category are MFI and MEL.
(b) Zeolites with cages separated by a window structure. The pore structure is formed by cavities connected through short channels. Usually, the size of the cavities (cages) is larger than that of the channels (windows). Examples of this category are CHA, ERI, FAU, and LTA framework types.
(c) Zeolites with a one-dimensional channel structure. Pore structure is constituted of essentially straight pore channels, which in some structures have side pockets. Framework types AFI, MOR, and TON are examples of zeolites belonging to this category.

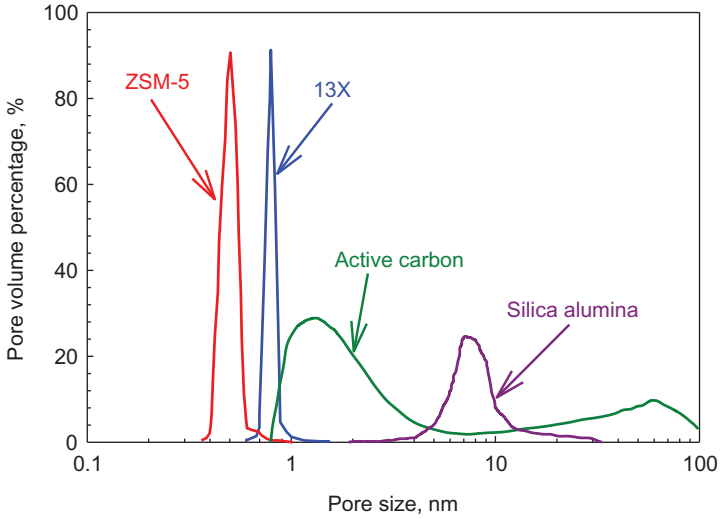

Fig. 18.6
Typical pore size distribution of different materials.

When a zeolite is arranged as a layer and it performs as a diffusion barrier, we have a zeolite membrane.

In general two types of zeolite membranes can be recognized:

- Polymeric zeolite filled membranes.
- Inorganic zeolite membranes.

For methanol synthesis, as discussed above, polymeric membranes are generally precluded because of their low temperature stability. Therefore only inorganic zeolite membranes seem to be suitable since they can stand at the high temperature and pressure needed for the methanol production process.

The quality and then the mass transport characteristics of the zeolite membrane mainly depend on the zeolite type and synthesis, presence of a support, and, obviously, the involved specie along with the operating conditions.

4.1 Zeolite Membrane Preparation

Zeolite membrane preparation is continuously improved as demonstrated by the average 40 papers per year on this topic reported in the last 10 years (see Scopus). Different papers report zeolite membrane formation on hollow fibers (Yu et al., 2017), on mixed ceramic supports (Vasanth et al., 2017), PVC (Danesh-Khorasgani and Nezamzadeh-Ejhieh, 2016), etc. An interested reader is referred to recent reviews on this topic (Pagis et al., 2016; Dragomirova and Wohlrab, 2015; Daer et al., 2015; Caro, 2016).

Generally zeolite membranes are supported on ceramic porous supports. The function of the support is to mechanically sustain the thin zeolite layer. It is mesoporous or more often macroporous so that no external mass transfer resistances are induced by the support itself (see Fig. 18.7).

Zeolite membranes can be produced via three different routes:

(a) Deposition or embedding of preformed crystals on a substrate.
(b) Hydrothermal synthesis (in situ synthesis).
(c) Deposition of seeds and hydrothermal synthesis (secondary growth).

For preparing membranes to be used in membrane reactors, the methods b and c are generally used. The in situ hydrothermal synthesis is generally used for preparation of zeolite MFI, ferrite, and zeolite A composite membranes on porous supports (Tavolaro and Tavolaro, 2009). By this method a prepared support and solution are put together into an autoclave. A gel layer is formed on the surface of the support by precipitation of the sol particles under certain concentration ranges and at given temperatures. The crystal grows into the gel layer consuming the gel until the growing crystals reach the support. The gel for the zeolite crystallization can either form a surface layer or it can get into the pore system of the support, forming zeolite plugs. In this case the mechanical stability of the zeolite improves (the layer is kind of anchored) but the flux through the membrane decreases (thicker layer) (Caro et al., 2000).

In order to improve the membrane performances, the membrane layer can be formed by different films grown in subsequent hydrothermal steps by following the so called multi in situ crystallization (MISC) method (Vroon et al., 1998) (see Fig. 18.8). The membranes produced by this method are, in general, defect-free membranes.

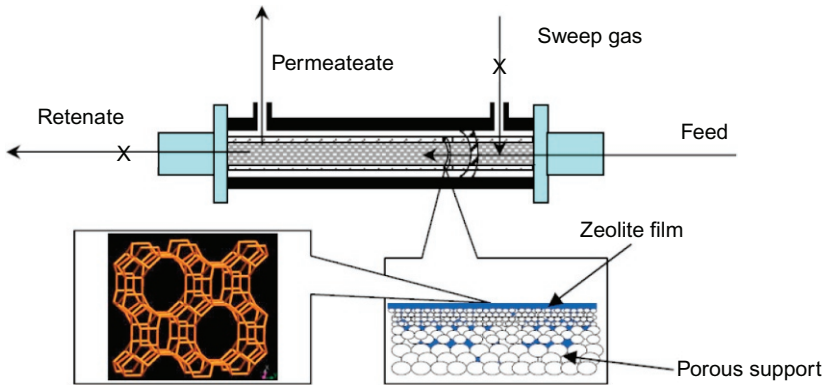

Fig. 18.7

Schematic of a membrane reactor with thin film supported zeolite membrane. *Reproduced from Tavolaro, A., Tavolaro, P., 2009.The preparation of transition metal-containing mordenite catalytic tubular composite membranes. Catal. Commun., 10. https://doi.org/10.1016/j.catcom.2008.10.041 with permission of Elsevier.*

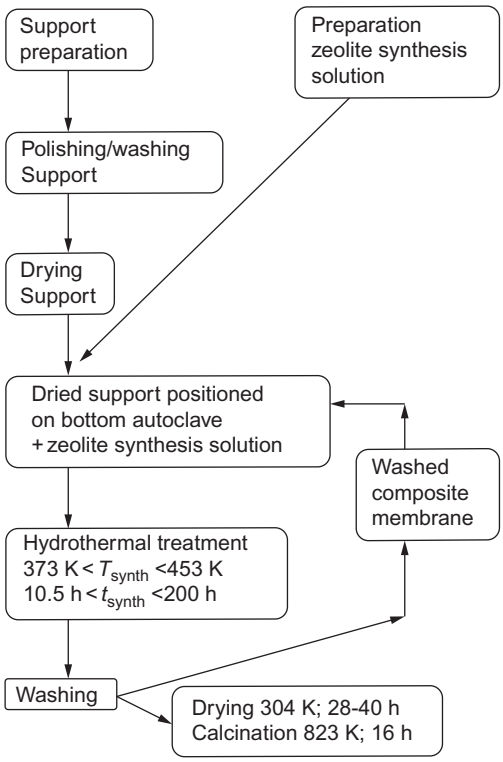

Fig. 18.8

Schematic illustration of the preparation of zeolite MFI membranes by the MISC method. *Reproduced from Vroon, Z.A.E., Keizer, K., Burggraaf, A. Verweij, H., 1998. Preparation and characterization of thin zeolite MFI membranes on porous supports. J. Memb. Sci., 144, 65–76. https://doi.org/10.1016/S0376-7388(98)00035-0 with permission of Elsevier.*

This MISC method allows producing thick layers, which have advantages and disadvantages. If it is possible to slowly remove the template from the thick layer, then the layer is defect free; otherwise cracks appear. The flow is generally very low.

To improve the flux through the membranes and avoid formation of cracks, thin zeolite layers should be produced. This can be achieved by the separation of the nucleation step and the growth step. This method, illustrated in Fig. 18.9, is called secondary growth. In such a way, one can optimize both seeding and growth steps and obtain defect-free thin membrane layers.

Other methods are used for zeolite membrane preparation that are not reported here, including vapor deposition, microwave-assisted deposition, etc. Without entering into a long description of the preparation methods used in literature, it is worth mentioning the work of Kim et al. (2016), who reported the method of producing in one step a zeolite membrane containing metal nanoparticles (and a nanocluster). This allows the production of catalytic

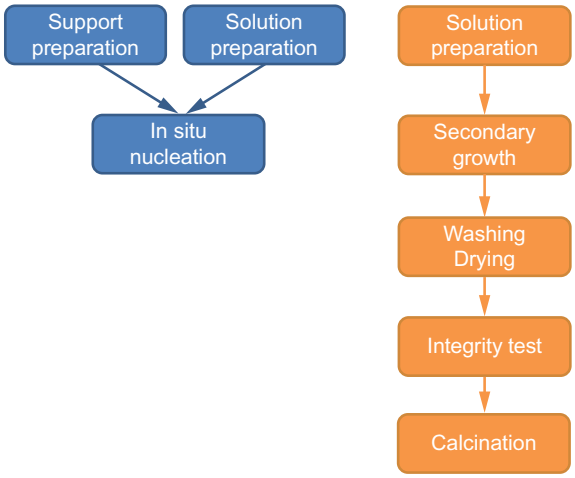

Fig. 18.9
Scheme of the secondary growth zeolite membrane preparation method.

membranes for membrane reactors, where both separation and the high surface area of the membrane are used for enhancing the conversion of chemicals.

Apart from the very ordered structure and narrow pore size distribution, the hydrophilicity and hydrophobicity of the membranes can also be tailored by selecting the right kind of zeolite. Hundreds of papers dealing with the preparation and use of zeolite membranes for gas separation and gas/vapor separation are present in literature. However, few practical examples of the use of zeolite membranes in membrane reactors can be found so far.

Masuda et al. (2003) used a zeolite catalytic membrane reactor for increasing the selectivity of olefins during the methanol conversion. First they synthesized a ZSM-5 zeolite by a three-step in situ hydrothermal synthesis (MISC) on the outer surface of a commercial cylindrical ceramic filter. The resulting membrane was free of defects, and they were successfully withdrawing the olefins from the reaction zone during the methanol conversion. In their paper, a method for testing the durability of membrane under a sequence of thermal and mechanical shocks is reported. Their membrane showed a quite high durability while the selectivity of olefins from methanol was increased up to 90%, even at high methanol conversion. The same group (Tago et al., 2005) further improved the use of ZSM-5 membranes for the MTO reaction. In fact, in order to decrease the production of paraffin and aromatics, the authors modified the acidic sites of their membrane by using the so-called catalytic cracking of silane (CSS) method. In this way the acidic sites of the zeolite are deactivated (by forming SiO_2 units) and the production of paraffin and aromatics (catalyzed by these acidic sites) was prevented.

Li et al. (2007) synthesized an LTA zeolite membrane for improving the performances of the Fisher-Tropsch (FT) reaction. Use of a hydrophilic membrane during the FT reaction can

allow the separation of water (a product of reaction) from the permanent gases resulting in an increase of the conversion per pass and, more important, avoiding the catalyst deactivation caused by the high amount of water present in the reaction system. The authors produced their LTA zeolite membrane with an in situ method improved with microwaves, on a α-Al_2O_3 tubular support. They obtained very high perm-selectivities over a broad range of experimental conditions. They also found that the water flux was only dependent on the pressure difference of water across the membrane. The authors also performed mixed-alcohols permeation tests and the permeate stream contained only water and a little methanol. The only problem faced by the authors was the fouling of the membrane by the long chain of hydrocarbon impurities, which of course occur during the FT synthesis.

The use of membranes for the FT reaction was also suggested by Espinoza et al. (2000). In their work, they studied the possibility of recovering water from the reaction system as well as increasing the catalyst lifetime and the conversion by using different types of membranes such as silicalite-1, Mordenite, and ZSM-5.

De Falco et al. (2017) simulated a zeolite membrane reactor for the production of dimethyl ether (DME). The authors simulated the behavior of the reactor in different conditions, demonstrating once more that the zeolite membrane reactor can be used for DME as a CO_2 reuse route. They reported a conversion enhancement compared to a conventional reactor of more than 30% (see Fig. 18.10). These results should, of course, be confirmed by an experimental study.

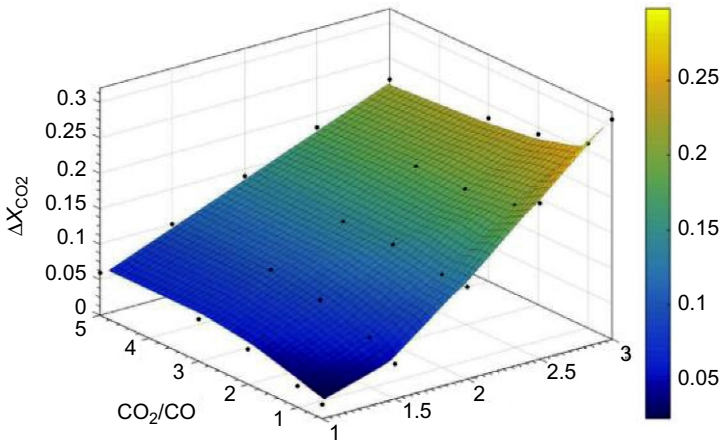

Fig. 18.10

CO_2 conversion enhancement varying the inlet feedstock composition for DME production.
Reproduced from De Falco, M., Capocelli, M., Basile, A., 2017. Selective membrane application for the industrial one-step DME production process fed by CO_2 rich streams : modeling and simulation. Int. J. Hydrogen Energy, 42, 6771–6786. https://doi.org/10.1016/j.ijhydene.2017.02.047 with permission of Elsevier.

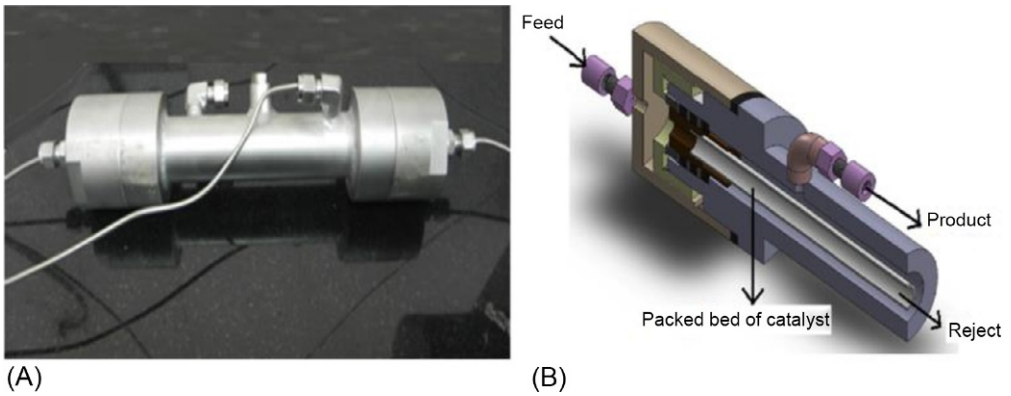

Fig. 18.11

(A) Membrane reactor assembly. (B) Membrane reactor cross-section. *Reproduced from Goswami, N., Bose, A., Das, N., Achary, S.N., Sahu, A.K., Karki, V., et al., 2017. DDR zeolite membrane reactor for enhanced HI decomposition in IS thermochemical process. Int. J. Hydrogen Energy 42 (16), 10867–10879. https://doi.org/10.1016/j.ijhydene.2017.02.175 with permission of Elsevier.*

On the other hand, the efficient synthesis of the DME in a membrane reactor already has been experimentally demonstrated by Zhou et al. (2016) by using a FAU-LTA dual-layer membrane in a membrane reactor. The authors were able to boost the conversion of methanol up to >90% at 100% DME selectivity in their membrane reactor.

Goswami et al. (2017) reported the use of a defect-free deca dodecasil rhombohedral zeolite membrane reactor (see Fig. 18.11) for the decomposition of HI, which is a thermodynamically limited reaction with conversion of around 22% at 700 K. The use of this zeolite membrane reactor increased the conversion of HI up to 95% in a single pass by extracting the hydrogen formed during the reaction.

4.2 Zeolite Membranes and Methanol Production

The use of a zeolite membrane for the methanol synthesis was also proposed in the literature. In fact, during the synthesis of methanol via hydrogenation of CO_2/CO, the following reactions take place:

$$CO + 2H_2 \Leftrightarrow CH_3OH \quad \Delta H_{298K} = -90.7 \text{ kJ/mol}$$

$$CO_2 + H_2 \Leftrightarrow CO + H_2O \quad \Delta H_{298K} = 41.19 \text{ kJ/mol}$$

$$CO_2 + 3H_2 \Leftrightarrow CH_3OH + H_2O \quad \Delta H_{298K} = -49.51 \text{ kJ/mol}$$

It is worth observing that the removal of methanol and/or water at high temperature from the reaction zone will allow the equilibrium limitation to be circumvented, resulting in a more efficient operation (lower sizes, higher conversion, higher selectivities).

A process design for the use of zeolite membranes in methanol production from CO_2 was proposed by Van Der Ham et al. (2012), where the authors decided to use a fluidized bed membrane reactor with a Zn-Cu based catalyst and a zeolite membrane for removal of the products. This obtained a yield of 25% per pass.

The scheme of the reactor used for their simulations is reported in Fig. 18.12.

Barbieri et al. (2002) have performed a thermodynamic analysis of the CO_2 hydrogenation into methanol by using zeolite membranes with different values of methanol and steam permeation. As indicated in Fig. 18.13, the authors found a sharp increase in carbon dioxide conversion while using the membrane reactors with respect to the conventional system. Additionally, the increase of methanol permeation in the membrane (compared to water) resulted in higher selectivity and methanol yield. The methanol yield (per pass) increased from 5.8% of a conventional system up to 13.7% in the best membrane reactor.

The modeling study from Barbieri and coworkers relied heavily on the permeation rates of methanol and water in zeolite membranes. The more reliable data available on this separation, the better modeling of membrane reactors can be achieved. In this sense, Sawamura et al. (2008)

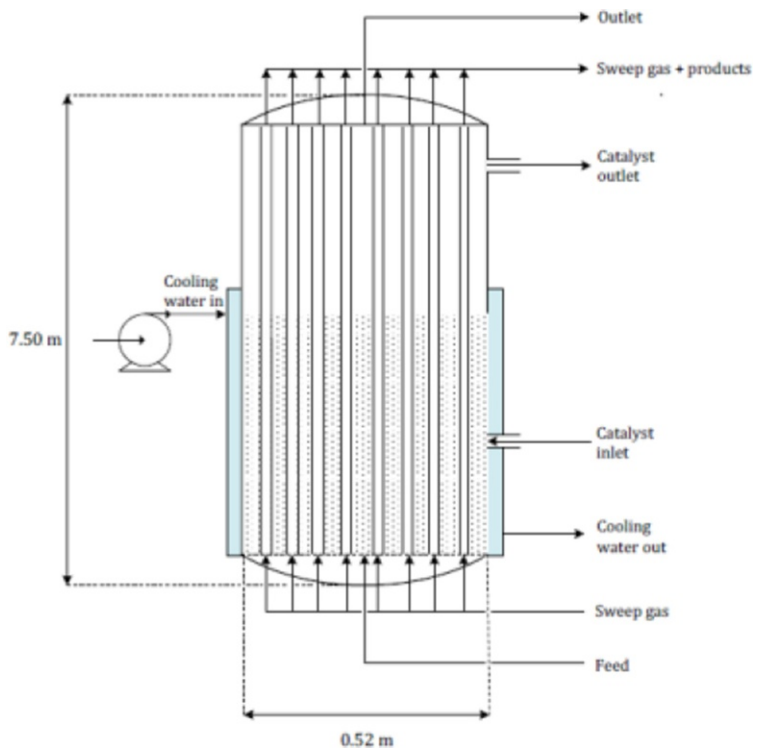

Fig. 18.12
Schematic representation of wall-cooled fluidized bed membrane reactor (Van Der Ham et al., 2012).

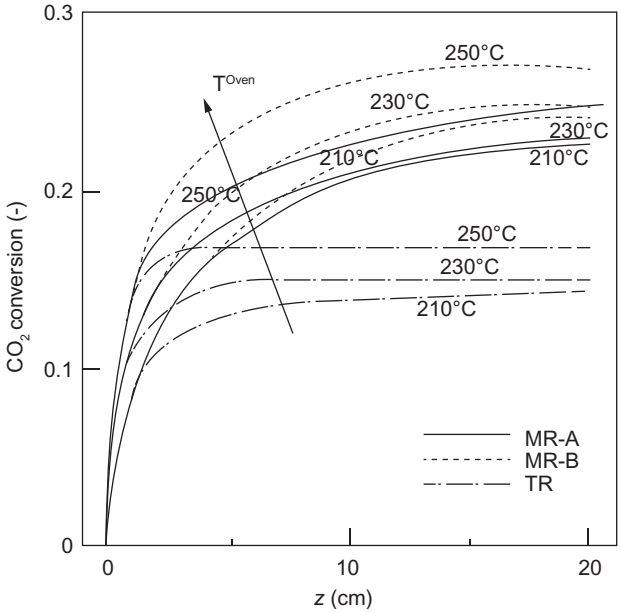

Fig. 18.13

CO_2 conversion profiles for MR and TR at oven temperatures of 210, 230, 250°C. Feed flow rate 400 cm^3 (STP)/min, sweep gas flow rate = 1000 cm^3 (STP)/min, H_2/CO_2 feed molar ratio = 3, $P_{Reaction} = P_{Permeation} = 10$ bar. *Reproduced from Barbieri, G., Marigliano, G., Golemme, G., Drioli, E., 2002. Simulation of CO_2 hydrogenation with CH_3OH removal in a zeolite membrane reactor. Chem. Eng. J., 85, 53–59. https://doi.org/10.1016/S1385-8947(01)00143-7 with permission of Elsevier.*

studied the selective removal of water from a water-methanol-hydrogen mixture by using a mordenite membrane. The membrane was prepared by a secondary growth method on the outer surface of a α-alumina commercial tube with an asymmetric structure.

The authors performed a permeation test with pure hydrogen and with mixtures in the setup shown in Fig. 18.14. When pure hydrogen was fed inside the membrane, the flux through the mordenite was really high. However, when the hydrogen was fed in a mixture with methanol and water vapors, the permeation of hydrogen decreased dramatically. This trend was observed up to 523 K. The mordenite membrane could then be used during the methanol synthesis with some interesting results. However, a membrane with high perm selectivity of both methanol and water could give better results in terms of CO_2 conversion and methanol selectivity.

As already reported above, the reactions considered are:

$$CO + 2H_2 \Leftrightarrow CH_3OH \quad \Delta H_{298K} = -90.7 \text{ kJ/mol} \tag{18.1}$$

$$CO_2 + H_2 \Leftrightarrow CO + H_2O \quad \Delta H_{298K} = 41.19 \text{ kJ/mol} \tag{18.2}$$

$$CO_2 + 3H_2 \Leftrightarrow CH_3OH + H_2O \quad \Delta H_{298K} = -49.51 \text{ kJ/mol} \tag{18.3}$$

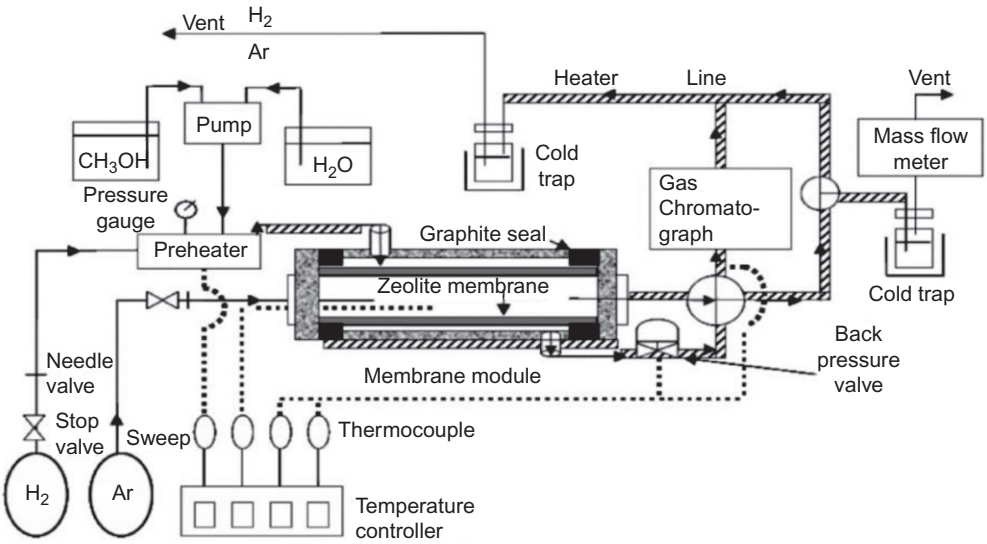

Fig. 18.14

Schematic diagram of the experimental apparatus for $H_2O/CH_3OH/H_2$ separation through a zeolite membrane. *Reproduced from Sawamura, K.-I., Shirai, T., Takada, M., Sekine, Y., Kikuchi, E., Matsukata, M., 2008. Selective permeation and separation of steam from water-methanol-hydrogen gas mixtures through mordenite membrane. Catal. Today., 132. https://doi.org/10.1016/j.cattod.2007.12.005 with permission of Elsevier.*

In Fig. 18.15, the CO_2 conversion of the reaction system versus the temperature is reported at different reaction pressures. It is clear that: (a) at a fixed temperature, CO_2 conversion increases with increasing pressure; (b) at a fixed pressure, each curve shows a minimum that moves along the temperature axis when pressure increases. In other words, with increasing pressure the minimum in CO_2 conversion shifts toward higher temperatures.

This behavior can be explained considering that the exothermic Eqs. (18.1), (18.3) proceed with a reduction of the total mole number. So, they are thermodynamically favored at high pressures and low temperatures, while a decreasing behavior of CO_2 conversion versus temperature is expected for these two reactions. Vice versa, the reverse WGS reaction (18.2) is an endothermic one, with no variation of the total moles number. It is thermodynamically favored at higher temperatures and is indifferent to pressure variations, so an increasing behavior of CO_2 conversion versus temperature is expected only for this reaction. In this way, for the overall reaction system at low temperature, the total CO_2 conversion is regulated by the equilibrium conversion of the exothermic reactions. While at high temperature, the total CO_2 conversion is close to the equilibrium conversion of the reverse WGS reaction. In fact, at $T = 160°C$, for example, the total CO_2 conversion shows a large range by varying the pressure from 5 to 30 bar, while at 300°C the same curves are in a narrower range.

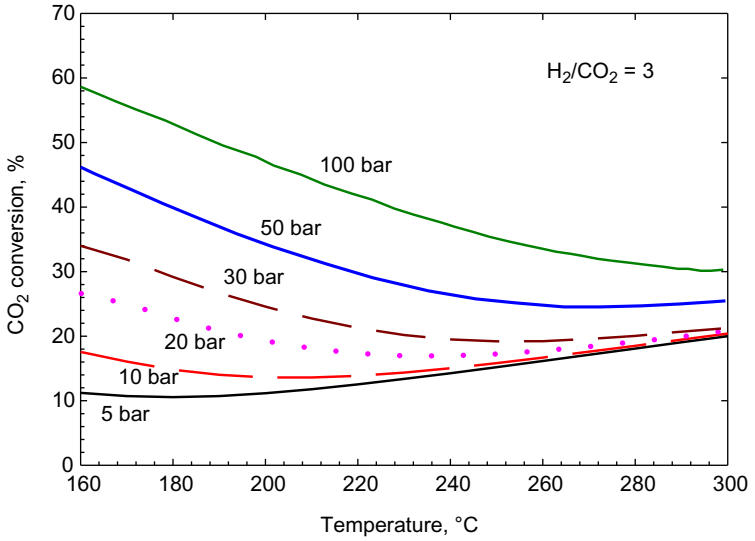

Fig. 18.15
CO_2 conversion versus temperature for thermodynamic equilibrium at different pressures, $H_2/CO_2 = 3$.

From the figure it can be observed that, even by increasing the pressure up to 100 bar, the maximum conversion attainable in the temperature range in which the catalysts are active (200–300°C), is hardly higher than 40%.

As demonstrated by Barbieri et al. (2002), the membrane reactor equipped with a zeolite membrane will be able to increase the conversion of a conventional system, depending on the amount of methanol and water permeating the membrane. It is thus possible to calculate the maximum amount of conversion and selectivity in a membrane reactor as a function of the membrane permeation as reported in Fig. 18.16. The figure shows the maximum CO_2 conversion and the methanol selectivity versus the reaction temperature, at $p = 20$ bar and $H_2/CO_2 = 3$ for different values of membrane permeation. In the same figure the equilibrium conversion and selectivity for a traditional system are also shown for comparison.

The methanol and water withdrawal (expressed by α in the figure) promote the shift of the thermodynamic equilibrium so that the maximum CO_2 conversion and methanol selectivity in a membrane reactor are higher than the ones of a traditional reactor. Of course the shift effect increases by increasing α.

At this point a kinetic model can be used to simulate the behavior of a membrane reactor providing that the value of α is known. For example, Fig. 18.17 shows the CO_2 conversion and methanol selectivity versus temperature at the fixed catalyst load at 20 bar, $\alpha = 40\%$, $H_2/CO_2 = 3$, time factor $= 0.04$ g_{cat} min/mL_{CO2}, and different permeation ratios H_2O/CH_3OH.

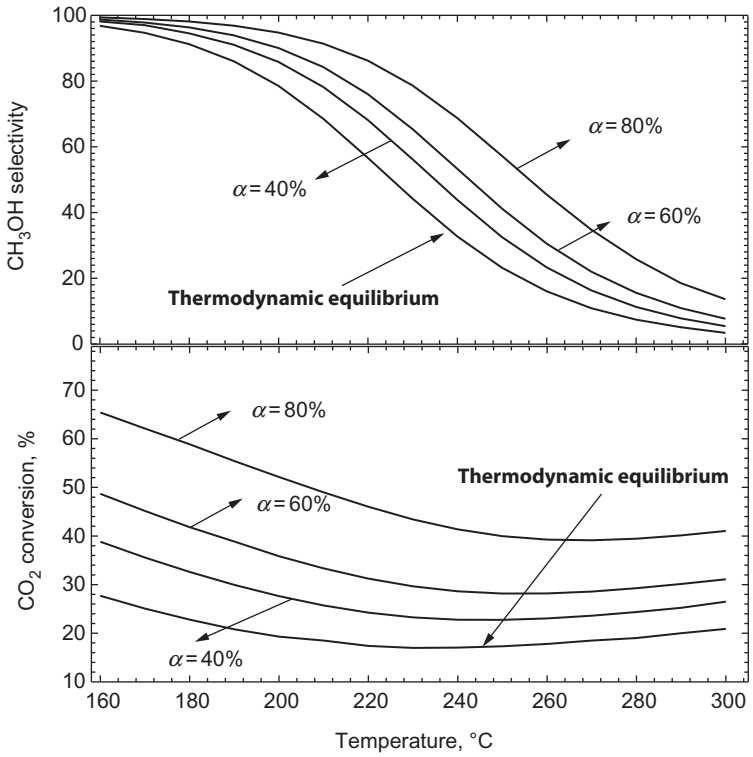

Fig. 18.16

CO_2 conversion and methanol selectivity versus temperature for dynamic equilibrium at different permeation coefficients (α), $H_2/CO_2 = 3$, $Q^0_{CO_2} = 200\,\text{mL/min}$, $p = 20$ bar.

The largest difference between equilibrium curve and kinetic curve is shown at 160°C; at this temperature, the catalyst is almost nonactive. Methanol selectivity is plotted at the same cited operative conditions. For both curves the trend is quite similar: methanol selectivity decreases by increasing temperature. Methanol selectivity is different for equilibrium and kinetic curves, but the difference is not so high. CO_2 might give low conversion to methanol but the methanol selectivity is high, favored by the low temperature.

The methanol production in zeolite membrane reactors has also been studied from an experimental point of view as reported by Gallucci et al. (2004).

Fig. 18.18 shows the behavior of CO_2 conversion versus temperature in terms of experimental results for both the traditional system and a membrane reactor, at 20 bar and at two different H_2/CO_2 feed ratios. A membrane reactor generally outperforms the traditional system. However, for temperatures higher than 230°C, membrane reactors tend to converge with traditional reactors. Two explanations can be given for this loss in performance. The first is related to the thermal stability of the zeolite membrane. However, another possible

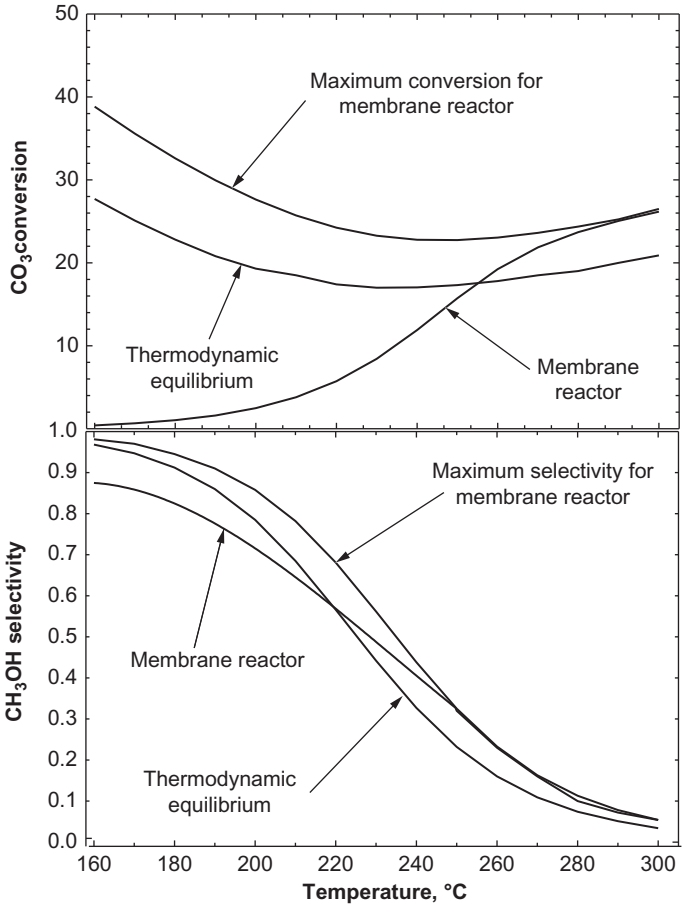

Fig. 18.17

CO_2 conversion and methanol selectivity versus temperature for thermodynamic and dynamic equilibrium, and membrane reactor model, at permeation coefficient $\alpha = 40\%$, $p = 20$ bar, $H_2/CO_2 = 3$, Time Factor $= 0.04\ g_{cat}\ min/mL_{CO2}$.

explanation is the impossibility, at high temperature, for methanol to condense inside the pores of the structure. Methanol has the critical temperature at 238°C, so at $T > 238$°C a behavior like a gas is expected. The critical temperature of water (374°C) assures that, in the range of temperature considered for experimental tests (200–263°C), only methanol is expected to change phase from vapor to gas when overcoming 238°C. Above 238°C, from this effect follows a weaker increase in CO_2 conversion versus temperature. In fact, at 255–263°C both membrane reactors and traditional reactors show similar CO_2 conversion.

Similar trends have been later reported demonstrating that an LTA zeolite membrane reactor is able to overcome the limitations of a conventional system and improve the conversion rates.

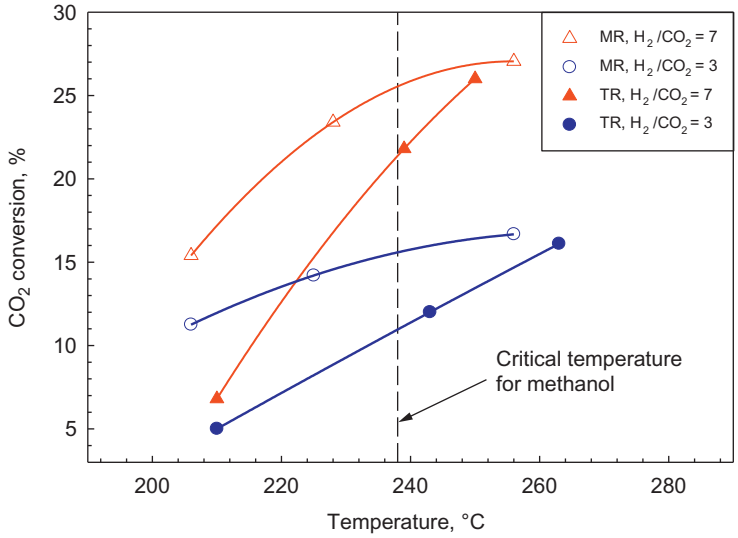

Fig. 18.18

CO_2 conversion versus temperature, for both membrane and traditional reactors, $p = 20$ bar, $H_2/CO_2 = 3$ and 7, Total feed rate = 800 mL/min, catalyst weight = 8 g. *Reproduced from Gallucci, F., Paturzo, L., Basile, A., 2004. An experimental study of CO_2 hydrogenation into methanol involving a zeolite membrane reactor. Chem. Eng. Process., 43, 1029–1036. https://doi.org/10.1016/j.cep.2003.10.005 with permission of Elsevier.*

Apart from these examples of membrane reactors for methanol production, several other papers have been recently published on membrane reactors for CO_2 hydrogenation or methanol synthesis.

Atsonios et al. (2016) recently reported on a process improvement using membrane reactors for methanol production. The authors reported a process flow diagram for methanol synthesis in membrane reactors as shown in Fig. 18.19. The authors reported that the adoption of a membrane reactor for methanol synthesis has no effect on the methanol plant thermal efficiency but increases the methanol yield Atsonios et al. (2016). Because of this increase in yield, the recycle stream is reduced and thus the reactors are smaller and the capital cost strongly reduced.

Recently, Wang et al. (2015) studied hydrophilic zeolite membranes for the selective removal of water for membrane reactor applications. As reported in Fig. 18.20, the authors reported good selectivity for the modified membranes such that could be directly used in a CO_2 feed membrane reactor for efficient methanol production.

Rahimpour and coworkers presented in recent years several membrane reactor concepts for methanol synthesis using inorganic membranes. In all these modeling studies, generally hydrogen membranes are used to feed the hydrogen to methanol synthesis. The models (see for instance Bayat et al., 2014) show an increase of methanol production compared with a

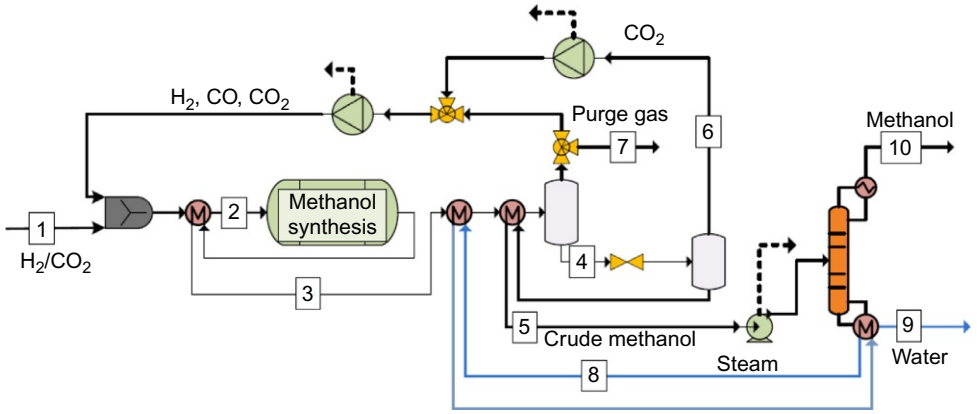

Fig. 18.19

Process flowsheet of the CO_2 to MeOH concept. *Reproduced from Atsonios, K., Panopoulos, K.D., Kakaras, E., 2016. Thermocatalytic CO_2 hydrogenation for methanol and ethanol production: process improvements. Int. J. Hydrogen Energy, 41, 792–806. https://doi.org/10.1016/j.ijhydene.2015.12.001 with permission of Elsevier.*

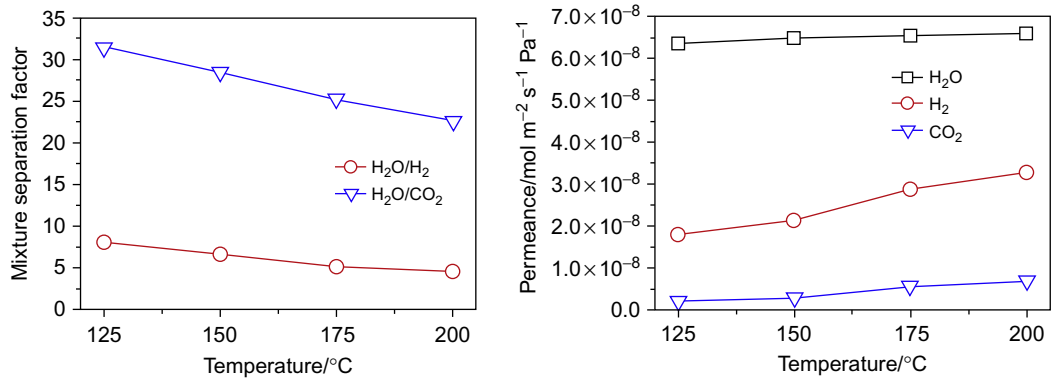

Fig. 18.20

Mixture separation factors of equimolar mixtures of H_2O/H_2 and H_2O/CO_2 as well as single gas permeances of H_2O, H_2, and CO_2 through a supported zeolite SOD membrane prepared by two-step repeated hydrothermal synthesis as a function of temperature. *Reproduced from Wang, N., Liu, Y., Huang, A., Caro, J., 2015. Hydrophilic SOD and LTA membranes for membrane-supported methanol, dimethylether and dimethylcarbonate synthesis. Microporous Mesoporous Mater., 207. https://doi.org/10.1016/j.micromeso.2014.12.028 with permission of Elsevier.*

conventional system. However, it is not yet clear if the overall cost of the systems presented is lower than conventional methanol production plants.

Farsi and Jahanmiri (2011) reported the use of a dual-membrane reactor for methanol production. In the concept reported in Fig. 18.21, two membranes are used, one for hydrogen feeding and one for water removal.

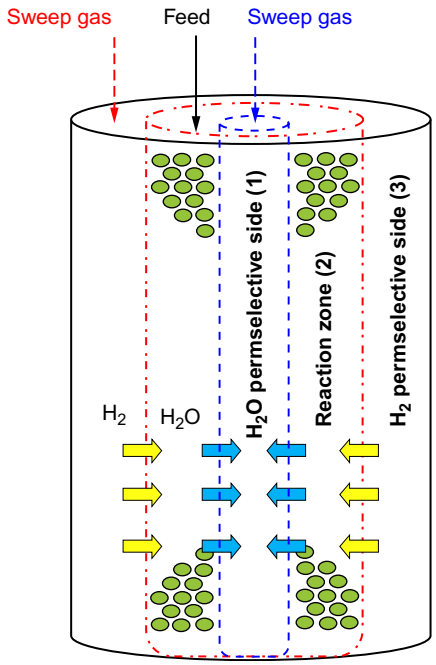

Fig. 18.21

Dual-membrane reactor. *Reproduced from Farsi, M., Jahanmiri, A., Methanol production in an optimized dual-membrane fixed-bed reactor, Chem. Eng. Process. Process Intensif. 50 (2011). https://doi.org/10.1016/j.cep.2011.08.011 with permission of Elsevier.*

According to the authors the advantages of the optimized dual-membrane reactor are both related to higher CO_2 conversion into methanol and lower methanol costs.

5 Conclusion and Future Trends

So far many reports have been published on the use of inorganic membranes for methanol production. Despite the large interest, however, minimal experimental data have been reported. These results are interesting, but far from being scaled up to an industrial scale. The main drawback so far is the lack of reproducible membranes with the right characteristics for methanol/water permeation under reactive conditions.

The future activities in this field should thus focus on production and scale-up of membranes able to effectively separate the products of the methanol production. This can be achieved either trying to prepare defect-free zeolite membranes or by increasing the work on carbon molecular sieves membranes, as these are cheaper and easier to prepare while the surface morphology can be tuned by working at specific temperatures/concentrations.

References

Atsonios, K., Panopoulos, K.D., Kakaras, E., 2016. Thermocatalytic CO_2 hydrogenation for methanol and ethanol production: process improvements. Int. J. Hydrog. Energy 41, 792–806. https://doi.org/10.1016/j.ijhydene.2015.12.001.

Barbieri, G., Marigliano, G., Golemme, G., Drioli, E., 2002. Simulation of CO_2 hydrogenation with CH_3OH removal in a zeolite membrane reactor. Chem. Eng. J. 85, 53–59. https://doi.org/10.1016/S1385-8947(01)00143-7.

Bayat, M., Dehghani, Z., Rahimpour, M.R., 2014. Membrane/sorption-enhanced methanol synthesis process: dynamic simulation and optimization. J. Ind. Eng. Chem. 20, 3256–3269. https://doi.org/10.1016/j.jiec.2013.12.007.

Bos, M.J., Brilman, D.W.F., 2015. A novel condensation reactor for efficient CO_2 to methanol conversion for storage of renewable electric energy. Chem. Eng. J. 278, 527–532. https://doi.org/10.1016/j.cej.2014.10.059.

Brunetti, A., Caravella, A., Barbieri, G., Drioli, E., 2007. Simulation study of water gas shift reaction in a membrane reactor. J. Membr. Sci. 306, 329–340.

Caro, J., Noack, M., Kölsch, P., Schäfer, R., 2000. Zeolite membranes—state of their development and perspective. Microporous Mesoporous Mater. 38, 3–24. https://doi.org/10.1016/S1387-1811(99)00295-4.

Caro, J., 2016. Supported Zeolite and MOF Molecular Sieve Membranes: Preparation, Characterization, Application. Elsevier, New York. https://doi.org/10.1016/B978-0-444-63506-8.00008-2.

Daer, S., Kharraz, J., Giwa, A., Hasan, S.W., 2015. Recent applications of nanomaterials in water desalination: a critical review and future opportunities. Desalination 367, 37–48. https://doi.org/10.1016/j.desal.2015.03.030.

Danesh-Khorasgani, M., Nezamzadeh-Ejhieh, A., 2016. PVC-zeolite nanoparticle-surfactant anion exchanger membrane: preparation, characterization, and its application in development of ion-selective electrode for detection of sulfate. J. Solid State Electrochem. 20, 2827–2833. https://doi.org/10.1007/s10008-016-3265-9.

Dragomirova, R., Wohlrab, S., 2015. Zeolite membranes in catalysis—from separate units to particle coatings. Catalysts 5, 2161–2222. https://doi.org/10.3390/catal5042161.

Espinoza, R.L., Toit, E.D., Santamaria, J., Menendez, M., Coronas, J., Irusta, S., 2000. Use of membranes in Fischer-Tropsch reactors. Stud. Surf. Sci. Catal. 130 (A), 389–394.

De Falco, M., Capocelli, M., Basile, A., 2017. Selective membrane application for the industrial one-step DME production process fed by CO_2 rich streams: modeling and simulation. Int. J. Hydrog. Energy 42, 6771–6786. https://doi.org/10.1016/j.ijhydene.2017.02.047.

Farbenindustrie Akt-Ges, I.G., 1932. Verfahren Zur Darstellung von Methanol und Seinen Homologen. German Patent 565,309, Issued November 30.

Farsi, M., Jahanmiri, A., 2011. Methanol production in an optimized dual-membrane fixed-bed reactor. Chem. Eng. Process. Process Intensif. 50, 1177–1185. https://doi.org/10.1016/j.cep.2011.08.011.

Gallucci, F., Paturzo, L., Basile, A., 2004. An experimental study of CO_2 hydrogenation into methanol involving a zeolite membrane reactor. Chem. Eng. Process. 43, 1029–1036. https://doi.org/10.1016/j.cep.2003.10.005.

Gallucci, F., Basile, A., Drioli, E., 2007. Methanol as an energy source and/or energy carrier in membrane processes. Sep. Purif. Rev. 36, 175–202.

Goswami, N., Bose, A., Das, N., Achary, S.N., Sahu, A.K., Karki, V., et al., 2017. DDR zeolite membrane reactor for enhanced HI decomposition in IS thermochemical process. Int. J. Hydrog. Energy 42 (16), 10867–10879. https://doi.org/10.1016/j.ijhydene.2017.02.175.

Van Der Ham, L.G.J., Van Den Berg, H., Benneker, A., Simmelink, G., Timmer, J., Van Weerden, S., 2012. Hydrogenation of carbon dioxide for methanol production. Chem. Eng. Trans. 29, 181–186. https://doi.org/10.3303/CET1229031.

Hanson, R.S., Hanson, T.E., 1996. Methanotrophic bacteria. Microbiol. Rev. 60, 439–471.

Kim, S.-J., Tan, S., Taborga Claure, M., Briones Gil, L., More, K.L., Liu, Y., et al., 2016. One-step synthesis of zeolite membranes containing catalytic metal nanoclusters. ACS Appl. Mater. Interfaces 8, 24671–24681. https://doi.org/10.1021/acsami.6b06576.

Kiss, A.A., Pragt, J.J., Vos, H.J., Bargeman, G., de Groot, M.T., 2016. Novel efficient process for methanol synthesis by CO_2 hydrogenation. Chem. Eng. J. 284, 260–269. https://doi.org/10.1016/j.cej.2015.08.101.

Krishna, R., 2006. The maxwell-stefan formulation of diffusion in zeolites. In: Conner, W.C., Fraissard, J. (Eds.), Fluid Transp. Nanoporous Mater. Springer Netherlands, Dordrecht, pp. 211–240. https://doi.org/10.1007/1-4020-4382-1_10.

Li, Y., Chen, H., Liu, J., Li, H., Yang, W., 2007. Pervaporation and vapor permeation dehydration of Fischer-Tropsch mixed-alcohols by LTA zeolite membranes. Sep. Purif. Technol. 57, 140–146. https://doi.org/10.1016/j.seppur.2007.03.027.

Llosa Tanco, M.A., Pacheco Tanaka, D.A., Mendes, A., 2015. Composite-alumina-carbon molecular sieve membranes prepared from novolac resin and boehmite. Part II. Effect of the carbonization temperature on the gas permeation properties. Int. J. Hydrog. Energy 40, 3485–3496. https://doi.org/10.1016/j.ijhydene.2014.11.025.

Masuda, T., Asanuma, T., Shouji, M., Mukai, S.R., Kawase, M., Hashimoto, K., 2003. Methanol to olefins using ZSM-5 zeolite catalyst membrane reactor. Chem. Eng. Sci. 58, 649–656. https://doi.org/10.1016/S0009-2509(02)00591-2.

Meier, W.M., 1986. Zeolites and Zeolite-Like Materials. Elsevier, New York. https://doi.org/10.1016/S0167-2991(09)60851-X.

Meier, W.M., 1991. Zeolite structure types: past-present-future. Stud. Surf. Sci. Catal. 65, 247–256. https://doi.org/10.1016/S0167-2991(08)62910-9.

Methanol.org, 2017. http://www.metanol.org/. Accessed in April 2017.

Pagis, C., Morgado Prates, A.R., Farrusseng, D., Bats, N., Tuel, A., 2016. Hollow zeolite structures: an overview of synthesis methods. Chem. Mater. 28, 5205–5223. https://doi.org/10.1021/acs.chemmater.6b02172.

RITE, 2017. The RITE website.

Sawamura, K.-I., Shirai, T., Takada, M., Sekine, Y., Kikuchi, E., Matsukata, M., 2008. Selective permeation and separation of steam from water-methanol-hydrogen gas mixtures through mordenite membrane. Catal. Today 132, 182–187. https://doi.org/10.1016/j.cattod.2007.12.005.

Struis, R.P.W.J., Stucki, S., Wiedorn, M., 1996. A membrane reactor for methanol synthesis. J. Membr. Sci. 113, 93–100. https://doi.org/10.1016/0376-7388(95)00222-7.

Tago, T., Iwakai, K., Morita, K., Tanaka, K., Masuda, T., 2005. Control of acid-site location of ZSM-5 zeolite membrane and its application to the MTO reaction. Catal. Today 105, 662–666. https://doi.org/10.1016/j.cattod.2005.06.009.

Tanaka, S., Yasuda, T., Katayama, Y., Miyake, Y., 2011. Pervaporation dehydration performance of microporous carbon membranes prepared from resorcinol/formaldehyde polymer. J. Membr. Sci. 379, 52–59. https://doi.org/10.1016/j.memsci.2011.05.046.

Tavolaro, A., Tavolaro, P., 2009. The preparation of transition metal-containing mordenite catalytic tubular composite membranes. Catal. Commun. 10, 586–591. https://doi.org/10.1016/j.catcom.2008.10.041.

Tijm, P.J., Waller, F., Brown, D., 2001. Methanol technology developments for the new millennium. Appl. Catal. A Gen. 221, 275–282. https://doi.org/10.1016/S0926-860X(01)00805-5.

Vasanth, D., Pugazhenthi, G., Uppaluri, R., 2017. Preparation, characterization, and performance evaluation of LTA zeolite-ceramic composite membrane by separation of BSA from aqueous solution. Sep. Sci. Technol. 52, 767–777. https://doi.org/10.1080/01496395.2016.1260142.

Vroon, Z.A.E., Keizer, K., Burggraaf, A., Verweij, H., 1998. Preparation and characterization of thin zeolite MFI membranes on porous supports. J. Membr. Sci. 144, 65–76. https://doi.org/10.1016/S0376-7388(98)00035-0.

Wang, N., Liu, Y., Huang, A., Caro, J., 2015. Hydrophilic SOD and LTA membranes for membrane-supported methanol, dimethylether and dimethylcarbonate synthesis. Microporous Mesoporous Mater. 207, 33–38. https://doi.org/10.1016/j.micromeso.2014.12.028.

Weitkamp, J., 2000. Zeolites and catalysis. Solid State Ionics 131, 175–188. https://doi.org/10.1016/S0167-2738(00)00632-9.

Wu, J., Saito, M., Takeuchi, M., Watanabe, T., 2001. The stability of Cu/ZnO-based catalysts in methanol synthesis from a CO_2-rich feed and from a CO-rich feed. Appl. Catal. A Gen. 218, 235–240. https://doi.org/10.1016/S0926-860X(01)00650-0.

Yu, L., Zeng, C., Wang, C., Zhang, L., 2017. In situ impregnation-gelation-hydrothermal crystallization synthesis of hollow fiber zeolite NaA membrane. Microporous Mesoporous Mater. 244, 278–283. https://doi.org/10.1016/j.micromeso.2016.10.047.

Zhang, B., Zhao, D., Wu, Y., Liu, H., Wang, T., Qiu, J., 2015. Fabrication and application of catalytic carbon membranes for hydrogen production from methanol steam reforming. Ind. Eng. Chem. Res. 54, 623–632. https://doi.org/10.1021/ie503094r.

Zhou, C., Wang, N., Qian, Y., Liu, X., Caro, J., Huang, A., 2016. Efficient synthesis of dimethyl ether from methanol in a bifunctional zeolite membrane reactor. Angew. Chem. Int. Ed. 55, 12678–12682. https://doi.org/10.1002/anie.201604753.

CHAPTER 19

Highly Conductive Structured Catalysts for the Intensification of Methanol Synthesis in Multitubular Reactors

Carlo G. Visconti*, Andrea Montebelli*, Gianpiero Groppi*, Enrico Tronconi*, Stefanie Kohler†

Dipartimento di Energia, Politecnico di Milano, Milano, Italy †Total Refining & Chemicals, Paris La Défense Cedex, France

Nomenclature

af	multiplying activity factor
CPSI	honeycomb monolith cell density (cells/in.^{2})
d_c	cell diameter (m)
d_h	pellet height (m)
d_p	catalyst pellet diameter (m)
d_{pa}	diameter of a sphere with the same surface as the pellet (m)
d_{pe}	diameter of a sphere with the same volumetric surface as the pellet (m)
d_{pv}	diameter of a sphere with the same volume as the pellet (m)
d_t	internal reactor tube diameter (m)
F	fresh feed molar flow rate to the reactor (mol/s)
HM	honeycomb monolith
h_w	wall heat transfer coefficient (W/m^2/K)
L	length (m)
M_F	stoichiometric number in fresh feed
n_{tubes}	number of reactor tubes
OF	open-cell foam
P	pressure (Pa)
PB	packed-bed
PD	foam pore density, expressed in PPI (i.e., pores/in.)
Pr	Prandtl number
r	reactor radial coordinate (m)
Re	Reynolds number

Methanol. https://doi.org/10.1016/B978-0-444-63903-5.00019-4

T	temperature (K)
U	1D length-averaged overall heat transfer coefficient ($W/m^2/K$)
W_{cat}	catalyst mass (kg)
z	reactor axial coordinate (m)

Greek symbols

ε	void fraction of bare substrate ($m^3_{void}/m^3_{substrate}$)
k_{ea}	axial effective thermal conductivity (W/m/K)
k_{er}	radial effective thermal conductivity (W/m/K)
ξ	catalyst volumetric fraction ($m^3_{catalyst}/m^3_{tube}$)

Superscripts

0	reactor inlet
out	reactor outlet

Subscripts

cat	catalyst
cl	centerline ($r=0$)
$cool$	coolant
g	referred to the gas phase
hs	hot-spot
hm	honeycomb-monolith
$MeOH$	methanol
OF	open-cell foams
PB	packed-bed
s	solid
t	tube
w	washcoat

1 Introduction

As discussed in the previous chapters, the low temperature-low pressure methanol synthesis from $H_2/CO/CO_2$ mixtures over $CuO/ZnO/Al_2O_3$ pelletized catalysts is a mature and well-developed commercial process used by many large industrial plants with capacities up to 10^7 kg per day. The synthesis is carried out at 250–300°C and 50–100 bar and is highly exothermic: at standard conditions, roughly 90 or 50 kJ/mol are released when a mole of methanol is produced from CO or CO_2, respectively. At these conditions, CO_x conversions per pass as well as the process yields are limited by thermodynamic equilibrium.

In the last few years, Politecnico di Milano and Total have worked jointly to design a compact reactor technology for methanol synthesis. Compact reactors for methanol synthesis are indeed particularly interesting for the exploitation of underutilized and therefore low-cost small gas reservoirs in remote areas, (which presently constitute 50% of the gas reserves, 50% of which are off-shore; Thackeray and Leckie, 2002), but also of other feedstocks available in limited amounts only, such as associated gas produced during oil extraction or syngas produced from biomass. This chapter provides an overview of the related work, which has involved both experimental activities and numerical reactor/process simulations.

2 State-of-the-Art of Multitubular Reactor Configurations for Methanol Synthesis

Several reactor designs are available on the market, but fixed-bed reactors with quench or multitubular cooling are generally preferred to run the methanol synthesis on an industrial scale (see Chapter 2). Among the two, multitubular reactors with external cooling represent the most flexible option. In these units, the possibility of tuning the coolant temperature provides a degree of freedom, which affords a better temperature control than quench reactors. This is fundamental for the catalyst lifetime (which is usually 5 years; Bartholomew and Farrauto, 2005), since $CuO/ZnO/Al_2O_3$ catalysts suffer significantly from sintering at 300°C (Spath and Dayton, 2003). Also, the possibility of tuning reactor productivity by varying the number of tubes represents a very interesting option for scaling the process.

One of the most widely used commercial technologies for methanol synthesis is the Lurgi externally cooled multitubular packed-bed (PB) reactor, which may achieve a capacity of 1.5×10^6 kg per day. In such a configuration, a few thousand tubes of 3–5 cm diameter are filled with catalyst pellets of a few millimeters in size and the heat of the reaction is removed by cooling with boiling water circulating externally to the tubes (Hartig and Keil, 1993).

These reactors have very interesting performances in terms of heat transfer. As shown in Fig. 19.1, the axial temperature profile measured within each tube is well controlled.

This result is achieved by maximizing the convective heat transfer (i.e., both the effective radial thermal conductivity k_{er} and the wall heat transfer coefficient h_w) within each tube. This implies the adoption of high flow rates, which typically imposes the use of long (i.e., 6–10 m) tubes, that seriously limits the possibilities for developing compact reactor configurations. In addition, multitubular fixed-bed reactors are operated with significantly overstoichiometric H_2/CO feed molar ratios (i.e., about 9–10). Indeed, H_2-rich syngas promotes CO conversion per pass and enables more efficient convective heat transfer due to its higher gas thermal conductivity. The large recycle of unconverted gas to ensure high overall syngas conversions (>90%–95%) results, however, in high investment and operating costs and large pressure drops (in the order of 1–10 bar) (Lange, 2001).

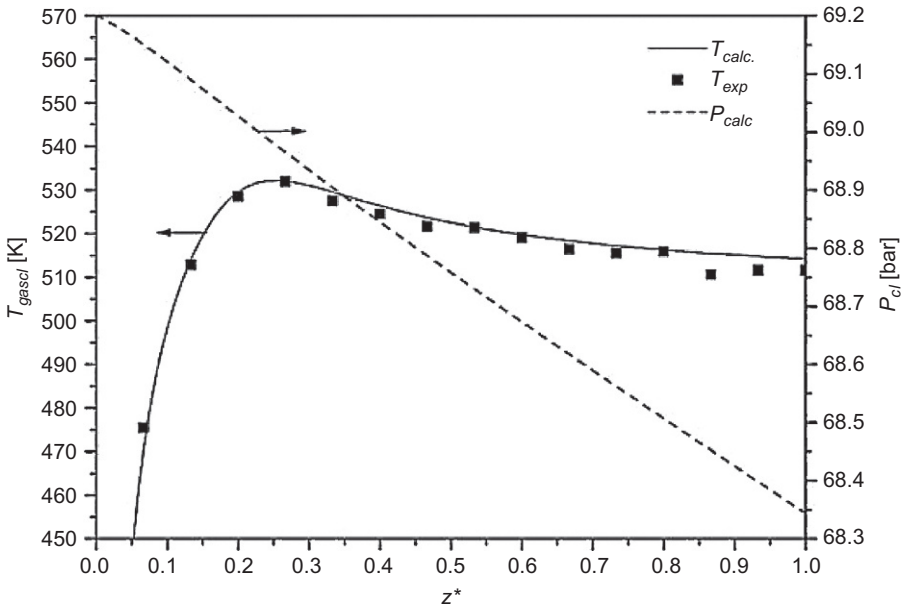

Fig. 19.1

Lurgi-type converter. Gas-phase temperature and pressure drop axial profiles at tube center line (*squares*: experimental T profile, *solid line*: calculated T profile, *dashed line*: calculated P profile). $T_g^0 = 323$ K, $T_{cool} = 511$ K, $P^0 = 69.2$ bar, $d_t = 4.2$ cm, $d_{pe} = 0.485$ cm (tablets with $d_p = 0.6$ cm and $d_h = 0.35$ cm), catalyst vol. fraction in the tube = 0.613, fresh feed composition: CO = 27.32%, $CO_2 = 3.55\%$, $H_2 = 68.64\%$, $N_2 + Ar + CH_4$ to balance. Feed flow rate is 25.9 Nl/s per tube. *Reprinted from Montebelli, A., Visconti, C.G., Groppi, G., Tronconi, E., Ferreira, C., Kohler, S., 2013. Enabling small-scale methanol synthesis reactors through the adoption of highly conductive structured catalysts. Catal. Today 215, 176–185 with permission from Elsevier.*

Therefore, it is clear that the intensification of methanol synthesis in compact reactors should aim at maximizing the syngas conversion per pass as well as the heat transfer in the reactor. Such a goal should be achieved without affecting the catalyst lifetime, and, at the same time, minimizing the selectivity toward byproducts (including dimethyl ether and methyl formate).

This chapter is focused on a possible strategy for improving the heat transfer in multitubular reactors for methanol synthesis. In particular, the adoption of highly conductive structured catalysts, washcoated with a catalytic layer and loaded in externally cooled multitubular reactors, will be addressed. For the other available options of intensifying methanol reactors, including: (i) the design of more active catalysts that operate at lower temperatures, thereby shifting the thermodynamic limit; (ii) the removal of methanol during the reaction to shift the equilibrium to higher CO conversions per pass, the reader is referred to dedicated literature, including Bartholomew and Farrauto (2005), Chapter 18, and references therein. For alternatives to highly conductive structured catalysts, the reader is referred to Tonkovich et al. (2007) and Bakhtiary-Davijany et al. (2011).

3 Highly Conductive Structured Reactors for Methanol Synthesis

For the sake of clarity, after a brief introduction on highly conductive structured catalysts and reactors (Section 3.1), in this section we will first present the results of a modeling study in which the performances of highly conductive structured reactors were compared to those of a commercial PB unit (i.e., of the Lurgi type, Section 3.2). An optimization study of the performances of compact conductive structured reactors follows, with a particular focus on the operation of such reactors at low catalyst loads (Section 3.3). Experimental activities are eventually reported (Section 3.4), showing that prototypes of conductive structured catalysts can be successfully prepared and operated in the methanol synthesis at industrially relevant conditions.

3.1 Highly Conductive Structured Catalysts and Reactors

Highly conductive structured catalysts consist in substrates made of highly conductive materials (usually metallic), shaped in the form of a monolithic matrix consisting of small (in the order of millimeters) interconnected cells or channels over which the catalytically active sites are properly dispersed. These materials have been widely studied in the last two decades because, thanks to their high void fraction, high geometric surface area substrates, and high intrinsic thermal conductivity, they have the potential: (i) of enabling low pressure drop; (ii) of diminishing the risk of intraporous mass transfer limitations; and (iii) of granting efficient heat removal in nonadiabatic applications (Groppi and Tronconi, 2000; Tronconi et al., 2014).

Highly conductive honeycombs and open-cell foams (OFs) are the two structured substrates with the greatest potential in multitubular fixed-bed reactors. Indeed, thanks to their highly conductive thermally connected matrix, they can introduce a new and more efficient heat transfer mechanism in these reactors, namely the heat conduction within the solid phase (Groppi and Tronconi, 2000, 2005; Tronconi et al., 2014; Bianchi et al., 2012, 2013). Such a mechanism, which is negligible in PB reactors where only point contacts exist among the pellets, is flow-independent. Accordingly, highly conductive structured catalysts are an interesting option for the operation of compact multitubular reactors, where scaling down the reactor requires shortening of the tubes.

The application of conductive structured catalysts to the methanol synthesis was scarcely investigated in the literature when, in 2010, Politecnico di Milano and Total started their collaboration in this field. The most relevant work before 2013 was that of Phan et al. (2010, 2011) who carried out the methanol synthesis over steel monoliths prepared from corrugated and flat Fecralloy sheets coated with a homemade $Cu/ZnO/Al_2O_3$ catalyst and loaded in a 0.5-in. stainless steel tubular reactor. By comparison with a conventional PB reactor, the authors claimed that the superior activity of the structured reactor was related to its higher

radial heat transfer rate, which provided a nearly isothermal catalytic bed for all the studied CO conversion levels (up to 30%).

In the following sections we will show by simulation that structured catalysts based on highly conductive OFs and honeycomb monoliths (HMs) can overcome conventional packed beds, especially when compact (i.e., short) externally cooled multitubular reactors are used.

In order to compare the performances of the different reactor configurations, we have used the commercial software gPROMS. For all reactors, we have adopted a two-dimensional steady-state heterogeneous pseudo-continuous description of the concentration and temperature gradients within one representative cylindrical tube along its axial and radial coordinates. We have also included the mathematical description of the intraporous concentration profiles according to an isothermal-isobaric intraporous reaction-diffusion model.

Heat transfer parameters have been estimated by using the following literature correlations:

Packed beds (Specchia and Sicardi, 1980):

$$k_{er,PB} = k_g \left(\varepsilon + \frac{1-\varepsilon}{0.220\varepsilon^2 + \frac{2}{3}\frac{k_g}{k_{cat}}} + \frac{Re_{d_{pa}} \cdot Pr}{8.65\frac{d_{pv}}{d_{pa}}\left(1 + 19.4\frac{d_{pa}^2}{d_t^2}\right)} \right) \tag{19.1}$$

$$h_{w,PB} = \frac{k_g}{d_{pv}} \left(2\varepsilon + \frac{1-\varepsilon}{0.0024\left(\frac{d_t}{d_{pv}}\right)^{1.58} + \frac{1}{3}\frac{k_g}{k_{cat}}} \right) + \frac{k_g}{d_{pa}} f(Re) \tag{19.2}$$

with

$$f(Re) = 0.0835 Re_{d_{pa}}^{0.91} \quad \text{if } Re_{d_{pa}} < 1200$$
$$f(Re) = 1.23 Re_{d_{pa}}^{0.53} \quad \text{if } Re_{d_{pa}} \geq 1200$$

Honeycomb monoliths (Groppi and Tronconi, 1996, 2005):

$$k_{er,HM} = k_s \left(\left(1 - \sqrt{\varepsilon+\xi}\right) + \frac{\sqrt{\varepsilon+\xi} - \sqrt{\varepsilon}}{\left(1 - \sqrt{\varepsilon+\xi}\right) + \frac{k_w}{k_s}\sqrt{\varepsilon+\xi}} + \frac{\sqrt{\varepsilon}}{\left(1 - \sqrt{\varepsilon+\xi}\right) + \frac{k_w}{k_s}\left(\sqrt{\varepsilon+\xi} - \sqrt{\varepsilon}\right) + \frac{k_g}{k_s}\sqrt{\varepsilon}} \right) \tag{19.3}$$

$$h_{w,HM} = 2410.1 k_g + 271.64 \tag{19.4}$$

Open foams (Bianchi et al., 2012, 2013):

$$k_{er,OF} = k_s\left(\frac{1-\varepsilon}{3}\right) \tag{19.5}$$

$$h_{w,OF} = \frac{k_g}{d_c}\left(7.18 + 0.029 Re_{d_c}^{0.8}\right) \tag{19.6}$$

Variables are defined in the "Nomenclature" section.

For the evaluation of the reaction rates in model equations we have considered the kinetic model proposed by Graaf et al. (1990), which includes reversible CO hydrogenation to methanol and reverse water-gas shift and CO_2 hydrogenation to methanol, respectively. A constant multiplying activity factor equal to 1.9 has been applied to account for the activity of modern commercial methanol synthesis catalysts (Montebelli et al., 2013). When a sensitivity analysis on the catalyst activity has been carried out, an additional multiplying factor (named "*af*") has been introduced in the rate expression.

The reactor has been simulated together with the whole methanol synthesis loop, which also includes: (i) an ideal condenser placed downstream to the reactor separating water and methanol produced in the reactor; (ii) a recycle stream to recover unconverted reactants; and (iii) a purge to prevent the accumulation of inerts (usually Ar, N_2, and CH_4) inside the loop. For more details on the reactor modeling the reader is referred to Montebelli et al. (2013, 2014a).

3.2 Performances of Highly Conductive Structured Catalysts in Full-Scale Reactors for Methanol Synthesis

To compare the performances of structured reactors—that is, washcoated HM and OF—with those of the PB reactor, we have assessed the performance of all the investigated reactors in terms of material balances (recycle ratio, overall CO conversion, methanol productivity) and thermal behavior (temperature profiles, heat transfer coefficients).

Considering that the effective radial conductivity of structured catalysts depends on the bulk thermal conductivity (k_s) of the material used to manufacture the substrate and on the relative density of the substrate ($1-\varepsilon$, see Eqs. 19.3 and 19.5), while the volumetric area of structured catalysts grows with their channel/pore density (CPSI and PPI), commercial structured substrates with the following properties have been preliminarily considered in our simulations: a copper ($k_s = 400$ W/m/K) OF with pore density of 40 PPI and void fraction $\varepsilon_{OF} = 0.88$ (Cristiani et al., 2005) and a copper HM with cell density of 400 CPSI and $\varepsilon_{HM} = 0.72$ (Tronconi et al., 2004). We have then assumed for both structured catalysts the same high catalyst inventory of PB (i.e., 0.613 $m^3_{catalyst}/m^3_{reactor}$), with a washcoat density equal to the bulk density of the pelletized catalyst in the PB reactor (i.e., 1712 kg/m^3). These assumptions imply diffusion lengths of 808, 229, and 74 μm for PB, HM, and OF, respectively.

Despite the thermodynamic constraint (CO conversion per pass always below 85%), simulation results show that, thanks to the process loop configuration, the overall CO conversion keeps very close to unity in all the reactors (99.0%–99.9%), with only a small amount of CO lost in the purge. This implies a very similar methanol productivity (variations well below 1%) for the three reactor configurations.

Concerning the internal mass transfer, due to the shorter diffusion length, structured reactors reveal instead performances better than PB. Both HM and OF reactors exhibit effectiveness factors close to unity (in the ranges of 0.85–1 and 0.95–1 for HM and OF, respectively) along the whole axial coordinate. This is not the case for the PB reactor, wherein the longer diffusion length of the pellets results in lower effectiveness factors (in the range of 0.6–0.95), especially in the hottest reactor zone. Such better efficiencies for structured reactors result in a closer approach to equilibrium at the reactor outlet, which in turn is responsible for slightly lower recycle ratios of structured (∼1.4) than PB (∼1.6) reactors.

As shown in Fig. 19.2, significant differences are observed in terms of the thermal behavior of the three reactors. For all the reactor types the same typical axial profile of externally cooled

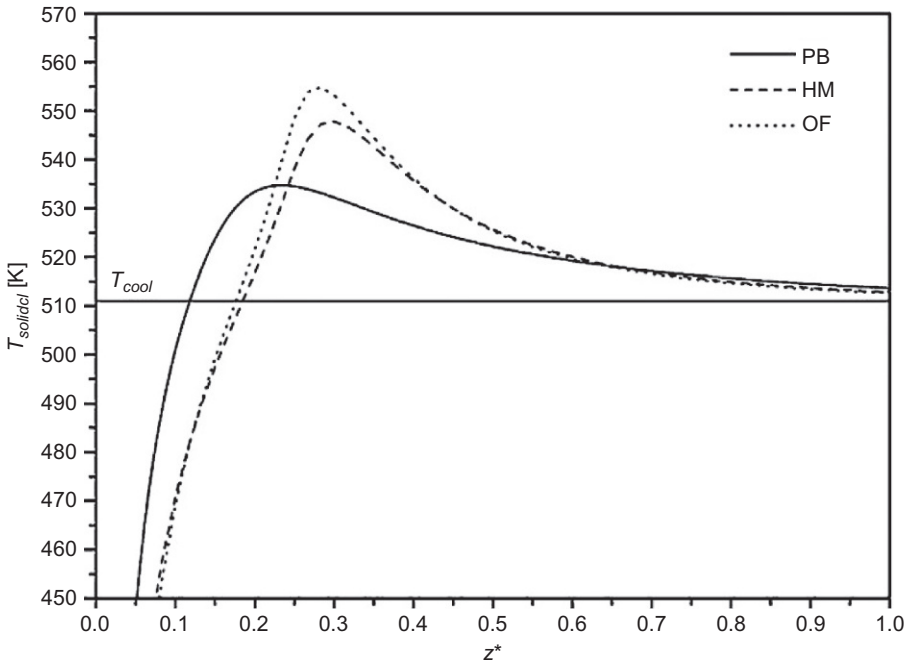

Fig. 19.2

Calculated gas-phase axial temperature profiles at center line. Process conditions as in Fig. 19.1. *Reprinted from Montebelli, A., Visconti, C.G., Groppi, G., Tronconi, E., Ferreira, C., Kohler, S., 2013. Enabling small-scale methanol synthesis reactors through the adoption of highly conductive structured catalysts. Catal. Today 215, 176–185 with permission from Elsevier.*

tubes in the presence of exothermic reactions is observed, showing a hotspot after some distance from the reactor inlet. The analysis of the temperature profile reveals, however, that the PB reactor exhibits better heat transfer performances, which are responsible for the earlier (shorter preheating length) and less pronounced hotspot. Worse performances were instead simulated for HM and OF, with OF showing the highest hotspot temperature.

This can be explained by analyzing the overall heat transfer coefficients, U, averaged on the reactor length, for the three reactors. According to Crider and Foss (1965), this coefficient, lumping the radial effective thermal conductivity and the wall heat transfer coefficient, is defined as shown in Eq. (19.7).

$$U = \left(\frac{1}{h_w} + \frac{d_t}{6.13\, k_{er}} \right)^{-1} \tag{19.7}$$

In fact, PB reactors always show the highest value of U ($\sim$600 W/m^2/K), which compares to $\sim$460 W/m^2/K of HM and $\sim$430 W/m^2/K of OF. In turn, these values of U are mainly due to the fact that, at the adopted process conditions, both the high gas thermal conductivity and the high velocity in the reactor tubes boost the wall heat transfer coefficient in PB ($\sim$1100 W/m^2/K), which plays a dominant role in the overall heat transfer resistance. This "boosting effect" is less pronounced in structured reactors, which are characterized by values of h_w of 520 and 490 W/m^2/K for OF and HM, respectively. These values adversely affect U, even in the presence of effective radial conductivities that, for structured catalysts (70 W/m/K for HM and 16 W/m/K for OF), are much higher than for the packed bed (9 W/m/K).

Based on these results, we conclude, therefore, that the existing industrial PB reactor outperforms both the considered structured reactors as far as the radial heat transfer efficiency is concerned. Anyway, variations in the thermal behavior are not dramatic: temperatures always remain below the limit where catalyst deactivation begins (i.e., 300°C).

3.3 Performances of Highly Conductive Structured Catalysts in Compact-Scale Reactors for Methanol Synthesis

In view of the development of compact-reactor configurations, we have then proceeded to a parametric analysis of the reactor's performances upon changing the tube length, while keeping constant the fresh feed flow rate to catalyst weight ratio ($F/W_{cat} = 103.47$ mol/s/kg$_{cat}$).

Fig. 19.3 shows that dramatically worse performances of the PB reactor are obtained when shortening the reactor tubes from full scale (FS) to FS/4 and FS/8. On the contrary, the behavior of HM and OF reactors is only slightly affected, both in terms of temperature profiles and of recycle ratios (RR).

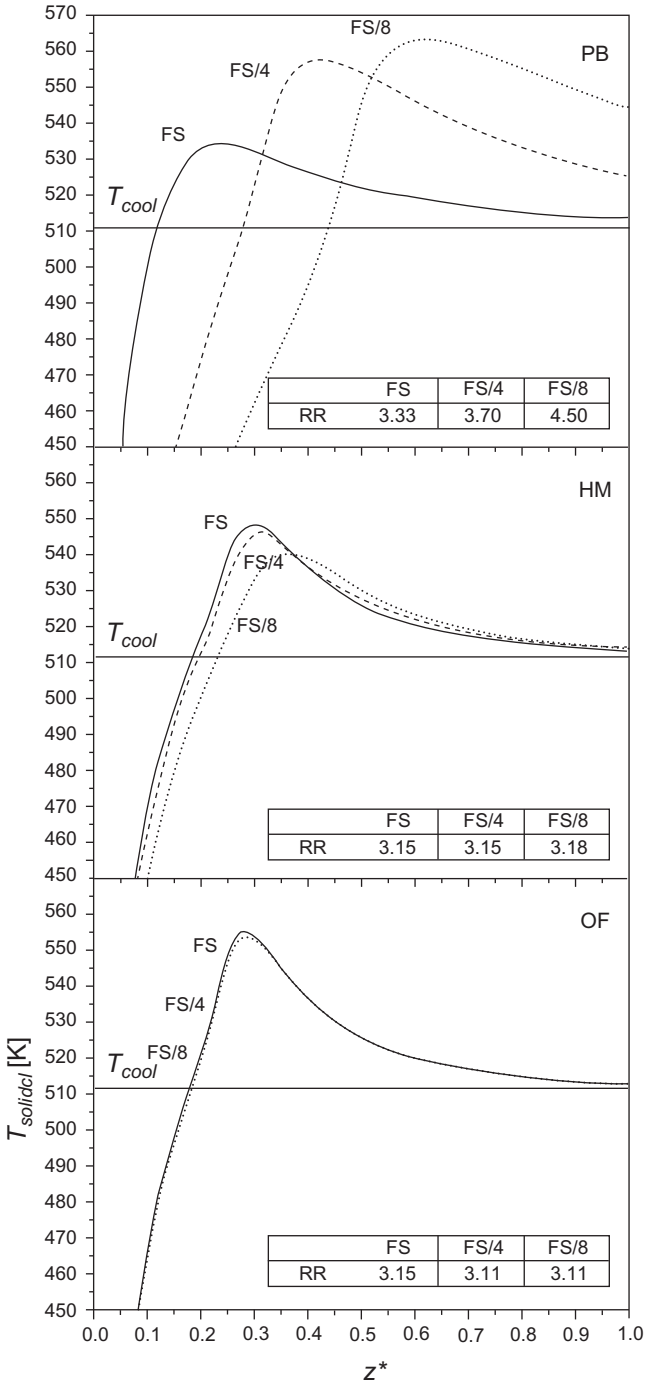

Fig. 19.3

Effect of tube length on solid-phase axial temperature profiles at center line and on recycle ratios. Process conditions as in Fig. 19.1. Fresh feed flow to catalyst weight ratio (F/W_{cat}) has been kept constant in the simulations. *Reprinted from Montebelli, A., Visconti, C.G., Groppi, G., Tronconi, E., Ferreira, C., Kohler, S., 2013. Enabling small-scale methanol synthesis reactors through the adoption of highly conductive structured catalysts. Catal. Today 215, 176–185 with permission from Elsevier.*

Such a different sensitivity is essentially due to the different heat transfer mechanisms prevailing in PB and structured reactors. Obeying to a convective mechanism, a PB reactor performs worse when low mass flow rates per tube are employed (i.e., for shorter reactors), resulting in longer preheating lengths as well as higher hotspots and outlet temperatures. On the other hand, structured reactors exchange heat mainly via a conductive mechanism, so they are unaffected by the reduction of the mass flow rate. As a result, hotspot and outlet temperatures remain practically the same. The only small deviation occurs in the case of the HM reactor, where a more significant contribution of axial conduction causes the temperature profile to flatten slightly as the tube length is reduced.

Notably, the longer preheating zone in a compact PB also affects the conversion efficiency, with the outlet composition remaining quite far from chemical equilibrium, leading to significantly higher recycle ratios.

From these simulation results we can conclude that, contrary to the case of industrial FS reactors, compact (short) structured reactors loaded with highly conductive structured supports have the potential to perform significantly better than PB reactors, granting lower recycle ratios and more limited hotspots.

Interestingly, Fig. 19.4 shows that while the hotspot temperature in PB significantly increases with the decreasing stoichiometric number M_F, structured reactors have hotspot temperatures less dependent on M_F. This is again mainly due to the different heat transfer mechanism controlling h_w and k_{er} in PB and in structured reactors. In particular, being that the heat transfer mechanism is dominated by heat conduction in the latter case, structured reactors exhibit temperature profiles almost independent of the recycle flow rate. On the contrary, in PB, where h_w and k_{er} show an almost linear dependence on the mass flow rate, the overall heat transfer coefficient markedly drops upon decreasing M_F.

Such a result is extremely important: it means that compact structured reactors enable operation of the methanol synthesis loop with less overstoichiometric feed streams, which implies smaller recycle ratios and more favorable process economics.

So far, the comparison of the performances of externally cooled methanol reactors loaded with a conventional random packing and with innovative highly conductive structured catalysts has been carried out using catalyst volumetric fractions as high as those typical of PB reactors (i.e., 0.613 $m^3_{catalyst}/m^3_{tube}$). These loadings are, however, hardly feasible when washcoating structured substrates (corresponding to washcoat thicknesses of about 331 and 214 μm in the case of HM and OF, respectively; Montebelli et al., 2014b), provided that the washcoat thickness cannot be too high (in general below 150 μm) to grant the necessary adhesion to the substrate. Accordingly, in the following, we will present the results of a parametric analysis of the catalyst volumetric fraction aiming at assessing the possibility of operating compact

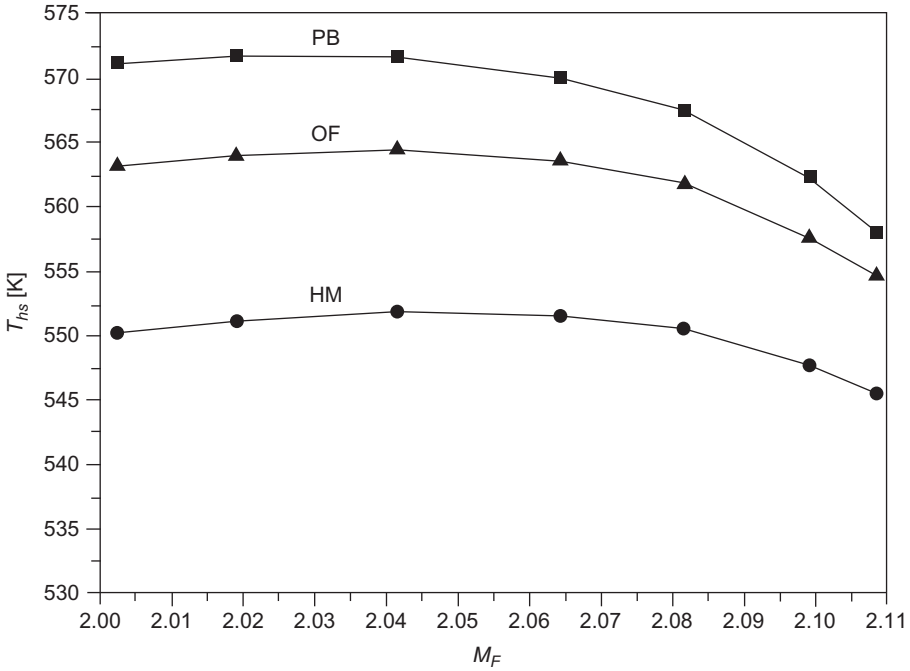

Fig. 19.4

Hotspot temperatures at center line as a function of the feed composition in compact reactors ($L_t = 1$ m). *Reprinted from Montebelli, A., Visconti, C.G., Groppi, G., Tronconi, E., Ferreira, C., Kohler, S., 2013. Enabling small-scale methanol synthesis reactors through the adoption of highly conductive structured catalysts. Catal. Today 215, 176–185 with permission from Elsevier.*

structured reactors with lower catalyst loads than in PBs. In particular we considered catalyst volumetric fractions as low as 0.3 $m^3_{catalyst}/m^3_{tube}$, which correspond to washcoat thicknesses around 130 μm for both the HM and the OF structures used in our simulations. Phan et al. (2011) experimentally obtained similar thickness values by coating a $Cu/ZnO/Al_2O_3$ methanol catalyst onto steel monoliths.

Fig. 19.5A shows the simulated axial temperature profiles for reactors with different catalyst inventories. The lower catalyst loads cause a significant drop in the activity within the reactor, which results in more limited axial temperature gradients (i.e., lower hotspot temperatures) in both HM and OF reactors. Also, the hot spot shifts towards the reactor outlet and the outlet temperature increases. Accordingly, lower CO conversions per pass are found, moving progressively away from equilibrium values (Fig. 19.6A).

To keep the overall methanol productivity constant, the synthesis loop is thus forced to operate at higher recycle ratios, where numerical values are essentially equivalent for the two

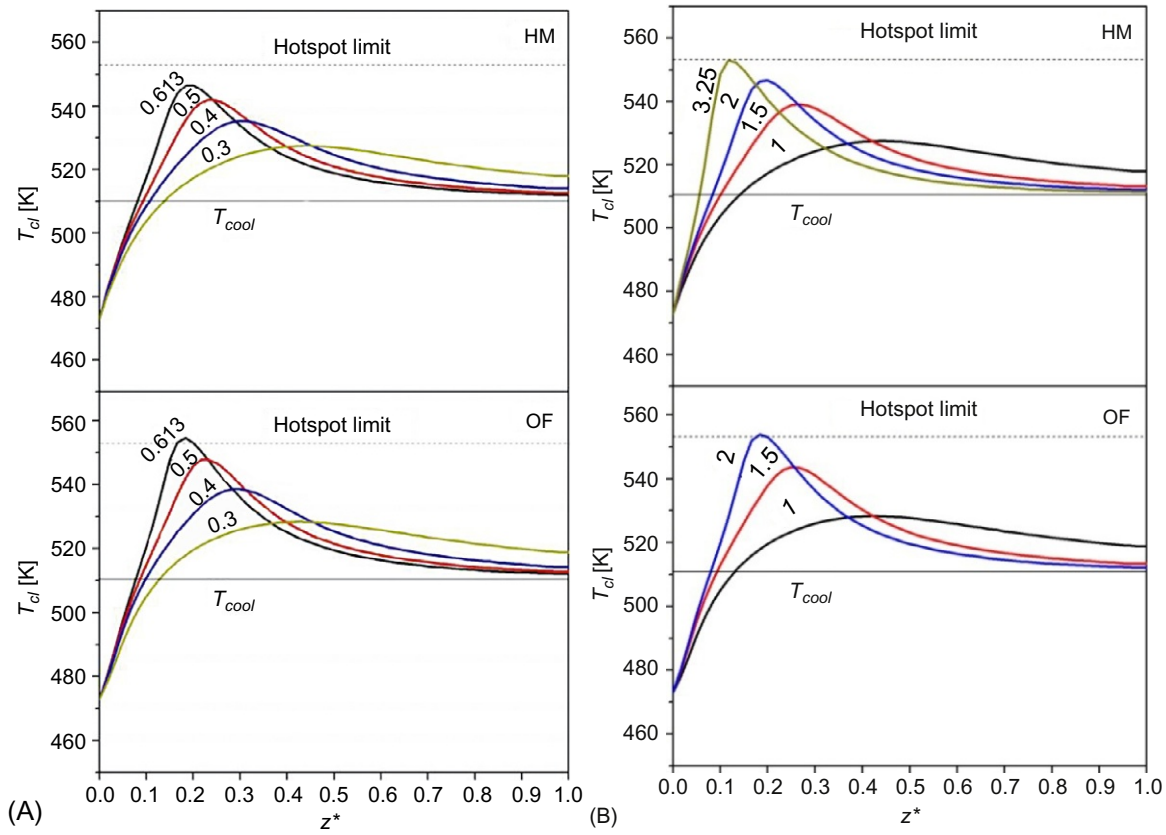

Fig. 19.5

Axial temperature profiles at center line of HM- and OF-based reactors with (A) different catalyst vol. fraction at constant activity factor (=1) or (B) different activity factors at constant catalyst inventory (= 0.3 $m^3_{catalyst}/m^3_{tube}$). $T_g^0 = 473$ K, $T_{cool} = 511$ K, $P^0 = 69.2$ bar, $d_t = 4.2$ cm, reactor length: FS/4. Fresh feed composition: CO = 27.32%, $CO_2 = 3.55\%$, $H_2 = 68.64\%$, $N_2 + Ar + CH_4$ to balance. Fresh feed flow rate has been kept constant in the simulations. *Reprinted from Montebelli, A., Visconti, C.G., Groppi, G., Tronconi, E., Ferreira, C., Kohler, S., 2014a. Optimisation of compact multitubular fixed-bed reactors for the methanol synthesis loaded with highly conductive structured catalysts. Chem. Eng. J. 255, 257–265 with permission from Elsevier.*

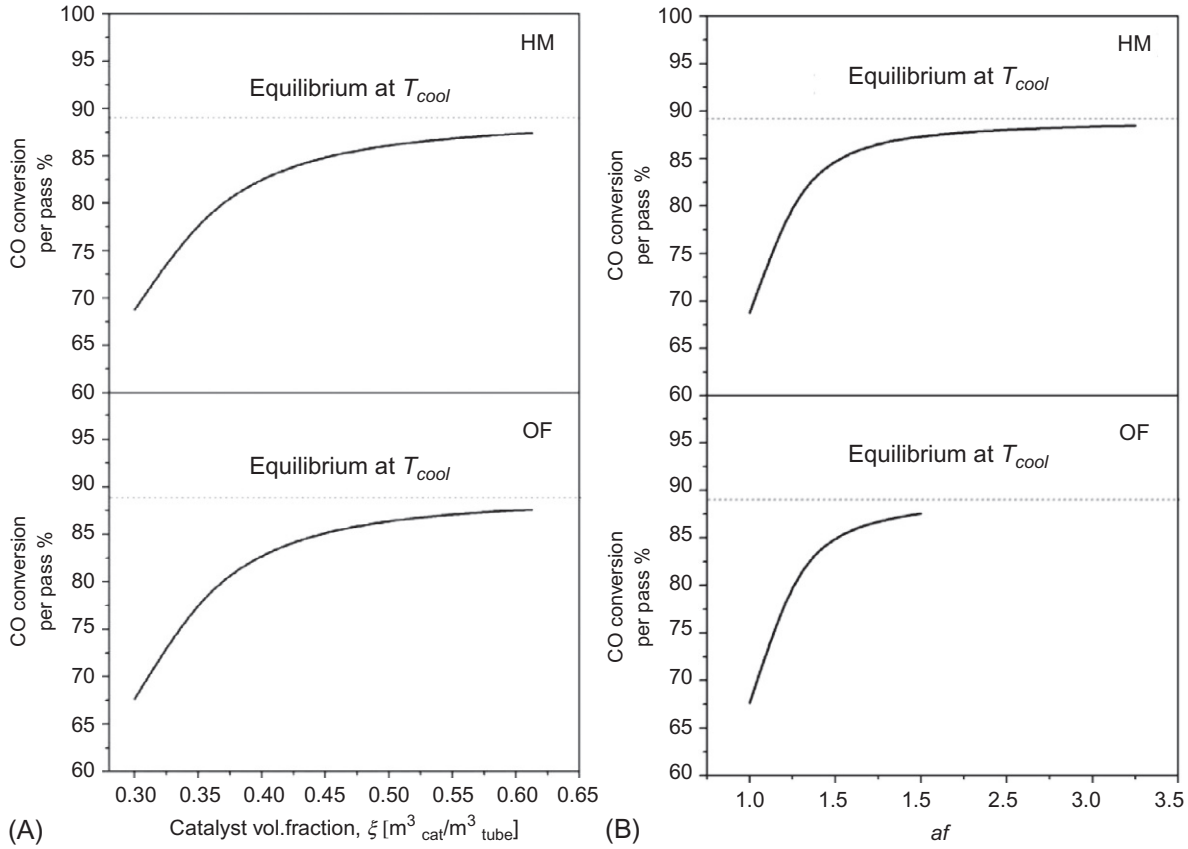

Fig. 19.6

CO conversion per pass in HM and OF reactors as a function of (A) the catalyst vol. fraction at constant activity factor (=1) and (B) the activity factor at constant catalyst inventory ($=0.3\ m^3_{catalyst}/m^3_{tube}$). CO conversion at equilibrium was evaluated at reactor outlet and at $T=T_{cool}$. Process conditions as in Fig. 19.5. *Reprinted from Montebelli, A., Visconti, C.G., Groppi, G., Tronconi, E., Ferreira, C., Kohler, S., 2014a. Optimisation of compact multitubular fixed-bed reactors for the methanol synthesis loaded with highly conductive structured catalysts. Chem. Eng. J. 255, 257–265 with permission from Elsevier.*

structured reactor configurations. This causes an increase in pressure drop, which, however, remains well below those typical of packed beds due to the high void fraction of the structured reactors. In addition, it is worth noting that the higher recycle ratios also contribute to increasing the gas advection term of the reactor energy balance, which is responsible for further mitigating the axial temperature gradients within the catalytic bed.

Interestingly, catalysts with enhanced intrinsic activity can be used to compensate for the decreased catalyst inventory in the reactor. As shown in Fig. 19.5B, the greater reactor activity results in steeper axial temperature profiles, being characterized by shorter preheating zones and more pronounced hotspot temperatures. As a result of the better approach to equilibrium at the reactor outlet (Fig. 19.6B), lower recycle ratios are required to keep the methanol productivity constant.

Notably, the simulated honeycomb-monolith catalyst performs better than the OFs at given activity in the reactor. Indeed, thanks to its higher effective radial thermal conductivity, which is over four times greater than that of OF (70 vs. 16 W/m/K), hotspot temperatures in the HM reactor stay below the safe hotspot limit of 553 K for activity factors up to 3.25, while the OF cannot be operated with activity factors exceeding 2 (Fig. 19.5B). These results should not be read as an indication of the superior heat transfer properties of highly conductive HM with respect to OF. Simulated performances are indeed strictly related to the geometric properties of the selected HM and OF structures, and in particular to their void fraction (at given material). OF with higher relative densities (i.e., lower void fraction) can perform similarly to the HM used in our simulations.

The outstanding heat transfer performances of the adopted structured catalysts further open the possibility of adopting multitubular reactors with bigger tubes.

Fig. 19.7 shows indeed that, as a consequence of the higher thermal loads generated per unit heat transfer surface area, in both structured reactors more pronounced axial temperature gradients are found by increasing the tube diameter. However, thanks to the effective radial heat transfer within the highly conductive substrates, the hot spot temperatures remain limited. Accordingly, lower recycle ratios are required to keep the methanol productivity constant.

Notably, coherently with the hotspot limit, Fig. 19.7 shows that tube diameters up to 63 mm could be adopted in the case of the OF reactor, which represents a 50% increase over those typical of commercial PB units. Even better, in HM the tube diameter can be increased up to 79.8 mm before approaching the hotspot limit. This would play an important role in decreasing the investment costs for the reactor (i.e., fewer tubes would be needed if larger diameters were adopted at fixed catalyst inventory), as both the number of tubes and the number of welding operations decrease with the square of the tube diameter at fixed catalyst inventory.

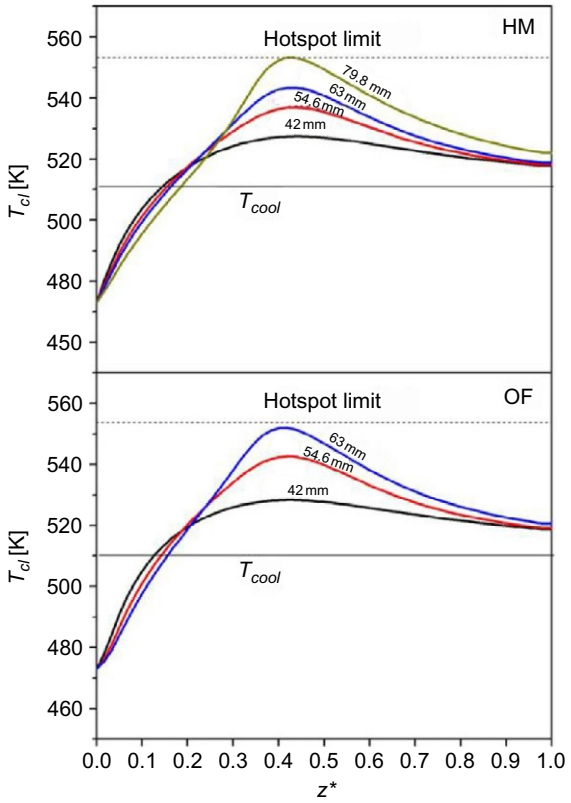

Fig. 19.7

Axial temperature profiles at center line of HM and OF-based reactors with tubes having diameters equal or larger than the typical value adopted in commercial units. Process conditions as in Fig. 19.5.

Reprinted from Montebelli, A., Visconti, C.G., Groppi, G., Tronconi, E., Ferreira, C., Kohler, S., 2014a. Optimisation of compact multitubular fixed-bed reactors for the methanol synthesis loaded with highly conductive structured catalysts. Chem. Eng. J. 255, 257–265 with permission from Elsevier.

3.4 Preparation and Testing of Highly Conductive Structured Catalysts for Methanol Synthesis

Once shown by simulation that highly conductive structured catalysts based on OF and HM, in addition to limited pressure drop and minimal impact of intraporous mass transfer limitations, enable compact multitubular reactors to operate with limited hotspot and recycle ratios with respect to conventional packings, we have experimentally investigated the preparation of conductive structured catalysts for methanol synthesis via washcoating (Montebelli et al., 2014b). In particular, we have focused on the preparation of prototype copper OFs coated with a commercial $Cu/ZnO/Al_2O_3$ catalyst. Prepared samples have then been tested in the low temperature-low pressure methanol synthesis at relevant industrial conditions, comparing their performances with those of the original commercial powdered catalyst.

Starting from the best recipe proposed by Germani et al. (2007) and the know-how developed in our labs (Cristiani et al., 2009), we prepared slurries by ball-milling a mixture containing 100 g of deionized water, 25.25 g of commercial powdered catalyst, and 0.7 g of Tylose MH 300 P2 as dispersant. To the scope, we used 3.5 g ZrO_2 spheres/g powder as grinding bodies (about 1 cm in diameter). We mixed the ingredients in a 250-ml polyethylene sealed jar, which was then kept rotating at 40 rpm for 24 h. Stable dispersions with a non-Newtonian shear-thinning behavior were obtained, which were used to washcoat some 45 PPI (average pore diameter = 0.564 mm, average cell diameter = 1.289 mm, average strut diameter = 0.212 mm) open-cell copper foam ($\varepsilon = 0.936$) supplied by Porvair (Fig. 19.8A) using the dip-blowing technique. More details on the preparation procedure can be found in Montebelli et al. (2014b).

Single-layer deposition on copper foams led to a washcoat load around 9 wt%. Optical microscopy images of washcoated foams evidenced homogeneous substrate coverage, with no

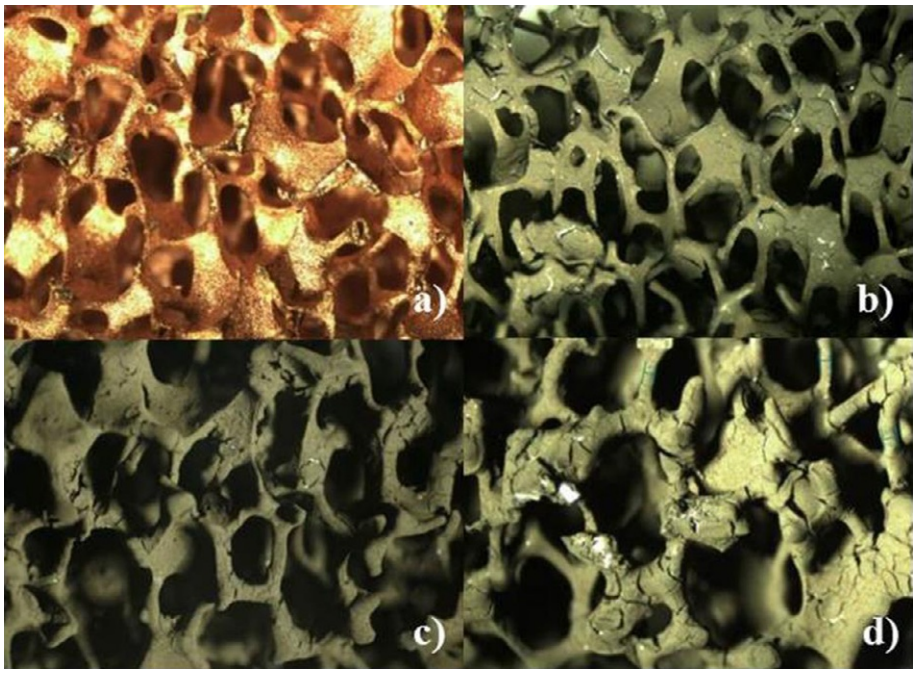

Fig. 19.8

Optical microscope images of the adopted copper OF. (A) Bare sample, (B) after one coating layer deposition, (C) after two coating layers deposition, and (D) after three coating layers deposition. Samples (B)–(D) were calcined from RT to 573 K for 2 h. *Reprinted from Montebelli, A., Visconti, C.G., Groppi, G., Tronconi, E., Ferreira, C., Kohler, S., Venvik, H.J., Myrstad, R., 2014b. Washcoating and chemical testing of a commercial Cu/ZnO/Al_2O_3 catalyst for the methanol synthesis over copper open-cell foams. Appl. Catal. A Gen. 481, 96–103 with permission from Elsevier.*

cracks and negligible pore blocking (Fig. 19.8B). Adhesion was satisfactory. The deposition of a second washcoat layer brought an increase of the washcoat load, approaching 14 wt%. Minor cracks were observed, but again did not significantly affect the washcoat adhesion (Fig. 19.8C). In view of increasing the washcoat load, a third deposition was attempted, but no significant weight increase occurred. Furthermore, the evident presence of cracks seriously compromised the washcoat adhesion in this case (Fig. 19.8D).

Accordingly, we decided to test the sample obtained after two coatings, which we estimated to be homogeneously covered by a washcoat with an average thickness of 75 μm (Montebelli et al., 2014b). For comparison purposes, we also tested the commercial powdered catalyst (CC) and the slurried powder (SP), that is the powders obtained by drying at 383 K for 24 h and calcining at 573 K for 2 h the slurry used for the washcoating. The results of the comparative testing are shown in Fig. 19.9 in terms of methanol productivity as a function of temperature.

As expected, the methanol productivity increased with increasing temperature over all three investigated catalysts, keeping reasonably far from thermodynamic equilibrium even at the highest investigated temperatures. OF as well as SP showed, however, lower methanol productivities than CC. This evidenced that the deposition procedure (i.e., dip-blowing) did not alter the catalyst activity. On the contrary, the slurry preparation and/or calcination procedure was responsible for a change in the catalytic performances.

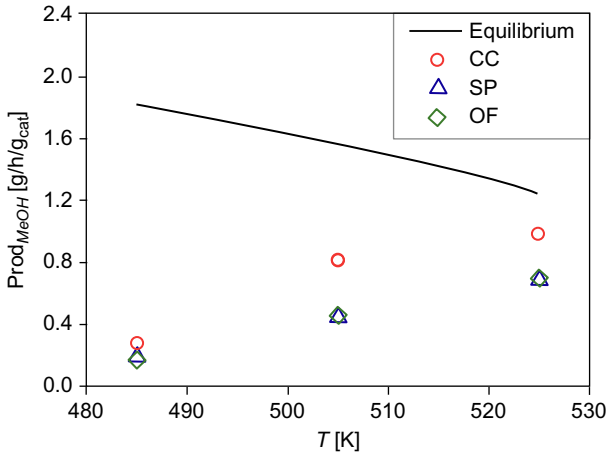

Fig. 19.9

Methanol productivity over the investigated catalysts as a function of temperature. $P = 50$ bar, GHSV = 15,000 Nl/h/kg$_{cat}$, feed composition: 8.3% CO, 2.6% CO_2, 73.2% H_2, 5.1% CH_4, N_2 to balance. *Reprinted from Montebelli, A., Visconti, C.G., Groppi, G., Tronconi, E., Ferreira, C., Kohler, S., Venvik, H.J., Myrstad, R., 2014b. Washcoating and chemical testing of a commercial Cu/ZnO/Al_2O_3 catalyst for the methanol synthesis over copper open-cell foams. Appl. Catal. A Gen. 481, 96–103 with permission from Elsevier.*

Overall, our experimental results proved that the manufacturing of washcoated structured catalysts with highly conductive supports for methanol synthesis is indeed a feasible option.

4 Conclusions

The simulation results presented in Sections 3.2 and 3.3, combined with the preliminary experimental proof-of-concept illustrated in Section 3.4, seem promising for the development of a new commercial technology for methanol synthesis in *compact* multitubular converters loaded with highly conductive OF or monolith structured catalysts. A key point worthy of emphasis is that the flow independent heat transfer properties of such conductive substrates enable the operation of tubular reactors with much shorter tubes than in existing full-scale converters. This is quite interesting in view of small-scale methanol synthesis units, as needed nowadays for decentralized and/or offshore GTL applications as well as for the exploitation of biomass.

On the other hand, the catalytic activation of conductive structured substrates still represents a critical aspect. We have shown that washcoating of metallic monoliths and OFs with commercial Cu-ZnO/Al_2O_3 catalyst powders is, in fact, practically feasible, leading to active and selective conductive catalytic systems. Nevertheless, washcoating has intrinsic limitations as far as the maximum volumetric fraction of the catalytically active phase in the reactor is concerned: typical washcoat thicknesses in the order of 100 μm correspond to a significantly smaller catalyst inventory than in PB reactors. In this respect, a possible alternative solution may come from the very recently proposed concept of "packed foams," wherein the catalytic activation of thermally conductive OFs is obtained by packing them with catalyst microparticles (Visconti et al., 2016).

References

Bakhtiary-Davijany, H., Hayer, F., Phan, X.K., Myrstad, R., Venvik, H.J., Pfeifer, P., Holmen, A., 2011. Characteristics of an integrated micro packed bed reactor-heat exchanger for methanol synthesis from syngas. Chem. Eng. J. 167, 496–503.

Bartholomew, C.H., Farrauto, R.J., 2005. Fundamentals of Industrial Catalytic Processes, second ed. John Wiley & Sons, Inc., Hoboken, NJ.

Bianchi, E., Heidig, T., Visconti, C.G., Groppi, G., Freund, H., Tronconi, E., 2012. An appraisal of the heat transfer properties of metallic open-cell foams for strongly exo-/endothermic catalytic processes in tubular reactors. Chem. Eng. J. 198–199, 512–528.

Bianchi, E., Heidig, T., Visconti, C.G., Groppi, G., Freund, H., Tronconi, E., 2013. Heat transfer properties of metal foam supports for structured catalysts: wall heat transfer coefficient. Catal. Today 216, 121–134.

Crider, J.E., Foss, A.S., 1965. Effective wall heat transfer coefficients and thermal resistances in mathematical models of packed beds. AIChE J. 11, 1012–1019.

Cristiani, C., Valentini, M., Merazzi, M., Neglia, S., Forzatti, P., 2005. Effect of ageing time on chemical and rheological evolution in γ-Al_2O_3 slurries for dip-coating. Catal. Today 105, 492–498.

Cristiani, C., Visconti, C.G., Finocchio, E., Stampino, P.G., Forzatti, P., 2009. Towards the rationalisation of the washcoating process conditions. Catal. Today 147, S24–S29.
Germani, G., Stefanescu, A., Schuurman, Y., van Veen, A.C., 2007. Preparation and characterization of porous alumina-based catalyst coatings in microchannels. Chem. Eng. Sci. 62, 5084–5091.
Graaf, G.H., Scholtens, H., Stamhuis, E.J., Beenackers, A.A.C.M., 1990. Intra-particle diffusion limitations in low-pressure methanol synthesis. Chem. Eng. Sci. 45, 773–783.
Groppi, G., Tronconi, E., 1996. Continuous vs. discrete models of nonadiabatic monolith catalysts. AIChE J. 42, 2382–2387.
Groppi, G., Tronconi, E., 2000. Design of novel monolith catalyst supports for gas/solid reactions with heat exchange. Chem. Eng. Sci. 55, 2161–2171.
Groppi, G., Tronconi, E., 2005. Honeycomb supports with high thermal conductivity for gas/solid chemical processes. Catal. Today 105, 297–304.
Hartig, F., Keil, F.J., 1993. Large-scale spherical fixed bed reactors: modeling and optimization. Ind. Eng. Chem. Res. 32, 424–437.
Lange, J.P., 2001. Methanol synthesis: a short review of technology improvements. Catal. Today 64, 3–8.
Montebelli, A., Visconti, C.G., Groppi, G., Tronconi, E., Ferreira, C., Kohler, S., 2013. Enabling small-scale methanol synthesis reactors through the adoption of highly conductive structured catalysts. Catal. Today 215, 176–185.
Montebelli, A., Visconti, C.G., Groppi, G., Tronconi, E., Ferreira, C., Kohler, S., 2014a. Optimisation of compact multitubular fixed-bed reactors for the methanol synthesis loaded with highly conductive structured catalysts. Chem. Eng. J. 255, 257–265.
Montebelli, A., Visconti, C.G., Groppi, G., Tronconi, E., Ferreira, C., Kohler, S., Venvik, H.J., Myrstad, R., 2014b. Washcoating and chemical testing of a commercial $Cu/ZnO/Al_2O_3$ catalyst for the methanol synthesis over copper open-cell foams. Appl. Catal. A Gen. 481, 96–103.
Phan, X.K., Bakhtiary-Davijany, H., Myrstad, R., Thormann, J., Pfeifer, P., Venvik, H.J., Holmen, A., 2010. Preparation and performance of a catalyst-coated stacked foil microreactor for the methanol synthesis. Ind. Eng. Chem. Res. 49, 10934–10941.
Phan, X.K., Bakhtiary-Davijany, H., Myrstad, R., Pfeifer, P., Venvik, H.J., Holmen, A., 2011. Preparation and performance of Cu-based monoliths for methanol synthesis. Appl. Catal. A Gen. 405 (1–2), 1–7.
Spath, P.L., Dayton, D.C., 2003. Preliminary screening – technical and economic assessment of synthesis gas to fuels and chemicals with emphasis on the potential for biomass-derived syngas. NREL/TP-510-34929 Report. http://www.nrel.gov/docs/fy04osti/34929.pdf (accessed 08.03.17).
Specchia, V., Sicardi, S., 1980. Modified correlation for the conductive contribution on thermal conductivity in packed bed reactors. Chem. Eng. Commun. 6, 131–139.
Thackeray, F., Leckie, G., 2002. Stranded gas: a vital resource. Pet. Econ. 69 (5), 10–12.
Tonkovich, A.L.Y., Jarosch, K., Arora, R., Silva, L., Perry, S., McDaniel, J., Daly, F., Litt, B., 2007. Methanol production FPSO plant concept using. multiple microchannel unit operations. Chem. Eng. J. 135S, S2–S8.
Tronconi, E., Groppi, G., Boger, T., Heibel, A., 2004. Monolithic catalysts with 'high conductivity' honeycomb supports for gas/solid exothermic reactions: characterization of the heat-transfer properties. Chem. Eng. Sci. 59, 4941–4949.
Tronconi, E., Groppi, G., Visconti, C.G., 2014. Structured catalysts for non-adiabatic applications. Curr. Opin. Chem. Eng. 5, 55–67.
Visconti, C.G., Groppi, G., Tronconi, E., 2016. Highly conductive "packed foams": a new concept for the intensification of strongly endo- and exo-thermic catalytic processes in compact tubular reactors. Catal. Today 273, 178–186.

CHAPTER 20

Methanol Production in Thermally Coupled, Fluidized-Bed, Bubble-Column and Membrane Reactors

Behnaz Rahmatmand, Mohammad R. Rahimpour
Shiraz University, Shiraz, Iran

Acronyms

MTBE	methyl tertiary butyl ether
DME	dimethyl ether
MTG	methanol to gasoline process
DMFC	direct methanol fuel cell
JMC	Johnson Matthey Catalyst
DPT	Davy Process Technology
MGC	Mitsubishi Gas Chemical
MCH	methylcyclohexane
TOL	toluene
H-SOD	hydroxy sodalite
TDCTMR	thermally double-coupled two-membrane reactor
TCDMR	thermally coupled dual methanol reactor
SBCR	slurry bubble column reactor
TBR	trickle bed reactor
F-T	Fischer-Tropsch
CFD	computational fluid dynamics
SBCR/FC	slurry bubble column reactor with a flash column
FSE-TCR	fluidized bed sorption enhanced thermally coupled reactor
CMR	conventional methanol reactor
TCMR	thermally coupled methanol reactor
TDCR	thermally double coupled reactor
TCMR	thermally coupled membrane reactor
TCDMR	thermally coupled double-membrane reactor

Methanol. https://doi.org/10.1016/B978-0-444-63903-5.00020-0

DE differential evolution
FTCMR fluidized-bed thermally coupled membrane reactor
OTCDMR optimized thermally coupled dual methanol reactor

1 Introduction

Nowadays, energy supply is one of the most important worldwide concerns. Fossil fuels are the main source of energy, but they are also nonrenewable fuels. Also, combustion of fossil fuels produces much of the pollutant gases in the atmosphere. So, it seems necessary to find alternative sources of energy. Recently, methanol has received much attention as a renewable and clean source of energy.

1.1 Methanol

Energy is an essential part of our life. Generally, the main part of energy is supplied by fossil fuels as a nonrenewable energy source (Rahimpour et al., 2011b). Fossil fuels contain coal, petroleum, and natural gas, which mainly consist of carbon (Eisenberg and Nocera, 2005). Fossil fuels are so useful because they are able to produce substantial amounts of energy. However, they are known as nonrenewable sources of energy because it takes a long time for nature to produce these fuels in comparison to their extraction and consumption rate. So, there is global concern about the continuity of fossil-fuel production (Farniaei et al., 2013). Moreover, recent investigations report that carbon dioxide (CO_2) emissions are increasing due to the rising trend of fossil fuels, so that CO_2 is introduced as one of the main pollutant gases in the atmosphere (Golkhar et al., 2013; Rahmatmand et al., 2016). Since energy demand is increasing due to industrial development and population growth, our dependence on fossil fuels as energy sources leads to substantial environmental problems such as CO_2 emission and a decrease in energy sources (Samimi et al., 2013; Rahimpour et al., 2011b). In order to find a solution for these problems, many studies have focused on finding alternative sources of energy (Taylor, 2008). Although energy sources such as wind, solar, and biomass energy can be considered as renewable energy sources, they are not easily available. So, they are not appropriate alternatives for fossil fuels (Jung and Gamwo, 2008; Samimi et al., 2013). Therefore, many studies have been carried out to find renewable and clean fuel as a desirable substitute for fossil fuels (Gómez-Castro et al., 2011). Since CO_2 is one of the main pollutant greenhouse gases, production of methanol from CO_2 can reduce pollutant gas emissions significantly. On the other hand, methanol can be a valuable clean fuel, a raw chemical for different industries, an intermediate for production of synthetic fuels, and a useful solvent (Semelsberger et al., 2006). Also, methanol is used to supply hydrogen for fuel cells. So, methanol can play a major role in providing global energy (Semelsberger et al., 2006). Mainly, methanol is produced by catalytic conversion of synthesis gas (H_2, CO_2, CO) (Chinchen et al., 1988). Regarding the major role of methanol in the energy sector, many studies have been

performed to introduce the advantages of methanol as an automotive fuel. These advantages are (Rahimpour et al., 2008):

- It is a clean-burning fuel (Samimi et al., 2013).
- Production of methanol can significantly reduce CO_2 emissions by conversion of CO_2 to methanol (Lange, 2001; Samimi et al., 2013).
- Since methanol is liquid under standard conditions, conversion of hydrogen to methanol can solve the drawbacks of hydrogen storage and transportation (Samimi et al., 2013).
- It can enhance the octane rating of gasoline, which leads to reduced "knock" in conventional combustion engines (Samimi et al., 2013).
- Conversion of natural gas to methanol is economically more profitable in comparison with transportation and shipping of liquefied natural gas (LNG) (Samimi et al., 2013).

Also, methanol is used to produce chemicals such as methyl tertiary butyl ether (MTBE), dimethyl ether (DME), and olefins. DME and olefins have wide demand while MTBE is the additive in gasoline. In the methanol-to-gasoline (MTG) process, methanol can be converted to synthetic fuel. Also, methanol has numerous applications in the production of biodiesel, formaldehyde, and acetic acid. Recently, methanol synthesis was the second source of hydrogen consumption after ammonia production (Zhang et al., 2003; Wang et al., 2005; Zhang and Zhao, 2006; Guo et al., 2007; Cheng, 1994; Semelsberger et al., 2006; Olah et al., 2011). Furthermore, the novel process of microchannel methanol steam reforming and direct methanol fuel cell (DMFC) have recently become attractive applications of methanol (Hao et al., 2011; Park et al., 2012).

In fact, methanol synthesis plays a major role in environmental protection by converting CO_2 pollutant gas to methanol, which is a clean-burning fuel (Lange, 2001; Samimi et al., 2014). The methanol demand has grown at an average annual rate of 10% since 2010, and this continues to increase (Alarifi et al., 2013). However, hydrogen could also be used as a clean fuel but there are some difficulties in transportation and storage. So, methanol has received much attention as a better alternative for fossil fuels in comparison with hydrogen in recent years (Bromberg and Cheng, 2010). Consequently, many companies have paid greater attention to the improvement of methanol synthesis (Alarifi et al., 2013). Methanol technologies are licensed by numerous companies such as Johnson Matthey Catalyst (JMC), Davy Process Technology (DPT), Mitsubishi Gas Chemical (MGC), Lurgi, and Haldor Topsoe (Alarifi et al., 2013). The enhancement of methanol production efficiency can lead to environmental protection, energy preservation, and greater profits (Schack et al., 1989). The methanol synthesis process contains two main steps: production of synthesis gas and conversion of synthesis gas to methanol (Tijm et al., 2001; Alarifi et al., 2013). The important difficulties in the industrial methanol synthesis process are the variation of the reacting gas composition, thermodynamic equilibrium limitations, and catalyst deactivation. In the reversible exothermic reactions of CO_2 conversion to methanol, a low temperature condition can lead to higher conversion, but

it also reduces the reaction rate and consequently a great amount of catalyst will be required. Even though raising the reaction temperature enhances the rate of reaction, it is also not applicable because increasing the temperature will allow the deteriorating effect of equilibrium conversion to emerge while also reducing methanol production (Rahimpour et al., 2003). Therefore, significant attention has been paid in the current studies to coupling reactors that lead to more profitable and efficient processes (Samimi et al., 2014).

1.2 Hydrogen

Due to global warming and the reduction of fossil-fuel resources, hydrogen has received much attention as an appropriate energy carrier for the near future (Jain et al., 2010). Hydrogen can be used as an efficient and environmentally friendly fuel (Lokurlu et al., 2003; Heinzel et al., 2002; Song, 2002; Brown, 2001). Hydrogen is introduced as an environmentally friendly energy source because the products of hydrogen combustion are only water and a tiny amount of NO_x. So, a negligible amount of greenhouse gas is produced (Mueller-Langer et al., 2007). Also, hydrogen has the highest calorific value compared to other fuels except nuclear fuels (Sun et al., 2012). However, transportation and storage of hydrogen present some difficulties (Rahimpour et al., 2011c). Because of the importance of hydrogen, different processes have been developed to enhance hydrogen production. It can be produced from processes such as coal and biomass gasification, electrolysis of water, and natural gas reforming (Sun et al., 2012). Pregger et al. (2009) has proposed some perspectives of hydrogen production enhancement. Recently, natural gas catalytic steam reforming has mainly been applied to produce hydrogen (Wang et al., 2008). But applying this process causes greenhouse gas emissions such as CO and CO_2 (Wang et al., 2008; Kariya et al., 2003). Another appropriate process for hydrogen storage and transportation is the dehydrogenation of organic hydrocarbons (Rahimpour et al., 2011c). The dehydrogenation reaction is a reversible reaction (Kang and Anderson, 1985). The positive points of the dehydrogenation process in comparison with steam reforming are (Kariya et al., 2003; Wang et al., 2008; Yolcular and Olgun, 2008; Khademi et al., 2009a; Rahimpour and Asgari, 2009):

- The products are only hydrogen and dehydrogenated hydrocarbons.
- Environmentally friendly process that produces no toxic, corrosive, or greenhouse gases.
- Pure hydrogen is produced without CO impurity.
- Oil tankers and gas stations can be used for storage and transportation of hydrogen. Also, hydrogen production by dehydrogenation is a reversible reaction and the products can again be converted to raw materials by the reverse hydrogenation reaction. This makes the dehydrogenation process more suitable than using metal hydrides.

Besides, cyclic hydrocarbons, which are used in dehydrogenation reactions, have a high hydrogen content (Rahimpour et al., 2011c). Chemical hydrides such as cyclohexane are suggested as convenient hydrogen carriers. They are more attractive than metal hydrides due to

the following advantages: (1) High hydrogen content (Rahimpour et al., 2011b). (2) Comfortable storage and transportation because of a high boiling point (80.7°C) (Rahimpour et al., 2011b). (3) The products can be easily hydrogenated and reused (Itoh et al., 2003). (4) They cause zero CO_2 emissions and eliminate the difficulties of hydrogen storage conditions (Jain et al., 2010; Khademi et al., 2009a). Today, from the environmental perspective, methylcyclohexane (MCH) has received excessive attention as a hydrogen carrier (Yolcular and Olgun, 2008). Hence, toluene (TOL) is preferred as the product of dehydrogenation reaction in comparison with benzene (Rahimpour et al., 2011c).

1.3 Methanol Synthesis

Methanol is largely produced from synthesis gas (CO, CO_2, and H_2) under reactions of CO and CO_2 hydrogenation and reverse water gas shift (WGS) reaction. Also, it can be produced from syngas through the Fisher-Tropsch (FT) process and also by pyrolysis of organic materials (Rahimpour et al., 2008). The shell and tube heat exchanger is a traditional fixed-bed methanol synthesis reactor in which the tubes are packed with a $CuO/ZnO/Al_2O_3$ catalyst (Jahanmiri and Eslamloueyan, 2002). The main problem with a conventional reactor is low methanol conversion. Circulating synthesis gas around the loop can diminish this problem but it imposes excessive operating costs. The methanol synthesis reaction is an exothermic reaction and the temperature and pressure of the reaction are 495–535 K and 5–8 MPa, respectively (Struis et al., 1996; Rahimpour and Ghader, 2003; Khademi et al., 2010). To eliminate this problem, which is caused by the equilibrium nature of the reaction, many attempts have been made to enhance the methanol production efficiency of the reactor. Many studies have been carried out to promote methanol reactor performance (Løvik et al., 1998; Velardi and Barresi, 2002). Multifunctional reactors are utilized in different industries to enhance the process. These reactors integrate in one vessel, one or more transport processes, and a reaction system (Agar, 1999; Zanfir and Gavriilidis, 2003). The multifunctional reactors help to achieve a more efficient process with lower operational and capital costs (Dautzenberg and Mukherjee, 2001). These reactors can be applied for coupling exothermic and endothermic reactions, so that the exothermic reaction supplies the necessary heat for the endothermic reaction. In recent years, much attention has been paid to the concept of exothermic and endothermic reaction coupling, which makes the process more profitable and efficient (Khademi et al., 2009b; Samimi et al., 2013).

1.4 Literature Review

Methanol has many applications such as antifreeze, a hydrate inhibitor in pipelines, and solvent. Also, it can be used as an environmentally friendly fuel (Rahimpour et al., 1998, 2005; Løvik et al., 1998; Semelsberger et al., 2006). First, methanol was introduced as wood alcohol because it was produced as a byproduct of wood distillation. In an advanced case, methanol

is produced from synthesis gases consisting of carbon monoxide, carbon dioxide, and hydrogen through a catalytic process (Farniaei et al., 2013). The equilibrium nature of this reaction reduces the methanol conversion of a conventional fixed-bed methanol synthesis reactor. Circulating the unreacted synthesis gas could enhance methanol conversion, but it causes excessive operating costs (Khademi et al., 2010). Another methanol production process is conversion of methane to methanol by using Cu-zeolites or other catalysts (Rezaie et al., 2005; Rahimpour and Ghader, 2003; Amandusson et al., 2001). By applying the concept of endothermic and exothermic reaction coupling, methanol can be synthesized more economically and efficiently. In this process, the exothermic reaction provides the necessary heat for the endothermic reaction side. Coupling the endothermic and exothermic reactions can also reduce the negative environmental effects of the methanol synthesis process (Zanfir and Gavriilidis, 2001; Dautzenberg and Mukherjee, 2001; Eigenberger et al., 2007; Harmsen, 2010). The advantages of this novel synthesis method are efficiency enhancement, the production of multiple products, the reduction of the reactor size, and striking the thermodynamic limitation (Dautzenberg and Mukherjee, 2001). The specific criteria of the exothermic reaction that should exist as a suitable reaction for coupling with the endothermic reaction are as follows (Rahimpour et al., 2012a):

- It should have a higher temperature and lower pressure than the endothermic one.
- The reaction rates should be definite.

Many studies have been carried out regarding coupling the exothermic and endothermic reaction (Kolios et al., 2002; Moustafa and Elnashaie, 2000; Ramaswamy et al., 2008; Altimari and Bildea, 2009; Iranshahi et al., 2010). Hunter and McGuire (1980) were among those who first studied coupling endothermic with exothermic reactions. They studied heat exchangers in which catalytic combustion or other exothermic reactions were thermally coupled with an endothermic reaction to supply the necessary heat for the endothermic side. Eigenberger's group investigated the coupling of methane combustion and methane steam reforming theoretically and experimentally in counter-current configuration (Frauhammer et al., 1999; Kolios et al., 2001, 2002). Van Sint Annaland and Nijssen (2002) investigated a new configuration in which highly heterogeneous exothermic catalytic gas-phase reactions coupled with endothermic reactions with a rapid and reversible catalyst deactivation rate. Fukuhara and Igarashi (2005) compared the efficiency of fixed-bed and wall-type reactors by a mathematical simulation and numerical method where methanol decomposition and methane combustion were coupled. Ramaswamy et al. (2006) applied a one-dimensional pseudo-homogeneous plug flow model to investigate the performance of cocurrent and counter-current heat exchanger reactors for coupling exothermic and endothermic reactions. Kirillov et al. (2007) analyzed the performance of coupled methane steam reforming by the fuel oxidation configuration. Also, a shortcut theory was presented by Glöckler et al. (2009) to analyze the performance of adiabatic fixed-bed reactors with reverse flow for coupling the exothermic and endothermic reactions.

In addition a membrane can be applied in the coupled reactors to overcome the reaction's thermodynamic limitation problem or separation of a desired product. For this purpose, a novel generation of reactors has been introduced that are called thermally coupled membrane reactors. These reactors help to improve productivity while also making it possible to produce multiple products (Rahimpour et al., 2011b). First, Itoh and Wu (1997) proposed an adiabatic type of palladium membrane reactor for coupling endothermic and exothermic reactions. Elnashaie et al. (2000) studied the performance of the membrane catalytic reactor in which catalytic sections were detached by a hydrogen-selective composite membrane to separate the hydrogen for the dehydrogenation of ethylbenzene to styrene. They compared the cocurrent and counter-current flow patterns. Patel and Sunol (2007) coupled methane steam reforming with exothermic methane combustion in a thermally coupled membrane reactor. Abo-Ghander et al. (2008) applied two fixed beds separated by a hydrogen-selective membrane to couple endothermic and exothermic reaction in cocurrent and counter-current modes so that hydrogen and heat were transferred across the membrane simultaneously. Also, Bhat and Sadhukhan (2009) investigated the effect of applying a membrane in the thermally coupled reactors in order to reduce heat transfer, mass transfer, and thermodynamic equilibrium limitations. Also, a model was developed to study the performance of a Pd/Ag membrane thermally coupled reactor. In this simulation, the dehydrogenation of cyclohexane to benzene reaction was coupled with the reaction of synthesis gas conversion to methanol in cocurrent mode (Khademi et al., 2009a). This new configuration has some important advantages in comparison to a conventional methanol reactor such as increasing methanol production efficiency and eliminating associated thermodynamics equilibrium limitations; production of pure hydrogen in the permeation side; production of additional valuable products; reduction of the reactor sizes; lowering the outlet temperature of product stream; and the establishment of autothermal conditions inside the reactors (Rahimpour et al., 2011b). Also, a hydrogen-perm-selective membrane and nonmembrane thermally coupled reactor by the differential evolution (DE) method was optimized in which the cyclohexane dehydrogenation endothermic reaction was coupled with a methanol synthesis exothermic reaction (Khademi et al., 2009b, 2010). Moreover, a thermally coupled hydrogen-perm selective membrane reactor was simulated to produce methanol, benzene, and pure hydrogen simultaneously from three separated sides of the reactor (Khademi et al., 2009a, 2010). Rahimpour and Pourazadi (2011) proposed a membrane heat exchanger reactor that consisted of three separated sides. Dehydrogenation of cyclohexane to benzene and methanol synthesis were carried out in endothermic and exothermic sides respectively. Hydrogen that was the product of the endothermic side permeated through the membrane to the third side. They compared cocurrent and counter-current modes. Furthermore, the hydrogen perm-selective membrane and dual-membrane thermally coupled reactors were studied in which methanol synthesis and cyclohexane dehydrogenation were thermally coupled (Rahimpour et al., 2011b). In addition, the thermally coupled double-membrane reactor is optimized by Amirabadi et al. (2013) by applying differential evolution strategy.

Since most studies have focused on coupling one exothermic and one endothermic reaction, a new generation of thermally coupled reactors was proposed to enhance the efficiency of methanol production by these rectors. Therefore, Rahimpour et al. (2013) introduced a thermally double-coupled reactor in which exothermic reactions of methanol and DME synthesis were coupled with dehydrogenation of cyclohexane as the endothermic reaction. It was shown that the efficiency of desired products greatly increases compared with conventional coupling. Also, a thermally double-coupled reactor was studied in which three different units of a multitubular reactor with 2962 three concentric tubes in cocurrent mode had been applied. Two exothermic reactions with one endothermic reaction were coupled to produce methanol, DME, and hydrogen simultaneously (Farniaei et al., 2014a). In one other study, the effects of hydroxy sodalite (H-SOD) and Pd/Ag membranes were studied in a thermally double-coupled two-membrane reactor (TDCTMR) as water and hydrogen perm-selective membranes respectively. Methanol and DME synthesis were considered as exothermic reactions that were thermally coupled with the endothermic reaction of cyclohexane dehydrogenation. In order to remove water from the methanol side and inject hydrogen to the DME side, H-SOD and Pd/Ag membranes were used respectively (Farniaei et al., 2014b). Furthermore, some of the studies focused on optimization of the autothermal dual-type methanol synthesis reactor and membrane dual-type methanol reactor in the presence of catalyst deactivation in order to achieve the optimal operating condition of these reactors (Askari et al., 2008; Rahimpour and Behjati, 2009). Mirvakili et al. (2012) proposed a new configuration of thermally coupled membrane reactors. They investigated methanol production by this reactor in which cyclohexane and hydrogen were turned around by a loop. This new configuration of thermally coupled membrane reactors benefits from the advantages of both hydrogen carrier specifications and multifunctional reactors simultaneously. This generation of reactor is called a thermally coupled dual-methanol reactor (TCDMR).

Due to the associated problems of gas-phase reactor designs, other systems such as slurry bubble-column reactors (SBCRs) and trickle-bed reactors (TBRs) have been suggested as a way to overcome the problems of gas-phase reactors (Zhai et al., 2008). In the 1970s, methanol was synthesized in the liquid phase by applying CO-rich syngas from coal gasification. In the 1980s, the American company Air Products and Chemicals used the three-phase SBCRs with a $CuO/ZnO/Al_2O_3$ catalyst to synthesis methanol. Then, they built an industrial plant in 1997 to attain the economic benefits of large-scale methanol production (Maretto and Krishna, 1999; van der Laan et al., 1999; Krishna and Sie, 2000; Li and Prakash, 2000; Wu and Gidaspow, 2000; Šetinc and Levec, 2001; Rados et al., 2003; Zhai et al., 2008; Wang et al., 2011; Rahimpour et al., 2012b). Generally, SBCRs are suitable for high exothermic reactions in order to absorb heat that is released during the reaction. SBCRs can lead to many advantages, such as perfect heat and mass transfer specifications due to small catalyst particle sizes (the size of catalyst particles are 5–150 mm), easy operating conditions, isothermal operation, low pressure drop, and low operating costs (Šetinc and Levec, 1999, 2001; Shaikh and Al-Dahhan, 2007; Wang et al., 2007).

In the recent years, SBCRs have been simulated by a number of researchers (Gamwo et al., 2003). One model was proposed to study the FT conversion of syngas in an SBCR (Gamwo et al., 2003). Furthermore, methanol production by SBCRs was simulated by Wu and Gidaspow (2000). They proposed a transient, two-dimensional hydrodynamic model. Gamwo et al. (2003) presented two computational fluid dynamics (CFD) models based on catalyst viscosity and the kinetic theory of granular flow (Gamwo et al., 2003). Zhao et al. (2007) used a $CuCr/CH_3ONa$ catalyst for the synthesis of methanol to investigate the effect of this catalytic reaction on the performance of low-temperature methanol synthesis in a slurry bubble-column reactor with a flash column (SBCR/FC). In this system methanol synthesis and the separation of reaction products were performed simultaneously. Moreover, Bakopoulos (2006) introduced a novel improved large-scale methanol production process by slurry bubble column. This large-scale slurry jet loop bubble column consisted of an auxiliary internal heat exchanger and a gas-liquid slurry jet-eductor mixing system with high efficiency. Salehi et al. (2014) studied the effects of CO injection to the feed on methanol production efficiency. Since water produced by CO_2 hydrogenation reaction during methanol synthesis causes catalyst deactivation due to the crystallization of the Cu/Zno-based catalyst, CO injection can reduce the crystallization of Cu and Zno in the catalyst. In fact, higher CO conversion leads to lower water production and catalyst deactivation during the methanol production process. Accordingly, CO injection in the feed could substantially improve the methanol production rate (Rahimpour and Ghader, 2003).

In methanol synthesis, a suitable idea to overcome the thermodynamic limitations is the sorption-enhanced reaction process in a fluidized-bed reactor. The sorption-enhanced process in the fixed-bed reactor has some noticeable problems, such as the large size of catalyst and adsorbent particles, dominant diffusion limitations due to the large size of particles, low efficiency, a difficult process of adsorbent substitution, an inconvenient regeneration reaction switch-type operation, and hotspot technical problems (Chao et al., 2012). A fluidized bed configuration can be used to eliminate these problems (Bayat et al., 2016). In this configuration, a high conversion is achieved by the addition of adsorbent solid particles to the reaction zone. The main advantages of the fluidized bed reactor are high heat transfer ability, low pressure drop, efficiency enhancement, and negligible diffusion limitations (Abashar, 2004). The idea of a fluidized-bed reactor was proposed 50 years ago in which fine solid particles (flowing solids) were in contact with gas inside the reactor (Retallick, 1963). Afterward, Wagialla and Elnashaie (1991) applied the fluidized-bed reactor for methanol synthesis to overcome some operational problems of industrial packed-bed reactors. Although the fluidized-bed configuration has many advantages, it also has some problems, such as the ablation of reactor internals, catalyst friction, and obstacles in reactor construction (Deshmukh et al., 2005). In a large number of new studies, zeolite 4A has been applied as a valuable selective water adsorbent for the methanol synthesis process. (Bayat et al., 2014a,b,c,d; Dehghani et al., 2014). The high water adsorption capacity of zeolite makes it suitable for water separation and

removal (Zhu et al., 2005). Therefore, Bayat et al. (2016) proposed an attractive idea of sorption-enhancement for methanol synthesis in the fluidized-bed reactor. They applied a fluidized-bed reactor with water adsorption capability as the exothermic side in which the methanol synthesis reaction was carried out to supply the necessary heat for the endothermic reaction side. In this configuration, which is called fluidized bed sorption, the enhanced thermally coupled reactor (FSE-TCR) and H_2O adsorption and removal lead to a higher conversion of CO_2 to methanol (Iliuta et al., 2011; Bayat et al., 2016). The continuous regeneration of zeolite 4A in the FSE-TCR configuration helps to eliminate the discontinuity of the reactor operation (Iliuta et al., 2011; Bayat et al., 2016). The results show that FSE-TCR improves methanol production significantly compared to the conventional methanol production process (Bayat et al., 2016). Also, Rahimpour and Bayat (2011) applied a fluidized-bed thermally coupled membrane reactor for production of hydrogen, methanol, and benzene simultaneously.

Biomass gasification has become one of the promising methods of methanol synthesis due to its advantages, such as low cost, high efficiency, and the production of methanol in a large scale (Turn et al., 1998; Gil et al., 1999; Rapagna et al., 2002; Courson et al., 2002; Guan et al., 2006; Shamsul et al., 2014). In this method, biomass can first be converted to syngas. Then, the syngas is synthesized to methanol (Zhang et al., 2009). For this purpose, Zhang et al. (2009) used interconnected fluidized-bed reactors to synthesize methanol from an H_2-rich biomass-derived syngas produced by biomass gasification. They simulated methanol production through biomass gasification in a fluidized-bed reactor with Aspen Plus software.

Obviously, methanol is an important chemical that can be widely used in different industries. It also has a significant effect on the reduction of negative environmental effects produced by fossil fuels. For these principal reasons, different reactors of methanol synthesis have been introduced in the current research.

2 Methanol Synthesis Reactors

In fact, methanol is a useful compound in different industries. Also, it has received much attention as a clean and renewable source of energy. Accordingly, different methanol synthesis reactors are presented in the following subsections.

2.1 Conventional Methanol Reactor (CMR)

Fig. 20.1 shows the schematic diagram of a single-stage CMR. This reactor contains tubes surrounded by a shell compartment. Boiling water flows in the shell and the tubes are packed with a catalyst. A $CuO/ZnO/Al_2O_3$ catalyst (35% copper, 15%–50% zinc, 4%–20% aluminum) is used for the methanol synthesis reaction as the exothermic reaction. Water is converted

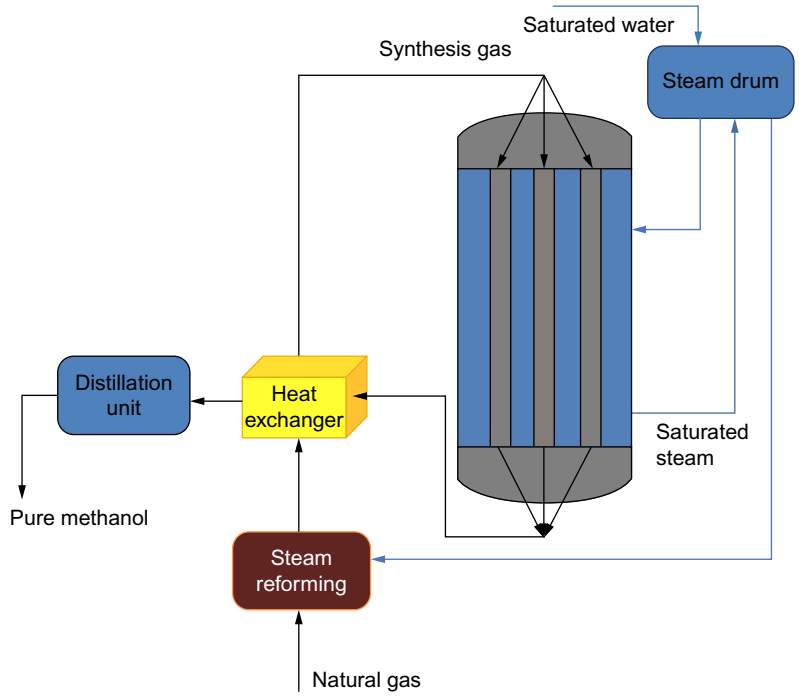

Fig. 20.1
Schematic diagram of CMR (Rahimpour et al., 2011c).

to vapor through absorbing heat from the exothermic reaction side. Table 20.1 shows the specific properties and operating conditions of the CMR (Rahimpour et al., 2011c).

2.2 Thermally Coupled Methanol Reactor (TCMR)

The thermally coupled reactor configuration is shown in Fig. 20.2. It is composed of shell and tube sections which are thermally coupled. The endothermic reaction is carried out in the shell side, while the exothermic reaction is performed in the tube side. Each section is filled with the appropriate catalyst for the reaction. Heat produced by the exothermic reaction is absorbed continuously by the endothermic reaction. The endothermic reaction of cyclohexane catalytic dehydrogenation to benzene is used in the shell side (Khademi et al., 2009b).

Fig. 20.3 shows one other configuration of TCMR. This reactor consists of two concentric tubes. The inner and outer tubes are the exothermic and endothermic sides, respectively. Methanol synthesis is used as the exothermic reaction and dehydrogenation of MCH is carried out as the endothermic one. The exothermic reaction supplies the necessary heat for the endothermic reaction continuously to produce hydrogen (Rahimpour et al., 2011c). A steady-state heterogeneous one-dimensional model has been applied to simulate this system. The results show that the coupled reactor has some advantages such as (Rahimpour et al., 2011c):

Table 20.1 Operating conditions and the properties of the catalyst for CMR (Rahimpour et al., 2011c)

Parameter	Value	Unit
Gas phase		
Feed composition (mole fraction)		
CH_3OH	0.0050	
CO_2	0.0940	
CO	0.0460	
H_2O	0.0004	
H_2	0.6590	
N_2	0.0930	
CH_4	0.1026	
Total molar flow rate	0.64	mol s^{-1}
Inlet pressure	76.98	bar
Catalyst particle Density	1770	kg m^{-3}
Particle diameter	5.47×10^{-3}	m
Heat capacity	5.0	kJ kg^{-1} K^{-1}
Thermal conductivity	.004	W m^{-1} K^{-1}
Specific surface area	626.98	m^2 m^{-3}
Ratio of void fraction to tortuosity of catalyst particle	0.123	
Length of reactor	7.022	m
Number of tubes	2962	
Bed void fraction	0.39	
Density of catalyst bed	1140	kg m^{-3}
Tube inner diameter	3.8×10^{-2}	m
Tube outer diameter	4.2×10^{-2}	m
Wall thermal conductivity	48	W $m^{-}1$ K^{-1}

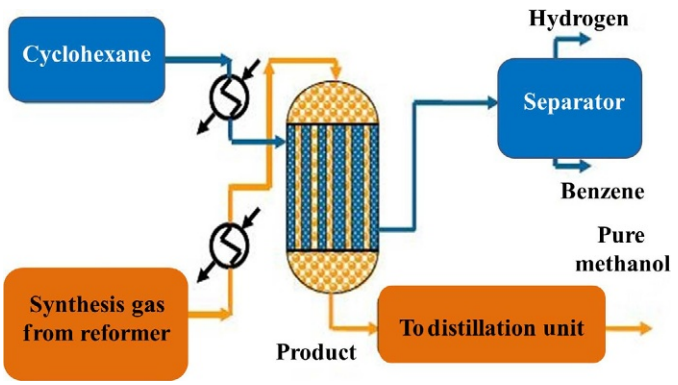

Fig. 20.2
A schematic diagram of a thermally coupled reactor configuration (Khademi et al., 2009b).

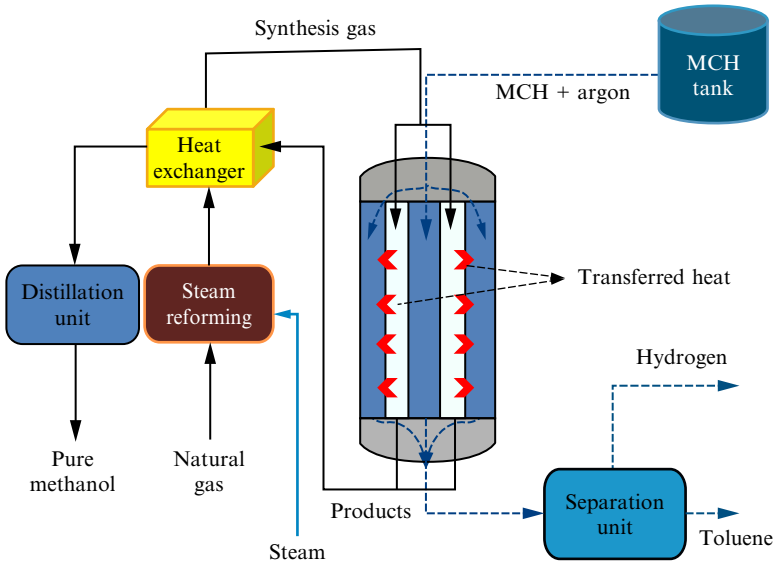

Fig. 20.3
Schematic diagram of TCMR (Rahimpour et al., 2011c).

- The catalyst deactivation rate is reduced due to the lower temperature profile of coupled reactors compared to CMRs.
- In addition to methanol, hydrogen is also produced as a valuable product.
- Reactor size and outlet temperature of the products are reduced.
- Autothermal condition is established in the reactor.

Besides, a higher degree of energy integration between exothermic and endothermic reactions can be achieved in the TCMR configuration (Khademi et al., 2009b).

2.3 Thermally Double-Coupled Reactor (TDCR)

TDCR is a multitubular reactor that contains 2962 three concentric tubes. In the central tube, heat is transferred from exothermic reactions to the endothermic reaction, which is carried out in the outer and inner tubes, respectively. In this configuration, three reactions with suitable temperature ranges are thermally coupled (Farniaei et al., 2014b). A thermally double-coupled reactor configuration is shown in Fig. 20.4. In this configuration methanol synthesis and FT synthesis are carried out in the inner and outer tubes as the two exothermic sides over $CuO/ZnO/Al_2O_3$ and Fe-HZSM5, respectively. On the other hand, a dehydrogenation of decline over the Pt-Sn/γ-Al_2O_3 catalyst occurs in the middle tube. Heat is transferred from two exothermic sides to the endothermic reaction in the middle tube (Samimi et al., 2013).

Due to the equilibrium limitation of the exothermal reaction conversion in the methanol synthesis reactor, it is essential to find a solution in order to drive the equilibrium reaction of

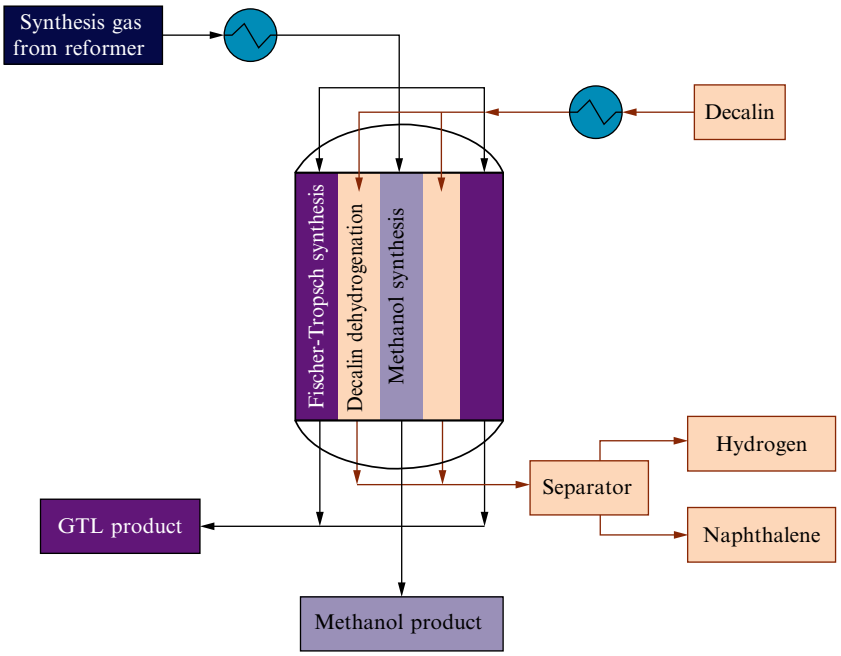

Fig. 20.4
Schematic diagram of integrated TDCR (Samimi et al., 2013).

methanol synthesis toward the product. For this reason, the membrane reactor has received much attention for methanol production in recent studies (Rahimpour et al., 2011b).

2.4 Membrane

Recently, membranes have been applied to enhance the conversion and selectivity of reactions. Membranes have many advantages such as (Farniaei et al., 2013):

- Because membranes don't need major phase change, they are less energy intensive.
- Membranes don't need solvent or absorbent.
- Membrane equipment is not complicated, so it can be widely used.
- Membranes don't require various maintenance operations.

2.5 Membrane Reactor

A semipermeable membrane is applied in the membrane reactor that leads to a more compact design and higher conversion. Today, membrane technology is used in the reaction systems that contain hydrogen and oxygen. Membranes are based on palladium and ceramic (Rohde et al., 2005). A Pd-Ag membrane is suitable for hydrogen removal (Mirvakili et al., 2012). The performance of H_2-selective Pd membranes was investigated by microsystem technology

(Gielens et al., 2007; Peters et al., 2008). On the other hand, the H-SOD membrane has excellent water selectivity compared to hydrogen. Moreover, the membrane seems to have high thermal and mechanical stability. Therefore, an H-SOD membrane can be a good choice for water removal in the FT process to provide the necessary H_2O/H_2 perm-selectivity (Rohde et al., 2008). The effect of water removal by an H-SOD membrane on the performance of the FT process has been proposed by Rahimpour et al. (2011a).

2.5.1 Pd/Ag membrane

The palladium membrane is a metallic tube that contains palladium and a silver alloy material. This property helps in that only hydrogen monoatomic gas is able to pass through the membrane lattice when it is heated above 300°C. Due to this characteristic, the Pd/Ag membrane is applied for hydrogen removal in dehydrogenation reactions (Shu et al., 1991). By hydrogen removal from the dehydrogenation reaction section through the Pd/Ag membrane, the reversible reaction of dehydrogenation drives toward the product. So, applying a membrane could enhance the conversion of the reversible reaction. The effect of a Pd/Ag membrane on the performance of hydrogenation and dehydrogenation reactions has also been studied (Uemiya et al., 1991). In addition, the hydrogen permeability of the Pd/Ag membrane is enhanced by increasing silver content so that the maximum permeability can be achieved when the silver content of the membrane is about 23 wt% (Graaf et al., 1988).

2.5.2 H-SOD membrane

A membrane has received much attention due to its advantages for chemical processes. As mentioned, the removal of byproducts from the reaction side by the membrane shifts the reversible reaction toward the product. As a result, the reaction conversion is increased by applying the membrane (Farsi and Jahanmiri, 2011). Water is one of the main byproducts of the methanol synthesis process. Therefore water removal enhances the methanol production rate. According to the studies, microporous zeolite membranes seem to be one of the best choices for this purpose. H-SOD is a microporous zeolite membrane produced by direct hydrothermal synthesis on α-Al_2O_3 supports (Rohde et al., 2008). H-SOD is suitable for small molecule removal such as water and helium (Baerlocher et al., 2007). An H-SOD membrane should have some properties such as thermal and mechanical stability, an economical price, and high selectivity of water to hydrogen (van Niekerk et al., 2007). In fact, the H-SOD membrane is approximately 100% selective for water removal from hydrogen or carbon monoxide gases (Rohde et al., 2008). Therefore, it is a promising candidate for in situ H_2O removal during methanol and DME synthesis processes (Samimi et al., 2014).

2.5.3 Thermally coupled membrane reactor (TCMR)

In this novel configuration, the exothermic reaction supplies the necessary heat for the endothermic reaction. Moreover, a membrane is used to remove byproducts or separate the desired product to shift the reversible reaction toward the higher conversion. The autothermal

condition inside the reactor, the production of multiple products, and conversion enhancement are some the advantages of thermally coupled membrane reactors (Rahimpour et al., 2011b). Khademi et al. (2010) introduced the hydrogen perm-selective membrane thermally coupled reactor. They applied catalytic dehydrogenation of cyclohexane to benzene as the endothermic reaction to absorb heat produced by the methanol synthesis reaction. Fig. 20.5 shows a schematic diagram of a TCMR configuration in the concurrent mode with three sides. The methanol synthesis exothermic reaction on the $CuO/ZnO/Al_2O_3$ catalyst is carried out in the first side. Endothermic reaction of cyclohexane dehydrogenation to benzene is performed on the Pt/Al_2O_3 catalyst in the second side. Finally, the third side is the permeation side. In the permeation side, sweep gas flows to remove the hydrogen that permeates through the Pd/Ag membrane. Also, exothermic and endothermic reactions are thermally coupled and heat is transferred from the exothermic reaction to the endothermic one. The valuable advantages of this integrated catalytic membrane reactor are multiple products can be achieved by applying the multiple reactants, pure hydrogen is also produced as a valuable product, and a higher degree of in situ energy integration is implemented between coupled exothermic and endothermic reactions. Moreover, a higher temperature is established in the first part of the reactor to achieve high kinetic constants. The temperature is then diminished piecemeal at the end parts of the reactor to enhance thermodynamic equilibrium. Due to the many advantages of this novel reactor, methanol production is enhanced significantly by applying TCMR.

Fig. 20.6 shows one other configuration of TCMR in which the H-SOD membrane is applied in the tube side to remove water produced in the reaction side (Mirvakili et al., 2012).

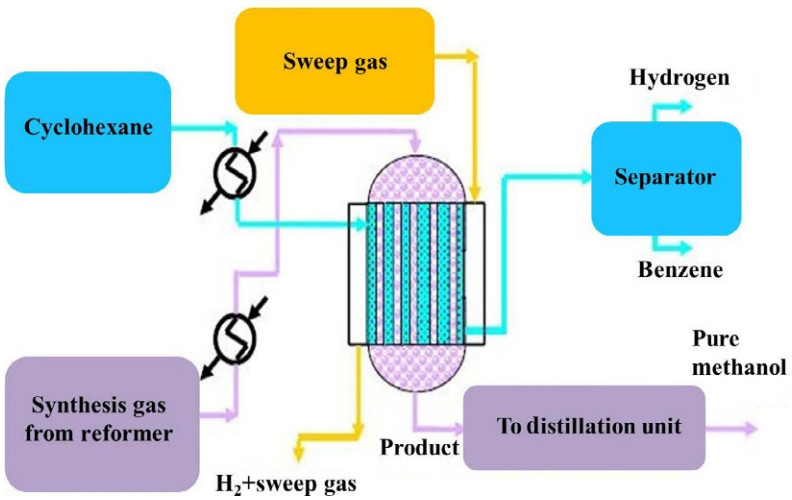

Fig. 20.5
A schematic diagram of TCMR (Khademi et al., 2010).

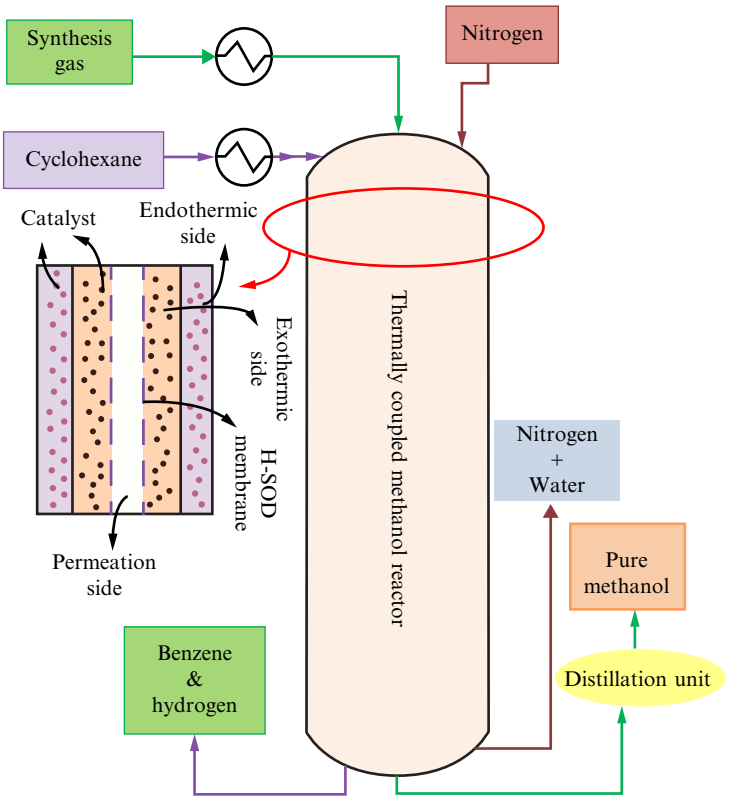

Fig. 20.6
Schematic diagram of TCMR (Mirvakili et al., 2012).

2.5.4 Thermally coupled double-membrane reactor (TCDMR)

Fig. 20.7 shows the schematic diagram of the integrated double-membrane reactor for simultaneous production of methanol and hydrogen. Basically, the procedure of TCDMR is similar to TCMR but there are some differences between them, such as:

First, the synthesis gas enters the shell side of the reactor as the exothermic section and the high-pressure product is routed from the recycle stream through tubes of this reactor in a cocurrent mode with reacting gas. Second, a hydrogen perm-selective membrane between the first and second tube helps hydrogen diffuse through the Pd/Ag membrane due to the pressure difference on both sides of the membrane as the driving force for diffusion. In fact, there are four concentric tubes so that the inner tube is separated from the second tube (exothermic side) by a hydrogen perm-selective membrane and the synthesis gas is fed into the inner tube. Methanol synthesis is carried out in the exothermic side, while catalytic dehydrogenation of cyclohexane to benzene occurs in the third tube. Each side is filled with a fixed bed of the appropriate catalyst. Synthesis gas passes through the exothermic side and then the product is

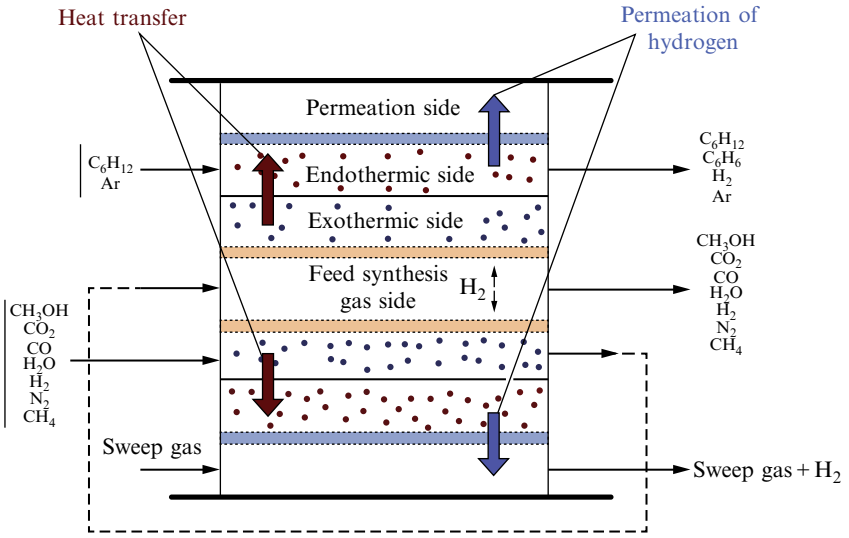

Fig. 20.7
Schematic diagram of the cocurrent mode for TCDMR (Rahimpour et al., 2011b).

conducted for recycling, then flows inside the inner tube. Hydrogen can permeate to the exothermic side due to its appropriate partial pressure in the recycle stream after compressing. Finally, the methanol product with high pressure is conducted from the recycle stream through the inner tube of the reactor, so that it is in a cocurrent mode with the reacting synthesis gas. Consequently, heat is transferred from the reacting synthesis gas to the recycle gas and reacting gas in the inner tube in the endothermic side, respectively. Furthermore, hydrogen diffuses from the endothermic side to the permeation side (outer tube) through the Pd/Ag membrane, which covers the wall of the endothermic side (Rahimpour et al., 2011b).

2.5.5 Thermally double-coupled two-membrane reactor (TDCTMR)

TDCTMR is a multitubular reactor that contains 2962 three concentric tubes. The inside and outside of each concentric tube is covered with two membranes. Fig. 20.8 demonstrates the schematic diagram of one three concentric tube in which the inside and outside of the tubes are covered with a membrane in cocurrent mode. This configuration is studied by Farniaei et al. (2013). They investigated a TDCTMR to produce methanol, hydrogen, and DME simultaneously by applying Pd/Ag membranes in cocurrent mode. In this novel configuration, methanol synthesis and DME synthesis from syngas as the exothermic reactions were coupled with the cyclohexane dehydrogenation endothermic reaction. Hydrogen is removed from the recycled gas and is added in the exothermic side by two Pd/Ag membranes to drive the reversible reaction toward the product. So, it helps to enhance the production efficiency of exothermic sides. The compressor is used to increase the pressure of the recycle stream up to 90 bar to provide the necessary driving force for hydrogen separation by Pd/Ag membranes.

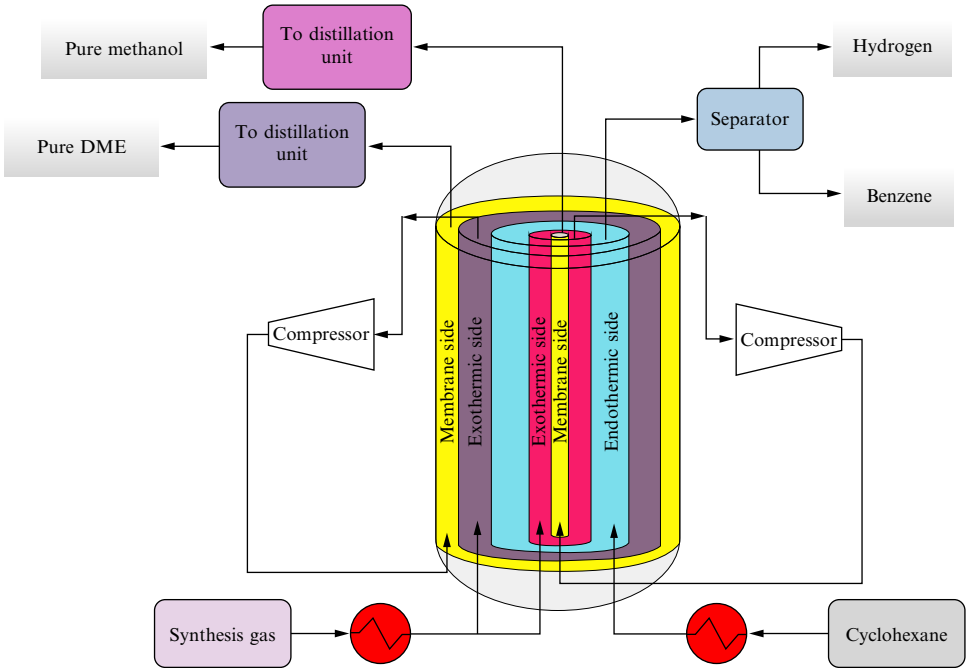

Fig. 20.8
A schematic diagram of one three concentric tubes with covered membrane inside and outside of it in TDCTMR (Farniaei et al., 2013).

Simulation results demonstrate that applying this novel reactor could enhance the methanol yield and methanol production substantially compared to CMR, TDCR, and TCMR.

Fig. 20.9 shows one other configuration of TDCTMR. This configuration contains five concentric tubes. Methanol and DME synthesis occur in the two exothermic sides by CuO/ZnO/Al_2O_3 and γ-Al_2O_3 catalysts, respectively. MCH dehydrogenation by a Pt/Al_2O_3 catalyst is carried out in the endothermic side, which is located between the exothermic sides. An H-SOD membrane is applied in the inner and outer walls of the exothermic sides to remove water from both sides. Heat produced by methanol synthesis and DME reactions supplies the necessary heat for the endothermic reaction of MCH dehydrogenation. Fig. 20.10 shows an elemental volume along the axial direction inside the thermally double-coupled dual-membrane reactor in order to make this configuration more obvious. Also, the performance of TDCTMR is compared with the optimized TDCR and CMR. The results show that applying TDCTMR leads to the improvement of a methanol mole fraction (Samimi et al., 2014).

In addition, the performance of TDCTMR with water and hydrogen perm-selective membranes was simulated via different recycle cases. In the mentioned study, methanol and direct DME synthesis from natural gas were carried out as the exothermic reactions. The exothermic reactions were thermally coupled with an endothermic reaction of cyclohexane

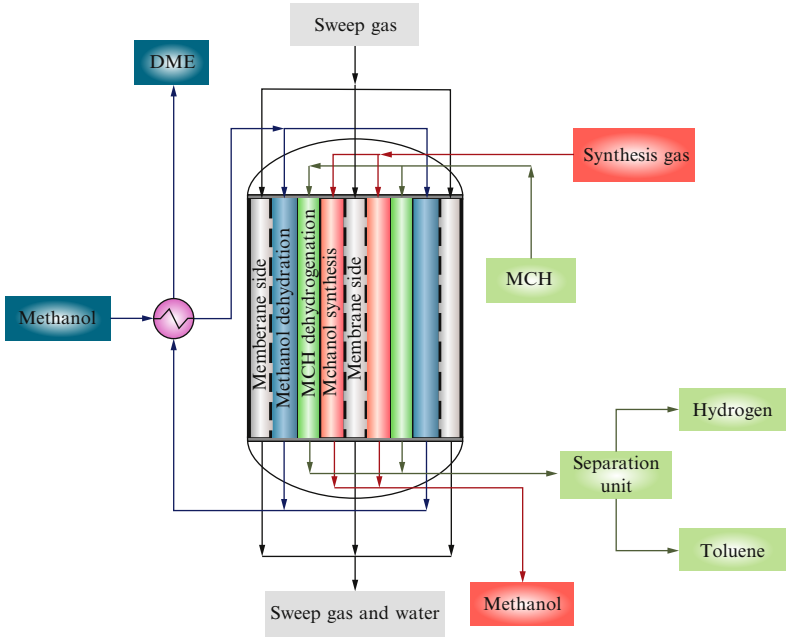

Fig. 20.9
A schematic diagram of integrated TDCTMR (Samimi et al., 2014).

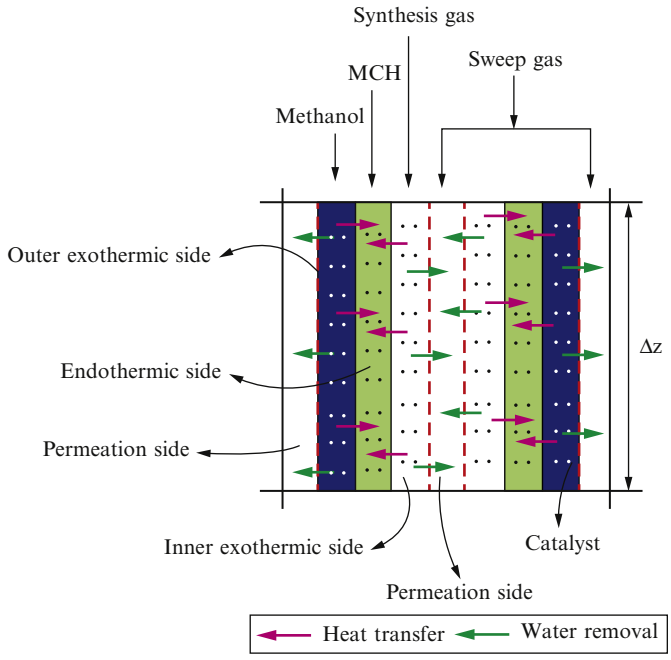

Fig. 20.10
An elemental volume along the axial direction inside the TDCTMR (Samimi et al., 2014).

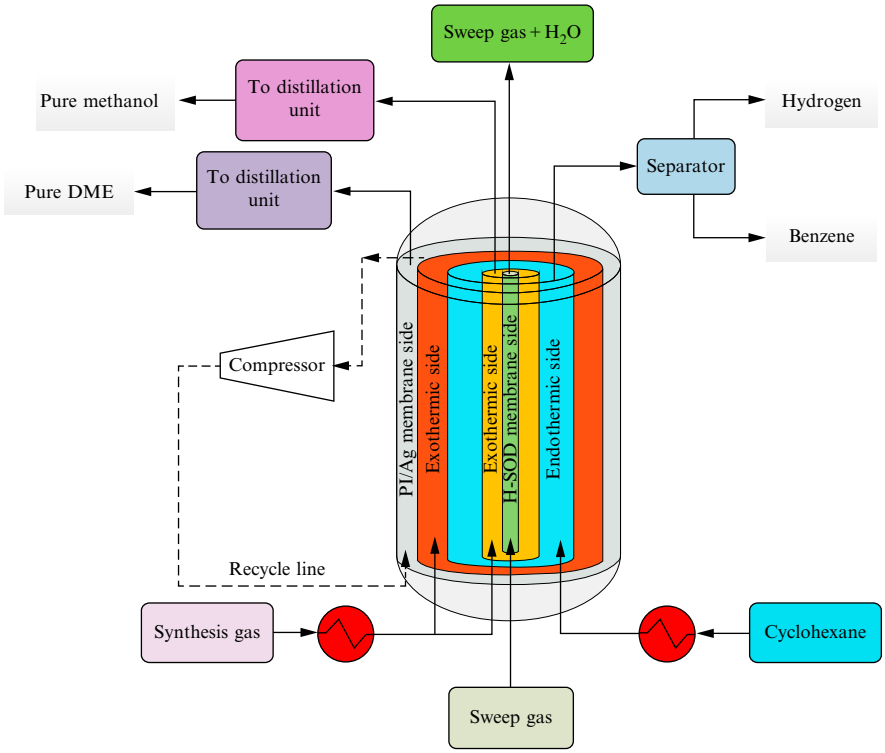

Fig. 20.11
Schematic diagram of TDCTMR-Case 1 (Farniaei et al., 2014b).

dehydrogenation. Water was removed from the methanol side by the H-SOD membrane and the Pd/Ag membrane was used for hydrogen diffusion to the DME side. Three different recycle stream cases of TDCTMR are demonstrated in Figs. 20.11–20.13. The simulation results show that methanol production by TDCTMR is higher than that of TDCR (Farniaei et al., 2014b).

2.5.6 Thermally coupled dual-methanol reactor (TCDMR)

This configuration is the new generation of TCMR that benefits from the advantages of both hydrogen carrier characteristics and multifunctional reactors. Mirvakili et al. (2012) optimized thermally coupled dual reactors associated with the cyclohexane and hydrogen loop approach for methanol production. They applied the DE method. Fig. 20.14 shows this configuration. It consists of two reactors. The cyclohexane dehydrogenation reaction is coupled with the methanol synthesis reactions in the first reactor. Hydrogen produced in the first reactor is used in the second reactor for the hydrogenation of benzene to cyclohexane. Also, the performance of the optimized thermally coupled dual-methanol reactor (OTCDMR) is compared with TCMR and CMR. The results demonstrate that the OTCDMR configuration is the best one.

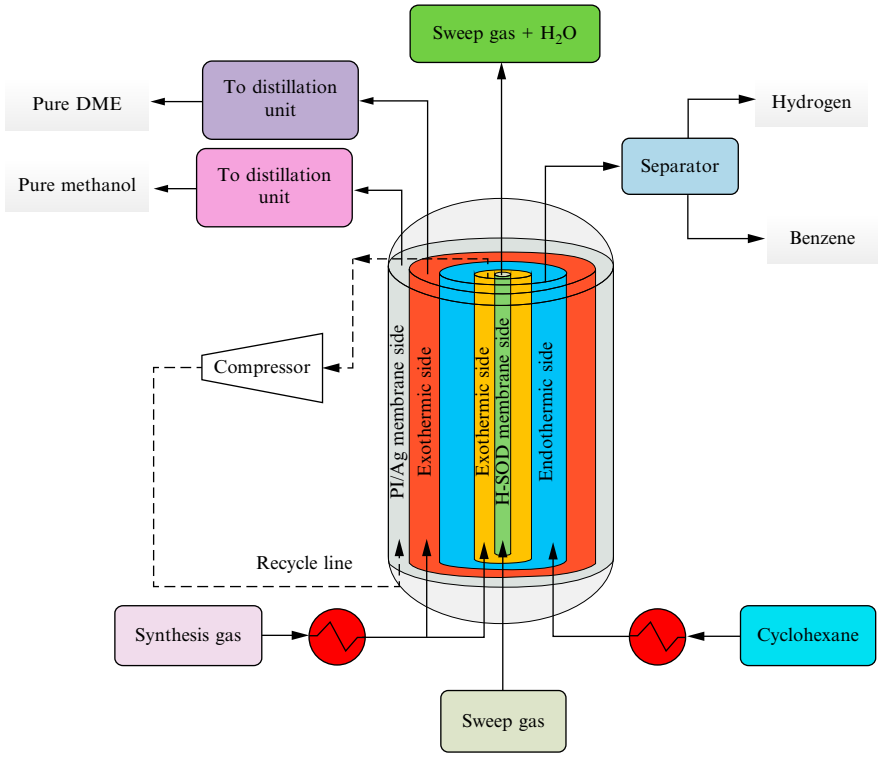

Fig. 20.12
Schematic diagram of TDCTMR-Case 2 (Farniaei et al., 2014b).

2.6 Slurry Bubble-Column Reactor (SBCR)

Fig. 20.15 shows a schematic diagram of an SBCR for methanol synthesis that is a liquid-phase reactor. The duty of liquid phase is the absorption of reaction heat, dispersion of catalyst particles, and transfer of gas bubbles through the liquid. The liquid phase contains liquids such as paraffin oil, paraffin wax, decahydronaphthalene, and tetrahydronaphthalene. Mass transfer occurs between liquid phase, gas bubbles, and solid catalyst particles that leads to the reaction on the catalyst surface (Wu and Gidaspow, 2000; Gamwo et al., 2003; Wang et al., 2007; Salehi et al., 2014). The advantages of SBCR are an easy scale-up, good heat transfer, low cost, online addition and withdrawal of catalyst, and simple construction. In fact, the most important advantages of SBCR are the isothermal operation condition and uniform temperature throughout the reactor. Since the methanol synthesis reaction is strongly exothermal, SBCR could be one of the best choices for a methanol synthesis reactor (Zhao et al., 2007).

2.7 Fluidized-Bed Methanol Reactor

It is obvious that industrial packed-bed methanol reactors have disadvantages such as undesirable heat transfer rate, pressure drop inside the reactor, low efficiency of catalyst particles due to the diffusion limitations, and consequently a low production rate

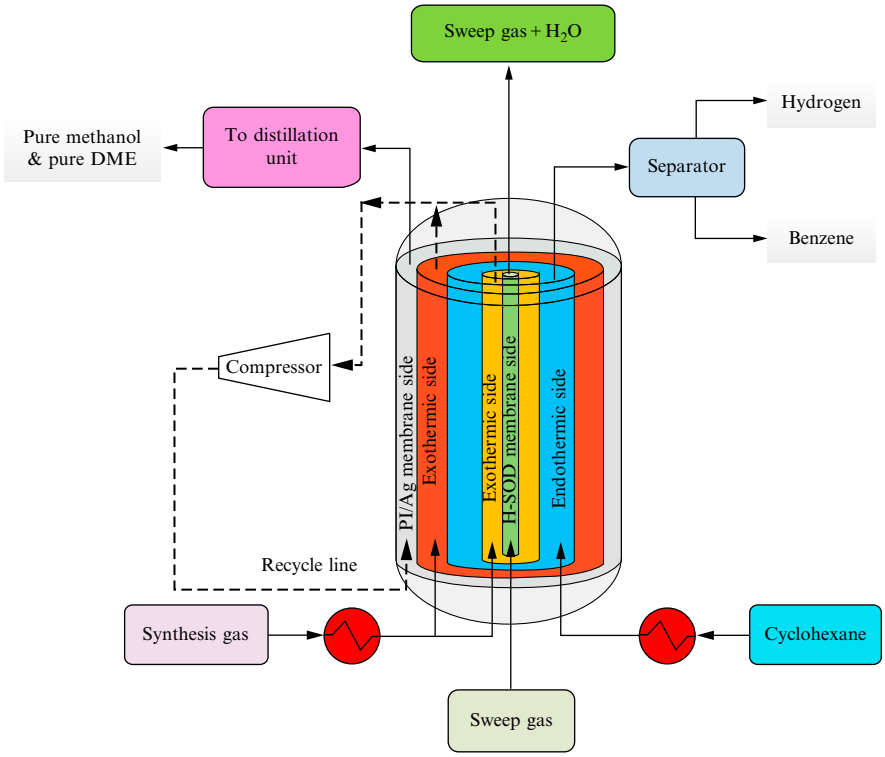

Fig. 20.13
Schematic diagram of TDCTMR-Case 3 (Farniaei et al., 2014b).

(Rahimpour and Alizadehhesari, 2008). It is impossible to apply smaller particle size in the fixed-bed systems due to the pressure drop, so that the effective diameter of catalyst particles in a fixed-bed reactor is usually over 3 mm to decrease internal mass transfer resistance. Due to the drawbacks of packed-bed methanol reactors, fluidized-bed reactors have received significant attention regarding their advantages such as low pressure drop, negligible diffusion limitations, desirable heat transfer, high conversion, and better compact design (Abashar, 2004). Wagialla and Elnashaie (1991) used the fluidized-bed reactor idea instead of a packed-bed system for methanol synthesis to eliminate the problems of industrial fixed-bed reactors. However, while a fluidized-bed reactor has many advantages, it also has some disadvantages such as erosion of reactor internals, difficulties in reactor construction, and catalyst friction (Deshmukh et al., 2005).

2.7.1 Fluidized-bed thermally coupled membrane reactor (FTCMR)

Fig. 20.16 shows the schematic of FTCMR that produces methanol and hydrogen simultaneously (Jeong et al., 2004; Koukou et al., 1997). It consists of three concentric tubes. The exothermic reaction of methanol synthesis by the $CuO/ZnO/Al_2O_3$ catalyst is carried out in the inner tube that is a fluidized-bed reactor to provide the necessary heat for the endothermic side. The second tube is the endothermic side in which catalytic dehydrogenation

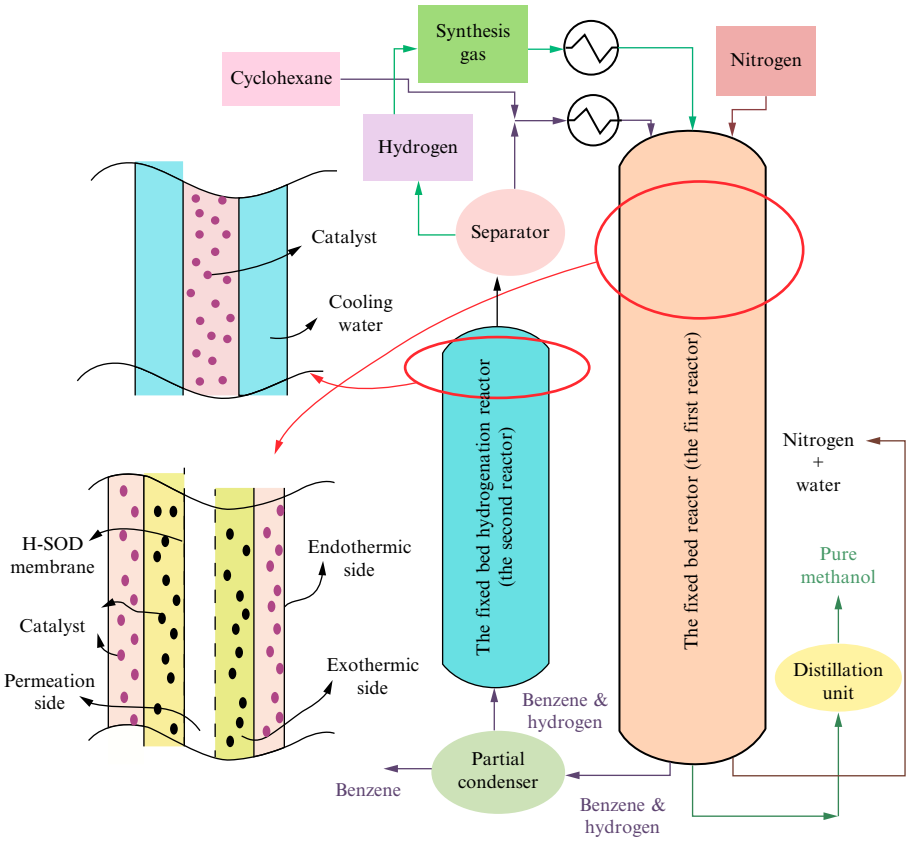

Fig. 20.14
Schematic diagrams of OTCDMR (Mirvakili et al., 2012).

of cyclohexane is carried out. Moreover, the Pd/Ag membrane is applied between the endothermic and penetration sides that make it possible for hydrogen to penetrate from the endothermic side to the penetration side. In fact, there is little difference between the FTCMR and TCMR configurations. These differences are as follows: a small catalyst size is used to fluidize the catalyst bed of the inner tube side; and the feed synthesis gas is entered at the bottom of the exothermic side in order to fluidize the catalyst bed. Accordingly, the sweep gases are feed gas and argon, which are entered to the endothermic and permeation sides from the bottom, respectively (Rahimpour and Bayat, 2011).

2.7.2 Fluidized-bed sorption enhanced thermally coupled reactor (FSE-TCR)

A schematic of the FSE-TCR configuration is shown in Fig. 20.17. Methanol synthesis takes place inside the fluidized bed reactor as the exothermic reaction, while the endothermic reaction of benzene synthesis occurs in the packed-bed endothermic side. The heat is continuously transferred from the exothermic side to the endothermic side. Flowing solids of

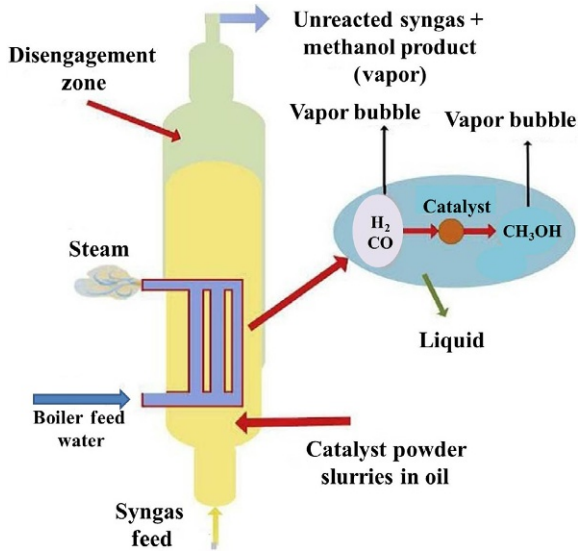

Fig. 20.15
Hydrodynamic of a SBCR for methanol synthesis (Salehi et al., 2014).

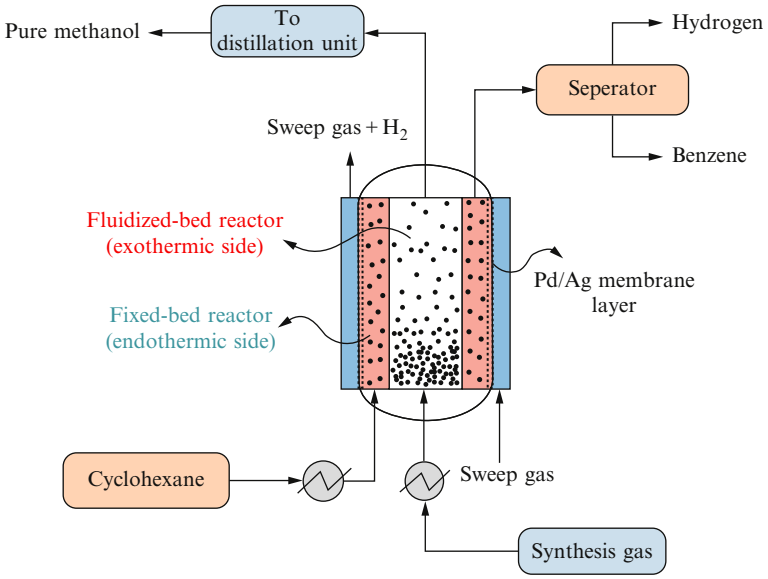

Fig. 20.16
Schematic diagram of the cocurrent mode for a FTCMR configuration (Rahimpour and Bayat, 2011).

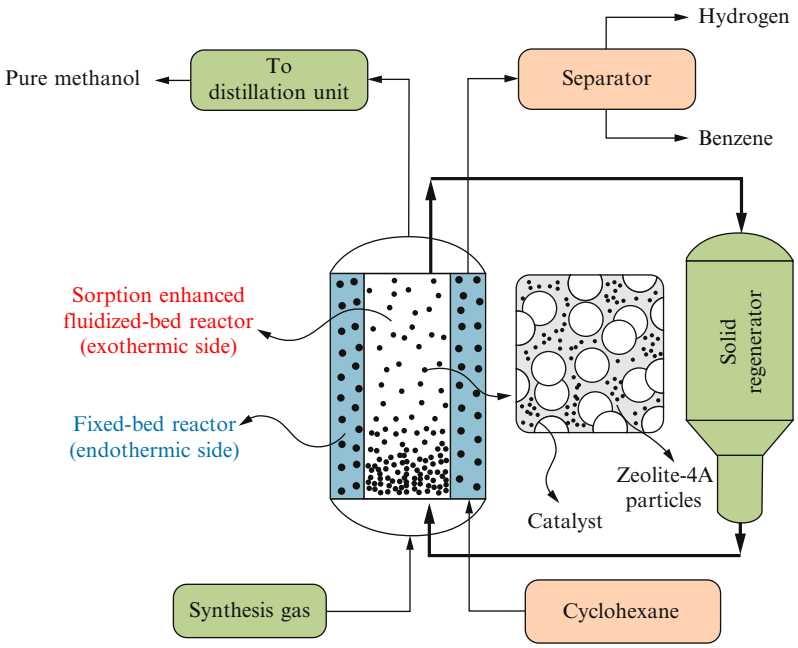

Fig. 20.17
A schematic diagram of FSE-TCR (Bayat et al., 2016).

zeolite 4A are used in the exothermic side as water adsorbents. The solid particles are continuously entered from the bottom of the reactor to adsorb the water vapor inside the tube. The adsorbent particles and catalyst can be separated due to their density difference, so that the light adsorbents prefer to rise and the heavy catalyst particles prefer to descend. In this way, the adsorbent particles enter the solid regenerator to revive, and again are fed to the methanol synthesis side as the fresh adsorbents. Regeneration of the adsorbent particles could be achieved continuously by depressurization in a regenerator (Bayat et al., 2016). Details of advanced regeneration technologies can be found in the literature (Xiu et al., 2002).

3 Conclusion and Future Trends

There are several theoretical and experimental studies regarding the synthesis of methane as a valuable product. The lack of fundamental studies for large-scale production plants is still felt (Bridgwater, 2012). It seems necessary to experimentally investigate the performance of a new generation of methanol synthesis reactors such as thermally coupled and membrane reactors for the large-scale industrial production of methanol.

References

Abashar, M., 2004. Coupling of steam and dry reforming of methane in catalytic fluidized bed membrane reactors. Int. J. Hydrog. Energy 29, 799–808.

Abo-Ghander, N.S., Grace, J.R., Elnashaie, S.S., Lim, C.J., 2008. Modeling of a novel membrane reactor to integrate dehydrogenation of ethylbenzene to styrene with hydrogenation of nitrobenzene to aniline. Chem. Eng. Sci. 63, 1817–1826.

Agar, D.W., 1999. Multifunctional reactors: old preconceptions and new dimensions. Chem. Eng. Sci. 54, 1299–1305.

Alarifi, A., Elkamel, A., Croiset, E., 2013. Steady-state simulation of a novel annular multitubular reactor for enhanced methanol production. Ind. Eng. Chem. Res. 52, 15387–15393.

Altimari, P., Bildea, C.S., 2009. Integrated design and control of plantwide systems coupling exothermic and endothermic reactions. Comput. Chem. Eng. 33, 911–923.

Amandusson, H., Ekedahl, L.-G., Dannetun, H., 2001. Hydrogen permeation through surface modified Pd and PdAg membranes. J. Membr. Sci. 193, 35–47.

Amirabadi, S., Kabiri, S., Vakili, R., Iranshahi, D., Rahimpour, M.R., 2013. Differential evolution strategy for optimization of hydrogen production via coupling of methylcyclohexane dehydrogenation reaction and methanol synthesis process in a thermally coupled double membrane reactor. Ind. Eng. Chem. Res. 52, 1508–1522.

Askari, F., Rahimpour, M.R., Jahanmiri, A., Khosravanipour Mostafazadeh, A., 2008. Dynamic simulation and optimization of a dual-type methanol reactor using genetic algorithms. Chem. Eng. Technol. 31, 513–524.

Baerlocher, C., Mccusker, L.B., Olson, D.H., 2007. Atlas of Zeolite Framework Types. Elsevier, Amsterdam.

Bakopoulos, A., 2006. Multiphase fluidization in large-scale slurry jet loop bubble columns for methanol and or dimethyl ether production. Chem. Eng. Sci. 61, 538–557.

Bayat, M., Dehghani, Z., Hamidi, M., Rahimpour, M.R., 2014a. Methanol synthesis via sorption-enhanced reaction process: modeling and multi-objective optimization. J. Taiwan Inst. Chem. Eng. 45, 481–494.

Bayat, M., Dehghani, Z., Rahimpour, M.R., 2014b. Membrane/sorption-enhanced methanol synthesis process: dynamic simulation and optimization. J. Ind. Eng. Chem. 20, 3256–3269.

Bayat, M., Dehghani, Z., Rahimpour, M.R., 2014c. Sorption-enhanced methanol synthesis in a dual-bed reactor: dynamic modeling and simulation. J. Taiwan Inst. Chem. Eng. 45, 2307–2318.

Bayat, M., Hamidi, M., Dehghani, Z., Rahimpour, M.R., Shariati, A., 2014d. Hydrogen/methanol production in a novel multifunctional reactor with in situ adsorption: modeling and optimization. Int. J. Energy Res. 38, 978–994.

Bayat, M., Heravi, M., Rahimpour, M.R., 2016. Sorption enhanced process by integrated heat-exchanger reactor assisted by fluidization concept for methanol synthesis. Chem. Eng. Process. Process Intensif. 110, 30–43.

Bhat, S.A., Sadhukhan, J., 2009. Process intensification aspects for steam methane reforming: an overview. AIChE J. 55, 408–422.

Bridgwater, A.V., 2012. Review of fast pyrolysis of biomass and product upgrading. Biomass Bioenergy 38, 68–94.

Bromberg, L., Cheng, W., 2010. Methanol as an Alternative Transportation Fuel in the US: Options for Sustainable and/or Energy-Secure Transportation. Sloan Automotive Laboratory, Massachusetts Institute of Technology, Cambridge, MA.

Brown, L.F., 2001. A comparative study of fuels for on-board hydrogen production for fuel-cell-powered automobiles. Int. J. Hydrog. Energy 26, 381–397.

Chao, Z., Wang, Y., Jakobsen, J.P., Fernandino, M., Jakobsen, H.A., 2012. Numerical investigation of the sorption enhanced steam methane reforming in a fluidized bed reactor. Energy Procedia 26, 15–21.

Cheng, W.-H., 1994. Methanol Production and Use. CRC Press, United States.

Chinchen, G., Denny, P., Jennings, J., Spencer, M., Waugh, K., 1988. Synthesis of methanol: Part 1. Catalysts and kinetics. Appl. Catal. 36, 1–65.

Courson, C., Udron, L., Świerczyński, D., Petit, C., Kiennemann, A., 2002. Hydrogen production from biomass gasification on nickel catalysts: tests for dry reforming of methane. Catal. Today 76, 75–86.

Dautzenberg, F., Mukherjee, M., 2001. Process intensification using multifunctional reactors. Chem. Eng. Sci. 56, 251–267.
Dehghani, Z., Bayat, M., Rahimpour, M.R., 2014. Sorption-enhanced methanol synthesis: dynamic modeling and optimization. J. Taiwan Inst. Chem. Eng. 45, 1490–1500.
Deshmukh, S., Laverman, J.A., Cents, A., Van Sint Annaland, M., Kuipers, J., 2005. Development of a membrane-assisted fluidized bed reactor. 1. Gas phase back-mixing and bubble-to-emulsion phase mass transfer using tracer injection and ultrasound experiments. Ind. Eng. Chem. Res. 44, 5955–5965.
Eigenberger, G., Kolios, G., Nieken, U., 2007. Thermal pattern formation and process intensification in chemical reaction engineering. Chem. Eng. Sci. 62, 4825–4841.
Eisenberg, R., Nocera, D.G., 2005. Preface: overview of the forum on solar and renewable energy. Inorg. Chem. 44, 6799–6801.
Elnashaie, S., Moustafa, T., Alsoudani, T., Elshishini, S., 2000. Modeling and basic characteristics of novel integrated dehydrogenation—hydrogenation membrane catalytic reactors. Comput. Chem. Eng. 24, 1293–1300.
Farniaei, M., Abbasi, M., Rahnama, H., Rahimpour, M.R., 2014a. Simultaneous production of methanol, DME and hydrogen in a thermally double coupled reactor with different endothermic reactions: application of cyclohexane, methylcyclohexane and decalin dehydrogenation reactions. J. Nat. Gas Sci. Eng. 19, 324–336.
Farniaei, M., Abbasi, M., Rasoolzadeh, A., Rahimpour, M.R., 2013. Enhancement of methanol, DME and hydrogen production via employing hydrogen permselective membranes in a novel integrated thermally double-coupled two-membrane reactor. J. Nat. Gas Sci. Eng. 14, 158–173.
Farniaei, M., Abbasi, M., Rasoolzadeh, A., Rahimpour, M.R., 2014b. Performance enhancement of thermally coupling of methanol synthesis, DME synthesis and cyclohexane dehydrogenation processes: employment of water and hydrogen perm-selective membranes via different recycle streams. Chem. Eng. Process. Process Intensif. 85, 24–37.
Farsi, M., Jahanmiri, A., 2011. Mathematical simulation and optimization of methanol dehydration and cyclohexane dehydrogenation in a thermally coupled dual-membrane reactor. Int. J. Hydrog. Energy 36, 14416–14427.
Frauhammer, J., Eigenberger, G., Hippel, L., Arntz, D., 1999. A new reactor concept for endothermic high-temperature reactions. Chem. Eng. Sci. 54, 3661–3670.
Fukuhara, C., Igarashi, A., 2005. Performance simulation of a wall-type reactor in which exothermic and endothermic reactions proceed simultaneously, comparing with that of a fixed-bed reactor. Chem. Eng. Sci. 60, 6824–6834.
Gamwo, I.K., Halow, J.S., Gidaspow, D., Mostofi, R., 2003. CFD models for methanol synthesis three-phase reactors: reactor optimization. Chem. Eng. J. 93, 103–112.
Gielens, F., Tong, H.D., Vorstman, M., Keurentjes, J., 2007. Measurement and modeling of hydrogen transport through high-flux Pd membranes. J. Membr. Sci. 289, 15–25.
Gil, J., Corella, J., Aznar, M.A.P., Caballero, M.A., 1999. Biomass gasification in atmospheric and bubbling fluidized bed: effect of the type of gasifying agent on the product distribution. Biomass Bioenergy 17, 389–403.
Glöckler, B., Kolios, G., Tellaeche, C., Nieken, U., 2009. A heat-integrated reverse-flow reactor concept for endothermic high-temperature syntheses. Part I: Fundamentals-short-cut theory and experimental verification of a traveling endothermic reaction zone. Chem. Eng. Technol. 32, 1339–1347.
Golkhar, A., Keshavarz, P., Mowla, D., 2013. Investigation of CO_2 removal by silica and CNT nanofluids in microporous hollow fiber membrane contactors. J. Membr. Sci. 433, 17–24.
Gómez-Castro, F.I., Rico-Ramírez, V., Segovia-Hernández, J.G., Hernández-Castro, S., 2011. Esterification of fatty acids in a thermally coupled reactive distillation column by the two-step supercritical methanol method. Chem. Eng. Res. Des. 89, 480–490.
Graaf, G., Stamhuis, E., Beenackers, A., 1988. Kinetics of low-pressure methanol synthesis. Chem. Eng. Sci. 43, 3185–3195.
Guan, Y., Guo, L., Zhang, X., Lu, Y., Hao, X., 2006. Gasification of biomass model compounds in supercritical water. J. Chem. Ind. Eng. 57, 1426.
Guo, X.-J., Li, L.-M., Liu, S.-M., Bao, G.-L., Hou, W.-H., 2007. Preparation of $CuO/ZnO/Al_2O_3$ catalysts for methanol synthesis using parallel-slurry-mixing method. J. Fuel Chem. Technol. 35, 329–333.

Hao, Y., Du, X., Yang, L.., Shen, Y., Yang, Y., 2011. Numerical simulation of configuration and catalyst-layer effects on micro-channel steam reforming of methanol. Int. J. Hydrog. Energy 36, 15611–15621.
Harmsen, J., 2010. Process intensification in the petrochemicals industry: drivers and hurdles for commercial implementation. Chem. Eng. Process. Process Intensif. 49, 70–73.
Heinzel, A., Vogel, B., Hübner, P., 2002. Reforming of natural gas—hydrogen generation for small scale stationary fuel cell systems. J. Power Sources 105, 202–207.
Hunter, J.B., Mcguire, G., 1980. Method and apparatus for catalytic heat exchange. Google Patents.
Iliuta, I., Iliuta, M.C., Larachi, F., 2011. Sorption-enhanced dimethyl ether synthesis—multiscale reactor modeling. Chem. Eng. Sci. 66, 2241–2251.
Iranshahi, D., Bahmanpour, A.M., Pourazadi, E., Rahimpour, M.R., 2010. Mathematical modeling of a multi-stage naphtha reforming process using novel thermally coupled recuperative reactors to enhance aromatic production. Int. J. Hydrog. Energy 35, 10984–10993.
Itoh, N., Tamura, E., Hara, S., Takahashi, T., Shono, A., Satoh, K., Namba, T., 2003. Hydrogen recovery from cyclohexane as a chemical hydrogen carrier using a palladium membrane reactor. Catal. Today 82, 119–125.
Itoh, N., Wu, T.-H., 1997. An adiabatic type of palladium membrane reactor for coupling endothermic and exothermic reactions. J. Membr. Sci. 124, 213–222.
Jahanmiri, A., Eslamloueyan, R., 2002. Optimal temperature profile in methanol synthesis reactor. Chem. Eng. Commun. 189, 713–741.
Jain, I., Lal, C., Jain, A., 2010. Hydrogen storage in Mg: a most promising material. Int. J. Hydrog. Energy 35, 5133–5144.
Jeong, B.-H., Sotowa, K.-I., Kusakabe, K., 2004. Modeling of an FAU-type zeolite membrane reactor for the catalytic dehydrogenation of cyclohexane. Chem. Eng. J. 103, 69–75.
Jung, J., Gamwo, I.K., 2008. Multiphase CFD-based models for chemical looping combustion process: fuel reactor modeling. Powder Technol. 183, 401–409.
Kang, D.B., Anderson, A.B., 1985. Theoretical interpretation of the cyclohexane .fwdarw. benzene reaction on the platinum (III) surface. J. Am. Chem. Soc. 107, 7858–7861.
Kariya, N., Fukuoka, A., Utagawa, T., Sakuramoto, M., Goto, Y., Ichikawa, M., 2003. Efficient hydrogen production using cyclohexane and decalin by pulse-spray mode reactor with Pt catalysts. Appl. Catal. A Gen. 247, 247–259.
Khademi, M., Jahanmiri, A., Rahimpour, M.R., 2009a. A novel configuration for hydrogen production from coupling of methanol and benzene synthesis in a hydrogen-permselective membrane reactor. Int. J. Hydrog. Energy 34, 5091–5107.
Khademi, M., Rahimpour, M.R., Jahanmiri, A., 2010. Differential evolution (DE) strategy for optimization of hydrogen production, cyclohexane dehydrogenation and methanol synthesis in a hydrogen-permselective membrane thermally coupled reactor. Int. J. Hydrog. Energy 35, 1936–1950.
Khademi, M., Setoodeh, P., Rahimpour, M.R., Jahanmiri, A., 2009b. Optimization of methanol synthesis and cyclohexane dehydrogenation in a thermally coupled reactor using differential evolution (DE) method. Int. J. Hydrog. Energy 34, 6930–6944.
Kirillov, V., Fadeev, S., Kuzin, N., Shigarov, A., 2007. Modeling of a heat-coupled catalytic reactor with co-current oxidation and conversion flows. Chem. Eng. J. 134, 131–137.
Kolios, G., Frauhammer, J., Eigenberger, G., 2001. A simplified procedure for the optimal design of autothermal reactors for endothermic high-temperature reactions. Chem. Eng. Sci. 56, 351–357.
Kolios, G., Frauhammer, J., Eigenberger, G., 2002. Efficient reactor concepts for coupling of endothermic and exothermic reactions. Chem. Eng. Sci. 57, 1505–1510.
Koukou, M., Chaloulou, G., Papayannakos, N., Markatos, N., 1997. Mathematical modelling of the performance of non-isothermal membrane reactors. Int. J. Heat Mass Transf. 40, 2407–2417.
Krishna, R., Sie, S., 2000. Design and scale-up of the Fischer-Tropsch bubble column slurry reactor. Fuel Process. Technol. 64, 73–105.
Lange, J.-P., 2001. Methanol synthesis: a short review of technology improvements. Catal. Today 64, 3–8.
Li, H., prakash, A., 2000. Influence of slurry concentrations on bubble population and their rise velocities in a three-phase slurry bubble column. Powder Technol. 113, 158–167.

Lokurlu, A., Grube, T., Höhlein, B., Stolten, D., 2003. Fuel cells for mobile and stationary applications—cost analysis for combined heat and power stations on the basis of fuel cells. Int. J. Hydrog. Energy 28, 703–711.
Løvik, I., Hillestad, M., Hertzberg, T., 1998. Long term dynamic optimization of a catalytic reactor system. Comput. Chem. Eng. 22, S707–S710.
Maretto, C., Krishna, R., 1999. Modelling of a bubble column slurry reactor for Fischer-Tropsch synthesis. Catal. Today 52, 279–289.
Mirvakili, A., Rostami, M., Paymooni, K., Rahimpour, M.R., Moghtaderi, B., 2012. Hydrogen looping approach in optimized methanol thermally coupled membrane reactor. Int. J. Hydrog. Energy 37, 235–249.
Moustafa, T., Elnashaie, S., 2000. Simultaneous production of styrene and cyclohexane in an integrated membrane reactor. J. Membr. Sci. 178, 171–184.
Mueller-Langer, F., Tzimas, E., Kaltschmitt, M., Peteves, S., 2007. Techno-economic assessment of hydrogen production processes for the hydrogen economy for the short and medium term. Int. J. Hydrog. Energy 32, 3797–3810.
Olah, G.A., Goeppert, A., Prakash, G.S., 2011. Beyond Oil and Gas: The Methanol Economy. John Wiley & Sons, Germany.
Park, Y.-C., Kim, D.-H., Lim, S., Kim, S.-K., Peck, D.-H., Jung, D.-H., 2012. Design of a MEA with multi-layer electrodes for high concentration methanol DMFCs. Int. J. Hydrog. Energy 37, 4717–4727.
Patel, K.S., Sunol, A.K., 2007. Modeling and simulation of methane steam reforming in a thermally coupled membrane reactor. Int. J. Hydrog. Energy 32, 2344–2358.
Peters, T., Stange, M., Klette, H., Bredesen, R., 2008. High pressure performance of thin Pd-23% Ag/stainless steel composite membranes in water gas shift gas mixtures; influence of dilution, mass transfer and surface effects on the hydrogen flux. J. Membr. Sci. 316, 119–127.
Pregger, T., Graf, D., Krewitt, W., Sattler, C., Roeb, M., Möller, S., 2009. Prospects of solar thermal hydrogen production processes. Int. J. Hydrog. Energy 34, 4256–4267.
Rados, N., Al-Dahhan, M.H., Dudukovic, M.P., 2003. Modeling of the Fischer-Tropsch synthesis in slurry bubble column reactors. Catal. Today 79, 211–218.
Rahimpour, M.R., Asgari, A., 2009. Production of hydrogen from purge gases of ammonia plants in a catalytic hydrogen-permselective membrane reactor. Int. J. Hydrog. Energy 34, 5795–5802.
Rahimpour, M.R., Bayat, M., 2011. Production of ultrapure hydrogen via utilizing fluidization concept from coupling of methanol and benzene synthesis in a hydrogen-permselective membrane reactor. Int. J. Hydrog. Energy 36, 6616–6627.
Rahimpour, M.R., Behjati, H.E., 2009. Dynamic optimization of membrane dual-type methanol reactor in the presence of catalyst deactivation using genetic algorithm. Fuel Process. Technol. 90, 279–291.
Rahimpour, M.R., Dehnavi, M., Allahgholipour, F., Iranshahi, D., Jokar, S., 2012a. Assessment and comparison of different catalytic coupling exothermic and endothermic reactions: a review. Appl. Energy 99, 496–512.
Rahimpour, M.R., Ghader, S., 2003. Theoretical investigation of a Pd-membrane reactor for methanol synthesis. Chem. Eng. Technol. 26, 902–907.
Rahimpour, M.R., Jokar, S., Jamshidnejad, Z., 2012b. A novel slurry bubble column membrane reactor concept for Fischer-Tropsch synthesis in GTL technology. Chem. Eng. Res. Des. 90, 383–396.
Rahimpour, M.R., Mirvakili, A., Paymooni, K., 2011a. A novel water perm-selective membrane dual-type reactor concept for Fischer-Tropsch synthesis of GTL (gas to liquid) technology. Energy 36, 1223–1235.
Rahimpour, M.R., Moghtaderi, B., Jahanmiri, A., Rezaie, N., 2005. Operability of an industrial methanol synthesis reactor with mixtures of fresh and partially deactivated catalyst. Chem. Eng. Technol. 28, 226–234.
Rahimpour, M.R., Mostafazadeh, A.K., Barmaki, M., 2008. Application of hydrogen-permselective Pd-based membrane in an industrial single-type methanol reactor in the presence of catalyst deactivation. Fuel Process. Technol. 89, 1396–1408.
Rahimpour, M.R., Pourazadi, E., 2011. A comparison of hydrogen and methanol production in a thermally coupled membrane reactor for co-current and counter-current flows. Int. J. Energy Res. 35, 863–882.
Rahimpour, M.R., Rahmani, F., Bayat, M., Pourazadi, E., 2011b. Enhancement of simultaneous hydrogen production and methanol synthesis in thermally coupled double-membrane reactor. Int. J. Hydrog. Energy 36, 284–298.

Rahimpour, M.R., Vakili, R., Pourazadi, E., Bahmanpour, A., Iranshahi, D., 2011c. Enhancement of hydrogen production via coupling of MCH dehydrogenation reaction and methanol synthesis process by using thermally coupled heat exchanger reactor. Int. J. Hydrog. Energy 36, 3371–3383.

Rahimpour, M.R., Alizadehhesari, K., 2008. A novel fluidized-bed membrane dual-type reactor concept for methanol synthesis. Chem. Eng. Technol. 31, 1775–1789.

Rahimpour, M.R., Farniaei, M., Abbasi, M., Javanmardi, J., Kabiri, S., 2013. Comparative study on simultaneous production of methanol, hydrogen, and DME using a novel integrated thermally double-coupled reactor. Energy Fuel 27, 1982–1993.

Rahimpour, M.R., Fathikalajahi, J., Jahanmiri, A., 1998. Selective kinetic deactivation model for methanol synthesis from simultaneous reaction of CO_2 and CO with H_2 on a commercial copper/zinc oxide catalyst. Can. J. Chem. Eng. 76, 753–761.

Rahimpour, M.R., Ghader, S., Baniadam, M., Fathi Kalajahi, J., 2003. Incorporation of flexibility in the design of a methanol synthesis loop in the presence of catalyst deactivation. Chem. Eng. Technol. 26, 672–678.

Rahmatmand, B., Keshavarz, P., Ayatollahi, S., 2016. Study of absorption enhancement of CO_2 by SiO_2, Al_2O_3, CNT, and Fe_3O_4 nanoparticles in water and amine solutions. J. Chem. Eng. Data 61, 1378–1387.

Ramaswamy, R., Ramachandran, P., Duduković, M., 2006. Recuperative coupling of exothermic and endothermic reactions. Chem. Eng. Sci. 61, 459–472.

Ramaswamy, R., Ramachandran, P., Duduković, M., 2008. Coupling exothermic and endothermic reactions in adiabatic reactors. Chem. Eng. Sci. 63, 1654–1667.

Rapagna, S., Provendier, H., Petit, C., Kiennemann, A., Foscolo, P., 2002. Development of catalysts suitable for hydrogen or syn-gas production from biomass gasification. Biomass Bioenergy 22, 377–388.

Retallick, W.B., 1963. Method for the production of hydrogen. Google Patents.

Rezaie, N., Jahanmiri, A., Moghtaderi, B., Rahimpour, M.R., 2005. A comparison of homogeneous and heterogeneous dynamic models for industrial methanol reactors in the presence of catalyst deactivation. Chem. Eng. Process. Process Intensif. 44, 911–921.

Rohde, M., Schaub, G., Khajavi, S., Jansen, J., Kapteijn, F., 2008. Fischer-Tropsch synthesis with in situ H_2O removal-directions of membrane development. Microporous Mesoporous Mater. 115, 123–136.

Rohde, M.P., Unruh, D., Schaub, G., 2005. Membrane application in Fischer-Tropsch synthesis reactors—overview of concepts. Catal. Today 106, 143–148.

Salehi, K., Jokar, S., Shariati, J., Bahmani, M., Sedghamiz, M., Rahimpour, M.R., 2014. Enhancement of CO conversion in a novel slurry bubble column reactor for methanol synthesis. J. Nat. Gas Sci. Eng. 21, 170–183.

Samimi, F., Kabiri, S., Mirvakili, A., Rahimpour, M.R., 2013. The concept of integrated thermally double coupled reactor for simultaneous production of methanol, hydrogen and gasoline via differential evolution method. J. Nat. Gas Sci. Eng. 14, 144–157.

Samimi, F., Kabiri, S., Rahimpour, M.R., 2014. The optimal operating conditions of a thermally double coupled, dual membrane reactor for simultaneous methanol synthesis, methanol dehydration and methyl cyclohexane dehydrogenation. J. Nat. Gas Sci. Eng. 19, 175–189.

Schack, C.J., Mcneil, M.A., Rinker, R.G., 1989. Methanol synthesis from hydrogen, carbon monoxide, and carbon dioxide over a $CuO/ZnO/Al_2O_3$ catalyst: I. Steady-state kinetics experiments. Appl. Catal. 50, 247–263.

Semelsberger, T.A., Borup, R.L., Greene, H.L., 2006. Dimethyl ether (DME) as an alternative fuel. J. Power Sources 156, 497–511.

Šetinc, M., Levec, J., 1999. On the kinetics of liquid-phase methanol synthesis over commercial $Cu/ZnO/Al_2O_3$ catalyst. Chem. Eng. Sci. 54, 3577–3586.

Šetinc, M., Levec, J., 2001. Dynamics of a mixed slurry reactor for the three-phase methanol synthesis. Chem. Eng. Sci. 56, 6081–6087.

Shaikh, A., Al-Dahhan, M.H., 2007. A review on flow regime transition in bubble columns. Int. J. Chem. React. Eng. 5.

Shamsul, N., Kamarudin, S.K., Rahman, N.A., Kofli, N.T., 2014. An overview on the production of bio-methanol as potential renewable energy. Renew. Sust. Energ. Rev. 33, 578–588.

Shu, J., Grandjean, B., Neste, A.V., KALIAGUINE, S., 1991. Catalytic palladium-based membrane reactors: a review. Can. J. Chem. Eng. 69, 1036–1060.
Song, C., 2002. Fuel processing for low-temperature and high-temperature fuel cells: challenges, and opportunities for sustainable development in the 21st century. Catal. Today 77, 17–49.
Struis, R.P.W.J., Stucki, S., Wiedorn, M., 1996. A membrane reactor for methanol synthesis. J. Membr. Sci. 113, 93–100.
Sun, Z.-Y., Liu, F.-S., Liu, X.-H., Sun, B.-G., Sun, D.-W., 2012. Research and development of hydrogen fuelled engines in China. Int. J. Hydrog. Energy 37, 664–681.
Taylor, A.M., 2008. Science review of internal combustion engines. Energy Policy 36, 4657–4667.
Tijm, P., Waller, F., Brown, D., 2001. Methanol technology developments for the new millennium. Appl. Catal. A Gen. 221, 275–282.
Turn, S., Kinoshita, C., Zhang, Z., Ishimura, D., Zhou, J., 1998. An experimental investigation of hydrogen production from biomass gasification. Int. J. Hydrog. Energy 23, 641–648.
Uemiya, S., Matsuda, T., Kikuchi, E., 1991. Hydrogen permeable palladium-silver alloy membrane supported on porous ceramics. J. Membr. Sci. 56, 315–325.
Van Der Laan, G.P., Beenackers, A.A., Krishna, R., 1999. Multicomponent reaction engineering model for Fe-catalyzed Fischer-Tropsch synthesis in commercial scale slurry bubble column reactors. Chem. Eng. Sci. 54, 5013–5019.
Van Niekerk, A., Zah, J., Breytenbach, J.C., Krieg, H.M., 2007. Direct crystallisation of a hydroxy sodalite membrane without seeding using a conventional oven. J. Membr. Sci. 300, 156–164.
Van Sint Annaland, M., Nijssen, R., 2002. A novel reverse flow reactor coupling endothermic and exothermic reactions: an experimental study. Chem. Eng. Sci. 57, 4967–4985.
Velardi, S.A., Barresi, A.A., 2002. Methanol synthesis in a forced unsteady-state reactor network. Chem. Eng. Sci. 57, 2995–3004.
Wagialla, K., Elnashaie, S., 1991. Fluidized-bed reactor for methanol synthesis. A theoretical investigation. Ind. Eng. Chem. Res. 30, 2298–2308.
Wang, B., Goodman, D.W., Froment, G.F., 2008. Kinetic modeling of pure hydrogen production from decalin. J. Catal. 253, 229–238.
Wang, J., Anthony, R.G., Akgerman, A., 2005. Mathematical simulations of the performance of trickle bed and slurry reactors for methanol synthesis. Comput. Chem. Eng. 29, 2474–2484.
Wang, T., Wang, J., Jin, Y., 2007. Slurry reactors for gas-to-liquid processes: a review. Ind. Eng. Chem. Res. 46, 5824–5847.
Wang, Y., Fan, W., Liu, Y., Zeng, Z., Xu, Y., Xiang, H., Li, Y., 2011. Modeling study for Fischer-Tropsch synthesis in slurry bubble column reactors. J. Fuel Chem. Technol. 39, 961–966.
Wu, Y., Gidaspow, D., 2000. Hydrodynamic simulation of methanol synthesis in gas-liquid slurry bubble column reactors. Chem. Eng. Sci. 55, 573–587.
Xiu, G.-H., Li, P., Rodrigues, A.E., 2002. Sorption-enhanced reaction process with reactive regeneration. Chem. Eng. Sci. 57, 3893–3908.
Yolcular, S., Olgun, Ö., 2008. Ni/Al_2O_3 catalysts and their activity in dehydrogenation of methylcyclohexane for hydrogen production. Catal. Today 138, 198–202.
Zanfir, M., Gavriilidis, A., 2001. Modelling of a catalytic plate reactor for dehydrogenation-combustion coupling. Chem. Eng. Sci. 56, 2671–2683.
Zanfir, M., Gavriilidis, A., 2003. Catalytic combustion assisted methane steam reforming in a catalytic plate reactor. Chem. Eng. Sci. 58, 3947–3960.
Zhai, X., Shamoto, J., Xie, H., Tan, Y., Han, Y., Tsubaki, N., 2008. Study on the deactivation phenomena of Cu-based catalyst for methanol synthesis in slurry phase. Fuel 87, 430–434.
Zhang, K., Song, H., Sun, D., Li, S., Yang, X., Zhao, Y., Huang, Z., Wu, Y., 2003. Low-temperature methanol synthesis in a circulating slurry bubble reactor. Fuel 82, 233–239.
Zhang, K., Zhao, Y., 2006. A scale-up strategy for low-temperature methanol synthesis in a circulating slurry bubble reactor. Chem. Eng. Sci. 61, 1459–1469.

Zhang, Y., Xiao, J., Shen, L., 2009. Simulation of methanol production from biomass gasification in interconnected fluidized beds. Ind. Eng. Chem. Res. 48, 5351–5359.

Zhao, Y., Huang, Z., Zhang, K., Li, S., 2007. Investigation of low-temperature methanol synthesis in a bubble column slurry reactor with a flash column. Fuel Process. Technol. 88, 137–142.

Zhu, W., Gora, L., Van Den Berg, A., Kapteijn, F., Jansen, J., Moulijn, J., 2005. Water vapour separation from permanent gases by a zeolite-4A membrane. J. Membr. Sci. 253, 57–66.

This page intentionally left blank

CHAPTER 21

Modeling of the Di Methyl Ether Production Reactors

Marjan Alavi, Nazanin Hamedi, Mohammad R. Rahimpour

Shiraz University, Shiraz, Iran

Acronyms

ANN	artificial neural network
DBM	data based models
DE	differential evolution
DME	dimethyl ether
FPM	first principle models
WHSV	weight hourly space velocity (kg kg_{cat}^{-1} h^{-1})

Symbols

C	molar concentration (mol $m^{-3)}$
D	reactor diameter (m)
K_{eq}	thermodynamic equilibrium constant (m^3 $kmol^{-1}$)
k_s	reaction rate constant (kmol kg^{-1} h^{-1})
K_i	adsorption constants of component i (m^3 $kmol^{-1}$)
L	reactor length (m)
P	pressure (bar)
R	gas constant (J mol^{-1} K^{-1})
r	reaction rate (mol kg^{-1} s^{-1})
T	temperature (K)

Greek letters

η	catalyst effectiveness factor (dimensionless)

Methanol. https://doi.org/10.1016/B978-0-444-63903-5.00021-2

1 Introduction

Dimethyl ether or methoxy methane is the simplest ether with the chemical formula of CH_3OCH_3. Its boiling point is −25°C and when it is pressurized above 0.5 MPa at ambient temperature, it condenses to the liquid phase (Semelsberger et al., 2006). DME synthesis has received more attention in the past decades due to its potential applications as a suitable fuel. During the combustion of DME, since no harmful components like NO_x smoke or particulates is formed, it is regarded as a clean energy source for the next generation of fuels (Fleisch et al., 1997). Natural gas, coal, and biomass are considered to be the resources for DME production that result in reducing the energy dependence on oil.

Two methods have been applied for DME production. In the first method, which is known as the direct method, DME is directly produced from the synthesis of gases. First the gases, which include CO, CO_2, and H_2, are synthesized to methanol, and then DME is produced by methanol dehydration (Cheng et al., 2011).

The conventional method, which is known as the indirect method, employs the dehydration of methanol over solid-acid catalysts such as HZSM-5 or γ-Al_2O_3 (Xu et al., 1997).

$$2CH_3OH \leftrightarrow CH_3OCH_3 + H_2O \quad -23.0\,kJ\,mol^{-1} \tag{21.1}$$

Al_2O_3 is used as a common catalyst because of its fine particle size, high surface area, surface catalytic activity, excellent thermal stability, high mechanical resistance, and wide range of chemical, physical, and catalytic properties among the various crystalline phases of Al_2O_3. γ-Al_2O_3 has received much attention due to the less generation of a by-product. In order to improve the acidity of γ-Al_2O_3, the addition of some dopants such as borate, silica, phosphorous, and fluorine has been studied. Also, some zeolites like ZSM-5 and HZSM-5 are used as proper catalysts for this reaction (Laugel et al., 2011).

DME can be produced in fluidized-beds (Lu et al., 2004) or fixed-bed reactors (Song et al., 2008). Fluidized-bed reactors have the best mass and heat transfer capabilities compared to the other class of reactors. However, they are more complex and expensive in design and operation.

The reaction rate equation and kinetics of methanol dehydration on acidic catalysts have been studied extensively. Bercic and Levec (1992) published the different reaction rate equations which are presented in Table 21.1.

Bercic claimed that most of these reaction rates have been provided in such experimental conditions that may not be common in industrial reactors. Since water is one of the main products and it can also be present in the methanol feed, most of these reaction rates are not useful for industrial scales. So, they performed some special studies on methanol dehydration reaction on γ-Al_2O_3, assuming the surface reaction to be the rate controlling step, and used the Langmuir-Hinshelwood mechanism to apply it, so the following global reaction rate was obtained (Bercic and Levec, 1993).

Table 21.1 Summery of the published reaction rate equations (Bercic and Levec, 1992)

Reference	The Reaction Rates
Kallo and Knozinger (1967)	$-r_M = K\dfrac{C_M^{1/2}}{C_M^{1/2} + k_2 C_W}$ [b]
Gates and Johanson (1971) Sinicyna at al. (1986)	$-r_M = \dfrac{K \cdot K_M^2 C_M^2}{(1 + K_M C_M + K_W C_W)^2}$ [a, b]
Figueras et al. (1971)	$-r_M = \dfrac{K \cdot K_M \cdot C_M^{1/2}}{\left(1 + K_M \cdot C_M^{1/2} + K_W \cdot C_W\right)}$ [b]
Than et al. (1972)	$-r_M = K\dfrac{K_M \cdot C_M^{1/2}}{(1 + K_M C_W)^2}$ [a]
Schmitz (1978)	$-r_M = K_1 + K_2 \cdot C_M$ [b]
Rubio et al. (1980)	$-r_M = K_1 C_M^{1/2} - K_2 C_W^{1/2}$ [b]
Klusacek and Schneider (1982)	$-r_M = \dfrac{K \cdot K_M C_M}{\left(1 + 2\sqrt{K_M C_M} + K_W C_W\right)^2}$
	$-r_M = \dfrac{K \cdot K_M C_M^2}{\left(1 + 2\sqrt{K_M C_M} + K_W C_W\right)^3}$ [a]
	$-r_M = \dfrac{K \cdot K_M C_M^2}{\left(1 + 2\sqrt{K_M C_M} + K_W C_W\right)^4}$

[a] Acidic ion exchange resin as catalyst.
[b] Alumina or silica-alumina as catalyst.

$$-r_M = \frac{k_s \cdot K_M^2 \left(C_M^2 - C_W \cdot C_D / K_{eq}\right)}{\left(1 + 2\sqrt{K_M C_M} + K_W C_W\right)^4} \tag{21.2}$$

C_M, C_W, and C_D are, respectively, the molar concentrations of methanol, water and, DME. k_s is the reaction rate constant and K_{eq} is the equilibrium constant. K_M and K_W are respectively, the adsorption constants of methanol and water and they can be calculated as follows:

$$k_s = 5.35 \times 10^{13} \exp(-17280/T) \tag{21.3}$$

$$K_M = 5.39 \times 10^{-4} \exp(8487/T) \tag{21.4}$$

$$K_W = 8.47 \times 10^{-2} \exp(5070/T) \tag{21.5}$$

Table 21.2 Equilibrium constants for methanol dehydration in literature (Diep and Wainwright, 1987)

Reference	Equilibrium Constant
Given (1943)	$\ln K_{eq} = 7300/RT - 4.8$
Hayashi and Moffat (1982)	$\ln K_{eq} = 3440/T - 1.67\ \ln T + 2.39 \times 10^{-4} T + 0.055 \times 10^{-6} T^2 + 5.496$
Diep and Wainwright (1987)	$\ln K_{eq} = 2835.2/T - 1.675\ \ln T - 2.39 \times 10^{-4} T - 0.21 \times 10^{-6} T^2 - 13.36$

Research indicates that this reaction rate is more global than other proposed ones.

Because of the exothermic and reversible nature of this reaction, yields are extremely subject to the thermodynamic behavior of the system. Several relationships describing the temperature dependence of the equilibrium constant for the dehydration of methanol have been introduced in the literature. Diep and Wainwright (1987) has extensively studied the thermodynamic and equilibrium condition of this reaction. A short summary of their investigations are in Table 21.2.

The equilibrium constant introduced by the Bercic and Levec model has been used widely in fixed-bed reactor modeling papers (Bercic and Levec, 1993).

$$\ln K_{eq} = 3138/T + 0.86\ \ln T + 1.33 \times 10^{-3} T - 1.23 \times 10^{-5} T^2 + 3.5 \times 10^{-10} T^3 \qquad (21.6)$$

2 Process Modeling

Reactor models are used in the design, operation, and optimization of industrial reactors. Reliable mathematical models and mathematical techniques are the key factors for the design of new equipment and the optimization of the existing ones. This task can be performed by three different types: first principle models (FPM), data based models (DBM), and hybrid models.

2.1 First Principle Models

To have a model that describes the behavior of a system properly, having complete and detailed knowledge of the process is necessary. Using this knowledge as the mass/energy/momentum balance and applying thermodynamic laws, leads to the first principle or white box model, which is the most accurate kind of model. The behavior of the process is well understood and is clearly perceptible. But it is sometimes impossible to take into account all the parameters affecting the process, so it will be necessary to apply a number of simplifications that may cause some inaccuracies.

White box modeling of chemical reactors are categorized into different groups due to the reactor state and conditions. When the only major transport mechanism is convection, the

model is referred to as a plug-flow model and is known as the one-dimensional model. In the two-dimensional model, the radial temperature and concentration profiles are also considered and the concentration and temperature profiles are available not only on the axial coordinate but also on the radial coordinate. When the ratio of L/D (reactor length to its diameter) is significantly high, for example more than 50, a one-dimensional approach is suitable (Farsi et al., 2011).

In a simple model, both phases can be assumed as one and a pseudo-homogenous model is constructed. All the models can be developed in static or dynamic states.

Pseudo-homogenous models are the simplest to use in catalytic fixed bed reactor modeling. The basic assumption made is that the reactor can be described as an entity consisting only of a single phase. Actually two phases are present: the solid catalytic phase and the bulk gas phase. In other words, this model assumes that all catalyst surfaces are totally exposed to the bulk conditions and have the same condition as the bulk fluid and can thus be fully described by bulk variables (temperature, concentration, pressure). This is strictly valid when (the catalyst effectiveness factor) $\eta = 1$ for all reactions and/or components (Ghavipour and Behbahani, 2014).

By considering the fluid as a different phase from the solid catalyst phase, a concentration and temperature difference will be present between the catalyst surface and the bulk phase so this is a heterogeneous model. Actually, it is necessary to distinguish between the bulk fluid phase and the catalyst surface as well as between the surface of the pellet and inside the catalyst pore. Thus mass and energy conversion equations are written separately for both phases.

In a general case, where the active material is dispersed through the pellet and the catalyst is porous, internal diffusion of the species within the pores must be included. In these conditions, $\eta \neq 1$ and must be calculated along the reactor.

Modeling the fixed-bed DME synthesis reactors have been considered in lots of research studies. A short summary of these researches are shown in Table 21.3.

Nasehi et al. (2006) considered an industrial adiabatic fixed-bed reactor for DME production from methanol dehydration in steady state condition, but their results showed little difference between one- and two-dimensional models.

An unsteady state heterogeneous model was developed by Farsi et al. (2011) to simulate the dynamic behavior of an industrial DME production reactor. The model was tested using real data from an industrial plant. A conventional feedback controller was designed to maintain the inlet temperature at the chosen value (Farsi et al., 2011).

Bercic and Levec (1993) introduced a pseudo homogenous and three heterogeneous one-dimensional steady state models for DME production in an adiabatic fixed bed reactor. They showed that a homogenous model, after neglecting the intra-particle gradients and assuming

Table 21.3 A summary of some published studies on the fixed bed reactor modeling of DME

Model Type	State	Balance			Ref.
		Mass	Energy	Momentum	
One-dimensional non adiabatic, pesudo-homogenious	Steady	●	●	●	Nasrollahi et al. (2013)
One-dimensional, heterogeneous	Unsteady	●	●	●	Farsi (2015)
One-dimensional, heterogeneous	Unsteady	●	●	●	Ghavipour and Behbahani (2014)
One-dimensional, pesudo-homogenious	Unsteady	●	●		Tavan et al. (2013)
One-dimensional, pesudo-homogenious	Steady	●			Pisarenko and Pisarenko (2014)
One-dimensional, heterogeneous	Unsteady	●	●	●	Farsi et al. (2011)

the amount of effectiveness factor of the catalysts to be one, can describe the behavior of the reactor correctly without having significant differences from the actual performance.

A one-dimensional steady state pseudo homogenous model was proposed by Fazlollahnejad et al. (2009) for a bench scale adiabatic reactor. Their model was validated with real data demonstrating the effects of the weight hourly space velocity (WHSV) and feed temperature on methanol conversion. The maximum conversion reported was approximately equal to 95.8% at 603.15 K with WHSV of 72.87 h^{-1}.

2.1.1 Data based models

When a set of experimental data rather than the full prior knowledge is available for a system, connecting the input, output data sets results in a model known as data-based model or black-box model. Very common examples in this category are fuzzy logic, nonlinear regression, and Artificial Neural Networks (ANN) (Baş et al., 2007).

Valeh-e-Sheyda et al. (2010) applied an ANN to estimate the reaction rate of MeOH dehydration to DME synthesis. The output of the network was the reaction rate. The ultimate ANN results showed a good agreement with the experimental data.

DBMs can be employed to predict the output of the whole system or combined with the first principle model. This combination called the hybrid model incorporates two configurations. In the serial configuration, the unknown parameters in the process are estimated by ANN and the output is fed to the first principle model as one of its inputs. In parallel configuration, the ANN model tries to decrease the error between the actual output of the system and the output calculated by FPM by compensating the difference in values (Psichogios and Ungar, 1992).

Alavi et al. (2014) found an optimum operating condition in the DME synthesis reactor that maximized methanol equilibrium conversion. In this work, a hybrid model and a first principle model were developed to simulate the adiabatic fixed-bed reactor for DME production. The results presented clearly show that the predicted outputs of the proposed hybrid model were almost close to the outputs obtained by the first principle model while the hybrid model operated about 20 times faster.

Though, despite the simplicity of DBMs, they are not perceptible and they can't perform well beyond the data being used, which results in poor generalization.

3 Process Intensification

In any process, a significant incentive to improve the overall result, leads to the applications of different process intensification techniques. Methanol conversion to DME conventionally takes place in an adiabatic, fixed bed reactor in which the feed uses the heat of the product stream to reach the designed temperature (Samimi et al., 2013a).

However, this reactor configuration has some problems, which can be overcome by means of various process intensification techniques. During the past years, many researchers have proposed different methods for improving the performance of the reactor of methanol conversion to DME. First, some of the most important process intensification techniques from this study will be briefly explained and afterwards the studies applying those techniques to the reactor of methanol conversion to DME will be reviewed.

When it comes to process intensification methods for improving a reactor performance, spherical reactors play a major role. Indeed, spherical reactors provide a larger cross sectional area in comparison with tubular reactors, leading to lower pressure drop. Thus, when a reactor has a huge pressure drop, spherical reactors are considerably useful. In fact, the lower pressure drop contributes to considerable advantages, which are listed as follows:

- Lower pressure drop in spherical reactors in comparison with tubular reactors, causes lower recompression power.
- Using smaller catalyst particles eliminates the internal mass transfer, and therefore improves the overall reaction rate and reactor performance. On the other hand, it causes a huge pressure drop in fixed bed reactors. Applying spherical reactors, and significantly lowering the pressure drop, allows the application of smaller catalyst particles.
- By lowering pressure drop, it is possible to use higher feed flow rate, resulting in more significant plant productivity.
- In spherical membrane reactors, the required membrane surface is considerably lower in comparison with tubular, membrane reactors.
- Because of the lower reactor thickness in spherical reactors, the fabrication cost would be reduced (Rahimpour et al., 2011).

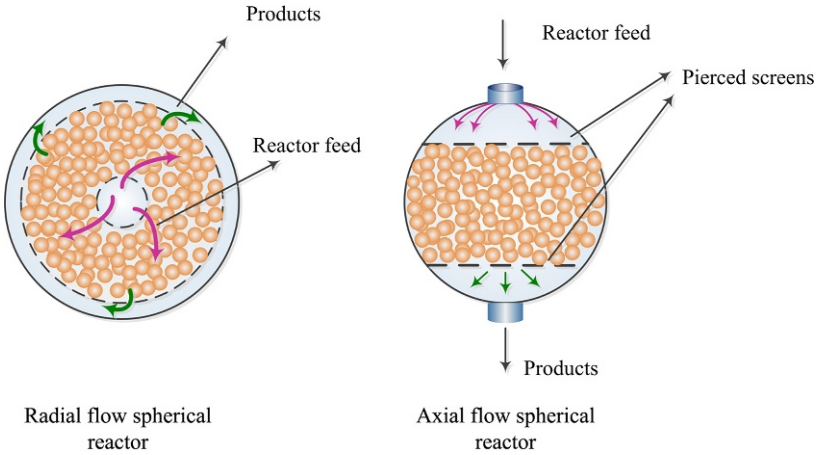

Fig. 21.1
A schematic diagram of axial and radial flow spherical reactors.

As shown in Fig. 21.1, the catalysts are held by two pierced screens, which mechanically support the catalyst and provide a uniform flow distribution. It is worth mentioning that based on the flow regime, spherical reactors are divided into axial and radial flow reactors.

One of the leading-edge technologies for process investigation is the concept of membrane reactors. Generally, in a membrane reactor, a specific reactant transfers through the membrane and is partially eliminated from the reaction medium. As a result, the reaction thermodynamically shifts towards the production side. Apart from their benefits of higher production rate, they also separate one of the products; hence, the separation step is much more cost effective. It should be noted that separation by membrane does not require any phase change, so it is more energy efficient and provides low maintenance operation (Iranshahi et al., 2012)

To take advantage of membrane reactors in methanol dehydration reactions, a suitable membrane should be chosen that is selective in water or DME. In view of this fact, hydroxy sodalite (HSOD) membrane has gained much attention, as it is a 100% selective membrane for water removal. HSOD is a zeolite-like material which works based on a molecular sieve, and enjoys very good thermal and mechanical stability. It is reported that the maximum possible permeation rate of this membrane is 10^{-6} mol/s m^2 Pa (Khajavi et al., 2009, 2010; Breck, 1973; Rohde et al., 2008). Obviously, a sweep gas must be applied to maintain the driving force high enough during the process. Usually, N_2 is used to sweep the permeated H_2O (Samimi et al., 2013a).

Besides using a membrane, another way to separate one of the products from the reaction media and, as a result shifting the equilibrium to the right, is the application of adsorbents. In this type of reactor, the gas phase (reactant and products) flows through a catalytic bed, along

with fine solid particles, flowing co-currently or counter-currently. The solid particles adsorb one of the products and increase the reaction conversion. The fluid dynamics of such systems are developed based on mass and heat transfer studies. Usually, these reactors are referred to as gas-flowing solids-fixed bed contactors, gas-solid-solid trickle flow contactors, or raining packed bed contactors (Westerterp and Kuczynski, 1987; Bayat et al., 2014).

Nowadays, the coupling of the exothermic and endothermic reactions in a single reactor is one of the methods, contributing to the improvement in energy efficiency and reduction of harmful emissions. These multifunctional reactors make the process more effective and reduce the costs (Agar, 1999). In these configurations, the heat generated by the exothermic reaction transmits to the endothermic side without any reactant mixing between these two sides (Kolios et al., 2002). As seen in Fig. 21.2, these reactors consist of two concentric tubes, and in order to avoid heat loss, usually the exothermic reaction is considered to take place in the inner tube. Since methanol conversion to DME is an exothermic reaction, it should be coupled with an appropriate endothermic reaction. Indeed, the two coupled reactions should be chosen in a way that heat transfers from the exothermic to the endothermic side; that is, the temperature of the exothermic side is higher than that of the endothermic side (Rahimpour et al., 2010; Patel and Sunol, 2007).

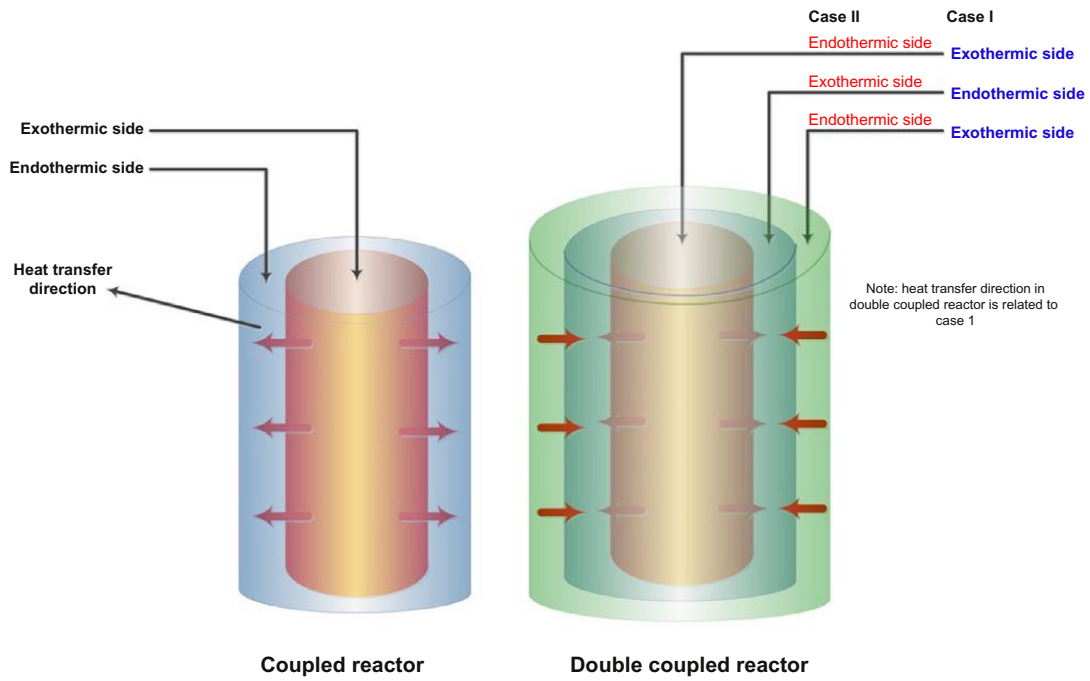

Fig. 21.2
A schematic diagram of coupled and double coupled reactors.

One of the state of the art process intensification techniques is double coupled reactors. In these reactor configurations, two exothermic and one endothermic reactions (or vice versa) are involved. In fact, the required heat for the endothermic sides is provided by the generated heat in the exothermic side (in the case of two endothermic and one exothermic reactions). Usually, in a double coupled reactor concept, three concentric cylinders are considered, in which the inner, middle, and outer tubes are, respectively, used for suitable exothermic, endothermic, and exothermic reactions, or vice versa (see Fig. 21.2). It is worth mentioning that a double coupled configuration is significantly beneficial for multi-objective reactors. In other words, this reactor configuration has the potential for simultaneous production of several components, leading to lower production cost and smaller reactors (Rahimpour et al., 2013; Farniaei et al., 2013)

Conventionally, the reaction of DME production from methanol takes place in an adiabatic, fixed bed reactor. However, this reactor configuration has some shortcomings. Given the fact that the reaction is exothermic, using an isothermal reactor would be clearly beneficial. This idea has been proposed by Farsi et al. (2010). They suggested an optimized, shell and tube, fixed bed reactor, in which saturated water was used to absorb the generated heat of the exothermic reaction of methanol dehydration to DME. Moreover, they applied a genetic algorithm to determine the optimum temperature profile along the reactor. Their result proved the superiority of the isothermal reactor rather than the conventional, adiabatic reactor.

Afterwards, the same group improved the reactor performance by suggesting an isothermal, membrane reactor (Farsi and Jahanmiri, 2011a). They proposed a one-dimensional, heterogeneous, steady state model which was based on mass and energy conservation laws. To verify the effect of the membrane, the obtained results of the isothermal, membrane reactor were compared with those of the isothermal and conventional, adiabatic reactors. Their study demonstrated that using the membrane caused higher methanol conversion and resulted in lower purification cost.

Subsequently, much attention has been paid to address a thermally coupled reactor configuration for methanol dehydration to DME. Khademi et al. (2011) conducted a study on an optimal thermally coupled heat exchanger reactor design for simultaneous production of DME and benzene. The reactions of DME production from methanol and cyclohexane dehydrogenation to benzene were respectively taken into account as the exothermic and endothermic reactions. Also, DE optimization method, as a heuristic useful optimization technique, was applied to find the optimum operating conditions, contributing to a higher reactor yield. As desired products, DME and benzene mole fractions were considered as the decision variables. Their study demonstrated a reactor design for simultaneous DME and benzene production, reducing the overall cost and size of the reactor.

Moreover, in the same year, Farsi and Jahanmiri (2011b) proposed a steady state, heterogeneous mathematical model to predict the performance of a thermally coupled dual membrane reactor. In the proposed reactor structure, the necessary heat of the reaction of dehydrogenation of cyclohexane to benzene was provided by the exothermic reaction of dehydration of methanol to DME. Both Pd/Ag and a composite membrane were applied to respectively separate hydrogen from the endothermic side and water vapor from the exothermic side. Furthermore, they applied DE optimization method to maximize the summation of DME mole fraction in the outlet of the exothermic side, benzene mole fraction in the outlet of endothermic side, and hydrogen mole fraction in the permeation side. Their study proved the feasibility and advantages of the optimized thermally coupled membrane reactor, in which methanol conversion was higher than that of the conventional reactor.

Apart from membrane and thermally coupled reactors, the concept of spherical reactors is extremely beneficial for the process of methanol conversion to DME. In 2013, Samimi et al. (2013a) proposed a novel axial-flow, spherical membrane reactor for methanol dehydration, which was constructed with two concentric spheres. The inner sphere filled with catalysts, where the reaction took place and it was surrounded by hydroxy sodalite membrane to separate water from the reaction medium. They used N_2 as the sweep gas, which flowed in the outer sphere to collect the separated H_2O. Then, the differential evolution (DE) optimization technique was applied to find the optimum value of operating conditions and length per radius, resulting in the maximum mole fraction of DME in the outlet stream. The results indicated the superiority of the optimized spherical membrane reactor in comparison with conventional, spherical, and nonoptimized configurations.

Subsequently, Farsi (2014) investigated the flow regime effect on the reactor performance, with the previous reactor configuration examined using a radial flow pattern. Their study focused on developing a suitable mathematical model for a spherical, membrane reactor with radial flow regime. In the proposed reactor configuration, two concentric spheres were considered, so that the inner sphere was used for feed distribution. The catalysts were placed between the two spheres, and this catalytic zone was radially divided by membranes, separating H_2O from the reaction zone and shifting the equilibrium to the production side. Both one and two stage reactor configurations were examined and their performances were compared. Their suggested reactor configurations offered the advantages of lower pressure drop, higher methanol conversion, and it reduced the next stage purification cost. The result showed that the two-stage, radial flow, membrane, and spherical reactors led to a higher DME production rate.

In terms of applying adsorbents to improve the reactor performance, Hamidi et al. (2015) used Zeolite 4A ($Na_{12}(Si_{12}Al_{12}O_{48})_{27}H_2O$) as a selective adsorbent for H_2O in the reactor of methanol conversion to DME. In other words, they suggested a trickle bed reactor in which the solid adsorbents and gas stream flowed co-currently over the fixed catalytic bed. The

adsorbents were continuously regenerated and fed to the top of the reactor. They applied a steady-state, one-dimensional mathematical model to predict the reactor behavior. They concluded that the H_2O removal by the adsorbent led to a higher DME production rate.

Recently, Bakhtyari et al. (2016a) went one step further and developed a reactor design in which three reactions were thermally coupled and HSOD water perm-selective membranes were applied in the inner and outer reactor walls. In their proposed reactor configuration, the exothermic reactions of DME production from syngas and methanol supplied the required heat for the endothermic reaction of methanol conversion to methyl formate. In addition, optimum operating conditions were found by means of the genetic algorithm optimization method. The superiority of the proposed reactor configuration was proved by reaching higher DME and methyl formate conversions.

The aforementioned research is just some of the published articles addressing the important topic of process intensification for the reactor of methanol conversion to DME. Most of the studies related to this topic are reviewed in Table 21.4.

4 Conclusion and Future Trends

Due to the growing concerns of environmental pollution, energy security, and future oil supplies, the global community is looking for nonpetroleum based alternative fuels to increase the efficiency of energy use. Compared to some of the other leading alternative fuel candidates (i.e., methane, methanol, ethanol, and Fischer-Tropsch fuels), DME has been proved to be a suitable candidate since it is a clean high-efficiency compression ignition fuel with reduced NO_x, SO_x, and particulate material. It can be efficiently converted to hydrogen at low temperatures, and does not have large concerns with toxicity, production, infrastructure, and transportation. On the other hand, DME has received much attention because of its possible application as a fuel and a chemical feedstock. It is well known that DME is a main intermediate formed from methanol dehydration in the mechanism studies of methanol to olefins. DME is also used in aerosol spray propellants as a chlorofluorocarbon replacement.

DME can be produced via methanol dehydration in a fixed bed reactor. Mathematical modeling this system is an excellent tool to simulate the physical and chemical behavior of the process. A good prior knowledge to the system must be in hand to be a reliable model. This prior knowledge decreases the unnecessary consumption of time and energy in the experiments.

Different modeling approaches for DME production in fixed bed reactors has been discussed in this chapter and the most recent findings in this area have been completely presented.

Table 21.4 A review of different studies related to process intensification methods for the reactor of methanol conversion to DME

Summary	Reactor Type	Flow Pattern	Membrane	Coupling Technique	Optimization Technique	Reference
A one-dimensional heterogeneous model was proposed for the isothermal reactor of methanol conversion to DME.	Shell and tube, fixed bed	Axial, concurrent	–	–	Genetic algorithm	Farsi et al. (2010)
The reactions of methanol dehydration and cyclohexane dehydrogenation were thermally coupled and optimized.	Multi-tubular	Axial, concurrent	–	The reaction of cyclohexane dehydrogenation was used as the endothermic reaction.	DE	Khademi et al. (2011)
A isothermal membrane reactor of methanol conversion to DME was examined.	Shell and tube, fixed bed, membrane	Axial, concurrent	Water-selective alumina-silica composite membrane	–	Genetic Algorithm	Farsi and Jahanmiri (2011a)
A thermally coupled, dual-membrane reactor for simultaneous production of hydrogen, dimethyl ether (DME) and benzene was investigated.	Multi-tubular	Axial, concurrent	Pd/Ag and composite membranes were respectively used for hydrogen and water separation in endothermic and exothermic sides.	The reaction of cyclohexane dehydrogenation was used as the endothermic reaction.	DE	Farsi and Jahanmiri (2011b)

Continued

Table 21.4 A review of different studies related to process intensification methods for the reactor of methanol conversion to DME—cont'd

Summary	Reactor Type	Flow Pattern	Membrane	Coupling Technique	Optimization Technique	Reference
DME, hydrogen, and benzene were simultaneously produced in a thermally coupled reactor.	Multi-tubular	Axial, concurrent	Pd/Ag membrane for hydrogen separation from the endothermic side.	The reaction of cyclohexane dehydrogenation was used as the endothermic reaction.	DE	Vakili et al. (2012)
An optimized, spherical membrane reactor was suggested, in which the membrane was selective for H_2O.	Spherical packed-bed membrane	Axial	Hydroxy sodalite membrane for H_2O removal.	–	DE	Samimi et al. (2013a)
Two serial spherical reactors were proposed for methanol conversion to DME.	Spherical, packed bed	Axial	–	–	DE	Samimi et al. (2014)
Three serial reactor configurations were considered for the reaction of DME synthesis from methanol.	Spherical, packed bed	Radial	–	–	Genetic algorithm	Farsi et al. (2014)

A thermally coupled dual membrane reactor was considered for the reactions of methanol dehydration and decalin dehydrogenation.	Multi-tubular	Axial, concurrent	A Pd/Ag membrane and a hydroxy sodalite (HSOD) membrane were used for hydrogen and H_2O removal, respectively.	The reaction of decalin dehydrogenation was used as the endothermic reaction.	DE	Samimi et al. (2013b)
A double-coupled, dual membrane reactor was proposed for simultaneous methanol synthesis, methanol dehydration, and methyl cyclohexane dehydrogenation.	Multi-tubular	Axial, concurrent	Hydroxy sodalite membrane for H_2O removal from both exothermic sides.	The exothermic reactions of methanol synthesis and methanol dehydration occurred in the inner and outer tubes while the methyl cyclohexane dehydrogenation, as a endothermic reaction, took place in the middle tube.	DE	Samimi et al. (2013c)
Multi-stage, spherical, membrane reactors were suggested for DME production from methanol.	Spherical, packed bed	Radial	Selective membrane for H_2O removal.	–	–	Farsi (2014)
The effect of Pd-Ag membrane was investigated in a thermally coupled reactor.	Multi-tubular membrane	Axial, concurrent	Pd-Ag membrane for H_2 removal from the endothermic side.	The endothermic reaction of methanol dehydrogenation to methyl formate and hydrogen was used in the thermally coupled reactor.	–	Bakhtyari et al. (2015)

Continued

Table 21.4 A review of different studies related to process intensification methods for the reactor of methanol conversion to DME—cont'd

Summary	Reactor Type	Flow Pattern	Membrane	Coupling Technique	Optimization Technique	Reference
A thermally coupled dual membrane reactor was proposed for simultaneous dimethyl ether, methyl formate, and hydrogen production.	Multi-tubular membrane	Axial, concurrent	A Hydroxy sodalite, water selective membrane and Pd-Ag membrane were used for H_2O and H_2 removal, respectively.	The endothermic reaction of methanol dehydrogenation to methyl formate and hydrogen was used in the thermally coupled reactor.	Genetic algorithm	Bakhtyari et al. (2016b)
The reactions of DME production from methanol, and syngas were thermally coupled with the reaction of methanol dehydrogenation to methyl formate, in which H_2O perm-selective membrane was used.	Multi-tubular membrane	Axial, concurrent	A Hydroxy sodalite, water selective membrane was used in both the exothermic sides.	A double-coupled reactor configuration was proposed, in which the endothermic reaction of methanol dehydration was coupled with two exothermic reactions of ME synthesis from syngas and methanol.	Genetic algorithm	Bakhtyari et al. (2016a)

References

Agar, D.W., 1999. Multifunctional reactors: old preconceptions and new dimensions. Chem. Eng. Sci. 54, 1299–1305.

Alavi, M., Jazayeri-Rad, H., Behbahani, R.M., 2014. Optimizing the feed conditions in a dimethyl ether production process to maximize methanol conversion using a hybrid first principle neural network approach. Chem. Eng. Commun. 201, 650–673.

Bakhtyari, A., Mohammadi, M., Rahimpour, M.R., 2015. Simultaneous production of dimethyl ether (DME), methyl formate (MF) and hydrogen from methanol in an integrated thermally coupled membrane reactor. J. Nat. Gas Sci. Eng. 26, 595–607.

Bakhtyari, A., Haghbakhsh, R., Rahimpour, M.R., 2016a. Investigation of thermally double coupled double membrane heat exchanger reactor to produce dimethyl ether and methyl formate. J. Nat. Gas Sci. Eng. 32, 185–197.

Bakhtyari, A., Parhoudeh, M., Rahimpour, M.R., 2016b. Optimal conditions in converting methanol to dimethyl ether, methyl formate, and hydrogen utilizing a double membrane heat exchanger reactor. J. Nat. Gas Sci. Eng. 28, 31–45.

Baş, D., Dudak, F.C., Boyaci, İ.H., 2007. Modeling and optimization III: reaction rate estimation using artificial neural network (ANN) without a kinetic model. J. Food Eng. 79, 622–628.

Bayat, M., Hamidi, M., Dehghani, Z., Rahimpour, M.R., Shariati, A., 2014. Hydrogen/methanol production in a novel multifunctional reactor with in situ adsorption: modeling and optimization. Int. J. Energy Res. 38, 978–994.

Bercic, G., Levec, J., 1992. Intrinsic and global reaction rate of methanol dehydration over .gamma.-alumina pellets. Ind. Eng. Chem. Res. 31, 1035–1040.

Bercic, G., Levec, J., 1993. Catalytic dehydration of methanol to dimethyl ether. Kinetic investigation and reactor simulation. Ind. Eng. Chem. Res. 32, 2478–2484.

Breck, D.W., 1973. Zeolite Molecular Sieves: Structure, Chemistry, and Use. Wiley, New York.

Cheng, C., Zhang, H., Ying, W., Fang, D., 2011. Intrinsic kinetics of one-step dimethyl ether synthesis from hydrogen-rich synthesis gas over bi-functional catalyst. Korean J. Chem. Eng. 28, 1511–1517.

Diep, B.T., Wainwright, M.S., 1987. Thermodynamic equilibrium constants for the methanol-dimethyl ether-water system. J. Chem. Eng. Data 32, 330–333.

Farniaei, M., Abbasi, M., Rasoolzadeh, A., Rahimpour, M.R., 2013. Enhancement of methanol, DME and hydrogen production via employing hydrogen permselective membranes in a novel integrated thermally double-coupled two-membrane reactor. J. Nat. Gas Sci. Eng. 14, 158–173.

Farsi, M., 2014. DME production in multi-stage radial flow spherical membrane reactors: reactor design and modeling. J. Nat. Gas Sci. Eng. 20, 366–372.

Farsi, M., 2015. Dynamic modeling and controllability analysis of DME production in an isothermal fixed bed reactor. Chem. Eng. Res. Bull. 17, 12.

Farsi, M., Jahanmiri, A., 2011a. Enhancement of DME production in an optimized membrane isothermal fixed-Bed reactor. Int. J. Chem. React. Eng. 9, 1–18

Farsi, M., Jahanmiri, A., 2011b. Mathematical simulation and optimization of methanol dehydration and cyclohexane dehydrogenation in a thermally coupled dual-membrane reactor. Int. J. Hydrog. Energy 36, 14416–14427.

Farsi, M., Jahanmiri, A., Eslamloueyan, R., 2010. Modeling and optimization of MeOH to DME in isothermal fixed-bed reactor. Int. J. Chem. React. Eng. 8, 1–14.

Farsi, M., Eslamloueyan, R., Jahanmiri, A., 2011. Modeling, simulation and control of dimethyl ether synthesis in an industrial fixed-bed reactor. Chem. Eng. Process. Process Intensif. 50, 85–94.

Farsi, M., Asemani, M., Rahimpour, M.R., 2014. Mathematical modeling and optimization of multi-stage spherical reactor configurations for large scale dimethyl ether production. Fuel Process. Technol. 126, 207–214.

Fazlollahnejad, M., Taghizadeh, M., Eliassi, A., Bakeri, G., 2009. Experimental study and modeling of an adiabatic fixed-bed reactor for methanol dehydration to dimethyl ether. Chin. J. Chem. Eng. 17, 630–634.

Figueras, F., Nohl, A., Mourgues, L., Trambouze, Y., 1971. Dehydration of methanol and tert-butyl alcohol on silica-alumina. Trans. Faraday SOC 67, 1155–1163.
Fleisch, T.H., Basu, A., Gradassi, M.J., Masin, J.G., 1997. Dimethyl ether: a fuel for the 21st century. Studies in Surface Science and Catalysis 107, 117–125.
Gates, B.C., Johanson, L.N., 1971. Lungmuir-hinshelwood kinetics of the dehydration of methanol catalyzed by cation exchange resin. AIChE J. 17, 981–983.
Ghavipour, M., Behbahani, R.M., 2014. Fixed-bed reactor modeling for methanol to dimethyl ether (DME) reaction over γ-alumina using a new practical reaction rate model. J. Ind. Eng. Chem. 20, 1942–1951.
Given, P.H., 1943. Note. J. Chem. Soc. 589–589.
Hamidi, M., Samimi, F., Rahimpour, M.R., 2015. Dimethyl ether synthesis in a gas-solid-solid trickle flow reactor with continuous adsorbent regeneration. J. Taiwan Inst. Chem. Eng. 47, 105–112.
Hayashi, H., Moffat, J.B., 1982. The properties of heteropoly acids and the conversion of methanol to hydrocarbons. J. Catal. 77, 473–484.
Iranshahi, D., Pourazadi, E., Paymooni, K., Rahimpour, M.R., 2012. A novel dynamic membrane reactor concept with radial-flow pattern for reacting material and axial-flow pattern for sweeping gas in catalytic naphtha reformers. AICHE J. 58, 1230–1247.
Kallo, D., Knozinger, H. Zur, 1967. Dehydratisierung von alkoholen an aliminiumoksid. Chem. Ing. Tech. 39, 676–680.
Khademi, M.H., Farsi, M., Rahimpour, M.R., Jahanmiri, A., 2011. DME synthesis and cyclohexane dehydrogenation reaction in an optimized thermally coupled reactor. Chem. Eng. Process. Process Intensif. 50, 113–123.
Khajavi, S., Jansen, J.C., Kapteijn, F., 2009. Application of hydroxy sodalite films as novel water selective membranes. J. Membr. Sci. 326, 153–160.
Khajavi, S., Jansen, J.C., Kapteijn, F., 2010. Application of a sodalite membrane reactor in esterification—coupling reaction and separation. Catal. Today 156, 132–139.
Klusacek, K., Schneider, P., 1982. Stationary catalytic kinetics via surface concentrations from transient data methanol dehydration. Chem. Eng. Sci. 37, 1523–1528.
Kolios, G., Frauhammer, J., Eigenberger, G., 2002. Efficient reactor concepts for coupling of endothermic and exothermic reactions. Chem. Eng. Sci. 57, 1505–1510.
Laugel, G., Nitsch, X., Ocampo, F., Louis, B., 2011. Methanol dehydration into dimethylether over ZSM-5 type zeolites: raise in the operational temperature range. Appl. Catal. A Gen. 402, 139–145.
Lu, W.-Z., Teng, L.-H., Xiao, W.-D., 2004. Simulation and experiment study of dimethyl ether synthesis from syngas in a fluidized-bed reactor. Chem. Eng. Sci. 59, 5455–5464.
Nasehi, S.M., Eslamloueyan, R., Jahanmiri, A., 2006. Simulation of DME reactor from methanol. In: 11th Chemical Engineering Conference.
Nasrollahi, F., Bakeri, G., Ismail, A.F., Rahimnejad, M., Imanian, M., 2013. Development of a model for dimethyl ether non-adiabatic reactors to improve methanol conversion. Korean J. Chem. Eng. 30, 1867–1875.
Patel, K.S., Sunol, A.K., 2007. Modeling and simulation of methane steam reforming in a thermally coupled membrane reactor. Int. J. Hydrog. Energy 32, 2344–2358.
Pisarenko, E.V., Pisarenko, V.N., 2014. Modeling the low-temperature synthesis of dimethyl ether from methanol. Theor. Found. Chem. Eng. 48, 249–253.
Psichogios, D.C., Ungar, L.H., 1992. A hybrid neural network-first principles approach to process modeling. AICHE J. 38, 1499–1511.
Rahimpour, M.R., Khademi, M.H., Bahmanpour, A.M., 2010. A comparison of conventional and optimized thermally coupled reactors for Fischer-Tropsch synthesis in GTL technology. Chem. Eng. Sci. 65, 6206–6214.
Rahimpour, M.R., Iranshahi, D., Pourazadi, E., Paymooni, K., Bahmanpour, A.M., 2011. The aromatic enhancement in the axial-flow spherical packed-bed membrane naphtha reformers in the presence of catalyst deactivation. AICHE J. 57, 3182–3198.
Rahimpour, M.R., Farniaei, M., Abbasi, M., Javanmardi, J., Kabiri, S., 2013. Comparative study on simultaneous production of methanol, hydrogen, and DME using a novel integrated thermally double-coupled reactor. Energy Fuel 27, 1982–1993.

Rohde, M.P., Schaub, G., Khajavi, S., Jansen, J.C., Kapteijn, F., 2008. Fischer-Tropsch synthesis with in situ H_2O removal—directions of membrane development. Microporous Mesoporous Mater. 115, 123–136.

Rubio, F.C., Diaz, S.D., Castillo, D.D., Trujillo, J.D., Alvarez, R.A., 1980. Deshidratacion catalitica de metanol en fase vapor. Ing. Quim. (Madrid) 12, 113–119.

Samimi, F., Bayat, M., Karimipourfard, D., Rahimpour, M.R., Keshavarz, P., 2013a. A novel axial-flow spherical packed-bed membrane reactor for dimethyl ether synthesis: simulation and optimization. J. Nat. Gas Sci. Eng. 13, 42–51.

Samimi, F., Kabiri, S., Mirvakili, A., Rahimpour, M., 2013b. Simultaneous dimethyl ether synthesis and decalin dehydrogenation in an optimized thermally coupled dual membrane reactor. J. Nat. Gas Sci. Eng. 14, 77–90.

Samimi, F., Kabiri, S., Mirvakili, A., Rahimpour, M.R., 2013c. Simultaneous dimethyl ether synthesis and decalin dehydrogenation in an optimized thermally coupled dual membrane reactor. J. Nat. Gas Sci. Eng. 14, 77–90.

Samimi, F., Bayat, M., Rahimpour, M.R., Keshavarz, P., 2014. Mathematical modeling and optimization of DME synthesis in two spherical reactors connected in series. J. Nat. Gas Sci. Eng. 17, 33–41.

Schmitz, G., 1978. Deshydration dumethanol sur silice-slumine. Chim. Phys. 75, 650–655.

Semelsberger, T.A., Borup, R.L., Greene, H.L., 2006. Dimethyl ether (DME) as an alternative fuel. J. Power Sources 156, 497–511.

Sinicyna, O.A., Cumakova, V.N., Moskovskaja, I.F., 1986. Kinetika degidratacii metanola do dimetilovogo efira na SVK ceolite. Kinet. Katal. 27, 1160–1162.

Song, D., Cho, W., Lee, G., Park, D.K., Yoon, E.S., 2008. Numerical analysis of a pilot-scale fixed-Bed reactor for dimethyl ether (DME) synthesis. Ind. Eng. Chem. Res. 47, 4553–4559.

Tavan, Y., Hosseini, S.H., Ghavipour, M., Khosravi NIKOU, M.R., Shariati, A., 2013. From laboratory experiments to simulation studies of methanol dehydration to produce dimethyl ether—Part I: Reaction kinetic study. Chem. Eng. Process. Process Intensif. 73, 144–150.

Than, L.N., Setinek, K., Beranek, L., 1972. Kinetics and adsorption on acid catalysts. IV. Kinetics of gas-phase dehydration of methanol on a sulphonated ion exchanger. Collect. Czech. Commun. 37, 3878–3884.

Vakili, R., Rahimpour, M.R., Eslamloueyan, R., 2012. Incorporating differential evolution (DE) optimization strategy to boost hydrogen and DME production rate through a membrane assisted single-step DME heat exchanger reactor. J. Nat. Gas Sci. Eng. 9, 28–38.

Valeh-E-Sheyda, P., Yaripour, F., Moradi, G., Saber, M., 2010. Application of artificial neural networks for estimation of the reaction rate in methanol dehydration. Ind. Eng. Chem. Res. 49, 4620–4626.

Westerterp, K.R., Kuczynski, M., 1987. A model for a countercurrent gas-solid-solid trickle flow reactor for equilibrium reactions. The methanol synthesis. Chem. Eng. Sci. 42, 1871–1885.

Xu, M., Lunsford, J.H., Goodman, D.W., Bhattacharyya, A., 1997. Synthesis of dimethyl ether (DME) from methanol over solid-acid catalysts. Appl. Catal. A Gen. 149, 289–301.

This page intentionally left blank

PART 4

Environment and Economy

This page intentionally left blank

CHAPTER 22

Methanol Economy: Environment, Demand, and Marketing With a Focus on the Waste-to-Methanol Process

Gaetano Iaquaniello[*,‡], **Gabriele Centi**[†], **Annarita Salladini**[†], **Emma Palo**[‡]

[*]*Processi Innovativi, L'Aquila, Italy* [†]*University of Messina and INSTM/CASPE, Messina, Italy*
[‡]*KT—Kinetics Technology S.p.A., Rome, Italy*

Acronyms

CAGR	compound annual growth rate
CAPEX	capital expenditure
CCR	carbon capture and reuse
CCS	carbon capture and storage
COP	cost of production
DICP	Dalian Institute of Chemical Physics Chinese Academy of Sciences
DME	dimethyl ether
DMFC	direct methanol fuel cell
DMTO	DICP methanol to olefins process
EU	Europe Union
GHG	greenhouse gas
GTL	gas-to-liquid
EMOGAS	Exxon Mobil Olefins to GASoline
EMRE	ExxonMobil Research and Engineering Co.
ETBE	ethanol tert buthyl alcohol
IRENA	International Renewable Energy Agency
HT	high temperature (converter)
KIT	Karlruhe Institute of Technology
kJ	kilojoule (10^3 Joule)
KM-CDR	Kansai Mitsubishi carbon dioxide recovery
LHV	lower heating value
MEA	mono-ethanol amine

Methanol. https://doi.org/10.1016/B978-0-444-63903-5.00022-4

MSW	municipal solid waste
M€	million Euro
Mt	million ton
MTBE	methyl tert-buthyl ether
MTA	methanol-to-aromatics
MTG	methanol-to-gasoline
MTO	methanol-to-olefin
MTP	methanol-to-propylene
MTT	triptane (2,2,3-trimethylbutane)
MW	megawatt (10^6 watt)
NG	natural gas
OCC	olefin catalytic cracking process
PET	polyethylene terephthalate
POM	polyoxometalate
PM	particulate matter
ppb	parts per billion
ppm	parts per million
PSA	pressure swing adsorption
Rdf	residue derived fuel
TAEE	*t*-amyl ethyl ether
TAME	tert-amyl-methyl-ether
TIGAS	Topsoe Integrated Gasoline Synthesis
t/d	ton per day (t/d)
WESP	wet electrostatic precipitator
WGS	water gas-shift reaction
WtE	waste-to-energy
WtM	waste-to-methanol

1 Introduction

Methanol is one of the most flexible chemicals, which makes it the crossroads of the future of sustainable chemical and energy production (Law et al., 2013; Bertau et al., 2010, 2014; Goeppert et al., 2014; Olah et al., 2009; Olah, 2005). Methanol can be used as:

- A chemical and raw material for large-volume chemicals.
- A fuel, both as a blending component or to produce a range of other components for fuels.

It may be produced both from (i) fossil fuels (methane and coal, the latter in rapid expansion in China) and (ii) non-fossil-fuel sources (residue/biomass/renewable + CO_2). Thus, methanol is one of the most important and versatile platform chemicals for the chemical industry. It is

also a key element in the transformation to a future of sustainable energy (i.e., trading renewable energy on the world scale) (Abate et al., 2015a,b; Barbato et al., 2014).

Methanol is much less flammable than gasoline, it can be blended with amounts of 10% or higher, and it is a biofuel competitive with ethanol or one that can be integrated with other biofuels to reach targets. Methanol is already included in standards for use in transportation fuels (in the European Union (EU) for example, directives provide additional incentives for waste and ligno-cellulosic derived biomethanol). The conversion of biomass to methanol is simpler and cheaper than for other biomass-to-liquid processes. Methanol production from CO_2 and H_2 is estimated to reach 40–70 Mt by the year 2050 (Faberi and Paolucci, 2014).

There are different pushes to promote greater methanol use, to exploit coal in Asian regions, to promote the use of renewables in Europe, and to utilize shale gas in a more flexible way in the United States. Methanol is one of the chemicals/fuels with the largest growth rate in the last decade, with its demand increasing from about 5 Mt in 2005 to more than 70 Mt in 2015. The compound annual growth rate (CAGR) nearly doubled in the last five years compared to the average in the decade before. A significant increase is shown to produce:

- formaldehyde, driven by the expansion in polymers and resins particular in Asian markets.
- olefins (methanol-to-olefin (MTO)/methanol-to-propylene (MTP) processes) in the last few years, particularly in China.
- Dimethyl ether (DME), also especially in China.
- gasoline/fuel/biodiesel, especially in Europe.

Methanol demand in the gasoline pool will increase from 5 Mt in 2012 to 11 Mt in 2022, with Northeast Asia, Europe, and North America being the largest methanol importers (80% of the total world trade) (Source: IHS Chemical Market Advisory Service–Global Methanol). Northeast Asia imports will triple from 2012 to 2022. Future MTO-, MTP-, and DME-integrated complexes will consume the largest amounts of methanol.

1.1 Paths for Methanol Use: Fuels

Methanol and DME are key intermediates to producing liquid fuels (gasoline, kerosene, gasoil) by different routes, which are currently being studied by many companies, as summarized in Fig. 22.1 (Bertau et al., 2010, 2014). DME can be synthetized either directly from syngas or in a two-step process via methanol (Azizi et al., 2014). The latter is the most used industrially.

The methanol dehydration reaction to DME is catalyzed by acidic compounds such as γ-alumina, silica-alumina, zeolites (HZSM-5, NaHZSM-5, HY, Ferrierite), mesoporous materials (MCM and SAPO families), or ZrO_2 (Sun et al., 2014). The main factors influencing the activity and selectivity are the acidic site's strength and structural characteristics (e.g., pore size distribution). High acidity strength is undesirable because it further catalyzes the DME

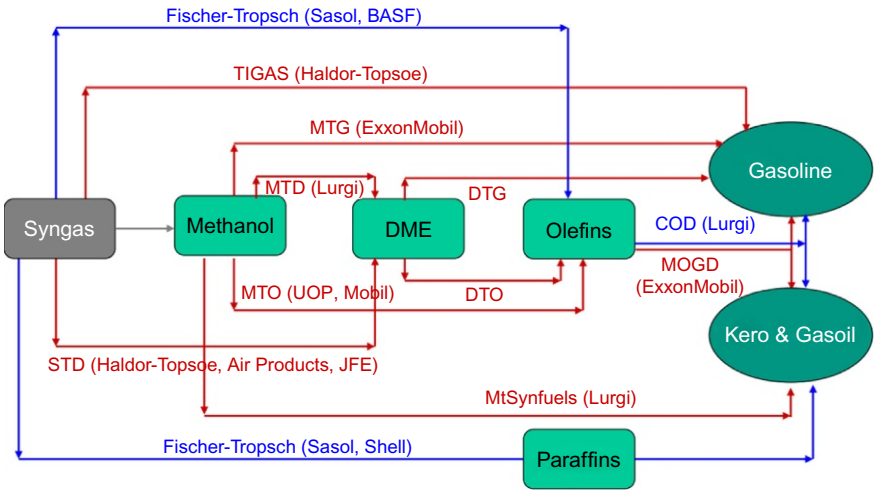

Fig. 22.1
Overview of the various routes investigated by different companies to produce liquid fuels from syngas, methanol, and DME.

conversion to hydrocarbons. Therefore, sites with medium acidity ensure a better performance. For this reason, the creation of mesoporosity to improve diffusivity may also enhance deactivation without a precise control of the type of acid sites created in the process. New and interesting catalysts that have been developed are based on polyoxometalate (POM). Among the industrial processes developed are Lurgi's MegaDME, BioDME, Mitsubishi DME, Air Product, and JFE DME processes based on the slurry bubble-column reactor. A number of solutions have been developed to achieve process intensification, including dividing-wall column catalytic distillation.

About three decades after the first (and only) plant was opened in New Zealand, a renewed interest is under way for methanol or better DME conversion to gasoline. Second-generation methanol-to-gasoline (MTG) technology incorporates improvements derived from the operation of that first plant. These improvements reduce the heat input, the compressor duty, and the heat exchange surface area, which also reduces capital by about 10%–15%. Fluidized-bed MTG technology, developed by Uhde/ExxonMobil and Sinopec Eng./EMRE, allows better control of temperature and deactivation. However, other companies such as Lurgi (MtSynfuels/COD) prefer a multitubular fixed-bed reactor. The DME to gasoline (DtG) process, developed by a consortium led by KIT, focuses on the direct use of DME as a raw material. KIT has also developed a route to convert methanol to diesel components, meaning oxymethylene ethers.

Improved catalysts have been developed by ExxonMobil Research and Engineering. Recent activities on catalysts for MTG synthesis focused on the modification of the ZSM-5 catalyst to develop nano-sized materials and/or with suitable mesoporosity and/or tuned acidity. Various advances have been made recently on the reaction and deactivation

mechanisms, and the nature of organic-type active catalytic centers involved in the "hydrocarbon poll" type mechanism of olefin, aromatics, and gasoline products from methanol/DME (Olsbye et al., 2012).

Alternative processes to MTG are (i) Mobil olefins-to-gasoline/diesel (distillate); (ii) Exxon Mobil Olefins to GASoline (EMOGAS); and (iii) Topsoe Integrated Gasoline Synthesis (TIGAS).

Methyl tert-buthyl ether (MTBE) has been widely used over the last 30 years to improve the octane number in gasoline, but its production is declining. Tert-amyl-methyl-ether (TAME) is one of the alternative ether additives to gasoline together with ethanol tert buthyl alcohol (ETBE) and t-amyl ethyl ether (TAEE). World TAME capacity is about 10% of MTBE capacity. Ether demand is expected to remain stable over the next decade, but with a shift toward the use of biomethanol to take advantage of renewable energy directives. Although the processes for synthesis of these ethers are well established, process advances allow us to improve the economics and energy savings. A valuable option is the use of reactive distillation to intensify the MTBE process.

Various routes and catalysts have been proposed to improve the first-generation biodiesel processes by transesterification with methanol using soluble base salts as catalysts. Base or acid solid catalysts are two of the routes being actively studied (Vonortas and Papayannakos, 2014; Santacesaria et al., 2012). However, the research and industrial interest is decreasing, for two reasons. First, most of the production of biodiesel by transesterification is made by companies with little interest in investing in new technologies due to uncertainties in the market. Second, the preference by refining companies is to develop second-generation processes for biodiesel production based on hydrogenation. Between recent developments, we may cite the use of engineered zirconia (ZrO_2) nanostructures with mesoscopic ordering to convert long-chain fatty acids to their Me esters (Das and El-Safty, 2013). A nearly 100% yield in biodiesel was obtained. Advances can also be found in the literature for the mechanism of transesterification and derived kinetics. Novel reactors for biodiesel process intensification have been proposed to reduce reaction times from hours to seconds.

Between the fuel additives, which can be obtained from methanol or DME, triptane is among the most interesting (Hazari et al., 2012). Triptane can be synthetized both homogeneously with soluble metal halide catalysts and heterogeneously over solid microporous acid catalysts. In both cases, hydrocarbon chains grow by successive methylation in a carbocation-based mechanism. Between the recent developments in this area, there is also the use of the Cu/BEA catalyst to convert DME to 2,2,3-trimethylbutane. A Cu-modified H-BEA catalyst is able to incorporate hydrogen from gas-phase cofed with DME into the desired branched alkane products while maintaining the high C4 and C7 carbon selectivity of the parent H-BEA.

Methanol can thus be considered the ideal energy vector to guarantee a smooth and effective transition from the actual oil-centric energy system to the new, more sustainable energy future.

Methanol use in chemical production is also of increasing relevance for the role of methanol as an ideal molecule to favor the energy transition. The latter indicates the transition from the current use of fossil fuels to the use of new "renewable" raw materials, via an extended use of fossil fuels (coal and unconventional fossil fuels, and CO_2 derived from fossil fuels). The new "renewable" raw materials are biomass and CO_2, with the latter deriving also from biomass processes and energy. The related challenge is to introduce renewable energy in the chemical industry and to trade renewable energy on a large-scale via chemical energy storage (Lanzafame et al., 2014; Perathoner and Centi, 2014).

1.2 Paths for Methanol Use: Chemicals

Chemical use of methanol may be distinguished between different branches (Bertau et al., 2010, 2014):

- *The acetic acid branch*. One important use of methanol is in the production of acetic acid by carbonylation of methanol. The largest use of acetic acid is as a feedstock for vinyl acetate, which is used for the production of a range of polymers used for such things as paint, adhesives, foam rubber, etc. The second largest use of acetic acid is as a solvent in the synthesis of terephthalic acid, which is the main component in polyethylene terephthalate (PET) bottles and nylon fibers.
- *The formaldehyde branch*. Methanol can be oxidized to its aldehyde. Formaldehyde is extensively used as a component in thermosetting resins and plastics together with phenols, urea, or melamine. Other uses include the production of high-performance plastics and fibers such as polyoxymethylene, Spandex, and polyurethanes.
- *The DME and olefin branch*. DME can be produced by dehydrating methanol. DME is used as an environmentally compatible propellant for spray cans, as a foaming agent for polystyrene insulating material, or as a low-boiling solvent. DME can be converted (or is intermediate when starting from methanol) in the MTO and derived MTP processes. Propylene is of particular interest recently, due to shortages causing a shift from naphtha to ethane in steam crackers. Propylene is the starting point for synthesis for a long range of plastics and chemicals including polypropylene, butanol, isopropanol, propylene oxide, acrylic acid, acrylonitrile, and cumene. It is further transformed for great use in products from reusable shopping bags to windshield fluid to absorbent material in a diaper. By adapting the MTO process (e.g., the catalyst), aromatics can be targeted as the main product.

MTO and analogous processes such as methanol-to-aromatics (MTA) are an emerging methanol demand segment (Funk et al., 2013; Tian et al., 2015). Olefin production from methanol/DME is growing fast, particularly in China, with several plants completed or in the advanced stage of construction for a total capacity of more than 18 MMT. Few of these are based on the second-generation processes that integrate a downstream stage to crack $\geq$C4 hydrocarbons to lighter ones. Total/UOP MTO process integrated with the olefin cracking

process (OCP) improves carbon yield to ethylene and propylene formation to over 85%. Similarly, the second-generation DICP methanol-to-olefins process (DMTO) developed by DICP (China). The MTO process is characterized by a high selectivity and yield to light olefins, particularly on zeolite catalysts such as SAPO-34, giving $>90\%$ selectivity to C2–C4 olefins. Fast deactivation and exothermicity requires the use of a fluid-bed reactor with continuous regeneration. Instead of a dense-phase fluidized-bed reactor (utilized in the DMTO process), riser and fast fluidized-bed reactors were also developed for the MTO process by ExxonMobil and UOP. A catalyst-gas contact time of about 2–3 s is necessary in order to avoid undesired byproducts in the MTO reaction. Such a short catalyst-gas contact time means that an industrial MTO reactor has to be operated at a gas velocity higher than 1 m/s, imposing a great challenge for engineering design. A turbulent fluidized-bed reactor offers operational advantages over the bubbling and fast fluidized bed due to the excellent catalyst-gas contact, high mass transfer efficiency, and large solids holdup.

Various commercial processes exist for MTO, in addition to DMTO and DMTO-II developed by the Dalian Institute of Chemical Physics (DICP) together with some Chinese companies (Tian et al., 2015). Among these are: (i) the UOP/Hydro (Norsk-Hydro, now Ineos) MTO process with the advanced MTO version that combines the UOP/Hydro MTO process and the Total/UOP olefin cracking process; and (ii) the SINOPEC MTO process (named S-MTO), which has high olefin selectivity, high methanol conversion, and low catalyst consumption. When combined with the OCC process to convert the heavier olefins, the overall yield of ethylene and propylene increases to $\sim$85%–87% and propylene-ethylene ratios of more than 1.5 are achievable.

SINOPEC has also developed a proprietary technology for MTP, based on the ZSM-5 catalyst, which has a very high carbon selectivity to propylene. The typical result of the MTP process is a conversion of methanol to propylene at 40%–50% carbon selectivity in a fixed-bed reactor for a single pass. The Tsinghua FMTP technology, based on fluidized bed and an SAPO-34 catalyst, has been developed by the Beijing Key Laboratory of Green Reaction Engineering and the Process of Department of Chemical Engineering, Tsinghua University, China. The Lurgi (AirLiquide) MTP process, based on a fixed-bed reactor with in situ regeneration, operates in mild conditions (1.5 bar, 425°C) and allows long catalyst cycle times based on a low coking zeolite catalyst (supplied by SudChemie, an alkaline-modified ZSM-5 by the addition of a small amount of ZnO and CdO).

The reaction mechanism, as in the methanol-to-hydrocarbon transformation, involves the formation of hydrocarbon intermediate within the zeolitic cage (Tian et al., 2015; Khadzhiev et al., 2014; Teketel et al., 2014; Lefevere et al., 2014; Chen et al., 2012). This intermediate is the active catalytic element, although the exact nature (hexamethylbenzene or other species) remains under debate. A large scientific interest exists in the literature in understanding the role of zeolite acting as a hosting center to create this active species and to limit side reactions

leading to deactivation. Among the active areas of research, we may cite: (i) the role of internal defects, that is the role of lattice defects in zeolite (silanol defects), particularly on deactivation and the creation of these defects during treatments to induce mesoporosity; (ii) the creation of mesoporosity; and (iii) the crystallization mechanism of SAPO-34. Among the many recent advances we may cite: (i) how P doping may restrict adsorption of aromatics and reduce deactivation; (ii) the effect of pore and cage size on the formation of aromatic intermediates during the MTO reaction; (iii) that both the aromatic-based cycle and the olefin-based cycle can proceed during the MTO reaction, but with the latter cycle being predominant; (iv) the use of multiple templating agents to enhance the performance of SAPO-34 catalysts; (v) the analysis of the reaction mechanism during the early period of the methanol-to-olefin conversion; and (vi) the preparation of nanosheet-like SAPO-34.

The future scenario for the use of methanol, driven largely from the MTO process, will develop the role of shale gas in this scenario, mainly out of Asia but also in parts of Asia. Nexant (2014) has developed a scenario for both cases, even though evidence already exists that the future development of shale gas has been overestimated. For this reason, a scenario has also been elaborated for higher petrochemical production from coal and biomass, where methanol plays the critical role. This high alternative feedstock scenario, presented in Fig. 22.2, would lead to further MTO developments in China but also in the United States; they would be more minor in Europe. MTA capacity could also develop, reducing investment in conventional naphtha-based steam cracking. Additional MTO production would substitute naphtha-based steam-crackers. MTO production of ethylene and propylene would reduce the propane requirement for propane dehydrogenation. Tecnon OrbiChem (Bann, 2015) estimated the viability of advanced MTO using imported methanol. The viability depends on the light olefins

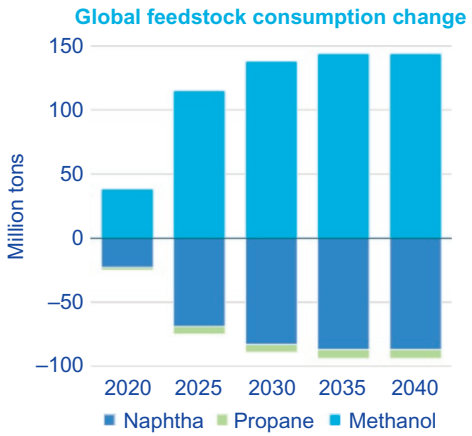

Fig. 22.2

A scenario of higher petrochemical production from coal and biomass. *Source: Nexant, 2014. Petrochemical outlook: challenges and opportunities, prepared for EU-OPEC energy dialogue (Dec. 2014). Available at: https://ec.europa.eu/energy/sites/ener/files/documents/OPEC%20presentation.pdf.*

spot price and methanol cost, which fluctuate greatly. On average, however, there is a positive margin of about 200 $/t.

Formaldehyde is produced industrially from methanol by the following catalytic technologies (Reuss et al., 2000): (i) Oxidative dehydrogenation with air in the presence of a silver catalyst, steam, and excess methanol at 680–720°C (BASF process, 97%–98% methanol conversion, single pass). (ii) Oxidative dehydrogenation with air in the presence of crystalline silver or silver gauze, steam, and excess methanol at 600–650°C (77%–87% primary conversion of methanol). The conversion is completed by distilling the product and recycling the unreacted methanol (process with recycle). (iii) Oxidation with excess air in the presence of a modified iron-molybdenum-vanadium oxide catalyst at 250–400°C (98–99% methanol conversion). This process, also known as the FORMOX process, is a highly exothermic process. Although catalysts are quite established for these reactions, some progress on their understanding has been reported recently.

Acetic acid can be produced by many routes, but methanol carbonylation dominates current acetic acid production (>75%). This is also a well-established process, although various evolutions of the original BASF process (based on cobalt-carbonyl, and operating at high temperature-pressure) and the Monsanto process (based on Rh complexes, but operating in milder conditions and with higher selectivity) are present. Among these are the Cativa process, which uses an iridium complex and shows higher activity and catalyst stability at low water concentrations, and the "low water" methanol carbonylation process commercialized by Celanese and Daicel. Heterogenization of the homogeneous catalysts is another of the process options actively investigated. The CT-ACETICA process developed by the Chiyoda Corporation includes, in addition to high-performance resin-supported rhodium catalysts, the use of bubble-column loop reactors designed for effective usage of resin catalysts.

Methanol homologation to ethanol was discovered by BASF, but there is some renewed interest. An indirect route to synthetize ethanol from methanol and syngas, based on three sequential steps (methanol dehydrogenation, DME carbonylation, and methyl acetate hydrogenolysis) has been also reported recently (Liu et al., 2013). Another possibility studied is the direct hydrogenation of acetic acid to ethanol utilizing a platinum/tin catalyst (Johnston et al., 2011). Celanese indicates his TCX ethanol process marks a "paradigm shift" in ethanol production. A 1 Mt total capacity with one to two greenfield industrial ethanol plants is in construction. Celanese claims that TCX ethanol is cheapest with respect to MTBE, Brazilian ethanol, and methanol to gasoline as well as corn ethanol and GTL. In addition, it has a low lifecycle water consumption and better energy conversion.

Various advances have also been presented recently in other routes of methanol conversion and use: (i) methanol to methyl chloride by hydrochlorination; (ii) methylamines by reaction of methanol with ammonia; (iii) sulfur derivatives of methanol; (iv) toluene alkylation with

methanol; (v) dimethoxymethane; (vi) dimethyl terephthalic acid; (vii) methyl methacrylate; and (viii) dimethyl carbonate.

Numerous established petrochemicals are accessible via methanol. It is also obvious from C1-chemistry that there is a link to C2-chemistry as well as to C3- and C4-chemistry. Via the established protocols of MTO, MTP, and MTA, higher C-numbers as well as aromatics can be obtained from this alternative chemical feedstock. It is thus evident that methanol has the potential to be a raw material, direct or indirectly, for a large part of the current petrochemical routes. With respect to the past, three main factors are changing the scenario of chemical production regarding the chemical utilization of methanol:

1. The possibility of cheap production from coal, and one of the best options to chemically exploit the use of coal.
2. The possibility for producing renewable methanol, that is from 100% fossil-fuel free resources. The motivations for this route are more political than economic, but this route offers advantages in terms of exploiting unused renewable energy resources as well as a way to move to a more carbon-efficient bioeconomy. In Europe, this likely will enhance the availability of methanol for chemical productions.
3. The possibility of decreasing the cost of "classical" methanol production due to the availability of shale gas. It is likely, however, that this will occur mainly in the U.S., while the impact of relevant potential shale-gas resources in China is still difficult to predict.

For different motivations in world regions, we may predict that the methanol chemistry impact as an economically viable alternative to the current routes will be significant.

2 Producing Methanol From Waste

Feedstock costs for methanol make up as much as 90% of the total cost and as such, access to low cost feedstock is the key to overall methanol economics. Methanol can be produced from other carbon-containing feedstock rather than fossil fuels, including biogas, biomass, waste streams, and CO_2 (Barbato et al., 2014). The main advantage of biomethanol is the reduction of fossil fuel and the possibility of converting by gasification a range of renewable feedstock into biomethanol. The production cost of biomethanol is estimated between 1.5/4.0 times higher than the cost of natural gas-based methanol (Production of Bio-methanol, 2013). Using waste as Rdf and other byproduct streams from industrial processes as feedstock offers the best way for improving such economies. Cofeeding of renewable feedstock in natural gas or coal-based methanol production facilities may also be very attractive while reducing the environmental impact of conventional methanol production.

The use of MSW or, even better, Rdf might already compete today for biofuel production if a proper policy is implemented that should include colabeling of biobased chemicals, a carbon tax, and information campaigns.

2.1 Assessing the Economic Performance of Biomethanol

Methanol demand and price have historically been highly variable and cyclical. Prices have been bounded on the low side by the price that marginal suppliers offer on the market. Today's low price dissuades supply and new projects. However, biomethanol supply and price are not strictly related to the conventional methanol market, but mainly aligned with the market of alternative fuels such as ethanol or ETBE. In Chapter 4, the possibility of converting waste-derived fuel into biomethanol was presented and analyzed. Here the cost of production (COP) of such a scheme is presented for a new 300 t/d methanol plant. Results are very interesting without considering the double count of bioenergy content value, and competitive against hydrocarbon-based production.

The conversion of Rdf into biomethanol results in an excess of CO_2. It then becomes of interest to integrate such a scheme in a conventional methanol unit based on natural gas feedstock that produces an excess of hydrogen. The balancing of two schemes allows reducing the COP even further than a stand-alone configuration. In general, such a process may also be identified as a carbon capture-and-reuse (CCR) process, and excess of CO_2 could be available for carbon capture-and-storage (CCS) deployment at a very attractive cost per ton of CO_2, confirming the increased interest in BIO-CCS (European Bio-fuels Technology Platform, 2012).

2.1.1 Plant configuration

A block diagram for the waste-derived fuel-to-methanol production was presented in Chapter 4 (Fig. 4.4). The core of the process is the high temperature converter where Rdf is mixed with oxygen to produce a syngas, followed by the methanol synthesis reactor where the syngas, following purification and R ratio control, is converted into raw methanol. The overall material balance for a 300 t/d methanol unit was shown in Chapter 4 (Fig. 4.7), where around 716 t/d were used as feedstock.

2.1.2 Key economic assumptions and parameters, and price derivation of biomethanol

Economic parameters used to estimate the COP of methanol are summarized in Table 22.1 for two cases presented: (A) 300 t/d new methanol production, and (B) the hybridization scheme with an existing 900 t/d methanol unit. The investment for the new plant has used a standard estimating tool and experience in building an industrial plant. Table 22.2A gives the cost of delivered equipment for the different process sections of the plant. Table 22.2B provides the overall capital expenditures (CAPEX), calculated as a percentage of the delivered equipment costs (Peters and Timmerhaus, 1980). This method is commonly used for the preliminary estimates with an accuracy of ±25%.

The overall cost estimate of the plant for a production of 300 MTPD of methanol is 189 M€. For the hybrid scheme, the CAPEX, which is relevant only to the Rdf conversion and purification (on two single lines), is reduced to 80 M€.

Table 22.1 Key economic assumptions and parameters

Rdf Price (Flock Type)	**70€ per t (Italian Basis)**	
Electricity price	50€ per MWh	
Natural gas	0.15€ per kg nat gas (11,500 kcal/kg)	
Slag disposal costs	20€ per t	
Case	(*A*)	(*B*)
Labor M€ per year	3 M€	1 M€
Methanol capacity t/y	105,000	55,000
Maintenance cost M€[a]	4.0	2.4
Plant factor	8400 h	
Depreciation factor based on a 20-year life and 6% interest rate	0.0875	
Other costs, M€	2.0	0.6
Calculated cost of excess CO_2 capture, € per t	15	

(A) 300 t/d new biomethanol plant.
(B) Hybridization with a natural gas-based 900 t/d methanol unit.
[a]Based on 1% of CAPEX for syngas-methanol section and 3% of the CAPEX for the conversion/purification section.

Table 22.2A Estimated cost of equipment for 300 t/d methanol

	M€
HT convertor reactor (three lines)	28
Syngas shift and CO_2 removal	8
Methanol synthesis	12
Air separator and compressor	10
TOTAL equipment costs	*58*

Table 22.2B Estimated investment costs

	M€	**% of Delivered Equipment Cost**
Equipment costs (delivered)	58	100
Bulk materials (piping, instrumentation, electrical)	40	70
Building and civil works	*12*	*20*
Total direct costs	110	190
Engineering and site supervision	13	22
Construction	41	71
Total direct and indirect costs (*tot*)	*164*	*283*
Contractor profit 5%	8	14
Contingency 10%	17	28
Fixed capital investment (*CAPEX*)	*189*	*325*

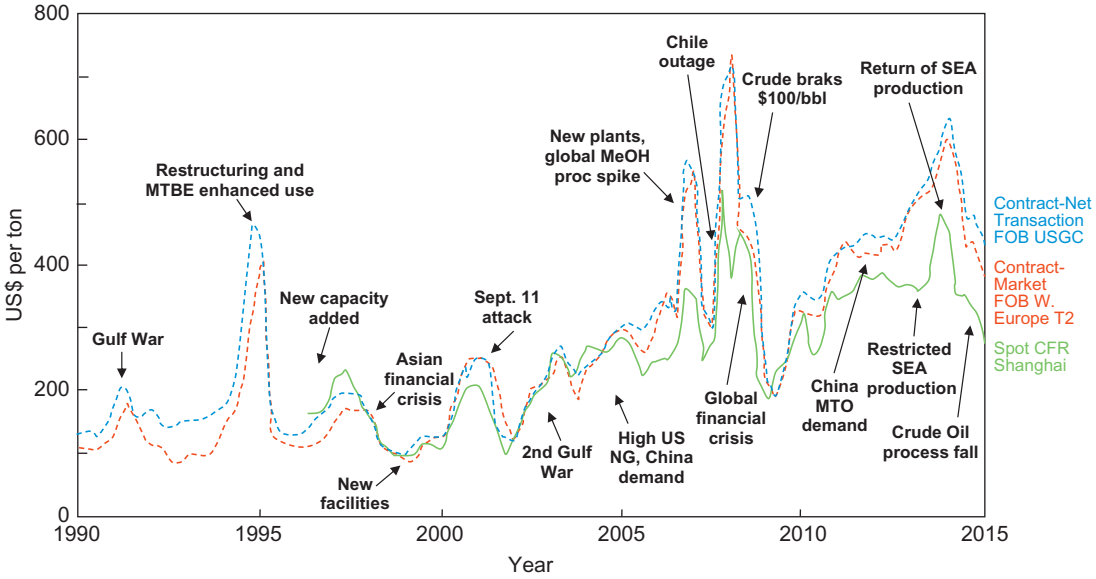

Fig. 22.3

Historical quarterly methanol prices, 1990 to present with an indication of some key factors driving price fluctuations: cost and freight (CFR), free on board (FOB), domestic (T2), US Gulf Coast (USGC), and Southeast Asia (SEA).

As far as the price of commercial methanol, on October 2016 and based on a Rotterdam delivery, it was around 225 €/t (Mithomex, 2016). A 10% increase may be considered for transportation costs and handling at an Italian port. In Fig. 22.3 the historical quarterly methanol prices have been reported (MMSA, 2015). However, biomethanol produced by wastes is qualified by the EU's RED for double recognition, so a supplier needs only half the quantity of such biofuel in place of first-generation ethanol to meet their obligations. The price of biomethanol is thus unlikely to fall like that of conventional ethanol. Such different market positions are going to generate a cap at least as high as 150–250 €/t (Market study, 2011).

2.1.3 Cost of production of methanol for a 300 t/d plant

Table 22.3 provides the cost of production for a ton of product based on the operating and economic parameters indicated in Fig. 22.2 and Table 22.1. The COP is calculated by deducting the annual operating costs from the income. About half of the operational costs are related to the depreciation while 20% goes to power consumption (ASU, syngas compression, etc.). As far as income is concerned, about 80% comes from Rdf with 20% from avoiding the cost of emitting CO_2. The estimated COP is around 111 € per ton of methanol for an Italian site.

Table 22.3 Cost of production per ton of methanol

COSTS	M€ per Year
Power	6.7
Slag disposal	1.0
Maintenance	4.0
Depreciation	16.5
Other costs	2.0
Labor	3.0
Total annual costs$^{(1)}$	*33.2*
Incomes	
Rdf disposal	17.5
CO_2 avoided	2.1
Excess CO_2 for bio-CSS	1.92
Total incomes$^{(2)}$	*21.52*
ANNUAL methanol production	105,000 MTP
COP = (1) − (2)	*111€/t of methanol*

2.1.4 Sensitivity analysis

For each ton of methanol produced, 2.4 tons of Rdf are consumed. This will imply the need for an urban area that produces around 700,000 Mt of municipal waste per year, assuming that 35% of that will be converted into waste-derived-fuel. In terms of population, we are talking about 1.5 million inhabitants.

The income generated by Rdf disposal is then the main driver in reducing the COP. Such a value may vary from country to country and is related to the distance from the installed incinerator capacity. It is quite evident that such a new architecture will have advantages where Rdf is landfilled and limited incineration capacity is available. In Fig. 22.4, the impact of the Rdf price

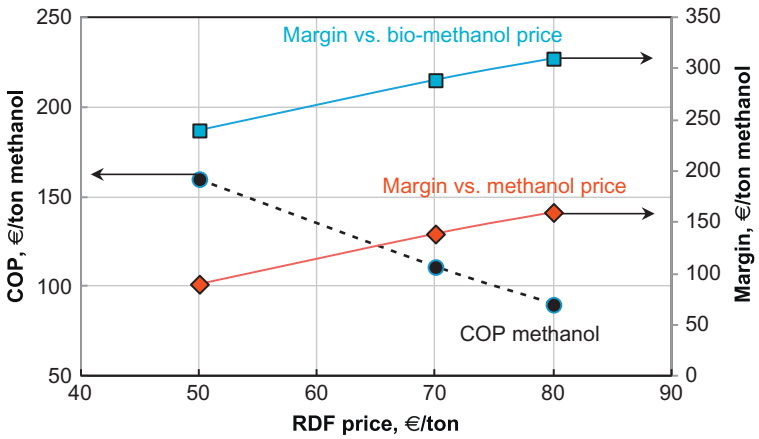

Fig. 22.4
Impact of RDF price on Methanol COP.

on the methanol COP is shown. Even at an Rdf price of 50€ per ton, the COP increases to less than 200€ per ton. In the same Fig. 22.4, industrial margins have been calculated considering the methanol price and that for biomethanol.

2.1.5 Return on investment (ROI)

Although under the ROI term it is possible to find a variety of definitions and applications, here we want to focus on the shareholder's point of view, which is interested in a return on shareholders' equity, to know about the payback time for the investment. In order to provide a simple ROI, previous data are reformulated in different ways and presented in Table 22.4. The simple ROI is around 29%, meaning the payback time of the investment is then slightly more than four years. By redoing the same calculation for a biomethanol plant having a capacity of 50,000 t/y, the ROI is around 18%.

2.2 Cost of Production of Methanol on a Hybrid Process

A block diagram of the proposed hybridization is presented in Fig. 22.5. Here, the concept is to install only a section of the plant, which provides high-temperature conversion and cleaning of Rdf, to produce a syngas with high CO/CO_2 content to balance the excess of hydrogen produced in a conventional methanol plant where natural gas is the feedstock. As a reference, a methanol plant having a capacity of 900 t/d has been selected. To balance such a plant, two lines of Rdf conversion have been envisioned to treat about 380 t/d of Rdf.

Based on the data from Section 2.1, the CAPEX for such a section is estimated at 80 M€. A reduction of natural gas with overall material balance is indicated in Fig. 22.6. Table 22.5 provides the cost of production where depreciation has been considered only for the new HT conversion section. In such favorable conditions, the COP becomes a profit even without

Table 22.4 Simple ROI calculation for 300 MTPD methanol unit.

Net sales[a]	42.0 M€
Other incomes	21.5 M€
Less costs	16.7 M€
Less loan repayment[b]	11.0 M€
Pretax profit	*35.7* M€
Tax 50%	17.9 M€
Net profit	*17.9* M€
ROI %[c]	*28.7*

[a]Based on a methanol price of 400€/t, 250€/t+150€ as cap.
[b]Loan is 2/3 of CAPEX, equity 1/3 of CAPEX. Repayment calculated on 20 years with 6% interest rate.
[c]Net profit/equity × 100.

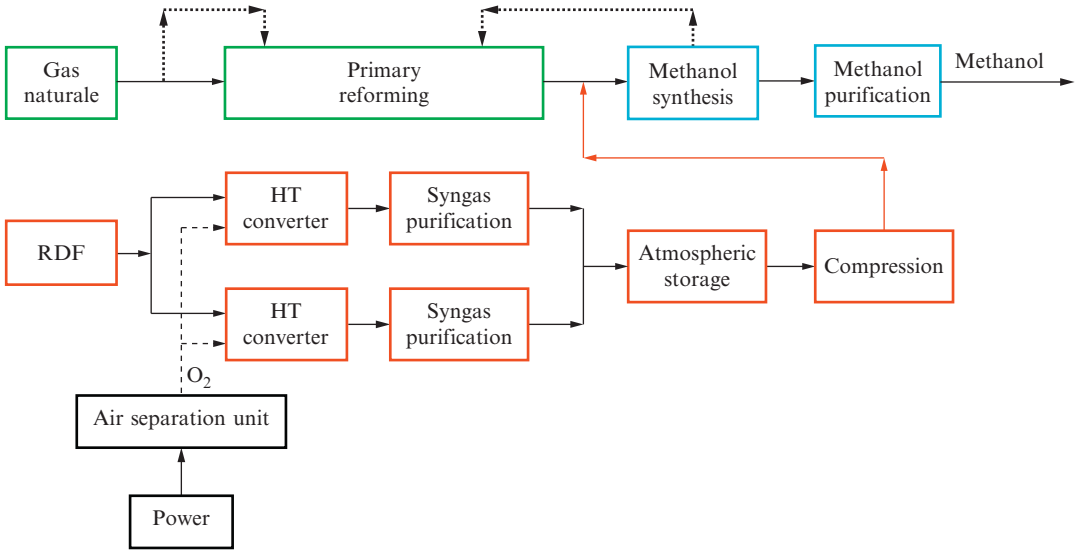

Fig. 22.5
Block diagram for the hybrid RDF/natural gas to methanol.

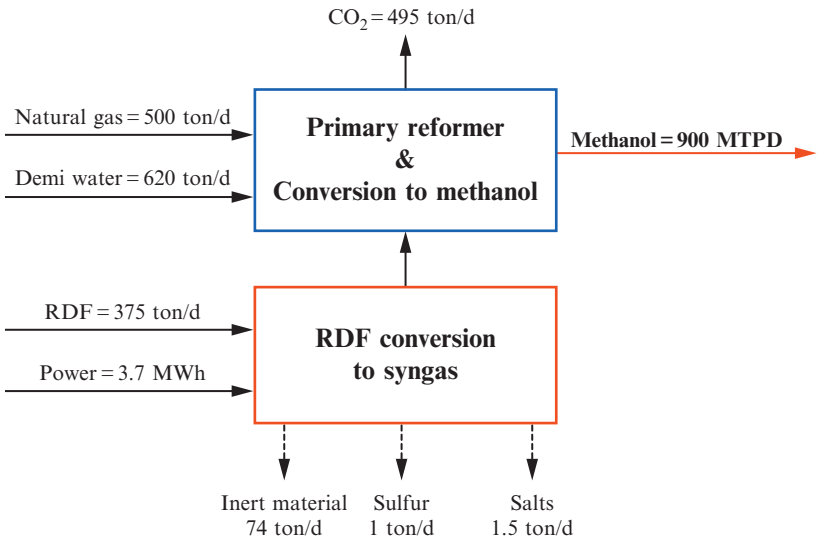

Fig. 22.6
Hybrid methanol unit: overall material balance.

considering the cap for biomethanol production. Although the proposed hybridization looks very attractive from an economic point of view, it is important to stress that availability of Rdf near a methanol plant is quite questionable and the number of plants where this could be implemented in such a way is limited.

Table 22.5 Cost of production per ton of methanol

Costs	M€ per Year
Power	3.5
Slag disposal	0.5
Maintenance	2.4
Labor	1.0
Other costs	0.6
Depreciation	8.0
Total annual costs(1)	*16.1*
Incomes	
Rdf disposal	9.3
CO_2 avoided	2.7
Reduction natural gas cost	7.7
Total incomes(2)	*19.7*
ANNUAL methanol production MTPY	55,300
COP = (1) − (2) = €/t	(−65)

3 Conclusion

Biobased manufacturing of commodities in most cases is not cost-competitive with today's hydrocarbon price. Conversely, wastes and waste-derived fuel as Rdf may already be competitive enough these days to attract new investments. In particular, biomethanol may also count double with its bioenergy content value, pushing its price to 400–450 €/t against a cost of production, which, in the worse case, does not exceed 200 €/t.

For a 300 MTPD methanol plant, a ROI of 29% is expected. For a 150 t/d capacity, the ROI is reduced to 18%.

References

Abate, S., Centi, G., Perathoner, S., 2015a. Chemical energy conversion as enabling factor to move to a renewable energy economy. Green 5, 43–54.

Abate, S., Centi, G., Perathoner, S., 2015b. Energy-related catalysis. Nat. Sci. Rev. 2, 143–145.

Azizi, Z., Rezaeimanesh, M., Tohidian, T., Rahimpour, M.R., 2014. Dimethyl ether: a review of technologies and production challenges. Chem. Eng. Process. 82, 150–172.

Bann, W., 2015. Methanol & ethanol—fuel or feedstock? In: Tecnon OrbiChem Marketing Seminar at APIC (2015), Seoul, 7 May. Available at:http://www.orbichem.com/userfiles/APIC%202015/2015_APIC_William_Bann.pdf.

Barbato, L., Centi, G., Iaquaniello, G., Mangiapane, A., Perathoner, S., 2014. Trading renewable energy by using CO_2: an effective option to mitigate climate change and increase the use of renewable energy sources. Energ. Technol. 2, 453–461.

Bertau, M., Effenberger, F.X., Keim, W., Menges, G., Offermanns, H., 2010. Methanol needs more attention as a fuel and raw material for the future. Chem. Ing. Tech. 82, 2055–2058.

Bertau, M., Offermanns, H., Plass, L., Schmidt, F., Wernicke, H.-J., 2014. Methanol: The Basic Chemical and Energy Feedstock of the Future. Springer Pub., Heidelberg.

Chen, D., Moljord, K., Holmen, A., 2012. A methanol to olefins review: diffusion, coke formation and deactivation on SAPO type catalysts. Microporous Mesoporous Mater. 164, 239–250.

Das, S.K., El-Saft, S.A., 2013. Development of mesoscopically assembled sulfated zirconia nanoparticles as promising heterogeneous and recyclable biodiesel catalysts. ChemCatChem 5, 3050–3059.
European Bio-fuels Technology Platform, June 2012. Biomass with CO_2 capture and storage (Bio-CSS).
Faberi, S., Paolucci, L., 2014. Methanol: a future transport fuel based on hydrogen and carbon dioxide? In: Science and Technology Options Assessment (STOA) of the European Parliament Study PE 527.377.
Funk, G.A., Myers, D., Vora, B., 2013. A different game plan. Hydrocarb. Process. 12, 25–28.
Goeppert, A., Czaun, M., Jones, J.-P., Surya Prakash, G.K., Olah, G.A., 2014. Recycling of carbon dioxide to methanol and derived products—closing the loop. Chem. Soc. Rev. 43, 7995–8048.
Hazari, N., Iglesia, E., Labinger, J.A., Simonetti, D.A., 2012. Selective homogeneous and heterogeneous catalytic conversion of methanol/dimethyl ether to triptane. Acc. Chem. Res. 45, 653–662.
Johnston, V.J., Chen, L., Kimmich, B.F., Chapman, J.T., Zink, J.H., 2011. Direct and selective production of ethanol from acetic acid utilizing a platinum/tin catalyst, US Patent 7863489 B2.
Khadzhiev, S.N., Magomedova, M.V., Peresypkina, E.G., 2014. Mechanism of olefin synthesis from methanol and dimethyl ether over zeolite catalysts: a review. Pet. Chem. 54, 245–269.
Lanzafame, P., Centi, G., Perathoner, S., 2014. Catalysis for biomass and CO_2 use through solar energy: opening new scenarios for a sustainable and low-carbon chemical production. Chem. Soc. Rev. 43, 7562–7580.
Law, K., Rosenfeld, J., Jackson, M., 2013. Methanol As A Renewable Energy Resource. White Paper. Methanol Institute, Alexandria, VA.
Lefevere, J., Mullens, S., Meynen, V., Van Noyen, J., 2014. Structured catalysts for methanol-to-olefins conversion: a review. Chem. Pap. 68, 1143–1153.
Liu, Y., Murata, K., Inaba, M., 2013. Synthesis of ethanol from methanol and syngas through an indirect route containing methanol dehydrogenation, DME carbonylation, and methyl acetate hydrogenolysis. Fuel Process. Technol. 110, 206–213.
Market study, 2011. Market study for the production of second generation Bioliquids—Wyton Energy Consulting for NEPIC, March 2011.
Mithomex, 2016. Mithomex Monthly Average Regional Posted Contract Price History, Oct. 2016.
MMSA, 2015. Global Insight, Asian Perspective. Chapter IX—397 Price Forecast.
Nexant, 2014. Petrochemical outlook: challenges and opportunities, prepared for EU-OPEC energy dialogue (Dec. 2014). Available at: https://ec.europa.eu/energy/sites/ener/files/documents/OPEC%20presentation.pdf.
Olah, G.A., 2005. Beyond oil and gas: the methanol economy. Angew. Chem. Int. Ed. 44, 2636–2639.
Olah, G.A., Goeppert, A., Surya Prakash, G.K., 2009. Chemical recycling of carbon dioxide to methanol and dimethyl ether: from greenhouse gas to renewable, environmentally carbon neutral fuels and synthetic hydrocarbons. J. Org. Chem. 74, 487–498.
Olsbye, U., Svelle, S., Bjorgen, M., Beato, P., Janssens, T.V.W., Joensen, F., Bordiga, S., Lillerud, K.P., 2012. Conversion of methanol to hydrocarbons: how zeolite cavity and pore size controls product selectivity. Angew. Chem. Int. Ed. 51, 5810–5831.
Perathoner, S., Centi, G., 2014. A new scenario for green & sustainable chemical production. J. Chin. Chem. Soc. 61, 719–730.
Peters, M.S., Timmerhaus, K.D., 1980. Plant Design and Economics for Chemical Engineers, third ed. McGraw-Hill Book Company, New York.
Production of Bio-methanol, January 2013. IEA-ETSAP and IRENA Technology Brief 108.
Reuss, G., Disteldorf, W., Gamer, A.O., Hilt, A., 2000. Formaldehyde. Ullmann's Encyclopedia of Industrial Chemistry, Vol. 15. Wiley Online Library. https://doi.org/10.1002/14356007.a11_619.
Santacesaria, E., Martinez Vicente, G., Di Serio, M., Tesser, R., 2012. Main technologies in biodiesel production: state of the art and future challenges. Catal. Today 195, 2–13.
Sun, J., Yang, G., Yoneyama, Y., Tsubaki, N., 2014. Catalysis chemistry of dimethyl ether synthesis. ACS Catal. 4, 3346–3356.
Teketel, S., Erichsen, M.W., Bleken, F.L., Lillerud, S.S.K.P., Olsbye, U., 2014. Shape selectivity in zeolite catalysis. The methanol to hydrocarbons (MTH) reaction. Catalysis 26, 179–217.
Tian, P., Wei, Y., Ye, M., Liu, Z., 2015. Methanol to olefins (MTO): from fundamentals to commercialization. ACS Catal. 5, 1922–1938.
Vonortas, A., Papayannakos, N., 2014. Comparative analysis of biodiesel versus green diesel. Wiley Interdiscip. Rev. Energy Environ. 3, 3–23.

CHAPTER 23

Economic Assessment of Methanol Production

Kamran Ghasemzadeh[*], Seyyed M. Sadati Tilebon[†], Mojtaba Nasirinezhad[*], Angelo Basile[‡]

[*] *Urmia University of Technology, Urmia, Iran* [†] *Iran University of Science & Technology, Tehran, Iran*
[‡] *Institute on Membrane Technology (ITM-CNR), Rende, Italy*

Acronyms

AEC	alkaline electrolyzer
AGR	acid gas removal
ASU	air separation unit
ATR	autothermal reforming
CCS	carbon capture and storage
DMAC	dimethylacetamide
DME	dimethyl ether
DMF	dimethylformamide
DMT	dimethyltryptamine
HCN	hydrogen cyanide
ICI	Imperial Chemical Industries
IGCC	integrated gasification combined cycles
MDI	1,3-dimethyl-2-imidazolidinone
MMA	methyl methacrylate
MSR	methanol steam reforming
MTBE	methyl-tert-butyl ether
PC	pulverized coal
PMMA	poly (methyl methacrylate)
RES	renewable energy sources
TMAH	tetramethylammonium hydroxide
VAM	vinyl acetage monomer
WGS	water gas shift

Methanol. https://doi.org/10.1016/B978-0-444-63903-5.00023-6

Symbols

D diameter (m)
g gravitational acceleration
H geodetic height (m)
P power (W)
ν wind velocity (m/s)
π pi
ρ density (kg/m^3)
η efficiency

1 Introduction

Methanol is an important product of petrochemical industries with a variety of applications. In 1830, the first commercial process for methanol production was initiated by the destructive distillation of wood method. In 1905, French chemist Paul Sabatier suggested a synthetic methanol route, which was commercialized in 1923. In the 1940s, the production of methanol by using synthetic gas from natural gas was introduced. A low-pressure methanol process was announced by Imperial Chemical Industries (ICI) in 1966. Since then, improvements to the methanol production system have been studied. One of the most important changes considered for methanol production is using environmentally friendly feeds (such as biomass) for methanol production instead of fossil fuels (Kung, 1994). However, methanol is mostly produced from fossil fuels and more than 85% of global methanol production is based on natural gas reforming and coal gasification. The main process, in this method, is synthetic gas (CO and H_2) and the reaction takes place over a copper/zinc oxide catalyst (Rivarolo et al., 2016).

Initially, the main application of methanol was as a fuel for lighting, cooking, and heating purposes, but this was quickly replaced by more economical fuels. Over time, the applications of methanol expanded and it was increasingly required by the chemical industry. Synthesis gas and a pathway for methanol production by the use of synthetic gas has solved the main problems of the old processes such as low productivity and cost effectiveness. In the old processes of methanol production, the feed of syngas production systems was light fossil fuels, especially natural gas. Early discoveries showed that syngas can be supplied via coal gasification. This process is catalytic and needs especially hard process conditions (zinc/chromium oxide catalyst, temperature of 300–400°C, and pressure of 250–350 atm). The first development of this process was in 1923, in Leuna, Germany. After this time, researchers focused on development of catalyst and process conditions. The goal of this activity is achieving a suitable process from an economic point of view. To our knowledge, methanol steam reforming (MSR) was introduced as the best process for syngas production. The main advantages of this pathway are purer syngas in product, the use of a more active Cu/ZnO

catalyst, and a decrease in the process temperature and pressure (about 300°C and 100 atm). These improvements made the methanol production method proposed by ICI in 1966 cost effective. Lurgi was the next process that improved the previous technology and showed that syngas can be produced in temperatures between 230–250°C and pressures of 40–50 atm (Kung, 1994; Bozzano and Manenti, 2016).

After the environmental crisis and problems were identified, attempts at using other sources instead of fossil fuels have increased. Methanol production by using coal has many disadvantages. Biomass is an environmentally friendly source for the gasification process. However, carbon dioxide is the best choice for methanol production. Methanol production by carbon dioxide is a mature technology because of a high level of methanol selectivity (over 99.8%) and good energy efficiency (around 75%) (Bozzano and Manenti, 2016; Ghasemzadeh et al., 2016).

The main reason for wide studies regarding an economical process of methanol production is a large variety of chemical production processes that require methanol. Formaldehyde is a major consumer of methanol. Indeed, about 70% of methanol worldwide is used for formaldehyde production. The next large consumer of methanol is methyl-tert-butyl ether (MTBE), which uses 20% of the total annually produced methanol. Acetic acid and dimethyl ether are the other main methanol consumers. In addition to these noted direct applications, there are many indirect applications that are dependent on methanol, including paints, resins, silicones, adhesives, antifreeze, plastics, etc. Moreover, methanol can be used as a transportation fuel in addition to gasoline. It has many positive qualities such as low pollutant emissions (hydrocarbons, NO_x, SO_x, particulate). More than 80% of the world's energy consumption comes from fossil fuels. This is the main reason for a wide range of environmental problems (Pachauri et al., 2014; Garrow, 2015). However, before being able to use pure methanol as fuel, many issues must be solved, including metal corrosion (in particular, aluminum, zinc and magnesium can be attacked) and/or cold engine start, which is related to the absence of highly volatile compounds. Experimental studies showed that adding a certain percentage of methanol can improve the quality of gasoline. In China in 2009, the marketing of a mixture of methanol and gasoline started (Bozzano and Manenti, 2016).

In the European Union, the production of biofuels and their use as a replacement for fossil fuels is a main goal to be reached by 2020 (Liu et al., 2007). The main reason for this activity is decreasing the pollutant emissions. Methanol has many good properties when it is used as a fuel. Of course, methanol energy density is half that of gasoline (20.1 MJ/kg for methanol, 44.3 MJ/kg for gasoline, Balki and Sayin, 2014) but a high octane number for methanol (108 for methanol, 95 for gasoline) introduced it as a suitable fuel. A high octane number leads to a higher compression ratio than traditional gasoline, therefore combustion will be more efficient and the emissions (CO and CO_2) will be reduced (Balki and Sayin, 2014; Celik et al., 2011; Gong et al., 2011). On the other hand, the main parameter for process industrialization that

should be satisfied is cost effectiveness. It should be noted that there are several methods for methanol production, but each of them has significant problems. Old methanol production has low productivity while modern commercial methanol production systems are dramatically complex (syngas production and then methanol production). Biobase processes for methanol production are the latest methods that have been recently introduced; studies of their feasibility continue. Hence, the economic assessment of methanol production methods is necessary. Therefore, in this chapter, after introducing different pathways for methanol production, the economic evaluation of them will also be discussed.

2 Methanol Production Methods

As indicated in Fig. 23.1, a wide range of feeds can be used for methanol production (natural gas, coal, biomass). Without consideration of the feed type, there are some basic processing steps that should occur for methanol production. The first step is gasification of the feed in the presence of little or no oxygen to produce syngas comprised of carbon monoxide and hydrogen (carbon dioxide, water and various other gases may be in the produced stream). The next step is conversion of the syngas to methanol. This process is catalytic and conditions are dependent on technology, equipment, and catalyst type.

A summary of methanol production methods regarding their feedstock, reactions, and catalysts is noted in Table 23.1 (Santos et al., 2015; Miguel et al., 2015; Dolan, 2013).

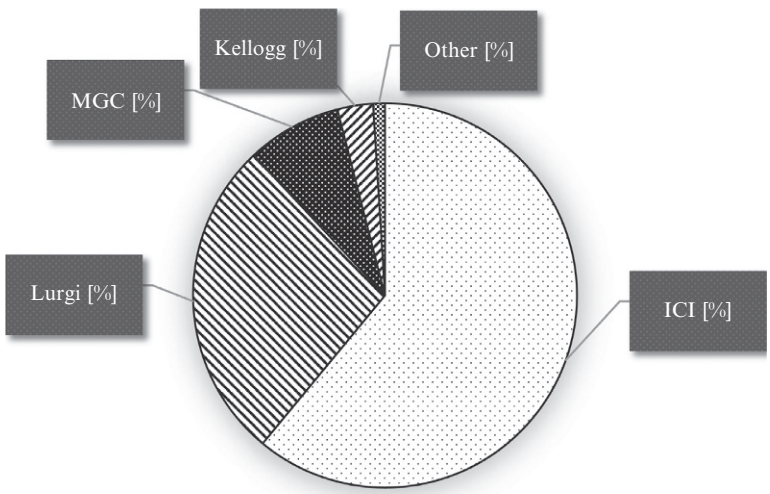

Fig. 23.1
Worldwide methanol production capacity by process.

Table 23.1 Characteristics (feedstocks, main reactions, catalysts) for production of methanol

Feedstocks	Processes and main reactions	Catalysts	Ref.
Syngas	Methanol synthesis: $CO + 2H_2 \rightleftharpoons CH_3OH$ $CO_2 + 3H_2 \rightleftharpoons CH_3OH + H_2O$	$Cu/ZnO/Al_2O_3$ $Cu/ZnO/Cr_2O_3$ or Zn/Cr	Behrens et al. (2012) and Dong et al. (2003)
Syngas	Two-step methanol synthesis: $CH_3OH + CO \rightleftharpoons HCOOCH_3$ Then $HCOOCH_3 + 2H_2 \rightleftharpoons 2CH_3OH$	Potassium methoxide, Cu chromite	Palekar et al. (1993)
Methane	Direct oxidation: $CH_4 + 0.5O_2$ (or N_2O) $\rightleftharpoons CH_3OH$	Metal oxides (e.g., MoO_3 based)	Foster (1985) and Soorholtz et al. (2013)
Methane	Bioprocessing	Enzymes (e.g., cytochrome P_{450}), methanotrophs	Hwang et al. (2014)

2.1 Steam Reforming of Methanol

As mentioned before, most of the world methanol production (about 85%) comes from steam reforming of natural gas. Two major methods are studied for the production of methanol by syngas and steam reformation. Direct and indirect syngas conversion are the main routes for methanol production by use of fossil fuels.

2.1.1 Indirect method

Production of methanol can be characterized by the two-step equation (Dolan, 2013):

$$CH_4 + 0.5O_2 \rightarrow CO + 2H_2 \tag{23.1}$$

$$CO + 2H_2 \rightarrow CH_3OH \tag{23.2}$$

This process is based on the production of syngas and methanol in two separated reactors. In this pathway, methanol production will occur in four basic steps. As shown in Fig. 23.2, these steps are:

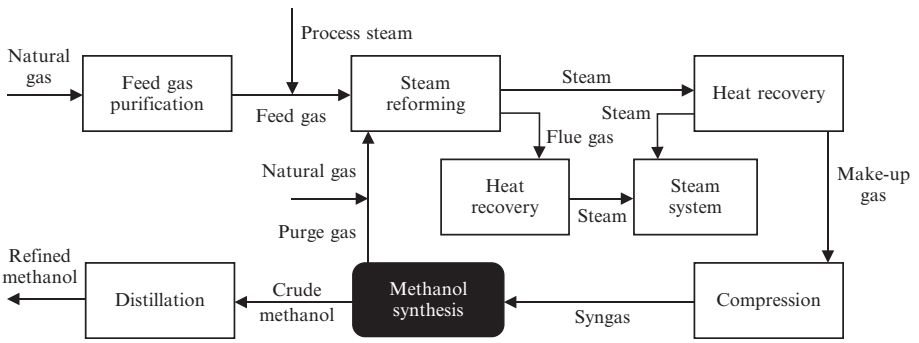

Fig. 23.2
Conventional methanol production.

i. Purification of feed gas in order to remove undesirable natural gas components such as sulfur. This step is absolutely important. The reactor is the heart of the process and the catalyst is the heart of reactor; sulfur can poison the catalysts.
ii. Steam reforming of natural gas and production of required syngas. The product of this process is a stream that is reached by carbon monoxide and hydrogen.
iii. Methanol synthesis by passing the synthesis gas over a catalyst bed at high temperatures and pressures to produce crude liquid methanol.
iv. The latest process is purification of produced methanol. During the process some unwanted components such as ethanol are produced. On the other hand, some of the process feed will be seen in the product stream (for example, water) that should separate from the product stream. Therefore, the final product of methanol production will be pure methanol (based on ASTM D-1152/97, required purity is 99.85%).

It should be noted that, usually for the syngas production process, a temperature higher than 800°C is required. Steam reforming is an endothermic process; therefore, a high temperature is suitable for the syngas production process. On the other hand, the required temperature for the methanol production process is 200–300°C. Production of methanol is an exothermic process. As indicated in Fig. 23.2, heat integration and recovery are important features of the process (Wu et al., 2005; Cheng, 1994; Kung, 1994).

Indeed, methanol production is one of the most important steps in the integrated process. Current low-pressure processes operate at 510 MPa in vapor phase using quench (ICI), tubular, or double-tube heat-exchange reactors. A single-pass conversion of syngas is low and is limited by equilibrium conversion. A high rate of gas recycling is needed. Cu/ZnO-based catalysts are industrial low-pressure methanol synthesis catalysts. In general, the selectivity of the catalysts decreases when operating at high pressures, high temperatures, high CO/H_2 or CO/CO_2 ratios, and low space velocities. Improved catalyst activity would allow a change in operational conditions in favor of high selectivity (Kung, 1994).

2.1.2 Direct method

Methanol production in a tow reactor increased the process problems. Increasing the number of process steps can lead to increases in the required space and equipment. Two systems for controlling the process will be needed. Therefore, an integrated process is desirable and can introduce a simplified process. In the past few years, there have been many active research programs around the world on the direct conversion of methane to methanol. Methanol and formaldehyde can be produced by partial oxidation of methane under controlled conditions in a homogeneous or catalytic reaction process. Many catalysts, such as Mo-based oxides, aluminosilicates, promoted superacids, and silicoferrate, have been used for the reaction. Since the activation energy for the subsequent oxidation of methanol to carbon oxides is usually smaller than that for partial oxidation, high selectivities for methanol have been demonstrated only at low methane conversions. Reaction conditions (e.g., O_2 or N_2O to CH_4 ratio,

temperature, resistance time) and surface area of supports play important roles in methanol yield. In general, low pressure favors the formation of formaldehyde. High pressure and low O_2/methane ratios favor the formation of methanol. The low yields achieved to date are a major obstacle to an economical commercialization of this route (Cheng, 1994; Cavalcanti et al., 1992).

2.2 Biomass Gasification

Methanol production from syngas leads to dramatic emissions of large amounts of greenhouse gases. Estimations show that about 3.8 kg CO_2/kg of methanol is produced in the coal-based process while for natural gas base methanol production, the amount of produced carbon dioxide is 1.6 kg per kg of methanol (Cifre and Badr, 2007). Furthermore, large amounts of coal and carbon dioxide are annually consumed in the world because these fuels are two of the most important energy sources. The production of methanol from renewable energy sources (RES) allows reducing the intensity of fossil fuels as the main feed of a methanol plant, mitigating the CO_2 emission as well (Rivarolo et al., 2016).

Production of biofuel, especially methanol from biomass as a feedstock, can occur by four basic pathways, including:

i. Biochemical conversion using enzymes and microorganisms to break down biomass into sugars used for fuel production.
ii. Thermochemical conversion employing heat energy and chemical catalysts to convert biomass into fuels.

iii. Gasification to dissociate biomass in a high-temperature, oxygen-starved environment to produce synthesis gas.
iv. Pyrolysis using high temperatures in an oxygen-free environment to encourage the decomposition of biomass.

Different dry biomass (such as forest things, waste wood, pulp mill byproducts, municipal solid waste) can be used in a methanol production system. Some of these processes can be utilized for methanol production but gasification of "dry biomass" is the most common process. In addition to dry biomass, wet biomass (like animal manure, wastewater, industrial wastewater, algae, seaweed) can be converted to ethanol by anaerobic digestion (Ray et al., 2015). The main goal for using biomass is a reduction in the consumption of fossil fuels that leads to reducing the pollutant emissions. In this method of methanol production, the synthesis reaction is reported below (Cifre and Badr, 2007; Van-Dal and Bouallou, 2013).

$$3H_2 + CO_2 \Leftrightarrow CH_3OH + H_2O \tag{23.3}$$

The methanol reaction is exothermic ($\triangle H_r = -49.2$ kJ/mol), meaning that higher methanol yields are obtained at low temperatures and high pressures. Industrially, the range of operating

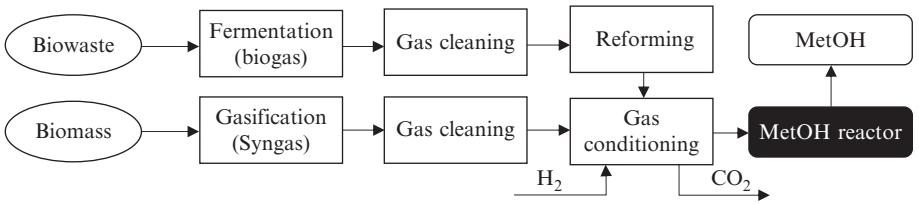

Fig. 23.3
Simplified schematic of methanol production by biomass-based feedstocks.

temperature and pressure are 200–300°C and 50–100 bar, respectively, and the catalyst commonly used is $CuO/ZnO/Al_2O_3$-based. A simplified schematic of methanol production by bio-based feedstocks is shown in Fig. 23.3 (Rivarolo et al., 2016).

Moreover, for biomass feedstocks, there are many activities that can improve the environmental friendliness of the process. One of them is to supply the required hydrogen by electrolysis. The most important subject for electrolysis use is providing the electricity. This electricity can be supplied by renewable sources such as wind and hydraulic turbines and photovoltaic panels (Sayah and Sayah, 2011).

Besides gasification for dry sources, the anaerobic fermentation system is another pathway for methanol production. Biogas can be produced by fermentation and is composed of 48% CO_2 and 52% CH_4 (+ impurities). CO_2 is a required component for methanol production; therefore a gas separation unit is necessary. The product of a biogas system should be sent to a gas separation unit for the removal of impurities and methane from the gas stream. Another component that is necessary for methanol production is H_2. This component is produced by a pressurized (30 bar) alkaline electrolyzer (AEC) fed by renewable electrical energy. The two reagents, H_2 and CO_2, are sent in the proper volume ratio (3:1) to the mixer and then to the methanol reactor that works at the operating condition of 240°C and 80 bar. The simplified plant layout is shown in Fig. 23.4. Wind, photovoltaic, and hydroelectric are the main renewable sources for electricity. The module calculates the electrical energy outlet according to the functions reported below (Rivarolo et al., 2016):

- Wind: $P = \frac{1}{2}\rho v^3 \cdot \pi \cdot \frac{D^2}{4} \cdot \eta$

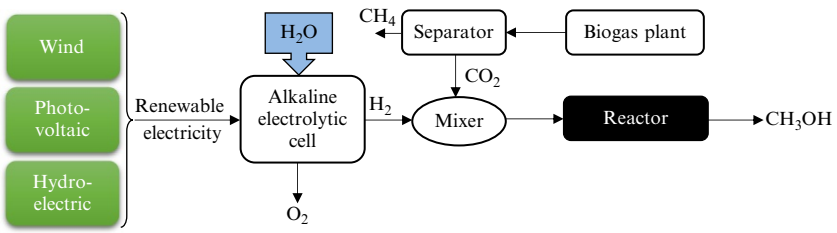

Fig. 23.4
Methanol production from biogas.

- Photovoltaic: $P = \text{Irradiation} \cdot \text{Area} \cdot \eta$
- Hydroelectric: $P = Q \cdot \rho g H \cdot \eta$

2.3 Atmospheric Carbon Dioxide

The reductive conversion of atmospheric carbon dioxide with hydrogen is noted in the below reaction. In this way, hydrogen can be stored by converting it into methanol with carbon dioxide from industrial effluents or the atmosphere. A schematic strategy of methanol production by using the atmospheric carbon dioxide method is presented in Fig. 23.5. There are many sources for supplying the required H_2. In this system, renewable electricity sources are used for H_2 production (Garrow, 2015).

$$CO_2 \xrightarrow{H_2 \text{ or } H_2O/e^-} CH_3OH \tag{23.4}$$

Supplying the required CO_2 is the key process for atmospheric carbon dioxide methanol production systems. Carbon dioxide is a greenhouse gas, which is a global concern. Many technologies have been studied for the prevention of CO_2 emissions into the atmosphere. Industrial approaches for capturing the CO_2 can be categorized into three systems: postcombustion, precombustion, and oxy-combustion. On the other hand, air contains about 0.04% (by volume) CO_2. This source can supply the needed CO_2 but air separation and separation of trace amounts of CO_2 are not cost effective. Therefore combustion systems are the main CO_2 providers for methanol production (CO_2 atmospheric method).

2.3.1 Precombustion

Precombustion technology can be widely used in chemical processes and integrated gasification combined cycles (IGCC) (Metz et al., 2005; Ghasemzadeh et al., 2015). In precombustion technology, fuel convert sto a stream of hydrogen and carbon dioxide. The next step in this process is gas separation for achieving pure hydrogen and carbon dioxide. After separation, hydrogen is used as a fuel. Carbon dioxide capture based on the precombustion method is shown in Fig. 23.6. The first step is the reaction of fuel with vapor and oxygen. An oxygen-rich flow (for liquid fuel) or air (for solid fuel) supplies oxygen for combustion.

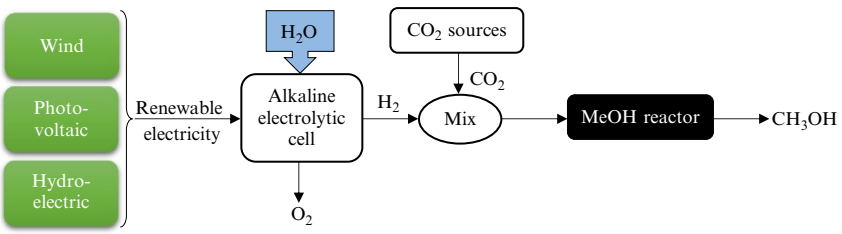

Fig. 23.5
Methanol production from pure CO_2 in atmospheric condition.

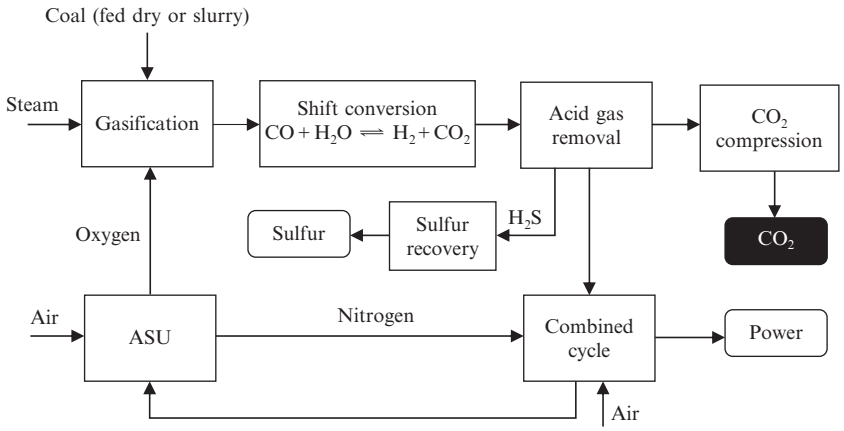

Fig. 23.6
Simple flow sheet for IGCC power plant with precombustion carbon dioxide capturing.

Operating conditions are high temperature (about 1100°C) and high pressure (about 500–800 psi) (Blomen et al., 2009; Metz et al., 2005).

The product of this process is synthesis gas. The next step is a water gas shift (WGS) that converts CO to CO_2. Due to impurities such as vapor, pretreatment is required for this stream. Pretreatment causes an increase in efficiency. An acid gas removal (AGR) section is used for separating carbon dioxide and hydrogen. Physical adsorbents are conventional methods for performing this. The product (carbon dioxide) purity of this process is near 80–90% (Gibbins and Chalmers, 2008; Sadati et al., 2015).

2.3.2 Oxy-combustion

Complete combustion of hydrocarbons (without impurities) in the presence of enough oxygen produces water vapor and carbon dioxide. Separation of water vapor from the gas stream is simple; condensation can provide the suitable separation. In precombustion technologies, combustion is made using pure oxygen (up to 97% purity); however, a small amount of nitrogen and argon remains. A big part of the exhaust gases is recycled in the boiler to maintain the usual temperature levels of pulverized coal (PC) without capture. This avoids full resizing of the boiler and its associated exchangers. The flow of uncycled CO_2 still contains water vapor, impurities (particularly some NO_x and SO_x amounts that remain in the exhaust gas of scrubbing systems), and incondensable gases such as oxygen, nitrogen, and argon. The latter originates from the ASU (air separation unit) and parasite air entries due to the lack of a seal of the PC cycle (combustion chamber, deduster, gas-gas heater, etc.). The content of CO_2 in these exhaust gases is about 75% (wet basis). The next step is to condense the water and purify the CO_2 until it is 99% pure so that it can be transported in the supercritical state. A simple schematic of the oxy-combustion system is shown in Fig. 23.7 (Sadati et al., 2015; Kanniche et al., 2010).

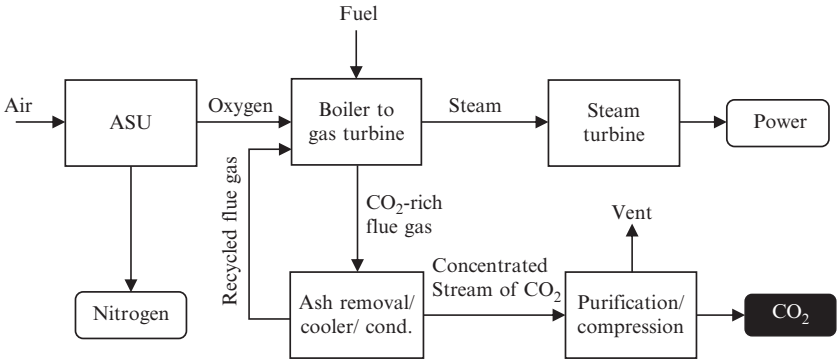

Fig. 23.7
Schematic of oxy-combustion process in an IGCC power plant.

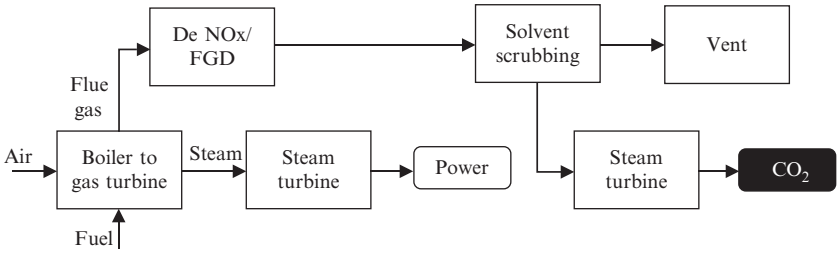

Fig. 23.8
Schematic of postcombustion process in an IGCC power plant.

2.4.3 Postcombustion

As shown in Fig. 23.8, postcombustion capture consists of treating exhaust gases on the output side of the fuel combustion. Technologies based on chemical absorption appear to be best adapted to this separation. However, other promising technologies, such as adsorption, membranes, and cryogenic processes can be used for the separation of carbon dioxide (Wang et al., 2011; Kanniche et al., 2010).

3 Methanol Applications

There are variety of applications for methanol. In the other word, production of hundreds of chemical components is dependent on methanol. Acetic acid and formaldehyde are some of the chemical components that utilize methanol (Dolan, 2013). It touches daily many products made by methanol or methanol used in its production process direction. The largest global market for methanol is as a feedstock for the production of formaldehyde. Engineered woods used in building our homes and furniture are bonded with resins produced from formaldehyde. In our cars, urethanes and plastics used in essential components also contain formaldehyde. Methanol is also used in the production of acetic acid, which is then used for making polyethylene

teraphthalate plastic used in beverage packaging. Acetic acid is the basic component of terapthalic acid, which is used in making polyester fiber for our clothing and carpets. Vinyl acetage monomer (VAM) is also produced for acetic acid and is used in the manufacture of water-based paints and adhesives. On a global basis, the fuel additive MTBE is still used to increase octane performance and reduce emissions in vehicles. MTBE is produced from methanol and butanes and continues to play an important role as a fuel oxygenate in Asia and the Middle East (Dolan, 2013). One of the most important applications of methanol for the future is transport fuel. Nowadays, the main drawback is the economy of fuel methanol. Studies showed that green methanol can improve the economy of methanol production methods. On the other hand, methanol has many suitable qualities for usage as a transportation fuel. Methanol has an octane number of 113 and its energy density is about half that of gasoline (by volume). The blend of 10% methanol with 90% gasoline can lead to an octane number up to 130. Pure methanol engines can reach efficiency close to 43% and maintain it above 40% in a wide speed and load range. Methanol can favor the transition from fossil fuels to renewable energies (Olah et al., 2011; Bozzano and Manenti, 2016). Global methanol consumption percentages are shown in Fig. 23.9. Moreover, methanol-derived chemical products and materials in detail are indicated in Fig. 23.10.

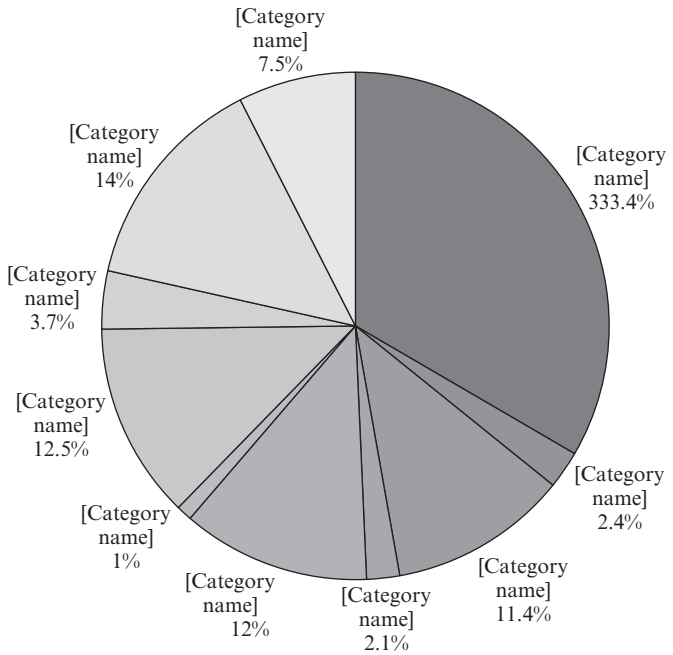

Fig. 23.9
Different global applications of methanol.

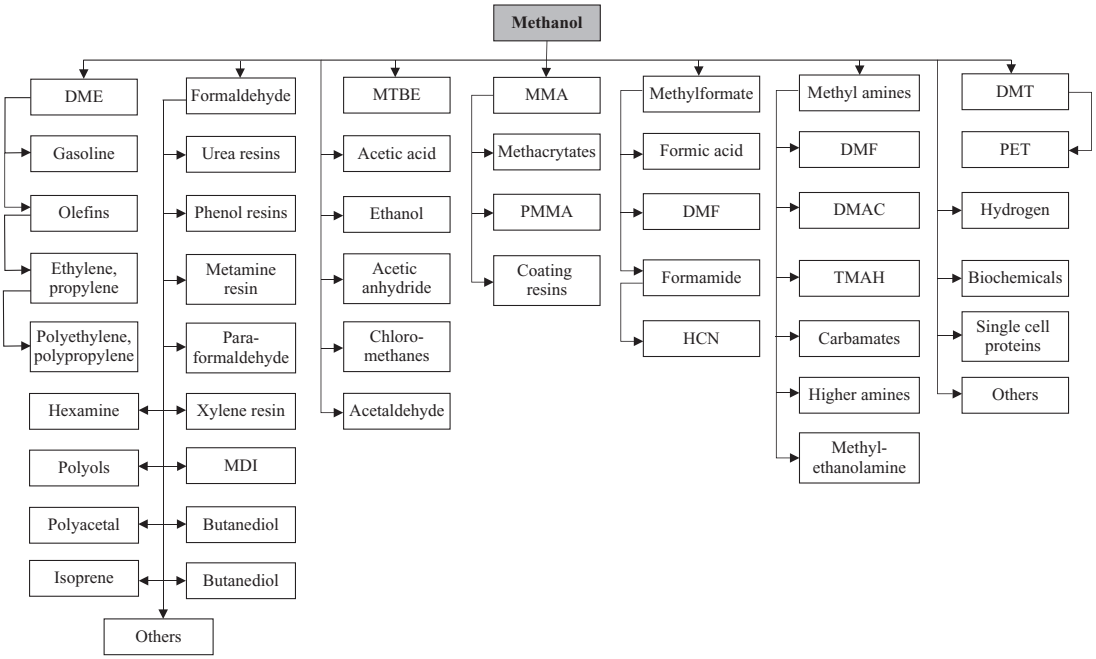

Fig. 23.10
Methanol-derived chemical products and materials.

4 Economic Assessment of Methanol Production

4.1 The Effect of Renewable Sources on Methanol Cost

For production of a chemical component, raw material feedstocks typically constitute up to 60%–70% of the manufacturing costs. Therefore, in an economic study of chemical processes, feedstock plays a significant role. As an example, acetic acid was predominantly produced from ethylene using the Wacker process, but during the early 1970s Monsanto introduced another process. By carbonylation of methanol using a Wilkinson's rhodium-phosphine catalyst and iodide (in the form of HI, CH_3I, or I_2), this process produces acetic acid with a conversion and selectivity close to 100%. Because of the high efficiency of this process and the lower cost of methanol compared to ethylene, most of the new acetic acid plants built worldwide since then are based on this technology (Olah et al., 2009).

Nowadays, renewable sources have been introduced as a suitable solution for the problems associated with fossil fuels. Renewable sources are environmentally sustainable and eliminate the worry of depleting nonrenewable sources. There are two different layouts of environmentally sustainable methanol production. Biomass and atmospheric carbon dioxide can lead to environmentally friendly processes for methanol production. Hence, the final cost effectivity of this process should be studied. Sayah and Sayah (2011) studied the

wind-hydrogen utilization for methanol production (an economic assessment in Iran). They investigated the feasibility of synthesizing methanol from its flue gas and wind hydrogen. The concept was to mitigate CO_2 emissions through flue gas recovery. Methanol production, on the other hand, requires hydrogen at the rate of 3 kmol/kmol of carbon dioxide. Electrolysis is one method by which hydrogen can be produced cleanly from a renewable source. Here it is assumed that the electrolysis unit is fed with electricity from neighbor wind farms. Oxygen will be produced as a byproduct in an electrolysis unit. However, electrolytic oxygen could be utilized for partial oxidation of methane in an autothermal reactor (ATR). Onboard water electrolysis facilitates the oxygen and hydrogen storage, delivery, and marketing. This study focuses on an integrated system of methanol production that enables green methanol production through a system with zero carbon emissions. Indeed, green methanol production is comprised of CO_2 capturing and recycling along with renewable hydrogen generation. The produced hydrogen and CO_2 will be directed to a methanol production unit. By employing the integrated system for methanol production, it can reduce the cost of using renewable energy technology. In this case, Rivarolo et al. (2016), investigated an economic analysis for methanol production from different renewable sources. One of the most important parameters for industrial processes is capital cost. Capital cost distribution for methanol production from CO_2 atmospheric purchasing and biogas are presented in Fig. 23.11.

It is clear that the majority of the total investment is consumed by the production of required hydrogen. Therefore, a hydrogen production system is a key point for environmental methanol production. Hydrogen production should be considered for the future studies about methanol production in order to accessing the best hydrogen production system in cost point of view.

As illustrated in Fig. 23.11, it's obvious that CO_2 production is not considered. As noted previously, the best method for supply the required CO_2 is a carbon capture and storage (CCS) project. This project can prevent CO_2 emissions from the main industrial carbon dioxide producers. Therefore, in order to study the economics of methanol production, a CO_2 production system should be considered. In other words, this comparison is not complete because the CO_2 production in the biogas method is considered, but the CO_2 system is ignored.

The energy source is an important parameter for discussion about methanol production from renewable sources. Three major sources for supplying the required energy are wind, hydroelectric, and photovoltaic. Each of these sources has some advantages and disadvantages. Daily distribution of output energy is one of the most important parameters. It's clear that all the noted sources are unstable in different months of the year. On the other hand, wind and photovoltaic are unstable at different times of the day. A comparison of stability or instability of wind, hydroelectric, and photovoltaic sources is shown in Fig. 23.12. In the Italian scenario, the best economic results were obtained with a hydroelectric source, which guarantees a higher number of equivalent operative hours (3000) than wind (1300) and solar (1100) energies. When renewable energy is not available, electrical energy to AEC should be purchased by the national grid (Dolan, 2013; Rivarolo et al., 2016).

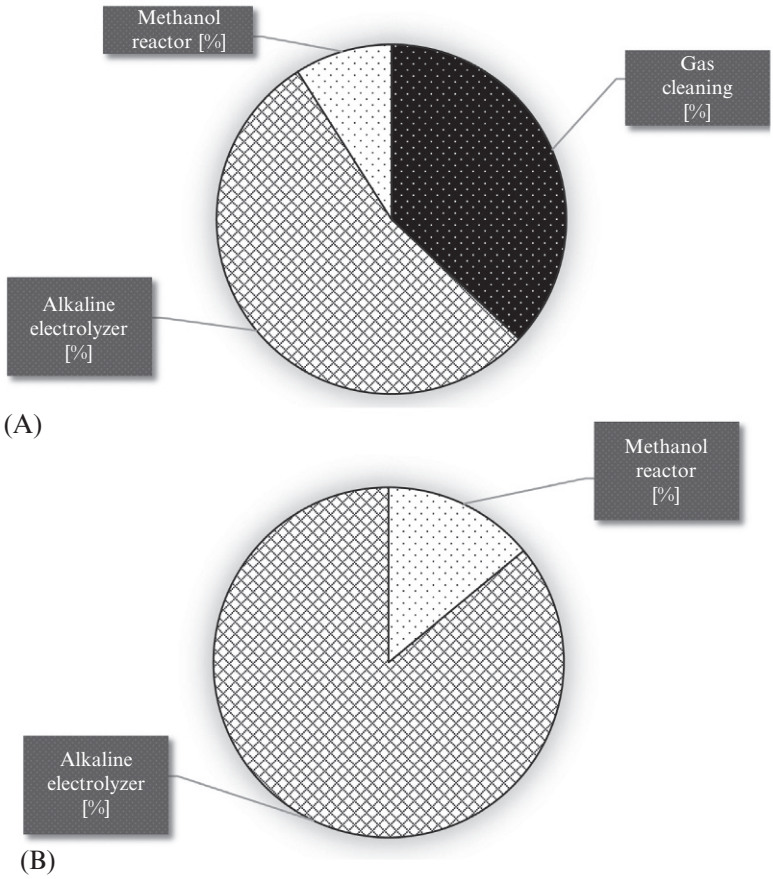

Fig. 23.11
Capital cost distribution percentages for methanol production from (A) Biogas and (B) CO_2 purchasing (total cost of (A) 3.8 M€ and (B) 2.5 M€).

Biomass gasification for methanol production is especially attractive as high carbon conversion rates and fuel yields mean that the biomass resource can be completely utilized. By comparison, conventional production processes for the biochemical conversion of plant starch and oil plants use only a small fraction of the biomass feedstock. For example, it is understood that production of ethanol from corn yields 7.2 dry tons/ha/year, or 76 GJ/ha/year, whereas the production of methanol from wood yields 15 dry tons/ha/year or the equivalent of 177 GJ/ha/year. In other words, through gasification, one ton of woody biomass can produce 165 gallons of methanol while the hoped-for yields for cellulosic ethanol are targeted at around 60–70 gallons of fuel per ton of biomass. As is noted in the reference (Dolan, 2013): "We need to move away from (the) first generation in ethanol manufacturing and further to (the) second and third generation, which is all about cellulose material and gasification, and this implies therefore room for methanol and synthetic diesel."

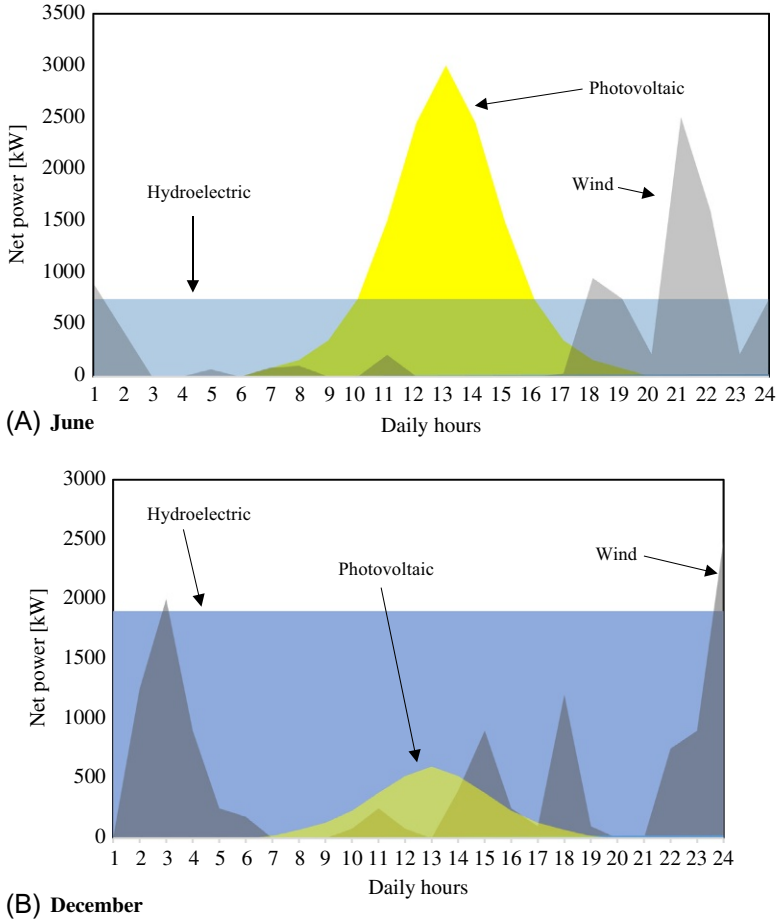

Fig. 23.12

Net power average production from different RES in summer (June) and winter (December).

4.2 Effect of Operating Conditions on Methanol Cost

Operating conditions can change the efficiency of the process. Temperature, pressure, and the contribution of each feed component in the feed stream are the main operating conditions. Perhaps a process could be independent of one of those denoted parameters, but it should be noted that most of the chemical processes are dependent on the denoted parameters. Hence, for methanol production systems, reaction temperature, reaction pressure, and circulation rate are the main variables that can change the economy of methanol production.

4.2.1 Reaction temperature

It is evident that various catalysts have different desirable temperatures. Methanol production is a catalytic process. Hence, the catalyst operating temperature has a marked effect on the rate of methanol production. New converter charges of a $Cu/Zn/Al_2O_3$ catalyst should be

operated as cool as possible at the inlet to preserve long-term life but generally not below 200°C. When equilibrium is not being achieved, an increase in the catalyst operating temperature gives a marked increase in methanol conversion. At design catalyst activity ("end of life"), the increase of a few degrees Celsius in the average bed temperature could result in a 35% increase in the rate of reaction and, therefore, the rate of methanol production. For a fresh catalyst, a 3°C increase in the average bed operating temperature can result in about 10% enhancement in methanol production. However, as equilibrium is attained, further increases in temperature result in a reduction in the rate of methanol production. Indeed, the temperature of the reactor should be controlled exactly to achieve suitable conversion (Kung, 1994; Hirano et al., 1998).

4.2.2 Reaction pressure

The feed of a methanol reactor is a gas stream, so reaction pressure is an effective parameter. Indeed, reaction pressure affects both equilibrium position and rate of reaction in methanol synthesis. From a total loop perspective, an increase (or decrease) in operating pressure affects more than merely the reaction conditions. It also affects the condensation of product (dew point) and recycling of methanol back to the converter system. Considering any given converter, however, calculations indicate that a 10% increase in operating pressure yields about a 10% increase in methanol production if equilibrium conditions exist. When the reaction is far from equilibrium and controlled by kinetics, the increase (or decrease) in methanol production is more than proportional to the increase (or decrease) in operating pressure. In particular, a 10% increase in pressure under these conditions, for example, yields about 20% improvement in methanol production (Kung, 1994; Graaf et al., 1988).

4.2.3 Circulation rate

In equilibrium reactions using a real system, access to the equilibrium condition is impossible. Therefore, it is necessary to help the process to achieve better conditions in the aspects of conversion and productivity. Circulation is one of the process conditions that should be controlled. When the reactor system in methanol production operates under kinetically controlled conditions, an increase in the circulating gas rate causes methanol production to decrease. If equilibrium is being achieved, however, one can expect that a 2.53% increase in production will be realized for a 5% enhancement in circulation and that a 56% increase in production will result from a 10% enhancement in circulation, and so forth (Kung, 1994).

5 Conclusion and Future Trends

Detailed studies of methanol production systems show that renewable sources have great potential for methanol production. Current studies were focused on the economy of methanol production from biomass. Two overall pathways for utilization of biomass for methanol production are suggested: biogas by wet biomass and gasification of dry biomass. It's clear that replacing fossil fuels with biomass can help the environment. On the other hand, CO_2 can

convert to methanol by an environmentally friendly process. Experimental studies show that the total cost of the biogas system is about 1.5 times more than the CO_2 purchasing system. It seems that an investment cost of the CO_2 capture process has not been considered. For production of methanol from CO_2, this component should separate and prevent emissions to the atmosphere. Therefore, an additional process should add to the CO_2 producer processes. This investment is effective on general cost effectivity of the process. However, without consideration of the CO_2 capture process investment, the plant configuration with CO_2 sequestration by biogas plant is characterized by higher investment costs, due to the plant complexity. On the other hand, revenues are higher and DPBP is lower than eight years in most of the scenarios, thanks to CH_4 selling. From the environmental point of view, both the solutions allow avoiding the consumption of methane and the emissions of CO_2 related to the standard methanol production from fossil fuels. The economic performances can be further improved considering the carbon tax related to CO_2 emissions.

Another important point for the life cycle of methanol production (environmentally friendly) is the H_2 producer system. Nowadays, electrolysis of water is considered as a suitable H_2 producer process. The main subject in this process is supplying the required electricity. Conventional methods for renewable electricity are photovoltaic, hydroelectric, and wind power base electricity. Photovoltaic and wind are unstable on a daily basis. Therefore preorganization and controlling these systems are difficult. In this point of view, the hydroelectric source is suitable, but this source has an availability problem. Therefore, for each area of the world, land use planning and studies are required for making a decision.

Finally it should be noted that economic studies results can't be considered for global programming. In other words, economic studies are location-dependent. For example, in one part of the world, installation may be more expensive while in another part, it could be feedstock. Therefore, overall parameters such as productivity, conversion, operating temperature, operating pressure, etc. should discussed for achieving economic effectivity.

References

Balki, M.K., Sayin, C., 2014. The effect of compression ratio on the performance, emissions and combustion of an SI (spark ignition) engine fueled with pure ethanol, methanol and unleaded gasoline. Energy 71, 194–201.

Behrens, M., et al., 2012. The active site of methanol synthesis over $Cu/ZnO/Al_2O_3$ industrial catalysts. Science 336 (6083), 893–897.

Blomen, E., Hendriks, C., Neele, F., 2009. Capture technologies: improvements and promising developments. Energy Procedia 1 (1), 1505–1512.

Bozzano, G., Manenti, F., 2016. Efficient methanol synthesis: perspectives, technologies and optimization strategies. Prog. Energy Combust. Sci. 56, 71–105.

Cavalcanti, F.A.P., Stakheev, A.Y., Sachtler, W.M.H., 1992. Direct synthesis of methanol, dimethyl ether, and paraffins from syngas over Pd/zeolite Y catalysts. J. Catal. 134 (1), 226–241.

Celik, M.B., Ozdalyan, B., Alkan, F., 2011. The use of pure methanol as fuel at high compression ratio in a single cylinder gasoline engine. Fuel 90 (4), 1591–1598.

Cheng, W.-H., 1994. Methanol Production and Use. CRC Press, United States.
Cifre, P.G., Badr, O., 2007. Renewable hydrogen utilisation for the production of methanol. Energy Convers. Manag. 48 (2), 519–527.
Dolan, G.A., 2013. Methanol production and markets: past, present, and future. The Toxicology of Methanol. John Wiley & Sons, United States, pp. 1–10.
Dong, X., et al., 2003. Highly active CNT-promoted Cu-ZnO-Al_2O_3 catalyst for methanol synthesis from H_2/CO/CO_2. Catal. Lett. 85 (3–4), 237–246.
Foster, N.R., 1985. Direct catalytic oxidation of methane to methanol—a review. Appl. Catal. 19 (1), 1–11.
Garrow, T., 2015. A methanol economy based on renewable resources. McGill Green Chem. J. 1, 87.
Ghasemzadeh, K., Basile, A., Tilebon, S.M.S., 2015. Membranes for IGCC power plants. In: Integrated Membrane Systems and Processes. John Wiley & Sons, United States, p. 255.
Ghasemzadeh, K., Tilebon, S.M.S., Basile, A., 2016. Membrane reactors for hydrogen production from biomass-derived oxygenates. In: Membrane Technologies for Biorefining. Woodhead Publishing, United Kingdom, p. 435.
Gibbins, J., Chalmers, H., 2008. Carbon capture and storage. Energy Policy 36 (12), 4317–4322.
Gong, C.-M., et al., 2011. Improvement of fuel economy of a direct-injection spark-ignition methanol engine under light loads. Fuel 90 (5), 1826–1832.
Graaf, G.H., Stamhuis, E.J., Beenackers, A., 1988. Kinetics of low-pressure methanol synthesis. Chem. Eng. Sci. 43 (12), 3185–3195.
Hirano, A., et al., 1998. Temperature effect on continuous gasification of microalgal biomass: theoretical yield of methanol production and its energy balance. Catal. Today 45 (1), 399–404.
Hwang, I.Y., et al., 2014. Biocatalytic conversion of methane to methanol as a key step for development of methane-based biorefineries. J. Microbiol. Biotechnol. 24 (12), 1597–1605.
Kanniche, M., et al., 2010. Pre-combustion, post-combustion and oxy-combustion in thermal power plant for CO_2 capture. Appl. Therm. Eng. 30 (1), 53–62.
Kung, H.H., 1994. Methanol Production and Use Chemical Industries. Northwestern University, Evanston, IL
Liu, S., et al., 2007. Study of spark ignition engine fueled with methanol/gasoline fuel blends. Appl. Therm. Eng. 27 (11), 1904–1910.
Metz, B., et al., 2005. IPCC special Report on Carbon Dioxide Capture and Storage. Prepared by Working Group III of the Intergovernmental Panel on Climate Change, IPCC. Cambridge University Press, Cambridge, United Kingdom/New York, USA, p. 4.
Miguel, C.V., et al., 2015. Direct CO_2 hydrogenation to methane or methanol from post-combustion exhaust streams-A thermodynamic study. J. Nat. Gas Sci. Eng. 22, 1–8.
Olah, G.A., Goeppert, A., Prakash, G.K., 2009. Methanol-based chemicals, synthetic hydrocarbons and materials. Beyond Oil and Gas: The Methanol Economy, second ed., Wiley-VCH, Germany, pp. 279–288.
Olah, G.A., Goeppert, A., Prakash, G.K.S., 2011. Beyond Oil and Gas: the Methanol Economy. John Wiley & Sons, United States.
Pachauri, R.K., et al. (2014). Climate Change 2014: Synthesis Report. Contribution of Working Groups I, II and III to the Fifth Assessment Report of the Intergovernmental Panel on Climate Change, IPCC.
Palekar, V.M., et al., 1993. Slurry phase synthesis of methanol with a potassium methoxide/copper chromite catalytic system. Appl. Catal. A Gen. 102 (1), 13–34.
Ray, S., et al., 2015. Design and analysis of a simulated methanol production plant. In: Industrial Engineering and Operations Management (IEOM), 2015 International Conference, pp. 1–7.
Rivarolo, M., et al., 2016. Feasibility study of methanol production from different renewable sources and thermo-economic analysis. Int. J. Hydrog. Energy 41 (4), 2105–2116.
Sadati, S., Vousoughi, P., Eyvazi, M., 2015. Hydrogen production: overview of technology options and membrane in auto-thermal reforming including partial oxidation and steam reforming. Int. J. Membr. Sci. Technol. 2 (1), 56–67.
Santos, B.A.V., et al., 2015. Methanol production by bi-reforming. Can. J. Chem. Eng. 93 (3), 510–526.
Sayah, A.K., Sayah, A.K., 2011. Wind-hydrogen utilization for methanol production: an economy assessment in Iran. Renew. Sust. Energ. Rev. 15 (8), 3570–3574.

Soorholtz, M., et al., 2013. Direct methane oxidation over Pt-modified nitrogen-doped carbons. Chem. Commun. 49 (3), 240–242.
Van-Dal, É.S., Bouallou, C., 2013. Design and simulation of a methanol production plant from CO_2 hydrogenation. J. Clean. Prod. 57, 38–45.
Wang, M., et al., 2011. Post-combustion CO_2 capture with chemical absorption: a state-of-the-art review. Chem. Eng. Res. Des. 89 (9), 1609–1624.
Wu, J., et al., 2005. Combined coal gasification and methane reforming for production of syngas in a fluidized-bed reactor. Energy Fuel 19 (2), 512–516.

CHAPTER 24

Cost Estimation of an Integrated System for Co-production of Electricity and Methanol

Kamran Ghasemzadeh[*], Seyyed M. Sadati Tilebon[†], Mojtaba Nasirinezhad[*], Angelo Basile[‡]

[*] *Urmia University of Technology, Urmia, Iran* [†] *Iran University of Science & Technology, Tehran, Iran*
[‡] *Institute on Membrane Technology (ITM-CNR), Rende, Italy*

Acronyms

ASU	air separation unit
CCS	carbon dioxide capture and storage
CGT	conventional flue gas treatment
EP-ASU	elevated pressure air separation unit
ESP	electrostatic precipitator
FGD	flue-gas desulfurization
HP	high pressure
HRSG	heat recovery steam generator
IGCC	Integrated gasification combined cycle
LCOE	levelized cost of the electricity
LHV	lower heating value
LP	low pressure
MP	medium pressure
NGCC	natural gas combined cycle
NPV	net present value
PC	pulverized coal
PLOX	pumped liquid oxygen
SCR	silicon-controlled rectifier
USC	ultra-supercritical
WGS	water gas shift

Methanol. https://doi.org/10.1016/B978-0-444-63903-5.00024-8

1 Introduction

In recent years, the most extensively discussed topic in environmental studies signifies a potentially serious threat to natural ecosystems and to the quality of human life on earth. Research studies predict that the adverse concerns of climate change induced by human activities will include some of the following in the future (Chen, 2005; Goldemberg, 2000):

- The average temperature of the global surface air will increase by 1.0–3.5°C during this century.
- The global mean sea level is likely to rise by about 6 cm per decade during this century, mainly due to the thermal expansion of the ocean and the melting of some land ice.
- Even though food production may increase in some areas, the high likelihood of its decrease in other areas, especially in the tropics and subtropics, will bring hardship to large segments of the population.
- Fast climate changes may result in the instability of ecosystems, causing natural disasters such as floods and droughts.
- Some diseases currently contained within certain areas may spread further to threaten new populations.

Environment safety is the most important responsibility for the future. Greenhouse gases are a serious problem for the future of the atmosphere and therefore the future of the world. Power plants are main greenhouse gases producers. Between different technologies, coal base power plants can emit a huge amount of pollutant and greenhouse gases such as CO_2 to atmosphere. Therefore, finding a way for the removal of CO_2 from the flue gas of power plants will be a valuable method for reduction of CO_2 emission (Wall, 2007; David and Herzog, 2000).

However, the cause of the discussion about coal base power plants is a second future problem named energy. Now, natural gas and petroleum is the main energy carrier that is used in many applications but burning is the worst usage of them. Coal is more accessible than natural gas and petroleum. Integrated gasification combined cycle (IGCC) power plants can convert the coal to electricity but there are some disadvantages such as air pollutants (Zhang et al., 2013; Kaldis et al., 2004). Consumption of low quality fuels such as heavy fossil feedstocks (petcoke, coal, and refinery residues) is a suitable solution for the limitations of natural gas and petroleum. Gasification is a favorite method for producing syngas from heavy fossil feedstocks. In the IGCC power plants, the feedstock, an oxidizer, and a temperature moderator (usually steam) react inside a gasifier to produce a syngas stream that is rich in CO and H_2, which is ultimately fed into a gas turbine-based combined cycle for power generation. Research on the IGCC power plant technology started in the 1970s, but coal-based IGCC power plants are still not fully commercial (Ghasemzadeh et al., 2015).

From the power generation point of view, estimations show that global power generation in 2030 will be about 1.6 times more than that of 2010. It's extensively expected that coal can play

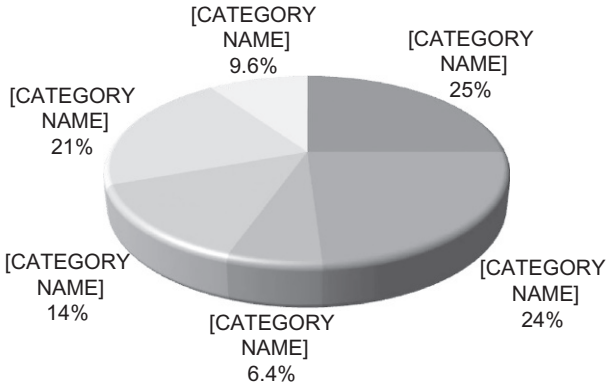

Fig. 24.1
Total GHG emissions in 2010 (49 Gt CO_2).

an important role to supply the additional required power. Coal, due to its stable and cheap price, large amounts of minable reserves, a good geographical distribution of coal mines and, depending on their location, being in politically stable regions, will remain a significant primary energy source for the future (Ghasemzadeh et al., 2015; Nagasaki et al., 2013). Hence, the IGCC power plants are being developed as an economical method of producing electricity, while simultaneously capturing CO_2 for sequestration. In these kinds of power plants, conventional cold absorption processes are the common technology for CO_2 separation from gasified coal syngas. Separation and sequestration of the CO_2 by these procedures increase the levelized cost of the electricity (LCOE) produced by about 30%. Separation of CO_2 leads to an environmental friendly process with better economic conditions (Ghasemzadeh et al., 2015). The main sources of CO_2 emissions are power generation, Agriculture, Forestry, and Other Land Use, industrial processes, transportation, and residential and commercial buildings, as illustrated in Fig. 24.1 (On Climate Change, 2015).

On the other hand, the main application of CO_2 capture is currently expected to be in power generation and large energy-consuming industries, particularly oil, gas processing, cement, iron, steel, and chemicals production. Captured CO_2 can be used in several applications, the same as enhanced oil recovery can. One of the newest applications for captured CO_2 is methanol production. However, economic assessment of the coproduction of electricity and methanol can be of interest for researchers and industrial engineers. Therefore, in this chapter, the integrated system for coproduction of electricity and methanol is discussed in from the economic point of view (IEA, 2003; Davison, 2007).

2 IGCC Plant Technology

As indicated in Fig. 24.2, the process flow diagram (PFD) of the IGCC plant is significantly complex. Typically, this process is required for the air separation unit (ASU), in which the required oxygen is provided for gasification. The gasifier converts the coal to syngas in high

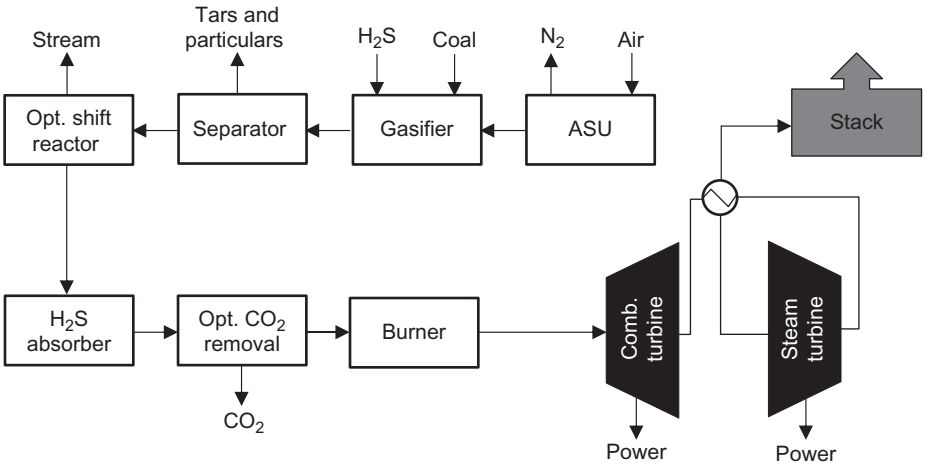

Fig. 24.2
PFD for a typical IGCC power plant.

pressure (HP) and temperature. It should be noted that coal contains some nonhydro-carbonic atoms such as N, Ar, and S. Therefore, in addition to the syngas product, the stream includes some other components, such as CO_2, N_2, CH_4, Ar, H_2S, particulates, and tars.

The gas stream is quenched and scrubbed to remove tar and particulates. If CO_2 capture or H_2 production is desired in the IGCC plant, regarding the water gas shift (WGS) reaction, high and low temperature shift reactors are used to convert CO and H_2O to H_2 and CO_2. Sulfur compounds, and optionally CO_2, are then eliminated by a low temperature absorption process. The high-pressure syngas stream is then burned with air and the hot high-pressure gas product stream is used to drive a gas turbine and generate electricity. The hot turbine exhaust stream is used to produce steam that provides additional electricity in a steam turbine. The cooled gas stream is vented into the atmosphere. In general, an IGCC plant has an overall heat-to-electrical power efficiency of about 45%, significantly better than the 35% efficiency of a conventional subcritical pulverized coal (PC) power plant. However, this advantage is more than outweighed by the higher capital cost of an IGCC plant (Merkel et al., 2012; Ghasemzadeh et al., 2016).

As noted previously, coal base power plants are main CO_2 producers. Therefore, from the CO_2 capturing point of view, the IGCC plant with and without a CO_2 capture unit are two types of the IGCC power plant. Block flow diagrams for both processes are presented in Figs. 24.3 and 24.4. It should be noted that the real benefit of the IGCC technology can be bold if a cost is placed on CO_2 emissions. This is because the CO_2 removal from high-pressure, high-concentration gasification streams will be significantly less costly than CO_2 removal from conventional PC power plant flue gas. Regarding the literature, several technologies were studied for the separation of CO_2, but the absorption process has been introduced as main commercial process.

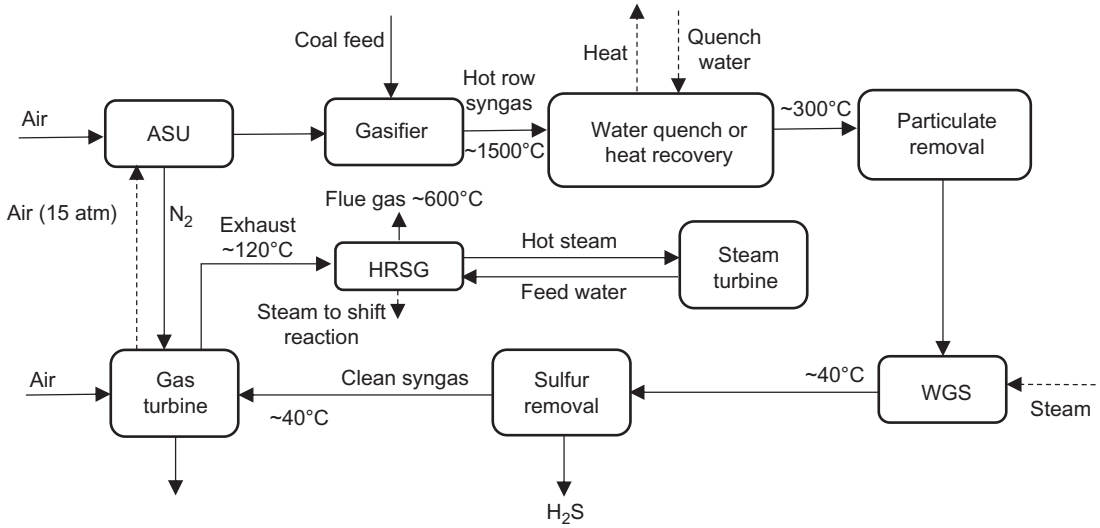

Fig. 24.3
The process scheme of an IGCC power plant without CO_2 capture processing.

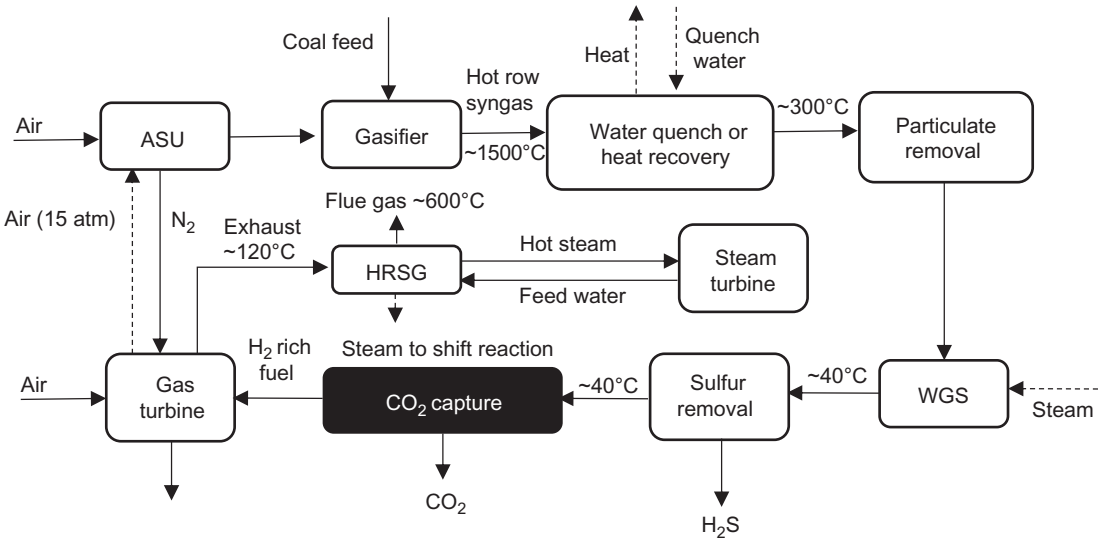

Fig. 24.4
The process scheme of an IGCC power plant with CO_2 capture processing.

There are many advantages and disadvantages for absorption such as simple technical base (as an advantage) and needs of tertiary component, complex and high-volume technology, unstable efficiency (as disadvantages). Membrane separation, as one of the new methods, can be used in gas separation instead of conventional methods and provides many suitable characteristics (Rezvani et al., 2009; Carbo et al., 2006).

3 Methanol Production in the IGCC Plant

There are three major technologies used to produce methanol, including the usage of syngas, biomass, and carbon dioxide. The main reactions for methanol production is the conversion of $CO+H_2$ or CO_2+H_2 to methanol (as shown in Eqs. 24.1 and 24.2). For the syngas method of methanol production, the required CO and H_2 is produced by a reformer. On the other hand, for the carbon dioxide method of methanol production, the needed CO_2 should be supplied by an external source. Power plants (especially those which consume coal) are principal CO_2 producers in the world. Therefore, consideration of a system for the separation of CO_2 and usage of it in methanol production will be a valuable improvement from the economic and environmental points of view. The overall flow diagram of a typical methanol production by power plant flue gas is displayed in Fig. 24.5 (Studt et al., 2014; Sakurai and Haruta, 1995; Obert and Dave, 1999).

$$CO+2H_2=CH_3OH \tag{24.1}$$

$$CO_2+3H_2=CH_3OH+H_2O \tag{24.2}$$

As discussed previously, in order to have simultaneous methanol and electricity production in an IGCC power plant, a CO_2 separation system should be considered. There are three main ideas for carbon dioxide capturing from IGCC power plants. These main methods for CO_2 separation from the IGCC power plant (as indicated in Fig. 24.6) include (Kanniche et al., 2010; Kunze and Spliethoff, 2012):

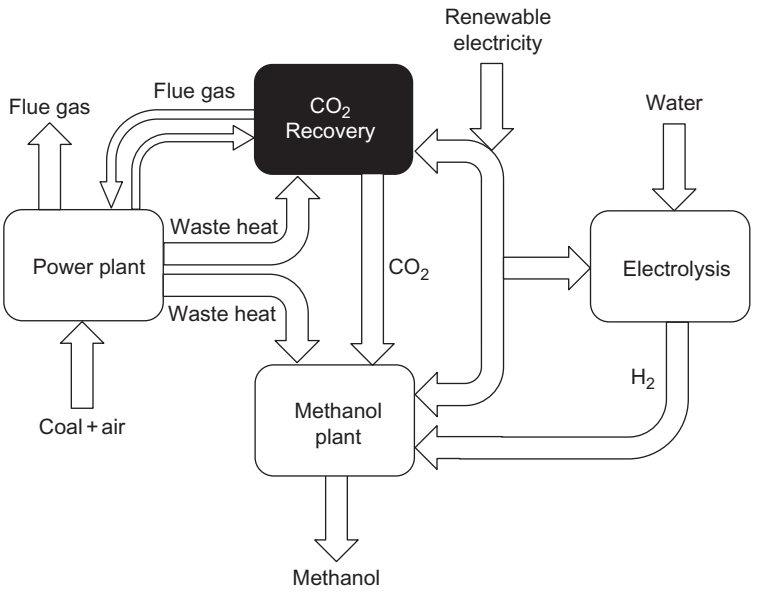

Fig. 24.5
Use of waste heat and renewable electricity to produce methanol from flue gas CO_2.

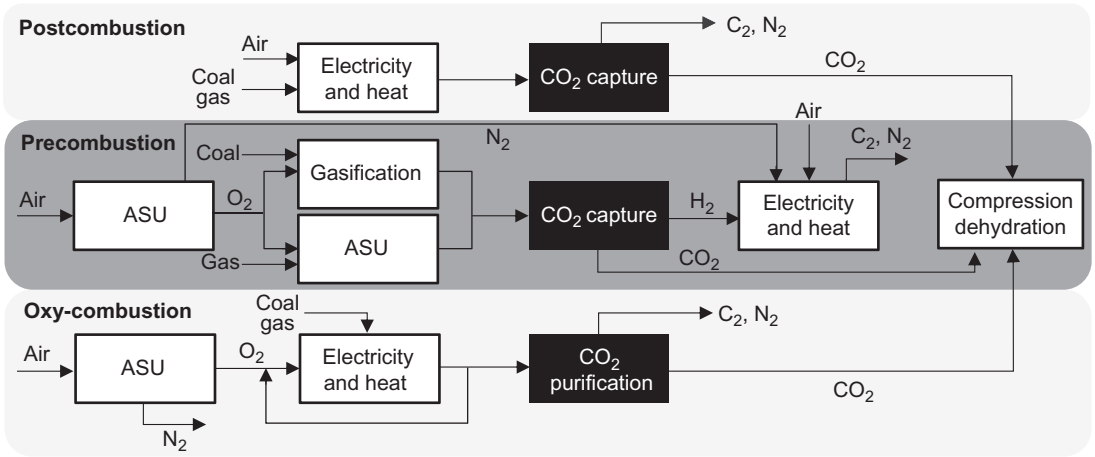

Fig. 24.6
The three CO_2 capture processes.

- *Precombustion capture*: To capture CO_2 in a synthesis gas after conversion of CO into CO_2. In this method, fossil fuel should convert to $CO+H_2$. Then H_2 is used as an energy source and CO_2, after WGS, will be separate (Babu et al., 2013; Kanniche et al., 2010; Ertesvåg et al., 2005).
- *Postcombustion capture*: To capture CO_2 in the exhaust gases after fully burning the fuel with air (Abanades et al., 2007; Puxty et al., 2009).
- *Capture in oxy-combustion*: Consisting of combustion in oxygen with recycling of exhaust gases (therefore, composed mainly of CO_2 and water) and purification of the CO_2 flow, to eliminate incondensable gases (Dillon et al., 2004; Fu and Gundersen, 2012; Kanniche et al., 2010).

After supplying the required CO_2, this stream will send in a methanol production reactor. So, by adding the H_2 in the presence of a suitable catalyst, it leads to methanol production.

3.1 Cases of CO_2 Capturing

3.1.1 Precombustion

Feeding the IGCC process with CO_2 precombustion capture can occur in two types: dry feeding and slurry feeding (see Figs. 24.7 and 24.8). Precombustion is based on syngas production. When a controlled amount of water is present, the syngas production reactor will be improved. The cause of this improvement is the WGS reaction that can consume the water and produce H_2 and CO_2. On the other hand, coal should enter through a crasher, then the powder of the coal enters the gasifier. It's clear that the operability of slurry powders is better than the dry powder. However, the dry operation of the IGCC plant needs steam for gasification. Because of the high

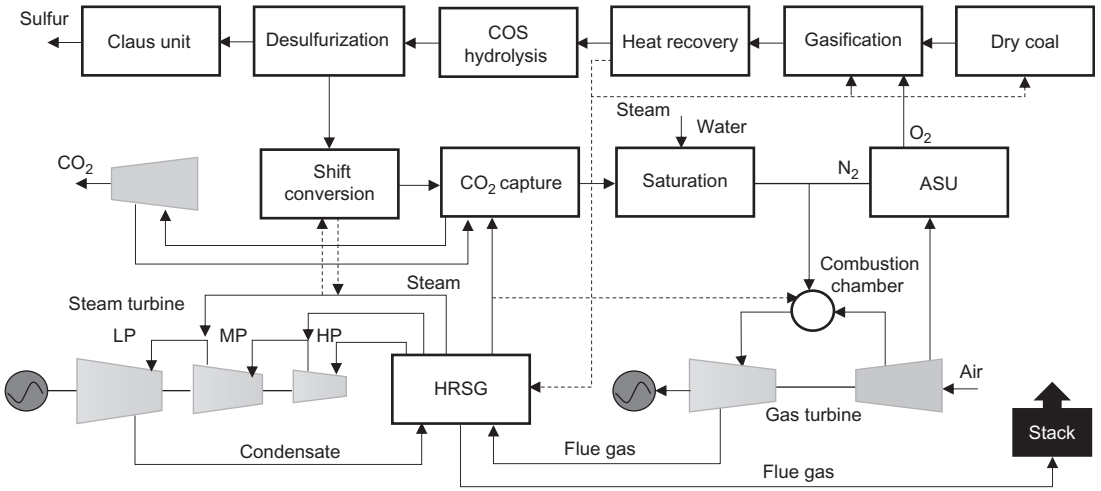

Fig. 24.7
Dry feeding IGCC with capture of CO_2 (precombustion).

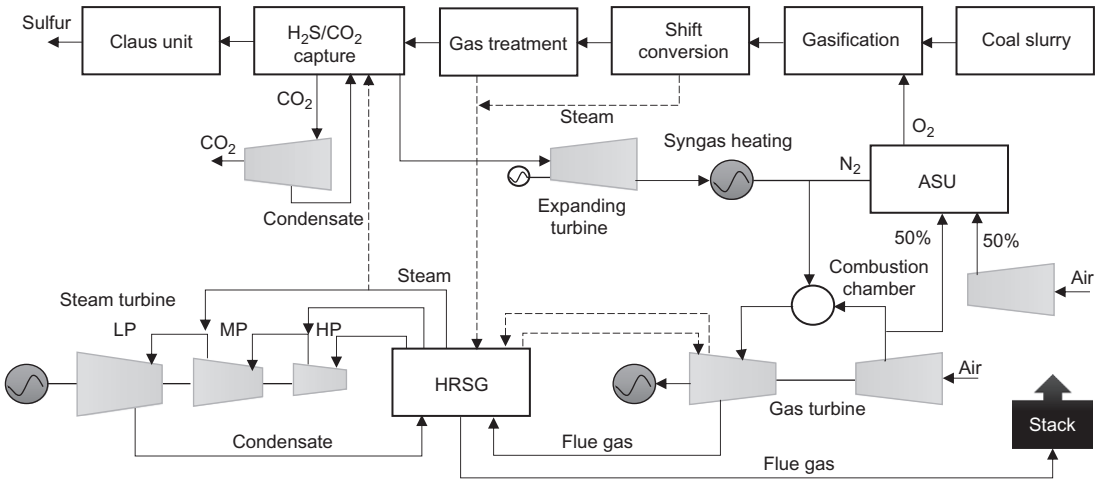

Fig. 24.8
Quench-IGCC-slurry with capture of CO_2 (precombustion).

temperature, the pressure of the steam is a positive parameter for gasification. All of these noted and non-noted parameters should be considered during the design stage (Carbo et al., 2009; Kim et al., 2011a,b).

The precombustion of CO_2 capturing is related to the treatment of a synthetic gas composed principally of CO and H_2. Gasification of coal or reforming of natural gas with oxygen leads to a mixture composed principally of $CO + H_2$ (on dry), and then after conversion of CO with steam, to a mixture of $CO_2 + H_2$. CO_2 can then be separated using a physical absorbent (which is less

expensive as an investment and less penalizing for the efficiency than if the exhaust gases are treated, because the gas is under pressure and there is no nitrogen). Indeed, CO_2 is sent to the compression unit, while H_2 is used as input to a combined cycle to produce electricity. However, this system is still handicapped by low availability and high investment and production costs (Kanniche et al., 2010).

The optimum separation process will be chosen as a function of the partial pressure of CO_2 in the gas to be treated. In the case of precombustion capture, the partial pressure of CO_2 depends on the IGCC process chosen for coal, or the pressure of the reforming process chosen for natural gas. However, the increase in pressure is not a free operation, and it must be assured that the gain in capture due to the HP is not cancelled out by the additional energy that must be supplied. The schematic of two different IGCC power plants with CO_2 capture is illustrated in Figs. 24.7 and 24.8. The first is precombustion CO_2 capturing in an IGCC. The partial pressure of CO_2 provided by this system is about 8 bars. The quench type gasification, the other alternative studied here, is fed with a mixture of coal and water (slurry), and the shift conversion is immediately inserted downstream the gasification system as the synthetic gas contains enough water to convert CO into CO_2 (Kanniche et al., 2010; Babu et al., 2013).

3.1.2 Postcombustion

As depicted in Fig. 24.9, postcombustion capture consists of treating exhaust gases on the output side of IGCC power plants. Several technologies like membrane separation, cryogenic separation, adsorption, and absorption can be used in postcombustion process. Technologies

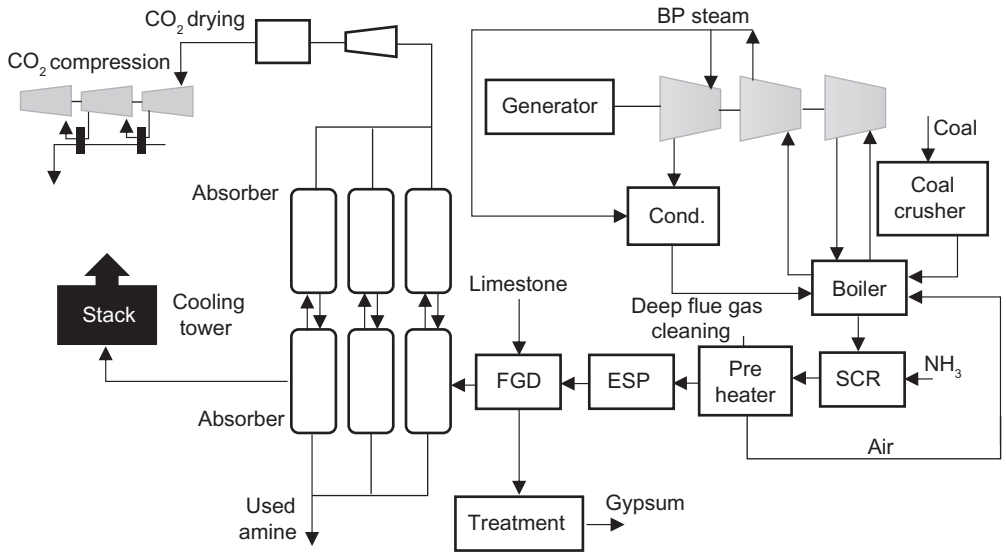

Fig. 24.9
CO_2 capturing in postcombustion of PC.

based on chemical absorption appear to be best adapted to this separation. Other technologies, adsorption, membranes, and cryogenic, are even less suitable for postcombustion capture than for precombustion capture. Researchers noted two reasons for this comparison (Kanniche et al., 2010):

- A much lower partial pressure of CO_2 in postcombustion exhaust gases than in synthetic gas originating from a gasifier or a reformer: 50–100 mbars in exhaust gases compared with 8–16 in synthetic gas.
- The presence of larger quantities of dust, impurities such as SO_x and NO_x, and incondensable gases, particularly oxygen (which do not exist or exist only in very small quantities in synthetic gas).

As noted before, the absorption process is (now but maybe not in the future due to fast development of separation technologies especially membrane separation) the best method for the postcombustion process. For choosing a suitable absorbent, partial pressure in flue gas is the main parameter. However, partial pressure of CO_2 in flue gas is usually low. This is the main reason for the choice of using the chemical absorption process (Kanniche et al., 2010; Ertesvåg et al., 2005).

Chemical absorption (processes with amines, Benfield process with potassium carbonate) is an industrial technology and has been used for decades, but in the past it has only been used to treat very clean gas mixtures containing few or no impurities such as dust, SO_x, NO_x, oxygen (ammonia industry and fertilizer industry, separation of CO_2 from natural gas), or only containing very small quantities of them. Therefore, chemical absorption will have to satisfy two challenges before it can be applied to the capture of CO_2 in exhaust gases from coal power stations, first related to its strong energy demand for the regeneration of the absorbent (increasing with decreasing of CO_2 partial pressure), and second the degradation of the absorbent by impurities contained in the exhaust gases to be treated. Degradation of chemical solvents will be treated subsequently in the chapter concerning technical limitations. In addition to these noted problems, coal contains a low amount of sulfur. Hence, absorbed gases will contain sulfur component. So, if sulfur component enters the reactor, it will deactivate the used catalysts (Kanniche et al., 2010).

3.1.3 Oxy-combustion

The importance of CO_2 partial pressure in flue gas was discussed in the previous section. Changing the partial pressure of CO_2 can affect the chosen separation method. The most significant goal of the oxy-combustion process is increasing the partial pressure of CO_2 in flue gas. In fact, the oxy-combustion process can provide a stream of flue gas (exhaust gases from combustion) by a high partial pressure of CO_2, because it avoids the dilution of exhaust gases with nitrogen in air. Therefore, an ASU unit as a pure oxygen provider is required. An APC oxy-combustion diagram is illustrated in Fig. 24.10 (Kim et al., 2011a,b; Erlach et al., 2011).

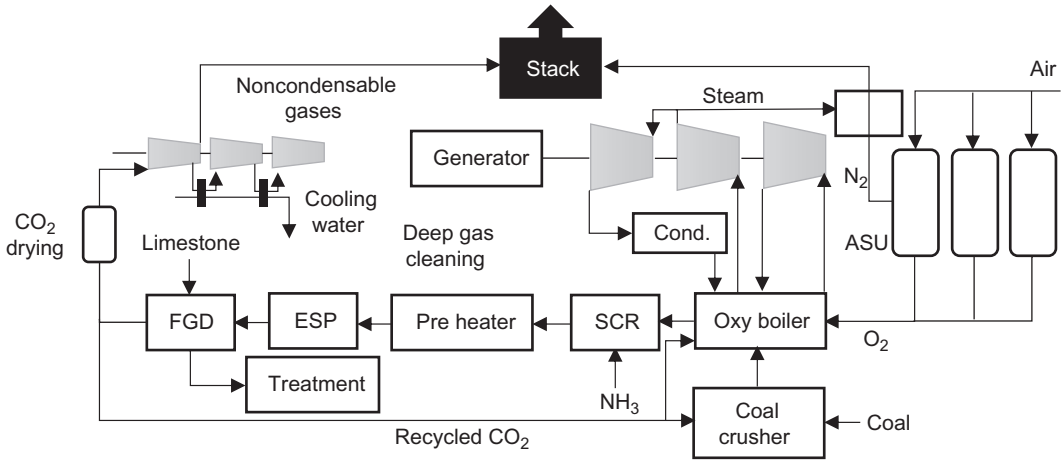

Fig. 24.10
CO_2 capturing in Oxy-combustion of PC.

In the oxy-combustion process, combustion is made using pure oxygen (up to 97% purity), but in which a small amount of nitrogen and argon remains. A big part of the exhaust gases are recycled in the boiler to maintain the usual temperature levels of PC without CO_2 capturing. This avoids full resizing of the boiler and its associated exchangers. The flow of uncycled CO_2 still contains water vapor, impurities (particularly some NO_x and SO_x amounts that remain in the exhaust gas of scrubbing systems), and incondensable gases such as oxygen, nitrogen, and argon. These latter gases originate from the ASU unit and parasite air entries due to the lack of seal of the PC cycle (combustion chamber, deduster, gas-gas heater, etc.). The content of CO_2 in these exhaust gases is of 75% on wet gas. The next step is to condense the water and purify the CO_2 until it is 99% pure so that it can be transported into the supercritical state. The presence of incondensable gases in the CO_2 flow transported by the pipeline in the supercritical state can cause vibrations and shock loads in the pipe, which can cause mechanical damage. However, no known study has attempted to specify critical concentrations of these incondensable gases. All that is agreed upon unanimously is the concentration of water and most works published on this subject agree upon a fixed limit of 20 ppm by mass (50 ppm by volume). Thus a dehydration system using triethylene glycol followed by a cryogenic impurity separation device can be integrated into the CO_2 compression/liquefaction step (Kanniche et al., 2010).

4 Economic Evaluation of an Integrated System for IGCC Plant

As mentioned in previous sections, coproduction of methanol and electricity within the IGCC power plant should take place in two steps. The first step is capturing the CO_2 during electricity production and the second step is the production of methanol by using captured CO_2. Therefore, an economic assessment of this type of system should be carried out in two separate sections:

the economic evaluation of the CO_2 capture process and the economic evaluation of methanol production using captured CO_2. The total cost obtained from these evaluations indicates a cost difference of the IGCC plant without CO_2 capturing.

4.1 Economic Evaluation of CO_2 Capture Process

It should be noted that various feeds can be used in the IGCC power plants. Kanniche et al. (2010), analyzed a detail comparison between an IGCC plant, a conventional combustion of PC, and a natural gas combined cycle (NGCC). In this research, two gasification types were studied:

- A current technology based on gasification of dry coal at 27 bars (Shell or GE/Texaco radiant type) integrated into a classical combined cycle.
- A future technology based on gasification of a coal-water mixture (slurry) that can be compressed to 64 bars integrated into an advanced combined cycle (type H with steam cooling of the combustion turbine blades).

Results demonstrate that the highest efficiency with CO_2 capture is obtained for NGCC in case of postcombustion capture, with an efficiency of 50% compared with 60% without capture. The next highest is the oxy-combustion in PC, with an efficiency of almost 35% compared with 45% without CO_2 capture, and then IGCC Puertollano with precombustion capture with an efficiency of the order of 33.5% compared with 44% without CO_2 capture. The lowest efficiency is obtained with postcombustion capture in PC, equal to 30% which is 15 points less than PC without CO_2 capture. Therefore, from a purely energetic point of view without considering economic figures, it would be recommended to only consider precombustion capture in IGCC, postcombustion in NGCC, and oxy-combustion in PC. Concerning economic investment, the least expensive technology comparative to PC investment cost which is given 100 as reference, remains NGCC with or without CO_2 capture, 40% of the PC for NGCC without capture, and 83% for NGCC with postcombustion capture. The PC and IGCC-slurry (GE/Texaco) are in second position at 169% for PC with oxy-combustion, 101% for IGCC-slurry without CO_2 capture, but only 164% for the IGCC-slurry with precombustion capture. The radiant type IGCC is more expensive than IGCC-slurry and PC, at 122% for the Puertollano type IGCC without CO_2 capture and 185% for the precombustion option. However, it should be noted that the additional investment costs induced by capture are much higher for NGCC (110% greater than NGCC cost without capture) than for radiant type IGCC (52% greater than IGCC-300 cost without capture), IGCC-slurry (62% greater than IGCC-1200 cost without capture), or oxy-combustion in PC (69% greater than PC-1200 cost without capture). The lowest production costs are obtained with oxy-combustion PC (148% of PC without capture) and IGCC-slurry with precombustion capture (154%). The production cost of radiant type IGCC with capture in precombustion is of the same order of magnitude as NGCC with postcombustion capture (162%). On the other hand, the lowest costs per ton of CO_2 avoided are

obtained with precombustion capture in IGCC-slurry (65% of the cost of CO_2 avoided in PC with postcombustion capture), oxy-combustion in PC (71%), and the radiant type IGCC with capture in precombustion (73%). The highest cost per ton of CO_2 (234%) is obtained using precombustion CO_2 capture in the NGCC plant (Kanniche et al., 2010).

Among different fossil fuels for power plants, natural gas is an ideal energy source and is a valuable matter with a majority of applications, while coal is an ideal energy source from the cost point of view but burning of the coal is difficult. Tola and Pettinau (2014) reported the techno-economic comparison between coal combustion and gasification technologies. They studied three configurations for comparison of the IGCC power plant with convectional power plants:

- Ultra-supercritical (USC) plant equipped with a conventional flue gas treatment (CGT) process.
- USC plant equipped with SNOX technology for a combined removal of sulfur and nitrogen oxides.
- IGCC plant based on a slurry-feed entrained-flow gasifier.

Each technology was analyzed in its configurations with and without CO_2 capture, referring to a commercial-scale of 1000 MWth. Technical assessment was carried out using simulation models implemented through Aspen Plus and Gate-Cycle tools, whereas economic assessment was performed through a properly developed simulation model. USC equipped with CGT systems shows an overall efficiency (43.7%) comparable to IGCC (43.9%), whereas introduction of SNOX technology increases USC efficiency up to 44.8%. Since the carbon dioxide capture and storage (CCS) energy penalties are significantly higher for USC (about 10.5% points vs. about 8.5 for IGCC), the IGCC with CCS is more efficient (35.3%) than the corresponding CO_2-free USC (34.2% for the SNOX-based configuration). Whereas, for the case study, USC is most profitable than IGCC (with a net present value, NPV, of 190 M€ vs. 54 M€) for a conventional configuration, CO_2-free IGCC shows a higher NPV (−673 M€) than USC (−711 M€). In any cases, the NPV of all the CO_2-free configurations is strongly negative: this means that, with the current market conditions, the introduction of a CCS system cannot be economically justified without a significant incentive.

On the other hand, the CO_2 capturing process is required for methanol production from the IGCC power plant. Therefore, the effect of the CCS system on overall efficiency of power plant is necessary. Martelli et al. (2009) compared the coal from the IGCC with and without CO_2 capture and storage. In this study, shell gasification with standard vs. partial water quench was considered. As a consequence, they noted that, in a conventional Shell coal IGCC with syngas coolers, adding CO_2 capture reduces plant efficiency by nearly 10% points. The partial water quench (with CCS) further decreases the efficiency by ∼1% point. The cost of Shell coal IGCC with CCS is estimated in the range of 2300–2500 USD/kWe, with the partial water quench near the lower end and the conventional design at the upper end.

Feed characteristics are effective on the overall efficiency of the IGCC power plants. Chen and Rubin (2009) considered four coals, including selections of bituminous, subbituminous and lignite, used to investigate the effects of coal quality on the performance and cost of an IGCC system design employing a slurry-fed quench gasifier. Although this gasifier type is able to process all four coals, the coal rank significantly influenced the gasification efficiency, thermal efficiency, and capital cost of the power plant. With low-rank coals, the total water input for the slurry-fed gasifier substantially lowered the gasification efficiency and increased total system cost.

In general, separation process is a key technology for industrial systems. In major plants, contribution of separation technologies in operating cost is higher than all of the other technologies. For an example in ethanol production, about 60%–80% of total operating cost is consumed for a separation system (Ghasemzadeh et al., 2015, 2016). Several parameters in separation systems are more significant. Some of them include (Ghasemzadeh et al., 2015; 2016):

- Energy consumption
- Required place
- Required humane resources
- Separation phase
- Efficiency of separation
- Product purity, etc.

As a general point of view, it should be noted that gas separation units are one of the most complex units in chemical processes. On the other hand, for IGCC power plants that are integrated by CO_2 capture (precombustion and oxy-combustion), an ASU unit is required. The ASU plays a key role in improving the efficiency, availability, and operability of an oxygen-fed IGCC power plant. An optimal integration between the ASU and the balance of the plant, especially the gasifier and the gas turbine, has significant potential for enhancing the overall plant efficiency. Considering the higher operating pressure of the gas turbine, an elevated pressure air separation unit (EP-ASU) is usually favored instead of the conventional low-pressure air separation units. In addition, a pumped liquid oxygen (PLOX) cycle is usually chosen if the operating pressure of the gasifier is high. A PLOX cycle helps to improve plant safety and availability and to decrease the capital cost by reducing the size of the oxygen compressor or by eliminating it completely. However, the refrigeration lost in withdrawn liquid oxygen must be efficiently recovered.

In this case, Jones et al. (2011) have considered five different configurations of an ASU with PLOX cycle and compares their power consumptions with an EP-ASU with a traditional gaseous oxygen (GOX) cycle. Their evaluation indicated that an optimally designed EP-ASU with a PLOX cycle can have similar power consumption to that of an EP-ASU with GOX cycle in the case of 100% nitrogen integration. In the case of an IGCC with precombustion CO_2 capture, the lower heating value (LHV) of the shifted syngas, both on a mass and volumetric

basis, is between the LHV of the unshifted syngas from an IGCC plant and the LHV of natural gas, for which the gas turbines are generally designed. The optimal air integration in the case of a shifted syngas is found to be much lower than that of an unshifted syngas.

Chen and Rubin (2009) denoted that a preliminary analysis of advanced IGCC systems showed that incorporation of advanced oxygen production and gas turbine technologies holds promise to significantly improve the performance and reduce the cost of future IGCC systems with and without CCS. For plants with CCS, simulation results presented that these two advanced technologies can yield a system that is more efficient than a current plant without CCS, and reduce, by approximately 50%, the cost penalties currently associated with CCS.

Noted parameters for separation and lack of achievement to them is the main drawback of separation techniques. Membrane separation is a suitable solution for this problem and there is no need to phase change (usually), therefore consumption of energy is not high for membrane processes. On the other hand, membranes can separate the matters in a molecular scale. It is clear that product purity will be extremely high. In addition to these noted advantages, good efficiency, good stability, no required human involvement in process time, etc. are some of the others. For methanol production from CO_2 in IGCC power plants, membrane separation can be a valuable technology. In this case, Sadati et al. (2015) and Ghasemzadeh et al. (2015) discussed membrane separation applications in hydrogen production systems (precombustion) and membranes for IGCC power plants. It is denoted that steam reforming is a suitable process for hydrogen production but purity of the product is a drawback of this system that can be solved by utilization of membrane separation. Studies show that the main units in IGCC power plants that can use the membranes are ASU, WGS, H_2 separation, and CO_2 separation. It was concluded that replacing the ASU with the ITM membrane system provides the oxygen for gasification. Integrating low temperature polymeric hydrogen membranes downstream in a WGS process is another application of membrane separation. Intensifying the CO_2 formation and separation by combining H_2 selective (Pd-based or silica) membranes with the WGS reaction process and integrating CO_2 selective membrane (silica and zeolite membranes) for precombustion process are other usable membranes for IGCC systems.

In addition to flue gas, atmospheric CO_2 can provide the required carbon dioxide for methanol production. It is clear that flue gas is a better choice because of higher partial pressure of CO_2 and suitable accessibility. As noted previously, CO_2 can be extracted from fuel by pre-, oxy-, or postcombustion processed. In all of these noted pathways, CO_2 separation from a gas stream is required. Because of the noted advantages of membranes, a CO_2-selective membrane can be a powerful instrument for CO_2 separation. Grainger and Hägg (2008) reported a carbon dioxide selective membrane. In this work, published data for an operating power plant, the ELCOGAS 315 MWe Puertollano plant was used as a basis for the simulation of an IGCC process with CO_2 capture. This incorporated a fixed site carrier polyvinylamine membrane to separate the CO_2 from a CO-shifted syngas stream. It appears that the modified process, using a sour shift catalyst prior to sulfur removal, could achieve greater than 85% CO_2 recovery at 95 vol% purity.

In similar study and for metallic membrane, Chiesa et al. (2007) investigated IGCC power plants with metallic membrane. As a main result, the membrane-based plants expected to have the following advantages over the commercially ready reference plant:

- superior efficiency,
- higher CO_2 capture efficiency, and
- reduction in plant capital cost.

Membrane reactors (MRs) are the next generation of convectional membrane separation technologies. MRs have many advantages in addition to traditional reactor (TR) (Ghasemzadeh et al., 2016). One of the most important advantages is feasibility of reaction simultaneous with separation. In the majority of chemical processes, equilibrium is a stop point for improvement of the efficiency of process. Therefore, MRs can change the economy of process impressively. Bracht et al. (1997) studied the WGS with MR in IGCC systems. From system optimization and cycle efficiency calculations it has been shown that the system proposed has a higher efficiency connected with lower costs compared to conventional options for CO_2 removal. In this study, net efficiency for IGCC with convectional CO_2 removal and membrane separation reported 40.5% and 42.8%. The literatures indicated that absorption is ideal technology for CO_2 separation. As noted previously, membranes are the next generation separation technology for CO_2 capture. Two types of membranes, CO_2-selective membranes and H_2 selective membranes are applicable in CO_2 capture.

In this case, Merkel et al. (2012) studied these methods and compared them. The results of this comparison are shown in Table 24.1.

On the other hand, simulation is an important method for the discussion about chemical process. Therefore, many researchers tried to improve the IGCC power plants with simulation tools. The next generation of traditional power plants is IGCC, and the next generation of them are IGCC with CO_2 capture.

In this case, Mondol et al.(2009) investigated a techno-economic evaluation of advanced IGCC lignite coal fueled power plants with CO_2 capture, the techno-economic evaluation of four novel IGCC power plants fueled with low rank lignite coal with CO_2 capture facility has been investigated using ECLIPSE process simulator. The performance of the proposed plants was compared with two conventional IGCC plants with and without CO_2 capture. The proposed plants include an advanced CO_2 capturing process based on the absorption enhanced reforming reaction and the regeneration of sorbent materials avoiding the need for sulfur removal component, shift reactor, and/or a high temperature gas cleaning process. The results show that the proposed CO_2 capture plants efficiencies were 18.5%–21% higher than the conventional IGCC CO_2 capture plant. For the proposed plants, the CO_2 capture efficiencies were found to be within 95.8%–97%. The CO_2 capture efficiency for the conventional IGCC plant was 87.7%. The specific investment costs for the proposed plants

Table 24.1 Comparison of energy use and capital costs for CO_2 capture from a 556 MWe IGCC plant using Selexol and various CO_2-selective and hydrogen-selective membrane processes (cost basis is 2007 USD) (Merkel et al., 2012)

System/Cost Parameter	Units	Selexol + CO_2 Compression	CO_2-Selective Membrane	H_2-Selective Membrane
Compression power used	MWe	31	31	18
Refrigeration (or steam) used	MWe	19	14	20
Total power used	MWe	50	45	38
Membrane area used	m^2	–	16,000	25,000
Membrane or Selexol equipment cost	USD million	74	8	12.5
Compression and/or refrigeration equipment cost	USD million	18	45	48
Bare erected plant cost	USD million	166	88	100
Engineering fees	USD million	16	8	9
Contingencies	USD million	69	21	26
Total plant cost	USD million	252	117	135
Estimated increase in LCOE	%	31	20	21

were between 1207 and 1479 and 1620 and 1134€/kWe for the conventional plants with and without CO_2 capture, respectively. Overall, the proposed IGCC plants are cleaner, more efficient, and produce electricity at a cheaper price than the conventional IGCC process.

Cormos (2012) studied a precombustion system for CO_2 separation in IGCC power plant. They noted that the introduction of the CCS step implies a 7%–9.5% energy penalty expressed in terms of net plant efficiency,10%–75% plant construction materials, 22%–24% capital costs increase, 10.5%–13.5% operational and maintenance costs increase, and 30%–35% LCOE increase for capturing about 90% of the feedstock carbon. One clear benefit of large scale deployment of CCS technologies in the power generation sector is the significant reduction of specific CO_2 emissions. A hydrogen and power cogeneration scenario as future developments of IGCC plants for implementation of low carbon economy was also described in term of key technical and economic indicators.

Nevertheless, the percentage and amount of CO_2 removal from IGCC power plants is effective on the total system economy. For the separation system, usually production of pure or ultra-pure product is very costly. On the other hand, it was shown that the integration of CCS with IGCC power plants can improve the net efficiency of the process. Therefore, there is an optimum point

for CO_2 removal. Chen and Rubin (2009) studied the effects of different CO_2 capture efficiencies on auxiliary power requirements, thermal efficiency, capital cost, COE, and CO_2 avoidance cost. For the case study plant, the CO_2 avoidance cost was lowest when the total CO_2 removal efficiency was approximately 90%, indicating this to be an optimal CO_2 capture efficiency for this plant design (Jones et al., 2011; Chen and Rubin, 2009). Between introduced technologies for CCS, pre-, and oxy-combustion need basic changes in the power plant. Indeed, for the precombustion, a reformer is required to produce CO_2 and H_2. After the separation of CO_2 and H_2, the hydrogen turbine should be used instead of conventional turbine. For the oxy-combustion process an ASU should be added to convectional system power plants. Among these methods, postcombustion is a valuable pathway for separation of CO_2 so there is no need to change the main process flow. Therefore, many research discussed about this system focused on the achievement for more efficient CCS processes.

Schach et al. (2010) investigated CO_2 separation from IGCC power plant by postcombustion process. Four different configurations of a CO_2-capture process based on an absorption/stripping cycle was investigated using Aspen Plus software. Based on the simulation results, the process options were technically and economically analyzed and compared with a defined reference case. The influence of the cost on innovative configurations was indicated, which was not clear due to a lack of information in this field. All alternative configurations presented a better performance than the basic process. Indeed, the alternative configurations paid for energy savings with higher investment costs. Investing in a certain option of process improvement needs a minimum of energy savings so that the process can be improved in terms of cost of CO_2 was avoided.

Meanwhile, at least, a comparison of IGCC with and without CCS seems necessary. Studies depict that net capacity of power plants with CCS will be reduced about 8%. Total capital requirement and cost of electricity will be increased by about 37.8% and 45.4%. By using a CCS system by the IGCC power plant, a decrease in thermal efficiency (about 13.7%) and CO_2 emission is predicted. CO_2 is a greenhouse gas and is a crisis for the future of the world. Power plants are the main CO_2 producer in the world. Using the CCS systems in power plants can decrease the emissions about 88.5%. A comparison of a IGCC plant with and without CO_2 capture is noted in Table 24.2 (Chen and Rubin, 2009).

Table 24.2 Comparison of a IGCC plant with and without CO_2 capture

Plant Design	Net Capacity (MW)	Total Capital Requirement (Jun. 2008 USD/kW)	Cost of Electricity (USD/MWh)	Thermal Efficiency (HHV) (%)	CO_2 Emission (kg/kWh)
Reference plant	538	1823	65.9	38.1	0.819
Capture plant (90% CO_2 capture)	495	2513	95.8	32.9	0.094
Change (%)	−8.0	37.8	45.4	−13.7	−88.5

Table 24.3 Power plant thermal efficiencies

Fuel	Power Generation Technology	CO2 Capture Technology	Gross Efficiency (%, LHV)	Auxiliary Consumption (% Fuel Feed)	Net Efficiency[a] (%, LHV)
Coal	Pulverized fuel	None	48.2	4.2	44.0
		Postcombustion, fluor	43.2	8.4	34.8
		Postcombustion, MHI	43.8	8.5	35.3
		Oxy-combustion	49.1	13.7	35.4
	IGCC, Shell	None	50.5	7.4	43.1
		Precombustion, Selexol	45.7	11.2	34.5
	IGCC, GE	None	45.4	7.4	38.0
		Precombustion, Selexol	41.9	10.4	31.5
Gas	Gas turbine combined cycle	None	57.3	1.7	55.6
		Postcombustion, fluor	53.0	5.6	47.4
		Postcombustion, MHI	54.3	4.7	49.6
		Oxy-combustion	58.4	13.7	44.7

[a]HHV efficiencies of the coal-fired plants are 0.956 times the LHV efficiencies. HHV efficiencies of the gas-fired plants are 0.904 times the LHV efficiencies.

In the other study, Davison (2007) compared various processes of power plants with CCS. The thermal efficiencies, on a lower heating value (LHV) basis, and the auxiliary power consumptions of power plants with and without CO_2 capture are shown in Table 24.3.

The thermal efficiencies of power plants with CO_2 capture based on the current technologies are 32%–35%, LHV basis, for bituminous coal fired plants, and 45%–50% for NGCC plants. The cost of electricity generation with CO_2 capture depends on various technical and economic factors including the fuel cost, which is highly variable at present. Based on predicted fuel prices for North West Europe for the next 25 years, the cost of electricity generation with CO_2 capture is estimated to be 6.9 c/kWh for the least cost coal technology (water quench IGCC) and 7.8 c/kWh for the least cost natural gas technology (combined cycle with postcombustion capture).

As a general assessment, the estimated cost of CO_2 capture and compression (excluding CO_2 transport and storage) is 27–39 USD/t of CO_2 emissions avoided for coal-fired plants and 48–102 USD/t for NGCC plants. The costs are 1.6–2.4 c/kWh for coal-fired plants and 1.5–3.7 c/kWh for gas-fired plants. An indicative cost of CO_2 transport and storage of 10 USD/t CO_2 stored would increase the cost of CO_2 avoided by 12–13 USD/t and increase the cost of electricity by about 0.8 c/kWh for coal-fired plants and 0.4 c/kWh for gas-fired plants.

The optimum power generation and CO_2 capture technologies will depend on various criteria which will depend on local circumstances and utilities' preferences. Further work is needed to assess the power generation with CO_2 capture at a range of different locations worldwide and to assess the abilities of capture processes to accommodate the present and future operational requirements of power utilities (Davison, 2007).

4.2 Economic Evaluation of Methanol Production

As mentioned before, the common feed for methanol production is CO and H_2 produced from gasified coal and natural gas. This methanol production pathway is a fossil fuel base process and can dramatically result in the emissions of GHGs. On the other hand, synthesis gas is a valuable product and requires an extremely complex process for production. Therefore, an alternative feed for methanol production is necessary. There are many reports about methanol production by CO_2. Moreover, methanol production by CO_2 has many advantages, for example:

- increasing the environmental sustainability of process,
- decreasing the CO_2 emission,
- middle process operating conditions,
- suitable methanol production rate and high selectivity.

In general, syngas production systems have many operating, design, and economic limitations. For methanol production systems, the rate of H_2/CO should be stable and about 2–3. However, this regulation is very problematic. Indeed, operating conditions of syngas production usually are very harsh (a high temperature, usually higher than 600°C). In a technology point of view, synthesis gas production is dramatically complex (reformer, high temperature WGS, and low temperature WGS) with many operating problems such as cocking. All of these aspects lead to the decrease of economic efficiency for methanol production from synthesis gas (Sadati et al., 2015).

In fact, subsequent generation of methanol production feed is CO_2. This pathway leads to CO_2 and H_2 as feed. Power plants (especially coal base power plants) are suitable goals for supplying the required CO_2 for methanol production. Unfortunately, in addition to CO_2, H_2 is required for methanol production. However, H_2 is expensive and has caused the reduction of the cost effectivity of the process. Hydrogen production from electrolysis is well known as the best method, but the main disadvantage is the supply of the required electricity. Inexpensive electricity obtained by natural energy, such as hydroelectric power, wind power, and geothermal power can be the best strategy for this problem. However, each of these sources have some advantages and disadvantages. In fact, hydroelectric power is ideal because of its stability for the seasons of the year. In addition to hydroelectric power, geothermal power is used widely for methanol production. In Iceland, the amount of methanol production by the

hydrogenation of CO_2 with geothermally generated electric power is scheduled to be 4000 t/year (Arena et al., 2007, 2008, 2009; Omae, 2012).

The construction of facilities was started in 2010 and during the hydrogenation of CO_2, methanol is produced at lower temperatures and under higher pressures. Several copper catalysts such as Cu/ZnO, CuO/ZnO, and CuO ZnO/ZrO_2 were studied. Other catalysts that have been studied include a Ni catalyst, an Al-based frustrated Lewis paired with ammonia borane, heterocyclic carbenes, and pyridinium and its derivatives. For example, Liu et al. (2007) reported a low-temperature methanol production process in a slurry-phased reactor over copper catalysts prepared by an oxalate-gel coprecipitation method. In another study, methanol production over Cu/ZnO/Al_2O_3 and operating conditions of 170°C and 20 h residence time was investigated. This reaction conversion is achieved to 15.7% with methanol selectivity of 78.7%. CO is a byproduct of methanol production by CO_2 as feed. Production of methanol by the hydrosilylation of CO_2 with N-heterocyclic carbenes as catalysts is illustrated in Fig. 24.11 (Chakraborty et al., 2010; Huang et al., 2010; Ménard and Stephan, 2010; Riduan et al., 2009).

As noted previously, mild operating conditions of methanol production by CO_2 is one of the most important advantages of this pathway. It should be noted that research to achieve better operating conditions and higher conversion and selectivity is being continued. Comparison of CO_2 and syngas feed for methanol production can show characteristics of each process. Syngas is a main feed for methanol production systems. Researchers denoted that CO conversion is one of the most important parameters that can change the economic conditions of process. Mahajan and Goland (2003) investigated integrating low-temperature methanol synthesis and CO_2 sequestration technologies and application to IGCC plants. In this study, methanol was synthesized by syngas in mild conditions (temperature lower than 150°C and pressure lower than 5 MPa). As main result of this study, CO conversion and methanol selectivity was reported

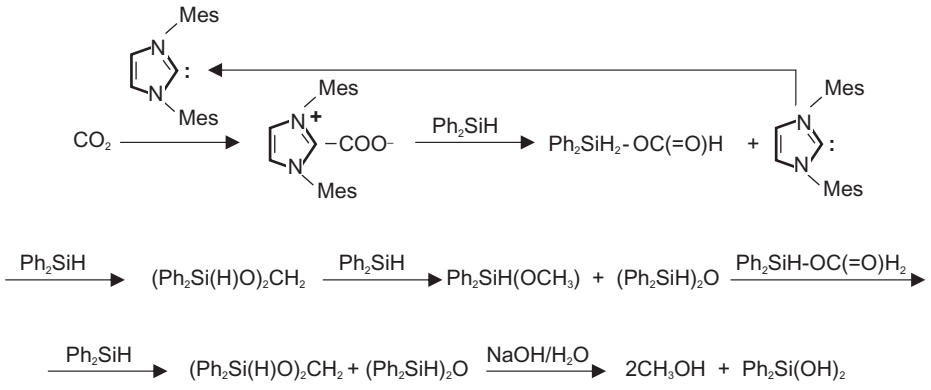

Fig. 24.11
Synthesis of methanol by the hydrosilylation of carbon dioxide with N-heterocyclic carbenes as catalysts.

to be 90% and 95%. In this study it was noted that conversion, methanol selectivity, and process conditions are effective on the economy of the process. Therefore, in CO_2 conversion cases (like CO conversion) effective parameters should be studied (Mahajan and Goland, 2003).

Mignard et al. (2003) conducted a feasibility study of methanol production from flue-gas CO_2 and renewable electricity. The twin requirements of reducing CO_2 emission levels and increasing the level of penetration of renewable energy will involve innovative technical and operational solutions. This work describes a novel but proven process which could be adapted to use, as input reagents, CO_2 emitted from fossil-fueled power stations and hydrogen from electrolysis of water by a zero-emissions electricity source, e.g., renewable and/or nuclear energy. This approach, in addition to addressing the above two issues, would produce methanol for which there is a ready and expanding market. A preliminary analysis is presented of the process economics and operational regimes necessary in the UK Electrical Supply Industry to accommodate the methanol plant. Four different designs are assessed, all based on a supply of renewable energy limited to 16 h/day when demand is off-peak. It is claimed that significant benefits might accrue from the successful development of a methanol process and that it may ease the absorption of increasing levels of embedded generation into the electricity supply network.

The most important advantage of methanol production from CO_2 is being an environmentally friendly process. However, for this procedure of methanol production, H_2 is required. Hence, the source of the H_2 is important because the environmentally sustainability of the process can change. Therefore, researchers have tried to supply the needed H_2 from renewable sources. The conventional pathway for H_2 production is electrolysis. In fact, the main energy consumer in this method of methanol production is the H_2 production system and its required electricity. Rivarolo et al. (2016) studied different renewable energy sources (hydroelectric, photovoltaic, and wind power) to supply the needed electricity for electrolysis and hydrogen production. This study considered two different configurations for economic analysis: biogas as CO_2 provider and flue gas as CO_2 provider. The results showed that capital cost is 3.8 M€ for biogas configuration and 2.5 M€ for flue gas CO_2 configuration. Therefore, the electrolyzer is the most important system in total cost of methanol production by CO_2. Of course, the required technologies for CO_2 removal from flue gas should be considered for achievement of a correct comparison. In addition to capital cost, different renewable sources for providing the required electricity were compared. This comparison shows that wind power and photovoltaic are unstable at different times of day. This is despite the fact that the electrolyzer needs stable electricity and in this point of view, hydroelectric power is suitable.

Moreover, Kim et al. (2011a,b) investigated the methanol production from CO_2 using solar-thermal energy. They described a novel solar-based process for the production of methanol from carbon dioxide and water. The system utilizes concentrated solar energy in a

thermochemical reactor to reenergize CO_2 into CO and then using WGS to produce syngas to feed a methanol synthesis reactor. Indeed, this work presents an initial assessment of energy efficiency and economic feasibility of this baseline configuration for an industrial-scale methanol plant. Using detailed sensitivity calculations, they determined that a breakeven price of the methanol produced using this approach would be 1.22 USD/kg, which, while higher than current market prices, is comparable to other renewable-resource-based alternatives. They also determined that if solar power is the sole primary energy source, then an overall process energy efficiency (solar-to-fuel) of 7.1% could be achieved, assuming the solar collector, and solar thermochemical reactor subsystem operates at 20% sunlight to chemical energy efficiency. This 7.1% system efficiency is significantly higher than can currently be achieved with photosynthesis-based processes, and illustrated the potential for solar thermochemical based strategies to overcome the resource limitations that arise for low-efficiency approaches.

Their analysis indicated that a solar-thermochemical pathway to fuels has significant potential, and points towards future research opportunities to increase efficiency, reduce balance of plant utilities, and reduce cost from this baseline. Particularly, it is evident that there is much room for improvement in the development of a less expensive solar concentrator/reactor subsystem; an opportunity that will benefit from the increasing deployment of concentrated solar power (electricity). In addition, significant advances are achievable through improved separations, combined CO_2 and H_2O splitting, different end products, and greater process integration and distribution. The baseline investigation here establishes a methodology for identifying opportunities, comparison, and assessment of impact on the efficiency, lifecycle impact, and economics for advanced system designs. For noted pathways, many economic studies were

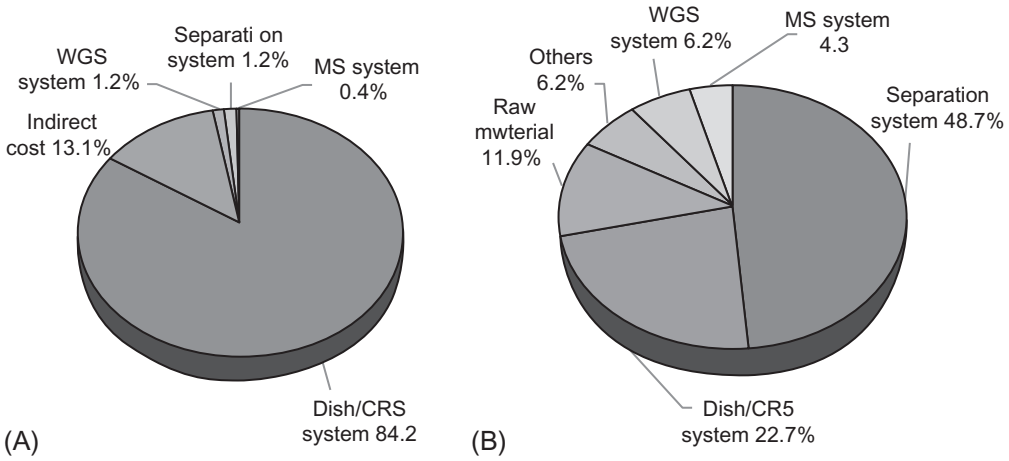

Fig. 24.12

(A, B) Distribution of capital cost and operating cost for the methanol production process. Indirect costs include engineering and supervision costs, construction expenses, other expenses, and contingency.

carried out. Results of different unit contributions in operating and capital cost are shown in Fig. 24.12.

4.3 Limitations

Unlike the discussed advantages, some disadvantages and limitations can be noted for methanol production from CO_2. The first problem of this system is the need for electricity. Electricity is the most ideal type of energy that can be used for the power distribution network. Therefore, a high-level of electricity requirement is not desirable.

In research, it is assumed that the specific problems that will be encountered in coal power stations with capture have been solved, although this is obviously not the case at the moment: problems remain with oxy-coal combustion boilers, hydrogen turbine for IGCC with CO_2 capture, degradation of amines, separation of incondensable gases in oxy-combustion. These main limitations are indicated in Table 24.4 (Kanniche et al., 2010).

The economic estimates are relevant for a comparison between the different systems, but their absolute values may vary significantly as a function of the cost of metals, the price of fuels, tension on the equipment market (availability of construction and supervision teams), etc. Similarly, the discount rate is different around the world. Fuel, equipment, and installation prices are usually lower in North America, but discount rates may be higher than those in Europe.

Table 24.4 Main limitations of IGCC process

	Technical Problems That Still Have to be Solved Effectively (R&D Necessary) But Which We Have Assumed to Have Been Solved for the Purposes of Our Studies	Technical Weak Points in the System	Financial Hard Points (What Is Most Expensive When Capture Is Added)
IGCC-slurry	Hydrogen turbine Acid gas shift conversion	Increased complexity for a process for which there are still problems with reliability without capture. Not well adapted to some coals (lignite, high ash and sulfur contents, etc.).	The shift conversion
Dry coal IGCC	Hydrogen turbine Acid gas shift conversion Badly adapted to high pressures	Increased complexity for a system for which there are still problems with reliability without capture.	The shift conversion

5 Conclusion and Future Trends

To reduce CO_2 emissions, various strategies are presented. One of the most promising solutions is CO_2 capturing from industrial plant sources that have a main role in the emission of CO_2 to the atmosphere. Among various CO_2 producer sources, the power plants have a major contribution. Hence, CO_2 capturing in the IGCC power plants can show important effects on the control of greenhouse gases in the world. However, economic aspects act as a barrier on the extending pathway of CO_2 capturing units in the IGCC power plants. Therefore, using an integrated system for coproduction of electricity and methanol can be improved cost-effectively for CO_2 capturing in the IGCC plant. Hence, in this chapter, a comprehensive review was carried out on integrated systems for the coproduction of electricity and methanol in the IGCC plant with reference to various aspects such as unit production capacity, CO_2 separation strategies, performance analysis, and especially economic assessment of this technology. Indeed, economic assessment results indicated that this strategy is cost-effective. However, depending on the separation method in AUS and CO_2 capturing in the IGCC plant, this result can be more highlighted. Regarding this study, membrane processes can be shown to have a critical effect on decreasing total costs of electricity production.

Therefore, future directions to improve this kind of integrated system should be focused on membrane technologies for CO_2 capture, O_2 enrichment, and methanol production by developing high-performing membranes that could achieve high selectivity and permeability, with recognition of the trade-off that exists between these two parameters. Moreover, presenting multistage or cascaded process designs to reach the desired selectivity and recovery with the aim to reduce the membrane area, which would decide its footprint, capital cost, and feasibility of integration with power plants that can have the effect to decrease the total cost of the integrated system for coproduction of electricity and methanol.

References

Abanades, J.C., et al., 2007. Cost structure of a postcombustion CO_2 capture system using CaO. Environ. Sci. Technol. 41 (15), 5523–5527.

Arena, F., et al., 2007. Synthesis, characterization and activity pattern of Cu-ZnO/ZrO_2 catalysts in the hydrogenation of carbon dioxide to methanol. J. Catal. 249 (2), 185–194.

Arena, F., et al., 2008. Solid-state interactions, adsorption sites and functionality of Cu-ZnO/ZrO_2 catalysts in the CO_2 hydrogenation to CH_3OH. Appl. Catal. A Gen. 350 (1), 16–23.

Arena, F., et al., 2009. Basic evidences for methanol-synthesis catalyst design. Catal. Today 143 (1), 80–85.

Babu, P., Kumar, R., Linga, P., 2013. Pre-combustion capture of carbon dioxide in a fixed bed reactor using the clathrate hydrate process. Energy 50, 364–373.

Bracht, M., et al., 1997. Water gas shift membrane reactor for CO_2 control in IGCC systems: techno-economic feasibility study. Energy Convers. Manage. 38, S159–S164.

Carbo, M.C., et al., 2006. Advanced membrane reactors in IGCC: H_2 or CO_2 separation. In: Fifth Annual Conference on Carbon Capture & Sequestration, Virginia.

Carbo, M.C., et al., 2009. Steam demand reduction of water-gas shift reaction in IGCC power plants with pre-combustion CO_2 capture. Int. J. Greenhouse Gas Control 3 (6), 712–719.
Chakraborty, S., et al., 2010. An efficient nickel catalyst for the reduction of carbon dioxide with a borane. J. Am. Chem. Soc. 132 (26), 8872–8873.
Chen, C., 2005. A Technical and Economic Assessment of CO_2 Capture Technology for IGCC Power Plants. PhD Thesis, Carnegie Mellon University.
Chen, C., Rubin, E.S., 2009. CO_2 control technology effects on IGCC plant performance and cost. Energy Policy 37 (3), 915–924.
Chiesa, P., Kreutz, T.G., Lozza, G.G., 2007. CO_2 sequestration from IGCC power plants by means of metallic membranes. J. Eng. Gas Turbines Power 129 (1), 123–134.
Cormos, C.-C., 2012. Integrated assessment of IGCC power generation technology with carbon capture and storage (CCS). Energy 42 (1), 434–445.
David, J., Herzog, H., 2000. The cost of carbon capture. In: Fifth International Conference on Greenhouse Gas Control Technologies, Cairns, Australia, pp. 13–16.
Davison, J., 2007. Performance and costs of power plants with capture and storage of CO_2. Energy 32 (7), 1163–1176.
Dillon, D.J., et al., 2004. Oxy-combustion processes for CO_2 capture from advanced supercritical PF and NGCC power plant. In: 7th International Conference on Greenhouse Gas Technologies, Vancouver, Canada.
Erlach, B., Schmidt, M., Tsatsaronis, G., 2011. Comparison of carbon capture IGCC with pre-combustion decarbonisation and with chemical-looping combustion. Energy 36 (6), 3804–3815.
Ertesvåg, I.S., Kvamsdal, H.M., Bolland, O., 2005. Exergy analysis of a gas-turbine combined-cycle power plant with precombustion CO_2 capture. Energy 30 (1), 5–39.
Fu, C., Gundersen, T., 2012. Using exergy analysis to reduce power consumption in air separation units for oxy-combustion processes. Energy 44 (1), 60–68.
Ghasemzadeh, K., Basile, A., Tilebon, S.M.S., 2015. Membranes for IGCC power plants. Integrated Membrane Systems and Processes. Wiley, p. 255.
Ghasemzadeh, K., Tilebon, S.M.S., Basile, A., 2016. Membrane reactors for hydrogen production from biomass-derived oxygenates. Membrane Technologies for Biorefining. Woodhead Publishing, p. 435.
Goldemberg, J., 2000. World Energy Assessment: Energy and the Challenge of Sustainability. United Nations Pubns, Agenda.
Grainger, D., Hägg, M.-B., 2008. Techno-economic evaluation of a PVAm CO_2-selective membrane in an IGCC power plant with CO_2 capture. Fuel 87 (1), 14–24.
Huang, F., et al., 2010. The catalytic role of N-heterocyclic carbene in a metal-free conversion of carbon dioxide into methanol: a computational mechanism study. J. Am. Chem. Soc. 132 (35), 12388–12396.
IEA, C.O., 2003. Emissions from Fuel Combustion 1997-2001. IEA/OECD, Paris, France.
Jones, D., et al., 2011. Optimal design and integration of an air separation unit (ASU) for an integrated gasification combined cycle (IGCC) power plant with CO_2 capture. Fuel Process. Technol. 92 (9), 1685–1695.
Kaldis, S.P., Skodras, G., Sakellaropoulos, G.P., 2004. Energy and capital cost analysis of CO_2 capture in coal IGCC processes via gas separation membranes. Fuel Process. Technol. 85 (5), 337–346.
Kanniche, M., et al., 2010. Pre-combustion, post-combustion and oxy-combustion in thermal power plant for CO_2 capture. Appl. Therm. Eng. 30 (1), 53–62.
Kim, J., et al., 2011a. Methanol production from CO_2 using solar-thermal energy: process development and techno-economic analysis. Energy Environ. Sci. 4 (9), 3122–3132.
Kim, S.M., et al., 2011b. Gas hydrate formation method to capture the carbon dioxide for pre-combustion process in IGCC plant. Int. J. Hydrogen Energy 36 (1), 1115–1121.
Kunze, C., Spliethoff, H., 2012. Assessment of oxy-fuel, pre- and post-combustion-based carbon capture for future IGCC plants. Appl. Energy 94, 109–116.
Liu, Y., et al., 2007. Efficient conversion of carbon dioxide to methanol using copper catalyst by a new low-temperature hydrogenation process. Chem. Lett. 36 (9), 1182–1183.

Mahajan, D., Goland, A.N., 2003. Integrating low-temperature methanol synthesis and CO_2 sequestration technologies: application to IGCC plants. Catal. Today 84 (1), 71–81.
Martelli, E., Kreutz, T., Consonni, S., 2009. Comparison of coal IGCC with and without CO_2 capture and storage: shell gasification with standard vs. partial water quench. Energy Procedia 1 (1), 607–614.
Ménard, G., Stephan, D.W., 2010. Room temperature reduction of CO_2 to methanol by Al-based frustrated Lewis pairs and ammonia borane. J. Am. Chem. Soc. 132 (6), 1796–1797.
Merkel, T.C., Zhou, M., Baker, R.W., 2012. Carbon dioxide capture with membranes at an IGCC power plant. J. Membr. Sci. 389, 441–450.
Mignard, D., et al., 2003. Methanol synthesis from flue-gas CO_2 and renewable electricity: a feasibility study. Int. J. Hydrogen Energy 28 (4), 455–464.
Mondol, J.D., et al., 2009. Techno-economic evaluation of advanced IGCC lignite coal fuelled power plants with CO_2 capture. Fuel 88 (12), 2495–2506.
Nagasaki, N., et al., 2013. Near-zero-emission IGCC Power Plant Technology. Hitachi Rev. 62 (1), 39–47.
Obert, R., Dave, B.C., 1999. Enzymatic conversion of carbon dioxide to methanol: enhanced methanol production in silica sol-gel matrices. J. Am. Chem. Soc. 121 (51), 12192–12193.
Omae, I., 2012. Recent developments in carbon dioxide utilization for the production of organic chemicals. Coord. Chem. Rev. 256 (13), 1384–1405.
On Climate Change, I.P., 2015. Climate Change 2014: Mitigation of Climate Change. PhD Thesis, Cambridge University Press, England.
Puxty, G., et al., 2009. Carbon dioxide postcombustion capture: a novel screening study of the carbon dioxide absorption performance of 76 amines. Environ. Sci. Technol. 43 (16), 6427–6433.
Rezvani, S., et al., 2009. Comparative assessment of coal fired IGCC systems with CO_2 capture using physical absorption, membrane reactors and chemical looping. Fuel 88 (12), 2463–2472.
Riduan, S.N., Zhang, Y., Ying, J.Y., 2009. Conversion of carbon dioxide into methanol with silanes over N-heterocyclic carbene catalysts. Angew. Chem. 121 (18), 3372–3375.
Rivarolo, M., et al., 2016. Feasibility study of methanol production from different renewable sources and thermo-economic analysis. Int. J. Hydrogen Energy 41 (4), 2105–2116.
Sadati, S., Vousoughi, P., Eyvazi, M., 2015. Hydrogen production: overview of technology options and membrane in auto-thermal reforming including partial oxidation and steam reforming. Int. J. Membr. Sci. Technol. 2 (1), 56–67.
Sakurai, H., Haruta, M., 1995. Carbon dioxide and carbon monoxide hydrogenation over gold supported on titanium, iron, and zinc oxides. Appl. Catal. A Gen. 127 (1–2), 93–105.
Schach, M.-O., et al., 2010. Techno-economic analysis of postcombustion processes for the capture of carbon dioxide from power plant flue gas. Ind. Eng. Chem. Res. 49 (5), 2363–2370.
Studt, F., et al., 2014. Discovery of a Ni-Ga catalyst for carbon dioxide reduction to methanol. Nat. Chem. 6 (4), 320–324.
Tola, V., Pettinau, A., 2014. Power generation plants with carbon capture and storage: a techno-economic comparison between coal combustion and gasification technologies. Appl. Energy 113, 1461–1474.
Wall, T.F., 2007. Combustion processes for carbon capture. Proc. Combust. Inst. 31 (1), 31–47.
Zhang, X., et al., 2013. Carbon chain analysis on a coal IGCC—CCS system with flexible multi-products. Fuel Process. Technol. 108, 146–153.

Further Reading

Sadati Tilebon, S.M., Ghasemzadeh, K., Jafarharasi, N., Vousoughi, P., 2014. An overview on the bioethanol production using membrane technologies. Int. J. Membr. Sci. Technol. 1, 9–22.

This page intentionally left blank

CHAPTER 25

Methanol Economy Versus Hydrogen Economy

Siddharth Gumber, Anand V.P. Gurumoorthy
VIT University, Vellore, India

Acronyms

ACS	American Chemical Society
DMFC	direct methanol fuel cell
DOE	Department of Energy
FC	fuel cell
ICI	Imperial Chemical Industries
LPG	liquefied petroleum gas
PEM	proton exchange membrane
PET	polyethylene terephthalate
WGS	water gas shift reaction

1 Introduction

> The world and its habits have evolved over time. There will be a paradigm shift from free oil to a paid alternative.

It is a challenging task to turn an invention into an innovation. This process demands high-end research and development over a significant time span. The present gasoline is a result of the advances in distillation over the years, so a fuel is desired which can fulfill the energy needs of the ecosystem and can haul it through a clean and economic pathway just as successfully as gasoline. The superior technology grows, reaching a maximum market penetration as it begins to be replaced by a better technology (Banholzer and Jones, 2013), which needs to happen with oil. Even after figuring out a practical solution to the problem, the advanced technology takes decades for adoption.

The quest for an appropriate fuel started with the wood and moss and ever since then, we haven't looked back. The industrial revolution brought in coal which was majorly used as a fuel due to its high calorific value. Oil and natural gas were added during the 20th century. Ample

Methanol. https://doi.org/10.1016/B978-0-444-63903-5.00025-X

stocks of reserves exist that would satisfy the dire demand for the next few decades. Though oil will not be exhausted overnight, market forces will inevitably drive prices up as demand will surpass supply, creating a true and lasting oil crisis (Olah et al., 2011).

Climate change, increasing oil prices, and altercations in the Middle East have given ominous hints to look for alternate fuels that could fulfill the energy demand for the latter centuries. There has been much debate on choosing the right fuel. Dennis Weaver had earlier commented that if we had a hydrogen economy worldwide, every nation on earth could create its own energy source to support its economy, and the threat of war over diminishing resources would just evaporate. This overtly highlights the utmost importance of hydrogen as a fuel in curbing imminent oil shortages. On the contrary, John Heywood, director of the Sloan Automotive Laboratory, argued that if hydrogen does not come from renewable sources, then it is simply not worth doing, environmentally or economically (Romm, 2004). From this viewpoint, it is clear that fuel selection has always been a highly debatable issue.

This chapter discusses the growing global trends in energy economy and reveals the crucial steps taken by different countries in order to solve the sustainability issues. Section 2 illustrates the hydrogen economy and its limitations. Section 3 discusses the growing methanol economy and its advantages to humankind. It also entails the various production methods of methanol. The following section presses on the importance of direct methanol fuel cell (DMFC) in the proposed methanol society. Section 4 lists the industrially important chemicals derived from methanol. Section 5 discusses the world methanol economy.

2 Hydrogen Economy and Its Limitations

> Future will see the solar-hydrogen economy at any bit of efficiency due to the abundance of solar and the miracles of hydrogen.

Hydrogen economy literally means producing and using hydrogen as a clean fuel. Despite its zero nontoxic emissions, we haven't been able to reach a cross-over point where it can compete with gasoline. Economic production, storage, and efficient combustion are the governing factors to regard any fuel as promising. The relatively low hydrogen density, together with the high gas pressures in the systems, are important drawbacks of the technically simple and, on the laboratory scale, well established high-pressure storage methods (Züttel, 2004). Hydrogen may not directly participate in greenhouse emissions but its production through fossil fuels, coal, etc. impart a significant carbon footprint. Also, a substantial amount of energy is lost during its storage and transportation which makes it economically nonviable when compared to oil.

Hydrogen poses some serious problems which demand intensive research before it can be a replacement to oil. They are:

1. *Production*: A significant amount of energy is required to produce hydrogen because it is not a primary energy resource. An ample amount of feedstock is the first requirement for any fuel to be considered as viable and economical. Secondly, the price of the raw material should be even-handed as compared to the value of fuel produced. For example, a photovoltaic solar panel integrated to a fuel cell (FC) can produce hydrogen by utilizing the electricity generated from the panel and reversibly produce electricity by consuming hydrogen during the night. Despite its renewable framework, the system is inefficient and economically not feasible. Putting in more energy into the creation of fuel than we get seems impractical as energy return on investment is a key parameter when talking about fuels (Banholzer and Jones, 2013).
2. *Storage*: Hydrogen has a low volumetric density which requires the development of advanced storage methods. The most common method of storage is high-pressure gasoline cylinders which have design pressures of up to 800 bar. Boil off and leakages are subsequent problems associated with high-pressure canisters. Peter Hall, a chemical engineer at the University of Strathclyde, UK, disparaged the Department of Energy (DOE) target of 10 wt% hydrogen storage at the ACS fall meeting in Boston due to significant anomalies linked to hydrogen production and management. Many car companies like Opel and General Motors have confirmed his statement. Fig. 25.1 depicts the overall feasibility of fuels in terms of gravimetric and volumetric density, diesel and gasoline have

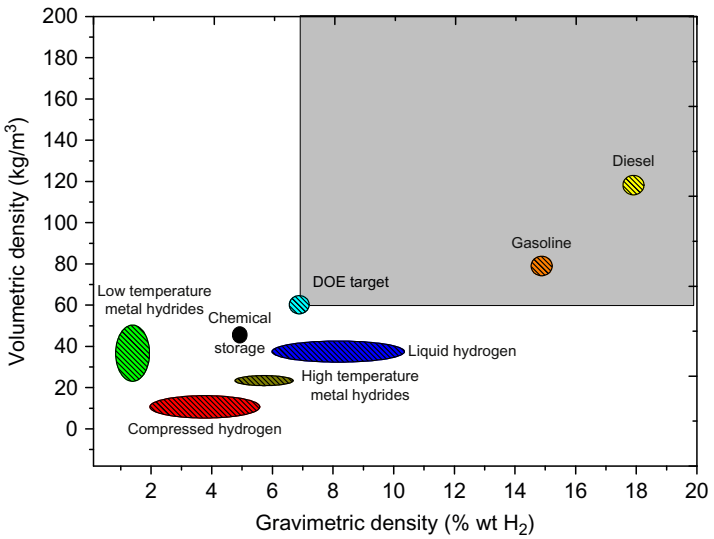

Fig. 25.1
Hydrogen storage methods and conventional fuels.

outweighed the available hydrogen/hydrogen storage methods. This clearly suggests that the material along with its tank and fittings should carry enough hydrogen to haul a conventional vehicle several hundred miles. It is also clear from the figure that liquid hydrogen has successfully crossed the DOE 2015 target of 10 wt% but liquid hydrogen requires a refrigeration unit to maintain a cryogenic state (Weast et al., 1988) thus adding weight and energy cost and around 40% loss in energy content (Trudeau, 1999).
A group of Mg-based hydrides is a potential candidate for mobile hydrogen storage with reversible hydrogen capacity of 7.6 wt% (Sakintuna et al., 2007). But this is still less than the DOE target and involves high desorption temperatures thereby reducing the efficiency and applicability in conventional vehicles.

3. An entirely new infrastructure needs to be developed to supply hydrogen to vehicles and meet the energy demands.
4. *Safety*: It is difficult to handle hydrogen in the gaseous phase.

It's plausible to say that the problems associated with sustainability which includes fuel production and safe and viable dispensing aren't just conventional engineering problems—they are "wicked" problems (Azapagic and Perdan, 2014). An affordable and viable alternative is methanol which has more hydrogen by mass in 1 L than in a liter of pure liquid hydrogen (98.8 g of hydrogen in 1 L of methanol at room temperature compared to 70.8 g in liquid hydrogen at −253°C) (Olah et al., 2011). Thus, it can be inferred that methanol is a safe carrier fuel for hydrogen. The reported octane number of methanol is 108.7 as compared to that of gasoline which is 91. This explicitly suggests that the methanol-air mixture can be compressed more before it's ignited. This boosts up the efficiency of the engine and ensures cleaner emissions. Unlike gasoline and diesel, methanol doesn't emit any soot or smoke on combustion. Also, methanol can acquire the same infrastructure as used for gas and diesel and thus can relieve infrastructure and dispensing costs. Such novel characteristics can solve the heated issues of evanescing fossil reserves and bring in a feasible "Methanol Economy."

3 The Methanol Economy and Its Advantages

> The Stone Age did not end for lack of stone, and the Oil Age will end long before the world runs out of oil
>
> ***Rapier (2012).***

Sheikh Yamani's prescient words assure us that the technology will solve the problem of evanescing oil reserves. Oil shall not serve as a primary energy source any longer but will be used to prepare other chemical products (Marbán and Valdés-Solís, 2007). "Methanol Economy" will eventually solve many of the tacit issues of climate change and oil shortage due to the following reasons:

1. Presently, methanol is prepared from synthesis gas (syngas or $CO + H_2$). Syngas is obtained from partial combustion of coal and natural gas. Coal will last for another 150–200 years.

2. Methanol can be effectively produced by methane via oxidation without the production of syngas.
3. Methanol can also be produced by reductive hydrogenation by utilizing CO_2. This is a crucial method as it can solve the problem of global warming by cutting the level of CO_2 that is being emitted through the industries.
4. Methanol has a higher "flame speed" which enables faster and more complete fuel combustion in the cylinders (Olah et al., 2011).
5. Methanol has a higher octane number than gasoline, an increased efficiency of the internal combustion engines.
6. Despite having half the energy density of gasoline, less than double the amount of methanol is necessary to achieve the same power output (Olah et al., 2011).
7. Using DMFC to obtain electricity without the need to produce hydrogen.

3.1 Methanol Production

3.1.1 Production from syngas

Today, methanol is mainly produced by syngas according to the following main equations:

$$\text{Methanol synthesis} \quad CO + 2H_2 \Leftrightarrow CH_3OH \quad \Delta H_R = -90.84 \text{ kJ/mole} \tag{25.1}$$

$$\text{Water-gas shift reaction} \quad CO + H_2O \Leftrightarrow CO_2 + H_2 \quad \Delta H_R = 41.27 \text{ kJ/mole} \tag{25.2}$$

Reaction (25.1) is exothermic as it is produced at low temperatures and higher pressures. The reaction is mediated by a copper catalyst. It has been proven that syngas and a minimal amount of CO_2 are required to produce methanol. Therefore, it's ensured that CO_2 is also produced to maintain the composition of syngas. The purity of syngas is measured by stoichiometric number S.

$$S = \frac{(\text{Moles of } H_2 - \text{Moles of } CO_2)}{(\text{Moles of } CO + \text{Moles of } CO_2)}$$

The value of S for methanol production lies in the vicinity of 2.0. An S value greater than 2.0 denotes more H_2 content and a lesser value denotes less hydrogen content. A value of 2.0 is considered to be an optimal and target value by methanol manufacturers. The catalyst is active at temperature and pressure conditions of around 230°C and 50–100 atm, respectively. These reaction parameters and the choice of catalyst were provided by Imperial Chemical Industries (ICI) in 1960 and since then this route is the lowest pressure route achievable in the history of methanol production. Reaction (25.2) is the water gas shift reaction (WGS) which aims to maintain the composition of H_2 in the syngas.

The synthetic gas used to produce methanol is obtained from partial oxidation of coal, petroleum, asphalt, and heavy oils, etc. (Olah et al., 2011).

3.1.2 Partial oxidation of natural gas (CH_4)

Production of methanol from natural gas without the need to convert into syngas is an appreciated and promising route due to the abundant natural gas reserves. Also, large reserves of methane are tied up in the hydrated form in vast areas of the subarctic tundra and under the seas in areas of the continental shelves (Olah et al., 2011). The reactions are given as follows:

$$\text{Methanol synthesis} \quad CH_4 + \frac{1}{2}O_2 \Rightarrow CH_3OH \quad \Delta H_{298} = -128 \text{ kJ/mole} \tag{25.3}$$

The above process has not been commercialized due to the poor selectivity of methanol. The difficulty in converting methane to methanol lies in activating the C–H bond. The methane molecule is a perfect tetrahedron and the four C–H bonds are uniform (Zhang et al., 2003). Another disadvantage linked to this process is the oxidation of CO and H_2 due to unwanted CO_2 and water. A large amount of heat is also wasted in this process. To increase the efficacy of the process, modern plants are using the released heat for steam reforming and partially oxidizing methane with oxygen and reformed steam.

3.1.3 Methanol from CO_2

Methanol has attracted researchers and climatologists over the global issues of surface warming by utilizing the CO_2 for its production using a homogenous catalyst. The reaction is:

$$\text{Methanol synthesis} \quad CH_4 + CO_2 \Rightarrow 2CO + H_2 \quad \Delta H = 70.7 \text{ kJ/mole} \tag{25.4}$$

The syngas obtained from the above reaction has low hydrogen content and so hydrogen has to be added from other sources to reach the adequate composition (Olah et al., 2011).

This methodology is a two-way scheme:

1. It solves the problem of global warming by taking up the greenhouse gas, i.e., CO_2.
2. Using the products of this reaction as raw materials to produce methanol.

The crucial factor involved in this mechanism is the choice of the right catalyst. The reaction a high temperature. Sintering and coking of the catalyst at high temperatures are other major associated limitations. As a future goal, researchers plan to introduce a catalyst that can withstand high temperatures and improve the kinetics of the process.

3.1.4 Methanol from formic acid and formaldehyde

The above reactions operate at extreme pressure and temperature conditions which are not suitable for many catalysts and also pose a risk of an industrial disaster. In order to reduce the working temperature and pressure needed for methanol synthesis, new pathways have been devised to convert syngas to methanol. One of the potential techniques is to produce methanol via methyl formate and successive hydrogenolysis (removal of substituent using hydrogen) of

methyl formate to methanol, leading to a net gain of one molecule of methanol (Marchionna et al., 1997). The reactions are:

$$\text{Methyl formate synthesis} \quad CH_3OH + CO \Rightarrow HCOOCH_3 \tag{25.5}$$

$$CH_3OH + H_2O \Rightarrow CO_2 + 6H^+ + 6e^- \quad E^{\circ}_{\text{anode}} = 0.046 \text{ V} \tag{25.6}$$

$$\text{Methanol synthesis} \quad HCOOCH_3 + 2H_2 \Rightarrow 2CH_3OH \tag{25.7}$$

A methanol molecule produces two methanol molecules. The carbonylation is carried out in the liquid phase using sodium or potassium methoxide as a homogenous catalyst (Olah et al., 2011).

3.2 Direct Methanol Fuel Cell

DMFC as a potential energy carrier is an important invention. A 20% efficient DMFC is three times more efficient than advanced lithium ion batteries (Jeong et al., 2008). Unlike FCs, DMFCs are not dependent upon the generation of hydrogen. The end products of a DMFC are CO_2 and water. CO_2 can be further sequestered to produce methanol. It is a challenging task to store hydrogen in present-day vehicles for onboard electricity generation and hence, FC is not a viable solution. On the contrary, methanol is a liquid and can occupy the conventional gasoline tanks in vehicles with minor modifications.

Methanol-proton exchange membrane (PEM) cells use a separate reformer to produce hydrogen, after which it is fed to the FC for electricity production (Olah et al., 2011). But the system is inefficient. DMFC is a simpler setup, consisting of two electrodes separated by a PEM. The electrodes are connected to an external circuitry for electricity supply. This technique scraps the need to produce and store hydrogen. Also, FCs are based on molten carbonate and solid oxide (SO) electrolytes, which have to be operated at a temperature spanning from 700 to 1000°C (Hogarth and Hards, 1996). Fig. 25.2 shows the construction of a DMFC. The anode is dipped in the methanol-water mixture and the cathode is exposed to oxygen in the air, either in ambient or in pressurized form. The anode and cathode are separated by a PEM which is impregnated with a catalyst on both sides.

Methanol and water react at the anode to produce CO_2, protons, and electrons. The CO_2 is rejected at the anode and the protons migrate to the cathode through PEM and react with O_2 to form water. The free electrons' electricity is supplied to the load connected to the DMFC. The theoretical open circuit voltage is 1.18 V which is substantially reduced in a real system due to the cell's internal resistance (poor kinetics and methanol cross-over). The limitations of this system are:

1. The reaction kinetics involved in the electricity generation is slow. Methanol permeates into the PEM and reaches the cathode catalyst layer, where it forms a mixed potential that

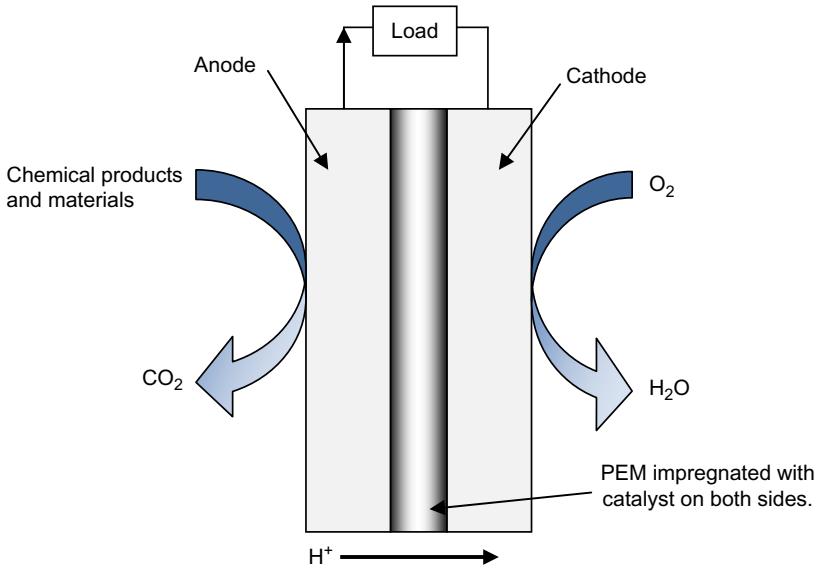

Fig. 25.2
Schematic representation of DMFC.

decreases the cell voltage (Jeong et al., 2008). Methanol may poison the cathode catalyst (Pt) and block its sites, thereby reducing its efficiency (Olah et al., 2011).

2. Flooding occurs at cathode due to excessive generation of water (Olah et al., 2011).

DMFCs are still in their preliminary design stage so not much efficiency and feasibility has been achieved so far. Researchers are focusing on:

1. Development of alternate catalysts which can resist a methanol attack.
2. Improvement in present membranes and electrolytes to prevent flooding at the cathode.

DMFCs are an important class of FCs in terms of its on-board electricity generation application. These are simple and compact setups, unlike conventional FCs which require a hydrogen infrastructure and storage facility. DMFCs can successfully serve over long distances once they are efficient enough as they run on clean and liquid methanol. On the contrary, conventional FCs need development in efficiency as well as in hydrogen storage capability before they can attract attention.

3.3 "Methanol Society" and Environment

The most promising and efficient method to produce methanol is through syngas produced from natural gas due to the abundance of natural gas reserves. People are trying to simplify the production process by directly converting methane to methanol. Partial oxidation of methanol is an innovative approach which requires significant research to make it more feasible and

usable. Methanol has a number of advantages over other alternate forms of fuel available as a replacement to the conventional oil. They are:

1. A significant reduction in the carbon footprint can be achieved by using DMFC which relies on cheap methanol rather than costly hydrogen.
2. The end product obtained from burning methanol is CO_2 which can be recycled to produce methanol again. Moreover, atmospheric CO_2 can also be captured and utilized in the production of methanol.
3. Methanol is a polar liquid and can rapidly degrade both in aerobic and anaerobic conditions, unlike crude oil which doesn't.
4. Oil spillage in water bodies reduces oxygen diffusion into the water which subsequently kills the aquatic life. The toxicity level of methanol is low as compared to oil.
5. It is safe to store methanol in double walled canisters but it is dangerous to store hydrogen in conventional containers as it tends to corrode steel and many other metals with time.
6. Methanol burns with a visible and controllable flame. Hence, safety precautions and mitigation operations can be performed in the affected areas, whereas hydrogen burns with an invisible flame and can attract difficulty in mitigating hydrogen fires. It becomes extremely difficult to control hydrogen fires because of the fuel's higher flame speed as compared to methanol.

The traditional fossil fuel society will undergo significant and viable changes when methanol becomes the primary energy source. The suggested "Methanol Society" is given in Fig. 25.3.

The features of the methanol society are illustrated below:

1. Oil will continue to serve as a secondary energy source. It will be used to produce other important hydrocarbon products. Coal and natural gas will serve as the major feedstock for electricity generation followed by hydroelectric, nuclear, geothermal, wind, and solar energies.
2. Natural gas will support the methanol society due to its abundant availability. The accessibility of biomass shall serve the methanol production only at selected locations.
3. The CO_2 emitted by industries and vehicles will be captured and used to produce methanol.

The "Methanol Society" will be able to control the energy issues through an economic and green pathway which would be fairly acceptable in the ecosystem without any unwanted forcing.

Methanol has some added disadvantages which may prove to be harmful if exploited. Some distinguishable points have been listed below:

1. Methanol is severely harmful if consumed. Higher doses can lead to death. Crude is equally dangerous if swallowed.

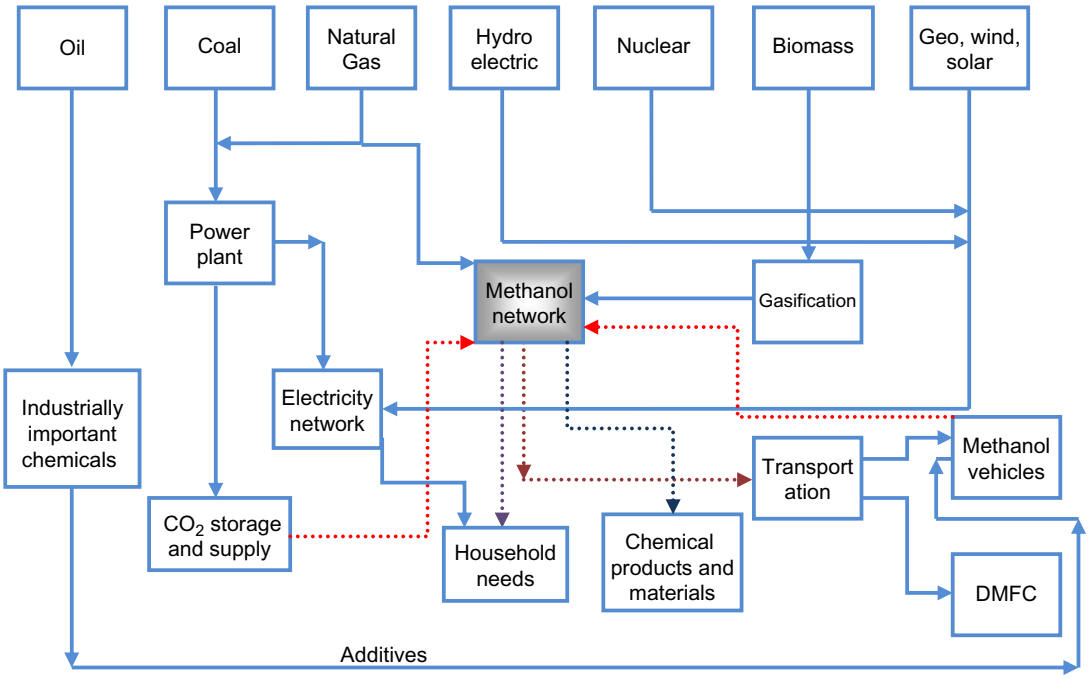

Fig. 25.3
Suggested "Methanol Society."

2. In methanol production, infrastructural modifications are required to meet the diverse energy needs and it will also require time and research before methanol economy is put into practice but these efforts are worthy and viable in order to shift to an alternate fuel.

Many new discoveries have been greeted with overenthusiasm with the hope that it will fulfill the diverse energy needs of the country but just because many possible solutions are available to a problem doesn't mean that all of them are viable. Hydrogen economy, bio-fuels, etc. are some of the proposed alternatives. A minor error in the conceptual stage can reflect as a major error in the final design. Such situations arise due to the misunderstanding of basic thermodynamic principles and conservation laws (Banholzer and Jones, 2013). Hence, energy economies should be handled with extreme care due to its larger penetration in the ecosystem.

4 Methanol Based Chemicals and Materials

As mentioned, methanol has a higher octane number than gasoline—it is a potential and clear substitution to gasoline and can be used as a blending agent. A commonly available blend includes M85, which is 85% methanol and 15% gasoline. Methanol can be chemically converted into gasoline, ethanol, liquefied petroleum gas (LPG), diesel, olefins, formates,

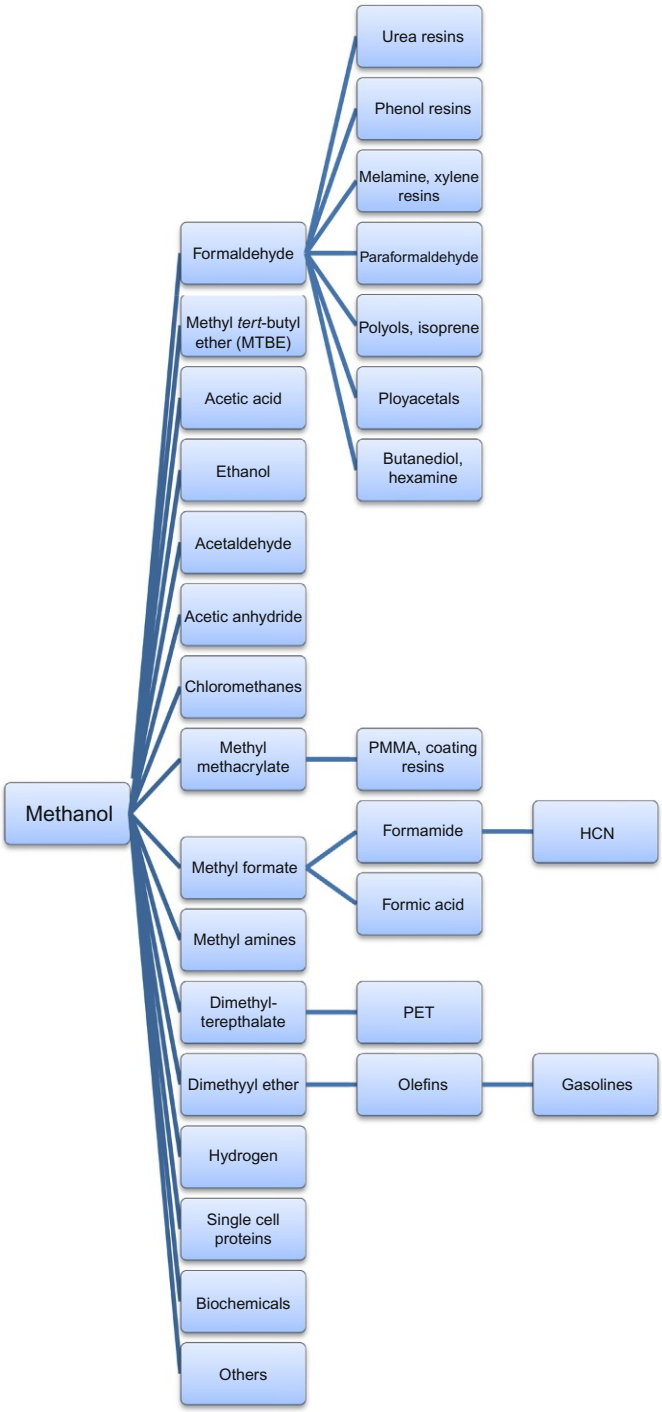

Fig. 25.4
Methanol-derived chemical products and materials.

anhydrides, etc. The methanol-derived chemical products and materials are listed in Fig. 25.4.

Formaldehyde is an important derivative from methanol and is used to manufacture a variety of industrially important materials such as urea resins, phenol resins, polyols, isoprene, polyacetals, etc. Coating resins used in paint industries are also derived from Methyl methacrylate which is produced from methanol. Crude oil based chemicals such as gasoline, olefins, and PET can be derived from dimethyl ether obtained from methanol, which is why methanol is an effective building block for the production of chemicals conventionally produced from petrochemical roots. The production of gasoline from methanol came out as an alternative to its production from natural gas and coal due to the issue of evanescing fossil reserves. The reactions are given in Eq. (25.8):

$$2CH_3OH \Leftrightarrow CH_3OCH_3 \rightarrow \text{Light Olefins} \rightarrow \text{Higher Olefins} \tag{25.8}$$

Methanol is converted to dimethyl ether, methanol, and water. The mixture is subsequently converted to light olefins and higher compounds. The higher gasoline compounds can be directly used in the gasoline pool without any refining.

There has been a paradigm shift in the energy needs of the world. The growing dependency on methanol cannot be disregarded. It would be fair enough to regard methanol economy as a "Revolution in evolution."

5 World Methanol Economy

The global methanol demand is 59 million tons (Methanex, 2015) and the volume of methanol used for crude oil substitution is estimated to increase from 32 to 39 Million Metric Tons by 2018 (ABAZAJIAN, 2015). The rate at which the methanol is substituting oil is sustaining due to the low prices of natural gas as compared to gasoline. The Chinese government is reportedly dependent on the methanol infrastructure in order to reduce the dependency on imported oil. A substitution of oil by methanol is growing rapidly. China is among the leaders to initiate several methanol projects which are continuing to develop whilst some are in the design stage. Fig. 25.5 depicts the methanol usage by region (Methanex, 2015). Besides China, Europe is blending up to 3% of methanol today. The methanol economy is penetrating into other parts of the world due to the competitive prices of methanol to gasoline and affordable infrastructure.

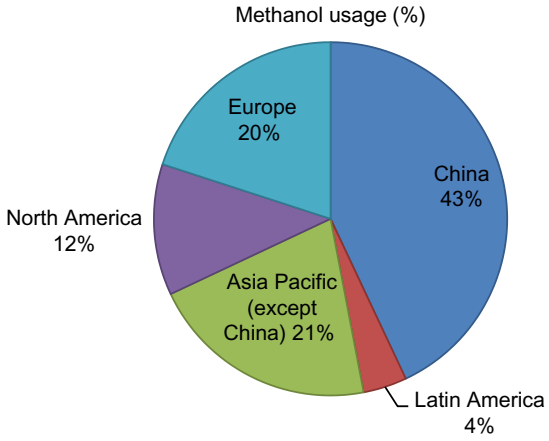

Fig. 25.5
Methanol usage by region.

6 Conclusion

Chemical engineering problems aren't just conceptual problems dealing with mass and energy balance but require a holistic analysis of the impacts of the solutions available to tackle critical issues of energy and food.

With the increasing human population, and development and higher standards of living, the energy demand is expected to grow to 21 TW in 2025 and about 30 TW in 2050 (Olah et al., 2011). It is important to note that older oil fields are running out of oil and newer oil fields are being discovered and explored to meet the energy demands. There has been a significant increase in the demand which has surpassed the overall exploration rates, to which we often conclude that the world is running out of oil. It is our responsibility to distinguish an efficient and virtuoso alternative amongst the many available choices. Just because we cannot feel and see energy like electricity, we have started creating hype about various economies.

There is a plausible explanation as to why we should be focusing upon methanol economy and not on the hydrogen economy. "Well to wheel analysis" is a crucial methodology used to trap the carbon footprint imparted by any fuel from its extraction to the final dispensing. Hydrogen may seem to win over other choices in terms of the final emissions but we cannot disregard its production and storage anomalies. On the other hand, methanol can solely depend upon natural gas for its production which will still last for another 100 years. It should be able to curb the increasing content of CO_2 in the atmosphere which has reached an alarming value of 400 ppm through improvement in the reaction kinetics. There have been suggestions about sequestering CO_2 under the aquifers and the bottom of the seas but we cannot simply implement a solution without doing an impact assessment. Storing the gas for a significant time span can cause absorption of the gas in the geographic layers of that eco-system

which may malign the life in that region. Another associated threat to underground storage is the gas leak which may also prove to be malignant. Such practices do not solve the Kyoto Protocol's argument of increasing CO_2 content in the atmosphere. Utilizing CO_2 for methanol production can provide a strong framework to the protocol's arguments. Finding efficient ways to store energy and to produce convenient hydrocarbon based fuels and products while mitigating global warming by recycling CO_2 is essential to our life and has long-range significance (Olah, 2005). Hence, it is strongly suggested to focus on methanol economy to serves as:

1. An energy carrier.
2. A nonpolluting fuel.
3. The initiator of industry important chemical products.

References

Abazajian, A., 2015. 'Methanol Economy' Gains Ground With Technology, Market Developments. Available: http://www.gasprocessingnews.com/features/201604/methanol-economy-gains-ground-with-technology,-market-developments.aspx (Last accessed February 2017).

Azapagic, A., Perdan, S., 2014. Sustainable chemical engineering: dealing with "wicked" sustainability problems. AIChE J. 60, 3998–4007.

Banholzer, W.F., Jones, M.E., 2013. Chemical engineers must focus on practical solutions. AIChE J. 59, 2708–2720.

Hogarth, M., Hards, G., 1996. Direct methanol fuel cells. Platinum Met. Rev. 40, 150–159.

Jeong, I., Kim, J., Pak, S., Nam, S.W., Moon, I., 2008. Optimum operating strategies for liquid-fed direct methanol fuel cells. J. Power Sources 185, 828–837.

Marbán, G., Valdés-Solís, T., 2007. Towards the hydrogen economy? Int. J. Hydrogen Energy 32, 1625–1637.

Marchionna, M., Lami, M., Galletti, A.M.R., 1997. Synthesizing methanol at lower temperatures. ChemTech 27 (4), 27–31.

Methanex, 2015. Methanex Investor Presentation. Available: http://www.gasprocessingnews.com/features/201604/methanol-economy-gains-ground-with-technology,-market-developments.aspx (Last accessed February 2017).

Olah, G.A., 2005. Beyond oil and gas: the methanol economy. Angew. Chem. Int. Ed. 44, 2636–2639.

Olah, G.A., Goeppert, A., Prakash, G.S., 2011. Beyond Oil and Gas: The Methanol Economy. John Wiley & Sons, Weinheim.

Rapier, R., 2012. Power Plays: Energy Options in the Age of Peak Oil. Apress, New York.

Romm, J.J., 2004. The Hype About Hydrogen: Fact and Fiction in the Race to Save the Climate. Island Press, Washington, DC.

Sakintuna, B., Lamari-Darkrim, F., Hirscher, M., 2007. Metal hydride materials for solid hydrogen storage: a review. Int. J. Hydrogen Energy 32, 1121–1140.

Trudeau, M.L., 1999. Advanced materials for energy storage. MRS Bull. 24, 23–26.

Weast, R.C., Astle, M.J., Beyer, W.H., 1988. CRC Handbook of Chemistry and Physics. CRC Press, Boca Raton, FL.

Zhang, Q., He, D., Zhu, Q., 2003. Recent progress in direct partial oxidation of methane to methanol. J. Nat. Gas Chem. 12, 81–89.

Züttel, A., 2004. Hydrogen storage methods. Naturwissenschaften 91, 157–172.

Index

Note: Page numbers followed by *f* indicate figures, and *t* indicate tables.

H

I

N

O

P

R

Z

Methanol
Science and Engineering

Edited by
Angelo Basile
Francesco Dalena

Timely, comprehensive reference on the most advanced production processes, properties, new technologies, and different applications of methanol

- Provides the latest developments on methanol research
- Reviews methanol production methods and their economics
- Outlines the use of methanol as an alternative green transportation fuel
- Includes new technologies and many new applications of methanol

Methanol: Science and Engineering provides a comprehensive review of the chemistry, properties, and current and potential uses and applications of methanol. Divided into four parts, the book begins with a detailed account of current production methods and their economics. The second part deals with the applications of methanol, providing useful insights into future applications. Modeling of the various reactor systems is covered in the next section, with final discussions in the book focusing on the economic and environmental impact of this chemical. Users will find *Methanol: Science and Engineering* to be a must-have resource for all researchers and engineers studying alternative energy sources.

Dr. Angelo Basile is a chemical engineer and senior researcher at the ITM-CNR, where he is responsible for research related to both ultra-pure hydrogen production and CO_2 capture using Pd-based Membrane Reactors. Dr. Basile serves as an associate editor and editor-in-chief of two international scientific journals and has participated in various national and international projects on membrane reactors and membrane science. Since 2014, Dr. Basile has been a full professor of chemical engineering processes.

Francesco Dalena, a European PhD, specializes in chemistry of advanced materials at the University of Calabria (Italy). His research field ranges from the bioenergy sector and inorganic membrane reactors to chemical kinetics. Dr. Dalena serves as a member of the editorial boards of two international scientific journals. Recently he was involved in a project concerning the functionalization of cellulose fibers that produced a patent.

ELSEVIER

elsevier.com/books-and-journals

ISBN 978-0-444-63903-5

9 780444 639035